Responses to United Wambo Submission of 14 April 2019, responding to the Rocky Hill and Wallarah 2 cases on climate change and greenhouse gas emissions

I have prepared this report following a request from EDO NSW acting on behalf of Hunter Environment Lobby Inc, to respond to the United Wambo Submission of 14 April 2019. This report follows on from my original expert report on the United Wambo project, dated 11 December 2018. In preparing this report I have been bound by Division 2 of Part 31 and the Expert Witness Code of Conduct under the *Uniform Civil Procedure Rules 2005*.

The numbers below refer to paragraphs in the United Wambo Submission

6.26. The carbon budget is the most scientifically robust approach to determining the cumulative amount of CO_2 that can be emitted globally for a given temperature target (see points 41-43 in my original expert report of 11 December 2018; Collins et al. 2013; IPCC 2013). That it is not required to be observed by the *Paris Agreement* in no way diminishes its scientific validity. National NDCs, such as Australia's, are influenced by a number of factors, and are not necessarily consistent with the scientific requirements to meet the Paris targets. In fact, the Climate Change Authority, based on the carbon budget framework, has determined that Australia's NDC is significantly weaker than what is required for Australia to do its fair share of emission reductions in meeting the Paris targets (CCA 2015).

6.27(a). This statement is incorrect. The carbon budget approach is directly relevant to any proposed projects that would emit greenhouse gases to the atmosphere.

6.27(b) This statement (the 'double counting argument') is incorrect. The carbon budget approach is directly applicable to the *Paris Agreement* in that it determines the cumulative amount of CO_2 that can be emitted globally to achieve the Paris temperature targets. The mechanisms by which nations reduce their emissions are indeed determined by the nations themselves, but the sum total (Scope 1 + Scope 2 + Scope 3) of emissions, no matter where the emissions occur, must meet the scientific requirements for a given temperature target. These emissions are counted only once (no matter where they occur) in the carbon budget approach so there is definitely no double counting. It is the temperature targets that nations have agreed to meet in signing the *Paris Agreement* (not a specific accounting protocol) and the carbon budget approach is the most scientifically robust way of determining what is required to meet the targets.

6.27(c)(i) There are indeed uncertainties around the carbon budget, as noted in my submission (point 44; Collins et al. 2013, Ciais et al. 2013; Steffen et al. 2018). However, in my analysis I have taken these uncertainties into account to produce a conclusion that gives a very generous (large) remaining carbon budget. More specifically:

- the analysis assumes a 67% probability of meeting the 2°C target; this means that there is a 33% probability of exceeding the 2°C target, which most scientists view as unacceptably high given their knowledge of the risks associated with higher temperature rises;
- non-CO_2 greenhouse gas emissions have not been included, given that they are much more difficult to reduce than CO_2;
- carbon cycle feedbacks (Steffen et al. 2018) have not been included, which leaves a larger CO_2 budget.

The overall outcome is that these assumptions regarding uncertainties leave a large, but limited, remaining CO_2 emission budget (205 GtC, taking 2018 emissions into account). Even with these assumptions, there is far more than enough CO_2 emissions built into existing fossil fuel developments to easily consume the entire budget of 205 GtC (e.g., McGlade and Ekins 2015). Therefore, the inescapable conclusion is that to meet the Paris 2°C target, no new fossil fuel developments can be allowed.

6.27(c)(ii). Technological advances can easily be accounted for in the carbon budget approach. For example, new technologies could increase the efficiency of the combustion process, thus reducing the coal burned, and thus the emissions, for a given amount of electricity produced. Such technologies would act to extend the lifetime of existing fossil fuel developments (but would result in the same cumulative emissions over the lifetime of the power plant) rather than to allow new ones. In addition, the technologies quoted in this point by the proponent (e.g., carbon capture and storage) do not yet exist at commercial costs and scales. The critical point for this argument of the Applicant is that such technologies are hypothetical at present. Furthermore, it is very unlikely that new, hypothetical technologies would be retrofitted onto existing fossil fuel facilities at the scale and rate needed to stay within the carbon budget.

6.27(c)(iii). The fact that the carbon budget approach is not formally recognised in the *Paris Agreement* is not at all a reflection on any deficiencies in the approach. Rather, it is reflection on the failure of nations to agree a current mitigation framework that is consistent with the best available science. Consistency with the science could be achieved if nations adopt more aggressive NDCs. For example, changing Australia's 2030 target from a 26-28% reduction (based on 2005 levels), our current NDC, to a 45-65% reduction on 2005 levels as a new NDC would then move our commitment into consistency with the carbon budget approach. This could be achieved via the 5-yearly 'ratcheting up' mechanism in the *Paris Agreement*.

8.6. This comment by the Applicant is based on faulty logic. The impacts of climate change are the result of millions of individual emissions of greenhouse gases from the combustion of fossil fuels. This proposed development would increase those emissions, thus contributing to the worsening of climate change impacts around the globe.

8.8. This comment directly contradicts the comment in 8.7. In 8.7, the Applicant agrees that action needs to be taken to reduce GHG emissions. Then in 8.8 the Applicant proposes to **increase** GHG emissions, using deficiencies in Australian or NSW laws as an excuse to open a new coal mine that would increase GHG emissions. This argument defies fundamental logic: one cannot reduce GHG emissions by increasing them. Furthermore, approval of this coal mine would be in contravention of the *Paris Agreement*, to which Australia is a signatory.

8.10-8.13. The Applicant's response is fundamentally flawed. The climate system is a single, highly integrated planetary system. It does not care where the emissions come from or how they are classified (Scope 1, 2 or 3); they all contribute to climate change. Greenhouse gas emissions anywhere affect the climate system everywhere. To meet the targets of the *Paris Agreement*, GHG emissions must be reduced deeply and rapidly, and any **NEW** sources of emissions are incompatible with that agreement, regardless of how they are assigned or what planning laws may or may not permit.

8.15. The question I raise here is the fundamental question of whether the IPC should make a merit-based decision to approve the project taking into account the overall objective of avoiding dangerous climate change as articulated by the *Paris Agreement*, in particular, the temperature targets. That is, if Australia (or any other country, for that matter) is serious about implementing the *Paris Agreement*, then no new fossil fuel development should be allowed. The absolutely clear, scientifically indisputable fact is that if the global average temperature rise is to be limited to "well below 2 degrees C" (the *Paris Agreement*), then expansion of the fossil fuel industry must end immediately and a phase-out period for fossil fuel usage of two-three decades must begin, at the end of which GHG emissions must have reached net-zero (please see the *IPCC SR1.5 report 2018* for the scientific justification for that statement).

8.19. This point misrepresents my position. I have never said that existing fossil fuel facilities should be halted. In fact, as noted above, I have argued that existing fossil fuel facilities need to be phased out in an orderly fashion over a two-three decade period, as recommended in the IPCC SR1.5 report. This would allow time for alternative energy sources to be put in place, thus avoiding the alleged deleterious effects on human populations (IPCC SR1.5). I would add that **<u>not</u>** refusing new fossil fuel developments and phasing out existing ones would, with a very high probability, result in crippling and devastating consequences for human populations and for intragenerational and intergenerational equity (see IPCC Fifth Assessment Report, WGII 2014).

Will Steffen
1 May 2019

Relevant References:

CCA (Climate Change Authority) (2015) Final Report on Australia's Future Emissions Reduction Targets, 2 July 2015. Accessed at: http://climatechangeauthority.gov.au/sites/prod.climatechangeauthority.gov.au/files/Final-report- Australias-future-emissions-reduction-targets.pdf.

Ciais P et al. (2013) Carbon and Other Biogeochemical Cycles, in Climate Change 2013: *The Physical Science Basis, Contribution of Working Group I to the Fifth Assessment Report of the Intergovernmental Panel on Climate Change*, edited by Stocker TF, Qin D, Plattner G-K, Tignor M, Allen SK, Boschung J, Nauels A, Xia Y, Bex V and Midgley PM, Cambridge and New York, Cambridge University Press, pp. 465–570, doi:10.1017/CBO9781107415324.015.

Collins, M. *et al.* (2013) Long-term climate change: Projections, commitments and irreversibility, in *Climate Change 2013: The Physical Science Basis*, *Contribution of Working Group I to the Fifth Assessment Report of the Intergovernmental Panel on Climate Change*, edited by Stocker, T.F., Qin, D., Plattner, G.-K., Tignor, M. Allen, S.K., Boschung, J. Nauels, A., Xia, Y., Bex, V. and Midgley, P.M., Cambridge and New York, Cambridge University Press, pp. 1029-1136.

IPCC (2013) Summary for Policymakers. In: *Climate Change 2013: The Physical Science Basis*, Contribution of Working Group I to the Fifth Assessment Report of the Intergovernmental Panel on Climate Change, edited by Stocker TF, et al. Cambridge and New York, Cambridge University Press, pp .

IPCC (2014) Summary for Policymakers. In Climate Change 2014: Impacts, Adaptation, and Vulnerability, Contribution of Working Group II to the Fifth Assessment Report of the Intergovernmental Panel on Climate Change, edited by Field CB, et al. Cambridge and New York, Cambridge University Press.

IPCC (2018) Global Warming of 1.5°C. IPCC Special Report on the impacts of global warming of 1.5°C above pre-industrial levels and related global greenhouse gas emission pathways, in the context of strengthening the global response to the threat of climate change, sustainable development, and efforts to eradicate poverty. Intergovernmental Panel on Climate Change.

Le Quéré C et al. (2017) Global Carbon Budget 2017. *Earth System Science Data Discussions* https://doi.org/10.5194/essdd-2017-123

McGlade C and Ekins P (2015) The geographical distribution of fossil fuels unused when limiting global warming to 2°C. *Nature* 517: 187-190.

Steffen W et al. (2018) Trajectories of the Earth System in the Anthropocene. *Proc. Natl. Acad. Sci. (USA)* doi/10.1073/pnas.1810141115

Australian Government
Climate Change Authority

FINAL REPORT ON AUSTRALIA'S FUTURE EMISSIONS REDUCTION TARGETS, 2 JULY 2015

In its Draft Report to the Minister for the Environment on 22 April on Australia's future greenhouse gas emissions reduction targets, the Authority recommended that at the upcoming Paris climate conference Australia commit to:

- a 2025 target of 30 per cent below 2000 levels; and
- further reductions by 2030 of between 40 and 60 per cent below 2000 levels.

The Authority indicated it would review these preliminary recommendations in the light of feedback from stakeholders and any new information that became available.

The consultative process elicited a good exchange of views, which helped to clarify the Authority's understanding of the positions of various stakeholders. From the Authority's perspective, these discussions—and the limited new information which has emerged in recent weeks—have strengthened the Authority's conviction in the overall appropriateness of its preliminary recommendations. In particular, a broad measure of agreement existed around the following points:

- the determination of targets should give most weight to what the scientific evidence is telling us we need to do, to what comparable countries are doing and, not least, to what is in the best interests of current and future generations of Australians;
- while the recommended targets for Australia are challenging, they are no more so than the targets many other developed countries have been pursuing in recent years, and are committing to in the post-2020 period;
- the costs of achieving particular targets (including their adverse impacts on certain industries) are best considered in the design of appropriate policy instruments, rather than through the acceptance of inadequate national targets;
- major benefits to Australia will accrue both from avoiding the harmful consequences of dangerous climate change and from participating in the opportunities and new technologies that will accompany the transition to a lower carbon world; and
- all countries, including Australia, will need to progressively lift their efforts to reduce emissions well beyond 2020 to maintain a reasonable chance of limiting global warming to less than 2 degrees above pre-industrial levels.

This brief final report addresses issues which have arisen since the release of the Authority's recent Draft Report, and indicates the Authority's responses to those issues.

Climate science

The Authority's recommendations for Australia's post-2020 emissions reduction targets are underpinned by the evidence from climate science that emissions of greenhouse gases from human activities are the dominant contributor to global warming. All countries have agreed to work together to reduce emissions to a level that keeps global warming below the 2 degrees threshold. Climate science also tells us that warming beyond that threshold is likely to have increasingly severe social, economic and environmental impacts, not least in a dry continent like Australia. Avoiding those impacts will require concerted global actions with all countries—Australia included—shouldering a fair share of the emissions reduction burden: unilateral insouciance is no protection against the encroachment of climate change.

Stakeholder feedback

Stakeholders were generally supportive of the 2 degree goal. In their submissions, AGL Energy, the Grattan Institute, the Australian Academy of Sciences, the Australian Industry Group and the Investor Group on Climate Change all indicated broad support for determining post-2020 targets in the light of this agreed goal; some (such as WWF and The Climate Institute) favoured stronger targets than those recommended by the Authority, arguing that Australia's emissions reduction targets should be aligned with a higher probability of limiting global warming to 2 degrees, and/or of keeping open the possibility of limiting warming to 1.5 degrees. Stakeholders generally agreed with the Authority's proposal that Australia's targets and policies should be reviewed periodically against global goals and action.

Comparability of action

In addition to their underpinning by climate science, the Authority's preliminary recommendations reflected a judgment that, as a proxy for its fair share of the overall emissions reduction task, Australia should broadly match the targets of other wealthy developed countries, including the United States and the European Union. It is the Authority's judgment that its recommended targets for 2025 and 2030 continue to satisfy this comparability test.

Recent developments

Since the Authority's Draft Report was released, some additional countries—including Canada and Japan—have announced post-2020 emissions reduction targets. Over the same period there has been a notable build-up—at many levels—both in concerns about the risks of dangerous climate change and in expectations for effective, ongoing policy actions to emerge from the Paris Conference in December.

Table 1 shows how the recently announced targets of Canada and Japan compare with those announced previously by several other developed countries. Canada's target is to reduce its emissions by 30 per cent from 2005 levels by 2030, with Japan proposing a 2030 target of 26 per cent below 2013 levels. While representing an improvement on their existing 2020 targets, these post-2020 targets for Canada and Japan are rather less ambitious than those announced by the United States and some other developed countries. In the case of Japan that country's emissions reduction efforts were dealt a serious blow by Japan's response to the Fukushima nuclear disaster, and the consequent increased reliance on coal for its electricity generation. Canada's national target is a good deal weaker than that which the Authority is recommending for Australia; the Canadian target suggests that much of the running on climate change in that country will remain with the provincial governments, some of which have adopted their own emissions reduction targets and policies.

Outside national governments, interest in reducing greenhouse gas emissions and bolstering the 2 degree goal continues to build. The G7 group resolved recently to phase out carbon emissions from fossil fuels by the close of the century. State and provincial governments—and major cities—in several countries are increasing their collaboration on ways to reduce their emissions; this includes Australian state and territory governments, as well as the cities of Sydney and Melbourne.

Business and community groups too have been sharpening their focus on the implications of ongoing climate change for their particular constituencies. Major fund managers, banks and other project financiers are now paying more attention to the financial risks surrounding long-life carbon-intensive assets, as well as to emerging opportunities to develop and market new low-emissions products and processes (such as improved battery storage technologies). In early June the Norwegian Parliament resolved to divest its $US880 billion sovereign wealth fund of shares in companies that generate more than 30 per cent of their turnover from coal.

Religious leaders of all faiths have also joined with other groups in calling for strong emissions reduction targets (including in Australia) to help reduce the risks of dangerous climate change, with the Pope (among others) reminding us that poor people and poor countries would suffer most if those risks were not contained.

A notable and potentially very encouraging development in Australia in the past week was the call by a broad coalition of business, social, environmental and other groups—under the umbrella of the Australian Climate Roundtable—for Australia to play its fair part in international efforts to achieve the 2 degree goal. It is, hopefully, a decisive step towards building the wide consensus and genuine commitment necessary to delivering this outcome.

Stakeholder feedback

Stakeholders generally acknowledged that many countries—including the United States and China, the world's two biggest emitters—were committing to strong actions to contain and reduce their emissions, even if the motivation in some cases stemmed as much from concerns about air pollution and energy security as from climate change per se.

As to the comparability of the Authority's recommended target reduction of 30 per cent by 2025 with the broad thrust of other developed countries' targets, a couple of stakeholders argued that this recommendation would require sharp reductions in the emissions intensity of the Australian economy, and impose severe burdens on certain industries. It has also been argued that the Authority's recommendation would require much greater reductions in the emissions intensity of the Australian economy than those required by other developed countries to meet their targets.

The Authority is not persuaded by such arguments. It is true (as shown in Figure 1) that Australia has a much higher emissions intensity than most other developed countries: to some extent, however, this measure (and Australia's highest ranking on the measure of per person emissions, also shown in Figure 1) illustrates the extent to which Australia is starting behind other developed countries and the extent of the 'catch-up' required. The relevant question is whether the 'catch-up' implicit in meeting the recommended target for 2025 is realistic. It is challenging, but not, in the judgment of the Authority, unrealistic, for the following reasons:

- Between 1990 and 2012 the emissions intensity of the Australian economy has approximately halved, in response to structural changes, new technologies, fuel switching and improvements in energy efficiency.
- These drivers of change can be expected to continue over the decade ahead, and to accommodate both larger absolute reductions in Australia's greenhouse gas emissions, and further substantial reductions in the emissions intensity of the Australian economy.
- On the Authority's figuring, achievement of the recommended target of a 30 per cent reduction in emissions by 2025 would still have Australia with a more emissions intensive economy (and higher per person emissions) than any major developed country other than Canada.

In any event, it is the reduction in a country's total emissions—not its emissions intensity—which is the most relevant measure in assessing that country's contribution to attaining the 2 degree goal. On this measure, the Authority reaffirms its recommended target of a 30 per cent reduction in Australia's greenhouse gas emissions in 2025, compared with the 2000 level. Such a commitment by Australia, together with those foreshadowed by other major countries, would help to move the world closer to a sustainable path towards the 2 degree goal.

Stakeholder feedback on two other matters raised in the Authority's draft report might be noted here. First, the Authority's recommended package of a specific target for 2025 and a target range out to 2030 received general support, combining as it would clear signals as to the Government's intentions in the earlier years with flexibility to adjust Australia's efforts in the latter years in the light of relevant developments. Secondly, stakeholders did not express strong views on any preferred base (or reference) year for Australia's targets. Several noted, however, that choosing particular base years could make targets appear stronger without necessarily entailing any stronger effort on the part of policymakers to reduce emissions (see Figure 2). The Authority has based its recommendations on the year 2000 to maintain consistency with Australia's previous commitments.

Benefits and Costs

In its Draft Report the Authority identified the major benefits to Australia of effective action to reduce global emissions as the avoidance of the adverse social, economic and environmental impacts of dangerous climate change. It is clearly in Australia's interests to strive towards this outcome: in doing so Australia would be playing a responsible international role in helping to reduce global emissions and, simultaneously, acting to protect vital interests of current and future generations of Australians. In addition, the transition to a low carbon world now underway carries with it the prospect of benefits of the more conventional kind—new technologies, skills, investments, industries and jobs—for Australia and other countries with the foresight and wit to seize these opportunities.

The Authority also acknowledged in its Draft Report that achieving the requisite reductions in Australia's greenhouse gas emissions would entail some costs, and these could impact more heavily on some industries and communities than others. The Authority argued that these costs would depend largely on the particular measures adopted to pursue the targets and, at least in the first instance, are best addressed through the design of those measures, not through scaling back the targets themselves.

Stakeholder feedback

Feedback from the discussions on the benefits and costs of the Authority's recommended targets tended to reflect the perceived implications of the targets for the balance sheets of particular stakeholders. Industry groups were obviously concerned that Australia's targets should not create heavy cost burdens for Australian businesses, or undermine their international competitiveness. A couple of stakeholders made the point that, given its highly emissions intensive economy, Australia would have to make greater efforts than many other countries to meet any nominated target, a point which was discussed earlier in this report.

Other stakeholders observed that Australia's future, including its economy, was about much more than mining, with some emphasizing avoidance of the harmful consequences of dangerous climate change, and others emphasising the opportunities for Australia to develop new industries through greater utilisation of the country's abundant renewable energy resources. Emissions intensive and trade exposed sectors currently generate a large share of Australia's exports but they make up rather less than 10 per cent of the whole economy.

The Authority had not looked for—or found—unanimity in stakeholder views on the benefits and costs of the Authority's recommended targets. This outcome was expected, not least because the costs of achieving any given emissions reduction target cannot be meaningfully assessed until the suite of measures to be adopted has been identified. The feedback was nonetheless helpful in a number of respects, including its considerable focus on the potential benefits and opportunities to be stacked up against the costs (when these can be sensibly estimated). It has also lent broad support for many of the propositions underlying the Authority's thinking in its Draft Report. In particular, that:

- the targets to be recommended by the Authority should be based primarily on the science of climate change and broad comparability with the efforts of other wealthy, developed countries;
- targets which are judged to be in the nation's best interests should not be scaled back to try to protect sectoral interests—possible threats to the cost base or competitiveness of particular activities should be addressed, in the first instance, through the design of the policies chosen to meet those targets; and
- the provision of any additional support that might be considered necessary to assist certain emissions-intensive activities to adjust to the ongoing transition to a low carbon world should not be at the discouragement of new investment in renewable energy—which could not be said to be the situation currently.

Endpiece

For the reasons discussed in its Draft Report and reiterated briefly here, the Authority confirms its preliminary recommendations that Australia commit to the following package at the forthcoming Paris Conference:

- a 2025 target of a 30 per cent reduction in its emissions below 2000 levels (or a 36 per cent reduction if the Government should choose 2005 as its preferred base year); and
- further reductions within a range of 40 to 60 per cent below 2000 levels by 2030 (or a range of approximately 45 to 65 per cent below 2005 levels).

The second and third parts of the Special Review commissioned by the Minister for the Environment require the Authority to report on possible policy actions to achieve Australia's post-2020 targets. As part of this exercise, a draft report on the case for an emissions trading scheme for Australia is to be completed by 30 November 2015. The third and final part of the Special Review specifically requires the Authority to report by 30 June 2016 on the full suite of actions Australia should take to meet its commitments arising out of the Paris Conference. That final report will be the vehicle for the Authority to present its analysis and recommendations on how Australia's actual post-2020 targets might be most appropriately and cost-effectively implemented.

At this time, however, attention is properly focussed on the targets themselves. The Authority believes its recommendations constitute a credible package for the Australian Government to take to the Paris Conference. It is credible in terms of what the science requires—and what many comparable countries are doing—to move the world back towards a global emissions reduction path consistent with a reasonable chance of limiting the increase in global warming to 2 degrees. It would also send a credible signal to domestic and international stakeholders alike that the Government is intent on playing a leadership role in guiding Australia's long-term transition to a sustainable, low carbon world.

Tables and Figures

Table 1: Announced post-2020 targets for emissions reductions

This table summarises announced and foreshadowed targets for emissions reductions post-2020; it reports the targets in the terms announced by the countries concerned. (Targets for developed countries alone are compared on a common base year in Figure 1.)

Country	Target
Canada	30 per cent below 2005 levels by 2030
China	peak CO_2 emissions by 2030 and to make best efforts to peak early; reduce emissions intensity per unit of GDP by 60 to 65 per cent from 2005 levels by 2030
European Union	at least 40 per cent below 1990 levels by 2030
Japan *proposed	26 per cent below 2013 levels by 2030
United States	26 to 28 per cent below 2005 levels by 2025
Andorra	37 per cent below BAU by 2030
Ethiopia	64 per cent below BAU by 2030
Gabon	50 per cent below BAU in 2025
Germany	55 per cent below 1990 levels by 2030
Liechtenstein	40 per cent below 1990 levels by 2030
Mexico	25 per cent reduction in greenhouse gases and short lived climate pollutants from BAU in 2030
Morocco	32 per cent below BAU by 2030
Norway	at least 40 per cent below 1990 levels by 2030
Republic of Korea	37 per cent below BAU in 2030
Russia	25 to 30 per cent below 1990 levels by 2030
South Africa	42 per cent below BAU by 2025
Switzerland	50 per cent below 1990 levels by 2030
United Kingdom	50 per cent below 1990 levels over the period 2023-27

Note: BAU: business-as-usual.
Source: CCA (2015) Table 4. Canada, China, Republic of Korea: UNFCCC INDC submissions (2015). Japan: Japanese government proposed INDC outline (draft) 2015.

Figure 1: How Australia Compares

The first chart in this figure compares the Authority's recommended 2025 target with the post-2020 targets of other wealthy, developed countries. The second and third charts compare the level of per person emissions and emissions intensity of each economy in 2005, and the levels implied by the announced post-2020 targets, based on projected population and economic growth. They also indicate the percentage change in level between 2005 and 2025. These years were selected to enable comparison: some countries have earlier base years and others have later target years, but all countries have announced reductions across this 20 year period.

Percentage change in total emissions, 2005-2025

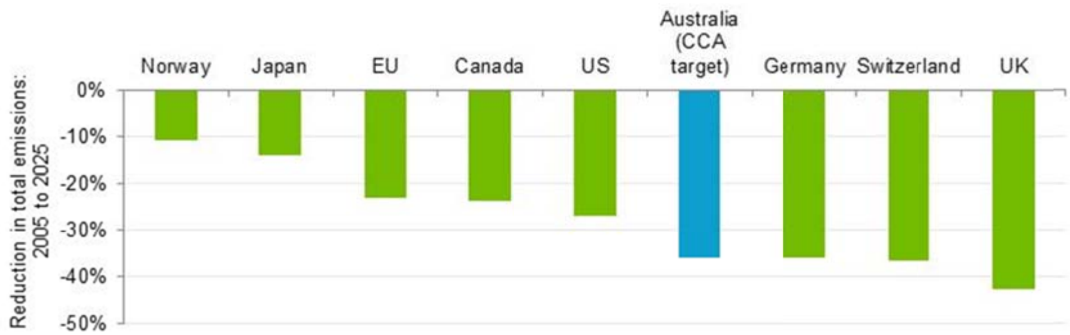

Level of emissions per person, 2005 and 2025

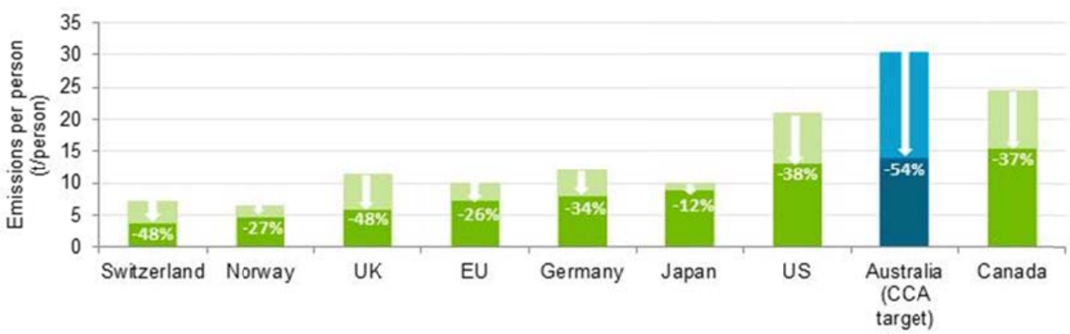

Level of emissions intensity of GDP, 2005 and 2025

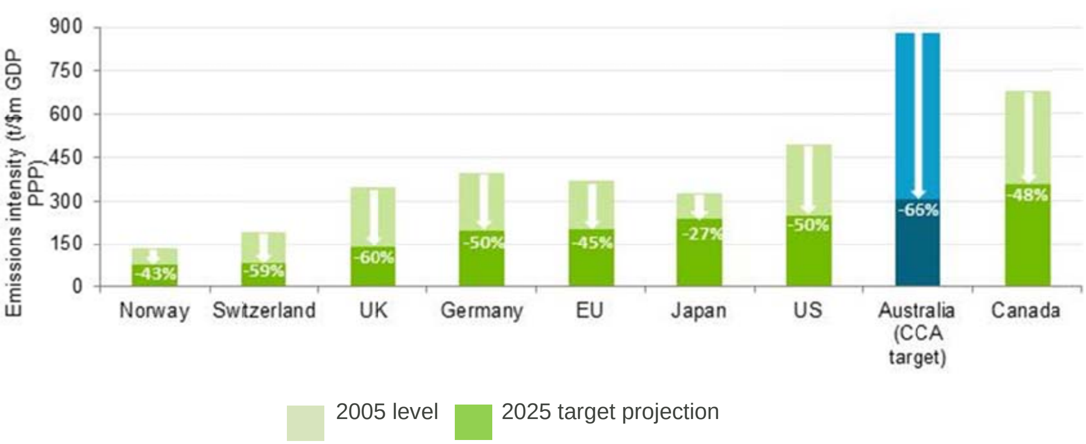

Notes: The US target is the midpoint of its 2025 target range. The EU, Norway, Switzerland, Germany, Japan and Canada targets are midpoints between their 2020 and 2030 targets. This figure uses UNFCCC emissions data (including land sector). This may not match countries' Kyoto Protocol emissions accounts (particularly for Norway).
Sources: CCA (2015) Figures 2 and 3. Additional emissions targets—as for Table 1.

Figure 2: Implications of Different Base Years

This figure shows that the Authority's recommended 2025 target of 30 per cent below 2000 levels (dotted green line) translates to 36 per cent below 2005 levels and 32 per cent below 2010.

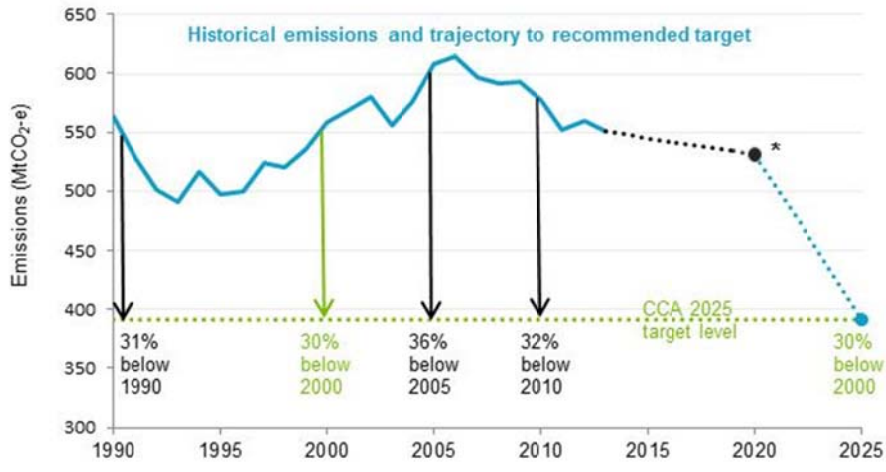

Source: Historical greenhouse gas emissions (DoE 2015)
Notes: This Figure uses historical data for Australia's emissions to 2013 and then straight line trajectories to the unconditional 2020 target and the Authority's recommended 2025 target.
***** The 2020 target shown here is Australia's "unconditional" 5 per cent reduction in emissions below 2000 levels provided for in the Copenhagen Accord; it is the figure which the Government consistently refers to as its emissions reduction target for 2020.
Under the Kyoto Protocol Australia agreed to undertakings in respect of the "first commitment period" (the five years 2008 to 2012) and the "second commitment period" (the eight years 2013 to 2020); the undertaking for the latter period is broadly consistent with the unconditional 5 per cent reduction target for 2020. Under the Kyoto Protocol countries which bettered their emissions reduction targets for the first commitment period can carryover their surplus emission units to the second period to help meet or strengthen their targets, or they can decide to cancel those units altogether. It is understood that the United Kingdom has chosen to cancel its carryover units, and that the EU as a whole is still considering its position.
Australia's carryover from the first Kyoto commitment period is currently estimated to be equivalent to about 4 percentage points of emissions reductions below 2000 levels in 2020. In its 2014 Targets and Progress Review the Authority recommended a minimum 2020 target of 15 per cent below 2000 levels, and utilizing Australia's carryover under the Kyoto Protocol to lift that figure to an effective target of 19 per cent. It is not clear at this time what part (if any) this carryover might play in meeting or strengthening the Government's unconditional 5 per cent reduction target.
For more information see CCA (2014), pp 110-11 and 209.

References

Climate Change Authority (CCA) 2014, *Reducing Australia's Greenhouse Gas Emissions: Targets and Progress Review*, Melbourne, http://www.climatechangeauthority.gov.au/reviews/targets-and-progress-review-3.

CCA 2015, *Special Review Draft Report: Australia's future emissions reduction targets*.

Department of the Environment (DoE) 2015, *Australia's emissions projections* 2014-15, Canberra.

Japanese government proposed INDC outline (draft) 2015, *Japan promised draft outline*, Japanese Government submission to the joint committee of MOE and METI on Apr. 30, 2015 (in Japanese), http://www.meti.go.jp/committee/sankoushin/sangyougijutsu/chikyu_kankyo/yakusoku_souan_wg/pdf/007_04_00.pdf.

United Nations Framework Convention on Climate Change (UNFCCC) 2015, *Intended Nationally Determined Contributions (INDCs)*, viewed 1 July 2015, http://unfccc.int/focus/indc_portal/items/8766.php.

6

Carbon and Other Biogeochemical Cycles

Coordinating Lead Authors:
Philippe Ciais (France), Christopher Sabine (USA)

Lead Authors:
Govindasamy Bala (India), Laurent Bopp (France), Victor Brovkin (Germany/Russian Federation), Josep Canadell (Australia), Abha Chhabra (India), Ruth DeFries (USA), James Galloway (USA), Martin Heimann (Germany), Christopher Jones (UK), Corinne Le Quéré (UK), Ranga B. Myneni (USA), Shilong Piao (China), Peter Thornton (USA)

Contributing Authors:
Anders Ahlström (Sweden), Alessandro Anav (UK/Italy), Oliver Andrews (UK), David Archer (USA), Vivek Arora (Canada), Gordon Bonan (USA), Alberto Vieira Borges (Belgium/Portugal), Philippe Bousquet (France), Lex Bouwman (Netherlands), Lori M. Bruhwiler (USA), Kenneth Caldeira (USA), Long Cao (China), Jérôme Chappellaz (France), Frédéric Chevallier (France), Cory Cleveland (USA), Peter Cox (UK), Frank J. Dentener (EU/Netherlands), Scott C. Doney (USA), Jan Willem Erisman (Netherlands), Eugenie S. Euskirchen (USA), Pierre Friedlingstein (UK/Belgium), Nicolas Gruber (Switzerland), Kevin Gurney (USA), Elisabeth A. Holland (Fiji/USA), Brett Hopwood (USA), Richard A. Houghton (USA), Joanna I. House (UK), Sander Houweling (Netherlands), Stephen Hunter (UK), George Hurtt (USA), Andrew D. Jacobson (USA), Atul Jain (USA), Fortunat Joos (Switzerland), Johann Jungclaus (Germany), Jed O. Kaplan (Switzerland/Belgium/USA), Etsushi Kato (Japan), Ralph Keeling (USA), Samar Khatiwala (USA), Stefanie Kirschke (France/Germany), Kees Klein Goldewijk (Netherlands), Silvia Kloster (Germany), Charles Koven (USA), Carolien Kroeze (Netherlands), Jean-François Lamarque (USA/Belgium), Keith Lassey (New Zealand), Rachel M. Law (Australia), Andrew Lenton (Australia), Mark R. Lomas (UK), Yiqi Luo (USA), Takashi Maki (Japan), Gregg Marland (USA), H. Damon Matthews (Canada), Emilio Mayorga (USA), Joe R. Melton (Canada), Nicolas Metzl (France), Guy Munhoven (Belgium/Luxembourg), Yosuke Niwa (Japan), Richard J. Norby (USA), Fiona O'Connor (UK/Ireland), James Orr (France), Geun-Ha Park (USA), Prabir Patra (Japan/India), Anna Peregon (France/Russian Federation), Wouter Peters (Netherlands), Philippe Peylin (France), Stephen Piper (USA), Julia Pongratz (Germany), Ben Poulter (France/USA), Peter A. Raymond (USA), Peter Rayner (Australia), Andy Ridgwell (UK), Bruno Ringeval (Netherlands/France), Christian Rödenbeck (Germany), Marielle Saunois (France), Andreas Schmittner (USA/Germany), Edward Schuur (USA), Stephen Sitch (UK), Renato Spahni (Switzerland), Benjamin Stocker (Switzerland), Taro Takahashi (USA), Rona L. Thompson (Norway/New Zealand), Jerry Tjiputra (Norway/Indonesia), Guido van der Werf (Netherlands), Detlef van Vuuren (Netherlands), Apostolos Voulgarakis (UK/Greece), Rita Wania (Austria), Sönke Zaehle (Germany), Ning Zeng (USA)

Review Editors:
Christoph Heinze (Norway), Pieter Tans (USA), Timo Vesala (Finland)

This chapter should be cited as:
Ciais, P., C. Sabine, G. Bala, L. Bopp, V. Brovkin, J. Canadell, A. Chhabra, R. DeFries, J. Galloway, M. Heimann, C. Jones, C. Le Quéré, R.B. Myneni, S. Piao and P. Thornton, 2013: Carbon and Other Biogeochemical Cycles. In: *Climate Change 2013: The Physical Science Basis. Contribution of Working Group I to the Fifth Assessment Report of the Intergovernmental Panel on Climate Change* [Stocker, T.F., D. Qin, G.-K. Plattner, M. Tignor, S.K. Allen, J. Boschung, A. Nauels, Y. Xia, V. Bex and P.M. Midgley (eds.)]. Cambridge University Press, Cambridge, United Kingdom and New York, NY, USA.

Table of Contents

Supplementary Material is available in online versions of the report.

Executive Summary

This chapter addresses the biogeochemical cycles of carbon dioxide (CO_2), methane (CH_4) and nitrous oxide (N_2O). The three greenhouse gases (GHGs) have increased in the atmosphere since pre-industrial times, and this increase is the main driving cause of climate change (Chapter 10). CO_2, CH_4 and N_2O altogether amount to 80% of the total radiative forcing from well-mixed GHGs (Chapter 8). The increase of CO_2, CH_4 and N_2O is caused by anthropogenic emissions from the use of fossil fuel as a source of energy and from land use and land use changes, in particular agriculture. The observed change in the atmospheric concentration of CO_2, CH_4 and N_2O results from the dynamic balance between anthropogenic emissions, and the perturbation of natural processes that leads to a partial removal of these gases from the atmosphere. Natural processes are linked to physical conditions, chemical reactions and biological transformations and they respond themselves to perturbed atmospheric composition and climate change. Therefore, the physical climate system and the biogeochemical cycles of CO_2, CH_4 and N_2O are coupled. This chapter addresses the present human-caused perturbation of the biogeochemical cycles of CO_2, CH_4 and N_2O, their variations in the past coupled to climate variations and their projected evolution during this century under future scenarios.

The Human-Caused Perturbation in the Industrial Era

CO_2 increased by 40% from 278 ppm about 1750 to 390.5 ppm in 2011. During the same time interval, CH_4 increased by 150% from 722 ppb to 1803 ppb, and N_2O by 20% from 271 ppb to 324.2 ppb in 2011. It is unequivocal that the current concentrations of atmospheric CO_2, CH_4 and N_2O exceed any level measured for at least the past 800,000 years, the period covered by ice cores. Furthermore, the average rate of increase of these three gases observed over the past century exceeds any observed rate of change over the previous 20,000 years. {2.2, 5.2, 6.1, 6.2}

Anthropogenic CO_2 emissions to the atmosphere were 555 ± 85 PgC (1 PgC = 10^{15} gC) between 1750 and 2011. Of this amount, fossil fuel combustion and cement production contributed 375 ± 30 PgC and land use change (including deforestation, afforestation and reforestation) contributed 180 ± 80 PgC. {6.3.1, Table 6.1}

With a *very high level of confidence*[1], the increase in CO_2 emissions from fossil fuel burning and those arising from land use change are the dominant cause of the observed increase in atmospheric CO_2 concentration. About half of the emissions remained in the atmosphere (240 ± 10 PgC) since 1750. The rest was removed from the atmosphere by sinks and stored in the natural carbon cycle reservoirs. The ocean reservoir stored 155 ± 30 PgC. Vegetation biomass and soils not affected by land use change stored 160 ± 90 PgC. {6.1, 6.3, 6.3.2.3, Table 6.1, Figure 6.8}

Carbon emissions from fossil fuel combustion and cement production increased faster during the 2000–2011 period than during the 1990–1999 period. These emissions were 9.5 ± 0.8 PgC yr^{-1} in 2011, 54% above their 1990 level. Anthropogenic net CO_2 emissions from land use change were 0.9 ± 0.8 PgC yr^{-1} throughout the past decade, and represent about 10% of the total anthropogenic CO_2 emissions. It is *more likely than not*[2] that net CO_2 emissions from land use change decreased during 2000–2011 compared to 1990–1999. {6.3, Table 6.1, Table 6.2, Figure 6.8}

Atmospheric CO_2 concentration increased at an average rate of 2.0 ± 0.1 ppm yr^{-1} during 2002–2011. This decadal rate of increase is higher than during any previous decade since direct atmospheric concentration measurements began in 1958. Globally, the size of the combined natural land and ocean sinks of CO_2 approximately followed the atmospheric rate of increase, removing 55% of the total anthropogenic emissions every year on average during 1958–2011. {6.3, Table 6.1}

After almost one decade of stable CH_4 concentrations since the late 1990s, atmospheric measurements have shown renewed CH_4 concentrations growth since 2007. The drivers of this renewed growth are still debated. The methane budget for the decade of 2000–2009 (bottom-up estimates) is 177 to 284 Tg(CH_4) yr^{-1} for natural wetlands emissions, 187 to 224 Tg(CH_4) yr^{-1} for agriculture and waste (rice, animals and waste), 85 to 105 Tg(CH_4) yr^{-1} for fossil fuel related emissions, 61 to 200 Tg(CH_4) yr^{-1} for other natural emissions including, among other fluxes, geological, termites and fresh water emissions, and 32 to 39 Tg(CH_4) yr^{-1} for biomass and biofuel burning (the range indicates the expanse of literature values). Anthropogenic emissions account for 50 to 65% of total emissions. By including natural geological CH_4 emissions that were not accounted for in previous budgets, the fossil component of the total CH_4 emissions (i.e., anthropogenic emissions related to leaks in the fossil fuel industry and natural geological leaks) is now estimated to amount to about 30% of the total CH_4 emissions (*medium confidence*). Climate driven fluctuations of CH_4 emissions from natural wetlands are the main drivers of the global interannual variability of CH_4 emissions (*high confidence*), with a smaller contribution from the variability in emissions from biomass burning during high fire years. {6.3.3, Figure 6.2, Table 6.8}

The concentration of N_2O increased at a rate of 0.73 ± 0.03 ppb yr^{-1} over the last three decades. Emissions of N_2O to the atmosphere are mostly caused by nitrification and de-nitrification reactions

6

[1] In this Report, the following summary terms are used to describe the available evidence: limited, medium, or robust; and for the degree of agreement: low, medium, or high. A level of confidence is expressed using five qualifiers: very low, low, medium, high, and very high, and typeset in italics, e.g., *medium confidence*. For a given evidence and agreement statement, different confidence levels can be assigned, but increasing levels of evidence and degrees of agreement are correlated with increasing confidence (see Section 1.4 and Box TS.1 for more details).

[2] In this Report, the following terms have been used to indicate the assessed likelihood of an outcome or a result: Virtually certain 99–100% probability, Very likely 90–100%, Likely 66–100%, About as likely as not 33–66%, Unlikely 0–33%, Very unlikely 0–10%, Exceptionally unlikely 0–1%. Additional terms (Extremely likely: 95–100%, More likely than not >50–100%, and Extremely unlikely 0–5%) may also be used when appropriate. Assessed likelihood is typeset in italics, e.g., *very likely* (see Section 1.4 and Box TS.1 for more details).

of reactive nitrogen in soils and in the ocean. Anthropogenic N_2O emissions increased steadily over the last two decades and were 6.9 (2.7 to 11.1) TgN (N_2O) yr^{-1} in 2006. Anthropogenic N_2O emissions are 1.7 to 4.8 TgN (N_2O) yr^{-1} from the application of nitrogenous fertilisers in agriculture, 0.2 to 1.8 TgN (N_2O) yr^{-1} from fossil fuel use and industrial processes, 0.2 to 1.0 TgN (N_2O) yr^{-1} from biomass burning (including biofuels) and 0.4 to 1.3 TgN (N_2O) yr^{-1} from land emissions due to atmospheric nitrogen deposition (the range indicates expand of literature values). Natural N_2O emissions derived from soils, oceans and a small atmospheric source are together 5.4 to 19.6 TgN (N_2O) yr^{-1}. {6.3, 6.3.4, Figure 6.4c, Figure 6.19, Table 6.9}

The human-caused creation of reactive nitrogen in 2010 was at least two times larger than the rate of natural terrestrial creation. The human-caused creation of reactive nitrogen is dominated by the production of ammonia for fertiliser and industry, with important contributions from legume cultivation and combustion of fossil fuels. Once formed, reactive nitrogen can be transferred to waters and the atmosphere. In addition to N_2O, two important nitrogen compounds emitted to the atmosphere are NH_3 and NO_x both of which influence tropospheric O_3 and aerosols through atmospheric chemistry. All of these effects contribute to radiative forcing. It is also *likely* that reactive nitrogen deposition over land currently increases natural CO_2 sinks, in particular forests, but the magnitude of this effect varies between regions. {6.1.3, 6.3, 6.3.2.6.5, 6.3.4, 6.4.6, Figures 6.4a and 6.4b, Table 6.9, Chapter 7}

Before the Human-Caused Perturbation

During the last 7000 years prior to 1750, atmospheric CO_2 from ice cores shows only very slow changes (increase) from 260 ppm to 280 ppm, in contrast to the human-caused increase of CO_2 since pre-industrial times. The contribution of CO_2 emissions from early anthropogenic land use is *unlikely* sufficient to explain the CO_2 increase prior to 1750. Atmospheric CH_4 from ice cores increased by about 100 ppb between 5000 years ago and around 1750. *About as likely as not*, this increase can be attributed to early human activities involving livestock, human-caused fires and rice cultivation. {6.2, Figures 6.6 and 6.7}

Further back in time, during the past 800,000 years prior to 1750, atmospheric CO_2 varied from 180 ppm during glacial (cold) up to 300 ppm during interglacial (warm) periods. This is well established from multiple ice core measurements. Variations in atmospheric CO_2 from glacial to interglacial periods were caused by decreased ocean carbon storage (500 to 1200 PgC), partly compensated by increased land carbon storage (300 to 1000 PgC). {6.2.1, Figure 6.5}

Future Projections

With *very high confidence*, ocean carbon uptake of anthropogenic CO_2 emissions will continue under all four Representative Concentration Pathways (RCPs) through to 2100, with higher uptake corresponding to higher concentration pathways. The future evolution of the land carbon uptake is much more uncertain, with a majority of models projecting a continued net carbon uptake under all RCPs, but with some models simulating a net loss of carbon by the land due to the combined effect of climate change and land use change. In view of the large spread of model results and incomplete process representation, there is *low confidence* on the magnitude of modelled future land carbon changes. {6.4.3, Figure 6.24}

There is *high confidence* that climate change will partially offset increases in global land and ocean carbon sinks caused by rising atmospheric CO_2. Yet, there are regional differences among Climate Modelling Intercomparison Project Phase 5 (CMIP5) Earth System Models, in the response of ocean and land CO_2 fluxes to climate. There is a high agreement between models that tropical ecosystems will store less carbon in a warmer climate. There is medium agreement between models that at high latitudes warming will increase land carbon storage, although none of the models account for decomposition of carbon in permafrost, which may offset increased land carbon storage. There is high agreement between CMIP5 Earth System models that ocean warming and circulation changes will reduce the rate of carbon uptake in the Southern Ocean and North Atlantic, but that carbon uptake will nevertheless persist in those regions. {6.4.2, Figures 6.21 and 6.22}

It is *very likely*, based on new experimental results {6.4.6.3} and modelling, that nutrient shortage will limit the effect of rising atmospheric CO_2 on future land carbon sinks, for the four RCP scenarios. There is *high confidence* that low nitrogen availability will limit carbon storage on land, even when considering anthropogenic nitrogen deposition. The role of phosphorus limitation is more uncertain. Models that combine nitrogen limitations with rising CO_2 and changes in temperature and precipitation thus produce a systematically larger increase in projected future atmospheric CO_2, for a given fossil fuel emissions trajectory. {6.4.6, 6.4.6.3, 6.4.8.2, Figure 6.35}

Taking climate and carbon cycle feedbacks into account, we can quantify the fossil fuel emissions compatible with the RCPs. Between 2012 and 2100, the RCP2.6, RCP4.5, RCP6.0, and RCP8.5 scenarios imply cumulative compatible fossil fuel emissions of 270 (140 to 410) PgC, 780 (595 to 1005) PgC, 1060 (840 to 1250) PgC and 1685 (1415 to 1910) PgC respectively (values quoted to nearest 5 PgC, range derived from CMIP5 model results). For RCP2.6, an average 50% (range 14 to 96%) emission reduction is required by 2050 relative to 1990 levels. By the end of the 21st century, about half of the models infer emissions slightly above zero, while the other half infer a net removal of CO_2 from the atmosphere. {6.4.3, Table 6.12, Figure 6.25}

There is *high confidence* that reductions in permafrost extent due to warming will cause thawing of some currently frozen carbon. However, there is *low confidence* on the magnitude of carbon losses through CO_2 and CH_4 emissions to the atmosphere, with a range from 50 to 250 PgC between 2000 and 2100 under the RCP8.5 scenario. The CMIP5 Earth System Models did not include frozen carbon feedbacks. {6.4.3.4, Chapter 12}

There is *medium confidence* that emissions of CH_4 from wetlands are *likely* to increase under elevated CO_2 and a warmer climate. But there is *low confidence* in quantitative projections of these changes. The likelihood of the future release of CH_4 from marine gas hydrates in response to seafloor warming is poorly understood. In the event of a significant release of CH_4 from hydrates in the sea floor by the end of the 21st century, it is *likely* that subsequent emissions to the atmosphere would be in the form of CO_2, due to CH_4 oxidation in the water column. {6.4.7, Figure 6.37}

It is *likely* that N_2O emissions from soils will increase due to the increased demand for feed/food and the reliance of agriculture on nitrogen fertilisers. Climate warming will *likely* amplify agricultural and natural terrestrial N_2O sources, but there is *low confidence* in quantitative projections of these changes. {6.4.6, Figure 6.32}

It is *virtually certain* that the increased storage of carbon by the ocean will increase acidification in the future, continuing the observed trends of the past decades. Ocean acidification in the surface ocean will follow atmospheric CO_2 while it will also increase in the deep ocean as CO_2 continues to penetrate the abyss. The CMIP5 models consistently project worldwide increased ocean acidification to 2100 under all RCPs. The corresponding decrease in surface ocean pH by the end of the 21st century is 0.065 (0.06 to 0.07) for RCP2.6, 0.145 (0.14 to 0.15) for RCP4.5, 0.203 (0.20 to 0.21) for RCP6.0, and 0.31 (0.30 to 0.32) for RCP8.5 (range from CMIP5 models spread). Surface waters become seasonally corrosive to aragonite in parts of the Arctic and in some coastal upwelling systems within a decade, and in parts of the Southern Ocean within 1 to 3 decades in most scenarios. Aragonite undersaturation becomes widespread in these regions at atmospheric CO_2 levels of 500 to 600 ppm. {6.4.4, Figures 6.28 and 6.29}

It is *very likely* that the dissolved oxygen content of the ocean will decrease by a few percent during the 21st century. CMIP5 models suggest that this decrease in dissolved oxygen will predominantly occur in the subsurface mid-latitude oceans, caused by enhanced stratification, reduced ventilation and warming. However, there is no consensus on the future development of the volume of hypoxic and suboxic waters in the open-ocean because of large uncertainties in potential biogeochemical effects and in the evolution of tropical ocean dynamics. {6.4.5, Figure 6.30}

Irreversible Long-Term Impacts of Human-Caused Emissions

With *very high confidence*, the physical, biogeochemical carbon cycle in the ocean and on land will continue to respond to climate change and rising atmospheric CO_2 concentrations created during the 21st century. Ocean acidification will *very likely* continue in the future as long as the oceans take up atmospheric CO_2. Committed land ecosystem carbon cycle changes will manifest themselves further beyond the end of the 21st century. In addition, it is *virtually certain* that large areas of permafrost will experience thawing over multiple centuries. There is, however, *low confidence* in the magnitude of frozen carbon losses to the atmosphere, and the relative contributions of CO_2 and CH_4 emissions. {6.4.4, 6.4.9, Chapter 12}

The magnitude and sign of the response of the natural carbon reservoirs to changes in climate and rising CO_2 vary substantially over different time scales. The response to rising CO_2 is to increase cumulative land and ocean uptake, regardless of the time scale. The response to climate change is variable, depending of the region considered because of different responses of the underlying physical and biological mechanisms at different time scales. {6.4, Table 6.10, Figures 6.14 and 6.17}

The removal of human-emitted CO_2 from the atmosphere by natural processes will take a few hundred thousand years (*high confidence*). Depending on the RCP scenario considered, about 15 to 40% of emitted CO_2 will remain in the atmosphere longer than 1,000 years. This very long time required by sinks to remove anthropogenic CO_2 makes climate change caused by elevated CO_2 irreversible on human time scale. {Box 6.1}

Geoengineering Methods and the Carbon Cycle

Unconventional ways to remove CO_2 from the atmosphere on a large scale are termed Carbon Dioxide Removal (CDR) methods. CDR could in theory be used to reduce CO_2 atmospheric concentrations but these methods have biogeochemical and technological limitations to their potential. Uncertainties make it difficult to quantify how much CO_2 emissions could be offset by CDR on a human time scale, although it is *likely* that CDR would have to be deployed at large-scale for at least one century to be able to significantly reduce atmospheric CO_2. In addition, it is *virtually certain* that the removal of CO_2 by CDR will be partially offset by outgassing of CO_2 from the ocean and land ecosystems. {6.5, Figures 6.39 and 6.40, Table 6.15, Box 6.1, FAQ 7.3}

The level of confidence on the side effects of CDR methods on carbon and other biogeochemical cycles is low. Some of the climatic and environmental effects of CDR methods are associated with altered surface albedo (for afforestation), de-oxygenation and enhanced N_2O emissions (for artificial ocean fertilisation). Solar Radiation Management (SRM) methods (Chapter 7) will not directly interfere with the effects of elevated CO_2 on the carbon cycle, such as ocean acidification, but will impact carbon and other biogeochemical cycles through their climate effects. {6.5.3, 6.5.4, 7.7, Tables 6.14 and 6.15}

6.1 Introduction

The radiative properties of the atmosphere are strongly influenced by the abundance of well-mixed GHGs (see Glossary), mainly carbon dioxide (CO_2), methane (CH_4) and nitrous oxide (N_2O), which have substantially increased since the beginning of the Industrial Era (defined as beginning in the year 1750), due primarily to anthropogenic emissions (see Chapter 2). Well-mixed GHGs represent the gaseous phase of global biogeochemical cycles, which control the complex flows and transformations of the elements between the different components of the Earth System (atmosphere, ocean, land, lithosphere) by biotic and abiotic processes. Since most of these processes are themselves also dependent on the prevailing environment, changes in climate and human impacts on ecosystems (e.g., land use and land use change) also modify the atmospheric concentrations of CO_2, CH_4 and N_2O. During the glacial-interglacial cycles (see Glossary), in absence of significant direct human impacts, long variations in climate also affected CO_2, CH_4 and N_2O and vice versa (see Chapter 5, Section 5.2.2). In the coming century, the situation would be quite different, because of the dominance of anthropogenic emissions that affect global biogeochemical cycles, and in turn, climate change (see Chapter 12). Biogeochemical cycles thus constitute feedbacks in the Earth System.

This chapter summarizes the scientific understanding of atmospheric budgets, variability and trends of the three major biogeochemical greenhouse gases, CO_2, CH_4 and N_2O, their underlying source and sink processes and their perturbations caused by direct human impacts, past and present climate changes as well as future projections of climate change. After the introduction (Section 6.1), Section 6.2 assesses the present understanding of the mechanisms responsible for the variations of CO_2, CH_4 and N_2O in the past emphasizing glacial-interglacial changes, and the smaller variations during the Holocene (see Glossary) since the last glaciation and over the last millennium. Section 6.3 focuses on the Industrial Era addressing the major source and sink processes, and their variability in space and time. This information is then used to evaluate critically the models of the biogeochemical cycles, including their sensitivity to changes in atmospheric composition and climate. Section 6.4 assesses future projections of carbon and other biogeochemical cycles computed, in particular, with CMIP5 Earth System Models. This includes a quantitative assessment of the direction and magnitude of the various feedback mechanisms as represented in current models, as well as additional processes that might become important in the future but which are not yet fully understood. Finally, Section 6.5 addresses the potential effects and uncertainties of deliberate carbon dioxide removal methods (see Glossary) and solar radiation management (see Glossary) on the carbon cycle.

6.1.1 Global Carbon Cycle Overview

6.1.1.1 Carbon Dioxide and the Global Carbon Cycle

Atmospheric CO_2 represents the main atmospheric phase of the global carbon cycle. The global carbon cycle can be viewed as a series of reservoirs of carbon in the Earth System, which are connected by exchange fluxes of carbon. Conceptually, one can distinguish two domains in the global carbon cycle. The first is a fast domain with large exchange fluxes and relatively 'rapid' reservoir turnovers, which consists of carbon in the atmosphere, the ocean, surface ocean sediments and on land in vegetation, soils and freshwaters. Reservoir turnover times, defined as reservoir mass of carbon divided by the exchange flux, range from a few years for the atmosphere to decades to millennia for the major carbon reservoirs of the land vegetation and soil and the various domains in the ocean. A second, slow domain consists of the huge carbon stores in rocks and sediments which exchange carbon with the fast domain through volcanic emissions of CO_2, chemical weathering (see Glossary), erosion and sediment formation on the sea floor (Sundquist, 1986). Turnover times of the (mainly geological) reservoirs of the slow domain are 10,000 years or longer. Natural exchange fluxes between the slow and the fast domain of the carbon cycle are relatively small (<0.3 PgC yr^{-1}, 1 PgC = 10^{15} gC) and can be assumed as approximately constant in time (volcanism, sedimentation) over the last few centuries, although erosion and river fluxes may have been modified by human-induced changes in land use (Raymond and Cole, 2003).

During the Holocene (beginning 11,700 years ago) prior to the Industrial Era the fast domain was close to a steady state, as evidenced by the relatively small variations of atmospheric CO_2 recorded in ice cores (see Section 6.2), despite small emissions from human-caused changes in land use over the last millennia (Pongratz et al., 2009). By contrast, since the beginning of the Industrial Era, fossil fuel extraction from geological reservoirs, and their combustion, has resulted in the transfer of significant amount of fossil carbon from the slow domain into the fast domain, thus causing an unprecedented, major human-induced perturbation in the carbon cycle. A schematic of the global carbon cycle with focus on the fast domain is shown in Figure 6.1. The numbers represent the estimated current pool sizes in PgC and the magnitude of the different exchange fluxes in PgC yr^{-1} averaged over the time period 2000–2009 (see Section 6.3).

In the atmosphere, CO_2 is the dominant carbon bearing trace gas with a current (2011) concentration of approximately 390.5 ppm (Dlugokencky and Tans, 2013a), which corresponds to a mass of 828 PgC (Prather et al., 2012; Joos et al., 2013). Additional trace gases include methane (CH_4, current content mass ~3.7 PgC) and carbon monoxide (CO, current content mass ~0.2 PgC), and still smaller amounts of hydrocarbons, black carbon aerosols and organic compounds.

The terrestrial biosphere reservoir contains carbon in organic compounds in vegetation living biomass (450 to 650 PgC; Prentice et al., 2001) and in dead organic matter in litter and soils (1500 to 2400 PgC; Batjes, 1996). There is an additional amount of old soil carbon in wetland soils (300 to 700 PgC; Bridgham et al., 2006) and in permafrost soils (see Glossary) (~1700 PgC; Tarnocai et al., 2009); albeit some overlap with these two quantities. CO_2 is removed from the atmosphere by plant photosynthesis (Gross Primary Production (GPP), 123±8 PgC yr^{-1}, (Beer et al., 2010)) and carbon fixed into plants is then cycled through plant tissues, litter and soil carbon and can be released back into the atmosphere by autotrophic (plant) and heterotrophic (soil microbial and animal) respiration and additional disturbance processes (e.g., sporadic fires) on a very wide range of time scales (seconds to millennia). Because CO_2 uptake by photosynthesis occurs only during the growing season, whereas CO_2 release by respiration occurs nearly year-round, the greater land mass in the Northern Hemisphere (NH) imparts

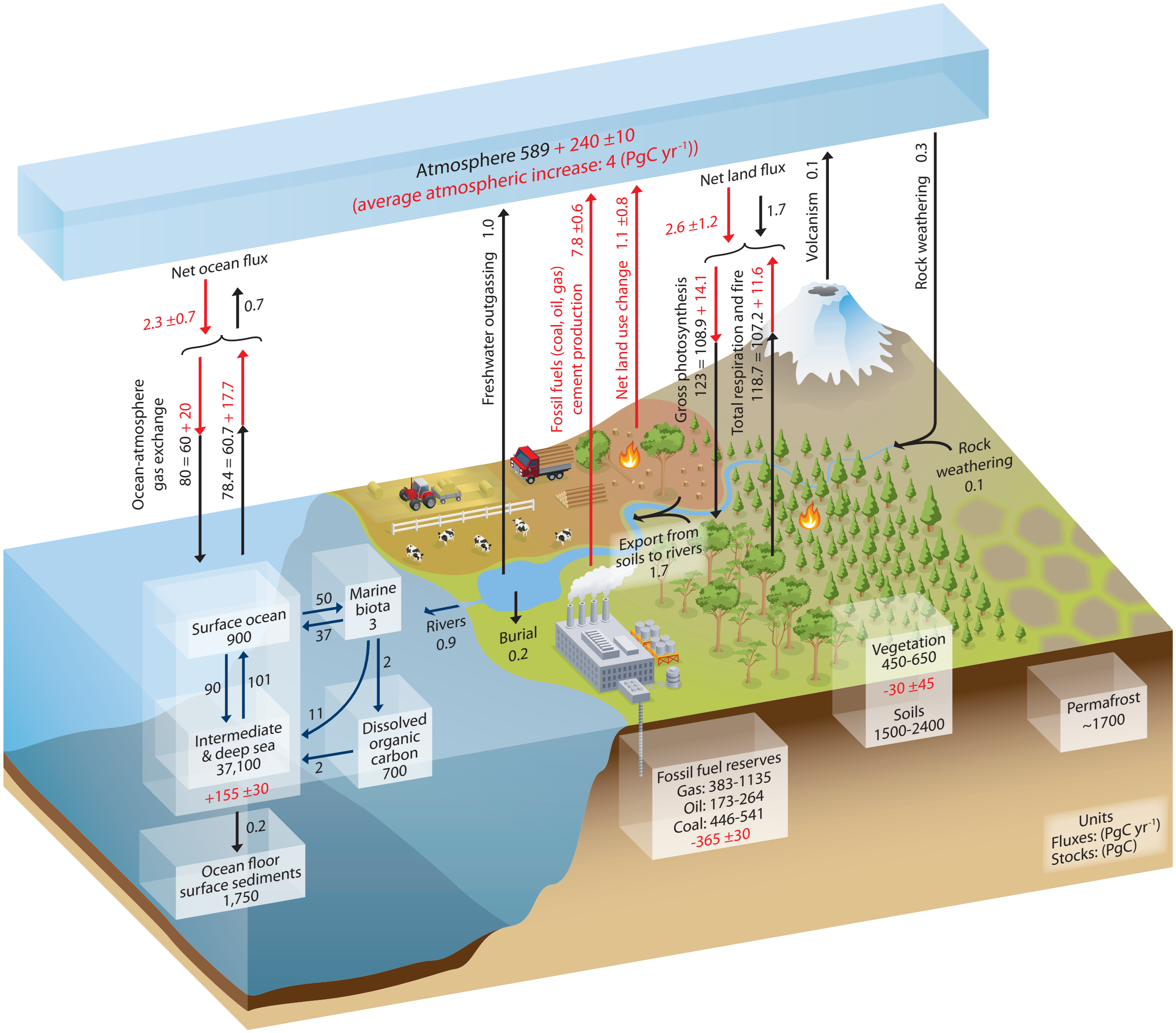

Figure 6.1 | Simplified schematic of the global carbon cycle. Numbers represent reservoir mass, also called 'carbon stocks' in PgC (1 PgC = 10^{15} gC) and annual carbon exchange fluxes (in PgC yr^{-1}). Black numbers and arrows indicate reservoir mass and exchange fluxes estimated for the time prior to the Industrial Era, about 1750 (see Section 6.1.1.1 for references). Fossil fuel reserves are from GEA (2006) and are consistent with numbers used by IPCC WGIII for future scenarios. The sediment storage is a sum of 150 PgC of the organic carbon in the mixed layer (Emerson and Hedges, 1988) and 1600 PgC of the deep-sea $CaCO_3$ sediments available to neutralize fossil fuel CO_2 (Archer et al., 1998). Red arrows and numbers indicate annual 'anthropogenic' fluxes averaged over the 2000–2009 time period. These fluxes are a perturbation of the carbon cycle during Industrial Era post 1750. These fluxes (red arrows) are: *Fossil fuel and cement emissions of CO_2* (Section 6.3.1), *Net land use change* (Section 6.3.2), and the *Average atmospheric increase* of CO_2 in the atmosphere, also called 'CO_2 growth rate' (Section 6.3). The uptake of anthropogenic CO_2 by the ocean and by terrestrial ecosystems, often called 'carbon sinks' are the red arrows part of *Net land flux* and *Net ocean flux*. Red numbers in the reservoirs denote cumulative changes of anthropogenic carbon over the Industrial Period 1750–2011 (column 2 in Table 6.1). By convention, a positive cumulative change means that a reservoir has gained carbon since 1750. The cumulative change of anthropogenic carbon in the terrestrial reservoir is the sum of carbon cumulatively lost through land use change and carbon accumulated since 1750 in other ecosystems (Table 6.1). Note that the mass balance of the two ocean carbon stocks *Surface ocean* and *Intermediate and deep ocean* includes a yearly accumulation of anthropogenic carbon (not shown). Uncertainties are reported as 90% confidence intervals. Emission estimates and land and ocean sinks (in red) are from Table 6.1 in Section 6.3. The change of gross terrestrial fluxes (red arrows of *Gross photosynthesis* and *Total respiration and fires*) has been estimated from CMIP5 model results (Section 6.4). The change in air–sea exchange fluxes (red arrows of ocean atmosphere gas exchange) have been estimated from the difference in atmospheric partial pressure of CO_2 since 1750 (Sarmiento and Gruber, 2006). Individual gross fluxes and their changes since the beginning of the Industrial Era have typical uncertainties of more than 20%, while their differences (*Net land flux* and *Net ocean flux* in the figure) are determined from independent measurements with a much higher accuracy (see Section 6.3). Therefore, to achieve an overall balance, the values of the more uncertain gross fluxes have been adjusted so that their difference matches the *Net land flux* and *Net ocean flux* estimates. Fluxes from volcanic eruptions, rock weathering (silicates and carbonates weathering reactions resulting into a small uptake of atmospheric CO_2), export of carbon from soils to rivers, burial of carbon in freshwater lakes and reservoirs and transport of carbon by rivers to the ocean are all assumed to be pre-industrial fluxes, that is, unchanged during 1750–2011. Some recent studies (Section 6.3) indicate that this assumption is likely not verified, but global estimates of the Industrial Era perturbation of all these fluxes was not available from peer-reviewed literature. The atmospheric inventories have been calculated using a conversion factor of 2.12 PgC per ppm (Prather et al., 2012).

6

a characteristic 'sawtooth' seasonal cycle in atmospheric CO_2 (Keeling, 1960) (see Figure 6.3). A significant amount of terrestrial carbon (1.7 PgC yr^{-1}; Figure 6.1) is transported from soils to rivers headstreams. A fraction of this carbon is outgassed as CO_2 by rivers and lakes to the atmosphere, a fraction is buried in freshwater organic sediments and the remaining amount (~0.9 PgC yr^{-1}; Figure 6.1) is delivered by rivers to the coastal ocean as dissolved inorganic carbon, dissolved organic carbon and particulate organic carbon (Tranvik et al., 2009).

Atmospheric CO_2 is exchanged with the surface ocean through gas exchange. This exchange flux is driven by the partial CO_2 pressure difference between the air and the sea. In the ocean, carbon is available predominantly as Dissolved Inorganic Carbon (DIC, ~38,000 PgC; Figure 6.1), that is carbonic acid (dissolved CO_2 in water), bicarbonate and carbonate ions, which are tightly coupled via ocean chemistry. In addition, the ocean contains a pool of Dissolved Organic Carbon (DOC, ~700 PgC), of which a substantial fraction has a turnover time of 1000 years or longer (Hansell et al., 2009). The marine biota, predominantly phytoplankton and other microorganisms, represent a small organic carbon pool (~3 PgC), which is turned over very rapidly in days to a few weeks.

Carbon is transported within the ocean by three mechanisms (Figure 6.1): (1) the 'solubility pump' (see Glossary), (2) the 'biological pump' (see Glossary), and (3) the 'marine carbonate pump' that is generated by the formation of calcareous shells of certain oceanic microorganisms in the surface ocean, which, after sinking to depth, are re-mineralized back into DIC and calcium ions. The marine carbonate pump operates counter to the marine biological soft-tissue pump with respect to its effect on CO_2: in the formation of calcareous shells, two bicarbonate ions are split into one carbonate and one dissolved CO_2 molecules, which increases the partial CO_2 pressure in surface waters (driving a release of CO_2 to the atmosphere). Only a small fraction (~0.2 PgC yr^{-1}) of the carbon exported by biological processes (both soft-tissue and carbonate pumps) from the surface reaches the sea floor where it can be stored in sediments for millennia and longer (Denman et al., 2007).

Box 6.1 | Multiple Residence Times for an Excess of Carbon Dioxide Emitted in the Atmosphere

On an average, CO_2 molecules are exchanged between the atmosphere and the Earth surface every few years. This fast CO_2 cycling through the atmosphere is coupled to a slower cycling of carbon through land vegetation, litter and soils and the upper ocean (decades to centuries); deeper soils and the deep sea (centuries to millennia); and geological reservoirs, such as deep-sea carbonate sediments and the upper mantle (up to millions of years) as explained in Section 6.1.1.1. Atmospheric CO_2 represents only a tiny fraction of the carbon in the Earth System, the rest of which is tied up in these other reservoirs. Emission of carbon from fossil fuel reserves, and additionally from land use change (see Section 6.3) is now rapidly increasing atmospheric CO_2 content. The removal of all the human-emitted CO_2 from the atmosphere by natural processes will take a few hundred thousand years (*high confidence*) as shown by the timescales of the removal process shown in the table below (Archer and Brovkin, 2008). For instance, an extremely long atmospheric CO_2 recovery time scale from a large emission pulse of CO_2 has been inferred from geological evidence when during the Paleocene–Eocene thermal maximum event about 55 million years ago a large amount of CO_2 was released to the atmosphere (McInerney and Wing, 2011). Based on the amount of CO_2 remaining in the atmosphere after a pulse of emissions (data from Joos et al. 2013) and on the magnitude of the historical and future emissions for each RCP scenario, we assessed that about 15 to 40% of CO_2 emitted until 2100 will remain in the atmosphere longer than 1000 years.

Box 6.1, Table 1 | The main natural processes that remove CO_2 consecutive to a large emission pulse to the atmosphere, their atmospheric CO_2 adjustment time scales, and main (bio)chemical reactions involved.

Processes	Time scale (years)	Reactions
Land uptake: Photosynthesis–respiration	$1–10^2$	$6CO_2 + 6H_2O + \text{photons} \rightarrow C_6H_{12}O_6 + 6O_2$ $C_6H_{12}O_6 + 6O_2 \rightarrow 6CO_2 + 6H_2O + \text{heat}$
Ocean invasion: Seawater buffer	$10–10^3$	$CO_2 + CO_3^{2-} + H_2O \rightleftharpoons 2HCO_3^-$
Reaction with calcium carbonate	$10^3–10^4$	$CO_2 + CaCO_3 + H_2O \rightarrow Ca^{2+} + 2HCO_3^-$
Silicate weathering	$10^4–10^6$	$CO_2 + CaSiO_3 \rightarrow CaCO_3 + SiO_2$

These processes are active on all time scales, but the relative importance of their role in the CO_2 removal is changing with time and depends on the level of emissions. Accordingly, the times of atmospheric CO_2 adjustment to anthropogenic carbon emissions can be divided into three phases associated with increasingly longer time scales.

Phase 1. Within several decades of CO_2 emissions, about a third to half of an initial pulse of anthropogenic CO_2 goes into the land and ocean, while the rest stays in the atmosphere (Box 6.1, Figure 1a). Within a few centuries, most of the anthropogenic CO_2 will be in the form of additional dissolved inorganic carbon in the ocean, thereby decreasing ocean pH (Box 6.1, Figure 1b). Within a thousand years, the remaining atmospheric fraction of the CO_2 emissions (see Section 6.3.2.4) is between 15 and 40%, depending on the amount of carbon released (Archer et al., 2009b). The carbonate buffer capacity of the ocean decreases with higher CO_2, so the larger the cumulative emissions, the higher the remaining atmospheric fraction (Eby et al., 2009; Joos et al., 2013). (continued on next page)

6

Box 6.1 (continued)

Phase 2. In the second stage, within a few thousands of years, the pH of the ocean that has decreased in Phase 1 will be restored by reaction of ocean dissolved CO_2 and calcium carbonate ($CaCO_3$) of sea floor sediments, partly replenishing the buffer capacity of the ocean and further drawing down atmospheric CO_2 as a new balance is re-established between $CaCO_3$ sedimentation in the ocean and terrestrial weathering (Box 6.1, Figure 1c right). This second phase will pull the remaining atmospheric CO_2 fraction down to 10 to 25% of the original CO_2 pulse after about 10 kyr (Lenton and Britton, 2006; Montenegro et al., 2007; Ridgwell and Hargreaves, 2007; Tyrrell et al., 2007; Archer and Brovkin, 2008).

Phase 3. In the third stage, within several hundred thousand years, the rest of the CO_2 emitted during the initial pulse will be removed from the atmosphere by silicate weathering, a very slow process of CO_2 reaction with calcium silicate ($CaSiO_3$) and other minerals of igneous rocks (e.g., Sundquist, 1990; Walker and Kasting, 1992).

Involvement of extremely long time scale processes into the removal of a pulse of CO_2 emissions into the atmosphere complicates comparison with the cycling of the other GHGs. This is why the concept of a single, characteristic atmospheric lifetime is not applicable to CO_2 (Chapter 8).

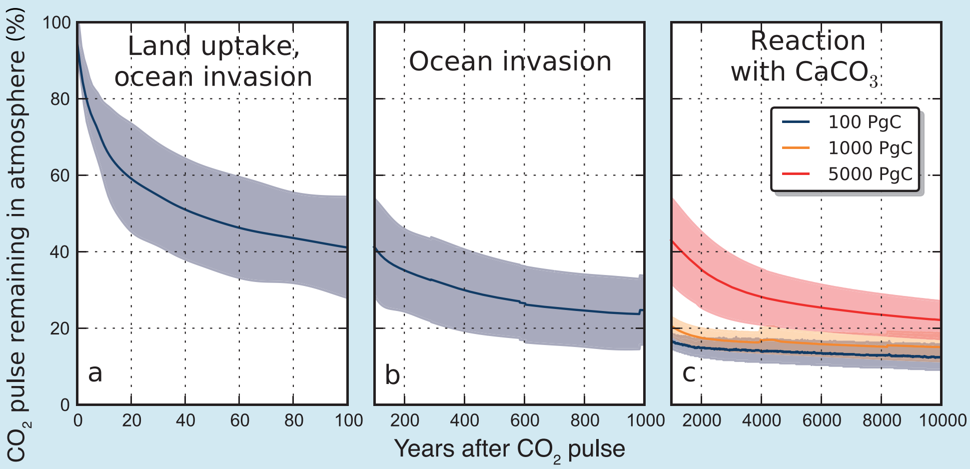

Box 6.1, Figure 1 | A percentage of emitted CO_2 remaining in the atmosphere in response to an idealised instantaneous CO_2 pulse emitted to the atmosphere in year 0 as calculated by a range of coupled climate–carbon cycle models. (Left and middle panels, a and b) Multi-model mean (blue line) and the uncertainty interval (±2 standard deviations, shading) simulated during 1000 years following the instantaneous pulse of 100 PgC (Joos et al., 2013). (Right panel, c) A mean of models with oceanic and terrestrial carbon components and a maximum range of these models (shading) for instantaneous CO_2 pulse in year 0 of 100 PgC (blue), 1000 PgC (orange) and 5000 PgC (red line) on a time interval up to 10 kyr (Archer et al., 2009b). Text at the top of the panels indicates the dominant processes that remove the excess of CO_2 emitted in the atmosphere on the successive time scales. Note that higher pulse of CO_2 emissions leads to higher remaining CO_2 fraction (Section 6.3.2.4) due to reduced carbonate buffer capacity of the ocean and positive climate–carbon cycle feedback (Section 6.3.2.6.6).

6.1.1.2 Methane Cycle

CH_4 absorbs infrared radiation relatively stronger per molecule compared to CO_2 (Chapter 8), and it interacts with photochemistry. On the other hand, the methane turnover time (see Glossary) is less than 10 years in the troposphere (Prather et al., 2012; see Chapter 7). The sources of CH_4 at the surface of the Earth (see Section 6.3.3.2) can be thermogenic including (1) natural emissions of fossil CH_4 from geological sources (marine and terrestrial seepages, geothermal vents and mud volcanoes) and (2) emissions caused by leakages from fossil fuel extraction and use (natural gas, coal and oil industry; Figure 6.2). There are also pyrogenic sources resulting from incomplete burning of fossil fuels and plant biomass (both natural and anthropogenic fires). The biogenic sources include natural biogenic emissions predominantly from wetlands, from termites and very small emissions from the ocean (see Section 6.3.3). Anthropogenic biogenic emissions occur from rice paddy agriculture, ruminant livestock, landfills, man-made lakes and wetlands and waste treatment. In general, biogenic CH_4 is produced from organic matter under low oxygen conditions by fermentation processes of methanogenic microbes (Conrad, 1996). Atmospheric CH_4 is removed primarily by photochemistry, through atmospheric chemistry reactions with the OH radicals. Other smaller removal processes of atmospheric CH_4 take place in the stratosphere through reaction with chlorine and oxygen radicals, by oxidation in well aerated soils, and possibly by reaction with chlorine in the marine boundary layer (Allan et al., 2007; see Section 6.3.3.3).

A very large geological stock (globally 1500 to 7000 PgC, that is 2 x 10^6 to 9.3 x 10^6 Tg(CH_4) in Figure 6.2; Archer (2007); with *low confidence* in estimates) of CH_4 exists in the form of frozen hydrate deposits ('clathrates') in shallow ocean sediments and on the slopes of continental shelves, and permafrost soils. These CH_4 hydrates are stable under conditions of low temperature and high pressure. Warming or changes in pressure could render some of these hydrates unstable with a potential release of CH_4 to the overlying soil/ocean and/or atmosphere. Possible future CH_4 emissions from CH_4 released by gas hydrates are discussed in Section 6.4.7.3.

6.1.2 Industrial Era

6.1.2.1 Carbon Dioxide and the Global Carbon Cycle

Since the beginning of the Industrial Era, humans have been producing energy by burning of fossil fuels (coal, oil and gas), a process that is releasing large amounts of CO_2 into the atmosphere (Rotty, 1983; Boden et al., 2011; see Section 6.3.2.1). The amount of fossil fuel CO_2 emitted to the atmosphere can be estimated with an accuracy of about 5 to 10% for recent decades from statistics of fossil fuel use (Andres et al., 2012). Total cumulative emissions between 1750 and 2011 amount to 375 ± 30 PgC (see Section 6.3.2.1 and Table 6.1), including a contribution of 8 PgC from the production of cement.

The second major source of anthropogenic CO_2 emissions to the atmosphere is caused by changes in land use (mainly deforestation), which causes globally a net reduction in land carbon storage, although recovery from past land use change can cause a net gain in in land

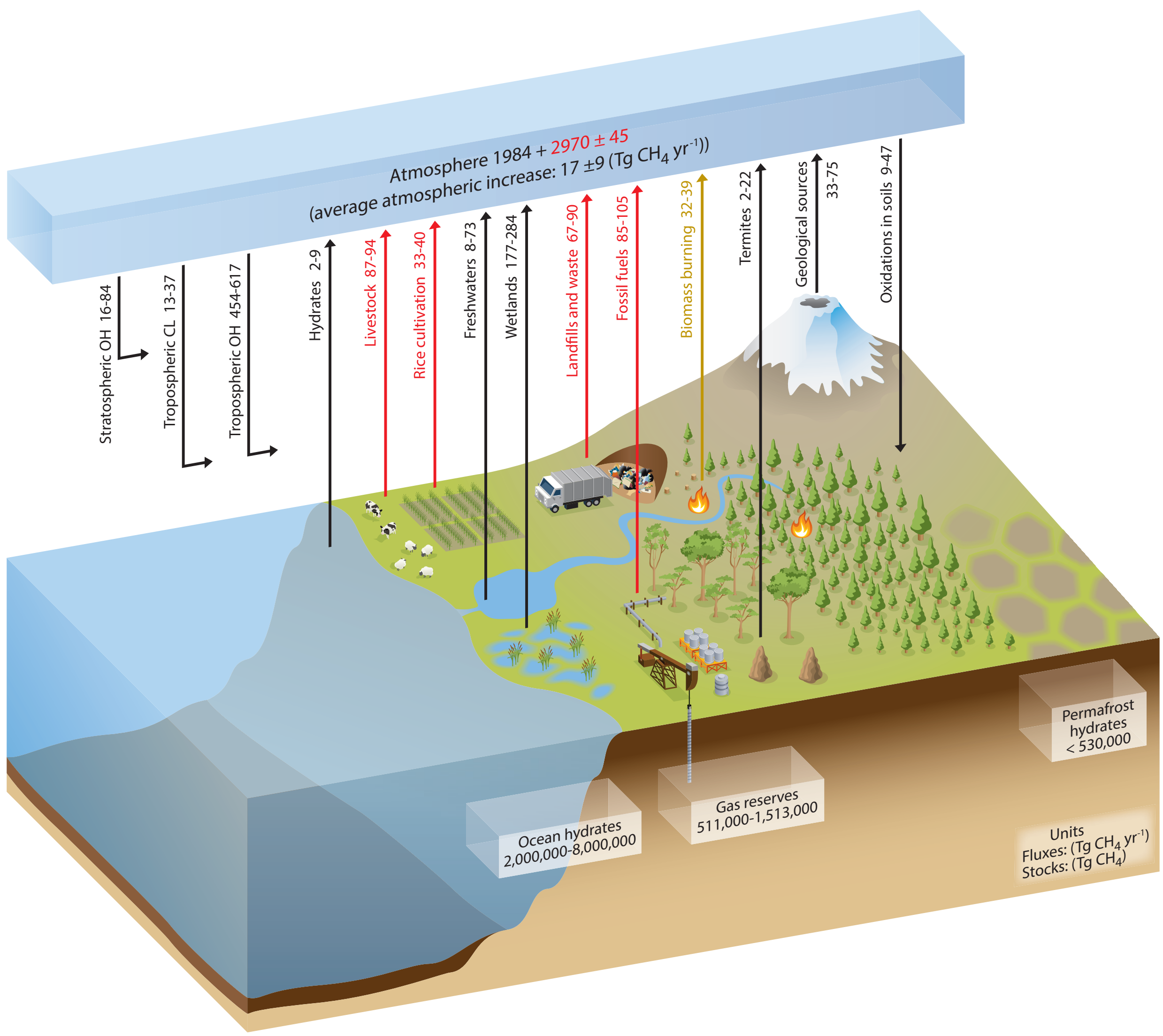

Figure 6.2 | Schematic of the global cycle of CH_4. Numbers represent annual fluxes in Tg(CH_4) yr^{-1} estimated for the time period 2000–2009 and CH_4 reservoirs in Tg (CH_4): the atmosphere and three geological reservoirs (hydrates on land and in the ocean floor and gas reserves) (see Section 6.3.3). Black arrows denote 'natural' fluxes, that is, fluxes that are not directly caused by human activities since 1750, red arrows anthropogenic fluxes, and the light brown arrow denotes a combined natural + anthropogenic flux. Note that human activities (e.g., land use) may have modified indirectly the global magnitude of the natural fluxes (Section 6.3.3). Ranges represent minimum and maximum values from cited references as given in Table 6.8 in Section 6.3.3. Gas reserves are from GEA (2006) and are consistent with numbers used by IPCC WG III for future scenarios. Hydrate reservoir sizes are from Archer et al. (2007). The atmospheric inventories have been calculated using a conversion factor of 2.7476 TgCH_4 per ppb (Prather et al., 2012). The assumed preindustrial annual mean globally averaged CH_4 concentration was 722 ± 25 ppb taking the average of the Antarctic Law Dome ice core observations (MacFarling-Meure et al., 2006) and the measurements from the GRIP ice core in Greenland (Blunier et al., 1995; see also Table 2.1). The atmospheric inventory in the year 2011 is based on an annual globally averaged CH_4 concentration of 1803 ± 4 ppb in the year 2011 (see Table 2.1). It is the sum of the atmospheric increase between 1750 and 2011 (in red) and of the pre-industrial inventory (in black). The *average atmospheric increase* each year, also called growth rate, is based on a measured concentration increase of 2.2 ppb yr^{-1} during the time period 2000–2009 (Dlugokencky et al., 2011).

carbon storage in some regions. Estimation of this CO_2 source to the atmosphere requires knowledge of changes in land area as well as estimates of the carbon stored per area before and after the land use change. In addition, longer term effects, such as the decomposition of soil organic matter after land use change, have to be taken into account (see Section 6.3.2.2). Since 1750, anthropogenic land use changes have resulted into about 50 million km^2 being used for cropland and pasture, corresponding to about 38% of the total ice-free land area (Foley et al., 2007, 2011), in contrast to an estimated cropland and pasture area of 7.5 to 9 million km^2 about 1750 (Ramankutty and Foley, 1999; Goldewijk, 2001). The cumulative net CO_2 emissions from land use changes between 1750 and 2011 are estimated at approximately 180 ± 80 PgC (see Section 6.3 and Table 6.1).

Multiple lines of evidence indicate that the observed atmospheric increase in the global CO_2 concentration since 1750 (Figure 6.3) is caused by the anthropogenic CO_2 emissions (see Section 6.3.2.3). The rising atmospheric CO_2 content induces a disequilibrium in the exchange fluxes between the atmosphere and the land and oceans respectively. The rising CO_2 concentration implies a rising atmospheric CO_2 partial pressure (pCO_2) that induces a globally averaged net-air-to-sea flux and thus an ocean sink for CO_2 (see Section 6.3.2.5). On land, the rising atmospheric CO_2 concentration fosters photosynthesis via the CO_2 fertilisation effect (see Section 6.3.2.6). However, the efficacy of these oceanic and terrestrial sinks does also depend on how the excess carbon is transformed and redistributed within these sink reservoirs. The magnitude of the current sinks is shown in Figure 6.1 (averaged over the years 2000–2009, red arrows), together with the cumulative reservoir content changes over the industrial era (1750–2011, red numbers) (see Table 6.1, Section 6.3).

6.1.2.2 Methane Cycle

After 1750, atmospheric CH_4 levels rose almost exponentially with time, reaching 1650 ppb by the mid-1980s and 1803 ppb by 2011. Between the mid-1980s and the mid-2000s the atmospheric growth of CH_4 declined to nearly zero (see Section 6.3.3.1, see also Chapter 2). More recently since 2006, atmospheric CH_4 is observed to increase again (Rigby et al., 2008); however, it is unclear if this is a short-term fluctuation or a new regime for the CH_4 cycle (Dlugokencky et al., 2009).

There is *very high* level of *confidence* that the atmospheric CH_4 increase during the Industrial Era is caused by anthropogenic activities. The massive increase in the number of ruminants (Barnosky, 2008), the emissions from fossil fuel extraction and use, the expansion of rice paddy agriculture and the emissions from landfills and waste are the dominant anthropogenic CH_4 sources. Total anthropogenic sources contribute at present between 50 and 65% of the total CH_4 sources (see Section 6.3.3). The dominance of CH_4 emissions located mostly in the NH (wetlands and anthropogenic emissions) is evidenced by the observed positive north–south gradient in CH_4 concentrations (Figure 6.3). Satellite-based CH_4 concentration measurements averaged over the entire atmospheric column also indicate higher concentrations of CH_4 above and downwind of densely populated and intensive agriculture areas where anthropogenic emissions occur (Frankenberg et al., 2011).

6.1.3 Connections Between Carbon and the Nitrogen and Oxygen Cycles

6.1.3.1 Global Nitrogen Cycle Including Nitrous Oxide

The biogeochemical cycles of nitrogen and carbon are tightly coupled with each other owing to the metabolic needs of organisms for these two elements. Changes in the availability of one element will influence not only biological productivity but also availability and requirements for the other element (Gruber and Galloway, 2008) and in the longer term, the structure and functioning of ecosystems as well.

Before the Industrial Era, the creation of reactive nitrogen Nr (all nitrogen species other than N_2) from non-reactive atmospheric N_2 occurred primarily through two natural processes: lightning and biological nitrogen fixation (BNF). BNF is a set of reactions that convert N_2 to ammonia in a microbially mediated process. This input of Nr to the land and ocean biosphere was in balance with the loss of Nr though denitrification, a process that returns N_2 back to the atmosphere (Ayres et al., 1994). This equilibrium has been broken since the beginning of the Industrial Era. Nr is produced by human activities and delivered to ecosystems. During the last decades, the production of Nr by humans has been much greater than the natural production (Figure 6.4a; Section 6.3.4.3). There are three main anthropogenic sources of Nr: (1) the Haber-Bosch industrial process, used to make NH_3 from N_2, for nitrogen fertilisers and as a feedstock for some industries; (2) the cultivation of legumes and other crops, which increases BNF; and (3) the combustion of fossil fuels, which converts atmospheric N_2 and fossil fuel nitrogen into nitrogen oxides (NO_x) emitted to the atmosphere and re-deposited at the surface (Figure 6.4a). In addition, there is a small flux from the mobilization of sequestered Nr from nitrogen-rich sedimentary rocks (Morford et al., 2011) (not shown in Figure 6.4a).

The amount of anthropogenic Nr converted back to non-reactive N_2 by denitrification is much smaller than the amount of Nr produced each year, that is, about 30 to 60% of the total Nr production, with a large uncertainty (Galloway et al., 2004; Canfield et al., 2010; Bouwman et al., 2013). What is more certain is the amount of N_2O emitted to the atmosphere. Anthropogenic sources of N_2O are about the same size as natural terrestrial sources (see Section 6.3.4 and Table 6.9 for the global N_2O budget). In addition, emissions of Nr to the atmosphere, as NH_3 and NO_x, are caused by agriculture and fossil fuel combustion. A portion of the emitted NH_3 and NO_x is deposited over the continents, while the rest gets transported by winds and deposited over the oceans. This atmospheric deposition flux of Nr over the oceans is comparable to the flux going from soils to rivers and delivered to the coastal ocean (Galloway et al., 2004; Suntharalingam et al., 2012). The increase of Nr creation during the Industrial Era, the connections among its impacts, including on climate and the connections with the carbon cycle are presented in Box 6.2.

For the global ocean, the best BNF estimate is 160 TgN yr^{-1}, which is roughly the midpoint of the minimum estimate of 140 TgN yr^{-1} of Deutsch et al. (2007) and the maximum estimate of 177 TgN yr^{-1} (Großkopf et al., 2012). The probability that this estimate will need an upward revision in the near future is high because several additional processes are not yet considered (Voss et al., 2013).

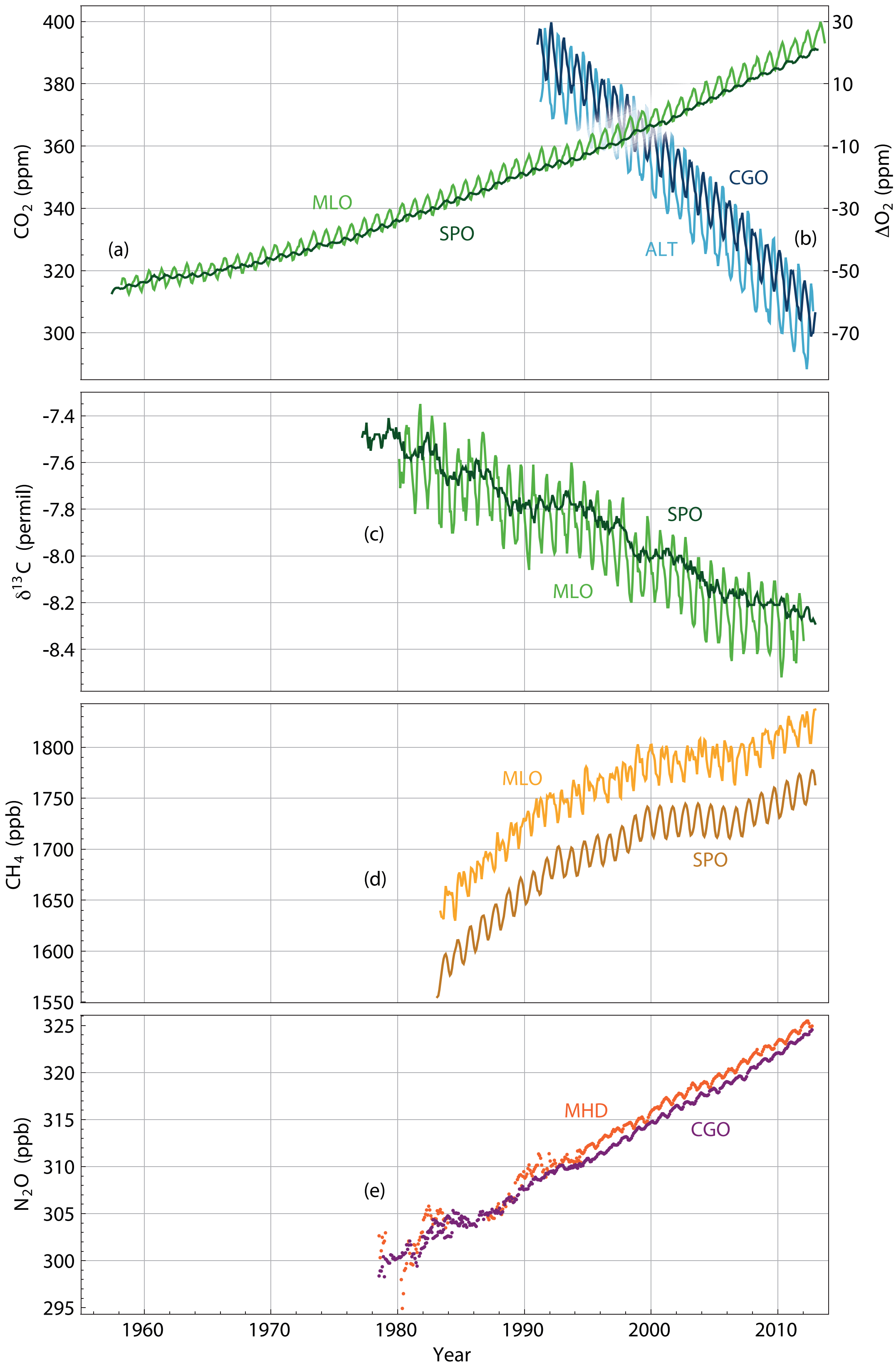

Figure 6.3 | Atmospheric concentration of CO_2, oxygen, $^{13}C/^{12}C$ stable isotope ratio in CO_2, CH_4 and N_2O recorded over the last decades at representative stations (a) CO_2 from Mauna Loa (MLO) Northern Hemisphere and South Pole Southern Hemisphere (SPO) atmospheric stations (Keeling et al., 2005). (b) O_2 from Alert Northern Hemisphere (ALT) and Cape Grim Southern Hemisphere (CGO) stations (http://scrippso2.ucsd.edu/ right axes, expressed relative to a reference standard value). (c) $^{13}C/^{12}C$: Mauna Loa, South Pole (Keeling et al., 2005). (d) CH_4 from Mauna Loa and South Pole stations (Dlugokencky et al., 2012). (e) N_2O from Mace-Head Northern Hemisphere (MHD) and Cape Grim stations (Prinn et al., 2000).

Box 6.2 | Nitrogen Cycle and Climate-Carbon Cycle Feedbacks

Human creation of reactive nitrogen by the Haber–Bosch process (see Sections 6.1.3 and 6.3.4), fossil fuel combustion and agricultural biological nitrogen fixation (BNF) dominate Nr creation relative to biological nitrogen fixation in natural terrestrial ecosystems. This dominance impacts on the radiation balance of the Earth (covered by the IPCC; see, e.g., Chapters 7 and 8), and affects human health and ecosystem health as well (EPA, 2011b; Sutton et al., 2011).

The Nr creation from 1850 to 2005 is shown in Box 6.2 (Figure 1). After mid-1970s, human production of Nr exceeded natural production. During the 2000s food production (mineral fertilisers, legumes) accounts for three-quarters of Nr created by humans, with fossil fuel combustion and industrial uses accounting equally for the remainder (Galloway et al., 2008; Canfield et al., 2010; Sutton et al., 2011).

The three most relevant questions regarding the anthropogenic perturbation of the nitrogen cycle with respect to global change are: (1) What are the interactions with the carbon cycle, and the effects on carbon sinks (see Sections 6.3.2.6.5 and 6.4.2.1), (2) What are the effects of increased Nr on the radiative forcing of nitrate aerosols (Chapter 7, 7.3.2) and tropospheric ozone (Chapters 8), (3) What are the impacts of the excess of Nr on humans and ecosystems (health, biodiversity, eutrophication, not treated in this report, but see, for example, EPA, 2011b; Sutton et al., 2011).

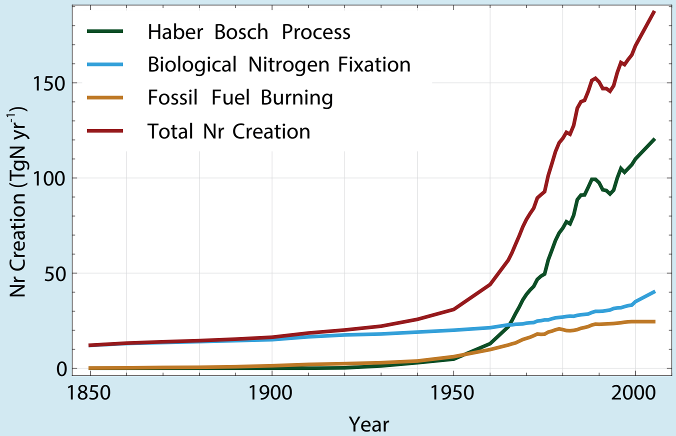

Box 6.2, Figure 1 | Anthropogenic reactive nitrogen (Nr) creation rates (in TgN yr^{-1}) from fossil fuel burning (orange line), cultivation-induced biological nitrogen fixation (blue line), Haber–Bosch process (green line) and total creation (red line). Source: Galloway et al. (2003), Galloway et al. (2008). Note that updates are given in Table 6.9. The only one with significant changes in the more recent literature is cultivation-induced BNF) which Herridge et al. (2008) estimated to be 60 TgN yr^{-1}. The data are only reported since 1850, as no published estimate is available since 1750.

Essentially all of the Nr formed by human activity is spread into the environment, either at the point of creation (i.e., fossil fuel combustion) or after it is used in food production and in industry. Once in the environment, Nr has a number of negative impacts if not converted back into N_2. In addition to its contributions to climate change and stratospheric ozone depletion, Nr contributes to the formation of smog; increases the haziness of the troposphere; contributes to the acidification of soils and freshwaters; and increases the productivity in forests, grasslands, open and coastal waters and open ocean, which can lead to eutrophication and reduction in biodiversity in terrestrial and aquatic ecosystems. In addition, Nr-induced increases in nitrogen oxides, aerosols, tropospheric ozone, and nitrates in drinking water have negative impacts on human health (Galloway et al., 2008; Davidson et al., 2012). Once the nitrogen atoms become reactive (e.g., NH_3, NO_x), any given Nr atom can contribute to all of the impacts noted above in sequence. This is called the nitrogen cascade (Galloway et al., 2003; Box 6.2, Figure 2). The nitrogen cascade is the sequential transfer of the same Nr atom through the atmosphere, terrestrial ecosystems, freshwater ecosystems and marine ecosystems that results in multiple effects in each reservoir. Because of the nitrogen cascade, the creation of any molecule of Nr from N_2, at any location, has the potential to affect climate, either directly or indirectly, as explained in this box This potential exists until the Nr gets converted back to N_2.

The most important processes causing direct links between anthropogenic Nr and climate change include (Erisman et al., 2011): (1) N_2O formation during industrial processes (e.g., fertiliser production), combustion, or microbial conversion of substrate containing nitrogen—notably after fertiliser and manure application to soils. N_2O is a strong greenhouse gas (GHG), (2) emission of anthropogenic NO_x leading to (a) formation of tropospheric O_3, (which is the third most important GHG), (b) a decrease of CH_4 and (c) the formation of nitrate aerosols. Aerosol formation affects radiative forcing, as nitrogen-containing aerosols have a direct cooling effect in addition to an indirect cooling effect through cloud formation and (3) NH_3 emission to the atmosphere which contributes to aerosol formation. The first process has a warming effect. The second has both a warming (as a GHG) and a cooling (through the formation of the OH radical in the troposphere which reacts with CH_4, and through aerosol formation) effect. The net effect of all three NO_x-related contributions is cooling. The third process has a cooling effect.

The most important processes causing an indirect link between anthropogenic Nr and climate change include: (1) nitrogen-dependent changes in soil organic matter decomposition and hence CO_2 emissions, affecting heterotrophic respiration; (2) alteration of the biospheric CO_2 sink due to increased supply of Nr. About half of the carbon that is emitted to the atmosphere is

(continued on next page)

6

Box 6.2 (continued)

taken up by the biosphere; Nr affects net CO_2 uptake from the atmosphere in terrestrial systems, rivers, estuaries and the open ocean in a positive direction (by increasing productivity or reducing the rate of organic matter breakdown) and negative direction (in situations where it accelerates organic matter breakdown). CO_2 uptake in the ocean causes ocean acidification, which reduces CO_2 uptake; (3) changes in marine primary productivity, generally an increase, in response to Nr deposition; and (4) O_3 formed in the troposphere as a result of NO_x and volatile organic compound emissions reduces plant productivity, and therefore reduces CO_2 uptake from the atmosphere. On the global scale the net influence of the direct and indirect contributions of Nr on the radiative balance was estimated to be –0.24 W m^{-2} (with an uncertainty range of +0.2 to –0.5 W m^{-2}) (Erisman et al., 2011).

Nr is required for both plants and soil microorganisms to grow, and plant and microbial processes play important roles in the global carbon cycle. The increasing concentration of atmospheric CO_2 is observed to increase plant photosynthesis (see Box 6.3) and plant growth, which drives an increase of carbon storage in terrestrial ecosystems. Plant growth is, however, constrained by the availability of Nr in soils (see Section 6.3.2.6.5). This means that in some nitrogen-poor ecosystems, insufficient Nr availability will limit carbon sinks, while the deposition of Nr may instead alleviate this limitation and enable larger carbon sinks (see Section 6.3.2.6.5). Therefore, human production of Nr has the potential to mitigate CO_2 emissions by providing additional nutrients for plant growth in some regions. Microbial growth can also be limited by the availability of Nr, particularly in cold, wet environments, so that human production of Nr also has the potential to accelerate the decomposition of organic matter, increasing release of CO_2. The availability of Nr also changes in response to climate change, generally increasing with warmer temperatures and increased precipitation (see Section 6.4.2.1), but with complex interactions in the case of seasonally inundated environments. This complex network of feedbacks is amenable to study through observation and experimentation (Section 6.3) and Earth System modelling (Section 6.4). Even though we do not yet have a thorough understanding of how nitrogen and carbon cycling will interact with climate change, elevated CO_2 and human Nr production in the future, given scenarios of human activity, current observations and model results all indicate that low nitrogen availability will limit carbon storage on land in the 21st century (see Section 6.4.2.1).

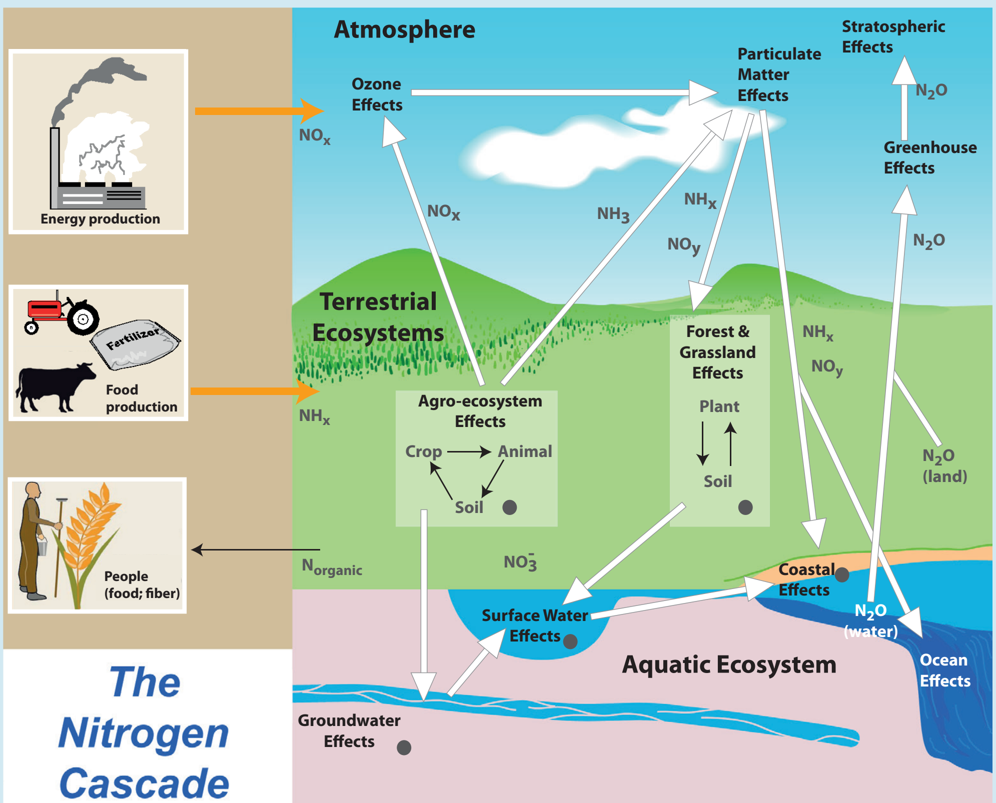

Box 6.2, Figure 2 | Illustration of the nitrogen cascade showing the sequential effects that a single atom of nitrogen in its various molecular forms can have in various reservoirs after it has been converted from nonreactive N_2 to a reactive form by energy and food production (orange arrows). Once created the reactive nitrogen has the potential to continue to contribute to impacts until it is converted back to N_2. The small black circle indicates that there is the potential for denitrification to occur within that reservoir. NH_3 = ammonia; NH_x = ammonia plus ammonium; NO_3^- = nitrate; NO_x = nitrogen oxides; NO_y = NO_x and other combinations of nitrogen and oxygen (except N_2O); N_2O = nitrous oxide. (Adapted with permission from the GEO Yearbook 2003, United Nations Environmental Programme (UNEP), 2004 which was based on Galloway et al., 2003.)

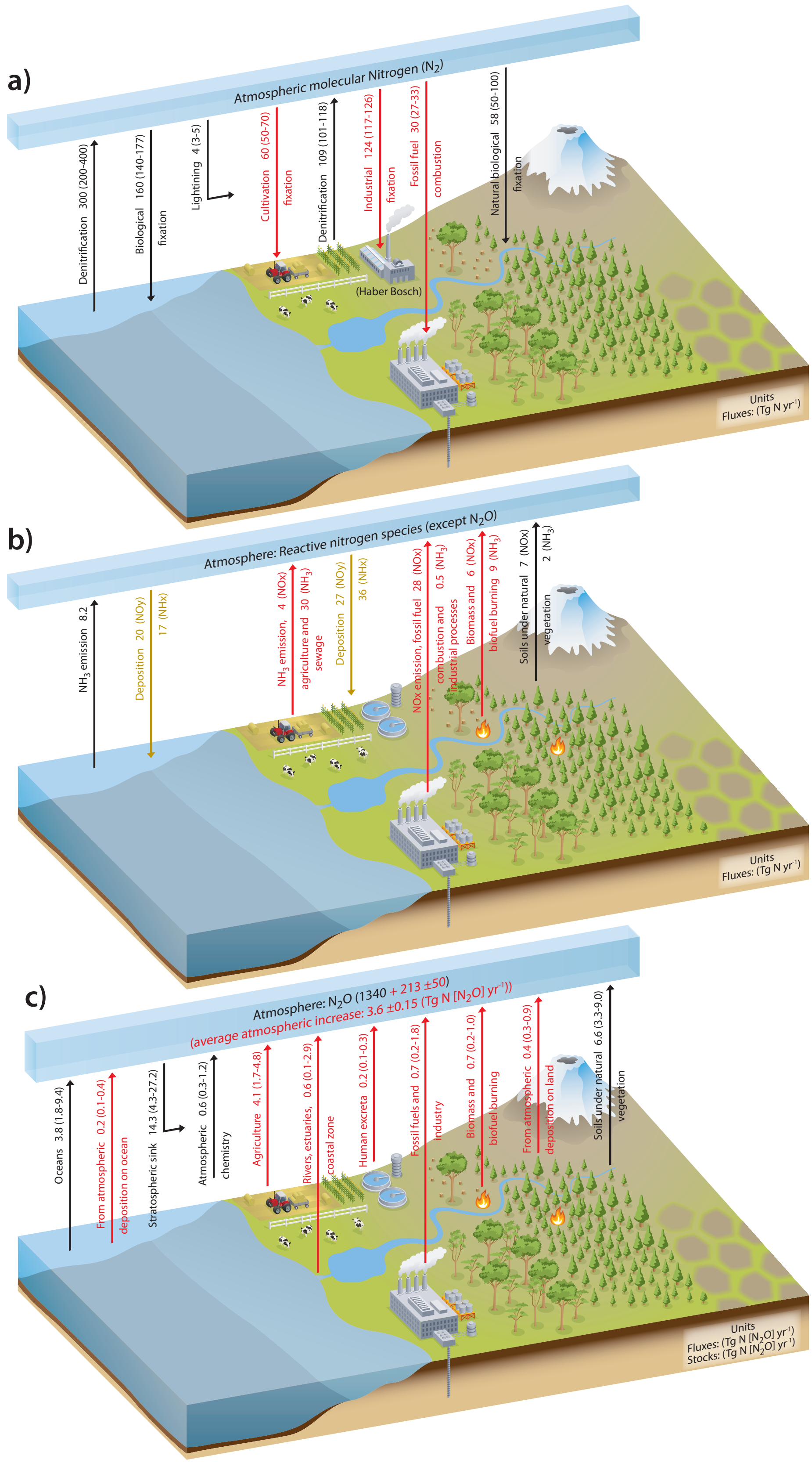

Figure 6.4 | Schematic of the global nitrogen cycle. (a) The natural and anthropogenic processes that create reactive nitrogen and the corresponding rates of denitrification that convert reactive nitrogen back to N_2. (b) The flows of the reactive nitrogen species NO_y and NH_x. (c) The stratospheric sink of N_2O is the sum of losses via photolysis and reaction with O(1D) (oxygen radical in the 1D excited state; Table 6.9). The global magnitude of this sink is adjusted here in order to be equal to the difference between the total sources and the observed growth rate. This value falls within literature estimates (Volk et al., 1997). The atmospheric inventories have been calculated using a conversion factor of 4.79 TgN (N_2O) per ppb (Prather et al., 2012).

A global denitrification rate is much more difficult to constrain than the BNF considering the changing paradigms of nitrogen cycling in the oxygen minimum zones or the unconstrained losses in permeable sediments on the continental shelves (Gao et al., 2012). The coastal ocean may have losses in the range of 100 to 250 (Voss et al., 2011). For the open and distal ocean Codispoti (2007) estimated an upper limit of denitrification of 400 TgN yr^{-1}. Voss et al. (2013) used a conservative estimate of 100 TgN yr^{-1} for the coastal ocean, and 200 to 300 TgN yr^{-1} for the open ocean. Because the upper limit in the global ocean is 400 TgN yr^{-1}, 300 ± 100 TgN yr^{-1} is the best estimate for global ocean losses of reactive nitrogen (Table 6.9).

This chapter does not describe the phosphorus and sulphur biogeochemical cycles, but phosphorus limitations on carbon sinks are briefly addressed in Section 6.4.8.2 and future sulphur deposition in Section 6.4.6.2.

6.1.3.2 Oxygen

Atmospheric oxygen is tightly coupled with the global carbon cycle (sometimes called a mirror of the carbon cycle). The burning of fossil fuels removes oxygen from the atmosphere in a tightly defined stoichiometric ratio depending on fuel carbon content. As a consequence of the burning of fossil fuels, atmospheric O_2 levels have been observed to decrease steadily over the last 20 years (Keeling and Shertz, 1992; Manning and Keeling, 2006) (Figure 6.3b). Compared to the atmospheric oxygen content of about 21% this decrease is very small; however, it provides independent evidence that the rise in CO_2 must be due to an oxidation process, that is, fossil fuel combustion and/or organic carbon oxidation, and is not caused by, for example, volcanic emissions or by outgassing of dissolved CO_2 from a warming ocean. The atmospheric oxygen measurements furthermore also show the north–south concentration O_2 difference (higher in the south and mirroring the CO_2 north–south concentration difference) as expected from the stronger fossil fuel consumption in the NH (Keeling et al., 1996).

On land, during photosynthesis and respiration, O_2 and CO_2 are exchanged in nearly a 1:1 ratio. However, with respect to exchanges with the ocean, O_2 behaves quite differently from CO_2, because compared to the atmosphere only a small amount of O_2 is dissolved in the ocean whereas by contrast the oceanic CO_2 content is much larger due to the carbonate chemistry. This different behaviour of the two gases with respect to ocean exchange provides a powerful method to assess independently the partitioning of the uptake of anthropogenic CO_2 by land and ocean (Manning and Keeling, 2006), Section 6.3.2.3.

6.2 Variations in Carbon and Other Biogeochemical Cycles Before the Fossil Fuel Era

The Earth System mechanisms that were responsible for past variations in atmospheric CO_2, CH_4, and N_2O will probably operate in the future as well. Past archives of GHGs and climate therefore provide useful knowledge, including constraints for biogeochemical models applied to the future projections described in Section 6.4. In addition, past archives of GHGs also show with *very high confidence* that the average rates of increase of CO_2, CH_4 and N_2O are larger during the Industrial Era (see Section 6.3) than during any comparable period of at least the past 22,000 years (Joos and Spahni, 2008).

6.2.1 Glacial–Interglacial Greenhouse Gas Changes

6.2.1.1 Processes Controlling Glacial Carbon Dioxide

Ice cores recovered from the Antarctic ice sheet reveal that the concentration of atmospheric CO_2 at the Last Glacial Maximum (LGM; see Glossary) at 21 ka was about one third lower than during the subsequent interglacial (Holocene) period started at 11.7 ka (Delmas et al., 1980; Neftel et al., 1982; Monnin et al., 2001). Longer (to 800 ka) records exhibit similar features, with CO_2 values of ~180 to 200 ppm during glacial intervals (Petit et al., 1999). Prior to 420 ka, interglacial CO_2 values were 240 to 260 ppm rather than 270 to 290 ppm after that date (Lüthi et al., 2008).

A variety of proxy reconstructions as well as models of different complexity from conceptual to complex Earth System Models (ESM; see Glossary) have been used to test hypotheses for the cause of lower LGM atmospheric CO_2 concentrations (e.g., Köhler et al., 2005; Sigman et al., 2010). The mechanisms of the carbon cycle during the LGM which lead to low atmospheric CO_2 can be broken down by individual drivers (Figure 6.5). It should be recognized, however, that this separation is potentially misleading, as many of the component drivers shown in Figure 6.5 may combine nonlinearly (Bouttes et al., 2011). Only well-established individual drivers are quantified (Figure 6.5), and discussed here.

6.2.1.1.1 Reduced land carbon

Despite local evidence of larger carbon storage in permafrost regions during glacial periods (Zimov et al., 2009; Zech et al., 2011), the $\delta^{13}C$ record of ocean waters as preserved in benthic foraminiferal shells has been used to infer that global terrestrial carbon storage was reduced in glacial times, thus opposite to recorded changes in atmospheric CO_2. Data-based estimates of the deficit between LGM and pre-industrial land carbon storage range from a few hundreds to 1000 PgC (e.g., Bird et al., 1996; Ciais et al., 2012). Dynamic vegetation models tend to simulate values at the higher end (~800 PgC) (Kaplan et al., 2002; Otto et al., 2002) and indicate a role for the physiological effects of low CO_2 on photosynthesis at the LGM at least as large as that of colder and dryer climate conditions in determining the past extent of forests (Prentice and Harrison, 2009).

6.2.1.1.2 Lower sea surface temperatures

Reconstructions of sea surface temperatures (SSTs) during the LGM suggest that the global surface ocean was on average 3°C to 5°C cooler compared to the Holocene. Because the solubility of CO_2 increases at colder temperature (Zeebe and Wolf-Gladrow, 2001), a colder glacial ocean will hold more carbon. However, uncertainty in reconstructing the LGM pattern of ocean temperature, particularly in the tropics (Archer et al., 2000; Waelbroeck et al., 2009), together with problems in transforming this pattern to the resolution of models in light of the nonlinear nature of the CO_2–temperature relationship

(Ridgwell, 2001), creates a large spread in modelled estimates, Most ocean general circulation models (OGCM) projections, however, cluster more tightly and suggest that lower ocean temperatures contribute to lower CO_2 values by 25 ppm during the LGM (Figure 6.5).

6.2.1.1.3 Lower sea level and increased salinity

During the LGM, sea level was about ~120 m lower than today, and this change in ocean volume had several well-understood effects on atmospheric CO_2 concentrations. Lower sea level impacts the LGM ocean carbon cycle in two main ways. First, the resulting higher LGM ocean surface salinity causes atmospheric CO_2 to be higher than during the Holocene. Second, the total dissolved inorganic carbon and alkalinity (a measure of the capacity of an aqueous solution to neutralize acid) become more concentrated in equal proportions, and this process also causes atmospheric CO_2 to be higher during the LGM. In total, lower sea level is estimated to contribute to higher CO_2 values by 15 ppm during the LGM (Figure 6.5), implying that other processes must explain the lower CO_2 values measured in ice cores.

6.2.1.1.4 Ocean circulation and sea ice

Reorganization in ocean circulation during glacial periods that promoted the retention of dissolved inorganic carbon in the deep ocean during the LGM has become the focus of most research on the glacial–interglacial CO_2 problem. That ocean circulation plays a key role in low glacial period atmospheric CO_2 concentration is exemplified by the tight coupling observed between reconstructed deep ocean temperatures and atmospheric CO_2 (Shackleton, 2000). Evidence from marine bore hole sites (Adkins et al., 2002) and from marine sediment cores (Jaccard et al., 2005; Skinner et al., 2010) show that the glacial ocean was highly stratified compared to interglacial conditions and may thus have held a larger store of carbon during glacial times. $\delta^{13}CO_2$ ice core records (Lourantou et al., 2010a, 2010b; Schmitt et al., 2012), as well as radiocarbon records from deep-sea corals demonstrate the role of a deep and stratified Southern Ocean in the higher LGM ocean carbon storage. However, conflicting hypotheses exist on the drivers of this increase in the Southern Ocean stratification, for example, northward shift and weakening of Southern Hemisphere (SH) westerly winds (Toggweiler et al., 2006), reduced air–sea buoyancy fluxes (Watson and Garabato, 2006) or massive brine rejections during sea ice formation (Bouttes et al., 2011, 2012). Ocean carbon cycle models have simulated a circulation-induced effect on LGM CO_2 that can explain lower values than during interglacial by 3 ppm (Bopp et al., 2003) to 57 ppm (Toggweiler, 1999).

A long-standing hypothesis is that increased LGM sea ice cover acted as a barrier to air–sea gas exchange and hence reduced the 'leakage' of CO_2 during winter months from the ocean to the atmosphere during glacial periods (Broecker and Peng, 1986). However, concurrent changes in ocean circulation and biological productivity complicate the estimation of the impact of increased sea ice extent on LGM atmospheric CO_2 (Kurahashi-Nakamura et al., 2007). With the exception of the results of an idealised box model (Stephens and Keeling, 2000), ocean carbon models are relatively consistent in projecting a small effect of higher sea ice extent on maintaining atmospheric CO_2 lower during LGM (Archer et al., 2003).

6.2.1.1.5 Iron fertilisation

Both marine and terrestrial sediment records indicate higher rates of deposition of dust and hence iron (Fe) supply at the LGM (Mahowald et al., 2006), implying a potential link between Fe fertilisation of marine productivity and lower glacial CO_2 (Martin, 1990). However, despite the fact that ocean carbon cycle models generally employ similar reconstructions of glacial dust fluxes (i.e., Mahowald et al., 1999; Mahowald et al., 2006), there is considerable disagreement among them in the associated CO_2 change. OGCM that include a description of the Fe cycle tend to cluster at the lower end of simulated CO_2 changes between glacial and interglacial (e.g., Archer at al., 2000; Bopp et al., 2003), whereas box models (e.g., Watson et al., 2000) or Earth System Models of Intermediate Complexity (EMICs, e.g., Brovkin et al., 2007) tend to produce CO_2 changes which are at the higher end (Parekh et al., 2008). An alternative view comes from inferences drawn from the timing and magnitude of changes in dust and CO_2 in ice cores (Röthlisberger et al., 2004), assigning a 20 ppm limit for the lowering of CO_2 during the LGM in response to an Southern Ocean Fe fertilisation effect, and a 8 ppm limit for the same effect in the North Pacific.

6.2.1.1.6 Other glacial carbon dioxide drivers

A number of further aspects of altered climate and biogeochemistry at the LGM are also likely to have affected atmospheric CO_2. Reduced bacterial metabolic rates and remineralization (see Glossary) of organic matter (Matsumoto, 2007; Menviel et al., 2012), increased glacial supply of dissolved silica (required by diatoms to form frustules) (Harrison, 2000), 'silica leakage' (Brzezinski et al., 2002; Matsumoto et al., 2002), changes in net global weathering rates (Berner, 1992; Munhoven, 2002), reduction in coral reef growth and other forms of shallow water $CaCO_3$ accumulation (Berger, 1982), carbonate compensation (Ridgwell and Zeebe, 2005) and changes in the $CaCO_3$ to organic matter 'rain ratio' to the sediments (Archer and Maier-Reimer, 1994) will act to amplify or diminish the effect of many of the aforementioned drivers on glacial CO_2.

6.2.1.1.7 Summary

All of the major drivers of the glacial-to-interglacial atmospheric CO_2 changes (Figure 6.5) are likely to have already been identified. However, Earth System Models have been unable to reproduce the full magnitude of the glacial-to-interglacial CO_2 changes. Significant uncertainties exist in glacial boundary conditions and on some of the primary controls on carbon storage in the ocean and in the land. These uncertainties prevent an unambiguous attribution of individual mechanisms as controllers of the low glacial CO_2 concentrations. Further assessments of the interplay of different mechanisms prior to deglacial transitions or in glacial inceptions will provide additional insights into the drivers and processes that caused the glacial decrease of CO_2. Because several of these identified drivers (e.g., organic matter remineralization, ocean stratification) are sensitive to climate change in general, improved understanding drawn from the glacial–interglacial cycles will help constrain the magnitude of future ocean feedbacks on atmospheric CO_2. Other drivers (e.g., iron fertilisation) are involved in geoengineering methods (see Glossary), such that improved under-

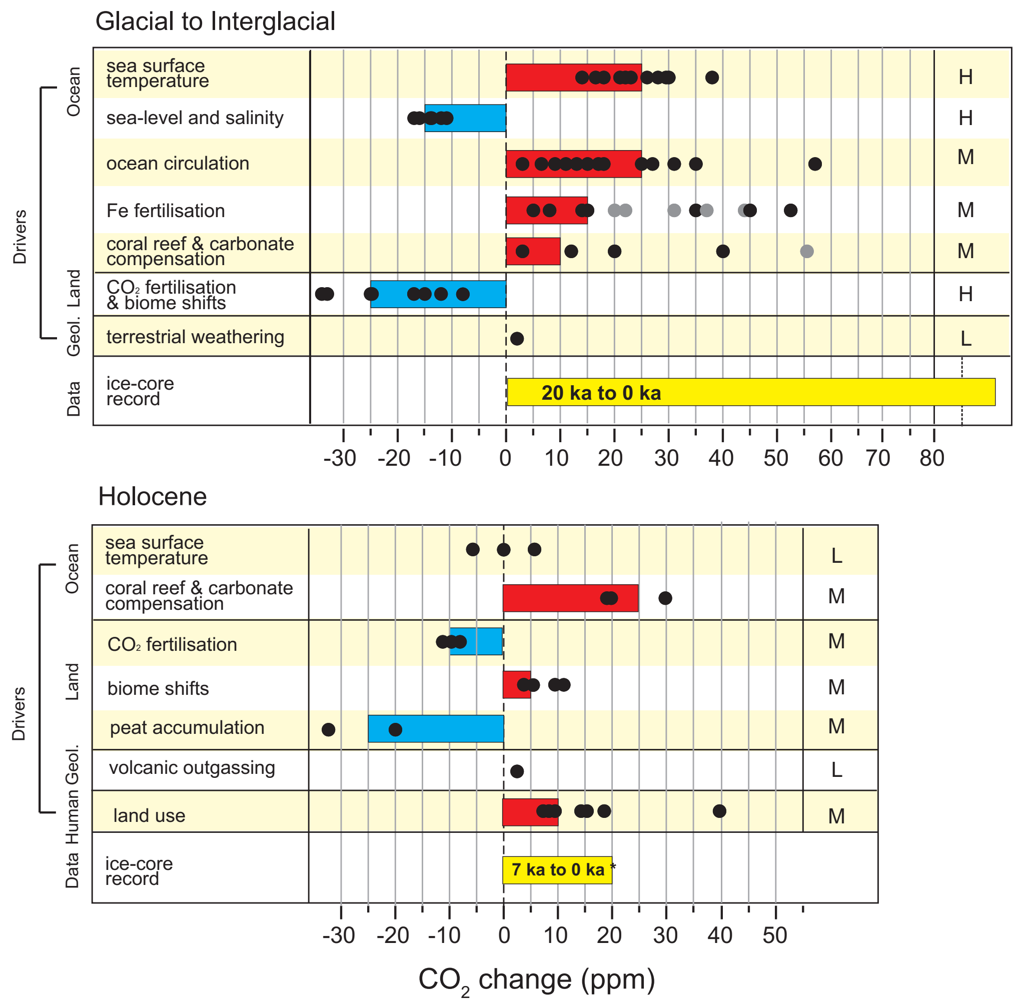

Figure 6.5 | Mechanisms contributing to carbon dioxide concentrations changes from Last Glacial Maximum (LGM) to late Holocene (top) and from early/mid Holocene (7 ka) to late Holocene (bottom). Filled black circles represent individual model-based estimates for individual ocean, land, geological or human mechanisms. Solid colour bars represent expert judgment (to the nearest 5 ppm) rather than a formal statistical average. References for the different model results used for explaining CO_2 changes from LGM to late Holocene are as per (Kohfeld and Ridgwell, 2009) with excluded model projections in grey. References for the different model results used for explaining CO_2 changes during the Holocene are: Joos et al. (2004), Brovkin et al. (2002, 2008), Kleinen et al. (2010, 2012), Broecker et al. (1999), Ridgwell et al. (2003), Schurgers et al. (2006), Yu (2011), Ruddiman (2003, 2007), Strassmann et al. (2008), Olofsson and Hickler (2008), Pongratz et al. (2009), Kaplan et al. (2011), Lemmen (2009), Stocker et al. (2011), Roth and Joos (2012). Confidence levels for each mechanism are indicated in the left column — H for *high confidence*, M for *medium confidence* and L for *low confidence*.

standing could also help constrain the potential and applicability of these methods (see Section 6.5.2).

6.2.1.2 Processes Controlling Glacial Methane and Nitrous Oxide

Ice core measurements show that atmospheric CH_4 and N_2O were much lower under glacial conditions compared to interglacial ones. Their reconstructed history encompasses the last 800 ka (Loulergue et al., 2008; Schilt et al., 2010a). Glacial CH_4 mixing ratios are in the 350 to 400 ppb range during the eight glacial maxima covered by the ice core record. This is about half the levels observed during interglacial conditions. The N_2O concentration amounts to 202 ± 8 ppb at the LGM, compared to the early Holocene levels of about 270 ppb (Flückiger et al., 1999).

CH_4 and N_2O isotopic ratio measurements in ice cores provide important constraints on the mechanisms responsible for their temporal changes. N_2O isotopes suggest a similar increase in marine and terrestrial N_2O emissions during the last deglaciation (Sowers et al., 2003). Marine sediment proxies of ocean oxygenation suggest that most of the observed N_2O deglacial rise was of marine origin (Jaccard and Galbraith, 2012). δD and ^{14}C isotopic composition measurements of CH_4 have shown that catastrophic methane hydrate degassing events are *unlikely* to have caused the last deglaciation CH_4 increase (Sowers, 2006; Petrenko et al., 2009; Bock et al., 2010). $\delta^{13}C$ and δD measurements of CH_4 combined with interpolar atmospheric CH_4 gradient changes (Greenland minus Antarctica ice cores) suggest that most of the deglacial CH_4 increase was caused by increased emissions from boreal and tropical wetlands and an increase in CH_4 atmospheric residence time due to a reduced oxidative capacity of the atmosphere (Fischer et al., 2008). The biomass burning source apparently changed little on the same time scale, whereas this CH_4 source experienced large fluctuations over the last millennium (Mischler et al., 2009; Wang et al., 2010b). Recent modelling studies, however, suggest that changes in the atmospheric oxidising capacity of the atmosphere at the LGM are probably negligible compared to changes in sources (Levine et al., 2011) and that tropical temperature influencing tropical wetlands and global vegetation were the dominant controls for CH_4 atmospheric changes on glacial–interglacial time scales (Konijnendijk et al., 2011).

6.2.1.3 Processes Controlling Changes in Carbon Dioxide, Methane, and Nitrous Oxide During Abrupt Glacial Events

Ice core measurements of CO_2, CH_4 and N_2O show sharp (millennial-scale) changes in the course of glaciations, associated with the so-called Dansgaard/Oeschger (DO) climatic events (see Section 5.7), but their amplitude, shape and timing differ. During these millennial scale climate events, atmospheric CO_2 concentrations varied by about 20 ppm, in phase with Antarctic, but not with Greenland temperatures. CO_2 increased during cold (stadial) periods in Greenland, several thousands years before the time of the rapid warming event in Greenland (Ahn and Brook, 2008). CH_4 and N_2O showed rapid transitions in phase with Greenland temperatures with little or no lag. CH_4 changes are in the 50 to 200 ppb range (Flückiger et al., 2004), in phase with Greenland temperature warming at a decadal time scale (Huber et al., 2006). N_2O changes are large, of same magnitude than glacial–interglacial changes, and for the warmest and longest DO events N_2O starts to increase several centuries before Greenland temperature and CH_4 (Schilt et al., 2010b).

Conflicting hypotheses exist on the drivers of these millennial-scale changes. Some model simulations suggest that both CO_2 and N_2O fluctuations can be explained by changes in the Atlantic meridional overturning ocean circulation (Schmittner and Galbraith, 2008), CO_2 variations being explained mainly by changes in the efficiency of the biological pump which affects deep ocean carbon storage (Bouttes et al., 2011), whereas N_2O variations could be due to changes in productivity and oxygen concentrations in the subsurface ocean (Schmittner and Galbraith, 2008). Other studies, however, suggest that the millennial-scale CO_2 fluctuations can be explained by changes in the land carbon storage (Menviel et al., 2008; Bozbiyik et al., 2011). For CH_4, models have difficulties in reproducing changes in wetland emissions compatible with DO atmospheric variations (Hopcroft et al., 2011), and the changes in the atmospheric oxidizing capacity of the atmosphere during DO events seem to be too weak to explain the CH_4 changes (Levine et al., 2012).

6.2.2 Greenhouse Gas Changes over the Holocene

6.2.2.1 Understanding Processes Underlying Holocene Carbon Dioxide Changes

The evolution of the atmospheric CO_2, CH_4, and N_2O concentrations during the Holocene, the interglacial period which began 11.7 ka, is known with high certainty from ice core measurements (Figure 6.6). A decrease in atmospheric CO_2 of about 7 ppm is measured in ice cores

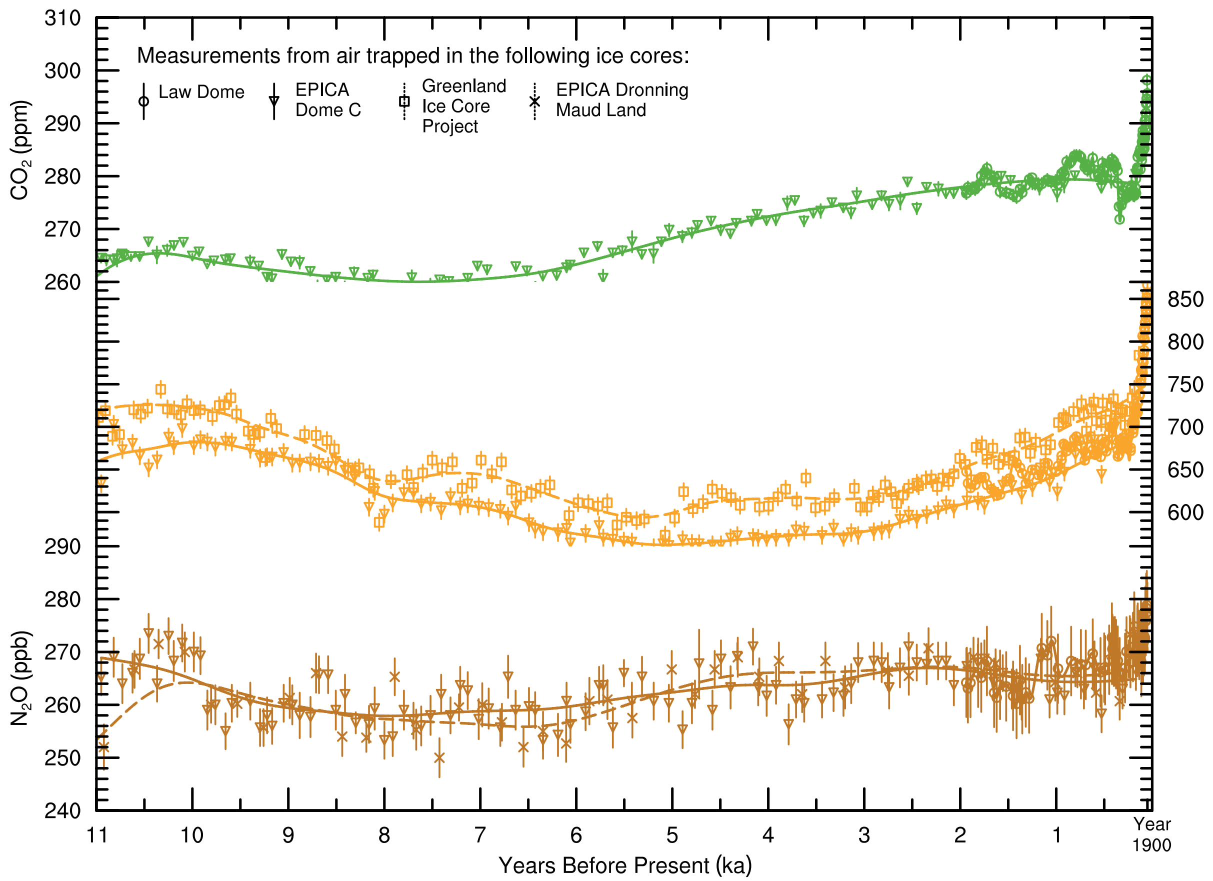

Figure 6.6 | Variations of CO_2, CH_4, and N_2O concentrations during the Holocene. The data are for Antarctic ice cores: European Programme for Ice Coring in Antarctica EPICA Dome C (Flückiger et al., 2002; Monnin et al., 2004), triangles; EPICA Dronning Maud Land (Schilt et al., 2010b), crosses; Law Dome (MacFarling-Meure et al., 2006), circles; and for Greenland Ice Core Project (GRIP) (Blunier et al., 1995), squares. Lines correspond to spline fits.

between 11 and 7 ka, followed by a 20 ppm CO_2 increase until the onset of the Industrial Era in 1750 (Indermühle et al., 1999; Monnin et al., 2004; Elsig et al., 2009). These variations in atmospheric CO_2 over the past 11 kyr preceding industrialisation are more than five times smaller than the CO_2 increase observed during the Industrial Era (see Section 6.3.2.3). Despite the small magnitude of CO_2 variations prior to the Industrial Era, these changes are nevertheless useful for understanding the role of natural forcing in carbon and other biogeochemical cycles during interglacial climate conditions.

Since the IPCC AR4, the mechanisms underlying the observed 20 ppm CO_2 increase between 7 ka and the Industrial Era have been a matter of intensive debate. During three interglacial periods prior to the Holocene, CO_2 did not increase, and this led to a hypothesis that pre-industrial anthropogenic CO_2 emissions could be associated with early land use change and forest clearing (Ruddiman, 2003, 2007). However, ice core CO_2 data (Siegenthaler et al., 2005b) indicate that during Marine Isotope Stage 11 (see Section 5.2.2), an interglacial period that lasted from 400 to 420 ka, CO_2 increased similarly to the Holocene period. Drivers of atmospheric CO_2 changes during the Holocene can be divided into oceanic and terrestrial processes (Figure 6.5) and their roles are examined below.

6.2.2.1.1 Oceanic processes

The change in oceanic carbonate chemistry could explain the slow atmospheric CO_2 increase during the Holocene since 7 ka. Proposed mechanisms include: (1) a shift of oceanic carbonate sedimentation from deep sea to the shallow waters due to sea level rise onto continental shelves causing accumulation of $CaCO_3$ on shelves including coral reef growth, a process that releases CO_2 to the atmosphere (Ridgwell et al., 2003; Kleinen et al., 2010), (2) a 'carbonate compensation' in response to the release of carbon from the deep ocean during deglaciation and to the buildup of terrestrial biosphere in the early Holocene (Broecker et al., 1999; Joos et al., 2004; Elsig et al., 2009; Menviel and Joos, 2012). Proxies for carbonate ion concentration in the deep sea (Yu et al., 2010) and a decrease in modern $CaCO_3$ preservation in equatorial Pacific sediments (Anderson et al., 2008) support the hypothesis that the ocean was a source of CO_2 to the atmosphere during the Holocene. Changes in SSTs over the last 7 kyr (Kim et al., 2004) could have contributed to slightly lower (Brovkin et al., 2008) or higher (Menviel and Joos, 2012) atmospheric CO_2 concentration but, *very likely*, SST-driven CO_2 change represents only a minor contribution to the observed CO_2 increase during the Holocene after 7 ka (Figure 6.5).

6.2.2.1.2 Terrestrial processes

The $\delta^{13}C$ of atmospheric CO_2 trapped in ice cores can be used to infer changes in terrestrial biospheric carbon pools. Calculations based on inferred $\delta^{13}C$ of atmospheric CO_2 during the Holocene suggest an increase in terrestrial carbon storage of about 300 PgC between 11 and 5 ka and small overall terrestrial changes thereafter (Elsig et al., 2009). Modelling studies suggest that CO_2 fertilisation (Box 6.3) in response to increasing atmospheric CO_2 concentration after 7 ka contributed to a substantially increased terrestrial carbon storage (>100 PgC) on Holocene time scales (Kaplan et al., 2002; Joos et al., 2004; Kleinen et al., 2010). Orbitally forced climate variability, including the intensification and decline of the Afro-Asian monsoon and the mid-Holocene warming of the high latitudes of the NH are estimated in models to have caused changes in vegetation distribution and hence of terrestrial carbon storage. These climate-induced carbon storage changes are estimated using models to have been smaller than the increase due to CO_2 fertilisation (Brovkin et al., 2002; Schurgers et al., 2006). The Holocene accumulation of carbon in peatlands has been reconstructed globally, suggesting a land carbon additional storage of several hundred petagrams of carbon between the early Holocene and the Industrial Era, although uncertainties remain on this estimate (Tarnocai et al., 2009; Yu, 2011; Kleinen et al., 2012). Volcanic CO_2 emissions to the atmosphere between 12 and 7 ka were estimated to be two to six times higher than during the last millennium, of about 0.1 PgC yr^{-1} (Huybers and Langmuir, 2009; Roth and Joos, 2012). However, a peak in the inferred volcanic emissions coincides with the period of decreasing atmospheric CO_2 and the *confidence* in changes of volcanic CO_2 emissions is *low*.

Global syntheses of the observational, paleoecological and archaeological records for Holocene land use change are not currently available (Gaillard et al., 2010). Available reconstructions of anthropogenic land use and land cover change (LULCC) prior to the last millennium currently extrapolate using models and assumptions from single regions to changes in all regions of the world (Goldewijk et al., 2011; Kaplan et al., 2011). Because of regional differences in land use systems and uncertainty in historical population estimates, the *confidence* in spatially explicit LULCC reconstructions is *low*.

Some recent studies focused on reconstructing LULCC and making very simple assumptions regarding the effect of land use on carbon (Olofsson and Hickler, 2008; Lemmen, 2009). Other studies relied on more sophisticated terrestrial biosphere models to simulate carbon storage and loss in response to pre-industrial LULCC during the late Holocene (Strassmann et al., 2008; Pongratz et al., 2009; Stocker et al., 2011). The conclusion of the aforementioned studies was that cumulative Holocene carbon emissions as a result of pre-industrial LULCC were not large enough (~50 to 150 PgC during the Holocene before 1850) to have had an influence larger than an increase of ~10 ppm on late Holocene observed CO_2 concentration increase (Figure 6.5). However, a modelling study by Kaplan et al. (2011) suggested that more than 350 PgC could have been released as a result of LULCC between 8 ka and 1850 as a result of a much stronger loss of soil carbon in response to land use change, than in other studies.

In addition to clearing of forests, large-scale biomass burning activity, inferred from synthesized charcoal records and bog sediments has been hypothesized to correlate with the observed Late Holocene atmospheric CO_2 (Carcaillet et al., 2002). A global extensive synthesis of charcoal records for the last 21 kyr (Power et al., 2008) and updates of those shows that fire activity followed climate variability on global (Marlon et al., 2008; Daniau et al., 2012) and regional scale (Archibald et al., 2009; Mooney et al., 2011; Marlon et al., 2012; Power et al., 2013). There is no evidence, however, for a distinct change in fire activity linked to human activity alone as hypothesized from a regional charcoal record synthesis for the tropical Americas (Nevle and Bird, 2008; Nevle et al., 2011). Fire being a newly studied component, no estimate for its role is given in Figure 6.5.

6.2.2.2 Holocene Methane and Nitrous Oxide Drivers

The atmospheric CH_4 levels decreased from the early Holocene to about 6 ka, were lowest at around 5 ka, and increased between 5 ka and year 1750 by about 100 ppb (Figure 6.6). Major Holocene agricultural developments, in particular rice paddy cultivation and widespread domestication of ruminants, have been proposed as an explanation for the Late Holocene CH_4 rise (Ruddiman, 2007). The most recent syntheses of archaeological data point to an increasing anthropogenic CH_4 source from domesticated ruminants after 5 ka and from rice cultivation after 4 ka (Ruddiman, 2007; Fuller et al., 2011). The modelling support for either natural or anthropogenic explanations of the Late Holocene increase in the atmospheric CH_4 concentration is equivocal. A study by Kaplan et al. (2006) suggested that a part of the Late Holocene CH_4 rise could be explained by anthropogenic sources. Natural wetland CH_4 models driven by simulated climate changes are able (Singarayer et al., 2011) or unable (Konijnendijk et al., 2011) to simulate Late Holocene increase in the CH_4 concentration, reflecting a large spread in present-day CH_4 emissions simulated by this type of models (Melton et al., 2013; see Section 6.3.3.2). Consequently, *about as likely as not,* the atmospheric CH_4 increase after 5000 years ago can be attributed to early human activities. The mechanisms causing the N_2O concentration changes during the Holocene are not firmly identified (Flückiger et al., 2002).

6.2.3 Greenhouse Gas Changes over the Last Millennium

6.2.3.1 A Decrease of Carbon Dioxide around Year 1600 and Possible Explanations for this Event

High resolution ice cores records reveal that atmospheric CO_2 during the last millennium varied with a drop in atmospheric CO_2 concentration by 7 to 10 ppm around year 1600, followed by a CO_2 increase during the 17th century (Trudinger et al., 2002; Siegenthaler et al., 2005a; MacFarling-Meure et al., 2006; Ahn et al., 2012). This is shown in Figure 6.7. The CO_2 decrease during the 17th century was used to evaluate the response of atmospheric CO_2 concentration to a century-scale shift in global temperature (Scheffer et al., 2006; Cox and Jones, 2008; Frank et al., 2010) which was found to be dependent on the choice of global temperature reconstructions used in the model.

One of the possible explanations for the drop in atmospheric CO_2 around year 1600 is enhanced land and/or ocean carbon uptake in response to the cooling caused by reduced solar irradiance during the Maunder Minimum (Section 5.3.5.3). However, simulations using Earth System Models of Intermediate Complexity (EMICs)(Gerber et al., 2003; Brovkin et al., 2004) and by complex Earth System Models (ESMs) (Jungclaus et al., 2010) suggest that solar irradiance forcing alone is not sufficient

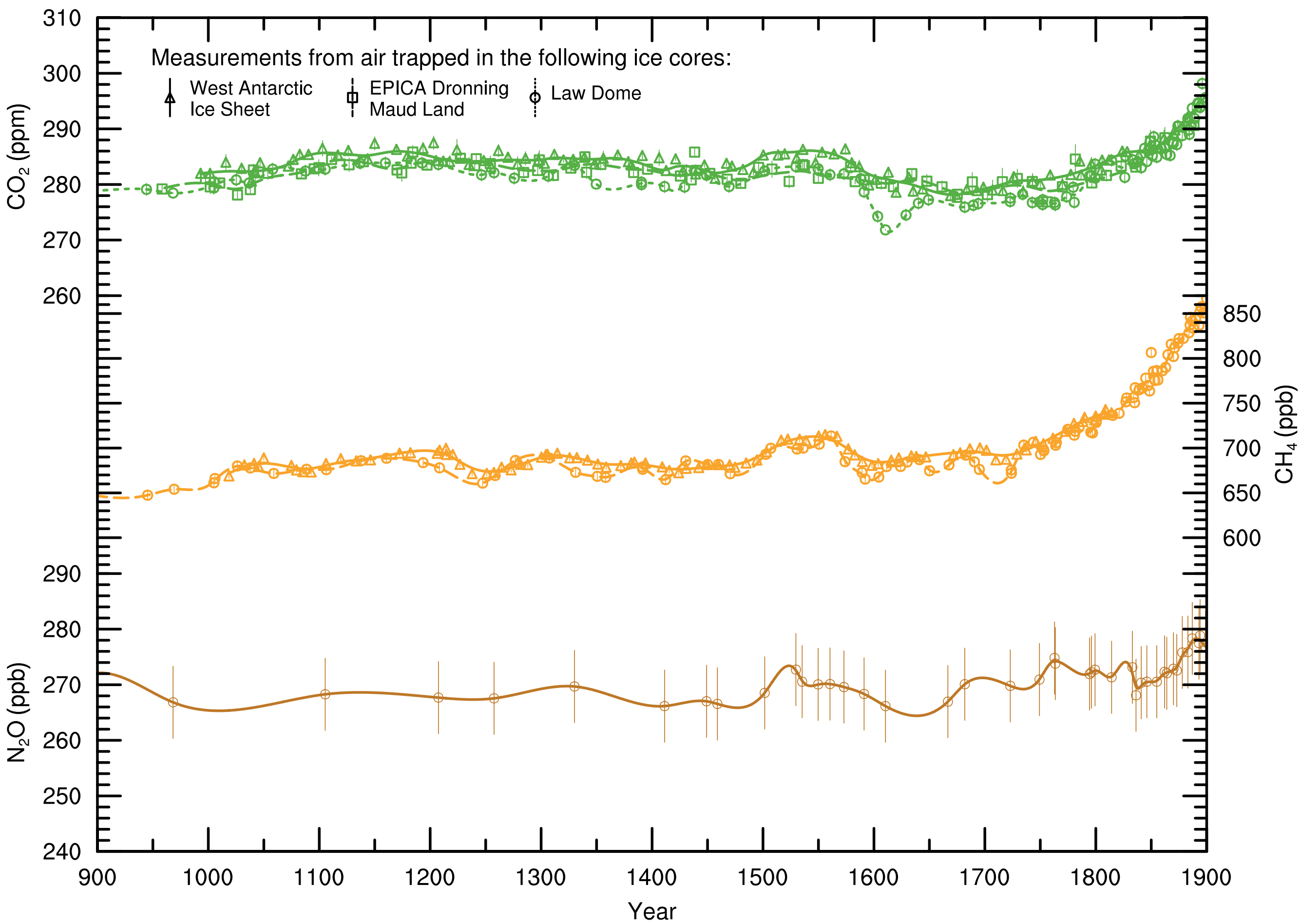

Figure 6.7 | Variations of CO_2, CH_4, and N_2O during 900–1900 from ice cores. The data are for Antarctic ice cores: Law Dome (Etheridge et al., 1996; MacFarling-Meure et al., 2006), circles; West Antarctic Ice Sheet (Mitchell et al., 2011; Ahn et al., 2012), triangles; Dronning Maud Land (Siegenthaler et al., 2005a), squares. Lines are spline fits to individual measurements.

to explain the magnitude of the CO_2 decrease. The drop in atmospheric CO_2 around year 1600 could also be caused by a cooling from increased volcanic eruptions (Jones and Cox, 2001; Brovkin et al., 2010; Frölicher et al., 2011). A third hypothesis calls for a link between CO_2 and epidemics and wars associated with forest regrowth over abandoned lands and increased carbon storage, especially in Central America. Here, results are model and scenario dependent. Simulations by Pongratz et al. (2011a) do not reproduce a decrease in CO_2, while simulations by Kaplan et al. (2011) suggest a considerable increase in land carbon storage around year 1600. The temporal resolution of Central American charcoal and pollen records is insufficient to support or falsify these model results (e.g., Nevle and Bird, 2008; Marlon et al., 2008).

Ensemble simulations over the last 1200 years have been conducted using an ESM (Jungclaus et al., 2010) and EMICs (Eby et al., 2013) including a fully interactive carbon cycle. The sensitivity of atmospheric CO_2 concentration to NH temperature changes in ESM was modeled to be of 2.7 to 4.4 ppm °C^{-1}, while EMICs show on average a higher sensitivity of atmospheric CO_2 to global temperature changes of 8.6 ppm °C^{-1}. These sensitivities fall within the range of 1.7 to 21.4 ppm °C^{-1} of a recent reconstruction based on tree-ring NH temperature reconstructions (Frank et al., 2010).

6.2.3.2 Mechanisms Controlling Methane and Nitrous Oxide during the Last Millennium

Recent high-resolution ice core records confirm a CH_4 decrease in the late 16th century by about 40 ppb (MacFarling-Meure et al., 2006; Mitchell et al., 2011), as shown in Figure 6.7. Correlations between this drop in atmospheric CH_4 and the lower temperatures reconstructed during the 15th and 16th centuries suggest that climate change may have reduced CH_4 emissions by wetlands during this period. In addition to changes in the wetland CH_4 source, changes in biomass burning have been invoked to explain the last millennium CH_4 record (Ferretti et al., 2005; Mischler et al., 2009), ice core CO and CO isotopes (Wang et al., 2010b) and global charcoal depositions (Marlon et al., 2008). Changes in anthropogenic CH_4 emissions during times of war and plague hypothetically contributed to variability in atmospheric CH_4 concentration (Mitchell et al., 2011). Ice core $\delta^{13}CH_4$ measurements suggested pronounced variability in both natural and anthropogenic CH_4 sources over the 1000–1800 period (Sapart et al., 2012). No studies are known about mechanisms of N_2O changes for the last millennium.

6.3 Evolution of Biogeochemical Cycles Since the Industrial Revolution

6.3.1 Carbon Dioxide Emissions and Their Fate Since 1750

Prior to the Industrial Era, that began in 1750, the concentration of atmospheric CO_2 fluctuated roughly between 180 ppm and 290 ppm for at least 2.1 Myr (see Section 5.2.2 and Hönisch et al., 2009; Lüthi et al., 2008; Petit et al., 1999). Between 1750 and 2011, the combustion of fossil fuels (coal, gas, oil and gas flaring) and the production of cement have released 375 ± 30 PgC (1 PgC = 10^{15} gC) to the atmosphere (Table 6. 1; Boden et al., 2011). Land use change activities, mainly deforestation, has released an additional 180 ± 80 PgC (Table 6.1). This carbon released by human activities is called anthropogenic carbon.

Of the 555 ± 85 PgC of anthropogenic carbon emitted to the atmosphere from fossil fuel and cement and land use change, less than half have accumulated in the atmosphere (240 ± 10 PgC) (Table 6.1). The remaining anthropogenic carbon has been absorbed by the ocean and

Table 6.1 | Global anthropogenic CO_2 budget, accumulated since the Industrial Revolution (onset in 1750) and averaged over the 1980s, 1990s, 2000s, as well as the last 10 years until 2011. By convention, a negative ocean or land to atmosphere CO_2 flux is equivalent to a gain of carbon by these reservoirs. The table does not include natural exchanges (e.g., rivers, weathering) between reservoirs. The uncertainty range of 90% confidence interval presented here differs from how uncertainties were reported in AR4 (68%).

	1750–2011 Cumulative PgC	1980–1989 PgC yr^{-1}	1990–1999 PgC yr^{-1}	2000–2009 PgC yr^{-1}	2002–2011 PgC yr^{-1}
Atmospheric increase[a]	240 ± 10[f]	3.4 ± 0.2	3.1 ± 0.2	4.0 ± 0.2	4.3 ± 0.2
Fossil fuel combustion and cement production[b]	375 ± 30[f]	5.5 ± 0.4	6.4 ± 0.5	7.8 ± 0.6	8.3 ± 0.7
Ocean-to-atmosphere flux[c]	–155 ± 30[f]	–2.0 ± 0.7	–2.2 ± 0.7	–2.3 ± 0.7	–2.4 ± 0.7
Land-to-atmosphere flux *Partitioned as follows*	30 ± 45[f]	–0.1 ± 0.8	–1.1 ± 0.9	–1.5 ± 0.9	–1.6 ± 1.0
Net land use change[d]	180 ± 80[f,g]	1.4 ± 0.8	1.5 ± 0.8	1.1 ± 0.8	0.9 ± 0.8
Residual land sink[e]	–160 ± 90[f]	–1.5 ± 1.1	–2.6 ± 1.2	–2.6 ± 1.2	–2.5 ± 1.3

Notes:

[a] Data from Charles D. Keeling, (http://scrippsco2.ucsd.edu/data/data.html), Thomas Conway and Pieter Tans, National Oceanic and Atmospheric Administration–Earth System Research Laboratory (NOAA–ESRL, www.esrl.noaa.gov/gmd/ccgg/trends/) using a conversion factor of 2.120 PgC per ppm (Prather et al., 2012). Prior to the atmospheric record in 1960, ice core data is used (Neftel et al., 1982; Friedli et al., 1986; Etheridge et al., 1996).

[b] Estimated by the Carbon Dioxide Information Analysis Center (CDIAC) based on UN energy statistics for fossil fuel combustion (up to 2009) and US Geological Survey for cement production (Boden et al., 2011), and updated to 2011 using BP energy statistics.

[c] Based on observations for 1990–1999, with the trends based on existing global estimates (see Section 6.3.2.5 and Table 6.4).

[d] Based on the "bookkeeping" land use change flux accounting model of Houghton et al. (2012) until 2010, and assuming constant LUC emissions for 2011, consistent with satellite-based fire emissions (Le Quéré et al., 2013; see Section 6.3.2.2 and Table 6.2).

[e] Calculated as the sum of the *Land-to-atmosphere flux* minus *Net land use change flux*, assuming the errors on each term are independent and added quadratically.

[f] The 1750–2011 estimate and its uncertainty is rounded to the nearest 5 PgC.

[g] Estimated from the cumulative net land use change emissions of Houghton et al. (2012) during 1850–2011 and the average of four publications (Pongratz at al., 2009; van Minnen et al., 2009; Shevliakova et al., 2009; Zaehle et al., 2011) during 1750–1850.

in terrestrial ecosystems: the carbon 'sinks' (Figure 6.8). The ocean stored 155 ± 30 PgC of anthropogenic carbon since 1750 (see Section 6.3.2.5.3 and Box 6.1). Terrestrial ecosystems that have not been affected by land use change since 1750, have accumulated 160 ± 90 PgC of anthropogenic carbon since 1750 (Table 6.1), thus not fully compensating the net CO_2 losses from terrestrial ecosystems to the atmosphere from land use change during the same period estimated of 180 ± 80 PgC (Table 6.1). The net balance of all terrestrial ecosystems, those affected by land use change and the others, is thus close to neutral since 1750, with an average loss of 30 ± 45 (see Figure 6.1). This increased storage in terrestrial ecosystems not affected by land use change is *likely* to be caused by enhanced photosynthesis at higher CO_2 levels and nitrogen deposition, and changes in climate favouring carbon sinks such as longer growing seasons in mid-to-high latitudes. Forest area expansion and increased biomass density of forests that result from changes in land use change are also carbon sinks, and they

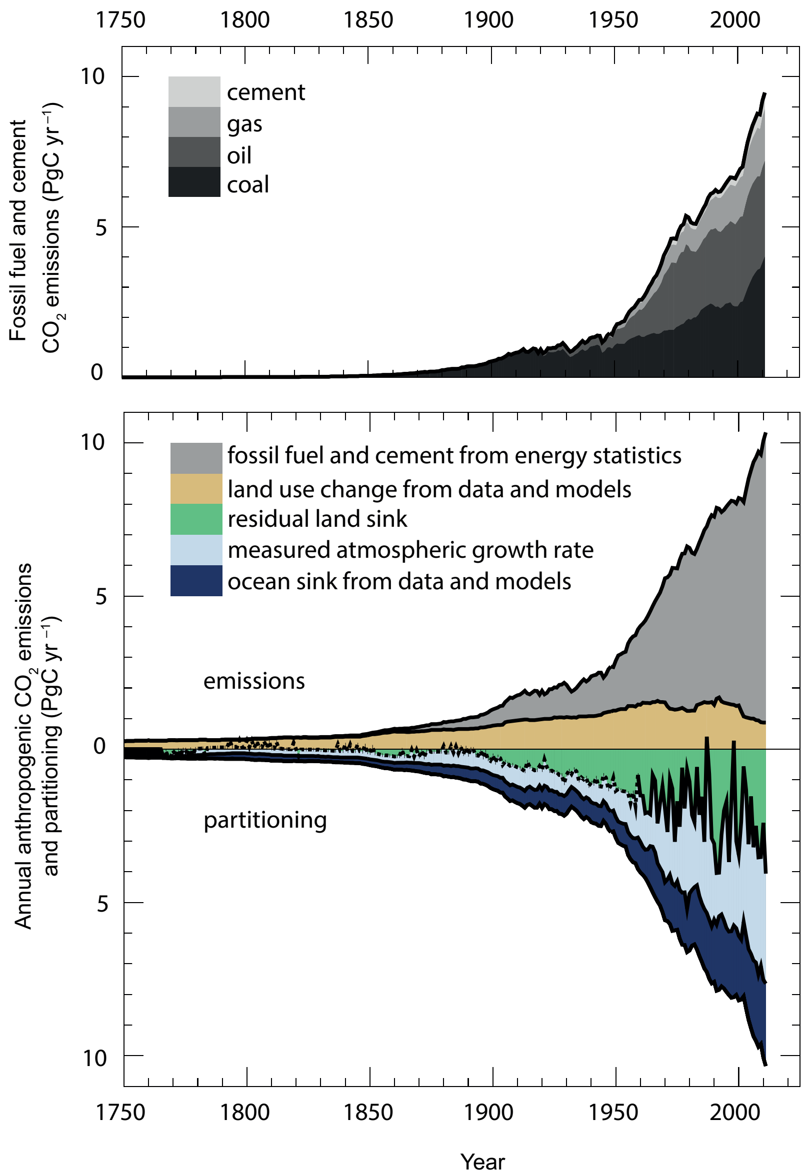

Figure 6.8 | Annual anthropogenic CO_2 emissions and their partitioning among the atmosphere, land and ocean (PgC yr^{-1}) from 1750 to 2011. (Top) Fossil fuel and cement CO_2 emissions by category, estimated by the Carbon Dioxide Information Analysis Center (CDIAC) based on UN energy statistics for fossil fuel combustion and US Geological Survey for cement production (Boden et al., 2011). (Bottom) Fossil fuel and cement CO_2 emissions as above. CO_2 emissions from net land use change, mainly deforestation, are based on land cover change data and estimated for 1750–1850 from the average of four models (Pongratz et al., 2009; Shevliakova et al., 2009; van Minnen et al., 2009; Zaehle et al., 2011) before 1850 and from Houghton et al. (2012) after 1850 (see Table 6.2). The atmospheric CO_2 growth rate (term in light blue 'atmosphere from measurements' in the figure) prior to 1959 is based on a spline fit to ice core observations (Neftel et al., 1982; Friedli et al., 1986; Etheridge et al., 1996) and a synthesis of atmospheric measurements from 1959 (Ballantyne et al., 2012). The fit to ice core observations does not capture the large interannual variability in atmospheric CO_2 and is represented with a dashed line. The ocean CO_2 sink prior to 1959 (term in dark blue 'ocean from indirect observations and models' in the figure) is from Khatiwala et al. (2009) and from a combination of models and observations from 1959 from (Le Quéré et al., 2013). The residual land sink (term in green in the figure) is computed from the residual of the other terms, and represents the sink of anthropogenic CO_2 in natural land ecosystems. The emissions and their partitioning only include the fluxes that have changed since 1750, and not the natural CO_2 fluxes (e.g., atmospheric CO_2 uptake from weathering, outgassing of CO_2 from lakes and rivers, and outgassing of CO_2 by the ocean from carbon delivered by rivers; see Figure 6.1) between the atmosphere, land and ocean reservoirs that existed before that time and still exist today. The uncertainties in the various terms are discussed in the text and reported in Table 6.1 for decadal mean values.

are accounted in Table 6.1 as part of the net flux from land use change. The increased terrestrial carbon storage in ecosystems not affected by land use change is called the *Residual land sink* in Table 6.1 because it is inferred from mass balance as the difference between fossil and net land use change emissions and measured atmospheric and oceanic storage increase.

6.3.2 Global Carbon Dioxide Budget

Since the IPCC AR4 (Denman et al., 2007), a number of new advancements in data availability and data-model synthesis have allowed the establishment of a more constrained anthropogenic CO_2 budget and better attribution of its flux components. The advancements are: (1) revised data on the rates of land use change conversion from country statistics (FAO, 2010) now providing an arguably more robust estimate of the land use change flux (Houghton et al., 2012; Section 6.3.2.2); (2) a new global compilation of forest inventory data that provides an independent estimate of the amount of carbon that has been gained by forests over the past two decades, albeit with very scarce measurements for tropical forest (Pan et al., 2011); (3) over 2 million new observations of the partial pressure of CO_2 (pCO_2) at the ocean surface have been taken and added to the global databases (Takahashi et al., 2009; Pfeil et al., 2013) and used to quantify ocean CO_2 sink variability and trends (Section 6.3.2.5) and to evaluate and constrain models (Schuster et al., 2013; Wanninkhof et al., 2013); and (4) the use of multiple constraints with atmospheric inversions and combined atmosphere–ocean

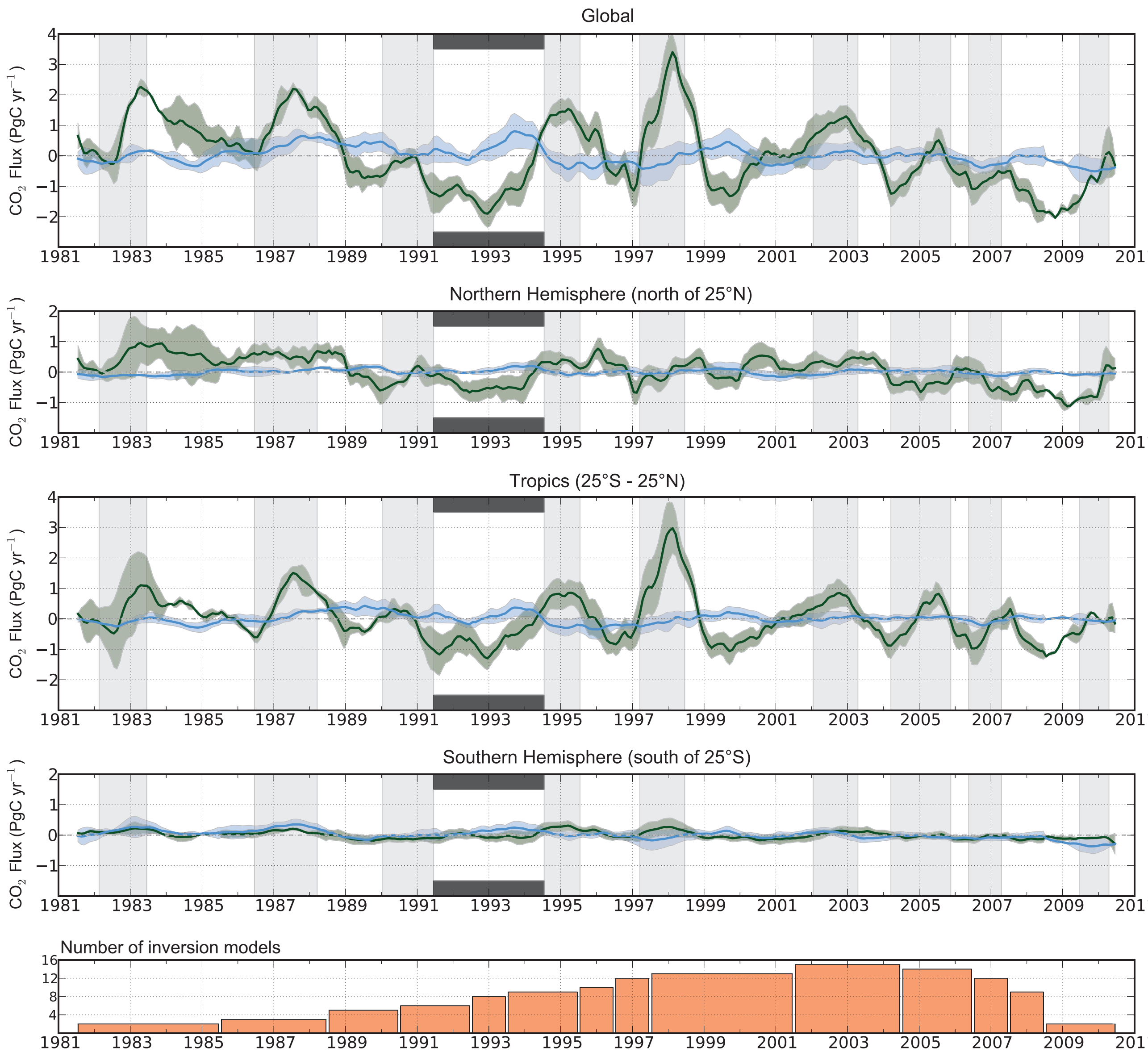

Figure 6.9 | Interannual surface CO_2 flux anomalies from inversions of the TRANSCOM project for the period 1981–2010 (Peylin et al., 2013). The ensemble of inversion results contains up to 17 atmospheric inversion models. The orange bars in the bottom panel indicate the number of available inversion models for each time period. The ensemble mean is bounded by the 1-σ inter-model spread in ocean–atmosphere (blue) and land–atmosphere (green) CO_2 fluxes (PgC yr^{-1}) grouped into large latitude bands, and the global. For each flux and each region, the CO_2 flux anomalies were obtained by subtracting the long-term mean flux from each inversion and removing the seasonal signal. Grey shaded regions indicate El Niño episodes, and the black bars indicate the cooling period following the Mt. Pinatubo eruption, during which the growth rate of CO_2 remained low. A positive flux means a larger than normal source of CO_2 to the atmosphere (or a smaller CO_2 sink).

inversions (so called top down approaches; Jacobson et al., 2007) and the up-scaling of reservoir-based observations using models (so called bottom up approaches) provides new coarse scale consistency checks on CO_2 flux estimates for land and ocean regions (McGuire et al., 2009; Piao et al., 2009b; Schulze et al., 2009; Ciais et al., 2010; Schuster et al., 2013). The causes of the year-to-year variability observed in the annual atmospheric CO_2 accumulation shown in Figure 6.8 are estimated with a *medium* to *high confidence* to be mainly driven by terrestrial processes occurring in tropical latitudes as inferred from atmospheric CO_2 inversions and supported by ocean data and models (Bousquet et al., 2000; Raupach et al., 2008; Sarmiento et al., 2010) (Figures 6.9 and 6.13; Section 6.3.2.5) and land models (Figure 6.16; Section 6.3.2.6).

6.3.2.1 Carbon Dioxide Emissions from Fossil Fuel Combustion and Cement Production

Global CO_2 emissions from the combustion of fossil fuels used for this chapter are determined from national energy consumption statistics and converted to emissions by fuel type (Marland and Rotty, 1984). Estimated uncertainty for the annual global emissions are on the order of ±8% (converted from ±10% uncertainty for 95% confidence intervals in Andres et al. (2012) to the 90% confidence intervals used here). The uncertainty has been increasing in recent decades because a larger fraction of the global emissions originate from emerging economies where energy statistics and emission factors per fuel type are more uncertain (Gregg et al., 2008). CO_2 emissions from cement production were 4% of the total emissions during 2000–2009, compared to 3% in the 1990s (Boden et al., 2011). Additional emissions from gas flaring represent <1% of the global emissions.

Global CO_2 emissions from fossil fuel combustion and cement production were 7.8 ± 0.6 PgC yr^{-1} on average during 2000–2009, 6.4 ± 0.5 PgC yr^{-1} during 1990–1999 and 5.5 ± 0.4 PgC yr^{-1} during 1980–1989 (Table 6.1; Figure 6.8). Global fossil fuel CO_2 emissions increased by 3.2% yr^{-1} on average during the decade 2000–2009 compared to 1.0% yr^{-1} in the 1990s and 1.9% yr^{-1} in the 1980s. Francey et al. (2013) recently suggested a cumulative underestimation of 8.8 PgC emissions during the period 1993–2004, which would reduce the contrast in emissions growth rates between the two decades. The global financial crisis in 2008–2009 induced only a short-lived drop in global emissions in 2009 (–0.3%), with the return to high annual growth rates of 5.1% and 3.0% in 2010 and 2011, respectively, and fossil fuel and cement CO_2 emissions of 9.2 ± 0.8 PgC in 2010 and 9.5 ± 0.8 PgC in 2011(Peters et al., 2013).

6.3.2.2 Net Land Use Change Carbon Dioxide Flux

CO_2 is emitted to the atmosphere by land use and land use change activities, in particular deforestation, and taken up from the atmosphere by other land uses such as afforestation (the deliberate creation of new forests) and vegetation regrowth on abandoned lands. A critical distinction in estimating land use change is the existence of gross and net fluxes. Gross fluxes are the individual fluxes from multiple processes involved in land use change that can be either emissions to or removals from the atmosphere occurring at different time scales. For example, gross emissions include instantaneous emissions from deforestation fires and long-term emissions from the decomposition of organic carbon; and they also include the long-term CO_2 uptake by forest regrowth and soil carbon storage on abandoned agricultural lands, afforestation and storage changes of wood products (Houghton et al., 2012; Mason Earles et al., 2012). The net flux of land use change is the balance among all source and sink processes involved in a given timeframe. The net flux of land use change is globally a net source to the atmosphere (Table 6.1; Figure 6.8).

Approaches to estimate global net CO_2 fluxes from land use fall into three categories: (1) the 'bookkeeping' method that tracks carbon in living vegetation, dead plant material, wood products and soils with cultivation, harvesting and reforestation using country-level reports on changes in forest area and biome-averaged biomass values (Houghton, 2003); (2) process-based terrestrial ecosystem models that simulate on a grid-basis the carbon stocks (biomass, soils) and exchange fluxes between vegetation, soil and atmosphere (see references in Table 6.2) and (3) detailed regional (primarily tropical forests) analyses based on satellite data that estimate changes in forest area or biomass (DeFries et al., 2002; Achard et al., 2004; Baccini et al., 2012; Harris et al., 2012). Satellite-derived estimates of CO_2 emissions to the atmosphere from so-called deforestation fires (van der Werf et al., 2010) provide additional constraints on the spatial attribution and variability of land use change gross emissions. Most global estimates do not include emissions from peat burning or decomposition after a land use change, which are estimated to be 0.12 PgC yr^{-1} over 1997–2006 for peat fires (van der Werf et al., 2008) and between 0.10 and 0.23 PgC yr^{-1} from the decomposition of drained peat (Hooijer et al., 2010). The processes and time scales captured by these methods to estimate net land use change CO_2 emissions are diverse, creating difficulties with comparison of different estimates (Houghton et al., 2012; Table 6.2). The bookkeeping method of Houghton et al. (2012) was used for Table 6.1 because it is closest to observations and includes the most extensive set of management practices (Table 6.2). Methods that do not include long-term 'legacy' fluxes from soils caused by deforestation (Table 6.2) underestimate net land use change CO_2 emissions by 13 to 62% depending on the starting year and decade (Ramankutty et al., 2006), and methods that do not include the fate of carbon wood harvest and shifting cultivation underestimate CO_2 emissions by 25 to 35% (Houghton et al., 2012).

Global net CO_2 emissions from land use change are estimated at 1.4, 1.5 and 1.1 PgC yr^{-1} for the 1980s, 1990s and 2000s, respectively, by the bookkeeping method of Houghton et al. (2012) (Table 6.2; Figure 6.10). This estimate is consistent with global emissions simulated by process-based terrestrial ecosystem models using mainly three land cover change data products as input for time-varying maps of land use change (Table 6.2). The bookkeeping method estimate is also generally consistent although higher than the satellite-based methods (tropics only). Part of the discrepancy can be accounted for by emissions from extratropical regions (~0.1 PgC yr^{-1}; Table 6.3) and by legacy fluxes for land cover change prior to 1980s (~0.2 PgC yr^{-1}) that are not covered by satellite-based methods used in Table 6.2, and by the fact that the bookkeeping method accounts for degradation and shifting agriculture CO_2 losses not detected in the satellite-based method reported in Table 6.2. We adopt an uncertainty of ±0.8 PgC yr^{-1} as representative of 90% uncertainty intervals. This is identical to the uncertainty of ±0.5 PgC yr^{-1} representing ±1-σ interval (68% if Gaussian distributed error)

6

from Houghton et al. (2012). This uncertainty of ±0.8 PgC yr^{-1} on net land use change CO_2 fluxes is smaller than the one that was reported in AR4 of 0.5 to 2.7 PgC yr^{-1} for the 1990s (68% confidence interval). In this chapter, uncertainty is estimated based on expert judgment of the available evidence, including improved accuracy of land cover change incorporating satellite data, the larger number of independent methods to quantify emissions and the consistency of the reported results (Table 6.2; Figure 6.10).

Different estimates of net land use change CO_2 emissions are shown in Figure 6.10. The lower net land use change CO_2 emissions reported in the 2000s compared to the 1990s, by 0.5 PgC yr^{-1} in the bookkeeping method based on FAO (2010), and by 0.3 to 0.5 PgC yr^{-1} from five process-based ecosystem models based on the HistorY Database of the global Environment (HYDE) land cover change data updated to 2009 (Goldewijk et al., 2011), are within the error bar of the data and methods. The bookkeeping method suggests that most of the LUC emissions

Table 6.2 | Estimates of net land to atmosphere CO_2 flux from land use change covering recent decades (PgC yr^{-1}). Positive values indicate CO_2 losses to the atmosphere. Various forms of land management are also included in the different estimates, including wood harvest (W), shifting cultivation (C) and harvesting (H) of crops and peat burning and peat drainage (P). All methods include the vegetation degradation after land clearance. Additional processes included are initial biomass loss during the year of deforestation (I), decomposition of slash and soil carbon during the year of initial loss (D), regrowth (R), change in storage in wood products pools (S), the effect of increasing CO_2, (C), the effect of observed climate variability between decades (M) and 'legacy' long-term decomposition flux carried over from land use change transitions prior to start of time period used for reporting in the table (L). In the absence of data on L in the assessed estimates, the studies have either assumed instantaneous loss of all biomass and soil carbon (I, a committed future flux) or did not consider the legacy flux L. Satellite-based methods have examined Land Use Change (LUC) emissions in the tropical regions only. Numbers in parentheses are ranges in uncertainty provided in some studies.

	Data for Land Use Change Area[a]	Biomass Data	Land Management Included	Processes Included	1980–1989 PgC yr^{-1}	1990–1999 PgC yr^{-1}	2000–2009 PgC yr^{-1}
Bookkeeping Method (global)							
Houghton et al. (2012)	FAO-2010	Observed[b]	W, C, H	I, D, R, S, L	1.4	1.5	1.1
Baccini et al. (2012)	FAO-2010	Satellite data	W, C, H	I, D, R, S, L			1.0
Satellite-based Methods (tropics only)							
Achard et al. (2004)	Landsat	Observed[b]		I, D, R, S, C, M		0.9 (0.5–1.4)[c]	
DeFries et al. (2002)	AVHRR	Observed[b]		I, D, R, S[d], C, M	0.6 (0.3–0.8)	0.9 (0.5–1.4)	
Van der Werf et al. (2010)	GFED	CASA[e]	P	I, D, C, M		1.2 (0.6–1.8)[f]	
Process Models (global)							
Shevliakova et al. (2009)	HYDE	LM3V	W, C	I, D, R, S, L, C	1.1	1.1	
Shevliakova et al. (2009)	SAGE	LM3V	W, C	I, D, R, S, L, C	1.4	1.3	
van Minnen et al. (2009)[g]	HYDE	IMAGE 2[e]	W	I, D, R, S, L, C	1.8	1.4	1.2
Strassmann et al. (2008)	HYDE	BernCC[e]		I, D, R, S, L, C	1.3	1.3	
Stocker et al. (2011)[g]	HYDE	BernCC[e]	H	I, D, R, S, L, C	1.4	0.9	0.6
Yang et al. (2010)	SAGE	ISAM[e]	W	I, D, R, S, L, C	1.7	1.7	
Yang et al. (2010)	FAO-2005	ISAM[e]	W	I, D, R, S, L, C	1.7	1.8	
Yang et al. (2010)[g]	HYDE	ISAM[e]	W	I, D, R, S, L, C	2.2	1.5	1.2
Arora and Boer (2010)	SAGE	CTEM[e]	H	I, D, R, S, L, C	1.1[h]	1.1[h]	
Arora and Boer (2010)[g]	HYDE	CTEM[e]	H	I, D, R, S, L, C	0.4[h]	0.4[h]	
Poulter et al. (2010)[g]	HYDE	LPJmL[e]		I, D, R, S, L, C	1.0	0.9	0.5
Kato et al. (2013)[g]	HYDE	VISIT[e]	C	I, D, R, S, L, C	1.2	1.0	0.5
Zaehle et al. (2011)	HYDE	O-CN		I, D, R, S, L, C	1.2	1.0	
Average of process models[i]					1.3 ± 0.7	1.2 ± 0.6	0.8 ± 0.6
Range of process models					[0.4–2.2]	[0.4–1.8]	[0.5–1.2]

Notes:

[a] References for the databases used: FAO (2010) as applied in Houghton et al. (2012); FAO (2005) as applied in Houghton (2003), updated; GFED (van der Werf et al., 2009); HYDE (Goldewijk et al., 2011), SAGE (Ramankutty and Foley, 1999). Landsat and AVHRR are satellite-based data and GFED is derived from satellite products as described in the references.

[b] Based on average estimates by biomes compiled from literature data (see details in corresponding references).

[c] 1990–1997 only.

[d] Legacy fluxes for land cover change prior to 1980 are not included and are estimated to add about 0.2 PgC yr^{-1} to the 1980s and 0.1 PgC yr^{-1} to the 1990s estimates, based on Ramankutty et al. (2006).

[e] The vegetation and soil biomass is computed using a vegetation model described in the reference.

[f] 1997–2006 average based on estimates of carbon emissions from deforestation and degradation fires, including peat fires and oxidation. Estimates were doubled to account for emissions other than fire including respiration of leftover plant materials and soil carbon following deforestation following (Olivier et al., 2005).

[g] Method as described in the reference but updated to 2010 using the land cover change data listed in column 2.

[h] The large variability produced by the calculation method is removed for comparison with other studies by averaging the flux over the two decades.

[i] Average of estimates from all process models and 90% confidence uncertainty interval; note that the spread of the different estimates does not follow a Gaussian distribution. AVHRR = Advanced Very High Resolution Radiometer; FAO = Food and Agriculture Organization (UN); GFED = Global Fire Emissions Database; HYDE = HistorY Database of the global Environment; SAGE = Center for Sustainability and the Global Environment.

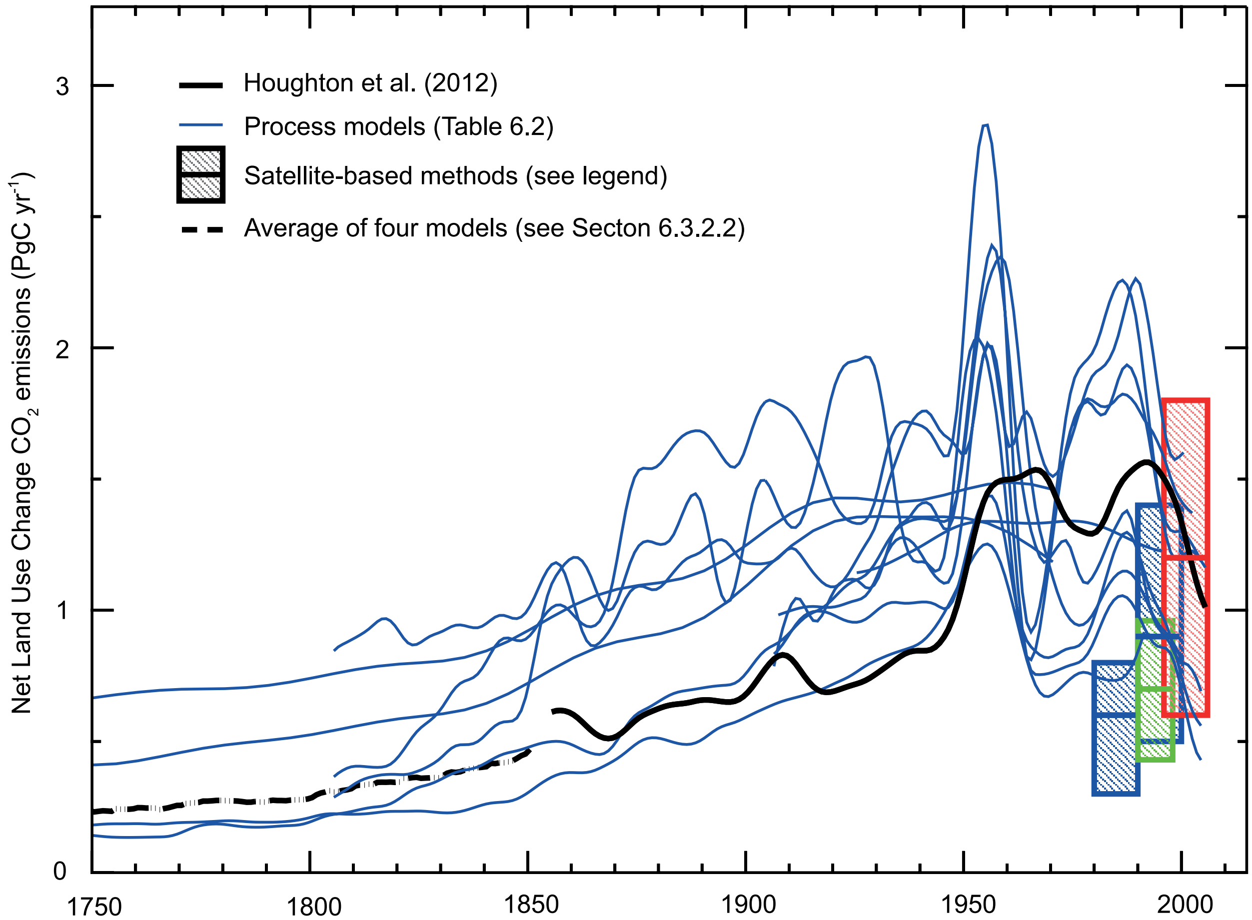

Figure 6.10 | Net land use change CO_2 emissions (PgC yr^{-1}). All methods are based on land cover change data (see Table 6.2) and are smoothed with a 10-year filter to remove interannual variability. The bookkeeping estimate of Houghton et al. (2012) (thick black over 1850–2011) and the average of four process models (dash black) over 1750–1850 (see 6.3.2.2) are used in Table 6.1. The process model results for net land use change CO_2 emissions from Table 6.2 are shown in blue. Satellite-based methods are available for the tropics only, from (red) van der Werf et al. (2010), (blue) DeFries et al. (2002), and (green) Achard et al. (2004). Note that the definitions of land use change fluxes vary between models (Table 6.2). The grey shading shows a constant uncertainty of ±0.8 PgC yr^{-1} around the mean estimate used in Table 6.3.

originate from Central and South America, Africa and Tropical Asia since the 1980s (Table 6.3). The process models based on the HYDE database allocate about 30% of the global land use change emissions to East Asia, but this is difficult to reconcile with the large afforestation programmes reported in this region. Inconsistencies in the available land cover change reconstructions and in the modelling results prevent a firm assessment of recent trends and their partitioning among regions (see regional data in Table 6.3).

In this chapter, we do not assess individual gross fluxes that sum up to make the net land use change CO_2 emission, because there are too few independent studies. Gross emissions from tropical deforestation and degradation were 3.0 ± 0.5 PgC yr^{-1} for the 1990s and 2.8 ± 0.5 PgC yr^{-1} for the 2000s using forest inventory data, FAO (2010) and the bookeeping method (Pan et al., 2011). These gross emissions are about double the net emissions because of the presence of a large regrowth that compensates for about half of the gross emissions. A recent analysis estimated a lower gross deforestation of 0.6 to 1.2 PgC yr^{-1} (Harris et al., 2012). That study primarily estimated permanent deforestation and excluded additional gross emissions from degraded forests, shifting agriculture and some carbon pools. In fact, gross emissions from permanent deforestation are in agreement between the bookkeeping method of Houghton et al. (2012) and the satellite data analysis of Harris et al. (2012).

Over the 1750–2011 period, cumulative net CO_2 emissions from land use change of 180 ± 80 PgC are estimated (Table 6.1): The uncertainty is based on the spread of the available estimates (Figure 6.10). The cumulative net CO_2 emissions from land use change have been dominated by deforestation and other land use change in the mid-northern latitudes prior to 1980s, and in the tropics since the 1980s, largely from deforestation in tropical America and Asia with smaller contributions from tropical Africa. Deforestation from 800 to 1750 has been estimated at 27 PgC using a process-based ecosystem model (Pongratz et al., 2009).

6.3.2.3 Atmospheric Carbon Dioxide Concentration Growth Rate

Since the beginning of the Industrial Era (1750), the concentration of CO_2 in the atmosphere has increased by 40%, from 278 ± 5 ppm to 390.5 ± 0.1 ppm in 2011 (Figure 6.11; updated from Ballantyne et al. (2012), corresponding to an increase in CO_2 of 240 ± 10 PgC in the atmosphere. Atmospheric CO_2 grew at a rate of 3.4 ± 0.2 PgC yr^{-1} in the 1980s, 3.1 ± 0.2 PgC yr^{-1} in the 1990s and 4.0 ± 0.2 PgC yr^{-1} in the 2000s (Conway and Tans, 2011) (Table 6.1). The increase of atmospheric CO_2 between 1750 and 1957, prior to direct measurements in the atmosphere, is established from measurements of CO_2 trapped in air bubbles in ice cores (e.g., Etheridge et al., 1996). After 1957, the increase of atmospheric CO_2 is established from highly precise continuous atmospheric CO_2 concentration measurements at background stations (e.g., Keeling et al., 1976).

The ice core record of atmospheric CO_2 during the past century exhibits interesting variations, which can be related to climate induced-changes in the carbon cycle. Most conspicuous is the interval from about 1940 to 1955, during which atmospheric CO_2 concentration stabilised

Table 6.3 | Estimates of net land to atmosphere flux from land use change (PgC yr^{-1}; except where noted) for decadal periods from 1980s to 2000s by region. Positive values indicate net CO_2 losses from land ecosystems affected by land use change to the atmosphere. Uncertainties are reported as 90% confidence interval (unlike 68% in AR4). Numbers in parentheses are ranges in uncertainty provided in some studies. Tropical Asia includes the Middle East, India and surrounding countries, Indonesia and Papua New Guinea. East Asia includes China, Japan, Mongolia and Korea.

	Land Cover Data	Central and South Americas	Africa	Tropical Asia	North America	Eurasia	East Asia	Oceania
2000s								
van der Werf et al. (2010)[a,b]	GFED	0.33	0.15	0.35				
DeFries and Rosenzweig (2010)[c]	MODIS	0.46	0.08	0.36				
Houghton et al. (2012)	FAO-2010	0.48	0.31[e]	0.25	0.01	–0.07[d]	0.01[e]	
van Minnen et al. (2009)[a]	HYDE	0.45	0.21	0.20	0.09	0.08	0.10	0.03
Stocker et al. (2011)[a]	HYDE	0.19	0.18	0.21	0.019	–0.067	0.12	0.011
Yang et al. (2010)[a]	HYDE	0.14	0.03	0.25	0.25	0.39	0.12	0.02
Poulter et al. (2010)[a]	HYDE	0.09	0.13	0.14	0.01	0.03	0.05	0.00
Kato et al. (2013)[a]	HYDE	0.36	–0.09	0.23	–0.05	–0.04	0.10	0.00
Average		0.31 ± 0.25	0.13 ± 0.20	0.25 ± 0.12	0.05 ± 0.17	0.12 ± 0.31	0.08 ± 0.07	0.01 ± 0.02
1990s								
DeFries et al. (2002)	AVHRR	0.5 (0.2–0.7)	0.1 (0.1–0.2)	0.4 (0.2–0.6)				
Achard et al. (2004)	Landsat	0.3 (0.3–0.4)	0.2 (0.1–0.2)	0.4 (0.3–0.5)				
Houghton et al. (2012)	FAO-2010	0.67	0.32[e]	0.45	0.05	–0.04[d]	0.05[e]	
van Minnen et al. (2009)[a]	HYDE	0.48	0.22	0.34	0.07	0.08	0.20	0.07
Stocker et al. (2011)[a]	HYDE	0.30	0.14	0.19	–0.072	0.11	0.27	0.002
Yang et al. (2010)[a]	HYDE	0.20	0.04	0.31	0.27	0.47	0.19	0.00
Poulter et al. (2010)[a]	HYDE	0.26	0.13	0.12	0.07	0.16	0.11	0.01
Kato et al. (2013)[a]	HYDE	0.53	0.07	0.25	–0.04	–0.01	0.16	0.02
Average		0.41 ± 0.27	0.15 ± 0.15	0.31 ± 0.19	0.08 ± 0.19	0.16 ± 0.30	0.16 ± 0.13	0.02 ± 0.05
1980s								
DeFries et al. (2002)	AVHRR	0.4 (0.2–0.5)	0.1 (0.08–0.14)	0.2 (01–0.3)				
Houghton et al. (2012)	FAO-2010	0.79	0.22[e]	0.32	0.04	0.00[d]	0.07[e]	
van Minnen et al. (2009)[a]	HYDE	0.70	0.18	0.43	0.07	0.06	0.37	0.04
Stocker et al. (2011)[a]	HYDE	0.44	0.16	0.25	0.085	0.11	0.40	0.009
Yang et al. (2010)[a]	HYDE	0.26	0.01	0.34	0.30	0.71	0.59	0.00
Poulter et al. (2010)[a]	HYDE	0.37	0.11	0.19	0.02	0.03	0.29	0.01
Kato et al. (2013)[a]	HYDE	0.61	0.07	0.25	–0.04	–0.02	0.35	0.01
Average		0.51 ± 0.32	0.12 ± 0.12	0.28 ± 0.14	0.08 ± 0.19	0.15 ± 0.46	0.35 ± 0.28	0.01 ± 0.03

Notes:

[a] Method as described in the reference but updated to 2010 using the HYDE land cover change data.

[b] 1997–2006 average based on estimates of CO_2 emissions from deforestation and degradation fires, including peat carbon emissions. Estimates were doubled to account for emissions other than fire including respiration of leftover plant materials and soil carbon following deforestation following (Olivier et al., 2005). Estimates include peat fires and peat soil oxidation. If peat fires are excluded, estimate in tropical Asia is 0.23 and Pan-tropical total is 0.71.

[c] CO_2 estimates were summed for dry and humid tropical forests, converted to C and normalized to annual values. Estimates are based on satellite-derived deforestation area (Hansen et al., 2010), and assume 0.6 fraction of biomass emitted with deforestation. Estimates do not include carbon uptake by regrowth or legacy fluxes from historical deforestation. Estimates cover emissions from 2000 to 2005.

[d] Includes China only.

[e] East Asia and Oceania are averaged in one region. The flux is split in two equally for computing the average; North Africa and the Middle East are combined with Eurasia. AVHRR = Advanced Very High Resolution Radiometer; FAO = Food and Agriculture Organization (UN); GFED = Global Fire Emissions Database; HYDE = HistorY Database of the global Environment; MODIS = Moderate Resolution Imaging Spectrometer.

(Trudinger et al., 2002), and the CH_4 and N_2O growth slowed down (MacFarling-Meure et al., 2006), possibly caused by slightly decreasing temperatures over land in the NH (Rafelski et al., 2009).

There is substantial evidence, for example, from ^{13}C carbon isotopes in atmospheric CO_2 (Keeling et al., 2005) that source/sink processes on land generate most of the interannual variability in the atmospheric CO_2 growth rate (Figure 6.12). The strong positive anomalies of the CO_2 growth rate in El Niño years (e.g., 1986–1987 and 1997–1998) originated in tropical latitudes (see Sections 6.3.6.3 and 6.3.2.5.4), while the anomalies in 2003 and 2005 originated in northern mid-latitudes, perhaps reflecting the European heat wave in 2003 (Ciais et al., 2005). Volcanic forcing also contributes to multi-annual variability in carbon storage on land and in the ocean (Jones and Cox, 2001; Gerber et al., 2003; Brovkin et al., 2010; Frölicher et al., 2011).

With a *very high confidence*, the increase in CO_2 emissions from fossil fuel burning and those arising from land use change are the dominant cause of the observed increase in atmospheric CO_2 concentration. Several lines of evidence support this conclusion:

- The observed decrease in atmospheric O_2 content over past two decades and the lower O_2 content in the northern compared to the SH are consistent with the burning of fossil fuels (see Figure 6.3 and Section 6.1.3.2; Keeling et al., 1996; Manning and Keeling, 2006).

- CO_2 from fossil fuels and from the land biosphere has a lower $^{13}C/^{12}C$ stable isotope ratio than the CO_2 in the atmosphere. This induces a decreasing temporal trend in the atmospheric $^{13}C/^{12}C$ ratio of atmospheric CO_2 concentration as well as, on annual average, slightly lower $^{13}C/^{12}C$ values in the NH (Figure 6.3). These signals are measured in the atmosphere.

- Because fossil fuel CO_2 is devoid of radiocarbon (^{14}C), reconstructions of the $^{14}C/C$ isotopic ratio of atmospheric CO_2 from tree rings

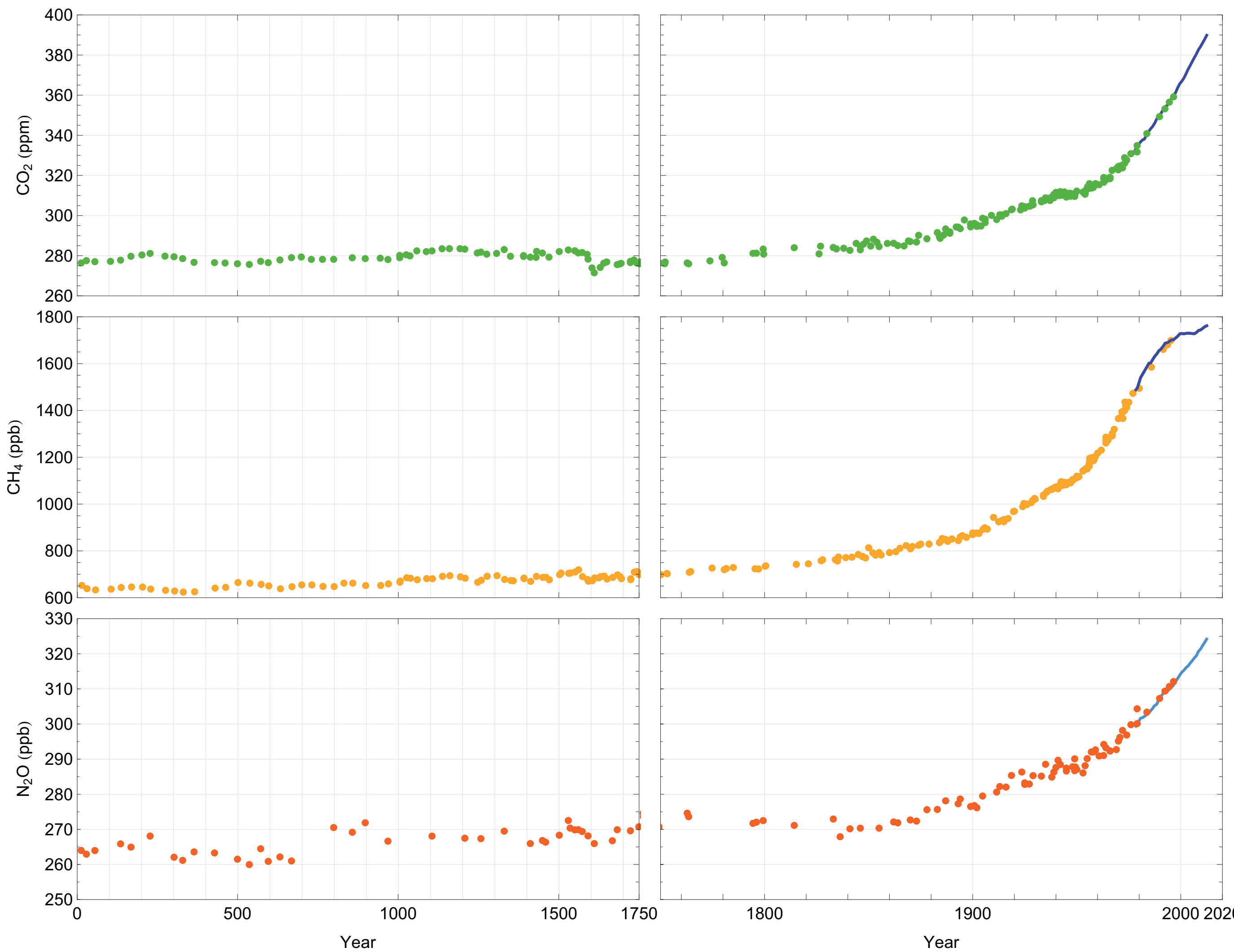

Figure 6.11 | Atmospheric CO_2, CH_4, and N_2O concentrations history over the industrial era (right) and from year 0 to the year 1750 (left), determined from air enclosed in ice cores and firn air (colour symbols) and from direct atmospheric measurements (blue lines, measurements from the Cape Grim observatory) (MacFarling-Meure et al., 2006).

show a declining trend, as expected from the addition of fossil CO_2 (Stuiver and Quay, 1981; Levin et al., 2010). Yet nuclear weapon tests in the 1950s and 1960s have been offsetting that declining trend signal by adding ^{14}C to the atmosphere. Since this nuclear weapon induced ^{14}C pulse in the atmosphere has been fading, the $^{14}C/C$ isotopic ratio of atmospheric CO_2 is observed to resume its declining trend (Naegler and Levin, 2009; Graven et al., 2012).

- Most of the fossil fuel CO_2 emissions take place in the industrialised countries north of the equator. Consistent with this, on annual average, atmospheric CO_2 measurement stations in the NH record increasingly higher CO_2 concentrations than stations in the SH, as witnessed by the observations from Mauna Loa, Hawaii, and the South Pole (see Figure 6.3). The annually averaged concentration difference between the two stations has increased in proportion of the estimated increasing difference in fossil fuel combustion emissions between the hemispheres (Figure 6.13; Keeling et al., 1989; Tans et al., 1989; Fan et al., 1999).

- The rate of CO_2 emissions from fossil fuel burning and land use change was almost exponential, and the rate of CO_2 increase in the atmosphere was also almost exponential and about half that of the emissions, consistent with a large body of evidence about changes of carbon inventory in each reservoir of the carbon cycle presented in this chapter.

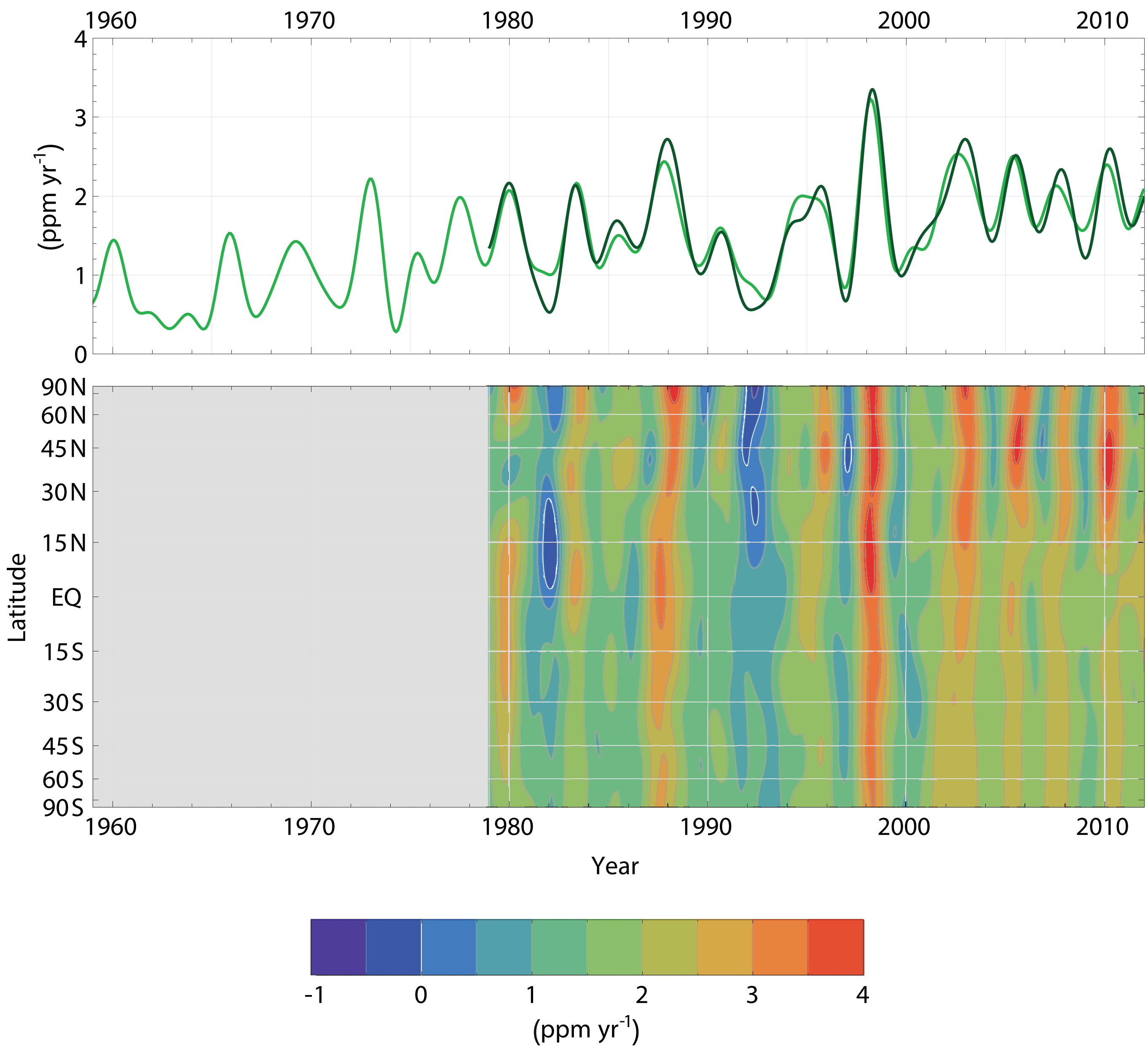

Figure 6.12 | (Top) Global average atmospheric CO_2 growth rate, computed from the observations of the Scripps Institution of Oceanography (SIO) network (light green line: Keeling et al. 2005, updated) and from the marine boundary layer air reference measurements of the National Oceanic and Atmospheric Administration –Global Monitoring Division (NOAA–GMD) network (dark green line: Conway et al., 1994; Dlugokencky and Tans, 2013b). (Bottom) Atmospheric growth rate of CO_2 as a function of latitude determined from the National Oceanic and Atmospheric Administration–Earth System Research Laboratory (NOAA–ESRL) network, representative of stations located in the marine boundary layer at each given latitude (Masarie and Tans, 1995; Dlugokencky and Tans, 2013b). Sufficient observations are available only since 1979.

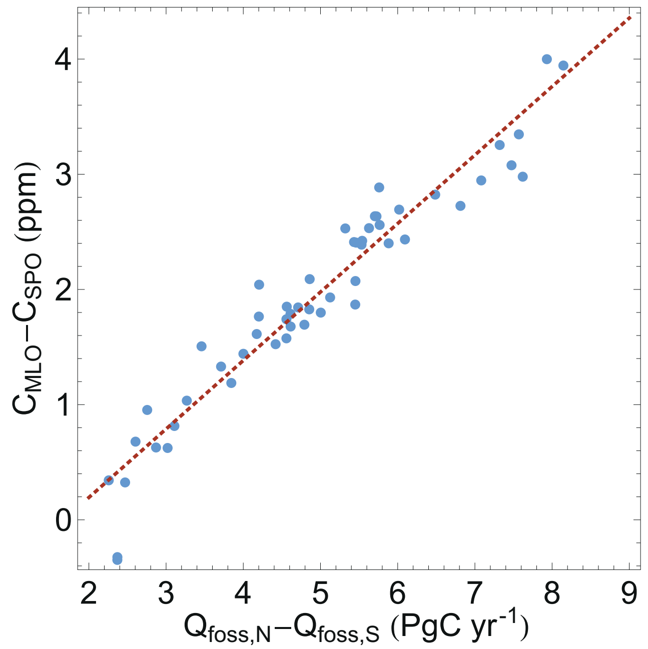

Figure 6.13 | Blue points: Annually averaged CO_2 concentration difference between the station Mauna Loa in the Northern Hemisphere and the station South Pole in the Southern Hemisphere (vertical axis; Keeling et al., 2005, updated) versus the difference in fossil fuel combustion CO_2 emissions between the hemispheres (Boden et al., 2011). Dark red dashed line: regression line fitted to the data points.

6.3.2.4 Carbon Dioxide Airborne Fraction

Until recently, the uncertainty in CO_2 emissions from land use change emissions was large and poorly quantified which led to the use of an airborne fraction (see Glossary) based on CO_2 emissions from fossil fuel only (e.g., Figure 7.4 in AR4 and Figure 6.26 of this chapter). However, reduced uncertainty of emissions from land use change and larger agreement in its trends over time (Section 6.3.2.2) allow making use of an airborne fraction that includes all anthropogenic emissions. The airborne fraction will increase if emissions are too fast for the uptake of CO_2 by the carbon sinks (Bacastow and Keeling, 1979; Gloor et al., 2010; Raupach, 2013). It is thus controlled by changes in emissions rates, and by changes in carbon sinks driven by rising CO_2, changes in climate and all other biogeochemical changes.

A positive trend in airborne fraction of ~0.3% yr^{-1} relative to the mean of 0.44 ±0.06 (or about 0.05 increase over 50 years) was found by all recent studies (Raupach et al., 2008, and related papers; Knorr, 2009; Gloor et al., 2010) using the airborne fraction of total anthropogenic CO_2 emissions over the approximately 1960–2010 period (for which the most accurate atmospheric CO_2 data are available). However, there is no consensus on the significance of the trend because of differences in the treatment of uncertainty and noise (Raupach et al., 2008; Knorr, 2009). There is also no consensus on the cause of the trend (Canadell et al., 2007b; Raupach et al., 2008; Gloor et al., 2010). Land and ocean carbon cycle model results attributing the trends of fluxes to underlying processes suggest that the effect of climate change and variability on ocean and land sinks have had a significant influence (Le Quéré et al., 2009), including the decadal influence of volcanic eruptions (Frölicher et al., 2013).

6.3.2.5 Ocean Carbon Dioxide Sink

6.3.2.5.1 Global ocean sink and decadal change

The estimated mean anthropogenic ocean CO_2 sink assessed in AR4 was 2.2 ± 0.7 PgC yr^{-1} for the 1990s based on observations (McNeil et al., 2003; Manning and Keeling, 2006; Mikaloff-Fletcher et al., 2006), and is supported by several contemporary estimates (see Chapter 3). Note that the uncertainty of ±0.7 PgC yr^{-1} reported here (90% confidence interval) is the same as the ±0.4 PgC yr^{-1} uncertainty reported in AR4 (68% confidence intervals). The uptake of anthropogenic CO_2 by the ocean is primarily a response to increasing CO_2 in the atmos-

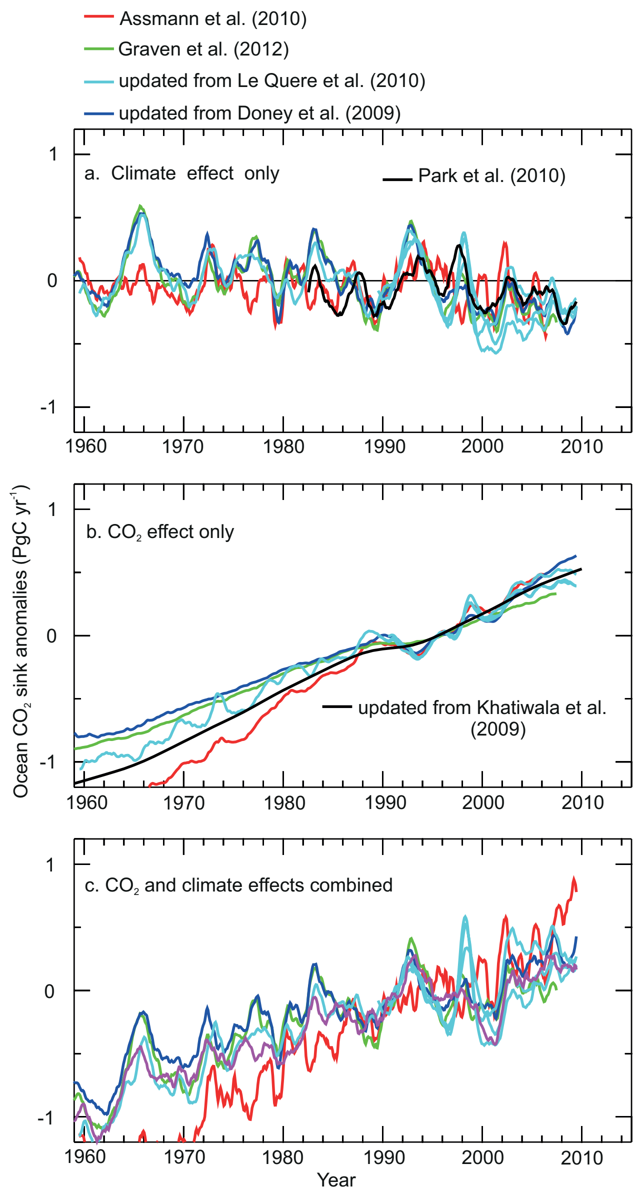

Figure 6.14 | Anomalies in the ocean CO_2 ocean-to-atmosphere flux in response to (a) changes in climate, (b) increasing atmospheric CO_2 and (c) the combined effects of increasing CO_2 and changes in climate (PgC yr^{-1}). All estimates are shown as anomalies with respect to the 1990–2000 averages. Estimates are updates from ocean models (in colours) and from indirect methods based on observations (Khatiwala et al., 2009; Park et al., 2010). A negative ocean-to-atmosphere flux represents a sink of CO_2, as in Table 6.1.

6

Table 6.4 | Decadal changes in the ocean CO_2 sink from models and from data-based methods (a positive change between two decades means an increasing sink with time). It is reminded that the total CO_2 sink for the 1990s is estimated at 2.2 ± 0.7 PgC yr^{-1} based on observations.

	Method	1990s Minus 1980s PgC yr^{-1}	2000s Minus 1990s PgC yr^{-1}
CO_2 effects only			
Khatiwala et al. (2009)	Data-based[c]	0.24	0.20
Mikaloff-Fletcher et al. (2006)[a]	Data-based[d]	0.40	0.44
Assmann et al. (2010) (to 2007 only)	Model	0.28	0.35
Graven et al. (2012)	Model	0.15	0.25
Doney et al. (2009)	Model	0.15	0.39
Le Quéré et al. (2010) NCEP	Model	0.16	0.32
Le Quéré et al. (2010) ECMWF	Model	—	0.39
Le Quéré et al. (2010) JPL	Model	—	0.32
Average[b]		0.23 ± 0.15	0.33 ± 0.13
Climate effects only			
Park et al. (2010)	Data-based[e]	—	–0.15
Assmann et al. (2010) (to 2007 only)	Model	0.07	0.00
Graven et al. (2012)	Model	0.02	–0.27
Doney et al. (2009)	Model	–0.02	–0.21
Le Quéré et al. (2010) NCEP	Model	0.02	–0.27
Le Quéré et al. (2010) ECMWF	Model	—	–0.14
Le Quéré et al. (2010) JPL	Model	—	–0.36
Average[b]		0.02 ± 0.05	–0.19 ± 0.18
CO_2 and climate effects combined		0.25 ± 0.16	0.14 ± 0.22

Notes:

[a] As published by Sarmiento et al. (2010).

[b] Average of all estimates ±90% confidence interval. The average includes results by Le Quéré et al. (2010)–NCEP only because the other Le Quéré et al. model versions do not differ sufficiently to be considered separately.

[c] Based on observed patterns of atmospheric minus oceanic pCO_2, assuming the difference increases with time following the increasing atmospheric CO_2.

[d] Ocean inversion, assuming constant oceanic transport through time.

[e] Based on observed fit between the variability in temperature and pCO_2, and observed variability in temperature.
ECMWF = European Centre for Medium-Range Weather Forecasts; JPL = Jet Propulsion Laboratory; NCEP = National Centers for Environmental Prediction.

phere and is limited mainly by the rate at which anthropogenic CO_2 is transported from the surface waters into the deep ocean (Sarmiento et al., 1992; Graven et al., 2012). This anthropogenic ocean CO_2 sink occurs on top of a very active natural oceanic carbon cycle. Recent climate trends, such as ocean warming, changes in ocean circulation and changes in marine ecosystems and biogeochemical cycles, can have affected both the anthropogenic ocean CO_2 sink as well as the natural air–sea CO_2 fluxes. We report a decadal mean uptake of 2.0 ± 0.7 PgC yr^{-1} for the 1980s and of 2.3 ± 0.7 PgC yr^{-1} for the 2000s (Table 6.4). The methods used are: (1) an empirical Green's function approach fitted to observations of transient ocean tracers (Khatiwala et al., 2009), (2) a model-based Green's function approach fitted to anthropogenic carbon reconstructions (Mikaloff-Fletcher et al., 2006), (3) estimates based on empirical relationships between observed ocean surface pCO_2 and temperature and salinity (Park et al., 2010) and (4) process-based global ocean biogeochemical models forced by observed meteorological fields (Doney et al., 2009; Assmann et al., 2010; Le Quéré et al., 2010; Graven et al., 2012). All these different methods suggest that in the absence of recent climate change and climate variability, the ocean anthropogenic CO_2 sink should have increased by 0.23 ± 0.15 PgC yr^{-1} between the 1980s and the 1990s, and by 0.33 ± 0.13 PgC yr^{-1} between the 1990s and the 2000s (Figure 6.14). The decadal estimates in the ocean CO_2 sink reported in Table 6.4 as 'CO_2 effects only' are entirely explained by the faster rate of increase of atmospheric CO_2 in the later decade. On the other hand, 'climate effects only' in Table 6.4 are assessed to have no noticeable effect on the sink difference between the 1980s and the 1990s (0.02 ± 0.05 PgC yr^{-1}), but are estimated to have reduced the ocean anthropogenic CO_2 sink by 0.19 ± 0.18 PgC yr^{-1} between the 1990s and the 2000s (Table 6.4).

6.3.2.5.2 Regional changes in ocean dissolved inorganic carbon

Observational-based estimates for the global ocean inventory of anthropogenic carbon are obtained from shipboard repeated hydrographic cross sections (Sabine et al., 2004; Waugh et al., 2006; Khatiwala et al., 2009). These estimates agree well among each other, with an average value of 155 ± 30 PgC of increased dissolved inorganic carbon for the period 1750–2011 (see Chapter 3). The uptake of anthropogenic carbon into the ocean is observed to be larger in the high latitudes than in the tropics and subtropics over the entire Industrial Era, because of the more vigorous ocean convection in the high latitudes (Khatiwala et al., 2009). A number of ocean cross sections have been repeated over the last decade, and the observed changes

Table 6.5 | Regional rates of change in inorganic carbon storage from shipboard repeated hydrographic cross sections.

Section	Time	Storage Rate (mol C m^{-2} yr^{-1})	Data Source
Global average (used in Table 6.1)	2007–2008	0.5 ± 0.2	Khatiwala et al. (2009)
Pacific Ocean			
Section along 30°S	1992–2003	1.0 ± 0.4	Murata et al. (2007)
N of 50°S, 120°W to 180°W	1974–1996	0.9 ± 0.3	Peng et al. (2003)
154°W, 20°N to 50°S	1991–2006	0.6 ± 0.1	Sabine et al. (2008)
140°E to 170°W, 45°S to 65°S	1968–1991/1996	0.4 ± 0.2	Matear and McNeil (2003)
149° W, 4°S to 10°N	1993–2005	0.3 ± 0.1	Murata et al. (2009)
149° W, 24°N to 30°N	1993–2005	0.6 ± 0.2	Murata et al. (2009)
Northeast Pacific	1973–1991	1.3 ± 0.5	Peng et al. (2003)
~160°E, ~45°N	1997–2008	0.4 ± 0.1	Wakita et al. (2010)
North of 20°N	1994–2004/2005	0.4 ± 0.2	Sabine et al. (2008)
150°W, 20°S to 20°N	1991/1992–2006	0.3 ± 0.1	Sabine et al. (2008)
Indian Ocean			
20°S to 10°S	1978–1995	0.1	Peng et al. (1998)
10°S to 5°N	1978–1995	0.7	Peng et al. (1998)
Section along 20°S	1995–2003/2004	1.0 ± 0.1	Murata et al. (2010)
Atlantic Ocean			
Section along 30°S	1992/1993–2003	0.6 ± 0.1	Murata et al. (2010)
~30°W, 56°S to 15°S	1989–2005	0.8	Wanninkhof et al. (2010)
20°W, 64°N to 15°N	1993–2003	0.6	Wanninkhof et al. (2010)
~25°W, 15°N to 15°S	1993–2003	0.2	Wanninkhof et al. (2010)
40°N to 65°N	1981–1997/1999	2.2 ± 0.7	Friis et al. (2005)
20°N to 40°N	1981–2004	1.2 ± 0.3	Tanhua et al. (2007)
Nordic Seas	1981–2002/2003	0.9 ± 0.2	Olsen et al. (2006)
Sub-decadal variations			
Irminger Sea	1981–1991	0.6 ± 0.4	Pérez et al. (2008)
Irminger Sea	1991–1996	2.3 ± 0.6	Pérez et al. (2008)
Irminger Sea	1997–2006	0.8 ± 0.2	Pérez et al. (2008)

in carbon storage (Table 6.5) suggest that some locations have rates of carbon accumulation that are higher and others that are lower than the global average estimated by Khatiwala et al. (2009). Model results suggest that there may be an effect of climate change and variability in the storage of total inorganic carbon in the ocean (Table 6.4), but that this effect is small (~2 PgC over the past 50 years; Figure 6.14) compared to the cumulative uptake of anthropogenic carbon during the same period.

6.3.2.5.3 Interannual variability in air-sea CO_2 fluxes

The interannual variability in the global ocean CO_2 sink is estimated to be of about ±0.2 PgC yr^{-1} (Wanninkhof et al., 2013) which is small compared to the interannual variability of the terrestrial CO_2 sink (see Sections 6.3.2.3 and 6.3.2.6.3; Figure 6.12). In general, the ocean takes up more CO_2 during El Niño episodes (Park et al., 2010) because of the temporary suppression of the source of CO_2 to the atmosphere over the eastern Pacific upwelling. Interannual variability of ~0.3 PgC yr^{-1} has been reported for the North Atlantic ocean region alone (Watson et al., 2009) but there is no agreement among estimates regarding the exact magnitude of driving factors of air–sea CO_2 flux variability in this region (Schuster et al., 2013). Interannual variability of 0.1 to 0.2 PgC yr^{-1} was also estimated by models and one atmospheric inversion in the Southern Ocean (Le Quéré et al., 2007), possibly driven by the Southern Annular Mode of climate variability (Lenton and Matear, 2007; Lovenduski et al., 2007; Lourantou and Metzl, 2011).

6.3.2.5.4 Regional ocean carbon dioxide partial pressure trends

Observations of the partial pressure of CO_2 at the ocean surface (pCO_2) show that ocean pCO_2 has been increasing generally at about the same rate as CO_2 in the atmosphere when averaged over large ocean regions during the past two to three decades (Yoshikawa-Inoue and Ishii, 2005; Takahashi et al., 2009; McKinley et al., 2011). However, analyses of regional observations highlight substantial regional and temporal variations around the mean trend.

In the North Atlantic, repeated observations show ocean pCO_2 increasing regionally either at the same rate or faster than atmospheric CO_2 between about 1990 and 2006 (Schuster et al., 2009), thus indicating a constant or decreasing sink for CO_2 in that region, in contrast to the increasing sink expected from the response of the ocean to increasing atmospheric CO_2 alone. The anomalous North Atlantic trends appear to be related to sea surface warming and its effect on solubility (Corbière et al., 2007) and/or changes in ocean circulation (Schuster and Watson, 2007; Schuster et al., 2009) and deep convection (Metzl et al., 2010). Recent changes have been associated with decadal variability in the North Atlantic Oscillation (NAO) and the Atlantic Multidecadal Variability (AMV) (Thomas et al., 2007; Ullman et al., 2009; McKinley et al., 2011; Tjiputra et al., 2012). A systematic analysis of trends estimated in this region show no agreement regarding the drivers of change (Schuster et al., 2013).

In the Southern Ocean, an approximately constant sink was inferred from atmospheric (Le Quéré et al., 2007) and oceanic (Metzl, 2009; Takahashi et al., 2009) CO_2 observations but the uncertainties are large (Law et al., 2008). Most ocean biogeochemistry models reproduce the constant sink and attribute it as a response to an increase in Southern Ocean winds driving increased upwards transport of carbon-rich deep waters (Lenton and Matear, 2007; Verdy et al., 2007; Lovenduski et al., 2008; Le Quéré et al., 2010). The increase in winds has been attributed to the depletion of stratospheric ozone (Thompson and Solomon, 2002) with a contribution from GHGs (Fyfe and Saenko, 2006).

Large decadal variability has been observed in the Equatorial Pacific (Ishii et al., 2009) associated with changes in the phasing of the Pacific Decadal Oscillation (see Glossary) and its impact on gas transfer velocity (Feely et al., 2006; Valsala et al., 2012). By contrast, ocean pCO_2 appears to have increased at a slower rate than atmospheric CO_2 (thus a growing ocean CO_2 sink in that region) in the northern North Pacific Ocean (Takahashi et al., 2006). There is less evidence available to attribute the observed changes in other regions to changes in underlying processes or climate change and variability.

6.3.2.5.5 Processes driving variability and trends in air–sea carbon dioxide fluxes

Three type of processes are estimated to have an important effect on the air–sea CO_2 fluxes on century time scales: (1) the dissolution of CO_2 at the ocean surface and its chemical equilibrium with other forms of carbon in the ocean (mainly carbonate and bicarbonate), (2) the transport of carbon between the surface and the intermediate and deep ocean and (3) changes in the cycling of carbon through marine ecosystem processes (the ocean biological pump; see Section 6.1.1.1). The surface dissolution and equilibration of CO_2 with the atmosphere is well understood and quantified. It varies with the surface ocean conditions, in particular with temperature (solubility effect) and alkalinity. The capacity of the ocean to take up additional CO_2 for a given alkalinity decreases at higher temperature (4.23% per degree warming; Takahashi et al., 1993) and at elevated CO_2 concentrations (about 15% per 100 ppm, computed from the so called Revelle factor; Revelle and Suess, 1957).

Recent changes in nutrient supply in the ocean are also thought to have changed the export of organic carbon from biological processes below the surface layer, and thus the ocean CO_2 sink (Duce et al., 2008). Anthropogenic reactive nitrogen Nr (see Box 6.2) entering the ocean via atmospheric deposition or rivers acts as a fertiliser and may enhance carbon export to depth and hence the CO_2 sink. This Nr contribution has been estimated to be between 0.1 and 0.4 PgC yr^{-1} around the year 2000 using models (Duce et al., 2008; Reay et al., 2008; Krishnamurthy et al., 2009; Suntharalingam et al., 2012). Similarly, increases in iron deposition over the ocean from dust generated by human activity is estimated to have enhanced the ocean cumulative CO_2 uptake by 8 PgC during the 20th century (or about 0.05 PgC yr^{-1} in the past decades) (Mahowald et al., 2010). Although changes in ocean circulation and in global biogeochemical drivers have the potential to alter the ocean carbon fluxes through changes in marine ecosystems, modelling studies show only small variability in ocean biological pump, which has not significantly impacted the response of the ocean carbon cycle over the recent period (Bennington et al., 2009).

Model studies suggest that the response of the air–sea CO_2 fluxes to climate change and variability in recent decades has decreased the rate at which anthropogenic CO_2 is absorbed by the ocean (Sarmiento et al. (2010); Figure 6.14 and Table 6.4). This result is robust to the model or climate forcing used (Figure 6.13), but no formal attribution to anthropogenic climate change has been made. There is insufficient data coverage to separate the impact of climate change on the global ocean CO_2 sink directly from observations, though the regional trends described in Section 6.3.2.5.4 suggest that surface ocean pCO_2 responds to changes in ocean properties in a significant and measurable way.

6.3.2.5.6 Model evaluation of global and regional ocean carbon balance

Ocean process-based carbon cycle models are capable of reproducing the mean air–sea fluxes of CO_2 derived from pCO_2 observations (Takahashi et al., 2009), including their general patterns and amplitude (Sarmiento et al., 2000), the anthropogenic uptake of CO_2 (Orr et al., 2001; Wanninkhof et al., 2013) and the regional distribution of air–sea fluxes (Gruber et al., 2009). The spread between different model results for air–sea CO_2 fluxes is the largest in the Southern Ocean (Matsumoto et al., 2004), where intense convection occurs. Tracer observations (Schmittner et al., 2009) and water mass analysis (Iudicone et al., 2011) have been used to reduce the model uncertainty associated with this process and improve the simulation of carbon fluxes. The models reproduce the observed seasonal cycle of pCO_2 in the sub-tropics but generally do poorly in sub-polar regions where the balance of processes is more difficult to simulate well (McKinley et al., 2006; Schuster et al., 2013). Less information is available to evaluate specifically the representation of biological fluxes in the models, outside of their realistic representation of surface ocean chlorophyll distributions. Ocean process-based carbon cycle models used in AR5 reproduce the relatively small interannual variability inferred from observations (Figure 6.12; Wanninkhof et al., 2013). See also Section 9.4.5.

Sensitivity of modelled air–sea fluxes to CO_2. Data-based studies estimated a cumulative carbon uptake of ~155 ± 30 PgC across studies for the 1750–2011 time period (Sabine et al., 2004; Waugh et al., 2006; Khatiwala et al., 2009), a mean anthropogenic CO_2 sink of 2.2 ± 0.7 PgC yr^{-1} for the 1990s, and decadal trends of 0.13 PgC yr^{-1} per decade during the two decades 1990–2009 (Wanninkhof et al., 2013; from atmospheric inversions), respectively. Models that have estimated these quantities give a total ocean uptake of 170 ± 25 PgC for

1750–2011 (from the model ensemble of Orr et al., (2005) until 1994, plus an additional 40 PgC from estimates in Table 6.4 for 1995–2011), a mean anthropogenic CO_2 sink of 2.1 ± 0.6 PgC yr^{-1} for 1990–1999 (Le Quéré et al., 2013) and a decadal trend of 0.14 PgC yr^{-1} per decade for 1990–2009 (Wanninkhof et al., 2013). Therefore, although the ocean models do not reproduce all the details of the regional structure and changes in air–sea CO_2 fluxes, their globally integrated ocean CO_2 sink and decadal rate of change of this sink is in good agreement with the available observations.

Sensitivity of modelled air–sea fluxes to climate. The relationship between air–sea CO_2 flux and climate is strongly dependent on the oceanic region and on the time scale. Ocean carbon cycle models of the type used in AR5 estimate a reduction in cumulative ocean CO_2 uptake of 1.6 to 5.4 PgC over the period 1959–2008 (1.5 to 5.4%) in response to climate change and variability compared to simulations with no changes in climate (Figure 6.14), partly due to changes in the equatorial Pacific and to changes in the Southern Ocean. The only observation-based estimate available to evaluate the climate response of the global air–sea CO_2 flux is from Park et al. (2010), which is at the low end of the model estimate for the past two decades (Table 6.4). However, this estimate does not include the nonlinear effects of changes in ocean circulation and warming on the global air–sea CO_2 flux, which could amplify the response of the ocean CO_2 sink to climate by 20 to 30% (Le Quéré et al., 2010; Zickfeld et al., 2011).

Processes missing in ocean models. The most important processes missing in ocean carbon cycle models used in the AR5 are those representing explicitly small-scale physical circulation (e.g., eddies, brine formation), which are parameterised in models. These processes have an important influence on the vertical transport of water, heat, salt and carbon (Loose and Schlosser, 2011; Sallée et al., 2012). In particular, changes in vertical transport in the Southern Ocean are thought to explain part of the changes in atmospheric CO_2 between glacial and interglacial conditions, a signal that is not entirely reproduced by models (Section 6.2) suggesting that the sensitivity of ocean models could be underestimated.

Processes related to marine ecosystems in global ocean models are also limited to the simulation of lower trophic levels, with crude parameterizations for sinking processes, bacterial and other loss processes at the surface and in the ocean interior and their temperature dependence (Kwon et al., 2009). Projected changes in carbon fluxes from the response of marine ecosystems to changes in temperature (Beaugrand et al., 2010), ocean acidification (Riebesell et al., 2009) (see Glossary) and pressure from fisheries (Pershing et al., 2010) are all considered potentially important, though not yet quantified. Several processes have been specifically identified that could lead to changes in the ocean CO_2 sink, in particular the temperature effects on marine ecosystem processes (Riebesell et al., 2009; Taucher and Oschlies, 2011) and the variable nutrient ratios induced by ocean acidification or ecosystem changes (Tagliabue et al., 2011). Coastal ocean processes are also poorly represented in global and may influence the ocean CO_2 sink. Nevertheless, the fit of ocean model results to the integrated CO_2 sink and decadal trends discussed above suggest that, up to now, the missing processes have not had a dominant effect on ocean CO_2 beyond the limits of the uncertainty of the data.

6.3.2.6 Land Carbon Dioxide Sink

6.3.2.6.1 Global residual land sink and atmosphere-to-land carbon dioxide flux

The residual land CO_2 sink, that is, the uptake of CO_2 in ecosystems excluding the effects of land use change, is 1.5 ± 1.1, 2.6 ± 1.2 and 2.6 ± 1.2 PgC yr^{-1} for the 1980s, 1990s and 2000s, respectively (Table 6.1). After including the net land use change emissions, the atmosphere-to-land flux of CO_2 (Table 6.1) corresponds to a net sink of CO_2 by all terrestrial ecosystems. This sink has intensified globally from a neutral CO_2 flux of 0.1 ± 0.8 PgC yr^{-1} in the 1980s to a net CO_2 sink of 1.1 ± 0.9 PgC yr^{-1} and 1.5 ± 0.9 PgC yr^{-1} during the 1990s and 2000s, respectively (Table 6.1; Sarmiento et al., 2010). This growing land sink is also supported by an atmospheric inversion (Gurney and Eckels, 2011) and by process-based models (Le Quéré et al., 2009).

6.3.2.6.2 Regional atmosphere-to-land carbon dioxide fluxes

The results from atmospheric CO_2 inversions, terrestrial ecosystem models and forest inventories consistently show that there is a large net CO_2 sink in the northern extratropics, albeit the very limited availability of observations in the tropics (Jacobson et al., 2007; Gurney and Eckels, 2011; Pan et al., 2011). Inversion estimates of atmosphere–land CO_2 fluxes show net atmosphere-to-land CO_2 flux estimates ranging from neutral to a net source of 0.5 to 1.0 PgC yr^{-1} (Jacobson et al., 2007; Gurney and Eckels, 2011) (Figure 6.15). However, Stephens et al. (2007) selected from an ensemble of inversion models those that were consistent with independent aircraft cross-validation data, and constrained an atmosphere-to-land CO_2 flux of 0.1 ± 0.8 PgC yr^{-1} during the period 1992–1996, and a NH net CO_2 sink of 1.5 ± 0.6 PgC yr^{-1}. These results shows that after subtracting emissions from land use change, tropical land ecosystems might also be large CO_2 sinks.

Based on repeated forest biomass inventory data, estimated soil carbon changes, and CO_2 emissions from land use change from the bookkeeping method of Houghton et al. (2012), Pan et al. (2011) estimated a global forest carbon accumulation of 0.5 ± 0.1 PgCyr^{-1} in boreal forests, and of 0.8 ± 0.1 PgC yr^{-1} in temperate forests for the period 2000–2007. Tropical forests were found to be near neutral with net emissions from land use change being compensated by sinks in established tropical forests (forests not affected by land use change), therefore consistent with the Stephens et al. (2007) inversion estimate of tropical atmosphere–land CO_2 fluxes.

Since AR4, a number of studies have compared and attempted to reconcile regional atmosphere-to-land CO_2 flux estimates from multiple approaches and so providing further spatial resolution of the regional contributions of carbon sources and sinks (Table 6.6). A synthesis of regional contributions estimated a 1.7 PgC yr^{-1} sink in the NH regions above 20°N with consistent estimates from terrestrial models and inventories (uncertainty: ±0.3 PgC yr^{-1}) and atmospheric CO_2 inversions (uncertainty: ±0.7 PgC yr^{-1}) (Ciais et al., 2010).

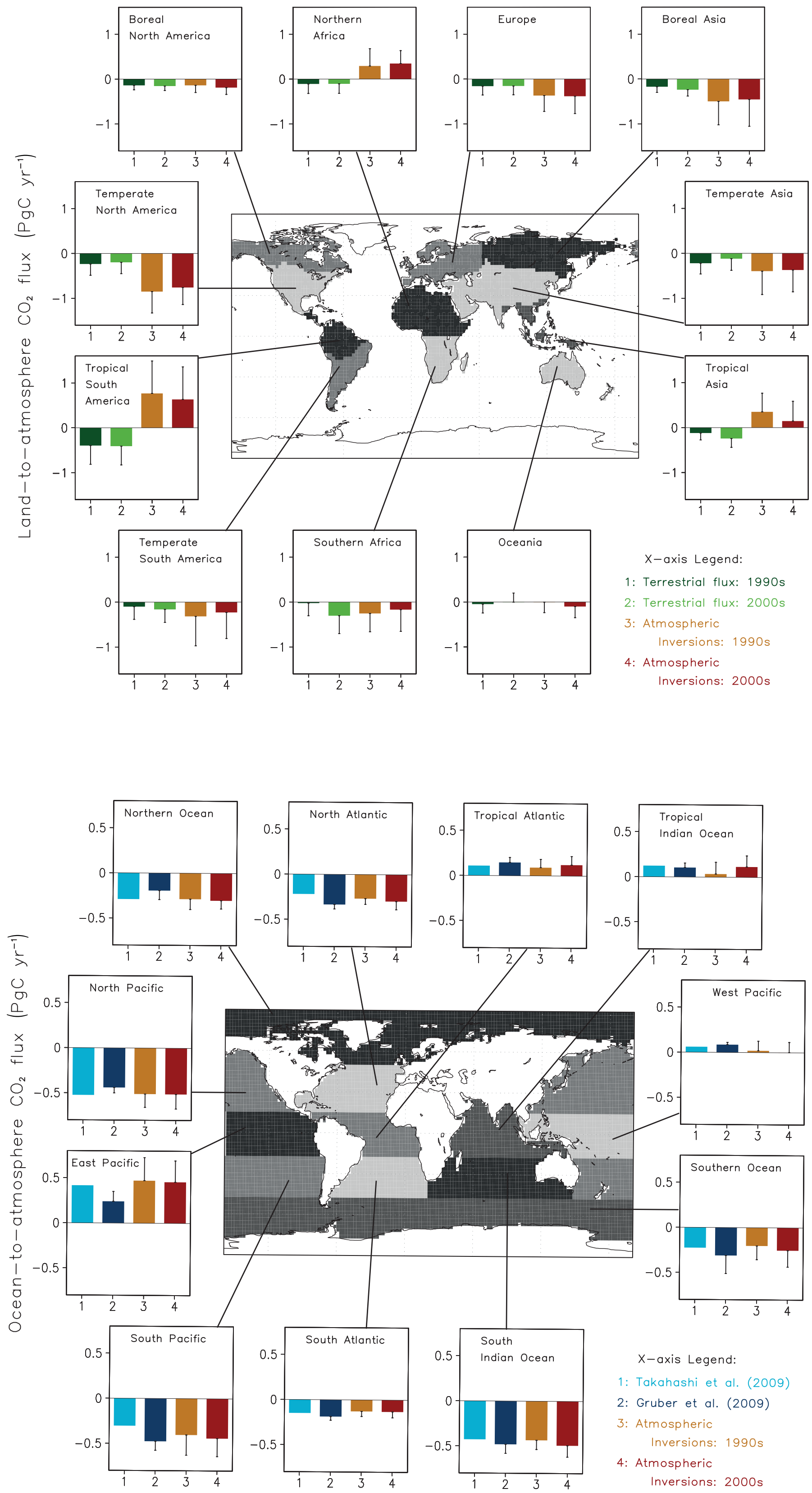

Figure 6.15 | (Top) Bar plots showing decadal average CO_2 fluxes for 11 land regions (1) as estimated by 10 different atmospheric CO_2 inversions for the 1990s (yellow) and 2000s (red) (Peylin et al., 2013; data source: http://transcom.lsce.ipsl.fr/), and (2) as simulated by 10 dynamic vegetation models (DGVMs) for the 1990s (green) and 2000s (light green) (Piao et al., 2013; data source: http://www-lscedods.cea.fr/invsat/RECCAP/). The divisions of land regions are shown in the map. (Bottom) Bar plots showing decadal average CO_2 fluxes for 11 ocean regions (1) as estimated by 10 different atmospheric CO_2 inversions for the 1990s (yellow) and 2000s (red) (data source: http://transcom.lsce.ipsl.fr/), (2) inversion of contemporary interior ocean carbon measurements using 10 ocean transport models (dark blue) (Gruber et al., 2009) and (3) surface ocean pCO_2 measurements based air-sea exchange climatology (Takahashi et al., 2009). The divisions of 11 ocean regions are shown in the map.

Table 6.6 | Regional CO_2 budgets using top-down estimates (atmospheric inversions) and bottom-up estimates (inventory data, biogeochemical modelling, eddy-covariance), excluding fossil fuel emissions. A positive sign indicates a flux from the atmosphere to the land (i.e., a land sink).

Region	CO_2 Sink (PgC yr^{-1})	Uncertainty[a]	Period	Reference
Artic Tundra	0.1	±0.3[b]	2000–2006	McGuire et al. (2012)
Australia	0.04	±0.03	1990–2009	Haverd et al. (2013)
East Asia	0.25	±0.1	1990–2009	Piao et al. (2012)
Europe	0.9	±0.2	2001–2005	Luyssaert et al. (2012)
North America	0.6	±0.02	2000–2005	King et al. (2012)
Russian Federation	0.6	–0.3 to –1.3	1990–2007	Dolman et al. (2012)
South Asia	0.15	±0.24	2000–2009	Patra et al. (2013)
South America	–0.3	±0.3	2000–2005	Gloor et al. (2012)

Notes:

[a] One standard deviation from mean unless indicated otherwise.

[b] Based on range provided.

6.3.2.6.3 Interannual variability in atmosphere-to-land carbon dioxide fluxes

The interannual variability of the residual land sink shown in Figures 6.12 and 6.16 accounts for most of the interannual variability of the atmospheric CO_2 growth rate (see Section 6.3.2.3). Atmospheric CO_2 inversion results suggest that tropical land ecosystems dominate the global CO_2 variability, with positive anomalies during El Niño episodes (Bousquet et al., 2000; Rödenbeck et al., 2003; Baker et al., 2006), which is consistent with the results of one inversion of atmospheric ^{13}C and CO_2 measurements (Rayner et al., 2008). A combined El Niño-Southern Oscillation (ENSO)–Volcanic index time series explains 75% of the observed variability (Raupach et al., 2008). A positive phase of ENSO (El Niño, see Glossary) is generally associated with enhanced land CO_2 source, and a negative phase (La Niña) with enhanced land CO_2 sink (Jones and Cox, 2001; Peylin et al., 2005). Observations from eddy covariance networks suggest that interannual carbon flux variability in the tropics and temperate regions is dominated by precipitation, while boreal ecosystem fluxes are more sensitive to temperature and shortwave radiation variation (Jung et al., 2011), in agreement with the results from process-based terrestrial ecosystem models (Piao et al., 2009a). Terrestrial biogeochemical models suggest that interannual net biome productivity (NBP) variability is dominated by GPP (see Glossary) rather than terrestrial ecosystem respiration (Piao et al., 2009b; Jung et al., 2011).

6.3.2.6.4 Carbon fluxes from inland water

Global analyses estimate that inland waters receive about 1.7 to 2.7 PgC yr^{-1} emitted by soils to rivers headstreams, of which, 0.2 to 0.6 PgC yr^{-1} is buried in aquatic sediments, 0.8 to 1.2 PgC yr^{-1} returns to the atmosphere as CO_2, and 0.9 PgC yr^{-1} is delivered to the ocean (Cole et al., 2007; Battin et al., 2009; Aufdenkampe et al., 2011). Estimates of the transport of carbon from land ecosystems to the coastal ocean by rivers are ~0.2 PgC yr^{-1} for Dissolved Organic Carbon (DOC), 0.3 PgC yr^{-1} for Dissolved Inorganic Carbon (DIC), and 0.1 to 0.4 PgC yr^{-1} for Particulate Organic Carbon (POC) (Seitzinger et al., 2005; Syvitski et al., 2005; Mayorga et al., 2010). For the DIC fluxes, only about two-thirds of it originates from atmospheric CO_2 and the rest of the carbon is supplied by weathered carbonate rocks (Suchet and Probst, 1995; Gaillardet et al., 1999; Oh and Raymond, 2006; Hartmann et al., 2009). Regional DIC concentrations in rivers has increased during the Industrial Era (Oh and Raymond, 2006; Hamilton et al., 2007; Perrin et al., 2008). Agricultural practices coupled with climate change can lead to large increases in regional scale DIC export in watersheds with a large agricultural footprint (Raymond et al., 2008). Furthermore, regional urbanization also elevates DIC fluxes in rivers (Baker et al., 2008; Barnes and Raymond, 2009), which suggests that anthropogenic activities have contributed a significant portion of the annual global river DIC flux to the ocean.

Land clearing and management are thought to produce an acceleration of POC transport, much of which is trapped in alluvial and colluvial deposition zones, lakes, reservoirs and wetlands (Stallard, 1998; Smith et al., 2001b; Syvitski et al., 2005). Numerous studies have demonstrated an increase in the concentration of DOC in rivers in the northeastern United States and northern/central Europe over the past two to four decades (Worrall et al., 2003; Evans et al., 2005; Findlay, 2005; Monteith et al., 2007; Lepistö et al., 2008). Owing to the important role of wetlands in DOC production, the mobilization of DOC due to human-induced changes in wetlands probably represents an important cause of changes in global river DOC fluxes to date (Seitzinger et al., 2005), although a global estimate of this alteration is not available. A robust partitioning between natural and anthropogenic carbon fluxes in freshwater systems is not yet possible, nor a quantification of the ultimate fate of carbon delivered by rivers to the coastal and open oceans.

6.3.2.6.5 Processes driving terrestrial atmosphere-to-land carbon dioxide fluxes

Assessment of experimental data, observations and model results suggests that the main processes responsible for the residual land sink include the CO_2 fertilisation effect on photosynthesis (see Box 6.3), nitrogen fertilisation by increased deposition (Norby, 1998; Thornton et al., 2007; Bonan and Levis, 2010; Zaehle and Dalmonech, 2011) and climate effects (Nemani et al., 2003; Gloor et al., 2009). It is *likely* that reactive nitrogen deposition over land currently increases natural CO_2 in particular in forests, but the magnitude of this effect varies between regions (Norby, 1998; Thornton et al., 2007; Bonan and Levis, 2010; Zaehle and Dalmonech, 2011). Processes responsible for the net atmosphere-to-land CO_2 sink on terrestrial ecosystems include, in addition, forest regrowth and afforestation (Myneni et al., 2001;

Box 6.3 | The Carbon Dioxide Fertilisation Effect

Elevated atmospheric CO_2 concentrations lead to higher leaf photosynthesis and reduced canopy transpiration, which in turn lead to increased plant water use efficiency and reduced fluxes of surface latent heat. The increase in leaf photosynthesis with rising CO_2, the so-called CO_2 fertilisation effect, plays a dominant role in terrestrial biogeochemical models to explain the global land carbon sink (Sitch et al., 2008), yet it is one of most unconstrained process in those models.

Field experiments provide a direct evidence of increased photosynthesis rates and water use efficiency (plant carbon gains per unit of water loss from transpiration) in plants growing under elevated CO_2. These physiological changes translate into a broad range of higher plant carbon accumulation in more than two-thirds of the experiments and with increased net primary productivity (NPP) of about 20 to 25% at double CO_2 from pre-industrial concentrations (Ainsworth and Long, 2004; Luo et al., 2004, 2006; Nowak et al., 2004; Norby et al., 2005;Canadell et al., 2007a; Denman et al., 2007; Ainsworth et al., 2012; Wang et al., 2012a). Since the AR4, new evidence is available from long-term Free-air CO_2 Enrichment (FACE) experiments in temperate ecosystems showing the capacity of ecosystems exposed to elevated CO_2 to sustain higher rates of carbon accumulation over multiple years (Liberloo et al., 2009; McCarthy et al., 2010; Aranjuelo et al., 2011; Dawes et al., 2011; Lee et al., 2011; Zak et al., 2011). However, FACE experiments also show the diminishing or lack of CO_2 fertilisation effect in some ecosystems and for some plant species (Dukes et al., 2005; Adair et al., 2009; Bader et al., 2009; Norby et al., 2010; Newingham et al., 2013). This lack of response occurs despite increased water use efficiency, also confirmed with tree ring evidence (Gedalof and Berg, 2010; Peñuelas et al., 2011).

Nutrient limitation is hypothesized as primary cause for reduced or lack of CO_2 fertilisation effect observed on NPP in some experiments (Luo et al., 2004; Dukes et al., 2005; Finzi et al., 2007; Norby et al., 2010). Nitrogen and phosphorus are *very likely* to play the most important role in this limitation of the CO_2 fertilisation effect on NPP, with nitrogen limitation prevalent in temperate and boreal ecosystems, and phosphorus limitation in the tropics (Luo et al., 2004; Vitousek et al., 2010; Wang et al., 2010a; Goll et al., 2012). Micronutrients interact in diverse ways with other nutrients in constraining NPP such as molybdenum and phosphorus in the tropics (Wurzburger et al., 2012). Thus, with *high confidence*, the CO_2 fertilisation effect will lead to enhanced NPP, but significant uncertainties remain on the magnitude of this effect, given the lack of experiments outside of temperate climates.

Pacala et al., 2001; Houghton, 2010; Bellassen et al., 2011; Williams et al., 2012a), changes in forest management and reduced harvest rates (Nabuurs et al., 2008).

Process attribution of the global land CO_2 sink is difficult due to limited availability of global data sets and biogeochemical models that include all major processes. However, regional studies shed light on key drivers and their interactions. The European and North American carbon sinks are explained by the combination of forest regrowth in abandoned lands and decreased forest harvest along with the fertilisation effects of rising CO_2 and nitrogen deposition (Pacala et al., 2001; Ciais et al., 2008; Sutton et al., 2008; Schulze et al., 2010; Bellassen et al., 2011; Williams et al., 2012a). In the tropics, there is evidence from forest inventories that increasing forest growth rates are not explained by the natural recovery from disturbances, suggesting that increasing atmospheric CO_2 and climate change play a role in the observed sink in established forests (Lewis et al., 2009; Pan et al., 2011). There is also recent evidence of tropical nitrogen deposition becoming more notable although its effects on the net carbon balance have not been assessed (Hietz et al., 2011).

The land carbon cycle is very sensitive to climate changes (e.g., precipitation, temperature, diffuse vs. direct radiation), and thus the changes in the physical climate from increasing GHGs as well as in the diffuse fraction of sunlight are *likely* to be causing significant changes in the carbon cycle (Jones et al., 2001; Friedlingstein et al., 2006; Mercado et al., 2009). Changes in the climate are also associated with disturbances such as fires, insect damage, storms, droughts and heat waves which are already significant processes of interannual variability and possibly trends of regional land carbon fluxes (Page et al., 2002; Ciais et al., 2005; Chambers et al., 2007; Kurz et al., 2008b; Clark et al., 2010; van der Werf et al., 2010; Lewis et al., 2011) (see Section 6.3.2.2).

Warming (and possibly the CO_2 fertilisation effect) has also been correlated with global trends in satellite greenness observations, which resulted in an estimated 6% increase of global NPP, or the accumulation of 3.4 PgC on land over the period 1982–1999 (Nemani et al., 2003). This enhanced NPP was attributed to the relaxation of climatic constraints to plant growth, particularly in high latitudes. Concomitant to the increased of NPP with warming, global soil respiration also increased between 1989 and 2008 (Bond-Lamberty and Thomson, 2010), reducing the magnitude of the net land sink. A recent study suggests a declining NPP trend over 2000–2009 (Zhao and Running, 2010) although the model used to reconstruct NPP trends from satellite observation has not been widely accepted (Medlyn, 2011; Samanta et al., 2011).

6.3.2.6.6 Model evaluation of global and regional terrestrial carbon balance

Evaluation of global process-based land carbon models was performed against ground and satellite observations including (1) measured CO_2

fluxes and carbon storage change at particular sites around the world, in particular sites from the Fluxnet global network (Baldocchi et al., 2001; Jung et al., 2007; Stöckli et al., 2008; Schwalm et al., 2010; Tan et al., 2010), (2) observed spatio-temporal change in leaf area index (LAI) (Lucht et al., 2002; Piao et al., 2006) and (3) interannual and seasonal change in atmospheric CO_2 (Randerson et al., 2009; Cadule et al., 2010).

Figure 6.16 compares the global land CO_2 sink driven by climate change and rising CO_2 as simulated by different process based carbon cycle models (without land use change), with the residual land sink computed as the sum of fossil fuel and cement emissions and land use change emissions minus the sum of CO_2 growth rate and ocean sink (Le Quéré et al., 2009; Friedlingstein et al., 2010). Although these two quantities are not the same, the multi-model mean reproduces well the trend and interannual variability of the residual land sink which is dominated by climate variability and climate trends and CO_2, respectively, both represented in models (Table 6.7). Limited availability of *in situ* measurements, particularly in the tropics, limits the progress towards reducing uncertainty on model parameterizations.

Regional and local measurements can be used to evaluate and improve global models. Regionally, forest inventory data show that the forest carbon sink density over Europe is of –89 ± 19 gC m^{-2} yr^{-1}, which is compatible with model estimates with afforestation (–63 gC m^{-2} yr^{-1}; Luyssaert et al., 2010), while modelled NPP was 43% larger than the inventory estimate. In North America, the ability of 22 terrestrial carbon cycle models to simulate the seasonal cycle of land–atmosphere CO_2 exchange from 44 eddy covariance flux towers was poor with a difference between observations and simulations of 10 times the observational uncertainty (Schwalm et al., 2010). Model shortcomings included spring phenology, soil thaw, snow pack melting and lag responses to extreme climate events (Keenan et al., 2012). In China, the magnitude of the carbon sink estimated by five terrestrial ecosystem models (–0.22 to –0.13 PgC yr^{-1}) was comparable to the observation-based estimate (–0.18 ± 0.73 PgC yr^{-1}; Piao et al., 2009a), but modelled interannual variation was weakly correlated to observed regional land–atmosphere CO_2 fluxes (Piao et al., 2011).

Sensitivity of the terrestrial carbon cycle to rising atmospheric carbon dioxide. An inter-comparison of 10 process-based models showed increased NPP by 3% to 10% over the last three decades, during which CO_2 increased by ~50 ppm (Piao et al., 2013). These results are consistent within the broad range of responses from experimental studies (see Box 6.3). However, Hickler et al. (2008) suggested that currently available FACE results (largely from temperate regions) are not applicable to vegetation globally because there may be large spatial heterogeneity in vegetation responses to CO_2 fertilisation.

Table 6.7 | Estimates of the land CO_2 sink from process-based terrestrial ecosystem models driven by rising CO_2 and by changes in climate. The land sink simulated by these models is close to but not identical to the terrestrial CO_2 sink from Table 6.1 because the models calculate the effect of CO_2 and climate over managed land, and many do not include nitrogen limitation and disturbances.

Model Name	Nitrogen Limitation	Natural Fire CO_2 Emissions	1980–1989	1990–1999	2000–2009
	(Yes/No)	(Yes/No)	PgC yr^{-1}	PgC yr^{-1}	PgC yr^{-1}
CLM4C[b,c]	No	Yes	1.98	2.11	2.64
CLM4CN[b,c]	Yes	Yes	1.27	1.25	1.67
Hyland[d]	No	No	2.21	2.92	3.99
LPJ[e]	No	Yes	1.14	1.90	2.60
LPJ_GUESS[f]	No	Yes	1.15	1.54	2.07
OCN[g]	Yes	No	1.75	2.18	2.36
ORC[h]	No	No	2.08	3.05	3.74
SDGVM[i]	Yes	Yes	1.25	1.95	2.30
TRIFFID[j]	No	No	1.85	2.52	3.00
VEGAS[k]	No	No	1.40	1.68	1.89
Average[a]			1.61 ± 0.65	2.11 ± 0.93	2.63 ± 1.22

Notes:

[a] Average of all models ±90% confidence interval.
[b] Oleson et al. (2010).
[c] Lawrence et al. (2011).
[d] Levy et al. (2004).
[e] Sitch et al. (2003).
[f] Smith et al. (2001a).
[g] Zaehle and Friend (2010).
[h] Krinner et al. (2005).
[i] Woodward and Lomas (2004).
[j] Cox (2001).
[k] Zeng (2003).

All of these models run are forced by rising CO_2 concentration and time-varying historical reconstructed weather and climate fields using the same protocol from the TRENDY project (Piao et al., 2013). (http://www.globalcarbonproject.org/global/pdf/DynamicVegetationModels.pdf).

CLM4C = Community Land Model for Carbon; CLM4CN = Community Land Model for Carbon–Nitrogen; GUESS = General Ecosystem Simulator; LPJ = Lund-Potsdam-Jena Dynamic Global Vegetation Model; OCN = Cycling of Carbon and Nitrogen on land, derived from ORCHIDEE model; ORC = ORCHIDEE, ORganizing Carbon and Hydrology in Dynamic EcosystEms model; SDGVM = Sheffield Dynamic Global Vegetation Model; TRIFFID = Top-down Representation of Interactive Foliage and Flora Including Dynamics; VEGAS = VEgetation-Global-Atmosphere-Soil terrestrial carbon cycle model.

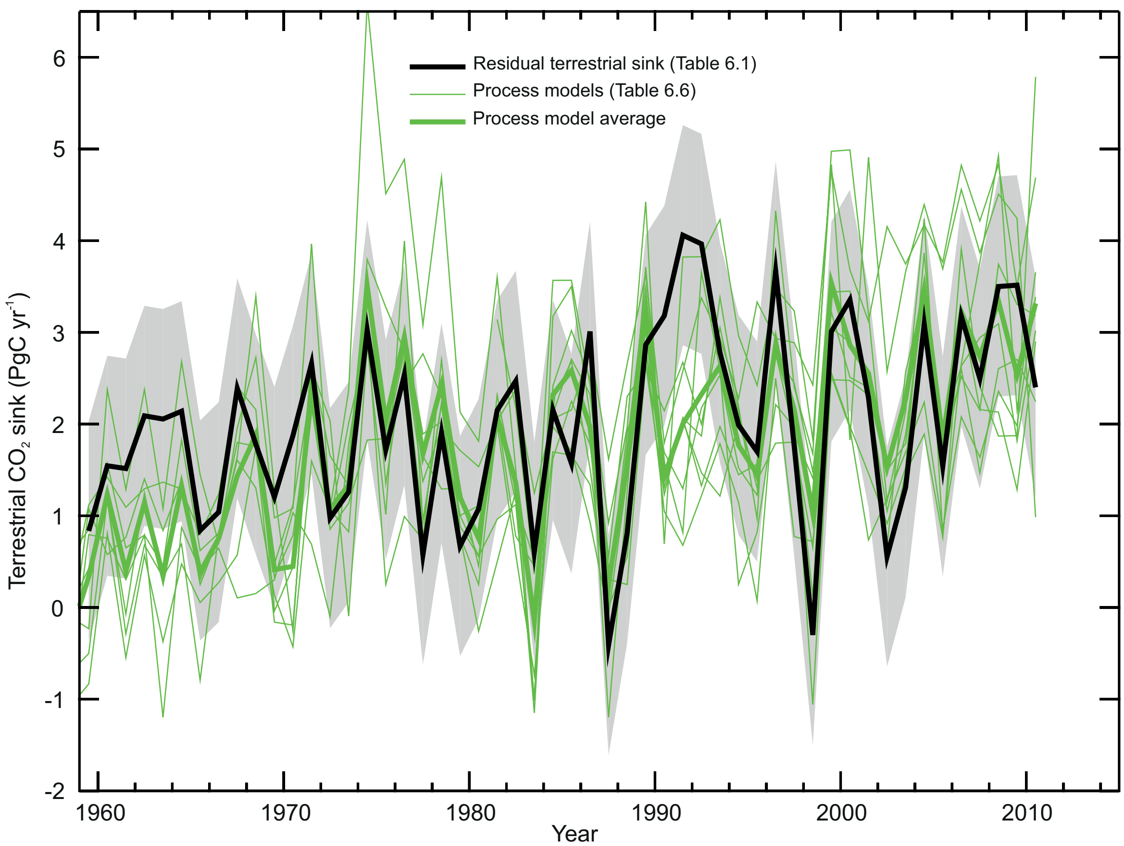

Figure 6.16 | The black line and gray shading represent the estimated value of the residual land sink (PgC yr^{-1}) and its uncertainty from Table 6.1, which is calculated from the difference between emissions from fossil fuel and land use change plus emissions from net land use change, minus the atmospheric growth rate and the ocean sink. The atmosphere-to-land flux simulated by process land ecosystem models from Table 6.7 are shown in thin green, and their average in thick green. A positive atmosphere-to-land flux represents a sink of CO_2. The definition of the atmosphere-to-land flux simulated by these models is close to but not identical to the residual land sink from Table 6.1 (see Table 6.7).

Sensitivity of terrestrial carbon cycle to climate trends and variability. Warming exerts a direct control on the net land–atmosphere CO_2 exchange because both photosynthesis and respiration are sensitive to changes in temperature. From estimates of interannual variations in the residual land sink, 1°C of positive global temperature anomaly leads to a decrease of 4 PgC yr^{-1} of the global land CO_2 sink (Figure 6.17). This observed interannual response is close to the response of the models listed in Table 6.7 (–3.5 ± 1.5 PgC yr^{-1}°C^{-1} in Piao et al., 2013), albeit individual models show a range going from –0.5 to –6.2 PgC yr^{-1} °C^{-1}. The sensitivity of atmospheric CO_2 concentration to century scale temperature change was estimated at about 3.6 to 45.6 PgC °C^{-1} (or 1.7 to 21.4 ppm CO_2 °C^{-1}) using the ice core observed CO_2 drop during the Little Ice Age (see Section 6.2; Frank et al., 2010).

Terrestrial carbon cycle models used in AR5 generally underestimate GPP in the water limited regions, implying that these models do not correctly simulate soil moisture conditions, or that they are too sensitive to changes in soil moisture (Jung et al., 2007). Most models (Table 6.7) estimated that the interannual precipitation sensitivity of the global land CO_2 sink to be higher than that of the observed residual land sink (–0.01 PgC yr^{-1} mm^{-1}; Figure 6.17).

Processes missing in terrestrial carbon cycle models. First, many models do not explicitly take into account the various forms of disturbances or ecosystem dynamics: migration, fire, logging, harvesting, insect outbreaks and the resulting variation in forest age structure which is known to affect the net carbon exchange (Kurz et al., 2008c; Bellassen et al., 2010; Higgins and Harte, 2012). Second, many key processes relevant to decomposition of carbon are missing in models (Todd-Brown et al., 2012), and particularly for permafrost carbon and for carbon in boreal and tropical wetlands and peatlands, despite the large amount of carbon stored in these ecosystems and their vulnerability to warming and land use change (Tarnocai et al., 2009; Hooijer et al., 2010; Page et al., 2011). However, progress has been made (Wania et al., 2009; Koven et al., 2011; Schaefer et al., 2011). Third, nutrient dynamics are taken into account only by few models despite the fact it is well established that nutrient constrains NPP and nitrogen deposition enhances NPP (Elser et al., 2007; Magnani et al., 2007; LeBauer and Treseder, 2008); see Section 6.3.2.6.5. Very few models have phosphorus dynamics (Zhang et al., 2011; Goll et al., 2012). Fourth, the negative effects of elevated tropospheric ozone on NPP have not been taken into account by most current carbon cycle models (Sitch et al., 2007). Fifth, transfer of radiation, water and heat in the vegetation–soil–atmosphere continuum are treated very simply in the global ecosystem models. Finally, processes that transport carbon at the surface (e.g., water and tillage erosion; Quinton et al., 2010) and human managements including fertilisation and irrigation (Gervois et al., 2008) are poorly or not represented at all. Broadly, models are still at their early stages in dealing with land use, land use change and forestry.

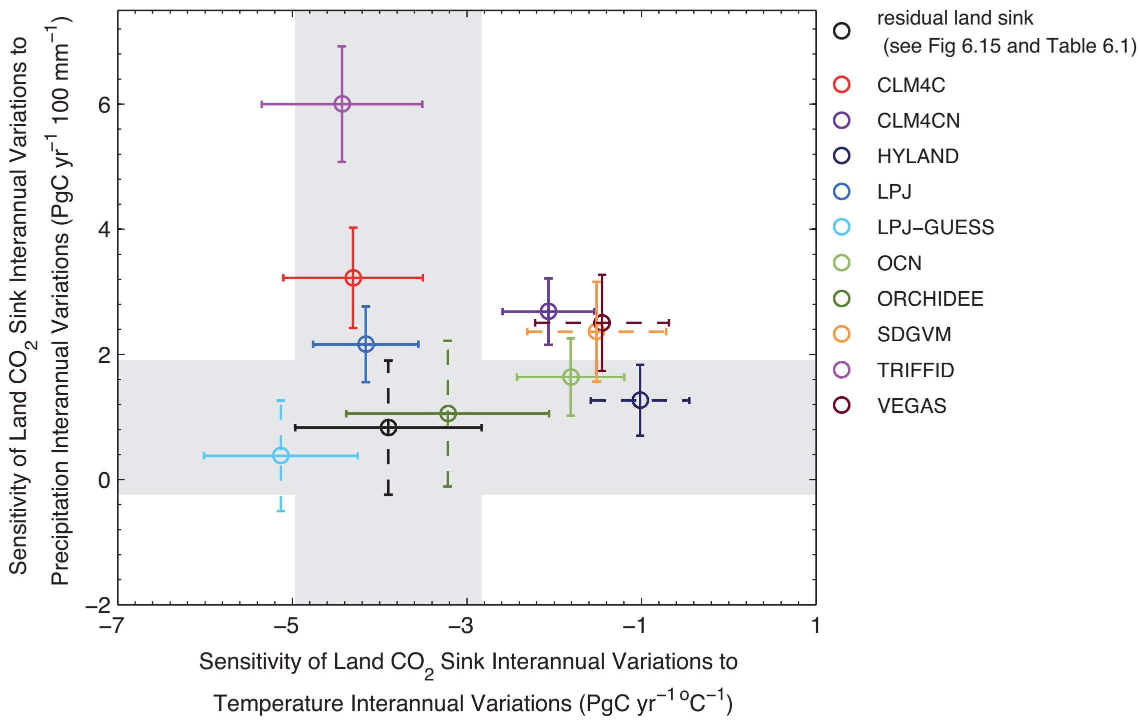

Figure 6.17 | The response of interannual land CO_2 flux anomaly to per 1°C interannual temperature anomaly and per 100 mm interannual precipitation anomaly during 1980–2009. Black circles show climate sensitivity of land CO_2 sink estimated from the residual land sink (see Figure 6.15 and Table 6.1), which is the sum of fossil fuel and cement emissions and land use change emissions minus the sum of observed atmospheric CO_2 growth rate and modeled ocean sink sink (Le Quéré et al., 2009; Friedlingstein and Prentice, 2010). Coloured circles show land CO_2 sink estimated by 10 process-based terrestrial carbon cycle models (CLM4C (Community Land Model for Carbon), CLM4CN (Community Land Model for Carbon–Nitrogen), HYLAND (HYbrid LAND terrestrial ecosystem model), LPJ (Lund-Potsdam-Jena Dynamic Global Vegetation Model), LPJ–GUESS (LPJ–General Ecosystem Simulator, OCN (Cycling of Carbon and Nitrogen on land, derived from ORCHIDEE model), ORCHIDEE (ORganizing Carbon and Hydrology in Dynamic EcosystEms model), SDGVM (Sheffield Dynamic Global Vegetation Model), TRIFFID (Top-down Representation of Interactive Foliage and Flora Including Dynamics) and VEGAS (terrestrial vegetation and carbon model)). Error bars show standard error of the sensitivity estimates. Dashed error bars indicate the estimated sensitivity by the regression approach is statistically insignificant ($P >$ 0.05). Grey area denoted the area bounded by the estimated climate sensitivity of the residual land sink ± the standard error of the estimated climate sensitivity of the residual land sink. The sensitivity of land CO_2 sink interannual variations to interannual variations of temperature (or precipitation) is estimated as the regression coefficient of temperature (or precipitation) in a multiple regression of detrended anomaly of land CO_2 sink against detrended anomaly of annual mean temperature and annual precipitation.

6.3.3 Global Methane Budget

AR5 is the first IPCC assessment report providing a consistent synthesis of the CH_4 budget per decade using multiple atmospheric CH_4 inversion models (top-down) and process-based models and inventories (bottom-up). Table 6.8 shows the budgets for the decades of 1980s, 1990s and 2000s. Uncertainties on emissions and sinks are listed using minimum and maximum of each published estimate for each decade. Bottom-up approaches are used to attribute decadal budgets to individual processes emitting CH_4 (see Section 6.1.1.2 for a general overview). Top-down inversions provide an atmospheric-based constraint mostly for the total CH_4 source per region, and the use of additional observations (e.g., isotopes) allows inferring emissions per source type. Estimates of CH_4 sinks in the troposphere by reaction with tropospheric OH, in soils and in the stratosphere are also presented. Despite significant progress since the AR4, large uncertainties remain in the present knowledge of the budget and its evolution over time.

6.3.3.1 Atmospheric Changes

Since the beginning of the Industrial Era, the atmospheric CH_4 concentration increased by a factor of 2.5 (from 722 ppb to 1803 ppb in 2011). CH_4 is currently measured by a network of more than 100 surface sites (Blake et al., 1982; Cunnold et al., 2002; Langenfelds et al., 2002; Dlugokencky et al., 2011), aircraft profiles (Brenninkmeijer et al., 2007), satellite (Wecht et al., 2012; Worden et al., 2012) and before 1979 from analyses of firn air and ice cores (see Sections 5.2.2 and Section 6.2, and Figure 6.11). The growth of CH_4 in the atmosphere is largely in response to increasing anthropogenic emissions. The vertically averaged atmospheric CH_4 concentration field can be mapped by remote sensing from the surface using Fourier Transform Infrared Spectroscopy (FTIR) instruments (Total Carbon Column Observing Network, TCCON, http://www.tccon.caltech.edu/) and from space by several satellite instruments: Atmospheric Infrared Sounder (AIRS, since 2002; http://airs.jpl.nasa.gov), Tropospheric Emission Spectrometer (TES, since 2004; http://tes.jpl.nasa.gov), Infrared Atmospheric Sounder Interferometer (IASI, since 2006; Crévoisier et al., 2009), Scanning Imaging Spectrometer for Atmospheric Cartography (SCIAMACHY, 2003–2012; Frankenberg et al., 2008), and Greenhouse Gases Observing Satellite-Thermal And Near infrared Sensor for carbon Observation Fourier-Transform Spectrometer (GOSAT-TANSO-FTS, since 2009; Morino et al., 2011). As an example, SCIAMACHY shows the column CH_4 gradient between the two hemispheres as well as increased concentrations over Southeast Asia, due to emissions from agriculture, wetlands, waste and energy production (Frankenberg et al., 2008). *In situ* observations provide very precise measurements (~0.2%) but unevenly located at the surface of the globe. Satellite data offer a global coverage at the cost of a lower precision on individual measurements (~2%) and possible biases (Bergamaschi et al., 2009).

The growth rate of CH_4 has declined since the mid-1980s, and a near zero growth rate (quasi-stable concentrations) was observed during 1999–2006, suggesting an approach to steady state where the sum of emissions are in balance with the sum of sinks (Dlugokencky et al., 2003; Khalil et al., 2007; Patra et al., 2011; Figure 6.18). The reasons for this growth rate decline after the mid-1980s are still debated, and results from various studies provide possible scenarios: (1) a reduction of anthropogenic emitting activities such as coal mining, gas industry and/or animal husbandry, especially in the countries of the former Soviet Union (Dlugokencky et al., 2003; Chen and Prinn, 2006; Savolainen et al., 2009; Simpson et al., 2012); (2) a compensation between increasing anthropogenic emissions and decreasing wetland emissions (Bousquet et al., 2006; Chen and Prinn, 2006); (3) significant (Rigby et al., 2008) to small (Montzka et al., 2011) changes in OH concentrations and/or based on two different $^{13}CH_4$ data sets; (4) reduced emissions from rice paddies attributed to changes in agricultural practices (Kai et al., 2011); or (5) stable microbial and fossil fuel emissions from 1990 to 2005 (Levin et al., 2012).

Since 2007, atmospheric CH_4 has been observed to increase again (Rigby et al., 2008; Dlugokencky et al., 2009) with positive anomalies of emissions of 21 Tg(CH_4) yr^{-1} and 18 Tg(CH_4) yr^{-1} estimated by inversions during 2007 and 2008, respectively (Bousquet et al., 2011) as compared to the 1999–2006 period. The increase of emissions in 2007–2008 was dominated by tropical regions (Bousquet et al., 2011), with a major contribution from tropical wetlands and some contribution from high-latitude wetlands during the 2007 anomaly (Dlugokencky et al., 2009; Bousquet et al., 2011). This increase is suggested by the growth rate over latitude in Figure 6.18 (Dlugokencky et al., 2009). The recent increase of CH_4 concentration since 2007 is also consistent

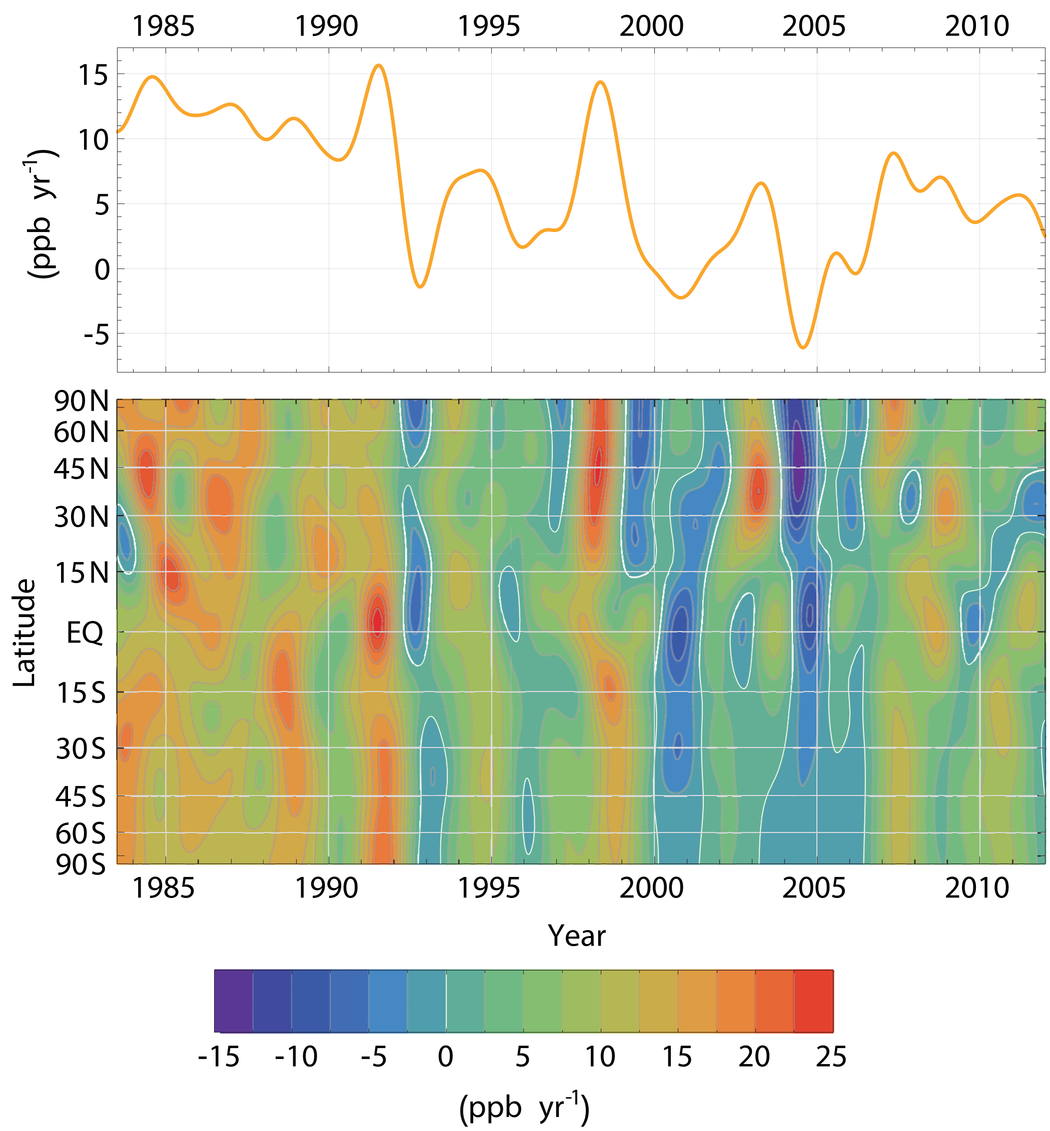

Figure 6.18 | (Top) Globally averaged growth rate of atmospheric CH_4 in ppb yr^{-1} determined from the National Oceanic and Atmospheric Administration–Earth System Research Laboratory (NOAA–ESRL) network, representative for the marine boundary layer. (Bottom) Atmospheric growth rate of CH_4 as a function of latitude (Masarie and Tans, 1995; Dlugokencky and Tans, 2013b).

Table 6.8 | Global CH_4 budget for the past three decades (in Tg(CH_4) yr^{-1}) and present day (2011)[38]. The bottom-up estimates for the decade of 2000–2009 are used in the Executive Summary and in Figure 6.2. T-D stands for Top-Down inversions and B-U for Bottom-Up approaches. Only studies covering at least 5 years of each decade have been used. Reported values correspond to the mean of the cited references and therefore not always equal (max-min)/2; likewise, ranges [in brackets] represent minimum and maximum values of the cited references. The sum of sources and sinks from B-U approaches does not automatically balance the atmospheric changes. For B-U studies, individual source types are also presented. For T-D inversions, the 1980s decade starts in 1984. As some atmospheric inversions did not reference their global sink, balance with the atmosphere and the sum of the sources has been assumed. One biomass burning estimate (Schultz et al., 2007) excludes biofuels (a). Stratospheric loss for B-U is the sum of the loss by OH radicals, a 10 Tg yr^{-1} loss due to O1D radicals (Neef et al., 2010) and a 20 to 35% contribution due to Cl radicals[24] (Allan et al., 2007). Present day budgets[39] adopt a global mean lifetime of 9.14 yr (±10%).

Tg(CH_4) yr^{-1}	1980–1989		1990–1999		2000–2009	
	Top-Down	Bottom-Up	Top-Down	Bottom-Up	Top-Down	Bottom-Up
Natural Sources	193 [150–267]	355 [244–466]	182 [167–197]	336 [230–465]	218 [179–273]	347 [238–484]
Natural wetlands	157 [115–231][1,2,3]	225 [183–266][4,5]	150 [144–160][1,28,29]	206 [169–265][4,5,27]	175 [142–208][1,29,33,34,35,36]	217 [177–284][4,5,27]
Other sources	36 [35–36][1,2]	130 [61–200]	32 [23–37][1,28,29]	130 [61–200]	43 [37–65][1,29,33,34,35,36]	130 [61–200]
Freshwater (lakes and rivers)		40 [8–73][6,7,8]		40 [8–73][6,7,8]		40 [8–73][6,7,8]
Wild animals		15 [15–15][9]		15 [15–15][9]		15 [15–15][9]
Wildfires		3 [1–5][9,10,11,12,13]		3 [1–5][9,10,11,12,13]		3 [1–5][9,10,11,12,13]
Termites		11 [2–22][9,10,14,15,x]		11 [2–22][9,10,14,15,x]		11 [2–22][9,10,14,15,x]
Geological (incl. oceans)		54 [33–75][10,16,17]		54 [33–75][10,16,17]		54 [33–75][10,16,17]
Hydrates		6 [2–9][9,18,19]		6 [2–9][9,18,19]		6 [2–9][9,18,19]
Permafrost (excl. lakes and wetlands)		1 [0–1][10]		1 [0–1][10]		1 [0–1][10]
Anthropogenic Sources	348 [305–383]	308 [292–323]	372 [290–453]	313 [281–347]	335 [273–409]	331 [304–368]
Agriculture and waste	208 [187–220][1,2,3]	185 [172–197][20]	239 [180–301][1,28,29]	187 [177–196][20,30,31]	209 [180–241][1,29,33,34,35,36]	200 [187–224][20,30,31]
Rice		45 [41–47][20]		35 [32–37][20,27,30,31]		36 [33–40][20,27,30,31]
Ruminants		85 [81–90][20]		87 [82–91][20,30,31]		89 [87–94][20,30,31]
Landfills and waste		55 [50–60][20]		65 [63–68][20,30,31]		75 [67–90][20,30,31]
Biomass burning (incl. biofuels)	46 [43–55][1,2,3]	34 [31–37][20,21,22a,38]	38 [26–45][1,28,29]	42 [38–45][13,20,21,22a,32,38]	30 [24–45][1,29,33,34,35,36]	35 [32–39][13,20,21,32,37,38]
Fossil fuels	94 [75–108][1,2,3]	89 [89–89][20]	95 [84–107][1,28,29]	84 [66–96][20,30,31]	96 [77–123][1,29,33,34,35,36]	96 [85–105][20,30,31]
Sinks						
Total chemical loss	490 [450–533][1,2,3]	539 [411–671][23,24,25,26]	515 [491–554][1,28,29]	571 [521–621][23,24,25,26]	518 [510–538][1,29,33,34,36]	604 [483–738][23,24,25,26]
Tropospheric OH		468 [382–567][26]		479 [457–501][26]		528 [454–617][25,26]
Stratospheric OH		46 [16–67][23,25,26]		67 [51–83][23,25,26]		51 [16–84][23,25,26]
Tropospheric Cl		25 [13–37][24]		25 [13–37][24]		25 [13–37][24]
Soils	21 [10–27][1,2,3]	28 [9–47][27,34,36]	27 [27–27][1]	28 [9–47][27,34,36]	32 [26–42][1,33,34,35,36]	28 [9–47][27,34,36]
Global						
Sum of sources	541 [500–592]	663 [536–789]	554 [529–596]	649 [511–812]	553 [526–569]	678 [542–852]
Sum of sinks	511 [460–559]	567 [420–718]	542 [518–579]	599 [530–668]	550 [514–560]	632 [592–785]
Imbalance (sources minus sinks)	30 [16–40]		12 [7–17]		3 [–4–19]	
Atmospheric growth rate	34		17		6	
Global top-down (year 2011)	2011 (AR5)[38]					
Burden (Tg CH_4)	4954±10					
Atmospheric loss (Tg CH_4 yr^{-1})	542±56					
Atmos. increase (Tg CH_4 yr^{-1})	14±3					
Total source (Tg CH_4 yr^{-1})	556±56					
Anthropogenic source (Tg CH_4 yr^{-1})	354±45					
Natural source (Tg CH_4 yr^{-1})	202±35					

References:

1 Bousquet et al. (2011)
2 Fung et al. (1991)
3 Hein et al. (1997)
4 Hodson et al. (2011)
5 Ringeval et al. (2011)
6 Bastviken et al. (2004)
7 Bastviken et al. (2011)
8 Walter et al. (2007)
9 Denman et al. (2007)
10 EPA (2010)

6

Table 6.8 References (continued)

[11] Hoelzemann et al. (2004)
[12] Ito and Penner (2004)
[13] van der Werf et al. (2010)
[14] Sanderson (1996)
[15] Sugimoto et al. (1998)
[16] Etiope et al. (2008)
[17] Rhee et al. (2009)
[18] Dickens (2003)
[19] Shakhova et al. (2010)
[20] EDGAR4-database (2009)
[21] Mieville et al. (2010)
[22] Schultz et al. (2007) (excluding biofuels)
[23] Neef et al. (2010)
[24] Allan et al. (2007)
[25] Williams et al. (2012b)
[26] Voulgarakis et al. (2013)
[27] Spahni et al. (2011)
[28] Chen and Prinn (2006)
[29] Pison et al. (2009)
[30] Dentener et al. (2005)
[31] EPA (2011a)
[32] van der Werf (2004)
[33] Bergamaschi et al. (2009)
[34] Curry (2007)
[35] Spahni et al. (2011)
[36] Ito and Inatomi (2012)
[37] Wiedinmyer et al. (2011)
[38] Andreae and Merlet (2001)
[39] Prather et al. (2012), updated to 2011 (Table 2.1) and used in Chapter 11 projections; uncertainties evaluated as 68% confidence intervals, see also Annex II.2.2 and II.4.2.

with anthropogenic emission inventories, which show more (EDGAR v4.2) or less (EPA, 2011a) rapidly increasing anthropogenic CH_4 emissions in the period 2000–2008. This is related to increased energy production in growing Asian economies (EDGAR, edgar.jrc.ec.europa.eu; EPA, http://www.epa.gov/nonco2/econ-inv/international.html). The atmospheric increase has continued after 2009, at a rate of 4 to 5 ppb yr^{-1} (Sussmann et al., 2012).

6.3.3.2 Methane Emissions

\The CH_4 growth rate results from the balance between emissions and sinks. Methane emissions around the globe are biogenic, thermogenic or pyrogenic in origin (Neef et al., 2010), and they can be the direct result of either human activities and/or natural processes (see Section 6.1.1.2 and Table 6.8). Biogenic sources are due to degradation of organic matter in anaerobic conditions (natural wetlands, ruminants, waste, landfills, rice paddies, fresh waters, termites). Thermogenic sources come from the slow transformation of organic matter into fossil fuels on geological time scales (natural gas, coal, oil). Pyrogenic sources are due to incomplete combustion of organic matter (biomass and biofuel burning). Some sources can eventually combine a biogenic and a thermogenic origin (e.g., natural geological sources such as oceanic seeps, mud volcanoes or hydrates). Each of these three types of emissions is characterized by ranges in its isotopic composition in^{13}C-CH_4: typically –55 to –70‰ for biogenic, –25 to –45‰ for thermogenic, and –13 to –25‰ for pyrogenic. These isotopic distinctions provide a basis for attempting to separate the relative contribution of different methane sources using the top-down approach (Bousquet et al., 2006; Neef et al., 2010; Monteil et al., 2011).

During the decade of the 2000s, natural sources of CH_4 account for 35 to 50% of the decadal mean global emissions (Table 6.8). The single most dominant CH_4 source of the global flux and interannual variability is CH_4 emissions from wetlands (177 to 284 Tg(CH_4) yr^{-1}). With *high confidence*, climate driven changes of emissions from wetlands are the main drivers of the global inter-annual variability of CH_4 emissions. The term 'wetlands' denotes here a variety of ecosystems emitting CH_4 in the tropics and the high latitudes: wet soils, swamps, bogs and peatlands. These emissions are highly sensitive to climate change and variability, as shown, for instance, from the high CH_4 growth rate in 2007–2008 that coincides with positive precipitation and temperature anomalies (Dlugokencky et al., 2009). Several process-based models of methane emissions from wetlands have been developed and improved since AR4 (Hodson et al., 2011; Ringeval et al., 2011; Spahni et al., 2011; Melton et al., 2013), yet the *confidence* in modeled wetland CH_4 emissions remains *low*, particularly because of limited observational data sets available for model calibration and evaluation. Spatial distribution and temporal variability of wetlands also remains highly unconstrained in spite the existence of some remote sensing products (Papa et al., 2010). It has been observed that wetland CH_4 emissions increase in response to elevated atmospheric CO_2 concentrations (van Groenigen et al., 2011). van Groenigen et al. attribute such an increase in CH_4 emissions from natural wetlands to increasing soil moisture due to the reduced plant demand for water under higher CO_2. However, the sign and magnitude of the CH_4 emission response to changes in temperature and precipitation vary among models but show, on average, a decrease of wetland area and CH_4 flux with increasing temperature, especially in the tropics, and a modest (~4%) increase of wetland area and CH_4 flux with increasing precipitation (Melton et al., 2013).

In AR4, natural geological sources were estimated between 4 and 19 Tg(CH_4) yr^{-1}. Since then, Etiope et al. (2008) provided improved emission estimates from terrestrial (13 to 29 Tg(CH_4) yr^{-1}) and marine (~20 Tg(CH_4) yr^{-1}) seepages, mud volcanoes (6 to 9 Tg(CH_4) yr^{-1}), hydrates (5 to 10 Tg(CH_4) yr^{-1}) and geothermal and volcanic areas (3 to 6 Tg(CH_4) yr^{-1}), which represent altogether between 42 and 64 Tg(CH_4) yr^{-1} (see Table 6.8 for full range of estimates). This contribution from natural, geological and partly fossil CH_4 is larger than in AR4 and consistent with a $^{14}CH_4$ reanalysis showing natural and anthropogenic fossil contributions to the global CH_4 budget to be around 30% (*medium confidence*) (Lassey et al., 2007) and not around 20% as previously estimated (e.g., AR4). However, such a large percentage was not confirmed by an analysis of the global atmospheric record of ethane (Simpson et al., 2012) which is co-emitted with geological CH_4.

Of the natural sources of CH_4, emissions from thawing permafrost and CH_4 hydrates in the northern circumpolar region will become potentially important in the 21st century because they could increase dramatically due to the rapid climate warming of the Arctic and the large carbon pools stored there (Tarnocai et al., 2009; Walter Anthony et al., 2012) (see Section 6.4.3.4). Hydrates are, however, estimated to represent only a very small emission, between 2 and 9 Tg(CH_4) yr^{-1} under the current time period (Table 6.8). Supersaturation of dissolved CH_4 at the bottom and surface waters in the East Siberian Arctic Shelf indicate some CH_4 activity across the region, with a net sea–air flux of 10.5 Tg(CH_4) yr^{-1} which is similar in magnitude to the flux for the entire ocean (Shakhova et al., 2010) but it is not possible to say whether this source has always been present or is a consequence of recent Arctic changes. The ebullition of CH_4 from decomposing, thawing lake sediments in north Siberia with an estimated flux of ~4 Tg(CH_4) yr^{-1} is another demonstration of the activity of this region and of its potential importance in the future (Walter et al., 2006; van Huissteden et al., 2011). The sum of all natural emission estimates other than wetlands is still very uncertain based on bottom-up studies [see Table 6.8, range of 238 to 484 Tg(CH_4) yr^{-1} for 2000–2009].

Pyrogenic sources of CH_4 (biomass burning in Table 6.8) are assessed to have a small contribution in the global flux for the 2000s (32 to 39 Tg(CH_4) yr^{-1}). Biomass burning of tropical and boreal forests (17 to 21 Tg(CH_4) yr^{-1}) play a much smaller role than wetlands in interannual variability of emissions, except during intensive fire periods (Langenfelds et al., 2002; Simpson et al., 2006). Only during the 1997–1998 record strong El Niño, burning of forests and peatland that took place in Indonesia and Malaysia, released ~12 Tg(CH_4) and contributed to the observed growth rate anomaly (Langenfelds et al., 2002; van der Werf et al., 2004). Other smaller fire CH_4 emissions positive anomalies were suggested over the northern mid-latitudes in 2002–2003, in particular over Eastern Siberia in 2003 (van der Werf et al., 2010) and Russia in 2010. Traditional biofuel burning is estimated to be a source of 14 to 17 Tg(CH_4) yr^{-1}(Andreae and Merlet, 2001; Yevich and Logan, 2003).

Keppler at al. (2006) reported that plants under aerobic conditions were able to emit CH_4, and thus potentially could constitute a large additional emission, which had not been previously considered in the global CH_4 budget. Later studies do not support plant emissions as a widespread mechanism (Dueck et al., 2007; Wang et al., 2008; Nisbet et al., 2009) or show small to negligible emissions in the context of the global CH_4 budget (Vigano et al., 2008; Nisbet et al., 2009; Bloom et al., 2010). Alternative mechanisms have been suggested to explain an apparent aerobic CH_4 production, which involve (1) adsorption and desorption (Kirschbaum and Walcroft, 2008; Nisbet et al., 2009), (2) degradation of organic matter under strong ultraviolet (UV) light (Dueck et al., 2007; Nisbet et al., 2009) and (3) methane in the groundwater emitted through internal air spaces in tree bodies (Terazawa et al., 2007). Overall, a significant emission of CH_4 by plants under aerobic conditions is *very unlikely*, and this source is not reported in Table 6.8.

Anthropogenic CH_4 sources are estimated to range between 50% and 65% of the global emissions for the 2000s (Table 6.8). They include rice paddies agriculture, ruminant animals, sewage and waste, landfills, and fossil fuel extraction, storage, transformation, transportation and use (coal mining, gas and oil industries). Anthropogenic sources are dominant over natural sources in top-down inversions (~65%) but they are of the same magnitude in bottom-up models and inventories (Table 6.8). Rice paddies emit between 33 to 40 Tg(CH_4) yr^{-1} and 90% of these emissions come from tropical Asia, with more than 50% from China and India (Yan et al., 2009). Ruminant livestock, such as cattle, sheep, goats, etc. produce CH_4 by food fermentation in their anoxic rumens with a total estimate of between 87 and 94 Tg(CH_4) yr^{-1}. Major regional contributions of this flux come from India, China, Brazil and the USA (EPA, 2006; Olivier and Janssens-Maenhout, 2012), EDGAR v4.2. India, with the world's largest livestock population emitted 11.8 Tg(CH_4) yr^{-1} in 2003, including emission from enteric fermentation (10.7 Tg(CH_4) yr^{-1}) and manure management (1.1 Tg(CH_4) yr^{-1}; Chhabra et al., 2013). Methanogenesis in landfills, livestock manure and waste waters produces between 67 and 90 Tg(CH_4) yr^{-1} due to anoxic conditions and a high availability of acetate, CO_2 and H_2. Loss of natural gas (~90% CH_4) is the largest contributor to fossil fuel related fugitive emissions, estimated between 85 and 105 Tg(CH_4) yr^{-1} in the USA (EPA, 2006; Olivier and Janssens-Maenhout, 2012), EDGAR v4.2.

6.3.3.3 Sinks of Atmospheric Methane

The main sink of atmospheric CH_4 is its oxidation by OH radicals, a chemical reaction that takes place mostly in the troposphere and stratosphere (Table 6.8). OH removes each year an amount of CH_4 equivalent to 90% of all surface emissions (Table 6.8), that is, 9% of the total burden of CH_4 in the atmosphere, which defines a partial atmospheric lifetime with respect to OH of 7 to 11 years for an atmospheric burden of 4800 Tg(CH_4) (4700 to 4900 TgCH_4 as computed by Atmospheric Chemistry and Climate Model Intercomparison Project (ACCMIP) atmospheric chemistry models in Voulgarakis et al. (2013), thus slightly different from Figure 6.2; see Section 8.2.3.3 for ACCMIP models). A recent estimate of the CH_4 lifetime is 9.1 ± 0.9 years (Prather et al., 2012). A small sink of atmospheric CH_4 is suspected, but still debated, in the marine boundary layer due to a chemical reaction with chlorine (Allan et al., 2007). Another small sink is the reaction of CH_4 with Cl radicals and O(1D) in the stratosphere (Shallcross et al., 2007; Neef et al., 2010). Finally, oxidation in upland soils (with oxygen) by methanotrophic bacterias removes about 9 to 47 Tg(CH_4) yr^{-1} (Curry, 2007; Dutaur and Verchot, 2007; Spahni et al., 2011; Ito and Inatomi, 2012).

There have been a number of published estimates of global OH concentrations and variations over the past decade (Prinn et al., 2001; Dentener et al., 2003; Bousquet et al., 2005; Prinn et al., 2005; Rigby et al., 2008; Montzka et al., 2011). The very short lifetime of OH makes it almost impossible to measure directly global OH concentrations in the atmosphere. Chemistry transport models (CTMs), chemistry climate models (CCMs) or proxy methods have to be used to obtain a global mean value and time variations. For the 2000s, CTMs and CCMs (Young et al., 2013) estimate a global chemical loss of methane due to OH of 604 Tg(CH_4) yr^{-1} (509 to 764 Tg(CH_4) yr^{-1}). This loss is larger, albeit compatible considering the large uncertainties, with a recent extensive analysis by Prather et al. (2012) inferring a global chemical loss of 554 ± 56 Tg(CH_4) yr^{-1}. Top-down inversions using methyl-chloroform (MCF) measurements to infer OH provide a smaller chemical loss of 518 Tg(CH_4) yr^{-1} with a more narrow range of 510 to 538 Tg(CH_4) yr^{-1} in the 2000s. However, inversion estimates probably do not account for all sources of uncertainties (Prather et al., 2012).

CCMs and CTMs simulate small interannual variations of OH radicals, typically of 1 to 3% (standard deviation over a decade) due to a high buffering of this radical by atmospheric photochemical reactions (Voulgarakis et al., 2013; Young et al., 2013). Atmospheric inversions show much larger variations for the 1980s and the 1990s (5 to 10%), because of their oversensitivity to uncertainties on MCF emissions, when measurements of this tracer are used to reconstruct OH (Montzka et al., 2011), although reduced variations are inferred after 1998 by Prinn et al. (2005). For the 2000s, the reduction of MCF in the atmosphere, due to the Montreal protocol (1987) and its further amendments, allows a consistent estimate of small OH variations between atmospheric inversions (<±5%) and CCMs/CTMs (<±3%). However, the very low atmospheric values reached by MCF (few ppt in 2010) impose the need to find another tracer to reconstruct global OH in the upcoming years. Finally, evidence for the role of changes in OH concentrations in explaining the increase in atmospheric methane since 2007 is variable, ranging from a significant contribution (Rigby et al., 2008) to only a small role (Bousquet et al., 2011).

6.3.3.4 Global Methane Budget for the 2000s

Based on the inversion of atmospheric measurements of CH_4 from surface stations, global CH_4 emissions for the 2000s are of 553 Tg(CH_4) yr^{-1}, with a range of 526 to 569 Tg(CH_4) yr^{-1} (Table 6.8). The total loss of atmospheric methane is of 550 Tg(CH_4) yr^{-1} with a range of 514 to 560 Tg(CH_4) yr^{-1}, determining a small imbalance of about 3 Tg(CH_4) yr^{-1}, in line with the small growth rate of 6 Tg(CH_4) yr^{-1} observed for the 2000s.

Based on bottom-up models and inventories, a larger global CH_4 emissions of 678 Tg(CH_4) yr^{-1} are found, mostly because of the still debated upward re-evaluation of geological (Etiope et al., 2008) and freshwater (Walter et al., 2007; Bastviken et al., 2011) emission sources. An averaged total loss of 632 Tg(CH_4) yr^{-1} is found, by an ensemble of Atmospheric Chemistry models (Lamarque et al., 2013) leading to an imbalance of about 45 Tg(CH_4) yr^{-1} during the 2000s, as compared to the observed mean growth rate of 6 Tg(CH_4) yr^{-1}(Table 6.8; Dlugokencky et al., 2011). There is no constraint that applies to the sum of emissions in the bottom-up approach, unlike for top-down inversions when these have constrained OH fields (e.g., from MCF). Therefore, top-down inversions can help constrain global CH_4 emissions in the global budget, although they do not resolve the same level of detail in the mix of sources than the bottom-up approaches, and thus provide more limited information about processes (Table 6.8).

6.3.4 Global Nitrogen Budgets and Global Nitrous Oxide Budget in the 1990s

The atmospheric abundance of N_2O has been increasing mainly as a result of agricultural intensification to meet the food demand for a growing human population. Use of synthetic fertiliser (primarily from the Haber–Bosch process) and manure applications increase the production of N_2O in soils and sediments, via nitrification and denitrification pathways, leading to increased N_2O emissions to the atmosphere. Increased emissions occur not only in agricultural fields, but also in aquatic systems after nitrogen leaching and runoff, and in natural soils and ocean surface waters as a result of atmospheric deposition of nitrogen originating from agriculture, fossil fuel combustion and industrial activities. Food production is *likely* responsible for 80% of the increase in atmospheric N_2O (Kroeze et al., 1999; Davidson, 2009; Williams and Crutzen, 2010; Syakila and Kroeze, 2011; Zaehle et al., 2011; Park et al., 2012), via the addition of nitrogen fertilisers. Global emissions of N_2O are difficult to estimate owing to heterogeneity in space and time. Table 6.9 presents global emissions based on upscaling of local flux measurements at the surface. Modelling of the atmospheric lifetime of N_2O and atmospheric inversions constrain global and regional N_2O budgets (Hirsch et al., 2006; Huang et al., 2008; Rhee et al., 2009; Prather et al., 2012), although there is uncertainty in these estimates because of uncertainty in the dominant loss term of N_2O, that is, the destruction of N_2O by photolysis and reaction with O(1D) in the stratosphere. The long atmospheric lifetime of N_2O (118 to 131 years, Volk et al., 1997; Hsu and Prather, 2010; Fleming et al., 2011; see Chapter 8) implies that it will take more than a century before atmospheric abundances stabilise after the stabilization of global emissions. This is of concern not only because of its contribution to the radiative forcing (see Glossary), but also because of the relative importance of N_2O and other GHGs in affecting the ozone layer (Ravishankara et al., 2009; Fleming et al., 2011).

Since AR4 (Table 6.9 for the 1990s), a number of studies allow us to update some of the N_2O emission estimates. First and most importantly, the IPCC Guidelines were revised in 2006 (De Klein et al., 2007) and in particular emission factors for estimating agricultural N_2O emissions. Applying these 2006 emission factors to global agricultural statistics results in higher direct emissions from agriculture (from fertilised soils and animal production) than in AR4, but into indirect emissions (associated with leaching and runoff of Nr resulting in N_2O emissions from groundwater, riparian zones and surface waters) that are considerably lower than reported in AR4 (Table 6.9). It should be noted that emissions of N_2O show large uncertainties when default emission factors are applied at the global scale (Crutzen et al., 2008; Davidson, 2009; Smith et al., 2012). Second, estimates of the anthropogenic source of N_2O from the open ocean have been made for the first time. These emissions result from atmospheric deposition of anthropogenic Nr (nitrogen oxides and ammonia/ammonium) (Duce et al., 2008; Suntharalingam et al., 2012). This anthropogenic ocean N_2O source was implicitly included as part of the natural ocean N_2O source in AR4, but is now given as a separate anthropogenic source of 0.2 (0.1 to 0.4) TgN yr^{-1} in Table 6.9. Finally, a first estimate of global N_2O uptake at the surface is now available (Syakila et al., 2010; Syakila and Kroeze, 2011), based on reviews of measurements of N_2O uptake in soils and sediments (Chapuis-Lardy et al., 2007; Kroeze et al., 2007). The uncertainty in this sink of N_2O is large. On the global scale, this surface sink is negligible, but at the local scale it may not be irrelevant.

6.3.4.1 Atmosphere Nitrous Oxide Burden and Growth Rate

The concentration of N_2O is currently 20% higher than pre-industrial levels (Figure 6.11; MacFarling-Meure et al., 2006). Figure 6.19 shows the annual growth rate of atmospheric N_2O estimated from direct measurements (National Oceanic and Atmospheric Administration – Global Monitoring Division (NOAA–GMD) network of surface stations). On decadal time scales, the concentration of N_2O has been increasing at a rate of 0.73 ± 0.03 ppb yr^{-1}. The interannual variability in mid- to high-latitude N_2O abundance in both the NH and SH was found to correlate with the strength of the stratospheric Brewer–Dobson circulation (Nevison et al., 2011). Variability in stratosphere to troposphere air mass exchange, coupled with the stratospheric N_2O sink is *likely* to be responsible for a fraction of the interannual variability in tropospheric N_2O, but the understanding of this process is poor (Huang et al., 2008). This removal process signal is obscured in the SH by the timing of oceanic thermal and biological ventilation signals (Nevison et al., 2011) and terrestrial sources (Ishijima et al., 2009). These two factors may thus also be important determinants of seasonal and interannual variability of N_2O in the atmosphere. Quantitative understanding of terrestrial N_2O emissions variability is poor, although emissions are known to be sensitive to soil water content (Ishijima et al., 2009). A first process model-based estimate suggests that the mainly climate-driven variability in the terrestrial source may account for only 0.07 ppb yr^{-1} variability in atmospheric N_2O growth rate, which would be difficult to detect in the observed growth rate (Zaehle et al., 2011).

Most N_2O is produced by biological (microbial) processes such as nitrification and denitrification in terrestrial and aquatic systems, including rivers, estuaries, coastal seas and the open ocean (Table 6.9; Freing et al., 2012). In general, more N_2O is formed when more reactive nitrogen is available. The production of N_2O shows large spatial and temporal variability. Emission estimates for tropical regions and for aquatic systems are relatively uncertain. Inverse modelling studies show that the errors in emissions are large, especially in (sub)-tropical regions (e.g., Hirsch et al., 2006; Huang et al., 2008). Emissions from rivers, estuaries and continental shelves have been the subject of debate for many years (Seitzinger and Kroeze, 1998; De Klein et al., 2007). Recent studies confirm that rivers can be important sources of N_2O, which could be a reason to reconsider recent estimates of aquatic N_2O emissions (Beaulieu et al., 2011; Rosamond et al., 2012).

Table 6.9 does not include the formation of atmospheric N_2O from abiotic decomposition of ammonium nitrate in the presence of light, appropriate relative humidity and a surface. This process recently has been proposed as a potentially important source of N_2O (Rubasinghege et al., 2011); however, a global estimate does not yet exist. Table 6.9 indicates that the global N_2O emissions in the mid-1990s amount to 17.5 (8.1 to 30.7) TgN (N_2O) yr^{-1}. The uncertainty range is consistent with that of atmospheric inversions studies (14.1 to 17.8) by Huang et al. (2008). The estimates of anthropogenic N_2O emissions of Table 6.9 are in line with the top-down estimates by Prather et al. (2012) of 6.5 ± 1.3 TgN (N_2O) yr^{-1}, and somewhat higher than their estimates for

Table 6.9 | Section 1 gives the global nitrogen budget (TgN yr^{-1}): (a) creation of reactive nitrogen, (b) emissions of NO_x, NH_3 in 2000s to atmosphere, (c) deposition of nitrogen to continents and oceans, (d) discharge of total nitrogen to coastal ocean and (e) conversion of Nr to N_2 by denitrification. Section 2 gives the N_2O budget for the year 2006, and for the 1990s compared to AR4. Unit: Tg(N_2O-N) yr^{-1}.

SECTION 1 (NO_y and NH_x)			
a. Conversion of N_2 to Nr	**2005**	**2005**	**References**
Anthropogenic sources			
Fossil fuel combustion	30 (27–33)		Fowler et al. (2013)
Haber–Bosch process			
Fertiliser	100 (95–100)		Galloway et al. (2008), Fowler et al. (2013)
Industrial feedstock	24 (22–26)		Galloway et al. (2008), Fowler et al. (2013)
Biological nitrogen fixation (BNF)	60 (50–70)		Herridge et al. (2008)
Anthropogenic total	**210**		
Natural sources			
BNF, terrestrial	58 (50–100)		Vitousek et al. (2013)
BNF, marine	160 (140–177)		Voss et al. (2013), Codispoti (2007)
Lightning	4 (3–5)		AR4
Natural total	**220**		
Total conversion of N_2 to reactive N	**440**		
b. Emissions to Atmosphere			
	NO_x	**NH_3**	
Fossil fuel combustion industrial processes	28.3	0.5	Dentener et al. (2006)
Agriculture	3.7	30.4	Dentener et al. (2006)
Biomass and biofuel burning	5.5	9.2	Dentener et al. (2006)
Anthropogenic total	**37.5**	**40.1**	
Natural sources			
Soils under natural vegetation	7.3 (5–8)	2.4 (1–10)	AR4
Oceans	—	8.2 (3.6)	AR4
Lightning	4 (3–5)	—	AR4
Natural total	**11.3**	**10.6**	AR4
Total sources	**48.8**	**50.7**	
c. Deposition from the Atmosphere			
	NO_y	**NH_x**	
Continents	27.1	36.1	Lamarque et al. (2010)
Oceans	19.8	17.0	Lamarque et al. (2010)
Total	**46.9**	**53.1**	
d. Discharge to Coastal Ocean			
Surface water N flux	45		Mayorga et al. (2010), Seitzinger et al. (2010)
e. Conversion of Nr to N_2 by Denitrification			
Continents	109 (101–118)		Bouwman et al. (2013)

(continued on next page)

Table 6.9 (continued)

SECTION 2 (N_2O)			
	AR5 (2006/2011)	AR5 (mid-1990s)	AR4 (1990s)
Anthropogenic sources			
Fossil fuel combustion and industrial processes	0.7 (0.2–1.8)[a]	0.7 (0.2–1.8)[a]	0.7 (0.2–1.8)
Agriculture	4.1 (1.7–4.8)[b]	3.7 (1.7–4.8) [b]	2.8(1.7–4.8)
Biomass and biofuel burning	0.7(0.2–1.0)[a]	0.7(0.2–1.0)[a]	0.7(0.2–1.0)
Human excreta	0.2 (0.1–0.3)[a]	0.2 (0.1–0.3)[a]	0.2 (0.1–0.3)
Rivers, estuaries, coastal zones	0.6 (0.1–2.9)[c]	0.6 (0.1–2.9)[c]	1.7(0.5–2.9)
Atmospheric deposition on land	0.4 (0.3–0.9)[d]	0.4 (0.3–0.9)[d]	0.6 (0.3–0.9)
Atmospheric deposition on ocean	0.2 (0.1–0.4)[e]	0.2 (0.1–0.4)[e]	—
Surface sink	–0.01 (0– -1)[f]	–0.01 (0– -1)[f]	—
Total anthropogenic sources	**6.9 (2.7–11.1)**	**6.5 (2.7–11.1)**	**6.7 (2.7–11.1)**
Natural sources[a]			
Soils under natural vegetation	6.6 (3.3–9.0)	6.6 (3.3–9.0)	6.6 (3.3–9.0)
Oceans	3.8(1.8–9.4)	3.8(1.8–9.4)	3.8(1.8–5.8)
Lightning	—	—	—
Atmospheric chemistry	0.6 (0.3–1.2)	0.6 (0.3–1.2)	0.6 (0.3–1.2)
Total natural sources	**11.0 (5.4–19.6)**	**11.0 (5.4–19.6)**	**11.0 (5.4–19.6)**
Total natural + anthropogenic sources	**17.9 (8.1–30.7)**	**17.5 (8.1–30.7)**	**17.7 (8.5–27.7)**
Stratospheric sink	**14.3 (4.3–27.2)[g]**		
Observed growth rate	**3.61 (3.5–3.8)[h]**		
Global top-down (year 2011)[i]			
Burden (Tg N)	**1553**		
Atmospheric Loss	**11.9±0.9**		
Atmospheric Increase	**4.0±0.5**		
Total Source	**15.8±1.0**		
Natural Source	**9.1±1.0**		
Anthropogenic Source	**6.7±1.3**		

Notes:

[a] All units for N_2O fluxes are in TgN (N_2O) yr^{-1} as in AR4 (not based on 2006 IPCC Guidelines). Lower end of range in the natural ocean from Rhee et al. (2009); higher end of the range from Bianchi et al. (2012) and Olivier and Janssens-Maenhout (2012); natural soils in line with Stocker et al. (2013).

[b] Direct soil emissions and emissions from animal production; calculated following 2006 IPCC Guidelines (Syakila and Kroeze, 2011); range from AR4 (Olivier and Janssens-Maenhout, 2012).

[c] Following 2006 IPCC Guidelines (Kroeze et al., 2010; Syakila and Kroeze, 2011). Higher end of range from AR4; lower end of range from 1996 IPCC Guidelines (Mosier et al., 1998). Note that a recent study indicates that emissions from rivers may be underestimated in the IPCC assessments (Beaulieu et al., 2011).

[d] Following 2006 IPCC Guidelines (Syakila and Kroeze, 2011).

[e] Suntharalingam et al. (2012).

[f] Syakila et al. (2010).

[g] The stratospheric sink regroups losses via photolysis and reaction with O(1D) that account for 90% and 10% of the sink, respectively (Minschwaner et al., 1993). The global magnitude of the stratospheric sink was adjusted in order to be equal to the difference between the total sources and the observed growth rate. This value falls within literature estimates (Volk et al., 1997).

[h] Data from Sections 6.1 and 6.3 (see Figure 6.4c). The range on the observed growth rate in this table is given by the 90% confidence interval of Figure 6.4c.

[i] Based on Prather et al. (2012), updated to 2011 (Table 2.1) and used in Chapter 11 projections; uncertainties evaluated as 68% confidence intervals, N_2O budget reduced based on recently published longer lifetimes of 131±10 yrs, see Annex II.2.3 and II.4.3.

natural (9.1 ± 1.3 TgN (N_2O) yr^{-1}) and total (15.7 ± 1.1 TgN (N_2O) yr^{-1}) emissions. Anthropogenic emissions have steadily increased over the last two decades and were 6.9 (2.7 to 11.1) TgN (N_2O) yr^{-1} in 2006, or 6% higher than the value in mid-1990s (Davidson, 2009; Zaehle et al., 2011) (see also Figure 6.4c). Overall, anthropogenic N_2O emissions are now a factor of 8 greater than their estimated level in 1900. These trends are consistent with observed increases in atmospheric N_2O (Syakila et al., 2010). Human activities strongly influence the source of N_2O, as nitrogen fertiliser used in agriculture is now the main source of nitrogen for nitrification and denitrification (Opdyke et al., 2009). Nitrogen stable isotope ratios confirm that fertilised soils are primarily responsible for the historic increase in N_2O (Röckmann and Levin, 2005; Sutka et al., 2006; Park et al., 2012).

6.3.4.2 Sensitivity of Nitrous Oxide Fluxes to Climate and Elevated Carbon Dioxide

Previous studies suggested a considerable positive feedback between N_2O and climate (Khalil and Rasmussen, 1989) supported by observed glacial–interglacial increases of ~70 ppb in atmospheric N_2O (Flückiger et al., 1999). Climate change influences marine and terrestrial N_2O sources, but their individual contribution and even the sign of their response to long-term climate variations are difficult to estimate (see Section 6.2). Simulations by terrestrial biosphere models suggest a moderate increase of global N_2O emissions with recent climate changes, related mainly to changes in land temperature (Zaehle and Dalmonech, 2011; Xu-Ri et al., 2012), thus suggesting a possible positive feedback to the climate system. Nonetheless, the recent change in atmospheric N_2O is largely dominated to anthropogenic reactive nitrogen (Nr) and industrial emissions (Holland et al., 2005; Davidson, 2009; Zaehle and Dalmonech, 2011). Stocker et al. (2013) have found, using a global coupled model of climate and biogeochemical cycles, that future climate change will amplify terrestrial N_2O emissions resulting from anthropogenic Nr additions, consistent with empirical understanding (Butterbach-Bahl and Dannenmann, 2011). This result suggests that the use of constant emission factors might underestimate future N_2O emission trajectories. Significant uncertainty remains in the N_2O–climate feedback from land ecosystems, given the poorly known response of emission processes to the changes in seasonal and frequency distribution of precipitation, and also because agricultural emissions themselves may also be sensitive to climate.

N_2O production will be affected by climate change through the effects on the microbial nitrification and denitrification processes (Barnard et al., 2005; Singh et al., 2010; Butterbach-Bahl and Dannenmann, 2011). Warming experiments tend to show enhanced N_2O emission (Lohila et al., 2010; Brown et al., 2011; Chantarel et al., 2011; Larsen et al., 2011). Elevated CO_2 predominantly increases N_2O emissions(van Groenigen et al., 2011); however, reductions have also been observed (Billings et al., 2002; Mosier et al., 2002), induced by changes in soil moisture, plant productivity and nitrogen uptake, as well as activity and composition of soil microbial and fungal communities (Barnard et al., 2005; Singh et al., 2010). The effect of interacting climate and atmospheric CO_2 change modulates and potentially dampens the individual responses to each driver (Brown et al., 2011). A terrestrial biosphere model that integrates the interacting effects of temperature, moisture and CO_2

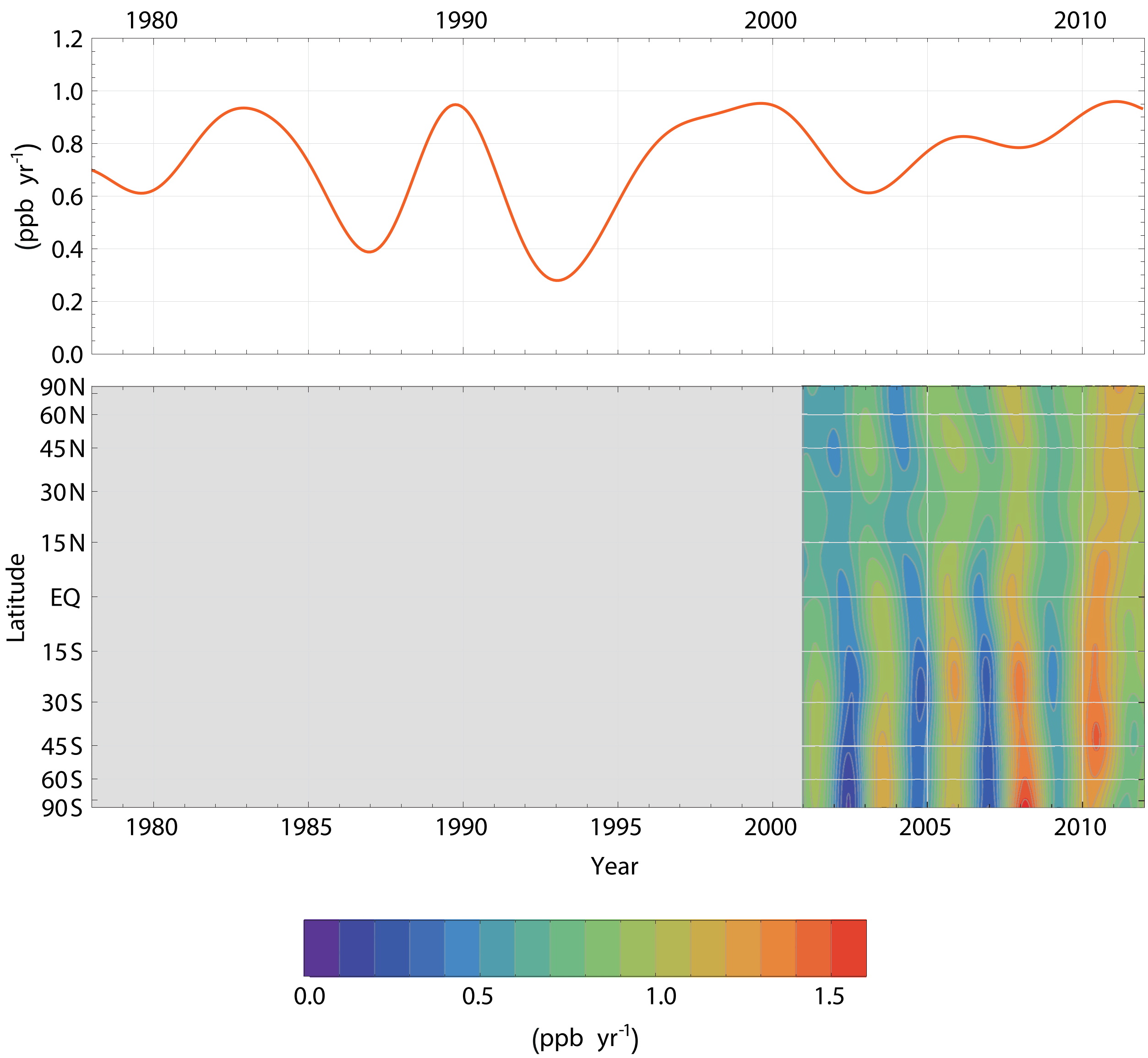

Figure 6.19 | (Top) Globally averaged growth rate of atmospheric N_2O in ppb yr^{-1} representative for the marine boundary layer. (Bottom) Atmospheric growth rate of N_2O as a function of latitude. Sufficient observations are available only since the year 2002. Observations from the National Oceanic and Atmospheric Administration–Earth System Research Laboratory (NOAA–ESRL) network (Masarie and Tans, 1995; Dlugokencky and Tans, 2013b).

changes is capable of qualitatively reproducing the observed sensitivities to these factors and their combinations (Xu-Ri et al., 2012). Thawing permafrost soils under particular hydrological settings may liberate reactive nitrogen and turn into significant sources of N_2O; however, the global significance of this source is not established (Elberling et al., 2010).

6.3.4.3 Global Nitrogen Budget

For base year 2010, anthropogenic activities created ~210 (190 to 230) TgN of reactive nitrogen Nr from N_2. This human-caused creation of reactive nitrogen in 2010 is at least 2 times larger than the rate of natural terrestrial creation of ~58 TgN (50 to 100 TgN yr^{-1}) (Table 6.9, Section 1a). Note that the estimate of natural terrestrial biological fixation (58 TgN yr^{-1}) is lower than former estimates (100 TgN yr^{-1}, Galloway et al., 2004), but the ranges overlap, 50 to 100 TgN yr^{-1}, vs. 90 to 120 TgN yr^{-1}, respectively). Of this created reactive nitrogen, NO_x and NH_3 emissions from anthropogenic sources are about fourfold greater than natural emissions (Table 6.9, Section 1b). A greater portion of the NH_3 emissions is deposited to the continents rather than to the oceans, relative to the deposition of NO_y, due to the longer atmospheric residence time of the latter. These deposition estimates are lower limits, as they do not include organic nitrogen species. New model and measurement information (Kanakidou et al., 2012) suggests that incomplete inclusion of emissions and atmospheric chemistry of reduced and oxidized organic nitrogen components in current models may lead to systematic underestimates of total global reactive nitrogen deposition by up to 35% (Table 6.9, Section 1c). Discharge of reactive nitrogen to the coastal oceans is ~45 TgN yr^{-1} (Table 6.9, Section 1d). Denitrification converts Nr back to atmospheric N_2. The current estimate for the production of atmospheric N_2 is 110 TgN yr^{-1} (Bouwman et al., 2013). Thus of the ~280 TgN yr^{-1} of Nr from anthropogenic and natural sources, ~40% gets converted to N_2 each year. The remaining 60% is stored in terrestrial ecosystems, transported by rivers and by atmospheric transport and deposition to the ocean, or emitted as N_2O (a small fraction of total Nr only despite the important forcing of increasing N_2O emissions for climate change). For the oceans, denitrification producing atmospheric N_2 is 200 to 400 TgN yr^{-1}, which is larger than the current uptake of atmospheric N_2 by ocean biological fixation of 140 to 177 TgN yr^{-1} (Table 6.9 Section 1e; Figure 6.4a).

6.4 Projections of Future Carbon and Other Biogeochemical Cycles

6.4.1 Introduction

In this section, we assess coupled model projections of changes in the evolution of CO_2, CH_4 and N_2O fluxes, and hence the role of carbon and other biogeochemical cycles in future climate under socioeconomic emission scenarios (see Box 6.4). AR4 reported how climate change can affect the natural carbon cycle in a way that could feed back onto climate itself. A comparison of 11 coupled climate–carbon cycle models of different complexity (Coupled Carbon Cycle Climate–Model Intercomparison Project (C4MIP); Friedlingstein et al., 2006) showed that all 11 models simulated a positive feedback. There is substantial quantitative uncertainty in future CO_2 and temperature, both across coupled carbon–climate models (Friedlingstein et al., 2006; Plattner et al., 2008) and within each model parametrizations (Falloon et al., 2011; Booth et al., 2012; Higgins and Harte, 2012). This uncertainty on the coupling between carbon cycle and climate is of comparable magnitude to the uncertainty caused by physical climate processes discussed in Chapter 12 of this Report (Denman et al., 2007; Gregory et al., 2009; Huntingford et al., 2009).

Other biogeochemical cycles and feedbacks play an important role in the future of the climate system, although the carbon cycle represents the strongest of these. Natural CH_4 emissions from wetland and fires are sensitive to climate change (Sections 6.2, 6.4.7 and 6.3.3.2). The fertilising effects of nitrogen deposition and rising CO_2 also affect CH_4 emissions by wetlands through increased plant productivity (Stocker et al., 2013). Changes in the nitrogen cycle, in addition to interactions with CO_2 sources and sinks, are *very likely* to affect the emissions of N_2O both on land and from the ocean (Sections 6.3.4.2 and 6.4.6) and potentially on the rate of CH_4 oxidation (Gärdenäs et al., 2011). A recent review highlighted the complexity of terrestrial biogeochemical feedbacks on climate change (Arneth et al., 2010) and used the methodology of Gregory et al. (2009) to express their magnitude in common units of W m^{-2} $°C^{-1}$ (Figure 6.20). A similar degree of complexity exists in the ocean and in interactions between land, atmosphere and ocean cycles. Many of these processes are not yet represented in coupled climate–biogeochemistry models. Leuzinger et al. (2011) observed a trend from manipulation experiments for higher-order interactions between feedbacks to reduce the magnitude of response. *Confidence* in the magnitude, and sometimes even the sign, of many of these feedbacks between climate and carbon and other biogeochemical cycles is *low*.

The response of land and ocean carbon storage to changes in climate, atmospheric CO_2 and other anthropogenic activities (e.g., land use change; Table 6.2) varies strongly on different time scales. This chapter has assessed carbon cycle changes across many time scales from millennial (see Section 6.2) to interannual and seasonal (see Section 6.3), and these are summarized in Table 6.10. A common result is that an increase in atmospheric CO_2 will *always* lead to an *increase* in land and ocean carbon storage, all other things being held constant. Cox et al. (2013) find an empirical relationship between short-term interannual variability and long-term land tropical carbon cycle sensitivity that may offer an observational constraint on the climate–carbon cycle response over the next century. Generally, however, changes in climate on different time scales do not lead to a consistent sign and magnitude of the response in carbon storage change owing to the many different mechanisms that operate. Thus, changes in carbon cycling on one time scale cannot be extrapolated to make projections on different time scales, but can provide valuable information on the processes at work and can be used to evaluate and improve models.

6.4.2 Carbon Cycle Feedbacks in Climate Modelling Intercomparison Project Phase 5 Models

6.4.2.1 Global Analysis

The carbon cycle response to future climate and CO_2 changes can be viewed as two strong and opposing feedbacks (Gregory et al., 2009).

The climate–carbon response (γ) determines changes in carbon storage due to changes in climate, and the concentration–carbon response (β) determines changes in storage due to elevated CO_2. Climate–carbon cycle feedback responses have been analyzed for eight CMIP5 ESMs that performed idealised simulations involving atmospheric CO_2 increasing at a prescribed rate of 1% yr^{-1} (Arora et al., 2013; Box 6.4). There is *high confidence* that increased atmospheric CO_2 will lead to increased land and ocean carbon uptake but by an uncertain amount. Models agree on the sign of land and ocean response to rising CO_2 but show only medium and low agreement for the magnitude of ocean and land carbon uptake respectively (Figure 6.21). Future climate change will decrease land and ocean carbon uptake compared to the case with constant climate (*medium confidence*). Models agree on the sign, globally, of land and ocean response to climate change but show low agreement on the magnitude of this response, especially for the land. Land and ocean carbon uptake may differ in sign between different regions and between models (Section 6.4.2.3). Inclusion of nitrogen cycle processes in two of the land carbon cycle model components out of these eight reduces the magnitude of the sensitivity to both CO_2 and climate (Section 6.4.6.3) and increases the spread across the CMIP5 ensemble. The CMIP5 spread in ocean sensitivity to CO_2 and climate appears reduced compared with C4MIP.

The role of the idealised experiment presented here is to study model processes and understand what causes the differences between models. Arora et al. (2013) assessed the global carbon budget from these idealised simulations and found that the CO_2 contribution to changes in land and ocean carbon storage sensitivity is typically four to five times larger than the sensitivity to climate across the CMIP5 ESMs. The land carbon-climate response (γ) is larger than the ocean carbon–climate

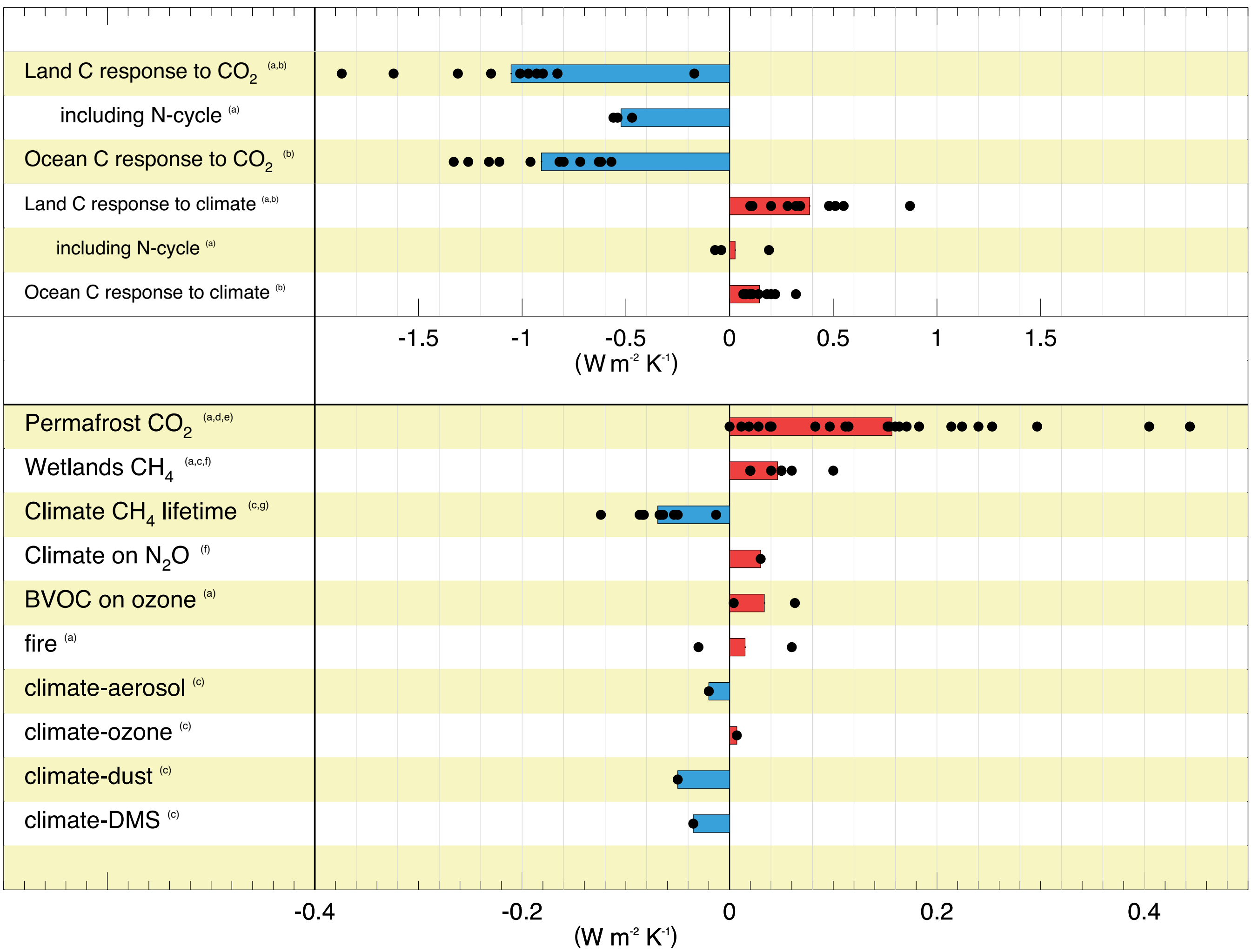

Figure 6.20 | A synthesis of the magnitude of biogeochemical feedbacks on climate. Gregory et al. (2009) proposed a framework for expressing non-climate feedbacks in common units (W m^{-2} °C^{-1}) with physical feedbacks, and Arneth et al. (2010) extended this beyond carbon cycle feedbacks to other terrestrial biogeochemical feedbacks. The figure shows the results compiled by Arneth et al. (2010), with ocean carbon feedbacks from the C4MIP coupled climate–carbon models used for AR4 also added. Some further biogeochemical feedbacks are also shown but this list is not exhaustive. Black dots represent single estimates, and coloured bars denote the simple mean of the dots with no weighting or assessment being made to likelihood of any single estimate. There is *low confidence* in the magnitude of the feedbacks in the lower portion of the figure, especially for those with few, or only one, dot. The role of nitrogen limitation on terrestrial carbon sinks is also shown—this is not a separate feedback, but rather a modulation to the climate–carbon and concentration–carbon feedbacks. These feedback metrics are also to be state or scenario dependent and so cannot always be compared like-for-like (see Section 6.4.2.2). Results have been compiled from (a) Arneth et al. (2010), (b) Friedlingstein et al. (2006), (c) Hadley Centre Global Environmental Model 2-Earth System (HadGEM2-ES, Collins et al., 2011) simulations, (d) Burke et al. (2013), (e) von Deimling et al. (2012), (f) Stocker et al. (2013), (g) Stevenson et al. (2006). Note the different *x*-axis scale for the lower portion of the figure.

Box 6.4 | Climate–Carbon Cycle Models and Experimental Design

What are coupled climate–carbon cycle models and why do we need them?
Atmosphere–Ocean General Circulation Models (AOGCMs; see Glossary) have long been used for making climate projections, and have formed the core of previous IPCC climate projection chapters (e.g., Meehl et al. (2007); see also Chapters 1, 9 and 12). For the 5th Coupled Model Intercomparison Project (CMIP5), many models now have an interactive carbon cycle. What exactly does this mean, how do they work and how does their use differ from previous climate models? AOGCMs typically represent the physical behaviour of the atmosphere and oceans but atmospheric composition, such as the amount of CO_2 in the atmosphere, is prescribed as an input to the model. This approach neglects the fact that changes in climate might affect the natural biogeochemical cycles, which control atmospheric composition, and so there is a need to represent these processes in climate projections.

At the core of coupled climate–carbon cycle models is the physical climate model, but additional components of land and ocean biogeochemistry respond to the changes in the climate conditions to influence in return the atmospheric CO_2 concentration. Input to themodels comes in the form of anthropogenic CO_2 emissions, which can increase the CO_2 and then the natural carbon cycle exchanges CO_2 between the atmosphere and land and ocean components. These 'climate–carbon cycle models' ('Earth System Models', ESMs; see Glossary) provide a predictive link between fossil fuel CO_2 emissions and future CO_2 concentrations and climate and are an important part of the CMIP5 experimental design (Hibbard et al., 2007; Taylor et al., 2012).

Apart from Earth System GCMs, so-called Earth System Models of Intermediate Complexity (EMICs) are often used to perform similar experiments (Claussen et al., 2002; Plattner et al., 2008). EMICs have reduced resolution or complexity but run much more quickly and can be used for longer experiments or large ensembles.

How are these models used?
The capability of ESMs to simulate carbon cycle processes and feedbacks, and in some models other biogeochemical cycles, allows for a greater range of quantities to be simulated such as changes in natural carbon stores, fluxes or ecosystem functioning. There may also be applications where it is desirable for a user to predefine the pathway of atmospheric CO_2 and prescribe it as a forcing to the ESMs. Thus, numerical simulations with ESM models can be either 'concentration driven' or 'emissions driven'.

Concentration-driven simulations follow the 'traditional' approach of prescribing the time-evolution of atmospheric CO_2 as an input to the model. This is shown schematically in Box 6.4 Figure 1 (left-hand side). Atmospheric CO_2 concentration is prescribed as input to the model from a given scenario and follows a predefined pathway regardless of changes in the climate or natural carbon cycle processes. The processes between the horizontal dashed lines in the figure represent the model components which are calculated during the concentration-driven simulation. Externally prescribed changes in atmospheric CO_2 concentration, which drive climate change, affect land and ocean carbon storage. By construction, changes in land and ocean storage, however, do not feed back on the atmospheric CO_2 concentration or on climate. The changes in natural carbon fluxes and stores are output by the model.

So-called 'compatible fossil fuel emissions', *E*, can be diagnosed afterwards from mass conservation by calculating the residual between the prescribed CO_2 pathway and the natural fluxes:

$$E = \left.\frac{dCO_2}{dt}\right|_{prescribed} + (\text{land\_carbon\_uptake} + \text{ocean\_carbon\_uptake}) \tag{6.1}$$

Land use change emissions cannot be diagnosed separately from a single simulation (see Section 6.4.3.2).

Emissions-driven simulations allow the full range of interactions in the models to operate and determine the evolution of atmospheric CO_2 and climate as an internal part of the simulation itself (Box 6.4, Figure 1, right-hand side). In this case emissions of CO_2 are the externally prescribed input to the model and the subsequent changes in atmospheric CO_2 concentration are simulated by it.

In *emissions-driven* experiments, the global atmospheric CO_2 growth rate is calculated within the model as a result of the net balance between the anthropogenic emissions, *E*, and natural fluxes:

$$\left.\frac{dCO_2}{dt}\right|_{simulated} = E - (\text{land\_carbon\_uptake} + \text{ocean\_carbon\_uptake}) \tag{6.2}$$

The effect of climate change on the natural carbon cycle will manifest itself either through changes in atmospheric CO_2 in the *emissions-driven* experiments or in the compatible emissions in the *concentration-driven* experiments.

(continued on next page)

Box 6.4 (continued)

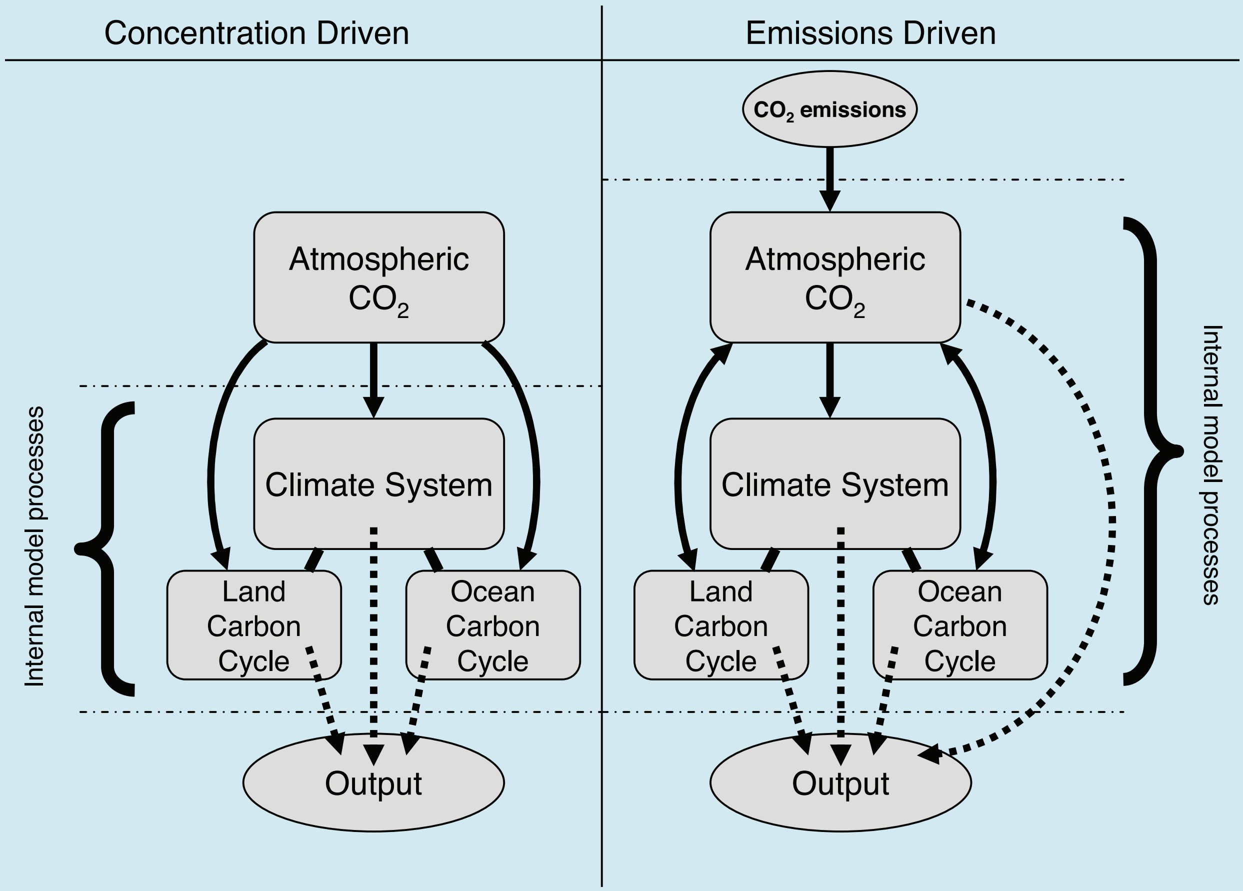

Box 6.4, Figure 1 | Schematic representation of carbon cycle numerical experimental design. Concentration-driven (left) and emissions-driven (right) simulation experiments make use of the same Earth System Models (ESMs), but configured differently. Concentration-driven simulations prescribe atmospheric CO_2 as a pre-defined input to the climate and carbon cycle model components, but their output does not affect the CO_2. Compatible emissions can be calculated from the output of the concentration-driven simulations. Emissions-driven simulations prescribe CO_2 emissions as the input and atmospheric CO_2 is an internally calculated element of the ESM.

Concentration-driven simulation experiments have the advantage that they can also be performed by GCMs without an interactive-carbon cycle and have been used extensively in previous assessments (e.g., Prentice et al., 2001). For this reason, most of the Representative Concentration Pathway (RCP) simulations (see Chapter 1) presented later in this chapter with carbon cycle models and in Chapter 12 with models that do not all have an interactive carbon cycle are performed this way. Emissions-driven simulations have the advantage of representing the full range of interactions in the coupled climate–carbon cycle models. The RCP8.5 pathway was repeated by many ESM models as an emissions-driven simulation (Chapter 12).

Feedback Analysis

The ESMs are made up of many 'components', corresponding to different processes or aspects of the system. To understand their behaviour, techniques have been applied to assess different aspects of the models' sensitivities (Friedlingstein et al., 2003, 2006; Arora et al., 2013). The two dominant emerging interactions are the sensitivity of the carbon cycle to changes in CO_2 and its sensitivity to changes in climate. These can be measured using two metrics: 'beta' (β) measures the strength of changes in carbon fluxes by land or ocean in response to changes in atmospheric CO_2; 'gamma' (γ) measures the strength of changes in carbon fluxes by land or ocean in response to changes in climate. These metrics can be calculated as cumulative changes in carbon storage (as in Friedlingstein et al., 2006) or instantaneous rates of change (Arora et al., 2013).

It is not possible to calculate these sensitivities in a single simulation, so it is necessary to perform 'decoupled' simulations in which some processes in the models are artificially disabled in order to be able to evaluate the changes in other processes. See Table 1 in Box 6.4.

(continued on next page)

Box 6.4 (continued)

A large positive value of β denotes that a model responds to increasing CO_2 by simulating large increases in natural carbon sinks. Negative values of γ denote that a model response to climate warming is to reduce CO_2 uptake from the atmosphere, while a positive value means warming acts to increase CO_2 uptake. β and γ values are not specified in a model, but are properties that emerge from the suite of complex processes represented in the model. The values of the β and γ metrics diagnosed from simulations can vary from place to place within the same model (see Section 6.4.2.3), although it is the average over the whole globe that determines the global extent of the climate–carbon cycle feedback.

Such an idealised analysis framework should be seen as a technique for assessing relative sensitivities of models and understanding their differences, rather than as absolute measures of invariant system properties. By design, these experiments exclude land use change.

The complex ESMs have new components and new processes beyond conventional AO GCMs and thus require additional evaluation to assess their ability to make climate projections. Evaluation of the carbon cycle model components of ESMs is presented in Section 6.3.2.5.6 for ocean carbon models and Section 6.3.2.6.6 for land carbon models. Evaluation of the fully coupled ESMs is presented in Chapter 9.

Box 6.4, Table 1 | Configurations of simulations designed for feedback analysis by allowing some carbon–climate interactions to operate but holding others constant. The curves denote whether increasing or constant CO_2 values are input to the radiation and carbon cycle model components. In a fully coupled simulation, the carbon cycle components of the models experience both changes in atmospheric CO_2 (see Box 6.3 on fertilisation) and changes in climate. In 'biogeochemically' coupled experiments, the atmospheric radiation experiences constant CO_2 (i.e., the radiative forcing of increased CO_2 is not activated in the simulation) whereas the carbon cycle model components experience increasing CO_2. This experiment quantifies the strength of the effect of rising CO_2 concentration alone on the carbon cycle (β). In a radiatively coupled experiment, the climate model's radiation scheme experiences an increase in the radiative forcing of CO_2 (and hence produces a change in climate) but CO_2 concentration is kept fixed to pre-industrial value as input to the carbon cycle model components. This simulation quantifies the effect of climate change alone on the carbon cycle (γ).

	CO_2 input to radiation scheme	CO_2 input to carbon-cycle scheme	Reason
Fully coupled	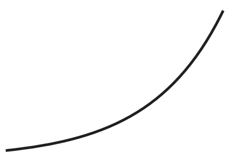	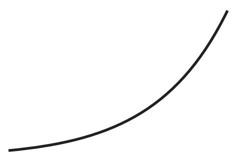	Simulates the fully coupled system
'Biogeochemically' coupled 'esmFixClim'		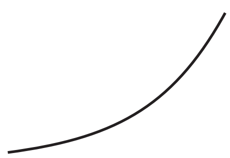	Isolates the carbon-cycle response to CO_2 (β) for land and oceans
Radiatively coupled 'esmFdbk'	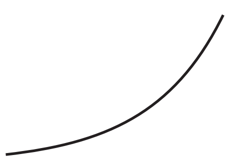		Isolates carbon-cycle response to climate change (γ) for land and for oceans

response in all models. Although land and ocean contribute equally to the total carbon–concentration response (β), the model spread in the land response is greater than for the ocean.

6.4.2.2 Scenario Dependence of Feedbacks

The values of carbon-cycle feedback metrics can vary markedly for different scenarios and as such cannot be used to compare model simulations over different time periods, nor to inter-compare model simulations with different scenarios (Arora et al., 2013). Gregory et al. (2009) demonstrated how sensitive the feedback metrics are to the rate of change of CO_2 for two models: faster rates of CO_2 increase lead to reduced β values as the carbon uptake (especially in the ocean) lags further behind the forcing. γ is much less sensitive to the scenario, as both global temperature and carbon uptake lag the forcing.

6.4.2.3 Regional Feedback Analysis

The linear feedback analysis with the β and γ metrics of Friedlingstein et al. (2006) has been applied at the regional scale to future carbon uptake by Roy et al. (2011) and Yoshikawa et al. (2008). Figure 6.22 shows this analysis extended to land and ocean points for the CMIP5 models under the 1% yr^{-1} CO_2 simulations.

6.4.2.3.1 Regional ocean response

Increased CO_2 is projected by the CMIP5 models to increase oceanic CO_2 sinks almost everywhere (positive β) (*high confidence*) with the exception of some very limited areas (Figure 6.22). The spatial distribution of the CO_2 ocean response, β_o, is consistent between the models and with the Roy et al. (2011) analysis. On average, the regions with

Table 6.10 | Comparison of the sign and magnitude of changes in carbon storage (PgC) by land and ocean over different time scales. These changes are shown as approximate numbers to allow a comparison across time scales. For more details see the indicated chapter section. An indication, where known, of what causes these changes (climate, CO_2, land use change) is also given with an indication of the sign: '+' means that an increase in CO_2 or global-mean temperature is associated with an increase in carbon storage (positive β or γ; see Section 6.4.2), and a '–' means an increase in CO_2 or global-mean temperature is associated with a decrease in carbon storage (negative β or γ). The processes that operate to drive these changes can vary markedly, for example, from seasonal phenology of vegetation to long-term changes in ice sheet cover or ocean circulation impacting carbon reservoirs. Some of these processes are 'reversible' in the context that they can increase and decrease cyclically, whereas some are 'irreversible' in the context that changes in one sense might be much longer than in the opposite direction.

Time Period	Duration	Land			Ocean		Section
		Climate	CO_2	Land Use	Climate	CO_2	
Seasonal cycle	Weeks to months	3–8[a]			2	1	6.3.2.5.1
		+				+	
Interannual variability	Months to years	2–4[b]			1	0.2	6.3.2.5.4
		–			+	+	
Historical (1750–Present)	Decades to centuries	150[c]		–180	2	155	6.3.2.5.3, Table 6.1
		–	+		?	+	
21st Century	Decades to centuries	100–400[d]		–100 to +100[e]	100–600[d]		6.4.3
		–	+		–	+	
Little Ice Age (LIA) [f]	Century	+5		+2 to +30			6.2.3
		–	+				
Holocene	10 kyr	+300		–50 to –150	+270 to –220[g]		6.2.2
		+	+				
Last Glacial Maximum/ glacial cycles	>10 kyr	+300 to +1000[h]			–500 to –1200[h]		6.2.1
		+	+		–	+	
Pulse [i], 100 PgC	1 kyr	+0 to +35		n/a	+48 to +75		6.2.2
			+		–	+	

Notes:

[a] Dominated by northern mid to high latitudes.

[b] Dominated by the tropics.

[c] 'Residual land sink', Table 6.1.

[d] Varies widely according to scenario. Climate effect estimated separately for RCP4.5 as –157 PgC (combined land and ocean), but not for other scenarios.

[e] Future scenarios may increase or decrease area of anthropogenic land use.

[f] Little Ice Age, 1500–1750.

[g] Shown here are two competing drivers of Holocene ocean carbon changes: carbonate accumulation on shelves (coral growth) and carbonate compensation to pre-Holocene changes. These are discussed in Section 6.2.2.

[h] Defined as positive if increasing from LGM to present, negative if decreasing.

[i] Idealised simulations with models to assess the response of the global carbon cycle to a sudden release of 100 PgC.

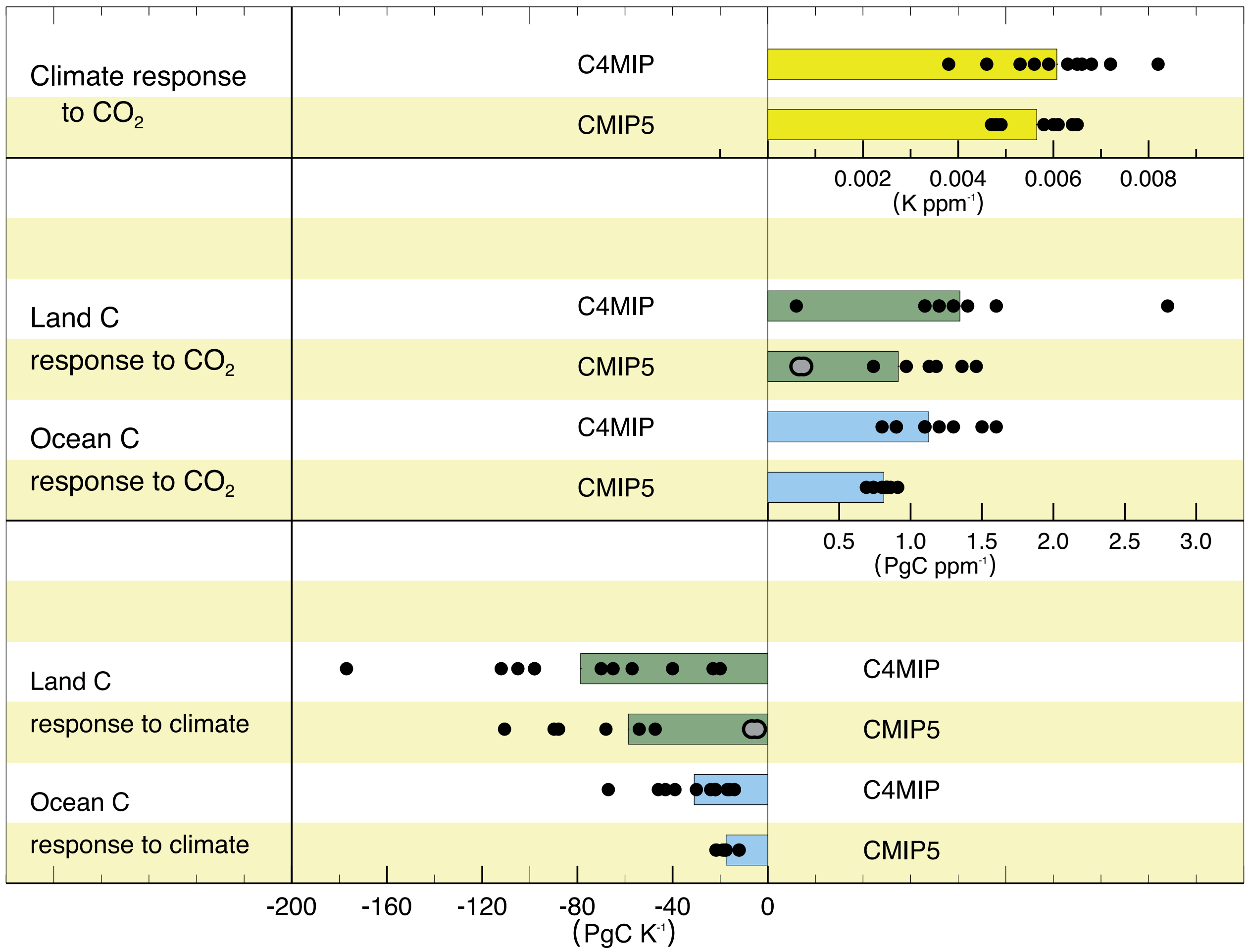

Figure 6.21 | Comparison of carbon cycle feedback metrics between the C4MIP ensemble of seven GCMs and four EMICs under the Special Report on Emission Scenario-A2 (SRES-A2) (Friedlingstein et al., 2006) and the eight CMIP5 models (Arora et al., 2013) under the 140-year 1% CO_2 increase per year scenario. Black dots represent a single model simulation and coloured bars the mean of the multi-model results; grey dots are used for models with a coupled terrestrial nitrogen cycle. The comparison with C4MIP is for context, but these metrics are known to be variable across different scenarios and rates of change (see Section 6.4.2.2). Some of the CMIP5 models are derived from models that contributed to C4MIP and some are new to this analysis. Table 6.11 lists the main attributes of each CMIP5 model used in this analysis. The SRES A2 scenario is closer in rate of change to a 0.5% yr^{-1} scenario and as such it should be expected that the CMIP5 γ terms are comparable, but the β terms are *likely* to be around 20% smaller for CMIP5 than for C4MIP due to lags in the ability of the land and ocean to respond to higher rates of CO_2 increase (Gregory et al., 2009). This dependence on scenario (Section 6.4.2.2) reduces confidence in any quantitative statements of how CMIP5 carbon cycle feedbacks differ from C4MIP. CMIP5 models used: Max Planck Institute–Earth System Model–Low Resolution (MPI–ESM–LR), Beijing Climate Center–Climate System Model 1 (BCC–CSM1), Hadley Centre Global Environmental Model 2–Earth System (HadGEM2–ES), Institute Pierre Simon Laplace–Coupled Model 5A–Low Resolution (IPSL–CM5A–LR), Canadian Earth System Model 2 (CanESM2), Norwegian Earth System Model– intermediate resolution with carbon cycle (NorESM–ME), Community Earth System Model 1–Biogeochemical (CESM1–BGC), Model for Interdisciplinary Research On Climate–Earth System Model (MIROC–ESM).

the strongest increase of oceanic CO_2 sinks in response to higher atmospheric CO_2 are the North Atlantic and the Southern Oceans. The magnitude and distribution of β_o in the ocean closely resemble the distribution of historical anthropogenic CO_2 flux from inversion studies and forward modelling studies (Gruber et al., 2009), with the dominant anthropogenic CO_2 uptake in the Southern Ocean (Section 6.3.2.5).

Climate warming is projected by the CMIP5 models to reduce oceanic carbon uptake in most oceanic regions (negative γ) (*medium confidence*) consistent with the Roy et al. (2011) analysis (Figure 6.22). This sensitivity of ocean CO_2 sinks to climate, γ_o, is mostly negative (i.e., a reduced regional ocean CO_2 sink in response to climate change) but with regions of positive values in the Arctic, the Antarctic and in the equatorial Pacific (i.e., climate change increases ocean CO_2 sink in these regions). The North Atlantic Ocean and the mid-latitude Southern Ocean have the largest negative γ_o values. Reduced CO_2 uptake in response to climate change in the sub-polar Southern Ocean and the tropical regions has been attributed to warming induced decreased CO_2 solubility, reduced CO_2 uptake in the mid latitudes to decreased CO_2 solubility and decreased water mass formation which reduces the absorption of anthropogenic CO_2 in intermediate and deep waters (Roy et al., 2011). Increased uptake in the Arctic Ocean and the polar Southern Ocean is partly associated with a reduction in the fractional sea ice coverage (Roy et al., 2011).

6.4.2.3.2 Regional land response

Increased CO_2 is projected by the CMIP5 models to increase land CO_2 sinks everywhere (positive β) (*medium confidence*). This response, β_L, has the largest values over tropical land, in humid rather than arid

Table 6.11 | CMIP5 model descriptions in terms of carbon cycle attributes and processes.

Model	Modelling Centre	Atmos Resolution	Ocean Resolution	Land-Carbon						Ocean Carbon			Reference
				Model Name	Dynamic Vegetation Cover?	No. of PFTs	Incl. LUC?	Nitrogen-Cycle	Fire	Model Name	No. of Plankton Types	Micronutrients?	
BCC-CSM1.1	BCC	≈2.8°, L26	0.3–1°, L40	BCC_AVIM1.0	N	15		N	N	OCMIP2	n/a	n/a	Wu et al. (2013)
CanESM2	CCCma	T63, L35	1.41° × 0.94°, L40	CTEM	N	9	Y	N	N	CMOC	1	N	Arora et al. (2011)
CESM1-BGC	NSF-DOE-NCAR	FV 0.9 × 1.25	1°	CLM4	N	15	Y	Y	Y	BEC	4	Y	Long et al. (2013)
GFDL-ESM2G	NOAA GFDL	2 × 2.5°, L24	1°, tri-polar, 1/3° at equator, L63.	LM3	Y	5	Y	N	Y	TOPAZ2	6	y	Dunne et al. (2012); Dunne et al. (2013)
GFDL-ESM2M	NOAA GFDL	2 × 2.5°, L24	1°, tri-polar, 1/3° at equator, L50.	LM3	Y	5	Y	N	Y	TOPAZ2	6	y	Dunne et al. (2012); Dunne et al. (2013)
HadGEM2-ES	MOHC	N96 (~ 1.6°), L38	1°, 1/3 ° at equator, L40	JULES	Y	5	Y	N	N	Diat-HadOCC	3	Y	Collins et al. (2011); Jones et al. (2011)
INMCM4	INM												
IPSL-CM5A-LR	IPSL	3.75 × 1.9 , L39	Zonal 2°, Meridional 2°–0.5° L31	ORCHIDEE	N	13	Y	N	Y	PISCES	2	Y	Dufresne et al. (2013)
MIROC-ESM	MIROC	T42, L80	Zonal: 1.4°, Meridional: 0.5–1.7°, Vertical: L43+BBL1	SEIB-DGVM	Y	13	Y	N	N	NPZD (Oschlies, 2001)	2 (Phytoplankton and Zoolo-plankton)	N	Watanabe et al. (2011)
MPI-ESM-LR	MPI-M	T63 (~ 1.9°), L47	ca.1.5°, L47	JSBACH	Y	12 (8 natural)	Y	N	Y	HAMOCC	2	Y	Raddatz et al. (2007), Brovkin et al. (2009), Maier-Reimer et al. (2005)
NorESM-ME	NCC	1.9 × 2.5°, L26	1°, L53	CLM4	N	16	Y	Y	Y	HAMOCC	2	N	Iversen et al. (2013)

6

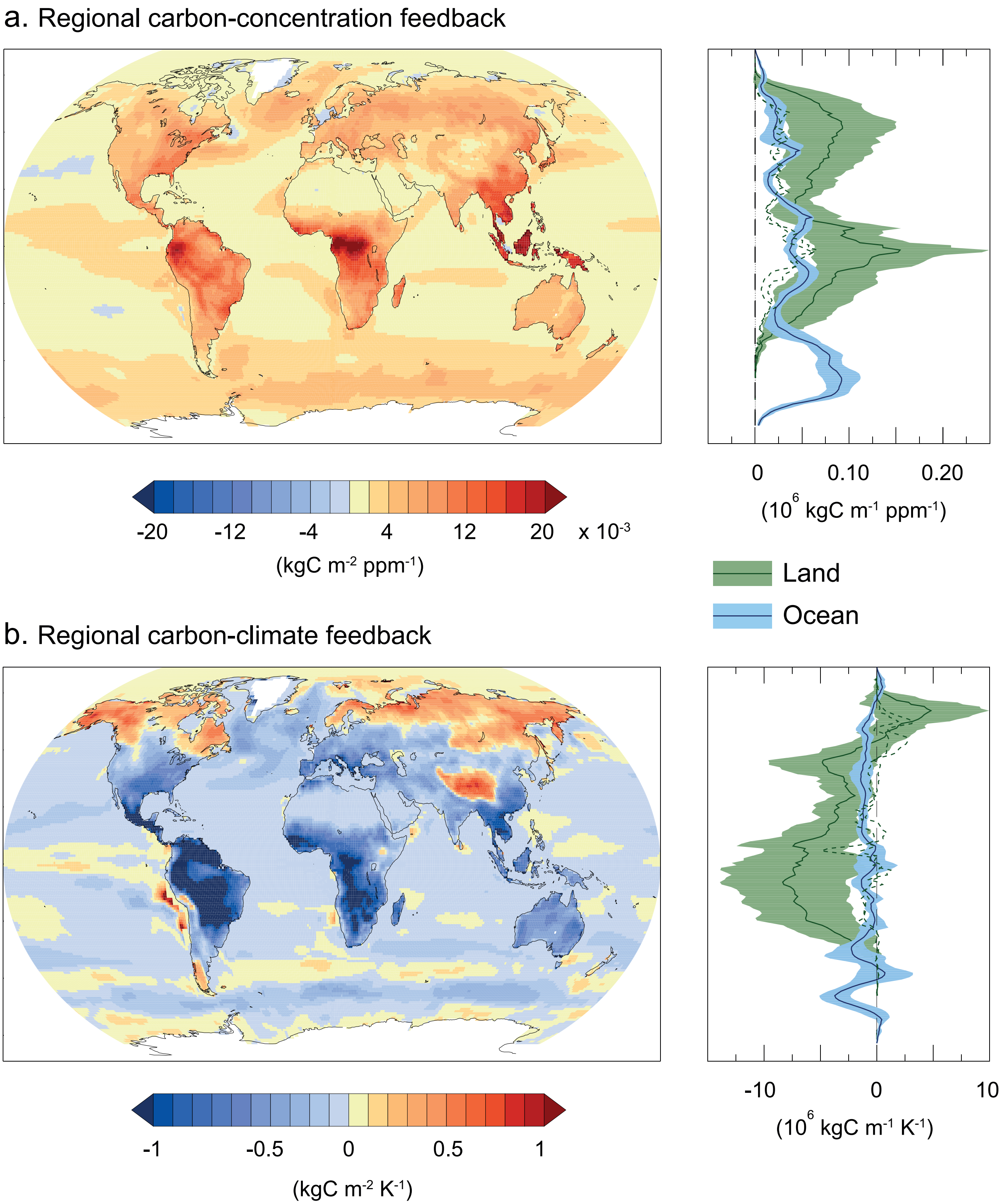

Figure 6.22 | The spatial distributions of multi-model-mean land and ocean β and γ for seven CMIP5 models using the *concentration-driven* idealised 1% yr^{-1} CO_2 simulations. For land and ocean, β and γ are defined from changes in terrestrial carbon storage and changes in air–sea integrated fluxes respectively, from 1 × CO_2 to 4 × CO_2, relative to global (not local) CO_2 and temperature change. In the zonal mean plots, the solid lines show the multi-model mean and shaded areas denote ±1 standard deviation. Models used: Beijing Climate Center–Climate System Model 1 (BCC–CSM1), Canadian Earth System Model 2 (CanESM2), Community Earth System Model 1–Biogeochemical (CESM1–BGC), Hadley Centre Global Environmental Model 2–Earth System (HadGEM2–ES), Institute Pierre Simon Laplace– Coupled Model 5A–Low Resolution (IPSL–CM5A-LR), Max Planck Institute–Earth System Model–Low Resolution (MPI–ESM–LR), Norwegian Earth System Model 1 (Emissions capable) (NorESM1–ME). The dashed lines show the models that include a land carbon component with an explicit representation of nitrogen cycle processes (CESM1-BGC, NorESM1-ME).

regions, associated with enhanced carbon uptake in forested areas of already high biomass. In the zonal totals, there is a secondary peak of high β_L values over NH temperate and boreal ecosystems, partly due to a greater land area there but also coincident with large areas of forest. Models agree on the sign of response but have low agreement on the magnitude.

The climate effect alone is projected by the CMIP5 models to reduce land CO_2 sinks in tropics and mid latitudes (negative γ) (*medium confidence*). CMIP5 models show medium agreement that warming may increase land carbon uptake in high latitudes but none of these models include representation of permafrost carbon pools which are projected to decrease in warmer conditions (Section 6.4.3.3); therefore *confidence* is *low* regarding the sign and magnitude of future high-latitude land carbon response to climate change. Matthews et al. (2005) showed that vegetation productivity is the major cause of C4MIP model spread, but this manifests itself as changes in soil organic matter (Jones and Falloon, 2009).

6.4.3 Implications of the Future Projections for the Carbon Cycle and Compatible Emissions

6.4.3.1 The RCP Future Carbon Dioxide Concentration and Emissions Scenarios

The CMIP5 simulations include four future scenarios referred to as Representative Concentration Pathways (RCPs; see Glossary) (Moss et al., 2010): RCP2.6, RCP4.5, RCP6.0, RCP8.5 (see Chapter 1). These future scenarios include CO_2 concentration and emissions, and have been generated by four Integrated Assessment Models (IAMs) and are labelled according to the approximate global radiative forcing level at 2100. These scenarios are described in more detail in Chapter 1 (Box 1.1) and Section 12.3 and also documented in Annex II.

van Vuuren et al. (2011) showed that the basic climate and carbon cycle responses of IAMs is generally consistent with the spread of climate and carbon cycle responses from ESMs. For the physical and biogeochemical components of the RCP scenarios 4.5, 6.0 and 8.5, the underlying IAMs are closely related. Only the Integrated Model to Assess the Global Environment (IMAGE) IAM, which created RCP2.6, differs markedly by using a more sophisticated carbon cycle sub-model for land and ocean. The Model for the Assessment of Greenhouse-gas Induced Climate Change 6 (MAGICC6) simple climate model was subsequently used to generate the CO_2 pathway for all four RCP scenarios using the CO_2 emissions output by the four IAMs (Meinshausen et al., 2011).

6.4.3.2 Land Use Changes in Future Scenarios

ESMs and IAMs use a diversity of approaches for representing land use changes, including different land use classifications, parameter settings, and geographical scales. To implement land use change in a consistent manner across ESMs, a 'harmonized' set of annual gridded land use change during the period 1500–2100 was developed for input to the CMIP5 ESMs (Hurtt et al., 2011).

Not all the CMIP5 ESMs used the full range of information available from the land use change scenarios, such as wood harvest projections or sub-grid scale shifting cultivation. Sensitivity studies indicated that these processes, along with the start date of the simulation, all strongly affect estimated carbon fluxes (Hurtt et al., 2011; Sentman et al., 2011).

Land use has been in the past and will be in the future a significant driver of forest land cover change and terrestrial carbon storage. Land use trajectories in the RCPs show very distinct trends and cover a wide range of projections. These land use trajectories are very sensitive to assumptions made by each individual IAM regarding the amount of land needed for food production (Figure 6.23). The area of cropland and pasture increases in RCP8.5 with the Model for Energy Supply Strategy Alternatives and their General Environmental Impact (MESSAGE) IAM model, mostly driven by an increasing global population, but cropland area also increases in the RCP2.6 with the IMAGE IAM model, as a result of bio-energy production and increased food demand as well. RCP6 with the AIM model shows an expansion of cropland but a decline in pasture land. RCP4.5 with the Global Change Assessment Model (GCAM) IAM is the only scenario to show a decrease in global cropland. Several studies (Wise et al., 2009; Thomson et al., 2010; Tilman et al., 2011) highlight the large sensitivity of future land use requirements to assumptions such as increases in crop yield, changes in diet, or how agricultural technology and intensification is applied.

Within the IAMs, land use change is translated into land use CO_2 emissions as shown in Figure 6.23(b). Cumulative emissions for the 21st century (Figure 6.23c) vary markedly across RCPs, with increasing cropland and pastureland areas in RCP2.6 and RCP8.5 giving rise to the highest emissions from land use change, RCP4.5 to intermediate emissions and RCP6.0 to close to zero net emissions. All scenarios suggest that 21st century land use emissions will be less than half of those from 1850 to the present day as rate of change of land conversion stabilises in future.

The adoption of widely differing approaches among ESMs for the treatment and diagnosis of land use and land cover change (LULCC) processes in terrestrial carbon cycle models leads to substantial between-model variation in the simulated impact on land carbon stocks. It is not yet possible to fully quantify LULCC fluxes from the CMIP5 model simulations. The harmonization process applied to LULCC data sets for CMIP5 has been an important step toward consistency among IAMs; however, among ESMs, and between IAMs and ESMs, assignment of meaningful uncertainty ranges to present-day and future LULCC fluxes and states remains a critical knowledge gap with implications for compatible emissions to achieve CO_2 pathways (Section 6.4.3.3; Jones et al., 2013).

6.4.3.3 Projections of Future Carbon Cycle Response by Earth System Models Under the Representative Concentration Pathway Scenarios

Simulated changes in land and ocean carbon uptake and storage under the four RCP scenarios are presented here using results from CMIP5 ESMs concentration-driven simulations (see Box 6.4). The implications of these changes on atmospheric CO_2 and climate as simulated by CMIP5 emissions-driven simulations are presented in Chapter 12.

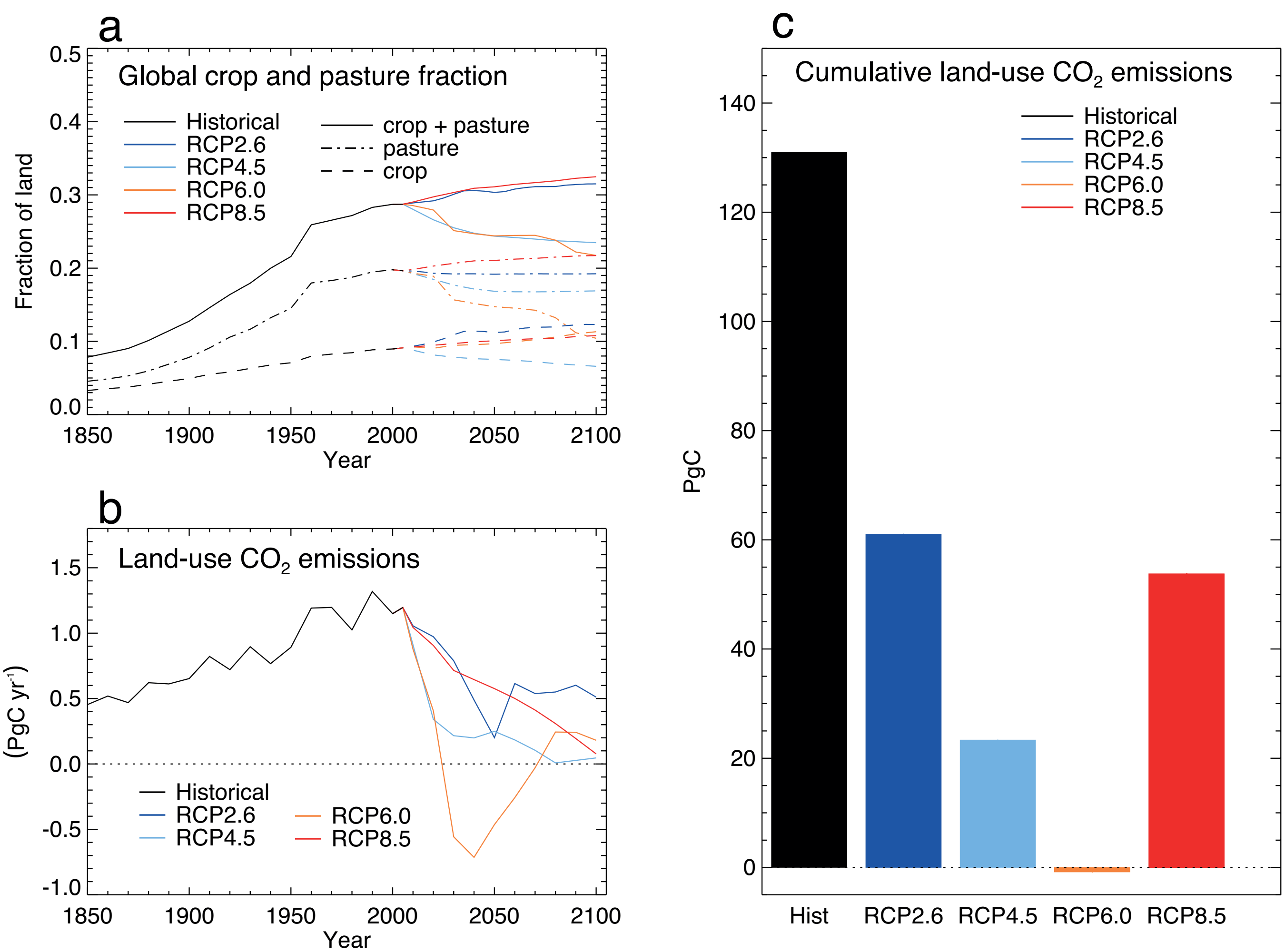

Figure 6.23 | Land use trends and CO_2 emissions according to the four different integrated assessment models (IAMs) used to define the RCP scenarios. Global changes in croplands and pasture from the historical record and the RCP scenarios (top left), and associated annual land use emissions of CO_2 (bottom left). Bars (right panel) show cumulative land use emissions for the historical period (defined here as 1850–2005) and the four RCP scenarios from 2006 to 2100.

The results of the *concentration-driven* CMIP5 ESMs simulations show medium agreement on the magnitude of cumulative ocean carbon uptake from 1850 to 2005 (Figure 6.24a): average 127 ± 28 PgC (1 standard deviation). The models show low agreement on the sign and magnitude of changes in land carbon storage (Figure 6.24a): average 2 ± 74 PgC (1 standard deviation). These central estimates are very close to observational estimates of 125 ± 25 PgC for the ocean and –5 ± 40 PgC for the net cumulative land–atmosphere flux respectively (see Table 6.12), but show a large spread across models. With *very high confidence*, for all four RCP scenarios, all models project continued ocean uptake throughout the 21st century, with higher uptake corresponding to higher concentration pathways. For RCP4.5, all the models also project an increase in land carbon uptake, but for RCP2.6, RCP6.0 and RCP8.5 a minority of models (4 out of 11 for RCP2.6, 1 out of 8 for RCP6.0 and 4 out of 15 for RCP8.5; Jones et al., 2013) project a decrease in land carbon storage at 2100 relative to 2005. Model spread in land carbon projections is much greater than model spread in ocean carbon projections, at least in part due to different treatment of land use change. Decade mean land and ocean fluxes are documented in Annex II, Table AII.3.1a, b. Important processes missing from many or all CMIP5 land carbon cycles include the role of nutrient cycles, permafrost, fire and ecosystem acclimation to changing climate. For this reason we assign *low confidence* to quantitative projections of future land uptake.

The *concentration-driven* ESM simulations can be used to quantify the compatible fossil fuel emissions required to follow the four RCP CO_2 pathways (Jones et al., 2013; see Box 6.4, Figure 6.25, Table 6.12, Annex II, Table AII.2.1a). There is significant spread between ESMs, but general consistency between ESMs and compatible emissions estimated by IAMs to define each RCP scenario. However, for RCP8.5 on average, the CMIP5 models project lower compatible emissions than the MESSAGE IAM. The IMAGE IAM predicts that global negative emissions are required to achieve the RCP2.6 decline in radiative forcing from 3 W m^{-2} to 2.6 W m^{-2} by 2100. All models agree that strong emissions reductions are required to achieve this after about 2020 (Jones et al., 2013). An average emission reduction of 50% (range 14 to 96%) is required by 2050 relative to 1990 levels. There is disagreement between those ESMs that performed this simulation over the necessity for global emissions in the RCP2.6 to become negative by

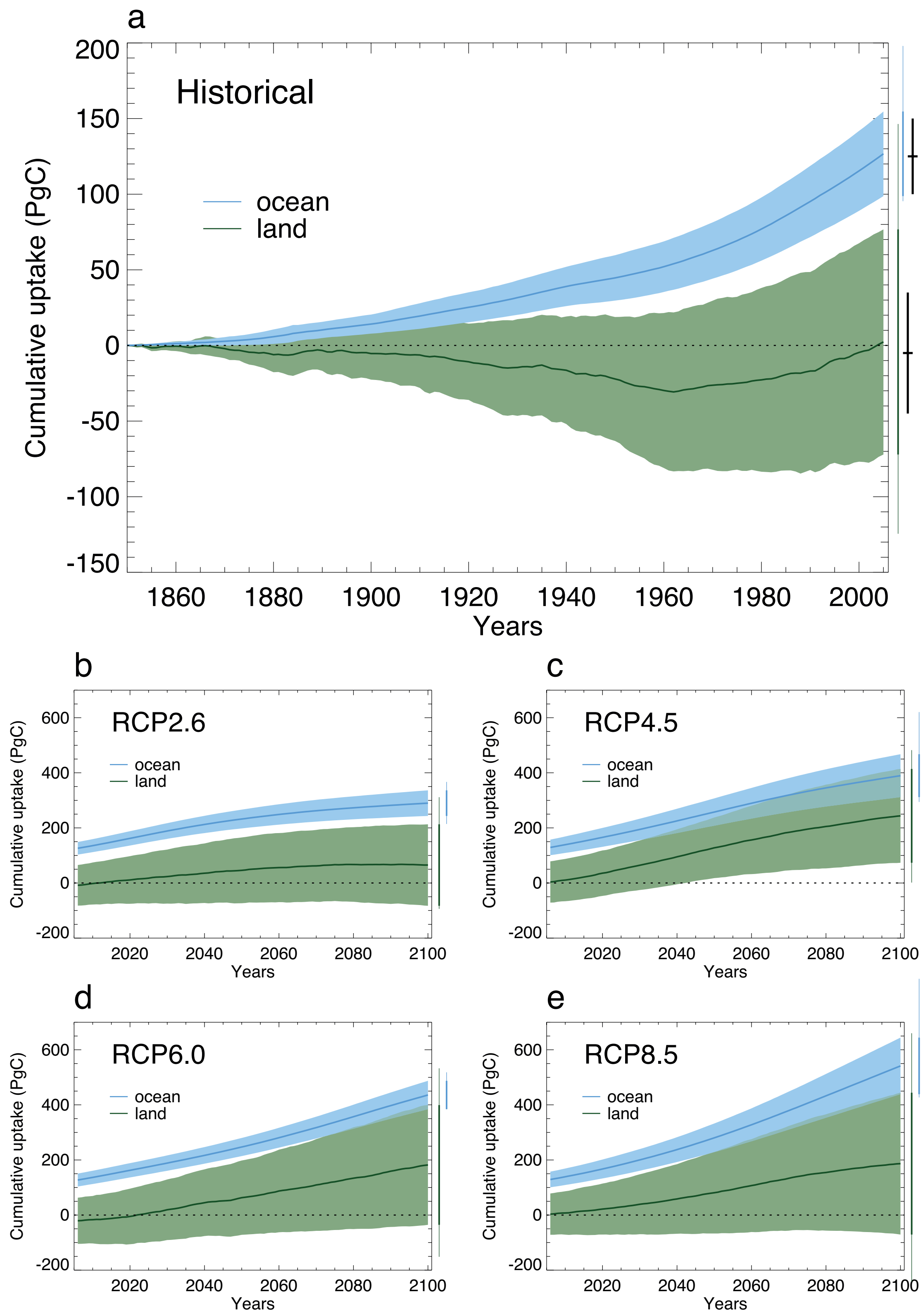

Figure 6.24 | Cumulative land and ocean carbon uptake simulated for the historical period 1850–2005 (top) and for the four RCP scenarios up to 2100 (b–e). Mean (thick line) and 1 standard deviation (shaded). Vertical bars on the right show the full model range as well as standard deviation. Black bars show observationally derived estimates for 2005. Models used: Canadian Earth System Model 2 (CanESM2), Geophysical Fluid Dynamics Laboratory–Earth System Model 2G (GFDL–ESM2G), Geophysical Fluid Dynamics Laboratory–Earth System Model 2M (GFDL–ESM2M), Hadley Centre Global Environmental Model 2–Carbon Cycle (HadGEM2-CC), Hadley Centre Global Environmental Model 2–Earth System (HadGEM2-ES), Institute Pierre Simon Laplace–Coupled Model 5A–Low Resolution (IPSL–CM5A–LR), Institute Pierre Simon Laplace–Coupled Model 5A–Medium Resolution (IPSL–CM5A–MR), Institute Pierre Simon Laplace–Coupled Model 5B–Low Resolution (IPSL–CM5B–LR), Model for Interdisciplinary Research On Climate–Earth System Model (MIROC–ESM–CHEM), Model for Interdisciplinary Research On Climate–Earth System Model (MIROC–ESM), Max Planck Institute–Earth System Model–Low Resolution (MPI–ESM–LR), Norwegian Earth System Model 1 (Emissions capable) (NorESM1–ME), Institute for Numerical Mathematics Coupled Model 4 (INMCM4), Community Earth System Model 1–Biogeochemical (CESM1–BGC), Beijing Climate Center–Climate System Model 1.1 (BCC–CSM1.1). Not every model performed every scenario simulation.

Table 6.12 | The range of compatible fossil fuel emissions (PgC) simulated by the CMIP5 models for the historical period and the four RCP scenarios, expressed as cumulative fossil fuel emission. To be consistent with Table 6.1 budgets are calculated up to 2011 for historical and 2012–2100 for future scenarios, and values are rounded to the nearest 5 PgC.

	Compatible Fossil Fuel Emissions Diagnosed from *Concentration-Driven* CMIP5 Simulations			Land Carbon Changes			Ocean Carbon Changes		
	Historical / RCP Scenario	CMIP5 ESM Mean	CMIP5 ESM Range	Historical / RCP Scenario	CMIP5 ESM Mean	CMIP5 ESM Range	Historical / RCP Scenario	CMIP5 ESM Mean	CMIP5 ESM Range
1850–2011	375[a]	350	235–455	5 ± 40[b]	10	–125 to 160	140 ± 25[b]	140	110–220
RCP2.6	275	270	140–410	[c]	65	–50 to 195	[c]	150	105–185
RCP4.5	735	780	595–1005		230	55 to 450		250	185–400
RCP6.0	1165	1060	840–1250		200	–80 to 370		295	265–335
RCP8.5	1855	1685	1415–1910		180	–165 to 500		400	320–635

Notes:

[a] Historical estimates of fossil fuel are as prescribed to all CMIP5 ESMs in the emissions-driven simulations (Andres et al., 2011).

[b] Estimate of historical net land and ocean carbon uptake from Table 6.1 but over the shorter 1850–2011 time period.

[c] IAM breakdown of future carbon changes by land and ocean are not available.

the end of the 21st century to achieve this, with six ESMs simulating negative compatible emissions and four ESM models simulating positive emissions from 2080 to 2100. The RCP2.6 scenario achieves this negative emission rate through use of large-scale bio-energy with carbon-capture and storage (BECCS). It is *as likely as not* that sustained globally negative emissions will be required to achieve the reductions in atmospheric CO_2 in the RCP2.6 scenario. This would be classed as a carbon dioxide removal (CDR) form of geoengineering under the definition used in this IPCC report, and is discussed further in Section 6.5.2. The ESMs themselves make no assumptions about how the compatible emissions could or would be achieved, but merely compute the global total emission that is required to follow the CO_2 concentration pathway, accounting for the carbon cycle response to climate and CO_2, and for land use change CO_2 emissions.

The dominant cause of future changes in the airborne fraction of fossil fuel emissions (see Section 6.3.2.4) is the emissions scenario and not carbon cycle feedbacks (Jones et al., 2013; Figure 6.26). Models show high agreement that 21st century cumulative airborne fraction will increase under rapidly increasing CO_2 in RCP8.5 and decreases under the peak-and-decline RCP2.6 scenarios. The airborne fraction declines slightly under RCP4.5 and remains of similar magnitude in the RCP6.0 scenario. Between-model spread in changes in the land-fraction is greater than between-scenario spread. Models show high agreement that the ocean fraction will increase under RCP2.6 and remain of similar magnitude in the other RCP scenarios.

Several studies (Jones et al., 2006; Matthews, 2006; Plattner et al., 2008; Miyama and Kawamiya, 2009) have shown that climate–carbon cycle feedbacks affect the compatible fossil fuel CO_2 emissions that are consistent with a given CO_2 concentration pathway. Using decoupled RCP4.5 simulations (see Box 6.4) five CMIP5 ESMs agree that the climate impact on carbon uptake by both land and oceans will reduce the compatible fossil fuel CO_2 emissions for that scenario by between 6% and 29% between 2006 and 2100 respectively (Figure 6.27), equating to an average of 157 ± 76 PgC (1 standard deviation) less carbon that can be emitted from fossil fuel use if climate feedback (see Glossary) is included. Compatible emissions would be reduced by a greater degree under higher CO_2 scenarios that exhibit a greater degree of climate change (Jones et al., 2006).

6.4.3.4 Permafrost Carbon

Current estimates of permafrost soil carbon stocks are ~1700 PgC (Tarnocai et al., 2009), the single largest component of the terrestrial carbon pool. Terrestrial carbon models project a land CO_2 sink with warming at high northern latitudes; however none of the models participating in C4MIP or CMIP5 included explicit representation of permafrost soil carbon decomposition in response to future warming. Including permafrost carbon processes into an ESM may change the sign of the high northern latitude carbon cycle response to warming from a sink to a source (Koven et al., 2011). Overall, there is *high confidence* that reductions in permafrost extent due to warming will cause thawing of some currently frozen carbon. However, there is *low confidence* on the magnitude of carbon losses through CO_2 and CH_4 emissions to the atmosphere. The magnitude of CO_2 and CH_4 emissions to the atmosphere is assessed to range from 50 to 250 PgC between 2000 and 2100 for RCP8.5. The magnitude of the source of CO_2 to the atmosphere from decomposition of permafrost carbon in response to warming varies widely according to different techniques and scenarios. Process models provide different estimates of the cumulative loss of permafrost carbon: 7 to 17 PgC (Zhuang et al., 2006) (not considered in the range given above because it corresponds only to contemporary tundra soil carbon), 55 to 69 Pg (Koven et al., 2011), 126 to 254 PgC (Schaefer et al., 2011) and 68 to 508 PgC (MacDougall et al., 2012) (not considered in the range given above because this estimate is not obtained from a concentration driven, but for emission driven RCP scenario and it is the only study of that type so far). Combining observed vertical soil carbon profiles with modeled thaw rates provides an estimate that the total quantity of newly thawed soil carbon by 2100 will be 246 PgC for RCP4.5 and 436 PgC for RCP8.5 (Harden et al., 2012), although not all of this amount will be released to the atmosphere on that time scale. Uncertainty estimates suggest the cumulative amount of thawed permafrost carbon could range from 33 to 114 PgC (68% range) under RCP8.5 warming (Schneider von Deimling et al., 2012), or 50 to 270 PgC (5th to 95th percentile range) (Burke et al., 2013).

6

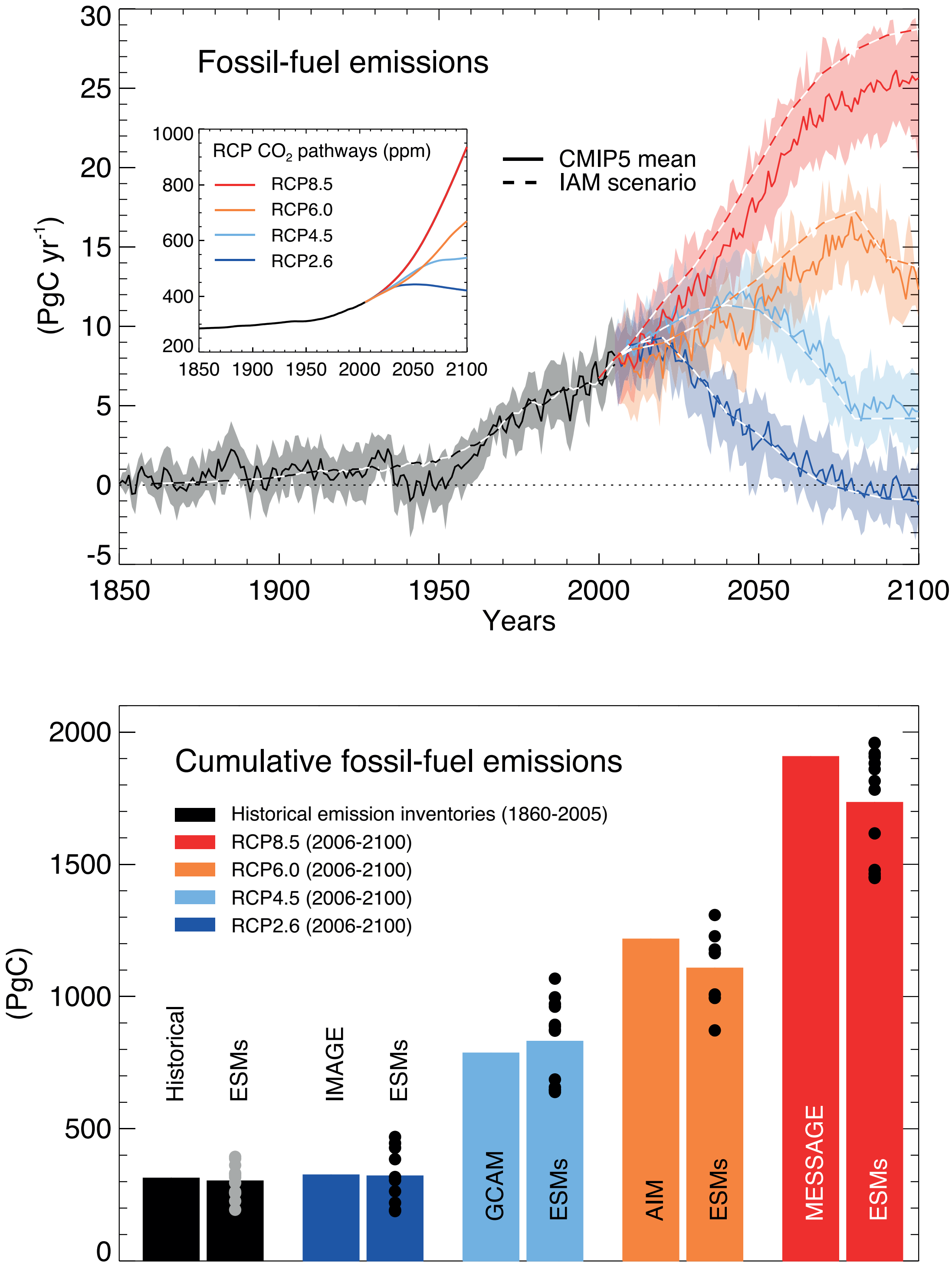

Figure 6.25 | Compatible fossil fuel emissions simulated by the CMIP5 ESMs for the four RCP scenarios. Top: time series of compatible emission rate (PgC yr^{-1}). Dashed lines represent the historical estimates and emissions calculated by the Integrated Assessment Models (IAMs) used to define the RCP scenarios, solid lines and plumes show results from CMIP5 ESMs (model mean, with 1 standard deviation shaded). Bottom: cumulative emissions for the historical period (1860–2005) and 21st century (defined in CMIP5 as 2006–2100) for historical estimates and RCP scenarios. Dots denote individual ESM results, bars show the multi-model mean. In the CMIP5 model results, total carbon in the land–atmosphere–ocean system can be tracked and changes in this total must equal fossil fuel emissions to the system (see Box 6.4). Models used: Canadian Earth System Model 2 (CanESM2), Geophysical Fluid Dynamics Laboratory–Earth System Model 2G (GFDL–ESM2G), Geophysical Fluid Dynamics Laboratory–Earth System Model 2M (GFDL–ESM2M), Hadley Centre Global Environmental Model 2–Carbon Cycle(HadGEM2-CC), Hadley Centre Global Environmental Model 2–Earth System (HadGEM2-ES), Institute Pierre Simon Laplace–Coupled Model 5A–Low Resolution (IPSL–CM5A–LR), Institute Pierre Simon Laplace–Coupled Model 5A–Medium Resolution (IPSL–CM5A–MR), Institute Pierre Simon Laplace–Coupled Model 5B–Low Resolution (IPSL–CM5B–LR), Model for Interdisciplinary Research On Climate–Earth System Model (MIROC–ESM–CHEM), Model for Interdisciplinary Research On Climate–Earth System Model (MIROC–ESM), Max Planck Institute–Earth System Model–Low Resolution (MPI–ESM–LR), Norwegian Earth System Model 1 (Emissions capable) (NorESM1–ME), Institute for Numerical Mathematics Coupled Model 4 (INMCM4), Community Earth System Model 1–Biogeochemical (CESM1–BGC), Beijing Climate Center–Climate System Model 1.1 (BCC–CSM1.1). Not every model performed every scenario simulation.

Sources of uncertainty for the permafrost carbon feedback include the physical thawing rates, the fraction of carbon that is released after being thawed and the time scales of release, possible mitigating nutrient feedbacks and the role of fine-scale processes such as spatial variability in permafrost degradation. It is also uncertain how much thawed carbon will decompose to CO_2 or to CH_4 (see Sections 6.4.7, 12.5.5.4 and 12.4.8.1).

6.4.4 Future Ocean Acidification

A fraction of CO_2 emitted to the atmosphere dissolves in the ocean, reducing surface ocean pH and carbonate ion concentrations. The associated chemistry response to a given change in CO_2 concentration is known with *very high confidence*. Overall, given evidence from Chapter 3 and model results from this chapter, it is *virtually certain* that the increased storage of carbon by the ocean will increase acidification in the future, continuing the observed trends of the past decades. Expected future changes are in line with what is measured at ocean time series stations (see Chapter 3). Multi-model projections using ocean process-based carbon cycle models discussed in AR4 demonstrate large decreases in pH and carbonate ion concentration [CO_3^{2-}] during the 21st century throughout the world oceans (Orr et al., 2005). The largest decrease in surface [CO_3^{2-}] occur in the warmer low and mid-latitudes, which are naturally rich in this ion (Feely et al., 2009). However, it is the low Ω_A waters in the high latitudes and in the upwelling regions that first become undersaturated with respect to aragonite (i.e., Ω_A <1,

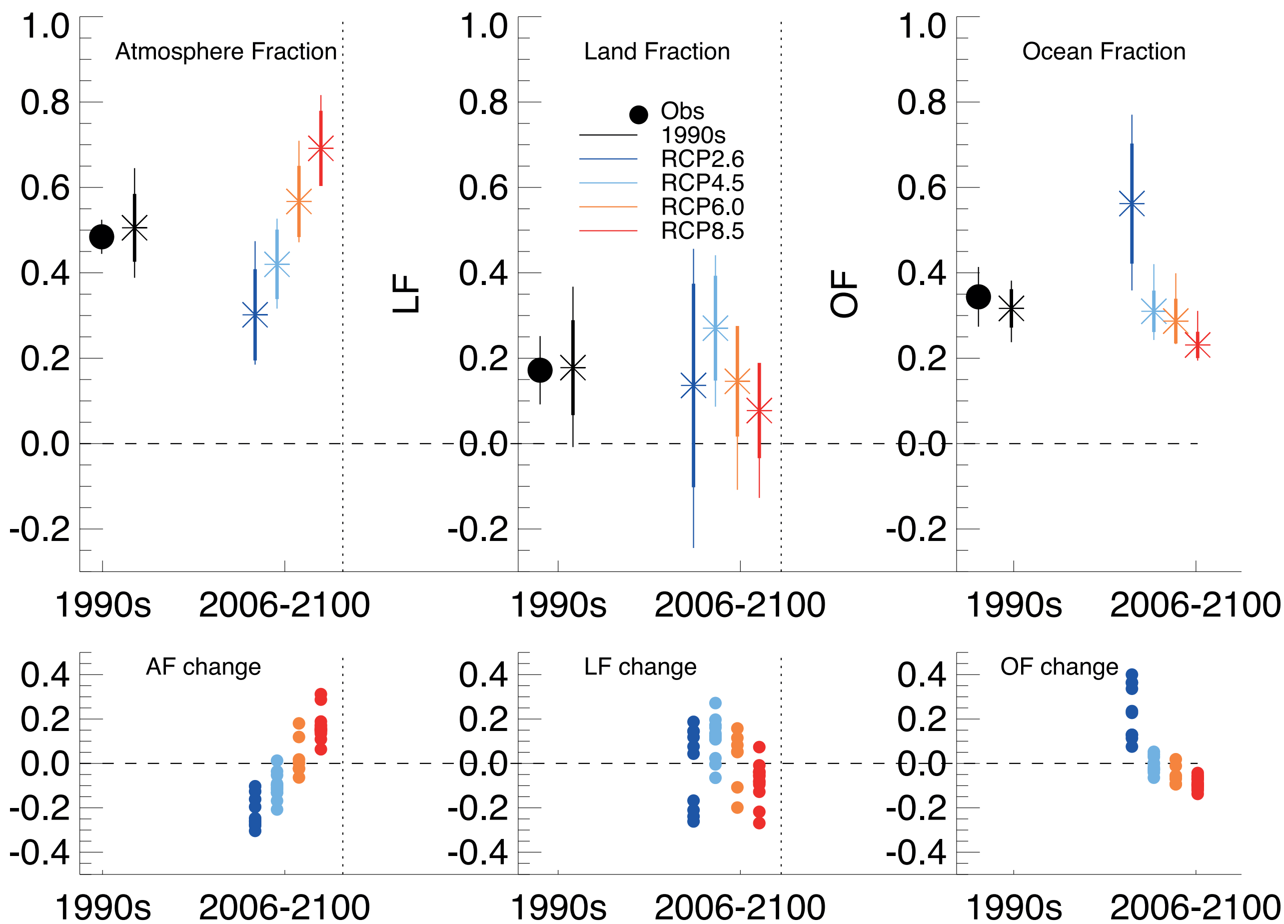

Figure 6.26 | Changes in atmospheric, land and ocean fraction of fossil fuel carbon emissions. The fractions are defined as the changes in storage in each component (atmosphere, land, ocean) divided by the compatible fossil fuel emissions derived from each CMIP5 simulation for the four RCP scenarios. Solid circles show the observed estimate based on Table 6.1 for the 1990s. The coloured bars denote the cumulative uptake fractions for the 21st century under the different RCP scenarios for each model. Multi-model mean values are shown as star symbols and the multi-model range (min-to-max) and standard deviation are shown by thin and thick vertical lines respectively. Owing to the difficulty of estimating land use emissions from the ESMs this figure uses a fossil fuel definition of airborne fraction, rather than the preferred definition of fossil and land use emissions discussed in Section 6.3.2.4. 21st century cumulative atmosphere, land and ocean fractions are shown here in preference to the more commonly shown instantaneous fractions because for RCP2.6 emissions reach and cross zero for some models and so an instantaneous definition of AF becomes singular at that point. Models used: Canadian Earth System Model 2 (CanESM2), Geophysical Fluid Dynamics Laboratory–Earth System Model 2G (GFDL–ESM2G), Geophysical Fluid Dynamics Laboratory–Earth System Model 2M (GFDL–ESM2M), Hadley Centre Global Environmental Model 2–Carbon Cycle (HadGEM2-CC), Hadley Centre Global Environmental Model 2–Earth System (HadGEM2-ES), Institute Pierre Simon Laplace–Coupled Model 5A–Low Resolution (IPSL–CM5A–LR), Institute Pierre Simon Laplace–Coupled Model 5A–Medium Resolution (IPSL–CM5A–MR), Institute Pierre Simon Laplace–Coupled Model 5B–Low Resolution (IPSL–CM5B–LR), Model for Interdisciplinary Research On Climate–Earth System Model (MIROC–ESM–CHEM), Model for Interdisciplinary Research On Climate–Earth System Model (MIROC–ESM), Max Planck Institute–Earth System Model–Low Resolution (MPI–ESM–LR), Norwegian Earth System Model 1 (Emissions capable) (NorESM1–ME), Institute for Numerical Mathematics Coupled Model 4 (INMCM4), Community Earth System Model 1–Biogeochemical (CESM1–BGC). Not every model performed every scenario simulation.

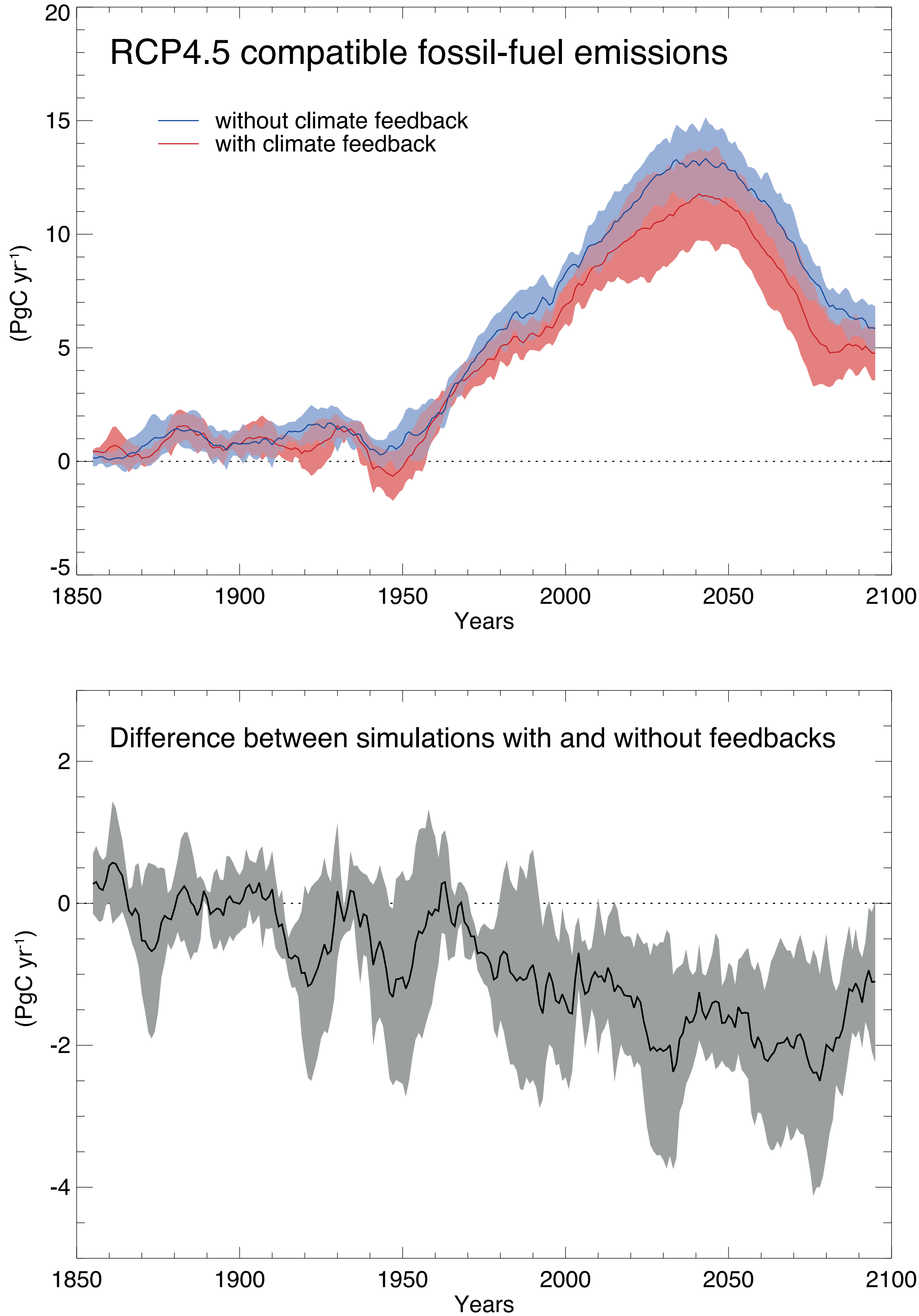

Figure 6.27 | Compatible fossil fuel emissions for the RCP4.5 scenario (top) in the presence (red) and absence (blue) of the climate feedback on the carbon cycle, and the difference between them (bottom). Multi-model mean, 10-year smoothed values are shown, with 1 standard deviation shaded. This shows the impact of climate change on the compatible fossil fuel CO_2 emissions to achieve the RCP4.5 CO_2 concentration pathway. Models used: Canadian Earth System Model 2 (CanESM2), Geophysical Fluid Dynamics Laboratory–Earth System Model 2M (GFDL-ESM2M), Hadley Centre Global Environmental Model 2–Earth System (HadGEM2-ES), Institute Pierre Simon Laplace–Coupled Model 5A–Low Resolution (IPSL-CM5A-LR) and Model for Interdisciplinary Research On Climate–Earth System Model (MIROC–ESM).

Frequently Asked Questions

FAQ 6.1 | Could Rapid Release of Methane and Carbon Dioxide from Thawing Permafrost or Ocean Warming Substantially Increase Warming?

Permafrost is permanently frozen ground, mainly found in the high latitudes of the Arctic. Permafrost, including the sub-sea permafrost on the shallow shelves of the Arctic Ocean, contains old organic carbon deposits. Some are relicts from the last glaciation, and hold at least twice the amount of carbon currently present in the atmosphere as carbon dioxide (CO_2). Should a sizeable fraction of this carbon be released as methane and CO_2, it would increase atmospheric concentrations, which would lead to higher atmospheric temperatures. That in turn would cause yet more methane and CO_2 to be released, creating a positive feedback, which would further amplify global warming.

The Arctic domain presently represents a net sink of CO_2—sequestering around 0.4 ± 0.4 PgC yr^{-1} in growing vegetation representing about 10% of the current global land sink. It is also a modest source of methane (CH_4): between 15 and 50 Tg(CH_4) yr^{-1} are emitted mostly from seasonally unfrozen wetlands corresponding to about 10% of the global wetland methane source. There is no clear evidence yet that thawing contributes significantly to the current global budgets of these two greenhouse gases. However, under sustained Arctic warming, modelling studies and expert judgments indicate with medium agreement that a potential combined release totalling up to 350 PgC as CO_2 equivalent could occur by the year 2100.

Permafrost soils on land, and in ocean shelves, contain large pools of organic carbon, which must be thawed and decomposed by microbes before it can be released—mostly as CO_2. Where oxygen is limited, as in waterlogged soils, some microbes also produce methane.

On land, permafrost is overlain by a surface 'active layer', which thaws during summer and forms part of the tundra ecosystem. If spring and summer temperatures become warmer on average, the active layer will thicken, making more organic carbon available for microbial decomposition. However, warmer summers would also result in greater uptake of carbon dioxide by Arctic vegetation through photosynthesis. That means the net Arctic carbon balance is a delicate one between enhanced uptake and enhanced release of carbon.

Hydrological conditions during the summer thaw are also important. The melting of bodies of excess ground ice may create standing water conditions in pools and lakes, where lack of oxygen will induce methane production. The complexity of Arctic landscapes under climate warming means we have *low confidence* in which of these different processes might dominate on a regional scale. Heat diffusion and permafrost melting takes time—in fact, the deeper Arctic permafrost can be seen as a relict of the last glaciation, which is still slowly eroding—so any significant loss of permafrost soil carbon will happen over long time scales.

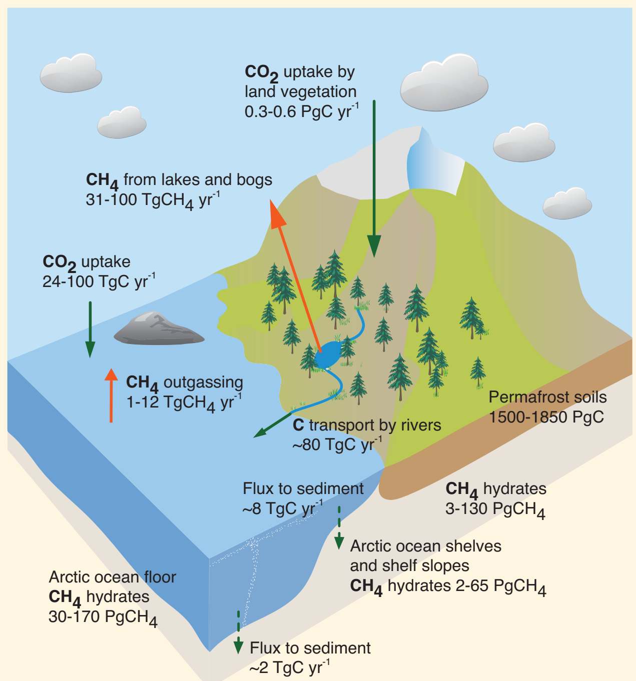

FAQ 6.1, Figure 1 | A simplified graph of current major carbon pools and flows in the Arctic domain, including permafrost on land, continental shelves and ocean. (Adapted from McGuire et al., 2009; and Tarnocai et al., 2009.) TgC = 10^{12} gC, and PgC = 10^{15} gC.

Given enough oxygen, decomposition of organic matter in soil is accompanied by the release of heat by microbes (similar to compost), which, during summer, might stimulate further permafrost thaw. Depending on carbon and ice content of the permafrost, and the hydrological regime, this mechanism could, under warming, trigger relatively fast local permafrost degradation. *(continued on next page)*

6

FAQ 6.1 (continued)

Modelling studies of permafrost dynamics and greenhouse gas emissions indicate a relatively slow positive feedback, on time scales of hundreds of years. Until the year 2100, up to 250 PgC could be released as CO_2, and up to 5 Pg as CH_4. Given methane's stronger greenhouse warming potential, that corresponds to a further 100 PgC of equivalent CO_2 released until the year 2100. These amounts are similar in magnitude to other biogeochemical feedbacks, for example, the additional CO_2 released by the global warming of terrestrial soils. However, current models do not include the full complexity of Arctic processes that occur when permafrost thaws, such as the formation of lakes and ponds.

Methane hydrates are another form of frozen carbon, occurring in deep permafrost soils, ocean shelves, shelf slopes and deeper ocean bottom sediments. They consist of methane and water molecule clusters, which are only stable in a specific window of low temperatures and high pressures. On land and in the ocean, most of these hydrates originate from marine or terrestrial biogenic carbon, decomposed in the absence of oxygen and trapped in an aquatic environment under suitable temperature–pressure conditions.

Any warming of permafrost soils, ocean waters and sediments and/or changes in pressure could destabilise those hydrates, releasing their CH_4 to the ocean. During larger, more sporadic releases, a fraction of that CH_4 might also be outgassed to the atmosphere. There is a large pool of these hydrates: in the Arctic alone, the amount of CH_4 stored as hydrates could be more than 10 times greater than the CH_4 presently in the global atmosphere.

Like permafrost thawing, liberating hydrates on land is a slow process, taking decades to centuries. The deeper ocean regions and bottom sediments will take still longer—between centuries and millennia to warm enough to destabilise the hydrates within them. Furthermore, methane released in deeper waters has to reach the surface and atmosphere before it can become climatically active, but most is expected to be consumed by microorganisms before it gets there. Only the CH_4 from hydrates in shallow shelves, such as in the Arctic Ocean north of Eastern Siberia, may actually reach the atmosphere to have a climate impact.

Several recent studies have documented locally significant CH_4 emissions over the Arctic Siberian shelf and from Siberian lakes. How much of this CH_4 originates from decomposing organic carbon or from destabilizing hydrates is not known. There is also no evidence available to determine whether these sources have been stimulated by recent regional warming, or whether they have always existed—it may be possible that these CH_4 seepages have been present since the last deglaciation. In any event, these sources make a very small contribution to the global CH_4 budget—less than 5%. This is also confirmed by atmospheric methane concentration observations, which do not show any substantial increases over the Arctic.

However modelling studies and expert judgment indicate that CH_4 and CO_2 emissions will increase under Arctic warming, and that they will provide a positive climate feedback. Over centuries, this feedback will be moderate: of a magnitude similar to other climate–terrestrial ecosystem feedbacks. Over millennia and longer, however, CO_2 and CH_4 releases from permafrost and shelves/shelf slopes are much more important, because of the large carbon and methane hydrate pools involved.

where $\Omega_A = [Ca^{+2}][CO_3^{2-}]/K_{sp}$, where K_{sp} is the solubility product for the metastable form of $CaCO_3$ known as aragonite; a value of $\Omega_A < 1$ thus indicates aragonite undersaturation). This aragonite undersaturation in surface waters is reached before the end of the 21st century in the Southern Ocean as highlighted in AR4, but occurs sooner and is more intense in the Arctic (Steinacher et al., 2009). Ten percent of Arctic surface waters are projected to become undersaturated when atmospheric CO_2 reaches 428 ppm (by 2025 under all IPCC SRES scenarios). That proportion increases to 50% when atmospheric CO_2 reaches 534 ppm (Steinacher et al., 2009). By 2100 under the A2 scenario, much of the Arctic surface is projected to become undersaturated with respect to calcite (Feely et al., 2009). Surface waters would then be corrosive to all $CaCO_3$ minerals. These general trends are confirmed by the latest projections from the CMIP5 Earth System models (Figure 6.28 and 6.29). Between 1986–2005 and 2081–2100, decrease in global-mean surface pH is 0.065 (0.06 to 0.07) for RCP2.6, 0.145 (0.14 to 0.15) for RCP4.5, 0.203 (0.20 to 0.21) for RCP6.0 and 0.31 (0.30 to 0.32) for RCP8.5 (range from CMIP5 models spread).

Surface $CaCO_3$ saturation also varies seasonally, particularly in the high latitudes, where observed saturation is higher in summer and lower in winter (Feely et al., 1988; Merico et al., 2006; Findlay et al., 2008). Future projections using ocean carbon cycle models indicate that undersaturated conditions will be reached first in winter (Orr et al., 2005). In the Southern Ocean, it is projected that wintertime undersaturation with respect to aragonite will begin when atmospheric CO_2 will reach 450 ppm, within 1-3 decades, which is about 100 ppm sooner (~30 years under the IS92a scenario) than for the annual mean undersaturation (McNeil and Matear, 2008). As well, aragonite undersaturation will be first reached during wintertime in parts (10%) of the Arctic when atmospheric CO_2 will reach 410 ppm, within a decade (Steinacher et al., 2009). Then, aragonite undersaturation will become widespread in these regions at atmospheric CO_2 levels of 500–600 ppm (Figure 6.28).

Although projected changes in pH are generally largest at the surface, the greatest pH changes in the subtropics occur between 200 and 300 m where subsurface increased loads of anthropogenic CO_2 are similar to surface changes but the carbonate buffering capacity is lower (Orr, 2011). This more intense projected subsurface pH reduction is consistent with the observed subsurface changes in pH in the subtropical North Pacific (Dore et al., 2009; Byrne et al., 2010; Ishii et al., 2011). As subsurface saturation states decline, the horizon separating undersaturated waters below from supersaturated waters above is projected to move upward (shoal). By 2100 under the RCP8.5 scenario, the median projection from 11 CMIP5 models is that this interface (aragonite saturation horizon) will shoal from 200 m up to 40 m in the subarctic Pacific, from 1000 m up to the surface in the Southern Ocean, and from 2850 m to 150 m in the North Atlantic (Figure 6.29), consistent with results from previous model comparison (Orr et al., 2005; Orr, 2011). Under the SRES A2 scenario, the volume of ocean with supersaturated waters is projected to decline from 42% in the preindustrial Era to 25% in 2100 (Steinacher et al., 2009). Yet even if atmospheric CO_2 does not go above 450 ppm, most of the deep ocean volume is projected to become undersaturated with respect to both aragonite and calcite after several centuries (Caldeira and Wickett, 2005). Nonetheless, the most recent projections under all RCPs scenarios but RCP8.5 illustrate that limiting atmospheric CO_2 will greatly reduce the level of ocean acidification that will be experienced (Joos et al., 2011).

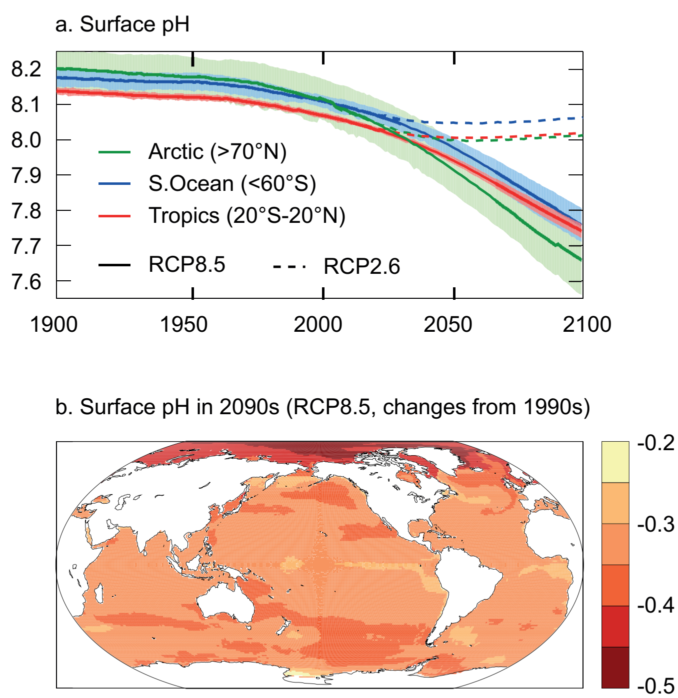

Figure 6.28 | Projected ocean acidification from 11 CMIP5 Earth System Models under RCP8.5 (other RCP scenarios have also been run with the CMIP5 models): (a) Time series of surface pH shown as the mean (solid line) and range of models (filled), given as area-weighted averages over the Arctic Ocean (green), the tropical oceans (red) and the Southern Ocean (blue). (b) Maps of the median model's change in surface pH from 1850 to 2100. Panel (a) also includes mean model results from RCP2.6 (dashed lines). Over most of the ocean, gridded data products of carbonate system variables (Key et al., 2004) are used to correct each model for its present-day bias by subtracting the model-data difference at each grid cell following (Orr et al., 2005). Where gridded data products are unavailable (Arctic Ocean, all marginal seas, and the ocean near Indonesia), the results are shown without bias correction. The bias correction reduces the range of model projections by up to a factor of 4, e.g., in panel (a) compare the large range of model projections for the Arctic (without bias correction) to the smaller range in the Southern Ocean (with bias correction).

In the open ocean, future reductions in surface ocean pH and $CaCO_3$ (calcite and aragonite) saturation states are controlled mostly by the invasion of anthropogenic carbon. Other effects due to future climate change counteract less than 10% of the reductions in $CaCO_3$ saturation induced by the invasion of anthropogenic carbon (Orr et al., 2005; McNeil and Matear, 2006; Cao et al., 2007). Warming dominates other effects from climate-change by reducing CO_2 solubility and thus by enhancing $[CO_3^{2-}]$. An exception is the Arctic Ocean where reductions in pH and $CaCO_3$ saturation states are projected to be exacerbated by effects from increased freshwater input due to sea ice melt, more precipitation, and greater air–sea CO_2 fluxes due to less sea ice cover (Steinacher et al., 2009; Yamamoto et al., 2012). The projected effect of freshening is consistent with current observations of lower saturation states and lower pH values near river mouths and in areas under substantial fresh-water influence (Salisbury et al., 2008; Chierici and Fransson, 2009; Yamamoto-Kawai et al., 2009).

Regional ocean carbon cycle models project that some nearshore systems are also highly vulnerable to future pH decrease. In the California Current System, an eastern boundary upwelling system, observations and model results show that strong seasonal upwelling of carbon-rich waters (Feely et al., 2008) renders surface waters as vulnerable to future ocean acidification as those in the Southern Ocean (Gruber et al., 2012). In the Northwestern European Shelf Seas, large spatio-temporal variability is enhanced by local effects from river input and organic matter degradation, exacerbating acidification from anthropogenic CO_2 invasion (Artioli et al., 2012). In the Gulf of Mexico and East China Sea, coastal eutrophication, another anthropogenic perturbation, has been shown to enhance subsurface acidification as additional respired carbon accumulates at depth (Cai et al., 2011).

6.4.5 Future Ocean Oxygen Depletion

It is *very likely* that global warming will lead to declines in dissolved O_2 in the ocean interior through warming-induced reduction in O_2 solubility and increased ocean stratification. This will have implications for nutrient and carbon cycling, ocean productivity and marine habitats (Keeling et al., 2010).

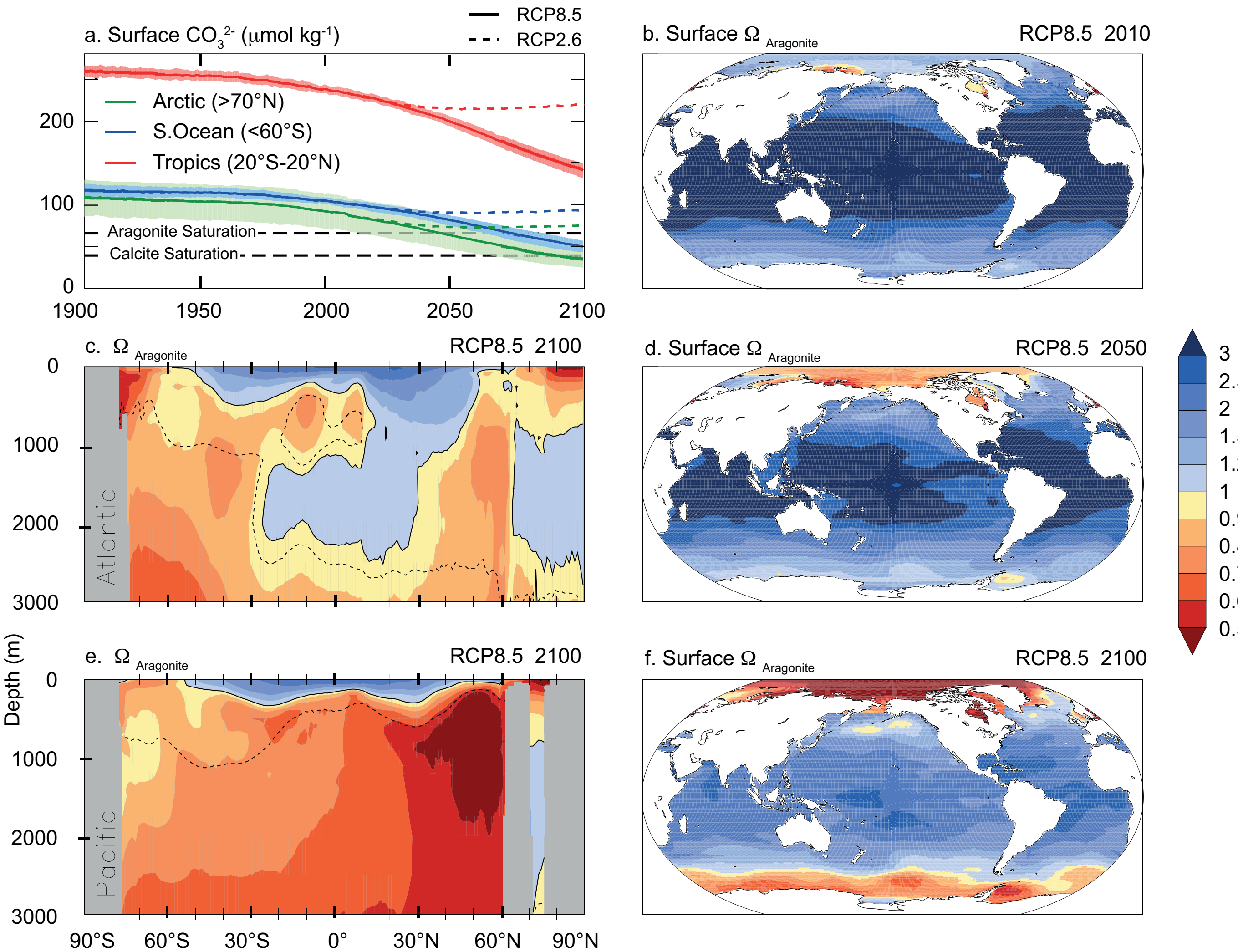

Figure 6.29 | Projected aragonite saturation state from 11 CMIP5 Earth System Models under RCP8.5 scenario: (a) time series of surface carbonate ion concentration shown as the mean (solid line) and range of models (filled), given as area-weighted averages over the Arctic Ocean (green), the tropical oceans (red), and the Southern Ocean (blue); maps of the median model's surface Ω_A in (b) 2010, (d) 2050 and (f) 2100; and zonal mean sections (latitude vs. depth) of Ω_A in 2100 over the (c) Atlantic and (e) Pacific, while the ASH is shown in 2010 (dotted line) as well as 2100 (solid line). Panel (a) also includes mean model results from RCP2.6 (dashed lines). As for Figure 6.28, gridded data products of carbonate system variables (Key et al., 2004) are used to correct each model for its present-day bias by subtracting the model-data difference at each grid cell following (Orr et al., 2005). Where gridded data products are unavailable (Arctic Ocean, all marginal seas, and the ocean near Indonesia), results are shown without bias correction.

Future changes in dissolved O_2 have been investigated using models of various complexity (see references in Table 6.13). The global ocean dissolved oxygen will decline significantly under future scenarios (Cocco et al., 2013). Simulated declines in mean dissolved O_2 concentration for the global ocean range from 6 to 12 µmol kg^{-1} by the year 2100 (Table 6.13), with a projection of 3 to 4 µmol kg^{-1} in one model with low climate sensitivity (Frölicher et al., 2009). This general trend is confirmed by the latest projections from the CMIP5 Earth System models, with reductions in mean dissolved O_2 concentrations from 1.5 to 4% (2.5 to 6.5 µmol kg^{-1}) in 2090s relative to 1990s for all RCPs (Figure 6.30a).

Most modelling studies (Table 6.13) explain the global decline in dissolved oxygen by enhanced surface ocean stratification leading to reductions in convective mixing and deep water formation and by a contribution of 18 to 50% from ocean warming-induced reduction in solubility. These two effects are in part compensated by a small increase in O_2 concentration from projected reductions in biological export production production (Bopp et al., 2001; Steinacher et al., 2010) or changes in ventilation age of the tropical thermocline (Gnanadesikan et al., 2007). The largest regional decreases in oxygen concentration (~20 to 100 µmol kg^{-1}) are projected for the intermediate (200 to 400 m) to deep waters of the North Atlantic, North Pacific and Southern Ocean for 2100 (Plattner et al., 2002; Matear and Hirst, 2003; Frölicher et al., 2009; Matear et al., 2010; Cocco et al., 2013), which is confirmed by the latest CMIP5 projections (Figure 6.30c and 6.30d).

It is *as likely as not* that the extent of open-ocean hypoxic (dissolved oxygen <60 to 80 µmol kg^{-1}) and suboxic (dissolved oxygen <5 µmol kg^{-1}) waters will increase in the coming decades. Most models show even some increase in oxygen in most O_2-poor waters and thus a slight decrease in the extent of suboxic waters under the SRES-A2 scenario (Cocco et al., 2013), as well as under RCP8.5 scenario (see the model-

Table 6.13 | Model configuration and projections for global marine O_2 depletion by 2100 (adapted from Keeling et al. (2010).

Study	Ocean Carbon Cycle Model	Forcing	Mean [O_2] Decrease (μmol kg^{-1})[a,b]	Solubility Contribution (%)
Sarmiento et al. (1998)	GFDL		7[c]	
Matear et al. (2000)	CSIRO	IS92a		18
Plattner et al. (2002)	Bern 2D	SRES A1	12	35
Bopp et al. (2002)	IPSL	SRES A2[d]	4	25
Matear and Hirst (2003)	CSIRO	IS92a	9	26
Schmittner et al. (2008)	UVic	SRES A2	9	
Oschlies et al. (2008)	UVic	SRES A2	9	
	UVic-variable C:N	SRES A2	12	
Frölicher et al. (2009)	NCAR CSM1.4-CCCM	SRES A2	4	50
		SRES B1	3	
Shaffer et al. (2009)	DCESS	SRES A2	10[e]	

Notes:

[a] Assuming a total ocean mass of 1.48 × 10^{21} kg.

[b] Relative to pre-industrial baseline in 1750.

[c] Model simulation ends at 2065.

[d] Radiative forcing of non-CO_2 GHGs is excluded from this simulation.

[e] For simulations with reduced ocean exchange.

CCCM = Coupled-Climate-Carbon Model; CSIRO = Commonwealth Scientific and Industrial Research Organisation; DCESS = Danish Center for Earth System Science; GFDL = Geophysical Fluid Dynamics Laboratory; IPSL = Institute Pierre Simon Laplace; NCAR = National Center for Atmospheric Research; IS92 = IPCC scenarios for 1992; SRES = Special Report on Emission Scenarios; UVic = University of Victoria.

mean increase of sub-surface O_2 in large parts of the tropical Indian and Atlantic Oceans, Figure 6.30d). This rise in oxygen in most suboxic waters has been shown to be caused in one model study by an increased supply of oxygen due to lateral diffusion (Gnanadesikan et al., 2012). Given limitations of global ocean models in simulating today's O_2 distribution (Cocco et al., 2013), as well as reproducing the measured changes in O_2 concentrations over the past 50 years (see Chapter 3, and Stramma et al., 2012), the model projections are uncertain, especially concerning the evolution of O_2 in and around oxygen minimum zones.

A number of biogeochemical ocean carbon cycle feedbacks, not yet included in most marine biogeochemical models (including CMIP5 models, see Section 6.3.2.5.6), could also impact future trends of ocean deoxygenation. For example, model experiments which include a pCO_2-sensitive C:N drawdown in primary production, as suggested by some mesocosm experiments (Riebesell et al., 2007), project future increases of up to 50% in the volume of the suboxic waters by 2100 (Oschlies et al., 2008; Tagliabue et al., 2011). In addition, future marine hypoxia could be amplified by changes in the $CaCO_3$ to organic matter 'rain ratio' in response to rising pCO_2 (Hofmann and Schellnhuber, 2009). Reduction in biogenic calcification due to ocean acidification would weaken the strength of $CaCO_3$ mineral ballasting effect, which could lead organic material to be remineralized at a shallower depth exacerbating the future expansion of shallow hypoxic waters.

The modeled estimates do not take into account processes that are specific to the coastal ocean and may amplify deoxygenation. Recent observations for the period 1976–2000 have shown that dissolved O_2 concentrations have declined at a faster rate in the coastal ocean (–0.28 μmol kg^{-1} yr^{-1}) than the open ocean (–0.02 μmol kg^{-1} y^{-1}, and a faster rate than in the period 1951–1975, indicating a worsening of hypoxia (Gilbert et al., 2010). Hypoxia in the shallow coastal ocean (apart from continental shelves in Eastern Boundary Upwelling Systems) is largely eutrophication driven and is controlled by the anthropogenic flux of nutrients (N and P) and organic matter from rivers. If continued industrialisation and intensification of agriculture yield larger nutrient loads in the future, eutrophication should intensify (Rabalais et al., 2010), and further increase the coastal ocean deoxygenation.

On longer time scales beyond 2100, ocean deoxygenation is projected to increase with some models simulating a tripling in the volume of suboxic waters by 2500 (Schmittner et al., 2008). Ocean deoxygenation and further expansion of suboxic waters could persist on millennial time scales, with average dissolved O_2 concentrations projected to reach minima of up to 56 μmol kg^{-1} below pre-industrial levels in experiments with high CO_2 emissions and high climate sensitivity (Shaffer et al., 2009).

A potential expansion of hypoxic or suboxic water over large parts of the ocean is *likely* to impact the marine cycling of important nutrients, particularly nitrogen. The intensification of low oxygen waters has been suggested to lead to increases in water column denitrification and N_2O emissions (e.g., Codispoti, 2010; Naqvi et al., 2010). Recent works, however, suggest that oceanic N_2O production is dominated by nitrification with a contribution of 7% by denitrification (Freing et al., 2012), Figure 6.4c) and that ocean deoxygenation in response to anthropogenic climate change could leave N_2O production relatively unchanged (Bianchi et al., 2012).

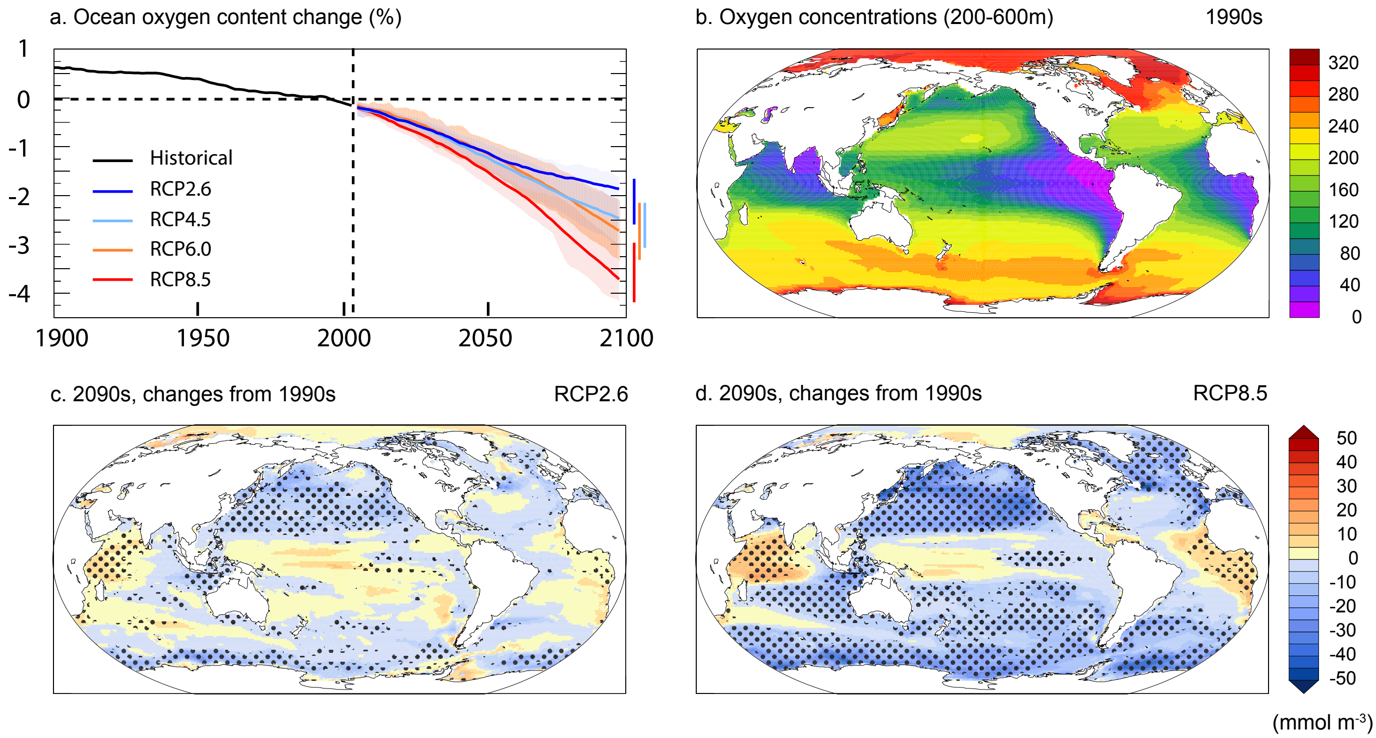

Figure 6.30 | (a) Simulated changes in dissolved O_2 (mean and model range as shading) relative to 1990s for RCP2.6, RCP4.5, RCP6.0 and RCP8.5. (b) Multi-model mean dissolved O_2 (µmol m^{-3}) in the main thermocline (200 to 600 m depth average) for the 1990s, and changes in 2090s relative to 1990s for RCP2.6 (c) and RCP8.5 (d). To indicate consistency in the sign of change, regions are stippled where at least 80% of models agree on the sign of the mean change. These diagnostics are detailed in Cocco et al. (2013) in a previous model intercomparison using the SRES-A2 scenario and have been applied to CMIP5 models here. Models used: Community Earth System Model 1–Biogeochemical (CESM1-BGC), Geophysical Fluid Dynamics Laboratory–Earth System Model 2G (GFDL-ESM2G), Geophysical Fluid Dynamics Laboratory–Earth System Model 2M (GFDL-ESM2M), Hadley Centre Global Environmental Model 2–Earth System (HadGEM2-ES), Institute Pierre Simon Laplace–Coupled Model 5A–Low Resolution (IPSL-CM5A-LR), Institute Pierre Simon Laplace–Coupled Model 5A–Medium Resolution (IPSL-CM5A-MR), Max Planck Institute–Earth System Model–Low Resolution (MPI-ESM-LR), Max Planck Institute–Earth System Model–Medium Resolution (MPI-ESM-MR), Norwegian Earth System Model 1 (Emissions capable) (NorESM1).

6.4.6 Future Trends in the Nitrogen Cycle and Impact on Carbon Fluxes

6.4.6.1 Projections for Formation of Reactive Nitrogen by Human Activity

Since the 1970s, food production, industrial activity and fossil fuel combustion have resulted in the creation of more reactive nitrogen (Nr) than natural terrestrial processes (Section 6.1; Box 6.2, Figure 1). Building on the general description of the set of AR4 Special Report on Emission (SRES) scenarios, Erisman et al. (2008) estimated anthropogenic nitrogen fertiliser consumption throughout the 21st century. Five driving parameters (population growth, consumption of animal protein, agricultural efficiency improvement and additional biofuel production) are used to project future nitrogen demands for four scenarios (A1, B1, A2 and B2) (Figure 6.31). Assigning these drivers to these four SRES scenarios, they estimated a production of Nr for agricultural use of 90 to 190 TgN yr^{-1} by 2100, a range that spans from slightly less to almost twice as much current fertiliser consumption rates (Section 6.1, Figure 6.4a, Figure 1 in Box 6.2).

Despite the uncertainties and the non-inclusion of many important drivers, three of the scenarios generated by the Erisman et al. (2008) model point towards an increase in future production of reactive nitrogen. In particular, the A1 scenario which assumes a world with rapid economic growth, a global population that peaks mid-century and rapid introduction of new and more efficient technologies ends up as the potentially largest contributor to nitrogen use, as a result of large amounts of biofuels required and the fertiliser used to produce it. This increase in nitrogen use is assumed to be largely in line with the RCP2.6 scenario, where it appears to have rather limited adverse effects like increasing N_2O emissions (van Vuuren et al., 2011).

N_2O emissions are projected to increase from increased anthropogenic Nr production. It is thus *likely* that N_2O emissions from soils will increase due to the increased demand for feed/food and the reliance of agriculture on nitrogen fertilisers. This is illustrated by the comparison of emissions from 1900 to those in 2000 and 2050, using the IAM IMAGE model that served to define the RCP2.6 pathway (Figure 6.32). The anthropogenic N_2O emission map IN 2050 shown in Figure 6.32 is established from the RCP4.5 scenario; the RCP8.5 and RCP6 scenarios have much higher emissions, and RCP2.6 much lower (van Vuuren et al., 2011). A spatially explicit inventory of soil nitrogen budgets in livestock and crop production systems using the IMAGE model (Bouwman et al., 2011) shows that between 1900 and 1950, the global soil Nr budget surplus almost doubled to 36 TgN yr^{-1}, and further increased to 138 TgN yr^{-1} between 1950 and 2000. The IMAGE model scenario from Bouwman et al. (2011) shown in Figure 6.32 portrays a world with a

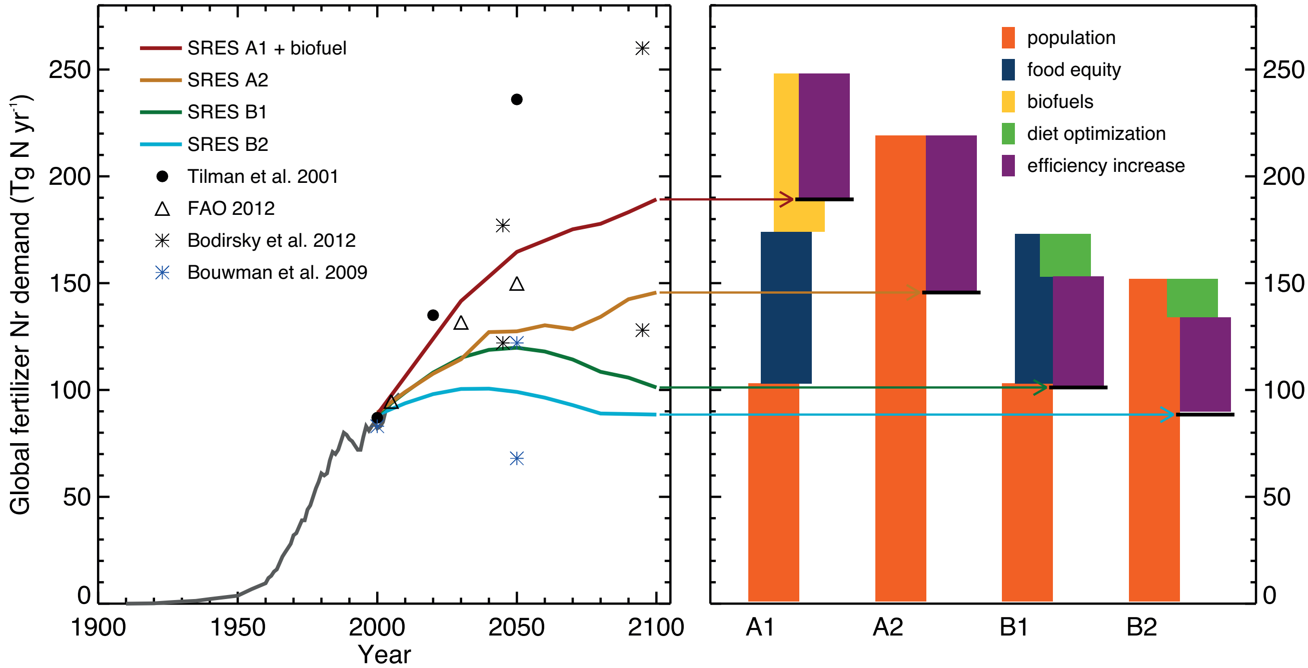

Figure 6.31 | Global nitrogen fertiliser consumption scenarios (left) and the impact of individual drivers on 2100 consumption (right). This resulting consumption is always the sum (denoted at the end points of the respective arrows) of elements increasing as well as decreasing nitrogen consumption. Other relevant estimates are presented for comparison. The A1, B1, A2 and B2 scenarios draw from the assumptions of the IPCC Special Report on Emission Scenarios (SRES) emission scenario storylines as explained in Erisman et al. (2008).

further increasing global crop production (+82% for 2000–2050) and livestock production (+115%). Despite the assumed rapid increase in nitrogen use efficiency in crop (+35%) and livestock (+35%) production, global agricultural Nr surpluses are projected to continue to increase (+23%), and associated emissions of N_2O to triple compared to 1900 levels.

Regional to global scale model simulations suggest a strong effect of climate variability on interannual variability of land N_2O emissions (Tian et al., 2010; Zaehle et al., 2011; Xu-Ri et al., 2012). Kesik et al. (2006) found for European forests that higher temperatures and lower soil moisture will decrease future N_2O emissions under scenarios of climate change, despite local increases of emission rates by up to 20%. Xu-Ri et al. (2012) show that local climate trends result in a spatially diverse pattern of increases and decreases of N_2O emissions, which globally integrated result in a net climate response of N_2O emissions of 1 TgN yr^{-1} per 1°C of land temperature warming. Using a further development of this model, Stocker et al. (2013) estimate increases in terrestrial N_2O from a pre-industrial terrestrial source of 6.9 TgN (N_2O) yr^{-1} to 9.8 to 11.1 TgN (N_2O) yr^{-1} (RCP 2.6) and 14.2 to 17.0 TgN (N_2O) yr^{-1} (RCP 8.5) by 2100. Of these increases, 1.1 to 2.4 TgN (N_2O) yr^{-1} (RCP 2.6) or 4.7 to 7.7 TgN (N_2O) yr^{-1} (RCP 8.5) are due to the interacting effects of climate and CO_2 on N_2O emissions from natural and agricultural ecosystems. An independent modelling study suggested a climate change related increase of N_2O emissions between 1860 and 2100 by 3.1 TgN (N_2O) yr^{-1} for the A2 SRES scenario (Zaehle, 2013) implying a slightly lower sensitivity of soil N_2O emissions to climate of 0.5 TgN (N_2O) yr^{-1} per 1°C warming. While the present-day contribution of these climate-mediated effects on the radiative forcing from N_2O is *likely* to be small (0.016 W m^{-2} °C^{-1}; Zaehle and Dalmonech, 2011). Modelling results (Stocker et al., 2013) suggest that the climate and CO_2-related amplification of terrestrial N_2O emissions imply a larger feedback of 0.03 to 0.05 W m^{-2} °C^{-1} by 2100.

With the continuing increases in the formation of Nr from anthropogenic activities will come increased Nr emissions and distribution of Nr by waters and the atmosphere. For the atmosphere, the main driver of future global nitrogen deposition is the emission trajectories of NO_y and NH_3. For all RCP scenarios except RCP2.6, nitrogen deposition is projected to remain relatively constant globally although there is a projected increase in NH_x deposition and decrease in NO_y deposition. On a regional basis, future decreases of NH_x and NOx are projected in North America and northern Europe, and increases in Asia (Figure 6.33). Spatially, projected changes in total nitrogen deposition driven primarily by increases in NH_x emissions occur over large regions of the world for all RCPs, with generally the largest in RCP8.5 and the smallest in RCP2.6 (Figure 6.33) (Supplementary Material has RCP4.5 and RCP6.0). Previous IPCC scenarios (SRES A2 or IS92a) project a near doubling of atmospheric nitrogen deposition over some world biodiversity hotspots with half of these hotspots subjected to deposition rates greater than 15 kgN ha^{-1} yr^{-1} (critical load threshold value) over at least 10% of their total area (Dentener et al., 2005; Phoenix et al., 2006; Bleeker et al., 2011).

Large uncertainties remain in our understanding and modelling of changes in Nr emissions, atmospheric transport and deposition processes, lead to *low confidence* in the projection of future Nr deposition fluxes, particularly in regions remote from anthropogenic emissions (Dentener et al., 2006). The large spread between atmospheric GCM models associated with precipitation projections confounds extraction

6

of a climate signal in deposition projections (Langner et al., 2005; Hedegaard et al., 2008).

6.4.6.2. Projected Changes in Sulphur Deposition

Given the tight coupling between the atmospheric nitrogen and sulphur cycles, and the impact on climate (Section 7.3) this Chapter also presents scenarios for sulphur deposition. Deposition of SO_x is projected to decrease in all RCP pathways (Figures 6.33 and 6.34). By contrast, scenarios established prior to RCPs indicated decreases of sulphur deposition in North America and Europe, but increases in South America, Africa, South and East Asia (Dentener et al., 2006; Tagaris et al., 2008). In all RCPs, sulphur deposition is lower by 2100 than in 2000 in all regions, with the largest decreases in North America, Europe and Asia (RCP2.6 and RCP 8.5 are seen in Figure 6.34; RCP4.5 and RCP6.0 are in the Supplementary Material) (Lamarque et al., 2011). Future hot spots of deposition are still evident in East and South East Asia, especially for RCP6.0.

Projected future increase of Nr input into terrestrial ecosystems also yields increased flux of Nr from rivers into coastal systems. As illustrated by the Global NEWS 2 model for 2050, by the base year 2000, the discharge of dissolved inorganic nitrogen (DIN) to marine coastal waters was >500 kg N km^{-2} of watershed area for most watershed systems downstream of either high population or extensive agricultural activity (Mayorga et al., 2010; Seitzinger et al., 2010). Additional information and the supporting figure are found in the Supplementary Material.

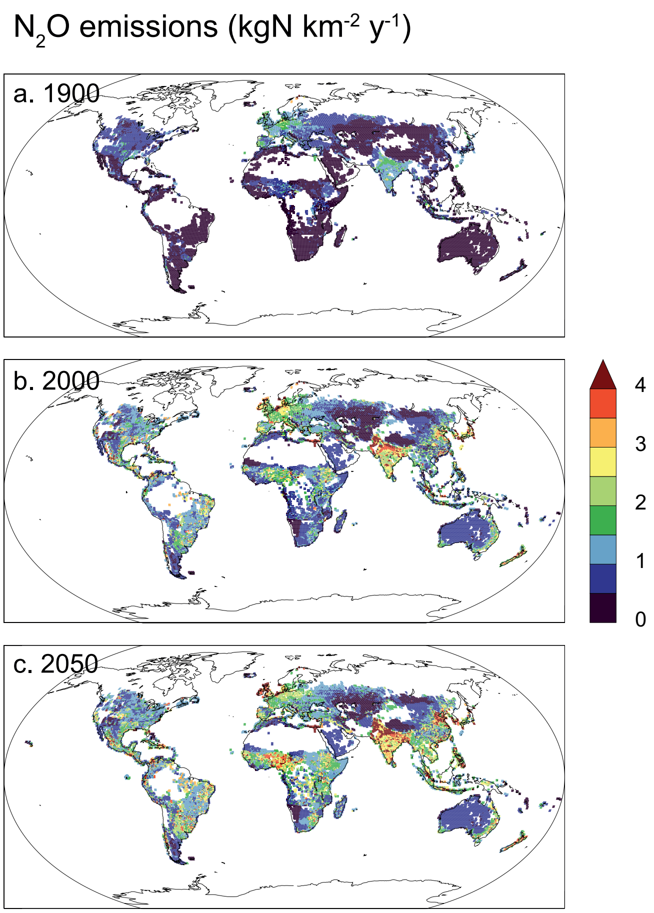

Figure 6.32 | N_2O emissions in 1900, 2000 and projected to 2050 (Bouwman et al., 2011). This spatially explicit soil nutrient budget and nitrogen gas emission scenario was elaborated with the Integrated Model to Assess the Global Environment (IMAGE) model on the basis of the International Assessment of Agricultural Knowledge, Science and Technology for Development (IAASTD) baseline scenario (McIntyre et al., 2009).

6.4.6.3 Impact of Future Changes in Reactive Nitrogen on Carbon Uptake and Storage

Anthropogenic Nr addition and natural nitrogen-cycle responses to global changes will have an important impact on the global carbon cycle. As a principal nutrient for plant growth, nitrogen can both limit future carbon uptake and stimulate it depending on changes in Nr availability. A range of global terrestrial carbon cycle models have been developed since AR4 that integrate nitrogen dynamics into the simulation of land carbon cycling (Thornton et al., 2007; Wang et al., 2007, 2010a; Sokolov et al., 2008; Xu-Ri and Prentice, 2008; Churkina et al., 2009; Jain et al., 2009; Fisher et al., 2010; Gerber et al., 2010; Zaehle and Friend, 2010; Esser et al., 2011). However, only two ESMs in CMIP5 (CESM1-BGC and NorESM1-ME) include a description of nitrogen–carbon interactions.

In response to climate warming, increased decomposition of soil organic matter increases nitrogen mineralisation, (*high confidence*) which can enhance Nr uptake and carbon storage by vegetation. Generally, higher C:N ratio in woody vegetation compared to C:N ratio of soil organic matter causes increased ecosystem carbon storage as increased Nr uptake shifts nitrogen from soil to vegetation (Melillo et al., 2011). In two studies (Sokolov et al., 2008; Thornton et al., 2009), this effect was strong enough to turn the carbon–climate interaction into a small negative feedback, that is, an increased land CO_2 uptake in response to climate warming (positive γ_L values in Figure 6.20), whereas in another study that described carbon–nitrogen interactions (Zaehle et al., 2010b) the carbon–climate interaction was reduced but remained positive, that is, decreased land CO_2 uptake in response to climate change (negative γ_L values in Figures 6.20, 6.21 and 6.22). The two CMIP5 ESMs which include terrestrial carbon–nitrogen interactions (Table 6.11) also simulate a small but positive climate–carbon feedback.

Consistent with the observational evidence (Finzi et al., 2006; Palmroth et al., 2006; Norby et al., 2010), modelling studies have shown a strong effect of Nr availability in limiting the response of plant growth and land carbon storage to elevated atmospheric CO_2 (e.g., Sokolov et al., 2008; Thornton et al., 2009; Zaehle and Friend, 2010). These analyses are affected by the projected future trajectories of anthropogenic Nr deposition. The effects of Nr deposition counteract the nitrogen limitation of CO_2 fertilisation (Churkina et al., 2009; Zaehle et al., 2010a). Estimates of the total net carbon storage on land due to Nr deposition between 1860 and 2100 range between 27 and 66 PgC (Thornton et al., 2009; Zaehle et al., 2010a).

It is *very likely* that, at the global scale, nutrient limitation will reduce the global land carbon storage projected by CMIP5 carbon-cycle only models. Only two of the current CMIP5 ESM models explicitly consider carbon–nitrogen interactions (CESM1-BGC and NorESM1-ME).

The effect of the nitrogen limitations on terrestrial carbon sequestration in the results of the other CMIP5 models may be approximated by comparing the implicit Nr requirement given plausible ranges of terrestrial C:N stoichiometry (Wang and Houlton, 2009) to plausible increases in terrestrial Nr supply due to increased biological nitrogen fixation (Wang and Houlton, 2009) and anthropogenic Nr deposition (Figure 6.35). For the ensemble of CMIP5 projections under the RCP 8.5 scenario, this implies a lack of available nitrogen of 1.3 to 13.1 PgN which would reduce terrestrial C sequestration by an average of 137 PgC over the period 1860–2100, with a range of 41 to 273 PgC among models. This represents an ensemble mean reduction in land carbon sequestration of 55%, with a large spread across models (14 to 196%). Inferred reductions in ensemble-mean land carbon sink over the same period for RCPs 6.0, 4.5 and 2.6 are 109, 117 and 85 PgC, respectively. Between-model variation in these inferred reduced land carbon sinks is similar for all RCPs, with ranges of 57 to 162 PgC, 38 to 208 PgC, and 32 to 171 PgC for RCPs 6.0, 4.5 and 2.6, respectively. The influence of nutrient addition for agriculture and pasture management is not addressed in this analysis. Results from the two CMIP5 models with explicit carbon–nitrogen interactions show even lower land carbon sequestration than obtained by this approximation method (Figure 6.35). More models with explicit carbon–nitrogen interactions are needed to understand between-model variation and construct an ensemble response.

The positive effect on land carbon storage due to climate-increased Nr mineralization is of comparable magnitude to the land carbon storage increase associated with increased anthropogenic Nr deposition. Models disagree, however, which of the two factors is more important, with both effects dependent on the choice of scenario. Crucially, the effect of nitrogen limitation on vegetation growth and carbon storage under elevated CO_2 is the strongest effect of the natural and disturbed nitrogen cycle on terrestrial carbon dynamics (Bonan and Levis, 2010; Zaehle et al., 2010a). In consequence, the projected atmospheric CO_2

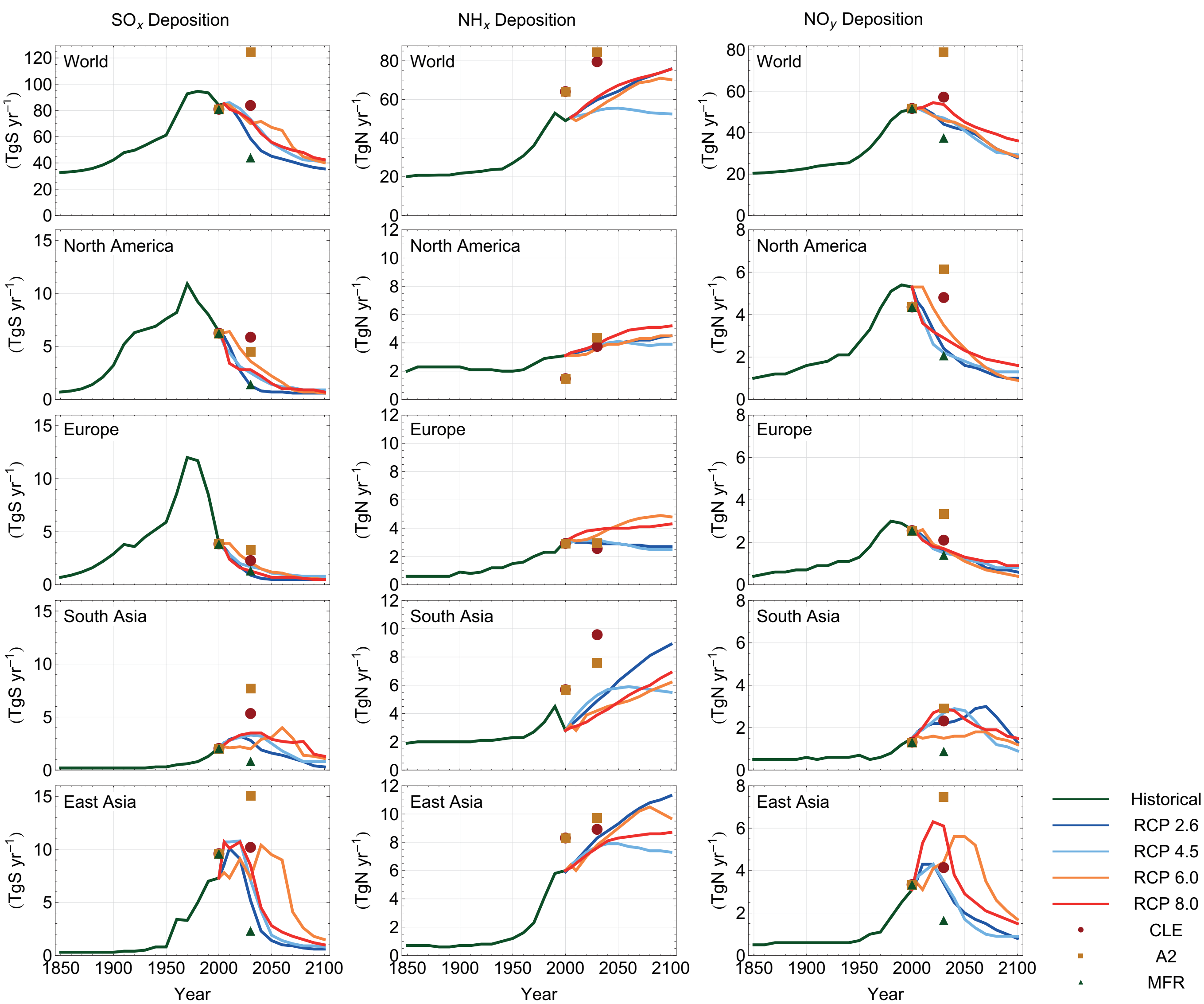

Figure 6.33 | Deposition of SO_x (left, $TgS\ yr^{-1}$), NH_x (middle, $TgN\ yr^{-1}$) and NO_y (right, $TgN\ yr^{-1}$) from 1850 to 2000 and projections of deposition to 2100 under the four RCP emission scenarios (Lamarque et al., 2011; van Vuuren et al., 2011). Also shown are the 2030 scenarios using the SRES B1/A2 energy scenario with assumed current legislation and maximum technically feasible air pollutant reduction controls (Dentener et al., 2006).

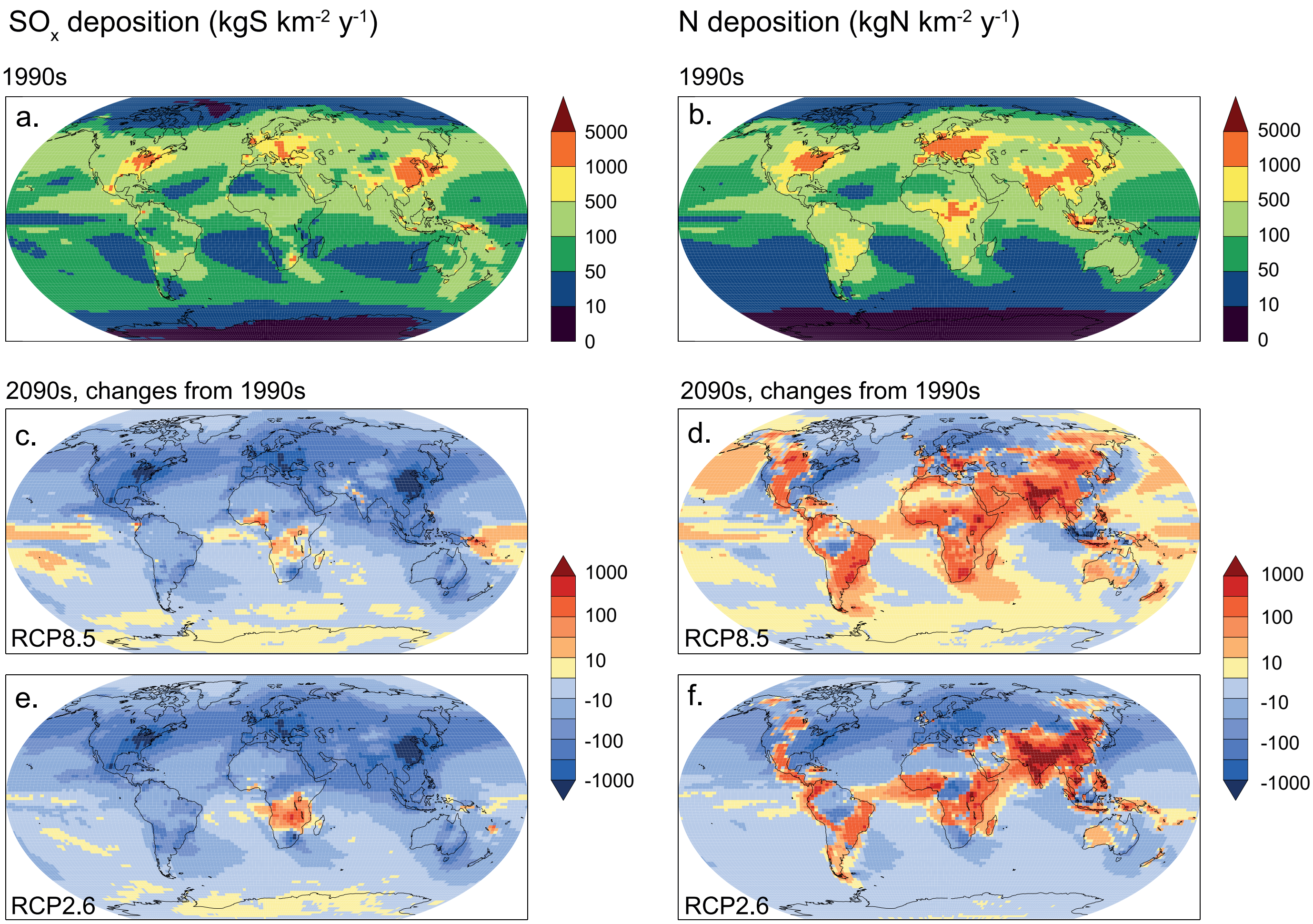

Figure 6.34 | Spatial variability of nitrogen and SO$_x$ deposition in 1990s with projections to the 2090s (shown as difference relative to the 1990s), using the RCP2.6 and RCP8.5 scenarios, kgN km^{-2} yr^{-1}, adapted from Lamarque et al. (2011). Note that no information on the statistical significance of the shown differences is available. This is of particular relevance for areas with small changes. The plots for all four of the RCP scenarios are in the Supplementary Material.

concentrations (and thus degree of climate change) in 2100 are higher in projections with models describing nitrogen limitations than in those same models without these interactions. The influence of current and future nitrogen deposition on the ocean sink for anthropogenic carbon is estimated to be rather small, with less than 5% of the ocean carbon sink in 2100 attributable to fertilisation from anthropogenic Nr deposition over the oceans (Reay et al., 2008).

None of the CMIP5 models include phosphorus as a limiting nutrient for land ecosystems, although this limitation and interactions with Nr availability are observed in many systems (Elser et al., 2007). Limitation by Nr availability alone may act as a partial surrogate for combined nitrogen–phosphorus limitation (Thornton et al., 2009; Section 6.4.8.2), but are *likely* to underestimate the overall nutrient limitation, especially in lowland tropical forest.

6.4.7 Future Changes in Methane Emissions

Future atmospheric CH_4 concentrations are sensitive to changes in both emissions and OH oxidation. Atmospheric chemistry is not covered in this chapter and we assess here future changes in natural CH_4 emissions in response to climate change (e.g., O'Connor et al., 2010; Figure 6.36). Projected increases in future fire occurrence (Section 6.4.8.1) suggest that CH_4 from fires may increase (*low confidence*). Future changes in anthropogenic emissions due to anthropogenic alteration of wetlands (e.g., peatland drainage) may also be important but are not assessed here.

6.4.7.1 Future Methane Emissions from Wetlands

Overall, there is *medium confidence* that emissions of CH_4 from wetlands are *likely* to increase in the future under elevated CO_2 and warmer climate. Wetland extent is determined by geomorphology and soil moisture, which depends on precipitation, evapotranspiration, drainage and runoff. All of these may change in the future. Increasing temperature can lead to higher rates of evapotranspiration, reducing soil moisture and therefore affect wetland extent, and temporary increasing aeration of existing wetlands with further consequences to methane emissions. Regional projections of precipitation changes are especially uncertain (see Chapter 12).

Direct effects on wetland CH_4 emissions include: higher NPP under higher temperature and higher atmospheric CO_2 concentrations leading to more substrate for methanogenesis (White et al., 2008); higher CH_4 production rates under higher temperature; and changes in CH_4 oxidation through changed precipitation that alters water table position (Melton et al., 2013). Wetland CH_4 emissions are also affected by changes in wetland area which may either increase (due to thawing permafrost or reduced evapotranspiration) or decrease (due to reduced precipitation or increased evaporation) regionally. In most models, elevated CO_2 has a stronger enhancement effect on CH_4 emissions than climate change. However, large uncertainties exist concerning the lack of wetland specific plant functional types in most models and the lack of understanding how wetland plants will react to CO_2 fertilisation (e.g., Berendse et al., 2001; Boardman et al., 2011; Heijmans et al., 2001, 2002a, 2002b).

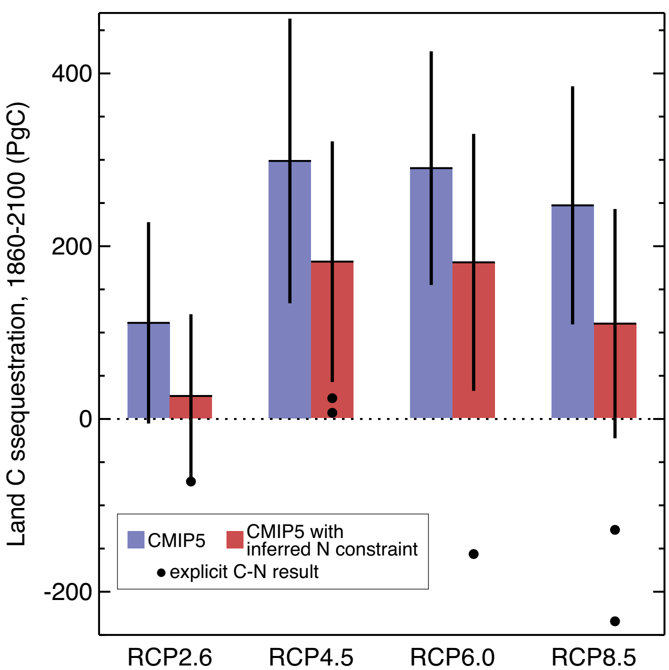

Figure 6.35 | Estimated influence of nitrogen availability on total land carbon sequestration over the period 1860–2100 (based on analysis method of Wang and Houlton (2009). Blue bars show, for each RCP scenario, the multi-model ensemble mean of land carbon sequestration, based on the carbon-only subset of CMIP5 models (Canadian Earth System Model 2 (CanESM2), Geophysical Fluid Dynamics Laboratory–Earth System Model 2G (GFDL-ESM2G), Geophysical Fluid Dynamics Laboratory–Earth System Model 2M (GFDL-ESM2M), Hadley Centre Global Environmental Model 2–Carbon Cycle(HadGEM2-CC), Hadley Centre Global Environmental Model 2–Earth System (HadGEM2-ES), Institute Pierre Simon Laplace–Coupled Model 5A–Low Resolution (IPSL-CM5A-LR), Institute Pierre Simon Laplace– Coupled Model 5A–Medium Resolution (IPSL-CM5A-MR), Institute Pierre Simon Laplace–Coupled Model 5B–Low Resolution (IPSL-CM5B-LR), Max Planck Institute–Earth System Model–Low Resolution (MPI-ESM-LR): not all models produced results for all scenarios). Red bars show, for each scenario, the mean land carbon sequestration from the same ensemble of carbon-only models after correcting for inferred constraints on carbon uptake due to limited availability of nitrogen. Black bars show ± one standard deviation around the means. Black symbols show individual model results from the two CMIP5 models with explicit carbon–nitrogen interactions (Community Earth System Model 1–Biogeochemical (CESM1-BGC) and Norwegian Earth System Model 1 (Emissions capable) (NorESM1-ME)). These two models have nearly identical representations of land carbon–nitrogen dynamics, and differences between them here (for RCP4.5 and RCP8.5, where both models contributed results) are due to differences in coupled system climate. All simulations shown here used prescribed atmospheric CO_2 concentrations.

Since AR4, several modelling studies have attempted to quantify the sensitivity of global wetland CH_4 emissions to environmental changes (see Figure 6.37). The studies cover a wide range of simulation results but there is high agreement between model results that the combined effect of CO_2 increase and climate change by the end of the 21st century will increase wetland CH_4 emissions. Using a common experimental protocol with spatially uniform changes in precipitation, temperature and CO_2 ("WETCHIMP"; Melton et al., 2013) seven models predict that the effect of increased temperature alone (red bars in Figure 6.37) may cause an increase or decrease of wetland CH_4 emissions, while the effect of increased precipitation alone (green bars in Figure 6.37) is always an increase, although generally small. The effect of increased atmospheric CO_2 concentration (fertilisation of NPP; Box 6.3; blue bars in Figure 6.37) always resulted in an increase of emissions (22 to 162%). Other studies assessed the effects of temperature and precipitation together (orange bars in Figure 6.37) and often found an increase in wetland CH_4 emissions (Eliseev et al., 2008; Gedney et al., 2004; Shindell et al., 2004; Volodin, 2008) although Ringeval et al. (2011) found a net decrease. The combined effect of climate and CO_2 resulted in an increase of wetland CH_4 emissions from 40% (Volodin (2008); fixed wetland area) to 68% (Ringeval et al., 2011); variable wetland area).

The models assessed here do not consider changes in soil hydrological properties caused by changes in organic matter content. Positive feedbacks from increased drainage due to organic carbon loss may

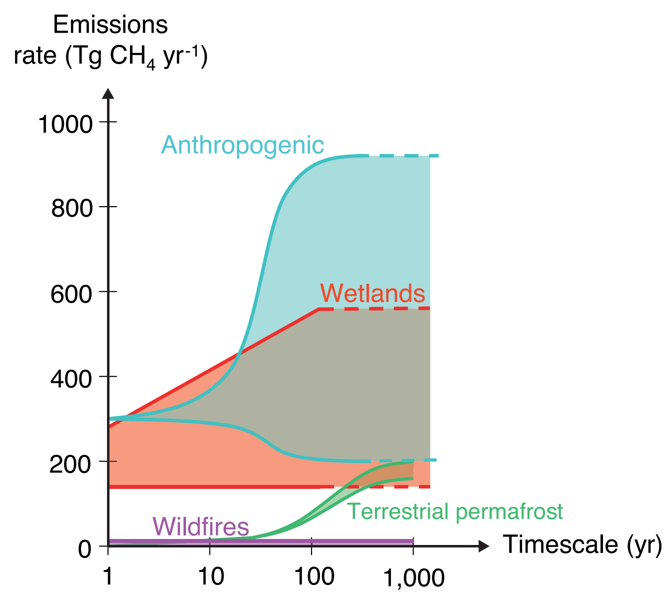

Figure 6.36 | Schematic synthesis of the magnitude and time scales associated with possible future CH_4 emissions (adapted from O'Connor et al., 2010). Uncertainty in these future changes is large, and so this figure demonstrates the relative magnitude of possible future changes. Anthropogenic emissions starting at a present-day level of 300 Tg(CH_4) yr^{-1} (consistent with Table 6.8) and increasing or decreasing according to RCP8.5 and RCP2.6 are shown for reference. Wetland emissions are taken as 140 to 280 Tg(CH_4) yr^{-1} present day values (Table 6.8) and increasing by between 0 and 100% (Section 6.4.7.1; Figure 6.37). Permafrost emissions may become important during the 21st century. CH_4 release from marine hydrates and subsea permafrost may also occur but uncertainty is sufficient to prevent plotting emission rates here. Large CH_4 hydrate release to the atmosphere is not expected during the 21st century. No quantitative estimates of future changes in CH_4 emissions from wildfires exist, so plotted here are continued present-day emissions of 1 to 5 Tg(CH_4) yr^{-1} (Table 6.8).

6

accelerate peat decomposition rates (Ise et al., 2008). However, carbon accumulation due to elevated NPP in wetland and permafrost regions may to some extent offset CH_4 emissions (Frolking and Roulet, 2007; Turetsky et al., 2007). None of the studies or models assessed here considers CH_4 emissions from mangroves.

The models also do not agree in their simulations of present day wetland extent or CH_4 emissions, and there are not adequate data sets to evaluate them thoroughly at the grid scale (typically 0.5°) (Melton et al., 2013). Hence despite high agreement between models of a strong positive response of wetland CH_4 emission rates to increasing atmospheric CO_2 we assign *low confidence* to quantitative projections of future wetland CH_4 emissions.

Soil CH_4 oxidation of about 30 Tg(CH_4) yr^{-1} (Table 6.8) represents the smallest of the three sinks for atmospheric methane (see Table 6.8) but is also sensitive to future environmental changes. Soil CH_4 oxidation is projected to increase by up to 23% under the SRES A1B due to rising atmospheric CH_4 concentrations, higher soil temperature and lower soil moisture (Curry, 2007, 2009).

6.4.7.2 Future Methane Emissions from Permafrost Areas

Permafrost thaw may lead to increased drainage and a net reduction in lakes and wetlands, a process that has already begun to be seen in lakes in the discontinuous permafrost zone (Smith et al., 2005; Jones et al., 2011) and has been projected to continue under future scenarios (Avis et al., 2011). Alternatively, small lakes or ponds and wetland growth may occur in continuous permafrost areas underlain by ice-rich material subject to thermokarst (Christensen et al., 2004; Jorgenson et al., 2006; Plug and West, 2009; Jones et al., 2011).

There is high agreement between land surface models that permafrost extent is expected to reduce during the 21st century, accompanying particularly rapid warming at high latitudes (Chapter 12). However, estimates vary widely as to the pace of degradation (Lawrence and Slater, 2005; Burn and Nelson, 2006; Lawrence et al., 2008). The LPJ-WHyMe model projected permafrost area loss of 30% (SRES B1) and 47% (SRES A2) by 2100 (Wania, 2007). Marchenko et al. (2008) calculate that by 2100, 57% of Alaska will lose permafrost within the top 2 m. For the RCP scenarios, the CMIP5 multi-model ensemble shows a wide range of projections for permafrost loss: 15 to 87% under RCP4.5 and 30 to 99% under RCP8.5 (Koven et al., 2013).

Hydrological changes may lead to tradeoffs between the CO_2 and CH_4 balance of ecosystems underlain by permafrost, with methane production rates being roughly an order of magnitude less than rates of oxic decomposition to CO_2 but CH_4 having a larger greenhouse warming potential (Frolking and Roulet, 2007). The extent of permafrost thaw simulated by climate models has been used to estimate possible subsequent carbon release (Burke et al., 2013; Harden et al., 2012; Section 6.4.3.4) but few studies explicitly partition this into CO_2 or CH_4 release

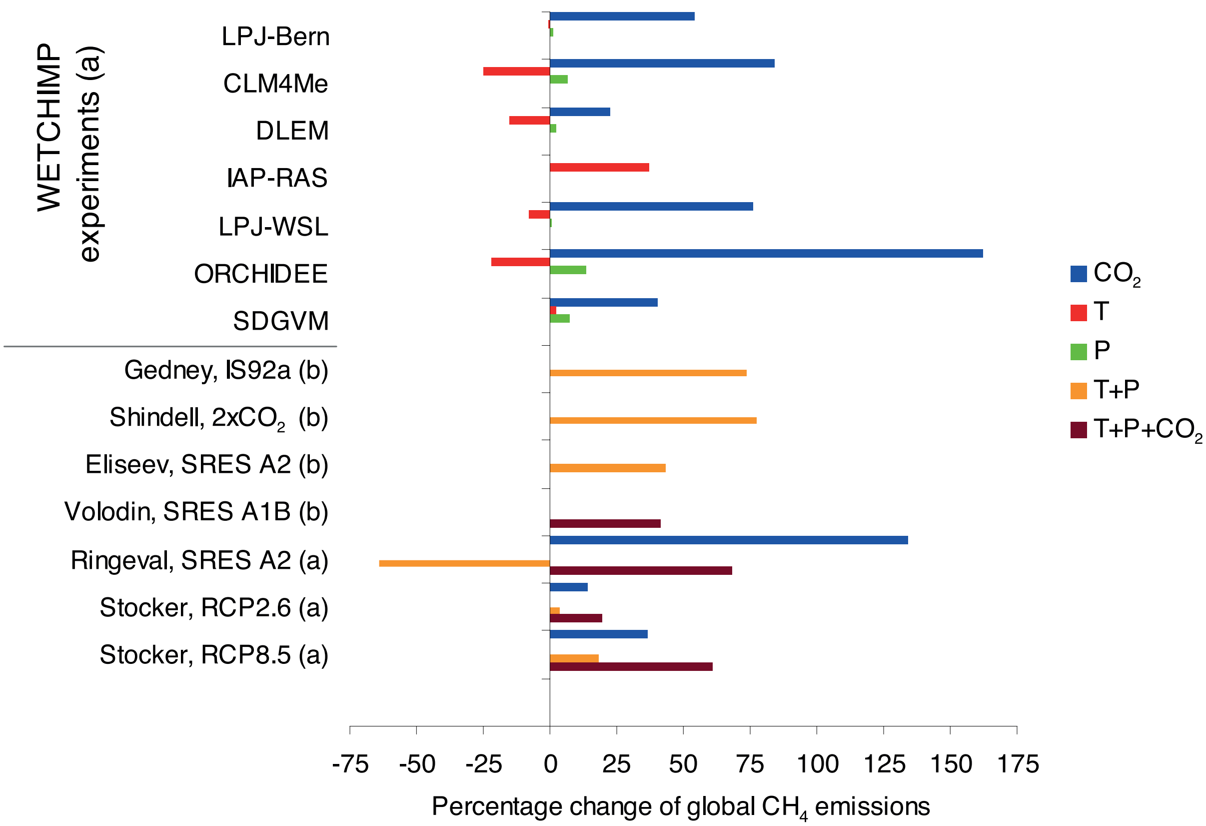

Figure 6.37 | Relative changes of global CH_4 emissions from either pre-industrial (a) or present-day (b) conditions and environmental changes that reflect potential conditions in 2100. The first seven models took part in the WETCHIMP intercomparison project and were run under a common protocol (Melton et al., 2013). Bars represent CH_4 emission changes associated with temperature-only changes (T), precipitation only (P), CO_2 only (CO_2) or combinations of multiple factors. Other studies as listed in the figure used different future scenarios: Eliseev et al. (2008), Gedney et al. (2004), Ringeval et al. (2011), Shindell et al. (2004), Volodin (2008), Stocker et al. (2013).

to the atmosphere. Schneider von Deimling et al. (2012) estimate cumulative CH_4 emissions by 2100 between 131 and 533 Tg(CH_4) across the 4 RCPs. CMIP5 projections of permafrost thaw do not consider changes in pond or lake formation. Thawing of unsaturated Yedoma carbon deposits (which contain large, but uncertain amounts of organic carbon in permafrost in northeast Siberia; Schirrmeister et al., 2011) was postulated to produce significant CH_4 emissions (Khvorostyanov et al., 2008), however more recent estimates with Yedoma carbon lability constrained by incubation observations (Dutta et al., 2006) argue for smaller emissions at 2100 (Koven et al., 2011).

6.4.7.3 Future Methane Hydrate Emissions

Substantial quantities of methane are believed to be stored within submarine hydrate deposits at continental margins (see also Section 6.1, FAQ 6.1). There is concern that warming of overlying waters may melt these deposits, releasing CH_4 into the ocean and atmosphere systems. Overall, it is *likely* that subsequent emissions to the atmosphere caused by hydrate destabilisation would be in the form of CO_2, due to CH_4 oxidation in the water column.

Considering a potential warming of bottom waters by 1°C, 3°C and 5°C during the next 100 years, Reagan and Moridis (2007) found that hydrates residing in a typical deep ocean setting (4°C and 1000 m depth) would be stable and in shallow low-latitude settings (6°C and 560 m) any sea floor CH_4 fluxes would be oxidized within the sediments. Only in cold-shallow Arctic settings (0.4°C and 320 m) would CH_4 fluxes exceed rates of benthic sediment oxidation. Simulations of heat penetration through the sediment by Fyke and Weaver (2006) suggest that changes in the gas hydrate stability zone will be small on century time scales except in high-latitude regions of shallow ocean shelves. In the longer term, Archer et al. (2009a) estimated that between 35 and 940 PgC could be released over several thousand years in the future following a 3°C seafloor warming.

Using multiple climate models (Lamarque, 2008), predicted an upper estimate of the global sea floor flux of between 560 and 2140 Tg(CH_4) yr^{-1}, mostly in the high latitudes. Hunter et al. (2013) also found 21st century hydrate dissociation in shallow Arctic waters and comparable in magnitude to Biastoch et al. (2011), although maximum CH_4 sea floor fluxes were smaller than Lamarque (2008), with emissions from 330 to 450 Tg(CH_4) yr^{-1} for RCP 4.5 to RCP8.5. Most of the sea floor flux of CH_4 is expected to be oxidised in the water column into dissolved CO_2. Mau et al. (2007) suggest only 1% might be released to the atmosphere but this fraction depends on the depth of water and ocean conditions. Elliott et al. (2011) demonstrated significant impacts of such sea floor release on marine hypoxia and acidity, although atmospheric CH_4 release was small.

Observations of CH_4 release along the Svalbard margin seafloor (Westbrook et al., 2009) suggest observed regional warming of 1°C during the last 30 years is driving hydrate disassociation, an idea supported by modelling (Reagan and Moridis, 2009). However, these studies do not consider subsea-permafrost hydrates suggested recently to be regionally significant sources of atmospheric CH_4 (Shakhova et al., 2010). There was no positive excursion in the methane concentration recorded in ice cores from the largest known submarine landslide, the Storegga slide of Norway 8200 years ago. Large methane hydrate release due to marine landslides is *unlikely* as any given landslide could release only a tiny fraction of the global inventory (Archer, 2007).

There is *low confidence* in modelling abilities to simulate transient changes in hydrate inventories, but large CH_4 release to the atmosphere during this century is *unlikely*.

6.4.8 Other Drivers of Future Carbon Cycle Changes

6.4.8.1 Changes in Fire under Climate Change/Scenarios of Anthropogenic Fire Changes

Regional studies for boreal regions suggest an increase in future fire risk (e.g., Amiro et al., 2009; Balshi et al., 2009; Flannigan et al., 2009a; Spracklen et al., 2009; Tymstra et al., 2007; Westerling et al., 2011; Wotton et al., 2010) with implications for carbon and nutrient storage (Certini, 2005). Kurz et al. (2008b) and Metsaranta et al. (2010) indicated that increased fire activity has the potential to turn the Canadian forest from a sink to a source of atmospheric CO_2. Models predict spatially variable responses in fire activity, including strong increases and decreases, due to regional variations in the climate–fire relationship, and anthropogenic interference (Scholze et al., 2006; Flannigan et al., 2009b; Krawchuk et al., 2009; Pechony and Shindell, 2010; Kloster et al., 2012). Wetter conditions can reduce fire activity, but increased biomass availability can increase fire emissions (Scholze et al., 2006; Terrier et al., 2013). Using a land surface model and future climate projections from two GCMs, Kloster et al. (2012) projected fire carbon emissions in 2075–2099 that exceed present-day emissions by 17 to 62% (0.3 to 1.0 PgC yr^{-1}) depending on scenario.

Future fire activity will also depend on anthropogenic factors especially related to land use change. For the Amazon it is estimated that at present 58% of the area is too humid to allow deforestation fires but climate change might reduce this area to 37% by 2050 (Le Page et al., 2010). Golding and Betts (2008) estimated that future Amazon forest vulnerability to fire may depend nonlinearly on combined climate change and deforestation.

6.4.8.2 Other Biogeochemical Cycles and Processes Impacting Future Carbon Fluxes

6.4.8.2.1 Phosphorus

On centennial time scales, the phosphoros (P) limitation of terrestrial carbon uptake could become more severe than the nitrogen limitation because of limited phosphorus sources. Model simulations have shown a shift after 2100 from nitrogen to phosphorus limitation at high latitudes (Goll et al., 2012).

6.4.8.2.2 Elevated surface ozone

Plants are known to suffer damage due to exposure to levels of ozone (O_3) above about 40 ppb (Ashmore, 2005). Model simulations of plant O_3 damage on the carbon cycle have found a reduction in terrestrial carbon storage between 2005 and 2100 ranging from 4 to 140 PgC (Felzer et al., 2005) and up to 260 PgC (Sitch et al., 2007).

6.4.8.2.3 Iron deposition to oceans

Changes in iron deposition may have affected ocean carbon uptake in the past (Section 6.2.1.1), but future projections of iron deposition from desert dust over the ocean are uncertain, even about the sign of changes (Tegen et al., 2004; Mahowald et al., 2009). Tagliabue et al. (2008) found relatively little impact of varying aeolian iron input on ocean CO_2 fluxes, but Mahowald et al. (2011) show projected changes in ocean productivity as large as those due to CO_2 increases and climate change.

6.4.8.2.4 Changes in the diffuse fraction of solar radiation at the surface

Mercado et al. (2009) estimated that variations in the diffuse fraction, associated largely with the 'global dimming' period (Stanhill and Cohen, 2001), enhanced the land carbon sink by approximately 25% between 1960 and 1999. Under heavily polluted or dark cloudy skies, plant productivity may decline as the diffuse effect is insufficient to offset decreased surface irradiance (UNEP, 2011). Under future scenarios involving reductions in aerosol emissions (Figures 6.33 and 6.34), the diffuse-radiation enhancement of carbon uptake will decline.

6.4.9 The Long-term Carbon Cycle and Commitments

With *very high confidence*, the physical, biogeochemical carbon cycle in the ocean and on land will continue to respond to climate change and rising atmospheric CO_2 concentrations created during the 21st century. Long-term changes in vegetation structure and induced carbon storage potentially show larger changes beyond 2100 than during the 21st century as the long time scale response of tree growth and ecosystem migrations means that by 2100 only a part of the eventual committed change will be realized (Jones et al., 2009). Holocene changes in tree-line lagged changes in climate by centuries (MacDonald et al., 2008). Long-term 'commitments' to ecosystems migration also carry long-term committed effects to changes in terrestrial carbon storage (Jones et al., 2010; Liddicoat et al., 2013) and permafrost (O'Connor et al., 2010; Sections 6.4.3.3 and 6.4.7).

Warming of high latitudes is common to most climate models (Chapter 12) and this may enable increased productivity and northward expansion of boreal forest ecosystems into present tundra regions depending on nutrient availability (Kellomäki et al., 2008; Kurz et al., 2008a; MacDonald et al., 2008). CMIP5 simulations by two ESMs with dynamic vegetation for extended RCP scenarios to 2300 (Meinshausen et al., 2011) allow analysis of this longer term response of the carbon cycle. Increases in tree cover and terrestrial carbon storage north of 60°N are shown in Figure 6.38.

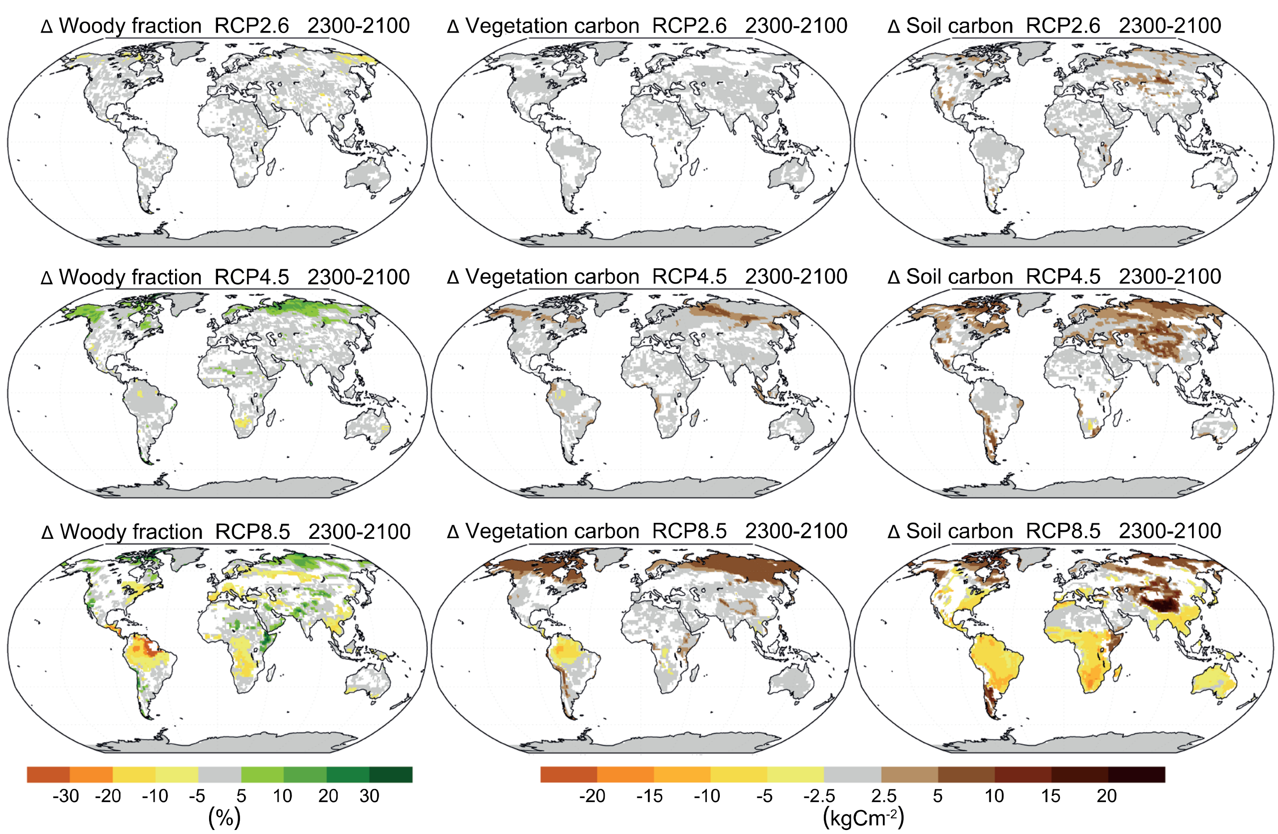

Figure 6.38 | Maps of changes in woody cover fraction, %, (left) and terrestrial carbon storage, kg C m^{-2} (vegetation carbon, middle; soil carbon, right) between years 2100 and 2300 averaged for two models, Hadley Centre Global Environmental Model 2-Earth System (HadGEM2-ES) and Max Planck Institute–Earth System Model (MPI-ESM), which simulate vegetation dynamics for three RCP extension scenarios 2.6 (top), 4.5 (middle), and 8.5 (bottom). Note the RCP6.0 extension was not a CMIP5 required simulation. Model results were interpolated on 1° × 1° grid; white colour indicates areas where models disagree in sign of changes. Anthropogenic land use in these extension scenarios is kept constant at 2100 levels, so these results show the response of natural ecosystems to the climate change.

Frequently Asked Questions

FAQ 6.2 | What Happens to Carbon Dioxide After It Is Emitted into the Atmosphere?

Carbon dioxide (CO_2), after it is emitted into the atmosphere, is firstly rapidly distributed between atmosphere, the upper ocean and vegetation. Subsequently, the carbon continues to be moved between the different reservoirs of the global carbon cycle, such as soils, the deeper ocean and rocks. Some of these exchanges occur very slowly. Depending on the amount of CO_2 released, between 15% and 40% will remain in the atmosphere for up to 2000 years, after which a new balance is established between the atmosphere, the land biosphere and the ocean. Geological processes will take anywhere from tens to hundreds of thousands of years—perhaps longer—to redistribute the carbon further among the geological reservoirs. Higher atmospheric CO_2 concentrations, and associated climate impacts of present emissions, will, therefore, persist for a very long time into the future.

CO_2 is a largely non-reactive gas, which is rapidly mixed throughout the entire troposphere in less than a year. Unlike reactive chemical compounds in the atmosphere that are removed and broken down by sink processes, such as methane, carbon is instead redistributed among the different reservoirs of the global carbon cycle and ultimately recycled back to the atmosphere on a multitude of time scales. FAQ 6.2, Figure 1 shows a simplified diagram of the global carbon cycle. The open arrows indicate typical timeframes for carbon atoms to be transferred through the different reservoirs.

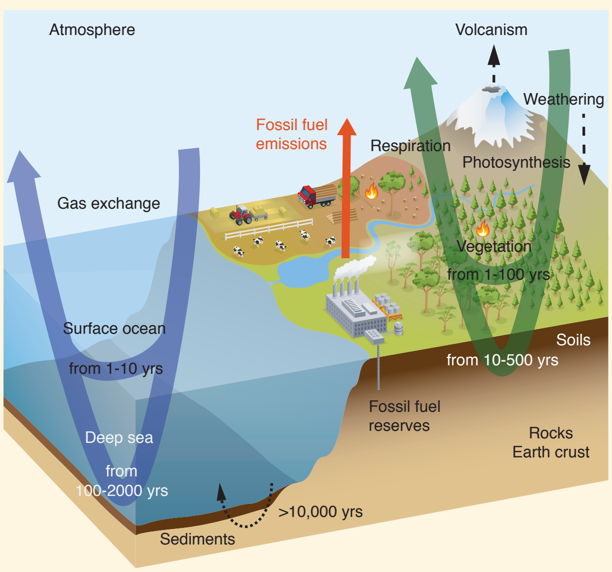

FAQ 6.2, Figure 1 | Simplified schematic of the global carbon cycle showing the typical turnover time scales for carbon transfers through the major reservoirs.

Before the Industrial Era, the global carbon cycle was roughly balanced. This can be inferred from ice core measurements, which show a near constant atmospheric concentration of CO_2 over the last several thousand years prior to the Industrial Era. Anthropogenic emissions of carbon dioxide into the atmosphere, however, have disturbed that equilibrium. As global CO_2 concentrations rise, the exchange processes between CO_2 and the surface ocean and vegetation are altered, as are subsequent exchanges within and among the carbon reservoirs on land, in the ocean and eventually, the Earth crust. In this way, the added carbon is redistributed by the global carbon cycle, until the exchanges of carbon between the different carbon reservoirs have reached a new, approximate balance.

Over the ocean, CO_2 molecules pass through the air-sea interface by gas exchange. In seawater, CO_2 interacts with water molecules to form carbonic acid, which reacts very quickly with the large reservoir of dissolved inorganic carbon—bicarbonate and carbonate ions—in the ocean. Currents and the formation of sinking dense waters transport the carbon between the surface and deeper layers of the ocean. The marine biota also redistribute carbon: marine organisms grow organic tissue and calcareous shells in surface waters, which, after their death, sink to deeper waters, where they are returned to the dissolved inorganic carbon reservoir by dissolution and microbial decomposition. A small fraction reaches the sea floor, and is incorporated into the sediments.

The extra carbon from anthropogenic emissions has the effect of increasing the atmospheric partial pressure of CO_2, which in turn increases the air-to-sea exchange of CO_2 molecules. In the surface ocean, the carbonate chemistry quickly accommodates that extra CO_2. As a result, shallow surface ocean waters reach balance with the atmosphere within 1 or 2 years. Movement of the carbon from the surface into the middle depths and deeper waters takes longer—between decades and many centuries. On still longer time scales, acidification by the invading CO_2 dissolves carbonate sediments on the sea floor, which further enhances ocean uptake. However, current understanding suggests that, unless substantial ocean circulation changes occur, plankton growth remains roughly unchanged because it is limited mostly by environmental factors, such as nutrients and light, and not by the availability of inorganic carbon it does not contribute significantly to the ocean uptake of anthropogenic CO_2. *(continued on next page)*

FAQ 6.2 (continued)

On land, vegetation absorbs CO_2 by photosynthesis and converts it into organic matter. A fraction of this carbon is immediately returned to the atmosphere as CO_2 by plant respiration. Plants use the remainder for growth. Dead plant material is incorporated into soils, eventually to be decomposed by microorganisms and then respired back into the atmosphere as CO_2. In addition, carbon in vegetation and soils is also converted back into CO_2 by fires, insects, herbivores, as well as by harvest of plants and subsequent consumption by livestock or humans. Some organic carbon is furthermore carried into the ocean by streams and rivers.

An increase in atmospheric CO_2 stimulates photosynthesis, and thus carbon uptake. In addition, elevated CO_2 concentrations help plants in dry areas to use ground water more efficiently. This in turn increases the biomass in vegetation and soils and so fosters a carbon sink on land. The magnitude of this sink, however, also depends critically on other factors, such as water and nutrient availability.

Coupled carbon-cycle climate models indicate that less carbon is taken up by the ocean and land as the climate warms constituting a positive climate feedback. Many different factors contribute to this effect: warmer seawater, for instance, has a lower CO_2 solubility, so altered chemical carbon reactions result in less oceanic uptake of excess atmospheric CO_2. On land, higher temperatures foster longer seasonal growth periods in temperate and higher latitudes, but also faster respiration of soil carbon.

The time it takes to reach a new carbon distribution balance depends on the transfer times of carbon through the different reservoirs, and takes place over a multitude of time scales. Carbon is first exchanged among the 'fast' carbon reservoirs, such as the atmosphere, surface ocean, land vegetation and soils, over time scales up to a few thousand years. Over longer time scales, very slow secondary geological processes—dissolution of carbonate sediments and sediment burial into the Earth's crust—become important.

FAQ 6.2, Figure 2 illustrates the decay of a large excess amount of CO_2 (5000 PgC, or about 10 times the cumulative CO_2 emitted so far since the beginning of the industrial Era) emitted into the atmosphere, and how it is redistributed among land and the ocean over time. During the first 200 years, the ocean and land take up similar amounts of carbon. On longer time scales, the ocean uptake dominates mainly because of its larger reservoir size (~38,000 PgC) as compared to land (~4000 PgC) and atmosphere (589 PgC prior to the Industrial Era). Because of ocean chemistry the size of the initial input is important: higher emissions imply that a larger fraction of CO_2 will remain in the atmosphere. After 2000 years, the atmosphere will still contain between 15% and 40% of those initial CO_2 emissions. A further reduction by carbonate sediment dissolution, and reactions with igneous rocks, such as silicate weathering and sediment burial, will take anything from tens to hundreds of thousands of years, or even longer.

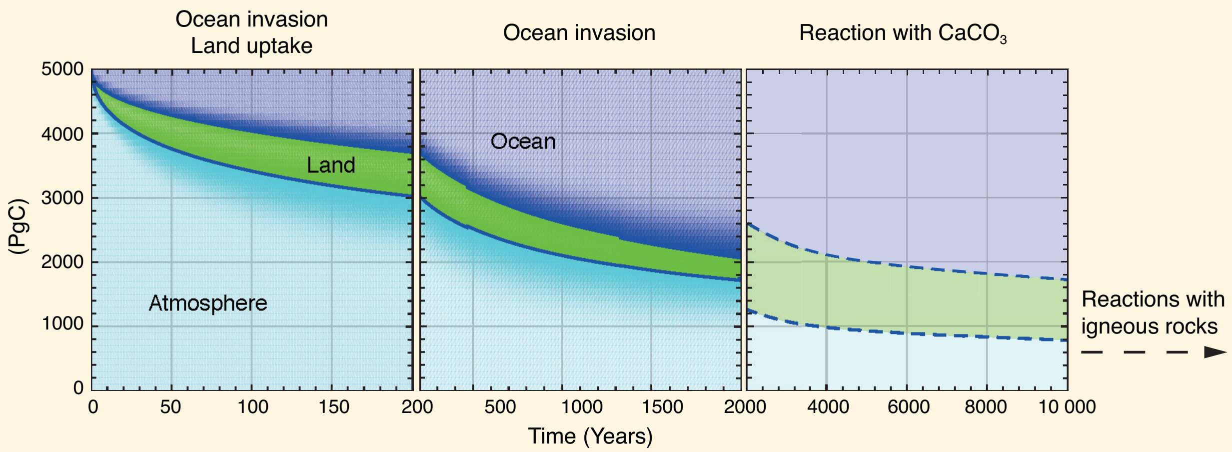

FAQ 6.2, Figure 2 | Decay of a CO_2 excess amount of 5000 PgC emitted at time zero into the atmosphere, and its subsequent redistribution into land and ocean as a function of time, computed by coupled carbon-cycle climate models. The sizes of the colour bands indicate the carbon uptake by the respective reservoir. The first two panels show the multi-model mean from a model intercomparison project (Joos et al., 2013). The last panel shows the longer term redistribution including ocean dissolution of carbonaceous sediments as computed with an Earth System Model of Intermediate Complexity (after Archer et al., 2009b).

Increases in fire disturbance or insect damage may drive loss of forest in temperate regions (Kurz et al., 2008c), but this process is poorly represented or not accounted at all in models. Recent evidence from models (Huntingford et al., 2013) and studies on climate variability (Cox et al., 2013) suggests that large scale loss of tropical forest as previously projected in some models (Cox et al., 2004; Scholze et al., 2006) is *unlikely*, but depends strongly on the predicted future changes in regional temperature (Galbraith et al., 2010) and precipitation (Good et al., 2011, 2013), although both models here simulate reduced tree cover and carbon storage for the RCP8.5 scenario. ESMs also poorly simulate resilience of ecosystems to climate changes and usually do not account for possible existence of alternative ecosystem states such as tropical forest or savannah (Hirota et al., 2011).

Regional specific changes in ecosystem composition and carbon storage are uncertain but it is *very likely* that ecosystems will continue to change for decades to centuries following stabilisation of GHGs and climate change.

6.5 Potential Effects of Carbon Dioxide Removal Methods and Solar Radiation Management on the Carbon Cycle

6.5.1 Introduction to Carbon Dioxide Removal Methods

To slow or perhaps reverse projected increases in atmospheric CO_2 (Section 6.4), several methods have been proposed to increase the removal of atmospheric CO_2 and enhance the storage of carbon in land, ocean and geological reservoirs. These methods are categorized as 'Carbon Dioxide Removal (CDR)' methods (see Glossary). Another class of methods involves the intentional manipulation of planetary solar absorption to counter climate change, and is called the 'Solar Radiation Management (SRM)' (discussed in Chapter 7, Section 7.7; see Glossary). In this section, CDR methods are discussed from the aspect of the carbon cycle processes (Section 6.5.2) and their impacts and side effects on carbon cycle and climate (Section 6.5.3). A brief discussion on the indirect carbon cycle effects of SRM methods is given in Section 6.5.4. Most of the currently proposed CDR methods are summarized in Table 6.14 and some are illustrated schematically in Chapter 7 (Section 7.7; FAQ 7.3 Figure 1). Since some CDR methods might operate on large spatial scales they are also called 'Geoengineering' proposals (Keith, 2001). Removal of CH_4 and N_2O has also been proposed to reduce climate change (Stolaroff et al., 2012). While the science of geoengineering methods is assessed in this section (CDR) and Chapter 7 (SRM), the benefits and risks of SRM are planned to be assessed in Chapter 19 of AR5 WGII report. Further, Chapter 6 of AR5 WGIII report plans to assess the cost and socioeconomic implications of some CDR and SRM methods for climate stabilization pathways.

Large-scale industrial methods such as carbon capture and storage (CCS), biofuel energy production (without CCS) and reducing emissions from deforestation and degradation (REDD) cannot be called CDR methods since they *reduce fossil fuel use or land use change CO_2 emissions* to the atmosphere but they do not involve a net removal of CO_2 that is already in the atmosphere. However, direct air capture of CO_2 using industrial methods (Table 6.14; and FAQ 7.3 Figure 1) will remove CO_2 from the atmosphere and is thus considered as a CDR method. The distinction between CDR and mitigation (see Glossary) is not clear and there could be some overlap between the two.

Insofar as the CDR-removed CO_2 is sequestered in a permanent reservoir, CDR methods could potentially reduce direct consequences of high CO_2 levels, including ocean acidification (see Section 6.4.4) (Matthews et al., 2009). However, the effects of CDR methods that propose to manipulate carbon cycle processes are slow (see Box 6.1) and hence the consequent climate effects would be slow. The climate system has a less than 5-years relaxation (e-folding) time scale for an assumed instantaneous reduction in radiative forcing to preindustrial levels (Held et al., 2010). While the climate effect of SRM could be rapid (Shepherd et al., 2009) given this time scale, at present, there is no known CDR method, including industrial direct air capture that can feasibly reduce atmospheric CO_2 to pre-industrial levels within a similar time scale. Therefore, CDR methods do not present an option for rapidly preventing climate change when compared to SRM. It is *likely* that CDR would have to be deployed at large-scale for at least one century to be able to significantly reduce atmospheric CO_2.

Important carbon cycle science considerations for evaluating CDR methods include the associated carbon storage capacity, the permanence of carbon storage and potential adverse side effects (Shepherd et al., 2009). Geological reservoirs could store several thousand PgC and the ocean may be able to store a few thousand PgC of anthropogenic carbon in the long-term (Metz et al., 2005; House et al., 2006; Orr, 2009) (see Box 6.1 and Archer et al., 2009b). The terrestrial biosphere may have a typical potential to store carbon equivalent to the cumulative historical land use loss of 180 ± 80 PgC (Table 6.1; Section 6.5.2.1).

In this assessment, we use "permanence" to refer to time scales larger than tens of thousands of years. CDR methods associated with either permanent or non-permanent carbon sequestration (see Table 6.14) have very different climate implications (Kirschbaum, 2003). Permanent sequestration methods have the potential to reduce the radiative forcing of CO_2 over time. By contrast, non-permanent sequestration methods will release back the temporarily sequestered carbon as CO_2 to the atmosphere, after some delayed time interval (Herzog et al., 2003). As a consequence, elevated levels of atmospheric CO_2 and climate warming will only be delayed and not avoided by the implementation of non-permanent CDR methods (Figure 6.39). Nevertheless, CDR methods that could create a temporary CO_2 removal (Table 6.14) may still have value (Dornburg and Marland, 2008) by reducing the cumulative impact of higher temperature.

Another important carbon cycle consequence of CDR methods is the 'rebound effect' (see Glossary). In the Industrial Era (since 1750) about half of the CO_2 emitted into the atmosphere from fossil fuel emissions has been taken up by land and ocean carbon reservoirs (see Section 6.3 and Table 6.1). As for current CO_2 emissions and the consequent CO_2 rise, which are currently *opposed* by uptake of CO_2 by natural reservoirs, any removal of CO_2 from the atmosphere by CDR will be *opposed* by release of CO_2 from natural reservoirs (Figure 6.40). It is thus *virtually certain* that the removal of CO_2 by CDR will be partially offset by outgassing of CO_2 from the ocean and land ecosystems. Therefore, return-

Table 6.14 | Examples of CDR methods and their implications for carbon cycle and climate. The list is non-exhaustive. A 'rebound' effect and a thermal inertia of climate system are associated with all CDR methods.

Carbon Cycle Process to be Modified Intentionally	CDR Method Name	Nature of CDR Removal Process	Storage Location	Storage Form	Some Carbon Cycle and Climate Implications
Enhanced biological production and storage on land	Afforestation / reforestation[a] Improved forest management[b] Sequestration of wood in buildings[c] Biomass burial[d] No till agriculture[e] Biochar[f] Conservation agriculture[g] Fertilisation of land plants[h] Creation of wetlands[i] Biomass Energy with Carbon Capture and Storage (BECCS)[j]	Biological	[a,b,h] Land (biomass, soils) [d] Land/ocean floor [e, f,g] Land (soils) [i] Land (wetland soils) [j]Ocean / geological formations	[a,b,c,d,e,f,g,h,i] Organic [j]Inorganic	[a,b,c,d,e,f,g,h,i,j] Alters surface albedo and evapotranspiration [a,b,c,e,f,g,h,i] Lack of permanence [d]Potentially permanent if buried on the ocean floor [j]Permanent if stored in geological reservoir
Enhanced biological production and storage in ocean	Ocean iron fertilisation[k] Algae farming and burial[l] Blue carbon (mangrove, kelp farming)[m] Modifying ocean upwelling to bring nutrients from deep ocean to surface ocean[n]	Biological	Ocean	[k,n] Inorganic [l,m] Organic	[k]May lead to expanded regions with low oxygen concentration, increased N_2O production, deep ocean acidification and disruptions to marine ecosystems and regional carbon cycle [n]Disruptions to regional carbon cycle
Accelerated weathering	Enhanced weathering over land[o] Enhanced weathering over ocean[p]	Chemical	[o]Soils and oceans [p]Ocean	[o,p]Inorganic	[o]Permanent removal; *likely* to change pH of soils, rivers, and ocean [p]Permanent removal; *likely* to change pH of ocean
Others	Direct-air capture with storage	Chemical	Ocean/geological formations	Inorganic	Permanent removal if stored in geological reservoirs

Notes

Superscripts in column 2 refer to the corresponding superscripts in columns 4, 5 and 6 of the same row.

ing to pre-industrial CO_2 levels would require permanently sequestering an amount of carbon equal to total anthropogenic CO_2 emissions that have been released before the time of CDR, roughly twice as much the excess of atmospheric CO_2 above pre-industrial level (Lenton and Vaughan, 2009; Cao and Caldeira, 2010b; Matthews, 2010).

6.5.2 Carbon Cycle Processes Involved in Carbon Dioxide Removal Methods

The CDR methods listed in Table 6.14 rely primarily on human management of carbon cycle processes to remove CO_2: (1) enhanced net biological uptake and subsequent sequestration by land ecosystems, (2) enhanced biological production in ocean and subsequent sequestration in the ocean and (3) accelerated chemical weathering reactions over land and ocean. The exceptional CDR method is industrial direct air capture of CO_2, for example, relying on chemistry methods. CO_2 removed by CDR is expected to be stored in organic form on land and in inorganic form in ocean and geological reservoirs (Table 6.14). This management of the carbon cycle however has other implications on ecosystems and biogeochemical cycles. The principle of different CDR methods listed in Table 6.14 is described below and the characteristics of some CDR methods are summarized in Table 6.15.

Some of the RCP scenarios used as a basis for future projections in this Assessment Report already include some CDR methods. To achieve the RCP2.6 CO_2 peak and decline the IMAGE integrated assessment model simulates widespread implementation of BECCS technology to achieve globally negative emissions after around 2080 (see Section 6.4.3). RCP4.5 also assumes some use of BECCS to stabilise CO_2 concentration by 2100. Therefore it should be noted that potentials for CDR assessed in this section cannot be seen as additional potential for CO_2 removal from the low RCPs as this is already included in those scenarios.

6.5.2.1 Enhanced Carbon Sequestration by Land Ecosystems

The key driver of these CDR methods is net primary productivity on land that currently produces biomass at a rate of approximately 50 to 60 PgC yr^{-1} (Nemani et al., 2003). The principle of these CDR methods is to increase net primary productivity and/or store a larger fraction of the biomass produced into ecosystem carbon pools with long turnover times, for example, under the form of wood or refractory organic matter in soils (Table 6.14). One variant is to harvest biomass for energy production and sequester the emitted CO_2 (BECCS). BECCS technology has not been tested at industrial scale, but is commonly included in Integrated Assessment Models and future scenarios that aim to achieve low CO_2 concentrations.

Estimates of the global potential for enhanced primary productivity over land are uncertain because the potential of any specific method will be severely constrained by competing land needs (e.g., agriculture, biofuels, urbanization and conservation) and sociocultural considerations. An order of magnitude of the upper potential of afforestation/reforestation would be the restoration of all the carbon released by historical land use (180 ± 80 PgC; Table 6.1; Section 6.3.2.2). House et al. (2002) estimated that the atmospheric CO_2 concentration by 2100 would be lowered by only about 40 to 70 ppm in that scenario (accounting for the 'rebound' effect).

The capacity for enhancing the soil carbon content on agricultural and degraded lands was estimated by one study at 50 to 60% of the historical soil carbon released, that is 42 to 78 PgC (Lal, 2004a). The proposed agricultural practices are the adoption of conservation tillage with cover crops and crop residue mulch, conversion of marginal lands into restorative land uses and nutrient cycling including the use of

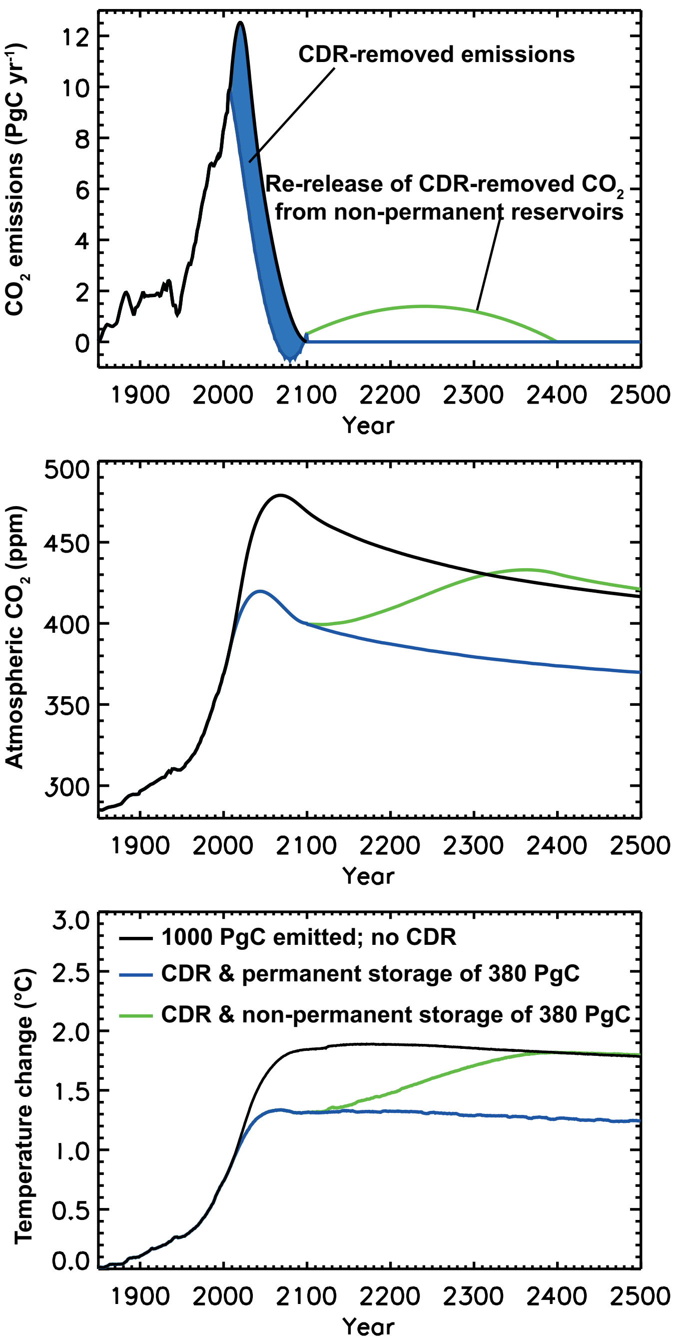

Figure 6.39 | Idealised model simulations (Matthews, 2010) to illustrate the effects of CDR methods associated with either permanent or non-permanent carbon sequestration. There is an emission of 1000 PgC in the reference case (black line) between 1800 and 2100, corresponding approximately to RCP4.5 scenario (Section 6.4). Permanent sequestration of 380 PgC, assuming no leakage of sequestered carbon would reduce climate change (blue line, compared to black line). By contrast, a non-permanent sequestration CDR method where carbon will be sequestered and later on returned to the atmosphere in three centuries would not. In this idealised non-permanent sequestration example scenario, climate change would only be delayed but the eventual magnitude of climate change will be equivalent to the no-sequestration case (green line, compared to black). Figure adapted from Figure 5 of Matthews (2010).

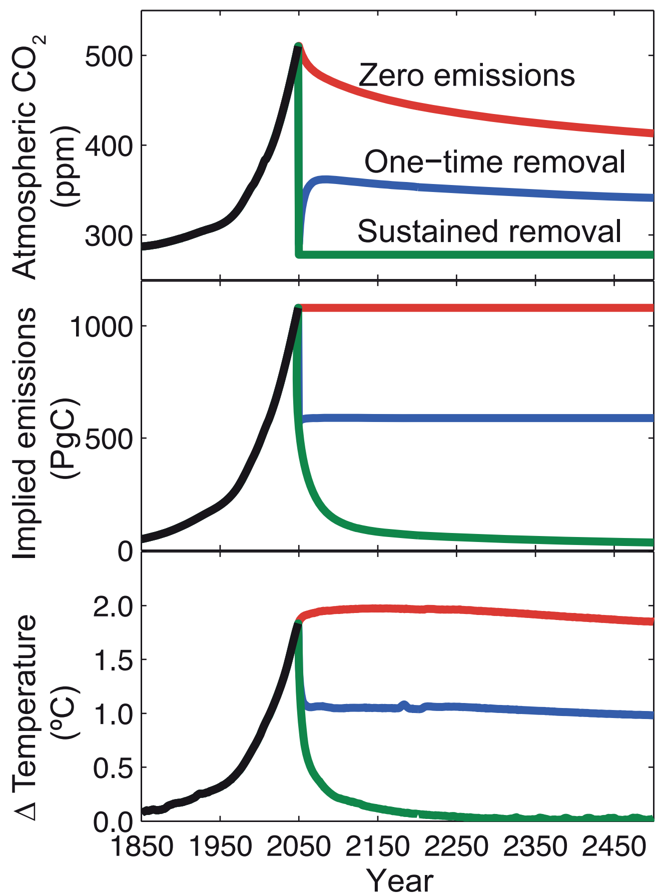

Figure 6.40 | Idealised simulations with a simple global carbon cycle model (Cao and Caldeira, 2010b) to illustrate the 'rebound effect'. Effects of an instantaneous cessation of CO_2 emissions in the year 2050 (amber line), one-time removal of the excess of atmospheric CO_2 over pre-industrial levels (blue line) and removal of this excess of atmospheric CO_2 followed by continued removal of all the CO_2 that degasses from the ocean (green line) are shown. For the years 1850–2010 observed atmospheric CO_2 concentrations are prescribed and CO_2 emissions are calculated from CO_2 concentrations and modeled carbon uptake. For the years 2011–2049, CO_2 emissions are prescribed following the SRES A2 scenario. Starting from year 2050, CO_2 emission is either set to zero or calculated from modeled CO_2 concentrations and CO_2 uptake. To a first approximation, a cessation of emissions would prevent further warming but would not lead to significant cooling on the century time scale. A one-time removal of excess atmospheric CO_2 would eliminate approximately only half of the warming experienced at the time of the removal because of CO_2 that outgases from the ocean (the rebound effect). To bring atmospheric CO_2 back to pre-industrial levels permanently, would require the removal of all previously emitted CO_2, that is, an amount equivalent to approximately twice the excess atmospheric CO_2 above pre-industrial level. (Figure adapted from Cao and Caldeira, 2010b.)

Table 6.15 | Characteristics of some CDR methods from peer-reviewed literature. Note that a variety of economic, environmental, and other constraints could also limit their implementation and net potential.

Carbon Dioxide Removal Method	Means of Removing CO_2 from Atmosphere	Carbon Storage / Form	Time Scale of Carbon Storage	Physical Potential of CO_2 Removed in a Century[a]	Reference	Unintended Side Effects
Afforestation and reforestation	Biological	Land /organic	Decades to centuries	40–70 PgC	House et al. (2002) Canadell and Raupach (2008)	Alters surface energy budget, depending on location; surface warming will be locally increased or decreased; hydrological cycle will be changed
Bio-energy with carbon-capture and storage (BECCS); biomass energy with carbon capture and storage	Biological	Geological or ocean /inorganic	Effectively permanent for geologic, centuries for ocean	125 PgC	See the footnote[b]	Same as above
Biochar creation and storage in soils	Biological	Land /organic	Decades to centuries	130 PgC	Woolf et al. (2010)	Same as above
Ocean fertilisation by adding nutrients to surface waters	Biological	Ocean / inorganic	Centuries to millennia	15–60 PgC 280 PgC	Aumont and Bopp (2006), Jin and Gruber (2003) Zeebe and Archer (2005) Cao and Caldeira (2010a)	Expanded regions with low oxygen concentration; enhanced N_2O emissions; altered production of dimethyl sulphide and non-CO_2 greenhouse gases; possible disruptions to marine ecosystems and regional carbon cycles
Ocean-enhanced upwelling bringing more nutrients to surface waters	Biological	Ocean / inorganic	Centuries to millennia	90 PgC 1–2 PgC	Oschlies et al. (2010a); Lenton and Vaughan (2009), Zhou and Flynn (2005)	*Likely* to cause changes to regional ocean carbon cycle opposing CO_2 removal, e.g., compensatory downwelling in other regions
Land-based increased weathering	Geochemical	Ocean (and some soils) / inorganic	Centuries to millennia for carbonates, permanent for silicate weathering	No determined limit 100 PgC	Kelemen and Matter (2008), Schuiling and Krijgsman (2006) Köhler et al. (2010)	pH of soils and rivers will increase locally, effects on terrestrial/freshwater ecosystems
Ocean-based increased weathering	Geochemical	Ocean / inorganic	Centuries to millennia for carbonates, permanent for silicate weathering	No determined limit	Rau (2008), Kheshgi (1995)	Increased alkalinity effects on marine ecosystems
Direct air capture	Chemical	Geological or ocean /inorganic	Effectively permanent for geologic, centuries for ocean	No determined limit	Keith et al. (2006), Shaffer (2010)	Not known

Notes:

[a] Physical potential does not account for economic or environmental constraints of CDR methods; for example, the value of the physical potential for afforestation and reforestation does not consider the conflicts with land needed for agricultural production. Potentials for BECCS and biochar are highly speculative.

[b] If 2.5 tC yr^{-1} per hectare can be harvested on a sustainable basis (Kraxner et al., 2003) on about 4% (~500 million hectares, about one tenth of global agricultural land area) of global land (13.4 billion hectares) for BECCS, approximately 1.25 PgC yr^{-1} could be removed or about 125 PgC in this century. Future CO_2 concentration pathways, especially RCP2.6 and RCP4.5 include some CO_2 removal by BECCS (Chapter 6 of AR5 WGIII) and hence the potentials estimated here cannot add on to existing model results (Section 6.4).

compost and manure. Recent estimates suggest a cumulative potential of 30 to 60 PgC of additional storage over 25 to 50 years (Lal, 2004b).

Finally, biochar and biomass burial methods aim to store organic carbon into very long turnover time ecosystem carbon pools. The maximum sustainable technical potential of biochar cumulative sequestration is estimated at 130 PgC over a century by one study (Woolf et al., 2010). The residence time of carbon converted to biochar and the additional effect of biochar on soil productivity are uncertain, and further research is required to assess the potential of this method (Shepherd et al., 2009).

6.5.2.2 Enhanced Carbon Sequestration in the Ocean

The principle here is to enhance the primary productivity of phytoplankton (biological pump; Section 6.1.1) so that a fraction of the extra organic carbon produced gets transported to the deep ocean. Some of the inorganic carbon in the surface ocean that is removed by the export of net primary productivity below the surface layer will be subsequently replaced by CO_2 pumped from the atmosphere, thus removing atmospheric CO_2. Ocean primary productivity is limited by nutrients (e.g., iron, nitrogen and phosphorus). Enhanced biological production in ocean CDR methods (Table 6.14) is obtained by adding nutrients that would otherwise be limiting (Martin, 1990). The expected increase in the downward flux of carbon can be partly sequestered as Dissolved Inorganic Carbon (DIC) after mineralization in the intermediate and deep waters. In other ocean-based CDR methods, algae and kelp farming and burial, carbon would be stored in organic form.

The effectiveness of ocean CDR through iron addition depends on the resulting increase of productivity and the fraction of this extra carbon exported to deep and intermediate waters, and its fate. Small-scale

(~10 km^2) experiments (Boyd et al., 2007) have shown only limited transient effects of iron addition in removing atmospheric CO_2. An increased productivity was indeed observed, but this effect was moderated either by other limiting elements, or by compensatory respiration from increased zooplankton grazing. Most of the carbon produced by primary productivity is oxidized (remineralized into DIC) in the surface layer, so that only a small fraction is exported to the intermediate and deep ocean (Lampitt et al., 2008) although some studies indicate little remineralization in the surface layer (Jacquet et al., 2008). A recent study (Smetacek et al., 2012) finds that at least half the extra carbon in plankton biomass generated by artificial iron addition sank far below a depth of 1000 m, and that a substantial portion is likely to have reached the sea floor. There are some indications that sustained natural iron fertilisation may have a higher efficiency in exporting carbon from surface to intermediate and deep ocean than short term blooms induced by artificial addition of iron (Buesseler et al., 2004; Blain et al., 2007; Pollard et al., 2009). Thus, there is no consensus on the efficiency of iron fertilisation from available field experiments.

Using ocean carbon models (see Section 6.3.2.5.6), the maximum drawdown of atmospheric CO_2 have been estimated from 15 ppm (Zeebe and Archer, 2005) to 33 ppm (Aumont and Bopp, 2006) for an idealised continuous (over 100 years) global ocean iron fertilisation, which is technically unrealistic. In other idealised simulations of ocean fertilisation in the global ocean or only in the Southern Ocean (Joos et al., 1991; Peng and Broecker, 1991; Watson et al., 1994; Cao and Caldeira, 2010a), atmospheric CO_2 was reduced by less than 100 ppm for ideal conditions. Jin and Gruber (2003) obtained an atmospheric drawdown of more than 60 ppm over 100 years from an idealised iron fertilisation scenario over the entire Southern Ocean. The radiative benefit from lower CO_2 could be offset by a few percent to more than 100% from an increase in N_2O emissions (Jin and Gruber, 2003). All the above estimates of maximum potential CO_2 removal account for the rebound effect from oceans but not from the land (thus overestimate the atmospheric CO_2 reduction).

One ocean CDR variant is to artificially supply more nutrients to the surface ocean in upwelling areas (Lovelock and Rapley, 2007; Karl and Letelier). The amount of carbon sequestered by these enhanced upwelling methods critically depends on their location (Yool et al., 2009). Idealised simulations suggest an atmospheric CO_2 removal at a net rate of about 0.9 PgC yr^{-1} (Oschlies et al., 2010b). This ocean-based CDR method has not been tested in the field, unlike iron addition experiments.

6.5.2.3 Accelerated Weathering

The removal of CO_2 by the weathering of silicate and carbonate minerals (Berner et al., 1983; Archer et al., 2009b) occurs on time scales from thousands to tens of thousands of years (see Box 6.1) and at a rate of ~ 0.3 PgC yr^{-1} (Figure 6.1; Gaillardet et al., 1999; Hartmann et al., 2009). This rate is currently much too small to offset the rate at which fossil fuel CO_2 is being emitted (Section 6.3).

The principle of accelerated weathering CDR on land is to dissolve *artificially* silicate minerals so drawdown of atmospheric CO_2 and geochemical equilibrium restoration could proceed on a much faster (century) time scale. For instance, large amounts of silicate minerals such as olivine ($(Mg,Fe)_2SiO_4$) could be mined, crushed, transported to and distributed on agricultural lands, to remove atmospheric CO_2 and form carbonate minerals in soils and/or bicarbonate ions that would be transported to the ocean by rivers (Schuiling and Krijgsman, 2006)l. Alternatively, CO_2 removal by weathering reactions might be enhanced by exposing minerals such as basalt or olivine to elevated CO_2, with potential CO_2 removal rates exceeding 0.25 PgC yr^{-1} (Kelemen and Matter, 2008). In the idealised case where olivine could be spread as a fine powder over all the humid tropics, potential removal rates of up to 1 PgC yr^{-1} have been estimated, despite limitations by the saturation concentration of silicic acid (Köhler et al., 2010). For the United Kingdom, the potential from silicate resources was estimated to be more than 100 PgC (Renforth, 2012).

Fossil fuel CO_2 released to the atmosphere leads to the addition of anthropogenic CO_2 in the ocean (Section 6.3.2.5). This anthropogenic CO_2 will eventually dissolve ocean floor carbonate sediments to reach geochemical equilibrium on a 10 kyr time scale (Archer et al., 1997). The principle of ocean based weathering CDR methods is to accelerate this process. For instance, carbonate rocks could be crushed, reacted with CO_2 (e.g., captured at power plants) to produce bicarbonate ions that would be released to the ocean (Rau and Caldeira, 1999; Caldeira and Rau, 2000; Rau, 2008). Alternatively, carbonate minerals could be directly released into the ocean (Kheshgi, 1995; Harvey, 2008). Strong bases, derived from silicate rocks, could also be released to ocean (House et al., 2007) to increase alkalinity and drawdown of atmospheric CO_2. Carbonate minerals such as limestone could be heated to produce lime ($Ca(OH)_2$); this lime could be added to the ocean to increase alkalinity as well (Kheshgi, 1995). While the level of *confidence* is *very high* for the scientific understanding of weathering chemical reactions, it is *low* for its effects and risks at planetary scale (Section 6.5.3.3).

6.5.2.4 Carbon Dioxide Removal by Direct Industrial Capture of Atmospheric Carbon Dioxide

Direct Air Capture refers to the chemical process by which a pure CO_2 stream is produced by capturing CO_2 from ambient air. The captured CO_2 could be sequestered in geological reservoirs or the deep ocean. At least three methods have been proposed to capture CO_2 from the atmosphere: (1) adsorption on solids (Gray et al., 2008; Lackner, 2009, 2010; Lackner et al., 2012); (2) absorption into highly alkaline solutions (Stolaroff et al., 2008; Mahmoudkhani and Keith, 2009) and (3) absorption into moderate alkaline solution with a catalyst (Bao and Trachtenberg, 2006). The main limitation to direct air capture is the thermodynamic barrier due to the low concentration of CO_2 in ambient air.

6.5.3 Impacts of Carbon Dioxide Removal Methods on Carbon Cycle and Climate

One impact common to all CDR methods is related to the thermal inertia of the climate system. Climate warming will indeed continue for at least decades after CDR is applied. Therefore, temperature (and climate change) will lag a CDR-induced decrease in atmospheric CO_2 (Boucher et al., 2012). Modelling the impacts of CDR on climate change is still in its infancy. Some of the first studies (Wu et al., 2010; Cao et al., 2011) showed that the global hydrological cycle could intensify in response to a reduction in atmospheric CO_2 concentrations.

6.5.3.1 Impacts of Enhanced Land Carbon Sequestration

In the case of land-based CDR, biomass in forests is a non-permanent ecosystem carbon pool and hence there is a risk that this carbon may return to the atmosphere, for example, by disturbances such as fire, or by future land use change. When considering afforestation/reforestation, it is also important to account for biophysical effects on climate that come together with carbon sequestration because afforestation/reforestation changes the albedo (see Glossary), evapotranspiration and the roughness of the surface (Bonan, 2008; Bernier et al., 2011). Modelling studies show that afforestation in seasonally snow covered boreal and temperate regions will decrease the land surface albedo and have a net (biophysical plus biogeochemical) warming effect, whereas afforestation in low latitudes (Tropics) is *likely* to enhance latent heat flux from evapotranspiration and have a net cooling effect (Bonan et al., 1992; Betts, 2000; Bala et al., 2007; Montenegro et al., 2009; Bathiany et al., 2010). Consequently, the location of land ecosystem based CDR methods needs to be considered carefully when evaluating their effects on climate (Bala et al., 2007; Arora and Montenegro, 2011; Lee et al., 2011; Pongratz et al., 2011b). In addition CDR in land ecosystems is *likely* to increase N_2O emissions (Li et al., 2005). Enhanced biomass production may also require more nutrients (fertilisers) which are associated with fossil fuel CO_2 emission from industrial fertiliser production and Nr impacts. Biochar-based CDR could reduce N_2O emissions but may increase CO_2 and CH_4 emissions from agricultural soils (Wang et al., 2012b). Addition of biochar could also promote a rapid loss of forest humus and soil carbon in some ecosystems during the first decades (Wardle et al., 2008).

6.5.3.2 Impacts of Enhanced Carbon Sequestration in the Ocean

In the case of ocean-based CDR using fertilisation, adding macronutrients such as nitrogen and phosphate in the fertilised region could lead to a decrease in production 'downstream' of the fertilised region (Gnanadesikan et al., 2003; Gnanadesikan and Marinov, 2008; Watson et al., 2008). Gnanadesikan et al. (2003) simulated a decline in export production of 30 tC for every ton removed from the atmosphere. A sustained global-ocean iron fertilisation for SRES A2 CO_2 emission scenario was also found to acidify the deep ocean (pH decrease of about 0.1 to 0.2) while mitigating surface pH change by only 0.06 (Cao and Caldeira, 2010a). Other environmental risks associated with ocean fertilisation include expanded regions with low oxygen concentration (Oschlies et al., 2010a), increased N_2O emission (Jin and Gruber, 2003), increased production of dimethylsulphide (DMS), isoprene, CO, N_2O, CH_4 and other non-CO_2 GHGs (Oschlies et al., 2010a) and possible disruptions to marine ecosystems (Denman, 2008).

In the case of enhanced ocean upwelling CDR methods there could be disturbance to the regional carbon balances, since the extra-upwelling will be balanced by extra-downwelling at another location. Along with growth-supporting nutrients, enhanced concentrations of DIC will also be brought to surface waters and partially offset the removal of CO_2 by increased biological pump. Further, in case artificially enhanced upwelling would be stopped, atmospheric CO_2 concentrations could rise rapidly because carbon removed from the atmosphere and stored in soils in the cooler climate caused by artificial upwelling could be rapidly released back (Oschlies et al., 2010b). The level of *confidence* on the impacts of the enhanced upwelling is *low*.

6.5.3.3 Impact of Enhanced Weathering

In the case of weathering-based CDR, the pH and carbonate mineral saturation of soils, rivers and ocean surface waters will increase where CDR is implemented. Köhler et al. (2010) simulated that the pH of the Amazon river would rise by 2.5 units if the dissolution of olivine in the entire Amazon basin was used to remove 0.5 PgC yr^{-1} from the atmosphere. In the marine environment, elevated pH and increased alkalinity could potentially counteract the effects of ocean acidification, which is beneficial. Changes in alkalinity could also modify existing ecosystems. There is uncertainty in our understanding of the net effect on ocean CO_2 uptake but there will be a partial offset of the abiotic effect by calcifying species. As for other CDR methods, the confidence level on the carbon cycle impacts of enhanced weathering is low.

6.5.4 Impacts of Solar Radiation Management on the Carbon Cycle

Solar radiation management (SRM) methods aim to reduce incoming solar radiation at the surface (discussed in Section 7.7 and in AR5, WG2, Chapter 19). Balancing reduced outgoing radiation by reduced incoming radiation may be able to cool global mean temperature but may lead to a less intense global hydrological cycle (Bala et al., 2008) with regionally different climate impacts (Govindasamy et al., 2003; Matthews and Caldeira, 2007; Robock et al., 2008; Irvine et al., 2010; Ricke et al., 2010). Therefore, SRM will not prevent the effects of climate change on the carbon and other biogeochemical cycles.

SRM could reduce climate warming but will not interfere with the direct biogeochemical effects of elevated CO_2 on the carbon cycle. For example, ocean acidification caused by elevated CO_2 (Section 6.4.4) and the CO_2 fertilisation of productivity (Box 6.3) will not be altered by SRM (Govindasamy et al., 2002; Naik et al., 2003; Matthews and Caldeira, 2007). Similarly, SRM will not interfere with the stomatal response of plants to elevated CO_2 (the CO_2-physiological effect) that leads to a decline in evapotranspiration, causing land temperatures to warm and runoff to increase (Gedney et al., 2006; Betts et al., 2007; Matthews and Caldeira, 2007; Piao et al., 2007; Cao et al., 2010; Fyfe et al., 2013).

However, due to carbon–climate feedbacks (Section 6.4), the implementation of SRM could affect the carbon cycle. For instance, carbon uptake by land and ocean could increase in response to SRM by reducing the negative effects of climate change on carbon sinks (Matthews and Caldeira, 2007). For instance, for the SRES A2 scenario with SRM, a lower CO_2 concentration of 110 ppm by year 2100 relative to a baseline case without SRM has been simulated by Matthews and Caldeira (2007). Land carbon sinks may be enhanced by increasing the amount of diffuse relative to direct radiation (Mercado et al., 2009) if SRM causes the fraction of diffuse light to increase (e.g., injection of aerosols into the stratosphere). However, reduction of total incoming solar radiation could decrease terrestrial CO_2 sinks as well.

6

6.5.5 Synthesis

CDR methods are intentional large scale methods to remove atmospheric CO_2 either by managing the carbon cycle or by direct industrial processes (Table 6.14). In contrast to SRM methods, CDR methods that manage the carbon cycle are *unlikely* to present an option for rapidly preventing climate change. The maximum (idealised) potential for atmospheric CO_2 removal by individual CDR methods is compiled in Table 6.15. In this compilation, note that unrealistic assumptions about the scale of deployment, such as fertilising the entire global ocean, are used, and hence large potentials are simulated. The 'rebound effect' in the natural carbon cycle is *likely* to diminish the effectiveness of all the CDR methods (Figure 6.40). The level of *confidence* on the effects of both CDR and SRM methods on carbon and other biogeochemical cycles is *very low*.

Acknowledgements

We wish to acknowledge Anna Peregon (LSCE, France) for investing countless hours compiling and coordinating input from all of the Chapter 6 Lead Authors. She was involved in the production of every aspect of the chapter and we could not have completed our task on time without her help. We also thank Brett Hopwood (ORNL, USA) for skilful and artistic edits of several graphical figures representing the global biogeochemical cycles in the Chapter 6 Introduction. We also thank Silvana Schott (Max Planck Institute for Biogeochemistry, Germany) for graphics artwork for several of the figures in Chapter 6.

References

Achard, F., H. D. Eva, P. Mayaux, H.-J. Stibig, and A. Belward, 2004: Improved estimates of net carbon emissions from land cover change in the tropics for the 1990s. *Global Biogeochem. Cycles*, **18**, GB2008.

Adair, E. C., P. B. Reich, S. E. Hobbie, and J. M. H. Knops, 2009: Interactive effects of time, CO_2, N, and diversity on total belowground carbon allocation and ecosystem carbon storage in a grassland community. *Ecosystems*, **12**, 1037–1052.

Adkins, J. F., K. McIntyre, and D. P. Schrag, 2002: The salinity, temperature and $\delta^{18}O$ of the glacial deep ocean. *Science*, **298**, 1769–1773.

Ahn, J. and E. J. Brook, 2008: Atmospheric CO_2 and climate on millennial time scales during the last glacial period. *Science*, **322**, 83–85.

Ahn, J., et al., 2012: Atmospheric CO_2 over the last 1000 years: A high resolution record from the West Antarctic Ice Sheet (WAIS) Divide ice core. *Global Biogeochem. Cycles*, **26**, GB2027.

Ainsworth, E. A. and S. P. Long, 2004: What have we learned from 15 years of free-air CO_2 enrichment (FACE)? A meta-analytic review of the responses of photosynthesis, canopy properties and plant production to rising CO_2. *New Phytologist*, **165**, 351–372.

Ainsworth, E. A., C. R. Yendrek, S. Sitch, W. J. Collins, and L. D. Emberson, 2012: The effects of tropospheric ozone on net primary productivity and implications for climate change. *Annu. Rev. Plant Biol.*, **63**, 637–661.

Allan, W., H. Struthers, and D. C. Lowe, 2007: Methane carbon isotope effects caused by atomic chlorine in the marine boundary layer: Global model results compared with Southern Hemisphere measurements. *J. Geophys. Res. Atmos.*, **112**, D04306.

Amiro, B. D., A. Cantin, M. D. Flannigan, and W. J. de Groot, 2009: Future emissions from Canadian boreal forest fires. *Can. J. Forest Res.*, **39**, 383–395.

Anderson, R. F., M. Q. Fleisher, Y. Lao, and G. Winckler, 2008: Modern $CaCO_3$ preservation in equatorial Pacific sediments in the context of late-Pleistocene glacial cycles. *Mar. Chem.*, **111**, 30–46.

Andreae, M. O. and P. Merlet, 2001: Emission of trace gases and aerosols from biomass burning. *Global Biogeochem. Cycles*, **15**, 955–966.

Andres, R. J., J. S. Gregg, L. Losey, G. Marland, and T. A. Boden, 2011: Monthly, global emissions of carbon dioxide from fossil fuel consumption. *Tellus B*, **63**, 309–327.

Andres, R. J., et al., 2012: A synthesis of carbon dioxide emissions from fossil-fuel combustion. *Biogeosciences*, **9**, 1845–1871.

Aranjuelo, I., et al., 2011: Maintenance of C sinks sustains enhanced C assimilation during long-term exposure to elevated [CO_2] in Mojave Desert shrubs. *Oecologia*, **167**, 339–354.

Archer, D., 2007: Methane hydrate stability and anthropogenic climate change. *Biogeosciences*, **4**, 521–544.

Archer, D. and E. Maier-Reimer, 1994: Effect of deep-sea sedimentary calcite preservation on atmospheric CO_2 concentration. *Nature*, **367**, 260–263.

Archer, D. and V. Brovkin, 2008: The millennial atmospheric lifetime of anthropogenic CO_2. *Clim. Change*, **90**, 283–297.

Archer, D., H. Kheshgi, and E. Maier-Reimer, 1997: Multiple timescales for neutralization of fossil fuel CO_2. *Geophys. Res. Lett.*, **24**, 405–408.

Archer, D., H. Kheshgi, and E. Maier-Reimer, 1998: Dynamics of fossil fuel CO_2 neutralization by marine $CaCO_3$. *Global Biogeochem. Cycles*, **12**, 259–276.

Archer, D., B. Buffett, and V. Brovkin, 2009a: Ocean methane hydrates as a slow tipping point in the global carbon cycle. *Proc. Natl. Acad. Sci. U.S.A.*, **106**, 20596–20601.

Archer, D., A. Winguth, D. Lea, and N. Mahowald, 2000: What caused the glacial/interglacial atmospheric pCO_2 cycles? *Rev. Geophys.*, **38**, 159–189.

Archer, D., et al., 2009b: Atmospheric lifetime of fossil fuel carbon dioxide. *Annu. Rev. Earth Planet. Sci.*, **37**, 117–134.

Archer, D. E., P. A. Martin, J. Milovich, V. Brovkin, G.-K. Plattner, and C. Ashendel, 2003: Model sensitivity in the effect of Antarctic sea ice and stratification on atmospheric pCO_2. *Paleoceanography*, **18**, 1012.

Archibald, S., D. P. Roy, B. W. van Wilgen, and R. J. Scholes, 2009: What limits fire? An examination of drivers of burnt area in Southern Africa. *Global Change Biol.*, **15**, 613–630.

Arneth, A., et al., 2010: Terrestrial biogeochemical feedbacks in the climate system. *Nature Geosci.*, **3**, 525–532.

Arora, V. K., and G. J. Boer, 2010: Uncertainties in the 20th century carbon budget associated with land use change. *Global Change Biol.*, **16**, 3327–3348.

Arora, V. K., and A. Montenegro, 2011: Small temperature benefits provided by realistic afforestation efforts. *Nature Geosci.*, **4**, 514–518.

Arora, V. K., et al., 2011: Carbon emission limits required to satisfy future representative concentration pathways of greenhouse gases. *Geophys. Res. Lett.*, **38**, L05805.

Arora, V. K., et al., 2013: Carbon-concentration and carbon-climate feedbacks in CMIP5 Earth system models. *J. Clim.*, **26**, 5289-5314.

Artioli, Y., et al., 2012: The carbonate system in the North Sea: Sensitivity and model validation. *J. Mar. Syst.*, **102–104**, 1–13.

Ashmore, M. R., 2005: Assessing the future global impacts of ozone on vegetation. *Plant Cell Environ.*, **28**, 949–964.

Assmann, K. M., M. Bentsen, J. Segschneider, and C. Heinze, 2010: An isopycnic ocean carbon cycle model. *Geosci. Model Dev.*, **3**, 143–167.

Aufdenkampe, A. K., et al., 2011: Rivering coupling of biogeochemical cycles between land, oceans and atmosphere. *Front. Ecol. Environ.*, **9**, 23–60.

Aumont, O., and L. Bopp, 2006: Globalizing results from ocean in situ iron fertilization studies. *Global Biogeochem. Cycles*, **20**, GB2017.

Avis, C. A., A. J. Weaver, and K. J. Meissner, 2011: Reduction in areal extent of high-latitude wetlands in response to permafrost thaw. *Nature Geosci.*, **4**, 444–448.

Ayres, R. U., W. H. Schlesinger, and R. H. Socolow, 1994: Human impacts on the carbon and nitrogen cycles.In: *Industrial Ecology and Global Change* [R. H. Socolow, C. Andrews, F. Berkhout and V. Thomas (eds.)]. Cambridge University Press, Cambridge, United Kingdom, and New York, NY, USA, pp. 121–155.

Bacastow, R. B., and C. D. Keeling, 1979: Models to predict future atmospheric CO_2 concentrations. In: *Workshop on the Global Effects of Carbon Dioxide from Fossil Fuels.* United States Department of Energy, Washington, DC, pp. 72–90.

Baccini, A., et al., 2012: Estimated carbon dioxide emissions from tropical deforestation improved by carbon-density maps. *Nature Clim. Change*, **2**, 182–185.

Bader, M., E. Hiltbrunner, and C. Körner, 2009: Fine root responses of mature deciduous forest trees to free air carbon dioxide enrichment (FACE). *Funct. Ecol.*, **23**, 913–921.

Baker, A., S. Cumberland, and N. Hudson, 2008: Dissolved and total organic and inorganic carbon in some British rivers. *Area*, **40**, 117–127.

Baker, D. F., et al., 2006: TransCom 3 inversion intercomparison: Impact of transport model errors on the interannual variability of regional CO_2 fluxes, 1988–2003. *Global Biogeochem. Cycles*, **20**, GB1002.

Bala, G., P. B. Duffy, and K. E. Taylor, 2008: Impact of geoengineering schemes on the global hydrological cycle. *Proc. Natl. Acad. Sci. U.S.A.*, **105**, 7664–7669.

Bala, G., K. Caldeira, M. Wickett, T. J. Phillips, D. B. Lobell, C. Delire, and A. Mirin, 2007: Combined climate and carbon-cycle effects of large-scale deforestation. *Proc. Natl. Acad. Sci. U.S.A.*, **104**, 6550–6555.

Baldocchi, D. D., et al., 2001: FLUXNET: A new tool to study the temporal and spatial variability of ecosystem-scale carbon dioxide, water vapor and energy flux densities. *Bull. Am. Meteorol. Soc.*, **82**, 2415–2435.

Ballantyne, A. P., C. B. Alden, J. B. Miller, P. P. Tans, and J. W. C. White, 2012: Increase in observed net carbon dioxide uptake by land and oceans during the last 50 years. *Nature*, **488**, 70–72.

Balshi, M. S., A. D. McGuire, P. Duffy, M. D. Flannigan, D. W. Kicklighter, and J. Melillo, 2009: Vulnerability of carbon storage in North American boreal forests to wildfires during the 21st century. *Global Change Biol.*, **15**, 1491–1510.

Bao, L. H., and M. C. Trachtenberg, 2006: Facilitated transport of CO_2 across a liquid membrane: Comparing enzyme, amine, and alkaline. *J. Membr. Sci.*, **280**, 330–334.

Barnard, R., P. W. Leadley, and B. A. Hungate, 2005: Global change, nitrification, and denitrification: A review. *Global Biogeochem. Cycles*, **19**, GB1007.

Barnes, R. T., and P. A. Raymond, 2009: The contribution of agricultural and urban activities to inorganic carbon fluxes within temperate watersheds. *Chem. Geol.*, **266**, 318–327.

Barnosky, A. D., 2008: Colloquium Paper: Megafauna biomass tradeoff as a driver of Quaternary and future extinctions. *Proc. Natl. Acad. Sci. U.S.A.*, **105**, 11543–11548.

Bastviken, D., J. Cole, M. Pace, and L. Tranvik, 2004: Methane emissions from lakes: Dependence of lake characteristics, two regional assessments, and a global estimate. *Global Biogeochem. Cycles*, **18**, GB4009.

Bastviken, D., L. J. Tranvik, J. A. Downing, P. M. Crill, and A. Enrich-Prast, 2011: Freshwater methane emissions offset the continental carbon sink. *Science*, **331**, 50.

Bathiany, S., M. Claussen, V. Brovkin, T. Raddatz, and V. Gayler, 2010: Combined biogeophysical and biogeochemical effects of large-scale forest cover changes in the MPI earth system model. *Biogeosciences*, **7**, 1383–1399.

Batjes, N. H., 1996: Total carbon and nitrogen in the soils of the world. *Eur. J. Soil Sci.*, **47**, 151–163.

Battin, T. J., S. Luyssaert, L. A. Kaplan, A. K. Aufdenkampe, A. Richter, and L. J. Tranvik, 2009: The boundless carbon cycle *Nature Geosci.*, **2**, 598–600.

Beaugrand, G., M. Edwards, and L. Legendre, 2010: Marine biodiversity, ecosystem functioning, and carbon cycles. *Proc. Natl. Acad. Sci. U.S.A.*, **107**, 10120–10124.

Beaulieu, J. J., et al., 2011: Nitrous oxide emission from denitrification in stream and river networks. *Proc. Natl. Acad. Sci. U.S.A.*, **108**, 214–219.

Beer, C., et al., 2010: Terrestrial gross carbon dioxide uptake: Global distribution and covariation with climate. *Science*, **329**, 834-838.

Bellassen, V., G. Le Maire, J. F. Dhote, P. Ciais, and N. Viovy, 2010: Modelling forest management within a global vegetation model. Part 1: Model structure and general behaviour. *Ecol. Model.*, **221**, 2458–2474.

Bellassen, V., N. Viovy, S. Luyssaert, G. Le Maire, M.-J. Schelhaas, and P. Ciais, 2011: Reconstruction and attribution of the carbon sink of European forests between 1950 and 2000. *Global Change Biol.*, **17**, 3274–3292.

Bennington, V., G. A. McKinley, S. Dutkiewicz, and D. Ullman, 2009: What does chlorophyll variability tell us about export and air-sea CO_2 flux variability in the North Atlantic? *Global Biogeochem. Cycles*, **23**, GB3002.

Berendse, F., et al., 2001: Raised atmospheric CO_2 levels and increased N deposition cause shifts in plant species composition and production in Sphagnum bogs. *Global Change Biol.*, **7**, 591–598.

Bergamaschi, P., et al., 2009: Inverse modeling of global and regional CH_4 emissions using SCIAMACHY satellite retrievals. *J. Geophys. Res.*, **114**, D22301.

Berger, W. H., 1982: Increase of carbon dioxide in the atmosphere during deglaciation: The coral-reef hypothesis. *Naturwissenschaften*, **69**, 87–88.

Berner, R. A., 1992: Weathering, plants, and the long-term carbon-cycle. *Geochim. Cosmochim. Acta*, **56**, 3225–3231.

Berner, R. A., A. C. Lasaga, and R. M. Garrels, 1983: The carbonate-silicate geochemical cycle and its effect on atmospheric carbon dioxide over the past 100 million years. *Am. J. Sci.*, **283**, 641–683.

Bernier, P. Y., R. L. Desjardins, Y. Karimi-Zindashty, D. E. Worth, A. Beaudoin, Y. Luo, and S. Wang, 2011: Boreal lichen woodlands: A possible negative feedback to climate change in Eastern North America. *Agr. Forest Meteorol.*, **151**, 521–528.

Betts, R. A., 2000: Offset of the potential carbon sink from boreal forestation by decreases in surface albedo. *Nature*, **408**, 187–190.

Betts, R. A., et al., 2007: Projected increase in continental runoff due to plant responses to increasing carbon dioxide. *Nature*, **448**, 1037–1041.

Bianchi, D., J. P. Dunne, J. L. Sarmiento, and E. D. Galbraith, 2012: Data-based estimates of suboxia, denitrification and N_2O production in the ocean and their sensitivity to dissolved O_2. *Global Biogeochem. Cycles*, **26**, GB2009.

Biastoch, A., et al., 2011: Rising Arctic Ocean temperatures cause gas hydrate destabilization and ocean acidification. *Geophys. Res. Lett.*, **38**, L08602.

Billings, S. A., S. M. Schaeffer, and R. D. Evans, 2002: Trace N gas losses and N mineralization in Mojave desert soils exposed to elevated CO_2. *Soil Biol. Biochem.*, **34**, 1777–1784.

Bird, M. I., J. Lloyd, and G. D. Farquhar, 1996: Terrestrial carbon storage from the last glacial maximum to the present. *Chemosphere*, **33**, 1675–1685.

Blain, S., et al., 2007: Effect of natural iron fertilization on carbon sequestration in the Southern Ocean. *Nature*, **446**, 1070–1074.

Blake, D. R., E. W. Mayer, S. C. Tyler, Y. Makide, D. C. Montague, and F. S. Rowland, 1982: Global increase in atmospheric methane concentrations between 1978 and 1980. *Geophys. Res. Lett.*, **9**, 477–480.

Bleeker, A., W. K. Hicks, F. Dentener, and J. Galloway, 2011: Nitrogen deposition as a threat to the World's protected areas under the Convention on Biological Diversity. *Environ. Pollut.*, **159**, 2280–2288.

Bloom, A. A., J. Lee-Taylor, S. Madronich, D. J. Messenger, P. I. Palmer, D. S. Reay, and A. R. McLeod, 2010: Global methane emission estimates from ultraviolet irradiation of terrestrial plant foliage. *New Phytologist*, **187**, 417–425.

Blunier, T., J. Chappellaz, J. Schwander, B. Stauffer, and D. Raynaud, 1995: Variations in atmospheric methane concentration during the Holocene epoch. *Nature*, **374**, 46–49.

Boardman, C. P., V. Gauci, J. S. Watson, S. Blake, and D. J. Beerling, 2011: Contrasting wetland CH_4 emission responses to simulated glacial atmospheric CO_2 in temperate bogs and fens. *New Phytologist*, **192**, 898–911.

Bock, M., J. Schmitt, L. Moller, R. Spahni, T. Blunier, and H. Fischer, 2010: Hydrogen isotopes preclude marine hydrate CH_4 emissions at the onset of Dansgaard-Oeschger events. *Science*, **328**, 1686–1689.

Boden, T., G. Marland, and R. Andres, 2011: Global CO_2 emissions from fossil-fuel burning, cement manufacture, and gas flaring: 1751–2008 (accessed at 2011.11.10). Oak Ridge National Laboratory, U. S. Department of Energy, Carbon Dioxide Information Analysis Center, Oak Ridge, TN, U.S.A., doi:10.3334/CDIAC/00001_V2011, http://cdiac.ornl.gov/trends/emis/overview_2008.html.

Bonan, G. B., 2008: *Ecological Climatology: Concepts and Applications.* Cambridge University Press, New York, NY, USA.

Bonan, G. B., and S. Levis, 2010: Quantifying carbon-nitrogen feedbacks in the Community Land Model (CLM4). *Geophys. Res. Lett.*, **37**, L07401.

Bonan, G. B., D. Pollard, and S. L. Thompson, 1992: Effects of boreal forest vegetation on global climate. *Nature*, **359**, 716–718.

Bond-Lamberty, B., and A. Thomson, 2010: Temperature-associated increases in the global soil respiration record. *Nature*, **464**, 579–U132.

Booth, B. B. B., et al., 2012: High sensitivity of future global warming to land carbon cycle processes. *Environ. Res. Lett.*, **7**, 024002.

Bopp, L., K. E. Kohfeld, C. Le Quéré, and O. Aumont, 2003: Dust impact on marine biota and atmospheric CO_2 during glacial periods. *Paleoceanography*, **18**, 1046.

Bopp, L., C. Le Quéré, M. Heimann, A. C. Manning, and P. Monfray, 2002: Climate-induced oceanic oxygen fluxes: Implications for the contemporary carbon budget. *Global Biogeochem. Cycles*, **16**, 1022.

Bopp, L., et al., 2001: Potential impact of climate change on marine export production. *Global Biogeochem. Cycles*, **15**, 81–99.

Boucher, O., et al., 2012: Reversibility in an Earth System model in response to CO_2 concentration changes. *Environ. Res. Lett.*, **7**, 024013.

Bousquet, P., D. A. Hauglustaine, P. Peylin, C. Carouge, and P. Ciais, 2005: Two decades of OH variability as inferred by an inversion of atmospheric transport and chemistry of methyl chloroform. *Atmos. Chem. Phys.*, **5**, 2635–2656.

Bousquet, P., P. Peylin, P. Ciais, C. Le Quéré, P. Friedlingstein, and P. P. Tans, 2000: Regional changes in carbon dioxide fluxes of land and oceans since 1980. *Science*, **290**, 1342–1346.

Bousquet, P., et al., 2006: Contribution of anthropogenic and natural sources to atmospheric methane variability. *Nature*, **443**, 439–443.

Bousquet, P., et al., 2011: Source attribution of the changes in atmospheric methane for 2006–2008. *Atmos. Chem. Phys.*, **11**, 3689–3700.

Bouttes, N., D. Paillard, D. M. Roche, V. Brovkin, and L. Bopp, 2011: Last Glacial Maximum CO_2 and $d^{13}C$ successfully reconciled. *Geophys. Res. Lett.*, **38**, L02705.

Bouttes, N., et al., 2012: Impact of oceanic processes on the carbon cycle during the last termination. *Clim. Past*, **8**, 149–170.

Bouwman, A. F., et al., 2013: Global trends and uncertainties in terrestrial denitrification and N_2O emissions. *Philos. Trans. R. Soc. London Ser. B, 368*, 20130112.

Bouwman, L., et al., 2011: Exploring global changes in nitrogen and phosphorus cycles in agriculture induced by livestock production over the 1900–2050 period. *Proc. Natl. Acad. Sci. U.S.A.*, doi:10.1073/pnas.1012878108.

Boyd, P. W., et al., 2007: Mesoscale iron enrichment experiments 1993–2005: Synthesis and future directions. *Science*, **315**, 612–617.

Bozbiyik, A., M. Steinacher, F. Joos, T. F. Stocker, and L. Menviel, 2011: Fingerprints of changes in the terrestrial carbon cycle in response to large reorganizations in ocean circulation. *Clim. Past*, **7**, 319–338.

Brenninkmeijer, C. A. M., et al., 2007: Civil Aircraft for the regular investigation of the atmosphere based on an instrumented container: The new CARIBIC system. *Atmos. Chem. Phys.*, **7**, 4953–4976.

Bridgham, S. D., J. P. Megonigal, J. K. Keller, N. B. Bliss, and C. Trettin, 2006: The carbon balance of North American wetlands. *Wetlands*, **26**, 889–916.

Broecker, W. S., and T.-H. Peng, 1986: Carbon cycle: 1985 glacial to interglacial changes in the operation of the global carbon cycle. *Radiocarbon*, **28**, 309–327.

Broecker, W. S., E. Clark, D. C. McCorkle, T.-H. Peng, I. Hajdas, and G. Bonani, 1999: Evidence for a reduction in the carbonate ion content of the deep sea during the course of the Holocene. *Paleoceanography*, **14**, 744–752.

Brovkin, V., A. Ganopolski, D. Archer, and S. Rahmstorf, 2007: Lowering of glacial atmospheric CO_2 in response to changes in oceanic circulation and marine biogeochemistry. *Paleoceanography*, **22**, PA4202.

Brovkin, V., J. H. Kim, M. Hofmann, and R. Schneider, 2008: A lowering effect of reconstructed Holocene changes in sea surface temperatures on the atmospheric CO_2 concentration. *Global Biogeochem. Cycles*, **22**, GB1016.

Brovkin, V., T. Raddatz, C. H. Reick, M. Claussen, and V. Gayler, 2009: Global biogeophysical interactions between forest and climate. *Geophys. Res. Lett.*, **36**, L07405.

Brovkin, V., S. Sitch, W. von Bloh, M. Claussen, E. Bauer, and W. Cramer, 2004: Role of land cover changes for atmospheric CO_2 increase and climate change during the last 150 years. *Global Change Biol.*, **10**, 1253–1266.

Brovkin, V., J. Bendtsen, M. Claussen, A. Ganopolski, C. Kubatzki, V. Petoukhov, and A. Andreev, 2002: Carbon cycle, vegetation, and climate dynamics in the Holocene: Experiments with the CLIMBER-2 model. *Global Biogeochem. Cycles*, **16**, 1139.

Brovkin, V., et al., 2010: Sensitivity of a coupled climate-carbon cycle model to large volcanic eruptions during the last millennium. *Tellus B*, **62**, 674–681.

Brown, J. R., et al., 2011: Effects of multiple global change treatments on soil N_2O fluxes. *Biogeochemistry*, **109**, 85–100.

Brzezinski, M. A., et al., 2002: A switch from $Si(OH)_4$ to NO_3 depletion in the glacial Southern Ocean. *Geophys. Res. Lett.*, **29**, 1564.

Buesseler, K. O., J. E. Andrews, S. M. Pike, and M. A. Charette, 2004: The effects of iron fertilization on carbon sequestration in the Southern Ocean. *Science*, **304**, 414–417.

Burke, E. J., C. D. Jones, and C. D. Koven, 2013: Estimating the permafrost-carbon-climate response in the CMIP5 climate models using a simplified approach. *J. Clim.*, **26**, 4897-4909.

Burn, C. R., and F. E. Nelson, 2006: Comment on "A projection of severe near-surface permafrost degradation during the 21st century" by David M. Lawrence and Andrew G. Slater. *Geophys. Res. Lett.*, **33**, L21503.

Butterbach-Bahl, K., and M. Dannenmann, 2011: Denitrification and associated soil N_2O emissions due to agricultural activities in a changing climate. *Curr. Opin. Environ. Sustain.*, **3**, 389–395.

Byrne, R. H., S. Mecking, R. A. Feely, and X. W. Liu, 2010: Direct observations of basin-wide acidification of the North Pacific Ocean. *Geophys. Res. Lett.*, **37**, L02601.

Cadule, P., et al., 2010: Benchmarking coupled climate-carbon models against long-term atmospheric CO_2 measurements. *Global Biogeochem. Cycles*, **24**, GB2016.

Cai, W.-J., et al., 2011: Acidification of subsurface coastal waters enhanced by eutrophication. *Nature Geosci*, **4**, 766–770.

Caldeira, K., and G. H. Rau, 2000: Accelerating carbonate dissolution to sequester carbon dioxide in the ocean: Geochemical implications. *Geophys. Res. Lett.*, **27**, 225–228.

Caldeira, K., and M. E. Wickett, 2005: Ocean model predictions of chemistry changes from carbon dioxide emissions to the atmosphere and ocean. *J. Geophys. Res. Oceans*, **110**, C09S04.

Canadell, J. G., and M. R. Raupach, 2008: Managing forests for climate change mitigation. *Science*, **320**, 1456–1457.

Canadell, J. G., et al., 2007a: Saturation of the terrestrial carbon sink. In: *Terrestrial Ecosystems in a Changing World.* [J. G. Canadell, D. Pataki and L. Pitelka (eds.)]. The IGBP Series. Springer-Verlag, Berlin and Heidelberg, Germany, pp. 59–78,

Canadell, J. G., et al., 2007b: Contributions to accelerating atmospheric CO_2 growth from economic activity, carbon intensity, and efficiency of natural sinks. *Proc. Natl. Acad. Sci. U.S.A.*, **104**, 18,866–18,870.

Canfield, D. E., A. N. Glazer, and P. G. Falkowski, 2010: The evolution and future of Earth's nitrogen cycle. *Science*, **330**, 192–196.

Cao, L., and K. Caldeira, 2010a: Can ocean iron fertilization mitigate ocean acidification? *Clim. Change*, **99**, 303–311.

Cao, L., and K. Caldeira, 2010b: Atmospheric carbon dioxide removal: Long-term consequences and commitment. *Environ. Res. Lett.*, **5**, 024011.

Cao, L., K. Caldeira, and A. K. Jain, 2007: Effects of carbon dioxide and climate change on ocean acidification and carbonate mineral saturation. *Geophys. Res. Lett.*, **34**, L05607.

Cao, L., G. Bala, and K. Caldeira, 2011: Why is there a short-term increase in global precipitation in response to diminished CO_2 forcing? *Geophys. Res. Lett.*, **38**, L06703.

Cao, L., G. Bala, K. Caldeira, R. Nemani, and G. Ban-Weiss, 2010: Importance of carbon dioxide physiological forcing to future climate change. *Proc. Natl. Acad. Sci. U.S.A.*, **107**, 9513–9518.

Carcaillet, C., et al., 2002: Holocene biomass burning and global dynamics of the carbon cycle. *Chemosphere*, **49**, 845–863.

Certini, G., 2005: Effects of fire on properties of forest soils: A review. *Oecologia*, **143**, 1–10.

Chambers, J. Q., J. I. Fisher, H. Zeng, E. L. Chapman, D. B. Baker, and G. C. Hurtt, 2007: Hurricane Katrina's carbon footprint on U.S. Gulf Coast forests. *Science*, **318**, 1107.

Chantarel, A. M., J. M. G. Bloor, N. Deltroy, and J.-F. Soussana, 2011: Effects of climate change drivers on nitrous oxide fluxes in an upland temperate grassland. *Ecosystems*, **14**, 223–233.

Chapuis-Lardy, L., N. Wrage, A. Metay, J. L. Chotte, and M. Bernoux, 2007: Soils, a sink for N_2O? A review. *Global Change Biol.*, **13**, 1–17.

Chen, Y. H., and R. G. Prinn, 2006: Estimation of atmospheric methane emissions between 1996 and 2001 using a three-dimensional global chemical transport model. *J. Geophys. Res. Atmos.*, **111**, D10307.

Chhabra, A., K. R. Manjunath, S. Panigrahy, and J. S. Parihar, 2013: Greenhouse gas emissions from Indian livestock. *Clim. Change*, **117**, 329–344.

Chierici, M., and A. Fransson, 2009: Calcium carbonate saturation in the surface water of the Arctic Ocean: Undersaturation in freshwater influenced shelves. *Biogeosciences*, **6**, 2421–2431.

Christensen, T. R., et al., 2004: Thawing sub-arctic permafrost: Effects on vegetation and methane emissions. *Geophys. Res. Lett.*, **31**, L04501.

Churkina, G., V. Brovkin, W. von Bloh, K. Trusilova, M. Jung, and F. Dentener, 2009: Synergy of rising nitrogen depositions and atmospheric CO_2 on land carbon uptake moderately offsets global warming. *Global Biogeochem. Cycles*, **23**, GB4027.

Ciais, P., P. Rayner, F. Chevallier, P. Bousquet, M. Logan, P. Peylin, and M. Ramonet, 2010: Atmospheric inversions for estimating CO_2 fluxes: methods and perspectives. *Clim. Change*, **103**, 69–92(24).

Ciais, P., et al., 2012: Large inert carbon pool in the terrestrial biosphere during the Last Glacial Maximum. *Nature Geosci.*, **5**, 74–79.

Ciais, P., et al., 2008: Carbon accumulation in European forests. *Nature Geosci.*, **1**, 425–429.

Ciais, P., et al., 2005: Europe-wide reduction in primary productivity caused by the heat and drought in 2003. *Nature*, **437**, 529–533.

Clark, D. B., D. A. Clark, and S. F. Oberbauer, 2010: Annual wood production in a tropical rain forest in NE Costa Rica linked to climatic variation but not to increasing CO_2. *Global Change Biol.*, **16**, 747–759.

Claussen, M., et al., 2002: Earth system models of intermediate complexity: Closing the gap in the spectrum of climate system models. *Clim. Dyn.*, **18**, 579–586.

Cocco, V., et al., 2013: Oxygen and indicators of stress for marine life in multi-model global warming projections. *Biogeosciences*, **10**, 1849–1868.

Codispoti, L. A., 2007: An oceanic fixed nitrogen sink exceeding 400 Tg N a^{-1} vs the concept of homeostasis in the fixed-nitrogen inventory. *Biogeosciences*, **4**, 233–253.

Codispoti, L. A., 2010: Interesting Times for Marine N_2O. *Science*, **327**, 1339–1340.

Cole, J. J., et al., 2007: Plumbing the global carbon cycle: Integrating inland waters into the terrestrial carbon budget. *Ecosystems*, **10**, 171–184.

Collins, W. J., et al., 2011: Development and evaluation of an Earth-System model—HadGEM2. *Geosci. Model Dev.*, **4**, 1051–1075.

Conrad, R., 1996: Soil microorganisms as controllers of atmospheric trace gases (H_2, CO, CH_4, OCS, N_2O, and NO). *Microbiol. Rev.*, **60**, 609–640.

Conway, T., and P. Tans, 2011: Global CO_2. National Oceanic and Atmospheric Administration, Earth System Research Library, Silver Spring, MD, USA.

Conway, T. J., P. P. Tans, L. S. Waterman, K. W. Thoning, D. R. Kitzis, K. A. Masarie, and N. Zhang, 1994: Evidence for interannual variability of the carbon cycle from the National Oceanic and Atmospheric Administration Climate Monitoring and Diagnostics Laboratory Global Air Sampling Network. *J. Geophys. Res. Atmos.*, **99**, 22831–22855.

Corbière, A., N. Metzl, G. Reverdin, C. Brunet, and A. Takahashi, 2007: Interannual and decadal variability of the oceanic carbon sink in the North Atlantic subpolar gyre. *Tellus B*, **59**, 168–178.

Cox, P., and C. Jones, 2008: Climate change. Illuminating the modern dance of climate and CO_2. *Science*, **321**, 1642–1644.

Cox, P. M., 2001: Description of the TRIFFID dynamic global vegetation model. Technical Note 24. Hadley Centre, Met Office, Exeter, Devon, UK.

Cox, P. M., R. A. Betts, M. Collins, P. P. Harris, C. Huntingford, and C. D. Jones, 2004: Amazonian forest dieback under climate-carbon cycle projections for the 21st century. *Theor. Appl. Climatol.*, **78**, 137–156.

Cox, P. M., D. Pearson, B. B. Booth, P. Friedlingstein, C. Huntingford, C. D. Jones, and C. M. Luke, 2013: Sensitivity of tropical carbon to climate change constrained by carbon dioxide variability. *Nature*, **494**, 341–344.

Crévoisier, C., D. Nobileau, A. M. Fiore, R. Armante, A. Chédin, and N. A. Scott, 2009: Tropospheric methane in the tropics – first year from IASI hyperspectral infrared observations. *Atmos. Chem. Phys.*, **9**, 6337–6350.

Crutzen, P. J., A. R. Mosier, K. A. Smith, and W. Winiwarter, 2008: N_2O release from agro-biofuel production negates global warming reduction by replacing fossil fuels. *Atmos. Chem. Phys.*, **8**, 389–395.

Cunnold, D. M., et al., 2002: In situ measurements of atmospheric methane at GAGE/AGAGE sites during 1985–2000 and resulting source inferences. *J. Geophys. Res. Atmos.*, **107**, ACH20–1, CiteID 4225.

Curry, C. L., 2007: Modeling the soil consumption of methane at the global scale. *Global Biogeochem. Cycles*, **21**, GB4012.

Curry, C. L., 2009: The consumption of atmospheric methane by soil in a simulated future climate. *Biogeosciences*, **6**, 2355–2367.

Daniau, A. L., et al., 2012: Predictability of biomass burning in response to climate changes. *Global Biogeochem. Cycles*, **26**, Gb4007.

Davidson, E. A., 2009: The contribution of manure and fertilizer nitrogen to atmospheric nitrous oxide since 1860. *Nature Geosci.*, **2**, 659–662.

Davidson, E. A., et al., 2012: Excess nitrogen in the U.S. environnement: Trends, risks, and solutions. Issues of Ecology, Report number 15. Ecological Society of America, Washington, DC.

Dawes, M. A., S. Hättenschwiler, P. Bebi, F. Hagedorn, I. T. Handa, C. Körner, and C. Rixen, 2011: Species-specific tree growth responses to 9 years of CO_2 enrichment at the alpine treeline. *J. Ecol.*, **99**, 383–394.

De Klein, C., et al., 2007: N_2O emissions from managed soils, and CO_2 emissions from lime and urea application. In: *2006 IPCC Guidelines for National Greenhouse Gas Inventories,* Vol. 4 [M. Gytarsky, T. Higarashi, W. Irving, T. Krug and J. Penman (eds.)]. Intergovernmental Panel on Climate Change, Geneva, Switzerland, pp. 11.1–11.54.

DeFries, R., and C. Rosenzweig, 2010: Toward a whole-landscape approach for sustainable land use in the tropics. *Proc. Natl. Acad. Sci. U.S.A.*, **107**, 19627–19632.

DeFries, R. S., R. A. Houghton, M. C. Hansen, C. B. Field, D. L. Skole, and J. Townshend, 2002: Carbon emissions from tropical deforestation and regrowth based on satellite observations for the 1980s and 1990s. *Proc. Natl. Acad. Sci. U.S.A.*, **99**, 14256–14261.

Delmas, R. J., J.-M. Ascencio, and M. Legrand, 1980: Polar ice evidence that atmospheric CO_2 20,000–yr BP was 50% of present. *Nature*, **284**, 155–157.

Denman, K. L., 2008: Climate change, ocean processes and ocean iron fertilization. *Mar. Ecol. Prog. Ser.*, **364**, 219–225.

Denman, K. L., et al., 2007: Couplings between changes in the climate system and biogeochemistry. In: *Climate Change 2007: The Physical Science Basis. Contribution of Working Group I to the Fourth Assessment Report of the Intergovernmental Panel on Climate Change* [Solomon, S., D. Qin, M. Manning, Z. Chen, M. Marquis, K. B. Averyt, M. Tignor and H. L. Miller (eds.)] Cambridge University Press, Cambridge, United Kingdom and New York, NY, USA, 499-587.

Dentener, F., W. Peters, M. Krol, M. van Weele, P. Bergamaschi, and J. Lelieveld, 2003: Interannual variability and trend of CH_4 lifetime as a measure for OH changes in the 1979–1993 time period. *J. Geophys. Res. Atmos.*, **108**, 4442.

Dentener, F., et al., 2005: The impact of air pollutant and methane emission controls on tropospheric ozone and radiative forcing: CTM calculations for the period 1990–2030. *Atmos. Chem. Phys.*, **5**, 1731–1755.

Dentener, F., et al., 2006: The global atmospheric environment for the next generation. *Environ. Sci. Technol.*, **40**, 3586–3594.

Deutsch, C., J. L. Sarmiento, D. M. Sigman, N. Gruber, and J. P. Dunne, 2007: Spatial coupling of nitrogen inputs and losses in the ocean. *Nature*, **445**, 163–167.

Dickens, G. R., 2003: A methane trigger for rapid warming? *Science*, **299**, 1017.

Dlugokencky, E., and P. P. Tans, 2013a: Recent CO_2, NOAA, ESRS. Retrieved from www.esrl.noaa.gov/gmd/ccgg/trends/global.html, accessed 01-02-2013.

Dlugokencky, E., and P. P. Tans, 2013b: Globally averaged marine surface annual mean data, NOAA/ESRL. Retrieved from www.esrl.noaa.gov/gmd/ccgg/trends/, accessed 01-02-2013.

Dlugokencky, E. J., E. G. Nisbet, R. Fisher, and D. Lowry, 2011: Global atmospheric methane: Budget, changes and dangers. *Philos. Trans. R. Soc. London Ser. A*, **369**, 2058–2072.

Dlugokencky, E. J., P. M. Lang, A. M. Crotwell, and K. A. Masarie, 2012: Atmospheric methane dry air mole fractions from the NOAA ESRL Carbon Cycle Cooperative Global Air Sampling Network, 1983–2011, version 2012-09-24. Version 2010-08-12 ed.

Dlugokencky, E. J., S. Houweling, L. Bruhwiler, K. A. Masarie, P. M. Lang, J. B. Miller, and P. P. Tans, 2003: Atmospheric methane levels off: Temporary pause or a new steady-state? *Geophys. Res. Lett.*, **30**, 1992.

Dlugokencky, E. J., et al., 2009: Observational constraints on recent increases in the atmospheric CH_4 burden. *Geophys. Res. Lett.*, **36**, L18803.

Dolman, A. J., et al., 2012: An estimate of the terrestrial carbon budget of Russia using inventory based, eddy covariance and inversion methods. *Biogeosciences*, **9**, 5323–5340.

Doney, S. C., et al., 2009: Mechanisms governing interannual variability in upper-ocean inorganic carbon system and air-sea CO_2 fluxes: Physical climate and atmospheric dust. *Deep-Sea Res. Pt. II*, **56**, 640–655.

Dore, J. E., R. Lukas, D. W. Sadler, M. J. Church, and D. M. Karl, 2009: Physical and biogeochemical modulation of ocean acidification in the central North Pacific. *Proc. Natl. Acad. Sci. U.S.A.*, **106**, 12235–12240.

Dornburg, V., and G. Marland, 2008: Temporary storage of carbon in the biosphere does have value for climate change mitigation: A response to the paper by Miko Kirschbaum. *Mitigat. Adapt. Strat. Global Change*, **13**, 211–217.

Duce, R. A., et al., 2008: Impacts of atmospheric anthropogenic nitrogen on the open ocean. *Science*, **320**, 893–897.

Dueck, T. A., et al., 2007: No evidence for substantial aerobic methane emission by terrestrial plants: A ^{13}C-labelling approach. *New Phytologist*, **175**, 29–35.

Dufresne, J.-L., et al., 2013: Climate change projections using the IPSL-CM5 Earth System Model: From CMIP3 to CMIP5. *Clim. Dyn.*, **40**, 2123-2165.

Dukes, J. S., et al., 2005: Responses of grassland production to single and multiple global environmental changes. *PloS Biol.*, **3**, 1829–1837.

Dunne, J. P., et al., 2012: GFDL's ESM2 global coupled climate-carbon Earth System Models Part I: Physical formulation and baseline simulation characteristics. *J. Clim.*, **25**, 6646–6665.

Dunne, J. P., et al., 2013: GFDL's ESM2 global coupled climate-carbon Earth System Models. Part II: Carbon system formation and baseline simulation characteristics. *J. Clim.*, **26**, 2247-2267.

Dutaur, L., and L. V. Verchot, 2007: A global inventory of the soil CH_4 sink. *Global Biogeochem. Cycles*, **21**, GB4013.

Dutta, K., E. A. G. Schuur, J. C. Neff, and S. A. Zimov, 2006: Potential carbon release from permafrost soils of Northeastern Siberia. *Global Change Biol.*, **12**, 2336–2351.

Eby, M., K. Zickfeld, A. Montenegro, D. Archer, K. J. Meissner, and A. J. Weaver, 2009: Lifetime of anthropogenic climate change: Millennial time scales of potential CO_2 and surface temperature perturbations. *J. Clim.*, **22**, 2501–2511.

Eby, M., et al., 2013: Historical and idealized climate model experiments: An EMIC intercomparison. *Clim. Past*, **9**, 1–30.

EDGAR4–database, 2009: Emission Database for Global Atmospheric Research (EDGAR), release version 4.0. http://edgar.jrc.ec.europa.eu, 2009. European Commission. Joint Research Centre (JRC) / Netherlands Environmental Assessment Agency (PBL).

Elberling, B., H. H. Christiansen, and B. U. Hansen, 2010: High nitrous oxide production from thawing permafrost. *Nature Geosci.*, **3**, 332–335.

Eliseev, A. V., I. I. Mokhov, M. M. Arzhanov, P. F. Demchenko, and S. N. Denisov, 2008: Interaction of the methane cycle and processes in wetland ecosystems in a climate model of intermediate complexity. *Izvestiya Atmos. Ocean. Phys.*, **44**, 139–152.

Elliott, S., M. Maltrud, M. Reagan, G. Moridis, and P. Cameron-Smith, 2011: Marine methane cycle simulations for the period of early global warming. *J. Geophys. Res. Biogeosci.*, **116**, G01010.

Elser, J. J., et al., 2007: Global analysis of nitrogen and phosphorus limitation of primary producers in freshwater, marine and terrestrial ecosystems. *Ecol. Lett.*, **10**, 1135–1142.

Elsig, J., et al., 2009: Stable isotope constraints on Holocene carbon cycle changes from an Antarctic ice core. *Nature*, **461**, 507–510.

Emerson, S., and J. I. Hedges, 1988: Processes controlling the organic carbon content of open ocean sediments. *Paleoceanography*, **3**, 621–634.

EPA, 2006: Global anthropogenic non-CO_2 greenhouse gas emissions. United States Environmental Protection Agency (US EPA, Washington, DC) Report EPA-430-R-06-003. Retrieved from http://nepis.epa.gov/EPA/html/DLwait.htm?url=/Adobe/PDF/2000ZL5G.PDF.

EPA, 2010: Methane and nitrous oxide emissions from natural sources. United States Environmental Protection Agency (EPA) Report. Washington, DC. http://www.epa.gov/outreach/pdfs/Methane-and-Nitrous-Oxide-Emissions-From-Natural-Sources.pdf

EPA, 2011a: Global anthropogenic non-CO_2 greenhouse gas emissions: 1990–2030, United States Environmental Protection Agency (US EPA) Report. Washington, DC. http://www.epa.gov/climatechange/Downloads/EPAactivities/EPA_Global_NonCO2_Projections_Dec2012.pdf

EPA, 2011b: Reactive nitrogen in the United States: An analysis of inputs, flows, consequences, and management options. Report EPA-SAB-11-013, Washington, DC, 140 pp. http://yosemite.epa.gov/sab/sabproduct.nsf/WebBOARD/INCFullReport/$File/Final%20INC%20Report_8_19_11%28without%20signatures%29.pdf

Erisman, J. W., M. S. Sutton, J. N. Galloway, Z. Klimont, and W. Winiwarter, 2008: A century of ammonia synthesis. *Nature Geosci.*, **1**, 1–4.

Erisman, J. W., J. Galloway, S. Seitzinger, A. Bleeker, and K. Butterbach-Bahl, 2011: Reactive nitrogen in the environment and its effect on climate change. *Curr. Opin. Environ. Sustain.*, **3**, 281–290.

Esser, G., J. Kattge, and A. Sakalli, 2011: Feedback of carbon and nitrogen cycles enhances carbon sequestration in the terrestrial biosphere. *Global Change Biol.*, **17**, 819–842.

Etheridge, D. M., L. P. Steele, R. L. Langenfelds, R. J. Francey, J.-M. Barnola, and V. I. Morgan, 1996: Natural and anthropogenic changes in atmospheric CO_2 over the last 1000 years from air in Antarctic ice and firn. *J. Geophys. Res.*, **101**, 4115–4128.

Etiope, G., K. R. Lassey, R. W. Klusman, and E. Boschi, 2008: Reappraisal of the fossil methane budget and related emission from geologic sources. *Geophys. Res. Lett.*, **35**, L09307.

Evans, C. D., D. T. Monteith, and D. M. Cooper, 2005: Long-term increses in surface water dissolved organic carbon: Observations, possible causes and environmental impacts. *Environ. Pollut.*, **137**, 55–71.

Falloon, P., C. Jones, M. Ades, and K. Paul, 2011: Direct soil moisture controls of future global soil carbon changes: An important source of uncertainty. *Global Biogeochem. Cycles*, **25**, GB3010.

Fan, S.-M., T. L. Blaine, and J. L. Sarmiento, 1999: Terrestrial carbon sink in the Northern Hemisphere estimated from the atmospheric CO_2 difference between Manna Loa and the South Pole since 1959. *Tellus B*, **51**, 863–870.

FAO, 2005: Global Forest Resource Assessment 2005. Progress toward sustainable forest management. FAO Forestry Paper 147. Food and Agriculture Organization of the United Nations, Rome, Italy, pp. 129–147.

FAO, 2010: Global Forest Resources Assessment 2010. Main report. FAO Forestry Paper 163, Food and Agriculture Organization of the United Nations, Rome, Italy, 340 pp.

Feely, R. A., S. C. Doney, and S. R. Cooley, 2009: Ocean acidification: Present conditions and future changes in a high-CO_2 world. *Oceanography*, **22**, 36–47.

Feely, R. A., C. L. Sabine, J. M. Hernandez-Ayon, D. Ianson, and B. Hales, 2008: Evidence for upwelling of corrosive "acidified" water onto the continental shelf. *Science*, **320**, 1490–1492.

Feely, R. A., R. H. Byrne, J. G. Acker, P. R. Betzer, C.-T. A. Chen, J. F. Gendron, and M. F. Lamb, 1988: Winter-summer variations of calcite and aragonite saturation in the northeast Pacific. *Mar. Chem.*, **25**, 227–241.

Feely, R. A., T. Takahashi, R. Wanninkhof, M. J. McPhaden, C. E. Cosca, S. C. Sutherland, and M. E. Carr, 2006: Decadal variability of the air-sea CO_2 fluxes in the equatorial Pacific Ocean. *J. Geophys. Res. Oceans*, **111**, C08S90.

Felzer, B., et al., 2005: Past and future effects of ozone on carbon sequestration and climate change policy using a global biogeochemical model. *Clim. Change*, **73**, 345–373.

Ferretti, D. F., et al., 2005: Unexpected changes to the global methane budget over the past 2000 years. *Science*, **309**, 1714–1717.

Findlay, H. S., T. Tyrrell, R. G. J. Bellerby, A. Merico, and I. Skjelvan, 2008: Carbon and nutrient mixed layer dynamics in the Norwegian Sea. *Biogeosciences*, **5**, 1395–1410.

Findlay, S. E. G., 2005: Increased carbon transport in the Hudson River: Unexpected consequence of nitrogen deposition? *Front. Ecol. Environ.*, **3**, 133–137.

Finzi, A. C., et al., 2006: Progressive nitrogen limitation of ecosystem processes under elevated CO_2 in a warm-temperate forest. *Ecology*, **87**, 15–25.

Finzi, A. C., et al., 2007: Increases in nitrogen uptake rather than nitrogen-use efficiency support higher rates of temperate forest productivity under elevated CO_2. *Proc. Natl. Acad. Sci. U.S.A.*, **104**, 14014–14019.

Fischer, H., et al., 2008: Changing boreal methane sources and constant biomass burning during the last termination. *Nature*, **452**, 864–867.

Fisher, J. B., S. Sitch, Y. Malhi, R. A. Fisher, C. Huntingford, and S. Y. Tan, 2010: Carbon cost of plant nitrogen acquisition: A mechanistic, globally applicable model of plant nitrogen uptake, retranslocation, and fixation. *Global Biogeochem. Cycles*, **24**, GB1014.

Flannigan, M. D., B. Stocks, M. Turetsky, and M. Wotton, 2009a: Impacts of climate change on fire activity and fire management in the circumboreal forest. *Global Change Biol.*, **15**, 549–560.

Flannigan, M. D., M. A. Krawchuk, W. J. de Groot, B. M. Wotton, and L. M. Gowman, 2009b: Implications of changing climate for global wildland fire. *Int. J. Wildland Fire*, **18**, 483–507.

Fleming, E. L., C. H. Jackman, R. S. Stolarski, and A. R. Douglass, 2011: A model study of the impact of source gas changes on the stratosphere for 1850–2100. *Atmos. Chem. Phys.*, **11**, 8515–8541.

Flückiger, J., A. Dällenbach, T. Blunier, B. Stauffer, T. F. Stocker, D. Raynaud, and J.-M. Barnola, 1999: Variations in atmospheric N_2O concentration during abrupt climate changes. *Science*, **285**, 227–230.

Flückiger, J., et al., 2002: High-resolution Holocene N_2O ice core record and its relationship with CH_4 and CO_2. *Global Biogeochem. Cycles*, **16**, 1–10.

Flückiger, J., et al., 2004: N_2O and CH_4 variations during the last glacial epoch: Insight into global processes. *Global Biogeochem. Cycles*, **18**, GB1020.

Foley, J. A., C. Monfreda, N. Ramankutty, and D. Zaks, 2007: Our share of the planetary pie. *Proc. Natl. Acad. Sci. U.S.A.*, **104**, 12585–12586.

Foley, J. A., et al., 2011: Solutions for a cultivated planet. *Nature*, **478**, 337–342.

Fowler, D., et al., 2013: The global nitrogen cycle in the 21th century. *Philos. Trans. R. Soc. London Ser. B*, **368**, 20130165.

Francey, R. J., et al., 2013: Atmospheric verification of anthropogenic CO_2 emission trends. *Nature Clim. Change*, **3**, 520-524.

Frank, D. C., J. Esper, C. C. Raible, U. Buntgen, V. Trouet, B. Stocker, and F. Joos, 2010: Ensemble reconstruction constraints on the global carbon cycle sensitivity to climate. *Nature*, **463**, 527–U143.

Frankenberg, C., et al., 2011: Global column-averaged methane mixing ratios from 2003 to 2009 as derived from SCIAMACHY: Trends and variability. *J. Geophys. Res.*, **116**, D04302.

Frankenberg, C., et al., 2008: Tropical methane emissions: A revised view from SCIAMACHY onboard ENVISAT. *Geophys. Res. Lett.*, **35**, L15811.

Freing, A., D. W. R. Wallace, and H. W. Bange, 2012: Global oceanic production of nitrous oxide. *Philos. Trans. R. Soc. London Ser. B*, **367**, 1245–1255.

Friedli, H., H. Lötscher, H. Oeschger, U. Siegenthaler, and B. Stauffer, 1986: Ice core record of the $^{13}C/^{12}C$ ratio of atmospheric CO_2 in the past two centuries. *Nature*, **324**, 237–238.

Friedlingstein, P., and I. C. Prentice, 2010: Carbon-climate feedbacks: A review of model and observation based estimates. *Curr. Opin. Environ. Sustain.*, **2**, 251–257.

Friedlingstein, P., J. L. Dufresne, P. M. Cox, and P. Rayner, 2003: How positive is the feedback between climate change and the carbon cycle? *Tellus B*, **55**, 692–700.

Friedlingstein, P., et al., 2010: Update on CO_2 emissions. *Nature Geosci.*, **3**, 811–812.

Friedlingstein, P., et al., 2006: Climate-carbon cycle feedback analysis: Results from the C^4MIP model intercomparison. *J. Clim.*, **19**, 3337–3353.

Friis, K., A. Körtzinger, J. Patsch, and D. W. R. Wallace, 2005: On the temporal increase of anthropogenic CO_2 in the subpolar North Atlantic. *Deep-Sea Res. Pt. I*, **52**, 681–698.

Frölicher, T. L., F. Joos, and C. C. Raible, 2011: Sensitivity of atmospheric CO_2 and climate to explosive volcanic eruptions. *Biogeosciences*, **8**, 2317–2339.

Frölicher, T. L., F. Joos, C. C. Raible, and J. L. Sarmiento, 2013: Atmospheric CO_2 response to volcanic eruptions: The role of ENSO, season, and variability. *Global Biogeochem. Cycles*, **27**, 239-251.

Frölicher, T. L., F. Joos, G. K. Plattner, M. Steinacher, and S. C. Doney, 2009: Natural variability and anthropogenic trends in oceanic oxygen in a coupled carbon cycle–climate model ensemble. *Global Biogeochem. Cycles*, **23**, GB1003.

Frolking, S., and N. T. Roulet, 2007: Holocene radiative forcing impact of northern peatland carbon accumulation and methane emissions. *Global Change Biol.*, **13**, 1079–1088.

Fuller, D. Q., et al., 2011: The contribution of rice agriculture and livestock pastoralism to prehistoric methane levels: An archaeological assessment. *The Holocene*, **21**, 743–759.

Fung, I., M. Prather, J. John, J. Lerner, and E. Matthews, 1991: Three-dimensional model synthesis of the global methane cycle. *J. Geophys. Res.*, **96**, 13033–13065.

Fyfe, J. C., and O. A. Saenko, 2006: Simulated changes in the extratropical Southern Hemisphere winds and currents. *Geophys. Res. Lett.*, **33**, L06701.

Fyfe, J. C., J. N. S. Cole, V. K. Arora, and J. F. Scinocca, 2013: Biogeochemical carbon coupling influences global precipitation in geoengineering experiments. *Geophys. Res. Lett.*, **40**, 651–655.

Fyke, J. G., and A. J. Weaver, 2006: The effect of potential future climate change on the marine methane hydrate stability zone. *J. Clim.*, **19**, 5903–5917.

Gaillard, M. J., et al., 2010: Holocene land-cover reconstructions for studies on land cover-climate feedbacks. *Clim. Past*, **6**, 483–499.

Gaillardet, J., B. Dupre, P. Louvat, and C. J. Allegre, 1999: Global silicate weathering and CO_2 consumption rates deduced from the chemistry of large rivers. *Chem. Geol.*, **159**, 3–30.

Galbraith, D., P. E. Levy, S. Sitch, C. Huntingford, P. Cox, M. Williams, and P. Meir, 2010: Multiple mechanisms of Amazonian forest biomass losses in three dynamic global vegetation models under climate change. *New Phytologist*, **187**, 647–665.

Galloway, J. N., J. D. Aber, J. W. Erisman, S. P. Seitzinger, R. W. Howarth, E. B. Cowling, and B. J. Cosby, 2003: The nitrogen cascade. *BioScience*, **53**, 341–356.

Galloway, J. N., et al., 2008: Transformation of the nitrogen cycle: Recent trends, questions, and potential solutions. *Science*, **320**, 889.

Galloway, J. N., et al., 2004: Nitrogen cycles: Past, present and future. *Biogeochemistry*, **70**, 153–226.

Gao, H., et al., 2012: Intensive and extensive nitrogen loss from intertidal permeable sediments of the Wadden Sea *Limnol. Oceanogr.*, **57**, 185–198.

Gärdenäs, A. I., et al., 2011: Knowledge gaps in soil carbon and nitrogen interactions—From molecular to global scale. *Soil Biol. Biochem.*, **43**, 702–717.

GEA, 2006: Energy resources and potentials. In: Global Energy Assessment—Toward a Sustainable Future. Cambridge University Press, Cambridge, United Kingdom, and New York, NY, USA, 425-512.

Gedalof, Z., and A. A. Berg, 2010: Tree ring evidence for limited direct CO_2 fertilization of forests over the 20th century. *Global Biogeochem. Cycles*, **24**, Gb3027.

Gedney, N., P. M. Cox, and C. Huntingford, 2004: Climate feedback from wetland methane emissions. *Geophys. Res. Lett.*, **31**, L20503.

Gedney, N., P. M. Cox, R. A. Betts, O. Boucher, C. Huntingford, and P. A. Stott, 2006: Detection of a direct carbon dioxide effect in continental river runoff records. *Nature*, **439**, 835–838.

Gerber, S., L. O. Hedin, M. Oppenheimer, S. W. Pacala, and E. Shevliakova, 2010: Nitrogen cycling and feedbacks in a global dynamic land model. *Global Biogeochem. Cycles*, **24**, GB1001.

Gerber, S., F. Joos, P. Brugger, T. F. Stocker, M. E. Mann, S. Sitch, and M. Scholze, 2003: Constraining temperature variations over the last millennium by comparing simulated and observed atmospheric CO_2. *Clim. Dyn.*, **20**, 281–299.

Gervois, S., P. Ciais, N. de Noblet-Ducoudre, N. Brisson, N. Vuichard, and N. Viovy, 2008: Carbon and water balance of European croplands throughout the 20th century. *Global Biogeochem. Cycles*, **22**, GB003018.

Gilbert, D., N. N. Rabalais, R. J. Diaz, and J. Zhang, 2010: Evidence for greater oxygen decline rates in the coastal ocean than in the open ocean. *Biogeosciences*, **7**, 2283–2296.

Gloor, M., J. L. Sarmiento, and N. Gruber, 2010: What can be learned about carbon cycle climate feedbacks from the CO_2 airborne fraction? *Atmos. Chem. Phys.*, **10**, 7739–7751.

Gloor, M., et al., 2012: The carbon balance of South America: A review of the status, decadal trends and main determinants. *Biogeosciences*, **9**, 5407–5430.

Gloor, M., et al., 2009: Does the disturbance hypothesis explain the biomass increase in basin-wide Amazon forest plot data? *Global Change Biol.*, **15**, 2418–2430.

Gnanadesikan, A., and I. Marinov, 2008: Export is not enough: Nutrient cycling and carbon sequestration. *Mar. Ecol. Prog. Ser.*, **364**, 289–294.

Gnanadesikan, A., J. L. Sarmiento, and R. D. Slater, 2003: Effects of patchy ocean fertilization on atmospheric carbon dioxide and biological production. *Global Biogeochem. Cycles*, **17**, 1050.

Gnanadesikan, A., J. L. Russell, and F. Zeng, 2007: How does ocean ventilation change under global warming? *Ocean Sci.*, **3**, 43–53.

Gnanadesikan, A., J. P. Dunne, and J. John, 2012: Understanding why the volume of suboxic waters does not increase over centuries of global warming in an Earth System Model. *Biogeosciences*, **9**, 1159–1172.

Goldewijk, K. K., 2001: Estimating global land use change over the past 300 years: The HYDE Database. *Global Biogeochem. Cycles*, **15**, 417–433.

Goldewijk, K. K., A. Beusen, G. van Drecht, and M. de Vos, 2011: The HYDE 3.1 spatially explicit database of human-induced global land-use change over the past 12,000 years. *Global Ecol. Biogeogr.*, **20**, 73–86.

Golding, N., and R. Betts, 2008: Fire risk in Amazonia due to climate change in the HadCM3 climate model: Potential interactions with deforestation. *Global Biogeochem. Cycles*, **22**, GB4007.

Goll, D. S., et al., 2012: Nutrient limitation reduces land carbon uptake in simulations with a model of combined carbon, nitrogen and phosphorus cycling. *Biogeosciences*, **9**, 3547–3569.

Good, P., C. Jones, J. Lowe, R. Betts, and N. Gedney, 2013: Comparing tropical forest projections from two generations of Hadley Centre Earth System Models, HadGEM2–ES and HadCM3LC. *J. Clim.*, **26**, 495–511.

Good, P., C. Jones, J. Lowe, R. Betts, B. Booth, and C. Huntingford, 2011: Quantifying environmental drivers of future tropical forest extent. *J. Clim.*, **24**, 1337–1349.

Govindasamy, B., K. Caldeira, and P. B. Duffy, 2003: Geoengineering Earth's radiation balance to mitigate climate change from a quadrupling of CO_2. *Global Planet. Change*, **37**, 157–168.

Govindasamy, B., S. Thompson, P. B. Duffy, K. Caldeira, and C. Delire, 2002: Impact of geoengineering schemes on the terrestrial biosphere. *Geophys. Res. Lett.*, **29**, 2061.

Graven, H. D., N. Gruber, R. Key, S. Khatiwala, and X. Giraud, 2012: Changing controls on oceanic radiocarbon: New insights on shallow-to-deep ocean exchange and anthropogenic CO_2 uptake. *J. Geophys. Res. Oceans*, **117**, C10005.

Gray, M. L., K. J. Champagne, D. Fauth, J. P. Baltrus, and H. Pennline, 2008: Performance of immobilized tertiary amine solid sorbents for the capture of carbon dioxide. *Int. J. Greenh. Gas Control*, **2**, 3–8.

Gregg, J. S., R. J. Andres, and G. Marland, 2008: China: Emissions pattern of the world leader in CO_2 emissions from fossil fuel consumption and cement production. *Geophys. Res. Lett.*, **35**, L08806.

Gregory, J. M., C. D. Jones, P. Cadule, and P. Friedlingstein, 2009: Quantifying carbon cycle feedbacks. *J. Clim.*, **22**, 5232–5250.

Groszkopf, T., et al., 2012: Doubling of marine dinitrogen-fixation rates based on direct measurements. *Nature*, **488**, 361–364.

Gruber, N., and J. N. Galloway, 2008: An Earth-system perspective of the global nitrogen cycle. *Nature*, **451**, 293–296.

Gruber, N., C. Hauri, Z. Lachkar, D. Loher, T. L. Frölicher, and G. K. Plattner, 2012: Rapid progression of ocean acidification in the California Current System. *Science*, **337**, 220–223.

Gruber, N., et al., 2009: Oceanic sources, sinks, and transport of atmospheric CO_2. *Global Biogeochem. Cycles*, **23**, GB1005.

Gurney, K. R., and W. J. Eckels, 2011: Regional trends in terrestrial carbon exchange and their seasonal signatures. *Tellus B*, **63**, 328–339.

Hamilton, S. K., A. L. Kurzman, C. Arango, L. Jin, and G. P. Robertson, 2007: Evidence for carbon sequestration by agricultural liming. *Global Biogeochem. Cycles*, **21**, GB2021.

Hansell, D. A., C. A. Carlson, D. J. Repeta, and R. Schlitzer, 2009: Dissolved organic matter in the ocean: A controversy stimulates new insights. *Oceanography*, **22**, 202–211.

Hansen, M. C., S. V. Stehman, and P. V. Potapov, 2010: Quantification of global gross forest cover loss. *Proc. Natl. Acad. Sci. U.S.A.*, **107**, 8650–8655.

Harden, J. W., et al., 2012: Field information links permafrost carbon to physical vulnerabilities of thawing. *Geophys. Res. Lett.*, **39**, L15704.

Harris, N. L., et al., 2012: Baseline map of carbon emissions from deforestation in tropical regions. *Science*, **336**, 1573–1576.

Harrison, K. G., 2000: Role of increased marine silica input on paleo-pCO_2 levels. *Paleoceanography*, **15**, 292–298.

Hartmann, J., N. Jansen, H. H. Dürr, S. Kempe, and P. Köhler, 2009: Global CO_2– consumption by chemical weathering: What is the contribution of highly active weathering regions? *Global Planet. Change*, **69**, 185–194.

Harvey, L. D. D., 2008: Mitigating the atmospheric CO_2 increase and ocean acidification by adding limestone powder to upwelling regions. *J. Geophys. Res.*, **113**, C04028.

Haverd, V., et al., 2013: The Australian terrestrial carbon budget. *Biogeosciences*, **10**, 851–869.

Hedegaard, G. B., J. Brandt, J. H. Christensen, L. M. Frohn, C. Geels, K. M. Hansen, and M. Stendel, 2008: Impacts of climate change on air pollution levels in the Northern Hemisphere with special focus on Europe and the Arctic. *Atmos. Chem. Phys.*, **8**, 3337–3367.

Heijmans, M. M. P. D., W. J. Arp, and F. Berendse, 2001: Effects of elevated CO_2 and vascular plants on evapotranspiration in bog vegetation. *Global Change Biol.*, **7**, 817–827.

Heijmans, M. M. P. D., H. Klees, and F. Berendse, 2002a: Competition between *Sphagnum magellanicum* and *Eriophorum angustifolium* as affected by raised CO_2 and increased N deposition. *Oikos*, **97**, 415–425.

Heijmans, M. M. P. D., H. Klees, W. de Visser, and F. Berendse, 2002b: Response of a *Sphagnum* bog plant community to elevated CO_2 and N supply. *Plant Ecol.*, **162**, 123–134.

Hein, R., P. J. Crutzen, and M. Heimann, 1997: An inverse modeling approach to investigate the global atmospheric methane cycle. *Global Biogeochem. Cycles*, **11**, 43–76.

Held, I. M., M. Winton, K. Takahashi, T. Delworth, F. Zeng, and G. K. Vallis, 2010: Probing the fast and slow components of global warming by returning abruptly to preindustrial forcing. *J. Clim.*, **23**, 2418–2427.

Herridge, D. F., M. B. Peoples, and R. M. Boddey, 2008: Global inputs of biological nitrogen fixation in agricultural systems. *Plant Soil*, **311**, 1–18.

Herzog, H., K. Caldeira, and J. Reilly, 2003: An issue of permanence: Assessing the effectiveness of temporary carbon storage. *Clim. Change*, **59**, 293–310.

Hibbard, K. A., G. A. Meehl, P. M. Cox, and P. Friedlingstein, 2007: A strategy for climate change stabilization experiments. *EOS Trans. Am. Geophys. Union*, **88**, 217-221.

Hickler, T., B. Smith, I. C. Prentice, K. Mjöfors, P. Miller, A. Arneth, and M. T. Sykes, 2008: CO_2 fertilization in temperate FACE experiments not representative of boreal and trophical forests. *Global Change Biol.*, **14**, 1531–1542.

Hietz, P., B. L. Turner, W. Wanek, A. Richter, C. A. Nock, and S. J. Wright, 2011: Long-term change in the nitrogen cycle of tropical forests. *Science*, **334**, 664-666.

Higgins, P. A. T., and J. Harte, 2012: Carbon cycle uncertainty increases climate change risks and mitigation challenges. *J. Clim.*, **25**, 7660–7668.

Hirota, M., M. Holmgren, E. H. Van Nes, and M. Scheffer, 2011: Global resilience of tropical forest and savanna to critical transitions. *Science*, **334**, 232–235.

Hirsch, A. I., A. M. Michalak, L. M. Bruhwiler, W. Peters, E. J. Dlugokencky, and P. P. Tans, 2006: Inverse modeling estimates of the global nitrous oxide surface flux from 1998 to 2001. *Global Biogeochem. Cycles*, **20**, GB1008.

Hodson, E. L., B. Poulter, N. E. Zimmermann, C. Prigent, and J. O. Kaplan, 2011: The El Nino-Southern Oscillation and wetland methane interannual variability. *Geophys. Res. Lett.*, **38**, L08810.

Hoelzemann, J. J., M. G. Schultz, G. P. Brasseur, C. Granier, and M. Simon, 2004: Global Wildland Fire Emission Model (GWEM): Evaluating the use of global area burnt satellite data. *J. Geophys. Res. Atmos.*, **109**, D14S04.

Hofmann, M., and H.-J. Schellnhuber, 2009: Oceanic acidification affects marine carbon pump and triggers extended marine oxygen holes. *Proc. Natl. Acad. Sci. U.S.A.*, **106**, 3017–3022.

Holland, E. A., J. Lee-Taylor, C. D. Nevison, and J. Sulzman, 2005: Global N cycle: Fluxes and N_2O mixing ratios originating from human activity. Data set. Oak Ridge National Laboratory Distributed Active Archive Center, Oak Ridge National Laboratory, Oak Ridge, TN. Retrieved from http://www.daac.ornl.gov

Hönisch, B., N. G. Hemming, D. Archer, M. Siddall, and J. F. McManus, 2009: Atmospheric carbon dioxide concentration across the mid-Pleistocene transition. *Science*, **324**, 1551–1554.

Hooijer, A., S. Page, J. G. Canadell, M. Silvius, J. Kwadijk, H. Wösten, and J. Jauhiainen, 2010: Current and future CO_2 emissions from drained peatlands in Southeast Asia. *Biogeosciences*, **7**, 1505–1514.

Hopcroft, P. O., P. J. Valdes, and D. J. Beerling, 2011: Simulating idealized Dansgaard-Oeschger events and their potential impacts on the global methane cycle. *Quat. Sci. Rev.*, **30**, 3258–3268.

Houghton, R. A., 2003: Revised estimates of the annual net flux of carbon to the atmosphere from changes in land use and land management 1850–2000. *Tellus B*, **55**, 378–390.

Houghton, R. A., 2010: How well do we know the flux of CO_2 from land-use change? *Tellus B*, **62**, 337–351.

Houghton, R. A., et al., 2012: Carbon emissions from land use and land-cover change. *Biogeosciences*, **9**, 5125–5142.

House, J. I., I. C. Prentice, and C. Le Quéré, 2002: Maximum impacts of future reforestation or deforestation on atmospheric CO_2. *Global Change Biol.*, **8**, 1047–1052.

House, K. Z., D. P. Schrag, C. F. Harvey, and K. S. Lackner, 2006: Permanent carbon dioxide storage in deep-sea sediments. *Proc. Natl. Acad. Sci. U.S.A.*, **103**, 14255.

House, K. Z., C. H. House, D. P. Schrag, and M. J. Aziz, 2007: Electrochemical acceleration of chemical weathering as an energetically feasible approach to mitigating anthropogenic climate change. *Environ. Sci. Technol.*, **41**, 8464–8470.

Hsu, J., and M. J. Prather, 2010: Global long-lived chemical modes excited in a 3-D chemistry transport model: Stratospheric N_2O, NOy, O_3 and CH_4 chemistry. *Geophys. Res. Lett.*, **37**, L07805.

Huang, J., et al., 2008: Estimation of regional emissions of nitrous oxide from 1997 to 2005 using multinetwork measurements: A chemical transport model, and an inverse method. *J. Geophys. Res.*, **113**, D17313.

Huber, C., et al., 2006: Isotope calibrated Greenland temperature record over Marine Isotope Stage 3 and its relation to CH_4. *Earth Planet. Sci. Lett.*, **243**, 504–519.

Hunter, S. J., A. M. Haywood, D. S. Goldobin, A. Ridgwell, and J. G. Rees, 2013: Sensitivity of the global submarine hydrate inventory to scenarious of future climate change. *Earth Planet. Sci. Lett.*, **367**, 105–115.

Huntingford, C., J. A. Lowe, B. B. B. Booth, C. D. Jones, G. R. Harris, L. K. Gohar, and P. Meir, 2009: Contributions of carbon cycle uncertainty to future climate projection spread. *Tellus B*, **61**, 355–360.

Huntingford, C., et al., 2013: Simulated resilience of tropical rainforests to CO_{2-} induced climate change. *Nature Geosci.*, **6**, 268–273.

Hurtt, G. C., et al., 2011: Harmonization of land-use scenarios for the period 1500–2100: 600 years of global gridded annual land-use transitions, wood harvest, and resulting secondary lands. *Clim. Change*, **109**, 117–161.

Huybers, P., and C. Langmuir, 2009: Feedback between deglaciation, volcanism, and atmospheric CO_2. *Earth Planet. Sci. Lett.*, **286**, 479–491.

Indermühle, A., et al., 1999: Holocene carbon-cycle dynamics based on CO_2 trapped in ice at Taylor Dome, Antarctica. *Nature*, **398**, 121–126.

Irvine, P. J., A. Ridgwell, and D. J. Lunt, 2010: Assessing the regional disparities in geoengineering impacts. *Geophys. Res. Lett.*, **37**, L18702.

Ise, T., A. L. Dunn, S. C. Wofsy, and P. R. Moorcroft, 2008: High sensitivity of peat decomposition to climate change through water-table feedback. *Nature Geosci.*, **1**, 763–766.

Ishii, M., N. Kosugi, D. Sasano, S. Saito, T. Midorikawa, and H. Y. Inoue, 2011: Ocean acidification off the south coast of Japan: A result from time series observations of CO_2 parameters from 1994 to 2008. *J. Geophys. Res. Oceans*, **116**, C06022.

Ishii, M., et al., 2009: Spatial variability and decadal trend of the oceanic CO_2 in the western equatorial Pacific warm/fresh water. *Deep-Sea Res. Pt. II*, **56**, 591–606.

Ishijima, K., T. Nakazawa, and S. Aoki, 2009: Variations of atmospheric nitrous oxide concentration in the northern and western Pacific. *Tellus B*, **61**, 408–415.

Ito, A., and J. E. Penner, 2004: Global estimates of biomass burning emissions based on satellite imagery for the year 2000. *J. Geophys. Res.*, **109**, D14S05.

Ito, A., and M. Inatomi, 2012: Use of a process-based model for assessing the methane budgets of global terrestrial ecosystems and evaluation of uncertainty. *Biogeosciences*, **9**, 759–773.

Iudicone, D., et al., 2011: Water masses as a unifying framework for understanding the Southern Ocean Carbon Cycle. *Biogeosciences*, **8**, 1031–1052.

Iversen, T., et al., 2013: The Norwegian Earth System Model, NorESM1–M. Part 2: Climate response and scenario projections. *Geosci. Model Dev.*, **6**, 389–415.

Jaccard, S. L., and E. D. Galbraith, 2012: Large climate-driven changes of oceanic oxygen concentrations during the last deglaciation. *Nature Geosci.*, **5**, 151-156.

Jaccard, S. L., G. H. Haug, D. M. Sigman, T. F. Pedersen, H. R. Thierstein, and U. Rδhl, 2005: Glacial/interglacial changes in subarctic North Pacific stratification. *Science*, **308**, 1003–1006.

Jacobson, A. R., S. E. Mikaloff Fletcher, N. Gruber, J. L. Sarmiento, and M. Gloor, 2007: A joint atmosphere-ocean inversion for surface fluxes of carbon dioxide: 2. Regional results. *Global Biogeochem. Cycles*, **21**, GB1020.

Jacquet, S. H. M., N. Savoye, F. Dehairs, V. H. Strass, and D. Cardinal, 2008: Mesopelagic carbon remineralization during the European Iron Fertilization Experiment. *Global Biogeochem. Cycles*, **22**, 1–9.

Jain, A., X. J. Yang, H. Kheshgi, A. D. McGuire, W. Post, and D. Kicklighter, 2009: Nitrogen attenuation of terrestrial carbon cycle response to global environmental factors. *Global Biogeochem. Cycles*, **23**, GB4028.

Jin, X., and N. Gruber, 2003: Offsetting the radiative benefit of ocean iron fertilization by enhancing N_2O emissions. *Geophys. Res. Lett.*, **30**, 24, 2249.

Jones, C., S. Liddicoat, and J. Lowe, 2010: Role of terrestrial ecosystems in determining CO_2 stabilization and recovery behaviour. *Tellus B*, **62**, 682–699.

Jones, C., M. Collins, P. M. Cox, and S. A. Spall, 2001: The carbon cycle response to ENSO: A coupled climate-carbon cycle model study. *J. Clim.*, **14**, 4113–4129.

Jones, C., J. Lowe, S. Liddicoat, and R. Betts, 2009: Committed terrestrial ecosystem changes due to climate change. *Nature Geosci.*, **2**, 484–487.

Jones, C., et al., 2013: 21th Century compatible CO_2 emissions and airborne fraction simulated by CMIP5 Earth System models under 4 Representative Concentration Pathways. *J. Clim.*, **26**, 4398-4413.

Jones, C. D., and P. M. Cox, 2001: Modeling the volcanic signal in the atmospheric CO_2 record. *Global Biogeochem. Cycles*, **15**, 453–465.

Jones, C. D., and P. Falloon, 2009: Sources of uncertainty in global modelling of future soil organic carbon storage. In: *Uncertainties in Environmental Modelling and Consequences for Policy Making* [P. Bavaye, J. Mysiak and M. Laba (eds.)]. Springer Science+Business Media, New York, NY, USA and Heidelberg, Germany, pp. 283–315.

Jones, C. D., P. M. Cox, and C. Huntingford, 2006: Impact of climate carbon cycle feedbacks on emission scenarios to achieve stabilization. In: *Avoiding Dangerous Climate Change* [H. J. Schellnhuber, W. Cramer, N. Nakicenovic, T. Wigley and G. Yohe (eds.)]. Cambridge University Press, Cambridge, United Kingdom, and New York, NY, USA, pp. 323–332.

Jones, C. D., et al., 2011: The HadGEM2–ES implementation of CMIP5 centennial simulations. *Geosci. Model Dev.*, **4**, 543–570.

Joos, F., and R. Spahni, 2008: Rates of change in natural and anthropogenic radiative forcing over the past 20,000 years. *Proc. Natl. Acad. Sci. U.S.A.*, **105**, 1425–1430.

Joos, F., J. L. Sarmiento, and U. Siegenthaler, 1991: Estimates of the effect of Southern-Ocean iron fertilization on atmospheric CO_2 concentrations. *Nature*, **349**, 772–775.

Joos, F., T. L. Frölicher, M. Steinacher, and G.-K. Plattner, 2011: Impact of climate change mitigation on ocean acidification projections. In: *Ocean Acidification* [J. P. Gattuso and L. Hansson (eds.)]. Oxford University Press, Oxford, United Kingdom, and New York, NY, USA, pp. 273-289.

Joos, F., S. Gerber, I. C. Prentice, B. L. Otto-Bliesner, and P. J. Valdes, 2004: Transient simulations of Holocene atmospheric carbon dioxide and terrestrial carbon since the Last Glacial Maximum. *Global Biogeochem. Cycles*, **18**, Gb2002.

Joos, F., et al., 2013: Carbon dioxide and climate impulse response functions for the computation of greenhouse gas metrics: A multi-model analysis. *Atmos. Chem. Phys.*, **13**, 2793–2825.

Jorgenson, M. T., Y. L. Shur, and E. R. Pullman, 2006: Abrupt increase in permafrost degradation in Arctic Alaska. *Geophys. Res. Lett.*, **33**, L02503.

Jung, M., et al., 2007: Assessing the ability of three land ecosystem models to simulate gross carbon uptake of forests from boreal to Mediterranean climate in Europe. *Biogeosciences*, **4**, 647–656.

Jung, M., et al., 2011: Global patterns of land-atmosphere fluxes of carbon dioxide, latent heat, and sensible heat derived from eddy covariance, satellite, and meteorological observations. *J. Geophys. Res. Biogeosci.*, **116**, G00J07.

Jungclaus, J. H., et al., 2010: Climate and carbon-cycle variability over the last millennium. *Clim. Past*, **6**, 723–737.

Kai, F. M., S. C. Tyler, J. T. Randerson, and D. R. Blake, 2011: Reduced methane growth rate explained by decreased Northern Hemisphere microbial sources. *Nature*, **476**, 194–197.

Kanakidou, M., et al., 2012: Atmospheric fluxes of organic N and P to the global ocean. *Global Biogeochem. Cycles*, **26**, GB3026.

Kaplan, J. O., G. Folberth, and D. A. Hauglustaine, 2006: Role of methane and biogenic volatile organic compound sources in late glacial and Holocene fluctuations of atmospheric methane concentrations. *Global Biogeochem. Cycles*, **20**, Gb2016.

Kaplan, J. O., I. C. Prentice, W. Knorr, and P. J. Valdes, 2002: Modeling the dynamics of terrestrial carbon storage since the Last Glacial Maximum. *Geophys. Res. Lett.*, **29**, 31-1-31-4.

Kaplan, J. O., K. M. Krumhardt, E. C. Ellis, W. F. Ruddiman, C. Lemmen, and K. Klein Goldewijk, 2011: Holocene carbon emissions as a result of anthropogenic land cover change. *Holocene*, **21**, 775–791.

Karl, D. M., and R. M. Letelier, 2008: Nitrogen fixation-enhanced carbon sequestration in low nitrate, low chlorophyll seascapes. *Mar. Ecol. Prog. Ser.*, **364**, 257–268.

Kato, E., T. Kinoshita, A. Ito, M. Kawamiya, and Y. Yamagata, 2013: Evaluation of spatially explicit emission scenario of land-use change and biomass burning using a process-based biogeochemical model. *J. Land Use Sci.*, **8**, 104–122.

Keeling, C. D., 1960: The concentration and isotopic abundances of carbon dioxide in the atmosphere. *Tellus B*, **12**, 200–203.

Keeling, C. D., S. C. Piper, and M. Heimann, 1989: A three dimensional model of atmospheric CO_2 transport based on observed winds: 4. Mean annual gradients and interannual variations. In: *Aspects of Climate Variability in the Pacific and the Western Americas* [D. H. Peterson (ed.)]. Geophysical Monograph Series, Vol. 55. American Geophysical Union, Washington, DC, pp. 305–363.

Keeling, C. D., R. B. Bacastow, A. E. Bainbridge, C. A. Ekdahl, P. R. Guenther, L. S. Waterman, and J. F. S. Chin, 1976: Atmospheric carbon-dioxide variations at Mauna-Loa Observatory, Hawaii. *Tellus*, **28**, 538–551.

Keeling, C. D., S. C. Piper, R. B. Bacastow, M. Wahlen, T. P. Whorf, M. Heimann, and H. A. Meijer, 2005: Atmospheric CO_2 and $^{13}CO_2$ exchange with the terrestrial biosphere and oceans from 1978 to 2000: Observations and carbon cycle implications. In: *A History of Atmospheric CO_2 and Its Effects on Plants, Animals, and Ecosystems* [J. R. Ehleringer, T. E. Cerling and M. D. Dearing (eds.)]. Springer Science+Business Media, New York, NY, USA, and Heidelberg, Germany, pp. 83–113.

Keeling, R. F., and S. R. Shertz, 1992: Seasonal and interannual variations in atmospheric oxygen and implications for the global carbon cycle. *Nature*, **358**, 723–727.

Keeling, R. F., S. C. Piper, and M. Heimann, 1996: Global and hemispheric CO_2 sinks deduced from changes in atmospheric O_2 concentration. *Nature*, **381**, 218–221.

Keeling, R. F., A. Körtzinger, and N. Gruber, 2010: Ocean deoxygenation in a warming world. *Annu. Rev. Mar. Sci.*, **2**, 199–229.

Keenan, T. F., et al., 2012: Terrestrial biosphere model performance for inter-annual variability of land-atmosphere CO_2 exchange. *Global Change Biol.*, **18**, 1971–1987.

Keith, D. W., 2001: Geoengineering. *Nature*, **409**, 420.

Keith, D. W., M. Ha-Duong, and J. K. Stolaroff, 2006: Climate strategy with CO_2 capture from the air. *Clim. Change*, **74**, 17–45.

Kelemen, P. B., and J. Matter, 2008: In situ carbonation of peridotite for CO_2 storage. *Proc. Natl. Acad. Sci. U.S.A.*, **105**, 17295–17300.

Kellomäki, S., H. Peltola, T. Nuutinen, K. T. Korhonen, and H. Strandman, 2008: Sensitivity of managed boreal forests in Finland to climate change, with implications for adaptive management. *Philos. Trans. R. Soc. London Ser. B*, **363**, 2341–2351.

Keppler, F., J. T. G. Hamilton, M. Braδ, and T. Röckmann, 2006: Methane emissions from terrestrial plants under aerobic conditions. *Nature*, **439**, 187–191.

Kesik, M., et al., 2006: Future scenarios of N_2O and NO emissions from European forest soils. *J. Geophys. Res. Biogeosci.*, **111**, G02018.

Key, R. M., et al., 2004: A global ocean carbon climatology: Results from Global Data Analysis Project (GLODAP). *Global Biogeochem. Cycles*, **18**, GB4031.

Khalil, M. A. K., and R. A. Rasmussen, 1989: Climate-induced feedbacks for the global cycles of methane and nitrous oxide. *Tellus B*, **41**, 554–559.

Khalil, M. A. K., C. L. Butenhoff, and R. A. Rasmussen, 2007: Atmospheric methane: Trends and cycles of sources and sinks. *Environ. Sci. Technol.*, **41**, 2131–2137.

Khatiwala, S., F. Primeau, and T. Hall, 2009: Reconstruction of the history of anthropogenic CO_2 concentrations in the ocean. *Nature*, **462**, 346–349.

Kheshgi, H. S., 1995: Sequestering atmospheric carbon-dioxide by increasing ocean alkalinity. *Energy*, **20**, 915–922.

Khvorostyanov, D., P. Ciais, G. Krinner, and S. Zimov, 2008: Vulnerability of east Siberia's frozen carbon stores to future warming. *Geophys. Res. Lett.*, **35**, L10703.

Kim, J. H., et al., 2004: North Pacific and North Atlantic sea-surface temperature variability during the Holocene. *Quat. Sci. Rev.*, **23**, 2141–2154.

King, A. W., D. J. Hayes, D. N. Huntzinger, T. O. West, and W. M. Post, 2012: North America carbon dioxide sources and sinks: Magnitude, attribution, and uncertainty. *Front. Ecol. Environ.*, **10**, 512–519.

Kirschbaum, M. U. F., 2003: Can trees buy time? An assessment of the role of vegetation sinks as part of the global carbon cycle. *Clim. Change*, **58**, 47–71.

Kirschbaum, M. U. F., and A. Walcroft, 2008: No detectable aerobic methane efflux from plant material, nor from adsorption/desorption processes. *Biogeosciences*, **5**, 1551–1558.

Kleinen, T., V. Brovkin, and R. J. Schuldt, 2012: A dynamic model of wetland extent and peat accumulation: Results for the Holocene. *Biogeosciences*, **9**, 235–248.

Kleinen, T., V. Brovkin, W. von Bloh, D. Archer, and G. Munhoven, 2010: Holocene carbon cycle dynamics. *Geophys. Res. Lett.*, **37**, L02705.

Kloster, S., N. M. Mahowald, J. T. Randerson, and P. J. Lawrence, 2012: The impacts of climate, land use, and demography on fires during the 21st century simulated by CLM-CN. *Biogeosciences*, **9**, 509–525.

Knorr, W., 2009: Is the airborne fraction of anthropogenic emissions increasing? *Geophys. Res. Lett.*, **36**, L21710.

Kohfeld, K. E., and A. Ridgwell, 2009: Glacial-interglacial variability in atmospheric CO_2. In: *Surface Ocean–Lower Atmospheres Processes* [C. Le Quéré and E. S. Saltzman (eds.)]. American Geophysical Union, Washington, DC, pp. 251-286.

Köhler, P., J. Hartmann, and D. A. Wolf-Gladrow, 2010: Geoengineering potential of artificially enhanced silicate weathering of olivine. *Proc. Natl. Acad. Sci. U.S.A.*, **107**, 20228–20233.

6

Köhler, P., H. Fischer, G. Munhoven, and R. E. Zeebe, 2005: Quantitative interpretation of atmospheric carbon records over the last glacial termination. *Global Biogeochem. Cycles*, **19**, GB4020.

Konijnendijk, T. Y. M., S. L. Weber, E. Tuenter, and M. van Weele, 2011: Methane variations on orbital timescales: A transient modeling experiment. *Clim. Past*, **7**, 635–648.

Koven, C. D., W. J. Riley, and A. Stern, 2013: Analysis of permafrost thermal dynamics and response to climate change in the CMIP5 Earth System Models. *J. Clim.*, **26**, 1877-1900.

Koven, C. D., et al., 2011: Permafrost carbon-climate feedbacks accelerate global warming. *Proc. Natl. Acad. Sci. U.S.A.*, **108**, 14769–14774.

Krawchuk, M. A., M. A. Moritz, M.-A. Parisien, J. Van Dorn, and K. Hayhoe, 2009: Global pyrogeography: The current and future distribution of wildfire. *PLoS ONE*, **4**, e5102.

Kraxner, F., S. Nilsson, and M. Obersteiner, 2003: Negative emissions from BioEnergy use, carbon capture and sequestration (BECS)—the case of biomass production by sustainable forest management from semi-natural temperate forests. *Biomass Bioenerg.*, **24**, 285–296.

Krinner, G., et al., 2005: A dynamic global vegetation model for studies of the coupled atmosphere-biosphere system. *Global Biogeochem. Cycles*, **19**, GB1015.

Krishnamurthy, A., J. K. Moore, N. Mahowald, C. Luo, S. C. Doney, K. Lindsay, and C. S. Zender, 2009: Impacts of increasing anthropogenic soluble iron and nitrogen deposition on ocean biogeochemistry. *Global Biogeochem. Cycles*, **23**, GB3016.

Kroeze, C., A. Mosier, and L. Bouwman, 1999: Closing the global N_2O budget: A retrospective analysis 1500–1994. *Global Biogeochem. Cycles*, **13**, 1–8.

Kroeze, C., L. Bouwman, and C. P. Slomp, 2007: Sinks for N_2O at the Earth's surface. In: *Greenhouse Gas Sinks* [D. S. Raey , M. Hewitt, J. Grace and K. A. Smith (eds.)]. CAB International, pp. 227–243.

Kroeze, C., E. Dumont, and S. P. Seitzinger, 2010: Future trends in emissions of N_2O from rivers and estuaries. *J. Integrat. Environ. Sci.*, **7**, 71–78.

Kurahashi-Nakamura, T., A. Abe-Ouchi, Y. Yamanaka, and K. Misumi, 2007: Compound effects of Antarctic sea ice on atmospheric pCO_2 change during glacial-interglacial cycle. *Geophys. Res. Lett.*, **34**, L20708.

Kurz, W. A., G. Stinson, and G. Rampley, 2008a: Could increased boreal forest ecosystem productivity offset carbon losses from increased disturbances? *Philos. Trans. R. Soc. London Ser. B*, **363**, 2261–2269.

Kurz, W. A., G. Stinson, G. J. Rampley, C. C. Dymond, and E. T. Neilson, 2008b: Risk of natural disturbances makes future contribution of Canada's forests to the global carbon cycle highly uncertain. *Proc. Natl. Acad. Sci. U.S.A.*, **105**, 1551–1555.

Kurz, W. A., et al., 2008c: Mountain pine beetle and forest carbon feedback to climate change. *Nature*, **452**, 987–990.

Kwon, E. Y., F. Primeau, and J. L. Sarmiento, 2009: The impact of remineralization depth on the air-sea carbon balance. *Nature Geosci.*, **2**, 630–635.

Lackner, K. S., 2009: Capture of carbon dioxide from ambient air. *Eur. Phys. J. Spec. Topics*, **176**, 93–106.

Lackner, K. S., 2010: Washing carbon out of the air. *Sci. Am.*, **302**, 66–71.

Lackner, K. S., S. Brennan, J. M. Matter, A.-H. A. Park, A. Wright, and B. van der Zwaan, 2012: The urgency of the development of CO_2 capture from ambient air. *Proc. Natl. Acad. Sci. U.S.A.*, **109**, 13156–13162.

Lal, R., 2004a: Soil carbon sequestration impacts on global climate change and food security. *Science*, **304**, 1623–1627.

Lal, R., 2004b: Soil carbon sequestration to mitigate climate change. *Geoderma*, **123**, 1–22.

Lamarque, J.-F., 2008: Estimating the potential for methane clathrate instability in the 1%-CO_2 IPCC AR-4 simulations. *Geophys. Res. Lett.*, **35**, L19806.

Lamarque, J.-F., et al., 2010: Historical (1850–2000) gridded anthropogenic and biomass burning emissions of reactive gases and aerosols: Methodology and application. *Atmos. Chem. Phys.*, **10**, 7017–7039.

Lamarque, J.-F., et al., 2013: The Atmospheric Chemistry and Climate Model Intercomparison Project (ACCMIP): Overview and description of models, simulations and climate diagnostics. *Geosci. Model Dev.*, **6**, 179–206.

Lamarque, J. F., et al., 2011: Global and regional evolution of short-lived radiatively-active gases and aerosols in the Representative Concentration Pathways. *Clim. Change*, **109**, 191–212.

Lampitt, R. S., et al., 2008: Ocean fertilization: A potential means of geoengineering? *Philos. Trans. R. Soc. London Ser. A*, **366**, 3919–3945.

Langenfelds, R. L., R. J. Francey, B. C. Pak, L. P. Steele, J. Lloyd, C. M. Trudinger, and C. E. Allison, 2002: Interannual growth rate variations of atmospheric CO_2 and its $d^{13}C$, H_2, CH_4, and CO between 1992 and 1999 linked to biomass burning. *Global Biogeochem. Cycles*, **16**, 1048.

Langner, J., R. Bergstrom, and V. Foltescu, 2005: Impact of climate change on surface ozone and deposition of sulphur and nitrogen in Europe. *Atmos. Environ.*, **39**, 1129–1141.

Larsen, K. S., et al., 2011: Reduced N cycling in response to elevated CO_2, warming, and drought in a Danish heathland: Synthesizing results of the CLIMAITE project after two years of treatments. *Global Change Biol.*, **17**, 1884–1899.

Lassey, K. R., D. C. Lowe, and A. M. Smith, 2007: The atmospheric cycling of radiomethane and the "fossil fraction" of the methane source. *Atmos. Chem. Phys.*, **7**, 2141–2149.

Law, R. M., R. J. Matear, and R. J. Francey, 2008: Comment on "Saturation of the Southern Ocean CO_2 sink due to recent climate change". *Science*, **319**, 570a.

Lawrence, D., et al., 2011: Parameterization improvements and functional and structural advances in version 4 of the Community Land Model. *J. Adv. Model. Earth Syst.*, **3**, M03001, 27 pp.

Lawrence, D. M., and A. G. Slater, 2005: A projection of severe near-surface permafrost degradation during the 21st century. *Geophys. Res. Lett.*, **32**, L24401.

Lawrence, D. M., A. G. Slater, V. E. Romanovsky, and D. J. Nicolsky, 2008: Sensitivity of a model projection of near-surface permafrost degradation to soil column depth and representation of soil organic matter. *J. Geophys. Res. Earth Surf.*, **113**, F02011.

Le Page, Y., G. R. van der Werf, D. C. Morton, and J. M. C. Pereira, 2010: Modeling fire-driven deforestation potential in Amazonia under current and projected climate conditions. *J. Geophys. Res. Biogeosci.*, **115**, G03012.

Le Quéré, C., T. Takahashi, E. T. Buitenhuis, C. Rodenbeck, and S. C. Sutherland, 2010: Impact of climate change and variability on the global oceanic sink of CO_2. *Global Biogeochem. Cycles*, **24**, GB4007.

Le Quéré, C., et al., 2007: Saturation of the southern ocean CO_2 sink due to recent climate change. *Science*, **316**, 1735–1738.

Le Quéré, C., et al., 2009: Trends in the sources and sinks of carbon dioxide. *Nature Geosci.*, **2**, 831–836.

Le Quéré, C., et al., 2013: The global carbon budget 1959–2011. *Earth Syst. Sci. Data*, **5**, 165–186.

LeBauer, D. S., and K. K. Treseder, 2008: Nitrogen limitation of net primary productivity in terrestrial ecosystems is globally distributed. *Ecology*, **89**, 371–379.

Lee, X., et al., 2011: Observed increase in local cooling effect of deforestation at higher latitudes. *Nature*, **479**, 384–387.

Lemmen, C., 2009: World distribution of land cover changes during Pre- and Protohistoric Times and estimation of induced carbon releases. *Geomorphol. Relief Proc. Environ.*, **4**, 303–312.

Lenton, A., and R. J. Matear, 2007: Role of the Southern Annular Mode (SAM) in Southern Ocean CO_2 uptake. *Global Biogeochem. Cycles*, **21**, Gb2016.

Lenton, T. M., and C. Britton, 2006: Enhanced carbonate and silicate weathering accelerates recovery from fossil fuel CO_2 perturbations. *Global Biogeochem. Cycles*, **20**, Gb3009.

Lenton, T. M., and N. E. Vaughan, 2009: The radiative forcing potential of different climate geoengineering options. *Atmos. Chem. Phys.*, **9**, 5539–5561.

Lepistö, A., P. Kortelainen, and T. Mattsson, 2008: Increased organic C and N leaching in a northern boreal river basin in Finland. *Global Biogeochem. Cycles*, **22**, GB3029.

LeQuere, C., T. Takahashi, E. T. Buitenhuis, C. Rodenbeck, and S. C. Sutherland, 2010: Impact of climate change and variability on the global oceanic sink of CO2. *Global Biogeochem. Cycles*, **24**.

Leuzinger, S., Y. Q. Luo, C. Beier, W. Dieleman, S. Vicca, and C. Körner, 2011: Do global change experiments overestimate impacts on terrestrial ecosystems? *Trends Ecol. Evol.*, **26**, 236–241.

Levin, I., et al., 2010: Observations and modelling of the global distribution and long-term trend of atmospheric $^{14}CO_2$. *Tellus B*, **62**, 26–46.

Levin, I., et al., 2012: No inter-hemispheric $\delta^{13}CH_4$ trend observed. *Nature*, **486**, E3–E4.

Levine, J. G., E. W. Wolff, P. O. Hopcroft, and P. J. Valdes, 2012: Controls on the tropospheric oxidizing capacity during an idealized Dansgaard-Oeschger event, and their implications for the rapid rises in atmospheric methane during the last glacial period. *Geophys. Res. Lett.*, **39**, L12805.

Levine, J. G., et al., 2011: Reconciling the changes in atmospheric methane sources and sinks between the Last Glacial Maximum and the pre-industrial era. *Geophys. Res. Lett.*, **38**, L23804.

Levy, P. E., M. G. R. Cannell, and A. D. Friend, 2004: Modelling the impact of future changes in climate, CO_2 concentration and land use on natural ecosystems and the terrestrial carbon sink. *Global Environ. Change*, **14**, 21–30.

Lewis, S. L., P. M. Brando, O. L. Phillips, G. M. van der Heijden, and D. Nepstad, 2011: The 2010 Amazon drought. *Science*, **331**, 554.

Lewis, S. L., et al., 2009: Increasing carbon storage in intact African tropical forests. *Nature*, **457**, 1003–1006.

Li, C., S. Frolking, and K. Butterbach-Bahl, 2005: Carbon sequestration can increase nitrous oxide emissions. *Clim. Change*, **72**, 321–338.

Liberloo, M., et al., 2009: Coppicing shifts CO_2 stimulation of poplar productivity to above-ground pools: A synthesis of leaf to stand level results from the POP/EUROFACE experiment. *New Phytologist*, **182**, 331–346.

Liddicoat, S., C. Jones, and E. Robertson, 2013: CO_2 emissions determined by HadGEM2–ES to be compatible with the Representative Concentration Pathway scenarious and their extension. *J. Clim.*, **26**, 4381-4397.

Lohila, A., M. Aurela, J. Hatakka, M. Pihlatie, K. Minkkinen, T. Penttilä, and T. Laurila, 2010: Responses of N_2O fluxes to temperature, water table and N deposition in a northern boreal fen. *Eur. J. Soil Sci.*, **61**, 651–661.

Long, M. C., K. Lindsay, S. Peacock, J. K. Moore, and S. C. Doney, 2013: Twentieth-century oceanic carbon uptake and storage in CESM1(BGC). *J. Clim.*, **26**, 6775-6800.

Loose, B., and P. Schlosser, 2011: Sea ice and its effect on CO_2 flux between the atmosphere and the Southern Ocean interior. *J. Geophys. Res. Oceans*, **116**, C11.

Loulergue, L., et al., 2008: Orbital and millennial-scale features of atmospheric CH_4 over the past 800,000 years. *Nature*, **453**, 383–386.

Lourantou, A., and N. Metzl, 2011: Decadal evolution of carbon sink within a strong bloom area in the subantarctic zone. *Geophys. Res. Lett.*, **38**, L23608.

Lourantou, A., J. Chappellaz, J.-M. Barnola, V. Masson-Delmotte, and D. Raynaud, 2010a: Changes in atmospheric CO_2 and its carbon isotopic ratio during the penultimate deglaciation. *Quat. Sci. Rev.*, **29**, 1983–1992.

Lourantou, A., et al., 2010b: Constraint of the CO_2 rise by new atmospheric carbon isotopic measurements during the last deglaciation. *Global Biogeochem. Cycles*, **24**, GB2015.

Lovelock, J. E., and C. G. Rapley, 2007: Ocean pipes could help the Earth to cure itself. *Nature*, **449**, 403–403.

Lovenduski, N. S., N. Gruber, and S. C. Doney, 2008: Towards a mechanistic understanding of the decadal trends in the Southern Ocean carbon sink. *Global Biogeochem. Cycles*, **22**, GB3016.

Lovenduski, N. S., N. Gruber, S. C. Doney, and I. D. Lima, 2007: Enhanced CO_2 outgassing in the Southern Ocean from a positive phase of the Southern Annular Mode. *Global Biogeochem. Cycles*, **21**, Gb2026.

Lucht, W., et al., 2002: Climatic control of the high-latitude vegetation greening trend and Pinatubo effect. *Science*, **296**, 1687–1689.

Luo, Y., D. Hui, and D. Zhang, 2006: Elevated carbon dioxide stimulates net accumulations of carbon and nitrogen in terrestrial ecosystems: A meta-analysis. *Ecology*, **87**, 53–63.

Luo, Y., et al., 2004: Progressive nitrogen limitation of ecosystem responses to rising atmospheric carbon dioxide. *BioScience*, **54**, 731–739.

Lüthi, D., et al., 2008: High-resolution carbon dioxide concentration record 650,000–800,000 years before present. *Nature*, **453**, 379–382.

Luyssaert, S., et al., 2010: The European carbon balance. Part 3: Forests. *Global Change Biol.*, **16**, 1429–1450.

Luyssaert, S., et al., 2012: The European land and inland water CO_2, CO, CH_4 and N_2O balance between 2001 and 2005. *Biogeosciences*, **9**, 3357–3380.

MacDonald, G. M., K. V. Kremenetski, and D. W. Beilman, 2008: Climate change and the northern Russian treeline zone. *Philos. Trans. R. Soc. London Ser. B*, **363**, 2285–2299.

MacDougall, A. H., C. A. Avis, and A. J. Weaver, 2012: Significant contribution to climate warming from the permafrost carbon feedback. *Nature Geosci.*, **5**, 719–721.

MacFarling-Meure, C., et al., 2006: Law Dome CO_2, CH_4 and N_2O ice core records extended to 2000 years BP. *Geophys. Res. Lett.*, **33**, L14810.

Magnani, F., et al., 2007: The human footprint in the carbon cycle of temperate and boreal forests. *Nature*, **447**, 848–850.

Mahmoudkhani, M., and D. W. Keith, 2009: Low-energy sodium hydroxide recovery for CO_2 capture from atmospheric air - Thermodynamic analysis. *Int. J. Greenh. Gas Cont.*, **3**, 376–384.

Mahowald, N., et al., 1999: Dust sources and deposition during the last glacial maximum and current climate: A comparison of model results with paleodata from ice cores and marine sediments. *J. Geophys. Res. Atmos*, **104**, 15895–15916.

Mahowald, N., et al., 2011: Desert dust and anthropogenic aerosol interactions in the Community Climate System Model coupled-carbon-climate model. *Biogeosciences*, **8**, 387–414.

Mahowald, N. M., D. R. Muhs, S. Levis, P. J. Rasch, M. Yoshioka, C. S. Zender, and C. Luo, 2006: Change in atmospheric mineral aerosols in response to climate: Last glacial period, preindustrial, modern, and doubled carbon dioxide climates. *J. Geophys. Res. Atmos.*, **111**, D10202.

Mahowald, N. M., et al., 2009: Atmospheric iron deposition: Global ddistribution, variability, and human perturbations. *Annu. Rev. Mar. Sci.*, **1**, 245–278.

Mahowald, N. M., et al., 2010: Observed 20th century desert dust variability: Impact on climate and biogeochemistry. *Atmos. Chem. Phys.*, **10**, 10875–10893.

Maier-Reimer, E., I. Kriest, J. Segschneider, and P. Wetzel, 2005: The HAMburg Ocean Carbon Cycle model HAMOCC 5.1 – Technical description, Release 1.1. Max-Planck Institute for Meteorology, Hamburg, Germany.

Manning, A. C., and R. F. Keeling, 2006: Global oceanic and land biotic carbon sinks from the Scripps atmospheric oxygen flask sampling network. *Tellus B*, **58**, 95–116.

Marchenko, S. S., V. Romanovsky, and G. S. Tipenko, 2008: Numerical modeling of spatial permafrost dynamics in Alaska, Proceedings of the Ninth International Conference on Permafrost, University of Alaska Fairbanks, June 29–July 3, 2008, 1125–1130.

Marland, G., and R. M. Rotty, 1984: Carbon dioxide emissions from fossil fuels: A procedure for estimation and results for 1950–1982. *Tellus B*, **36**, 232–261.

Marlon, J. R., et al., 2008: Climate and human influences on global biomass burning over the past two millennia. *Nature Geosci.*, **1**, 697–702.

Marlon, J. R., et al., 2012: Long-term perspective on wildfires in the western USA. *Proc. Natl. Acad. Sci. U.S.A.*, **109**, E535–E543.

Martin, J. H., 1990: Glacial-interglacial CO_2 change: The iron hypothesis. *Paleoceanography*, **5**, 1–13.

Masarie, K. A., and P. P. Tans, 1995: Extension and integration of atmospheric carbon-dioxide data into a globally consistent measurement record. *J. Geophys. Res. Atmos.*, **100**, 11593–11610.

Mason Earles, J., S. Yeh, and K. E. Skog, 2012: Timing of carbon emissions from global forest clearance. *Nature Clim. Change*, **2**, 682–685.

Matear, R. J., and B. I. McNeil, 2003: Decadal accumulation of anthropogenic CO_2 in the Southern Ocean: A comparison of CFC-age derived estimates to multiple-linear regression estimates. *Global Biogeochem. Cycles*, **17**, 1113.

Matear, R. J., and A. C. Hirst, 2003: Long-term changes in dissolved oxygen concentrations in the ocean caused by protracted global warming. *Global Biogeochem. Cycles*, **17**, 1125.

Matear, R. J., A. C. Hirst, and B. I. McNeil, 2000: Changes in dissolved oxygen in the Southern Ocean with climate change. *Geochem. Geophys. Geosyst.*, **1**, 1050.

Matear, R. J., Y.-P. Wang, and A. Lenton, 2010: Land and ocean nutrient and carbon cycle interactions. *Curr. Opin. Environ. Sustain.*, **2**, 258–263.

Matsumoto, K., 2007: Biology-mediated temperature control on atmospheric pCO_2 and ocean biogeochemistry. *Geophys. Res. Lett.*, **34**, L20605.

Matsumoto, K., J. L. Sarmiento, and M. A. Brzezinski, 2002: Silicic acid leakage from the Southern Ocean: A possible explanation for glacial atmospheric pCO_2. *Global Biogeochem. Cycles*, **16**, 1031.

Matsumoto, K., et al., 2004: Evaluation of ocean carbon cycle models with data-based metrics. *Geophys. Res. Lett.*, **31**, L007303.

Matthews, H. D., 2006: Emissions targets for CO_2 stabilization as modified by carbon cycle feedbacks. *Tellus B*, **58**, 591–602.

Matthews, H. D., 2010: Can carbon cycle geoengineering be a useful complement to ambitious climate mitigation? *Carbon Management*, **1**, 135–144.

Matthews, H. D., and K. Caldeira, 2007: Transient climate-carbon simulations of planetary geoengineering. *Proc. Natl. Acad. Sci. U.S.A.*, **104**, 9949–9954.

Matthews, H. D., A. J. Weaver, and K. J. Meissner, 2005: Terrestrial carbon cycle dynamics under recent and future climate change. *J. Clim.*, **18**, 1609–1628.

Matthews, H. D., L. Cao, and K. Caldeira, 2009: Sensitivity of ocean acidification to geoengineered climate stabilization. *Geophys. Res. Lett.*, **36**, L10706.

Mau, S., D. Valentine, J. Clark, J. Reed, R. Camilli, and L. Washburn, 2007: Dissolved methane distributions and air-sea flux in the plume of a massive seep field, Coal Oil Point, California. *Geophys. Res. Lett.*, **34**, L22603.

Mayorga, E., et al., 2010: Global nutrient export from WaterSheds 2 (NEWS 2): Model development and implementation. *Environ. Model. Software*, **25**, 837–853.

McCarthy, H. R., et al., 2010: Re-assessment of plant carbon dynamics at the Duke free-air CO_2 enrichment site: Interactions of atmospheric CO_2 with nitrogen and water availability over stand development. *New Phytologist*, **185**, 514–528.

McGuire, A. D., et al., 2009: Sensitivity of the carbon cycle in the Arctic to climate change. *Ecol. Monogr.*, **79**, 523–555.

McGuire, A. D., et al., 2012: An assessment of the carbon balance of Arctic tundra: Comparisons among observations, process models, and atmospheric inversions. *Biogeosciences*, **9**, 3185–3204.

McInerney, F. A., and S. L. Wing, 2011: The Paleocene-Eocene thermal maximum: A perturbation of carbon cycle, climate, and biosphere with implications for the future. *Annu. Rev. Earth Planet. Sci.*, **39**, 489–516.

McIntyre, B. D., H. R. Herren, J. Wakhungu, and R. T. Watson, 2009: International assessment of agricultural knowledge, science and technology for development (IAASTD): Global report. International Assessment of Agricultural Knowledge, Science and Technology for Development, 590 pp.

McKinley, G. A., A. R. Fay, T. Takahashi, and N. Metzl, 2011: Convergence of atmospheric and North Atlantic carbon dioxide trends on multidecadal timescales. *Nature Geosci.*, **4**, 606–610.

McKinley, G. A., et al., 2006: North Pacific carbon cycle response to climate variability on seasonal to decadal timescales. *J. Geophys. Res. Oceans*, **111**, C07s06.

McNeil, B. I., and R. J. Matear, 2006: Projected climate change impact on oceanic acidification. *Carbon Bal. Manag.*, **1**.

McNeil, B. I., and R. J. Matear, 2008: Southern Ocean acidification: A tipping point at 450–ppm atmospheric CO_2. *Proc. Natl. Acad. Sci. U.S.A.*, **105**, 18860–18864.

McNeil, B. I., R. J. Matear, R. M. Key, J. L. Bullister, and J. L. Sarmiento, 2003: Anthropogenic CO_2 uptake by the ocean based on the global chlorofl uorocarbon data set. *Science*, **299**, 235–239.

Medlyn, B. E., 2011: Comment on "Drought-induced reductions in global terrestrial net primary production from 2000 through 2009". *Science*, **333**, 1093.

Meehl, G. H., et al., 2007: Global Climate Projections. In: *Climate Change 2007: The Physical Science Basis. Contribution of Working Group I to the Fourth Assessment Report of the Intergovernmental Panel on Climate Change* [Solomon, S., D. Qin, M. Manning, Z. Chen, M. Marquis, K. B. Averyt, M. Tignor and H. L. Miller (eds.)] Cambridge University Press, Cambridge, United Kingdom and New York, NY, USA, pp. 747–846.

Meinshausen, M., et al., 2011: The RCP greenhouse gas concentrations and their extensions from 1765 to 2300. *Clim. Change*, **109**, 213–241.

Melillo, J. M., et al., 2011: Soil warming, carbon-nitrogen interactions, and forest carbon budgets. *Proc. Natl. Acad. Sci. U.S.A.*, **108**, 9508–9512.

Melton, J. R., et al., 2013: Present state of global wetland extent and wetland methane modelling: Conclusions from a model intercomparison project (WETCHIMP). *Biogeosciences*, **10**, 753-788.

Menviel, L., and F. Joos, 2012: Toward explaining the Holocene carbon dioxide and carbon isotope records: Results from transient ocean carbon cycle-climate simulations. *Paleoceanography*, **27**, PA1207.

Menviel, L., F. Joos, and S. P. Ritz, 2012: Simulating atmospheric CO_2, C^{13} and the marine carbonate cycle during the last Glacial-Interglacial cycle: Possible role for a deepening of the mean remineralization depth and an increase in the oceanic nutrient inventory. *Quat. Sci. Rev.*, **56**, 46–68.

Menviel, L., A. Timmermann, A. Mouchet, and O. Timm, 2008: Meridional reorganizations of marine and terrestrial productivity during Heinrich events. *Paleoceanography*, **23**, PA1203.

Mercado, L. M., N. Bellouin, S. Sitch, O. Boucher, C. Huntingford, M. Wild, and P. M. Cox, 2009: Impact of changes in diffuse radiation on the global land carbon sink. *Nature*, **458**, 1014–1017.

Merico, A., T. Tyrrell, and T. Cokacar, 2006: Is there any relationship between phytoplankton seasonal dynamics and the carbonate system? *J. Mar. Syst.*, **59**, 120–142.

Metsaranta, J. M., W. A. Kurz, E. T. Neilson, and G. Stinson, 2010: Implications of future disturbance regimes on the carbon balance of Canada's managed forest (2010–2100). *Tellus B*, **62**, 719–728.

Metz, B., O. Davidson, H. C. De Coninck, M. Loss, and L. A. Meyer, 2005: *IPCC Special Report on Carbon Dioxide Capture and Storage* Cambridge University Press, Cambridge, United Kingdom, and New York, NY, USA, 442 pp.,

Metzl, N., 2009: Decadal increase of oceanic carbon dioxide in Southern Indian Ocean surface waters (1991–2007). *Deep-Sea Res. Pt. II*, **56**, 607–619.

Metzl, N., et al., 2010: Recent acceleration of the sea surface fCO_2 growth rate in the North Atlantic subpolar gyre (1993–2008) revealed by winter observations. *Global Biogeochem. Cycles*, **24**, GB4004.

Mieville, A., et al., 2010: Emissions of gases and particles from biomass burning during the 20th century using satellite data and an historical reconstruction. *Atmos. Environ.*, **44**, 1469–1477.

Mikaloff-Fletcher, S. E., et al., 2006: Inverse estimates of anthropogenic CO_2 uptake, transport, and storage by the ocean. *Global Biogeochem. Cycles*, **20**, GB2002.

Minschwaner, K., R. J. Salawitch, and M. B. McElroy, 1993: Absorption of solar radiation by O_2: Implications for O_3 and lifetimes of N_2O, $CFCl_3$, and CF_2Cl_2. *J. Geophys. Res. Atmos.*, **98**, 10543–10561.

Mischler, J. A., et al., 2009: Carbon and hydrogen isotopic composition of methane over the last 1000 years. *Global Biogeochem. Cycles*, **23**, GB4024.

Mitchell, L. E., E. J. Brook, T. Sowers, J. R. McConnell, and K. Taylor, 2011: Multidecadal variability of atmospheric methane, 1000–1800 C.E. *J. Geophys. Res. Biogeosci.*, **116**, G02007.

Miyama, T., and M. Kawamiya, 2009: Estimating allowable carbon emission for CO_2 concentration stabilization using a GCM-based Earth system model. *Geophys. Res. Lett.*, **36**, L19709.

Monnin, E., et al., 2001: Atmospheric CO_2 concentrations over the last glacial termination. *Science*, **291**, 112–114.

Monnin, E., et al., 2004: Evidence for substantial accumulation rate variability in Antarctica during the Holocene through synchronization of CO_2 in the Taylor Dome, Dome C and DML ice cores. *Earth Planet. Sci. Lett.*, **224**, 45–54.

Monteil, G., S. Houweling, E. J. Dlugockenky, G. Maenhout, B. H. Vaughn, J. W. C. White, and T. Rockmann, 2011: Interpreting methane variations in the past two decades using measurements of CH_4 mixing ratio and isotopic composition. *Atmos. Chem. Phys.*, **11**, 9141–9153.

Monteith, D. T., et al., 2007: Dissolved organic carbon trends resulting from changes in atmospheric deposition chemistry. *Nature*, **450**, 537–U539.

Montenegro, A., V. Brovkin, M. Eby, D. Archer, and A. J. Weaver, 2007: Long term fate of anthropogenic carbon. *Geophys. Res. Lett.*, **34**, L19707.

Montenegro, A., M. Eby, Q. Z. Mu, M. Mulligan, A. J. Weaver, E. C. Wiebe, and M. S. Zhao, 2009: The net carbon drawdown of small scale afforestation from satellite observations. *Global Planet. Change*, **69**, 195–204.

Montzka, S. A., M. Krol, E. Dlugokencky, B. Hall, P. Joeckel, and J. Lelieveld, 2011: Small interannual variability of global atmospheric hydroxyl. *Science*, **331**, 67–69.

Mooney, S. D., et al., 2011: Late Quaternary fire regimes of Australasia. *Quat. Sci. Rev.*, **30**, 28–46.

Morford, S. L., B. Z. Houlton, and R. A. Dahlgren, 2011: Increased forest ecosystem carbon and nitrogen storage from nitrogen rich bedrock. *Nature*, **477**, 78–81.

Morino, I., et al., 2011: Preliminary validation of column-averaged volume mixing ratios of carbon dioxide and methane retrieved from GOSAT short-wavelength infrared spectra. *Atmos. Measure. Techn.*, **3**, 5613–5643.

Mosier, A., C. Kroeze, C. Nevison, O. Oenema, S. Seitzinger, and O. van Cleemput, 1998: Closing the global N_2O budget: Nitrous oxide emissions through the agricultural nitrogen cycle - OECD/IPCC/IEA phase II development of IPCC guidelines for national greenhouse gas inventory methodology. *Nutr. Cycl. Agroecosyst.*, **52**, 225–248.

Mosier, A. R., J. A. Morgan, J. Y. King, D. R. LeCain, and D. G. Milchunas, 2002: Soil-atmosphere exchange of CH_4, CO_2, NOx, and N_2O in the Colorado shortgrass steppe under elevated CO_2. *Plant Soil*, **240**, 201–211.

Moss, R. H., et al., 2010: The next generation of scenarios for climate change research and assessment. *Nature*, **463**, 747–756.

Munhoven, G., 2002: Glacial-interglacial changes of continental weathering: Estimates of the related CO_2 and HCO^{3-} flux variations and their uncertainties. *Global Planet. Change*, **33**, 155–176.

Murata, A., Y. Kumamoto, S. Watanabe, and M. Fukasawa, 2007: Decadal increases of anthropogenic CO_2 in the South Pacific subtropical ocean along 32 degrees S. *J. Geophys. Res. Oceans*, **112**, C05033.

Murata, A., Y. Kumamoto, K.-i. Sasaki, S. Watanabe, and M. Fukasawa, 2009: Decadal increases of anthropogenic CO_2 along 149 degrees E in the western North Pacific. *J. Geophys. Res. Oceans*, **114**, C04018.

Murata, A., Y. Kumamoto, K. Sasaki, S. Watanabe, and M. Fukasawa, 2010: Decadal increases in anthropogenic CO_2 along 20 degrees S in the South Indian Ocean. *J. Geophys. Res. Oceans*, **115**, C12055.

Myneni, R. B., et al., 2001: A large carbon sink in the woody biomass of Northern forests. *Proc. Natl. Acad. Sci. U.S.A.*, **98**, 14784–14789.

Nabuurs, G. J., et al., 2008: Hotspots of the European forests carbon cycle. *Forest Ecol. Manage.*, **256**, 194–200.

Naegler, T., and I. Levin, 2009: Observation-based global biospheric excess radiocarbon inventory 1963–2005. *J. Geophys. Res.*, **114**, D17302.

Naik, V., D. J. Wuebbles, E. H. De Lucia, and J. A. Foley, 2003: Influence of geoengineered climate on the terrestrial biosphere. *Environ. Manage.*, **32**, 373–381.

Naqvi, S. W. A., H. W. Bange, L. Farias, P. M. S. Monteiro, M. I. Scranton, and J. Zhang, 2010: Coastal hypoxia/anoxia as a source of CH_4 and N_2O. *Biogeosciences*, **7**, 2159–2190.

Neef, L., M. van Weele, and P. van Velthoven, 2010: Optimal estimation of the present-day global methane budget. *Global Biogeochem. Cycles*, **24**, GB4024.

Neftel, A., H. Oeschger, J. Schwander, B. Stauffer, and R. Zumbrunn, 1982: Ice core sample measurements give atmospheric CO_2 content during the past 40,000 yr. *Nature*, **295**, 220–223.

Nemani, R. R., et al., 2003: Climate-driven increases in global terrestrial net primary production from 1982 to 1999. *Science*, **300**, 1560–1563.

Nevison, C. D., et al., 2011: Exploring causes of interannual variability in the seasonal cycles of tropospheric nitrous oxide. *Atmos. Chem. Phys.*, **11**, 3713–3730.

Nevle, R. J., and D. K. Bird, 2008: Effects of syn-pandemic fire reduction and reforestation in the tropical Americas on atmospheric CO_2 during European conquest. *Palaeogeogr. Palaeoclimatol. Palaeoecol.* **264**, 25–38.

Nevle, R. J., D. K. Bird, W. F. Ruddiman, and R. A. and Dull, 2011: Neotropical human landscape interactions, fire, and atmospheric CO_2 during European conquest. *Holocene*, **21**, 853–864.

Newingham, B. A., C. H. Vanier, T. N. Charlet, K. Ogle, S. D. Smith, and R. S. Nowak, 2013: No cumulative effect of ten years of elevated CO_2 on perennial plant biomass components in the Mojave Desert. *Global Change Biol.*, **19**, 2168-2181..

Nisbet, R. E. R., et al., 2009: Emission of methane from plants. *Proc. R. Soc. Ser. B*, **276**, 1347–1354.

Norby, R. J., 1998: Nitrogen deposition: A component of global change analysis. *New Phytologist*, **139**, 189–200.

Norby, R. J., J. M. Warren, C. M. Iversen, B. E. Medlyn, and R. E. McMurtrie, 2010: CO_2 enhancement of forest productivity constrained by limited nitrogen availability. *Proc. Natl. Acad. Sci. U.S.A.*, **107**, 19368–19373.

Norby, R. J., et al., 2005: Forest response to elevated CO_2 is conserved across a broad range of productivity. *Proc. Natl. Acad. Sci. U.S.A.*, **102**, 18052–18056.

Nowak, R. S., D. S. Ellsworth, and S. D. Smith, 2004: Functional responses of plants to elevated atmospheric CO_2—do photosynthetic and productivity data from FACE experiments support early predictions? *New Phytologist*, **162**, 253–280.

O'Connor, F. M., et al., 2010: Possible role of wetlands, permafrost, and methane hydrates in the methane cycle under future climate change: A review. *Rev. Geophys.*, **48**, RG4005.

Oh, N.-H., and P. A. Raymond, 2006: Contribution of agricultural liming to riverine bicarbonate export and CO_2 sequestration in the Ohio River basin. *Global Biogeochem. Cycles*, **20**, GB3012.

Oleson, K. W., et al., 2010: Technical description of version 4.0 of the Community Land Model (CLM), NCAR Technical Note NCAR/TN-478+STR, National Center for Atmospheric Research, Boulder, CO, USA, 257 pp.

Olivier, J., J. Aardenne, F. Dentener, L. Ganzeveld, and J. Peters, 2005: Recent trends in global greenhouse emissions: Regional trends 1970–2000 and spatial distribution of key sources in 2000. *Environ. Sci.*, **2**, 81–99.

Olivier, J. G. J., and G. Janssens-Maenhout, 2012: Part III: Greenhouse gas emissions: 1. Shares and trends in greenhouse gas emissions; 2. Sources and Methods; Total greenhouse gas emissions. In: *CO_2 Emissions from Fuel Combustion, 2012 Edition*. International Energy Agency (IEA), Paris, France, III.1–III.51.

Olofsson, J., and T. Hickler, 2008: Effects of human land-use on the global carbon cycle during the last 6,000 years. *Veget. Hist. Archaeobot.*, **17**, 605–615.

Olsen, A., et al., 2006: Magnitude and origin of the anthropogenic CO_2 increase and ^{13}C Suess effect in the Nordic seas since 1981. *Global Biogeochem. Cycles*, **20**, GB3027.

Opdyke, M. R., N. E. Ostrom, and P. H. Ostrom, 2009: Evidence for the predominance of denitrification as a source of N_2O in temperate agricultural soils based on isotopologue measurements. *Global Biogeochem. Cycles*, **23**, Gb4018.

Orr, F. M. J., 2009: Onshore geologic storage of CO_2. *Science*, **325**, 1656–1658.

Orr, J. C., 2011: Recent and future changes in ocean carbonate chemistry. In: *Ocean Acidification* [J.-P. Gattuso and L. Hansson (eds.)]. Oxford University Press, Oxford, United Kingdom, and New York, NY, USA, pp. 41-66.

Orr, J. C., et al., 2001: Estimates of anthropogenic carbon uptake from four three-dimensional global ocean models. *Global Biogeochem. Cycles*, **15**, 43–60.

Orr, J. C., et al., 2005: Anthropogenic ocean acidification over the twenty-first century and its impact on calcifying organisms. *Nature*, **437**, 681–686.

Oschlies, A., 2001: Model-derived estimates of new production: New results point towards lower values. *Deep-Sea Res. Pt. II*, **48**, 2173–2197.

Oschlies, A., K. G. Schulz, U. Riebesell, and A. Schmittner, 2008: Simulated 21st century's increase in oceanic suboxia by CO_2-enhanced biotic carbon export. *Global Biogeochem. Cycles*, **22**, GB4008.

Oschlies, A., W. Koeve, W. Rickels, and K. Rehdanz, 2010a: Side effects and accounting aspects of hypothetical large-scale Southern Ocean iron fertilization. *Biogeosciences*, **7**, 4017–4035.

Oschlies, A., M. Pahlow, A. Yool, and R. J. Matear, 2010b: Climate engineering by artificial ocean upwelling: Channelling the sorcerer's apprentice. *Geophys. Res. Lett.*, **37**, L04701.

Otto, D., D. Rasse, J. Kaplan, P. Warnant, and L. Francois, 2002: Biospheric carbon stocks reconstructed at the Last Glacial Maximum: Comparison between general circulation models using prescribed and computed sea surface temperatures. *Global Planet. Change*, **33**, 117–138.

Pacala, S. W., et al., 2001: Consistent land- and atmosphere-based U.S. carbon sink estimates. *Science*, **292**, 2316–2320.

Page, S. E., J. O. Rieley, and C. J. Banks, 2011: Global and regional importance of the tropical peatland carbon pool. *Global Change Biol.*, **17**, 798–818.

Page, S. E., F. Siegert, J. O. Rieley, H.-D. V. Boehm, A. Jaya, and S. Limin, 2002: The amount of carbon released from peat and forest fires in Indonesia during 1997. *Nature*, **420**, 61–65.

Palmroth, S., et al., 2006: Aboveground sink strength in forests controls the allocation of carbon below ground and its [CO_2]-induced enhancement. *Proc. Natl. Acad. Sci. U.S.A.*, **103**, 19362–19367.

Pan, Y. D., et al., 2011: A large and persistent carbon sink in the world's forests. *Science*, **333**, 988–993.

Papa, F., C. Prigent, F. Aires, C. Jimenez, W. B. Rossow, and E. Matthews, 2010: Interannual variability of surface water extent at the global scale, 1993–2004. *J. Geophys. Res.Atmos.*, **115**, D12111.

Parekh, P., F. Joos, and S. A. Müller, 2008: A modeling assessment of the interplay between aeolian iron fluxes and iron-binding ligands in controlling carbon dioxide fluctuations during Antarctic warm events. *Paleoceanography*, **23**, PA4202.

Park, G.-H., et al., 2010: Variability of global net air-sea CO_2 fluxes over the last three decades using empirical relationships. *Tellus B*, **62**, 352–368.

Park, S., et al., 2012: Trends and seasonal cycles in the isotopic composition of nitrous oxide since 1940. *Nature Geosci.*, **5**, 261–265.

Patra, P. K., et al., 2013: The carbon budget of South Asia. *Biogeosciences*, **10**, 513–527.

Patra, P. K., et al., 2011: TransCom model simulations of CH_4 and related species: Linking transport, surface flux and chemical loss with CH_4 variability in the troposphere and lower stratosphere. *Atmos. Chem. Phys.*, **11**, 12813–12837.

Pechony, O., and D. T. Shindell, 2010: Driving forces of global wildfires over the past millennium and the forthcoming century. *Proc. Natl. Acad. Sci. U.S.A.*, **107**, 19167–19170.

Peng, T.-H., and W. S. Broecker, 1991: Dynamic limitations on the Antarctic iron fertilization strategy. *Nature*, **349**, 227–229.

Peng, T.-H., R. Wanninkhof, J. L. Bullister, R. A. Feely, and T. Takahashi, 1998: Quantification of decadal anthropogenic CO_2 uptake in the ocean based on dissolved inorganic carbon measurements. *Nature*, **396**, 560–563.

Peng, T. H., R. Wanninkhof, and R. A. Feely, 2003: Increase of anthropogenic CO_2 in the Pacific Ocean over the last two decades. *Deep-Sea Res. Pt. II*, **50**, 3065–3082.

Peñuelas, J., J. G. Canadell, and R. Ogaya, 2011: Increased water-use-efficiency during the 20th century did not translate into enhanced tree growth. *Global Ecol. Biogeogr.*, **20**, 597–608.

Pérez, F. F., M. Vázquez-Rodríguez, E. Louarn, X. A. Padin, H. Mercier, and A. F. Rios, 2008: Temporal variability of the anthropogenic CO_2 storage in the Irminger Sea. *Biogeosciences*, **5**, 1669–1679.

Perrin, A.-S., A. Probst, and J.-L. Probst, 2008: Impact of nitrogenous fertilizers on carbonate dissolution in small agricultural catchments: Implications for weathering CO_2 uptake at regional and global scales. *Geochim. Cosmochim. Acta*, **72**, 3105–3123.

Pershing, A. J., L. B. Christensen, N. R. Record, G. D. Sherwood, and P. B. Stetson, 2010: The impact of whaling on the ocean carbon cycle: Why bigger was better. *PLoS ONE*, **5**, e12444.

Peters, G. P., et al., 2013: The challenge to keep global warming below 2°C. *Nature Clim. Change*, **3**, 4–6.

Petit, J. R., et al., 1999: Climate and atmospheric history of the past 420,000 years from the Vostok ice core, Antarctica. *Nature*, **399**, 429–436.

Petrenko, V. V., et al., 2009: $^{14}CH_4$ Measurements in Greenland ice: Investigating Last Glacial Termination CH_4 sources. *Science*, **324**, 506–508.

Peylin, P., et al., 2005: Multiple constraints on regional CO_2 flux variations over land and oceans. *Global Biogeochem. Cycles*, **19**, GB1011.

Peylin, P., et al., 2013: Global atmospheric carbon budget: Results from an ensemble of atmospheric CO_2 inversions. *Biogeosci. Discuss.*, **10**, 5301–5360.

Pfeil, G. B., et al., 2013: A uniform, quality controlled Surface Ocean CO_2 Atlas (SOCAT). *Earth Syst. Sci. Data*, **5**, 125–143.

Phoenix, G. K., et al., 2006: Atmospheric nitrogen deposition in world biodiversity hotspots: The need for a greater global perspective in assessing N deposition impacts. *Global Change Biol.*, **12**, 470–476.

Piao, S., et al., 2011: Contribution of climate change and rising CO_2 to terrestrial carbon balance in East Asia: A multi-model analysis. *Global Planet. Change*, **75**, 133–142.

Piao, S., et al., 2013: Evaluation of terrestrial carbon cycle models for their response to climate variability and CO_2 trends. *Global Change Biol.*, **19**, 2117-2132..

Piao, S. L., P. Friedlingstein, P. Ciais, L. M. Zhou, and A. P. Chen, 2006: Effect of climate and CO_2 changes on the greening of the Northern Hemisphere over the past two decades. *Geophys. Res. Lett.*, **33**, L23402.

Piao, S. L., P. Friedlingstein, P. Ciais, N. de Noblet-Ducoudré, D. Labat, and S. Zaehle, 2007: Changes in climate and land use have a larger direct impact than rising CO_2 on global river runoff trends. *Proc. Natl. Acad. Sci. U.S.A.*, **104**, 15242–15247.

Piao, S. L., P. Ciais, P. Friedlingstein, N. de Noblet-Ducoudré, P. Cadule, N. Viovy, and T. Wang, 2009a: Spatiotemporal patterns of terrestrial carbon cycle during the 20th century. *Global Biogeochem. Cycles*, **23**, Gb4026.

Piao, S. L., J. Y. Fang, P. Ciais, P. Peylin, Y. Huang, S. Sitch, and T. Wang, 2009b: The carbon balance of terrestrial ecosystems in China. *Nature*, **458**, 1009–U82.

Piao, S. L., et al., 2012: The carbon budget of terrestrial ecosystems in East Asia over the last two decades. *Biogeosciences*, **9**, 3571–3586.

Pison, I., P. Bousquet, F. Chevallier, S. Szopa, and D. Hauglustaine, 2009: Multi-species inversion of CH_4, CO and H_2 emissions from surface measurements. *Atmos. Chem. Phys.*, **9**, 5281–5297.

Plattner, G.-K., et al., 2008: Long-term climate commitments projected with climate-carbon cycle models. *J. Clim.*, **21**, 2721-2751.

Plattner, G. K., F. Joos, and T. Stocker, 2002: Revision of the global carbon budget due to changing air-sea oxygen fluxes. *Global Biogeochem. Cycles*, **16**, 1096.

Plug, L. J., and J. J. West, 2009: Thaw lake expansion in a two-dimensional coupled model of heat transfer, thaw subsidence, and mass movement. *J. Geophys. Res.*, **114**, F01002.

Pollard, R. T., et al., 2009: Southern Ocean deep-water carbon export enhanced by natural iron fertilization. *Nature*, **457**, 577–580.

Pongratz, J., C. H. Reick, T. Raddatz, and M. Claussen, 2009: Effects of anthropogenic land cover change on the carbon cycle of the last millennium. *Global Biogeochem. Cycles*, **23**, Gb4001.

Pongratz, J., K. Caldeira, C. H. Reick, and M. Claussen, 2011a: Coupled climate-carbon simulations indicate minor global effects of wars and epidemics on atmospheric CO_2 between AD 800 and 1850. *Holocene*, **21**, 843–851.

Pongratz, J., C. H. Reick, T. Raddatz, K. Caldeira, and M. Claussen, 2011b: Past land use decisions have increased mitigation potential of reforestation. *Geophys. Res. Lett.*, **38**, L15701.

Poulter, B., et al., 2010: Net biome production of the Amazon Basin in the 21st century. *Global Change Biol.*, **16**, 2062–2075.

Power, M. J., et al., 2013: Climatic control of the biomass-burning decline in the Americas after AD 1500. *Holocene*, **23**, 3–13.

Power, M. J., et al., 2008: Changes in fire regimes since the Last Glacial Maximum: An assessment based on a global synthesis and analysis of charcoal data. *Clim. Dyn.*, **30**, 887–907.

Prather, M. J., C. D. Holmes, and J. Hsu, 2012: Reactive greenhouse gas scenarios: Systematic exploration of uncertainties and the role of atmospheric chemistry. *Geophys. Res. Lett.*, **39**, L09803.

Prentice, I. C., and S. P. Harrison, 2009: Ecosystem effects of CO_2 concentration: Evidence from past climates. *Clim. Past*, **5**, 297–307.

Prentice, I. C., et al., 2001: The carbon cycle and atmospheric carbon dioxide. In: *Climate Change 2001: The Scientific Basis. Contribution of Working Group I to the Third Assessment Report of the Intergovernmental Panel on Climate Change* [J. T. Houghton, Y. Ding, D. J. Griggs, M. Noquer, P. J. van der Linden, X. Dai, K. Maskell and C. A. Johnson (eds.)]. Cambridge University Press, Cambridge, United Kingdom and New York, NY, USA, pp. 183–237.

Prinn, R. G., et al., 2001: Evidence for substantial variations of atmospheric hydroxyl radicals in the past two decades. *Science*, **292**, 1882–1888.

Prinn, R. G., et al., 2005: Evidence for variability of atmospheric hydroxyl radicals over the past quarter century. *Geophys. Res. Lett.*, **32**, L07809.

Prinn, R. G., et al., 2000: A history of chemically and radiatively important gases in air deduced from ALE/GAGE/AGAGE. *J. Geophys. Res. Atmos.*, **105**, 17751–17792.

Quinton, J. N., G. Govers, K. Van Oost, and R. D. Bardgett, 2010: The impact of agricultural soil erosion on biogeochemical cycling. *Nature Geosci.*, **3**, 311–314.

Rabalais, N. N., R. J. Diaz, L. A. Levin, R. E. Turner, D. Gilbert, and J. Zhang, 2010: Dynamics and distribution of natural and human-caused hypoxia. *Biogeosciences*, **7**, 585–619.

Raddatz, T. J., et al., 2007: Will the tropical land biosphere dominate the climate-carbon cycle feedback during the twenty-first century? *Clim. Dyn.*, **29**, 565–574.

Rafelski, L. E., S. C. Piper, and R. F. Keeling, 2009: Climate effects on atmospheric carbon dioxide over the last century. *Tellus B*, **61**, 718–731.

Ramankutty, N., and J. A. Foley, 1999: Estimating historical changes in global land cover: Croplands from 1700 to 1992. *Global Biogeochem. Cycles*, **13**, 997–1027.

Ramankutty, N., C. Delire, and P. Snyder, 2006: Feedbacks between agriculture and climate: An illustration of the potential unintended consequences of human land use activities. *Global Planet. Change*, **54**, 79–93.

Randerson, J. T., et al., 2009: Systematic assessment of terrestrial biogeochemistry in coupled climate-carbon models. *Global Change Biol.*, **15**, 2462–2484.

Rau, G. H., 2008: Electrochemical splitting of calcium carbonate to increase solution alkalinity: Implications for mitigation of carbon dioxide and ocean acidity. *Environ. Sci. Technol.*, **42**, 8935–8940.

Rau, G. H., and K. Caldeira, 1999: Enhanced carbonate dissolution: A means of sequestering waste CO_2 as ocean bicarbonate. *Energ. Conv. Manage.*, **40**, 1803–1813.

Raupach, M. R., 2013: The exponential eigenmodes of the carbon-climate system, and their implications for ratios of responses to forcings *Earth Syst. Dyn.*, **4**, 31–49.

Raupach, M. R., J. G. Canadell, and C. Le Quéré, 2008: Anthropogenic and biophysical contributions to increasing atmospheric CO_2 growth rate and airborne fraction. *Biogeosciences*, **5**, 1601–1613.

Ravishankara, A. R., J. S. Daniel, and R. W. Portmann, 2009: Nitrous oxide (N_2O): The dominant ozone-depleting substance emitted in the 21st century. *Science*, **326**, 123–125.

Raymond, P. A., and J. J. Cole, 2003: Increase in the export of alkalinity from North America's largest river. *Science*, **301**, 88–91.

Raymond, P. A., N.-H. Oh, R. E. Turner, and W. Broussard, 2008: Anthropogenically enhanced fluxes of water and carbon from the Mississippi River. *Nature*, **451**, 449–452.

Rayner, P. J., R. M. Law, C. E. Allison, R. J. Francey, C. M. Trudinger, and C. Pickett-Heaps, 2008: Interannual variability of the global carbon cycle (1992–2005) inferred by inversion of atmospheric CO_2 and δ^{13} CO_2 measurements. *Global Biogeochem. Cycles*, **22**, GB3008.

Reagan, M. T., and G. J. Moridis, 2007: Oceanic gas hydrate instability and dissociation under climate change scenarios. *Geophys. Res. Lett.*, **34**, L22709.

Reagan, M. T., and G. J. Moridis, 2009: Large-scale simulation of methane hydrate dissociation along the West Spitsbergen Margin. *Geophys. Res. Lett.*, **36**, L23612.

Reay, D. S., F. Dentener, P. Smith, J. Grace, and R. A. Feely, 2008: Global nitrogen deposition and carbon sinks. *Nature Geosci.*, **1**, 430–437.

Renforth, P., 2012: The potential of enhanced weathering in the UK. *Int. J. Greenh. Gas Cont.*, **10**, 229–243.

Revelle, R., and H. E. Suess, 1957: Carbon dioxide exchange between atmosphere and ocean and the question of an increase of atmospheric CO_2 during the past decades. *Tellus*, **9**, 18–27.

Rhee, T. S., A. J. Kettle, and M. O. Andreae, 2009: Methane and nitrous oxide emissions from the ocean: A reassessment using basin-wide observations in the Atlantic. *J. Geophys. Res.*, **114**, D12304.

Ricke, K. L., M. G. Morgan, and M. R. Allen, 2010: Regional climate response to solar-radiation management. *Nature Geosci.*, **3**, 537–541.

Ridgwell, A., and R. E. Zeebe, 2005: The role of the global carbonate cycle in the regulation and evolution of the Earth system. *Earth Planet. Sci. Lett.*, **234**, 299–315.

Ridgwell, A., and J. C. Hargreaves, 2007: Regulation of atmospheric CO_2 by deep-sea sediments in an Earth system model. *Global Biogeochem. Cycles*, **21**, Gb2008.

Ridgwell, A. J., 2001: Glacial-interglacial perturbations in the global carbon cycle. PhD Thesis, University of East Anglia, Norwich, United Kingdom, 134 pp.

Ridgwell, A. J., A. J. Watson, M. A. Maslin, and J. O. Kaplan, 2003: Implications of coral reef buildup for the controls on atmospheric CO_2 since the Last Glacial Maximum. *Paleoceanography*, **18**, 1083.

Riebesell, U., A. Körtzinger, and A. Oschlies, 2009: Sensitivities of marine carbon fluxes to ocean change. *Proc. Natl. Acad. Sci. U.S.A.*, **106**, 20602–20609.

Riebesell, U., et al., 2007: Enhanced biological carbon consumption in a high CO_2 ocean. *Nature*, **450**, 545–548.

Rigby, M., et al., 2008: Renewed growth of atmospheric methane. *Geophys. Res. Lett.*, **35**, L22805.

Ringeval, B., P. Friedlingstein, C. Koven, P. Ciais, N. de Noblet-Ducoudre, B. Decharme, and P. Cadule, 2011: Climate-CH_4 feedback from wetlands and its interaction with the climate-CO_2 feedback. *Biogeosciences*, **8**, 2137–2157.

Robock, A., L. Oman, and G. L. Stenchikov, 2008: Regional climate responses to geoengineering with tropical and Arctic SO_2 injections. *J. Geophys. Res.*, **113**, D16101.

Röckmann, T., and I. Levin, 2005: High-precision determination of the changing isotopic composition of atmospheric N_2O from 1990 to 2002. *J. Geophys. Res. Atmos.*, **110**, D21304.

Rödenbeck, C., S. Houweling, M. Gloor, and M. Heimann, 2003: CO_2 flux history 1982–2001 inferred from atmospheric data using a global inversion of atmospheric transport. *Atmos. Chem. Phys.*, **3**, 1919–1964.

Rosamond, M. S., S. J. Thuss, and S. L. Schiff, 2012: Dependence of riverine nitrous oxide emissions on dissolved oxygen levels. *Nature Geosci.*, **5**, 715–718.

Roth, R., and F. Joos, 2012: Model limits on the role of volcanic carbon emissions in regulating glacial-interglacial CO_2 variations. *Earth Planet. Sci. Lett.*, **329–330**, 141–149.

Röthlisberger, R., M. Bigler, E. W. Wolff, F. Joos, E. Monnin, and M. A. Hutterli, 2004: Ice core evidence for the extent of past atmospheric CO_2 change due to iron fertilisation. *Geophys. Res. Lett.*, **31**, L16207.

Rotty, R. M., 1983: Distribution of and changes in industrial carbon-cycle production. *J. Geophys. Res. Oceans*, **88**, 1301–1308.

Roy, T., et al., 2011: Regional impacts of climate change and atmospheric CO_2 on future ocean carbon uptake: A multimodel linear feedback analysis. *J. Clim.*, **24**, 2300–2318.

Rubasinghege, G., S. N. Spak, C. O. Stanier, G. R. Carmichael, and V. H. Grassian, 2011: Abiotic mechanism for the formation of atmospheric nitrous oxide from ammonium nitrate. *Environ. Sci. Technol.*, **45**, 2691–2697.

Ruddiman, W. F., 2003: The anthropogenic greenhouse era began thousands of years ago. *Clim. Change*, **61**, 261–293.

Ruddiman, W. F., 2007: The early anthropogenic hypothesis: Challenges and responses. *Rev. Geophys.*, **45**, RG4001.

Sabine, C. L., R. A. Feely, F. J. Millero, A. G. Dickson, C. Langdon, S. Mecking, and D. Greeley, 2008: Decadal changes in Pacific carbon. *J. Geophys. Res. Oceans*, **113**, C07021.

Sabine, C. L., et al., 2004: The oceanic sink for anthropogenic CO_2. *Science*, **305**, 367–371.

Salisbury, J., M. Green, C. Hunt, and J. Campbell, 2008: Coastal acidification by rivers: A threat to shellfish? *EOS Trans. AGU*, **89**, 513.

Sallée, J.-B., R. J. Matear, S. R. Rintoul, and A. Lenton, 2012: Localized subduction of anthropogenic carbon dioxide in the Southern Hemisphere oceans. *Nature Geosci.*, **5**, 579–584.

Samanta, A., M. H. Costa, E. L. Nunes, S. A. Viera, L. Xu, and R. B. Myneni, 2011: Comment on "Drought-induced reduction in global terrestrial net primary production from 2000 through 2009". *Science*, **333**, 1093.

Sanderson, M. G., 1996: Biomass of termites and their emissions of methane and carbon dioxide: A global database. *Global Biogeochem. Cycles*, **10**, 543–557.

Sapart, C. J., et al., 2012: Natural and anthropogenic variations in methane sources during the past two millennia. *Nature*, **490**, 85–88.

Sarmiento, J. L., and N. Gruber, 2006: *Ocean Biogeochemical Dynamics.* Princeton University Press, Princeton, NJ, USA.

Sarmiento, J. L., J. C. Orr, and U. Siegenthaler, 1992: A perturbation simulation of CO_2 uptake in an Ocean General Circulation Model. *J. Geophys. Res.*, **97**, 3621–3645.

Sarmiento, J. L., T. M. C. Hughes, R. J. Stouffer, and S. Manabe, 1998: Simulated response of the ocean carbon cycle to anthropogenic climate warming. *Nature*, **393**, 245–249.

Sarmiento, J. L., P. Monfray, E. Maier-Reimer, O. Aumont, R. Murnane, and J. C. Orr, 2000: Sea-air CO_2 fluxes and carbon transport: A comparison of three ocean general circulation models. *Global Biogeochem. Cycles*, **14**, 1267–1281.

Sarmiento, J. L., et al., 2010: Trends and regional distributions of land and ocean carbon sinks. *Biogeosciences*, **7**, 2351–2367.

Savolainen, I., S. Monni, and S. Syri, 2009: The mitigation of methane emissions from the industrialised countries can explain the atmospheric concentration level-off. *Int. J. Energ. Clean Environ.*, **10**, 193–201.

Schaefer, K., T. Zhang, L. Bruhwiler, and A. P. Barrett, 2011: Amount and timing of permafrost carbon release in response to climate warming. *Tellus B*, **63**, 165–180.

Scheffer, M., V. Brovkin, and P. M. Cox, 2006: Positive feedback between global warming and atmospheric CO_2 concentration inferred from past climate change. *Geophys. Res. Lett.*, **33**, L10702.

Schilt, A., M. Baumgartner, T. Blunier, J. Schwander, R. Spahni, H. Fischer, and T. F. Stocker, 2010a: Glacial-interglacial and millennial-scale variations in the atmospheric nitrous oxide concentration during the last 800,000 years. *Quat. Sci. Rev.*, **29**, 182–192.

Schilt, A., et al., 2010b: Atmospheric nitrous oxide during the last 140,000 years. *Earth Planet. Sci. Lett.*, **300**, 33–43.

Schirrmeister, L., G. Grosse, S. Wetterich, P. P. Overduin, J. Strauss, E. A. G. Schuur, and H.-W. Hubberten, 2011: Fossil organic matter characteristics in permafrost deposits of the northeast Siberian Arctic. *J. Geophys. Res.*, **116**, G00M02.

Schmitt, J., et al., 2012: Carbon isotope constraints on the deglacial CO_2 rise from ice cores. *Science*, **336**, 711–714.

Schmittner, A., and E. D. Galbraith, 2008: Glacial greenhouse-gas fluctuations controlled by ocean circulation changes. *Nature*, **456**, 373–376.

Schmittner, A., A. Oschlies, H. D. Matthews, and E. D. Galbraith, 2008: Future changes in climate, ocean circulation, ecosystems, and biogeochemical cycling simulated for a business-as-usual CO_2 emission scenario until year 4000 AD. *Global Biogeochem. Cycles*, **22**, GB1013.

Schmittner, A., N. M. Urban, K. Keller, and D. Matthews, 2009: Using tracer observations to reduce the uncertainty of ocean diapycnal mixing and climate-carbon cycle projections. *Global Biogeochem. Cycles*, **23**, GB4009.

Schneider von Deimling, T. S., M. Meinshausen, A. Levermann, V. Huber, K. Frieler, D. M. Lawrence, and V. Brovkin, 2012: Estimating the near-surface permafrost-carbon feedback on global warming. *Biogeosciences*, **9**, 649–665.

Scholze, M., W. Knorr, N. W. Arnell, and I. C. Prentice, 2006: A climate-change risk analysis for world ecosystems. *Proc. Natl. Acad. Sci. U.S.A.*, **103**, 13116–13120.

Schuiling, R. D., and P. Krijgsman, 2006: Enhanced weathering: An effective and cheap tool to sequester CO_2. *Clim. Change*, **74**, 349–354.

Schultz, M. G., et al., 2007: Emission data sets and methodologies for estimating emissions. *REanalysis of the TROpospheric chemical composition over the past 40 years.* A long-term global modeling study of tropospheric chemistry funded under the 5th EU framework programme EU-Contract EVK2-CT-2002–00170.

Schulze, E. D., S. Luyssaert, P. Ciais, A. Freibauer, and I. A. Janssens, 2009: Importance of methane and nitrous oxide for Europe's terrestrial greenhouse-gas balance. *Nature Geosci.*, **2**, 842–850.

Schulze, E. D., et al., 2010: The European carbon balance. Part 4: Integration of carbon and other trace-gas fluxes. *Global Change Biol.*, **16**, 1451–1469.

Schurgers, G., U. Mikolajewicz, M. Gröger, E. Maier-Reimer, M. Vizcaino, and A. Winguth, 2006: Dynamics of the terrestrial biosphere, climate and atmospheric CO_2 concentration during interglacials: A comparison between Eemian and Holocene. *Clim. Past*, **2**, 205–220.

Schuster, U., and A. J. Watson, 2007: A variable and decreasing sink for atmospheric CO_2 in the North Atlantic. *J. Geophys. Res. Oceans*, **112**, C11006.

Schuster, U., et al., 2009: Trends in North Atlantic sea-surface fCO_2 from 1990 to 2006. *Deep-Sea Res. Pt. II*, **56**, 620–629.

Schuster, U., et al., 2013: An assessment of the Atlantic and Arctic sea-air CO_2 fluxes, 1990–2009. *Biogeosciences*, **10**, 607–627.

Schwalm, C. R., et al., 2010: A model-data intercomparison of CO_2 exchange across North America: Results from the North American Carbon Program site synthesis. *J. Geophys. Res.*, **115**, G00H05.

Seitzinger, S. P., and C. Kroeze, 1998: Global distribution of nitrous oxide production and N inputs in freshwater and coastal marine ecosystems. *Global Biogeochem. Cycles*, **12**, 93–113.

Seitzinger, S. P., J. A. Harrison, E. Dumont, A. H. W. Beusen, and A. F. Bouwman, 2005: Sources and delivery of carbon, nitrogen, and phosphorus to the coastal zone: An overview of Global Nutrient Export from Watersheds (NEWS) models and their application. *Global Biogeochem. Cycles*, **19**, Gb4s01.

Seitzinger, S. P., et al., 2010: Global river nutrient export: A scenario analysis of past and future trends. *Global Biogeochem. Cycles*, **24**, GB0A08.

Sentman, L. T., E. Shevliakova, R. J. Stouffer, and S. Malyshev, 2011: Time scales of terrestrial carbon response related to land-use application: Implications for initializing an Earth System Model. *Earth Interactions*, **15**, 1–16.

Shackleton, N. J., 2000: The 100,000–year ice-age cycle identified and found to lag temperature, carbon dioxide, and orbital eccentricity. *Science*, **289**, 1897–1902.

Shaffer, G., 2010: Long-term effectiveness and consequences of carbon dioxide sequestration. *Nature Geosci.*, **3**, 464–467.

Shaffer, G., S. M. Olsen, and J. O. P. Pedersen, 2009: Long-term ocean oxygen depletion in response to carbon dioxide emission from fossil fuels. *Nature Geosci.*, **2**, 105–109.

Shakhova, N., I. Semiletov, A. Salyuk, V. Yusupov, D. Kosmach, and O. Gustafsson, 2010: Extensive methane venting to the atmosphere from sediments of the East Siberian Arctic shelf. *Science*, **327**, 1246–1250.

Shallcross, D. E., M. A. K. Khalil, and C. L. Butenhoff, 2007: The atmospheric methane sink. In: *Greenhouse Gas Sinks* [D. Reay (ed.)] CAB International, pp. 171-183.

Shepherd, J., et al., 2009: Geoengineering the climate: Science, governance and uncertainty. Report of the Royal Society, London, 98 pp.

Shevliakova, E., et al., 2009: Carbon cycling under 300 years of land use change: Importance of the secondary vegetation sink. *Global Biogeochem. Cycles*, **23**, GB2022.

Shindell, D. T., B. P. Walter, and G. Faluvegi, 2004: Impacts of climate change on methane emissions from wetlands. *Geophys. Res. Lett.*, **31**, L21202.

Siegenthaler, U., et al., 2005a: Supporting evidence from the EPICA Dronning Maud Land ice core for atmospheric CO_2 changes during the past millennium. *Tellus B*, **57**, 51–57.

Siegenthaler, U., et al., 2005b: Stable carbon cycle-climate relationship during the late Pleistocene. *Science*, **310**, 1313–1317.

Sigman, D. M., M. P. Hain, and G. H. Haug, 2010: The polar ocean and glacial cycles in atmospheric CO_2 concentration. *Nature*, **466**, 47–55.

Simpson, I. J., F. S. Rowland, S. Meinardi, and D. R. Blake, 2006: Influence of biomass burning during recent fluctuations in the slow growth of global tropospheric methane. *Geophys. Res. Lett.*, **33**, L22808.

Simpson, I. J., et al., 2012: Long-term decline of global atmospheric ethane concentrations and implications for methane. *Nature*, **488**, 490–494.

Singarayer, J. S., P. J. Valdes, P. Friedlingstein, S. Nelson, and D. J. Beerling, 2011: Late Holocene methane rise caused by orbitally controlled increase in tropical sources. *Nature*, **470**, 82–85.

Singh, B. K., R. D. Bardgett, P. Smith, and D. S. Reay, 2010: Microorganisms and climate change: Terrestrial feedbacks and mitigation options. *Nature Rev. Microbiol.*, **8**, 779–790.

Sitch, S., P. M. Cox, W. J. Collins, and C. Huntingford, 2007: Indirect radiative forcing of climate change through ozone effects on the land-carbon sink. *Nature*, **448**, 791–794.

Sitch, S., et al., 2003: Evaluation of ecosystem dynamics, plant geography and terrestrial carbon cycling in the LPJ Dynamic Global Vegetation Model. *Global Change Biol.*, **9**, 161–185.

Sitch, S., et al., 2008: Evaluation of the terrestrial carbon cycle, future plant geography and climate-carbon cycle feedbacks using five Dynamic Global Vegetation Models (DGVMs). *Global Change Biol.*, **14**, 2015–2039.

Skinner, L. C., S. Fallon, C. Waelbroeck, E. Michel, and S. Barker, 2010: Ventilation of the deep Southern ocean and deglacial CO_2 rise. *Science*, **328**, 1147–1151.

Smetacek, V., et al., 2012: Deep carbon export from a Southern Ocean iron-fertilized diatom bloom. *Nature*, **487**, 313–319.

Smith, B., I. C. Prentice, and M. T. Sykes, 2001a: Representation of vegetation dynamics in the modelling of terrestrial ecosystems: Comparing two contrasting approaches within European climate space. *Global Ecol. Biogeogr.*, **10**, 621–637.

Smith, K. A., A. R. Mosier, P. J. Crutzen, and W. Winiwarter, 2012: The role of N_2O derived from crop-based biofuels, and from agriculture in general, in Earth's climate. *Philos. Trans. R. Soc. London B*, **367**, 1169–1174.

Smith, L. C., Y. Sheng, G. M. MacDonald, and L. D. Hinzman, 2005: Disappearing Arctic lakes. *Science*, **308**, 1429.

Smith, S. V., W. H. Renwick, R. W. Buddemeier, and C. J. Crossland, 2001b: Budgets of soil erosion and deposition for sediments and sedimentary organic carbon across the conterminous United States. *Global Biogeochem. Cycles*, **15**, 697–707.

Sokolov, A. P., D. W. Kicklighter, J. M. Melillo, B. S. Felzer, C. A. Schlosser, and T. W. Cronin, 2008: Consequences of considering carbon-nitrogen interactions on the feedbacks between climate and the terrestrial carbon cycle. *J. Clim.*, **21**, 3776–3796.

Sowers, T., 2006: Late quaternary atmospheric CH_4 isotope record suggests marine clathrates are stable. *Science*, **311**, 838–840.

Sowers, T., R. B. Alley, and J. Jubenville, 2003: Ice core records of atmospheric N_2O covering the last 106,000 years. *Science*, **301**, 945–948.

Spahni, R., et al., 2011: Constraining global methane emissions and uptake by ecosystems. *Biogeosciences*, **8**, 1643–1665.

Spracklen, D. V., L. J. Mickley, J. A. Logan, R. C. Hudman, R. Yevich, M. D. Flannigan, and A. L. Westerling, 2009: Impacts of climate change from 2000 to 2050 on wildfire activity and carbonaceous aerosol concentrations in the western United States. *J. Geophys. Res. Atmos.*, **114**, D20301.

Stallard, R. F., 1998: Terrestrial sedimentation and the carbon cycle: Coupling weathering and erosion to carbon burial. *Global Biogeochem. Cycles*, **12**, 231–257.

Stanhill, G., and S. Cohen, 2001: Global dimming: A review of the evidence for a widespread and significant reduction in global radiation with discussion of its probable causes and possible agricultural consequences. *Agr. Forest Meteorol.*, **107**, 255–278.

Steinacher, M., F. Joos, T. L. Frölicher, G.-K. Plattner, and S. C. Doney, 2009: Imminent ocean acidification in the Arctic projected with the NCAR global coupled carbon cycle-climate model. *Biogeosciences*, **6**, 515–533.

Steinacher, M., et al., 2010: Projected 21st century decrease in marine productivity: A multi-model analysis. *Biogeosciences*, **7**, 979–1005.

Stephens, B. B., and R. F. Keeling, 2000: The influence of Antarctic sea ice on glacial-interglacial CO_2 variations. *Nature*, **404**, 171–174.

Stephens, B. B., et al., 2007: Weak northern and strong tropical land carbon uptake from vertical profiles of atmospheric CO_2. *Science*, **316**, 1732–1735.

Stevenson, D. S., et al., 2006: Multimodel ensemble simulations of present-day and near-future tropospheric ozone. *J. Geophys. Res.*, **111**, D08301.

Stocker, B. D., K. Strassmann, and F. Joos, 2011: Sensitivity of Holocene atmospheric CO_2 and the modern carbon budget to early human land use: Analyses with a process-based model. *Biogeosciences*, **8**, 69–88.

Stocker, B. D., et al., 2013: Multiple greenhouse gas feedbacks from the land biosphere under future climate change scenarious. *Nature Clim. Change*, **3**, 666-672.

Stöckli, R., et al., 2008: Use of FLUXNET in the Community Land Model development. *J. Geophys. Res.Biogeosci.*, **113**, G01025.

Stolaroff, J. K., D. W. Keith, and G. V. Lowry, 2008: Carbon dioxide capture from atmospheric air using sodium hydroxide spray. *Environ. Sci. Technol.*, **42**, 2728–2735.

Stolaroff, J. K., S. Bhattacharyya, C. A. Smith, W. L. Bourcier, P. J. Cameron-Smith, and R. D. Aines, 2012: Review of methane mitigation technologies with application to rapid release of methane from the Arctic. *Environ. Sci. Technol.*, **46**, 6455–6469.

Stramma, L., A. Oschlies, and S. Schmidtko, 2012: Mismatch between observed and modeled trends in dissolved upper-ocean oxygen over the last 50 years. *Biogeosciences*, **9**, 4045–4057.

Strassmann, K. M., F. Joos, and G. Fischer, 2008: Simulating effects of land use changes on carbon fluxes: Past contributions to atmospheric CO_2 increases and future commitments due to losses of terrestrial sink capacity. *Tellus B*, **60**, 583–603.

Stuiver, M., and P. D. Quay, 1981: Atmospheric ^{14}C changes resulting from fossil-fuel CO_2 release and cosmic-ray flux variability. *Earth Planet. Sci. Lett.*, **53**, 349–362.

Suchet, P. A., and J. L. Probst, 1995: A Global model for present-day atmospheric soil CO_2 consumption by chemical erosion of continental rocks (GEM-CO_2). *Tellus B*, **47**, 273–280.

Sugimoto, A., T. Inoue, N. Kirtibutr, and T. Abe, 1998: Methane oxidation by termite mounds estimated by the carbon isotopic composition of methane. *Global Biogeochem. Cycles*, **12**, 595–605.

Sundquist, E. T., 1986: Geologic analogs: Their value and limitations in carbon dioxide research. In: *The Changing Carbon Cycle* [J. R. Trabalka and D. E. Reichle (eds.)], Springer-Verlag, New York, pp. 371–402.

Sundquist, E. T, 1990: Influence of deep-sea benthic processes on atmospheric CO_2. *Philos. Trans. R. Soc. London Series A*, **331**, 155–165.

Suntharalingam, P., et al., 2012: Quantifying the impact of anthropogenic nitrogen deposition on oceanic nitrous oxide. *Geophys. Res. Lett.*, **39**, L07605.

Sussmann, R., F. Forster, M. Rettinger, and P. Bousquet, 2012: Renewed methane increase for five years (2007–2011) observed by solar FTIR spectrometry. *Atmos. Chem. Phys.*, **112**, 4885–4891.

Sutka, R. L., N. E. Ostrom, P. H. Ostrom, J. A. Breznak, H. Gandhi, A. J. Pitt, and F. Li, 2006: Distinguishing nitrous oxide production from nitrification and denitrification on the basis of isotopomer abundances. *Appl. Environ. Microbiol.*, **72**, 638–644.

Sutton, M. A., D. D. Simpson, P. E. Levy, R. I. Smith, S. Reis, M. Van Oijen, and W. De Vries, 2008: Uncertainties in the relationship between atmospheric nitrogen deposition and forest carbon sequestration. *Global Change Biol.*, **14**, 2057–2063.

Sutton, M. A., et al., 2011: *The European Nitrogen Assessment —Sources, Effects and Policy Perspectives.* Cambridge University Press, Cambridge, United Kingdom, and New York, NY, USA, 664 pp.

Syakila, A., and C. Kroeze, 2011: The global N_2O budget revisited. *Greenh. Gas Measure. Manage.*, **1**, 17–26.

Syakila, A., C. Kroeze, and C. P. Slomp, 2010: Neglecting sinks for N_2O at the earth's surface: Does it matter? *J. Integrat. Environ. Sci.*, **7**, 79–87.

Syvitski, J. P. M., C. J. Vörösmarty, A. J. Kettner, and P. Green, 2005: Impact of humans on the flux of terrestrial sediment to the global coastal ocean. *Science*, **308**, 376–380.

Tagaris, E., K.-J. Liao, K. Manomaiphiboon, J.-H. Woo, S. He, P. Amar, and A. G. Russell, 2008: Impacts of future climate change and emissions reductions on nitrogen and sulfur deposition over the United States. *Geophys. Res. Lett.*, **35**, L08811.

Tagliabue, A., L. Bopp, and O. Aumont, 2008: Ocean biogeochemistry exhibits contrasting responses to a large scale reduction in dust deposition. *Biogeosciences*, **5**, 11–24.

Tagliabue, A., L. Bopp, and M. Gehlen, 2011: The response of marine carbon and nutrient cycles to ocean acidification: Large uncertainties related to phytoplankton physiological assumptions. *Global Biogeochem. Cycles*, **25**, GB3017.

Takahashi, T., S. C. Sutherland, R. A. Feely, and R. Wanninkhof, 2006: Decadal change of the surface water pCO_2 in the North Pacific: A synthesis of 35 years of observations. *J. Geophys. Res. Oceans*, **111**, C07s05.

Takahashi, T., J. Olafsson, J. G. Goddard, D. W. Chipman, and S. C. Sutherland, 1993: Seasonal variation of CO_2 and nutrients in the high-latitude surface oceans—A comparative study. *Global Biogeochem. Cycles*, **7**, 843–878.

Takahashi, T., et al., 2009: Climatological mean and decadal change in surface ocean pCO_2, and net sea-air CO_2 flux over the global oceans. *Deep-Sea Res. Pt. II*, **56**, 554–577.

Tan, K., et al., 2010: Application of the ORCHIDEE global vegetation model to evaluate biomass and soil carbon stocks of Qinghai-Tibetan grasslands. *Global Biogeochem. Cycles*, **24**, GB1013.

Tanhua, T., A. Körtzinger, K. Friis, D. W. Waugh, and D. W. R. Wallace, 2007: An estimate of anthropogenic CO_2 inventory from decadal changes in oceanic carbon content. *Proc. Natl. Acad. Sci. U.S.A.*, **104**, 3037–3042.

Tans, P. P., T. J. Conway, and T. Nakazawa, 1989: Latitudinal distribution of the sources and sinks of atmospheric carbon dioxide derived from surface observations and an atmospheric transport model. *J. Geophys. Res. Atmos.*, **94**, 5151–5172.

Tarnocai, C., J. G. Canadell, E. A. G. Schuur, P. Kuhry, G. Mazhitova, and S. Zimov, 2009: Soil organic carbon pools in the northern circumpolar permafrost region. *Global Biogeochem. Cycles*, **23**, Gb2023.

Taucher, J., and A. Oschlies, 2011: Can we predict the direction of marine primary production change under global warming? *Geophys. Res. Lett.*, **38**, L02603.

Taylor, K. E., R. J. Stouffer, and G. A. Meehl, 2012: An overview of CMIP5 and the experiment design. *Bull. Am. Meteorol. Soc.*, **93**, 485–498.

Tegen, I., M. Werner, S. P. Harrison, and K. E. Kohfeld, 2004: Relative importance of climate and land use in determining present and future global soil dust emission. *Geophys. Res. Lett.*, **31**, L05105.

Terazawa, K., S. Ishizuka, T. Sakata, K. Yamada, and M. Takahashi, 2007: Methane emissions from stems of *Fraxinus mandshurica* var. *japonica* trees in a floodplain forest. *Soil Biology and Biochemistry*, **39**, 2689–2692.

Terrier, A., M. P. Girardin, C. Périé, P. Legendre, and Y. Bergeron, 2013: Potential changes in forest composition could reduce impacts of climate change on boreal wildfires. *Ecol. Appl.*, **23**, 21–35.

Thomas, H., et al., 2007: Rapid decline of the CO_2 buffering capacity in the North Sea and implications for the North Atlantic Ocean. *Global Biogeochem. Cycles*, **21**, GB4001.

Thompson, D. W. J., and S. Solomon, 2002: Interpretation of recent Southern Hemisphere climate change. *Science*, **296**, 895–899.

Thomson, A. M., et al., 2010: Climate mitigation and food production in tropical landscapes. Special feature: Climate mitigation and the future of tropical landscapes. *Proc. Natl. Acad. Sci. U.S.A.*, **107**, 19633–19638.

Thornton, P. E., J.-F. Lamarque, N. A. Rosenbloom, and N. M. Mahowald, 2007: Influence of carbon-nitrogen cycle coupling on land model response to CO_2 fertilization and climate variability. *Global Biogeochem. Cycles*, **21**, Gb4018.

Thornton, P. E., et al., 2009: Carbon-nitrogen interactions regulate climate-carbon cycle feedbacks: Results from an atmosphere-ocean general circulation model. *Biogeosciences*, **6**, 2099–2120.

Tian, H., X. Xu, M. Liu, W. Ren, C. Zhang, G. Chen, and C. Lu, 2010: Spatial and temporal patterns of CH_4 and N_2O fluxes in terrestrial ecosystems of North America during 1979–2008: Application of a global biogeochemistry model. *Biogeosciences*, **7**, 2673–2694.

Tilman, D., C. Balzer, J. Hill, and B. L. Befort, 2011: Global food demand and the sustainable intensification of agriculture. *Proc. Natl. Acad. Sci. U.S.A.*, **108**, 20260–20264.

Tjiputra, J. F., A. Olsen, K. Assmann, B. Pfeil, and C. Heinze, 2012: A model study of the seasonal and long-term North Atlantic surface pCO_2 variability. *Biogeosciences*, **9**, 907–923.

Todd-Brown, K., F. M. Hopkins, S. N. Kivlin, J. M. Talbot, and S. D. Allison, 2012: A framework for representing microbial decomposition in coupled climate models. *Biogeoschemistry*, **109**, 19–33.

Toggweiler, J. R., 1999: Variation of atmospheric CO_2 by ventilation of the ocean's deepest water. *Paleoceanography*, **14**, 571–588.

Toggweiler, J. R., J. L. Russell, and S. R. Carson, 2006: Midlatitude westerlies, atmospheric CO_2, and climate change during the ice ages. *Paleoceanography*, **21**, PA2005.

Tranvik, L. J., et al., 2009: Lakes and reservoirs as regulators of carbon cycling and climate. *Limnol. Oceanogr.*, **54**, 2298–2314.

Trudinger, C. M., I. G. Enting, P. J. Rayner, and R. J. Francey, 2002: Kalman filter analysis of ice core data – 2. Double deconvolution of CO_2 and δ13C measurements. *J. Geophys. Res.*, **107**, D20.

Turetsky, M. R., R. K. Wieder, D. H. Vitt, R. J. Evans, and K. D. Scott, 2007: The disappearance of relict permafrost in boreal north America: Effects on peatland carbon storage and fluxes. *Global Change Biol.*, **13**, 1922–1934.

Tymstra, C., M. D. Flannigan, O. B. Armitage, and K. Logan, 2007: Impact of climate change on area burned in Alberta's boreal forest. *Int. J. Wildland Fire*, **16**, 153–160.

Tyrrell, T., J. G. Shepherd, and S. Castle, 2007: The long-term legacy of fossil fuels. *Tellus B*, **59**, 664–672.

Ullman, D. J., G. A. McKinley, V. Bennington, and S. Dutkiewicz, 2009: Trends in the North Atlantic carbon sink: 1992–2006. *Global Biogeochem. Cycles*, **23**, Gb4011.

UNEP, 2011: Integrated assessment of black carbon and tropospheric ozone: Summary for decision makers. United Nations Environment Programme and World Meterological Association, 38 pp.

Valsala, V., S. Maksyutov, M. Telszewski, S. Nakaoka, Y. Nojiri, M. Ikeda, and R. Murtugudde, 2012: Climate impacts on the structures of the North Pacific air-sea CO_2 flux variability. *Biogeosciences*, **9**, 477–492.

van der Werf, G. R., et al., 2004: Continental-scale partitioning of fire emissions during the 1997 to 2001 El Niño/La Niña period. *Science*, **303**, 73–76.

van der Werf, G. R., et al., 2009: CO_2 emissions from forest loss. *Nature Geosci.*, **2**, 737–738.

van der Werf, G. R., et al., 2010: Global fire emissions and the contribution of deforestation, savanna, forest, agricultural, and peat fires (1997–2009). *Atmos. Chem. Phys.*, **10**, 11707–11735.

van der Werf, G. R., et al., 2008: Climate regulation of fire emissions and deforestation in equatorial Asia *Proc. Natl. Acad. Sci. U.S.A.*, **105**, 20350–20355.

van Groenigen, K. J., C. W. Osenberg, and B. A. Hungate, 2011: Increased soil emissions of potent greenhouse gases under increased atmospheric CO_2. *Nature*, **475**, 214–216.

van Huissteden, J., C. Berrittella, F. J. W. Parmentier, Y. Mi, T. C. Maximov, and A. J. Dolman, 2011: Methane emissions from permafrost thaw lakes limited by lake drainage. *Nature Clim. Change*, **1**, 119–123.

van Minnen, J. G., K. Klein Goldewijk, E. Stehfest, B. Eickhout, G. van Drecht, and R. Leemans, 2009: The importance of three centuries of land-use change for the global and regional terrestrial carbon cycle. *Clim. Change*, **97**, 123–144.

van Vuuren, D. P., L. F. Bouwman, S. J. Smith, and F. Dentener, 2011: Global projections for anthropogenic reactive nitrogen emissions to the atmosphere: An assessment of scenarios in the scientific literature. *Curr. Opin. Environ. Sustain.*, **3**, 359–369.

Verdy, A., S. Dutkiewicz, M. J. Follows, J. Marshall, and A. Czaja, 2007: Carbon dioxide and oxygen fluxes in the Southern Ocean: Mechanisms of interannual variability. *Global Biogeochem. Cycles*, **21**, Gb2020.

Vigano, I., H. van Weelden, R. Holzinger, F. Keppler, A. McLeod, and T. Röckmann, 2008: Effect of UV radiation and temperature on the emission of methane from plant biomass and structural components. *Biogeosciences*, **5**, 937–947.

Vitousek, P. M., S. Porder, B. Z. Houlton, and O. A. Chadwick, 2010: Terrestrial phosphorus limitation: Mechanisms, implications, and nitrogen-phosphorus interactions. *Ecol. Appl.*, **20**, 5–15.

Vitousek, P. M., D. N. L. Menge, S. C. Reed, and C. C. Cleveland, 2013: Biological nitrogen fixation: Rates, patterns, and ecological controls in terrestrial ecosystems. *Philos. Trans. R. Soc. London B,368,* 20130119.

Volk, C. M., et al., 1997: Evaluation of source gas lifetimes from stratospheric observations. *J. Geophys. Res.: Atmos.*, **102**, 25543–25564.

Volodin, E. M., 2008: Methane cycle in the INM RAS climate model. *Izvestiya Atmos. Ocean. Phys.*, **44**, 153–159.

Voss, M., H. W. Bange, J. W. Dippner, J. J. Middelburg, J. P. Montoya, and B. Ward, 2013: The marine nitrogen cycle: Recent discoveries, uncertainties and the potential relevance of climate change. *Philos. Trans. R. Soc. London B*, **368**, 20130121.

Voss, M., et al., 2011: Nitrogen processes in coastal and marine ecosystems. In: *The European Nitrogen Assessment: Sources, Effects, and Policy Perspectives.* [M. A. Sutton, C. M. Howard, J. W. Erisman, G. Billen, A. Bleeker, P. Grennfelt, H. van Grinsven and B. Grizetti (eds.)]. Cambridge University Press, Cambridge, United Kingdom, and New York, NY, USA, pp. 147–176.

Voulgarakis, A., et al., 2013: Analysis of present day and future OH and methane lifetime in the ACCMIP simulations. *Atmos. Chem. Phys.*, **13**, 2563–2587.

Waelbroeck, C., et al., 2009: Constraints on the magnitude and patterns of ocean cooling at the Last Glacial Maximum. *Nature Geosci.*, **2**, 127–132.

Wakita, M., S. Watanabe, A. Murata, N. Tsurushima, and M. Honda, 2010: Decadal change of dissolved inorganic carbon in the subarctic western North Pacific Ocean. *Tellus B*, **62**, 608–620.

Walker, J. C. G., and J. F. Kasting, 1992: Effects of fuel and forest conservation on future levels of atmospheric carbon dioxide. *Palaeogeogr. Palaeoclimat. Palaeoecol.* (*Global Planet. Change Sect.*), **97**, 151–189.

Walter Anthony, K. M., P. Anthony, G. Grosse, and J. Chanton, 2012: Geologic methane seeps along boundaries of Arctic permafrost thaw and melting glaciers. *Nature Geosci.*, **5**, 419-426.

Walter, K. M., L. C. Smith, and F. Stuart Chapin, 2007: Methane bubbling from northern lakes: Present and future contributions to the global methane budget. *Philos. Trans. R. Soc. A*, **365**, 1657–1676.

Walter, K. M., S. A. Zimov, J. P. Chanton, D. Verbyla, and F. S. I. Chapin, 2006: Methane bubbling from Siberian thaw lakes as a positive feedback to climate warming. *Nature*, **443**, 71–75.

Wang, D., S. A. Heckathorn, X. Wang, and S. M. Philpott, 2012a: A meta-analysis of plant physiological and growth responses to temperature and elevated CO_2. *Oecologia*, **169**, 1–13.

Wang, J., X. Pan, Y. Liu, X. Zhang, and Z. Xiong, 2012b: Effects of biochar amendment in two soils on greenhouse gas emissions and crop production. *Plant Soil*, **360**, 287–298.

Wang, Y.-P., and B. Z. Houlton, 2009: Nitrogen constraints on terrestrial carbon uptake: Implications for the global carbon-climate feedback. *Geophys. Res. Lett.*, **36**, L24403.

Wang, Y. P., B. Z. Houlton, and C. B. Field, 2007: A model of biogeochemical cycles of carbon, nitrogen, and phosphorus including symbiotic nitrogen fixation and phosphatase production. *Global Biogeochem. Cycles*, **21**, GB1018.

Wang, Y. P., R. M. Law, and B. Pak, 2010a: A global model of carbon, nitrogen and phosphorus cycles for the terrestrial biosphere. *Biogeosciences*, **7**, 2261–2282.

Wang, Z., J. Chappellaz, K. Park, and J. E. Mak, 2010b: Large variations in Southern Hemisphere biomass burning during the last 650 years. *Science*, **330**, 1663–1666.

Wang, Z. P., X. G. Han, G. G. Wang, Y. Song, and J. Gulledge, 2008: Aerobic methane emission from plants in the Inner Mongolia steppe. *Environ. Sci. Technol.*, **42**, 62–68.

Wania, R., 2007: *Modelling Northern Peatland Land Surface Processes, Vegetation Dynamics and Methane Emissions*. Ph.D. Thesis, Bristol, UK.

Wania, R., I. Ross, and I. C. Prentice, 2009: Integrating peatlands and permafrost into a dynamic global vegetation model: 1. Evaluation and sensitivity of physical land surface processes. *Global Biogeochem. Cycles*, **23**, GB3014.

Wanninkhof, R., S. C. Doney, J. L. Bullister, N. M. Levine, M. Warner, and N. Gruber, 2010: Detecting anthropogenic CO_2 changes in the interior Atlantic Ocean between 1989 and 2005. *J. Geophys. Res. Oceans*, **115**, C11028.

Wanninkhof, R., et al., 2013: Global ocean carbon uptake: Magnitude, variability and trends. *Biogeosciences*, **10**, 1983–2000.

Wardle, D. A., M.-C. Nilsson, and O. Zackrisson, 2008: Fire-derived charcoal causes loss of forest humus. *Science*, **320**, 629.

Watanabe, S., et al., 2011: MIROC-ESM 2010: Model description and basic results of CMIP5–20c3m experiments. *Geosci. Model Dev.*, **4**, 845–872.

Watson, A. J., and A. C. N. Garabato, 2006: The role of Southern Ocean mixing and upwelling in glacial-interglacial atmospheric CO_2 change. *Tellus B*, **58**, 73–87.

Watson, A. J., D. C. E. Bakker, A. J. Ridgwell, P. W. Boyd, and C. S. Law, 2000: Effect of iron supply on Southern Ocean CO_2 uptake and implications for glacial atmospheric CO_2. *Nature*, **407**, 730–733.

Watson, A. J., P. W. Boyd, S. M. Turner, T. D. Jickells, and P. S. Liss, 2008: Designing the next generation of ocean iron fertilization experiments. *Mar. Ecol. Prog. Ser.*, **364**, 303–309.

Watson, A. J., et al., 1994: Minimal effect of iron fertilization on sea-surface carbon-dioxide concentartions. *Nature*, **371**, 143–145.

Watson, A. J., et al., 2009: Tracking the variable North Atlantic sink for atmospheric CO_2. *Science*, **326**, 1391–1393.

Waugh, D. W., T. M. Hall, B. I. McNeil, R. Key, and R. J. Matear, 2006: Anthropogenic CO_2 in the oceans estimated using transit time distributions. *Tellus B*, **58**, 376–389.

Wecht, K. J., et al., 2012: Validation of TES methane with HIPPO aircraft observations: Implications for inverse modeling of methane sources. *Atmos. Chem. Phys.*, **12**, 1823–1832.

Westbrook, G. K., et al., 2009: Escape of methane gas from the seabed along the West Spitsbergen continental margin. *Geophys. Res. Lett.*, **36**, L15608.

Westerling, A. L., M. G. Turner, E. A. H. Smithwick, W. H. Romme, and M. G. Ryan, 2011: Continued warming could transform Greater Yellowstone fire regimes by mid-21st century. *Proc. Natl. Acad. Sci. U.S.A.*, **108**, 13165–13170.

White, J. R., R. D. Shannon, J. F. Weltzin, J. Pastor, and S. D. Bridgham, 2008: Effects of soil warming and drying on methane cycling in a northern peatland mesocosm study. *J. Geophys. Res. Biogeosci.*, **113**, G00A06.

Wiedinmyer, C., S. K. Akagi, R. J. Yokelson, L. K. Emmons, J. A. Al-Saadi, J. J. Orlando, and A. J. Soja, 2011: The Fire INventory from NCAR (FINN): A high resolution global model to estimate the emissions from open burning. *Geosci. Model Dev.*, **4**, 625–641.

Williams, C. A., G. J. Collatz, J. Masek, and S. N. Goward, 2012a: Carbon consequences of forest disturbance and recovery across the conterminous United States. *Global Biogeochem. Cycles*, **26**, GB1005.

Williams, J., and P. J. Crutzen, 2010: Nitrous oxide from aquaculture. *Nature Geosci.*, **3**, 143.

Williams, J. E., A. Strunk, V. Huijnen, and M. van Weele, 2012b: The application of the Modified Band Approach for the calculation of on-line photodissociation rate constants in TM5: Implications for oxidative capacity. *Geosci. Model Dev.*, **5**, 15–35.

Wise, M., et al., 2009: Implications of limiting CO_2 concentrations for land Uue and energy. *Science*, **324**, 1183–1186.

Woodward, F. I., and M. R. Lomas, 2004: Simulating vegetation processes along the Kalahari transect. *Global Change Biol.*, **10**, 383–392.

Woolf, D., J. E. Amonette, F. A. Street-Perrott, J. Lehmann, and S. Joseph, 2010: Sustainable biochar to mitigate global climate change. *Nature Commun.*, **1**, 1–9.

Worden, J., et al., 2012: Profiles of CH_4, HDO, H_2O, and N_2O with improved lower tropospheric vertical resolution from Aura TES radiances. *Atmos. Measure. Techn.*, **5**, 397–411

Worrall, F., T. Burt, and R. Shedden, 2003: Long term records of riverine dissolved organic matter. *Biogeochemistry*, **64**, 165–178.

Wotton, B. M., C. A. Nock, and M. D. Flannigan, 2010: Forest fire occurrence and climate change in Canada. *Int. J. Wildland Fire*, **19**, 253–271.

Wu, P. L., R. Wood, J. Ridley, and J. Lowe, 2010: Temporary acceleration of the hydrological cycle in response to a CO_2 rampdown. *Geophys. Res. Lett.*, **37**, L12705.

Wu, T., et al., 2013: Global Carbon budgets simulated by the Beijing Climate Center Climate System Model for the last Century. *J. Geophys. Res. Atmos.*, doi:10.1002/jgrd.50320, in press.

Wurzburger, N., J. P. Bellenger, A. M. L. Kraepiel, and L. O. Hedin, 2012: Molybdenum and phosphorus interact to constrain asymbiotic nitrogen fixation in tropical forests. *PLoS ONE*, **7**, e33710.

Xu-Ri, and I. C. Prentice, 2008: Terrestrial nitrogen cycle simulation with a dynamic global vegetation model. *Global Change Biol.*, **14**, 1745–1764.

Xu-Ri, I. C. Prentice, R. Spahni, and H. S. Niu, 2012: Modelling terrestrial nitrous oxide emissions and implications for climate feedback. *New Phytologist*, **196**, 472–488.

Yamamoto-Kawai, M., F. A. McLaughlin, E. C. Carmack, S. Nishino, and K. Shimada, 2009: Aragonite undersaturation in the Arctic Ocean: Effects of ocean acidification and sea ice melt. *Science*, **326**, 1098–1100.

Yamamoto, A., M. Kawamiya, A. Ishida, Y. Yamanaka, and S. Watanabe, 2012: Impact of rapid sea-ice reduction in the Arctic Ocean on the rate of ocean acidification. *Biogeosciences*, **9**, 2365–2375.

Yan, X., H. Akiyama, K. Yagi, and H. Akimoto, 2009: Global estimations of the inventory and mitigation potential of methane emissions from rice cultivation conducted using the 2006 Intergovernmental Panel on Climate Change Guidelines. *Global Biogeochem. Cycles*, **23**, GB2002.

Yang, X., T. K. Richardson, and A. K. Jain, 2010: Contributions of secondary forest and nitrogen dynamics to terrestrial carbon uptake. *Biogeosciences*, **7**, 3041-3050.

Yevich, R., and J. A. Logan, 2003: An assessment of biofuel use and burning of agricultural waste in the developing world. *Global Biogeochem. Cycles*, **17**, 1095.

Yool, A., J. G. Shepherd, H. L. Bryden, and A. Oschlies, 2009: Low efficiency of nutrient translocation for enhancing oceanic uptake of carbon dioxide. *J. Geophys. Res. Oceans*, **114**, C08009.

Yoshikawa-Inoue, H. Y., and M. Ishii, 2005: Variations and trends of CO_2 in the surface seawater in the Southern Ocean south of Australia between 1969 and 2002. *Tellus B*, *57*, 58–69.

Yoshikawa, C., M. Kawamiya, T. Kato, Y. Yamanaka, and T. Matsuno, 2008: Geographical distribution of the feedback between future climate change and the carbon cycle. *J. Geophys. Res. Biogeosci.*, **113**, G03002.

Young, P., et al., 2013: Pre-industrial to end 21st century projections of tropospheric ozone from the Atmospheric Chemistry and Climate Model Intercomparison Project (ACCMIP). *Atmos. Chem. Phys.*, **4**, 2063–2090.

Yu, J., W. S. Broecker, H. Elderfield, Z. Jin, J. McManus, and F. Zhang, 2010: Loss of carbon from the deep sea since the Last Glacial Maximum. *Science*, **330**, 1084–1087.

Yu, Z., 2011: Holocene carbon flux histories of the world's peatlands: Global carbon-cycle implications. *Holocene*, **21**, 761–774.

Zaehle, S., 2013: Terrestrial nitrogen-carbon cycle interactions at the global scale, *Philos. Trans. R. Soc. London B*, **368**, 20130125.

Zaehle, S., and A. D. Friend, 2010: Carbon and nitrogen cycle dynamics in the O-CN land surface model: 1. Model description, site-scale evaluation, and sensitivity to parameter estimates. *Global Biogeochem. Cycles*, **24**, GB1005.

Zaehle, S., and D. Dalmonech, 2011: Carbon-nitrogen interactions on land at global scales: Current understanding in modelling climate biosphere feedbacks. *Curr. Opin. Environ. Sustain.*, **3**, 311–320.

Zaehle, S., P. Friedlingstein, and A. D. Friend, 2010a: Terrestrial nitrogen feedbacks may accelerate future climate change. *Geophys. Res. Lett.*, **37**, L01401.

Zaehle, S., P. Ciais, A. D. Friend, and V. Prieur, 2011: Carbon benefits of anthropogenic reactive nitrogen offset by nitrous oxide emissions. *Nature Geosci.*, **4**, 601–605.

Zaehle, S., A. D. Friend, P. Friedlingstein, F. Dentener, P. Peylin, and M. Schulz, 2010b: Carbon and nitrogen cycle dynamics in the O-CN land surface model: 2. Role of the nitrogen cycle in the historical terrestrial carbon balance. *Global Biogeochem. Cycles*, **24**, GB1006.

Zak, D. R., K. S. Pregitzer, M. E. Kubiske, and A. J. Burton, 2011: Forest productivity under elevated CO_2 and O_3: Positive feedbacks to soil N cycling sustain decade-long net primary productivity enhancement by CO_2. *Ecol. Lett.*, **14**, 1220–1226.

Zech, R., Y. Huang, M. Zech, R. Tarozo, and W. Zech, 2011: High carbon sequestration in Siberian permafrost loess-paleosoils during glacials. *Clim. Past*, **7**, 501–509.

Zeebe, R. E., and D. Wolf-Gladrow, 2001: *CO_2 in Seawater: Equilibrium, Kinetics, Isotopes.* Elsevier Science, Amsterdam, Netherlands, and Philadelphia, PA, USA.

Zeebe, R. E., and D. Archer, 2005: Feasibility of ocean fertilization and its impact on future atmospheric CO_2 levels. *Geophys. Res. Lett.*, **32**, L09703.

Zeng, N., 2003: Glacial-interglacial atmospheric CO_2 change —The glacial burial hypothesis. *Adv. Atmos. Sci.*, **20**, 677–693.

Zhang, Q., Y. P. Wang, A. J. Pitman, and Y. J. Dai, 2011: Limitations of nitrogen and phosphorous on the terrestrial carbon uptake in the 20th century. *Geophys. Res. Lett.*, **38**, L22701.

Zhao, M., and S. W. Running, 2010: Drought-induced reduction in global terrestrial net primary production from 2000 through 2009. *Science*, **329**, 940–943.

Zhou, S., and P. C. Flynn, 2005: Geoengineering downwelling ocean currents: A cost assessment. *Clim. Change*, **71**, 203–220.

Zhuang, Q. L., et al., 2006: CO_2 and CH_4 exchanges between land ecosystems and the atmosphere in northern high latitudes over the 21st century. *Geophys. Res. Lett.*, **33**, L17403.

Zickfeld, K., M. Eby, H. D. Matthews, A. Schmittner, and A. J. Weaver, 2011: Nonlinearity of carbon cycle feedbacks. *J. Clim.*, **24**, 4255–4275.

Zimov, N. S., S. A. Zimov, A. E. Zimova, G. M. Zimova, V. I. Chuprynin, and F. S. Chapin, 2009: Carbon storage in pernafrost and soils of the mammoth tundra-steppe biome: Role in the global carbon budget. *Geophys. Res. Lett.*, **36**, L02502.

12

Long-term Climate Change: Projections, Commitments and Irreversibility

Coordinating Lead Authors:
Matthew Collins (UK), Reto Knutti (Switzerland)

Lead Authors:
Julie Arblaster (Australia), Jean-Louis Dufresne (France), Thierry Fichefet (Belgium), Pierre Friedlingstein (UK/Belgium), Xuejie Gao (China), William J. Gutowski Jr. (USA), Tim Johns (UK), Gerhard Krinner (France/Germany), Mxolisi Shongwe (South Africa), Claudia Tebaldi (USA), Andrew J. Weaver (Canada), Michael Wehner (USA)

Contributing Authors:
Myles R. Allen (UK), Tim Andrews (UK), Urs Beyerle (Switzerland), Cecilia M. Bitz (USA), Sandrine Bony (France), Ben B.B. Booth (UK), Harold E. Brooks (USA), Victor Brovkin (Germany), Oliver Browne (UK), Claire Brutel-Vuilmet (France), Mark Cane (USA), Robin Chadwick (UK), Ed Cook (USA), Kerry H. Cook (USA), Michael Eby (Canada), John Fasullo (USA), Erich M. Fischer (Switzerland), Chris E. Forest (USA), Piers Forster (UK), Peter Good (UK), Hugues Goosse (Belgium), Jonathan M. Gregory (UK), Gabriele C. Hegerl (UK/Germany), Paul J. Hezel (Belgium/USA), Kevin I. Hodges (UK), Marika M. Holland (USA), Markus Huber (Switzerland), Philippe Huybrechts (Belgium), Manoj Joshi (UK), Viatcheslav Kharin (Canada), Yochanan Kushnir (USA), David M. Lawrence (USA), Robert W. Lee (UK), Spencer Liddicoat (UK), Christopher Lucas (Australia), Wolfgang Lucht (Germany), Jochem Marotzke (Germany), François Massonnet (Belgium), H. Damon Matthews (Canada), Malte Meinshausen (Germany), Colin Morice (UK), Alexander Otto (UK/Germany), Christina M. Patricola (USA), Gwenaëlle Philippon-Berthier (France), Prabhat (USA), Stefan Rahmstorf (Germany), William J. Riley (USA), Joeri Rogelj (Switzerland/Belgium), Oleg Saenko (Canada), Richard Seager (USA), Jan Sedláček (Switzerland), Len C. Shaffrey (UK), Drew Shindell (USA), Jana Sillmann (Canada), Andrew Slater (USA/Australia), Bjorn Stevens (Germany/USA), Peter A. Stott (UK), Robert Webb (USA), Giuseppe Zappa (UK/Italy), Kirsten Zickfeld (Canada/Germany)

Review Editors:
Sylvie Joussaume (France), Abdalah Mokssit (Morocco), Karl Taylor (USA), Simon Tett (UK)

This chapter should be cited as:
Collins, M., R. Knutti, J. Arblaster, J.-L. Dufresne, T. Fichefet, P. Friedlingstein, X. Gao, W.J. Gutowski, T. Johns, G. Krinner, M. Shongwe, C. Tebaldi, A.J. Weaver and M. Wehner, 2013: Long-term Climate Change: Projections, Commitments and Irreversibility. In: *Climate Change 2013: The Physical Science Basis. Contribution of Working Group I to the Fifth Assessment Report of the Intergovernmental Panel on Climate Change* [Stocker, T.F., D. Qin, G.-K. Plattner, M. Tignor, S.K. Allen, J. Boschung, A. Nauels, Y. Xia, V. Bex and P.M. Midgley (eds.)]. Cambridge University Press, Cambridge, United Kingdom and New York, NY, USA.

Table of Contents

Executive Summary

This chapter assesses long-term projections of climate change for the end of the 21st century and beyond, where the forced signal depends on the scenario and is typically larger than the internal variability of the climate system. Changes are expressed with respect to a baseline period of 1986–2005, unless otherwise stated.

Scenarios, Ensembles and Uncertainties

The Coupled Model Intercomparison Project Phase 5 (CMIP5) presents an unprecedented level of information on which to base projections including new Earth System Models with a more complete representation of forcings, new Representative Concentration Pathways (RCP) scenarios and more output available for analysis. The four RCP scenarios used in CMIP5 lead to a total radiative forcing (RF) at 2100 that spans a wider range than that estimated for the three Special Report on Emission Scenarios (SRES) scenarios (B1, A1B, A2) used in the Fourth Assessment Report (AR4), RCP2.6 being almost 2 W m^{-2} lower than SRES B1 by 2100. The magnitude of future aerosol forcing decreases more rapidly in RCP scenarios, reaching lower values than in SRES scenarios through the 21st century. Carbon dioxide (CO_2) represents about 80 to 90% of the total anthropogenic forcing in all RCP scenarios through the 21st century. The ensemble mean total effective RFs at 2100 for CMIP5 concentration-driven projections are 2.2, 3.8, 4.8 and 7.6 W m^{-2} for RCP2.6, RCP4.5, RCP6.0 and RCP8.5 respectively, relative to about 1850, and are close to corresponding Integrated Assessment Model (IAM)-based estimates (2.4, 4.0, 5.2 and 8.0 W m^{-2}). {12.2.1, 12.3, Table 12.1, Figures 12.1, 12.2, 12.3, 12.4}

New experiments and studies have continued to work towards a more complete and rigorous characterization of the uncertainties in long-term projections, but the magnitude of the uncertainties has not changed significantly since AR4. There is overall consistency between the projections based on CMIP3 and CMIP5, for both large-scale patterns and magnitudes of change. Differences in global temperature projections are largely attributable to a change in scenarios. Model agreement and confidence in projections depend on the variable and spatial and temporal averaging. The well-established stability of large-scale geographical patterns of change during a transient experiment remains valid in the CMIP5 models, thus justifying pattern scaling to approximate changes across time and scenarios under such experiments. Limitations remain when pattern scaling is applied to strong mitigation scenarios, to scenarios where localized forcing (e.g., aerosols) are significant and vary in time and for variables other than average temperature and precipitation. {12.2.2, 12.2.3, 12.4.2, 12.4.9, Figures 12.10, 12.39, 12.40, 12.41}

Projections of Temperature Change

Global mean temperatures will continue to rise over the 21st century if greenhouse gas (GHG) emissions continue unabated. Under the assumptions of the concentration-driven RCPs, global mean surface temperatures for 2081–2100, relative to 1986–2005 will *likely*[1] be in the 5 to 95% range of the CMIP5 models; 0.3°C to 1.7°C (RCP2.6), 1.1°C to 2.6°C (RCP4.5), 1.4°C to 3.1°C (RCP6.0), 2.6°C to 4.8°C (RCP8.5). Global temperatures averaged over the period 2081–2100 are projected to *likely* exceed 1.5°C above 1850-1900 for RCP4.5, RCP6.0 and RCP8.5 (*high confidence*), are *likely* to exceed 2°C above 1850-1900 for RCP6.0 and RCP8.5 (*high confidence*) and are *more likely than not* to exceed 2°C for RCP4.5 (*medium confidence*). Temperature change above 2°C under RCP2.6 is *unlikely* (*medium confidence*). Warming above 4°C by 2081–2100 is *unlikely* in all RCPs (*high confidence*) except for RCP8.5, where it is *about as likely as not* (*medium confidence*). {12.4.1, Tables 12.2, 12.3, Figures 12.5, 12.8}

Temperature change will not be regionally uniform. There is *very high confidence*[2] that globally averaged changes over land will exceed changes over the ocean at the end of the 21st century by a factor that is *likely* in the range 1.4 to 1.7. In the absence of a strong reduction in the Atlantic Meridional Overturning, the Arctic region is projected to warm most (*very high confidence*). This polar amplification is not found in Antarctic regions due to deep ocean mixing, ocean heat uptake and the persistence of the Antarctic ice sheet. Projected regional surface air temperature increase has minima in the North Atlantic and Southern Oceans in all scenarios. One model exhibits marked cooling in 2081–2100 over large parts of the Northern Hemisphere (NH), and a few models indicate slight cooling locally in the North Atlantic. Atmospheric zonal mean temperatures show warming throughout the troposphere, especially in the upper troposphere and northern high latitudes, and cooling in the stratosphere. {12.4.2, 12.4.3, Table 12.2, Figures 12.9, 12.10, 12.11, 12.12}

It is *virtually certain* that, in most places, there will be more hot and fewer cold temperature extremes as global mean temperatures increase. These changes are expected for events defined as extremes on both daily and seasonal time scales. Increases in the frequency, duration and magnitude of hot extremes along with heat stress are expected; however, occasional cold winter extremes will continue to occur. Twenty-year return values of low temperature events are projected to increase at a rate greater than winter mean temperatures in most regions, with the largest changes in the return values of low temperatures at high latitudes. Twenty-year return values for high temperature events are projected to increase at a rate similar to or greater than the rate of increase of summer mean temperatures in most regions. Under RCP8.5 it is *likely* that, in most land regions, a current 20-year high temperature event will occur more frequently by the end of the 21st

[1] In this Report, the following terms have been used to indicate the assessed likelihood of an outcome or a result: Virtually certain 99–100% probability, Very likely 90–100%, Likely 66–100%, About as likely as not 33–66%, Unlikely 0–33%, Very unlikely 0–10%, Exceptionally unlikely 0–1%. Additional terms (Extremely likely: 95–100%, More likely than not >50–100%, and Extremely unlikely 0–5%) may also be used when appropriate. Assessed likelihood is typeset in italics, e.g., *very likely* (see Section 1.4 and Box TS.1 for more details).

[2] In this Report, the following summary terms are used to describe the available evidence: limited, medium, or robust; and for the degree of agreement: low, medium, or high. A level of confidence is expressed using five qualifiers: very low, low, medium, high, and very high, and typeset in italics, e.g., *medium confidence*. For a given evidence and agreement statement, different confidence levels can be assigned, but increasing levels of evidence and degrees of agreement are correlated with increasing confidence (see Section 1.4 and Box TS.1 for more details).

century (at least doubling its frequency, but in many regions becoming an annual or 2-year event) and a current 20-year low temperature event will become exceedingly rare. {12.4.3, Figures 12.13, 12.14}

Changes in Atmospheric Circulation

Mean sea level pressure is projected to decrease in high latitudes and increase in the mid-latitudes as global temperatures rise. In the tropics, the Hadley and Walker Circulations are *likely* to slow down. Poleward shifts in the mid-latitude jets of about 1 to 2 degrees latitude are *likely* at the end of the 21st century under RCP8.5 in both hemispheres (*medium confidence*), with weaker shifts in the NH. In austral summer, the additional influence of stratospheric ozone recovery in the Southern Hemisphere opposes changes due to GHGs there, though the net response varies strongly across models and scenarios. Substantial uncertainty and thus *low confidence* remains in projecting changes in NH storm tracks, especially for the North Atlantic basin. The Hadley Cell is *likely* to widen, which translates to broader tropical regions and a poleward encroachment of subtropical dry zones. In the stratosphere, the Brewer–Dobson circulation is *likely* to strengthen. {12.4.4, Figures 12.18, 12.19, 12.20}

Changes in the Water Cycle

It is *virtually certain* that, in the long term, global precipitation will increase with increased global mean surface temperature. Global mean precipitation will increase at a rate per degree Celsius smaller than that of atmospheric water vapour. It will *likely* increase by 1 to 3% $°C^{-1}$ for scenarios other than RCP2.6. For RCP2.6 the range of sensitivities in the CMIP5 models is 0.5 to 4% $°C^{-1}$ at the end of the 21st century. {12.4.1, Figures 12.6, 12.7}

Changes in average precipitation in a warmer world will exhibit substantial spatial variation. Some regions will experience increases, other regions will experience decreases and yet others will not experience significant changes at all. There is *high confidence* that the contrast of annual mean precipitation between dry and wet regions and that the contrast between wet and dry seasons will increase over most of the globe as temperatures increase. The general pattern of change indicates that high latitude land masses are *likely* to experience greater amounts of precipitation due to the increased specific humidity of the warmer troposphere as well as increased transport of water vapour from the tropics by the end of this century under the RCP8.5 scenario. Many mid-latitude and subtropical arid and semi-arid regions will *likely* experience less precipitation and many moist mid-latitude regions will *likely* experience more precipitation by the end of this century under the RCP8.5 scenario. Globally, for short-duration precipitation events, a shift to more intense individual storms and fewer weak storms is *likely* as temperatures increase. Over most of the mid-latitude land-masses and over wet tropical regions, extreme precipitation events will *very likely* be more intense and more frequent in a warmer world. The global average sensitivity of the 20-year return value of the annual maximum daily precipitation increases ranges from 4% $°C^{-1}$ of local temperature increase (average of CMIP3 models) to 5.3% $°C^{-1}$ of local temperature increase (average of CMIP5 models) but regionally there are wide variations. {12.4.5, Figures 12.10, 12.22, 12.26, 12.27}

Annual surface evaporation is projected to increase as global temperatures rise over most of the ocean and is projected to change over land following a similar pattern as precipitation. Decreases in annual runoff are *likely* in parts of southern Europe, the Middle East, and southern Africa by the end of the 21st century under the RCP8.5 scenario. Increases in annual runoff are *likely* in the high northern latitudes corresponding to large increases in winter and spring precipitation by the end of the 21st century under the RCP8.5 scenario. Regional to global-scale projected decreases in soil moisture and increased risk of agricultural drought are *likely* in presently dry regions and are projected with *medium confidence* by the end of the 21st century under the RCP8.5 scenario. Prominent areas of projected decreases in evaporation include southern Africa and north western Africa along the Mediterranean. Soil moisture drying in the Mediterranean, southwest USA and southern African regions is consistent with projected changes in Hadley Circulation and increased surface temperatures, so surface drying in these regions as global temperatures increase is *likely* with *high confidence* by the end of this century under the RCP8.5 scenario. In regions where surface moistening is projected, changes are generally smaller than natural variability on the 20-year time scale. {12.4.5, Figures 12.23, 12.24, 12.25}

Changes in Cryosphere

It is *very likely* that the Arctic sea ice cover will continue shrinking and thinning year-round in the course of the 21st century as global mean surface temperature rises. At the same time, in the Antarctic, a decrease in sea ice extent and volume is expected, but with *low confidence*. Based on the CMIP5 multi-model ensemble, projections of average reductions in Arctic sea ice extent for 2081–2100 compared to 1986–2005 range from 8% for RCP2.6 to 34% for RCP8.5 in February and from 43% for RCP2.6 to 94% for RCP8.5 in September (*medium confidence*). A nearly ice-free Arctic Ocean (sea ice extent less than 1×10^6 km^2 for at least 5 consecutive years) in September before mid-century is *likely* under RCP8.5 (*medium confidence*), based on an assessment of a subset of models that most closely reproduce the climatological mean state and 1979–2012 trend of the Arctic sea ice cover. Some climate projections exhibit 5- to 10-year periods of sharp summer Arctic sea ice decline—even steeper than observed over the last decade—and it is *likely* that such instances of rapid ice loss will occur in the future. There is little evidence in global climate models of a tipping point (or critical threshold) in the transition from a perennially ice-covered to a seasonally ice-free Arctic Ocean beyond which further sea ice loss is unstoppable and irreversible. In the Antarctic, the CMIP5 multi-model mean projects a decrease in sea ice extent that ranges from 16% for RCP2.6 to 67% for RCP8.5 in February and from 8% for RCP2.6 to 30% for RCP8.5 in September for 2081–2100 compared to 1986–2005. There is, however, *low confidence* in those values as projections because of the wide inter-model spread and the inability of almost all of the available models to reproduce the mean annual cycle, interannual variability and overall increase of the Antarctic sea ice areal coverage observed during the satellite era. {12.4.6, 12.5.5, Figures 12.28, 12.29, 12.30, 12.31}

It is *very likely* that NH snow cover will reduce as global temperatures rise over the coming century. A retreat of permafrost extent with rising global temperatures is *virtually certain*. Snow cover changes result from precipitation and ablation changes, which are sometimes opposite. Projections of the NH spring snow covered area by the end of the 21st century vary between a decrease of 7% (RCP2.6) and a decrease of 25% (RCP8.5), with a pattern that is fairly consistent between models. The projected changes in permafrost are a response not only to warming but also to changes in snow cover, which exerts a control on the underlying soil. By the end of the 21st century, diagnosed near-surface permafrost area is projected to decrease by between 37% (RCP2.6) and 81% (RCP8.5) (*medium confidence*). {12.4.6, Figures 12.32, 12.33}

Changes in the Ocean

The global ocean will warm in all RCP scenarios. The strongest ocean warming is projected for the surface in subtropical and tropical regions. At greater depth the warming is projected to be most pronounced in the Southern Ocean. Best estimates of ocean warming in the top one hundred meters are about 0.6°C (RCP2.6) to 2.0°C (RCP8.5), and about 0.3°C (RCP2.6) to 0.6°C (RCP8.5) at a depth of about 1 km by the end of the 21st century. For RCP4.5 by the end of the 21st century, half of the energy taken up by the ocean is in the uppermost 700 m and 85% is in the uppermost 2000 m. Due to the long time scales of this heat transfer from the surface to depth, ocean warming will continue for centuries, even if GHG emissions are decreased or concentrations kept constant. {12.4.7, 12.5.2–12.5.4, Figure 12.12}

It is *very likely* that the Atlantic Meridional Overturning Circulation (AMOC) will weaken over the 21st century but it is *very unlikely* that the AMOC will undergo an abrupt transition or collapse in the 21st century. Best estimates and ranges for the reduction from CMIP5 are 11% (1 to 24%) in RCP2.6 and 34% (12 to 54%) in RCP8.5. There is *low confidence* in assessing the evolution of the AMOC beyond the 21st century. {12.4.7, Figure 12.35}

Carbon Cycle

When forced with RCP8.5 CO_2 emissions, as opposed to the RCP8.5 CO_2 concentrations, 11 CMIP5 Earth System Models with interactive carbon cycle simulate, on average, a 50 ppm (min to max range –140 to +210 ppm) larger atmospheric CO_2 concentration and 0.2°C (min to max range –0.4 to +0.9°C) larger global surface temperature increase by 2100. {12.4.8, Figures 12.36, 12.37}

Long-term Climate Change, Commitment and Irreversibility

Global temperature equilibrium would be reached only after centuries to millennia if RF were stabilized. Continuing GHG emissions beyond 2100, as in the RCP8.5 extension, induces a total RF above 12 W m^{-2} by 2300. Sustained negative emissions beyond 2100, as in RCP2.6, induce a total RF below 2 W m^{-2} by 2300. The projected warming for 2281–2300, relative to 1986–2005, is 0.0°C to 1.2°C for RCP2.6 and 3.0°C to 12.6°C for RCP8.5 (*medium confidence*). In much the same way as the warming to a rapid increase of forcing is delayed, the cooling after a decrease of RF is also delayed. {12.5.1, Figures 12.43, 12.44}

A large fraction of climate change is largely irreversible on human time scales, unless net anthropogenic CO_2 emissions were strongly negative over a sustained period. For scenarios driven by CO_2 alone, global average temperature is projected to remain approximately constant for many centuries following a complete cessation of emissions. The positive commitment from CO_2 may be enhanced by the effect of an abrupt cessation of aerosol emissions, which will cause warming. By contrast, cessation of emission of short-lived GHGs will contribute a cooling. {12.5.3, 12.5.4, Figures 12.44, 12.45, 12.46, FAQ 12.3}

Equilibrium Climate Sensitivity and Transient Climate Response

Estimates of the equilibrium climate sensitivity (ECS) based on observed climate change, climate models and feedback analysis, as well as paleoclimate evidence indicate that ECS is *likely* in the range 1.5°C to 4.5°C with *high confidence*, *extremely unlikely* less than 1°C (*high confidence*) and *very unlikely* greater than 6°C (*medium confidence*). The transient climate response (TCR) is *likely* in the range 1°C to 2.5°C and *extremely unlikely* greater than 3°C, based on observed climate change and climate models. {Box 12.2, Figures 1, 2}

Climate Stabilization

The principal driver of long-term warming is total emissions of CO_2 and the two quantities are approximately linearly related. The global mean warming per 1000 PgC (transient climate response to cumulative carbon emissions (TCRE)) is *likely* between 0.8°C to 2.5°C per 1000 PgC, for cumulative emissions less than about 2000 PgC until the time at which temperatures peak. To limit the warming caused by anthropogenic CO_2 emissions alone to be *likely* less than 2°C relative to the period 1861-1880, total CO_2 emissions from all anthropogenic sources would need to be limited to a cumulative budget of about 1000 PgC since that period. About half [445 to 585 PgC] of this budget was already emitted by 2011. Accounting for projected warming effect of non-CO_2 forcing, a possible release of GHGs from permafrost or methane hydrates, or requiring a higher likelihood of temperatures remaining below 2°C, all imply a lower budget. {12.5.4, Figures 12.45, 12.46, Box 12.2}

Some aspects of climate will continue to change even if temperatures are stabilized. Processes related to vegetation change, changes in the ice sheets, deep ocean warming and associated sea level rise and potential feedbacks linking for example ocean and the ice sheets have their own intrinsic long time scales and may result in significant changes hundreds to thousands of years after global temperature is stabilized. {12.5.2 to 12.5.4}

Abrupt Change

Several components or phenomena in the climate system could potentially exhibit abrupt or nonlinear changes, and some are known to have done so in the past. Examples include the AMOC, Arctic sea ice, the Greenland ice sheet, the Amazon forest and monsoonal circulations. For some events, there is information on potential consequences, but in general there is *low confidence* and little consensus on the likelihood of such events over the 21st century. {12.5.5, Table 12.4}

12.1 Introduction

Projections of future climate change are not like weather forecasts. It is not possible to make deterministic, definitive predictions of how climate will evolve over the next century and beyond as it is with short-term weather forecasts. It is not even possible to make projections of the frequency of occurrence of all possible outcomes in the way that it might be possible with a calibrated probabilistic medium-range weather forecast. Projections of climate change are uncertain, first because they are dependent primarily on scenarios of future anthropogenic and natural forcings that are uncertain, second because of incomplete understanding and imprecise models of the climate system and finally because of the existence of internal climate variability. The term climate projection tacitly implies these uncertainties and dependencies. Nevertheless, as greenhouse gas (GHG) concentrations continue to rise, we expect to see future changes to the climate system that are greater than those already observed and attributed to human activities. It is possible to understand future climate change using models and to use models to characterize outcomes and uncertainties under specific assumptions about future forcing scenarios.

This chapter assesses climate projections on time scales beyond those covered in Chapter 11, that is, beyond the mid-21st century. Information from a range of different modelling tools is used here; from simple energy balance models, through Earth System Models of Intermediate Complexity (EMICs) to complex dynamical climate and Earth System Models (ESMs). These tools are evaluated in Chapter 9 and, where possible, the evaluation is used in assessing the validity of the projections. This chapter also summarizes some of the information on leading-order measures of the sensitivity of the climate system from other chapters and discusses the relevance of these measures for climate projections, commitments and irreversibility.

Since the AR4 (Meehl et al., 2007b) there have been a number of advances:

- New scenarios of future forcings have been developed to replace the Special Report on Emissions Scenarios (SRES). The Representative Concentration Pathways (RCPs, see Section 12.3) (Moss et al., 2010), have been designed to cover a wide range of possible magnitudes of climate change in models rather than being derived sequentially from storylines of socioeconomic futures. The aim is to provide a range of climate responses while individual socioeconomic scenarios may be derived, scaled and interpolated (some including explicit climate policy). Nevertheless, many studies that have been performed since AR4 have used SRES and, where appropriate, these are assessed. Simplified scenarios of future change, developed strictly for understanding the response of the climate system rather than to represent realistic future outcomes, are also synthesized and the understanding of leading-order measures of climate response such as the equilibrium climate sensitivity (ECS) and the transient climate response (TCR) are assessed.

- New models have been developed with higher spatial resolution, with better representation of processes and with the inclusion of more processes, in particular processes that are important in simulating the carbon cycle of the Earth. In these models, emissions of GHGs may be specified and these gases may be chemically active in the atmosphere or be exchanged with pools in terrestrial and oceanic systems before ending up as an airborne concentration (see Figure 10.1 of AR4).

- New types of model experiments have been performed, many coordinated by the Coupled Model Intercomparison Project Phase 5 (CMIP5) (Taylor et al., 2012), which exploit the addition of these new processes. Models may be driven by emissions of GHGs, or by their concentrations with different Earth System feedback loops cut. This allows the separate assessment of different feedbacks in the system and of projections of physical climate variables and future emissions.

- Techniques to assess and quantify uncertainties in projections have been further developed but a full probabilistic quantification remains difficult to propose for most quantities, the exception being global, temperature-related measures of the system sensitivity to forcings, such as ECS and TCR. In those few cases, projections are presented in the form of probability density functions (PDFs). We make the distinction between the spread of a multi-model ensemble, an *ad hoc* measure of the possible range of projections and the quantification of uncertainty that combines information from models and observations using statistical algorithms. Just like climate models, different techniques for quantifying uncertainty exist and produce different outcomes. Where possible, different estimates of uncertainty are compared.

Although not an advance, as time has moved on, the baseline period from which climate change is expressed has also moved on (a common baseline period of 1986–2005 is used throughout, consistent with the 2006 start-point for the RCP scenarios). Hence climate change is expressed as a change with respect to a recent period of history, rather than a time before significant anthropogenic influence. It should be borne in mind that some anthropogenically forced climate change had already occurred by the 1986–2005 period (see Chapter 10).

The focus of this chapter is on global and continental/ocean basin-scale features of climate. For many aspects of future climate change, it is possible to discuss generic features of projections and the processes that underpin them for such large scales. Where interesting or unique changes have been investigated at smaller scales, and there is a level of agreement between different studies of those smaller-scale changes, these may also be assessed in this chapter, although where changes are linked to climate phenomena such as El Niño, readers are referred to Chapter 14. Projections of atmospheric composition, chemistry and air quality for the 21st century are assessed in Chapter 11, except for CO_2 which is assessed in this chapter. An innovation for AR5 is Annex I: Atlas of Global and Regional Climate Projections, a collection of global and regional maps of projected climate changes derived from model output. A detailed commentary on each of the maps presented in Annex I is not provided here, but some discussion of generic features is provided.

Projections from regional models driven by boundary conditions from global models are not extensively assessed but may be mentioned in this chapter. More detailed regional information may be found in Chapter 14 and is also now assessed in the Working Group II report, where it can more easily be linked to impacts.

12.2 Climate Model Ensembles and Sources of Uncertainty from Emissions to Projections

12.2.1 The Coupled Model Intercomparison Project Phase 5 and Other Tools

Many of the figures presented in this chapter and in others draw on data collected as part of CMIP5 (Taylor et al., 2012). The project involves the worldwide coordination of ESM experiments including the coordination of input forcing fields, diagnostic output and the hosting of data in a distributed archive. CMIP5 has been unprecedented in terms of the number of modelling groups and models participating, the number of experiments performed and the number of diagnostics collected. The archive of model simulations began being populated by mid-2011 and continued to grow during the writing of AR5. The production of figures for this chapter draws on a fixed database of simulations and variables that was available on 15 March 2013 (the same as the cut-off date for the acceptance of the publication of papers). Different figures may use different subsets of models and there are unequal numbers of models that have produced output for the different RCP scenarios. Figure 12.1 gives a summary of which output was available from which model for which scenario. Where multiple runs are performed with exactly the same model but with different initial conditions, we choose only one ensemble member (usually the first but in cases where that was not available, the first available member is chosen) in order not to weight models with more ensemble members than others unduly in the multi-model synthesis. Rather than give an exhaustive account of which models were used to make which figures, this summary information is presented as a guide to readers.

In addition to output from CMIP5, information from a coordinated set of simulations with EMICs is also used (Zickfeld et al., 2013) to investigate long-term climate change beyond 2100. Even more simplified energy balance models or emulation techniques are also used, mostly to estimate responses where ESM experiments are not available (Meinshausen et al., 2011a; Good et al., 2013). An evaluation of the models used for projections is provided in Chapter 9 of this Report.

12.2.2 General Concepts: Sources of Uncertainties

The understanding of the sources of uncertainty affecting future climate change projections has not substantially changed since AR4, but many experiments and studies since then have proceeded to explore and characterize those uncertainties further. A full characterization,

Figure 12.1 | A summary of the output used to make the CMIP5 figures in this chapter (and some figures in Chapter 11). The climate variable names run along the horizontal axis and use the standard abbreviations in the CMIP5 protocol (Taylor et al., 2012, and online references therein). The climate model names run along the vertical axis. In each box the shading indicates the number of ensemble members available for historical, RCP2.6, RCP4.5, RCP6.0, RCP8.5 and pre-industrial control experiments, although only one ensemble member per model is used in the relevant figures.

Frequently Asked Questions

FAQ 12.1 | Why Are So Many Models and Scenarios Used to Project Climate Change?

Future climate is partly determined by the magnitude of future emissions of greenhouse gases, aerosols and other natural and man-made forcings. These forcings are external to the climate system, but modify how it behaves. Future climate is shaped by the Earth's response to those forcings, along with internal variability inherent in the climate system. A range of assumptions about the magnitude and pace of future emissions helps scientists develop different emission scenarios, upon which climate model projections are based. Different climate models, meanwhile, provide alternative representations of the Earth's response to those forcings, and of natural climate variability. Together, ensembles of models, simulating the response to a range of different scenarios, map out a range of possible futures, and help us understand their uncertainties.

Predicting socioeconomic development is arguably even more difficult than predicting the evolution of a physical system. It entails predicting human behaviour, policy choices, technological advances, international competition and cooperation. The common approach is to use scenarios of plausible future socioeconomic development, from which future emissions of greenhouse gases and other forcing agents are derived. It has not, in general, been possible to assign likelihoods to individual forcing scenarios. Rather, a set of alternatives is used to span a range of possibilities. The outcomes from different forcing scenarios provide policymakers with alternatives and a range of possible futures to consider.

Internal fluctuations in climate are spontaneously generated by interactions between components such as the atmosphere and the ocean. In the case of near-term climate change, they may eclipse the effect of external perturbations, like greenhouse gas increases (see Chapter 11). Over the longer term, however, the effect of external forcings is expected to dominate instead. Climate model simulations project that, after a few decades, different scenarios of future anthropogenic greenhouse gases and other forcing agents—and the climate system's response to them—will differently affect the change in mean global temperature (FAQ 12.1, Figure 1, left panel). Therefore, evaluating the consequences of those various scenarios and responses is of paramount importance, especially when policy decisions are considered.

Climate models are built on the basis of the physical principles governing our climate system, and empirical understanding, and represent the complex, interacting processes needed to simulate climate and climate change, both past and future. Analogues from past observations, or extrapolations from recent trends, are inadequate strategies for producing projections, because the future will not necessarily be a simple continuation of what we have seen thus far.

Although it is possible to write down the equations of fluid motion that determine the behaviour of the atmosphere and ocean, it is impossible to solve them without using numerical algorithms through computer model simulation, similarly to how aircraft engineering relies on numerical simulations of similar types of equations. Also, many small-scale physical, biological and chemical processes, such as cloud processes, cannot be described by those equations, either because we lack the computational ability to describe the system at a fine enough resolution to directly simulate these processes or because we still have a partial scientific understanding of the mechanisms driving these processes. Those need instead to be approximated by so-called parameterizations within the climate models, through which a mathematical relation between directly simulated and approximated quantities is established, often on the basis of observed behaviour.

There are various alternative and equally plausible numerical representations, solutions and approximations for modelling the climate system, given the limitations in computing and observations. This diversity is considered a healthy aspect of the climate modelling community, and results in a range of plausible climate change projections at global and regional scales. This range provides a basis for quantifying uncertainty in the projections, but because the number of models is relatively small, and the contribution of model output to public archives is voluntary, the sampling of possible futures is neither systematic nor comprehensive. Also, some inadequacies persist that are common to all models; different models have different strength and weaknesses; it is not yet clear which aspects of the quality of the simulations that can be evaluated through observations should guide our evaluation of future model simulations. *(continued on next page)*

FAQ 12.1 (continued)

Models of varying complexity are commonly used for different projection problems. A faster model with lower resolution, or a simplified description of some climate processes, may be used in cases where long multi-century simulations are required, or where multiple realizations are needed. Simplified models can adequately represent large-scale average quantities, like global average temperature, but finer details, like regional precipitation, can be simulated only by complex models.

The coordination of model experiments and output by groups such as the Coupled Model Intercomparison Project (CMIP), the World Climate Research Program and its Working Group on Climate Models has seen the science community step up efforts to evaluate the ability of models to simulate past and current climate and to compare future climate change projections. The 'multi-model' approach is now a standard technique used by the climate science community to assess projections of a specific climate variable.

FAQ 12.1, Figure 1, right panels, shows the temperature response by the end of the 21st century for two illustrative models and the highest and lowest RCP scenarios. Models agree on large-scale patterns of warming at the surface, for example, that the land is going to warm faster than ocean, and the Arctic will warm faster than the tropics. But they differ both in the magnitude of their global response for the same scenario, and in small scale, regional aspects of their response. The magnitude of Arctic amplification, for instance, varies among different models, and a subset of models show a weaker warming or slight cooling in the North Atlantic as a result of the reduction in deepwater formation and shifts in ocean currents.

There are inevitable uncertainties in future external forcings, and the climate system's response to them, which are further complicated by internally generated variability. The use of multiple scenarios and models have become a standard choice in order to assess and characterize them, thus allowing us to describe a wide range of possible future evolutions of the Earth's climate.

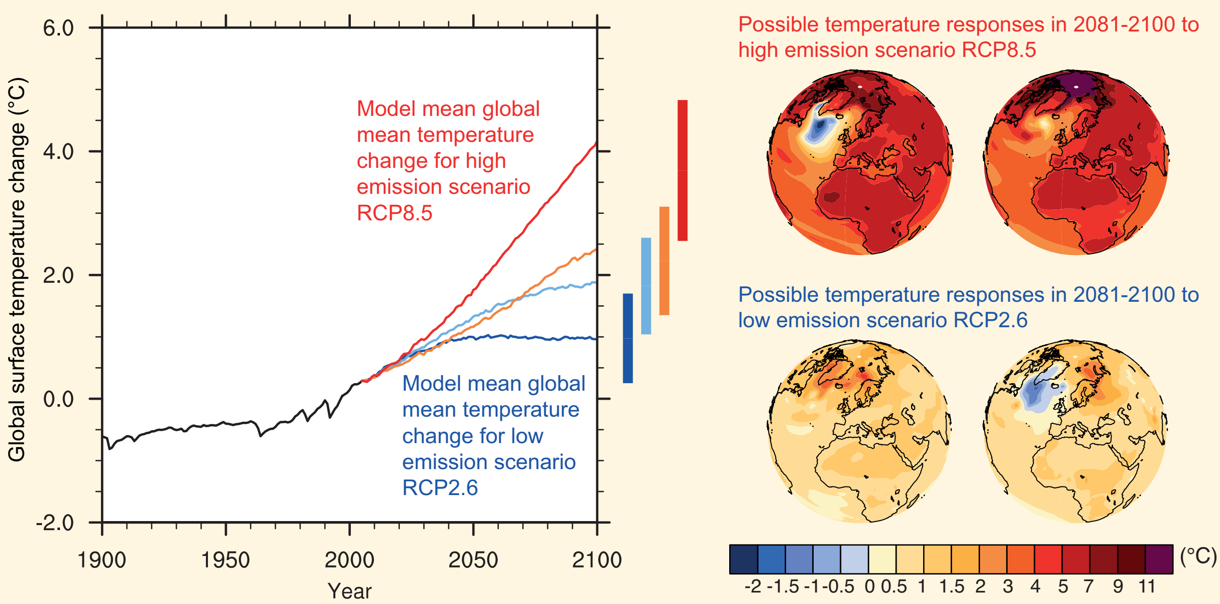

FAQ 12.1, Figure 1 | Global mean temperature change averaged across all Coupled Model Intercomparison Project Phase 5 (CMIP5) models (relative to 1986–2005) for the four Representative Concentration Pathway (RCP) scenarios: RCP2.6 (dark blue), RCP4.5 (light blue), RCP6.0 (orange) and RCP8.5 (red); 32, 42, 25 and 39 models were used respectively for these 4 scenarios. *Likely* ranges for global temperature change by the end of the 21st century are indicated by vertical bars. Note that these ranges apply to the difference between two 20-year means, 2081–2100 relative to 1986–2005, which accounts for the bars being centred at a smaller value than the end point of the annual trajectories. For the highest (RCP8.5) and lowest (RCP2.6) scenario, illustrative maps of surface temperature change at the end of the 21st century (2081–2100 relative to 1986–2005) are shown for two CMIP5 models. These models are chosen to show a rather broad range of response, but this particular set is not representative of any measure of model response uncertainty.

12

qualitative and even more so quantitative, involves much more than a measure of the range of model outcomes, because additional sources of information (e.g., observational constraints, model evaluation, expert judgement) lead us to expect that the uncertainty around the future climate state does not coincide straightforwardly with those ranges. In fact, in this chapter we highlight wherever relevant the distinction between model uncertainty evaluation, which encompasses the understanding that models have intrinsic shortcoming in fully and accurately representing the real system, and cannot all be considered independent of one another (Knutti et al., 2013), and a simpler descriptive quantification, based on the range of outcomes from the ensemble of models.

Uncertainty affecting mid- to long-term projections of climatic changes stems from distinct but possibly interacting sources. Figure 12.2 shows a schematic of the chain from scenarios, through ESMs to projections. Uncertainties affecting near-term projections of which some aspect are also relevant for longer-term projections are discussed in Section 11.3.1.1 and shown in Figure 11.8.

Future anthropogenic emissions of GHGs, aerosol particles and other forcing agents such as land use change are dependent on socioeconomic factors including global geopolitical agreements to control those emissions. Systematic studies that attempt to quantify the likely ranges of anthropogenic emission have been undertaken (Sokolov et al., 2009) but it is more common to use a scenario approach of different but plausible—in the sense of technically feasible—pathways, leading to the concept of *scenario uncertainty*. AR4 made extensive use of the SRES scenarios (IPCC, 2000) developed using a sequential approach, that is, socioeconomic factors feed into emissions scenarios which are then used either to directly force the climate models or to determine concentrations of GHGs and other agents required to drive these models. This report also assesses outcomes of simulations that use the new RCP scenarios, developed using a parallel process (Moss et al., 2010) whereby different targets in terms of RF at 2100 were selected (2.6, 4.5, 6.0 and 8.5 W m^{-2}) and GHG and aerosol emissions consistent with those targets, and their corresponding socioeconomic drivers were developed simultaneously (see Section 12.3). Rather than being identified with one socioeconomic storyline, RCP scenarios are consistent with many possible economic futures (in fact, different combinations of GHG and aerosol emissions can lead to the same RCP). Their development was driven by the need to produce scenarios that could be input to climate model simulations more expediently while corresponding socioeconomic scenarios would be developed in parallel, and to produce a wide range of model responses that may be scaled and interpolated to estimate the response under other scenarios, involving different measures of adaptation and mitigation.

In terms of the uncertainties related to the RCP emissions scenarios, the following issues can be identified:

- No probabilities or likelihoods have been attached to the alternative RCP scenarios (as was the case for SRES scenarios). Each of them should be considered plausible, as no study has questioned their technical feasibility (see Chapter 1).

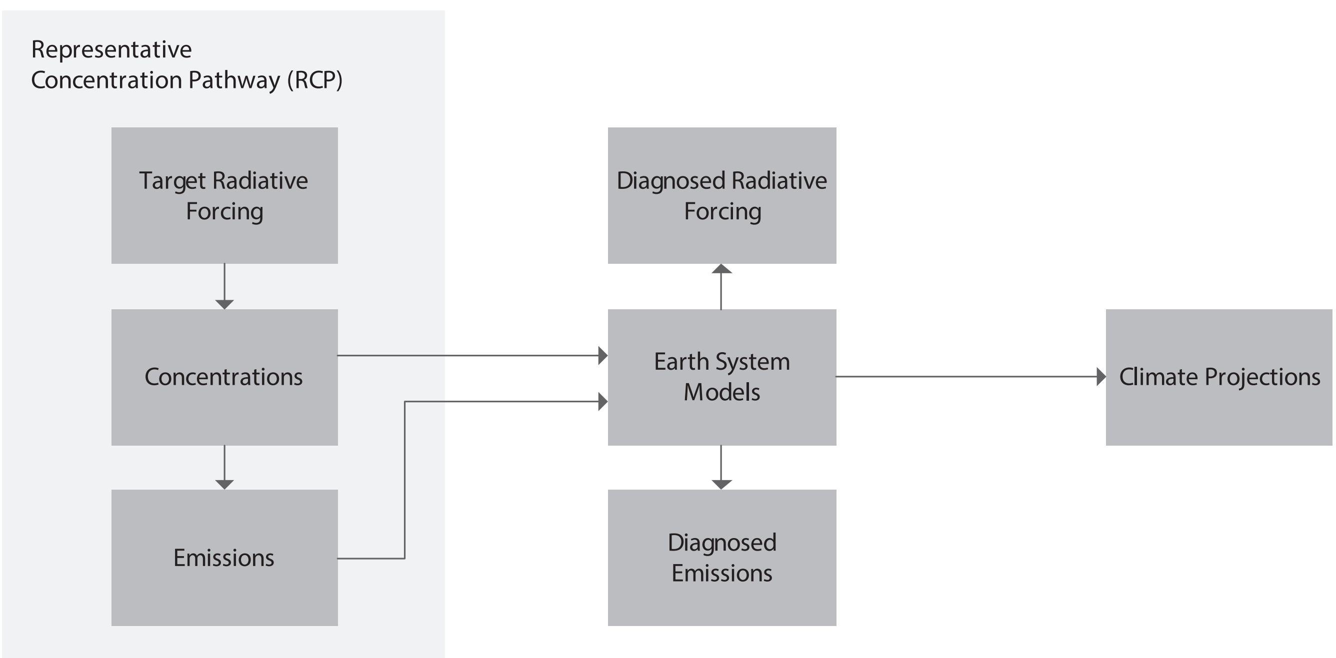

Figure 12.2 | Links in the chain from scenarios, through models to climate projections. The Representative Concentration Pathways (RCPs) are designed to sample a range of radiative forcing (RF) of the climate system at 2100. The RCPs are translated into both concentrations and emissions of greenhouse gases using Integrated Assessment Models (IAMs). These are then used as inputs to dynamical Earth System Models (ESMs) in simulations that are either concentration-driven (the majority of projection experiments) or emissions-driven (only for RCP8.5). Aerosols and other forcing factors are implemented in different ways in each ESM. The ESM projections each have a potentially different RF, which may be viewed as an output of the model and which may not correspond to precisely the level of RF indicated by the RCP nomenclature. Similarly, for concentration-driven experiments, the emissions consistent with those concentrations diagnosed from the ESM may be different from those specified in the RCP (diagnosed from the IAM). Different models produce different responses even under the same RF. Uncertainty propagates through the chain and results in a spread of ESM projections. This spread is only one way of assessing uncertainty in projections. Alternative methods, which combine information from simple and complex models and observations through statistical models or expert judgement, are also used to quantify that uncertainty.

- Despite the naming of the RCPs in terms of their target RF at 2100 or at stabilization (Box 1.1), climate models translate concentrations of forcing agents into RF in different ways due to their different structural modelling assumptions. Hence a model simulation of RCP6.0 may not attain exactly a RF of 6 W m^{-2}; more accurately, an RCP6.0 forced model experiment may not attain exactly the same RF as was intended by the specification of the RCP6.0 forcing inputs. Thus in addition to the scenario uncertainty there is RF uncertainty in the way the RCP scenarios are implemented in climate models.

- Some model simulations are concentration-driven (GHG concentrations are specified) whereas some models, which have Earth Systems components, convert emission scenarios into concentrations and are termed emissions-driven. Different ESMs driven by emissions may produce different concentrations of GHGs and aerosols because of differences in the representation and/or parameterization of the processes responsible for the conversion of emissions into concentrations. This aspect may be considered a facet of forcing uncertainty, or may be compounded in the category of model uncertainty, which we discuss below. Also, aerosol loading and land use changes are not dictated intrinsically by the RCP specification. Rather, they are a result of the Integrated Assessment Model that created the emission pathway for a given RCP.

SRES and RCPs account for future changes only in anthropogenic forcings. With regard to solar forcing, the 1985–2005 solar cycle is repeated. Neither projections of future deviations from this solar cycle, nor future volcanic RF and their uncertainties are considered.

Any climate projection is subject to sampling uncertainties that arise because of internal variability. In this chapter, the prediction of, for example, the amplitude or phase of some mode of variability that may be important on long time scales is not addressed (see Sections 11.2 and 11.3). Any climate variable projection derived from a single simulation of an individual climate model will be affected by internal variability (stemming from the chaotic nature of the system), whether it be a variable that involves a long time average (e.g., 20 years), a snapshot in time or some more complex diagnostic such as the variance computed from a time series over many years. No amount of time averaging can reduce internal variability to zero, although for some EMICs and simplified models, which may be used to reproduce the results of more complex model simulations, the representation of internal variability is excluded from the model specification by design. For different variables, and different spatial and time scale averages, the relative importance of internal variability in comparison with other sources of uncertainty will be different. In general, internal variability becomes more important on shorter time scales and for smaller scale variables (see Section 11.3 and Figure 11.2). The concept of signal-to-noise ratio may be used to quantify the relative magnitude of the forced response (signal) versus internal variability (noise). Internal variability may be sampled and estimated explicitly by running ensembles of simulations with slightly different initial conditions, designed explicitly to represent internal variability, or can be estimated on the basis of long control runs where external forcings are held constant. In the case of both multi-model and perturbed physics ensembles (see below), there is an implicit perturbation in the initial state of each run considered, which means that these ensembles sample both modelling uncertainty and internal variability jointly.

The ability of models to mimic nature is achieved by simplification choices that can vary from model to model in terms of the fundamental numeric and algorithmic structures, forms and values of parameterizations, and number and kinds of coupled processes included. Simplifications and the interactions between parameterized and resolved processes induce ‘errors’ in models, which can have a leading-order impact on projections. It is possible to characterize the choices made when building and running models into structural—indicating the numerical techniques used for solving the dynamical equations, the analytic form of parameterization schemes and the choices of inputs for fixed or varying boundary conditions—and parametric—indicating the choices made in setting the parameters that control the various components of the model. The community of climate modellers has regularly collaborated in producing coordinated experiments forming multi-model ensembles (MMEs), using both global and regional model families, for example, CMIP3/5 (Meehl et al., 2007a), ENSEMBLES (Johns et al., 2011) and Chemistry–Climate Model Validation 1 and 2 (CCM-Val-1 and 2; Eyring et al., 2005), through which structural uncertainty can be at least in part explored by comparing models, and perturbed physics ensembles (PPEs, with e.g., Hadley Centre Coupled Model version 3 (HadCM3; Murphy et al., 2004), Model for Interdiciplinary Research On Climate (MIROC; Yokohata et al., 2012), Community Climate System Model 3 (CCSM3; Jackson et al., 2008; Sanderson, 2011)), through which uncertainties in parameterization choices can be assessed in a given model. As noted below, neither MMEs nor PPEs represent an adequate sample of all the possible choices one could make in building a climate model. Also, current models may exclude some processes that could turn out to be important for projections (e.g., methane clathrate release) or produce a common error in the representation of a particular process. For this reason, it is of critical importance to distinguish two different senses in which the uncertainty terminology is used or misused in the literature (see also Sections 1.4.2, 9.2.2, 9.2.3, 11.2.1 and 11.2.2). A narrow interpretation of the concept of model uncertainty often identifies it with the range of responses of a model ensemble. In this chapter this type of characterization is referred as model range or model spread. A broader concept entails the recognition of a fundamental uncertainty in the representation of the real system that these models can achieve, given their necessary approximations and the limits in the scientific understanding of the real system that they encapsulate. When addressing this aspect and characterizing it, this chapter uses the term model uncertainty.

The relative role of the different sources of uncertainty—model, scenario and internal variability—as one moves from short- to mid- to long-term projections and considers different variables at different spatial scales has to be recognized (see Section 11.3). The three sources exchange relevance as the time horizon, the spatial scale and the variable change. In absolute terms, internal variability is generally estimated, and has been shown in some specific studies (Hu et al., 2012) to remain approximately constant across the forecast horizon, with model ranges and scenario/forcing variability increasing over time. For forecasts of global temperatures after mid-century, scenario and model ranges dominate the amount of variation due to internally generated variability, with scenarios accounting for the largest source of uncertainty in projections by the end of the century. For global average precipitation projections, scenario uncertainty has a much smaller role even by the end of the 21st century and model range maintains the largest share across all projection horizons. For temperature and precipitation projections at smaller spatial scales, internal variability may remain a significant source of uncertainty up until middle of the 21st century in some regions (Hawkins and Sutton, 2009, 2011; Rowell, 2012; Knutti and Sedláček, 2013). Within single model experiments, the persistently significant role of internally generated variability for regional projections even beyond short- and mid-term horizons has been documented by analyzing relatively large ensembles sampling initial conditions (Deser et al., 2012a, 2012b).

12.2.3 From Ensembles to Uncertainty Quantification

Ensembles like CMIP5 do not represent a systematically sampled family of models but rely on self-selection by the modelling groups. This opportunistic nature of MMEs has been discussed, for example, in Tebaldi and Knutti (2007) and Knutti et al. (2010a). These ensembles are therefore not designed to explore uncertainty in a coordinated manner, and the range of their results cannot be straightforwardly interpreted as an exhaustive range of plausible outcomes, even if some studies have shown how they appear to behave as well calibrated probabilistic forecasts for some large-scale quantities (Annan and Hargreaves, 2010). Other studies have argued instead that the tail of distributions is by construction undersampled (Räisänen, 2007). In general, the difficulty in producing quantitative estimates of uncertainty based on multiple model output originates in their peculiarities as a statistical sample, neither random nor systematic, with possible dependencies among the members (Jun et al., 2008; Masson and Knutti, 2011; Pennell and Reichler, 2011; Knutti et al., 2013) and of spurious nature, that is, often counting among their members models with different degrees of complexities (different number of processes explicitly represented or parameterized) even within the category of general circulation models.

Agreement between multiple models can be a source of information in an uncertainty assessment or confidence statement. Various methods have been proposed to indicate regions where models agree on the projected changes, agree on no change or disagree. Several of those methods are compared in Box 12.1. Many figures use stippling or hatching to display such information, but it is important to note that confidence cannot be inferred from model agreement alone.

Perturbed physics experiments (PPEs) differ in their output interpretability for they can be, and have been, systematically constructed and as such lend themselves to a more straightforward treatment through statistical modelling (Rougier, 2007; Sanso and Forest, 2009). Uncertain parameters in a single model to whose values the output is known to be sensitive are targeted for perturbations. More often it is the parameters in the atmospheric component of the model that are varied (Collins et al., 2006a; Sanderson et al., 2008), and to date have in fact shown to be the source of the largest uncertainties in large-scale response, but lately, with much larger computing power expense, also parameters within the ocean component have been perturbed (Collins et al., 2007; Brierley et al., 2010). Parameters in the land surface schemes have also been subject to perturbation studies (Fischer et al., 2011; Booth et al., 2012; Lambert et al., 2012). Ranges of possible values are explored and often statistical models that fit the relationship between parameter values and model output, that is, emulators, are trained on the ensemble and used to predict the outcome for unsampled parameter value combinations, in order to explore the parameter space more thoroughly that would otherwise be computationally affordable (Rougier et al., 2009). The space of a single model simulations (even when filtered through observational constraints) can show a large range of outcomes for a given scenario (Jackson et al., 2008). However, multi-model ensembles and perturbed physics ensembles produce modes and distributions of climate responses that can be different from one another, suggesting that one type of ensemble cannot be used as an analogue for the other (Murphy et al., 2007; Sanderson et al., 2010; Yokohata et al., 2010; Collins et al., 2011).

Many studies have made use of results from these ensembles to characterize uncertainty in future projections, and these will be assessed and their results incorporated when describing specific aspects of future climate responses. PPEs have been uniformly treated across the different studies through the statistical framework of analysis of computer experiments (Sanso et al., 2008; Rougier et al., 2009; Harris et al., 2010) or, more plainly, as a thorough exploration of alternative responses reweighted by observational constraints (Murphy et al., 2004; Piani et al., 2005; Forest et al., 2008; Sexton et al., 2012). In all cases the construction of a probability distribution is facilitated by the systematic nature of the experiments. MMEs have generated a much more diversified treatment (1) according to the choice of applying weights to the different models on the basis of past performance or not (Weigel et al., 2010) and (2) according to the choice between treating the different models and the truth as indistinguishable or treating each model as a version of the truth to which an error has been added (Annan and Hargreaves, 2010; Sanderson and Knutti, 2012). Many studies can be classified according to these two criteria and their combination, but even within each of the four resulting categories different studies produce different estimates of uncertainty, owing to the preponderance of *a priori* assumptions, explicitly in those studies that approach the problem through a Bayesian perspective, or only implicit in the choice of likelihood models, or weighting. This makes the use of probabilistic and other results produced through statistical inference necessarily dependent on agreeing with a particular set of assumptions (Sansom et al., 2013), given the lack of a full exploration of the robustness of probabilistic estimates to varying these assumptions.

In summary, there does not exist at present a single agreed on and robust formal methodology to deliver uncertainty quantification estimates of future changes in all climate variables (see also Section 9.8.3 and Stephenson et al., 2012). As a consequence, in this chapter, statements using the calibrated uncertainty language are a result of the expert judgement of the authors, combining assessed literature results with an evaluation of models demonstrated ability (or lack thereof) in simulating the relevant processes (see Chapter 9) and model consensus (or lack thereof) over future projections. In some cases when a significant relation is detected between model performance and reliability of its future projections, some models (or a particular parametric configuration) may be excluded (e.g., Arctic sea ice; Section 12.4.6.1 and Joshi et al., 2010) but in general it remains an open research question to find significant connections of this kind that justify some form of weighting across the ensemble of models and produce aggregated

Box 12.1 | Methods to Quantify Model Agreement in Maps

The climate change projections in this report are based on ensembles of climate models. The ensemble mean is a useful quantity to characterize the average response to external forcings, but does not convey any information on the robustness of this response across models, its uncertainty and/or likelihood or its magnitude relative to unforced climate variability. In the IPCC AR4 WGI contribution (IPCC, 2007) several criteria were used to indicate robustness of change, most prominently in Figure SPM.7. In that figure, showing projected precipitation changes, stippling marked regions where at least 90% of the CMIP3 models agreed on the sign of the change. Regions where less than 66% of the models agreed on the sign were masked white. The resulting large white area was often misinterpreted as indicating large uncertainties in the different models' response to external forcings, but recent studies show that, for the most part, the disagreement in sign among models is found where projected changes are small and still within the modelled range of internal variability, that is, where a response to anthropogenic forcings has not yet emerged locally in a statistically significant way (Tebaldi et al., 2011; Power et al., 2012).

A number of methods to indicate model robustness, involving an assessment of the significance of the change when compared to internal variability, have been proposed since AR4. The different methods share the purpose of identifying regions with large, significant or robust changes, regions with small changes, regions where models disagree or a combination of those. They do, however, use different assumptions about the statistical properties of the model ensemble, and therefore different criteria for synthesizing the information from it. Different methods also differ in the way they estimate internal variability. We briefly describe and compare several of these methods here.

Method (a): The default method used in Chapters 11,12 and 14 as well as in the Annex I (hatching only) is shown in Box 12.1, Figure 1a, and is based on relating the climate change signal to internal variability in 20-year means of the models as a reference[3]. Regions where the multi-model mean change exceeds two standard deviations of internal variability and where at least 90% of the models agree on the sign of change are stippled and interpreted as 'large change with high model agreement'. Regions where the model mean is less than one standard deviation of internal variability are hatched and interpreted as 'small signal or low agreement of models'. This can have various reasons: (1) changes in individual models are smaller than internal variability, or (2) although changes in individual models are significant, they disagree about the sign and the multi-model mean change remains small. Using this method, the case where all models scatter widely around zero and the case where all models agree on near zero change therefore are both hatched (e.g., precipitation change over the Amazon region by the end of the 21st century, which the following methods mark as 'inconsistent model response').

Method (b): Method (a) does not distinguish the case where all models agree on no change and the case where, for example, half of the models show a significant increase and half a decrease. The distinction may be relevant for many applications and a modification of method (a) is to restrict hatching to regions where there is high agreement among the models that the change will be 'small', thus eliminating the ambiguous interpretation 'small or low agreement' in (a). In contrast to method (a) where the model mean is compared to variability, this case (b) marks regions where at least 80% of the individual models show a change smaller than two standard deviations of variability with hatching. Grid points where many models show significant change but don't agree are no longer hatched (Box 12.1, Figure 1b).

Method (c): Knutti and Sedláček (2013) define a dimensionless robustness measure, R, which is inspired by the signal-to-noise ratio and the ranked probability skill score. It considers the natural variability and agreement on magnitude and sign of change. A value of $R = 1$ implies perfect model agreement; low or negative values imply poor model agreement (note that by definition R can assume any negative value). Any level of R can be chosen for the stippling. For illustration, in Box 12.1, Figure 1c, regions with $R > 0.8$ are marked with small dots, regions with $R > 0.9$ with larger dots and are interpreted as 'robust large change'. This yields similar results to method (a) for the end of the century, but with some areas of moderate model robustness ($R > 0.8$) already for the near-term projections, even though the signal is still within the noise. Regions where at least 80% of the models individually show no significant change are hatched and interpreted as 'changes unlikely to emerge from variability'[4]. There is less hatching in this method than in method (a),

(continued on next page)

[3] The internal variability in this method is estimated using pre-industrial control runs for each of the models which are at least 500 years long. The first 100 years of the pre-industrial are ignored. Variability is calculated for every grid point as the standard deviation of non-overlapping 20-year means, multiplied by the square root of 2 to account for the fact that the variability of a difference in means is of interest. A quadratic fit as a function of time is subtracted from these at every grid point to eliminate model drift. This is by definition the standard deviation of the difference between two independent 20-year averages having the same variance and estimates the variation of that difference that would be expected due to unforced internal variability. The median across all models of that quantity is used.

[4] Variability in methods b–d is estimated from interannual variations in the base period within each model.

Box 12.1 (continued)

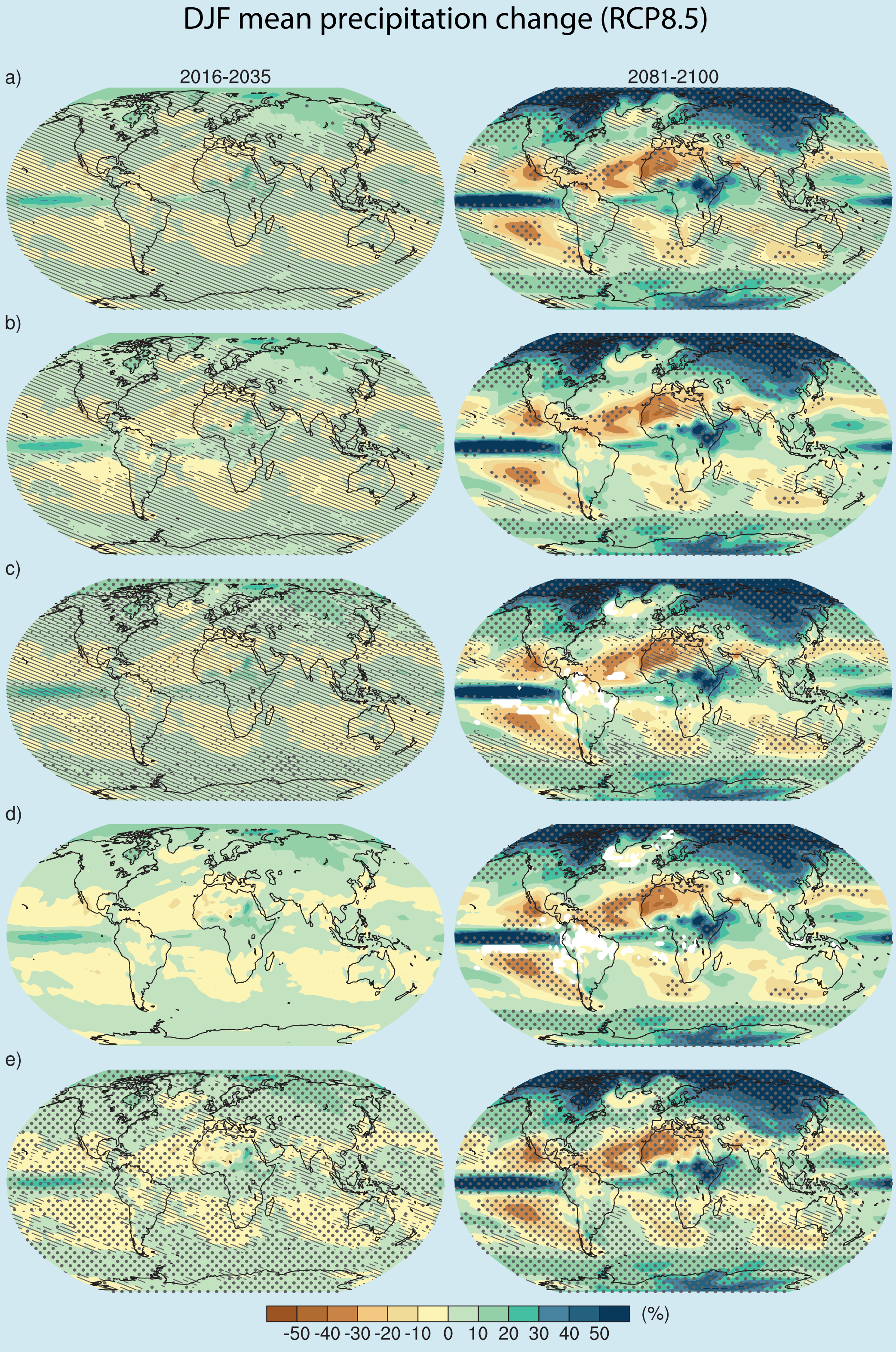

Box 12.1, Figure 1 | Projected change in December to February precipitation for 2016–2035 and 2081–2100, relative to 1986–2005 from CMIP5 models. The choice of the variable and time frames is just for illustration of how the different methods compare in cases with low and high signal-to-noise ratio (left and right column, respectively). The colour maps are identical along each column and only stippling and hatching differ on the basis of the different methods. Different methods for stippling and hatching are shown determined (a) from relating the model mean to internal variability, (b) as in (a) but hatching here indicates high agreement for 'small change', (c) by the robustness measure by Knutti and Sedláček (2013), (d) by the method proposed by Tebaldi et al. (2011) and (e) by the method by Power et al. (2012). Detailed technical explanations for each method are given in the text. 39 models are used in all panels.

Box 12.1 (continued)

because it requires 80% of the models to be within variability, not just the model average. Regions where at least 50% of the models show significant change but $R < 0.5$ are masked as white to indicate 'models disagreeing on the projected change projections' (Box 12.1, Figure 1c).

Method (d): Tebaldi et al. (2011) start from IPCC AR4 SPM7 but separate lack of model agreement from lack of signal (Box 12.1, Figure 1e). Grid points are stippled and interpreted as 'robust large change' when more than 50% of the models show significant change and at least 80% of those agree on the sign of change. Grid points where more than 50% of the models show significant change but less than 80% of those agree on the sign of change are masked as white and interpreted as 'unreliable'. The results are again similar to the methods above. No hatching was defined in that method (Box 12.1 Figure 1d). (See also Neelin et al., 2006 for a similar approach applied to a specific regional domain.)

Method (e): Power et al. (2012) identify three distinct regions using various methods in which projections can be very loosely described as either: 'statistically significant', 'small (relative to temporal variability) or zero, but not statistically significant' or 'uncertain'. The emphasis with this approach is to identify robust signals taking the models at face value and to address the questions: (1) What will change? (2) By how much? and (3) What will not change? The underlying consideration here is that statistical testing under the assumption of model independence provides a worthwhile, albeit imperfect, line of evidence that needs to be considered in conjunction with other evidence (e.g., degree of interdependence, ability of models to simulate the past), in order to assess the degree of confidence one has in a projected change.

The examples given here are not exhaustive but illustrate the main ideas. Other methods include simply counting the number of models agreeing on the sign (Christensen et al., 2007), or varying colour hue and saturation to indicate magnitude of change and robustness of change separately (Kaye et al., 2012). In summary, there are a variety of ways to characterize magnitude or significance of change, and agreement between models. There is also a compromise to make between clarity and richness of information. Different methods serve different purposes and a variety of criteria can be justified to highlight specific properties of multi-model ensembles. Clearly only a subset of information regarding robust and uncertain change can be conveyed in a single plot. The methods above convey some important pieces of this information, but obviously more information could be provided if more maps with additional statistics were provided. In fact Annex I provides more explicit information on the range of projected changes evident in the models (e.g., the median, and the upper and lower quartiles). For most of the methods there is a necessity to choose thresholds for the level of agreement that cannot be identified objectively, but could be the result of individual, application-specific evaluations. Note also that all of the above methods measure model agreement in an ensemble of opportunity, and it is impossible to derive a confidence or likelihood statement from the model agreement or model spread alone, without considering consistency with observations, model dependence and the degree to which the relevant processes are understood and reflected in the models (see Section 12.2.3).

The method used by Power et al. (2012) differs from the other methods in that it tests the statistical significance of the ensemble mean rather than a single simulation. As a result, the area where changes are significant increases with an increasing number of models. Already for the period centred on 2025, most of the grid points when using this method show significant change in the ensemble mean whereas in the other methods projections for this time period are classified as changes not exceeding internal variability. The reason is that the former produces a statement about the mean of the distribution being significantly different from zero, equivalent to treating the ensemble as 'truth plus error', that is, assuming that the models are independent and randomly distributed around reality. Methods a–d, on the other hand, use an 'indistinguishable' interpretation, in which each model and reality are drawn from the same distribution. In that case, the stippling and hatching characterize the likelihood of a single member being significant or not, rather than the ensemble mean. There is some debate in the literature on how the multi-model ensembles should be interpreted statistically. This and past IPCC reports treat the model spread as some measure of uncertainty, irrespective of the number of models, which implies an 'indistinguishable' interpretation. For a detailed discussion readers are referred to the literature (Tebaldi and Knutti, 2007; Annan and Hargreaves, 2010; Knutti et al., 2010a, 2010b; Annan and Hargreaves, 2011a; Sanderson and Knutti, 2012).

future projections that are significantly different from straightforward one model–one vote (Knutti, 2010) ensemble results. Therefore, most of the analyses performed for this chapter make use of all available models in the ensembles, with equal weight given to each of them unless otherwise stated.

12.2.4 Joint Projections of Multiple Variables

While many of the key processes relevant to the simulation of single variables are understood, studies are only starting to focus on assessing projections of joint variables, especially when extremes or variability in the individual quantities are of concern. A few studies have addressed projected changes in joint variables, for example, by combining mean temperature and precipitation (Williams et al., 2007; Tebaldi and Lobell, 2008; Tebaldi and Sanso, 2009; Watterson, 2011; Watterson and Whetton, 2011a; Sexton et al., 2012), linking soil moisture, precipitation and temperature mean and variability (Seneviratne et al., 2006; Fischer and Schär, 2009; Koster et al., 2009b, 2009c), combining temperature and humidity (Diffenbaugh et al., 2007; Fischer and Schär, 2010; Willett and Sherwood, 2012), linking summertime temperature and soil moisture to prior winter snowpack (Hall et al., 2008) or linking precipitation change to circulation, moisture and moist static energy budget changes (Neelin et al., 2003; Chou and Neelin, 2004; Chou et al., 2006, 2009). Models may have difficulties simulating all relevant interactions between atmosphere and land surface and the water cycle that determine the joint response, observations to evaluate models are often limited (Seneviratne et al., 2010), and model uncertainties are therefore large (Koster et al., 2006; Boé and Terray, 2008; Notaro, 2008; Fischer et al., 2011). In some cases, correlations between, for example, temperature and precipitation or accumulated precipitation and temperature have found to be too strong in climate models (Trenberth and Shea, 2005; Hirschi et al., 2011). The situation is further complicated by the fact that model biases in one variable affect other variables. The standard method for model projections is to subtract model biases derived from control integrations (assuming that the bias remains constant in a future scenario integration). Several studies note that this may be problematic when a consistent treatment of biases in multiple variables is required (Christensen et al., 2008; Buser et al., 2009), but there is no consensus at this stage for a methodology addressing this problem (Ho et al., 2012). More generally the existence of structural errors in models according to which an unavoidable discrepancy (Rougier, 2007) between their simulations and reality cannot be avoided is relevant here, as well as for univariate projections. In the recent literature an estimate of this discrepancy has been proposed through the use of MMEs, using each model in turn as a surrogate for reality, and measuring the distance between it and the other models of the ensemble. Some summary statistic of these measures is then used to estimate the distance between models and the real world (Sexton and Murphy, 2012; Sexton et al., 2012; Sanderson, 2013). Statistical frameworks to deal with multivariate projections are challenging even for just two variables, as they have to address a trade-off between modelling the joint behavior at scales that are relevant for impacts—that is, fine spatial and temporal scales, often requiring complex spatio-temporal models—and maintaining computational feasibility. In one instance (Tebaldi and Sanso, 2009) scales were investigated at the seasonal and sub-continental level, and projections of the forced response of temperature and precipitation at those scales did not show significant correlations, likely because of the heterogeneity of the relation between the variables within those large averaged regions and seasons. In Sexton et al. (2012) the spatial scale focussed on regions of Great Britain and correlation emerged as more significant, for example, between summer temperatures and precipitation amounts. Fischer and Knutti (2013) estimated strong relationships between variables making up impact relevant indices (e.g., temperature and humidity) and showed how in some cases, uncertainties across models are larger for a combined variable than if the uncertainties in the individual underlying variables were treated independently (e.g., wildfires), whereas in other cases the uncertainties in the combined variables are smaller than in the individual ones (e.g., heat stress for humans).

Even while recognizing the need for joint multivariate projections, the above limitations at this stage prevent a quantitative assessment for most cases. A few robust qualitative relationships nonetheless emerge from the literature and these are assessed, where appropriate, in the rest of the chapter. For applications that are sensitive to relationships between variables, but still choose to use the multi-model framework to determine possible ranges for projections, sampling from univariate ranges may lead to unrealistic results when significant correlations exist. IPCC assessments often show model averages as best estimates, but such averages can underestimate spatial variability, and more in general they neither represent any of the actual model states (Knutti et al., 2010a) nor do they necessarily represent the joint best estimate in a multivariate sense. Impact studies usually need temporally and spatially coherent multivariate input from climate model simulations. In those cases, using each climate model output individually and feeding it into the impact model, rather than trying to summarise a multivariate distribution from the MME and sample from it, is likely to be more consistent, assuming that the climate model itself correctly captures the spatial covariance, the temporal co-evolution and the relevant feedbacks.

12.3 Projected Changes in Forcing Agents, Including Emissions and Concentrations

The experiments that form the basis of global future projections discussed in this chapter are extensions of the simulations of the observational record discussed in Chapters 9 and 10. The scenarios assessed in AR5, introduced in Chapter 1, include four new scenarios designed to explore a wide range of future climate characterized by representative trajectories of well-mixed greenhouse gas (WMGHG) concentrations and other anthropogenic forcing agents. These are described further in Section 12.3.1. The implementation of forcing agents in model projections, including natural and anthropogenic aerosols, ozone and land use change are discussed in Section 12.3.2, with a strong focus on CMIP5 experiments. Global mean emissions, concentrations and RFs applicable to the historical record simulations assessed in Chapters 8, 9 and 10, and the future scenario simulations assessed here, are listed in Annex II. Global mean RF for the 21st century consistent with these scenarios, derived from CMIP5 and other climate model studies, is discussed in Section 12.3.3.

12.3.1 Description of Scenarios

Long-term climate change projections reflect how human activities or natural effects could alter the climate over decades and centuries. In this context, defined scenarios are important, as using specific time series of emissions, land use, atmospheric concentrations or RF across multiple models allows for coherent climate model intercomparisons and synthesis. Some scenarios present a simple stylized future (not accompanied by a socioeconomic storyline) and are used for process understanding. More comprehensive scenarios are produced by Integrated Assessment Models (IAMs) as internally consistent sets of emissions and socioeconomic assumptions (e.g., regarding population and socioeconomic development) with the aim of presenting several plausible future worlds (see Section 1.5.2 and Box 1.1). In general it is these scenarios that are used for policy relevant climate change, impact, adaptation and mitigation analysis. It is beyond the scope of this report to consider the full range of currently published scenarios and their implications for mitigation policy and climate targets—that is covered by the Working Group III contribution to the AR5. Here, we focus on the RCP scenarios used within the CMIP5 intercomparison exercise (Taylor et al. 2012) along with the SRES scenarios (IPCC, 2000) developed for the IPCC Third Assessment Report (TAR) but still widely used by the climate community.

12.3.1.1 Stylized Concentration Scenarios

A 1% per annum compound increase of atmospheric CO_2 concentration until a doubling or a quadrupling of its initial value has been widely used since the second phase of CMIP (Meehl et al., 2000) and the Second Assessment Report (Kattenberg et al., 1996). This stylized scenario is a useful benchmark for comparing coupled model climate sensitivity, climate feedback and transient climate response, but is not used directly for future projections. The exponential increase of CO_2 concentration induces approximately a linear increase in RF due to a 'saturation effect' of the strong absorbing bands (Augustsson and Ramanathan, 1977; Hansen et al., 1988; Myhre et al., 1998). Thus, a linear ramp function in forcing results from these stylized pathways, adding to their suitability for comparative diagnostics of the models' climate feedbacks and inertia. The CMIP5 intercomparison project again includes such a stylized pathway, in which the CO_2 concentration reaches twice the initial concentration after 70 years and four times the initial concentration after 140 years. The corresponding RFs are 3.7 W m^{-2} (Ramaswamy et al., 2001) and 7.4 W m^{-2} respectively with a range of ±20% accounting for uncertainties in radiative transfer calculations and rapid adjustments (see Section 8.3.2.1), placing them within the range of the RFs at the end of the 21st century for the future scenarios presented below. The CMIP5 project also includes a second stylized experiment in which the CO_2 concentration is quadrupled instantaneously, which allows a distinction between effective RFs and longer-term climate feedbacks (Gregory et al., 2004).

12.3.1.2 The Socioeconomic Driven Scenarios from the Special Report on Emission Scenarios

The climate change projections undertaken as part of CMIP3 and discussed in AR4 were based primarily on the SRES A2, A1B and B1 scenarios (IPCC, 2000). These scenarios were developed using IAMs and resulted from specific socioeconomic scenarios, that is, from storylines about future demographic and economic development, regionalization, energy production and use, technology, agriculture, forestry, and land use. All SRES scenarios assumed that no climate mitigation policy would be undertaken. Based on these SRES scenarios, global climate models were then forced with corresponding WMGHG and aerosol concentrations, although the degree to which models implemented these forcings differed (Meehl et al., 2007b, Table 10.1). The resulting climate projections, together with the socioeconomic scenarios on which they are based, have been widely used in further analysis by the impact, adaptation and vulnerability research communities.

12.3.1.3 The New Concentration Driven Representative Concentration Pathway Scenarios, and Their Extensions

As introduced in Box 1.1 and mentioned in Section 12.1, a new parallel process for scenario development was proposed in order to facilitate the interactions between the scientific communities working on climate change, adaptation and mitigation (Hibbard et al., 2007; Moss et al., 2008, 2010; van Vuuren et al., 2011). These new scenarios, Representative Concentration Pathways, are referred to as pathways in order to emphasize that they are not definitive scenarios, but rather internally consistent sets of time-dependent forcing projections that could potentially be realized with more than one underlying socioeconomic scenario. The primary products of the RCPs are concentrations but they also provide gas emissions. They are representative in that they are one of several different scenarios, sampling the full range of published scenarios (including mitigation scenarios) at the time they were defined, that have similar RF and emissions characteristics. They are identified by the approximate value of the RF (in W m^{-2}) at 2100 or at stabilization after 2100 in their extensions, relative to pre-industrial (Moss et al., 2008; Meinshausen et al., 2011c). RCP2.6 (the lowest of the four, also referred to as RCP3-PD) peaks at 3.0 W m^{-2} and then declines to 2.6 W m^{-2} in 2100, RCP4.5 (medium-low) and RCP6.0 (medium-high) stabilize after 2100 at 4.2 and 6.0 W m^{-2} respectively, while RCP8.5 (highest) reaches 8.3 W m^{-2} in 2100 on a rising trajectory (see also Figure 12.3a which takes into account the efficacies of the various anthropogenic forcings). The primary objective of these scenarios is to provide all the input variables necessary to run comprehensive climate models in order to reach a target RF (Figure 12.2). These scenarios were developed using IAMs that provide the time evolution of a large ensemble of anthropogenic forcings (concentration and emission of gas and aerosols, land use changes, etc.) and their individual RF values (Moss et al., 2008, 2010; van Vuuren et al., 2011). Note that due to the substantial uncertainties in RF, these forcing values should be understood as comparative 'labels', not as exact definitions of the forcing that is effective in climate models. This is because concentrations or emissions, rather than the RF itself, are prescribed in the CMIP5 climate model runs. The forcing as manifested in climate models is discussed in Section 12.3.3.

Various steps were necessary to turn the selected 'raw' RCP scenarios from the IAMs into data sets usable by the climate modelling community. First, harmonization with historical data was performed for emissions of reactive gases and aerosols (Lamarque et al., 2010; Granier et al., 2011; Smith et al., 2011), land use (Hurtt et al., 2011), and for GHG emissions and concentrations (Meinshausen et al., 2011c). Then

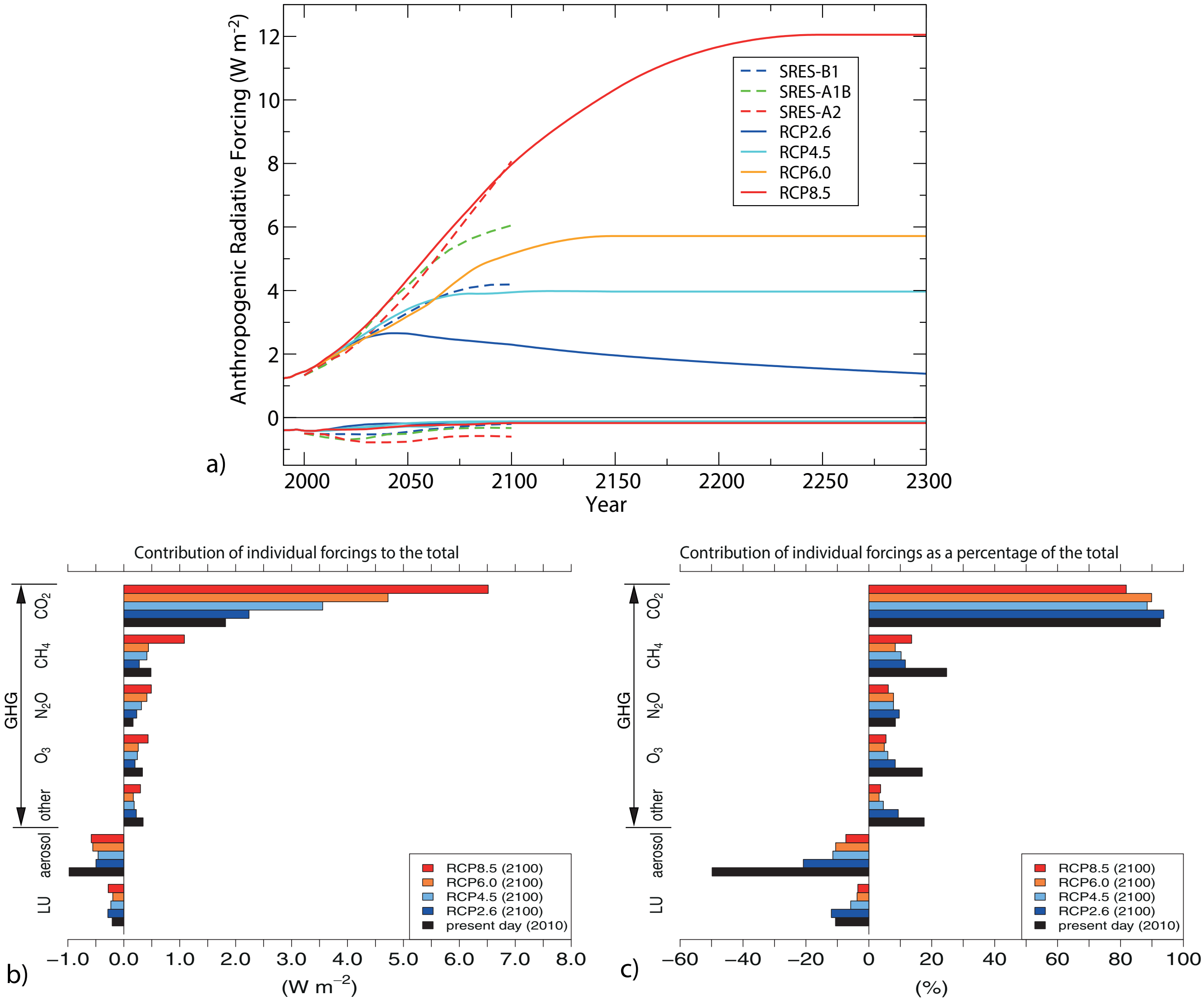

Figure 12.3 | (a) Time evolution of the total anthropogenic (positive) and anthropogenic aerosol (negative) radiative forcing (RF) relative to pre-industrial (about 1765) between 2000 and 2300 for RCP scenarios and their extensions (continuous lines), and SRES scenarios (dashed lines) as computed by the Integrated Assessment Models (IAMs) used to develop those scenarios. The four RCP scenarios used in CMIP5 are: RCP2.6 (dark blue), RCP4.5 (light blue), RCP6.0 (orange) and RCP8.5 (red). The three SRES scenarios used in CMIP3 are: B1 (blue, dashed), A1B (green, dashed) and A2 (red, dashed). Positive values correspond to the total anthropogenic RF. Negative values correspond to the forcing from all anthropogenic aerosol–radiation interactions (i.e., direct effects only). The total RF of the SRES and RCP families of scenarios differs in 2000 because the number of forcings represented and our knowledge about them have changed since the TAR. The total RF of the RCP family is computed taking into account the efficacy of the various forcings (Meinshausen et al., 2011a). (b) Contribution of the individual anthropogenic forcings to the total RF in year 2100 for the four RCP scenarios and at present day (year 2010). The individual forcings are gathered into seven groups: carbon dioxide (CO_2), methane (CH_4), nitrous oxide (N_2O), ozone (O_3), other greenhouse gases, aerosol (all effects unlike in (a), i.e., aerosol–radiation and aerosol–cloud interactions, aerosol deposition on snow) and land use (LU). (c) As in (b), but the individual forcings are relative to the total RF (i.e., RF_x/RF_{tot}, in %, with RF_x individual RFs and RF_{tot} total RF). Note that the RFs in (b) and (c) are not efficacy adjusted, unlike in (a). The values shown in (a) are summarized in Table AII.6.8. The values shown in (b) and (c) have been directly extracted from data files (hosted at http://tntcat.iiasa.ac.at:8787/RcpDb/) compiled by the four modelling teams that developed the RCP scenarios and are summarized in Tables AII.6.1 to AII.6.3 for CO_2, CH_4 and N_2O respectively.

atmospheric chemistry runs were performed to estimate ozone and aerosol distributions (Lamarque et al., 2011). Finally, a single carbon cycle model with a representation of carbon–climate feedbacks was used in order to provide consistent values of CO_2 concentration for the CO_2 emission provided by a different IAM for each of the scenarios. This methodology was used to produce consistent data sets across scenarios but does not provide uncertainty estimates for them. After these processing steps, the final RCP data sets comprise land use data, harmonized GHG emissions and concentrations, gridded reactive gas and aerosol emissions, as well as ozone and aerosol abundance fields. These data are used as forcings in individual climate models. The number and type of forcings included primarily depend on the experiment. For instance, while the CO_2 concentration is prescribed in most experiments, CO_2 emissions are prescribed in some others (see Box 6.4 and Section 12.3.2.1). Which of these forcings are included in individual CMIP5 models, and variations in their implementation, is described in Section 12.3.2.2.

During this development process, the total RF and the RF of individual forcing agents have been estimated by the IAMs and made available via the RCP database (Meinshausen et al., 2011c). Each individual anthropogenic forcing varies from one scenario to another. They have been aggregated into a few groups in Figure 12.3b and c. The total anthropogenic RF estimated by the IAMs in 2010 is about 0.15 W m^{-2} lower than Chapter 8's best estimate of ERF in 2010 (2.2 W m^{-2}), the difference arising from a revision of the RF due to aerosols and land use in the current assessment compared to AR4. All the other individual forcings are consistent to within 0.02 W m^{-2}. The change in CO_2 concentration is the main cause of difference in the total RF among the scenarios (Figure 12.3b). The relative contribution[5] of CO_2 to the total anthropogenic forcing is currently (year 2010) about 80 to 90% and does not vary much across the scenarios (Figure 12.3c), as was also the case for SRES scenarios (Ramaswamy et al., 2001). Aerosols have a large negative contribution to the total forcing (about –40 to –50% in 2010), but this contribution decreases (in both absolute and relative terms) in the future for all the RCPs scenarios. This means that while anthropogenic aerosols have had a cooling effect in the past, their decrease in all RCP scenarios relative to current levels is expected to have a net warming effect in the future (Levy II et al., 2013; see also Figure 8.20). The 21st century decrease in the magnitude of future aerosol forcing was not as large and as rapid in the SRES scenarios (Figure 12.3a). However, even in the SRES scenarios, aerosol effects were expected to have a diminishing role in the future compared to GHG forcings, mainly because of the accumulation of GHG in the atmosphere (Dufresne et al., 2005). Other forcings do not change much in the future, except CH_4 which increases in the RCP8.5 scenario. Note that the estimates of all of these individual RFs are subject to many uncertainties (see Sections 7.5, 8.5 and 11.3.6). In this section and in Table AII.6.8, the RF values for RCP scenarios are derived from published equivalent-CO_2 (CO_2eq) concentration data that aggregates all anthropogenic forcings including GHGs and aerosols. The conversion to RF uses the formula: RF = $3.71/\ln(2) \cdot \ln(CO_2eq/278)$ W m^{-2}, where CO_2eq is in ppmv.

The four RCPs (Meinshausen et al., 2011c) are based on IAMs up to the end of the 21st century only. In order to investigate longer-term climate change implications, these RCPs were also extended until 2300. The extensions, formally named Extended Concentration Pathways (ECPs) but often simply referred to as RCP extensions, use simple assumptions about GHG and aerosol emissions and concentrations beyond 2100 (such as stabilization or steady decline) and were designed as hypothetical 'what-if' scenarios, not as an outcome of an IAM assuming socioeconomic considerations beyond 2100 (Meinshausen et al., 2011c) (see Box 1.1). In order to continue to investigate a broad range of possible climate futures, RCP2.6 assumes small constant net negative emissions after 2100 and RCP8.5 assumes stabilization with high emissions between 2100 and 2150, then a linear decrease until 2250. The two middle RCPs aim for a smooth stabilization of concentrations by 2150. RCP8.5 stabilizes concentrations only by 2250, with CO_2 concentrations of approximately 2000 ppmv, nearly seven times the pre-industrial level. As RCP2.6 implies net negative CO_2 emissions after around 2070 and throughout the extension, CO_2 concentrations slowly reduce towards 360 ppmv by 2300.

12.3.1.4 Comparison of Special Report on Emission Scenarios and Representative Concentration Pathway Scenarios

The four RCP scenarios used in CMIP5 lead to RF values that range from 2.3 to 8.0 W m^{-2} at 2100, a wider range than that of the three SRES scenarios used in CMIP3 which vary from 4.2 to 8.1 W m^{-2} at 2100 (see Table AII.6.8 and Figure 12.3). The SRES scenarios do not assume any policy to control climate change, unlike the RCP scenarios. The RF of RCP2.6 is hence lower by 1.9 W m^{-2} than the three SRES scenarios and very close to the ENSEMBLES E1 scenario (Johns et al., 2011). RCP4.5 and SRES B1 have similar RF at 2100, and comparable time evolution (within 0.2 W m^{-2}). The RF of SRES A2 is lower than RCP8.5 throughout the 21st century, mainly due to a faster decline in the radiative effect of aerosols in RCP8.5 than SRES A2, but they converge to within 0.1 W m^{-2} at 2100. RCP6.0 lies in between SRES B1 and SRES A1B. Results obtained with one General Circulation Model (GCM) (Dufresne et al., 2013) and with a reduced-complexity model (Rogelj et al., 2012) confirm that the differences in temperature responses are consistent with the differences in RFs estimates. RCP2.6, which assumes strong mitigation action, yields a smaller temperature increase than any SRES scenario. The temperature increase with the RCP4.5 and SRES B1 scenarios are close and the temperature increase is larger with RCP8.5 than with SRES A2. The spread of projected global mean temperature for the RCP scenarios (Section 12.4.1) is considerably larger (at both the high and low response ends) than for the three SRES scenarios used in CMIP3 (B1, A1B and A2) as a direct consequence of the larger range of RF across the RCP scenarios compared to that across the three SRES scenarios (see analysis of SRES versus RCP global temperature projections in Section 12.4.9 and Figure 12.40).

12.3.2 Implementation of Forcings in Coupled Model Intercomparison Project Phase 5 Experiments

The CMIP5 experimental protocol for long-term transient climate experiments prescribes a common basis for a comprehensive set of anthropogenic forcing agents acting as boundary conditions in three experimental phases—historical, RCPs and ECPs (Taylor et al., 2012). To permit common implementations of this set of forcing agents in CMIP5 models, self-consistent forcing data time series have been computed and provided to participating models (see Sections 9.3.2.2 and 12.3.1.3) comprising emissions or concentrations of GHGs and related compounds, ozone and atmospheric aerosols and their chemical precursors, and land use change.

The forcing agents implemented in Atmosphere–Ocean General Circulation Models (AOGCMs) and ESMs used to make long-term climate projections in CMIP5 are summarized in Table 12.1. The number of CMIP5 models listed here is about double the number of CMIP3 models listed in Table 10.1 of AR4 (Meehl et al., 2007b).

Natural forcings (arising from solar variability and aerosol emissions via volcanic activity) are also specified elements in the CMIP5 experimental protocol, but their future time evolutions are not prescribed

12

[5] The range of the relative contribution of CO_2 and aerosols to the total anthropogenic forcing is derived here from the RF values given by the IAMs and the best estimate assessed in Chapter 8.

Table 12.1 | Radiative forcing agents in the CMIP5 multi-model global climate projections. See Table 9.A.1 for descriptions of the models and main model references. Earth System Models (ESMs) are highlighted in bold. Numeric superscripts indicate model-specific references that document forcing implementations. Forcing agents are mostly implemented in close conformance with standard prescriptions (Taylor et al., 2012) and recommended data sets (Lamarque et al., 2010; Cionni et al., 2011; Lamarque et al., 2011; Meinshausen et al., 2011c) provided for CMIP5. Variations in forcing implementations are highlighted with superscripts and expanded in the table footnotes. Entries mean: n.a.: Forcing agent is not included in either the historical or future scenario simulations; Y: Forcing agent included (via prescribed concentrations, distributions or time series data); E: Concentrations of forcing agent calculated interactively driven by prescribed emissions or precursor emissions; Es: Concentrations of forcing agent calculated interactively constrained by prescribed surface concentrations. For a more detailed classification of ozone chemistry and ozone forcing implementations in CMIP5 models see Eyring et al. (2013).

Model	Forcing Agents																
	Greenhouse Gases						Aerosols									Other	
	CO_2 [ce]	CH_4	N_2O	Trop O_3	Strat O_3	CFCs	SO_4	Black carbon	Organic carbon	Nitrate	Cloud albedo effect [ac]	Cloud lifetime effect [ac]	Dust	Volcanic	Sea salt	Land use	Solar
ACCESS-1.0 [1]	Y [p]	Y	Y	Y [b]	Y [b]	Y	E	E	E	n.a.	Y	Y	Y [pd]	Y [v5]	Y [pd]	n.a.	Y
ACCESS-1.3 [1]	Y [p]	Y	Y	Y [b]	Y [b]	Y	E	E	E	n.a.	Y	Y	n.a.	Y [v5]	Y [pd]	n.a.	Y
BCC-CSM1.1 [2]	Y/E [p]	Y	Y	Y [b]	Y [b]	Y	Y [a]	Y [a]	Y [a]	n.a.	n.a.	n.a.	Y [a]	Y [v0]	Y [a]	n.a.	Y
BCC-CSM1.1(m) [2]	Y/E [p]	Y	Y	Y [b]	Y [b]	Y	Y [a]	Y [a]	Y [a]	n.a.	n.a.	n.a.	Y [a]	Y [v0]	Y [a]	n.a.	Y
BNU-ESM	Y/E [p]	Y	Y	Y [a]	Y [a]	Y	Y [a]	Y [a]	Y [a]	n.a.	n.a.	n.a.	Y [a]	Y [v0]	Y [a]	n.a.	Y
CanCM4	Y	Y	Y	Y [b]	Y [b]	Y	E	E	E	n.a.	Y [so]	n.a.	Y [pd]	Y/E [st,v0]	Y [pd]	n.a.	Y
CanESM2	Y/E [p]	Y	Y	Y [b]	Y [b]	Y	E	E	E	n.a.	Y [so]	n.a.	Y [pd]	Y/E [st,v0]	Y [pd]	Y [cr]	Y
CCSM4 [3]	Y [p]	Y	Y	Y [a]	Y [a]	Y	Y [a]	Y [a]	Y [a]	n.a.	n.a.	n.a.	Y [a]	Y [v0]	Y [a]	Y	Y
CESM1(BGC) [4]	Y/E [p]	Y	Y	Y [a]	Y [a]	Y	Y [a]	Y [a]	Y [a]	n.a.	n.a.	n.a.	Y [a]	Y [v0]	Y [a]	Y	Y
CESM1(CAM5) [5]	Y [p]	Y	Y	Y [a]	Y [a]	Y	E	E	E	n.a.	Y	Y	E	Y [v0]	E	Y	Y
CESM1(CAM5.1,FV2) [5]	Y [p]	Y	Y	Y [a]	Y [a]	Y	E	E	E	n.a.	Y	Y	E	Y [v0]	E	Y	Y
CESM1(FASTCHEM)	Y [p]	Y [a]	Y	E	E	Y	E	Y [a]	Y [a]	n.a.	n.a.	n.a.	Y [a]	Y [v0]	Y [a]	Y	Y
CESM1(WACCM) [6]	Es [p]	Es	Es	E/Es [op]	E/Es [op]	Es	Y	Y	Y	n.a.	n.a.	n.a.	Y [a]	Y [v0]	Y [a]	Y	Y
CMCC-CESM [7]	Y	Y	Y	Y [b]	Y [b]	Y	Y [a]	n.a.	n.a.	n.a.	Y [so]	n.a.	Y [fx]	n.a.	Y [fx]	n.a.	Y [or]
CMCC-CM	Y	Y	Y	Y [b]	Y [b]	Y	Y [a]	n.a.	n.a.	n.a.	Y [so]	n.a.	Y [fx]	n.a.	Y [fx]	n.a.	Y [or]
CMCC-CMS	Y	Y	Y	Y [b]	Y [b]	Y	Y [a]	n.a.	n.a.	n.a.	Y [so]	n.a.	Y [fx]	n.a.	Y [fx]	n.a.	Y [or]
CNRM-CM5 [8]	Y	Y	Y	Y [c]	Y [c]	Y	Y [e]	Y [e]	Y [e]	n.a.	Y [so,ic]	n.a.	Y [e]	Y [v1]	Y [e]	n.a.	Y
CSIRO-Mk3.6.0 [9]	Y	Y	Y	Y [b]	Y [b]	Y	E	E	E	n.a.	Y	Y	Y [pd]	Y [v0]	Y [pd]	n.a.	Y
EC-EARTH [10]	Y	Y	Y	Y [b]	Y [b]	Y	Y [a]	Y [a]	Y [a]	n.a.	n.a.	n.a.	Y [a]	Y [v1]	Y [a]	Y	Y
FGOALS-g2 [11]	Y	Y	Y	Y [b]	Y [b]	Y	Y [a]	Y [a]	Y [a]	n.a.	Y	Y	Y [a]	n.a.	Y [a]	n.a.	Y
FGOALS-s2 [12]	Y/E	Y	Y	Y [b]	Y [b]	Y	Y [a]	Y [a]	Y [a]	n.a.	n.a.	n.a.	Y [a]	Y [v0]	Y [a]	n.a.	Y
FIO-ESM	Y/E	Y	Y	Y [a]	Y [a]	Y	Y [a]	Y [a]	Y [a]	n.a.	n.a.	n.a.	Y [a]	Y [v0]	Y [a]	n.a.	Y
GFDL-CM3 [13]	Y [p]	Y/Es [rc]	Y/Es [rc]	E	E	Y/Es [rc]	E	E	E	n.a./E [rc]	Y	Y	E [pd]	Y/E [st,v0]	E [pd]	Y	Y
GFDL-ESM2G	Y/E [p]	Y	Y	Y [b]	Y [b]	Y	Y [a]	Y [a]	Y [a]	n.a.	n.a.	n.a.	Y [fx]	Y [v0]	Y [fx]	Y	Y
GFDL-ESM2M	Y/E [p]	Y	Y	Y [b]	Y [b]	Y	Y [a]	Y [a]	Y [a]	n.a.	n.a.	n.a.	Y [fx]	Y [v0]	Y [fx]	Y	Y
GISS-E2-p1 [14]	Y	Y	Y	Y [d]	Y [d]	Y	Y	Y	Y	Y	Y	n.a.	Y [fx]	Y [v4]	Y [fx]	Y	Y [or]
GISS-E2-p2 [14]	Y	Es/E [hf]	Es	E	E	Es/E [hf]	E	E	E	E	Y	n.a.	Y [pd]	Y [v4]	Y [pd]	Y	Y [or]

(continued on next page)

Table 12.1 (continued)

Model	Forcing Agents															
	Greenhouse Gases						*Aerosols*								*Other*	
	CO_2 [ce]	CH_4	N_2O	Trop O_3	Strat O_3	CFCs	SO_4	Black carbon	Organic carbon	Nitrate	Cloud albedo effect [ac]	Cloud lifetime effect [ac]	Dust	Volcanic	Sea salt	Land use	Solar
GISS-E2-p3 [14]	Y	Es/E [hf]	Es	E	E	Es/E [hf]	E	E	E	E	Y	n.a.	Y [pd]	Y [v4]	Y [pd]	Y	Y [or]
HadCM3	Y [p]	Y	Y	Y [b]	Y [b]	Y	E	n.a.	n.a.	n.a.	Y [so]	n.a.	n.a.	Y [v2]	n.a.	n.a.	Y
HadGEM2-AO [15]	Y [p]	Y	Y	Y [b]	Y [b]	Y	E	E	E	n.a.	Y	Y	Y [pd]	Y [v2]	Y [pd]	Y	Y
HadGEM2-CC [16,17]	Y [p]	Y	Y	Y [b]	Y [b]	Y	E	E	E	n.a.	Y	Y	Y [pd]	Y [v2]	Y [pd]	Y	Y
HadGEM2-ES [16]	Y/E [p]	Es	Y	E	Y [b]	Y	E	E	E	n.a.	Y	Y	Y [pd]	Y [v2]	Y [pd]	Y	Y
INM-CM4	Y/E	Y	Y	Y [b]	Y [b]	n.a.	Y [fx]	n.a.	n.a.	n.a.	Y [so]	n.a.	n.a.	Y [v0]	n.a.	Y	Y
IPSL-CM5A-LR [18]	Y/E [p]	Y	Y	Y [e]	Y [e]	Y	Y [e]	Y [e]	Y [e]	n.a.	Y	n.a.	Y [e]	Y [v1]	Y [e]	Y	Y
IPSL-CM5A-MR [18]	Y/E [p]	Y	Y	Y [e]	Y [e]	Y	Y [e]	Y [e]	Y [e]	n.a.	Y	n.a.	Y [e]	Y [v1]	Y [e]	Y	Y
IPSL-CM5B-LR [18]	Y [p]	Y	Y	Y [e]	Y [e]	Y	Y [e]	Y [e]	Y [e]	n.a.	Y	n.a.	Y [e]	Y [v1]	Y [e]	Y	Y
MIROC-ESM [19]	Y/E [p]	Y	Y	Y [f]	Y [f]	Y	E	E	E	n.a.	Y [ic]	Y [ic]	Y [pd]	Y [v3]	Y [pd]	Y	Y
MIROC-ESM-CHEM [19]	Y [p]	Y	Y	E	E	Y	E	E	E	n.a.	Y [ic]	Y [ic]	Y [pd]	Y [v3]	Y [pd]	Y	Y
MIROC4h [20]	Y [p]	Y	Y	Y [g]	Y [g]	Y	E	E	E	n.a.	Y	Y	Y [pd]	Y [v3]	Y [pd]	Y [cr]	Y
MIROC5 [20]	Y [p]	Y	Y	Y [f]	Y [f]	Y	E	E	E	n.a.	Y [ic]	Y [ic]	Y [pd]	Y [v3]	Y [pd]	Y [cr]	Y
MPI-ESM-LR	Y/E [p]	Y	Y	Y [b]	Y [b]	Y	Y [h]	Y [h]	Y [h]	Y [h]	n.a.	n.a.	Y [h]	Y [v0]	Y [h]	Y	Y [or]
MPI-ESM-MR	Y [p]	Y	Y	Y [b]	Y [b]	Y	Y [h]	Y [h]	Y [h]	Y [h]	n.a.	n.a.	Y [h]	Y [v0]	Y [h]	Y	Y [or]
MPI-ESM-P	Y [p]	Y	Y	Y [b]	Y [b]	Y	Y [h]	Y [h]	Y [h]	Y [h]	n.a.	n.a.	Y [h]	Y [v0]	Y [h]	Y	Y [or]
MRI-CGCM3 [21]	Y	Y	Y	Y [b]	Y [b]	Y	E	E	E	n.a.	Y [ic]	Y [ic]	E [pd]	E [v0]	E [pd]	Y	Y
MRI-ESM1 [22]	E	Y	Y	E	E	Es	E	E	E	n.a.	Y [ic]	Y [ic]	E [pd]	E [v0]	E [pd]	Y	Y
NorESM1-M [23]	Y [p]	Y	Y	Y [a]	Y [a]	Y	E	E	E	n.a.	Y	Y	E	Y/E [st,v1]	E [pd]	Y	Y
NorESM1-ME [23]	Y/E [p]	Y	Y	Y [a]	Y [a]	Y	E	E	E	n.a.	Y	Y	E	Y/E [st,v1]	E [pd]	Y	Y

Notes:

Model-specific references relating to forcing implementations:

1 Dix et al. (2013)
2 Wu et al. (2013); Xin et al. (2013a, 2013b)
3 Meehl et al. (2012); Gent et al. (2011)
4 Long et al. (2013); Meehl et al. (2012)
5 Meehl et al. (2013)
6 Calvo et al. (2012); Meehl et al. (2012)
7 Cagnazzo et al. (2013)
8 Voldoire et al. (2013)
9 Rotstayn et al. (2012)
10 Hazeleger et al. (2013)
11 Li et al. (2013c)
12 Bao et al. (2013)
13 Levy II et al. (2013)
14 Shindell et al. (2013a). GISS-E2-R and GISS-E2-H model variants are forced similarly and both represented here as GISS-E2. Both -R and -H model versions have three variants: in physics version 1 (p1) aerosols and ozone are specified from pre-computed transient aerosol and ozone fields, in physics version 2 (p2) aerosols and atmospheric chemistry are calculated online as a function of atmospheric state and transient emissions inventories, while in physics version 3 (p3) atmospheric composition is calculated as for p2 but the aerosol impacts on clouds (and hence the aerosol indirect effect) is calculated interactively. In p1 and p2 variants the aerosol indirect effect is parameterized following Hansen et al. (2005b).
15 HadGEM2-AO is forced in a similar way to HadGEM2-ES and HadGEM2-CC following Jones et al. (2011), but tropospheric ozone, stratospheric ozone and land cover are prescribed.
16 Jones et al. (2011)
17 Hardiman et al. (2012)
18 Dufresne et al. (2013)
19 Watanabe et al. (2011)
20 Komuro et al. (2012)
21 Yukimoto et al. (2012)
22 Adachi et al. (2013)
23 Iversen et al. (2013); Kirkevåg et al. (2013); Tjiputra et al. (2013)

(continued on next page)

Table 12.1 (continued)

Additional notes:

[ce] Separate entries for CO_2 denote 'concentration-driven' and 'emissions-driven' experiments as indicated.

[ac] 'Cloud albedo effect' and 'Cloud lifetime effect' are classical terms (as used in AR4) to describe indirect effects of radiative forcing associated with aerosols. They relate to the revised terminologies defined in Chapter 7 and used in AR5: 'Radiative forcing from aerosol–cloud interactions (RFaci)' and 'Effective radiative forcing from aerosol–cloud interactions (ERFaci)'. RFaci equates to cloud albedo effect, while ERFaci is the effective forcing resulting from cloud albedo effect plus cloud lifetime effect, including all rapid adjustments to cloud lifetime and thermodynamics (Section 7.1.3, Figure 7.3).

[p] Physiological forcing effect of CO_2 via plant stomatal response and evapotranspiration (Betts et al., 2007) included.

[rc] Separate entries denote different treatments used for radiation and chemistry respectively.

[hf] Separate entries denote treatment for historical and future (RCPs) respectively.

[a] Three-dimensional tropospheric ozone, stratospheric ozone, methane, and/or aerosol distributions specified as monthly 10-year mean concentrations, computed off-line using CAM-Chem – a modified version of CAM3.5 with interactive chemistry – driven with specified emissions for the historical period (Lamarque et al., 2010) and RCPs (Lamarque et al., 2011) with sea surface temperature and sea ice boundary conditions based on CCSM3's projections for the closest corresponding AR4 scenarios.

[b] Ozone prescribed using the original or slightly modified IGAC/SPARC ozone data set (Cionni et al., 2011); in some models this data set is modified to add a future solar cycle and in some models tropospheric ozone is zonally averaged.

[c] Linearized 2D ozone chemistry scheme (Cariolle and Teyssedre, 2007) including transport and photochemistry, reactive to stratospheric chlorine concentrations but not tropospheric chemical emissions.

[d] Ozone prescribed using the data set described in Hansen et al. (2007), with historical tropospheric ozone being calculated by a CCM and stratospheric ozone taken from Randel and Wu (2007) in the past. Tropospheric ozone is held constant from 1990 onwards, while stratospheric ozone is constant from 1997 to 2003 and then returned linearly to its 1979 value over the period 2004 to 2050.

[e] For IPSL-CM5 model versions, ozone and aerosol concentrations are calculated semi-offline with the atmospheric general circulation model including interactive chemistry and aerosol, following the four RCPs in the future (Dufresne et al., 2013; Szopa et al., 2013). The same aerosol concentration fields (but not ozone) are also prescribed for the CNRM-CM5 model.

[f] Ozone concentrations computed off-line by Kawase et al. (2011) using a CCM forced with CMIP5 emissions.

[g] Ozone concentrations computed off-line by Sudo et al. (2003) for the historical period and Kawase et al. (2011) for the future.

[h] Time dependent climatology based on simulations and observations; aerosols are distinguished only with respect to coarse and fine mode, and anthropogenic and natural origins, not with respect to composition.

[op] Separate entries denote different ozone chemistry precursors.

[so] RFaci from sulphate aerosol only.

[st] Separate entries denote stratosphere and troposphere respectively.

[ic] Radiative effects of aerosols on ice clouds are represented.

[pd] Prognostic or diagnostic scheme for dust/sea salt aerosol with emissions/concentrations determined by the model state rather than externally prescribed.

[fx] Fixed prescribed climatology of dust/sea salt aerosol concentrations with no year-to-year variability.

[v0] Explosive volcanic aerosol returns rapidly in future to zero (or near-zero) background, like that in the pre-industrial control experiment.

[v1] Explosive volcanic aerosol returns rapidly in future to constant (average volcano) background, the same as in the pre-industrial control experiment.

[v2] Explosive volcanic aerosol returns slowly in future (over several decades) to constant (average volcano) background like that in the pre-industrial control experiment.

[v3] Explosive volcanic aerosol returns rapidly in future to near-zero background, below that in the pre-industrial control experiment.

[v4] Explosive volcanic aerosol set to zero in future, but constant (average volcano) background in the pre-industrial control experiment.

[v5] Explosive volcanic aerosol returns slowly in future (over several decades) to constant (average volcano) background, but zero background in the pre-industrial control experiment.

[cr] Land use change represented via crop change only.

[or] Realistic time-varying orbital parameters for solar forcing (in historical period only for GISS-E2).

very precisely. A repeated 11-year cycle for total solar irradiance (Lean and Rind, 2009) is suggested for future projections but the periodicity is not specified precisely as solar cycles vary in length. Some models include the effect of orbital variations as well, but most do not. For volcanic eruptions, no specific CMIP5 prescription is given for future emissions or concentration data, the general recommendation being that volcanic aerosols should either be omitted entirely both from the control experiment and future projections or the same background volcanic aerosols should be prescribed in both. This provides a consistent framework for model intercomparison given a lack of knowledge of when future large eruptions will occur. In general models have adhered to this guidance, but there are variations in the background volcanic aerosol levels chosen (zero or an average volcano background in general) and some cases, for example, Australian Community Climate and Earth System Simulator (ACCESS)1.0 and ACCESS1.3 (Dix et al., 2013), where the background volcanic aerosol in future differs significantly from that in the control experiment, with a small effect on future RF.

For the other natural aerosols (dust, sea-salt, etc.), no emission or concentration data are recommended. The emissions are potentially computed interactively by the models themselves and may change with climate, or prescribed from separate model simulations carried out in the implementation of CMIP5 experiments, or simply held constant. Natural aerosols (mineral dust and sea salt) are in a few cases prescribed with no year-to-year variation (giving no transient forcing effect), in some cases prescribed from data sets computed off-line as described above, and in other cases calculated interactively via prognostic or diagnostic calculations. The degree to which natural aerosol emissions are interactive is effectively greater in some such models than others, however, as mineral dust emissions are more constrained when land vegetation cover is specified (e.g., as in Commonwealth Scientific and Industrial Research Organisation (CSIRO)-Mk3.6.0) (Rotstayn et al., 2012) than when vegetation is allowed to evolve dynamically (e.g., as in Hadley Centre new Global Environmental Model 2-ES (HadGEM2-ES)) (Jones et al., 2011) (Table 9.A.1).

12.3.2.1 'Emissions-Driven' versus 'Concentration Driven' Experiments

A novel feature within the CMIP5 experimental design is that experiments with prescribed anthropogenic emissions are included in addition to classical experiments with prescribed concentration pathways for WMGHGs (Taylor et al., 2012). The essential features of these two classes of experiment are described in Box 6.4. The CMIP5 protocol includes experiments in which 'ESMs' (models possessing at least a carbon cycle, allowing for interactive calculation of atmospheric CO_2 or compatible emissions) and AOGCMs (that do not possess such an interactive carbon cycle) are both forced with WMGHG concentration pathways to derive a range of climate responses consistent with those pathways from the two types of model. The range of climate responses including climate–carbon cycle feedbacks can additionally be explored in ESMs driven with emissions rather than concentrations, analogous to Coupled Climate Carbon Cycle Model Intercomparison Project (C^4MIP) experiments (Friedlingstein et al., 2006)—see Box 6.4. Results from the two types of experiment cannot be compared directly, but they provide complementary information. Uncertainties in the forward climate response driven with specified emissions or concentrations can be derived from all participating models, while concentration-driven ESM experiments also permit a policy-relevant diagnosis of the range of anthropogenic carbon emissions compatible with the imposed concentration pathways (Hibbard et al., 2007; Moss et al., 2010).

WMGHG forcing implementations in CMIP5 concentration-driven experiments conform closely in almost all cases to the standard protocol (Table 12.1; CO_2, CH_4, N_2O, chlorofluorocarbons (CFCs)), imposing an effective control over the RF due to WMGHGs across the multi-model ensemble, apart from the model spread arising from radiative transfer codes (Collins et al., 2006b; Meehl et al., 2007b). The ability of ESMs to determine their own WMGHG concentrations in emissions-driven experiments means that RF due to WMGHGs is less tightly controlled in such experiments. Even in concentration-driven experiments, many models implement some emissions-driven forcing agents (more often aerosols, but also ozone in some cases), leading to a potentially greater spread in both the concentrations and hence RF of those emissions-driven agents.

12.3.2.2 Variations Between Model Forcing Implementations

Apart from the distinction between concentration-driven and emissions-driven protocols, a number of variations are present in the implementation of forcing agents listed in Table 12.1, which generally arise due to constraining characteristics of the model formulations, various computational efficiency considerations or local implementation decisions. In a number of models, off-line modelling using an aerosol chemistry climate model has been used to convert emissions into concentrations compatible with the specific model formulation or characteristics. As a result, although detailed prescriptions are given for the forcing agents in CMIP5 experiments in emissions terms, individual modelling approaches lead to considerable variations in their implementations and consequential RFs. This was also the case in the ENSEMBLES multi-model projections, in which similar forcing agents to CMIP5 models were applied but again with variations in the implementation of aerosol, ozone and land use forcings, prescribing the SRES A1B and E1 scenarios in a concentration-driven protocol (Johns et al., 2011) akin to the CMIP5 protocol.

Methane, nitrous oxide and CFCs (typically with some aggregation of the multiple gases) are generally prescribed in CMIP5 models as well-mixed concentrations following the forcing data time series provided for the given scenarios. In a number of models (CESM1(WACCM), GFDL-CM3, GISS-E2-p2, GISS-E2-p3, HadGEM2-ES and MRI-ESM1) the three-dimensional concentrations in the atmosphere of some species evolve interactively driven by the full emissions/sinks cycle (in some cases constrained by prescribed concentrations at the surface, e.g., HadGEM2-ES for methane). In cases where the full emissions/sinks cycle is modelled, the radiation scheme is usually passed the time-varying 3-D concentrations, but some models prescribe different concentrations for the purpose of radiation.

Eyring et al. (2013) document, in greater detail than Table 12.1, the implementations of tropospheric and stratospheric ozone in CMIP5 models, including their ozone chemistry schemes and modifications applied to reference data sets in models driven by concentrations. In most models that prescribe ozone, concentrations are based on the original or slightly modified CMIP5 standard ozone data set computed as part of the International Global Atmospheric Chemistry/Stratospheric Processes and their Role in Climate (IGAC/SPARC) activity (Cionni et al., 2011). In the stratosphere, this data set is based on observations of the past (Randel and Wu, 2007) continued into the future with the multi-model mean of 13 chemistry–climate models (CCMs) projections following the SRES A1B (IPCC, 2000) and SRES A1 adjusted halogen scenario (WMO, 2007). The stratospheric zonal mean ozone field is merged with a 3-D tropospheric ozone time series generated as the mean of two CCMs (Goddard Institute of Space Studies-Physical Understanding of Composition-Climate Interactions and Impacts (GISS-PUCCINI), Shindell et al., 2006; CAM3.5, Lamarque et al., 2010) in the past and continued by one CCM (CAM3.5) in the future. Some CMIP5 models (MIROC-ESM, MIROC4h, MIROC5 and GISS-E2-p1) prescribe ozone concentrations using different data sets but again following just one GHG scenario in the future for the projection of stratospheric ozone. In other models (e.g., Institut Pierre Simon Laplace (IPSL)-CM5, CCSM4) ozone is again prescribed, but supplied as concentrations from off-line computations using a related CCM. Some models determine ozone interactively from specified emissions via on-line atmospheric chemistry (CESM1(FASTCHEM), CESM1(WACCM), CNRM-CM5, GFDL-CM3, GISS-E2-p2, GISS-E2-p3, MIROC-ESM-CHEM, MRI-ESM1; and HadGEM2-ES for tropospheric ozone only). Computing ozone concentrations interactively allows the fast coupling between chemistry and climate to be captured, but modelling of chemistry processes is sometimes simplified (CNRM-CM5, CESM(FASTCHEM)) in comparison with full complexity CCMs to reduce the computational cost. Compared to CMIP3, in which all models prescribed ozone and around half of them used a fixed ozone climatology, this leads to substantial improvement to ozone forcings in CMIP5, although differences remain among the models with interactive chemistry.

For atmospheric aerosols, either aerosol precursor emissions-driven or concentration-driven forcings are applied depending on individual model characteristics (see Sections 7.3 and 7.4 for an assessment of aerosols processes including aerosol–radiation and aerosol–cloud interactions). A larger fraction of models in CMIP5 than CMIP3 prescribe aerosol precursor emissions rather than concentrations. Many still prescribe concentrations pre-computed either using a directly related aerosol CCM or from output of another, complex, emissions-driven aerosol chemistry model within the CMIP5 process. As for ozone, aerosol concentrations provided from off-line simulations help to reduce the computational burden of the projections themselves. For several of the concentration-driven models (CCSM4, IPSL-CM5A variants, MPI-ESM-LR, MPI-ESM-MR), additional emissions-driven simulations have been undertaken to tailor the prescribed concentrations closely to the model's individual aerosol–climate characteristics. Lamarque et al. (2010, 2011) provided the recommended CMIP5 aerosols data set which has been used in several of the models driven by concentrations. Compared with the CMIP3 models, a much larger fraction of CMIP5 models now incorporate black and organic carbon aerosol forcings. Also, a larger fraction of CMIP5 than CMIP3 models now includes a range of processes that combine in the effective RF from aerosol–cloud interactions (ERFaci; see Section 7.1.3 and Figure 7.3). Previously such processes were generally termed aerosol indirect effects, usually separated into cloud albedo (or first indirect) effect and cloud lifetime (or second indirect) effect. Many CMIP5 models only include the interaction between sulphate aerosol and cloud, and the majority of them only model the effect of aerosols on cloud albedo rather than cloud lifetime (Table 12.1). No CMIP5 models represent urban aerosol pollution explicitly so that is not listed in Table 12.1 (see Section 11.3.5.2 for discussion of future air quality). Only one model (GISS-E2) explicitly includes nitrate aerosol as a separate forcing, though it is also included within the total aerosol mixture in the Max Planck Institute-Earth System Model (MPI-ESM) model versions.

Land use change is typically applied by blending anthropogenic land surface disturbance via crop and pasture fraction changes with underlying land cover maps of natural vegetation, but model variations in the underlying land cover maps and biome modelling mean that the land use forcing agent is impossible to impose in a completely common way at present (Pitman et al., 2009). Most CMIP5 models represent crop and pasture disturbance separately, while some (Canadian Earth System Model (CanESM2), MIROC4h, MIROC5) represent crop but not pasture. Some models (e.g., HadGEM2-ES, MIROC-ESM and MPI-ESM versions) allow a dynamical representation of natural vegetation changes alongside anthropogenic disturbance (see also Sections 9.4.4.3 and 9.4.4.4).

Treatment of the CO_2 emissions associated with land cover changes is also model dependent. Some models do not account for land cover changes at all, some simulate the biophysical effects but are still forced externally by land cover change induced CO_2 emissions (in emissions-driven simulations), while the most advanced ESMs simulate both biophysical effects of land cover changes and their associated CO_2 emissions.

12.3.3 Synthesis of Projected Global Mean Radiative Forcing for the 21st Century

Quantification of future global mean RF is of interest as it is directly related to changes in the global energy balance of the climate system and resultant climate change. Chapter 8 discusses RF concepts and methods for computing it that form the basis of analysis directly from the output of model projections.

We assess three related estimates of projected global mean forcing and its range through the 21st century in the context of forcing estimated for the recent past (Figure 12.4). The estimates used are: the total forcings for the defined RCP scenarios, harmonized to RF in the past (Meinshausen et al., 2011a; Meinshausen et al., 2011c); the total effective radiative forcing (ERF) estimated from CMIP5 models through the 21st century for the four RCP experiments (Forster et al., 2013); and that estimated from models in the Atmospheric Chemistry and Climate Model Intercomparison Project (ACCMIP; Lamarque et al., 2013—see Section 8.2.2) for RCP time-slice experiments (Shindell et al., 2013b). Methodological differences mean that whereas CMIP5 estimates include both natural and anthropogenic forcings based entirely on ERF, ACCMIP estimates anthropogenic composition forcing only (neglecting forcing changes due to natural, i.e., solar and volcanic, and land use factors) based on a combination of ERF for aerosols and RF for WMGHG (see Section 8.5.3). Note also that total forcing for the defined RCP scenarios is based on Meinshausen et al. (2011c) but combining total anthropogenic ERF (allowing for efficacies of the various anthropogenic forcings as in Figure 12.3) with natural (solar and volcanic) RF.

The CMIP5 multi-model ensemble mean ERF at 2100 (relative to an 1850–1869 base period) is 2.2, 3.8, 4.8 and 7.6 W m^{-2} respectively for RCP2.6, RCP4.5, RCP6.0 and RCP8.5 concentration-driven projections, with a 1-σ range based on annual mean data for year 2100 of about ±0.5 to 1.0 W m^{-2} depending on scenario (lowest for RCP2.6 and highest for RCP8.5). The CMIP5-based ERF estimates are close to the total forcing at 2100 (relative to an 1850–1859 base period) of 2.4, 4.0, 5.2 and 8.0 W m^{-2} as defined for the four RCPs.

The spread in ERF indicated from CMIP5 model results with specified GHG concentration pathways is broadly consistent with that found for CMIP3 models for the A1B scenario using the corresponding method (Forster and Taylor, 2006). As for CMIP3 models, part of the forcing spread in CMIP5 models (Forster et al., 2013) is consistent with differences in GHG forcings arising from the radiative transfer codes (Collins et al., 2006b). Aerosol forcing implementations in CMIP5 models also vary considerably, however (Section 12.3.2), leading to a spread in aerosol concentrations and forcings which contributes to the overall model spread. A further small source of spread in CMIP5 results possibly arises from an underlying ambiguity in the CMIP5 experimental design regarding the volcanic forcing offset between the historical experiment versus the pre-industrial control experiment. Most models implement zero volcanic forcing in the control experiment but some use constant negative forcing equal to the time-mean of historical volcanic forcing (see Table 12.1 and Section 12.3.2). The effect of this volcanic forcing offset persists into the future projections.

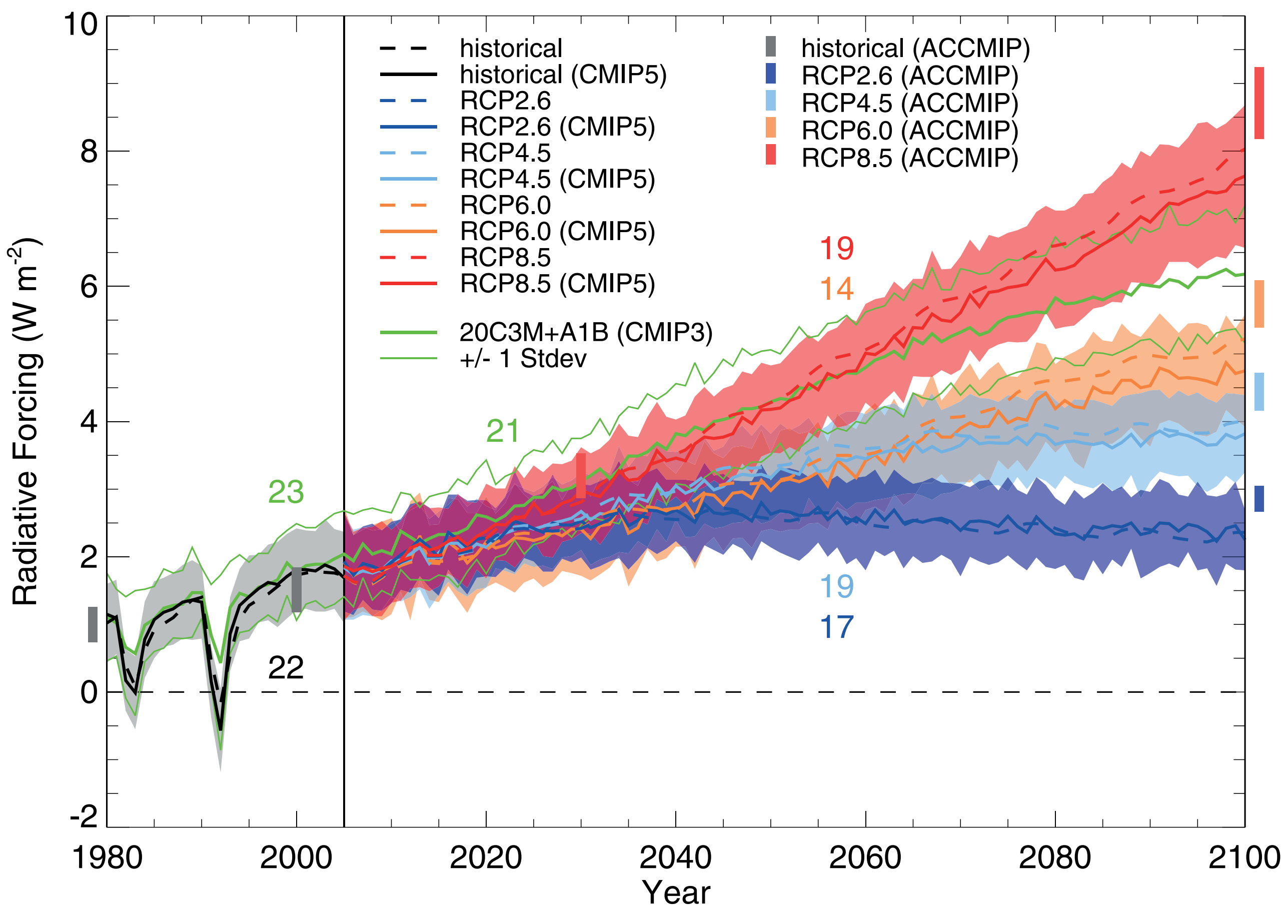

Figure 12.4 | Global mean radiative forcing (RF, W m^{-2}) between 1980 and 2100 estimated by alternative methods. The baseline is circa 1850 but dependent on the methods. Dashed lines indicate the total anthropogenic plus natural (solar and volcanic) RF for the RCP scenarios as defined by Meinshausen et al. (2011c), taking into account the efficacies of the various anthropogenic forcings (Meinshausen et al., 2011a), normalized by the mean between 1850 and 1859. Solid lines are multi-model mean effective radiative forcing (ERF) realized in a subset of CMIP5 models for the concentration-driven historical experiment and RCP scenarios, normalized either with respect to the 1850–1869 base period or with respect to the pre-industrial control simulation (Forster et al., 2013). (The subset of CMIP5 models included is defined by Table 1 of Forster et al. (2013) but omitting the FGOALS-s2 (Flexible Global Ocean-Atmosphere-Land System) model, the historical and RCP simulations of which were subsequently withdrawn from the CMIP5 archive.) This CMIP5-based estimate assumes each model has an invariant climate feedback parameter, calculated from abrupt 4 × CO_2 experiments using the method of Gregory et al. (2004). Each individual CMIP5 model's forcing estimate is an average over all available ensemble members, and a 1-σ inter-model range around the multi-model mean is shaded in light colour. Grey or coloured vertical bars illustrate the 1-σ range (68% confidence interval) of anthropogenic composition forcing (excluding natural and land use change forcings, based on ERF for aerosols combined with RF for WMGHG) estimated in ACCMIP models (Shindell et al., 2013b) for time slice experiments at 1980, 2000, 2030 (RCP8.5 only) and 2100 (all RCPs). The ACCMIP ranges plotted have been converted from the 5 to 95% ranges given in Shindell et al. (2013b) (Table 8) to a 1-σ range. Note that the ACCMIP bars at 1980 and 2100 are shifted slightly to aid clarity. The mean ERF diagnosed from 21 CMIP3 models for the SRES A1B scenario, as in Forster and Taylor (2006), is also shown (thick green line) with a 1-σ range (thinner green lines). The number of models included in CMIP3 and CMIP5 ensemble means is shown colour coded. (See Tables AII.6.8 to AII.6.10. Note that the CMIP5 model ranges given in Table AII.6.10 are based on decadal averages and therefore differ slightly from the ranges based on annual data shown in this figure.)

12

ACCMIP projected forcing at 2030 (for RCP8.5) and 2100 (all RCPs) is systematically higher than corresponding CMIP5 ERF, although with some overlap between 1-σ ranges. CMIP5 and ACCMIP comprise different sets of models and they are related in many but not all cases (Section 8.2.2). Confining analysis to a subset of closely related models also gives higher forcing estimates from ACCMIP compared to CMIP5 so the discrepancy in multi-model ensemble mean forcings appears unrelated to the different model samples associated with the two methods of estimation. The discrepancy is thought to originate mostly from differences in the underlying methodologies used to estimate RF, but is not yet well understood (see also Section 8.5.3).

There is *high confidence* in projections from ACCMIP models (Shindell et al., 2013b) based on the GISS-E2 CMIP5 simulations (Shindell et al., 2013a) and an earlier study with a version of the HadGEM2-ES model related to that used in CMIP5 (Bellouin et al., 2011), consistent with understanding of the processes controlling nitrate formation (Adams et al., 2001), that nitrate aerosols (which provide a negative forcing) will increase substantially over the 21st century under the RCPs (Section 8.5.3, Figure 8.20). The magnitude of total aerosol-related forcing (also negative in sign) will therefore tend to be underestimated in the CMIP5 multi-model mean ERF, as nitrate aerosol has been omitted as a forcing from almost all CMIP5 models.

Natural RF variations are, by their nature, difficult to project reliably (see Section 8.4). There is *very high confidence* that Industrial Era natural forcing has been a small fraction of the (positive) anthropogenic forcing except for brief periods following large volcanic eruptions (Sections 8.5.1 and 8.5.2). Based on that assessment and the assumption that variability in natural forcing remains of a similar magnitude and character to that over the Industrial Era, total anthropogenic forcing relative to pre-industrial, for any of the RCP scenarios through the 21st century, is *very likely* to be greater in magnitude than changes in natural (solar plus volcanic) forcing on decadal time scales.

In summary, global mean forcing projections derived from climate models exhibit a substantial range for the given RCP scenarios in concentration-driven experiments, contributing to the projected global mean temperature range (Section 12.4.1). Forcings derived from ACCMIP models for 2100 are systematically higher than those estimated from CMIP5 models for reasons that are not fully understood but are partly due to methodological differences. The multi-model mean estimate of combined anthropogenic plus natural forcing from CMIP5 is consistent with indicative RCP forcing values at 2100 to within 0.2 to 0.4 W m^{-2}.

12.4 Projected Climate Change over the 21st Century

12.4.1 Time-Evolving Global Quantities

12.4.1.1 Projected Changes in Global Mean Temperature and Precipitation

A consistent and robust feature across climate models is a continuation of global warming in the 21st century for all the RCP scenarios (Figure 12.5 showing changes in concentration-driven model simulations). Temperature increases are almost the same for all the RCP scenarios during the first two decades after 2005 (see Figure 11.25). At longer time scales, the warming rate begins to depend more on the specified GHG concentration pathway, being highest (>0.3°C per decade) in the highest RCP8.5 and significantly lower in RCP2.6, particularly after about 2050 when global surface temperature response stabilizes (and declines thereafter). The dependence of global temperature rise on GHG forcing at longer time scales has been confirmed by several studies (Meehl et al., 2007b). In the CMIP5 ensemble mean, global warming under RCP2.6 stays below 2°C above 1850-1900 levels throughout the 21st century, clearly demonstrating the potential of mitigation policies (note that to translate the anomalies in Figure 12.5 into anomalies with respect to that period, an assumed 0.61°C of observed warming since 1850–1900, as discussed in Section 2.4.3, should be added). This is in agreement with previous studies of aggressive mitigation scenarios (Johns et al., 2011; Meehl et al., 2012). Note, however, that some individual ensemble members do show warming exceeding 2°C above 1850-1900 (see Table 12.3). As for the other pathways, global warming exceeds 2°C within the 21st century under RCP4.5, RCP6.0 and RCP8.5, in qualitative agreement with previous studies using the SRES A1B and A2 scenarios (Joshi et al., 2011). Global mean temperature increase exceeds 4°C under RCP8.5 by 2100. The CMIP5 concentration-driven global temperature projections are broadly similar to CMIP3 SRES scenarios discussed in AR4 (Meehl et al., 2007b) and Section 12.4.9, although the overall range of the former is larger primarily because of the low-emission mitigation pathway RCP2.6 (Knutti and Sedláček, 2013).

The multi-model global mean temperature changes under different RCPs are summarized in Table 12.2. The relationship between cumulative anthropogenic carbon emissions and global temperature is assessed in Section 12.5 and only concentration-driven models are

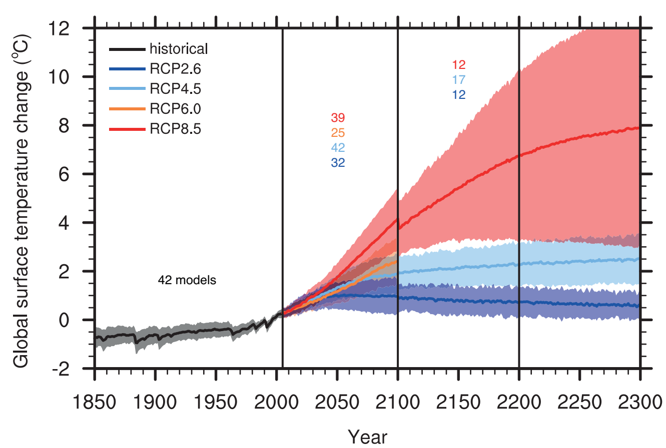

Figure 12.5 | Time series of global annual mean surface air temperature anomalies (relative to 1986–2005) from CMIP5 concentration-driven experiments. Projections are shown for each RCP for the multi-model mean (solid lines) and the 5 to 95% range (±1.64 standard deviation) across the distribution of individual models (shading). Discontinuities at 2100 are due to different numbers of models performing the extension runs beyond the 21st century and have no physical meaning. Only one ensemble member is used from each model and numbers in the figure indicate the number of different models contributing to the different time periods. No ranges are given for the RCP6.0 projections beyond 2100 as only two models are available.

12

Table 12.2 | CMIP5 annual mean surface air temperature anomalies (°C) from the 1986–2005 reference period for selected time periods, regions and RCPs. The multi-model mean ±1 standard deviation ranges across the individual models are listed and the 5 to 95% ranges from the models' distribution (based on a Gaussian assumption and obtained by multiplying the CMIP5 ensemble standard deviation by 1.64) are given in brackets. Only one ensemble member is used from each model and the number of models differs for each RCP (see Figure 12.5) and becomes significantly smaller after 2100. No ranges are given for the RCP6.0 projections beyond 2100 as only two models are available. Using Hadley Centre/Climate Research Unit gridded surface temperature data set 4 (HadCRUT4) and its uncertainty estimate (5 to 95% confidence interval), the observed warming to the 1986–2005 reference period (see Section 2.4.3) is 0.61°C ± 0.06°C (1850–1900), 0.30°C ± 0.03°C (1961–1990), 0.11°C ± 0.02°C (1980–1999). Decadal values are provided in Table AII.7.5, but note that percentiles of the CMIP5 distributions cannot directly be interpreted in terms of calibrated language.

		RCP2.6 (ΔT in °C)	RCP4.5 (ΔT in °C)	RCP6.0 (ΔT in °C)	RCP8.5 (ΔT in °C)
Global:	2046–2065	1.0 ± 0.3 (0.4, 1.6)	1.4 ± 0.3 (0.9, 2.0)	1.3 ± 0.3 (0.8, 1.8)	2.0 ± 0.4 (1.4, 2.6)
	2081–2100	1.0 ± 0.4 (0.3, 1.7)	1.8 ± 0.5 (1.1, 2.6)	2.2 ± 0.5 (1.4, 3.1)	3.7 ± 0.7 (2.6, 4.8)
	2181–2200	0.7 ± 0.4 (0.1, 1.3)	2.3 ± 0.5 (1.4, 3.1)	3.7 ± 0.7 (-,-)	6.5 ± 2.0 (3.3, 9.8)
	2281–2300	0.6 ± 0.3 (0.0, 1.2)	2.5 ± 0.6 (1.5, 3.5)	4.2 ± 1.0 (-,-)	7.8 ± 2.9 (3.0, 12.6)
Land: 2081–2100		1.2 ± 0.6 (0.3, 2.2)	2.4 ± 0.6 (1.3, 3.4)	3.0 ± 0.7 (1.8, 4.1)	4.8 ± 0.9 (3.4, 6.2)
Ocean: 2081–2100		0.8 ± 0.4 (0.2, 1.4)	1.5 ± 0.4 (0.9, 2.2)	1.9 ± 0.4 (1.1, 2.6)	3.1 ± 0.6 (2.1, 4.0)
Tropics: 2081–2100		0.9 ± 0.3 (0.3, 1.4)	1.6 ± 0.4 (0.9, 2.3)	2.0 ± 0.4 (1.3, 2.7)	3.3 ± 0.6 (2.2, 4.4)
Polar: Arctic: 2081–2100		2.2 ± 1.7 (-0.5, 5.0)	4.2 ± 1.6 (1.6, 6.9)	5.2 ± 1.9 (2.1, 8.3)	8.3 ± 1.9 (5.2, 11.4)
Polar: Antarctic: 2081–2100		0.8 ± 0.6 (-0.2, 1.8)	1.5 ± 0.7 (0.3, 2.7)	1.7 ± 0.9 (0.2, 3.2)	3.1 ± 1.2 (1.1, 5.1)

included here. Warming in 2046–2065 is slightly larger under RCP4.5 compared to RCP6.0, consistent with its greater total anthropogenic forcing at that time (see Table A.II.6.12). For all other periods the magnitude of global temperature change increases from RCP2.6 to RCP8.5. Beyond 2100, RCP2.6 shows a decreasing trend whereas under all other RCPs warming continues to increase. Also shown in Table 12.2 are projected changes at 2081–2100 averaged over land and ocean separately as well as area-weighted averages over the Tropics (30°S to 30°N), Arctic (67.5°N to 90°N) and Antarctic (90°S to 55°S) regions. Surface air temperatures over land warm more than over the ocean, and northern polar regions warm more than the tropics. The excess of land mass in the Northern Hemisphere (NH) in comparison with the Southern Hemisphere (SH), coupled with the greater uptake of heat by the Southern Ocean in comparison with northern ocean basins means that the NH generally warms more than the SH. Arctic warming is much greater than in the Antarctic, due to the presence of the Antarctic ice sheet and differences in local responses in snow and ice. Mechanisms behind these features of warming are discussed in Section 12.4.3. Maps and time series of regional temperature changes are displayed in Annex I and regional averages are discussed in Section 14.8.1.

Global annual multi-model mean temperature changes above 1850-1900 are listed in Table 12.3 for the 2081–2100 period (assuming 0.61°C warming since 1850–1900 as discussed in Section 2.4.3) along with the percentage of 2081–2100 projections from the CMIP5 models exceeding policy-relevant temperature levels under each RCP. These complement a similar discussion for the near-term projections in Table 11.3 which are based on the CMIP5 ensemble as well as evidence (discussed in Sections 10.3.1, 11.3.2.1.1 and 11.3.6.3) that some CMIP5 models have a higher sensitivity to GHGs and a larger response to other anthropogenic forcings (dominated by the effects of aerosols) than the real world (*medium confidence*). The percentage calculations for the long-term projections in Table 12.3 are based solely on the CMIP5 ensemble, using one ensemble member for each model. For these long-term projections, the 5 to 95% ranges of the CMIP5 model ensemble are considered the *likely* range, an assessment based on the fact that the 5 to 95% range of CMIP5 models' TCR coincides with the assessed *likely* range of the TCR (see Section 12.4.1.2 below and Box 12.2). Based on this assessment, global mean temperatures averaged in the period 2081–2100 are projected to *likely* exceed 1.5°C above 1850-1900 for RCP4.5, RCP6.0 and RCP8.5 (*high confidence*). They are also *likely* to exceed 2°C above 1850-1900 for RCP6.0 and RCP8.5 (*high confidence*) and *more likely than not* to exceed 2°C for RCP4.5 (*medium confidence*). Temperature change above 2°C under RCP2.6 is *unlikely* but is assessed only with *medium confidence* as some CMIP5 ensemble members do produce a global mean temperature change above 2°C. Warming above 4°C by 2081–2100 is *unlikely* in all RCPs (*high confidence*) except RCP8.5. Under the latter, the 4°C global temperature level is exceeded in more than half of ensemble members, and is assessed to be *about as likely as not* (*medium confidence*). Note that the likelihoods of exceeding specific temperature levels show some sensitivity to the choice of reference period (see Section 11.3.6.3).

CMIP5 models on average project a gradual increase in global precipitation over the 21st century: change exceeds 0.05 mm day^{-1} (~2% of global precipitation) and 0.15 mm day^{-1} (~5% of global precipitation) by 2100 in RCP2.6 and RCP8.5, respectively. The relationship between global precipitation and global temperature is approximately linear (Figure 12.6). The precipitation sensitivity, that is, the change of global precipitation with temperature, is about 1 to 3% °C^{-1} in most models, tending to be highest for RCP2.6 and RCP4.5 (Figure 12.7; note that only global values are discussed in this section, ocean and land changes are discussed in Section 12.4.5.2). These behaviours are consistent with previous studies, including CMIP3 model projections for SRES scenarios and AR4 constant composition commitment experiments (Meehl et al., 2007b), and ENSEMBLES multi-model results for SRES A1B and E1 scenarios (Johns et al., 2011).

The processes that govern global precipitation changes are now well understood and have been presented in Section 7.6. They are briefly summarized here and used to interpret the long-term projected changes. The precipitation sensitivity (about 1 to 3% °C^{-1}) is very different from the water vapour sensitivity (~7% °C^{-1}) as the main physical

Table 12.3 | CMIP5 global annual mean temperature changes above 1850-1900 for the 2081–2100 period of each RCP scenario (mean, ±1 standard deviation and 5 to 95% ranges based on a Gaussian assumption and obtained by multiplying the CMIP5 ensemble standard deviation by 1.64), assuming 0.61°C warming has occurred prior to 1986–2005 (second column). For a number of temperature levels (1°C, 1.5°C, 2°C, 3°C and 4°C), the proportion of CMIP5 model projections for 2081–2100 above those levels under each RCP scenario are listed. Only one ensemble member is used for each model.

	ΔT (°C) 2081–2100	$\Delta T > +1.0$°C	$\Delta T > +1.5$°C	$\Delta T > +2.0$°C	$\Delta T > +3.0$°C	$\Delta T > +4.0$°C
RCP2.6	1.6 ± 0.4 (0.9, 2.3)	94%	56%	22%	0%	0%
RCP4.5	2.4 ± 0.5 (1.7, 3.2)	100%	100%	79%	12%	0%
RCP6.0	2.8 ± 0.5 (2.0, 3.7)	100%	100%	100%	36%	0%
RCP8.5	4.3 ± 0.7 (3.2, 5.4)	100%	100%	100%	100%	62%

laws that drive these changes also differ. Water vapour increases are primarily a consequence of the Clausius–Clapeyron relationship associated with increasing temperatures in the lower troposphere (where most atmospheric water vapour resides). In contrast, future precipitation changes are primarily the result of changes in the energy balance of the atmosphere and the way that these later interact with circulation, moisture and temperature (Mitchell et al., 1987; Boer, 1993; Vecchi and Soden, 2007; Previdi, 2010; O'Gorman et al., 2012). Indeed, the radiative cooling of the atmosphere is balanced by latent heating (associated with precipitation) and sensible heating. Since AR4, the changes in heat balance and their effects on precipitation have been analyzed in detail for a large variety of forcings, simulations and models (Takahashi, 2009a; Andrews et al., 2010; Bala et al., 2010; Ming et al., 2010; O'Gorman et al., 2012; Bony et al., 2013).

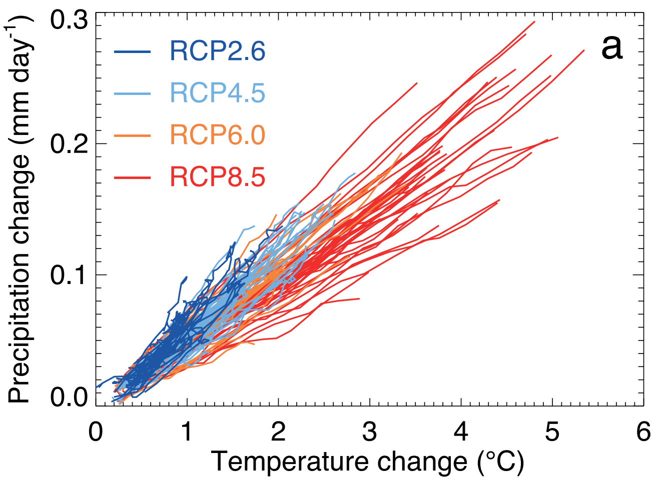

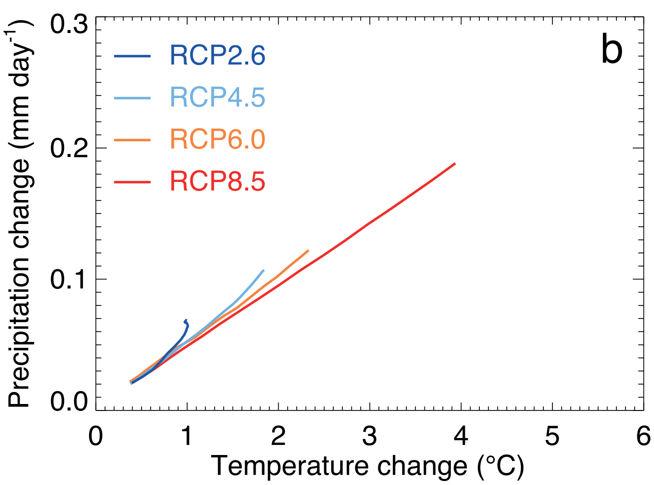

Figure 12.6 | Global mean precipitation (mm day^{-1}) versus temperature (°C) changes relative to 1986–2005 baseline period in CMIP5 model concentrations-driven projections for the four RCPs for (a) means over decadal periods starting in 2006 and overlapped by 5 years (2006–2015, 2011–2020, up to 2091–2100), each line representing a different model (one ensemble member per model) and (b) corresponding multi-model means for each RCP.

An increase of CO_2 decreases the radiative cooling of the troposphere and reduces precipitation (Andrews et al., 2010; Bala et al., 2010). On longer time scales than the fast hydrological adjustment time scale (Andrews et al., 2010; Bala et al., 2010; Cao et al., 2012; Bony et al., 2013), the increase of CO_2 induces a slow increase of temperature and water vapour, thereby enhancing the radiative cooling of the atmosphere and increasing global precipitation (Allen and Ingram, 2002; Yang et al., 2003; Held and Soden, 2006). Even after the CO_2 forcing stabilizes or begins to decrease, the ocean continues to warm, which then drives up global temperature, evaporation and precipitation. In addition, nonlinear effects also affect precipitation changes (Good et al., 2012). These different effects explain the steepening of the precipitation versus temperature relationship in RCP2.6 and RCP4.5 scenarios (Figure 12.6), as RF stabilizes and/or declines from the mid-century (Figure 12.4). In idealized CO_2 ramp-up/ramp-down experiments, this effect produces an hydrological response overshoot (Wu et al., 2010). An increase of absorbing aerosols warms the atmosphere and reduces precipitation, and the surface temperature response may be too small to compensate this decrease (Andrews et al., 2010; Ming et al., 2010; Shiogama et al., 2010a). Change in scattering aerosols or incoming solar radiation modifies global precipitation mainly via the response of the surface temperature (Andrews et al., 2009; Bala et al., 2010).

The main reasons for the inter-model spread of the precipitation sensitivity estimate among GCMs have not been fully understood. Nevertheless, spread in the changes of the cloud radiative effect has been shown to have an impact (Previdi, 2010), although the effect is less important for precipitation than it is for the climate sensitivity estimate (Lambert and Webb, 2008). The lapse rate plus water vapour feedback and the response of the surface heat flux (Previdi, 2010; O'Gorman et al., 2012), the shortwave absorption by water vapour (Takahashi, 2009b) or by aerosols, have been also identified as important factors.

Global precipitation sensitivity estimates from observations are very sensitive to the data and the time period considered. Some

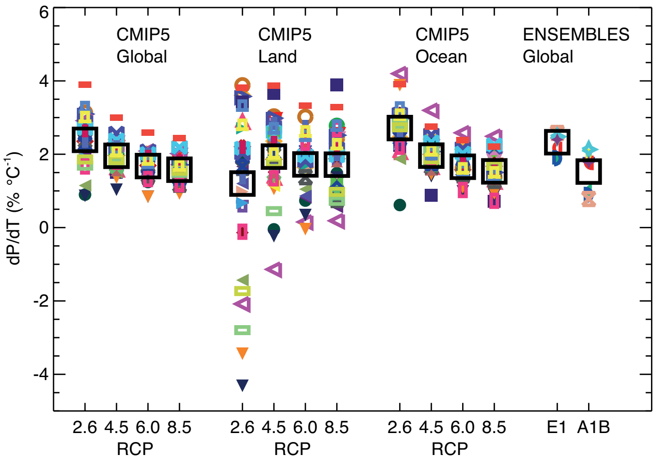

Figure 12.7 | Percentage changes over the 21st century in global, land and ocean precipitation per degree Celsius of global warming in CMIP5 model concentration-driven projections for the four RCP scenarios. Annual mean changes are calculated for each year between 2006 and 2100 from one ensemble member per model relative to its mean precipitation and temperature for the 1986–2005 baseline period, and the gradient of a least-squares fit through the annual data is derived. Land and ocean derived values use global mean temperature in the denominator of $\delta P/\delta T$. Each coloured symbol represents a different model, the same symbol being used for the same model for different RCPs and larger black squares being the multi-model mean. Also shown for comparison are global mean results for ENSEMBLES model concentrations-driven projections for the E1 and A1B scenarios (Johns et al., 2011), in this case using a least-squares fit derived over the period 2000–2099 and taking percentage changes relative to the 1980–1999 baseline period. Changes of precipitation over land and ocean are discussed in Section 12.4.5.2.

observational studies suggest precipitation sensitivity values higher than model estimates (Wentz et al., 2007; Zhang et al., 2007), although more recent studies suggest consistent values (Adler et al., 2008; Li et al., 2011b).

12.4.1.2 Uncertainties in Global Quantities

Uncertainties in global mean quantities arise from variations in internal natural variability, model response and forcing pathways. Table 12.2 gives two measures of uncertainty in the CMIP5 model projections, the standard deviation and the 5 to 95% range across the ensemble's distribution. Because CMIP5 was not designed to explore fully the uncertainty range in projections (see Section 12.2), neither its standard deviation nor its range can be interpreted directly as an uncertainty statement about the corresponding real quantities, and other techniques and arguments to assess uncertainty in future projections must be considered. Figure 12.8 summarizes the uncertainty ranges in global mean temperature changes at the end of the 21st century under the various scenarios quantified by various methods. Individual CMIP5 models are shown by red crosses. Red bars indicate mean and 5 to 95% percentiles based on assuming a normal distribution for the CMIP5 sample (i.e., ±1.64 standard deviations). Estimates from the simple climate carbon cycle Model for the Assessment of Greenhouse Gas-Induced Climate Change (MAGICC; Meinshausen et al., 2011a; Meinshausen et al., 2011b) calibrated to C[4]MIP (Friedlingstein et al., 2006) carbon cycle models, assuming a PDF for climate sensitivity that corresponds to the assessment of IPCC AR4 (Meehl et al., 2007b, Box 10.2), are given as yellow bars (Rogelj et al., 2012). Note that not all models have simulated all scenarios. To test the effect of undersampling, and to generate a consistent set of uncertainties across scenarios, a step response method that estimates the total warming as sum of responses to small forcing steps (Good et al., 2011a) is used to emulate 23 CMIP5 models under the different scenarios (those 23 models that supplied the necessary simulations to compute the emulators, i.e., CO_2 step change experiments). This provides means and ranges (5 to 95%) that are comparable across scenarios (blue). See also Section 12.4.9 for a discussion focussed on the differences between CMIP3 and CMIP5 projections of global average temperature changes.

For the CO_2 concentration-driven simulations (Figure 12.8a), the dominant driver of uncertainty in projections of global temperature for the higher RCPs beyond 2050 is the transient climate response (TCR), for RCP2.6, which is closer to equilibrium by the end of the century, it is both the TCR and the equilibrium climate sensitivity (ECS). In a transient situation, the ratio of temperature to forcing is approximately constant and scenario independent (Meehl et al., 2007b, Appendix 10.A.1; Gregory and Forster, 2008; Knutti et al., 2008b; Good et al., 2013). Therefore, the uncertainty in TCR maps directly into the uncertainty in global temperature projections for the RCPs other than RCP2.6. The assessed *likely* range of TCR based on various lines of evidence (see Box 12.2) is similar to the 5 to 95% percentile range of TCR in CMIP5. In addition, the assessed *likely* range of ECS is also consistent with the CMIP5 range (see Box 12.2). There is little evidence that the CMIP5 models are significantly over- or underestimating the RF. The RF uncertainty is small compared to response uncertainty (see Figure 12.4), and is considered by treating the 5 to 95% as a *likely* rather than *very likely* range. Kuhlbrodt and Gregory (2012) suggest that models might be overestimating ocean heat uptake, as previously suggested by Forest et al. (2006), but observationally constrained estimates of TCR are unaffected by that. The ocean heat uptake efficiency does not contribute much to the spread of TCR (Knutti and Tomassini, 2008; Kuhlbrodt and Gregory, 2012).

Therefore, for global mean temperature projections only, the 5 to 95% range (estimated as 1.64 times the sample standard deviation) of the CMIP5 projections can also be interpreted as a *likely* range for future temperature change between about 2050 and 2100. *Confidence* in this assessment is *high* for the end of the century because the warming then is dominated by CO_2 and the TCR. *Confidence* is only *medium* for mid-century when the contributions of RF and initial conditions to the total temperature response uncertainty are larger. The *likely* ranges are an expert assessment, taking into account many lines of evidence, in much the same way as in AR4 (Figure SPM.5), and are not probabilistic. The *likely* ranges for 2046–2065 do not take into account the possible influence of factors that lead to near-term (2016–2035) projections of global mean surface temperature (GMST) that are somewhat cooler than the 5 to 95% model ranges (see Section 11.3.6), because the influence of these factors on longer term projections cannot be quantified. A few recent studies indicate that some of the models with the strongest transient climate response might overestimate the near term warming (Otto et al., 2013; Stott et al., 2013) (see Sections 10.8.1, 11.3.2.1.1), but there is little evidence of whether and how much that affects the long-term warming response. One perturbed physics ensemble combined with observations indicates warming that exceeds the AR4 at the top end but used a relatively short time period of warming

12

(50 years) to constrain the models' projections (Rowlands et al., 2012) (see Sections 11.3.2.1.1 and 11.3.6.3). GMSTs for 2081–2100 (relative to 1986–2005) for the CO_2 concentration driven RCPs is therefore assessed to *likely* fall in the range 0.3°C to 1.7°C (RCP2.6), 1.1°C to 2.6°C (RCP4.5), 1.4°C to 3.1°C (RCP6.0), and 2.6°C to 4.8°C (RCP8.5) estimated from CMIP5. Beyond 2100, the number of CMIP5 simulations is insufficient to estimate a *likely* range. Uncertainties before 2050 are assessed in Section 11.3.2.1.1. The assessed *likely* range is very similar to the range estimated by the pulse response model, suggesting that the different sample of models for the different RCPs are not strongly affecting the result, and providing further support that this pulse response technique can be used to emulate temperature and ocean heat uptake in Chapter 13 and Section 12.4.9. The results are consistent with the probabilistic results from MAGICC, which for the lower RCPs have a slightly narrower range due to the lack of internal variability in the simple model, and the fact that non-CO_2 forcings are treated more homogeneously than in CMIP5 (Meinshausen et al., 2011a, 2011b). This is particularly pronounced for RCP2.6 where the CMIP5 range is substantially larger, partly due to the larger fraction of non-CO_2 forcings in that scenario.

The uncertainty estimate in AR4 for the SRES scenarios was –40% to +60% around the CMIP3 means (shown here in grey for comparison). That range was asymmetric and wider for the higher scenarios because it included the uncertainty in carbon cycle climate feedbacks. The SRES scenarios are based on the assumption of prescribed emissions, which then translates to uncertainties in concentrations that propagate through to uncertainties in the temperature response. The RCP scenarios assume prescribed concentrations. For scenarios that stabilize (RCP2.6) that approach of constant fractional uncertainty underestimates the uncertainty and is no longer applicable, mainly because internal variability has a larger relative contribution to the total uncertainty (Good et al., 2013; Knutti and Sedláček, 2013). For the RCPs, the carbon cycle climate feedback uncertainty is not included because the simulations are driven by concentrations. Furthermore, there is no clear evidence that distribution of CMIP5 global temperature changes deviates from a normal distribution. For most other variables the shape of the distribution is unclear, and standard deviations are simply used as an indication of model spread, not representing a formal uncertainty assessment.

Simulations with prescribed CO_2 emissions rather than concentrations are only available for RCP8.5 (Figure 12.8b) and from MAGICC. The projected temperature change in 2100 is slightly higher and the uncertainty range is wider as a result of uncertainties in the carbon cycle climate feedbacks. The CMIP5 range is consistent with the uncertainty range given in AR4 for SRES A2 in 2100. Further details about emission versus concentration driven simulations are given in Section 12.4.8.

In summary, the projected changes in global temperature for 2100 in the RCP scenarios are very consistent with those obtained by CMIP3 for SRES in IPCC AR4 (see Section 12.4.9) when taking into account the differences in scenarios. The *likely* uncertainty ranges provided here are similar for RCP4.5 and RCP6.0 but narrower for RCP8.5 compared to AR4. There was no scenario as low as RCP2.6 in AR4. The uncertainties in global temperature projections have not decreased significantly in CMIP5 (Knutti and Sedláček, 2013), but the assessed ranges cannot be

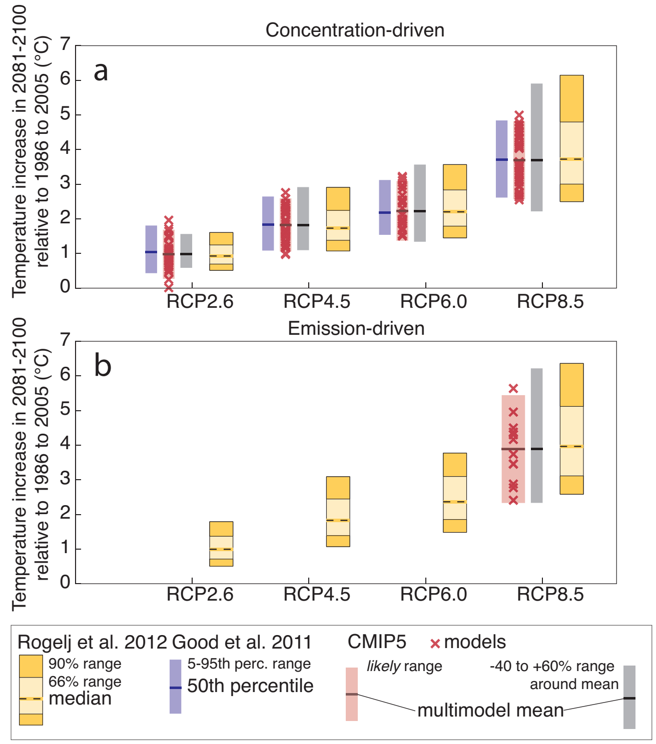

Figure 12.8 | Uncertainty estimates for global mean temperature change in 2081–2100 with respect to 1986–2005. Red crosses mark projections from individual CMIP5 models. Red bars indicate mean and 5 to 95% ranges based on CMIP5 (1.64 standard deviations), which are considered as a *likely* range. Blue bars indicate 5 to 95% ranges from the pulse response emulation of 21 models (Good et al., 2011a). Grey bars mark the range from the mean of CMIP5 minus 40% to the mean +60%, assessed as *likely* in AR4 for the SRES scenarios. The yellow bars show the median, 17 to 83% range and 5 to 95% range based on Rogelj et al. (2012). See also Figures 12.39 and 12.40.

compared between AR4 and AR5. The main reason is that uncertainties in carbon cycle feedbacks are not considered in the concentration driven RCPs. In contrast, the *likely* range in AR4 included those. The assessed *likely* ranges are therefore narrower for the high RCPs. The differences in the projected warming are largely attributable to the difference in scenarios (Knutti and Sedláček, 2013), and the change in the future and reference period, rather than to developments in modelling since AR4. A detailed comparison between the SRES and RCP scenarios and the CMIP3 and CMIP5 models is given in Section 12.4.9.

12.4.2 Pattern Scaling

12.4.2.1 Definition and Use

In this chapter we show geographical patterns of projected changes in climate variables according to specific scenarios and time horizons. Alternative scenarios and projection times can be inferred from those shown by using some established approximation methods. This is especially the case for large-scale regional patterns of average temperature and—with additional caveats—precipitation changes. In fact, 'pattern scaling' is an approximation that has been explicitly suggested in the description of the RCPs (Moss et al., 2010) as a method for deriving impact-relevant regional projections for scenarios that have not been simulated by global and regional climate models. It was first proposed by Santer et al. (1990) and revisited later by numerous studies (e.g., Huntingford and Cox, 2000). It relies on the existence of robust geographical patterns of change, emerging at the time when the response to external forcings emerges from the noise, and persisting across the length of the simulation, across different scenarios, and even across models, modulated by the corresponding changes in global average temperature. The robustness of temperature change patterns has been amply documented from the original paper onward. An example is given in Figure 12.9 for surface air temperature from each of the CMIP5 models highlighting both similarities and differences between the responses of different models. The precipitation pattern was shown to scale linearly with global average temperature to a sufficient accuracy in CMIP3 models (Neelin et al., 2006) for this to be useful for projections related to the hydrological cycle. Shiogama et al. (2010b) find similar results with the caution that in the early stages of warming aerosols modify the pattern. A more mixed evaluation can be found in

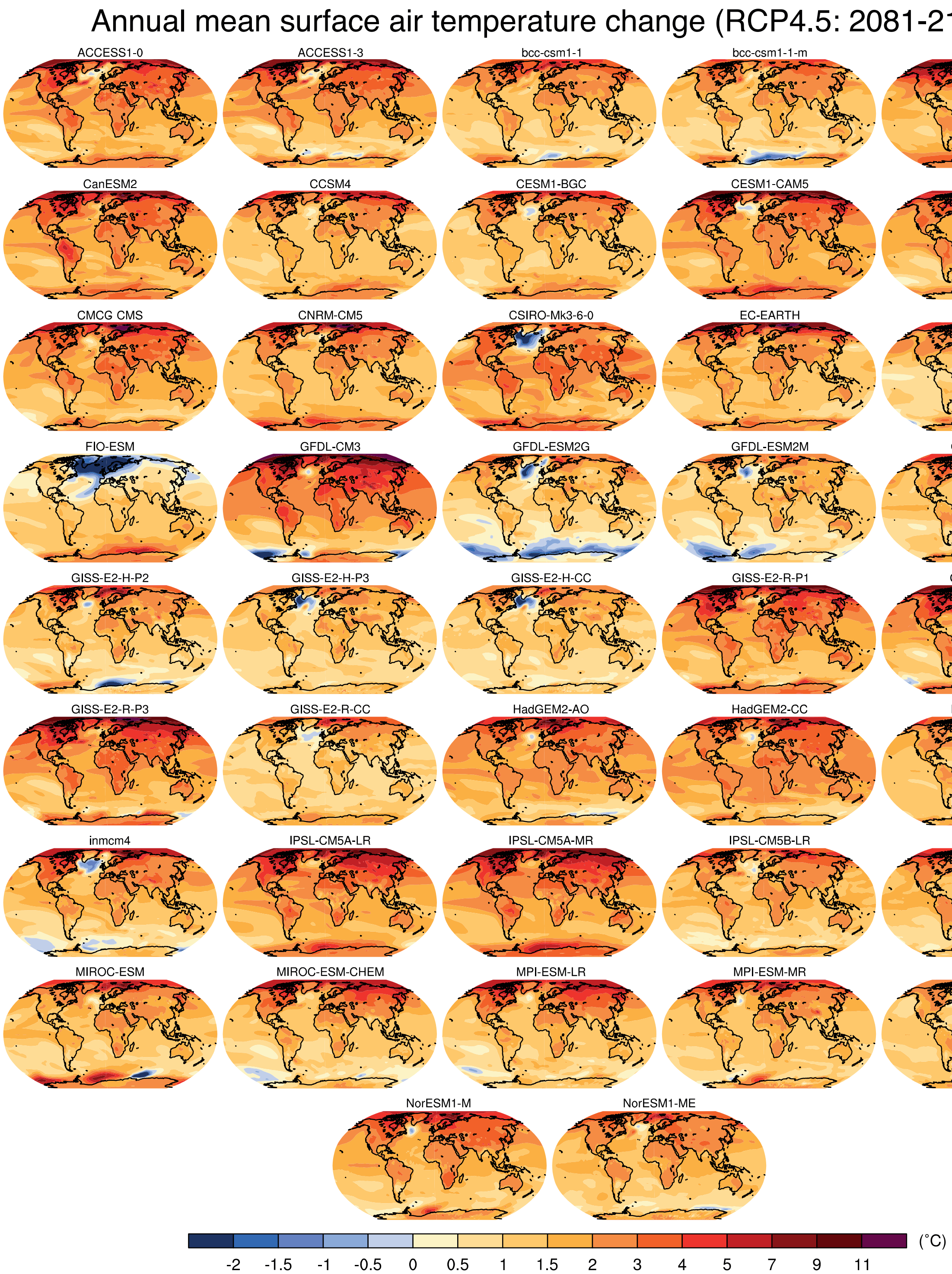

Figure 12.9 | Surface air temperature change in 2081–2100 displayed as anomalies with respect to 1986–2005 for RCP4.5 from one ensemble member of each of the concentration-driven models available in the CMIP5 archive.

12

Good et al. (2012), where some land areas in the low latitudes exhibit a nonlinear relation to global average temperature, but, largely, average precipitation change over the remaining regions can be well approximated by a grid-point specific linear function of global average temperature change. It is in the latter quantity that the dependence of the evolution of the change in time on the model (e.g., its climate sensitivity) and the forcing (e.g., the emission scenario) is encapsulated.

In analytical terms, it is assumed that the following relation holds:

$$C(t,\xi) = T_G(t)\,\chi(\xi) + R(t,\xi)$$

where the symbol ξ identifies the geographic location (model grid point or other spatial coordinates) and possibly the time of year (e.g., a June–July–August average). The index t runs along the length of the forcing scenario of interest. $T_G(t)$ indicates global average temperature change at time t under this scenario; $\chi(\xi)$ is the time-invariant geographic pattern of change per 1°C global surface temperature change for the variable of interest (which represents the forced component of the change) and $C(t,\xi)$ is the actual field of change for that variable at the specific time t under this scenario. The $R(t,\xi)$ is a residual term and highlights the fact that pattern scaling cannot reconstruct model behaviour with complete accuracy due to both natural variability and because of limitations of the methodology discussed below. This way, regionally and temporally differentiated results under different scenarios or climate sensitivities can be approximated by the product of a spatial pattern, constant over time, scenario and model characteristics, and a time evolving global mean change in temperature. Model and scenario dependence are thus captured through the global mean temperature response, and simple climate models calibrated against fully coupled climate models can be used to simulate the latter, at a great saving in computational cost. The spatial pattern can be estimated through the available coupled model simulations under the assumption that it does not depend on the specific scenario(s) used.

The choice of the pattern in the studies available in the literature can be as simple as the ensemble average field of change (across models and/or across scenarios, for the coupled experiments available), normalized by the corresponding change in global average temperature, choosing a segment of the simulations when the signal has emerged from the noise of natural variability from a baseline of reference (e.g., the last 20 years of the 21st century compared to pre-industrial or current climate) and taking the difference of two multi-decadal means. Similar properties and results have been obtained using more sophisticated multivariate procedures that optimize the variance explained by the pattern (Holden and Edwards, 2010). The validity of this approximation is discussed by Mitchell et al. (1999) and Mitchell (2003). Huntingford and Cox (2000) evaluate the quality of the approximation for numerous variables, showing that the technique performs best for temperature, downward longwave radiation, relative humidity, wind speeds and surface pressure while showing relatively larger limitations for rainfall rate anomalies. Joshi et al. (2013) have recently shown that the accuracy of the approximation, especially across models, is improved by adding a second term, linear in the land–sea surface warming ratio, another quantity that can be easily estimated from existing coupled climate model simulations. There exist of course differences between the patterns generated by different GCMs (documented for example for CMIP3 in Watterson and Whetton, 2011b), but uncertainty can be characterized, for example, by the inter-model spread in the pattern $\chi(\xi)$. Recent applications of the methodology to probabilistic future projections have in fact sought to fully quantify errors introduced by the approximation, on the basis of the available coupled model runs (Harris et al., 2006).

Pattern scaling and its applications have been documented in IPCC WGI Reports before (IPCC, 2001, Section 13.5.2.1; Meehl et al., 2007b, Section 10.3.2). It has been used extensively for regional temperature and precipitation change projections, for example, Murphy et al. (2007), (Watterson, 2008), Giorgi (2008), Harris et al. (2006, 2010), May (2008a), Ruosteenoja et al. (2007), Räisänen and Ruokolainen (2006), Cabre et al. (2010) and impact studies, for example, as described in Dessai et al. (2005) and Fowler et al. (2007b). Recent studies have focussed on patterns linked to warming at certain global average temperature change thresholds (e.g., May, 2008a; Sanderson et al., 2011) and patterns derived under the RCPs (Ishizaki et al., 2012).

There are basic limitations to this approach, besides a degradation of its performance as the regional scale of interest becomes finer and in the presence of regionally specific forcings. Recent work with MIROC3.2 (Shiogama et al., 2010a; Shiogama et al., 2010b) has revealed a dependence of the precipitation sensitivity (global average precipitation change per 1°C of global warming—see Figure 12.6) on the scenario, due to the precipitation being more sensitive to carbon aerosols than WMGHGs. In fact, there are significant differences in black and organic carbon aerosol forcing between the emission scenarios investigated by Shiogama et al. (2010a; 2010b). Levy II et al. (2013) confirm that patterns of precipitation change are spatially correlated with the sources of aerosol emissions, in simulations where the indirect effect is represented. This is a behaviour that is linked to a more general limitation of pattern scaling, which breaks down if aerosol forcing is significant. The effects of aerosols have a regional nature and are thus dependent on the future sources of pollution which are likely to vary geographically in the future and are difficult to predict (May, 2008a). For example, Asian and North American aerosol production are likely to have different time histories and future projections. Schlesinger et al. (2000) extended the methodology of pattern scaling by isolating and recombining patterns derived by dedicated experiments with a coupled climate model where sulphate aerosols were increased for various regions in turn. More recently, in an extension of pattern scaling into a probabilistic treatment of model, scenario and initial condition uncertainties, Frieler et al. (2012) derived joint probability distributions for regionally averaged temperature and precipitation changes as linear functions of global average temperature and additional predictors including regionally specific sulphate aerosol and black carbon emissions.

Pattern scaling is less accurate for strongly mitigated stabilization scenarios. This has been shown recently by May (2012), comparing patterns of temperature change under a scenario limiting global warming since pre-industrial times to 2°C and patterns produced by a scenario that reaches 4.5°C of global average temperature change. The limitations of pattern scaling in approximating changes while the climate system approaches equilibrium have found their explanation in Manabe and Wetherald (1980) and Mitchell et al. (1999). Both studies point out that as the temperatures of the deep oceans reach equilibrium (over multiple centuries) the geographical distribution of warming changes as well, for example, showing a larger warming of the high latitudes in the SH than in the earlier periods of the transient response, relative to the global mean warming. More recently, Held et al. (2010) showed how this slow warming pattern is in fact present during the initial transient response of the system as well, albeit with much smaller amplitude. Further, Gillett et al. (2011) show how in a simulation in which emissions cease, regional temperatures and precipitation patterns exhibit ongoing changes, even though global mean temperature remains almost constant. Wu et al. (2010) showed that the global precipitation response shows a nonlinear response to strong mitigation scenarios, with the hydrological cycle continuing to intensify even after atmospheric CO_2 concentration, and thus global average temperature, start decreasing. Regional nonlinear responses to mitigation scenarios of precipitation and sea surface temperatures (SSTs) are shown by Chadwick et al. (2013).

Other areas where pattern scaling shows a lack of robustness are the edges of polar ice caps and sea extent, where at an earlier time in the simulation ice melts and regions of sharp gradient surface, while later in the simulation, in the absence of ice, the gradient will become less steep. Different sea ice representations in models also make the location of such regions much less robust across the model ensembles and the scenarios.

Pattern scaling has not been as thoroughly explored for quantities other than average temperature and precipitation. Impact relevant extremes, for example, seem to indicate a critical dependence on the scale at which their changes are evaluated, with studies showing that some aspects of their statistics change in a close-to-linear way with mean temperature (Kharin et al., 2007; Lustenberger et al., 2013) while others have documented the dependence of their changes on moments of their statistical distribution other than the mean (Ballester et al., 2010a), which would make pattern scaling inadequate.

12.4.2.2 Coupled Model Intercomparison Project Phase 5 Patterns Scaled by Global Average Temperature Change

On the basis of CMIP5 simulations, we show geographical patterns (Figure 12.10) of warming and precipitation change and indicate measures of their variability across models and across RCPs. The patterns are scaled to 1°C global mean surface temperature change above the reference period 1986–2005 for 2081–2100 (first row) and for a period of approximate stable temperature, 2181–2200 (thus excluding RCP8.5, which does not stabilize by that time) (second row). Spatial correlation of fields of temperature and precipitation change range from 0.93 to 0.99 when considering ensemble means under different RCPs. The lower values are found when computing correlation between RCP2.6 and the higher RCPs, and may be related to the high mitigation

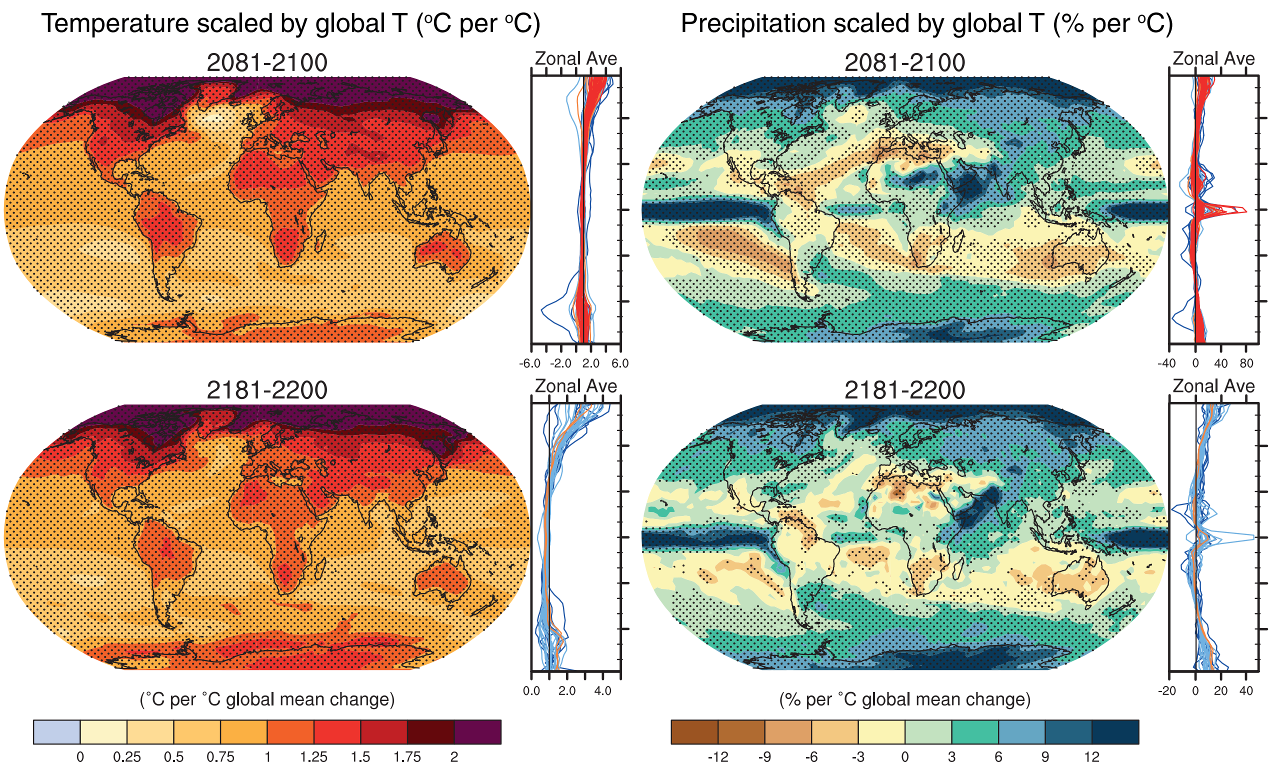

Figure 12.10 | Temperature (left) and precipitation (right) change patterns derived from transient simulations from the CMIP5 ensembles, scaled to 1°C of global mean surface temperature change. The patterns have been calculated by computing 20-year averages at the end of the 21st (top) and 22nd (bottom) centuries and over the period 1986–2005 for the available simulations under all RCPs, taking their difference (percentage difference in the case of precipitation) and normalizing it, grid-point by grid-point, by the corresponding value of global average temperature change for each model and scenario. The normalized patterns have then been averaged across models and scenarios. The colour scale represents degrees Celsius (in the case of temperature) and percent (in the case of precipitation) per 1°C of global average temperature change. Stippling indicates where the mean change averaged over all realizations is larger than the 95% percentile of the distribution of models. Zonal means of the geographical patterns are shown for each individual model for RCP2.6 (blue), 4.5 (light blue), 6.0 (orange) and 8.5 (red). RCP8.5 is excluded from the stabilization figures. The RCP2.6 simulation of the FIO-ESM (First Institute of Oceanography) model was excluded because it did not show any warming by the end of the 21st century, thus not complying with the method requirement that the pattern be estimated at a time when the temperature change signal from CO_2 increase has emerged.

12

enacted under RCP2.6 from early in the 21st century. Pattern correlation varies between 0.91 and 0.98 for temperature and between 0.91 and 0.96 for precipitation when comparing patterns computed by averaging and normalizing changes at the end of the 21st, 22nd and 23rd centuries, with the largest value representing the correlation between the patterns at the end of the 22nd and 23rd centuries, the lowest representing the correlation between the pattern at the end of the 21st and the pattern at the end of the 23rd century. The zonal means shown to the side of each plot represent each model by one line, colour coding the four different scenarios. They show good agreement of models and scenarios over low and mid-latitudes for temperature, but higher spread across models and especially across scenarios for the areas subject to polar amplification, for which the previous discussion about the sensitivity of the patterns to the sea ice edge may be relevant. A comparison of the mean of the lines to their spread indicates overall the presence of a strong mean signal with respect to the spread of the ensemble. Precipitation shows an opposite pattern of inter-model spread, with larger variations in the low latitudes and around the equator, and smaller around the high latitudes. Precipitation has also a lower signal-to-noise ratio (measured as above by comparing the ensemble mean change magnitude to the spread across models and scenarios of these zonal mean averages).

As already mentioned, although we do not explicitly use pattern scaling in the sections that follow, we consider it a useful approximation when the need emerges to interpolate or extrapolate results to different scenarios or time periods, noting the possibility that the scaling may break down at higher levels of global warming, and that the validity of the approximation is limited to broad patterns of change, as opposed to local scales. An important caveat is that pattern scaling only applies to the climate response that is externally forced. The actual response is a combination of forced change and natural variability, which is not and should not be scaled up or down by the application of this technique, which becomes important on small spatial scales and shorter time scales, and whose relative magnitude compared to the forced component also depends on the variable (Hawkins and Sutton, 2009, 2011; Mahlstein et al., 2011; Deser et al., 2012a, 2012b; Mahlstein et al., 2012) (see Section 11.2). One approach to produce projections that include both components is to estimate natural variability separately, scale the forced response and add the two.

12.4.3 Changes in Temperature and Energy Budget

12.4.3.1 Patterns of Surface Warming: Land–Sea Contrast, Polar Amplification and Sea Surface Temperatures

Patterns of surface air temperature change for various RCPs show widespread warming during the 21st century (Figure 12.11; see Annex I for seasonal patterns). A key feature that has been present throughout the history of coupled modelling is the larger warming over land compared to oceans, which occurs in both transient and equilibrium climate change (e.g., Manabe et al., 1990). The degree to which warming is larger over land than ocean is remarkably constant over time under transient warming due to WMGHGs (Lambert and Chiang, 2007; Boer, 2011; Lambert et al., 2011) suggesting that heat capacity differences between land and ocean do not play a major role in the land–sea warming contrast (Sutton et al., 2007; Joshi et al., 2008, 2013). The phenomenon is predominantly a feature of the surface and lower atmosphere (Joshi et al., 2008). Studies have found it occurs due to contrasts in surface sensible and latent fluxes over land (Sutton et al., 2007), land–ocean contrasts in boundary layer lapse rate changes (Joshi et al., 2008), boundary layer relative humidity and associated low-level cloud cover changes over land (Doutriaux-Boucher et al., 2009; Fasullo, 2010) and soil moisture reductions (Dong et al., 2009; Clark et al., 2010) under climate change. The land–sea warming contrast is also sensitive to aerosol forcing (Allen and Sherwood, 2010; Joshi et al., 2013). Globally averaged warming over land and ocean is identified separately in Table 12.2 for the CMIP5 models and the ratio of land to ocean warming is *likely* in the range of 1.4 to 1.7, consistent with previous studies (Lambert et al., 2011). The CMIP5 multi-model mean ratio is approximately constant from 2020 through to 2100 (based on an update of Joshi et al., 2008 from available CMIP5 models).

Amplified surface warming in Arctic latitudes is also a consistent feature in climate model integrations (e.g., Manabe and Stouffer, 1980). This is often referred to as polar amplification, although numerous studies have shown that under transient forcing, this is primarily an Arctic phenomenon (Manabe et al., 1991; Meehl et al., 2007b). The lack of an amplified transient warming response in high Southern polar latitudes has been associated with deep ocean mixing, strong ocean heat uptake and the persistence of the vast Antarctic ice sheet. In equilibrium simulations, amplified warming occurs in both polar regions.

On an annual average, and depending on the forcing scenario (see Table 12.2), the CMIP5 models show a mean Arctic (67.5°N to 90°N) warming between 2.2 and 2.4 times the global average warming for 2081–2100 compared to 1986–2005. Similar polar amplification factors occurred in earlier coupled model simulations (e.g., Holland and Bitz, 2003; Winton, 2006a). This factor in models is slightly higher than the observed central value, but it is within the uncertainty of the best estimate from observations of the recent past (Bekryaev et al., 2010). The uncertainty is large in the observed factor because station records are short and sparse (Serreze and Francis, 2006) and the forced signal is contaminated by the noise of internal variability. By contrast, model trends in surface air temperature are 2.5 to 5 times higher than observed over Antarctica, but here also the observational estimates have a very large uncertainty, so, for example, the CMIP3 ensemble mean is consistent with observations within error estimates (Monaghan et al., 2008). Moreover, recent work suggests more widespread current West Antarctic surface warming than previously estimated (Bromwich et al., 2013).

The amplified Arctic warming in models has a distinct seasonal character (Manabe and Stouffer, 1980; Rind, 1987; Holland and Bitz, 2003; Lu and Cai, 2009; Kumar et al., 2010). Arctic amplification (defined as the 67.5 N° to 90°N warming compared to the global average warming for 2081–2100 versus 1986–2005) peaks in early winter (November to December) with a CMIP5 RCP4.5 multi-model mean warming for 67.5°N to 90°N exceeding the global average by a factor of more than 4. The warming is smallest in summer when excess heat at the Arctic surface goes into melting ice or is absorbed by the ocean, which has a relatively large thermal inertia. Simulated Arctic warming also has a consistent vertical structure that is largest in the lower troposphere

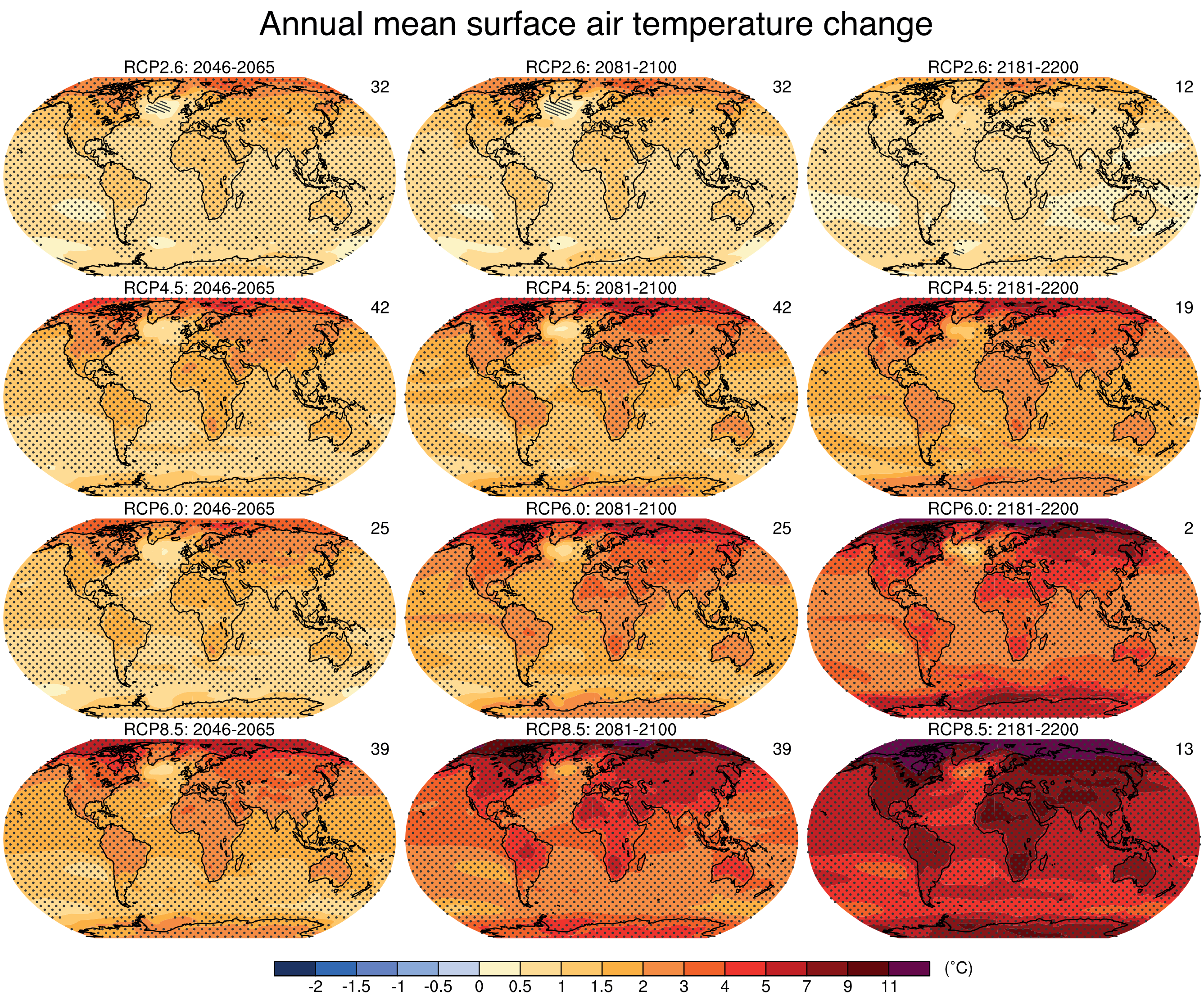

Figure 12.11 | Multi-model ensemble average of surface air temperature change (compared to 1986–2005 base period) for 2046–2065, 2081–2100, 2181–2200 for RCP2.6, 4.5, 6.0 and 8.5. Hatching indicates regions where the multi-model mean change is less than one standard deviation of internal variability. Stippling indicates regions where the multi-model mean change is greater than two standard deviations of internal variability and where at least 90% of the models agree on the sign of change (see Box 12.1). The number of CMIP5 models used is indicated in the upper right corner of each panel.

(e.g., Manabe et al., 1991; Kay et al., 2012). This is in agreement with recent observations (Serreze et al., 2009; Screen and Simmonds, 2010) but contrary to an earlier study that suggested a larger warming aloft (Graversen et al., 2008). The discrepancy in observed vertical structure may reflect inadequacies in data sets (Bitz and Fu, 2008; Grant et al., 2008; Thorne, 2008) and sensitivity to the time period used for averaging (see also Box 2.3).

As also discussed in Box 5.1, there are many mechanisms that contribute to Arctic amplification, some of which were identified in early modelling studies (Manabe and Stouffer, 1980). Feedbacks associated with changes in sea ice and snow amplify surface warming near the poles (Hall, 2004; Soden et al., 2008; Graversen and Wang, 2009; Kumar et al., 2010). The longwave radiation changes in the top of the atmosphere associated with surface warming opposes surface warming at all latitudes, but less so in the Arctic (Winton, 2006a; Soden et al., 2008). Rising temperature globally is expected to increase the horizontal latent heat transport by the atmosphere into the Arctic (Flannery, 1984; Alexeev et al., 2005; Cai, 2005; Langen and Alexeev, 2007; Kug et al., 2010), which warms primarily the lower troposphere. On average, CMIP3 models simulate enhanced latent heat transport (Held and Soden, 2006), but north of about 65°N, the sensible heat transport declines enough to more than offset the latent heat transport increase (Hwang et al., 2011). Increased atmospheric heat transport into the Arctic and subsidence warming has been associated with a teleconnection driven by enhanced convection in the tropical western Pacific (Lee et al., 2011). Ocean heat transport plays a role in the simulated Arctic amplification, with both large late 20th century transport (Mahlstein and Knutti, 2011) and increases over the 21st century (Hwang et al., 2011; Bitz et al., 2012) associated with higher amplification. As noted by Held and Soden (2006), Kay et al. (2012), and Alexeev and Jackson (2012), diagnosing the role of various factors in amplified warming is complicated by coupling in the system in which local feedbacks interact with poleward heat transports.

Although models consistently exhibit Arctic amplification as global mean temperatures rise, the multitude of physical processes described above mean that they differ considerably in the magnitude. Previous work has implicated variations across climate models in numerous factors including inversion strength (Boé et al., 2009a), ocean heat transport (Holland and Bitz, 2003; Mahlstein and Knutti, 2011), albedo feedback (Winton, 2006a), longwave radiative feedbacks (Winton, 2006a) and shortwave cloud feedback (Crook et al., 2011; Kay et al., 2012) as playing a role in the across-model scatter in polar amplification. The magnitude of amplification is generally higher in models with less extensive late 20th century sea ice in June, suggesting that the initial ice state influences the 21st century Arctic amplification. The pattern of simulated Arctic warming is also associated with the initial ice state, and in particular with the location of the winter sea ice edge (Holland and Bitz, 2003; Räisänen, 2007; Bracegirdle and Stephenson, 2012). This relationship has been suggested as a constraint on projected Arctic warming (Abe et al., 2011; Bracegirdle and Stephenson, 2012), although, in general, the ability of models to reproduce observed climate and its trends is not a sufficient condition for attributing *high confidence* to the projection of future trends (see Section 9.8).

Minima in surface warming occur in the North Atlantic and Southern Oceans under transient forcing in part due to deep ocean mixed layers in those regions (Manabe et al., 1990; Xie et al., 2010). Trenberth and Fasullo (2010) find that the large biases in the Southern Ocean energy budget in CMIP3 coupled models negatively correlate with equilibrium climate sensitivity (see Section 12.5.3), suggesting that an improved mean state in the Southern Ocean is needed before warming there can be understood. In the equatorial Pacific, warming is enhanced in a narrow band which previous assessments have described as 'El Niño-like', as may be expected from the projected decrease in atmospheric tropical circulations (see Section 12.4.4). However, DiNezio et al. (2009) highlight that the tropical Pacific warming in the CMIP3 models is not 'El Niño-like' as the pattern of warming and associated teleconnections (Xie et al., 2010; Section 12.4.5.2) is quite distinct from that of an El Niño event. Instead the pattern is of enhanced equatorial warming and is due to a meridional minimum in evaporative damping on the equator (Liu et al., 2005) and ocean dynamical changes that can be decoupled from atmospheric changes (DiNezio et al., 2009) (see also further discussion in Section 12.4.7).

In summary, there is robust evidence over multiple generations of models and *high confidence* in these large-scale warming patterns. In the absence of a strong reduction in the Atlantic Meridional Overturning Circulation (AMOC), there is *very high confidence* that the Arctic region is projected to warm most.

12.4.3.2 Zonal Average Atmospheric Temperature

Zonal temperature changes at the end of the 21st century show warming throughout the troposphere and, depending on the scenario, a mix of warming and cooling in the stratosphere (Figure 12.12). The maximum warming in the tropical upper troposphere is consistent with theoretical explanations and associated with a decline in the moist adiabatic lapse rate of temperature in the tropics as the climate warms (Bony et al., 2006). The northern polar regions also experience large warming in the lower atmosphere, consistent with the mechanisms discussed in Section 12.4.3.1. The tropospheric patterns are similar to those in the TAR and AR4 with the RCP8.5 changes being up to several degrees warmer in the tropics compared to the A1B changes appearing in the AR4. Similar tropospheric patterns appear in the RCP 2.6 and 4.5 changes, but with reduced magnitudes, suggesting some degree of scaling with forcing change in the troposphere, similar to behaviour discussed in the AR4 and Section 12.4.2. The consistency of tropospheric patterns over multiple generations of models indicates *high confidence* in these projected changes.

In the stratosphere, the models show similar tropical patterns of change, with magnitudes differing according to the degree of climate forcing. Substantial differences appear in polar regions. In the north, RCP8.5 and 4.5 yield cooling, though it is more significant in the RCP8.5 ensemble. In contrast, RCP2.6 shows warming, albeit weak and with little significance. In the southern polar region, RCP 2.6 and 4.5 both show significant warming, and RCP8.5 is the outlier, with significant cooling. The polar stratospheric warming, especially in the SH, is similar to that found by Butchart et al. (2010) and Meehl et al. (2012) in GCM simulations that showed effects of ozone recovery in determining the patterns (Baldwin et al., 2007; Son et al., 2010). Eyring et al. (2013) find behaviour in the CMIP5 ensemble both for models with and without interactive chemistry that supports the contention that the polar stratospheric changes in Figure 12.12 are strongly influenced by ozone recovery. Overall, the stratospheric temperature changes do not exhibit pattern scaling with global temperature change and are dependent on ozone recovery.

Away from the polar stratosphere, there is physical and pattern consistency in temperature changes between different generations of models assessed here and in the TAR and AR4. The consistency is especially clear in the northern high latitudes and, coupled with physical understanding, indicates that some of the greatest warming is *very likely* to occur here. There is also consistency across generations of models in relatively large warming in the tropical upper troposphere. Allen and Sherwood (2008) and Johnson and Xie (2010) have presented dynamic and thermodynamic arguments, respectively, for the physical robustness of the tropical behaviour. However, there remains uncertainty about the magnitude of warming simulated in the tropical upper troposphere because large observational uncertainties and contradictory analyses limit a confident assessment of model accuracy in simulating temperature trends in the tropical upper troposphere (Section 9.4.1.4.2). The combined evidence indicates that relatively large warming in the tropical upper troposphere is *likely*, but with *medium confidence*.

12.4.3.3 Temperature Extremes

As the climate continues to warm, changes in several types of temperature extremes have been observed (Donat et al., 2013), and are expected to continue in the future in concert with global warming (Seneviratne et al., 2012). Extremes occur on multiple time scales, from a single day or a few consecutive days (a heat wave) to monthly and seasonal events. Extreme temperature events are often defined by indices (see Box 2.4 for the common definitions used), for example, percentage of days in a year when maximum temperature is above the 90th percentile of a present day distribution or by long period return values. Although changes in temperature extremes are a very robust

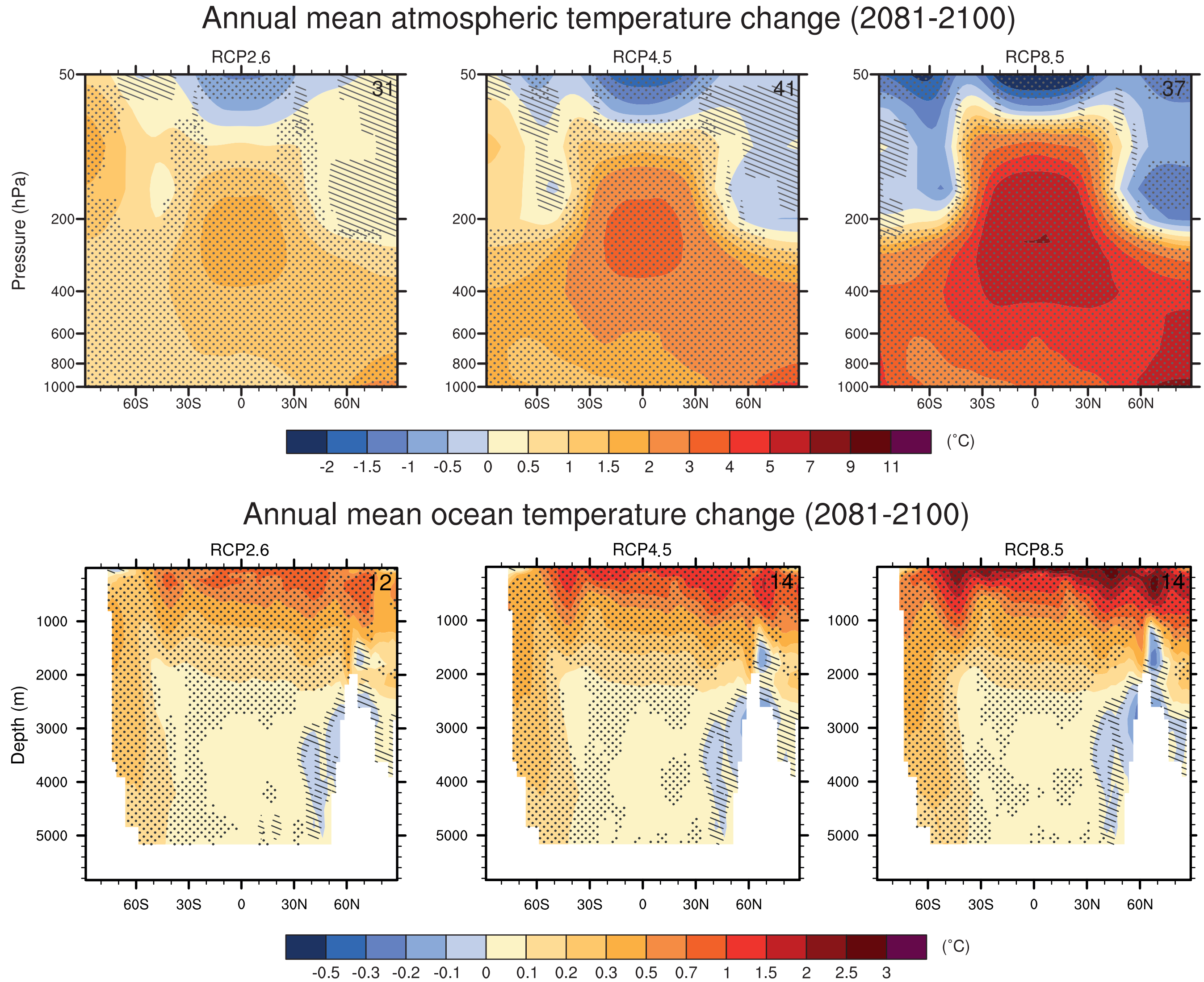

Figure 12.12 | CMIP5 multi-model changes in annual mean zonal mean temperature in the atmosphere and ocean relative to 1986–2005 for 2081–2100 under the RCP2.6 (left), RCP4.5 (centre) and RCP8.5 (right) forcing scenarios. Hatching indicates regions where the multi-model mean change is less than one standard deviation of internal variability. Stippling indicates regions where the multi-model change mean is greater than two standard deviations of internal variability and where at least 90% of the models agree on the sign of change (see Box 12.1).

signature of anthropogenic climate change (Seneviratne et al., 2012), the magnitude of change and consensus among models varies with the characteristics of the event being considered (e.g., time scale, magnitude, duration and spatial extent) as well as the definition used to describe the extreme.

Since the AR4 many advances have been made in establishing global observed records of extremes (Alexander et al., 2006; Perkins et al., 2012; Donat et al., 2013) against which models can be evaluated to give context to future projections (Sillmann and Roeckner, 2008; Alexander and Arblaster, 2009). Numerous regional assessments of future changes in extremes have also been performed and a comprehensive summary of these is given in Seneviratne et al. (2012). Here we summarize the key findings from this report and assess updates since then.

It is *virtually certain* that there will be more hot and fewer cold extremes as global temperature increases (Caesar and Lowe, 2012; Orlowsky and Seneviratne, 2012; Sillmann et al., 2013), consistent with previous assessments (Solomon et al., 2007; Seneviratne et al., 2012). Figure 12.13 shows multi-model mean changes in the absolute temperature indices of the coldest day of the year and the hottest day of the year and the threshold-based indices of frost days and tropical nights from the CMIP5 ensemble (Sillmann et al., 2013). A robust increase in warm temperature extremes and decrease in cold temperature extremes is found at the end of the 21st century, with the magnitude of the changes increasing with increased anthropogenic forcing. The coldest night of the year undergoes larger increases than the hottest day in the globally averaged time series (Figure 12.13b and d). This tendency is consistent with the CMIP3 model results shown in Figure 12.13, which use different models and the SRES scenarios (see Seneviratne et al. (2012) for earlier CMIP3 results). Similarly, increases in the frequency of warm nights are greater than increases in the frequency of warm days (Sillmann et al., 2013). Regionally, the largest increases in the coldest night of the year are projected in the high latitudes of the NH under the RCP8.5 scenario (Figure 12.13a). The subtropics and mid-latitudes exhibit the greatest projected changes in the hottest day of the year, whereas changes in tropical nights and the frequency of warm days and warm nights are largest in the tropics (Sillmann et al., 2013). The number of frost days declines in all regions while significant increases in tropical nights are seen in southeastern North America, the Mediterranean and central Asia.

It is *very likely* that, on average, there will be more record high than record cold temperatures in a warmer average climate. For example, Meehl et al. (2009) find that the current ratio of 2 to 1 for record daily high maxima to low minima over the USA becomes approximately 20 to 1 by the mid-21st century and 50 to 1 by late century in their model simulation of the SRES A1B scenario. However, even at the end of the century daily record low minima continue to be broken, if in a small number, consistent with Kodra et al. (2011), who conclude that cold extremes will continue to occur in a warmer climate, even though their frequency will decline.

It is also *very likely* that heat waves, defined as spells of days with temperature above a threshold determined from historical climatology, will occur with a higher frequency and duration, mainly as a direct consequence of the increase in seasonal mean temperatures (Barnett et al., 2006; Ballester et al., 2010a, 2010b; Fischer and Schär, 2010). Changes in the absolute value of temperature extremes are also *very likely* and expected to regionally exceed global temperature increases by far, with substantial changes in hot extremes projected even for moderate (<2.5°C above present day) average warming levels (Clark et al., 2010; Diffenbaugh and Ashfaq, 2010). These changes often differ from the mean temperature increase, as a result of changes in variability and shape of the temperature distribution (Hegerl et al., 2004; Meehl and Tebaldi, 2004; Clark et al., 2006). For example, summer temperature extremes over central and southern Europe are projected to warm substantially more than the corresponding mean local temperatures as a result of enhanced temperature variability at interannual to intraseasonal time scales (Schär et al., 2004; Clark et al., 2006; Kjellstrom et al., 2007; Vidale et al., 2007; Fischer and Schär, 2009, 2010; Nikulin et al., 2011; Fischer et al., 2012a). Several recent studies have also argued that the probability of occurrence of a Russian heat wave at least as severe as the one in 2010 increases substantially (by a factor of 5 to 10 by the mid-century) along with increasing mean temperatures and enhanced temperature variability (Barriopedro et al., 2011; Dole et al., 2011).

Since the AR4, an increased understanding of mechanisms and feedbacks leading to projected changes in extremes has been gained (Seneviratne et al., 2012). Climate models suggest that hot extremes are amplified by soil moisture-temperature feedbacks (Seneviratne et al., 2006; Diffenbaugh et al., 2007; Lenderink et al., 2007; Vidale et al., 2007; Fischer and Schär, 2009; Fischer et al., 2012a) in northern mid-latitude regions as the climate warms, consistent with previous assessments. Changes in temperature extremes may also be impacted by changes in land–sea contrast, with Watterson et al. (2008) showing an amplification of southern Australian summer warm extremes over the mean due to anomalous temperature advection from warmer continental interiors. The largest increases in the magnitude of warm extremes are simulated over mid-latitude continental areas, consistent with the drier conditions, and the associated reduction in evaporative cooling from the land surface projected over these areas (Kharin et al., 2007). The representation of the latter constitutes a major source of model uncertainty for projections of the absolute magnitude of temperature extremes (Clark et al., 2010; Fischer et al., 2011).

Winter cold extremes also warm more than the local mean temperature over northern high latitudes (Orlowsky and Seneviratne, 2012; Sillmann et al., 2013) as a result of reduced temperature variability related to declining snow cover (Gregory and Mitchell, 1995; Kjellstrom et al., 2007; Fischer et al., 2011) and decreases in land–sea contrast (de Vries et al., 2012). Changes in atmospheric circulation, induced by remote surface heating can also modify the temperature distribution (Haarsma et al., 2009). Sillmann and Croci-Maspoli (2009) note that cold winter extremes over Europe are in part driven by atmospheric blocking and changes to these blocking patterns in the future lead to changes in the frequency and spatial distribution of cold temperature extremes as global temperatures increase. Occasional cold winters will continue to occur (Räisänen and Ylhaisi, 2011).

Human discomfort, morbidity and mortality during heat waves depend not only on temperature but also specific humidity. Heat stress, defined as the combined effect of temperature and humidity, is expected to increase along with warming temperatures and dominates the local decrease in summer relative humidity due to soil drying (Diffenbaugh et al., 2007; Fischer et al., 2012b; Dunne et al., 2013). Areas with abundant atmospheric moisture availability and high present-day temperatures such as Mediterranean coastal regions are expected to experience the greatest heat stress changes because the heat stress response scales with humidity which thus becomes increasingly important to heat stress at higher temperatures (Fischer and Schär, 2010; Sherwood and Huber, 2010; Willett and Sherwood, 2012). For some regions, simulated heat stress indicators are remarkably robust, because those models with stronger warming simulate a stronger decrease in atmospheric relative humidity (Fischer and Knutti, 2013).

Changes in rare temperature extremes can be assessed using extreme value theory based techniques (Seneviratne et al., 2012). Kharin et al. (2007), in an analysis of CMIP3 models, found large increases in the 20-year return values of the annual maximum and minimum daily averaged surface air temperatures (i.e., the size of an event that would be expected on average once every 20 years, or with a 5% chance every year) with larger changes over land than ocean. Figure 12.14 displays the end of 21st century change in the magnitude of these rare events from the CMIP5 models in the RCP2.6, 4.5 and 8.5 scenarios (Kharin et al., 2013). Comparison to the changes in summer mean temperature shown in Figure AI.5 and A1.7 of Annex I Supplementary Material reveals that rare high temperature events are projected to change at rates similar to or slightly larger than the summertime mean temperature in many land areas. However, in much of Northern Europe 20-year return values of daily high temperatures are projected to increase 2°C or more than JJA mean temperatures under RCP8.5, consistent with previous studies (Sterl et al., 2008; Orlowsky and Seneviratne, 2012). Rare low temperature events are projected to experience significantly larger increases than the mean in most land regions, with a pronounced effect at high latitudes. Twenty-year return values of cold extremes increase significantly more than

12

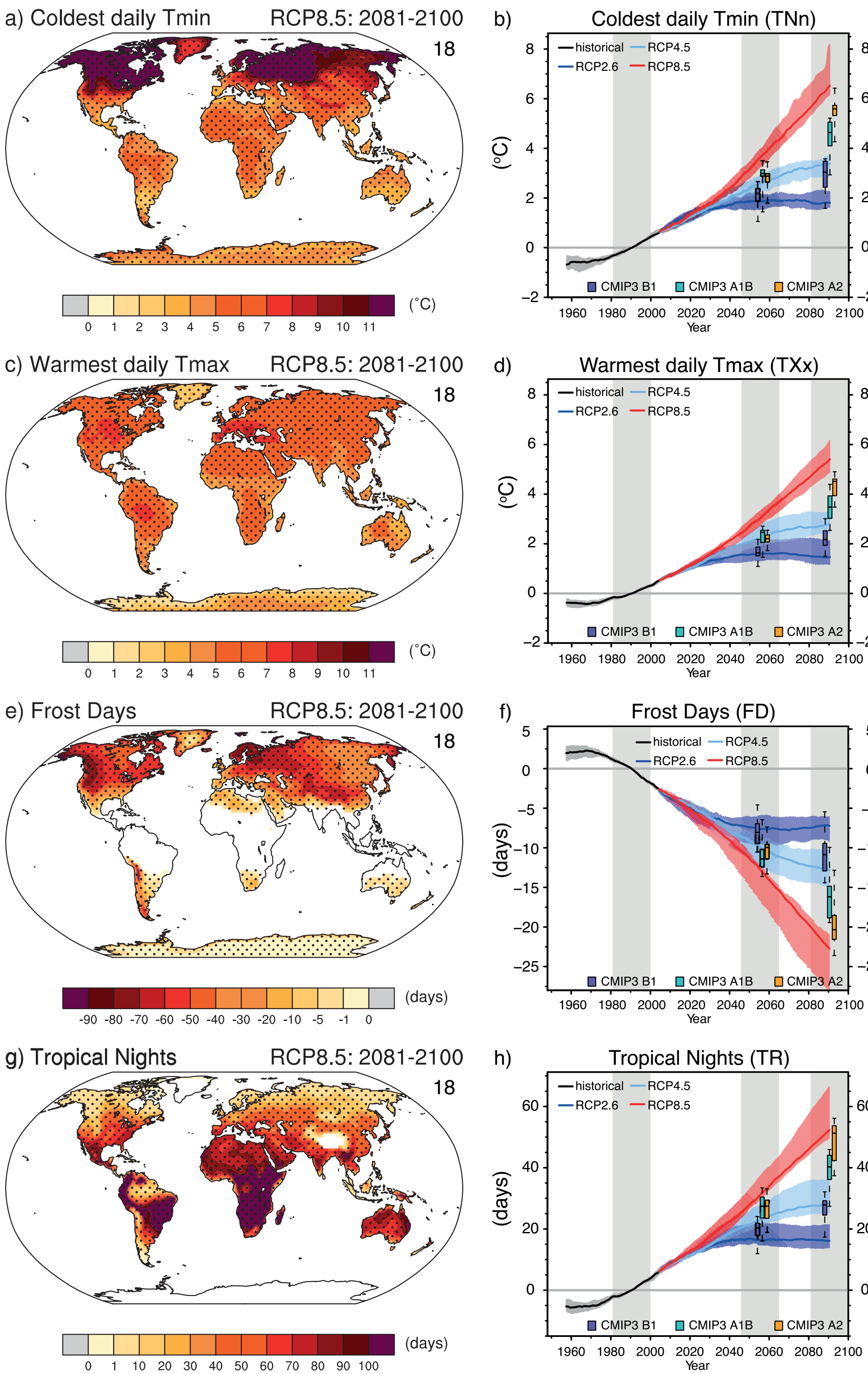

Figure 12.13 | CMIP5 multi-model mean geographical changes (relative to a 1981–2000 reference period in common with CMIP3) under RCP8.5 and 20-year smoothed time series for RCP2.6, RCP4.5 and RCP8.5 in the (a, b) annual minimum of daily minimum temperature, (c, d) annual maximum of daily maximum temperature, (e, f) frost days (number of days below 0°C) and (g, h) tropical nights (number of days above 20°C). White areas over land indicate regions where the index is not valid. Shading in the time series represents the interquartile ensemble spread (25th and 75th quantiles). The box-and-whisker plots show the interquartile ensemble spread (box) and outliers (whiskers) for 11 CMIP3 model simulations of the SRES scenarios A2 (orange), A1B (cyan), and B1 (purple) globally averaged over the respective future time periods (2046–2065 and 2081–2100) as anomalies from the 1981–2000 reference period. Stippling indicates grid points with changes that are significant at the 5% level using a Wilcoxon signed-ranked test. (Updated from Sillmann et al. (2013), excluding the FGOALS-s2 model.)

12

winter mean temperature changes, particularly over parts of North America and Europe. Kharin et al. (2013) concluded from the CMIP5 models that it is *likely* that in most land regions a current 20 year maximum temperature event is projected to become a one-in-two-year event by the end of the 21st century under the RCP4.5 and RCP8.5 scenarios, except for some regions of the high latitudes of the NH where it is *likely* to become a one-in-five-year event (see also Seneviratne et al. (2012) Figure 3.5). Current 20-year minimum temperature events are projected to become exceedingly rare, with return periods *likely* increasing to more than 100 years in almost all locations under RCP8.5 (Kharin et al., 2013). Section 10.6.1.1 notes that a number of detection and attribution studies since SREX suggest that the model changes may tend to be too large for warm extremes and too small for cold extremes and thus these likelihood statements are somewhat less strongly stated than a direct interpretation of model output and its ranges. The CMIP5 analysis shown in Figure 12.14 reinforces this assessment of large changes in the frequency of rare events, particularly in the RCP8.5 scenario (Kharin et al., 2013).

There is high consensus among models in the sign of the future change in temperature extremes, with recent studies confirming this conclusion from the previous assessments (Tebaldi et al., 2006; Meehl et al., 2007b; Orlowsky and Seneviratne, 2012; Seneviratne et al., 2012; Sillmann et al., 2013). However, the magnitude of the change remains uncertain owing to scenario and model (both structural and parameter) uncertainty (Clark et al., 2010) as well as internal variability. These uncertainties are much larger than corresponding uncertainties in the magnitude of mean temperature change (Barnett et al., 2006; Clark et al., 2006; Fischer and Schär, 2010; Fischer et al., 2011).

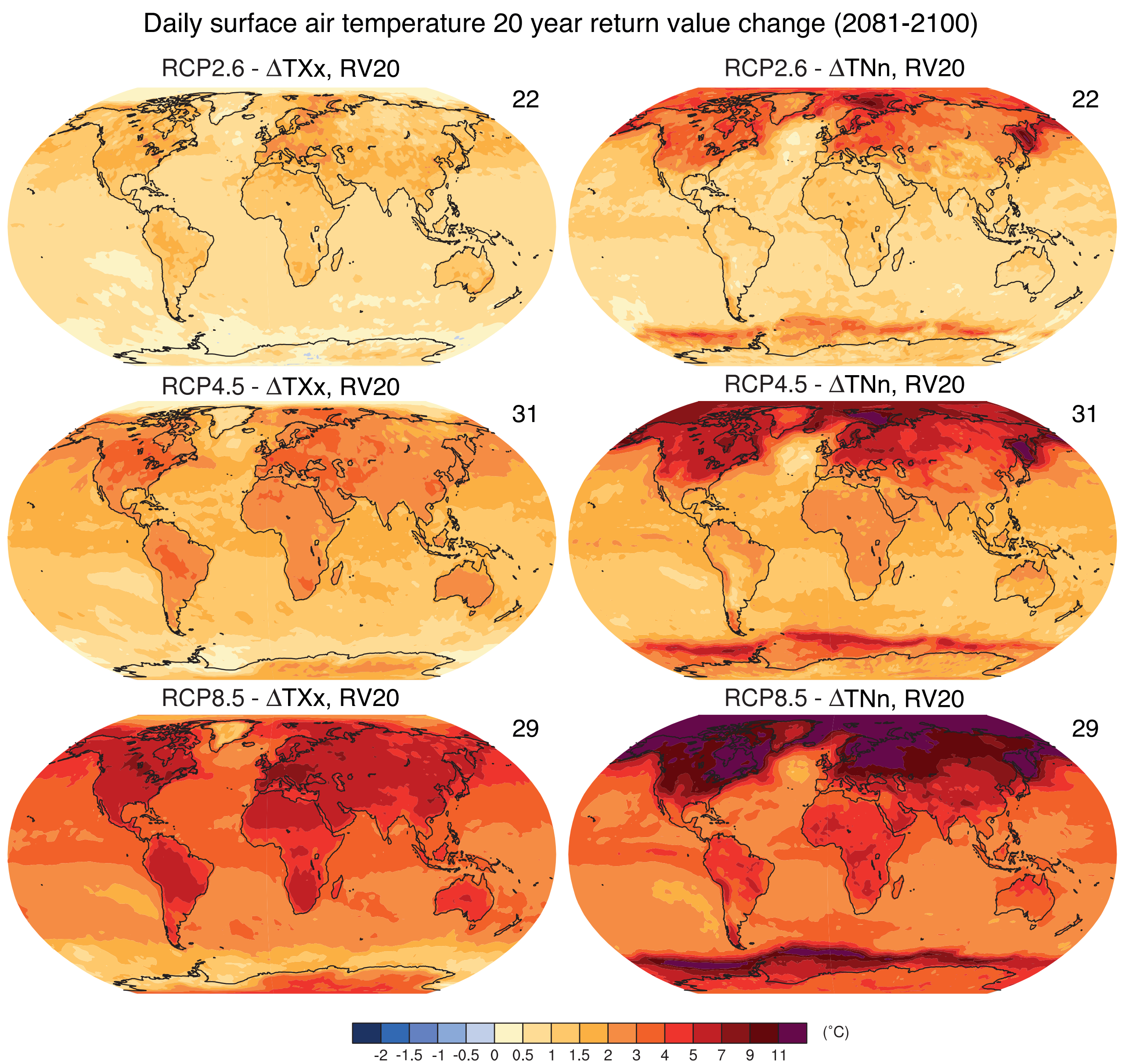

Figure 12.14 | The CMIP5 multi-model median change in 20-year return values of annual warm temperature extremes (left-hand panels) and cold temperature extremes (right-hand panels) as simulated by CMIP5 models in 2081–2100 relative to 1986–2005 in the RCP2.6 (top), RCP4.5 (middle panels), and RCP8.5 (bottom) experiments.

12.4.3.4 Energy Budget

Anthropogenic or natural perturbations to the climate system produce RFs that result in an imbalance in the global energy budget at the top of the atmosphere (TOA) and affect the global mean temperature (Section 12.3.3). The climate responds to a change in RF on multiple time scales and at multiyear time scales the energy imbalance (i.e., the energy heating or cooling the Earth) is very close to the ocean heat uptake due to the much lower thermal inertia of the atmosphere and the continental surfaces (Levitus et al., 2005; Knutti et al., 2008a; Murphy et al., 2009; Hansen et al., 2011). The radiative responses of the fluxes at TOA are generally analysed using the forcing-feedback framework and are presented in Section 9.7.2.

CMIP5 models simulate a small increase of the energy imbalance at the TOA over the 20th century (see Box 3.1, Box 9.2 and Box 13.1). The future evolution of the imbalance is very different depending on the scenario (Figure 12.15a): for RCP8.5 it continues to increase rapidly, much less for RCP6.0, it is almost constant for RCP4.5 and decreases for RCP2.6. This latter negative trend reveals the quasi-stabilization characteristic of RCP2.6. (In a transient scenario simulation, the TOA imbalance is always less than the RF because of the slow rate of ocean heat uptake.)

The rapid fluctuations that are simulated during the 20th century originate from volcanic eruptions that are prescribed in the models (see Section 12.3.2). These aerosols reflect solar radiation and thus decrease the amount of SW radiation absorbed by the Earth (Figure 12.15c). The minimum of shortwave (SW) radiation absorbed by the Earth during the period 1960–2000 is due mainly to two factors: a sequence of volcanic eruptions and an increase of the reflecting aerosol burden due to human activities (see Sections 7.5, 8.5 and 9.4.6). During the 21st century, the absorbed SW radiation monotonically increases for the RCP8.5 scenario, and increases and subsequently stabilizes for the other scenarios, consistent with what has been previously obtained with CMIP3 models and SRES scenarios (Trenberth and Fasullo, 2009). The two main contributions to the SW changes are the change of clouds (see Section 12.4.3.5) and the change of the cryosphere (see Section 12.4.6) at high latitudes. In the longwave (LW) domain (Figure 12.15b), the net flux at TOA represents the opposite of the flux that is emitted by the Earth's surface and atmosphere toward space, i.e., a negative anomaly represents an increase of the emitted

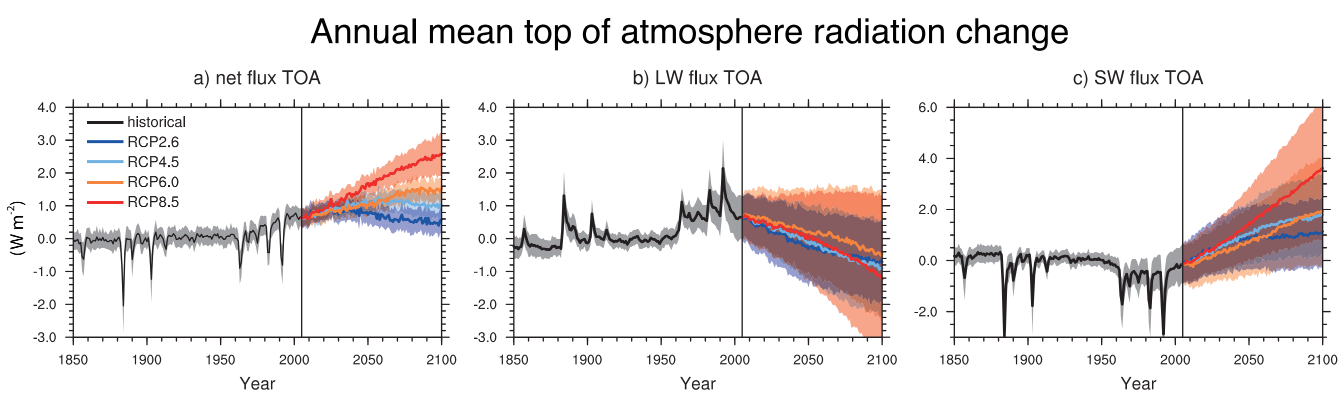

Figure 12.15 | Time series of global and annual multi-model mean (a) net total radiation anomaly at the top of the atmosphere (TOA), (b) net longwave radiation anomaly at the TOA and (c) net shortwave radiation anomaly at the TOA from the CMIP5 concentration-driven experiments for the historical period (black) and the four RCP scenarios. All the fluxes are positive downward and units are W m^{-2}. The anomalies are calculated relative to the 1900–1950 base period as this is a common period to all model experiments with few volcanic eruptions and relatively small trends. One ensemble member is used for each individual CMIP5 model and the ± standard deviation across the distribution of individual models is shaded.

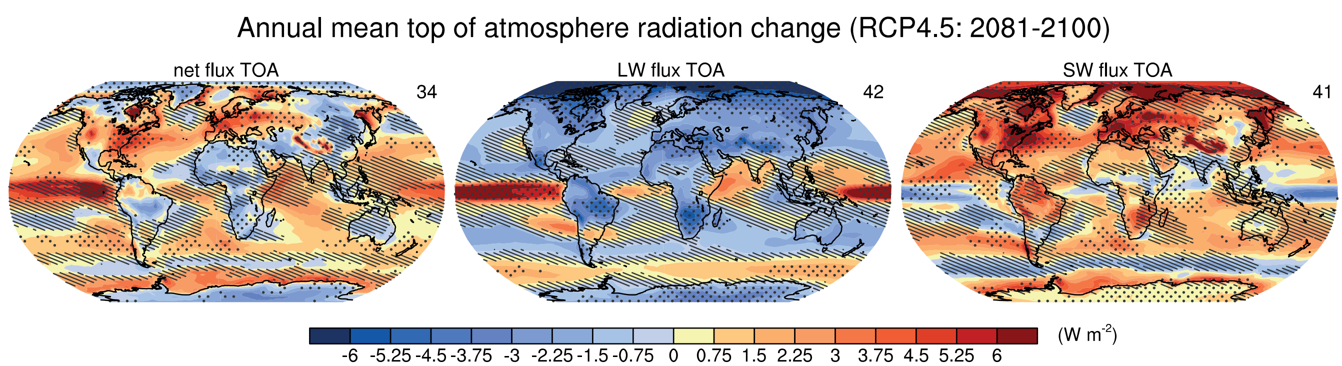

Figure 12.16 | Multi-model CMIP5 average changes in annual mean (left) net total radiation anomaly at the top of the atmosphere (TOA), (middle) net longwave radiation anomaly at the TOA and (right) net shortwave radiation anomaly at the TOA for the RCP4.5 scenario averaged over the periods 2081–2100. All fluxes are positive downward, units are W m^{-2}. The net radiation anomalies are computed with respect to the 1900–1950 base period. Hatching indicates regions where the multi-model mean change is less than one standard deviation of internal variability. Stippling indicates regions where the multi-model mean change is greater than two standard deviations of internal variability and where at least 90% of models agree on the sign of change (see Box 12.1).

LW radiation. The LW net flux depends mainly on two factors: the surface temperature and the magnitude of the greenhouse effect of the atmosphere. During the 20th century, the rapid fluctuations of LW radiation are driven by volcanic forcings, which decrease the absorbed SW radiation, surface temperature, and the LW radiation emitted by the Earth toward space. During the period 1960–2000, the fast increase of GHG concentrations also decreases the radiation emitted by the Earth. In response to this net heating of the Earth, temperatures warm and thereby increase emitted LW radiation although the change of the temperature vertical profile, water vapour, and cloud properties modulate this response (e.g., Bony et al., 2006; Randall et al., 2007).

12.4.3.5 Clouds

This section provides a summary description of future changes in clouds and their feedbacks on climate. A more general and more precise description and assessment of the role of clouds in the climate system is provided in Chapter 7, in particular Section 7.2 for cloud processes and feedbacks and Section 7.4 for aerosol–cloud interactions. Cloud feedbacks and adjustments are presented in Section 7.2.5 and a synthesis is provided in Section 7.2.6. Clouds are a major component of the climate system and play an important role in climate sensitivity (Cess et al., 1990; Randall et al., 2007), the diurnal temperature range (DTR) over land (Zhou et al., 2009), and land–sea contrast (see Section 12.4.3.1). The observed global mean cloud RF is about –20 W m^{-2} (Loeb et al., 2009) (see Section 7.2.1), that is, clouds have a net cooling effect. Current GCMs simulate clouds through various complex parameterizations (see Section 7.2.3), and cloud feedback is a major source of the spread of the climate sensitivity estimate (Soden and Held, 2006; Randall et al., 2007; Dufresne and Bony, 2008) (see Section 9.7.2).

Under future projections the multi-model pattern of total cloud amount shows consistent decreases in the subtropics, in conjunction with a decrease of the relative humidity there, and increases at high latitudes. Another robust pattern is an increase in cloud cover at all latitudes in the vicinity of the tropopause, a signature of the increase of the altitude of high level clouds in convective regions (Wetherald and Manabe, 1988; Meehl et al., 2007b; Soden and Vecchi, 2011; Zelinka et al., 2012). Low-level clouds were identified as a primary cause of inter-model spread in cloud feedbacks in CMIP3 models (Bony and Dufresne, 2005; Webb et al., 2006; Wyant et al., 2006). Since AR4, these results have been confirmed along with the positive feedbacks due to high level clouds in the CMIP3 or CFMIP models (Zelinka and Hartmann, 2010; Soden and Vecchi, 2011; Webb et al., 2013) and CMIP5 models (Vial et al., 2013). Since AR4, the response of clouds has been partitioned in a direct or 'rapid' response of clouds to CO_2 and a 'slow' response of clouds to the surface temperature increase (i.e., the usual feedback response) (Gregory and Webb, 2008). The radiative effect of clouds depends mainly on their fraction, optical depth and temperature. The contribution of these variables to the cloud feedback has been quantified for the multi-model CMIP3 (Soden and Vecchi, 2011) and CFMIP1 database (Zelinka et al., 2012). These findings are consistent with the radiative changes obtained with the CMIP5 models (Figure 12.16) and may be summarized as follows (see Section 7.2.5 for more details).

The dominant contributor to the SW cloud feedback is the change in cloud fraction. The reduction of cloud fraction between 50°S and 50°N, except along the equator and the eastern part of the ocean basins (Figure 12.17), contributes to an increase in the absorbed solar radiation (Figure 12.16c). Physical mechanisms and the role of different parameterizations have been proposed to explain this reduction of low-level clouds (Zhang and Bretherton, 2008; Caldwell and Bretherton, 2009; Brient and Bony, 2013; Webb et al., 2013). Poleward of 50°S, the cloud fraction and the cloud optical depth increases, thereby increasing cloud reflectance. This leads to a decrease of solar absorption around Antarctica where the ocean is nearly ice free in summer (Figure 12.16c). However, there is *low confidence* in this result because GCMs do not reproduce the nearly 100% cloud cover observed there and the negative feedback could be overestimated (Trenberth and Fasullo, 2010) or, at the opposite, underestimated because the cloud optical depth simulated by models is biased high there (Zelinka et al., 2012).

In the LW domain, the tropical high cloud changes exert the dominant effect. A lifting of the cloud top with warming is simulated consistently across models (Meehl et al., 2007b) which leads to a positive feedback whereby the LW emissions from high clouds decrease as they cool (Figure 12.16b). The dominant driver of this effect is the increase of tropopause height and physical explanations have been proposed (Hartmann and Larson, 2002; Lorenz and DeWeaver, 2007; Zelinka

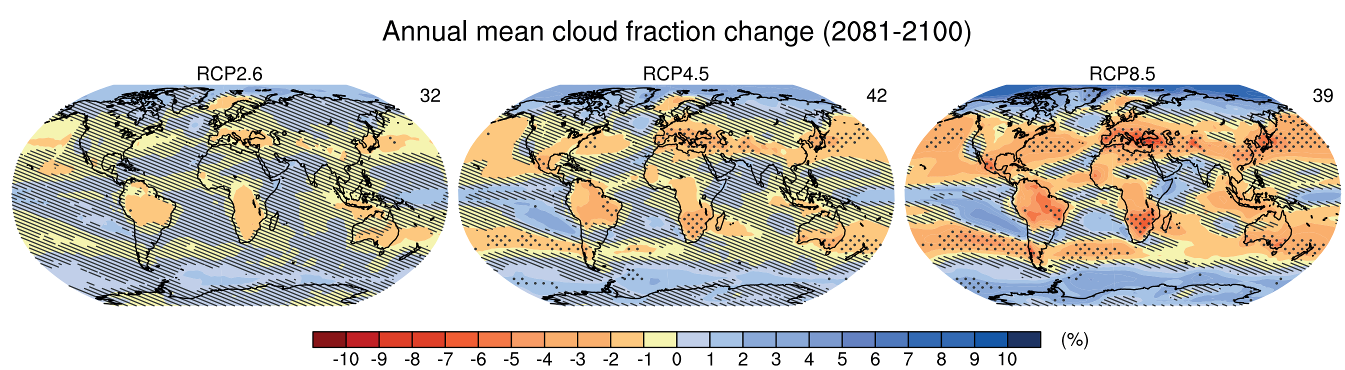

Figure 12.17 | CMIP5 multi-model changes in annual mean total cloud fraction (in %) relative to 1986–2005 for 2081–2100 under the RCP2.6 (left), RCP4.5 (centre) and RCP8.5 (right) forcing scenarios. Hatching indicates regions where the multi-model mean change is less than one standard deviation of internal variability. Stippling indicates regions where the multi-model mean change is greater than two standard deviations of internal variability and where 90% of the models agree on the sign of change (see Box 12.1). The number of CMIP5 models used is indicated in the upper right corner of each panel.

and Hartmann, 2010). Although the decrease in cloudiness generally increases outgoing longwave radiation and partly offsets the effect of cloud rising, the net effect is a consistent positive global mean LW cloud feedback across CMIP and CFMIP models. Global mean SW cloud feedbacks range from slightly negative to strongly positive (Soden and Vecchi, 2011; Zelinka et al., 2012), with an inter-model spread in net cloud feedback being mainly attributable to low-level cloud changes.

In summary, both the multi-model mean and the inter-model spread of the cloud fraction and radiative flux changes simulated by the CMIP5 models are consistent with those previously obtained by the CMIP3 models. These include decreases in cloud amount in the subtropics, increases at high latitudes and increases in the altitude of high level clouds in convective regions. Many of these changes have been understood primarily as responses to large-scale circulation changes (see Section 7.2.6).

12.4.4 Changes in Atmospheric Circulation

Projected changes in energy and water cycles couple with changes in atmospheric circulation and mass distribution. Understanding this coupling is necessary to assess physical behaviour underlying projected changes, particularly at regional scales, revealing why changes occur and the realism of the changes. The focus in this section is on atmospheric circulation behaviour that CMIP5 GCMs resolve well. Thus, the section includes discussion of extratropical cyclones but not tropical cyclones: extratropical cyclones are fairly well resolved by most CMIP5 GCMs, whereas tropical cyclones are not, requiring resolutions finer than used by the large majority of CMIP5 GCMs (see Section 9.5.4.3). Detailed discussion of tropical cyclones appears in Section 14.6.1 (see also Section 11.3.2.5.3 for near term changes and Section 3.4.4 in Seneviratne et al. (2012)). Regional detail concerning extratropical storm tracks, including causal processes, appears in Section 14.6.2 (see also Section 11.3.2.4 for near-term changes and Seneviratne et al. (2012) for an assessment of projected changes related to weather and climate extremes).

12.4.4.1 Mean Sea Level Pressure and Upper-Air Winds

Sea level pressure gives an indication of surface changes in atmospheric circulation (Figure 12.18). As in previous assessments, a robust feature of the pattern of change is a decrease in high latitudes and increases in the mid-latitudes, associated with poleward shifts in the SH mid-latitude storm tracks (Section 12.4.4.3) and positive trends in the annular modes (Section 14.5) as well as an expansion of the Hadley Cell (Section 12.4.4.2). Similar patterns of sea level pressure change are found in observed trends over recent decades, suggesting an already detectable change (Gillett and Stott, 2009; Section 10.3.3.4), although the observed patterns are influenced by both natural and anthropogenic forcing as well as internal variability and the relative importance of these influences is likely to change in the future. Internal variability has been found to play a large role in uncertainties of future sea level pressure projections, particularly at higher latitudes (Deser et al., 2012a).

In boreal winter, decreases of sea level pressure over NH high latitudes are slightly weaker in the CMIP5 ensemble compared to previous assessments, consistent with Scaife et al. (2012) and Karpechko and Manzini (2012), who suggest that improvements in the representation of the stratosphere can influence this pattern. In austral summer, the SH projections are impacted by the additional influence of stratospheric ozone recovery (see Section 11.3.2.4.2) which opposes changes due to GHGs. Under the weaker GHG emissions of RCP2.6, decreases in sea level pressure over the SH mid-latitudes and increases over SH high latitudes are consistent with expected changes from ozone recovery (Arblaster et al., 2011; McLandress et al., 2011; Polvani et al., 2011). For

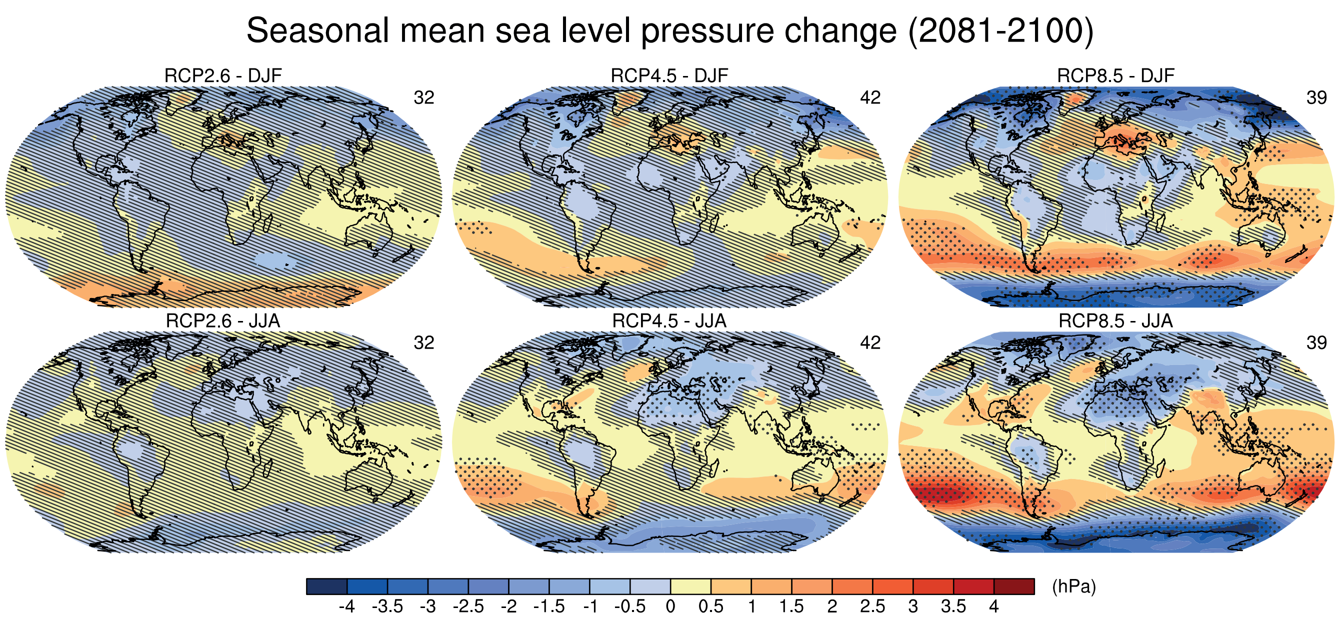

Figure 12.18 | CMIP5 multi-model ensemble average of December, January and February (DJF, top row) and June, July and August (JJA, bottom row) mean sea level pressure change (2081–2100 minus 1986–2005) for, from left to right, RCP2.6, 4.5 and 8.5. Hatching indicates regions where the multi-model mean change is less than one standard deviation of internal variability. Stippling indicates regions where the multi-model mean change is greater than two standard deviations of internal variability and where at least 90% of models agree on the sign of change (see Box 12.1).

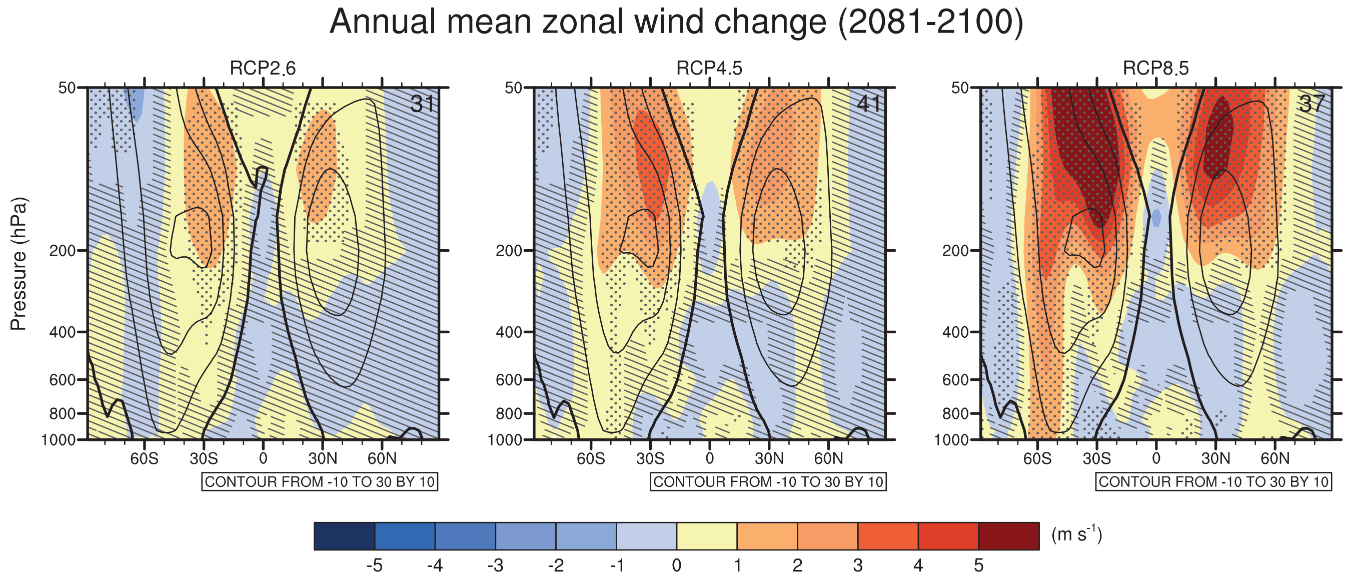

Figure 12.19 | Coupled Model Intercomparison Project Phase 5 (CMIP5) multi-model ensemble average of zonal and annual mean wind change (2081–2100 minus 1986–2005) for, from left to right, Representative Concentration Pathway 2.6 (RCP2.6), 4.5 and 8.5. Black contours represent the multi-model average for the 1986–2005 base period. Hatching indicates regions where the multi-model mean change is less than one standard deviation of internal variability. Stippling indicates regions where the multi-model mean change is greater than two standard deviations of internal variability and where at least 90% of models agree on the sign of change (see Box 12.1).

all other RCPs, the magnitude of SH extratropical changes scales with the RF, as found in previous model ensembles (Paeth and Pollinger, 2010; Simpkins and Karpechko, 2012).

Large increases in seasonal sea level pressure are also found in regions of sub-tropical drying such as the Mediterranean and northern Africa in DJF and Australia in JJA. Projected changes in the tropics are less consistent across the models; however, a decrease in the eastern equatorial Pacific and increase over the maritime continent, associated with a weakening of the Walker Circulation (Vecchi and Soden, 2007; Power and Kociuba, 2011b), is found in all RCPs.

Future changes in zonal and annual mean zonal winds (Figure 12.19) are seen throughout the atmosphere with stronger changes in higher RCPs. Large increases in winds are evident in the tropical stratosphere and a poleward shift and intensification of the SH tropospheric jet is seen under RCP4.5 and RCP8.5, associated with an increase in the SH upper tropospheric meridional temperature gradient (Figure 12.12) (Wilcox et al., 2012). In the NH, the response of the tropospheric jet is weaker and complicated by the additional thermal forcing of polar amplification (Woollings, 2008). Barnes and Polvani (2013) evaluate changes in the annual mean mid-latitude jets in the CMIP5 ensemble, finding consistent poleward shifts in both hemispheres under RCP8.5 for the end of the 21st century. In the NH, the poleward shift is ~1°, similar to that found for the CMIP3 ensemble (Woollings and Blackburn, 2012). In the SH, the annual mean mid-latitude jet shifts poleward by ~2° under RCP8.5 at the end of the 21st century in the CMIP5 multi-model mean (Barnes and Polvani, 2013), with a similar shift of 1.5° in the surface westerlies (Swart and Fyfe, 2012). A strengthening of the SH surface westerlies is also found under all RCPs except RCP2.6 (Swart and Fyfe, 2012), with largest changes in the Pacific basin (Bracegirdle et al., 2013). In austral summer, ozone recovery offsets changes in GHGs to some extent, with a weak reversal of the jet shift found in the multi-model mean under the low emissions scenario of RCP2.6 (Swart and Fyfe, 2012) and weak or poleward shifts in other RCPs (Swart and Fyfe, 2012; Wilcox et al., 2012). Eyring et al. (2013) note the sensitivity of the CMIP5 SH summertime circulation changes to both the strength of the ozone recovery (simulated by some models interactively) and the rate of GHG increases.

Although the poleward shift of the tropospheric jets are robust across models and *likely* under increased GHGs, the dynamical mechanisms behind these projections are still not completely understood and have been explored in both simple and complex models (Chen et al., 2008; Lim and Simmonds, 2009; Butler et al., 2010). The shifts are associated with a strengthening in the upper tropospheric meridional temperature gradient (Wilcox et al., 2012) and hypotheses for associated changes in planetary wave activity and/or synoptic eddy characteristics that impact on the position of the jet have been put forward (Gerber et al., 2012). Equatorward biases in the position of the SH jet (Section 9.5.3.2), while somewhat improved over similar biases in the CMIP3 models (Kidston and Gerber, 2010) still remain, limiting our confidence in the magnitude of future changes.

In summary, poleward shifts in the mid-latitude jets of about 1 to 2 degrees latitude are *likely* at the end of the 21st century under RCP8.5 in both hemispheres (*medium confidence*) with weaker shifts in the NH and under lower emission scenarios. Ozone recovery will *likely* weaken the GHG-induced changes in the SH extratropical circulation in austral summer.

12.4.4.2 Planetary-Scale Overturning Circulations

Large-scale atmospheric overturning circulations and their interaction with other atmospheric mechanisms are significant in determining tropical climate and regional changes in response to enhanced RF. Observed changes in tropical atmospheric circulation are assessed in Section 2.7.5, while Section 10.3.3 discusses attribution of these observed changes to anthropogenic forcing. Evidence is inconclusive on recent trends in the strength of the Hadley (Stachnik and Schumacher, 2011) and Walker Circulations (Vecchi et al., 2006; Sohn and Park, 2010; Merrifield, 2011; Luo et al., 2012; Tokinaga et al., 2012), though there is *medium confidence* of an anthropogenic influence on the observed widening of the Hadley Circulation (Hu and Fu, 2007; Johanson and Fu, 2009; Davis and Rosenlof, 2012). In the projections, there are indications of a weakening of tropical overturning of air as the climate warms (Held and Soden, 2006; Vecchi and Soden, 2007; Gastineau et al., 2008, 2009; Chou and Chen, 2010; Chadwick et al., 2012; Bony et al., 2013). In the SRES A1B scenario, CMIP3 models show a remarkable agreement in simulating a weakening of the tropical atmospheric overturning circulation (Vecchi and Soden, 2007). CMIP5 models also show a consistent weakening (Chadwick et al., 2012). Along the ascending branches of tropical overturning cells, a reduction in convective mass flux from the boundary layer to the free atmosphere is implied by the differential response to global warming of the boundary-layer moisture content and surface evaporation. This weakening of vertical motion along the ascending regions of both the tropical meridional and near-equatorial zonal cells is associated with an imbalance in the rate of atmospheric moisture increase and that of global mean precipitation (Held and Soden, 2006). A reduction in the compensating climatological subsidence along the downward branches of overturning circulations, where the rate of increase of static stability exceeds radiative cooling, is implied.

Several mechanisms have been suggested for the changes in the intensity of the tropical overturning circulation. The weakening of low-level convective mass flux along ascending regions of tropical overturning cells has been ascribed to changes in the hydrologic cycle (Held and Soden, 2006; Vecchi and Soden, 2007). Advection of dry air from subsidence regions towards the ascending branches of large-scale tropical circulation has been suggested to be a feasible mechanism weakening ascent along the edges of convection regions (Chou et al., 2009). A deepening of the tropical troposphere in response to global warming increases the vertical extent of convection, which has been shown to increase the atmosphere's moist stability and thus also weakening overturning cells (Chou and Chen, 2010). An imbalance between the increase in diabatic heating of the troposphere and in static stability whereby the latter increases more rapidly has also been thought to play a role in weakening tropical ascent (Lu et al., 2008). Mean advection of enhanced vertical stratification under GHG forcing which involves cooling of convective regions and warming of subsidence regions has been shown to slow down tropical cells (Ma et al., 2012). The latest findings using CMIP5 models reveal that an increase in GHGs (particularly CO_2) contributes significantly to weakening tropical overturning cells by reducing radiative cooling in the upper atmosphere (Bony et al., 2013). SST gradients have also been found to play a role in altering the strength of tropical cells (Tokinaga et al., 2012; Ma and Xie, 2013). Evidence has been provided suggesting that the SH Hadley Cell may strengthen in response to meridional SST gradients featuring reduced warming in the SH subtropical oceans relative to the NH, particularly over the Pacific and Indian Oceans (Ma and Xie, 2013). The north-to-south SST warming gradients are a source of intermodel differences in their projections of changes in the SH Hadley Circulation.

Apart from changes in Hadley Circulation strength, a robust feature in 21st century climate model simulations is an increase in the cell's depth and width (Mitas and Clement, 2006; Frierson et al., 2007; Lu et al., 2007; Lu et al., 2008), with the latter change translating to a broadening of tropical regions (Seidel and Randel, 2007; Seidel et al., 2008) and a poleward displacement of subtropical dry zones (Lu et al., 2007; Scheff and Frierson, 2012). The increase in the cell's depth is consistent with a tropical tropopause rise. The projected increase in the height of the tropical tropopause and the associated increase in meridional temperature gradients close to the tropopause slope have been proposed to be an important mechanism behind the Hadley cell expansion and the poleward displacement of the subtropical westerly jet (Lu et al., 2008; Johanson and Fu, 2009). An increase in subtropical and mid-latitude static stability has been found to be an important factor widening the Hadley Cell by shifting baroclinic eddy activity and the associated eddy-driven jet and subsidence poleward (Mitas and Clement, 2006; Lu et al., 2008). The projected widening of the Hadley Cell is consistent with late 20th century observations, where ~2° to 5° latitude expansion was found (Fu et al., 2006; Johanson and Fu, 2009). The consistency of simulated changes in CMIP3 and CMIP5 models and the consistency of Hadley Cell changes with the projected tropopause rise and increase in subtropical and mid-latitude static stability indicate that a widening and weakening of the NH Hadley Cell by the late 21st century is *likely*.

The zonally asymmetric Walker Circulation is projected to weaken under global warming (Power and Kociuba, 2011a, 2011b), more than the Hadley Circulation (Lu et al., 2007; Vecchi and Soden, 2007). The consistency of the projected Walker Circulation slowdown from CMIP3 to CMIP5 suggests that its change is robust (Ma and Xie, 2013). Almost everywhere around the equatorial belt, changes in the 500 hPa vertical motion oppose the climatological background motion, notably over the maritime continent (Vecchi and Soden, 2007; Shongwe et al., 2011). Around the Indo-Pacific warm pool, in response to a spatially uniform SST warming, the climatological upper tropospheric divergence weakens (Ma and Xie, 2013). Changes in the strength of the Walker Circulation also appear to be linked to differential warming between the Indian and Pacific Ocean warming at low latitudes (Luo et al., 2012). Over the equatorial Pacific Ocean, where mid-tropospheric ascent is projected to strengthen, changes in zonal SST and hence sea level pressure gradients induce low-level westerly wind anomalies that act to weaken the low-level branch of the Pacific Walker Circulation. These projected changes in the tropical Pacific circulation are already occurring (Zhang and Song, 2006). However, the projected weakening of the Pacific Walker Cell does not imply an increase in the frequency and/or magnitude of El Niño events (Collins et al., 2010). The consistency of simulated changes in CMIP3 and CMIP5 models and the consistency of Walker Cell changes with equatorial SST and pressure-gradient changes that are already observed indicate that a weakening of the Walker Cell by the late 21st century is *likely*.

In the upper atmosphere, a robust feature of projected stratospheric circulation change is that the Brewer–Dobson circulation will *likely* strengthen in the 21st century (Butchart et al., 2006, 2010; Li et al., 2008; McLandress and Shepherd, 2009; Shepherd and McLandress, 2011). In a majority of model experiments, the projected changes in the large-scale overturning circulation in the stratosphere feature an intensification of tropical upward mass flux, which may extend to the upper stratosphere. The proposed driver of the increase in mass flux at the tropical lower stratosphere is the enhanced propagation of wave activity, mainly resolved planetary waves, associated with a positive trend in zonal wind structure (Butchart and Scaife, 2001; Garcia and Randel, 2008). In the 21st century, increases in wave excitation from diabatic heating in the upper tropical troposphere could reinforce the wave forcing on the tropical upwelling branch of the stratospheric mean meridional circulation (Calvo and Garcia, 2009). Parameterized orographic gravity waves that result from strengthening of subtropical westerly jets and cause more waves to propagate into the lower stratosphere also play a role (Sigmond et al., 2004; Butchart et al., 2006). The projected intensification in tropical upwelling is counteracted by enhanced mean extratropical/polar lower stratospheric subsidence. In the NH high latitudes, the enhanced downwelling is associated with an increase in stationary planetary wave activities (McLandress and Shepherd, 2009). The intensification of the stratospheric meridional residual circulation has already been reported in studies focussing on the last decades of the 20th century (Garcia and Randel, 2008; Li et al., 2008; Young et al., 2012). The projected increase in troposphere-to-stratosphere mass exchange rate (Butchart et al., 2006) and stratospheric mixing associated with the strengthening of the Brewer–Dobson circulation will *likely* result in a decrease in the mean age of air in the lower stratosphere. In the mid-latitude lower stratosphere, quasi-horizontal mixing is a significant contributor to reducing the lifetimes of air. There are some suggestions that the changes in stratospheric overturning circulation could lead to a reduction in tropical ozone concentrations and an increase at high latitudes (Jiang et al., 2007) and an increase in the amplitude of the annual cycle of stratospheric ozone (Randel et al., 2007).

12.4.4.3 Extratropical Storms: Tracks and Influences on Planetary-Scale Circulation and Transports

Since the AR4, there has been continued evaluation of changes in extratropical storm tracks under projected warming using both CMIP3 and, more recently, CMIP5 simulations, as well as supporting studies using single models or idealized simulations. CMIP3 analyses use a variety of methods for diagnosing storm tracks, but diagnosis of changes in the tracks appears to be relatively insensitive to methods used (Ulbrich et al., 2013). Analyses of SH storm tracks generally agree with earlier studies, showing that extratropical storm tracks will tend to shift poleward (Bengtsson et al., 2009; Gastineau et al., 2009; Gastineau and Soden, 2009; Perrie et al., 2010; Schuenemann and Cassano, 2010; Chang et al., 2012b). The behaviour is consistent with a *likely* trend in observed storm-track behaviour (see Section 2.7.6). Similar behaviour appears in CMIP5 simulations for the SH (Figure 12.20c, d). In SH winter there is a clear poleward shift in storm tracks of several degrees and a reduction in storm frequency of only a few percent (not shown). The poleward shift at the end of the century is consistent with a poleward shift in the SH of the latitudes with strongest tropospheric jets (Figure 12.19). This appears to coincide with shifts in baroclinic dynamics governing extratropical storms (Frederiksen et al., 2011), though the degree of jet shift appears to be sensitive to bias in a model's contemporary-climate storm tracks (Chang et al., 2012a, 2012b). Although there is thus some uncertainty in the degree of shift, the consistency of behaviour with observation-based trends, consistency between CMIP5 and CMIP3 projections under a variety of diagnostics and the physical consistency of the storm response with other climatic changes gives *high confidence* that a poleward shift of several degrees in SH storm tracks is *likely* by the end of the 21st century under the RCP8.5 scenario.

In the NH winter (Figure 12.20a, b), the CMIP5 multi-model ensemble shows an overall reduced frequency of storms and less indication of a poleward shift in the tracks. The clearest poleward shift in the NH winter at the end of the 21st century occurs in the Asia-Pacific storm track, where intensification of the westerly jet promotes more intense cyclones in an ensemble of CMIP5 models (Mizuta, 2012). Otherwise, changes in winter storm-track magnitude, as measured by band-pass sea level pressure fluctuations, show only small change relative to interannual and inter-decadal variability by the end of the 21st century in SRES A1B and RCP4.5 simulations for several land areas over the NH (Harvey et al., 2012). Consistency in CMIP3 and CMIP5 changes seen in the SH are absent in the NH (Chang et al., 2012a). Factors identified that affect changes in the North Atlantic basin's storm track include horizontal resolution (Colle et al., 2013) and how models simulate changes in the Atlantic's meridional overturning circulation (Catto et al., 2011; Woollings et al., 2012), the zonal jet and Hadley Circulation (Mizuta, 2012; Zappa et al., 2013) and subtropical upper troposphere temperature (Haarsma et al., 2013). Substantial uncertainty and thus *low confidence* remains in projecting changes in NH winter storm tracks, especially for the North Atlantic basin.

Additional analyses of CMIP3 GCMs have determined other changes in properties of extratropical storms. Most analyses find that the frequency of storms decreases in projected climates (Finnis et al., 2007; Favre and Gershunov, 2009; Dowdy et al., 2013), though the occurrence of strong storms may increase in some regions (Pinto et al., 2007; Bengtsson et al., 2009; Ulbrich et al., 2009; Zappa et al., 2013). Many studies focus on behaviour of specific regions, and results of these studies are detailed in Section 14.6.2.

Changes in extratropical storms in turn may influence other large-scale climatic changes. Kug et al. (2010) in a set of time-slice simulations show that a poleward shift of storm tracks in the NH could enhance polar warming and moistening. The Arctic Oscillation (AO) is sensitive to synoptic eddy vorticity flux, so that projected changes in storm tracks can alter the AO (Choi et al., 2010). The net result is that changes in extratropical storms alter the climate in which they are embedded, so that links between surface warming, extratropical storms and their influence on climate are more complex than simple responses to changes in baroclinicity (O'Gorman, 2010).

12.4.5 Changes in the Water Cycle

The water cycle consists of water stored on the Earth in all its phases, along with the movement of water through the Earth's climate system. In the atmosphere, water occurs primarily as gaseous water vapour, but it also occurs as solid ice and liquid water in clouds. The ocean is primarily liquid water, but is partly covered by ice in polar regions. Terrestrial water in liquid form appears as surface water (lakes, rivers), soil moisture and groundwater. Solid terrestrial water occurs in ice sheets, glaciers, frozen lakes, snow and ice on the surface and permafrost.

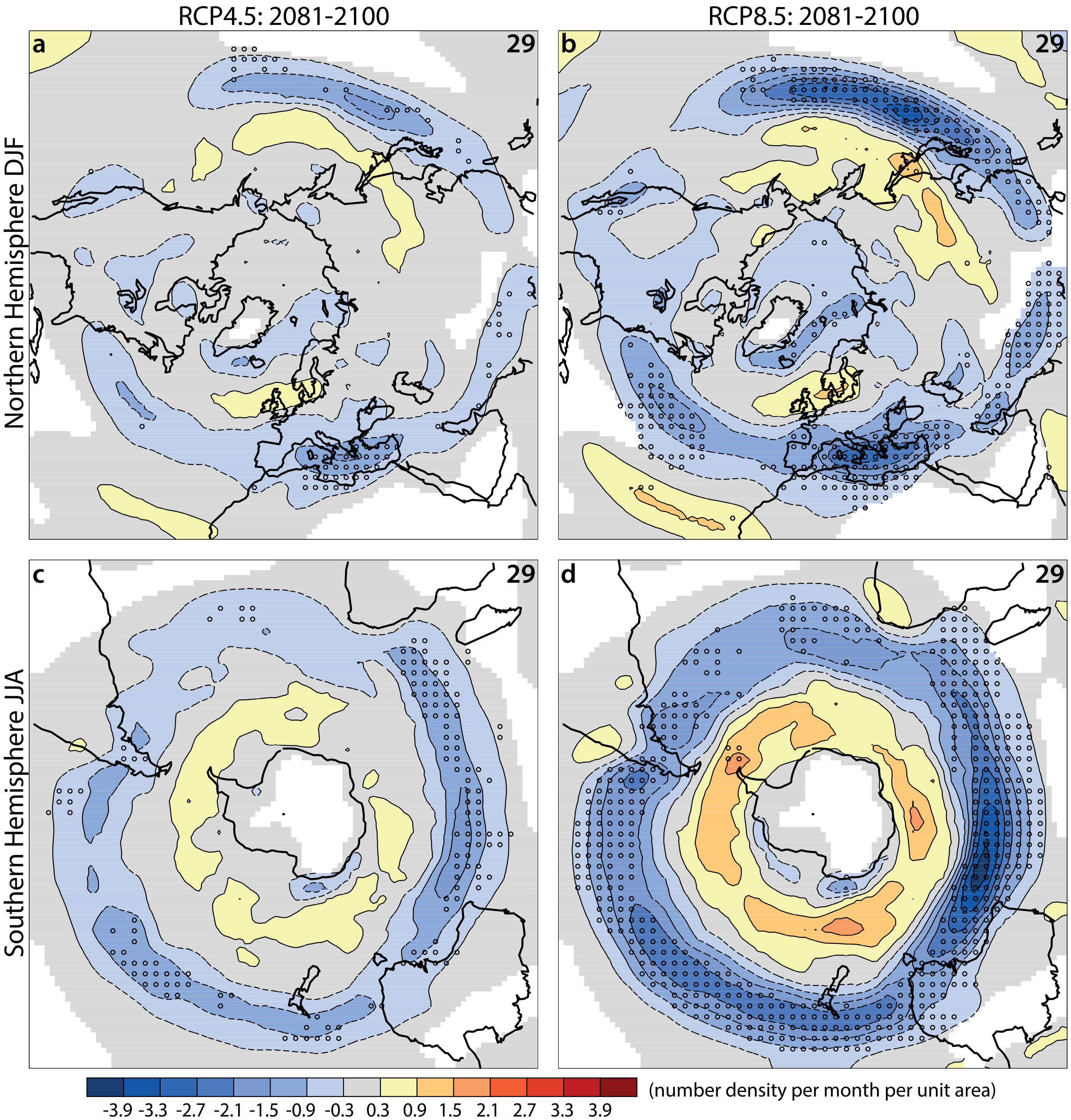

Figure 12.20 | Change in winter, extratropical storm track density (2081–2100) – (1986–2005) in CMIP5 multi-model ensembles: (a) RCP4.5 Northern Hemisphere December, January and February (DJF) and (b) RCP8.5 Northern Hemisphere DJF, (c) RCP4.5 Southern Hemisphere June, July and August (JJA) and (d) RCP8.5 Southern Hemisphere JJA. Storm-track computation uses the method of Bengtsson et al. (2006, their Figure 13a) applied to 6-hourly 850 hPa vorticity computed from horizontal winds in the CMIP5 archive. The number of models used appears in the upper right of each panel. DJF panels include data for December 1985 and 2080 and exclude December 2005 and December 2100 for in-season continuity. Stippling marks locations where at least 90% of the models agree on the sign of the change; note that this criterion differs from that used for many other figures in this chapter, due to the small number of models providing sufficient data to estimate internal variability of 20-year means of storm-track statistics. Densities have units (number density per month per unit area), where the unit area is equivalent to a 5° spherical cap (~10^6 km^2). Locations where the scenario or contemporary-climate ensemble average is below 0.5 density units are left white.

Projections of future changes in the water cycle are inextricably connected to changes in the energy cycle (Section 12.4.3) and atmospheric circulation (Section 12.4.4).

Saturation vapour pressure increases with temperature, but projected future changes in the water cycle are far more complex than projected temperature changes. Some regions of the world will be subject to decreases in hydrologic activity while others will be subject to increases. There are important local seasonal differences among the responses of the water cycle to climate change as well.

At first sight, the water cycles simulated by CMIP3/5 models may appear to be inconsistent, particularly at regional scales. Anthropogenic changes to the water cycle are superimposed on complex naturally varying modes of the climate (such as El Niño-Southern Oscillation (ENSO), AO, Pacific Decadal Oscillation (PDO), etc.) aggravating the differences between model projections. However, by careful consideration of the interaction of the water cycle with changes in other aspects of the climate system, the mechanisms of change are revealed, increasing confidence in projections.

12.4.5.1 Atmospheric Humidity

Atmospheric water vapour is the primary GHG in the atmosphere. Its changes affect all parts of the water cycle. However, the amount of water vapour is dominated by naturally occurring processes and not significantly affected directly by human activities. A common experience from past modelling studies is that relative humidity (RH) remains approximately constant on climatological time scales and planetary space scales, implying a strong constraint by the Clausius–Clapeyron relationship on how specific humidity will change. The AR4 stated that 'a broad-scale, quasi-unchanged RH response [to climate change] is uncontroversial' (Randall et al., 2007). However, underlying this fairly straightforward behaviour are changes in RH that can influence changes in cloud cover and atmospheric convection (Sherwood, 2010). More recent analysis provides further detail and insight on RH changes. Analysis of CMIP3 and CMIP5 models shows near-surface RH decreasing over most land areas as temperatures increase with the notable exception of parts of tropical Africa (O'Gorman and Muller, 2010) (Figure 12.21). The prime contributor to these decreases in RH over land is the larger temperature increases over land than over ocean in the RCP scenarios (Joshi et al., 2008; Fasullo, 2010; O'Gorman and Muller, 2010). The specific humidity of air originating over more slowly warming oceans will be governed by saturation temperatures of oceanic air. As this air moves over land and is warmed, its relative humidity drops as any further moistening of the air over land is insufficient to maintain constant RH, a behaviour Sherwood et al. (2010) term a last-saturation-temperature constraint. The RH decrease over most land areas by the end of the 21st century is consistent with a last-saturation-temperature constraint and with observed behaviour during the first decade of the current century (Section 2.5.5; Simmons et al., 2010). Land–ocean differences in warming are projected to continue through the 21st century, and although the CMIP5 projected changes are small, they are consistent with a last-saturation constraint, indicating with *medium confidence* that reductions in near-surface RH over many land areas are *likely*.

12.4.5.2 Patterns of Projected Average Precipitation Changes

Global mean precipitation changes have been presented in Section 12.4.1.1. The processes that govern large-scale changes in precipitation are presented in Section 7.6, and are used here to interpret the

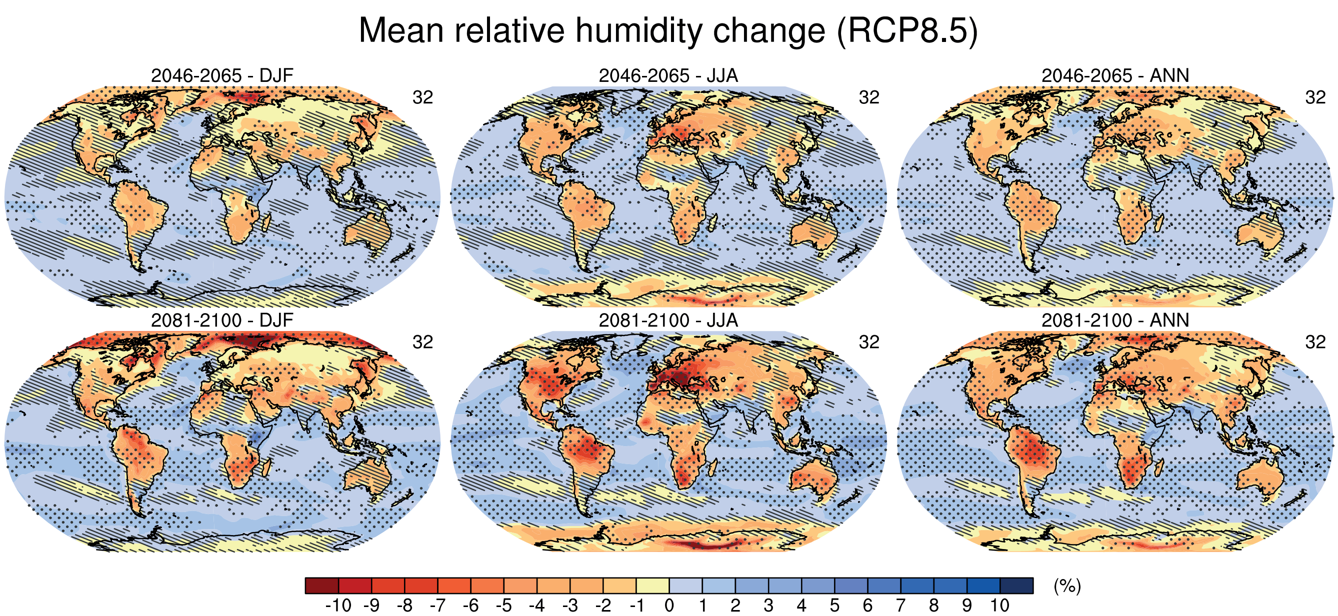

Figure 12.21 | Projected changes in near-surface relative humidity from the CMIP5 models under RCP8.5 for the December, January and February (DJF, left), June, July and August (JJA, middle) and annual mean (ANN, right) averages relative to 1986–2005 for the periods 2046–2065 (top row), 2081–2100 (bottom row). The changes are differences in relative humidity percentage (as opposed to a fractional or relative change). Hatching indicates regions where the multi-model mean change is less than one standard deviation of internal variability. Stippling indicates regions where the multi-model mean change is greater than two standard deviations of internal variability and where at least 90% of models agree on the sign of change (see Box 12.1).

projected changes in RCP scenarios. Changes in precipitation extremes are presented in Section 12.4.5.5. Further discussion of regional changes, in particular the monsoon systems, is presented in Chapter 14.

Figure 12.22 shows the CMIP5 multi-model average percentage change in seasonal mean precipitation in the middle of the 21st century, at the end of the 21st century and at the end of the 22nd century for the RCP8.5 scenario relative to the 1986–2005 average. Precipitation changes for all the scenarios are shown in Annex I Supplementary Material and scale approximately with the global mean temperature (Section 12.4.2). In many regions, changes in precipitation exhibit strong seasonal characteristics so that, in regions where the sign of the precipitation changes varies with the season, the annual mean values (Figure 12.10) may hide some of these seasonal changes, resulting in weaker confidence than seasonal mean values (Chou et al., 2013; Huang et al., 2013).

The patterns of multi-model precipitation changes displayed in Figure 12.22 tend to smooth and decrease the spatial contrast of precipitation changes simulated by each model, in particular over regions where model results disagree. Thus the amplitude of the multi-model ensemble mean precipitation response significantly underestimates the median amplitude computed from each individual model (Neelin et al., 2006; Knutti et al., 2010a). The CMIP3/5 multi-model ensemble precipitation projections must be interpreted in the context of uncertainty. Multi-model projections are not probabilistic statements about the likelihood of changes. Maps of multi-model projected changes are smoothly varying but observed changes are and will continue to be much more granular.

To analyze the patterns of projected precipitation changes, a useful framework consists in decomposing them into a part that is related to atmospheric circulation changes and a part that is related mostly to water vapour changes, referred to as dynamical and thermodynamical components, respectively. However, the definition of these two components may differ among studies. At the time of the AR4, the robust changes of the difference between precipitation and evaporation ($P - E$) were interpreted as a wet-get-wetter and dry-get-drier type of response (Mitchell et al., 1987; Chou and Neelin, 2004; Held and Soden, 2006). The theoretical background, which is more relevant over oceans than over land, is that the lower-tropospheric water vapour increase with temperature enhances the moisture transported by the circulation. This leads to additional moisture convergence within the convergence zones and to additional moisture divergence in the descent zones, increasing the contrast in precipitation minus evaporation values between moisture convergence and divergence regions. A weakening of the tropical overturning circulation (see Section 12.4.4.2) partially opposes this thermodynamic response (Chou and Neelin, 2004; Held and Soden, 2006; Vecchi and Soden, 2007; Chou et al., 2009; Seager et al., 2010; Allan, 2012; Bony et al., 2013). At the regional scale the dynamic response may be larger than the thermodynamic response, and this has been analyzed in more detail since the AR4 (Chou et al., 2009; Seager et al., 2010; Xie et al., 2010; Muller and O'Gorman, 2011; Chadwick et al., 2012; Scheff and Frierson, 2012; Bony et al., 2013; Ma and Xie, 2013). Over continents, this simple wet-get-wetter and dry-get-drier type of response fails for some important regions such as the Amazon. At the global scale, the net water vapour transport from oceans to land increases, and therefore the average $P - E$ over continents also increases (Liepert and Previdi, 2012).

In the mid and high latitudes, a common feature across generations of climate models is a simulated increased precipitation. The thermodynamical component explains most of the projected increase (Emori and Brown, 2005; Seager et al., 2010). This is consistent with theoretical explanations assuming fixed atmospheric flow patterns but increased water vapour in the lower troposphere (Held and Soden, 2006). In addition to this thermodynamical effect, water transport may be modified by the poleward shift of the storm tracks and by the increase of their intensity (Seager et al., 2010; Wu et al., 2011b), although confidence in such changes in storm tracks may not be high (see Section 12.4.4). On seasonal time scales, the minimum and maximum values of precipitation both increase, with a larger increase of the maximum and therefore an increase of the annual precipitation range (Seager et al., 2010; Chou and Lan, 2012). In particular, the largest changes over northern Eurasia and North America are projected to occur during winter. At high latitudes of the NH, the precipitation increase may lead to an increase of snowfall in the colder regions and a decrease of snowfall in the warmer regions due to the decreased number of freezing days (see Section 12.4.6.2).

Most models simulate a large increase of the annual mean precipitation over the equatorial ocean and an equatorward shift of the Intertropical Convergence Zone (ITCZ), in both summer and winter seasons, that are mainly explained by atmospheric circulation changes (Chou et al., 2009; Seager et al., 2010; Sobel and Camargo, 2011). The changes of the atmospheric circulation have different origins. Along the margins of the convection zones, spatial inhomogeneities, including local convergence feedback or the rate at which air masses from dry regions tend to flow into the convection zone, can yield a considerable sensitivity in precipitation response (Chou et al., 2006; Neelin et al., 2006). Along the equator, atmosphere–ocean interactions yield to a maximum of SST warming and a large precipitation increase there (Xie et al., 2010; Ma and Xie, 2013). Model studies with idealized configurations suggest that tropical precipitation changes should be interpreted as responses to changes of the atmospheric energy budget rather than responses to changes of SST (Kang and Held, 2012). All of these atmospheric circulation changes, and therefore precipitation changes, can differ considerably from model to model. This is the case over both ocean and land. For instance, the spread of model projections in the Sahel region, West Africa, is large in both the CMIP3 and CMIP5 multi-model data base (Roehrig et al., 2013).

In the subtropical dry regions, there is a robust decrease of $P - E$ that is accounted for by the thermodynamic contribution (Chou and Neelin, 2004; Held and Soden, 2006; Chou et al., 2009; Seager et al., 2010; Bony et al., 2013). Over ocean, the spatial heterogeneity of temperature increase impacts the lower-tropospheric water vapour increase, which impacts both the thermodynamic and the dynamic responses (Xie et al., 2010; Ma and Xie, 2013). In addition, the pattern of precipitation changes in dry regions may be different from that of $P - E$ because the contribution of evaporation changes can be as large (but of opposite sign) as the moisture transport changes (Chou and Lan, 2012; Scheff and Frierson, 2012; Bony et al., 2013). This is especially the case over the subsidence regions during the warm season over land where the agreement between models is the smallest (Chou et al., 2009; Allan, 2012). A robust feature is the decline of precipitation on the poleward flanks of the subtropical dry zones as a consequence of the Hadley Cell expansion, with possible additional decrease from a poleward shift of the mid latitude storm tracks (Seager et al., 2010; Scheff and Frierson, 2012). On seasonal time scales, the minimum and the maximum values of precipitation both increase, with a larger increase of the maximum and therefore an increase of the annual precipitation range (Sobel and Camargo, 2011; Chou and Lan, 2012).

Long-term precipitation changes are driven mainly by the increase of the surface temperature, as presented above, but other factors also contribute to them. Recent studies suggest that CO_2 increase has a significant direct influence on atmospheric circulation, and therefore on global and tropical precipitation changes (Andrews et al., 2010; Bala et al., 2010; Cao et al., 2012; Bony et al., 2013). Over the ocean, the positive RF from increased atmospheric CO_2 reduces the radiative cooling of the troposphere and the large scale rising motion and hence reduces precipitation in the convective regions. Over large landmasses, the direct effect of CO_2 on precipitation is the opposite owing to the small thermal inertia of land surfaces (Andrews et al., 2010; Bala et al., 2010; Cao et al., 2012; Bony et al., 2013). Regional precipitation changes are also influenced by aerosol and ozone (Ramanathan et al., 2001; Allen et al., 2012; Shindell et al., 2013a) through both local and large-scale processes, including changes in the circulation. Stratospheric ozone depletion contributes to the poleward expansion of the Hadley Cell and the related change of precipitation in the SH (Kang et al., 2011) whereas black carbon and tropospheric ozone increases are major contributors in the NH (Allen et al., 2012). Regional precipitation changes depend on regional forcings and on how models simulate their local and remote effects. Based on CMIP3 results, the inter-model spread of the estimate of precipitation changes over land is larger than the inter-scenario spread except in East Asia (Frieler et al., 2012).

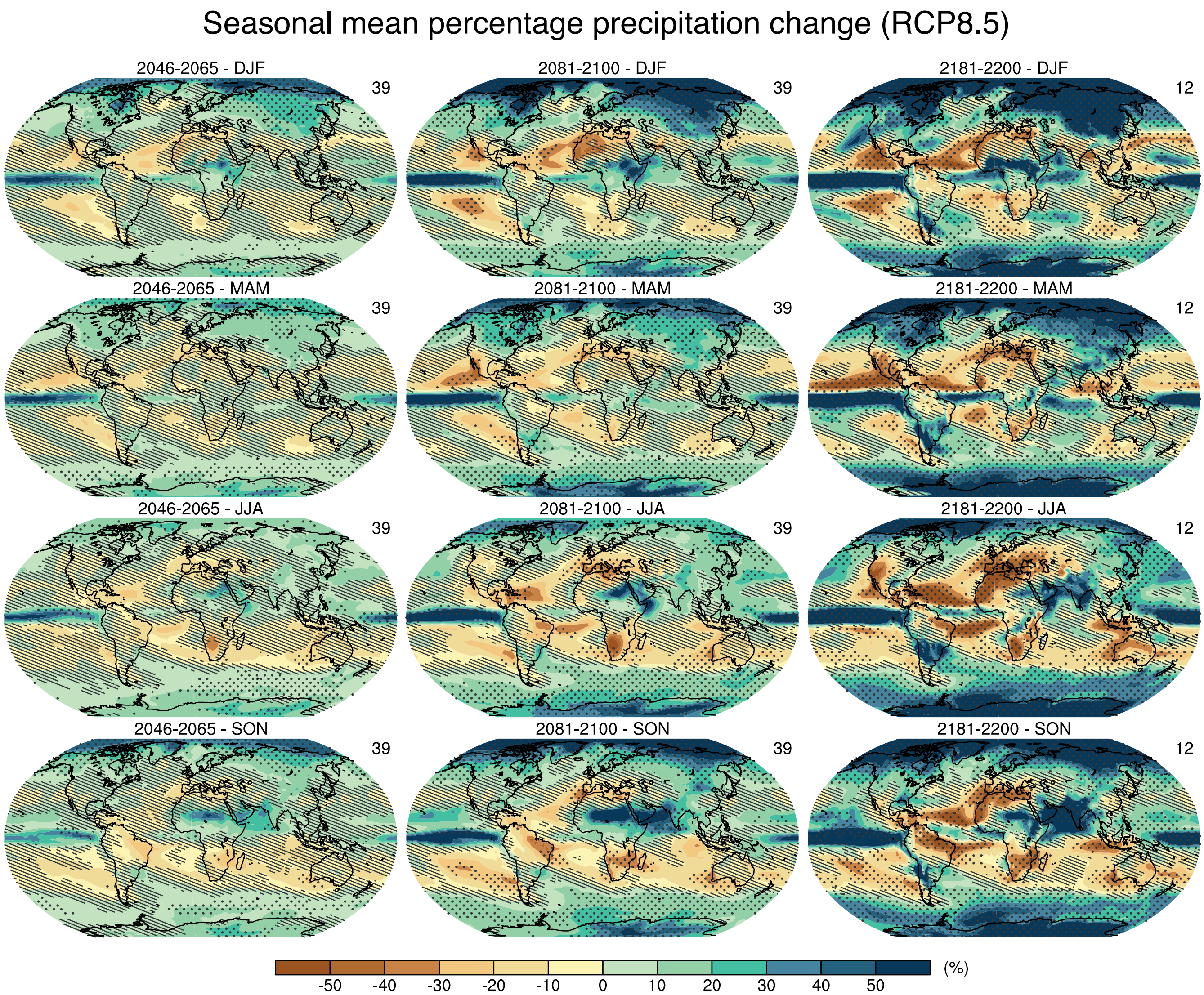

Figure 12.22 | Multi-model CMIP5 average percentage change in seasonal mean precipitation relative to the reference period 1986–2005 averaged over the periods 2045–2065, 2081–2100 and 2181–2200 under the RCP8.5 forcing scenario. Hatching indicates regions where the multi-model mean change is less than one standard deviation of internal variability. Stippling indicates regions where the multi-model mean change is greater than two standard deviations of internal variability and where at least 90% of models agree on the sign of change (see Box 12.1).

Projected precipitation changes vary greatly between models, much more so than for temperature projections. Part of this variance is due to genuine differences between the models including their ability to replicate observed precipitation patterns (see Section 9.4.1.1). However, a large part of it is also the result of the small ensemble size from each model (Rowell, 2012). This is especially true for regions of small projected changes located between two regions: one experiencing significant increases while the other experiences significant decreases. Individual climate model realizations will differ in their projection of future precipitation changes in these regions simply owing to their internal variability (Deser et al., 2012b; Deser et al., 2012a). Multi-model projections containing large numbers of realizations would tend to feature small changes in these regions, and hatching in Figure 12.22 indicates regions where the projected multi-model mean change is less than one standard deviation of internal variability (method (a), Box 12.1). Confidence in projections in regions of limited or no change in precipitation may be more difficult to obtain than confidence in regions of large projected changes. However, Power et al. (2012) and Tebaldi et al. (2011) show that for some of the regions featuring small multi-model average projected changes, effective consensus in projections may be better than the metrics reported in AR4 would imply.

Since the AR4, progress has been made in the understanding of the processes that control large scale precipitation changes. There is *high confidence* that the contrast of seasonal mean precipitation between dry and wet regions will increase in a warmer climate over most of the globe although there may be regional exceptions to this general pattern. This response is particularly robust when considering $P - E$ changes as a function of atmospheric dynamical regimes. However, it is important to note that significant exceptions can occur in specific regions especially along the equator and on the poleward edges of the subtropical dry zone. In these regions, atmospheric circulation changes lead to shifts of the precipitation patterns. There is *high confidence* that the contrast between wet and dry seasons will increase over most of the globe as temperatures increase. Over the mid- and high-latitude regions, projected precipitation increases in winter are larger than in summer. Over most of the subtropical oceans, projected precipitation increases in summer are larger than in winter.

The changes in precipitation shown in Figure 12.22 exhibit patterns that become more pronounced and confidence in them increases as temperatures increase. More generally, the spatial and temporal changes in precipitation between two scenarios or within two periods of a given scenario exhibit the pattern scaling behavior and limitations described in Section 12.4.2. The patterns and the associated multi-model spreads in CMIP5 for the RCP scenarios are very similar to those in CMIP3 for the SRES scenarios discussed in the AR4, with the projections in CMIP5 being slightly more consistent over land than those from CMIP3 (Knutti and Sedláček, 2013). The largest percentage changes are at the high latitudes. By the end of the 21st century, over the large northern land masses, increased precipitation is *likely* under the RCP8.5 scenario in the winter and spring poleward of 50°N. The robustness across scenarios, the magnitude of the projected changes versus natural variability and physical explanations described above yield *high confidence* that the projected changes would be larger than natural 20-year variations (see Box 12.1). In the tropics, precipitation changes exhibit strong regional contrasts, with increased precipitation over the equatorial Pacific and Indian Oceans and decreases over much of the subtropical ocean. However, decreases are not projected to be larger than natural 20-year variations anywhere until the end of this century under the RCP8.5 scenario. Decreased precipitation in the Mediterranean, Caribbean and Central America, southwestern United States and South Africa is *likely* under the RCP8.5 scenario and is projected with *medium confidence* to be larger than natural variations by the end of the 22nd century in some seasons (Box 12.1). The CMIP3 models' historical simulations of zonal mean precipitation trends were shown to underestimate observed trends (Gillett et al., 2004; Lambert et al., 2005; Zhang et al., 2007; Liepert and Previdi, 2009) (see Section 10.3.2.2). Therefore it is *more likely than not* that the magnitude of the projected future changes in Figure 12.22 based on the multi-model mean is underestimated. Observational uncertainties including limited global coverage and large natural variability, in addition to challenges in precipitation modelling, limit confidence in assessment of climatic changes in precipitation.

12.4.5.3 Soil Moisture

Near-surface soil moisture is the net result of a suite of complex processes (e.g., precipitation evapotranspiration, drainage, overland flow, infiltration), and heterogeneous and difficult-to-characterize aboveground and belowground system properties (e.g., slope, soil texture). As a result, regional to global-scale simulations of soil moisture and drought remain relatively uncertain (Burke and Brown, 2008; Henderson-Sellers et al., 2008). The AR4 (Section 8.2.3.2) discussed the lack of assessments of global-scale models in their ability to simulate soil moisture, and this problem appears to have persisted (Section 9.4.4.2). Furthermore, consistent multi-model projections of total soil moisture are difficult to make owing to substantial differences between climate models in the depth of their soil. However, Koster et al. (2009a) argued that once climatological statistics affecting soil moisture were accounted for, different models tend to agree on soil moisture projections.

The AR4 summarized multi-model projections of 21st century annual mean soil moisture changes as decreasing in the subtropics and Mediterranean region, and increasing in east Africa and central Asia. Dai (2013) found similar changes in an ensemble of 11 CMIP5 GCMs under RCP4.5. Figure 12.23 shows projected changes in surface soil moisture (upper 10 cm) in the CMIP5 ensemble at the end of the 21st century under the RCPs 2.6, 4.5, 6.0 and 8.5. We focus on this new CMIP5 specification because it describes soil moisture at a consistent depth across all CMIP5 models. The broad patterns are moderately consistent across the RCPs, with the changes tending to become stronger as the strength of the forcing change increases. The agreement among CMIP5 models and the consistency with other physical features of climate change indicate *high confidence* in certain regions where surface soils are projected to dry. There is little-to-no confidence anywhere in projections of moister surface soils. Under RCP8.5, with the largest projected change, individual ensemble members (not shown) show consistency across the ensemble for drying in the Mediterranean region, northeast and southwest South America, southern Africa, and southwestern USA. However, ensemble members show disagreement on the sign of change in large regions such as central Asia or the high northern latitudes. The Mediterranean, southwestern USA, northeast South America and southern African drying regions are consistent with

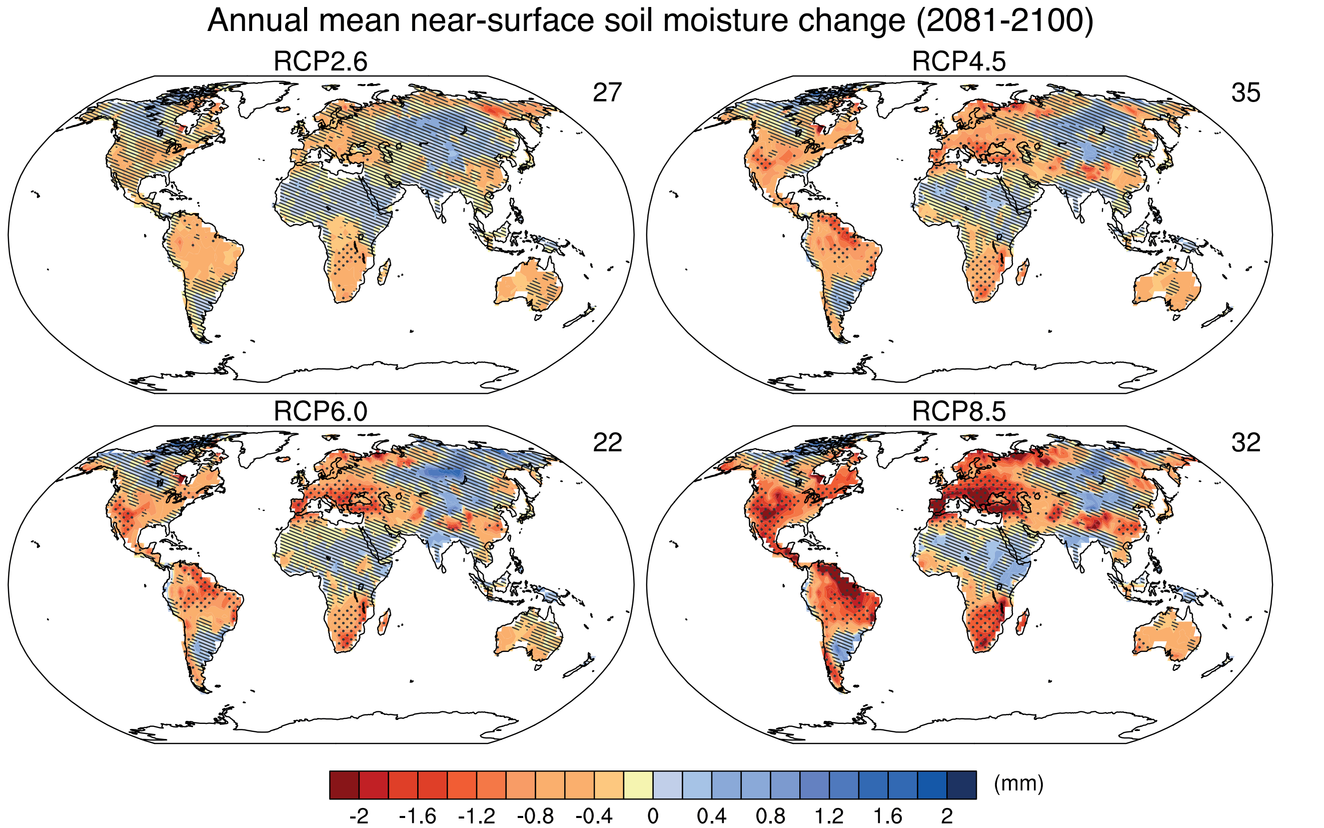

Figure 12.23 | Change in annual mean soil moisture (mass of water in all phases in the uppermost 10 cm of the soil) (mm) relative to the reference period 1986–2005 projected for 2081–2100 from the CMIP5 ensemble. Hatching indicates regions where the multi-model mean change is less than one standard deviation of internal variability. Stippling indicates regions where the multi-model mean change is greater than two standard deviations of internal variability and where at least 90% of models agree on the sign of change (see Box 12.1). The number of CMIP5 models used is indicated in the upper right corner of each panel.

projected widening of the Hadley Circulation that shifts downwelling, thus inhibiting precipitation in these regions. The large-scale drying in the Mediterranean, southwest USA, and southern Africa appear across generations of projections and climate models and is deemed *likely* as global temperatures rise and will increase the risk of agricultural drought. In addition, an analysis of CMIP3 and CMIP5 projections of soil moisture in five drought-prone regions indicates that the differences in future forcing scenarios are the largest source of uncertainty in such regions rather than differences between model responses (Orlowsky and Seneviratne, 2012).

Other recent assessments include multi-model ensemble approaches, dynamical downscaling, and regional climate models applied around the globe and illustrate the variety of issues influencing soil moisture changes. Analyses of the southwestern USA using CMIP3 models (Christensen and Lettenmaier, 2007; Seager et al., 2007) show consistent projections of drying, primarily due to a decrease in winter precipitation. In contrast, Kellomaki et al. (2010) find that SRES A2 projections for Finland yield decreased snow depth, but soil moisture generally increases, consistent with the general increase in precipitation occurring in high northern latitudes. Kolomyts and Surova (2010), using projections from the CMIP3 models, GISS and HadCM2, under the SRES A2 forcing, show that vegetation type has substantial influence on the development of pronounced drying over the 21st century in Middle Volga Region forests.

Projected changes in soil moisture from the CMIP3/5 models also show substantial seasonal variation. For example, soil moisture changes in the North American midlatitudes, coupled with projected warming, increases the strength of land–atmosphere coupling during spring and summer in 15 GCMs under RCP8.5 (Dirmeyer et al., 2013). For the Cline River watershed in western Canada, Kienzle et al. (2012) find decreases in summer soil moisture content, but annual increases averaging 2.6% by the 2080s using a suite of CMIP3 GCMs simulating B1, A1B and A2 scenarios to drive a regional hydrology model. Hansen et al. (2007), using dynamical downscaling of one GCM running the A2 scenario, find summer soil moisture decreases in Mongolia of up to 6% due to increased potential evaporation in a warming climate and decreased precipitation and decreased precipitation.

Soil moisture projections in high latitude permafrost regions are critically important for assessing future climate feedbacks from trace-gas emissions (Zhuang et al., 2004; Riley et al., 2011) and vegetation changes (Chapin et al., 2005). In addition to changes in precipitation, snow cover and evapotranspiration, future changes in high-latitude soil moisture also will depend on permafrost degradation, thermokarst evolution, rapid changes in drainage (Smith et al., 2005), and changes in plant communities and their water demands. Current understanding of these interacting processes at scales relevant to climate is poor, so that full incorporation in current GCMs is lacking.

12.4.5.4 Runoff and Evaporation

In the AR4, 21st century model-projected runoff consistently showed decreases in southern Europe, the Middle East, and southwestern USA and increases in Southeast Asia, tropical East Africa and at high northern latitudes. The same general features appear in the CMIP5 ensemble of GCMs for all four RCPs shown in Figure 12.24, with the areas of most robust change typically increasing with magnitude of forcing change. However, the robustness of runoff decreases in the southwestern USA is less in the CMIP5 models compared to the AR4. The large decreases in runoff in southern Europe and southern Africa are consistent with changes in the Hadley Circulation and related precipitation decreases and warming-induced evapotranspiration increases. The high northern latitude runoff increases are *likely* under RCP8.5 and consistent with the projected precipitation increases (Figure 12.22). The consistency of changes across different generations of models and different forcing scenarios, together with the physical consistency of change indicates that decreases are also *likely* in runoff in southern Europe, the Middle East, and southern Africa in this scenario.

A number of reports since the AR4 have updated findings from CMIP3 models and analyzed a large set of mechanisms affecting runoff. Several studies have focussed on the Colorado River basin in the United States (Christensen and Lettenmaier, 2007; McCabe and Wolock, 2007; Barnett and Pierce, 2008; Barnett et al., 2008) showing that runoff reductions that do happen under global warming occur through a combination of evapotranspiration increases and precipitation decreases, with the overall reduction in river flow exacerbated by human water demands on the basin's supply.

A number of CMIP3 analyses have examined trends and seasonal shifts in runoff. For example, Kienzle et al. (2012) studied climate change scenarios over the Cline River watershed in western Canada and projected (1) spring runoff and peak streamflow up to 4 weeks earlier than in 1961–1990; (2) significantly higher streamflow between October and June; and (3) lower streamflow between July and September. For the Mediterranean basin, an ensemble of regional climate models driven by several GCMs using the A1B scenario have a robust decrease in runoff emerging only after 2050 (Sanchez-Gomez et al., 2009).

Annual mean surface evaporation in the models assessed in AR4 showed increases over most of the ocean and increases or decreases over land with largely the same pattern over land as increases and decreases in precipitation. Similar behaviour occurs in an ensemble of CMIP5 models (Figure 12.25). Evaporation increases over most of the ocean and land, with prominent areas of decrease over land occurring in southern Africa and northwestern Africa along the Mediterranean. The areas of decrease correspond to areas with reduced precipitation. There is some uncertainty about storm-track changes over Europe (see Sections 12.4.3 and 14.6.2). However, the consistency of the decreases across different generations of models and different forcing scenarios along with the physical basis for the precipitation decrease

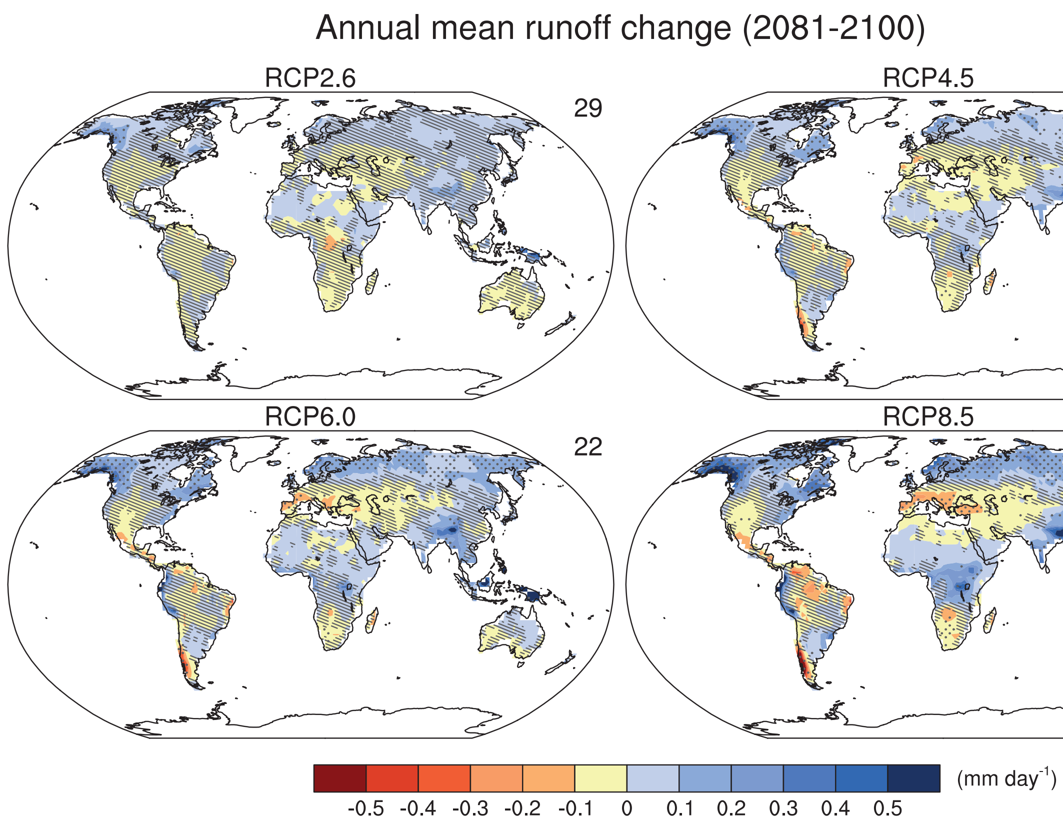

Figure 12.24 | Change in annual mean runoff relative to the reference period 1986–2005 projected for 2081–2100 from the CMIP5 ensemble. Hatching indicates regions where the multi-model mean change is less than one standard deviation of internal variability. Stippling indicates regions where the multi-model mean change is greater than two standard deviations of internal variability and where at least 90% of models agree on the sign of change (see Box 12.1). The number of CMIP5 models used is indicated in the upper right corner of each panel.

12

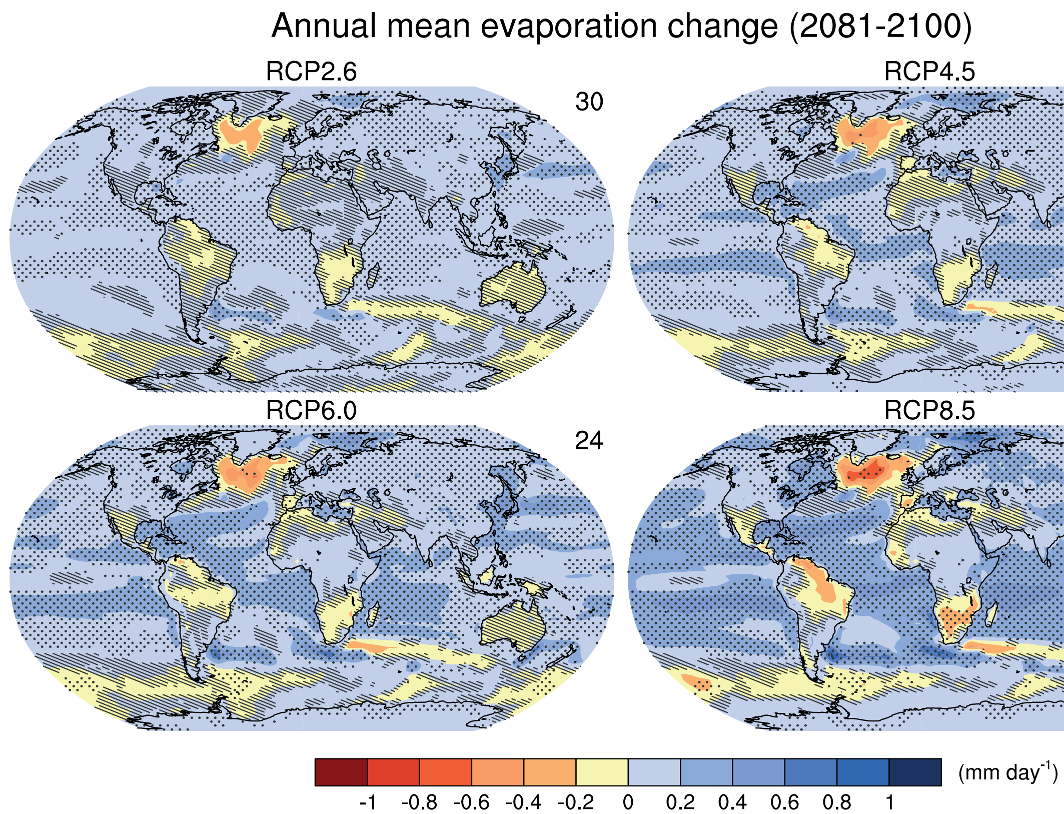

Figure 12.25 | Change in annual mean evaporation relative to the reference period 1986–2005 projected for 2081–2100 from the CMIP5 ensemble. Hatching indicates regions where the multi-model mean change is less than one standard deviation of internal variability. Stippling indicates regions where the multi-model mean change is greater than two standard deviations of internal variability and where at least 90% of models agree on the sign of change (see Box 12.1). The number of CMIP5 models used is indicated in the upper right corner of each panel.

indicates that these decreases in annual mean evaporation are *likely* under RCP8.5, but with *medium confidence.* Annual mean evaporation increases over land in the northern high latitudes are consistent with the increase in precipitation and the overall warming that would increase potential evaporation. For the northern high latitudes, the physical consistency and the similar behaviour across multiple generations and forcing scenarios indicates that annual mean evaporation increases there are *likely*, with *high confidence*.

Evapotranspiration changes partly reflect changes in precipitation. However, some changes might come from altered biological processes. For example, increased atmospheric CO_2 promotes stomatal closure and reduced transpiration (Betts et al., 2007; Cruz et al., 2010) which can potentially yield increased runoff. There is potential for substantial feedback between vegetation changes and regional water cycles, though the impact of such feedback remains uncertain at this point due to limitations on modelling crop and other vegetation processes in GCMs (e.g., Newlands et al., 2012) and uncertainties in plant response, ecosystem shifts and land management changes.

12.4.5.5 Extreme Events in the Water Cycle

In addition to the changes in the seasonal pattern of mean precipitation described above, the distribution of precipitation events is projected to undergo profound changes (Gutowski et al., 2007; Sun et al., 2007; Boberg et al., 2010). At daily to weekly scales, a shift to more intense individual storms and fewer weak storms is projected (Seneviratne et al., 2012). At seasonal or longer time scales, increased evapotranspiration over land can lead to more frequent and more intense periods of agricultural drought.

A general relationship between changes in total precipitation and extreme precipitation does not exist (Seneviratne et al., 2012). Two possible mechanisms controlling short-term extreme precipitation amounts are discussed at length in the literature and are similar to the thermodynamic and dynamical mechanisms detailed above for changes in average precipitation.

The first considers that extreme precipitation events occur when most of the available atmospheric water vapour rapidly precipitates out in a single storm. The maximum amount of water vapour in air (saturation) is determined by the Clausius–Clapeyron relationship. As air temperature increases, this saturated amount of water also increases (Allen and Ingram, 2002; Pall et al., 2007; Allan and Soden, 2008; Kendon et al., 2010). Kunkel et al. (2013) examined the CMIP5 model RCP4.5 and 8.5 projections for changes in maximum water vapour concentrations, a principal factor controlling the probable bound on maximum precipitation, concluding that maximum water vapour changes are comparable to mean water vapour changes but that the potential for changes in dynamical factors is less compelling. Such increases in atmospheric water vapour are expected to increase the intensity of individual precipitation events, but have less impact on their frequency. As a result projected increases in extreme precipitation may be more reliable than similar projections of changes in mean precipitation in some regions (Kendon et al., 2010).

A second mechanism for extreme precipitation put forth by O'Gorman and Schneider (2009a, 2009b) is that such events are controlled by anomalous horizontal moisture flux convergence and associated convective updrafts which would change in a more complicated fashion in a warmer world (Sugiyama et al., 2010). Emori and Brown (2005) showed that the thermodynamic mechanism dominated over the dynamical mechanism nearly everywhere outside the tropical warm pool. However, Utsumi et al. (2011) used gridded observed daily data to find that daily extreme precipitation monotonically increases with temperature only at high latitudes, with the opposite behaviour in the tropics and a mix in the mid-latitudes. Li et al. (2011a) found that both mechanisms contribute to extreme precipitation in a high-resolution aquaplanet model with updrafts as the controlling element in the tropics and air temperature controlling the mid-latitudes consistent with the results by Chou et al. (2012). Using a high-resolution regional model, Berg et al. (2009) found a seasonal dependence in Europe with the Clausius–Clapeyron relationship providing an upper limit to daily precipitation intensity in winter but water availability rather than storage capacity is the controlling factor in summer. Additionally, Lenderink and Van Meijgaard (2008) found that very short (sub-daily) extreme precipitation events increase at a rate twice the amount predicted by Clausius–Clapeyron scaling in a very high-resolution model over Europe suggesting that both mechanisms can interact jointly. Gastineau and Soden (2009) found in the CMIP3 models that the updrafts associated with the most extreme tropical precipitation events actually weaken despite an increase in the frequency of the heaviest rain rates further complicating simple mechanistic explanations. See also Sections 7.6.5 and 11.3.2.5.2.

Projections of changes in future extreme precipitation may be larger at the regional scales than for future mean precipitation, but natural variability is also larger causing a tendency for signal-to-noise ratios to decrease when considering increasingly extreme metrics. However, mechanisms of natural variability still are a large factor in assessing the robustness of projections (Kendon et al., 2008). In addition, large-scale circulation changes, which are uncertain, could dominate over the above mechanisms depending on the rarity and type of events considered. However, analysis of CMIP3 models suggests circulation changes are potentially insufficient to offset the influence of increasing atmospheric water vapour on extreme precipitation change over Europe at least on large spatial scales (Kendon et al., 2010). An additional shift of the storm track has been shown in models with a better representation of the stratosphere, and this is found to lead to an enhanced increase in extreme rainfall over Europe in winter (Scaife et al., 2012).

Similar to temperature extremes (Section 12.4.3.3), the definition of a precipitation extreme depends very much on context and is often used in discussion of particular climate-related impacts (Seneviratne et al. (2012), Box 3.1). Consistently, climate models project future episodes of more intense precipitation in the wet seasons for most of the land areas, especially in the NH and its higher latitudes, and the monsoon regions of the world, and at a global average scale. The actual magnitude of the projected change is dependent on the model used,

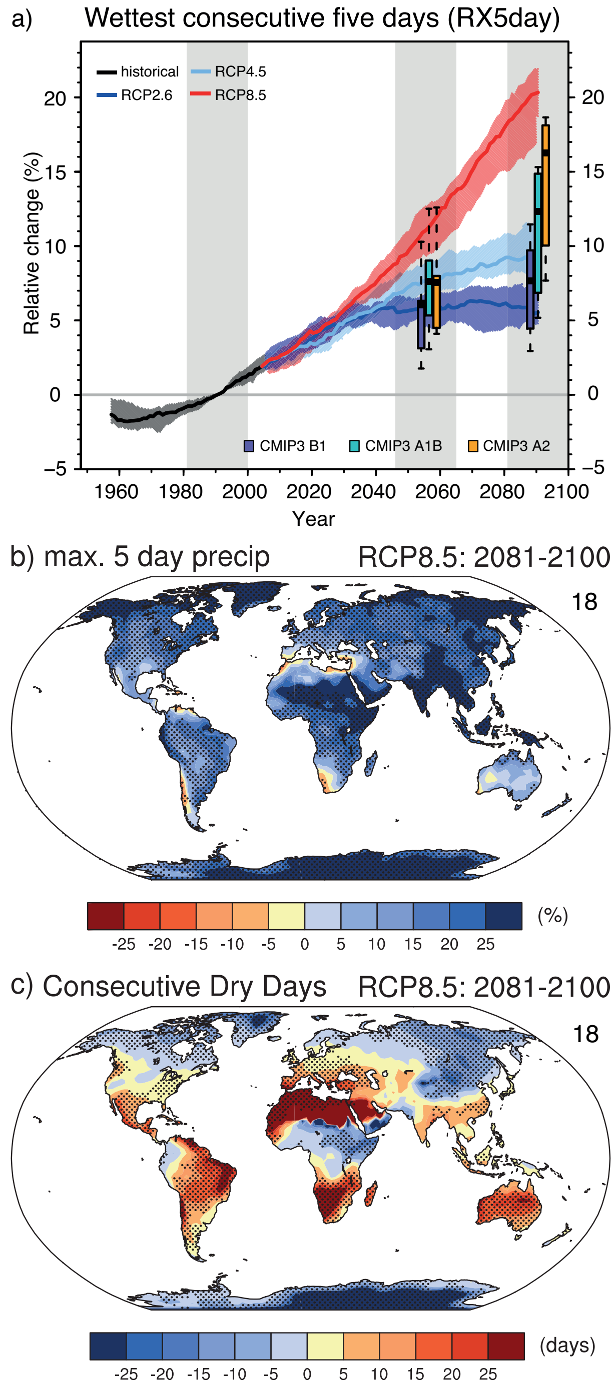

Figure 12.26 | (a, b) Projected percent changes (relative to the 1981–2000 reference period in common with CMIP3) from the CMIP5 models in RX5day, the annual maximum five-day precipitation accumulation. (a) Global average percent change over land regions for the RCP2.6, RCP4.5 and RCP8.5 scenarios. Shading in the time series represents the interquartile ensemble spread (25th and 75th quantiles). The box-and-whisker plots show the interquartile ensemble spread (box) and outliers (whiskers) for 11 CMIP3 model simulations of the SRES scenarios A2 (orange), A1B (cyan) and B1 (purple) globally averaged over the respective future time periods (2046–2065 and 2081–2100) as anomalies from the 1981–2000 reference period. (b) Percent change over the 2081–2100 period in the RCP8.5 scenario. (c) Projected change in annual CDD, the maximum number of consecutive dry days when precipitation is less than 1 mm, over the 2081–2100 period in the RCP8.5 scenario (relative to the 1981–2000 reference period) from the CMIP5 models. Stippling indicates gridpoints with changes that are significant at the 5% level using a Wilcoxon signed-ranked test. (Updated from Sillmann et al. (2013), excluding the FGOALS-s2 model.)

12

Frequently Asked Questions

FAQ 12.2 | How Will the Earth's Water Cycle Change?

The flow and storage of water in the Earth's climate system are highly variable, but changes beyond those due to natural variability are expected by the end of the current century. In a warmer world, there will be net increases in rainfall, surface evaporation and plant transpiration. However, there will be substantial differences in the changes between locations. Some places will experience more precipitation and an accumulation of water on land. In others, the amount of water will decrease, due to regional drying and loss of snow and ice cover.

The water cycle consists of water stored on the Earth in all its phases, along with the movement of water through the Earth's climate system. In the atmosphere, water occurs primarily as a gas—water vapour—but it also occurs as ice and liquid water in clouds. The ocean, of course, is primarily liquid water, but the ocean is also partly covered by ice in polar regions. Terrestrial water in liquid form appears as surface water—such as lakes and rivers—soil moisture and groundwater. Solid terrestrial water occurs in ice sheets, glaciers, snow and ice on the surface and in permafrost and seasonally frozen soil.

Statements about future climate sometimes say that the water cycle will accelerate, but this can be misleading, for strictly speaking, it implies that the cycling of water will occur more and more quickly with time and at all locations. Parts of the world will indeed experience intensification of the water cycle, with larger transports of water and more rapid movement of water into and out of storage reservoirs. However, other parts of the climate system will experience substantial depletion of water, and thus less movement of water. Some stores of water may even vanish.

As the Earth warms, some general features of change will occur simply in response to a warmer climate. Those changes are governed by the amount of energy that global warming adds to the climate system. Ice in all forms will melt more rapidly, and be less pervasive. For example, for some simulations assessed in this report, summer Arctic sea ice disappears before the middle of this century. The atmosphere will have more water vapour, and observations and model results indicate that it already does. By the end of the 21st century, the average amount of water vapour in the atmosphere could increase by 5 to 25%, depending on the amount of human emissions of greenhouse gases and radiatively active particles, such as smoke. Water will evaporate more quickly from the surface. Sea level will rise due to expansion of warming ocean waters and melting land ice flowing into the ocean (see FAQ 13.2).

These general changes are modified by the complexity of the climate system, so that they should not be expected to occur equally in all locations or at the same pace. For example, circulation of water in the atmosphere, on land and in the ocean can change as climate changes, concentrating water in some locations and depleting it in others. The changes also may vary throughout the year: some seasons tend to be wetter than others. Thus, model simulations assessed in this report show that winter precipitation in northern Asia may increase by more than 50%, whereas summer precipitation there is projected to hardly change. Humans also intervene directly in the water cycle, through water management and changes in land use. Changing population distributions and water practices would produce further changes in the water cycle.

12

Water cycle processes can occur over minutes, hours, days and longer, and over distances from metres to kilometres and greater. Variability on these scales is typically greater than for temperature, so climate changes in precipitation are harder to discern. Despite this complexity, projections of future climate show changes that are common across many models and climate forcing scenarios. Similar changes were reported in the AR4. These results collectively suggest well understood mechanisms of change, even if magnitudes vary with model and forcing. We focus here on changes over land, where changes in the water cycle have their largest impact on human and natural systems.

Projected climate changes from simulations assessed in this report (shown schematically in FAQ 12.2, Figure 1) generally show an increase in precipitation in parts of the deep tropics and polar latitudes that could exceed 50% by the end of the 21st century under the most extreme emissions scenario. In contrast, large areas of the subtropics could have decreases of 30% or more. In the tropics, these changes appear to be governed by increases in atmospheric water vapour and changes in atmospheric circulation that further concentrate water vapour in the tropics and thus promote more tropical rainfall. In the subtropics, these circulation changes simultaneously promote less rainfall despite warming in these regions. Because the subtropics are home to most of the world's deserts, these changes imply increasing aridity in already dry areas, and possible expansion of deserts. *(continued on next page)*

FAQ 12.2 (continued)

Increases at higher latitudes are governed by warmer temperatures, which allow more water in the atmosphere and thus, more water that can precipitate. The warmer climate also allows storm systems in the extratropics to transport more water vapour into the higher latitudes, without requiring substantial changes in typical wind strength. As indicated above, high latitude changes are more pronounced during the colder seasons.

Whether land becomes drier or wetter depends partly on precipitation changes, but also on changes in surface evaporation and transpiration from plants (together called evapotranspiration). Because a warmer atmosphere can have more water vapour, it can induce greater evapotranspiration, given sufficient terrestrial water. However, increased carbon dioxide in the atmosphere reduces a plant's tendency to transpire into the atmosphere, partly counteracting the effect of warming.

In the tropics, increased evapotranspiration tends to counteract the effects of increased precipitation on soil moisture, whereas in the subtropics, already low amounts of soil moisture allow for little change in evapotranspiration. At higher latitudes, the increased precipitation generally outweighs increased evapotranspiration in projected climates, yielding increased annual mean runoff, but mixed changes in soil moisture. As implied by circulation changes in FAQ 12.2, Figure 1, boundaries of high or low moisture regions may also shift.

A further complicating factor is the character of rainfall. Model projections show rainfall becoming more intense, in part because more moisture will be present in the atmosphere. Thus, for simulations assessed in this report, over much of the land, 1-day precipitation events that currently occur on average every 20 years could occur every 10 years or even more frequently by the end of the 21st century. At the same time, projections also show that precipitation events overall will tend to occur less frequently. These changes produce two seemingly contradictory effects: more intense downpours, leading to more floods, yet longer dry periods between rain events, leading to more drought.

At high latitudes and at high elevation, further changes occur due to the loss of frozen water. Some of these are resolved by the present generation of global climate models (GCMs), and some changes can only be inferred because they involve features such as glaciers, which typically are not resolved or included in the models. The warmer climate means that snow tends to start accumulating later in the fall, and melt earlier in the spring. Simulations assessed in this report show March to April snow cover in the Northern Hemisphere is projected to decrease by approximately 10 to 30% on average by the end of this century, depending on the greenhouse gas scenario. The earlier spring melt alters the timing of peak springtime flow in rivers receiving snowmelt. As a result, later flow rates will decrease, potentially affecting water resource management. These features appear in GCM simulations.

Loss of permafrost will allow moisture to seep more deeply into the ground, but it will also allow the ground to warm, which could enhance evapotranspiration. However, most current GCMs do not include all the processes needed to simulate well permafrost changes. Studies analysing soils freezing or using GCM output to drive more detailed land models suggest substantial permafrost loss by the end of this century. In addition, even though current GCMs do not explicitly include glacier evolution, we can expect that glaciers will continue to recede, and the volume of water they provide to rivers in the summer may dwindle in some locations as they disappear. Loss of glaciers will also contribute to a reduction in springtime river flow. However, if annual mean precipitation increases—either as snow or rain—then these results do not necessarily mean that annual mean river flow will decrease.

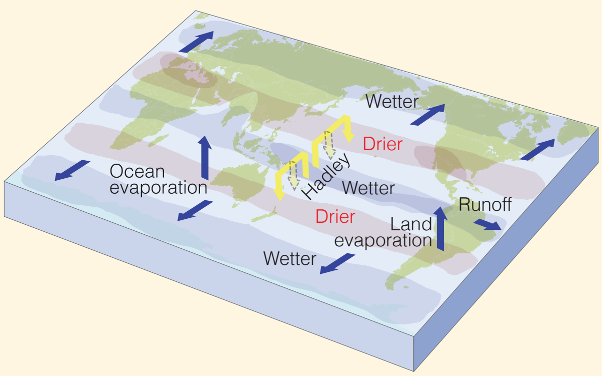

FAQ 12.2, Figure 1 | Schematic diagram of projected changes in major components of the water cycle. The blue arrows indicate major types of water movement changes through the Earth's climate system: poleward water transport by extratropical winds, evaporation from the surface and runoff from the land to the oceans. The shaded regions denote areas more likely to become drier or wetter. Yellow arrows indicate an important atmospheric circulation change by the Hadley Circulation, whose upward motion promotes tropical rainfall, while suppressing subtropical rainfall. Model projections indicate that the Hadley Circulation will shift its downward branch poleward in both the Northern and Southern Hemispheres, with associated drying. Wetter conditions are projected at high latitudes, because a warmer atmosphere will allow greater precipitation, with greater movement of water into these regions.

12

but there is strong agreement across the models over the direction of change (Tebaldi et al., 2006; Goubanova and Li, 2007; Chen and Knutson, 2008; Haugen and Iversen, 2008; May, 2008b; Kysely and Beranova, 2009; Min et al., 2011; Sillmann et al., 2013). Regional details are less robust in terms of the relative magnitude of changes but remain in good accord across models in terms of the sign of the change and the large-scale geographical patterns (Meehl et al., 2005a; CCSP, 2008a). In semi-arid regions of the midlatitudes and subtropics such as the Mediterranean, the southwest USA, southwestern Australia, southern Africa and a large portion of South America, the tendency manifested in the majority of model simulations is for longer dry periods and is consistent with the average decreases shown in Figure 12.22. Figure 12.26 shows projected percent changes in RX5day, the annual maximum of consecutive 5-day precipitation over land regions obtained from the CMIP5 models (Box 2.4, Table 1). Globally averaged end of 21st century changes over land range from 5% (RCP2.6) to 20% (RCP8.5) more precipitation during very wet 5-day periods. Results from the CMIP3 models are shown for comparison (see Section 12.4.9). Locally, the few regions where this index of extreme precipitation decreases in the late 21st century RCP8.5 projection coincide with areas of robust decreases in the mean precipitation of Figure 12.22.

Drought is discussed extensively in the SREX report (Seneviratne et al., 2012) and the conclusions about future drought risk described there based on CMIP3 models are reinforced by the CMIP5 models. As noted in the SREX reports, assessments of changes in drought characteristics with climate change should be made in the context of specific impacts questions. The risk of future agricultural drought episodes is increased in the regions of robust soil moisture decrease described in Section 12.4.5.3 and shown in Figure 12.23. Other measures in the literature of future agricultural drought are largely focussed on the Palmer Drought Severity Index (Wehner et al., 2011; Schwalm et al., 2012; Dai, 2013) and project 'extreme' drought as the normal climatological state by the end of the 21st century under the high emission scenarios in many mid-latitude locations. However, this measure of agricultural drought has been criticized as overly sensitive to increased temperatures due to a simplified soil moisture model (Hoerling et al., 2012). The consecutive dry-day index (CDD) is the length of the longest period of consecutive days with precipitation less than 1 mm (Box 2.4, Table 1). CMIP5 projected changes in CDD over the 2081–2100 period under the RCP8.5 scenario (relative to the 1981–2000 reference period in common with CMIP3) from the CMIP5 models are shown in Figure 12.26c and exhibit patterns similar to projected changes in both precipitation and soil moisture (Sillmann et al., 2013). Substantial increases in this measure of meteorological drought are projected in the Mediterranean, Central America, Brazil, South Africa and Australia while decreases are projected in high northern latitudes.

Truly rare precipitation events can cause very significant impacts. The statistics of these events at the tails of the precipitation distribution are well described by Extreme Value (EV) Theory although there are significant biases in the direct comparison of gridded model output and actual station data (Smith et al., 2009). There is also strong evidence that model resolution plays a key role in replicating EV quantities estimated from gridded observational data, suggesting that high-resolution models may provide somewhat more confidence in projection of changes in rare precipitation events (Fowler et al., 2007a; Wehner et al., 2011). Figure 12.27 shows the late 21st century changes per degree Celsius in local warming in 20-year return values of annual maximum daily precipitation relative to the late 20th century (left) and the associated return periods of late 20th century 20-year return values at the end of the 21st century from the CMIP5 models. Across future emission scenarios, the global average of the CMIP5 multi-model median return value sensitivity is an increase of 5.3% $°C^{-1}$ (Kharin et al., 2013). The CMIP5 land average is close to the CMIP3 value of 4% $°C^{-1}$ reported by Min et al. (2011) for a subset of CMIP3 models. Corresponding with this change, the global average of return periods of late 20th century 20-year return values is reduced from 20 years to 14 years for a 1°C local warming. Return periods are projected to be reduced by about 10 to 20% $°C^{-1}$ over the most of the mid-latitude land masses with larger reductions over wet tropical regions (Kharin et al., 2013). Hence, extreme precipitation events will *very likely* be more intense

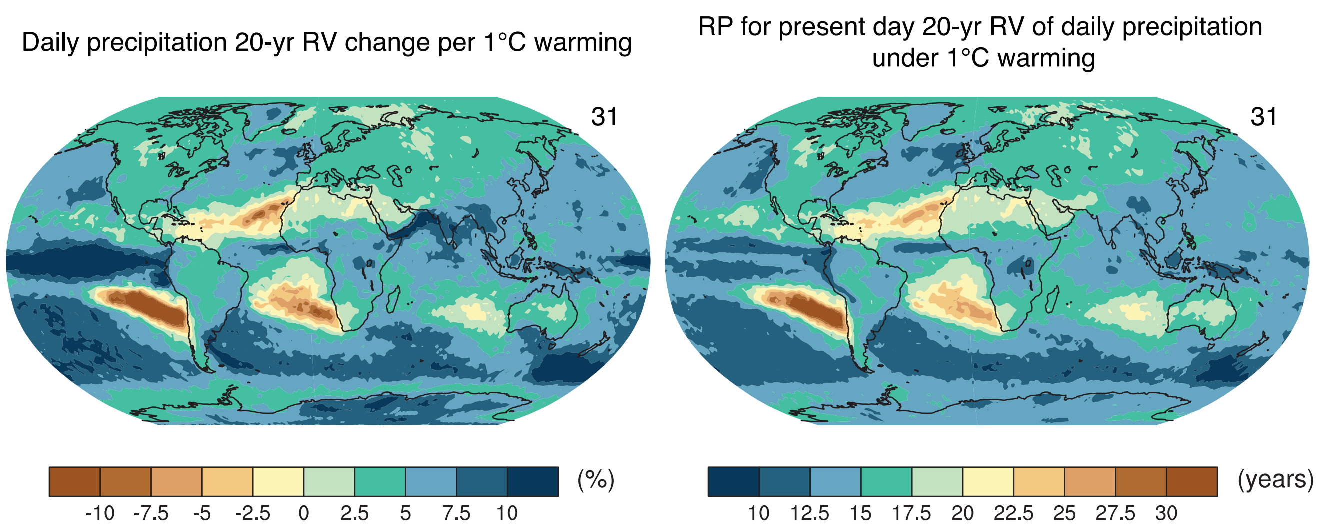

Figure 12.27 | (Left) The CMIP5 2081–2100 multi-model ensemble median percent change in 20-year return values of annual maximum daily precipitation per 1°C of local warming relative to the 1986–2005 reference period. (Right) The average 2081–2100 CMIP5 multi-model ensemble median of the return periods (years) of 1986–2005 20-year return values of annual maximum daily precipitation corresponding to 1°C of local warming. Regions of no change would have return periods of 20 years.

and more frequent in these regions in a warmer climate. Reductions in return values (or equivalently, increases in return period) are confined to convergent oceanic regions where circulation changes have reduced the available water vapour.

Severe thunderstorms, associated with large hail, high winds, and tornadoes, are another example of extreme weather associated with the water cycle. The large-scale environments in which they occur are characterized by large Convective Available Potential Energy (CAPE) and deep tropospheric wind shear (Brooks et al., 2003; Brooks, 2009). Del Genio et al. (2007), Trapp et al. (2007, 2009), and Van Klooster and Roebber (2009) found a general increase in the energy and decrease in the shear terms from the late 20th century to the late 21st century over the USA using a variety of regional model simulations embedded in global model SRES scenario simulations. The relative change between these two competing factors would tend to favour more environments that would support severe thunderstorms, providing storms are initiated. Trapp et al. (2009), for example, found an increase in favourable thunderstorm conditions for all regions of the USA east of the Rocky Mountains. Large variability in both the energy and shear terms means that statistical significance is not reached until late in the 21st century under high forcing scenarios. One way of assessing the possibility of a change in the frequency of future thunderstorms is to look at historical records of observed tornado, hail and wind occurrence with respect to the environmental conditions (Brooks, 2013). This indicates that an increase in the fraction of severe thunderstorms containing non-tornadic winds would be consistent with the model projections of increased energy and decreased shear, but there has not been enough research to make a firm conclusion regarding future changes in frequency or magnitude.

Less work has been done on projected changes outside of the USA. Marsh et al. (2009) found that mean energy decreased in the warm season in Europe while it increased in the cool season. Even though the energy decreases in the warm season, the number of days with favourable environments for severe thunderstorms increases because of an increasing number of days with relatively large values of available energy. For Europe, with the Mediterranean Sea and Sahara Desert to the south, questions remain about changes in boundary layer moisture, a main driver of the energy term. Niall and Walsh (2005) examined changes in CAPE, which may be associated with hailstorm occurrence in southeastern Australia using a global model, and found little change under warmer conditions. Leslie et al. (2008) reconsidered the southeastern Australia hail question by nesting models with 1 km horizontal grid spacing and using sophisticated microphysical parameterizations and found an increase in the frequency of large hail by 2050 under the SRES A1B scenario, but with extremely large internal variability in the environments and hail size.

Overall, for all parts of the world studied, the results are suggestive of a trend toward environments favouring more severe thunderstorms, but the small number of analyses precludes any likelihood estimate of this change.

12.4.6 Changes in Cryosphere

12.4.6.1 Changes in Sea Ice Cover

Based on the analysis of CMIP3 climate change simulations (e.g., Arzel et al., 2006; Zhang and Walsh, 2006), the AR4 concludes that the Arctic and Antarctic sea ice covers are projected to shrink in the 21st century under all SRES scenarios, with a large range of model responses (Meehl et al., 2007b). It also stresses that, in some projections, the Arctic Ocean becomes almost entirely ice-free in late summer during the second half of the 21st century. These conclusions were confirmed by further analyses of the CMIP3 archives (e.g., Stroeve et al., 2007; Bracegirdle et al., 2008; Lefebvre and Goosse, 2008; Boé et al., 2009b; Sen Gupta et al., 2009; Wang and Overland, 2009; Zhang, 2010b; NRC, 2011; Körper et al., 2013). Figures 12.28 and 12.29 and the studies of Maksym et al. (2012), Massonnet et al. (2012), Stroeve et al. (2012) and Wang and Overland (2012) show that the CMIP5 AOGCMs/ESMs as a group also project decreases in sea ice extent through the end of this century in both hemispheres under all RCPs. However, as in the case of CMIP3, the inter-model spread is considerable.

In the NH, in accordance with CMIP3 results, the absolute rate of decrease of the CMIP5 multi-model mean sea ice areal coverage is greatest in September. The reduction in sea ice extent between the time periods 1986–2005 and 2081–2100 for the CMIP5 multi-model average ranges from 8% for RCP2.6 to 34% for RCP8.5 in February and from 43% for RCP2.6 to 94% for RCP8.5 in September. *Medium confidence* is attached to these values as projections of sea ice extent decline in the real world due to errors in the simulation of present-day sea ice extent (mean and trends—see Section 9.4.3) and because of the large spread of model responses. About 90% of the available CMIP5 models reach nearly ice-free conditions (sea ice extent less than 1×10^6 km^2 for at least 5 consecutive years) during September in the Arctic before 2100 under RCP8.5 (about 45% under RCP4.5). By the end of the 21st century, the decrease in multi-model mean sea ice volume ranges from 29% for RCP2.6 to 73% for RCP8.5 in February and from 54% for RCP2.6 to 96% for RCP8.5 in September. *Medium confidence* is attached to these values as projections of the real world sea ice volume. In February, these percentages are much higher than the corresponding ones for sea ice extent, which is indicative of a substantial sea ice thinning.

A frequent criticism of the CMIP3 models is that, as a group, they strongly underestimate the rapid decline in summer Arctic sea ice extent observed during the past few decades (e.g., Stroeve et al., 2007; Winton, 2011), which suggests that the CMIP3 projections of summer Arctic sea ice areal coverage might be too conservative. As shown in Section 9.4.3 and Figure 12.28b, the magnitude of the CMIP5 multi-model mean trend in September Arctic sea ice extent over the satellite era is more consistent with, but still underestimates, the observed one (see also Massonnet et al., 2012; Stroeve et al., 2012; Wang and Overland, 2012; Overland and Wang, 2013). Owing to the shortness of the observational record, it is difficult to ascertain the relative influence of natural variability on this trend. This hinders the comparison between modelled and observed trends, and hence the estimate of the sensitivity of the September Arctic sea ice extent to global surface temperature change (i.e., the decrease in sea ice extent per degree global warming) (Kay et al., 2011; Winton, 2011; Mahlstein and Knutti, 2012). This sensitivity may be crucial for determining future sea ice losses. Indeed, a clear relationship exists at longer than decadal time scales in climate change simulations between the annual mean or September mean Arctic sea ice extent and the annual mean global surface temperature change for ice extents larger than ~1 × 10^6 km^2 (e.g., Ridley et al., 2007; Zhang, 2010b; NRC, 2011; Winton, 2011; Mahlstein and Knutti, 2012). This relationship is illustrated in Figure 12.30 for both CMIP3 and CMIP5 models. From this figure, it can be seen that the sea ice sensitivity varies significantly from model to model and is generally larger and in better agreement among models in CMIP5.

A complete and detailed explanation for what controls the range of Arctic sea ice responses in models over the 21st century remains elusive, but the Arctic sea ice provides an example where process-based constraints can be used to reduce the spread of model projections (Overland et al., 2011; Collins et al., 2012; Hodson et al., 2012). For CMIP3 models, results indicate that the changes in Arctic sea ice mass budget over the 21st century are related to the late 20th century mean sea ice thickness distribution (Holland et al., 2010), average sea ice thickness (Bitz, 2008; Hodson et al., 2012), fraction of thin ice cover (Boé et al., 2009b) and oceanic heat transport to the Arctic (Mahlstein and Knutti, 2011). For CMIP5 models, Massonnet et al. (2012) showed that the time needed for the September Arctic sea ice areal coverage to drop below a certain threshold is highly correlated with the September sea ice extent and annual mean sea ice volume averaged over the past several decades (Figure 12.31a, b). The timing of a seasonally ice-free Arctic Ocean or the fraction of remaining sea ice in September at any time during the 21st century were also found to correlate with the past trend in September Arctic sea ice extent and the amplitude of the mean seasonal cycle of sea ice extent (Boé et al., 2009b; Collins et al., 2012; Massonnet et al., 2012) (Figure 12.31c, d). All these empirical

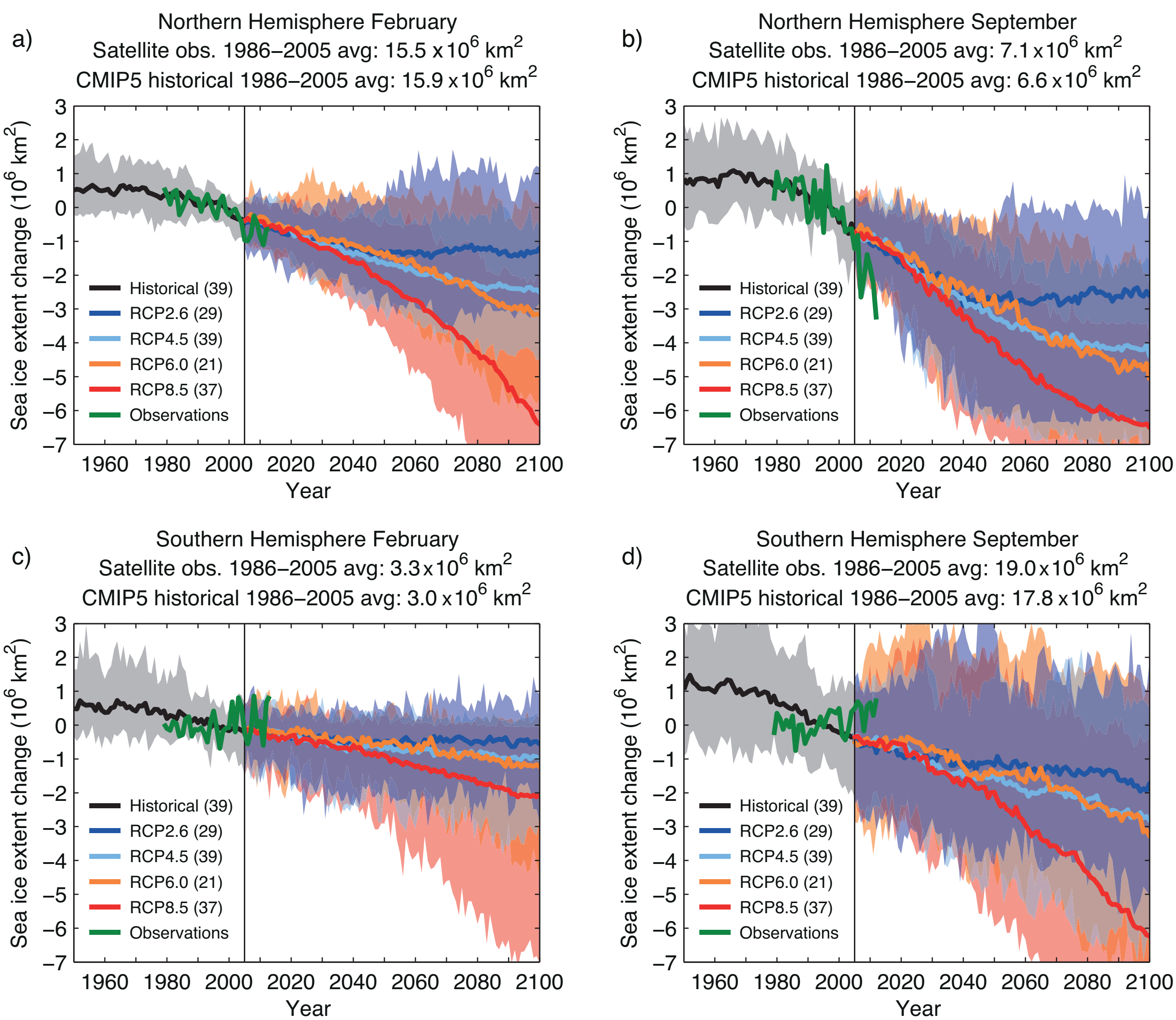

Figure 12.28 | Changes in sea ice extent as simulated by CMIP5 models over the second half of the 20th century and the whole 21st century under RCP2.6, RCP4.5, RCP6.0 and RCP8.5 for (a) Northern Hemisphere February, (b) Northern Hemisphere September, (c) Southern Hemisphere February and (d) Southern Hemisphere September. The solid curves show the multi-model means and the shading denotes the 5 to 95% range of the ensemble. The vertical line marks the end of CMIP5 historical climate change simulations. One ensemble member per model is taken into account in the analysis. Sea ice extent is defined as the total ocean area where sea ice concentration exceeds 15% and is calculated on the original model grids. Changes are relative to the reference period 1986–2005. The number of models available for each RCP is given in the legend. Also plotted (solid green curves) are the satellite data of Comiso and Nishio (2008, updated 2012) over 1979–2012.

relationships can be understood on simple physical grounds (see the aforementioned references for details).

These results lend support for weighting/recalibrating the models based on their present-day Arctic sea ice simulations. Today, the optimal approach for constraining sea ice projections from climate models is unclear, although one notes that these methods should have a credible underlying physical basis in order to increase confidence in their results (see Section 12.2). In addition, they should account for the potentially large imprint of natural variability on both observations and model simulations when these two sources of information are to be compared (see Section 9.8.3). This latter point is particularly critical if the past sea ice trend or sensitivity is used in performance metrics given the relatively short observational period (Kay et al., 2011; Overland et al., 2011; Mahlstein and Knutti, 2012; Massonnet et al., 2012; Stroeve et al., 2012). A number of studies have applied such metrics to the CMIP3 and CMIP5 models. Stroeve et al. (2007) and Stroeve et al. (2012) rejected several CMIP3 and CMIP5 models, respectively, on

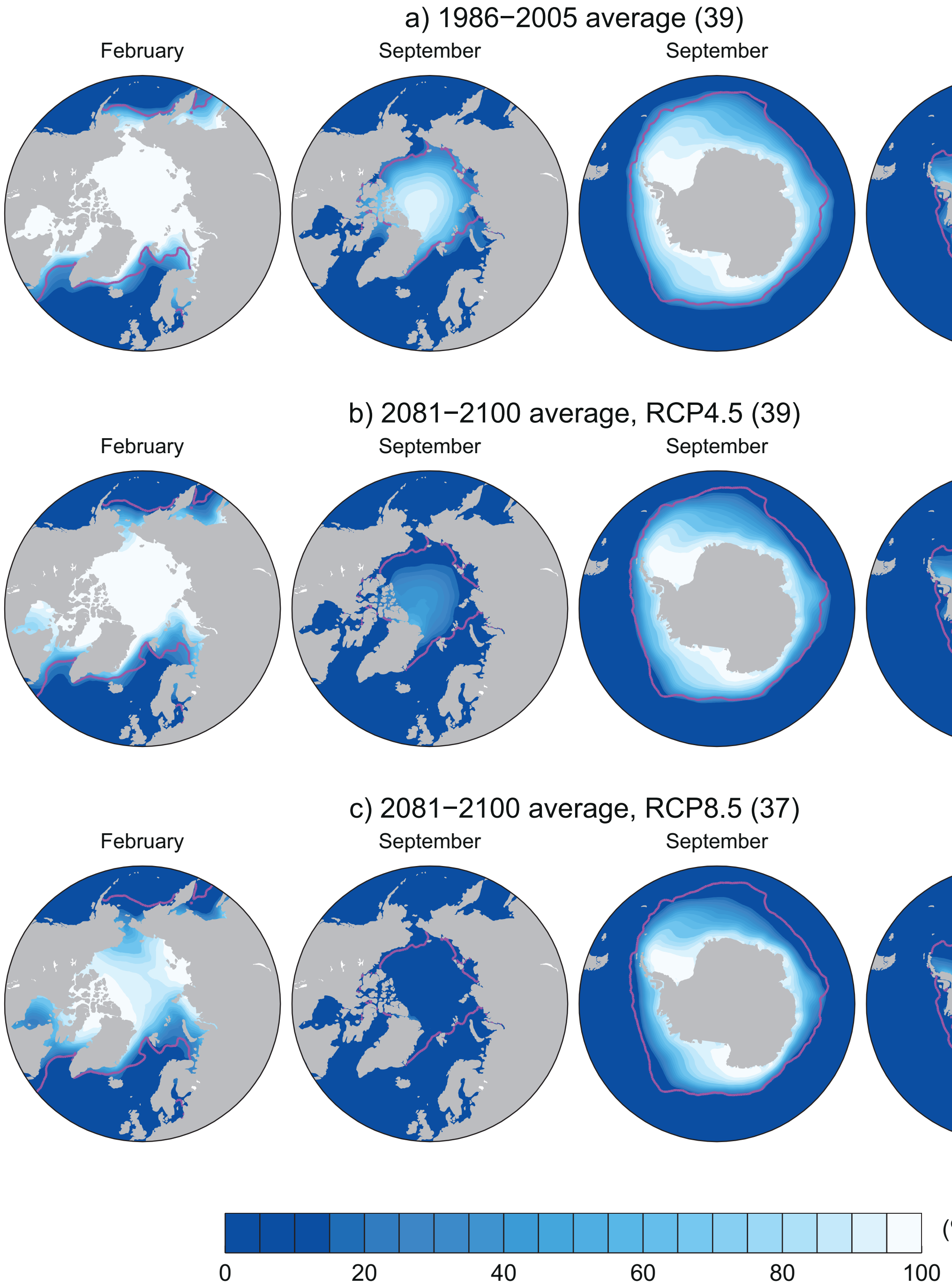

Figure 12.29 | February and September CMIP5 multi-model mean sea ice concentrations (%) in the Northern and Southern Hemispheres for the periods (a) 1986–2005, (b) 2081–2100 under RCP4.5 and (c) 2081–2100 under RCP8.5. The model sea ice concentrations are interpolated onto a 1° × 1° regular grid. One ensemble member per model is taken into account in the analysis, and the multi-model mean sea ice concentration is shown where it is larger than 15%. The number of models available for each RCP is given in parentheses. The pink lines indicate the observed 15% sea ice concentration limits averaged over 1986–2005 (Comiso and Nishio, 2008, updated 2012).

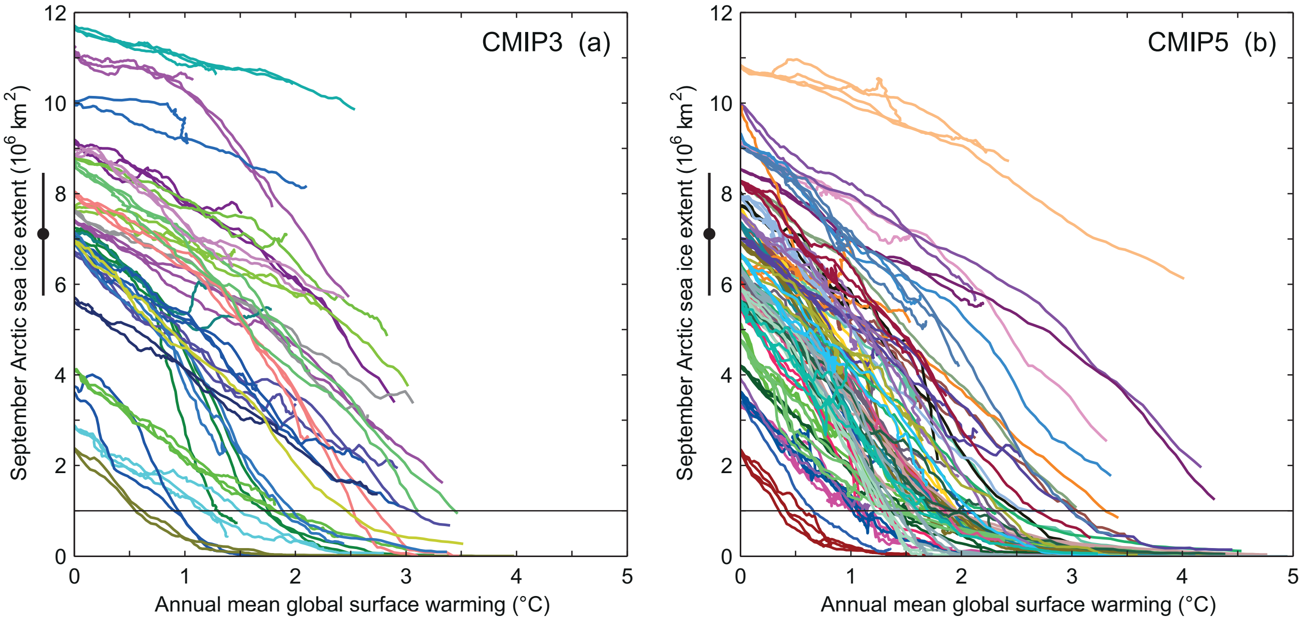

Figure 12.30 | September Arctic sea ice extent as a function of the annual mean global surface warming relative to the period 1986–2005 for (a) CMIP3 models (all SRES scenarios) and (b) CMIP5 models (all RCPs). The ice extents and global temperatures are computed on a common latitude-longitude grid for CMIP3 and on the original model grids for CMIP5. One ensemble member per model is taken into account in the analysis. A 21-year running mean is applied to the model output. The full black circle and vertical bar on the left-hand side of the *y*-axis indicate the mean and ±2 standard deviations about the mean of the observed September Arctic sea ice extent over 1986–2005, respectively (Comiso and Nishio, 2008, updated 2012). The horizontal line corresponds to a nearly ice-free Arctic Ocean in September.

the basis of their simulated late 20th century mean September Arctic sea ice extent. Wang and Overland (2009) selected a subset of CMIP3 models (and Wang and Overland (2012) did the same for the CMIP5 models) based on their fidelity to the observed mean seasonal cycle of Arctic sea ice extent in the late 20th century and then scaled the chosen models to the recently observed September sea ice extent. Zhang (2010b) retained a number of CMIP3 models based on the regression between summer sea ice loss and Arctic surface temperature change. Boé et al. (2009b) and Mahlstein and Knutti (2012) did not perform a model selection but rather recalibrated the CMIP3 Arctic sea ice projections on available observations of September Arctic sea ice trend and sensitivity to global surface temperature change, respectively. Finally, Massonnet et al. (2012) selected a subset of CMIP5 models on the basis of the four relationships illustrated in Figure 12.31a–d.

These various methods all suggest a faster rate of summer Arctic sea ice decline than the multi-model mean. Although they individually provide a reduced range for the year of near disappearance of the September Arctic sea ice compared to the original CMIP3/CMIP5 multi-model ensemble, they lead to different timings (Overland and Wang, 2013). Consequently, the time interval obtained when combining all these studies remains wide: 2020–2100$^+$ (2100$^+$ = not before 2100) for the SRES A1B scenario and RCP4.5 (Stroeve et al., 2007, 2012; Boé et al., 2009b; Wang and Overland, 2009, 2012; Zhang, 2010b; Massonnet et al., 2012) and 2020–2060 for RCP8.5 (Massonnet et al., 2012; Wang and Overland, 2012). The method proposed by Massonnet et al. (2012) is applied here to the full set of models that provided the CMIP5 database with sea ice output. The natural variability of each of the four diagnostics shown in Figure 12.31a–d is first estimated by averaging over all available models with more than one ensemble member the diagnostic standard deviations derived from the model ensemble members. Then, for each model, a ±2 standard deviation interval is constructed around the ensemble mean or single realization of the diagnostic considered. A model is retained if, for each diagnostic, either this interval overlaps a ±20% interval around the observed/reanalysed value of the diagnostic or at least one ensemble member from that model gives a value for the diagnostic that falls within ±20% of the observational/reanalysed data. The outcome is displayed in Figure 12.31e for RCP8.5. Among the five selected models (ACCESS1.0, ACCESS1.3, GFDL-CM3, IPSL-CM5A-MR, MPI-ESM-MR), four project a nearly ice-free Arctic Ocean in September before 2050 (2080) for RCP8.5 (RCP4.5), the earliest and latest years of near disappearance of the sea ice pack being about 2040 and about 2060 (about 2040 and 2100$^+$), respectively. It should be mentioned that Maslowski et al. (2012) projected that it would take only until about 2016 to reach a nearly ice-free Arctic Ocean in summer, based on a linear extrapolation into the future of the recent sea ice volume trend from a hindcast simulation conducted with a regional model of the Arctic sea ice–ocean system. However, such an extrapolation approach is problematic as it ignores the negative feedbacks that can occur when the sea ice cover becomes thin (e.g., Bitz and Roe, 2004; Notz, 2009) and neglects the effect of year-to-year or longer-term variability (Overland and Wang, 2013). Mahlstein and Knutti (2012) encompassed the dependence of sea ice projections on the forcing scenario by determining the annual mean global surface warming threshold for nearly ice-free conditions in September. Their best estimate of ~2°C above the present derived from both CMIP3 models and observations is consistent with the 1.6 to 2.1°C range (mean value: 1.9°C) obtained from the CMIP5 model subset shown in Figure 12.31e (see also Figure 12.30b). The reduction in September Arctic sea ice extent by the end of the 21st century, averaged over this subset of models, ranges from 56% for RCP2.6 to 100% for RCP8.5.

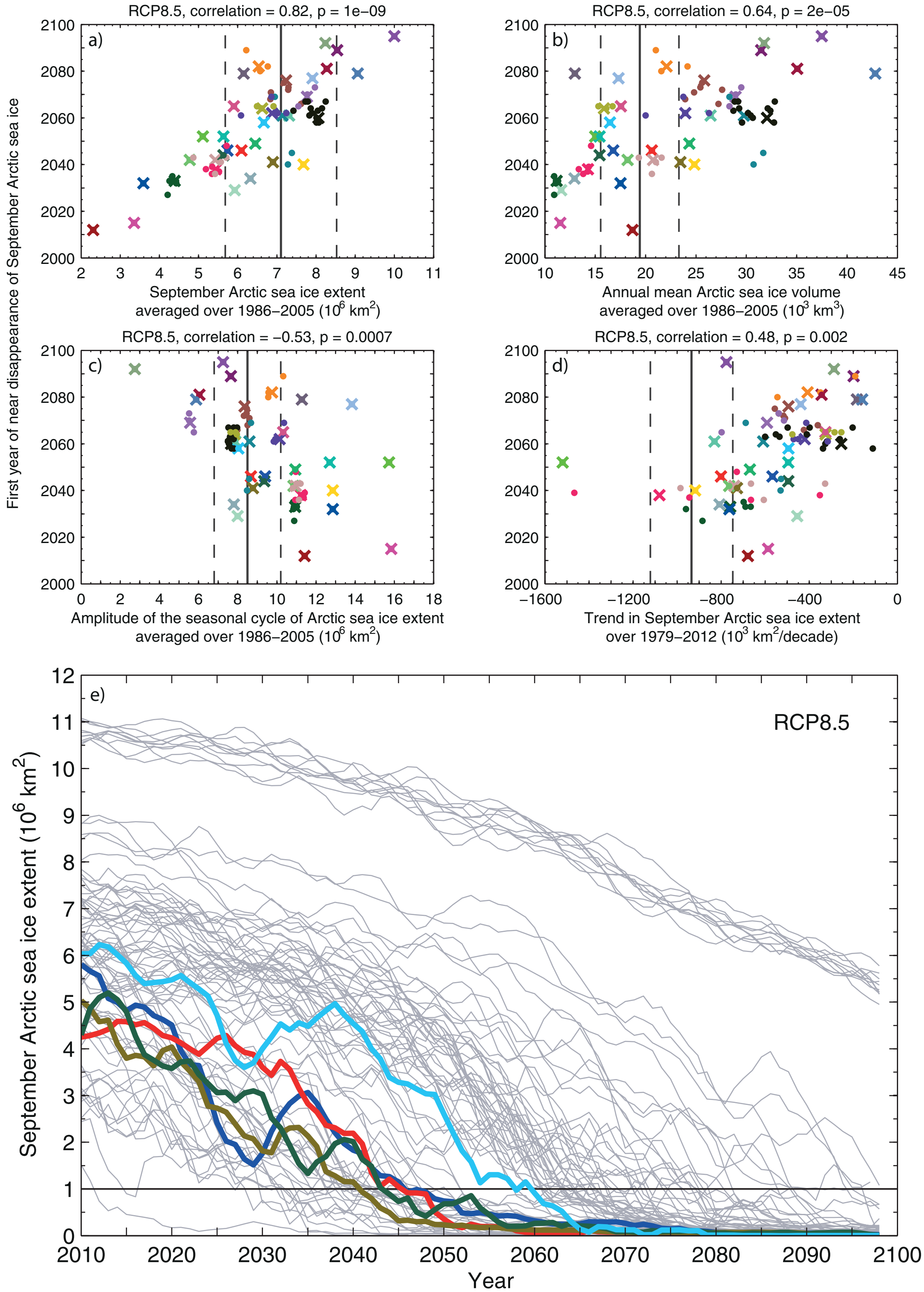

Figure 12.31 | (a–d) First year during which the September Arctic sea ice extent falls below 1×10^6 km^2 in CMIP5 climate projections (37 models, RCP8.5) as a function of (a) the September Arctic sea ice extent averaged over 1986–2005, (b) the annual mean Arctic sea ice volume averaged over 1986–2005, (c) the amplitude of the 1986–2005 mean seasonal cycle of Arctic sea ice extent and (d) the trend in September Arctic sea ice extent over 1979–2012. The sea ice diagnostics displayed are calculated on the original model grids. The correlations and one-tailed *p*-values are computed from the multi-member means for models with several ensemble members (coloured crosses), but the ensemble members of individual models are also depicted (coloured dots). The vertical solid and dashed lines show the corresponding observations or bias-adjusted PIOMAS (Pan-Arctic Ice-Ocean Modelling and Assimilation System) reanalysis data (a, c and d: Comiso and Nishio, 2008, updated 2012; b: Schweiger et al., 2011) and the ±20% interval around these data, respectively. (e) Time series of September Arctic sea ice extent (5-year running mean) as simulated by all CMIP5 models and their ensemble members under RCP8.5 (thin curves). The thick, coloured curves correspond to a subset of five CMIP5 models selected on the basis of panels a–d following Massonnet et al. (2012) (see text for details). Note that each of these models provides only one ensemble member for RCP8.5.

In light of all these results, it is *very likely* that the Arctic sea ice cover will continue to shrink and thin all year round during the 21st century as the annual mean global surface temperature rises. It is also *likely* that the Arctic Ocean will become nearly ice-free in September before the middle of the century for high GHG emissions such as those corresponding to RCP8.5 (*medium confidence*). The potential irreversibility of the Arctic sea ice loss and the possibility of an abrupt transition toward an ice-free Arctic Ocean are discussed in Section 12.5.5.7.

In the SH, the decrease in sea ice extent between 1986–2005 and 2081–2100 projected by the CMIP5 models as a group varies from 16% for RCP2.6 to 67% for RCP8.5 in February and from 8% to 30% in September. In contrast with the NH, the absolute rate of decline is greatest in wintertime. Eisenman et al. (2011) argue that this hemispheric asymmetry in the seasonality of sea ice loss is fundamentally related to the geometry of coastlines. For each forcing scenario, the relative changes in multi-model mean February and September Antarctic sea ice volumes by the end of the century are of the same order as the corresponding ones for sea ice extent. About 75% of the available CMIP5 models reach a nearly ice-free state in February within this century under RCP8.5 (about 60% under RCP4.5). For RCP8.5, only small portions of the Weddell and Ross Seas stay ice-covered in February during 2081–2100 in those models that do not project a seasonally ice-free Southern Ocean (see Figure 12.29c). Nonetheless, there is *low confidence* in these Antarctic sea ice projections because of the wide range of model responses and the inability of almost all of the models to reproduce the mean seasonal cycle, interannual variability and overall increase of the Antarctic sea ice areal coverage observed during the satellite era (see Section 9.4.3; Maksym et al., 2012; Turner et al., 2013; Zunz et al., 2013).

12.4.6.2 Changes in Snow Cover and Frozen Ground

Excluding ice sheets and glaciers, analyses of seasonal snow cover changes generally focus on the NH, where the configuration of the continents on the Earth induces a larger maximum seasonal snow cover extent (SCE) and a larger sensitivity of SCE to climate changes. Seasonal snow cover extent and snow water equivalent (SWE) respond to both temperature and precipitation. At the beginning and the end of the snow season, SCE decreases are closely linked to a shortening of the seasonal snow cover duration, while SWE is more sensitive to snowfall amount (Brown and Mote, 2009). Future widespread reductions of SCE, particularly in spring, are simulated by the CMIP3 models (Roesch, 2006; Brown and Mote, 2009) and confirmed by the CMIP5 ensemble (Brutel-Vuilmet et al., 2013). The NH spring (March-April average) snow cover area changes are coherent in the CMIP5 models although there is considerable scatter. Relative to the 1986–2005 reference period, the CMIP5 models simulate a weak decrease of about 7 ± 4% (one-σ inter-model dispersion) for RCP2.6 during the last two decades of the 21st century, while SCE decreases of about 13 ± 4% are simulated for RCP4.5, 15 ± 5% for RCP6.0, and 25 ± 8% for RCP8.5 (Figure 12.32). There is *medium confidence* in these numbers because of the considerable inter-model scatter mentioned above and because snow processes in global climate models are strongly simplified.

Projections for the change in annual maximum SWE are more mixed. Warming decreases SWE both by reducing the fraction of precipitation that falls as snow and by increasing snowmelt, but projected increases in precipitation over much of the northern high latitudes during winter months act to increase snow amounts. Whether snow covering the ground will become thicker or thinner depends on the balance between these competing factors. Both in the CMIP3 (Räisänen, 2008) and in the CMIP5 models (Brutel-Vuilmet et al., 2013), annual maximum SWE tends to increase or only marginally decrease in the coldest

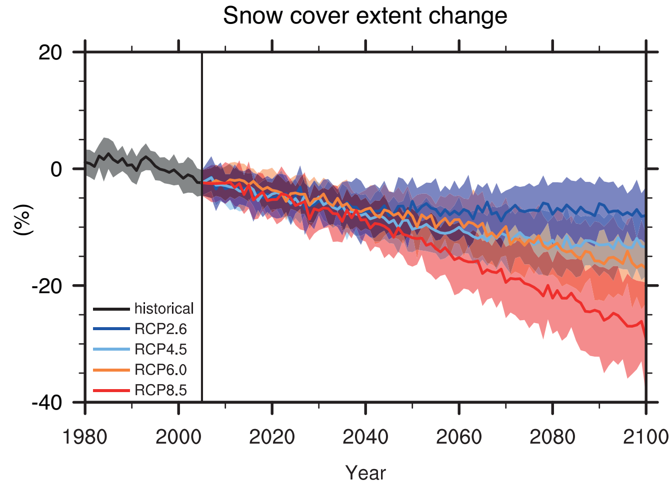

Figure 12.32 | Northern Hemisphere spring (March to April average) snow cover extent change (in %) in the CMIP5 ensemble, relative to the simulated extent for the 1986–2005 reference period. Thick lines mark the multi-model average, shading indicates the inter-model spread (one standard deviation). The observed March to April average snow cover extent for the 1986–2005 reference period is $32.6 \cdot 10^6$ km^2 (Brown and Robinson, 2011).

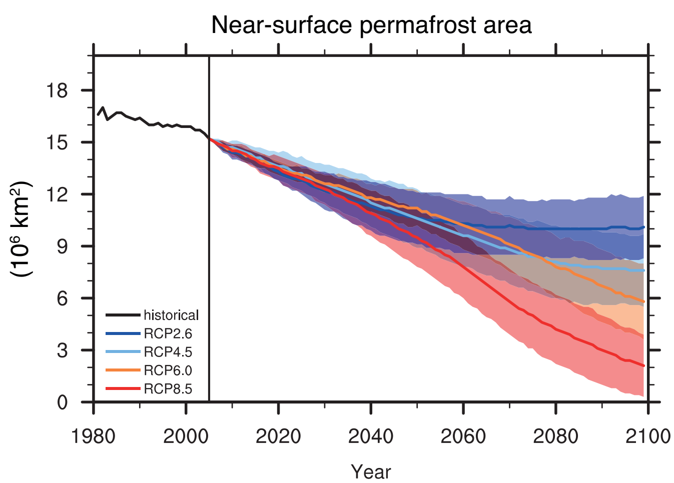

Figure 12.33 | Northern Hemisphere near-surface permafrost area, diagnosed for the available CMIP5 models by Slater and Lawrence (2013) following Nelson and Outcalt (1987) and using 20-year average bias-corrected monthly surface air temperatures and snow depths. Thick lines: multi-model average. Shading and thin lines indicate the inter-model spread (one standard deviation). The black line for the historical period is diagnosed from the average of the European Centre for Medium range Weather Forecast (ECMWF) reanalysis of the global atmosphere and surface conditions (ERA), Japanese ReAnalysis (JRA), Modern Era Retrospective-analysis for Research and Applications (MERRA) and Climate Forecast System Reanalysis and Reforecast (CFSRR) reanalyses (Slater and Lawrence, 2013). Estimated present permafrost extent is between 12 and 17 million km^2 (Zhang et al., 2000).

regions, while annual maximum SWE decreases are strong closer to the southern limit of the seasonally snow-covered area.

It is thus *very likely* (*high confidence*) that by the end of the 21st century, NH spring snow cover extent will be substantially lower than today if anthropogenic climate forcing is similar to the stronger scenarios considered here. Conversely, there is only *medium confidence* in the latitudinal pattern of annual maximum SWE changes (increase or little change in the coldest regions, stronger decrease further to the South) because annual maximum SWE is influenced by competing factors (earlier melt onset, higher solid precipitation rates in some regions).

The strong projected warming across the northern high latitudes in climate model simulations has implications for frozen ground. Recent projections of the extent of near-surface permafrost (see Glossary) degradation continue to vary widely depending on the underlying climate forcing scenario and model physics, but virtually all of them indicate substantial near-surface permafrost degradation and thaw depth deepening over much of the permafrost area (Saito et al., 2007; Lawrence et al., 2008a, 2012; Koven et al., 2011, 2013; Eliseev et al., 2013; Slater and Lawrence, 2013). Permafrost at greater depths is less directly relevant to the surface energy and water balance, and its degradation naturally occurs much more slowly (Delisle, 2007). Climate models are beginning to represent permafrost physical processes and properties more accurately (Alexeev et al., 2007; Nicolsky et al., 2007; Lawrence et al., 2008a; Rinke et al., 2008; Koven et al., 2009; Gouttevin et al., 2012), but there are large disagreements in the calculation of current frozen soil extent and active layer depth due to differences in the land model physics in the CMIP5 ensemble (Koven et al., 2013). The projected changes in permafrost are a response not only to warming, but also to changes in snow conditions because snow properties and their seasonal evolution exert significant control on soil thermal state (Zhang, 2005; Lawrence and Slater, 2010; Shkolnik et al., 2010; Koven et al., 2013). Applying the surface frost index method (Nelson and Outcalt, 1987) to coupled climate model anomalies from the CMIP5 models (Slater and Lawrence, 2013) yields a reduction of the diagnosed 2080–2099 near-surface permafrost area (continuous plus discontinuous near-surface permafrost) by 37 ± 11% (RCP2.6), 51 ± 13% (RCP4.5), 58 ± 13% (RCP6.0), and 81±12% (RCP8.5), compared to the 1986–2005 diagnosed near-surface permafrost area, with *medium confidence* in the numbers as such because of the strongly simplified soil physical processes in current-generation global climate models (Figure 12.33). The uncertainty range given here is the 1-σ inter-model dispersion. Applying directly the model output to diagnose permafrost extent and its changes over the 21st century yields similar relative changes (Koven et al., 2013). In summary, based on high agreement across CMIP5 and older model projections, fundamental process understanding, and paleoclimatic evidence (e.g., Vaks et al., 2013), it appears *virtually certain* (*high confidence*) that near-surface permafrost extent will shrink as global climate warms. However, the amplitude of the projected reductions of near-surface permafrost extent not only depends on the emission scenario and the global climate model response, but also very much on the permafrost-related soil processes taken into account in the models.

12.4.7 Changes in the Ocean

12.4.7.1 Sea Surface Temperature, Salinity and Ocean Heat Content

Projected increase of SST and heat content over the next two decades is relatively insensitive to the emissions trajectory. However, projected outcomes diverge as the 21st century progresses. When SSTs increase as a result of external forcing, the interior water masses respond to the integrated signal at the surface, which is then propagated down to greater depth (Gleckler et al., 2006; Gregory, 2010). Changes in globally averaged ocean heat content currently account for about 90% of the change in global energy inventory since 1970 (see Box 3.1). Heat is transported within the interior of the ocean by its large-scale general circulation and by smaller-scale mixing processes. Changes in transports lead to redistribution of existing heat content and can cause local cooling even though the global mean heat content is rising (Banks and Gregory, 2006; Lowe and Gregory, 2006; Xie and Vallis, 2012).

Figure 12.12 shows the multi-model mean projections of zonally averaged ocean temperature change under three emission scenarios. The differences in projected ocean temperature changes for different RCPs manifest themselves more markedly as the century progresses. The largest warming is found in the top few hundred metres of the subtropical gyres, similar to the observed pattern of ocean temperature changes (Levitus et al., 2012, see also Section 3.2). Surface warming varies considerably between the emission scenarios ranging from about 1°C (RCP2.6) to more than 3°C in RCP8.5. Mixing and advection processes gradually transfer the additional heat to deeper levels of about 2000 m at the end of the 21st century. Depending on the emission scenario, global ocean warming between 0.5°C (RCP2.6) and 1.5°C (RCP8.5) will reach a depth of about 1 km by the end of the century. The strongest warming signal is found at the surface in subtropical and tropical regions. At depth the warming is most pronounced in the Southern Ocean. From an energy point of view, for RCP4.5 by the end of the 21st century, half of the energy taken up by the ocean is in the uppermost 700 m, and 85% is in the uppermost 2000 m.

In addition to the upper-level warming, the patterns are further characterized by a slight cooling in parts of the northern mid- and high latitudes below 1000 m and a pronounced heat uptake in the deep Southern Ocean at the end of the 21st century. The cooling may be linked to the projected decrease of the strength of the AMOC (see Section 12.4.7.2; 13.4.1; Banks and Gregory, 2006).

The response of ocean temperatures to external forcing comprises mainly two time scales: a relatively fast adjustment of the ocean mixed layer and the slow response of the deep ocean (Hansen et al., 1985; Knutti et al., 2008a; Held et al., 2010). Simulations with coupled ocean–atmosphere GCMs suggest time-scales of several millennia until the deep ocean is in equilibrium with the external forcing (Stouffer, 2004; Hansen et al., 2011; Li et al., 2013a). Thus, the long time-scale of the ocean response to external forcing implies an additional commitment to warming for many centuries when GHG emissions are decreased or concentrations kept constant (see Section 12.5.2). Further assessment of ocean heat uptake and its relationship to projections of sea level rise is presented in Section 13.4.1.

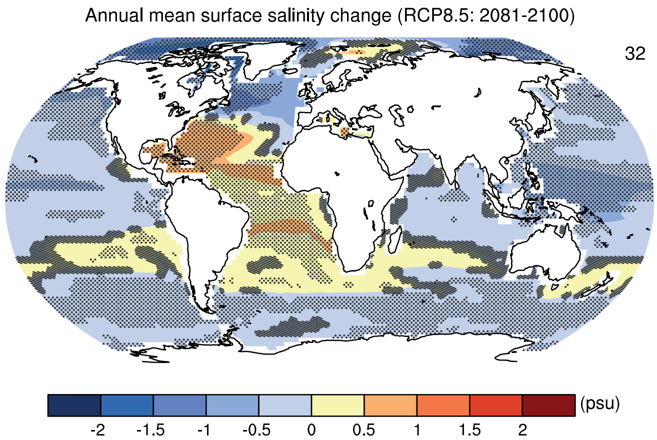

Figure 12.34 | Projected sea surface salinity differences 2081–2100 for RCP8.5 relative to 1986–2005 from CMIP5 models. Hatching indicates regions where the multi-model mean change is less than one standard deviation of internal variability. Stippling indicates regions where the multi-model mean change is greater than two standard deviations of internal variability and where at least 90% of the models agree on the sign of change (see Box 12.1). The number of CMIP5 models used is indicated in the upper right corner.

Durack and Wijffels (2010) and Durack et al. (2012) examined trends in global sea surface salinity (SSS) changes over the period 1950–2008. Their analysis revealed strong, spatially coherent trends in SSS over much of the global ocean, with a pattern that bears striking resemblance to the climatological SSS field and is associated with an intensification of the global water cycle (see Sections 3.3.2.1, 10.4.2 and 12.4.5). The CMIP5 climate model projections available suggest that high SSS subtropical regions that are dominated by net evaporation are typically getting more saline; lower SSS regions at high latitudes are typically getting fresher. They also suggest a continuation of this trend in the Atlantic where subtropical surface waters become more saline as the century progresses (Figure 12.34) (see also Terray et al., 2012). At the same time, the North Pacific is projected to become less saline.

12.4.7.2 Atlantic Meridional Overturning

Almost all climate model projections reveal an increase of high latitude temperature and high latitude precipitation (Meehl et al., 2007b). Both of these effects tend to make the high latitude surface waters lighter and hence increase their stability. As seen in Figure 12.35, all models show a weakening of the AMOC over the course of the 21st century (see Section 12.5.5.2 for further analysis). Projected changes in the strength of the AMOC at high latitudes appear stronger in Geophysical Fluid Dynamics Laboratory (GFDL) CM2.1 when density is used as a vertical coordinate instead of depth (Zhang, 2010a). Once the RF is stabilized, the AMOC recovers, but in some models to less than its pre-industrial level. The recovery may include a significant overshoot (i.e., a weaker circulation may persist) if the anthropogenic RF is eliminated (Wu et al., 2011a). Gregory et al. (2005) found that for all eleven models

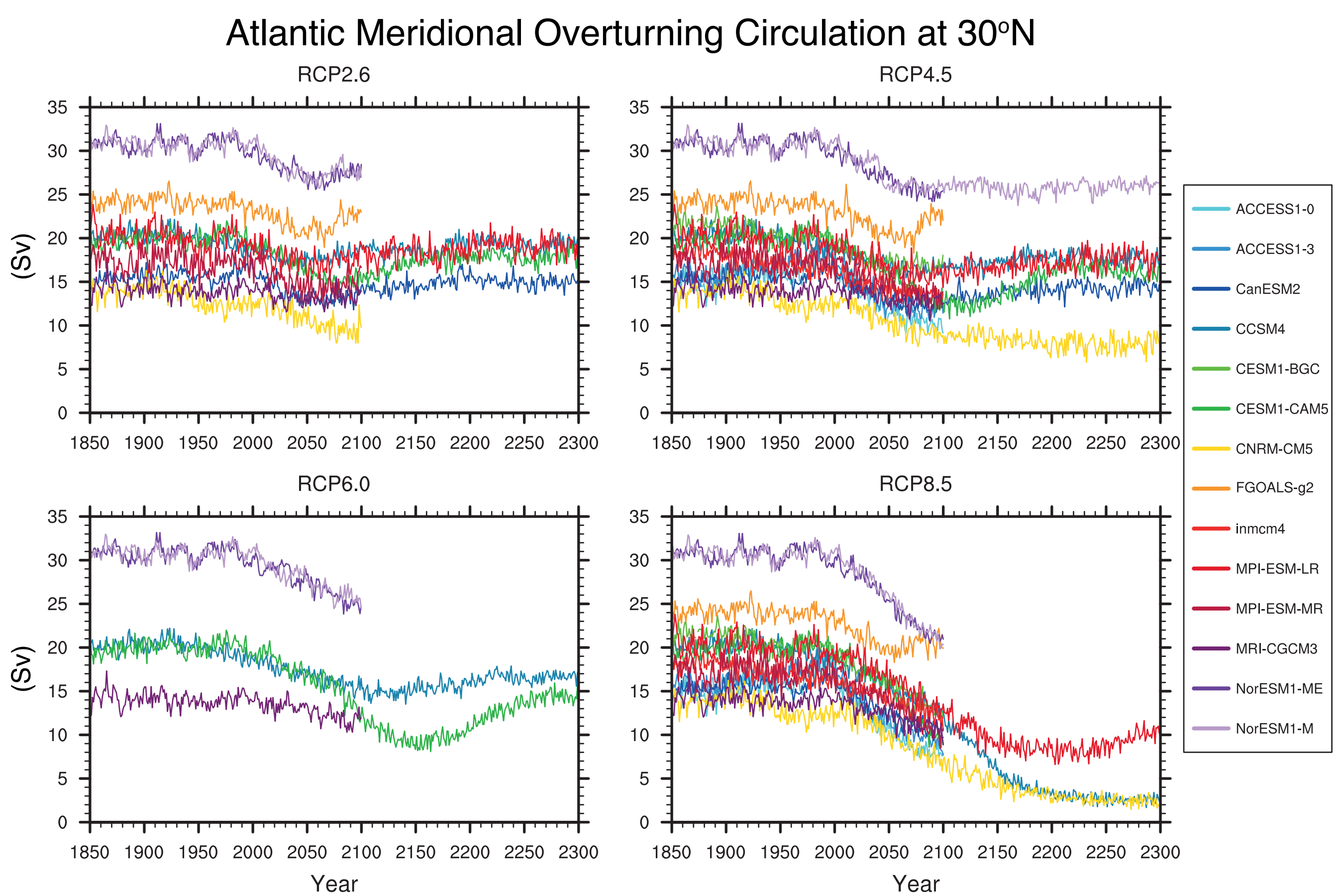

Figure 12.35 | Multi-model projections of Atlantic Meridional Overturning Circulation (AMOC) strength at 30°N from 1850 through to the end of the RCP extensions. Results are based on a small number of CMIP5 models available. Curves show results from only the first member of the submitted ensemble of experiments.

analysed (six from CMIP2/3 and five EMICs), the AMOC reduction was caused more by changes in surface heat flux than changes in surface freshwater flux. They further found that models with a stronger AMOC in their control run exhibited a larger weakening (see also Gregory and Tailleux, 2011).

Based on the assessment of the CMIP5 RCP simulations and on our understanding gleaned from analysis of CMIP3 models, observations and our understanding of physical mechanisms, it is *very likely* that the AMOC will weaken over the 21st century. Best estimates and ranges for the reduction from CMIP5 are 11% (1 to 24%) in RCP2.6 and 34% (12 to 54%) in RCP8.5. There is *low confidence* in assessing the evolution of the AMOC beyond the 21st century.

12.4.7.3 Southern Ocean

A dominant and robust feature of the CMIP3 climate projections assessed in AR4 is the weaker surface warming at the end of the 21st century in the Southern Ocean area compared to the global mean. Furthermore, the Antarctic Circumpolar Current (ACC) moves southward in most of the climate projections analysed in response to the simulated southward shift and strengthening of the SH mid-latitude westerlies (Meehl et al., 2007b).

The additional analyses of the CMIP3 model output performed since the release of AR4 confirm and refine the earlier findings. The displacement and intensification of the mid-latitude westerlies contribute to a large warming between 40°S and 60°S from the surface to mid-depths (Fyfe et al., 2007; Sen Gupta et al., 2009). Part of this warming has been attributed to the southward translation of the Southern Ocean current system (Sen Gupta et al., 2009). Moreover, the wind changes influence the surface temperature through modifications of the latent and sensible heat fluxes and force a larger northward Ekman transport of relatively cold polar surface water (Screen et al., 2010). This also leads to a stronger upwelling that brings southward and upward relatively warm and salty deep water, resulting in a subsurface salinity increase at mid-depths south of 50°S (Sen Gupta et al., 2009; Screen et al., 2010).

Overall, CMIP3 climate projections exhibit a decrease in mixed layer depth at southern mid- and high latitudes by the end of the 21st century. This feature is a consequence of the enhanced stratification resulting from surface warming and freshening (Lefebvre and Goosse, 2008; Sen Gupta et al., 2009; Capotondi et al., 2012). Despite large inter-model differences, there is a robust weakening of Antarctic Bottom Water production and its northward outflow, which is consistent with the decrease in surface density and is manifest as a warming signal close to the Antarctic margin that reaches abyssal depths (Sen Gupta et al., 2009).

In the vicinity of the Antarctic ice sheet, CMIP3 models project an average warming of ~0.5C° at depths of 200–500 m in 2091–2100 compared to 1991–2000 for the SRES A1B scenario, which has the potential to impact the mass balance of ice shelves (Yin et al., 2011). More detailed regional modelling using the SRES A1B scenario indicates that a redirection of the coastal current into the cavities underlying the Filchner-Ronne ice shelf during the second half of the 21st century might enhance the average basal melting rate there from 0.2 m yr^{-1} to almost 4 m yr^{-1} (Hellmer et al., 2012; see Section 13.4.4.2).

There are very few published analyses of CMIP5 climate projections focusing on the Southern Ocean. Meijers et al. (2012) found a wide variety of ACC responses to climate warming scenarios across CMIP5 models. Models show a high correlation between the changes in ACC strength and position, with a southward (northward) shift of the ACC core as the ACC gets stronger (weaker). No clear relationship between future changes in wind stress and ACC strength was identified, while the weakening of the ACC transport simulated at the end of the 21st century by many models was found to correlate with the strong decrease in the surface heat and freshwater fluxes in the ACC region (Meijers et al., 2012; Downes and Hogg, 2013). In agreement with the CMIP3 assessment (Sen Gupta et al., 2009), subtropical gyres generally strengthen under RCP4.5 and RCP8.5 and all expand southward, inducing a southward shift of the northern boundary of the ACC at most longitudes in the majority of CMIP5 models (Meijers et al., 2012). As in CMIP3 climate projections, an overall shallowing of the deep mixed layers that develop on the northern edge of the ACC in winter is observed, with larger shallowing simulated by models with deeper mixed layers during 1976–2005 (Sallée et al., 2013a). Sallée et al. (2013b) reported a warming of all mode, intermediate and deep water masses in the Southern Ocean. The largest temperature increase is found in mode and intermediate water layers. Consistently with CMIP3 projections (Downes et al., 2010), these water layers experience a freshening, whereas bottom water becomes slightly saltier. Finally, Sallée et al. (2013b) noted an enhanced upwelling of circumpolar deep water and an increased subduction of intermediate water that are nearly balanced by interior processes (diapycnal fluxes).

A number of studies suggest that oceanic mesoscale eddies might influence the response of the Southern Ocean circulation, meridional heat transport and deep water formation to changes in wind stress and surface buoyancy flux (Böning et al., 2008; Farneti et al., 2010; Downes et al., 2011; Farneti and Gent, 2011; Saenko et al., 2012; Spence et al., 2012). These eddies are not explicitly resolved in climate models and their role in future circulation changes still needs to be precisely quantified. Some of the CMIP5 models have output the meridional overturning due to the Eulerian mean circulation and that induced by parameterized eddies, thus providing a quantitative estimate of the role of the mesoscale circulation in a warming climate. On this basis, Downes and Hogg (2013) found that, under RCP8.5, the strengthening (weakening) of the upper (lower) Eulerian mean meridional overturning cell in the Southern Ocean is significantly correlated with the increased overlying wind stress and surface warming and is partly compensated at best by changes in eddy-induced overturning.

None of the CMIP3 and CMIP5 models include an interactive ice sheet component. When climate–ice sheet interactions are accounted for in an EMIC under a 4 × CO_2 scenario, the meltwater flux from the Antarctic ice sheet further reduces the surface density close to Antarctica and the rate of Antarctic Bottom Water formation. This ultimately results in a smaller surface warming at high southern latitudes compared to a simulation in which the freshwater flux from the melting ice sheet is not taken into account (Swingedouw et al., 2008). Nevertheless, in this study, this effect becomes significant only after more than one century.

12.4.8 Changes Associated with Carbon Cycle Feedbacks and Vegetation Cover

Climate change may affect the global biogeochemical cycles changing the magnitude of the natural sources and sinks of major GHGs. Numerous studies investigated the interactions between climate change and the carbon cycle (e.g., Friedlingstein et al., 2006), methane cycle (e.g., O'Connor et al., 2010), ozone (Cionni et al., 2011) or aerosols (e.g., Carslaw et al., 2010). Many CMIP5 ESMs now include a representation of the carbon cycle as well as atmospheric chemistry, allowing interactive projections of GHGs (mainly CO_2 and O_3) and aerosols. With such models, projections account for the imposed changes in anthropogenic emissions, but also for changes in natural sources and sinks as they respond to changes in climate and atmospheric composition. If included in ESMs, the impact on projected concentration, RF and hence on climate can be quantified. Climate-induced changes on the carbon cycle are assessed below, while changes in natural emissions of CH_4 are assessed in Chapter 6, changes in atmospheric chemistry in Chapter 11, and climate–aerosol interactions are assessed in Chapter 7.

12.4.8.1 Carbon Dioxide

As presented in Section 12.3, the CMIP5 experimental design includes, for the RCP8.5 scenario, experiments driven either by prescribed anthropogenic CO_2 emissions or concentration. The historical and 21st century emission-driven simulations allow evaluating the climate response of the Earth system when atmospheric CO_2 and the climate response are interactively being calculated by the ESMs. In such ESMs, the atmospheric CO_2 is calculated as the difference between the imposed anthropogenic emissions and the sum of land and ocean carbon uptakes. As most of these ESMs account for land use changes and their CO_2 emissions, the only external forcing is fossil fuel CO_2 emissions (along with all non-CO_2 forcings as in the C-driven RCP8.5 simulations). For a given ESM, the emission driven and concentration driven simulations would show different climate projections if the simulated atmospheric CO_2 in the emission driven run is significantly different from the one prescribed for the concentration driven runs. This would happen if the ESMs carbon cycle is different from the one simulated by MAGICC6, the model used to calculate the CMIP5 GHGs concentrations from the emissions for the four RCPs (Meinshausen et al., 2011c). When driven by CO_2 concentration, the ESMs can calculate the fossil fuel CO_2 emissions that would be compatible with the prescribed atmospheric CO_2 trajectory, allowing comparison with the set of CO_2 emissions initially estimated by the IAMs (Arora et al., 2011; Jones et al., 2013) (see Section 6.4.3, Box 6.4).

Figure 12.36 shows the simulated atmospheric CO_2 and global average surface air temperature warming (relative to the 1986–2005 reference period) for the RCP8.5 emission driven simulations from the CMIP5 ESMs, compared to the concentration driven simulations from the same models. Most (seven out of eleven) of the models estimate a larger CO_2 concentration than the prescribed one. By 2100, the multi-model average CO_2 concentration is 985 ± 97 ppm (full range 794 to 1142 ppm), while the CO_2 concentration prescribed for the RCP8.5 is 936 ppm. Figure 12.36 also shows the range of atmospheric CO_2 projections when the MAGICC6 model, used to provide the RCP concentrations, is tuned to emulate combinations of climate sensitivity uncertainty taken from 19 CMIP3 models and carbon cycle feedbacks uncertainty taken from 10 C^4MIP models, generating 190 model simulations (Meinshausen et al., 2011c; Meinshausen et al., 2011b). The emulation of the CMIP3/C^4MIP models shows for the RCP8.5, a range of simulated CO_2 concentrations of 794 to 1149 ppm (90% confidence level), extremely similar to what is obtained with the CMIP5 ESMs, with atmospheric concentration as high as 1150 ppm by 2100, that is, more than 200 ppm above the prescribed CO_2 concentration.

Global warming simulated by the E-driven runs show higher upper ends than when atmospheric CO_2 concentration is prescribed. For the models assessed here, the global surface temperature change (2081–2100 average relative to 1986–2005 average) ranges between 2.6°C and 4.7°C, with a multi-model average of 3.7°C ± 0.7°C for the concentration driven simulations, while the emission driven simulations give a range of 2.5°C to 5.6°C, with a multi-model average of 3.9°C ± 0.9°C, that is, 5% larger than for the concentration driven runs. The models that simulate the largest CO_2 concentration by 2100 have the largest warming amplification in the emission driven simulations, with an additional warming of more than 0.5°C.

The uncertainty on the carbon cycle has been shown to be of comparable magnitude to the uncertainty arising from physical climate processes (Gregory et al., 2009). Huntingford et al. (2009) used a simple model to characterize the relative role of carbon cycle and climate sensitivity uncertainties in contributing to the range of future temperature changes, concluding that the range of carbon cycle processes represent about 40% of the physical feedbacks. Perturbed parameter ensembles systematically explore land carbon cycle parameter uncertainty and illustrate that a wide range of carbon cycle responses are consistent with the same underlying model structures and plausible parameter ranges (Booth et al., 2012; Lambert et al., 2012). Figure 12.37 shows how the comparable range of future climate change (SRES A1B) arises from parametric uncertainty in land carbon cycle and atmospheric feedbacks. The same ensemble shows that the range of atmospheric CO_2 in the land carbon cycle ensemble is wider than the full SRES concentration range (B1 to A1FI scenario).

The CMIP5 ESMs described above do not include the positive feedback arising from the carbon release from high latitudes permafrost thawing under a warming scenario, which could further increase the atmospheric CO_2 concentration and the warming. Two recent studies investigated the climate–permafrost feedback from simulations with models of intermediate complexity (EMICs) that accounts for a permafrost carbon module (MacDougall et al., 2012; Schneider von Deimling et al., 2012). Burke et al. (2012) also estimated carbon loss from permafrost, from a diagnostic of the present-day permafrost carbon store and future soil warming as simulated by CMIP5 models. However, this last study did not quantify the effect on global temperature. Each of these studies found that the range of additional warming due to the permafrost carbon loss is quite large, because of uncertainties in future high latitude soil warming, amount of carbon stored in permafrost soils, vulnerability of freshly thawed organic material, the proportion of soil carbon that might be emitted as carbon dioxide via aerobic decomposition or as methane via anaerobic decomposition (Schneider von Deimling et al., 2012). For the RCP8.5, the additional warming from permafrost ranges between 0.04°C and 0.69°C by 2100 although

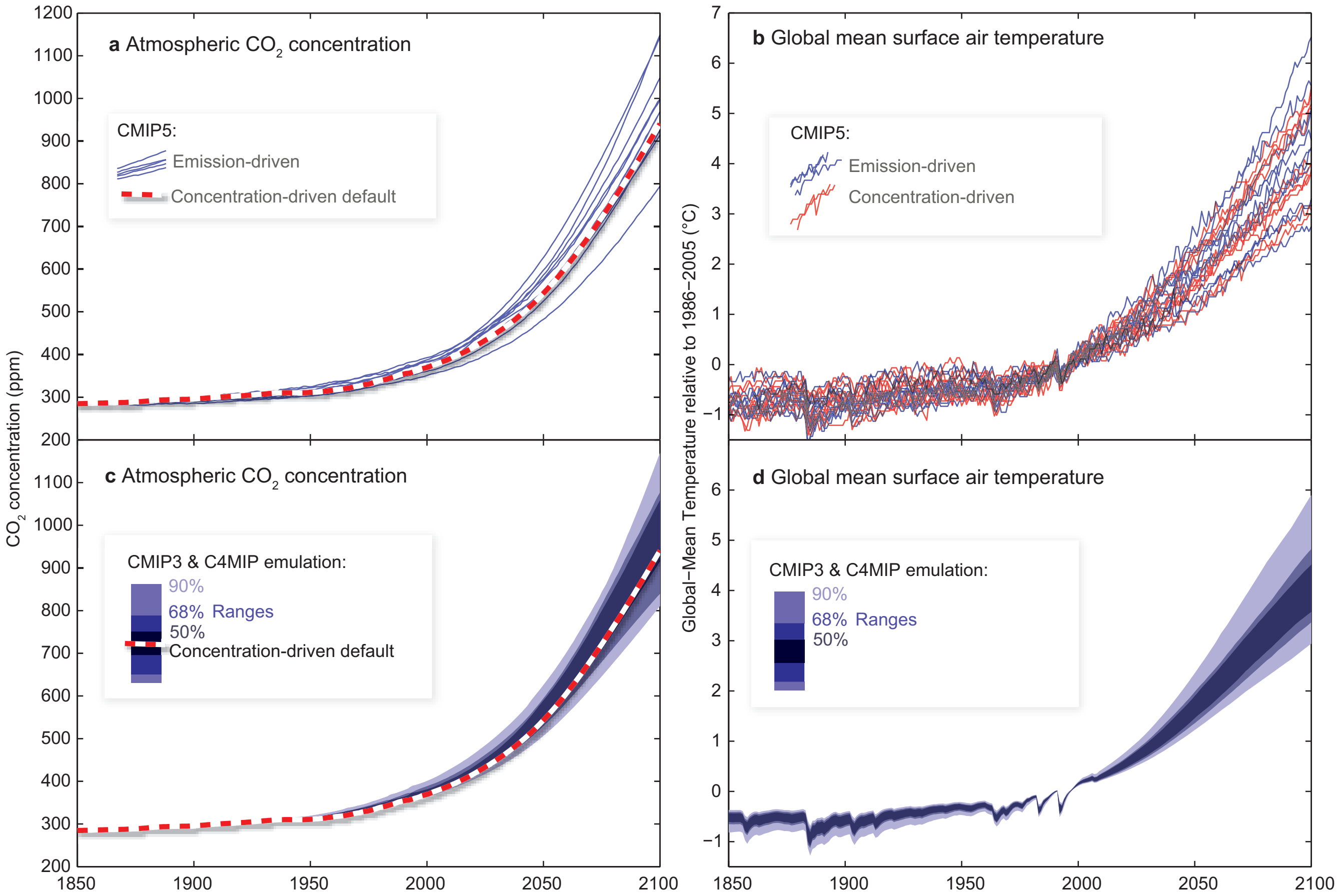

Figure 12.36 | Simulated changes in (a) atmospheric CO_2 concentration and (b) global averaged surface temperature (°C) as calculated by the CMIP5 Earth System Models (ESMs) for the RCP8.5 scenario when CO_2 emissions are prescribed to the ESMs as external forcing (blue). Also shown (b, in red) is the simulated warming from the same ESMs when directly forced by atmospheric CO_2 concentration (a, red white line). Panels (c) and (d) show the range of CO_2 concentrations and global average surface temperature change simulated by the Model for the Assessment of Greenhouse Gas-Induced Climate Change 6 (MAGICC6) simple climate model when emulating the CMIP3 models climate sensitivity range and the Coupled Climate Carbon Cycle Model Intercomparison Project (C[4]MIP) models carbon cycle feedbacks. The default line in (c) is identical to the one in (a).

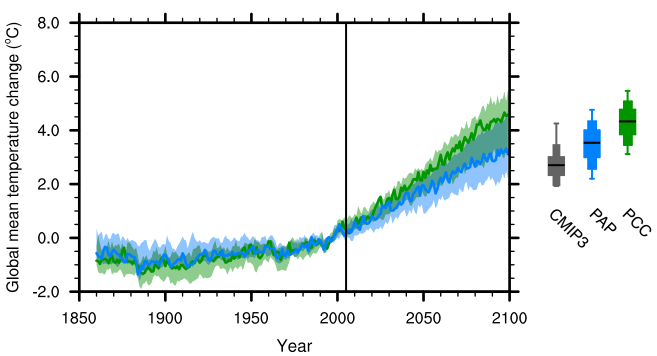

Figure 12.37 | Uncertainty in global mean temperature from Met Office Hadley Centre climate prediction model 3 (HadCM3) results exploring atmospheric physics and terrestrial carbon cycle parameter perturbations under the SRES A1B scenario (Murphy et al., 2004; Booth et al., 2012). Relative uncertainties in the Perturbed Carbon Cycle (PCC, green plume) and Perturbed Atmospheric Processes (PAP, blue plume) on global mean anomalies of temperature (relative to the 1986–2005 period). The standard simulations from the two ensembles, HadCM3 (blue solid) and HadCM3C (green solid) are also shown. Three bars are shown on the right illustrating the 2100 temperature anomalies associated with the CMIP3/AR4 ensemble (black) the PAP ensemble (blue) and PCC ensemble (green). The ranges indicate the full range, 10th to 90th, 25th to 75th and 50th percentiles.

there is *medium confidence* in these numbers as are the ones on the amount of carbon released (see Section 12.5.5.4) (MacDougall et al., 2012; Schneider von Deimling et al., 2012).

12.4.8.2 Changes in Vegetation Cover

Vegetation cover can also be affected by climate change, with forest cover potentially being decreasing (e.g., in the tropics) or increasing (e.g., in high latitudes). In particular, the Amazon forest has been the subject of several studies, generally agreeing that future climate change would increase the risk tropical Amazon forest being replaced by seasonal forest or even savannah (Huntingford et al., 2008; Jones et al., 2009; Malhi et al., 2009). Increase in atmospheric CO_2 would partly reduce such risk, through increase in water efficiency under elevated CO_2 (Lapola et al., 2009; Malhi et al., 2009). Recent multi-model estimates based on different CMIP3 climate scenarios and different dynamic global vegetation models predict a moderate risk of tropical forest reduction in South America and even lower risk for African and Asian tropical forests (see also Section 12.5.5.6) (Gumpenberger et al., 2010; Huntingford et al., 2013).

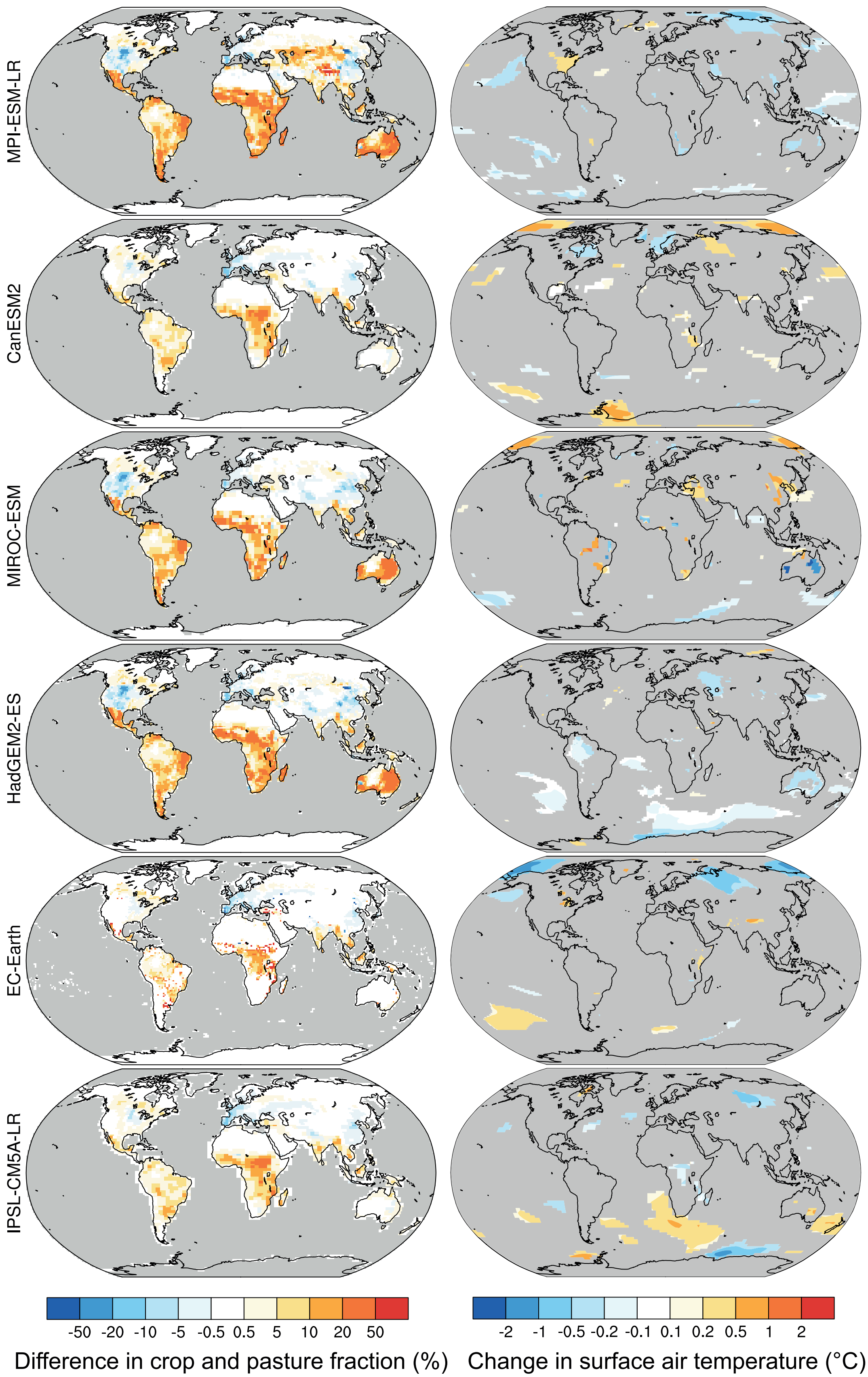

Figure 12.38 | Impact of land use change on surface temperature. LUCID-CMIP5 experiments where six ESMs were forced either with or without land use change beyond 2005 under the RCP8.5 scenario. Left maps of changes in total crop and pasture fraction (%) in the RCP8.5 simulations between 2006 and 2100 as implemented in each ESM. Right maps show the differences in surface air temperature (averaged over the 2071–2100 period) between the simulations with and without land use change beyond 2005. Only statistically significant changes ($p < 0.05$) are shown.

ESMs simulations with interactive vegetation confirmed known biophysical feedback associated with large-scale changes in vegetation. In the northern high latitudes, warming-induced vegetation expansion reduces surface albedo, enhancing the warming over these regions (Falloon et al., 2012; Port et al., 2012), with potentially larger amplification due to ocean and sea ice response (Swann et al., 2010). Over tropical forest, reduction of forest coverage would reduce evapotranspiration, also leading to a regional warming (Falloon et al., 2012; Port et al., 2012).

CMIP5 ESMs also include human induced land cover changes (deforestation, reforestation) affecting the climate system through changes in land surface physical properties (Hurtt et al., 2011). Future changes in land cover will have an impact on the climate system through biophysical and biogeochemical processes (e.g., Pongratz et al., 2010). Biophysical processes include changes in surface albedo and changes in partitioning between latent and sensible heat, while biogeochemical feedbacks essentially include change in CO_2 sources and sinks but could potentially also include changes in N_2O or CH_4 emissions. The biophysical response to future land cover changes has been investigated within the SRES scenarios. Using the SRES A2 2100 land cover, Davin et al. (2007) simulated a global cooling of 0.14 K relatively to a simulation with present-day land cover, the cooling being largely driven by change in albedo. Regional analyses have been performed in order to quantify the biophysical impact of biofuels plantation generally finding a local to regional cooling when annual crops are replaced by bioenergy crops, such as sugar cane (Georgescu et al., 2011; Loarie et al., 2011). However, some energy crops require nitrogen inputs for their production, leading inevitably to nitrous oxide (N_2O) emissions, potentially reducing the direct cooling effect and the benefit of biofuels as an alternative to fossil fuel emissions. Such emission estimates are still uncertain, varying strongly for different crops, management methods, soil types and reference systems (St. Clair et al., 2008; Smeets et al., 2009).

In the context of the Land-Use and Climate, IDentification of robust impacts (LUCID) project (Pitman et al., 2009) ESMs performed additional CMIP5 simulations in order to separate the biophysical from the biogeochemical effects of land use changes in the RCP scenarios. The LUCID–CMIP5 experiments were designed to complement RCP8.5 and RCP2.6 simulations of CMIP5, both of which showing an intensification of land use change over the 21st century. The LUCID–CMIP5 analysis was focussed on a difference in climate and land-atmosphere fluxes between the average of ensemble of simulations with and without land use changes by the end of 21st century (Brovkin et al., 2013). Due to different interpretation of land use classes, areas of crops and pastures were specific for each ESM (Figure 12.38, left). On the global scale, simulated biophysical effects of land use changes projected in the CMIP5 experiments with prescribed CO_2 concentrations were not significant. However, these effects were significant for regions with land use changes >10%. Only three out of six participating models, CanESM2, HadGEM2-ES and MIROC-ESM, reveal statistically significant changes in regional mean annual mean surface air temperature for the RCP8.5 scenario (Figure 12.38, right). However, there is *low confidence* on the overall effect as there is no agreement among the models on the sign of the global average temperature change due to the biophysical effects of land use changes (Brovkin et al., 2013). Changes in land surface albedo, available energy, latent and sensible heat fluxes were relatively small but significant in most of ESMs for regions with substantial land use changes. The scale of climatic effects reflects a small magnitude of land use changes in both the RCP2.6 and 8.5 scenarios and their limitation mainly to the tropical and subtropical regions where differences between biophysical effects of forests and grasslands are less pronounced than in mid- and high latitudes. LUCID-CMIP5 did not perform similar simulations for the RCP4.5 or RCP6.0 scenarios. As these two scenarios show a global decrease of land use area, one might expect their climatic impact to be different from the one seen in the RC2.6 and RCP8.5.

12.4.9 Consistency and Main Differences Between Coupled Model Intercomparison Project Phase 3/ Coupled Model Intercomparison Project Phase 5 and Special Report on Emission Scenarios/ Representative Concentration Pathways

In the experiments collected under CMIP5, both models and scenario have changed with respect to CMIP3 making a comparison with earlier results and the scientific literature they generated (on which some of this chapter's content is still based) complex. The set of models used in AR4 (the CMIP3 models) have been superseded by the new CMIP5 models (Table 12.1; Chapter 9) and the SRES scenarios have been replaced by four RCPs (Section 12.3.1). In addition, the baseline period used to compute anomalies has advanced 6 years, from 1980–1999 to 1986–2005.

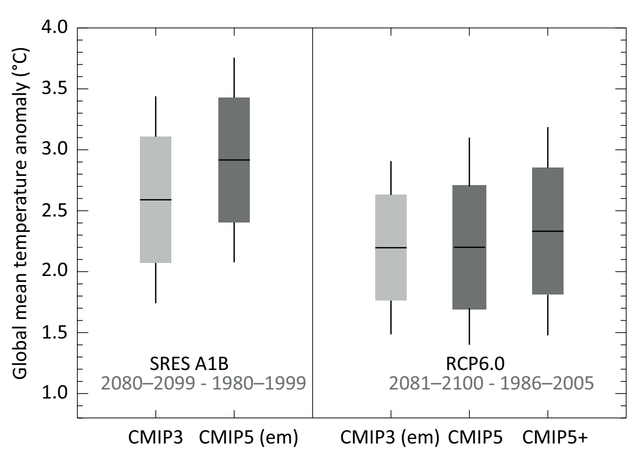

Figure 12.39 | Global mean temperature anomalies at the end of the 21st century from General Circulation Model (GCM) experiments and emulators comparing CMIP3/ CMIP5 responses under SRES A1B and RCP6.0. The boxes and whiskers indicate the 5th percentile, mean value – 1 standard deviation, mean, mean value + 1 standard deviation and 95th percentile of the distributions. The first box-and-whiskers on the left is computed directly from the CMIP3 ensemble and corresponds to the numbers quoted in AR4. The emulated SRES A1B projections (second from left) of CMIP5 are obtained by the method of Good et al. (2011a) and are calculated for the period 2080-2099 expressed with respect to the AR4 baseline period of 1980–1999. Because of the method, the subset of CMIP5 that are emulated are restricted to those with pre-industrial control, abrupt 4 × CO_2, historical, RCP4.5 and RCP8.5 simulations. The emulated RCP6.0 projections of CMIP3 (third from left, see also Figure 12.8) are from Knutti and Sedláček (2013) obtained using the method of Meinshausen et al. (2011b; 2011c) and are calculated for the slightly different future period 2081–2100 to be consistent with the rest of this chapter, and are expressed with respect to the AR5 baseline period of 1986–2005. The box-and-whiskers fourth from the left are a graphical representation of the numbers shown in Table 12.2. The final box-and-whiskers on the right is a combination of CMIP5 model output and emulation of CMIP5 RCP6.0 numbers for those models that did not run RCP6.0.

It would be extremely costly computationally to rerun the full CMIP3 ensemble under the new RCPs and/or the full CMIP5 ensemble under the old SRES scenarios in order to separate model and scenario effects. In the absence of a direct comparison, we rely on simplified modelling frameworks to emulate CMIP3/5 SRES/RCP model behaviour and compare them. Figure 12.39 shows an emulation of the global mean temperature response at the end of the 21st century that one would expect from the CMIP5 models if they were run under SRES A1B. In this case, anomalies are computed with respect to 1980–1999 for direct comparison with the values reported in AR4 (Meehl et al., 2007b) which used that baseline. The method used to emulate the SRES A1B response of the CMIP5 is documented by Good et al. (2011a; 2013). Ensemble-mean A1B RF was computed from CMIP3 projections using the Forster and Taylor (2006) method, scaled to ensure consistency with the forcing required by the method. The simple model is only used to predict the temperature difference between A1B and RCP8.5, and between A1B and RCP4.5 separately for each model. These differences are then added to CMIP5 GCM simulations of RCP8.5 and RCP4.5 respectively, and averaged to give a single A1B estimate. The emulated CMIP5 SRES A1B results show a slightly larger mean response than the actual CMIP3 models, with a similar spread (±1 standard deviation is used in this case). The main reason for this is the slightly larger mean transient climate response (TCR) in the subset of CMIP5 models available in comparison with the AR4 CMIP3 models. An alternative emulation is presented by Knutti and Sedláček (2013) who use the simplified MAGICC models with parameters chosen to emulate the response of the CMIP3 models to RCP6.0 forcing, with anomalies expressed with respect to the 1986–2005 baseline period (Figure 12.39). They too find a larger mean response in the CMIP5 case but also a larger spread (±1 standard deviation) in CMIP5. Uncertainties in the different approaches to emulating climate model simulations, for example estimating the non-GHG RF, and the small sample sizes of CMIP3 and CMIP5 make it difficult to draw conclusions on the statistical significance of the differences displayed in Figure 12.39, but the same uncertainties lead us to conclude that on the basis of these analyses there appears to be no fundamental difference between the behaviour of the CMIP5 ensemble, in comparison with CMIP3.

Meinshausen et al. (2011a; 2011b) tuned MAGICC6 to emulate 19 GCMs from CMIP3. The results are temperature projections and their uncertainties (based on the empirical distribution of the ensemble) under each of the RCPs, extended to year 2500 (under constant emissions for the lowest RCP and constant concentrations for the remaining three). In the same paper, an ensemble produced by combining carbon cycle parameter calibration to nine C[4]MIP models with the 19 CMIP3 model parameter calibrations is also used to estimate the emissions implied by the various concentration pathways, had the CMIP3 models included a carbon cycle component. Rogelj et al. (2012) used the same tool but performed a fully probabilistic analysis of the SRES and RCP scenarios using a parameter space that is consistent with

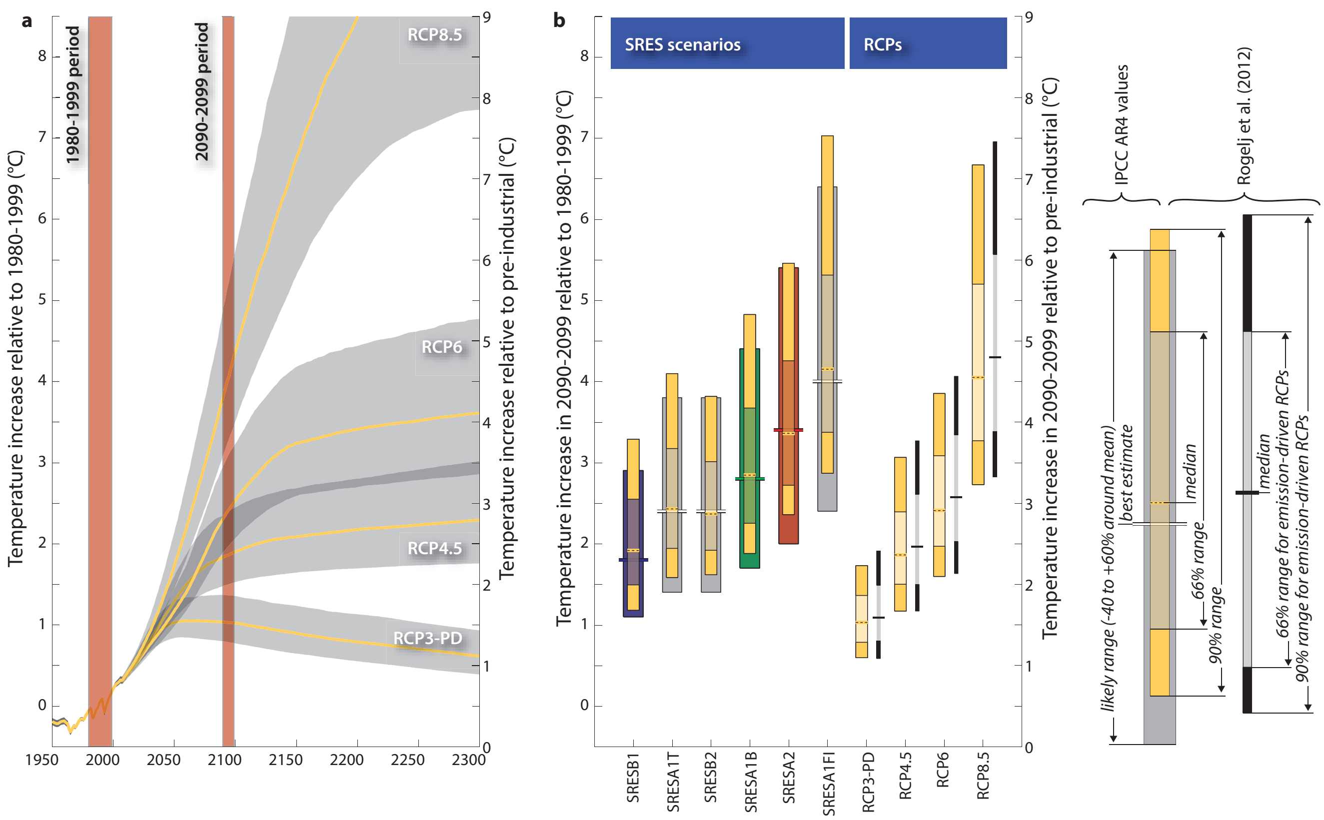

Figure 12.40 | Temperature projections for SRES scenarios and the RCPs. (a) Time-evolving temperature distributions (66% range) for the four RCP scenarios computed with the ECS distribution from Rogelj et al. (2012) and a model setup representing closely the carbon-cycle and climate system uncertainty estimates of the AR4 (grey areas). Median paths are drawn in yellow. Red shaded areas indicate time periods referred to in panel b. (b) Ranges of estimated average temperature increase between 2090 and 2099 for SRES scenarios and the RCPs respectively. Note that results are given both relative to 1980–1999 (left scale) and relative to pre-industrial (right scale). Yellow ranges indicate results obtained by Rogelj et al. (2012). Colour-coding of AR4 ranges is chosen to be consistent with AR4 (Meehl et al., 2007b). RCP2.6 is labelled as RCP3-PD here.

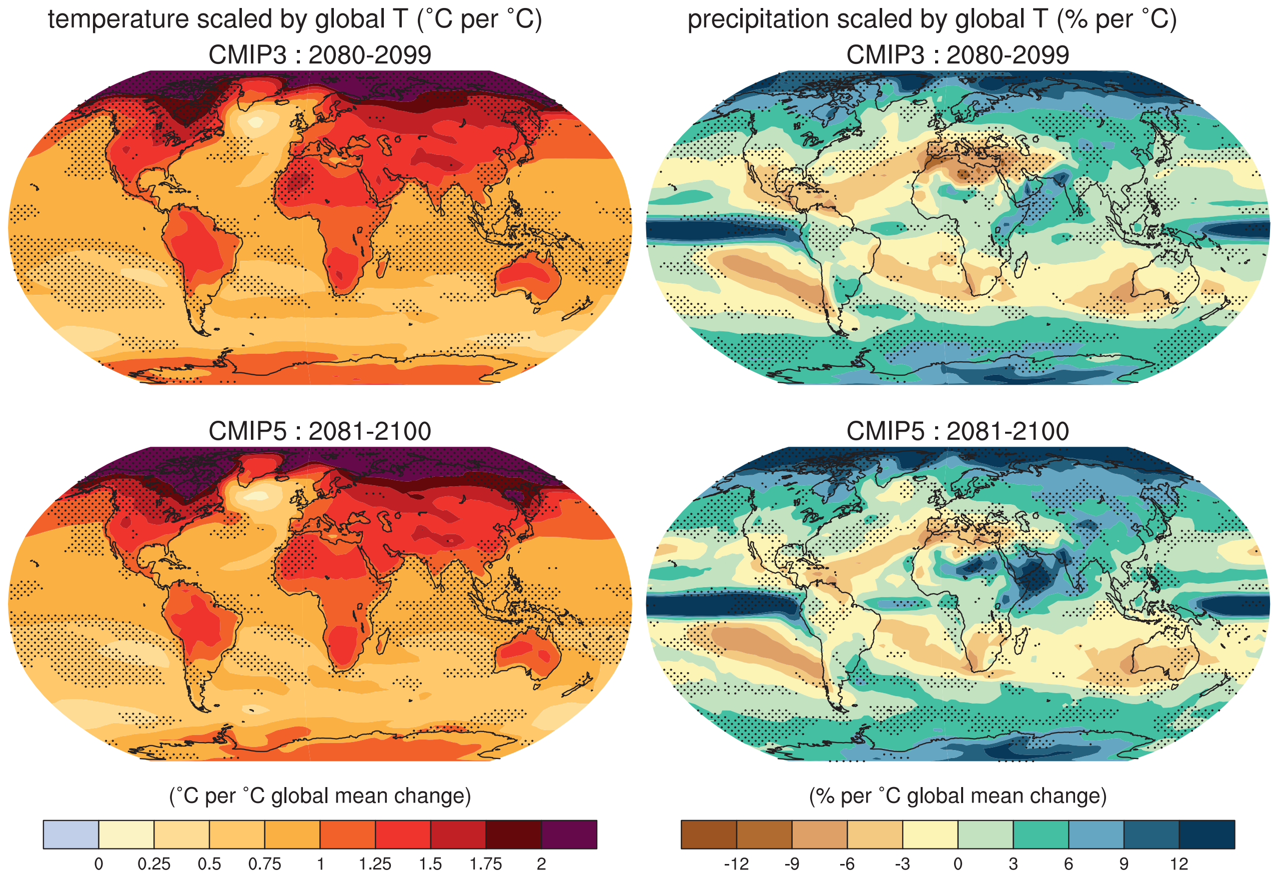

Figure 12.41 | Patterns of temperature (left column) and percent precipitation change (right column) for the CMIP3 models average (first row) and CMIP5 models average (second row), scaled by the corresponding global average temperature changes. The patterns are computed in both cases by taking the difference between the averages over the last 20 years of the 21st century experiments (2080–2099 for CMIP3 and 2081–2100 for CMIP5) and the last twenty years of the historic experiments (1980–1999 for CMIP3, 1986–2005 for CMIP5) and rescaling each difference by the corresponding change in global average temperature. This is done first for each individual model, and then the results are averaged across models. For the CMIP5 patterns, the RCP2.6 simulation of the FIO-ESM model was excluded because it did not show any warming by the end of the 21st century, thus not complying with the method requirement that the pattern be estimated at a time when the temperature change signal from CO_2 increase has emerged. Stippling indicates a measure of significance of the difference between the two corresponding patterns obtained by a bootstrap exercise. Two subsets of the pooled set of CMIP3 and CMIP5 ensemble members of the same size as the original ensembles, but without distinguishing CMIP3 from CMIP5 members, were randomly sampled 500 times. For each random sample we compute the corresponding patterns and their difference, then the true difference is compared, grid-point by grid-point, to the distribution of the bootstrapped differences, and only grid-points at which the value of the difference falls in the tails of the bootstrapped distribution (less than the 2.5 percentiles or the 97.5 percentiles) are stippled.

CMIP3/C[4]MIP but a more general uncertainty characterization for key quantities like equilibrium climate sensitivity, similarly to the approach utilized by Meinshausen et al. (2009). Observational or other historical constraints are also used in this study and the analysis is consistent with the overall assessment of sources and ranges of uncertainties for relevant quantities (equilibrium climate sensitivity above all) from AR4 (Meehl et al., 2007b , Box 10.2). Figure 12.40 summarizes results of this probabilistic comparison for global temperature. The RCPs span a large range of stabilization, mitigation and non-mitigation pathways and the resulting range of temperature changes are larger than those produced under SRES scenarios, which do not consider mitigation options. The SRES results span an interval between just above 1.0°C and 6.5°C when considering the respective *likely* ranges of all scenarios, including B1 as the lowest and A1FI as the highest. Emissions under RCP8.5 are highest and the resulting temperature changes *likely* range from 4.0°C to 6.1°C by 2100. The lowest RCP2.6 assumes significant mitigation and the global temperature change *likely* remains below 2°C.

Similar temperature change projections by the end of the 21st century are obtained under RCP8.5 and SRES A1FI, RCP6 and SRES B2 and RCP4.5 and SRES B1. There remain large differences though in the transient trajectories, with rates of change slower or faster for the different pairs. These differences can be traced back to the interplay of the (negative) short-term effect of sulphate aerosols and the (positive) effect of long-lived GHGs. Impact studies may be sensitive to the differences in these temporal profiles so care should be taken in approximating SRES with RCPs and vice versa.

While simple models can separate the effect of the scenarios and the model response, no studies are currently available that allow an attribution of the CMIP3-CMIP5 differences to changes in the transient climate response, the carbon cycle, and the inclusion of new processes (chemistry, land surface, vegetation). The fact that these sets of CMIP3 and CMIP5 experiments do not include emission-driven runs would suggest that differences in the representation of the carbon cycle are very unlikely to explain differences in the simulations, since the only effect of changes in the carbon cycle representation would affect the land surface, and thus would have only a minor effect on the climate response at the global scale.

Figure 12.41 shows a comparison of the patterns of warming and precipitation change from CMIP3 (using 23 models and three SRES scenarios) and CMIP5 (using 46 models and four RCPs), utilizing the pattern scaling methodology (Section 12.4.2). The geographic patterns of mean change are very similar across the two ensembles of models, with pattern correlations of 0.98 for temperature and 0.90 for precipitation changes. However there exist significant differences in the absolute values of the patterns, if not in their geographic shapes. A simple bootstrapping exercise that pooled together all models and scenarios and resampled 500 times the same numbers of models/scenarios divided into two groups, but without distinguishing CMIP3 from CMIP5 (and thus SRES from RCPs) allows to compute a measure of significance of the actual differences in the patterns. Stippling in Figure 12.41 marks the large regions where the difference is significant for temperature and precipitation patterns. The temperature pattern from CMIP5 shows significantly larger warming per degree Celsius of global mean temperature change in the NH and less warming per degree Celsius in the SH compared to the corresponding pattern from CMIP3. For precipitation patterns, CMIP5 shows significantly larger increases per degree Celsius in the NH and significantly larger decreases per degree Celsius in the SH compared to CMIP3. Even in this case we do not have studies that allow tracing the source of these differences to specific changes in models' configurations, processes represented or scenarios run.

Knutti and Sedláček (2013) attempt to identify or rule out at least some of these sources. Differences in model projections spread or its counterpart, robustness, between CMIP3 and CMIP5 are discussed, and it is shown that by comparing the behaviour of only a subset of 11 models, contributed to the two CMIPs by the same group of institutions, the robustness of CMIP5 versus that of CMIP3 actually decreases slightly. This would suggest that the enhanced robustness of CMIP5 is not clearly attributable to advances in modelling, and may be a result of the fact that the CMIP5 ensemble contains different versions of the same model that are counted as independent in this measure of robustness.

A comparison of CMIP3 and CMIP5 results for extreme indices is provided in Sections 12.4.3.3 and Figure 12.13 for temperature extremes, and Section 12.4.5.5 and Figure 12.26 for extremes in the water cycle.

12.5 Climate Change Beyond 2100, Commitment, Stabilization and Irreversibility

This section discusses the long term (century to millennia) climate change based on the RCP scenario extensions and idealized scenarios, the commitment from current atmospheric composition and from past emissions, the concept of cumulative carbon and the resulting constraints on emissions for various temperature targets. The term irreversibility is used in various ways in the literature. This report defines a perturbed state as irreversible on a given time scale if the recovery time scale from this state due to natural processes is significantly longer than the time it takes for the system to reach this perturbed state (see Glossary), for example, the climate change resulting from the long residence time of a CO_2 perturbation in the atmosphere. These results are discussed in Sections 12.5.2 to 12.5.4. Aspects of irreversibility in the context of abrupt change, multiple steady states and hysteresis are discussed in Section 12.5.5 and in Chapter 13 for ice sheets and sea level rise.

12.5.1 Representative Concentration Pathway Extensions

The CMIP5 intercomparison project includes simulations extending the four RCP scenarios to the year 2300 (see Section 12.3.1). This allows exploring the longer-term climate response to idealized GHG and aerosols forcings (Meinshausen et al., 2011c). Continuing GHG emissions beyond 2100 as in the RCP8.5 extension induces a total RF above 12 W m^{-2} by 2300, while sustaining negative emissions beyond 2100, as in the RCP2.6 extension, induces a total RF below 2 W m^{-2} by 2300. The projected warming for 2281–2300, relative to 1986–2005, is 0.6°C (range 0.0°C to 1.2°C) for RCP2.6, 2.5°C (range 1.5°C to 3.5°C) for RCP4.5, and 7.8°C (range 3.0°C to 12.6°C) for RCP8.5 (*medium confidence*, based on a limited number of CMIP5 simulations) (Figures 12.3 and 12.5, Table 12.2).

EMICs simulations have been performed following the same CMIP5 protocol for the historical simulation and RCP scenarios extended to 2300 (Zickfeld et al., 2013). These scenarios have been prolonged beyond 2300 to investigate longer-term commitment and irreversibility (see below). Up to 2300, projected warming and the reduction of the AMOC as simulated by the EMICs are similar to those simulated by the CMIP5 ESMs (Figures 12.5 and 12.42).

12.5.2 Climate Change Commitment

Climate change commitment, the fact that the climate will change further after the forcing or emissions have been eliminated or held constant, has attracted increased attention by scientists and policymakers shortly before the completion of IPCC AR4 (Hansen et al., 2005a; Meehl et al., 2005b, 2006; Wigley, 2005) (see also AR4 Section 10.7.1). However, the argument that the surface response would lag the RF due to the large thermal reservoir of the ocean in fact goes back much longer (Bryan et al., 1982; Hansen et al., 1984, 1985; Siegenthaler and Oeschger, 1984; Schlesinger, 1986; Mitchell et al., 2000; Wetherald et al., 2001). The discussion in this section is framed largely in terms of temperature change, but other changes in the climate system (e.g., precipitation) are closely related to changes in temperature (see Sections 12.4.1.1 and 12.4.2). A summary of how past emissions relate to future warming is also given in FAQ 12.3.

The Earth system has multiple response time scales related to different thermal reservoirs (see also Section 12.5.3). For a step change in forcing (instantaneous increase in the magnitude of the forcing and constant forcing after that), a large fraction of the total of the surface temperature response will be realized within years to a few decades (Brasseur and Roeckner, 2005; Knutti et al., 2008a; Murphy et al., 2009; Hansen et al., 2011). The remaining response, realized over centuries, is controlled by the slow mixing of the energy perturbation into the ocean (Stouffer, 2004). The response time scale depends on the amount of ocean mixing

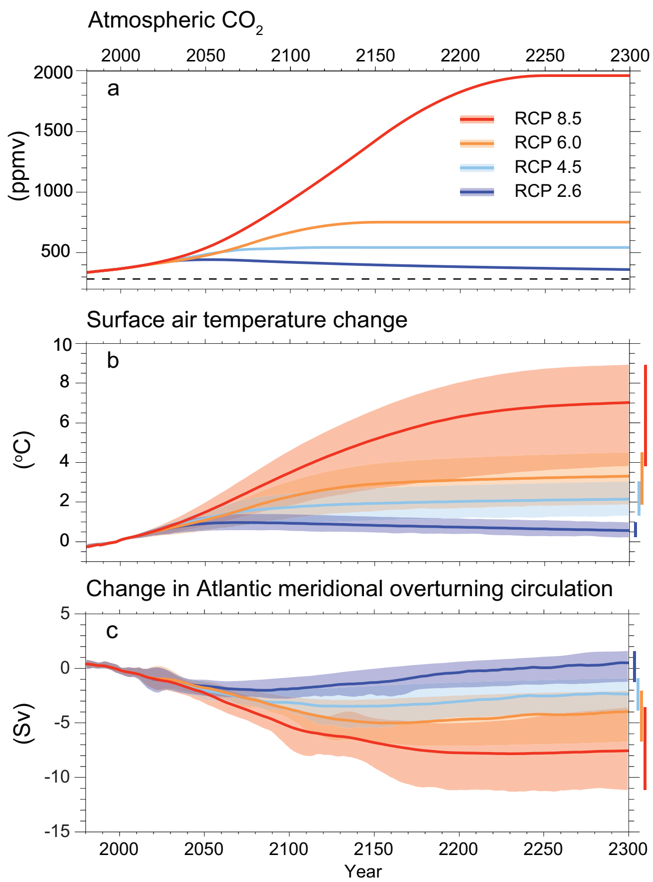

Figure 12.42 | (a) Atmospheric CO_2, (b) projected global mean surface temperature change and (c) projected change in the Atlantic meridional overturning circulation, as simulated by EMICs for the four RCPs up to 2300 (Zickfeld et al., 2013). A 10-year smoothing was applied. Shadings and bars denote the minimum to maximum range. The dashed line on (a) indicates the pre-industrial CO_2 concentration.

and the strength of climate feedbacks, and is longer for higher climate sensitivity (Hansen et al., 1985; Knutti et al., 2005). The transient climate response is therefore smaller than the equilibrium response, in particular for high climate sensitivities. This can also be interpreted as the ocean heat uptake being a negative feedback (Dufresne and Bony, 2008; Gregory and Forster, 2008). Delayed responses can also occur due to processes other than ocean warming, for example, vegetation change (Jones et al., 2009) or ice sheet melt that continues long after the forcing has been stabilized (see Section 12.5.3).

Several forms of commitment are often discussed in the literature. The most common is the 'constant composition commitment', the warming that would occur after stabilizing all radiative constituents at a given year (for example year 2000) levels. For year 2000 commitment, AOGCMs estimated a most likely value of about 0.6°C for 2100 (relative to 1980–1999, AR4 Section 10.7.1). A present-day composition commitment simulation is not part of CMIP5, so direct comparison with CMIP3 is not possible. However, the available CMIP5 results based on the RCP4.5 extension with constant RF (see Section 12.5.1) are consistent with those numbers, with an additional warming of about 0.5°C 200 years after stabilization of the forcing (Figures 12.5 and 12.42).

A measure of constant composition commitment is the fraction of realized warming which can be estimated as the ratio of the warming at a given time to the long-term equilibrium warming (e.g., Stouffer, 2004; Meehl et al., 2007b, Section 10.7.2; Eby et al., 2009; Solomon et al., 2009). EMIC simulations have been performed with RCPs forcing up to 2300 prolonged until the end of the millennium with a constant forcing set at the value reached by 2300 (Figure 12.43). When the forcing stabilizes, the fraction of realized warming is significantly below unity. However, the fraction of realized warming depends on the history of the forcing. For the RCP4.5 and RCP6.0 extension scenarios with early stabilization, it is about 75% at the time of forcing stabilization; while for RCP8.5, with stabilization occurring later, it is about 85% (see Figure 12.43); but for a 1% yr^{-1} CO_2 increase to 2 × CO_2 or 4 × CO_2 and constant forcing thereafter, the fraction of realized warming is much smaller, about 40 to 70% at the time when the forcing is kept constant. The fraction of realized warming rises typically by 10% over the century following the stabilization of forcing. Due to the long time scales in the deep ocean, full equilibrium is reached only after hundreds to thousands of years (Hansen et al., 1985; Gregory et al., 2004; Stouffer, 2004; Meehl et al., 2007b, Section 10.7.2; Knutti et al., 2008a; Danabasoglu and Gent, 2009; Held et al., 2010; Hansen et al., 2011; Li et al., 2013a).

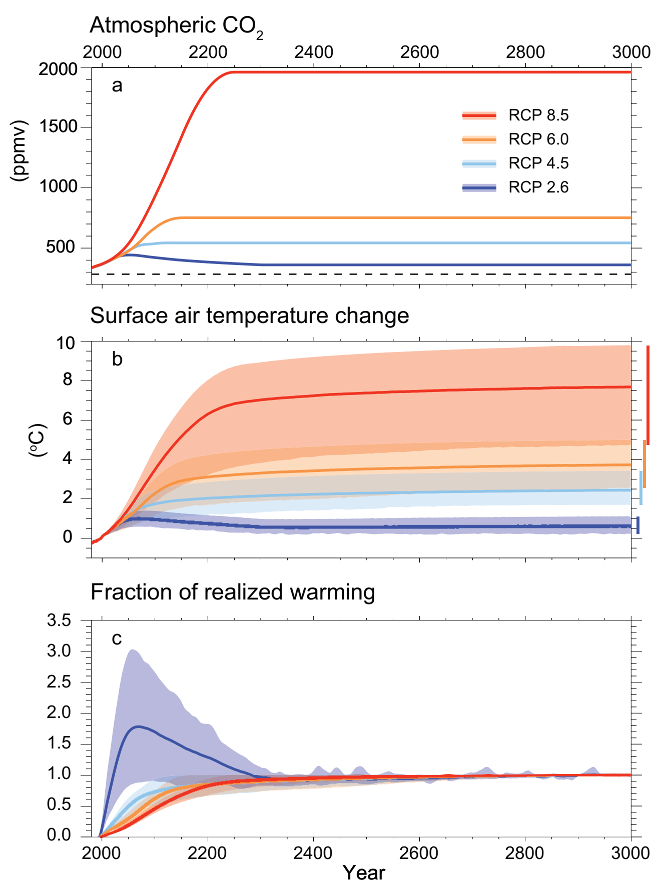

Figure 12.43 | (a) Atmospheric CO_2, (b) projected global mean surface temperature change and (c) fraction of realized warming calculated as the ratio of global temperature change at a given time to the change averaged over the 2980–2999 time period, as simulated by Earth System Models of Intermediate Complexity (EMICs) for the 4 RCPs up to 2300 followed by a constant (year 2300 level) radiative forcing up to the year 3000 (Zickfeld et al., 2013). A 10-year smoothing was applied. Shadings and bars denote the minimum to maximum range. The dashed line on (a) indicates the pre-industrial CO_2 concentration.

12

'Constant emission commitment' is the warming that would result from maintaining annual anthropogenic emissions at the current level. Few studies exist but it is estimated to be about 1°C to 2.5°C by 2100 assuming constant (year 2010) emissions in the future, based on the MAGICC model calibrated to CMIP3 and C[4]MIP models (Meinshausen et al., 2011a; Meinshausen et al., 2011b) (see FAQ 12.3). Such a scenario is different from non-intervention economic scenarios, and it does not stabilize global temperature, as any plausible emission path after 2100 would cause further warming. It is also different from a constant cumulative emission scenario which implies zero emissions in the future.

Another form of commitment involves climate change when anthropogenic emissions are set to zero ('zero emission commitment'). Results from a variety of models ranging from EMICs (Meehl et al., 2007b; Weaver et al., 2007; Matthews and Caldeira, 2008; Plattner et al., 2008; Eby et al., 2009; Solomon et al., 2009; Friedlingstein et al., 2011) to ESMs (Frölicher and Joos, 2010; Gillett et al., 2011; Gillett et al., 2013) show that abruptly setting CO_2 emissions to zero (keeping other forcings constant if accounted for) results in approximately constant global temperature for several centuries onward. Those results indicate that past emissions commit us to persistent warming for hundreds of years, continuing at about the level of warming that has been realized. On near equilibrium time scales of a few centuries to about a millennium, the temperature response to CO_2 emissions is controlled by climate sensitivity (see Box 12.2) and the cumulative airborne fraction of CO_2 over these time scales. After about a thousand years (i.e., near thermal equilibrium) and cumulative CO_2 emissions less than about 2000 PgC, approximately 20 to 30% of the cumulative anthropogenic carbon emissions still remain in the atmosphere (Montenegro et al., 2007; Plattner et al., 2008; Archer et al., 2009; Frölicher and Joos, 2010; Joos et al., 2013) (see Box 6.1) and maintain a substantial temperature response long after emissions have ceased (Friedlingstein and Solomon, 2005; Hare and Meinshausen, 2006; Weaver et al., 2007; Matthews and Caldeira, 2008; Plattner et al., 2008; Eby et al., 2009; Lowe et al., 2009; Solomon et al., 2009, 2010; Frölicher and Joos, 2010; Zickfeld et al., 2012). In the transient phase, on a 100- to 1000-year time scale, the approximately constant temperature results from a compensation between delayed commitment warming (Meehl et al., 2005b; Wigley, 2005) and the reduction in atmospheric CO_2 resulting from ocean and land carbon uptake as well as from the nonlinear dependence of RF on atmospheric CO_2 (Meehl et al., 2007b; Plattner et al., 2008; Solomon et al., 2009; Solomon et al., 2010). The commitment associated with past emissions depends, as mentioned above, on the value of climate sensitivity and cumulative CO_2 airborne fraction, but it also depends on the choices made for other RF constituents. In a CO_2 only case and for equilibrium climate sensitivities near 3°C, the warming commitment (i.e., the warming relative to the time when emissions are stopped) is near zero or slightly negative. For high climate sensitivities, and in particular if aerosol emissions are eliminated at the same time, the commitment from past emission can be significantly positive, and is a superposition of a fast response to reduced aerosols emissions and a slow response associated with high climate sensitivities (Brasseur and Roeckner, 2005; Hare and Meinshausen, 2006; Armour and Roe, 2011; Knutti and Plattner, 2012; Matthews and Zickfeld, 2012) (see FAQ 12.3). In the real world, the emissions of CO_2 and non-CO_2 forcing agents are of course coupled. All of the above studies support the conclusion that temperatures would decrease only very slowly (if at all), even for strong reductions or complete elimination of CO_2 emissions, and might even increase temporarily for an abrupt reduction of the short-lived aerosols (FAQ 12.3). The implications of this fact for climate stabilization are discussed in Section 12.5.4.

New EMIC simulations with pre-industrial CO_2 emissions and zero non-CO_2 forcings after 2300 (Zickfeld et al., 2013) confirm this behaviour (Figure 12.44) seen in many earlier studies (see above). Switching off anthropogenic CO_2 emissions in 2300 leads to a continuous slow decline of atmospheric CO_2, to a significantly slower decline of global temperature and to a continuous increase in ocean thermal expansion

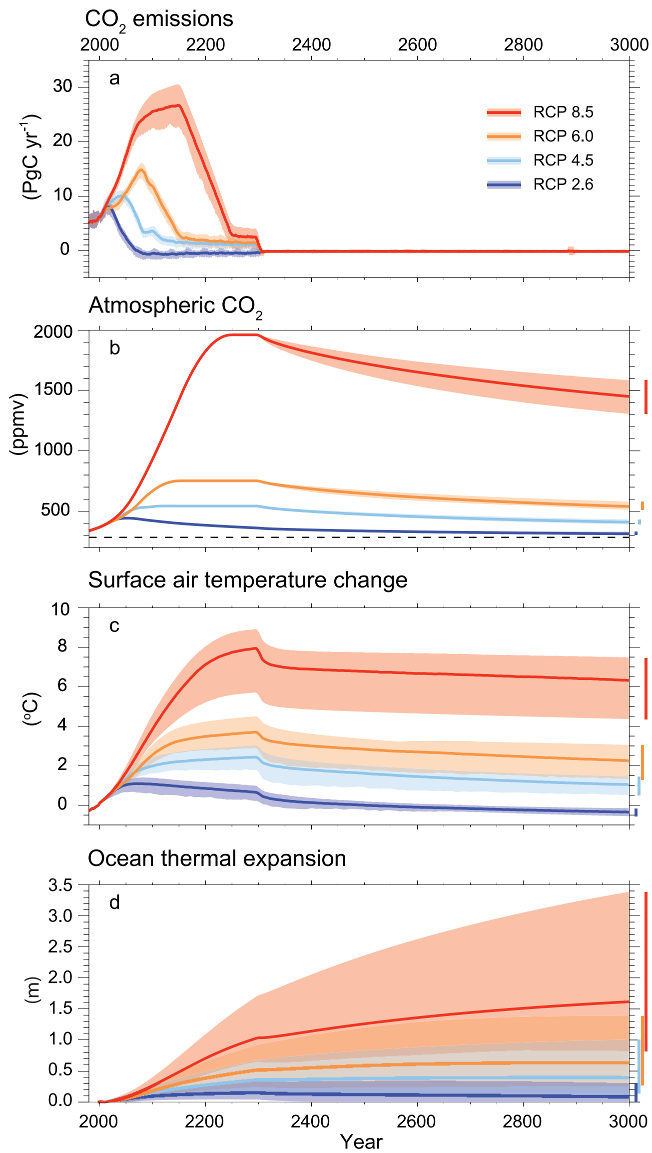

Figure 12.44 | (a) Compatible anthropogenic CO_2 emissions up to 2300, followed by zero emissions after 2300, (b) prescribed atmospheric CO_2 concentration up to 2300 followed by projected CO_2 concentration after 2300, (c) global mean surface temperature change and (d) ocean thermal expansion as simulated by Earth System Models of Intermediate Complexity (EMICs) for the four concentration driven RCPs with all forcings included (Zickfeld et al., 2013). A 10-year smoothing was applied. The drop in temperature in 2300 is a result of eliminating all non-CO_2 forcings along with CO_2 emissions. Shadings and bars denote the minimum to maximum range. The dashed line on (b) indicates the pre-industrial CO_2 concentration.

over the course of the millennium. Larger forcings induce longer delays before the Earth system would reach equilibrium. For RCP8.5, by year 3000 (700 years after emissions have ceased) global temperature has decreased only by 1°C to 2°C (relative to its peak value by 2300) and ocean thermal expansion has almost doubled (relative to 2300) and is still increasing (Zickfeld et al., 2013).

The previous paragraph discussed climate change commitment from GHGs that have already been emitted. Another form of commitment refers to climate change associated with heat and carbon that has gone into the land surface and oceans. This would be relevant to the consequences of a one-time removal of all of the excess CO_2 in the atmosphere and is computed by taking a transient simulation and instantaneously setting atmospheric CO_2 concentrations to initial (pre-industrial) values (Cao and Caldeira, 2010). In such an extreme case, there would be a net flux of CO_2 from the ocean and land surface to the atmosphere, releasing an amount of CO_2 representing about 30% of what was removed from the atmosphere, i.e., the airborne fraction applies equally to positive and negative emissions, and it depends on the emissions history. A related form of experiment investigates the consequences of an initial complete removal followed by sustained removal of any CO_2 returned to the atmosphere from the land surface and oceans, and is computed by setting atmospheric CO_2 concentrations to pre-industrial values and maintaining this concentration (Cao and Caldeira, 2010). In this case, only about one-tenth of the pre-existing temperature perturbation persists for more than half of a century. A similar study performed with a GFDL AOGCM where forcing was instantaneously returned to its pre-industrial value, found larger residual warming, up to 30% of the pre-existing warming (Held et al., 2010).

Several studies on commitment to past emissions have demonstrated that the persistence of warming is substantially longer than the lifetime of anthropogenic GHGs themselves, as a result of nonlinear absorption effects as well as the slow heat transfer into and out of the ocean. In much the same way as the warming to a step increase of forcing is delayed, the cooling after setting RF to zero is also delayed. Loss of excess heat from the ocean will lead to a positive surface air temperature anomaly for decades to centuries (Held et al., 2010; Solomon et al., 2010; Bouttes et al., 2013).

A more general form of commitment is the question of how much warming we are committed to as a result of inertia and hence commitments related to the time scales for energy system transitions and other societal, economic and technological aspects (Grubb, 1997; Washington et al., 2009; Davis et al., 2010). For example, Davis et al. (2010) estimated climate commitment of 1.3°C (range 1.1°C to 1.4°C, relative to pre-industrial) from existing CO_2-emitting devices under specific assumptions regarding their lifetimes. These forms of commitment, however, are strongly based on political, economic and social assumptions that are outside the domain of IPCC WGI and are not further considered here.

12.5.3 Forcing and Response, Time Scales of Feedbacks

Equilibrium climate sensitivity (ECS), transient climate response (TCR) and climate feedbacks are useful concepts to characterize the response of a model to an external forcing perturbation. However, there are limitations to the concept of RF (Joshi et al., 2003; Shine et al., 2003; Hansen et al., 2005b; Stuber et al., 2005), and the separation of forcings and fast (or rapid) responses (e.g., clouds changing almost instantaneously as a result of CO_2-induced heating rates rather than as a response to the slower surface warming) is sometimes difficult (Andrews and Forster, 2008; Gregory and Webb, 2008). Equilibrium warming also depends on the type of forcing (Stott et al., 2003; Hansen et al., 2005b; Davin et al., 2007). ECS is time or state dependent in some models (Senior and Mitchell, 2000; Gregory et al., 2004; Boer et al., 2005; Williams et al., 2008; Colman and McAvaney, 2009; Colman and Power, 2010), and in some but not all models climate sensitivity from a slab ocean version differs from that of coupled models or the effective climate sensitivity (see Glossary) diagnosed from a transient coupled integration (Gregory et al., 2004; Danabasoglu and Gent, 2009; Li et al., 2013a). The computational cost of coupled AOGCMs is often prohibitively large to run simulations to full equilibrium, and only a few models have performed those (Manabe and Stouffer, 1994; Voss and Mikolajewicz, 2001; Gregory et al., 2004; Danabasoglu and Gent, 2009; Li et al., 2013a). Because of the time dependence of effective climate sensitivity, fitting simple models to AOGCMs over the first few centuries may lead to errors when inferring the response on multi-century time scales. In the HadCM3 case the long-term warming would be underestimated by 30% if extrapolated from the first century (Gregory et al., 2004), in other models the warming of the slab and coupled model is almost identical (Danabasoglu and Gent, 2009). The assumption that the response to different forcings is approximately additive appears to be justified for large-scale temperature changes but limited for other climate variables (Boer and Yu, 2003; Sexton et al., 2003; Gillett et al., 2004; Meehl et al., 2004; Jones et al., 2007). A more complete discussion of the concept of ECS and the limitations is given in Knutti and Hegerl (2008). The CMIP5 model estimates of ECS and TCR are also discussed in Section 9.7. Despite all limitations, the ECS and TCR remain key concepts to characterize the transient and near equilibrium warming as a response to RF on time scales of centuries. Their overall assessment is given in Box 12.2.

A number of recent studies suggest that equilibrium climate sensitivities determined from AOGCMs and recent warming trends may significantly underestimate the true Earth system sensitivity (see Glossary) which is realized when equilibration is reached on millennial time scales (Hansen et al., 2008; Rohling et al., 2009; Lunt et al., 2010; Pagani et al., 2010; Rohling and Members, 2012). The argument is that slow feedbacks associated with vegetation changes and ice sheets have their own intrinsic long time scales and are not represented in most models (Jones et al., 2009). Additional feedbacks are mostly thought to be positive but negative feedbacks of smaller magnitude are also simulated (Swingedouw et al., 2008; Goelzer et al., 2011). The climate sensitivity of a model may therefore not reflect the sensitivity of the full Earth system because those feedback processes are not considered (see also Sections 10.8, 5.3.1 and 5.3.3.2; Box 5.1). Feedbacks determined in very different base state (e.g., the Last Glacial Maximum) differ from those in the current warm period (Rohling and Members, 2012), and relationships between observables and climate sensitivity are model dependent (Crucifix, 2006; Schneider von Deimling et al., 2006; Edwards et al., 2007; Hargreaves et al., 2007, 2012). Estimates of climate sensitivity based on paleoclimate archives (Hansen

Frequently Asked Questions

FAQ 12.3 | What Would Happen to Future Climate if We Stopped Emissions Today?

Stopping emissions today is a scenario that is not plausible, but it is one of several idealized cases that provide insight into the response of the climate system and carbon cycle. As a result of the multiple time scales in the climate system, the relation between change in emissions and climate response is quite complex, with some changes still occurring long after emissions ceased. Models and process understanding show that as a result of the large ocean inertia and the long lifetime of many greenhouse gases, primarily carbon dioxide, much of the warming would persist for centuries after greenhouse gas emissions have stopped.

When emitted in the atmosphere, greenhouse gases get removed through chemical reactions with other reactive components or, in the case of carbon dioxide (CO_2), get exchanged with the ocean and the land. These processes characterize the lifetime of the gas in the atmosphere, defined as the time it takes for a concentration pulse to decrease by a factor of e (2.71). How long greenhouse gases and aerosols persist in the atmosphere varies over a wide range, from days to thousands of years. For example, aerosols have a lifetime of weeks, methane (CH_4) of about 10 years, nitrous oxide (N_2O) of about 100 years and hexafluoroethane (C_2F_6) of about 10,000 years. CO_2 is more complicated as it is removed from the atmosphere through multiple physical and biogeochemical processes in the ocean and the land; all operating at different time scales. For an emission pulse of about 1000 PgC, about half is removed within a few decades, but the remaining fraction stays in the atmosphere for much longer. About 15 to 40% of the CO_2 pulse is still in the atmosphere after 1000 years.

As a result of the significant lifetimes of major anthropogenic greenhouse gases, the increased atmospheric concentration due to past emissions will persist long after emissions are ceased. Concentration of greenhouse gases would not return immediately to their pre-industrial levels if emissions were halted. Methane concentration would return to values close to pre-industrial level in about 50 years, N_2O concentrations would need several centuries, while CO_2 would essentially never come back to its pre-industrial level on time scales relevant for our society. Changes in emissions of short-lived species like aerosols on the other hand would result in nearly instantaneous changes in their concentrations.

The climate system response to the greenhouse gases and aerosols forcing is characterized by an inertia, driven mainly by the ocean. The ocean has a very large capacity of absorbing heat and a slow mixing between the surface and the deep ocean. This means that it will take several centuries for the whole ocean to warm up and to reach equilibrium with the altered radiative forcing. The surface ocean (and hence the continents) will continue to warm until it reaches a surface temperature in equilibrium with this new radiative forcing. The AR4 showed that if concentration of greenhouse gases were held constant at present day level, the Earth surface would still continue to warm by about 0.6°C over the 21st century relative to the year 2000. This is the climate commitment to current concentrations (or constant composition commitment), shown in grey in FAQ 12.3, Figure 1. Constant emissions at current levels would further increase the atmospheric concentration and result in much more warming than observed so far (FAQ 12.3, Figure 1, red lines).

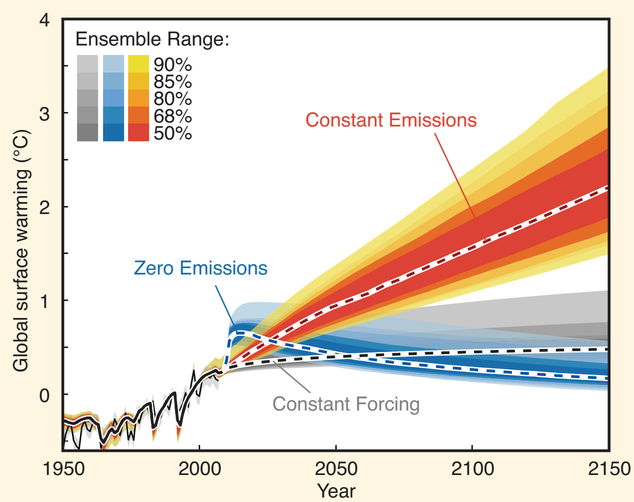

FAQ 12.3, Figure 1 | Projections based on the energy balance carbon cycle model Model for the Assessment of Greenhouse Gas-Induced Climate Change (MAGICC) for constant atmospheric composition (constant forcing, grey), constant emissions (red) and zero future emissions (blue) starting in 2010, with estimates of uncertainty. Figure adapted from Hare and Meinshausen (2006) based on the calibration of a simple carbon cycle climate model to all Coupled Model Intercomparison Project Phase 3 (CMIP3) and Coupled Climate Carbon Cycle Model Intercomparison Project (C4MIP) models (Meinshausen et al., 2011a; Meinshausen et al., 2011b). Results are based on a full transient simulation starting from pre-industrial and using all radiative forcing components. The thin black line and shading denote the observed warming and uncertainty.

Even if anthropogenic greenhouses gas emissions were halted now, the radiative forcing due to these long-lived greenhouse gases concentrations would only slowly decrease in the future, at a rate determined by the lifetime of the gas (see above). Moreover, the

(continued on next page)

FAQ 12.3 (continued)

climate response of the Earth System to that radiative forcing would be even slower. Global temperature would not respond quickly to the greenhouse gas concentration changes. Eliminating CO_2 emissions only would lead to near constant temperature for many centuries. Eliminating short-lived negative forcings from sulphate aerosols at the same time (e.g., by air pollution reduction measures) would cause a temporary warming of a few tenths of a degree, as shown in blue in FAQ 12.3, Figure 1. Setting all emissions to zero would therefore, after a short warming, lead to a near stabilization of the climate for multiple centuries. This is called the commitment from past emissions (or zero future emission commitment). The concentration of GHG would decrease and hence the radiative forcing as well, but the inertia of the climate system would delay the temperature response.

As a consequence of the large inertia in the climate and carbon cycle, the long-term global temperature is largely controlled by total CO_2 emissions that have accumulated over time, irrespective of the time when they were emitted. Limiting global warming below a given level (e.g., 2°C above pre-industrial) therefore implies a given budget of CO_2, that is, higher emissions earlier implies stronger reductions later. A higher climate target allows for a higher CO_2 concentration peak, and hence larger cumulative CO_2 emissions (e.g., permitting a delay in the necessary emission reduction).

Global temperature is a useful aggregate number to describe the magnitude of climate change, but not all changes will scale linearly global temperature. Changes in the water cycle for example also depend on the type of forcing (e.g., greenhouse gases, aerosols, land use change), slower components of the Earth system such as sea level rise and ice sheet would take much longer to respond, and there may be critical thresholds or abrupt or irreversible changes in the climate system.

et al., 2008; Rohling et al., 2009; Lunt et al., 2010; Pagani et al., 2010; Schmittner et al., 2011; Rohling and Members, 2012), most but not all based on climate states colder than present, are therefore not necessarily representative for an estimate of climate sensitivity today (see also Sections 5.3.1, 5.3.3.2, Box 5.1). Also it is uncertain on which time scale some of those Earth system feedbacks would become significant.

Equilibrium climate sensitivity undoubtedly remains a key quantity, useful to relate a change in GHGs or other forcings to a global temperature change. But the above caveats imply that estimates based on past climate states very different from today, estimates based on time scales different than those relevant for climate stabilization (e.g., estimates based on climate response to volcanic eruptions), or based on forcings other than GHGs (e.g., spatially non-uniform land cover changes, volcanic eruptions or solar forcing) may differ from the climate sensitivity measuring the climate feedbacks of the Earth system today, and this measure, in turn, may be slightly different from the sensitivity of the Earth in a much warmer state on time scales of millennia. The TCR and the transient climate response to cumulative carbon emissions (TCRE) are often more directly relevant to evaluate short term changes and emission reductions needed for stabilization (see Section 12.5.4).

12.5.4 Climate Stabilization and Long-term Climate Targets

This section discusses the relation between emissions and climate targets, in the context of the uncertainties characterizing both the transient and the equilibrium climate responses to emissions. 'Climate targets' considered here are both stabilizing temperature at a specified value and avoiding a warming beyond a predefined threshold. The latter idea of limiting peak warming is a more general concept than stabilization of temperature or atmospheric CO_2, and one that is more realistic than an exact climate stabilization which would require perpetual non-zero positive emissions to counteract the otherwise unavoidable long-term slow decrease in global temperature (Matsuno et al., 2012a) (Figure 12.44).

12.5.4.1 Background

The concept of stabilization is strongly linked to the ultimate objective of the UNFCCC, which is 'to achieve […] stabilization of greenhouse gas concentrations in the atmosphere at a level that would prevent dangerous anthropogenic interference with the climate system'. Recent policy discussions focussed on a global temperature increase, rather than on GHG concentrations. The most prominent target currently discussed is the 2°C temperature target, that is, to limit global temperature increase relative to pre-industrial times to below 2°C. The 2°C target has been used first by the European Union as a policy target in 1996 but can be traced further back (Jaeger and Jaeger, 2010; Randalls, 2010). Climate impacts however are geographically diverse (Joshi et al., 2011) and sector specific, and no objective threshold defines when dangerous interference is reached. Some changes may be delayed or irreversible, and some impacts are likely to be beneficial. It is thus not possible to define a single critical threshold without value judgments and without assumptions on how to aggregate current and future costs and benefits. Targets other than 2°C have been proposed (e.g., 1.5°C global warming relative to pre-industrial), or targets based on CO_2 concentration levels, for example, 350 ppm (Hansen et al., 2008). The rate of change may also be important (e.g., for adaptation). This section does not advocate or defend any threshold, nor does it judge the economic or political feasibility of such goals, but simply assesses the implications of different illustrative climate targets on allowed carbon emissions, based on our current understanding of climate and carbon cycle feedbacks.

12.5.4.2 Constraints on Cumulative Carbon Emissions

The current RF from GHGs maintained indefinitely (i.e., the commitment from constant greenhouse gas concentrations) would correspond to approximately 2°C warming. That, however, does not imply that the commitment from past emissions has already exceeded 2°C. Part of the positive RF from GHGs is currently compensated by negative aerosol forcing, and stopping GHG emissions would lead to a decrease in the GHG forcing. Actively removing CO_2 from the atmosphere, for example by the combined use of biomass energy and carbon capture and storage, would further accelerate the decrease in GHG forcing.

The total amount of anthropogenic CO_2 released in the atmosphere (often termed cumulative carbon emission) is a good indicator of the atmospheric CO_2 concentration and hence of the global warming response to CO_2. The ratio of global temperature change to total cumulative anthropogenic CO_2 emissions (TCRE) is relatively constant over time and independent of the scenario, but is model dependent as it depends on the model cumulative airborne fraction of CO_2 and ECS/TCR (Matthews and Caldeira, 2008; Allen et al., 2009; Gregory et al., 2009; Matthews et al., 2009; Meinshausen et al., 2009; Zickfeld et al., 2009; Bowerman et al., 2011; Knutti and Plattner, 2012; Zickfeld et al., 2012, 2013). This is consistent with an earlier study indicating that the global warming potential of CO_2 is approximately independent of the scenario (Caldeira and Kasting, 1993). The concept of a constant ratio of cumulative emissions of CO_2 to temperature holds well only until temperatures peak (see Figure 12.45e) and only for smoothly varying cumulative CO_2 emissions (Gillett et al., 2013). It does not hold for stabilization on millennial time scales or for non-CO_2 forcings, and there is limited evidence for its applicability for cumulative emissions exceeding 2000 PgC owing to limited simulations available (Plattner et al., 2008; Hajima et al., 2012; Matsuno et al., 2012b; Gillett et al., 2013; Zickfeld et al., 2013). For non-CO_2 forcings with shorter atmospheric life times than CO_2 the rate of emissions at the time of peak warming is more important than the cumulative emissions over time (Smith et al., 2012).

Assuming constant climate sensitivity and fixed carbon cycle feedbacks, long-term (several centuries to millennium) stabilization of global temperatures requires eventually the stabilization of atmospheric concentrations (or decreasing concentrations if the temperature should be stabilized more quickly). This requires decreasing emissions to near-zero (Jones et al., 2006; Meehl et al., 2007b; Weaver et al., 2007; Matthews and Caldeira, 2008; Plattner et al., 2008; Allen et al., 2009; Matthews et al., 2009; Meinshausen et al., 2009; Zickfeld et al., 2009; Friedlingstein et al., 2011; Gillett et al., 2011; Roeckner et al., 2011; Knutti and Plattner, 2012; Matsuno et al., 2012a).

The relationships between cumulative emissions and temperature for various studies are shown in Figure 12.45. Note that some lines mark the evolution of temperature as a function of emissions over time while other panels show peak temperatures for different simulations. Also some models prescribe only CO_2 emissions while others use multi gas scenarios, and the time horizons differ. The warming is usually larger if non-CO_2 forcings are considered, since the net effect of the non-CO_2 forcings is positive in most scenarios (Hajima et al., 2012). Not all numbers are therefore directly comparable. Matthews et al. (2009) estimated the TCRE as 1°C to 2.1°C per 1000 PgC (TtC, or 10^{12} metric tonnes of carbon) (5 to 95%) based on the C^{4}MIP model range (Figure 12.45a). The ENSEMBLES E1 show a range of 1°C to 4°C per 1000 PgC (scaled from 0.5°C to 2°C for 500 PgC, Figure 12.45d) (Johns et al., 2011). Rogelj et al. (2012) estimate a 5 to 95% range of about 1°C to 2°C per 1000 PgC (Figure 12.45e) based on the MAGICC model calibrated to the C^{4}MIP model range and the *likely* range of 2°C to 4.5°C for climate sensitivity given in AR4. Allen et al. (2009) used a simple model and found 1.3°C to 3.9°C per 1000 PgC (5 to 95%) for peak warming (Figure 12.45g) and 1.4°C to 2.5°C for TCRE. The EMICs TCRE simulations suggest a range of about 1.4°C to 2.5°C per 1000 PgC and a mean of 1.9°C per 1000 PgC (Zickfeld et al., 2013) (Figure 12.45h). The results of Meinshausen et al. (2009) confirm the approximate linearity between temperature and CO_2 emissions (Figure 12.45b). Their results are difficult to compare owing to the shorter time period considered, but the model was found to be consistent with that of Allen et al. (2009). Zickfeld et al. (2009), using an EMIC, find a best estimate of about 1.5°C per 1000 PgC. Gillett et al. (2013) find a range of 0.8°C to 2.4°C per 1000 PgC in 15 CMIP5 models and derive an observationally constrained range of 0.7°C to 2.0°C per 1000 PgC. Results from much earlier model studies support the near linear relationship of cumulative emissions and global temperature, even though these studies did not discuss the linear relationship. An example is given in Figure 12.45c based on data shown in IPCC TAR Figure 13.3 (IPCC, 2001) and IPCC AR4 Figure 10.35 (Meehl et al., 2007b). The relationships between cumulative CO_2 emissions and temperature in CMIP5 are shown in Figure 12.45f for the 1% yr^{-1} CO_2 increase scenarios and in Figure 12.45i for the RCP8.5 emission driven ESM simulations (Gillett et al., 2013). Compatible emissions from concentration driven CMIP5 ESMs are discussed in Section 6.4.3.3.

Expert judgement based on the available evidence therefore suggests that the TCRE is *likely* between 0.8°C to 2.5°C per 1000 PgC, for cumulative CO_2 emissions less than about 2000 PgC until the time at which temperature peaks. Under these conditions, and for low to medium estimates of climate sensitivity, the TCRE is nearly identical to the peak climate response to cumulative carbon emissions. For high climate sensitivity, strong carbon cycle climate feedbacks or large cumulative emissions, the peak warming can be delayed and the peak response may be different from TCRE, but is often poorly constrained by models and observations. The range of TCRE assessed here is consistent with other recent attempts to synthesize the available evidence (NRC, 2011; Matthews et al., 2012). The results by Schwartz et al. (2010, 2012) imply a much larger warming for the carbon emitted over the historical period and have been questioned by Knutti and Plattner (2012) for neglecting the relevant response time scales and combining a transient airborne fraction with an equilibrium climate sensitivity.

The TCRE can be compared to the temperature response to emissions on a time scale of about 1000 years after emissions cease. This can be estimated from the *likely* range of equilibrium climate sensitivity (1.5°C to 4.5°C) and a cumulative CO_2 airborne fraction after about

1000 years of about 25 ± 5% (Archer et al., 2009; Joos et al., 2013). Again combining the extreme values would suggest a range of 0.6°C to 2.7°C per 1000 PgC, and 1.5°C per 1000 PgC for an ECS of 3°C and a cumulative airborne fraction of 25%. However, this equilibrium estimate is based on feedbacks estimated for the present day climate. Climate and carbon cycle feedbacks may increase substantially on long time scales and for high cumulative CO_2 emissions (see Section 12.5.3), introducing large uncertainties in particular on the upper bound. Based on paleoclimate data and an analytical model, Goodwin et al. (2009) estimate a long term RF of 1.5 W m^{-2} for an emission of 1000 PgC. For an equilibrium climate sensitivity of 3°C this corresponds to a warming of 1.2°C on millennial time scales, consistent with the climate carbon cycle models results discussed above.

The uncertainty in TCRE is caused by the uncertainty in the physical feedbacks and ocean heat uptake (reflected in TCR) and uncertainties in carbon cycle feedbacks (affecting the cumulative airborne fraction of CO_2). TCRE only characterizes the warming due to CO_2 emissions, and contributions from non-CO_2 gases need to be considered separately when estimating likelihoods to stay below a temperature limit. Warming as a function of cumulative CO_2 emissions is similar in the four RCP scenarios, and larger than that due to CO_2 alone, since non-CO_2 forcings contribute warming in these scenarios (compare Figure 12.45 f, i) (Hajima et al., 2012).

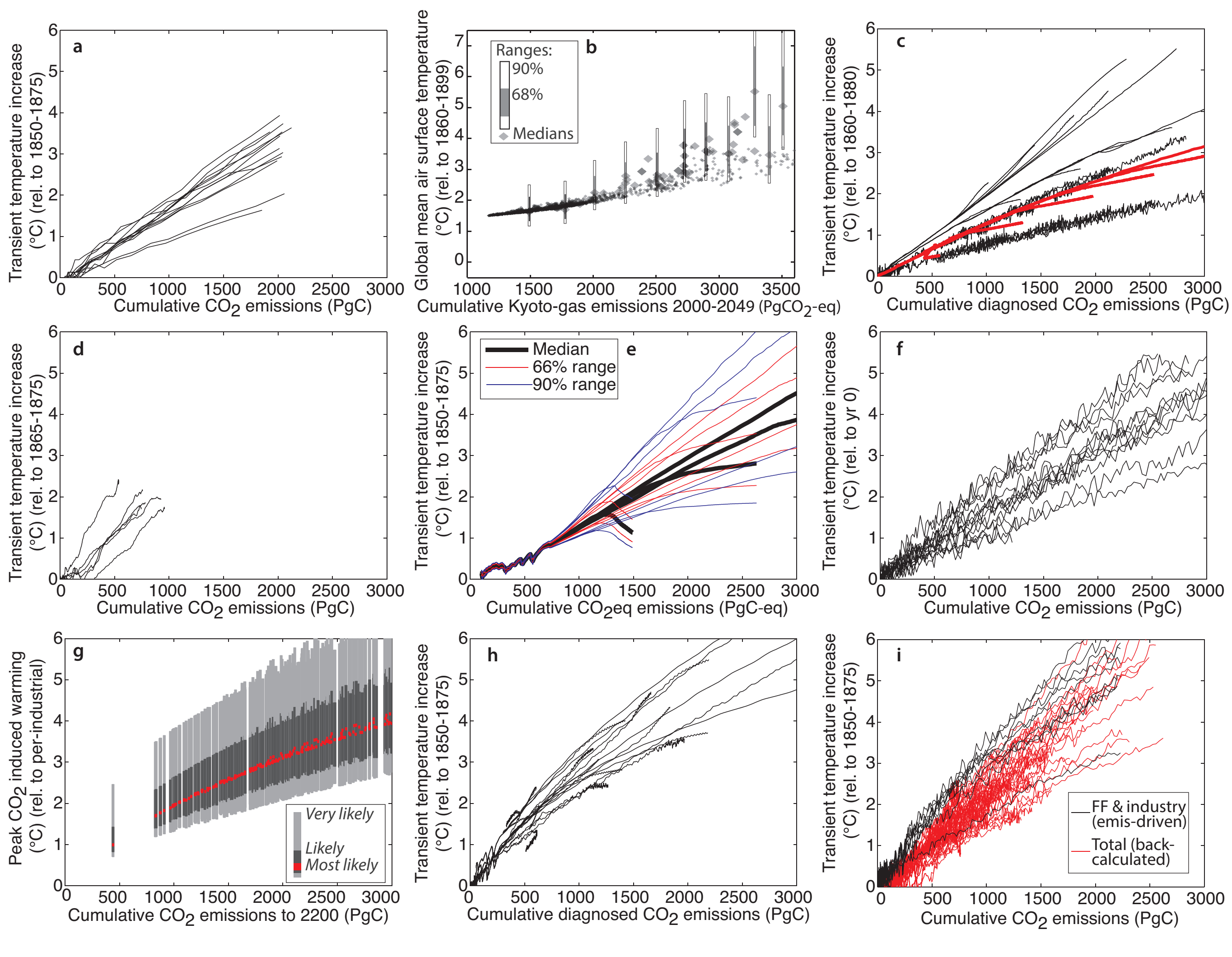

Figure 12.45 | Global temperature change vs. cumulative carbon emissions for different scenarios and models. (a) Transient global temperature increase vs. cumulative CO_2 emissions for Coupled Climate Carbon Cycle Model Intercomparison Project (C^4MIP) (Matthews et al., 2009). (b) Maximum temperature increase until 2100 vs. cumulative Kyoto-gas emissions (CO_2 equivalent; note that all other panels are given in C equivalent) (Meinshausen et al., 2009). (c) Transient temperature increase vs. cumulative CO_2 emissions for IPCC TAR models (red, IPCC TAR Figure 13.3) and IPCC AR4 Earth System Models of Intermediate Complexity (EMICs, black: IPCC AR4 Figure 10.35). (d) As in (a) but for the ENSEMBLES E1 scenario (Johns et al., 2011). (e) Transient temperature increase for the RCP scenarios based on the Model for the Assessment of Greenhouse Gas-Induced Climate Change (MAGICC) model constrained to C^4MIP, observed warming, and the IPCC AR4 climate sensitivity range (Rogelj et al., 2012). (f) Transient temperature change from the CMIP5 1% yr^{-1} concentration driven simulations. (g) Peak CO_2 induced warming vs. cumulative CO_2 emissions to 2200 (Allen et al., 2009; Bowerman et al., 2011). (h) Transient temperature increase from the new EMIC RCP simulations (Zickfeld et al., 2013). (i) Transient temperature change from the CMIP5 historical and RCP8.5 emission driven simulations (black) and transient temperature change in all concentration-driven CMIP5 RCP simulations with back-calculated emissions (red). Note that black lines in panel (i) do not include land use CO_2 and that warming in (i) is higher than in (f) due to additional non-CO_2 forcings.

Box 12.2 | Equilibrium Climate Sensitivity and Transient Climate Response

Equilibrium climate sensitivity (ECS) and transient climate response (TCR) are useful metrics summarizing the global climate system's temperature response to an externally imposed radiative forcing (RF). ECS is defined as the equilibrium change in annual mean global surface temperature following a doubling of the atmospheric CO_2 concentration (see Glossary), while TCR is defined as the annual mean global surface temperature change at the time of CO_2 doubling following a linear increase in CO_2 forcing over a period of 70 years (see Glossary). Both metrics have a broader application than these definitions imply: ECS determines the eventual warming in response to stabilization of atmospheric composition on multi-century time scales, while TCR determines the warming expected at a given time following any steady increase in forcing over a 50- to 100-year time scale.

ECS and TCR can be estimated from various lines of evidence. The estimates can be based on the values of ECS and TCR diagnosed from climate models (Section 9.7.1; Table 9.5), or they can be constrained by analysis of feedbacks in climate models (see Section 9.7.2), patterns of mean climate and variability in models compared to observations (Section 9.7.3.3), temperature fluctuations as reconstructed from paleoclimate archives (Sections 5.3.1 and 5.3.3.2; Box 5.1), observed and modelled short-term perturbations of the energy balance like those caused by volcanic eruptions (Section 10.8), and the observed surface and ocean temperature trends since pre-industrial (see Sections 10.8.1 and 10.8.2; Figure 10.20). For many applications, the limitations of the forcing-feedback analysis framework and the dependence of feedbacks on time scales and the climate state (see Section 12.5.3) must be kept in mind. Some studies estimate the TCR as the ratio of global mean temperature change to RF (Section 10.8.2.2) (Gregory and Forster, 2008; Padilla et al., 2011; Schwartz, 2012). Those estimates are scaled by the RF of 2 × CO_2 (3.7 W m^{-2}; Myhre et al., 1998) to be comparable to TCR in the following discussion.

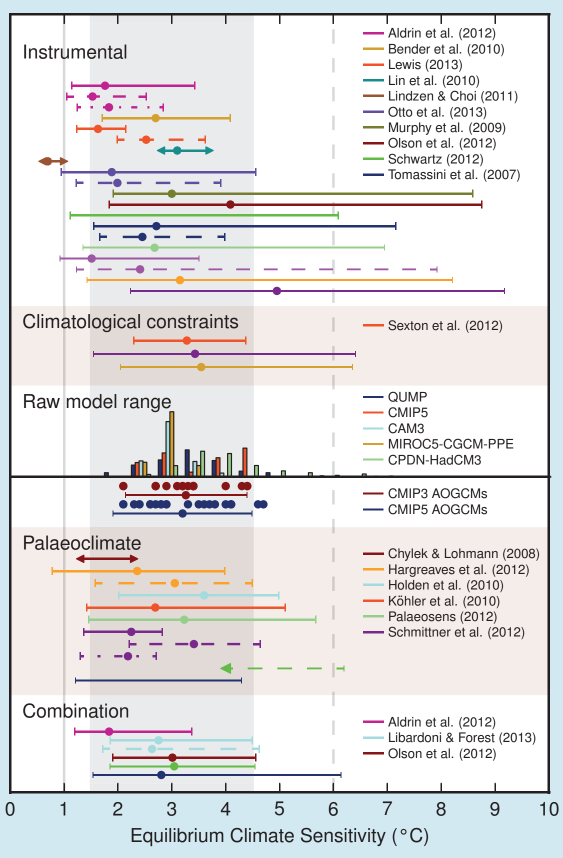

Box 12.2, Figure 1 | Probability density functions, distributions and ranges for equilibrium climate sensitivity, based on Figure 10.20b plus climatological constraints shown in IPCC AR4 (Meehl et al., 2007b; Box 10.2, Figure 1), and results from CMIP5 (Table 9.5). The grey shaded range marks the *likely* 1.5°C to 4.5°C range, and the grey solid line the *extremely unlikely* less than 1°C, the grey dashed line the *very unlikely* greater than 6°C. See Figure 10.20b and Chapter 10 Supplementary Material for full caption and details. Labels refer to studies since AR4. Full references are given in Section 10.8.

Newer studies of constraints based on the observed warming since pre-industrial, analysed using simple and intermediate complexity models, improved statistical methods, and several different and newer data sets, are assessed in detail in Section 10.8.2. Together with results from feedback analysis and paleoclimate constraints (Sections 5.3.1 and 5.3.3.2; Box 5.1), but without considering the CMIP based evidence, these studies show ECS is *likely* between 1.5°C to 4.5°C (*medium confidence*) and *extremely unlikely* less than 1.0°C (see Section 10.8.2). A few studies argued for very low values of climate sensitivity, but many of them have received criticism in the literature (see Section 10.8.2). Estimates based on AOGCMs and feedback analysis indicate a range of 2°C to 4.5°C, with the CMIP5 model mean at 3.2°C, similar to CMIP3. A summary of published ranges and PDFs of ECS is given in Box 12.2, Figure 1. Distributions and ranges for the TCR are shown in Box 12.2, Figure 2.

Simultaneously imposing different constraints from the observed warming trends, volcanic eruptions, model climatology, and paleoclimate, for example, by using a distribution obtained from the Last Glacial Maximum as a prior for the 20th century analysis, yields a more narrow range for climate sensitivity (see Figure 10.20; Section 10.8.2.5) (e.g., Annan and Hargreaves, 2006, 2011b; Hegerl et al., 2006; Aldrin et al., 2012). However, such methods are sensitive to assumptions of independence of the various lines of evidence, which might have shared biases (Lemoine, 2010), and the assumption that each individual line of evidence is unbiased and its uncertainties are captured completely. Expert elicitations for PDFs of climate sensitivity exist (Morgan and Keith, 1995; Zickfeld et al., 2010), but have also received some criticism (Millner et al., 2013). They are not used formally here because the experts base their opinion on the same studies as we assess. The peer-reviewed literature provides no consensus on a

(continued on next page)

Box 12.2 (continued)

formal statistical method to combine different lines of evidence. All methods in general are sensitive to the assumed prior distributions. These limitations are discussed in detail in Section 10.8.2.

Based on the combined evidence from observed climate change including the observed 20th century warming, climate models, feedback analysis and paleoclimate, ECS is *likely* in the range 1.5°C to 4.5°C with *high confidence*. The combined evidence increases the confidence in this final assessment compared to that based on the observed warming and paleoclimate only. ECS is positive, *extremely unlikely* less than 1°C (*high confidence*), and *very unlikely* greater than 6°C (*medium confidence*). The upper limit of the *likely* range is unchanged compared to AR4. The lower limit of the *likely* range of 1.5°C is less than the lower limit of 2°C in AR4. This change reflects the evidence from new studies of observed temperature change, using the extended records in atmosphere and ocean. These studies suggest a best fit to the observed surface and ocean warming for ECS values in the lower part of the *likely* range. Note that these studies are not purely observational, because they require an estimate of the response to RF from models. In addition, the uncertainty in ocean heat uptake remains substantial (see Section 3.2, Box 13.1). Accounting for short term variability in simple models remains challenging, and it is important not to give undue weight to any short time period that might be strongly affected by internal variability (see Box 9.2). On the other hand, AOGCMs show very good agreement with observed climatology with ECS values in the upper part of the 1.5°C to 4.5°C range (Section 9.7.3.3), but the simulation of key feedbacks like clouds remains challenging in those models. The estimates from the observed warming, paleoclimate, and from climate models are consistent within their uncertainties, each is supported by many studies and multiple data sets, and in combination they provide *high confidence* for the assessed *likely* range. Even though this assessed range is similar to previous reports (Charney, 1979; IPCC, 2001), confidence today is much higher as a result of high quality and longer observational records with a clearer anthropogenic signal, better process understanding, more and better understood evidence from paleoclimate reconstructions, and better climate models with higher resolution that capture many more processes more realistically. Box 12.2 Figure 1 illustrates that all these lines of evidence individually support the assessed *likely* range of 1.5°C to 4.5°C.

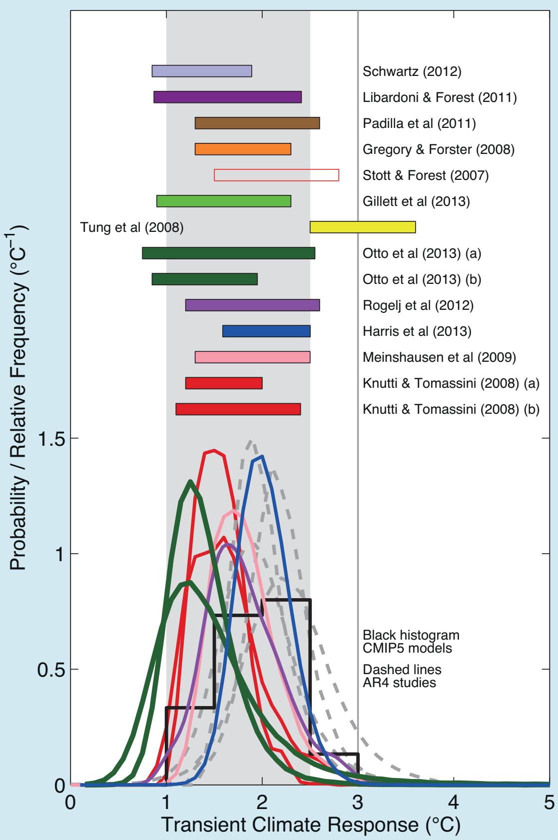

Box 12.2, Figure 2 | Probability density functions, distributions and ranges (5 to 95%) for the transient climate response from different studies, based on Figure 10.20a, and results from CMIP5 (black histogram; Table 9.5). The grey shaded range marks the *likely* 1°C to 2.5°C range, and the grey solid line marks the *extremely unlikely* greater than 3°C. See Figure 10.20a and Chapter 10 Supplementary Material for full caption and details. Full references are given in Section 10.8.

The tails of the ECS distribution are now better understood. Multiple lines of evidence provide *high confidence* that an ECS value less than 1°C is *extremely unlikely*. The assessment that ECS is *very unlikely* greater than 6°C is an expert judgment informed by several lines of evidence. First, the comprehensive climate models used in the CMIP5 exercise produce an ECS range of 2.1°C to 4.7°C (Table 9.5), very similar to CMIP3. Second, comparisons of perturbed-physics ensembles against the observed climate find that models with ECS values in the range 3°C to 4°C show the smallest errors for many fields (Section 9.7.3.3). Third, there is increasing evidence that the aerosol RF of the 20th century is not strongly negative, which makes it unlikely that the observed warming was caused by a very large ECS in response to a very small net forcing. Fourth, multiple and at least partly independent observational constraints from the satellite period, instrumental period and palaeoclimate studies continue to yield very low probabilities for ECS larger than 6°C, particularly when including most recent ocean and atmospheric data (see Box 12.2, Figure 1).

Analyses of observations and simulations of the instrumental period are estimating the effective climate sensitivity (a measure of the strengths of the climate feedbacks today, see Glossary), rather than ECS directly. In some climate models ECS tends to be higher than the effective climate sensitivity (see Section 12.5.3), because the feedbacks that are represented in the models (water vapour, lapse

(continued on next page)

12

Box 12.2 (continued)

rate, albedo and clouds) vary with the climate state. On time scales of many centuries, additional feedbacks with their own intrinsic time scales (e.g., vegetation, ice sheets; see Sections 5.3.3 and 12.5.3) (Jones et al., 2009; Goelzer et al., 2011) may become important but are not usually modelled. The resulting Earth system sensitivity is less well constrained but likely to be larger than ECS (Hansen et al., 2008; Rohling et al., 2009; Lunt et al., 2010; Pagani et al., 2010; Rohling and Members, 2012), implying that lower atmospheric CO_2 concentrations are needed to meet a given temperature target on multi-century time scales. A number of caveats, however, apply to those studies (see Section 12.5.3). Those long-term feedbacks have their own intrinsic time scales, and are less likely to be proportional to global mean temperature change.

For scenarios of increasing RF, TCR is a more informative indicator of future climate than ECS (Frame et al., 2005; Held et al., 2010). This assessment concludes with *high confidence* that the TCR is *likely* in the range 1°C to 2.5°C, close to the estimated 5 to 95% range of CMIP5 (1.2°C to 2.4°C; see Table 9.5), is positive and *extremely unlikely* greater than 3°C. As with the ECS, this is an expert-assessed range, supported by several different and partly independent lines of evidence, each based on multiple studies, models and data sets. TCR is estimated from the observed global changes in surface temperature, ocean heat uptake and RF, the detection/attribution studies identifying the response patterns to increasing GHG concentrations (Section 10.8.1), and the results of CMIP3 and CMIP5 (Section 9.7.1). Estimating TCR suffers from fewer difficulties in terms of state- or time-dependent feedbacks (see Section 12.5.3), and is less affected by uncertainty as to how much energy is taken up by the ocean. Unlike ECS, the ranges of TCR estimated from the observed warming and from AOGCMs agree well, increasing our confidence in the assessment of uncertainties in projections over the 21st century.

Another useful metric relating directly CO_2 emissions to temperature is the transient climate response to cumulative carbon emission (TCRE) (see Sections 12.5.4 and 10.8.4). This metric is useful to determine the allowed cumulative carbon emissions for stabilization at a specific global temperature. TCRE is defined as the annual mean global surface temperature change per unit of cumulated CO_2 emissions, usually 1000 PgC, in a scenario with continuing emissions (see Glossary). It considers physical and carbon cycle feedbacks and uncertainties, but not additional feedbacks associated for example with the release of methane hydrates or large amounts of carbon from permafrost. The assessment based on climate models as well as the observed warming suggests that the TCRE is *likely* between 0.8°C to 2.5°C per 1000 PgC (10^{12} metric tons of carbon), for cumulative CO_2 emissions less than about 2000 PgC until the time at which temperatures peak. Under these conditions, and for low to medium estimates of climate sensitivity, the TCRE gives an accurate estimate of the peak global mean temperature response to cumulated carbon emissions. TCRE has the advantage of directly relating global mean surface temperature change to CO_2 emissions, but as a result of combining the uncertainty in both TCR and the carbon cycle response, it is more uncertain. It also ignores non-CO_2 forcings and the fact that other components of the climate system (e.g., sea level rise, ice sheets) have their own intrinsic time scales, resulting in climate change not avoided by limiting global temperature change.

12

12.5.4.3 Conclusions and Limitations

One difficulty with the concepts of climate stabilization and targets is that stabilization of global temperature does not imply stabilization for all aspects of the climate system. For example, some models show significant hysteresis behaviour in the global water cycle, because global precipitation depends on both atmospheric CO_2 and temperature (Wu et al., 2010). Processes related to vegetation changes (Jones et al., 2009) or changes in the ice sheets (Charbit et al., 2008; Ridley et al., 2010) as well as ocean acidification, deep ocean warming and associated sea level rise (Meehl et al., 2005b; Wigley, 2005; Zickfeld et al., 2013) (see Figure 12.44d), and potential feedbacks linking, for example, ocean and the ice sheets (Gillett et al., 2011; Goelzer et al., 2011), have their own intrinsic long time scales. Those will result in significant changes hundreds to thousands of years after global temperature is stabilized. Thermal expansion, in contrast to global mean temperature, also depends on the evolution of surface temperature (Stouffer and Manabe, 1999; Bouttes et al., 2013; Zickfeld et al., 2013).

The simplicity of the concept of a cumulative carbon emission budget makes it attractive for policy (WBGU, 2009). The principal driver of long term warming is the total cumulative emission of CO_2 over time. To limit warming caused by CO_2 emissions to a given temperature target, cumulative CO_2 emissions from all anthropogenic sources therefore need to be limited to a certain budget. Higher emissions in earlier decades simply imply lower emissions by the same amount later on. This is illustrated in the RCP2.6 scenario in Figure 12.46a/b. Two idealized emission pathways with initially higher emissions (even sustained at high level for a decade in one case) eventually lead to the same warming if emissions are then reduced much more rapidly. Even a stepwise emission pathway with levels constant at 2010 and zero near mid-century would eventually lead to a similar warming as they all have identical cumulative emissions.

However, several aspects related to the concept of a cumulative carbon emission budget should be kept in mind. The ratio of global temperature and cumulative carbon is only approximately constant. It is the result of an interplay of several compensating carbon cycle and climate feedback processes operating on different time scales (a cancellation of variations in the increase in RF per ppm of CO_2, the ocean heat uptake efficiency and the airborne fraction) (Gregory et al., 2009; Matthews et al., 2009; Solomon et al., 2009). It depends on the modelled climate sensitivity and carbon cycle feedbacks. Thus, the allowed emissions for a given temperature target are uncertain (see Figure 12.45) (Matthews et al., 2009; Zickfeld et al., 2009; Knutti and Plattner, 2012). Nevertheless, the relationship is nearly linear in all models. Most models do not consider the possibility that long term feedbacks (Hansen et al., 2007; Knutti and Hegerl, 2008) may be different (see Section 12.5.3). Despite the fact that stabilization refers to equilibrium, the results assessed here are primarily relevant for the next few centuries and may differ for millennial scales. Notably, many of these limitations apply similarly to other policy targets, for example, stabilizing the atmospheric CO_2 concentration.

Non-CO_2 forcing constituents are important, which requires either assumptions on how CO_2 emission reductions are linked to changes in other forcings (Meinshausen et al., 2006; Meinshausen et al., 2009; McCollum et al., 2013), or separate emission budgets and climate modelling for short-lived and long-lived gases. So far, many studies ignored non-CO_2 forcings altogether. Those that consider them find significant effects, in particular warming of several tenths of a degree for abrupt reductions in emissions of short-lived species, like aerosols (Brasseur and Roeckner, 2005; Hare and Meinshausen, 2006; Zickfeld et al., 2009; Armour and Roe, 2011; Tanaka and Raddatz, 2011) (see also FAQ 12.3). Other studies, which model reductions that explicitly target warming from short-lived non-CO_2 species only, find important short-term cooling benefits shortly after the reduction of these species (Shindell et al., 2012), but do not extend beyond 2030.

The concept of cumulative carbon also implies that higher initial emissions can be compensated by a faster decline in emissions later or by negative emissions. However, in the real world short-term and long-term goals are not independent and mitigation rates are limited by economic constraints and existing infrastructure (Rive et al., 2007; Mignone et al., 2008; Meinshausen et al., 2009; Davis et al., 2010; Friedlingstein et al., 2011; Rogelj et al., 2013). An analysis of 193 published emission pathways with an energy balance model (UNEP, 2010; Rogelj et al., 2011) is shown in Figure 12.46c, d. Those emission pathways that *likely* limit warming below 2°C (above pre-industrial) by 2100 show emissions of about 31 to 46 Pg(CO_2-eq) yr^{-1} and 17 to 23 Pg(CO_2-eq) yr^{-1} by 2020 and 2050, respectively. Median 2010 emissions of all models are 48 Pg(CO_2-eq) yr^{-1}. Note that, as opposed to Figure 12.46a, b, many scenarios still have positive emissions in 2100. As these will not be zero immediately after 2100, they imply that the warming may exceed the target after 2100.

The aspects discussed above do not limit the robustness of the overall scientific assessment, but highlight factors that need to be considered when determining cumulative CO_2 emissions consistent with a given temperature target. In conclusion, taking into account the available information from multiple lines of evidence (observations, models and process understanding), the near linear relationship between cumulative CO_2 emissions and peak global mean temperature is well established in the literature and robust for cumulative total CO_2 emissions up to about 2000 PgC. It is consistent with the relationship inferred from past cumulative CO_2 emissions and observed warming, is supported by process understanding of the carbon cycle and global energy balance, and emerges as a robust result from the entire hierarchy of models.

Using a best estimate for the TCRE would provide a most likely value for the cumulative CO_2 emissions compatible with stabilization at a given temperature. However, such a budget would imply about 50% probability for staying below the temperature target. Higher probabilities for staying below a temperature or concentration target require significantly lower budgets (Knutti et al., 2005; Meinshausen et al., 2009; Rogelj et al., 2012). Based on the assessment of TCRE (assuming a normal distribution with a ±1 standard deviation range of 0.8-2.5°C per 1000 PgC), limiting the warming caused by anthropogenic CO_2 emissions alone (i.e., ignoring other radiative forcings) to less than 2°C since the period 1861–1880 with a probability of >33%, >50% and >66%, total CO_2 emissions from all anthropogenic sources would need to be below a cumulative budget of about 1570 PgC, 1210 PgC and 1000 PgC since 1870, respectively. An amount of 515 [445 to 585] PgC was emitted between 1870 and 2011. Accounting for non-CO_2 forcings contributing to peak warming, or requiring a higher likelihood of temperatures remaining below 2°C, both imply lower cumulative CO_2 emissions. A possible release of GHGs from permafrost or methane hydrates, not accounted for in current models, would also further reduce the anthropogenic CO_2 emissions compatible with a given temperature target. When accounting for the non-CO_2 forcings as in the RCP scenarios, compatible carbon emissions since 1870 are reduced to about 900 PgC, 820 PgC and 790 PgC to limit warming to less than 2°C since the period 1861–1880 with a probability of >33%, >50%, and >66%, respectively. These estimates were derived by computing the fraction of CMIP5 ESMs and EMICs that stay below 2°C for given cumulative emissions following RCP8.5, as shown in TFE.8 Figure 1c. The non-CO_2 forcing in RCP8.5 is higher than in RCP2.6. Because all likelihood statements in calibrated IPCC language are open intervals, the provided estimates are thus both conservative and consistent choices valid for non-CO_2 forcings across all RCP scenarios. There is no RCP scenario which limits warming to 2°C with probabilities of >33% or >50%, and which could be used to directly infer compatible cumulative emissions. For a probability of >66% RCP2.6 can be used as a comparison. Combining the average back-calculated fossil fuel carbon emissions for RCP2.6 between 2012 and 2100 (270 PgC) with the average historical estimate of 515 PgC gives a total of 785 PgC, i.e., 790 PgC when rounded to 10 PgC. As the 785 PgC estimate excludes an explicit assessment of future land-use change emissions, the 790 PgC value also remains a conservative estimate consistent with the overall likelihood assessment. The ranges of emissions for these three likelihoods based on the RCP scenarios are rather narrow, as they are based on a single scenario and on the limited sample of models available (TFE.8 Figure 1c). In contrast to TCRE they do not include observational constraints or account for sources of uncertainty not sampled by the models. The concept of a fixed cumulative CO_2 budget holds not just for 2°C, but for any temperature level explored with models so far (up to about 5°C; see Figures 12.44 to 12.46), with higher temperature levels implying larger budgets.

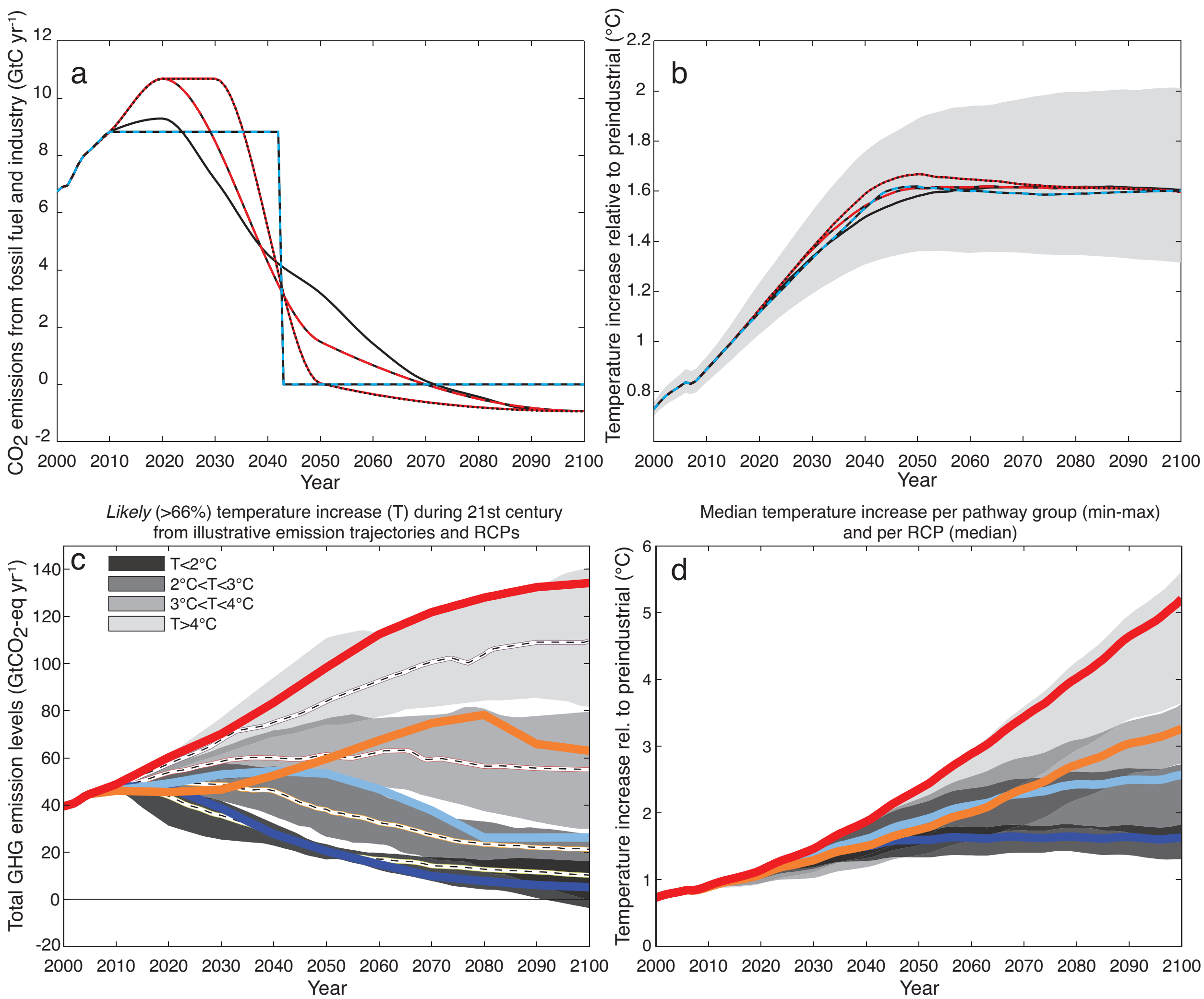

Figure 12.46 | (a) CO_2 emissions for the RCP2.6 scenario (black) and three illustrative modified emission pathways leading to the same warming. (b) Global temperature change relative to pre-industrial for the pathways shown in panel (a). (c) Grey shaded bands show Integrated Assessment Model (IAM) emission pathways over the 21st century. The pathways were grouped based on ranges of *likely* avoided temperature increase in the 21st century. Pathways in the darkest three bands *likely* stay below 2°C, 3°C, 4°C by 2100, respectively (see legend), while those in the lightest grey band are higher than that. Emission corridors were defined by, at each year, identifying the 15th to 85th percentile range of emissions and drawing the corresponding bands across the range. Individual scenarios that follow the upper edge of the bands early on tend to follow the lower edge of the band later on. Black-white lines show median paths per range. (d) Global temperature relative to pre-industrial for the pathways in (c). (Data in (c) and (d) based on Rogelj et al. (2011).) Coloured lines in (c) and (d) denote the four RCP scenarios.

12.5.5 Potentially Abrupt or Irreversible Changes

12.5.5.1 Introduction

This report adopts the definition of abrupt climate change used in Synthesis and Assessment Product 3.4 of the U.S. Climate Change Science Program CCSP (CCSP, 2008b). We define *abrupt climate change* as a large-scale change in the climate system that takes place over a few decades or less, persists (or is anticipated to persist) for at least a few decades, and causes substantial disruptions in human and natural systems (see Glossary). Other definitions of abrupt climate change exist. For example, in the AR4 climate change was defined as abrupt if it occurred faster than the typical time scale of the responsible forcing.

A number of components or phenomena within the Earth system have been proposed as potentially possessing critical thresholds (sometimes referred to as tipping points (Lenton et al., 2008)), beyond which abrupt or nonlinear transitions to a different state ensues. The term irreversibility is used in various ways in the literature. The AR5 report defines a perturbed state as *irreversible* on a given time scale if the recovery time scale from this state due to natural processes is significantly longer than the time it takes for the system to reach this perturbed state (see Glossary). In that context, most aspects of the climate change resulting from CO_2 emissions are irreversible, due to the long residence time of the CO_2 perturbation in the atmosphere and the resulting warming (Solomon et al., 2009). These results are discussed in Sections 12.5.2 to 12.5.4. Here, we also assess aspects of irreversibility in the context of abrupt change, multiple steady states and hysteresis, i.e., the question whether a change (abrupt or not) would be reversible if the forcing was reversed or removed (e.g., Boucher et al., 2012). Irreversibility of ice sheets and sea level rise are also assessed in Chapter 13.

Table 12.4 | Components in the Earth system that have been proposed in the literature as potentially being susceptible to abrupt or irreversible change. Column 2 defines whether or not a potential change can be considered to be abrupt under the AR5 definition. Column 3 states whether or not the process is irreversible in the context of abrupt change, and also gives the typical recovery time scales. Column 4 provides an assessment, if possible, of the likelihood of occurrence of abrupt change in the 21st century for the respective components or phenomena within the Earth system, for the scenarios considered in this chapter.

Change in climate system component	Potentially abrupt (AR5 definition)	Irreversibility if forcing reversed	Projected likelihood of 21st century change in scenarios considered
Atlantic MOC collapse	Yes	Unknown	*Very unlikely* that the AMOC will undergo a rapid transition (*high confidence*)
Ice sheet collapse	No	Irreversible for millennia	*Exceptionally unlikely* that either Greenland or West Antarctic Ice sheets will suffer near-complete disintegration (*high confidence*)
Permafrost carbon release	No	Irreversible for millennia	Possible that permafrost will become a net source of atmospheric greenhouse gases (*low confidence*)
Clathrate methane release	Yes	Irreversible for millennia	*Very unlikely* that methane from clathrates will undergo catastrophic release (*high confidence*)
Tropical forests dieback	Yes	Reversible within centuries	*Low confidence* in projections of the collapse of large areas of tropical forest
Boreal forests dieback	Yes	Reversible within centuries	*Low confidence* in projections of the collapse of large areas of boreal forest
Disappearance of summer Arctic sea ice	Yes	Reversible within years to decades	*Likely* that the Arctic Ocean becomes nearly ice-free in September before mid-century under high forcing scenarios such as RCP8.5 (*medium confidence*)
Long-term droughts	Yes	Reversible within years to decades	*Low confidence* in projections of changes in the frequency and duration of megadroughts
Monsoonal circulation	Yes	Reversible within years to decades	*Low confidence* in projections of a collapse in monsoon circulations

In this section we examine the main components or phenomena within the Earth system that have been proposed in the literature as potentially being susceptible to abrupt or irreversible change (see Table 12.4). Abrupt changes that arise from nonlinearities within the climate system are inherently difficult to assess and their timing, if any, of future occurrences is difficult to predict. Nevertheless, progress is being made exploring the potential existence of early warning signs for abrupt climate change (see e.g., Dakos et al., 2008; Scheffer et al., 2009).

12.5.5.2 The Atlantic Meridional Overturning

EMICs for which the stability has been systematically assessed by suitably designed hysteresis experiments robustly show a threshold beyond which the Atlantic thermohaline circulation cannot be sustained (Rahmstorf et al., 2005). This is also the case for one low-resolution ESM (Hawkins et al., 2011). However, proximity to this threshold is highly model dependent and influenced by factors that are currently poorly understood. There is some indication that the CMIP3 climate models may generally overestimate the stability of the Atlantic Ocean circulation (Hofmann and Rahmstorf, 2009; Drijfhout et al., 2010). In particular, De Vries and Weber (2005), Dijkstra (2007), Weber et al. (2007), Huisman et al. (2010), Drijfhout et al. (2010) and Hawkins et al. (2011) suggest that the sign of net freshwater flux into the Atlantic transported through its southern boundary via the overturning circulation determines whether or not the AMOC is in a mono-stable or bi-stable state. For the pre-industrial control climate of most of the CMIP3 models, Drijfhout et al. (2010) found that the salt flux was negative (implying a positive freshwater flux), indicating that they were in a mono-stable regime. However, this is not the case in the CMIP5 models where Weaver et al. (2012) found that the majority of the models were in a bi-stable regime during RCP integrations. Observations suggest that the present day ocean is in a bi-stable regime, thereby allowing for multiple equilibria and a stable 'off' state of the AMOC (Bryden et al., 2011; Hawkins et al., 2011).

In addition to the main threshold for a complete breakdown of the circulation, others may exist that involve more limited changes, such as a cessation of Labrador Sea deep water formation (Wood et al., 1999). Rapid melting of the Greenland ice sheet causes increases in freshwater runoff, potentially weakening the AMOC. None of the CMIP5 simulations include an interactive ice sheet component. However, Jungclaus et al. (2006), Mikolajewicz et al. (2007), Driesschaert et al. (2007) and Hu et al. (2009) found only a slight temporary effect of increased melt water fluxes on the AMOC, that was either small compared to the effect of enhanced poleward atmospheric moisture transport or only noticeable in the most extreme scenarios.

Although many more model simulations have been conducted since the AR4 under a wide range of forcing scenarios, projections of the AMOC behaviour have not changed. Based on the available CMIP5 models, EMICs and the literature, it remains *very likely* that the AMOC will weaken over the 21st century relative to pre-industrial. Best estimates and ranges for the reduction from CMIP5 are 11% (1 to 24%) in RCP2.6 and 34% (12 to 54%) in RCP8.5 (Weaver et al., 2012) (see Section 12.4.7.2, Figure 12.35). But there is *low confidence* in the magnitude of the weakening. Drijfhout et al. (2012) show that the AMOC decrease per degree global mean temperature rise varies from 1.5 to 1.9 Sv (10^6 m^3 s^{-1}) for the CMIP5 multi-model ensemble members they considered depending on the scenario, but that the standard deviation in this regression is almost half the signal.

The FIO-ESM model shows cooling over much of the NH that may be related to a strong reduction of the AMOC in all RCP scenarios (even RCP2.6), but the limited output available from the model precludes an assessment of the response and realism of this response. Hence it is not included the overall assessment of the likelihood of abrupt changes.

It is *unlikely* that the AMOC will collapse beyond the end of the 21st century for the scenarios considered but a collapse beyond the 21st century for large sustained warming cannot be excluded.There is *low confidence* in assessing the evolution of the AMOC beyond the 21st century. Two of the CMIP5 models revealed an eventual slowdown of the AMOC to an off state (Figure 12.35). But this did not occur abruptly.

As assessed by Delworth et al. (2008), for an abrupt transition of the AMOC to occur, the sensitivity of the AMOC to forcing would have to be far greater that seen in current models. Alternatively, significant ablation of the Greenland ice sheet greatly exceeding even the most aggressive of current projections would be required (Swingedouw et al., 2007; Hu et al., 2009). While neither possibility can be excluded entirely, it is *unlikely* that the AMOC will collapse beyond the end of the 21st century because of global warming based on the models and range of scenarios considered.

12.5.5.3 Ice Sheets

As detailed in Section 13.4.3, all available modelling studies agree that the Greenland ice sheet will significantly decrease in area and volume in a warmer climate as a consequence of increased melt rates not compensated for by increased snowfall rates and amplified by positive feedbacks. Conversely, the surface mass balance of the Antarctic ice sheet is projected to increase in most projections because increased snowfall rates outweigh melt increase (see Section 13.4.4).

Irreversibility of ice sheet volume and extent changes can arise because of the surface-elevation feedback that operates when a decrease of the elevation of the ice sheet induces a decreased surface mass balance (generally through increased melting), and therefore essentially applies to Greenland. As detailed in Section 13.4.3.3, several stable states of the Greenland ice sheet might exist (Charbit et al., 2008; Ridley et al., 2010; Langen et al., 2012; Robinson et al., 2012; Solgaard and Langen, 2012), and the ice sheet might irreversibly shrink to a stable smaller state once a warming threshold is crossed for a certain amount of time, with the critical duration depending on how far the temperature threshold has been exceeded. Based on the available evidence (see Section 13.4.3.3), an irreversible decrease of the Greenland ice sheet due to surface mass balance changes appears *very unlikely* in the 21st century but *likely* on multi-centennial to millennial time scales in the strongest forcing scenarios.

In theory (Weertman, 1974; Schoof, 2007) ice sheet volume and extent changes can be abrupt because of the grounding line instability that can occur in coastal regions where bedrock is retrograde (i.e., sloping towards the interior of the ice sheet) and below sea level (see Section 4.4.4 and Box 13.2). This essentially applies to West Antarctica, but also to parts of Greenland and East Antarctica. Furthermore, ice shelf decay induced by oceanic or atmospheric warming might lead to abruptly accelerated ice flow further inland (De Angelis and Skvarca, 2003). Because ice sheet growth is usually a slow process, such changes could also be irreversible in the definition adopted here. The available evidence (see Section 13.4) suggests that it is *exceptionally unlikely* that the ice sheets of either Greenland or West Antarctica will suffer a near-complete disintegration during the 21st century. More generally, the potential for abrupt and/or irreversible ice sheet changes (or the initiation thereof) during the 21st century and beyond is discussed in detail in Sections 13.4.3 and 13.4.4.

12.5.5.4 Permafrost Carbon Storage

Since the IPCC AR4, estimates of the amount of carbon stored in permafrost have been significantly revised upwards (Tarnocai et al., 2009), putting the permafrost carbon stock to an equivalent of twice the atmospheric carbon pool (Dolman et al., 2010). Because of low carbon input at high latitudes, permafrost carbon is to a large part of Pleistocene (Zimov et al., 2006) or Holocene (Smith et al., 2004) origin, and its potential vulnerability is dominated by decomposition (Eglin et al., 2010). The conjunction of a long carbon accumulation time scale on one hand and potentially rapid permafrost thawing and carbon decomposition under warmer climatic conditions (Zimov et al., 2006; Schuur et al., 2009; Kuhry et al., 2010) on the other hand suggests potential irreversibility of permafrost carbon decomposition (leading to an increase of atmospheric CO_2 and/or CH_4 concentrations) on time scales of hundreds to thousands of years in a warming climate. Indeed, recent observations (Dorrepaal et al., 2009; Kuhry et al., 2010) suggest that this process, induced by widespread permafrost warming and thawing (Romanovsky et al., 2010), might be already occurring. However, the existing modelling studies of permafrost carbon balance under future warming that take into account at least some of the essential permafrost-related processes (Khvorostyanov et al., 2008; Wania et al., 2009; Koven et al., 2011; Schaefer et al., 2011; MacDougall et al., 2012; Schneider von Deimling et al., 2012) do not yield coherent results beyond the fact that present-day permafrost might become a net emitter of carbon during the 21st century under plausible future warming scenarios (*low confidence*). This also reflects an insufficient understanding of the relevant soil processes during and after permafrost thaw, including processes leading to stabilization of unfrozen soil carbon (Schmidt et al., 2011), and precludes a firm assessment of the amplitude of irreversible changes in the climate system potentially related to permafrost degassing and associated global feedbacks at this stage (see also Sections 6.4.3.4 and 6.4.7.2 and FAQ 6.1).

12.5.5.5 Atmospheric Methane from Terrestrial and Oceanic Clathrates

Model simulations (Fyke and Weaver, 2006; Reagan and Moridis, 2007; Lamarque, 2008; Reagan and Moridis, 2009) suggest that clathrate deposits in shallow regions (in particular at high latitude regions and in the Gulf of Mexico) are susceptible to destabilization via ocean warming. However, concomitant sea level rise due to changes in ocean mass enhances clathrate stability in the ocean (Fyke and Weaver, 2006). A recent assessment of the potential for a future abrupt release of methane was undertaken by the U.S. Climate Change Science Program (Synthesis and Assessment Product 3.4 see Brooke et al., 2008). They concluded that it was *very unlikely* that such a catastrophic release would occur this century. However, they argued that anthropogenic warming will *very likely* lead to enhanced methane emissions from both terrestrial and oceanic clathrates (Brooke et al., 2008). Although difficult to formally assess, initial estimates of the 21st century positive feedback from methane clathrate destabilization are small but not insignificant (Fyke and Weaver, 2006; Archer, 2007; Lamarque, 2008). Nevertheless, on multi-millennial time scales, the positive feedback to anthropogenic warming of such methane emissions is potentially larger (Archer and Buffett, 2005; Archer, 2007; Brooke et al., 2008). Once more, due to the difference between release and accumulation time scales, such emissions are irreversible. See also FAQ 6.1.

12.5.5.6 Tropical and Boreal Forests

12.5.5.6.1 Tropical forests

In today's climate, the strongest growth in the Amazon rainforest occurs during the dry season when strong insolation is combined with water drawn from underground aquifers that store the previous wet season's rainfall (Huete et al., 2006). AOGCMs do not agree about how the dry season length in the Amazon may change in the future under the SRES A1 scenario (Bombardi and Carvalho, 2009), but simulations with coupled regional climate/potential vegetation models are consistent in simulating an increase in dry season length, a 70% reduction in the areal extent of the rainforest by the end of the 21st century using the SRES A2 scenario, and an eastward expansion of the Caatinga vegetation (Cook and Vizy, 2008; Sorensson et al., 2010). In addition, some models have demonstrated the existence of multiple equilibria of the tropical South American climate–vegetation system (e.g., Oyama and Nobre, 2003). The transition could be abrupt when the dry season becomes too long for the vegetation to survive, although the resilience of the vegetation to a longer dry period may be increased by the CO_2 fertilization effect (Zelazowski et al., 2011). Deforestation may also increase dry season length (Costa and Pires, 2010) and drier conditions increase the likelihood of wildfires that, combined with fire ignition associated with human activity, can undermine the forest's resiliency to climate change (see also Section 6.4.8.1). If climate change brings drier conditions closer to those supportive of seasonal forests rather than rainforest, fire can act as a trigger to abruptly and irreversibly change the ecosystem (Malhi et al., 2009). However, the existence of refugia is an important determinant of the potential for the re-emergence of the vegetation (Walker et al., 2009).

Analysis of projected change in the climate–biome space of current vegetation distributions suggest that the risk of Amazonian forest dieback is small (Malhi et al., 2009), a finding supported by modelling when strong carbon dioxide fertilization effects on Amazonian vegetation are assumed (Rammig et al., 2010). However, the strength of CO_2 fertilization on tropical vegetation is poorly known (see Box 6.3). Uncertainty concerning the existence of critical thresholds in the Amazonian and other tropical rainforests purely driven by climate change therefore remains high, and so the possibility of a critical threshold being crossed in precipitation volume cannot be ruled out (Nobre and Borma, 2009; Good et al., 2011b, 2011c). Nevertheless, there is still some question as to whether a transition of the Amazonian or other tropical rainforests into a lower biomass state could result from the combined effects of limits to carbon fertilization, climate warming, potential precipitation decline in interaction with the effects of human land use.

12.5.5.6.2 Boreal forest

Evidence from field observations and biogeochemical modelling make it scientifically conceivable that regions of the boreal forest could tip into a different vegetation state under climate warming, but uncertainties on the likelihood of this occurring are very high (Lenton et al., 2008; Allen et al., 2010). This is mainly due to large gaps in knowledge concerning relevant ecosystemic and plant physiological responses to warming (Niinemets, 2010). The main response is a potential advancement of the boreal forest northward and the potential transition from a forest to a woodland or grassland state on its dry southern edges in the continental interiors, leading to an overall increase in herbaceous vegetation cover in the affected parts of the boreal zone (Lucht et al., 2006). The proposed potential mechanisms for decreased forest growth and/or increased forest mortality are: increased drought stress under warmer summer conditions in regions with low soil moisture (Barber et al., 2000; Dulamsuren et al., 2009, 2010); desiccation of saplings with shallow roots due to summer drought periods in the top soil layers, causing suppression of forest reproduction (Hogg and Schwarz, 1997); leaf tissue damage due to high leaf temperatures during peak summer temperatures under strong climate warming; and increased insect, herbivory and subsequent fire damage in damaged or struggling stands (Dulamsuren et al., 2008). The balance of effects controlling standing biomass, fire type and frequency, permafrost thaw depth, snow volume and soil moisture remains uncertain. Although the existence of, and the thresholds controlling, a potential critical threshold in the boreal forest are extremely uncertain, its existence cannot at present be ruled out.

12.5.5.7 Sea Ice

Several studies based on observational data or model hindcasts suggest that the rapidly declining summer Arctic sea ice cover might reach or might already have passed a tipping point (Lindsay and Zhang, 2005; Wadhams, 2012; Livina and Lenton, 2013). Identifying Arctic sea ice tipping points from the short observational record is difficult due to high interannual and decadal variability. In some climate projections, the decrease in summer Arctic sea ice areal coverage is not gradual but is instead punctuated by 5- to10- year periods of strong ice loss (Holland et al., 2006; Vavrus et al., 2012; Döscher and Koenigk, 2013). Still, these abrupt reductions do not necessarily require the existence of a tipping point in the system or further imply an irreversible behaviour (Amstrup et al., 2010; Lenton, 2012). The 5- to 10-year events discussed by Holland et al. (2006) arise when large natural climate variability in the Arctic reinforces the anthropogenically-forced change (Holland et al., 2008). Positive trends on the same time scale also occur when internal variability counteracts the forced change until the middle of the 21st century (Holland et al., 2008; Kay et al., 2011; Vavrus et al., 2012).

Further work using single-column energy-balance models (Merryfield et al., 2008; Eisenman and Wettlaufer, 2009; Abbot et al., 2011) yielded mixed results about the possibility of tipping points and bifurcations in the transition from perennial to seasonal sea ice cover. Thin ice and snow covers promote strong longwave radiative loss to space and high ice growth rates (e.g., Bitz and Roe, 2004; Notz, 2009; Eisenman, 2012). These stabilizing negative feedbacks can be large enough to overcome the positive surface–albedo feedback and/or cloud feedback, which act to amplify the forced sea ice response. In such low-order models, the emergence of multiple stable states with increased climate forcing is a parameter-dependent feature (Abbot et al., 2011; Eisenman, 2012). For example, Eisenman (2012) showed with a single-column energy-balance model that certain parameter choices that cause thicker ice or warmer ocean under a given climate forcing make the model more prone to bifurcations and hence irreversible behaviour.

The reversibility of sea ice loss with respect to global or hemispheric mean surface temperature change has been directly assessed in AOGCMs/ESMs by first raising the CO_2 concentration until virtually all sea ice disappears year-round and then lowering the CO_2 level at the same rate as during the ramp-up phase until it reaches again the initial value (Armour et al., 2011; Boucher et al., 2012; Ridley et al., 2012; Li et al., 2013b). None of these studies show evidence of a bifurcation leading to irreversible changes in Arctic sea ice. AOGCMs have also been used to test summer Arctic sea ice recovery after either sudden or very rapid artificial removal, and all had sea ice return within a few years (Schröder and Connolley, 2007; Sedláček et al., 2011; Tietsche et al., 2011). In the Antarctic, as a result of the strong coupling between the Southern Ocean's surface and the deep ocean, the sea ice areal coverage in some of the models integrated with ramp-up and ramp-down atmospheric CO_2 concentration exhibits a significant lag relative to the global or hemispheric mean surface temperature (Ridley et al., 2012; Li et al., 2013b), so that its changes may be considered irreversible on centennial time scales.

Diagnostic analyses of a few global climate models have shown abrupt sea ice losses in the transition from seasonal to year-round Arctic ice-free conditions after raising CO_2 to very high levels (Winton, 2006b; Ridley et al., 2008; Li et al., 2013b), but without evidence for irreversible changes. Winton (2006b, 2008) hypothesized that the small ice cap instability (North, 1984) could cause such an abrupt transition. With a low-order Arctic sea ice model, Eisenman and Wettlaufer (2009) also found an abrupt change behaviour in the transition from seasonal ice to year-round ice-free conditions, accompanied by an irreversible bifurcation to a new stable, annually ice-free state. They concluded that the cause is a loss of the stabilizing effect of sea ice growth when the ice season shrinks in time. The Arctic sea ice may thus experience a sharp transition to annually ice-free conditions, but the irreversible nature of this transition seems to depend on the model complexity and structure.

In conclusion, rapid summer Arctic sea ice losses are *likely* to occur in the transition to seasonally ice-free conditions. These abrupt changes might have consequences throughout the climate system as noted by Vavrus et al. (2011) for cloud cover and Lawrence et al. (2008b) for the high-latitude ground state. Furthermore, the interannual-to-decadal variability in the summer Arctic sea ice extent is projected to increase in response to global warming (Holland et al., 2008; Goosse et al., 2009). These studies suggest that large anomalies in Arctic sea ice areal coverage, like the ones that occurred in 2007 and 2012, might become increasingly frequent. However, there is little evidence in global climate models of a tipping point (or critical threshold) in the transition from a perennially ice-covered to a seasonally ice-free Arctic Ocean beyond which further sea ice loss is unstoppable and irreversible.

12.5.5.8 Hydrologic Variability: Long-Term Droughts and Monsoonal Circulation

12.5.5.8.1 Long-term Droughts

As noted in Section 5.5.5, long-term droughts (often called mega-droughts, see Glossary) are a recurring feature of Holocene paleoclimate records in North America, East and South Asia, Europe, Africa and India. The transitions into and out of the long-term droughts take many years. Because the long-term droughts all ended, they are not irreversible. Nonetheless transitions over years to a decade into a state of long-term drought would have impacts on human and natural systems.

AR4 climate model projections (Milly et al., 2008) and CMIP5 ensembles (Figure 12.23) both suggest widespread drying and drought across most of southwestern North America and many other subtropical regions by the mid to late 21st century (see Section 12.4.5), although without abrupt change. Some studies suggest that this subtropical drying may have already begun in southwestern North America (Seager et al., 2007; Seidel and Randel, 2007; Barnett et al., 2008; Pierce et al., 2008). More recent studies (Hoerling et al., 2010; Seager and Vecchi, 2010; Dai, 2011; Seager and Naik, 2012) suggest that regional reductions in precipitation are due primarily to internal variability and that the anthropogenic forced trends are currently weak in comparison.

While previous long-term droughts in southwest North America arose from natural causes, climate models project that this region will undergo progressive aridification as part of a general drying and poleward expansion of the subtropical dry zones driven by rising GHGs (Held and Soden, 2006; Seager et al., 2007; Seager and Vecchi, 2010). The models project the aridification to intensify steadily as RF and global warming progress without abrupt changes. Because of the very long lifetime of the anthropogenic atmospheric CO_2 perturbation, such drying induced by global warming would be largely irreversible on millennium time scale (Solomon et al., 2009; Frölicher and Joos, 2010; Gillett et al., 2011) (see Sections 12.5.2 and 12.5.4). For example, Solomon et al. (2009) found in a simulation where atmospheric CO_2 increases to 600 ppm followed by zero emissions, that the 15% reduction in precipitation in areas such as southwest North America, southern Europe and western Australia would persist long after emissions ceased. This, however, is largely a consequence of the warming persisting for centuries after emissions cease rather than an irreversible behaviour of the water cycle itself.

12.5.5.8.2 Monsoonal circulation

Climate model simulations and paleo-reconstructions provide evidence of past abrupt changes in Saharan vegetation, with the 'green Sahara' conditions (Hoelzmann et al., 1998) of the African Humid Period (AHP) during the mid-Holocene serving as the most recent example. However, Mitchell (1990) and Claussen et al. (2003) note that the mid-Holocene is not a direct analogue for future GHG-induced climate change since the forcings are different: a increased shortwave forcing in the NH summer versus a globally and seasonally uniform atmospheric CO_2 increase, respectively. Paleoclimate examples suggest that a strong radiative or SST forcing is needed to achieve a rapid climate change, and that the rapid changes are reversible when the forcing is withdrawn. Both the abrupt onset and termination of the AHP were triggered when northern African summer insolation was 4.2% higher than present day, representing a local increase of about 19 W m^{-2} (deMenocal et al., 2000). Note that the globally averaged radiative anthropogenic forcing from 1750 to 2011 (Table 8.6) is small compared to this local increase in insolation. A rapid Saharan greening has been simulated in a climate model of intermediate complexity forced by a rapid increase in atmospheric CO_2, with the overall extent of greening depending on the equilibrium atmospheric CO_2 level reached (Claussen et al., 2003).

Abrupt Saharan vegetation changes of the Younger Dryas are linked with a rapid AMOC weakening which is considered *very unlikely* during the 21st century and *unlikely* beyond that as a consequence of global warming.

Studies with conceptual models (Zickfeld et al., 2005; Levermann et al., 2009) have shown that the Indian summer monsoon can operate in two stable regimes: besides the 'wet' summer monsoon, a stable state exists which is characterized by low precipitation over India. These studies suggest that any perturbation of the radiative budget that tends to weaken the driving pressure gradient has the potential to induce abrupt transitions between these two regimes.

Numerous studies with coupled ocean–atmosphere models have explored the potential impact of anthropogenic forcing on the Indian monsoon (see also Section 14.2). When forced with anticipated increases in GHG concentrations, the majority of these studies show an intensification of the rainfall associated with the Indian summer monsoon (Meehl and Washington, 1993; Kitoh et al., 1997; Douville et al., 2000; Hu et al., 2000; May, 2002; Ueda et al., 2006; Kripalani et al., 2007; Stowasser et al., 2009; Cherchi et al., 2010). Despite the intensification of precipitation, several of these modelling studies show a weakening of the summer monsoon circulation (Kitoh et al., 1997; May, 2002; Ueda et al., 2006; Kripalani et al., 2007; Stowasser et al., 2009; Cherchi et al., 2010). The net effect is nevertheless an increase of precipitation due to enhanced moisture transport into the Asian monsoon region (Ueda et al., 2006). In recent years, studies with GCMs have also explored the direct effect of aerosol forcing on the Indian monsoon (Lau et al., 2006; Meehl et al., 2008; Randles and Ramaswamy, 2008; Collier and Zhang, 2009). Considering absorbing aerosols (black carbon) only, Meehl et al. (2008) found an increase in pre-monsoonal precipitation, but a decrease in summer monsoon precipitation over parts of South Asia. In contrast, Lau et al. (2006) found an increase in May–June–July precipitation in that region. If an increase in scattering aerosols only is considered, the monsoon circulation weakens and precipitation is inhibited (Randles and Ramaswamy, 2008). More recently, Bollasina et al. (2011) showed that anthropogenic aerosols played a fundamental role in driving the recent observed weakening of the summer monsoon. Given that the effect of increased atmospheric regional loading of aerosols is opposed by the concomitant increases in GHG concentrations, it is *unlikely* that an abrupt transition to the dry summer monsoon regime will be triggered in the 21st century.

Acknowledgements

We especially acknowledge the input of Contributing Authors Urs Beyerle for maintaining the database of CMIP5 output, Jan Sedláček for producing a large number of CMIP5 figures, and Joeri Rogelj for preparing synthesis figures. Chapter technical assistants Oliver Stebler, Franziska Gerber and Barbara Aellig, provided great help in assembling the chapter and Sébastien Denvil and Jérôme Raciazek provided technical assistance in downloading the CMIP5 data.

References

Abbot, D. S., M. Silber, and R. T. Pierrehumbert, 2011: Bifurcations leading to summer Arctic sea ice loss. *J. Geophys. Res.*, **116**, D19120.

Abe, M., H. Shiogama, T. Nozawa, and S. Emori, 2011: Estimation of future surface temperature changes constrained using the future-present correlated modes in inter-model variability of CMIP3 multimodel simulations. *J. Geophys. Res.*, **116**, D18104.

Adachi, Y., et al., 2013: Basic performance of a new earth system model of the Meteorological Research Institute (MRI-ESM1). *Papers Meteorol. Geophys.*, doi:10.2467/mripapers.64.

Adams, P. J., J. H. Seinfeld, D. Koch, L. Mickley, and D. Jacob, 2001: General circulation model assessment of direct radiative forcing by the sulfate-nitrate-ammonium-water inorganic aerosol system. *J. Geophys. Res.*, **106**, 1097–1111.

Adler, R. F., G. J. Gu, J. J. Wang, G. J. Huffman, S. Curtis, and D. Bolvin, 2008: Relationships between global precipitation and surface temperature on interannual and longer timescales (1979–2006). *J. Geophys. Res.*, **113**, D22104.

Aldrin, M., M. Holden, P. Guttorp, R. B. Skeie, G. Myhre, and T. K. Berntsen, 2012: Bayesian estimation of climate sensitivity based on a simple climate model fitted to observations of hemispheric temperatures and global ocean heat content. *Environmetrics*, **23**, 253–271.

Alexander, L. V., and J. M. Arblaster, 2009: Assessing trends in observed and modelled climate extremes over Australia in relation to future projections. *Int. J. Climatol.*, **29**, 417–435.

Alexander, L. V., et al., 2006: Global observed changes in daily climate extremes of temperature and precipitation. *J. Geophys. Res.*, **111**, D05109.

Alexeev, V., and C. Jackson, 2012: Polar amplification: Is atmospheric heat transport important? *Clim. Dyn.*, doi:10.1007/s00382-012-1601-z.

Alexeev, V., D. Nicolsky, V. Romanovsky, and D. Lawrence, 2007: An evaluation of deep soil configurations in the CLM3 for improved representation of permafrost. *Geophys. Res. Lett.*, **34**, L09502.

Alexeev, V. A., P. L. Langen, and J. R. Bates, 2005: Polar amplification of surface warming on an aquaplanet in "ghost forcing" experiments without sea ice feedbacks. *Clim. Dyn.*, **24**, 655–666.

Allan, R., and B. Soden, 2008: Atmospheric warming and the amplification of precipitation extremes. *Science*, **321**, 1481–1484.

Allan, R. P., 2012: Regime dependent changes in global precipitation. *Clim. Dyn.*, doi:10.1007/s00382-011-1134-x.

Allen, C., et al., 2010: A global overview of drought and heat-induced tree mortality reveals emerging climate change risks for forests. *Forest Ecol. Manage.*, **259**, 660–684.

Allen, M. R., and W. J. Ingram, 2002: Constraints on future changes in climate and the hydrologic cycle. *Nature*, **419**, 224–232.

Allen, M. R., D. J. Frame, C. Huntingford, C. D. Jones, J. A. Lowe, M. Meinshausen, and N. Meinshausen, 2009: Warming caused by cumulative carbon emissions towards the trillionth tonne. *Nature*, **458**, 1163–1166.

Allen, R. J., and S. C. Sherwood, 2008: Warming maximum in the tropical upper troposphere deduced from thermal winds. *Nature Geosci.*, **1**, 399–403.

Allen, R. J., and S. C. Sherwood, 2010: Aerosol-cloud semi-direct effect and land-sea temperature contrast in a GCM. *Geophys. Res. Lett.*, **37**, L07702.

Allen, R. J., S. C. Sherwood, J. R. Norris, and C. S. Zender, 2012: Recent Northern Hemisphere tropical expansion primarily driven by black carbon and tropospheric ozone. *Nature*, **485**, 350–354.

Amstrup, S., E. DeWeaver, D. Douglas, B. Marcot, G. Durner, C. Bitz, and D. Bailey, 2010: Greenhouse gas mitigation can reduce sea-ice loss and increase polar bear persistence. *Nature*, **468**, 955–958.

Andrews, T., and P. M. Forster, 2008: CO_2 forcing induces semi-direct effects with consequences for climate feedback interpretations. *Geophys. Res. Lett.*, **35**, L04802.

Andrews, T., P. M. Forster, and J. M. Gregory, 2009: A surface energy perspective on climate change. *J. Clim.*, **22**, 2557–2570.

Andrews, T., P. Forster, O. Boucher, N. Bellouin, and A. Jones, 2010: Precipitation, radiative forcing and global temperature change. *Geophys. Res. Lett.*, **37**, L14701.

Annan, J. D., and J. C. Hargreaves, 2006: Using multiple observationally-based constraints to estimate climate sensitivity. *Geophys. Res. Lett.*, **33**, L06704.

Annan, J. D., and J. C. Hargreaves, 2010: Reliability of the CMIP3 ensemble. *Geophys. Res. Lett.*, **37**, L02703.

Annan, J. D., and J. C. Hargreaves, 2011a: Understanding the CMIP3 multi-model ensemble. *J. Clim.*, **24**, 4529–4538.

Annan, J. D., and J. C. Hargreaves, 2011b: On the generation and interpretation of probabilistic estimates of climate sensitivity. *Clim. Change*, **104**, 423–436.

Arblaster, J. M., G. A. Meehl, and D. J. Karoly, 2011: Future climate change in the Southern Hemisphere: Competing effects of ozone and greenhouse gases. *Geophys. Res. Lett.*, **38**, L02701.

Archer, D., 2007: Methane hydrate stability and anthropogenic climate change. *Biogeosciences*, **4**, 521–544.

Archer, D., and B. Buffett, 2005: Time-dependent response of the global ocean clathrate reservoir to climatic and anthropogenic forcing. *Geochem. Geophys. Geosyst.*, **6**, Q03002.

Archer, D., et al., 2009: Atmospheric lifetime of fossil fuel carbon dioxide. *Annu. Rev. Earth Planet. Sci.*, **37**, 117–134.

Armour, K., and G. Roe, 2011: Climate commitment in an uncertain world. *Geophys. Res. Lett.*, **38**, L01707.

Armour, K., I. Eisenman, E. Blanchard-Wrigglesworth, K. McCusker, and C. Bitz, 2011: The reversibility of sea ice loss in a state-of-the-art climate model. *Geophys. Res. Lett.*, **38**, L16705.

Arora, V. K., et al., 2011: Carbon emission limits required to satisfy future representative concentration pathways of greenhouse gases. *Geophys. Res. Lett.*, **38**, L05805.

Arzel, O., T. Fichefet, and H. Goosse, 2006: Sea ice evolution over the 20th and 21st centuries as simulated by current AOGCMs. *Ocean Model.*, **12**, 401–415.

Augustsson, T., and V. Ramanathan, 1977: Radiative-convective model study of CO_2 climate problem. *J. Atmos. Sci.*, **34**, 448–451.

Bala, G., K. Caldeira, and R. Nemani, 2010: Fast versus slow response in climate change: Implications for the global hydrological cycle. *Clim. Dyn.*, **35**, 423–434.

Baldwin, M. P., M. Dameris, and T. G. Shepherd, 2007: Atmosphere—How will the stratosphere affect climate change? *Science*, **316**, 1576–1577.

Ballester, J., F. Giorgi, and X. Rodo, 2010a: Changes in European temperature extremes can be predicted from changes in PDF central statistics. *Clim. Change*, **98**, 277–284.

Ballester, J., X. Rodo, and F. Giorgi, 2010b: Future changes in Central Europe heat waves expected to mostly follow summer mean warming. *Clim. Dyn.*, **35**, 1191–1205.

Banks, H. T., and J. M. Gregory, 2006: Mechanisms of ocean heat uptake in a coupled climate model and the implications for tracer based predictions of ocean heat uptake. *Geophys. Res. Lett.*, **33**, L07608.

Bao, Q., et al., 2013: The Flexible Global Ocean-Atmosphere-Land system model, Spectral Version 2: FGOALS-s2. *Adv. Atmos. Sci.*, **30**, 561–576.

Barber, V., G. Juday, and B. Finney, 2000: Reduced growth of Alaskan white spruce in the twentieth century from temperature-induced drought stress. *Nature*, **405**, 668–673.

Barnes, E. A., and L. M. Polvani, 2013: Response of the midlatitude jets and of their variability to increased greenhouse gases in the CMIP5 models. *J. Clim.*, doi:10.1175/JCLI-D-12-00536.1.

Barnett, D. N., S. J. Brown, J. M. Murphy, D. M. H. Sexton, and M. J. Webb, 2006: Quantifying uncertainty in changes in extreme event frequency in response to doubled CO_2 using a large ensemble of GCM simulations. *Clim. Dyn.*, **26**, 489–511.

Barnett, T., and D. Pierce, 2008: When will Lake Mead go dry? *Water Resour. Res.*, **44**, W03201.

Barnett, T. P., et al., 2008: Human-induced changes in the hydrology of the western United States. *Science*, **319**, 1080–1083.

Barriopedro, D., E. M. Fischer, J. Luterbacher, R. Trigo, and R. Garcia-Herrera, 2011: The hot summer of 2010: Redrawing the temperature record map of Europe. *Science*, **332**, 220–224.

Bekryaev, R. V., I. V. Polyakov, and V. A. Alexeev, 2010: Role of polar amplification in long-term surface air temperature variations and modern Arctic warming. *J. Clim.*, **23**, 3888–3906.

Bellouin, N., J. Rae, A. Jones, C. Johnson, J. Haywood, and O. Boucher, 2011: Aerosol forcing in the Hadley Centre CMIP5 simulations and the role of ammonium nitrate. *J. Geophys. Res.*, **116**, D20206.

Bengtsson, L., K. I. Hodges, and E. Roeckner, 2006: Storm tracks and climate change. *J. Clim.*, **19**, 3518–3543.

Bengtsson, L., K. I. Hodges, and N. Keenlyside, 2009: Will extratropical storms intensify in a warmer climate? *J. Clim.*, **22**, 2276–2301.

Berg, P., J. O. Haerter, P. Thejll, C. Piani, S. Hagemann, and J. H. Christensen, 2009: Seasonal characteristics of the relationship between daily precipitation intensity and surface temperature. *J. Geophys. Res.*, **114**, D18102.

Betts, R., et al., 2007: Projected increase in continental runoff due to plant responses to increasing carbon dioxide. *Nature*, **448**, 1037–1041.

Bitz, C., and G. Roe, 2004: A mechanism for the high rate of sea ice thinning in the Arctic Ocean. *J. Clim.*, **17**, 3623–3632.

Bitz, C., and Q. Fu, 2008: Arctic warming aloft is data set dependent. *Nature*, **455**, E3–E4.

Bitz, C. M., 2008: Some aspects of uncertainty in predicting sea ice thinning. In: *Arctic Sea Ice Decline: Observations, Projections, Mechanisms, and Implications* [E. T. DeWeaver, C. M. Bitz and L. B. Tremblay (eds.)]. American Geophysical Union, Washington, DC, pp. 63–76.

Bitz, C. M., J. K. Ridley, M. M. Holland, and H. Cattle, 2012: Global climate models and 20th and 21st century Arctic climate change. In: *Arctic Climate Change – The ACSYS Decade and Beyond* [P. Lemke (ed.)]. Springer Science+Business Media, Dordrecht, Netherlands, pp. 405–436.

Boberg, F., P. Berg, P. Thejll, W. Gutowski, and J. Christensen, 2010: Improved confidence in climate change projections of precipitation evaluated using daily statistics from the PRUDENCE ensemble. *Clim. Dyn.*, **35**, 1097–1106.

Boé, J., and L. Terray, 2008: Uncertainties in summer evapotranspiration changes over Europe and implications for regional climate change. *Geophys. Res. Lett.*, **35**, L05702.

Boé, J., A. Hall, and X. Qu, 2009a: Current GCMs' unrealistic negative feedback in the Arctic. *J. Clim.*, **22**, 4682–4695.

Boé, J. L., A. Hall, and X. Qu, 2009b: September sea-ice cover in the Arctic Ocean projected to vanish by 2100. *Nature Geosci.*, **2**, 341–343.

Boer, G. J., 1993: Climate change and the regulation of the surface moisture and energy budgets. *Clim. Dyn.*, **8**, 225–239.

Boer, G. J., 2011: The ratio of land to ocean temperature change under global warming. *Clim. Dyn.*, **37**, 2253–2270.

Boer, G. J., and B. Yu, 2003: Climate sensitivity and response. *Clim. Dyn.*, **20**, 415–429.

Boer, G. J., K. Hamilton, and W. Zhu, 2005: Climate sensitivity and climate change under strong forcing. *Clim. Dyn.*, **24**, 685–700.

Bollasina, M. A., Y. Ming, and V. Ramaswamy, 2011: Anthropogenic aerosols and the weakening of the South Asian summer monsoon. *Science*, **334**, 502–505.

Bombardi, R., and L. Carvalho, 2009: IPCC global coupled model simulations of the South America monsoon system. *Clim. Dyn.*, **33**, 893–916.

Böning, C., A. Dispert, M. Visbeck, S. Rintoul, and F. Schwarzkopf, 2008: The response of the Antarctic Circumpolar Current to recent climate change. *Nature Geosci.*, **1**, 864–869.

Bony, S., and J. L. Dufresne, 2005: Marine boundary layer clouds at the heart of tropical cloud feedback uncertainties in climate models. *Geophys. Res. Lett.*, **32**, L20806.

Bony, S., G. Bellon, D. Klocke, S. Sherwood, S. Fermepin, and S. Denvil, 2013: Robust direct effect of carbon dioxide on tropical circulation and regional precipitation. *Nature Geosci.*, doi:10.1038/ngeo1799.

Bony, S., et al., 2006: How well do we understand and evaluate climate change feedback processes? *J. Clim.*, **19**, 3445–3482.

Booth, B. B. B., et al., 2012: High sensitivity of future global warming to land carbon cycle processes. *Environ. Res. Lett.*, **7**, 024002.

Boucher, O., et al., 2012: Reversibility in an Earth System model in response to CO_2 concentration changes. *Environ. Res. Lett.*, **7**, 024013.

Bouttes, N., J. M. Gregory, and J. A. Lowe, 2013: The reversibility of sea level rise. *J. Clim.*, **26**, 2502–2513.

Bowerman, N., D. Frame, C. Huntingford, J. Lowe, and M. Allen, 2011: Cumulative carbon emissions, emissions floors and short-term rates of warming: Implications for policy. *Philos. Trans. R. Soc. A*, **369**, 45–66.

Bracegirdle, T., and D. Stephenson, 2012: Higher precision estimates of regional polar warming by ensemble regression of climate model projections. *Clim. Dyn.*, **39**, 2805–2821.

Bracegirdle, T., W. Connolley, and J. Turner, 2008: Antarctic climate change over the twenty first century. *J. Geophys. Res.*, **113**, D03103.

Bracegirdle, T. J., et al., 2013: Assessment of surface winds over the Atlantic, Indian, and Pacific Ocean sectors of the Southern Ocean in CMIP5 models: Historical bias, forcing response, and state dependence. *J. Geophys. Res.*, **118**, 547–562.

Brasseur, G., and E. Roeckner, 2005: Impact of improved air quality on the future evolution of climate. *Geophys. Res. Lett.*, **32**, L23704.

Brient, F., and S. Bony, 2013: Interpretation of the positive low-cloud feedback predicted by a climate model under global warming. *Clim. Dyn.*, **40**, 2415–2431.

Brierley, C. M., M. Collins, and A. J. Thorpe, 2010: The impact of perturbations to ocean-model parameters on climate and climate change in a coupled model. *Clim. Dyn.*, **34**, 325–343.

Bromwich, D. H., J. P. Nicolas, A. J. Monaghan, M. A. Lazzara, L. M. Keller, G. A. Weidner, and A. B. Wilson, 2013: Central West Antarctica among the most rapidly warming regions on Earth. *Nature Geosci.*, **6**, 139–145.

Brooke, E., D. Archer, E. Dlugokencky, S. Frolking, and D. Lawrence, 2008: Potential for abrupt changes in atmospheric methane. *Abrupt Climate Change: A Report by the U.S. Climate Change Science Program and the Subcommittee on Global Change Research*. U.S. Geological Survey, Washington, DC, pp. 163–201.

Brooks, H. E., 2009: Proximity soundings for severe convection for Europe and the United States from reanalysis data. *Atmos. Res.*, **93**, 546–553.

Brooks, H. E., 2013: Severe thunderstorms and climate change. *Atmos. Res.*, **123**, 129–138.

Brooks, H. E., J. W. Lee, and J. P. Craven, 2003: The spatial distribution of severe thunderstorm and tornado environments from global reanalysis data. *Atmos. Res.*, **67–68**, 73–94.

Brovkin, V., et al., 2013: Effect of anthropogenic land-use and land cover changes on climate and land carbon storage in CMIP5 projections for the 21st century. *J. Clim.*, doi:10.1175/JCLI-D-12–00623.1.

Brown, R., and P. Mote, 2009: The response of Northern Hemisphere snow cover to a changing climate. *J. Clim.*, **22**, 2124–2145.

Brown, R. D., and D. A. Robinson, 2011: Northern Hemisphere spring snow cover variability and change over 1922–2010 including an assessment of uncertainty. *Cryosphere*, **5**, 219–229.

Brutel-Vuilmet, C., M. Menegoz, and G. Krinner, 2013: An analysis of present and future seasonal Northern Hemisphere land snow cover simulated by CMIP5 coupled climate models. *Cryosphere*, **7**, 67–80.

Bryan, K., F. G. Komro, S. Manabe, and M. J. Spelman, 1982: Transient climate response to increasing atmospheric carbon-dioxide. *Science*, **215**, 56–58.

Bryden, H. L., B. A. King, and G. D. McCarthy, 2011: South Atlantic overturning circulation at 24S. *J. Mar. Res.*, **69**, 38–55.

Burke, E., and S. Brown, 2008: Evaluating uncertainties in the projection of future drought. *J. Hydrometeorol.*, **9**, 292–299.

Burke, E. J., C. D. Jones, and C. D. Koven, 2012: Estimating the permafrost-carbon-climate response in the CMIP5 climate models using a simplified approach. *J. Clim.*, doi:10.1175/JCLI-D-12-00550.1.

Buser, C. M., H. R. Kunsch, D. Luthi, M. Wild, and C. Schär, 2009: Bayesian multi-model projection of climate: Bias assumptions and interannual variability. *Clim. Dyn.*, **33**, 849–868.

Butchart, N., and A. A. Scaife, 2001: Removal of chlorofluorocarbons by increased mass exchange between the stratosphere and troposphere in a changing climate. *Nature*, **410**, 799–802.

Butchart, N., et al., 2006: Simulations of anthropogenic change in the strength of the Brewer-Dobson circulation. *Clim. Dyn.*, **27**, 727–741.

Butchart, N., et al., 2010: Chemistry-climate model simulations of twenty-first century stratospheric climate and circulation changes. *J. Clim.*, **23**, 5349–5374.

Butler, A. H., D. W. J. Thompson, and R. Heikes, 2010: The steady-state atmospheric circulation response to climate change-like thermal forcings in a simple General Circulation Model. *J. Clim.*, **23**, 3474–3496.

Cabre, M. F., S. A. Solman, and M. N. Nunez, 2010: Creating regional climate change scenarios over southern South America for the 2020's and 2050's using the pattern scaling technique: Validity and limitations. *Clim. Change*, **98**, 449–469.

Caesar, J., and J. A. Lowe, 2012: Comparing the impacts of mitigation versus non-intervention scenarios on future temperature and precipitation extremes in the HadGEM2 climate model. *J. Geophys. Res.*, **117**, D15109.

Cagnazzo, C., E. Manzini, P. G. Fogli, M. Vichi, and P. Davini, 2013: Role of stratospheric dynamics in the ozone–carbon connection in the Southern Hemisphere. *Clim. Dyn.*, doi:10.1007/s00382-013-1745-5.

Cai, M., 2005: Dynamical amplification of polar warming. *Geophys. Res. Lett.*, **32**, L22710.

Caldeira, K., and J. F. Kasting, 1993: Insensitivity of global warming potentials to carbon-dioxide emission scenarios. *Nature*, **366**, 251–253.

Caldwell, P., and C. S. Bretherton, 2009: Response of a subtropical stratocumulus-capped mixed layer to climate and aerosol changes. *J. Clim.*, **22**, 20–38.

Calvo, N., and R. R. Garcia, 2009: Wave forcing of the tropical upwelling in the lower stratosphere under increasing concentrations of greenhouse gases. *J. Atmos. Sci.*, **66**, 3184–3196.
Calvo, N., R. R. Garcia, D. R. Marsh, M. J. Mills, D. E. Kinnison, and P. J. Young, 2012: Reconciling modeled and observed temperature trends over Antarctica. *Geophys. Res. Lett.*, **39**, L16803.
Cao, L., and K. Caldeira, 2010: Atmospheric carbon dioxide removal: Long-term consequences and commitment. *Environ. Res. Lett.*, **5**, 024011.
Cao, L., G. Bala, and K. Caldeira, 2012: Climate response to changes in atmospheric carbon dioxide and solar irradiance on the time scale of days to weeks. *Environ. Res. Lett.*, **7**, 034015.
Capotondi, A., M. Alexander, N. Bond, E. Curchitser, and J. Scott, 2012: Enhanced upper ocean stratification with climate change in the CMIP3 models. *J. Geophys. Res.*, **117**, C04031.
Cariolle, D., and H. Teyssedre, 2007: A revised linear ozone photochemistry parameterization for use in transport and general circulation models: Multi-annual simulations. *Atmos. Chem. Phys.*, **7**, 2183–2196.
Carslaw, K., O. Boucher, D. Spracklen, G. Mann, J. Rae, S. Woodward, and M. Kulmala, 2010: A review of natural aerosol interactions and feedbacks within the Earth system. *Atmos. Chem. Phys.*, **10**, 1701–1737.
Catto, J. L., L. C. Shaffrey, and K. I. Hodges, 2011: Northern Hemisphere extratropical cyclones in a warming climate in the HiGEM high-resolution climate model. *J. Clim.*, **24**, 5336–5352.
CCSP, 2008a: *Weather and Climate Extremes in a Changing Climate: A Report by the U.S. Climate Change Science Program and the Subcommittee on Global Change Research*. Department of Commerce, NOAA's National Climatic Data Center, College Park, MD, 164 pp.
CCSP, 2008b: *Abrupt Climate Change*. *A Report by the U.S. Climate Change Science Program and the Subcommittee on Global Change Research*. U.S. Geological Survey, Washington, DC, 459 pp.
Cess, R., et al., 1990: Intercomparison and interpretation of climate feedback processes in 19 atmospheric general-circulation models. *J. Geophys. Res.*, **95**, 16601–16615.
Chadwick, R., I. Boutle, and G. Martin, 2012: Spatial patterns of precipitation change in CMIP5: Why the rich don't get richer in the Tropics. *J. Clim.*, doi:10.1175/JCLI-D-12-00543.1.
Chadwick, R., P. Wu, P. Good, and T. Andrews, 2013: Asymmetries in tropical rainfall and circulation patterns in idealised CO_2 removal experiments. *Clim. Dyn.*, **40**, 295–316.
Chang, E. K. M., Y. Guo, and X. Xia, 2012a: CMIP5 multimodel ensemble projection of storm track change under global warming. *J. Geophys. Res.*, **117**, D23118.
Chang, E. K. M., Y. Guo, X. Xia, and M. Zheng, 2012b: Storm track activity in IPCC AR4/CMIP3 model simulations. *J. Clim.*, **26**, 246–260.
Chapin, F., et al., 2005: Role of land-surface changes in Arctic summer warming. *Science*, **310**, 657–660.
Charbit, S., D. Paillard, and G. Ramstein, 2008: Amount of CO_2 emissions irreversibly leading to the total melting of Greenland. *Geophys. Res. Lett.*, **35**, L12503.
Charney, J. G., 1979: *Carbon Dioxide and Climate: A Scientific Assessment.* National Academies of Science Press, Washington, DC, 22 pp.
Chen, C. T., and T. Knutson, 2008: On the verification and comparison of extreme rainfall indices from climate models. *J. Clim.*, **21**, 1605–1621.
Chen, G., J. Lu, and D. M. W. Frierson, 2008: Phase speed spectra and the latitude of surface westerlies: Interannual variability and global warming trend. *J. Clim.*, **21**, 5942–5959.
Cherchi, A., A. Alessandri, S. Masina, and A. Navarra, 2010: Effect of increasing CO_2 levels on monsoons. *Clim. Dyn.*, **37**, 83–101.
Choi, D. H., J. S. Kug, W. T. Kwon, F. F. Jin, H. J. Baek, and S. K. Min, 2010: Arctic Oscillation responses to greenhouse warming and role of synoptic eddy feedback. *J. Geophys. Res. Atmos.*, **115**, D17103.
Chou, C., and J. D. Neelin, 2004: Mechanisms of global warming impacts on regional tropical precipitation. *J. Clim.*, **17**, 2688–2701.
Chou, C., and C. Chen, 2010: Depth of convection and the weakening of tropical circulation in global warming. *J. Clim.*, **23**, 3019–3030.
Chou, C., and C.-W. Lan, 2012: Changes in the annual range of precipitation under global warming. *J. Clim.*, **25**, 222–235.
Chou, C., J. D. Neelin, J. Y. Tu, and C. T. Chen, 2006: Regional tropical precipitation change mechanisms in ECHAM4/OPYC3 under global warming. *J. Clim.*, **19**, 4207–4223.
Chou, C., J. D. Neelin, C. A. Chen, and J. Y. Tu, 2009: Evaluating the "Rich-Get-Richer" mechanism in tropical precipitation change under global warming. *J. Clim.*, **22**, 1982–2005.
Chou, C., C. Chen, P.-H. Tan, and K.-T. Chen, 2012: Mechanisms for global warming impacts on precipitation frequency and intensity. *J. Clim.*, **25**, 3291–3306.
Chou, C., J. C. H. Chiang, C.-W. Lan, C.-H. Chung, Y.-C. Liao, and C.-J. Lee, 2013: Increase in the range between wet and dry season precipitation. *Nature Geosci.*, **6**, 263–267.
Christensen, J. H., F. Boberg, O. B. Christensen, and P. Lucas-Picher, 2008: On the need for bias correction of regional climate change projections of temperature and precipitation. *Geophys. Res. Lett.*, **35**, L20709.
Christensen, J. H., et al., 2007: Regional climate projections. In: *Climate Change 2007: The Physical Science Basis. Contribution of Working Group I to the Fourth Assessment Report of the Intergovernmental Panel on Climate Change* [Solomon, S., D. Qin, M. Manning, Z. Chen, M. Marquis, K. B. Averyt, M. Tignor and H. L. Miller (eds.)] Cambridge University Press, Cambridge, United Kingdom and New York, NY, USA, pp. 847–940.
Christensen, N., and D. Lettenmaier, 2007: A multimodel ensemble approach to assessment of climate change impacts on the hydrology and water resources of the Colorado River Basin. *Hydrol. Earth Syst. Sci.*, **11**, 1417–1434.
Cionni, I., et al., 2011: Ozone database in support of CMIP5 simulations: Results and corresponding radiative forcing. *Atmos. Chem. Phys.*, **11**, 11267–11292.
Clark, R. T., S. J. Brown, and J. M. Murphy, 2006: Modeling Northern Hemisphere summer heat extreme changes and their uncertainties using a physics ensemble of climate sensitivity experiments. *J. Clim.*, **19**, 4418–4435.
Clark, R. T., J. M. Murphy, and S. J. Brown, 2010: Do global warming targets limit heatwave risk? *Geophys. Res. Lett.*, **37**, L17703.
Claussen, M., V. Brovkin, A. Ganopolski, C. Kubatzki, and V. Petoukhov, 2003: Climate change in northern Africa: The past is not the future. *Clim. Change*, **57**, 99–118.
Colle, B. A., Z. Zhang, K. A. Lombardo, E. Chang, P. Liu, and M. Zhang, 2013: Historical evaluation and future prediction of eastern North America and western Atlantic extratropical cyclones in the CMIP5 models during the cool season. *J. Clim.*, doi:10.1175/JCLI-D-12-00498.1.
Collier, J., and G. Zhang, 2009: Aerosol direct forcing of the summer Indian monsoon as simulated by the NCAR CAM3. *Clim. Dyn.*, **32**, 313–332.
Collins, M., C. M. Brierley, M. MacVean, B. B. B. Booth, and G. R. Harris, 2007: The sensitivity of the rate of transient climate change to ocean physics perturbations. *J. Clim.*, **20**, 2315–2320.
Collins, M., B. B. B. Booth, G. Harris, J. M. Murphy, D. M. H. Sexton, and M. J. Webb, 2006a: Towards quantifying uncertainty in transient climate change. *Clim. Dyn.*, **27**, 127–147.
Collins, M., R. E. Chandler, P. M. Cox, J. M. Huthnance, J. Rougier, and D. B. Stephenson, 2012: Quantifying future climate change. *Nature Clim. Change*, **2**, 403–409.
Collins, M., B. Booth, B. Bhaskaran, G. Harris, J. Murphy, D. Sexton, and M. Webb, 2011: Climate model errors, feedbacks and forcings: A comparison of perturbed physics and multi-model ensembles. *Clim. Dyn.*, **36**, 1737–1766.
Collins, M., et al., 2010: The impact of global warming on the tropical Pacific ocean and El Nino. *Nature Geosci.*, **3**, 391–397.
Collins, W. D., et al., 2006b: Radiative forcing by well-mixed greenhouse gases: Estimates from climate models in the Intergovernmental Panel on Climate Change (IPCC) Fourth Assessment Report (AR4). *J. Geophys. Res.*, **111**, D14317.
Colman, R., and B. McAvaney, 2009: Climate feedbacks under a very broad range of forcing. *Geophys. Res. Lett.*, **36**, L01702.
Colman, R., and S. Power, 2010: Atmospheric radiative feedbacks associated with transient climate change and climate variability. *Clim. Dyn.*, **34**, 919–933.
Comiso, J. C., and F. Nishio, 2008: Trends in the sea ice cover using enhanced and compatible AMSR-E, SSM/I, and SMMR data. *J. Geophys. Res.*, **113**, C02S07.
Cook, K., and E. Vizy, 2008: Effects of twenty-first-century climate change on the Amazon rain forest. *J. Clim.*, **21**, 542–560.
Costa, M., and G. Pires, 2010: Effects of Amazon and Central Brazil deforestation scenarios on the duration of the dry season in the arc of deforestation. *Int. J. Climatol.*, **30**, 1970–1979.
Crook, J. A., P. M. Forster, and N. Stuber, 2011: Spatial patterns of modeled climate feedback and contributions to temperature response and polar amplification. *J. Clim.*, **24**, 3575–3592.
Crucifix, M., 2006: Does the Last Glacial Maximum constrain climate sensitivity? *Geophys. Res. Lett.*, **33**, L18701.

Cruz, F. T., A. J. Pitman, J. L. McGregor, and J. P. Evans, 2010: Contrasting regional responses to increasing leaf-level atmospheric carbon dioxide over Australia. *J. Hydrometeorol.*, **11**, 296–314.

Dai, A., 2011: Drought under global warming: A review. *WIREs Clim. Change*, **2**, 45–65.

Dai, A., 2013: Increasing drought under global warming in observations and models. *Nature Clim. Change*, **3**, 52–58.

Dakos, V., M. Scheffer, E. H. van Nes, V. Brovkin, V. Petoukhov, and H. Held, 2008: Slowing down as an early warning signal for abrupt climate change. *Proc. Natl. Acad. Sci. U.S.A.*, **105**, 14308–14312.

Danabasoglu, G., and P. Gent, 2009: Equilibrium climate sensitivity: Is it accurate to use a slab ocean model? *J. Clim.*, **22**, 2494–2499.

Davin, E. L., N. de Noblet-Ducoudre, and P. Friedlingstein, 2007: Impact of land cover change on surface climate: Relevance of the radiative forcing concept. *Geophys. Res. Lett.*, **34**, L13702.

Davis, S., K. Caldeira, and H. Matthews, 2010: Future CO_2 emissions and climate change from existing energy infrastructure. *Science*, **329**, 1330–1333.

Davis, S. M., and K. H. Rosenlof, 2012: A multidiagnostic intercomparison of tropical-width time series using reanalyses and satellite observations. *J. Clim.*, **25**, 1061–1078.

De Angelis, H., and P. Skvarca, 2003: Glacier surge after ice shelf collapse. *Science*, **299**, 1560–1562.

de Vries, H., R. J. Haarsma, and W. Hazeleger, 2012: Western European cold spells in current and future climate. *Geophys. Res. Lett.*, **39**, L04706.

de Vries, P., and S. Weber, 2005: The Atlantic freshwater budget as a diagnostic for the existence of a stable shut down of the meridional overturning circulation. *Geophys. Res. Lett.*, **32**, L09606.

Del Genio, A. D., M.-S. Yao, and J. Jonas, 2007: Will moist convection be stronger in a warmer climate? *Geophys. Res. Lett.*, **34**, L16703.

Delisle, G., 2007: Near-surface permafrost degradation: How severe during the 21st century? *Geophys. Res. Lett.*, **34**, L09503.

Delworth, T. L., et al., 2008: The potential for abrupt change in the Atlantic meridional overturning circulation. In: *Abrupt Climate Change: A Report by the U.S. Climate Change Science Program and the Subcommittee on Global Change Research*, U.S. Geological Survey, Washington, DC, pp. 258–359.

deMenocal, P., J. Ortiz, T. Guilderson, J. Adkins, M. Sarnthein, L. Baker, and M. Yarusinsky, 2000: Abrupt onset and termination of the African Humid Period: Rapid climate responses to gradual insolation forcing. *Quaternary Science Reviews*, **19**, 347–361.

Deser, C., A. Phillips, V. Bourdette, and H. Teng, 2012a: Uncertainty in climate change projections: The role of internal variability. *Clim. Dyn.*, **38**, 527–546.

Deser, C., R. Knutti, S. Solomon, and A. S. Phillips, 2012b: Communication of the role of natural variability in future North American climate. *Nature Clim. Change*, **2**, 775–779.

Dessai, S., X. F. Lu, and M. Hulme, 2005: Limited sensitivity analysis of regional climate change probabilities for the 21st century. *J. Geophys. Res. Atmos.*, **110**, D19108.

Diffenbaugh, N. S., and M. Ashfaq, 2010: Intensification of hot extremes in the United States. *Geophys. Res. Lett.*, **37**, L15701.

Diffenbaugh, N. S., J. S. Pal, F. Giorgi, and X. J. Gao, 2007: Heat stress intensification in the Mediterranean climate change hotspot. *Geophys. Res. Lett.*, **34**, L11706.

Dijkstra, H., 2007: Characterization of the multiple equilibria regime in a global ocean model. *Tellus A*, **59**, 695–705.

DiNezio, P. N., A. C. Clement, G. A. Vecchi, B. J. Soden, and B. P. Kirtman, 2009: Climate response of the equatorial Pacific to global warming. *J. Clim.*, **22**, 4873–4892.

Dirmeyer, P. A., Y. Jin, B. Singh, and X. Yan, 2013: Evolving land-atmosphere interactions over North America from CMIP5 simulations. *J. Clim.*, doi:10.1175/JCLI-D-12-00454.1.

Dix, M., et al., 2013: The ACCESS Coupled Model: Documentation of core CMIP5 simulations and initial results. *Aust. Meteorol. Oceanogr. J.*, **63,** 83-199.

Dole, R., et al., 2011: Was there a basis for anticipating the 2010 Russian heat wave? *Geophys. Res. Lett.*, **38**, L06702.

Dolman, A., G. van der Werf, M. van der Molen, G. Ganssen, J. Erisman, and B. Strengers, 2010: A carbon cycle science update since IPCC AR-4. *Ambio*, **39**, 402–412.

Donat, M. G., et al., 2013: Updated analyses of temperature and precipitation extreme indices since the beginning of the twentieth century: The HadEX2 dataset. *J. Geophys. Res.*, **118**, 2098–2118.

Dong, B. W., J. M. Gregory, and R. T. Sutton, 2009: Understanding land-sea warming contrast in response to increasing greenhouse gases. Part I: Transient adjustment. *J. Clim.*, **22**, 3079–3097.

Dorrepaal, E., S. Toet, R. van Logtestijn, E. Swart, M. van de Weg, T. Callaghan, and R. Aerts, 2009: Carbon respiration from subsurface peat accelerated by climate warming in the subarctic. *Nature*, **460**, 616–619.

Döscher, R., and T. Koenigk, 2013: Arctic rapid sea ice loss events in regional coupled climate scenario experiments. *Ocean Sci.*, **9**, 217–248.

Doutriaux-Boucher, M., M. J. Webb, J. M. Gregory, and O. Boucher, 2009: Carbon dioxide induced stomatal closure increases radiative forcing via a rapid reduction in low cloud. *Geophys. Res. Lett.*, **36**, L02703.

Douville, H., J. F. Royer, J. Polcher, P. Cox, N. Gedney, D. B. Stephenson, and P. J. Valdes, 2000: Impact of CO_2 doubling on the Asian summer monsoon: Robust versus model-dependent responses. *J. Meteorol. Soc. Jpn.*, **78**, 421–439.

Dowdy, A. J., G. A. Mills, B. Timbal, and Y. Wang, 2013: Changes in the risk of extratropical cyclones in Eastern Australia. *J. Clim.*, **26**, 1403–1417.

Downes, S., A. Budnick, J. Sarmiento, and R. Farneti, 2011: Impacts of wind stress on the Antarctic Circumpolar Current fronts and associated subduction. *Geophys. Res. Lett.*, **38**, L11605.

Downes, S. M., and A. M. Hogg, 2013: Southern Ocean circulation and eddy compensation in CMIP5 models. *J. Clim.*, doi:10.1175/JCLI-D-12-00504.1.

Downes, S. M., N. L. Bindoff, and S. R. Rintoul, 2010: Changes in the subduction of Southern Ocean water masses at the end of the twenty-first century in eight IPCC models. *J. Clim.*, **23**, 6526–6541.

Driesschaert, E., et al., 2007: Modeling the influence of Greenland ice sheet melting on the Atlantic meridional overturning circulation during the next millennia. *Geophys. Res. Lett.*, **34**, L10707.

Drijfhout, S., G. J. van Oldenborgh, and A. Cimatoribus, 2012: Is a decline of AMOC causing the warming hole above the North Atlantic in observed and modeled warming patterns? *J. Clim.*, **25**, 8373–8379.

Drijfhout, S. S., S. Weber, and E. van der Swaluw, 2010: The stability of the MOC as diagnosed from the model projections for the pre-industrial, present and future climate. *Clim. Dyn.*, **37**, 1575–1586.

Dufresne, J.-L., et al., 2013: Climate change projections using the IPSL-CM5 Earth system model: From CMIP3 to CMIP5. *Clim. Dyn.*, **40**, 2123–2165.

Dufresne, J., J. Quaas, O. Boucher, S. Denvil, and L. Fairhead, 2005: Contrasts in the effects on climate of anthropogenic sulfate aerosols between the 20th and the 21st century. *Geophys. Res. Lett.*, **32**, L21703.

Dufresne, J. L., and S. Bony, 2008: An assessment of the primary sources of spread of global warming estimates from coupled atmosphere-ocean models. *J. Clim.*, **21**, 5135–5144.

Dulamsuren, C., M. Hauck, and M. Muhlenberg, 2008: Insect and small mammal herbivores limit tree establishment in northern Mongolian steppe. *Plant Ecol.*, **195**, 143–156.

Dulamsuren, C., M. Hauck, and C. Leuschner, 2010: Recent drought stress leads to growth reductions in *Larix sibirica* in the western Khentey, Mongolia. *Global Change Biol.*, **16**, 3024–3035.

Dulamsuren, C., et al., 2009: Water relations and photosynthetic performance in *Larix sibirica* growing in the forest-steppe ecotone of northern Mongolia. *Tree Physiol.*, **29**, 99–110.

Dunne, J. P., R. J. Stouffer, and J. G. John, 2013: Reductions in labour capacity from heat stress under climate warming. *Nature Clim. Change*, doi:10.1038/nclimate1827.

Durack, P., and S. Wijffels, 2010: Fifty-year trends in global ocean salinities and their relationship to broad-scale warming. *J. Clim.*, **23**, 4342–4362.

Durack, P. J., S. E. Wijffels, and R. J. Matear, 2012: Ocean salinities reveal strong global water cycle intensification during 1950 to 2000. *Science*, **336**, 455–458.

Eby, M., K. Zickfeld, A. Montenegro, D. Archer, K. Meissner, and A. Weaver, 2009: Lifetime of anthropogenic climate change: Millennial time scales of potential CO_2 and surface temperature perturbations. *J. Clim.*, **22**, 2501–2511.

Edwards, T., M. Crucifix, and S. Harrison, 2007: Using the past to constrain the future: How the palaeorecord can improve estimates of global warming. *Prog. Phys. Geogr.*, **31**, 481–500.

Eglin, T., et al., 2010: Historical and future perspectives of global soil carbon response to climate and land-use changes. *Tellus B*, **62**, 700–718.

Eisenman, I., 2012: Factors controlling the bifurcation structure of sea ice retreat. *J. Geophys. Res.*, **117**, D01111.

Eisenman, I., and J. Wettlaufer, 2009: Nonlinear threshold behavior during the loss of Arctic sea ice. *Proc. Natl. Acad. Sci. U.S.A.*, **106**, 28–32.

Eisenman, I., T. Schneider, D. S. Battisti, and C. M. Bitz, 2011: Consistent changes in the sea ice seasonal cycle in response to global warming. *J. Clim.*, **24**, 5325–5335.
Eliseev, A., P. Demchenko, M. Arzhanov, and I. Mokhov, 2013: Transient hysteresis of near-surface permafrost response to external forcing. *Clim. Dyn.*, doi:10.1007/s00382–013–1672–5.
Emori, S., and S. Brown, 2005: Dynamic and thermodynamic changes in mean and extreme precipitation under changed climate. *Geophys. Res. Lett.*, **32**, L17706.
Eyring, V., et al., 2005: A strategy for process-oriented validation of coupled chemistry-climate models. *Bull. Am. Meteorol. Soc.*, **86**, 1117–1133.
Eyring, V., et al., 2013: Long-term ozone changes and associated climate impacts in CMIP5 simulations. *J. Geophys. Res.*, doi:10.1002/jgrd.50316.
Falloon, P. D., R. Dankers, R. A. Betts, C. D. Jones, B. B. B. Booth, and F. H. Lambert, 2012: Role of vegetation change in future climate under the A1B scenario and a climate stabilisation scenario, using the HadCM3C Earth system model. *Biogeosciences*, **9**, 4739–4756.
Farneti, R., and P. Gent, 2011: The effects of the eddy-induced advection coefficient in a coarse-resolution coupled climate model. *Ocean Model.*, **39**, 135–145.
Farneti, R., T. Delworth, A. Rosati, S. Griffies, and F. Zeng, 2010: The role of mesoscale eddies in the rectification of the Southern Ocean response to climate change. *J. Phys. Oceanogr.*, **40**, 1539–1557.
Fasullo, J. T., 2010: Robust land-ocean contrasts in energy and water cycle feedbacks. *J. Clim.*, **23**, 4677–4693.
Favre, A., and A. Gershunov, 2009: North Pacific cyclonic and anticyclonic transients in a global warming context: Possible consequences for Western North American daily precipitation and temperature extremes. *Clim. Dyn.*, **32**, 969–987.
Finnis, J., M. M. Holland, M. C. Serreze, and J. J. Cassano, 2007: Response of Northern Hemisphere extratropical cyclone activity and associated precipitation to climate change, as represented by the Community Climate System Model. *J. Geophys. Res.*, **112**, G04S42.
Fischer, E. M., and C. Schär, 2009: Future changes in daily summer temperature variability: Driving processes and role for temperature extremes. *Clim. Dyn.*, **33**, 917–935.
Fischer, E. M., and C. Schär, 2010: Consistent geographical patterns of changes in high-impact European heatwaves. *Nature Geosci.*, **3**, 398–403.
Fischer, E. M., and R. Knutti, 2013: Robust projections of combined humidity and temperature extremes. *Nature Clim. Change*, **3**, 126–130.
Fischer, E. M., D. M. Lawrence, and B. M. Sanderson, 2011: Quantifying uncertainties in projections of extremes—A perturbed land surface parameter experiment. *Clim. Dyn.*, **37**, 1381–1398.
Fischer, E. M., J. Rajczak, and C. Schär, 2012a: Changes in European summer temperature variability revisited. *Geophys. Res. Lett.*, **39**, L19702.
Fischer, E. M., K. W. Oleson, and D. M. Lawrence, 2012b: Contrasting urban and rural heat stress responses to climate change. *Geophys. Res. Lett.*, **39**, L03705.
Flannery, B. P., 1984: Energy-balance models incorporating transport of thermal and latent energy. *J. Atmos. Sci.*, **41**, 414–421.
Forest, C. E., P. H. Stone, and A. P. Sokolov, 2006: Estimated PDFs of climate system properties including natural and anthropogenic forcings. *Geophys. Res. Lett.*, **33**, L01705.
Forest, C. E., P. H. Stone, and A. P. Sokolov, 2008: Constraining climate model parameters from observed 20th century changes. *Tellus A*, **60**, 911–920.
Forster, P., and K. Taylor, 2006: Climate forcings and climate sensitivities diagnosed from coupled climate model integrations. *J. Clim.*, **19**, 6181–6194.
Forster, P. M., T. Andrews, P. Good, J. M. Gregory, L. S. Jackson, and M. Zelinka, 2013: Evaluating adjusted forcing and model spread for historical and future scenarios in the CMIP5 generation of climate models. *J. Geophys. Res.*, **118**, 1139–1150.
Fowler, H., M. Ekstrom, S. Blenkinsop, and A. Smith, 2007a: Estimating change in extreme European precipitation using a multimodel ensemble. *J. Geophys. Res.*, **112**, D18104.
Fowler, H. J., S. Blenkinsop, and C. Tebaldi, 2007b: Linking climate change modelling to impacts studies: Recent advances in downscaling techniques for hydrological modelling. *Int. J. Climatol.*, **27**, 1547–1578.
Frame, D., B. Booth, J. Kettleborough, D. Stainforth, J. Gregory, M. Collins, and M. Allen, 2005: Constraining climate forecasts: The role of prior assumptions. *Geophys. Res. Lett.*, **32**, L09702.
Frederiksen, C. S., J. S. Frederiksen, J. M. Sisson, and S. L. Osbrough, 2011: Australian winter circulation and rainfall changes and projections. *Int. J. Clim. Change Strat. Manage.*, **3**, 170–188.
Friedlingstein, P., and S. Solomon, 2005: Contributions of past and present human generations to committed warming caused by carbon dioxide. *Proc. Natl. Acad. Sci. U.S.A.*, **102**, 10832–10836.
Friedlingstein, P., S. Solomon, G. Plattner, R. Knutti, P. Ciais, and M. Raupach, 2011: Long-term climate implications of twenty-first century options for carbon dioxide emission mitigation. *Nature Clim. Change*, **1**, 457–461.
Friedlingstein, P., et al., 2006: Climate-carbon cycle feedback analysis: Results from the C^4MIP model intercomparison. *J. Clim.*, **19**, 3337–3353.
Frieler, K., M. Meinshausen, M. Mengel, N. Braun, and W. Hare, 2012: A scaling approach to probabilistic assessment of regional climate. *J. Clim.*, **25**, 3117–3144.
Frierson, D., J. Lu, and G. Chen, 2007: Width of the Hadley cell in simple and comprehensive general circulation models. *Geophys. Res. Lett.*, **34**, L18804.
Frölicher, T., and F. Joos, 2010: Reversible and irreversible impacts of greenhouse gas emissions in multi-century projections with the NCAR global coupled carbon cycle-climate model. *Clim. Dyn.*, **35**, 1439–1459.
Fu, Q., C. M. Johanson, J. M. Wallace, and T. Reichler, 2006: Enhanced mid-latitude tropospheric warming in satellite measurements. *Science*, **312**, 1179–1179.
Fyfe, J., O. Saenko, K. Zickfeld, M. Eby, and A. Weaver, 2007: The role of poleward-intensifying winds on Southern Ocean warming. *J. Clim.*, **20**, 5391–5400.
Fyke, J., and A. Weaver, 2006: The effect of potential future climate change on the marine methane hydrate stability zone. *J. Clim.*, **19**, 5903–5917.
Garcia, R. R., and W. J. Randel, 2008: Acceleration of the Brewer-Dobson circulation due to increases in greenhouse gases. *J. Atmos. Sci.*, **65**, 2731–2739.
Gastineau, G., and B. J. Soden, 2009: Model projected changes of extreme wind events in response to global warming. *Geophys. Res. Lett.*, **36**, L10810.
Gastineau, G., H. Le Treut, and L. Li, 2008: Hadley circulation changes under global warming conditions indicated by coupled climate models. *Tellus A*, **60**, 863–884.
Gastineau, G., L. Li, and H. Le Treut, 2009: The Hadley and Walker circulation changes in global warming conditions described by idealized atmospheric simulations. *J. Clim.*, **22**, 3993–4013.
Gent, P. R., et al., 2011: The Community Climate System Model Version 4. *J. Clim.*, **24**, 4973–4991.
Georgescu, M., D. Lobell, and C. Field, 2011: Direct climate effects of perennial bioenergy crops in the United States. *Proc. Natl. Acad. Sci. U.S.A.*, **109**, 4307–4312.
Gerber, E. P., et al., 2012: Assessing and understanding the impact of stratospheric dynamics and variability on the Earth system. *Bull. Am. Meteorol. Soc.*, **93**, 845–859.
Gillett, N., M. Wehner, S. Tett, and A. Weaver, 2004: Testing the linearity of the response to combined greenhouse gas and sulfate aerosol forcing. *Geophys. Res. Lett.*, **31**, L14201.
Gillett, N. P., and P. A. Stott, 2009: Attribution of anthropogenic influence on seasonal sea level pressure. *Geophys. Res. Lett.*, **36**, L23709.
Gillett, N. P., V. K. Arora, D. Matthews, and M. R. Allen, 2013: Constraining the ratio of global warming to cumulative CO_2 emissions using CMIP5 simulations. *J. Clim.*, doi:10.1175/JCLI-D-12-00476.1.
Gillett, N. P., V. K. Arora, K. Zickfeld, S. J. Marshall, and A. J. Merryfield, 2011: Ongoing climate change following a complete cessation of carbon dioxide emissions. *Nature Geosci.*, **4**, 83–87.
Giorgi, F., 2008: A simple equation for regional climate change and associated uncertainty. *J. Clim.*, **21**, 1589–1604.
Gleckler, P. J., K. AchutaRao, J. M. Gregory, B. D. Santer, K. E. Taylor, and T. M. L. Wigley, 2006: Krakatoa lives: The effect of volcanic eruptions on ocean heat content and thermal expansion. *Geophys. Res. Lett.*, **33**, L17702.
Goelzer, H., P. Huybrechts, M. Loutre, H. Goosse, T. Fichefet, and A. Mouchet, 2011: Impact of Greenland and Antarctic ice sheet interactions on climate sensitivity. *Clim. Dyn.*, **37**, 1005–1018.
Good, P., J. M. Gregory, and J. A. Lowe, 2011a: A step-response simple climate model to reconstruct and interpret AOGCM projections. *Geophys. Res. Lett.*, **38**, L01703.
Good, P., J. M. Gregory, J. A. Lowe, and T. Andrews, 2013: Abrupt CO_2 experiments as tools for predicting and understanding CMIP5 representative concentration pathway projections. *Clim. Dyn.*, **40**, 1041–1053.
Good, P., C. Jones, J. Lowe, R. Betts, B. Booth, and C. Huntingford, 2011b: Quantifying environmental drivers of future tropical forest extent. *J. Clim.*, **24**, 1337–1349.
Good, P., et al., 2012: A step-response approach for predicting and understanding non-linear precipitation changes. *Clim. Dyn.*, **39**, 2789–2803.

Good, P., et al., 2011c: A review of recent developments in climate change science. Part I: Understanding of future change in the large-scale climate system. *Prog. Phys. Geogr.*, **35**, 281–296.
Goodwin, P., R. Williams, A. Ridgwell, and M. Follows, 2009: Climate sensitivity to the carbon cycle modulated by past and future changes in ocean chemistry. *Nature Geosci.*, **2**, 145–150.
Goosse, H., O. Arzel, C. Bitz, A. de Montety, and M. Vancoppenolle, 2009: Increased variability of the Arctic summer ice extent in a warmer climate. *Geophys. Res. Lett.*, **36**, L23702.
Goubanova, K., and L. Li, 2007: Extremes in temperature and precipitation around the Mediterranean basin in an ensemble of future climate scenario simulations. *Global Planet. Change*, **57**, 27–42.
Gouttevin, I., G. Krinner, P. Ciais, J. Polcher, and C. Legout, 2012: Multi-scale validation of a new soil freezing scheme for a land-surface model with physically-based hydrology. *Cryosphere*, **6**, 407–430.
Granier, C., et al., 2011: Evolution of anthropogenic and biomass burning emissions at global and regional scales during the 1980–2010 period. *Clim. Change*, **109**, 163–190.
Grant, A., S. Brönnimann, and L. Haimberger, 2008: Recent Arctic warming vertical structure contested. *Nature*, **455**, E2–E3.
Graversen, R., and M. Wang, 2009: Polar amplification in a coupled climate model with locked albedo. *Clim. Dyn.*, **33**, 629–643.
Graversen, R., T. Mauritsen, M. Tjernstrom, E. Kallen, and G. Svensson, 2008: Vertical structure of recent Arctic warming. *Nature*, **541**, 53–56.
Gregory, J., and M. Webb, 2008: Tropospheric adjustment induces a cloud component in CO_2 forcing. *J. Clim.*, **21**, 58–71.
Gregory, J., and P. Forster, 2008: Transient climate response estimated from radiative forcing and observed temperature change. *J. Geophys. Res.*, **113**, D23105.
Gregory, J. M., 2010: Long-term effect of volcanic forcing on ocean heat content. *Geophys. Res. Lett.*, **37**, L22701.
Gregory, J. M., and J. F. B. Mitchell, 1995: Simulation of daily variability of surface-temperature and precipitation over Europe in the current and $2xCO_2$ climates using the UKMO climate model. *Q. J. R. Meteorol. Soc.*, **121**, 1451–1476.
Gregory, J. M., and R. Tailleux, 2011: Kinetic energy analysis of the response of the Atlantic meridional overturning circulation to CO_2-forced climate change. *Clim. Dyn.*, **37**, 893–914.
Gregory, J. M., C. D. Jones, P. Cadule, and P. Friedlingstein, 2009: Quantifying carbon cycle feedbacks. *J. Clim.*, **22**, 5232–5250.
Gregory, J. M., et al., 2004: A new method for diagnosing radiative forcing and climate sensitivity. *Geophys. Res. Lett.*, **31**, L03205.
Gregory, J. M., et al., 2005: A model intercomparison of changes in the Atlantic thermohaline circulation in response to increasing atmospheric CO_2 concentration. *Geophys. Res. Lett.*, **32**, L12703.
Grubb, M., 1997: Technologies, energy systems and the timing of CO_2 emissions abatement—An overview of economic issues. *Energy Policy*, **25**, 159–172.
Gumpenberger, M., et al., 2010: Predicting pan-tropical climate change induced forest stock gains and losses-implications for REDD. *Environ. Res. Lett.*, **5**, 014013.
Gutowski, W., K. Kozak, R. Arritt, J. Christensen, J. Patton, and E. Takle, 2007: A possible constraint on regional precipitation intensity changes under global warming. *J. Hydrometeorol.*, **8**, 1382–1396.
Haarsma, R. J., F. Selten, and G. J. van Oldenborgh, 2013: Anthropogenic changes of the thermal and zonal flow structure over Western Europe and Eastern North Atlantic in CMIP3 and CMIP5 models. *Clim. Dyn.*, doi:10.1007/s00382–013-1734-8.
Haarsma, R. J., F. Selten, B. V. Hurk, W. Hazeleger, and X. L. Wang, 2009: Drier Mediterranean soils due to greenhouse warming bring easterly winds over summertime central Europe. *Geophys. Res. Lett.*, **36**, L04705.
Hajima, T., T. Ise, K. Tachiiri, E. Kato, S. Watanabe, and M. Kawamiya, 2012: Climate change, allowable emission, and Earth system response to representative concentration pathway scenarios. *J. Meteorol. Soc. Jpn.*, **90**, 417–433.
Hall, A., 2004: The role of surface albedo feedback in climate. *J. Clim.*, **17**, 1550–1568.
Hall, A., X. Qu, and J. Neelin, 2008: Improving predictions of summer climate change in the United States. *Geophys. Res. Lett.*, **35**, L01702.
Hansen, J., M. Sato, P. Kharecha, and K. von Schuckmann, 2011: Earth's energy imbalance and implications. *Atmos. Chem. Phys.*, **11**, 13421–13449.
Hansen, J., G. Russell, A. Lacis, I. Fung, D. Rind, and P. Stone, 1985: Climate response-times—Dependence on climate sensitivity and ocean mixing. *Science*, **229**, 857–859.
Hansen, J., M. Sato, P. Kharecha, G. Russell, D. Lea, and M. Siddall, 2007: Climate change and trace gases. *Philos. Trans. R. Soc. A*, **365**, 1925–1954.
Hansen, J., et al., 1984: Climate sensitivity: Analysis of feedback mechanisms. In: *Climate Processes and Climate Sensitivity* [J. Hansen and T. Takahashi (eds.)]. American Geophysical Union, Washington, DC, pp. 130–163.
Hansen, J., et al., 1988: Global climate changes as forecast by Goddard Institute for Space Studies 3-dimensional model. *J. Geophys. Res. Atmos.*, **93**, 9341–9364.
Hansen, J., et al., 2008: Target atmospheric CO_2: Where should humanity aim? *Open Atmos. Sci. J.*, **2**, 217–231.
Hansen, J., et al., 2005a: Earth's energy imbalance: Confirmation and implications. *Science*, **308**, 1431–1435.
Hansen, J., et al., 2005b: Efficacy of climate forcings. *J. Geophys. Res.*, **110**, D18104.
Hardiman, S., N. Butchart, T. Hinton, S. Osprey, and L. Gray, 2012: The effect of a well resolved stratosphere on surface climate: Differences between CMIP5 simulations with high and low top versions of the Met Office climate model. *J. Clim.*, **35**, 7083–7099.
Hare, B., and M. Meinshausen, 2006: How much warming are we committed to and how much can be avoided? *Clim. Change*, **75**, 111–149.
Hargreaves, J. C., A. Abe-Ouchi, and J. D. Annan, 2007: Linking glacial and future climates through an ensemble of GCM simulations. *Clim. Past*, **3**, 77–87.
Hargreaves, J. C., J. D. Annan, M. Yoshimori, and A. Abe-Ouchi, 2012: Can the Last Glacial Maximum constrain climate sensitivity? *Geophys. Res. Lett.*, **39**, L24702.
Harris, G. R., M. Collins, D. M. H. Sexton, J. M. Murphy, and B. B. B. Booth, 2010: Probabilistic projections for 21st century European climate. *Nat. Hazards Earth Syst. Sci.*, **10**, 2009–2020.
Harris, G. R., D. M. H. Sexton, B. B. B. Booth, M. Collins, J. M. Murphy, and M. J. Webb, 2006: Frequency distributions of transient regional climate change from perturbed physics ensembles of general circulation model simulations. *Clim. Dyn.*, **27**, 357–375.
Hartmann, D. L., and K. Larson, 2002: An important constraint on tropical cloud-climate feedback. *Geophys. Res. Lett.*, **29**, 1951.
Harvey, B. J., L. C. Shaffrey, T. J. Woollings, G. Zappa, and K. I. Hodges, 2012: How large are projected 21st century storm track changes? *Geophys. Res. Lett.*, **39**, L18707.
Haugen, J., and T. Iversen, 2008: Response in extremes of daily precipitation and wind from a downscaled multi-model ensemble of anthropogenic global climate change scenarios. *Tellus A*, **60**, 411–426.
Hawkins, E., and R. Sutton, 2009: The potential to narrow uncertainty in regional climate predictions. *Bull. Am. Meteorol. Soc.*, **90**, 1095–1107.
Hawkins, E., and R. Sutton, 2011: The potential to narrow uncertainty in projections of regional precipitation change. *Clim. Dyn.*, **37**, 407–418.
Hawkins, E., R. Smith, L. Allison, J. Gregory, T. Woollings, H. Pohlmann, and B. de Cuevas, 2011: Bistability of the Atlantic overturning circulation in a global climate model and links to ocean freshwater transport. *Geophys. Res. Lett.*, **38**, L16699.
Hazeleger, W., et al., 2013: Multiyear climate predictions using two initialisation strategies. *Geophys. Res. Lett.*, doi:10.1002/grl.50355.
Hegerl, G., T. Crowley, W. Hyde, and D. Frame, 2006: Climate sensitivity constrained by temperature reconstructions over the past seven centuries. *Nature*, **440**, 1029–1032.
Hegerl, G. C., F. W. Zwiers, P. A. Stott, and V. V. Kharin, 2004: Detectability of anthropogenic changes in annual temperature and precipitation extremes. *J. Clim.*, **17**, 3683–3700.
Held, I., and B. Soden, 2006: Robust responses of the hydrological cycle to global warming. *J. Clim.*, **19**, 5686–5699.
Held, I. M., M. Winton, K. Takahashi, T. Delworth, F. R. Zeng, and G. K. Vallis, 2010: Probing the fast and slow components of global warming by returning abruptly to preindustrial forcing. *J. Clim.*, **23**, 2418–2427.
Hellmer, H. H., F. Kauker, R. Timmermann, J. Determann, and J. Rae, 2012: Twenty-first-century warming of a large Antarctic ice-shelf cavity by a redirected coastal current. *Nature*, **484**, 225–228.
Henderson-Sellers, A., P. Irannejad, and K. McGuffie, 2008: Future desertification and climate change: The need for land-surface system evaluation improvement. *Global and Planetary Change*, **64**, 129–138.
Hibbard, K. A., G. A. Meehl, P. A. Cox, and P. Friedlingstein, 2007: A strategy for climate change stabilization experiments. *EOS Transactions AGU*, **88**, 217–221.
Hirschi, M., et al., 2011: Observational evidence for soil-moisture impact on hot extremes in southeastern Europe. *Nature Geosci.*, **4**, 17–21.

Ho, C. K., D. B. Stephenson, M. Collins, C. A. T. Ferro, and S. J. Brown, 2012: Calibration strategies: A source of additional uncertainty in climate change projections. *Bull. Am. Meteorol. Soc.*, **93**, 21–26.

Hodson, D. L. R., S. P. E. Keeley, A. West, J. Ridley, E. Hawkins, and H. T. Hewitt, 2012: Identifying uncertainties in Arctic climate change projections. *Clim. Dyn.*, doi:10.1007/s00382-012-1512-z.

Hoelzmann, P., D. Jolly, S. Harrison, F. Laarif, R. Bonnefille, and H. Pachur, 1998: Mid-Holocene land-surface conditions in northern Africa and the Arabian Peninsula: A data set for the analysis of biogeophysical feedbacks in the climate system. *Global Biogeochem. Cycles*, **12**, 35–51.

Hoerling, M., J. Eischeid, and J. Perlwitz, 2010: Regional precipitation trends: Distinguishing natural variability from anthropogenic forcing. *J. Clim.*, **23**, 2131–2145.

Hoerling, M. P., J. K. Eischeid, X.-W. Quan, H. F. Diaz, R. S. Webb, R. M. Dole, and D. R. Easterling, 2012: Is a transition to semipermanent drought conditions imminent in the US Great Plains? *J. Clim.*, **25**, 8380–8386.

Hofmann, M., and S. Rahmstorf, 2009: On the stability of the Atlantic meridional overturning circulation. *Proc. Natl. Acad. Sci. U.S.A.*, **106**, 20584–20589.

Hogg, E., and A. Schwarz, 1997: Regeneration of planted conifers across climatic moisture gradients on the Canadian prairies: Implications for distribution and climate change. *J. Biogeogr.*, **24**, 527–534.

Holden, P. B., and N. R. Edwards, 2010: Dimensionally reduced emulation of an AOGCM for application to integrated assessment modelling. *Geophys. Res. Lett.*, **37**, L21707.

Holland, M., C. Bitz, and B. Tremblay, 2006: Future abrupt reductions in the summer Arctic sea ice. *Geophys. Res. Lett.*, **33**, L23503.

Holland, M., M. Serreze, and J. Stroeve, 2010: The sea ice mass budget of the Arctic and its future change as simulated by coupled climate models. *Clim. Dyn.*, **34**, 185–200.

Holland, M. M., and C. M. Bitz, 2003: Polar amplification of climate change in coupled models. *Clim. Dyn.*, **21**, 221–232.

Holland, M. M., C. M. Bitz, B. Tremblay, and D. A. Bailey, 2008: The role of natural versus forced change in future rapid summer Arctic ice loss. In: *Arctic Sea Ice Decline: Observations, Projections, Mechanisms, and Implications* [E. T. DeWeaver, C. M. Bitz and L. B. Tremblay (eds.)]. American Geophysical Union, Washington, DC, pp. 133–150.

Hu, A., G. Meehl, W. Han, and J. Yin, 2009: Transient response of the MOC and climate to potential melting of the Greenland ice sheet in the 21st century. *Geophys. Res. Lett.*, **36**, L10707.

Hu, Y., and Q. Fu, 2007: Observed poleward expansion of the Hadley circulation since 1979. *Atmos. Chem. Phys.*, **7**, 5229–5236.

Hu, Z.-Z., M. Latif, E. Roeckner, and L. Bengtsson, 2000: Intensified Asian summer monsoon and its variability in a coupled model forced by increasing greenhouse gas concentrations. *Geophys. Res. Lett.*, **27**, 2681–2684.

Hu, Z. Z., A. Kumar, B. Jha, and B. H. Huang, 2012: An analysis of forced and internal variability in a warmer climate in CCSM3. *J. Clim.*, **25**, 2356–2373.

Huang, P., S.-P. Xie, K. Hu, G. Huang, and R. Huang, 2013: Patterns of the seasonal response of tropical rainfall to global warming. *Nature Geosci.*, **6**, 357–361.

Huete, A. R., et al., 2006: Amazon rainforests green-up with sunlight in dry season. *Geophys. Res. Lett.*, **33**, L06405.

Huisman, S., M. den Toom, H. Dijkstra, and S. Drijfhout, 2010: An indicator of the multiple equilibria regime of the Atlantic meridional overturning circulation. *J. Phys. Oceanogr.*, **40**, 551–567.

Huntingford, C., and P. M. Cox, 2000: An analogue model to derive additional climate change scenarios from existing GCM simulations. *Clim. Dyn.*, **16**, 575–586.

Huntingford, C., J. Lowe, B. Booth, C. Jones, G. Harris, L. Gohar, and P. Meir, 2009: Contributions of carbon cycle uncertainty to future climate projection spread. *Tellus B*, **61**, 355–360.

Huntingford, C., et al., 2008: Towards quantifying uncertainty in predictions of Amazon 'dieback'. *Philos. Trans. R. Soc. B*, **363**, 1857–1864.

Huntingford, C., et al., 2013: Simulated resilience of tropical rainforests to CO_2-induced climate change. *Nature Geosci.*, **6**, 268–273.

Hurtt, G., et al., 2011: Harmonization of land-use scenarios for the period 1500–2100: 600 years of global gridded annual land-use transitions, wood harvest, and resulting secondary lands. *Clim. Change*, **109**, 117–161.

Hwang, Y.-T., D. M. W. D.M.W. Frierson, B. J. Soden, and I. M. Held, 2011: Corrigendum for Held and Soden (2006). *J. Clim.*, **24**, 1559–1560.

IPCC, 2000: *IPCC Special Report on Emissions Scenarios. Prepared by Working Group III of the Intergovernmental Panel on Climate Change.* Cambridge University Press, Cambridge, United Kingdom, and New York, NY, USA.

IPCC, 2001: *Climate Change 2001: The Scientific Basis. Contribution of Working Group I to the Third Assessment Report of the Intergovernmental Panel on Climate Change* [J. T. Houghton, Y. Ding, D. J. Griggs, M. Noquer, P. J. van der Linden, X. Dai, K. Maskell and C. A. Johnson (eds.)]. Cambridge University Press, Cambridge, United Kingdom and New York, NY, USA, 881 pp.

IPCC, 2007: *Climate Change 2007: The Physical Science Basis. Contribution of Working Group I to the Fourth Assessment Report of the Intergovernmental Panel on Climate Change* [Solomon, S., D. Qin, M. Manning, Z. Chen, M. Marquis, K. B. Averyt, M. Tignor and H. L. Miller (eds.)]. Cambridge University Press, Cambridge, United Kingdom and New York, NY, USA, 996 pp.

Ishizaki, Y., et al., 2012: Temperature scaling pattern dependence on representative concentration pathway emission scenarios. *Clim. Change*, **112**, 535–546.

Iversen, T., et al., 2013: The Norwegian Earth System Model, NorESM1–M – Part 2: Climate response and scenario projections. *Geosci. Model Dev.*, **6**, 389–415.

Jackson, C. S., M. K. Sen, G. Huerta, Y. Deng, and K. P. Bowman, 2008: Error reduction and convergence in climate prediction. *J. Clim.*, **21**, 6698–6709.

Jaeger, C., and J. Jaeger, 2010: Three views of two degrees. *Clim. Change Econ.*, **3**, 145–166.

Jiang, X., S. J. Eichelberger, D. L. Hartmann, R. Shia, and Y. L. Yung, 2007: Influence of doubled CO_2 on ozone via changes in the Brewer-Dobson circulation. *J. Atmos. Sci.*, **64**, 2751–2755.

Johanson, C. M., and Q. Fu, 2009: Hadley Cell widening: Model simulations versus observations. *J. Clim.*, **22**, 2713–2725.

Johns, T. C., et al., 2011: Climate change under aggressive mitigation: The ENSEMBLES multi-model experiment. *Clim. Dyn.*, **37**, 1975–2003.

Johnson, N. C., and S.-P. Xie, 2010: Changes in the sea surface temperature threshold for tropical convection. *Nature Geosci.*, **3**, 842–845.

Jones, A., J. Haywood, and O. Boucher, 2007: Aerosol forcing, climate response and climate sensitivity in the Hadley Centre climate model. *J. Geophys. Res.*, **112**, D20211.

Jones, C., P. Cox, and C. Huntingford, 2006: Climate-carbon cycle feedbacks under stabilization: Uncertainty and observational constraints. *Tellus B*, **58**, 603–613.

Jones, C., J. Lowe, S. Liddicoat, and R. Betts, 2009: Committed terrestrial ecosystem changes due to climate change. *Nature Geosci.*, **2**, 484–487.

Jones, C. D., et al., 2013: 21st Century compatible CO_2 emissions and airborne fraction simulated by CMIP5 Earth System models under 4 Representative Concentration Pathways. *J. Clim.*, doi:10.1175/JCLI-D-12-00554.1.

Jones, C. D., et al., 2011: The HadGEM2–ES implementation of CMIP5 centennial simulations. *Geosci. Model Dev.*, **4**, 543–570.

Joos, F., et al., 2013: Carbon dioxide and climate impulse response functions for the computation of greenhouse gas metrics: A multi-model analysis. *Atmos. Chem. Phys.*, **13**, 2793–2825.

Joshi, M., E. Hawkins, R. Sutton, J. Lowe, and D. Frame, 2011: Projections of when temperature change will exceed 2°C above pre-industrial levels. *Nature Clim. Change*, **1**, 407–412.

Joshi, M., K. Shine, M. Ponater, N. Stuber, R. Sausen, and L. Li, 2003: A comparison of climate response to different radiative forcings in three general circulation models: Towards an improved metric of climate change. *Clim. Dyn.*, **20**, 843–854.

Joshi, M. M., F. H. Lambert, and M. J. Webb, 2013: An explanation for the difference between twentieth and twenty-first century land–sea warming ratio in climate models. *Clim. Dyn.*, doi:10.1007/s00382-013-1664-5.

Joshi, M. M., M. J. Webb, A. C. Maycock, and M. Collins, 2010: Stratospheric water vapour and high climate sensitivity in a version of the HadSM3 climate model. *Atmos. Chem. Phys.*, **10**, 7161–7167.

Joshi, M. M., J. M. Gregory, M. J. Webb, D. M. H. Sexton, and T. C. Johns, 2008: Mechanisms for the land/sea warming contrast exhibited by simulations of climate change. *Clim. Dyn.*, **30**, 455–465.

Jun, M., R. Knutti, and D. W. Nychka, 2008: Spatial analysis to quantify numerical model bias and dependence: How many climate models are there? *J. Am. Stat. Assoc. Appl. Case Stud.*, **103**, 934–947.

Jungclaus, J., H. Haak, M. Esch, E. Röckner, and J. Marotzke, 2006: Will Greenland melting halt the thermohaline circulation? *Geophys. Res. Lett.*, **33**, L17708.

Kang, S. M., and I. M. Held, 2012: Tropical precipitation, SSTs and the surface energy budget: A zonally symmetric perspective. *Clim. Dyn.*, **38**, 1917–1924.

Kang, S. M., L. M. Polvani, J. C. Fyfe, and M. Sigmond, 2011: Impact of polar ozone depletion on subtropical precipitation. *Science*, **332**, 951–954.

Karpechko, A. Y., and E. Manzini, 2012: Stratospheric influence on tropospheric climate change in the Northern Hemisphere. *J. Geophys. Res.*, **117**, D05133.

Kattenberg, A., et al., 1996: Climate models—Projections of future climate. In: *Climate Change 1995: The Science of Climate Change. Contribution of WGI to the Second Assessment Report of the Intergovernmental Panel on Climate Change* [J. T. Houghton, L. G. Meira . A. Callander, N. Harris, A. Kattenberg and K. Maskell (eds.)]. Cambridge University Press, Cambridge, United Kingdom, and New York, NY, USA, pp. 285–357.

Kawase, H., T. Nagashima, K. Sudo, and T. Nozawa, 2011: Future changes in tropospheric ozone under Representative Concentration Pathways (RCPs). *Geophys. Res. Lett.*, **38**, L05801.

Kay, J., M. Holland, and A. Jahn, 2011: Inter-annual to multi-decadal Arctic sea ice extent trends in a warming world. *Geophys. Res. Lett.*, **38**, L15708.

Kay, J. E., M. M. Holland, C. Bitz, E. Blanchard-Wrigglesworth, A. Gettelman, A. Conley, and D. Bailey, 2012: The influence of local feedbacks and northward heat transport on the equilibrium Arctic climate response to increased greenhouse gas forcing in coupled climate models. *J. Clim.*, **25**, 5433–5450.

Kaye, N., A. Hartley, and D. Hemming, 2012: Mapping the climate: Guidance on appropriate techniques to map climate variables and their uncertainty. *Geosci. Model Dev.*, **5**, 245–256.

Kellomaki, S., M. Maajarvi, H. Strandman, A. Kilpelainen, and H. Peltola, 2010: Model computations on the climate change effects on snow cover, soil moisture and soil frost in the boreal conditions over Finland. *Silva Fennica*, **44**, 213–233.

Kendon, E., D. Rowell, and R. Jones, 2010: Mechanisms and reliability of future projected changes in daily precipitation. *Clim. Dyn.*, **35**, 489–509.

Kendon, E., D. Rowell, R. Jones, and E. Buonomo, 2008: Robustness of future changes in local precipitation extremes. *J. Clim.*, **17**, 4280–4297.

Kharin, V. V., F. W. Zwiers, X. B. Zhang, and G. C. Hegerl, 2007: Changes in temperature and precipitation extremes in the IPCC ensemble of global coupled model simulations. *J. Clim.*, **20**, 1419–1444.

Kharin, V. V., F. W. Zwiers, X. Zhang, and M. Wehner, 2013: Changes in temperature and precipitation extremes in the CMIP5 ensemble. *Clim. Change*, doi:10.1007/s10584-013-0705-8.

Khvorostyanov, D., P. Ciais, G. Krinner, and S. Zimov, 2008: Vulnerability of east Siberia's frozen carbon stores to future warming. *Geophys. Res. Lett.*, **35**, L10703.

Kidston, J., and E. P. Gerber, 2010: Intermodel variability of the poleward shift of the austral jet stream in the CMIP3 integrations linked to biases in 20th century climatology. *Geophys. Res. Lett.*, **37**, L09708.

Kienzle, S., M. Nemeth, J. Byrne, and R. MacDonald, 2012: Simulating the hydrological impacts of climate change in the upper North Saskatchewan River basin, Alberta, Canada. *J. Hydrol.*, **412**, 76–89.

Kirkevåg, K., et al., 2013: Aerosol–climate interactions in the Norwegian Earth System Model – NorESM1–M. *Geosci. Model Dev.*, **6**, 207–244.

Kitoh, A., S. Yukimoto, A. Noda, and T. Motoi, 1997: Simulated changes in the Asian summer monsoon at times of increased atmospheric CO_2. *J. Meteorol. Soc. Jpn.*, **75**, 1019–1031.

Kjellstrom, E., L. Barring, D. Jacob, R. Jones, G. Lenderink, and C. Schär, 2007: Modelling daily temperature extremes: Recent climate and future changes over Europe. *Clim. Change*, **81**, 249–265.

Knutti, R., 2010: The end of model democracy? *Clim. Change*, **102**, 395–404.

Knutti, R., and G. C. Hegerl, 2008: The equilibrium sensitivity of the Earth's temperature to radiation changes. *Nature Geosci.*, **1**, 735–743.

Knutti, R., and L. Tomassini, 2008: Constraints on the transient climate response from observed global temperature and ocean heat uptake. *Geophys. Res. Lett.*, **35**, L09701.

Knutti, R., and G.-K. Plattner, 2012: Comment on 'Why hasn't Earth warmed as much as expected?' by Schwartz et al. 2010. *J. Clim.*, **25**, 2192–2199.

Knutti, R., and J. Sedláček, 2013: Robustness and uncertainties in the new CMIP5 climate model projections. *Nature Clim. Change*, **3**, 369–373.

Knutti, R., D. Masson, and A. Gettelman, 2013: Climate model genealogy: Generation CMIP5 and how we got there. *Geophys. Res. Lett.*, **40**, 1194–1199.

Knutti, R., S. Krähenmann, D. Frame, and M. Allen, 2008a: Comment on "Heat capacity, time constant, and sensitivity of Earth's climate system" by S. E. Schwartz. *J. Geophys. Res.*, **113**, D15103.

Knutti, R., F. Joos, S. Müller, G. Plattner, and T. Stocker, 2005: Probabilistic climate change projections for CO_2 stabilization profiles. *Geophys. Res. Lett.*, **32**, L20707.

Knutti, R., R. Furrer, C. Tebaldi, J. Cermak, and G. A. Meehl, 2010a: Challenges in combining projections from multiple climate models. *J. Clim.*, **23**, 2739–2758.

Knutti, R., G. Abramowitz, M. Collins, V. Eyring, P. J. Gleckler, B. Hewitson, and L. Mearns, 2010b: Good practice guidance paper on assessing and combining multi model climate projections. *Meeting Report of the Intergovernmental Panel on Climate Change Expert Meeting on Assessing and Combining Multi-Model Climate Projections*. IPCC Working Group I Technical Support Unit, University of Bern, Bern, Switzerland.

Knutti, R., et al., 2008b: A review of uncertainties in global temperature projections over the twenty-first century. *J. Clim.*, **21**, 2651–2663.

Kodra, E., K. Steinhaeuser, and A. R. Ganguly, 2011: Persisting cold extremes under 21st-century warming scenarios. *Geophys. Res. Lett.*, **38**, L08705.

Kolomyts, E., and N. Surova, 2010: Predicting the impact of global warming on soil water resources in marginal forests of the middle Volga region. *Water Resour.*, **37**, 89–101.

Komuro, Y., et al., 2012: Sea-ice in twentieth-century simulations by new MIROC coupled models: A comparison between models with high resolution and with ice thickness distribution. *J. Meteorol. Soc. Jpn.*, **90A**, 213–232.

Körper, J., et al., 2013: The effects of aggressive mitigation on steric sea level rise and sea ice changes. *Clim. Dyn.*, **40**, 531–550.

Koster, R., Z. Guo, R. Yang, P. Dirmeyer, K. Mitchell, and M. Puma, 2009a: On the nature of soil moisture in land surface models. *J. Clim.*, **22**, 4322–4335.

Koster, R., et al., 2006: GLACE: The Global Land-Atmosphere Coupling Experiment. Part I: Overview. *J. Hydrometeorol.*, **7**, 590–610.

Koster, R. D., S. D. Schubert, and M. J. Suarez, 2009b: Analyzing the concurrence of meteorological droughts and warm periods, with implications for the determination of evaporative regime. *J. Clim.*, **22**, 3331–3341.

Koster, R. D., H. L. Wang, S. D. Schubert, M. J. Suarez, and S. Mahanama, 2009c: Drought-induced warming in the continental United States under different SST regimes. *J. Clim.*, **22**, 5385–5400.

Koven, C., P. Friedlingstein, P. Ciais, D. Khvorostyanov, G. Krinner, and C. Tarnocai, 2009: On the formation of high-latitude soil carbon stocks: Effects of cryoturbation and insulation by organic matter in a land surface model. *Geophys. Res. Lett.*, **36**, L21501.

Koven, C. D., W. J. Riley, and A. Stern, 2013: Analysis of permafrost thermal dynamics and response to climate change in the CMIP5 Earth system models. *J. Clim.*, **26**, 1877–1900.

Koven, C. D., et al., 2011: Permafrost carbon-climate feedbacks accelerate global warming. *Proc. Natl. Acad. Sci. U.S.A.*, **108**, 14769–14774.

Kripalani, R., J. Oh, A. Kulkarni, S. Sabade, and H. Chaudhari, 2007: South Asian summer monsoon precipitation variability: Coupled climate model simulations and projections under IPCC AR4. *Theor. Appl. Climatol.*, **90**, 133–159.

Kug, J., D. Choi, F. Jin, W. Kwon, and H. Ren, 2010: Role of synoptic eddy feedback on polar climate responses to the anthropogenic forcing. *Geophys. Res. Lett.*, **37**, L14704.

Kuhlbrodt, T., and J. M. Gregory, 2012: Ocean heat uptake and its consequences for the magnitude of sea level rise and climate change. *Geophys. Res. Lett.*, **39**, L18608.

Kuhry, P., E. Dorrepaal, G. Hugelius, E. Schuur, and C. Tarnocai, 2010: Potential remobilization of belowground permafrost carbon under future global warming. *Permafr. Periglac. Process.*, **21**, 208–214.

Kumar, A., et al., 2010: Contribution of sea ice loss to Arctic amplification. *Geophys. Res. Lett.*, **37**, L21701.

Kunkel, K. E., T. R. Karl, D. R. Easterling, K. Redmond, J. Young, X. Yin, and P. Hennon, 2013: Probable Maximum Precipitation (PMP) and climate change. *Geophys. Res. Lett.*, **40**, 1402–1408.

Kysely, J., and R. Beranova, 2009: Climate-change effects on extreme precipitation in central Europe: Uncertainties of scenarios based on regional climate models. *Theor. Appl. Climatol.*, **95**, 361–374.

Lamarque, J.-F., et al., 2011: Global and regional evolution of short-lived radiatively-active gases and aerosols in the Representative Concentration Pathways. *Clim. Change*, **109**, 191–212.

Lamarque, J., 2008: Estimating the potential for methane clathrate instability in the 1%-CO_2 IPCC AR-4 simulations. *Geophys. Res. Lett.*, **35**, L19806.

Lamarque, J., et al., 2010: Historical (1850–2000) gridded anthropogenic and biomass burning emissions of reactive gases and aerosols: Methodology and application. *Atmos. Chem. Phys.*, **10**, 7017–7039.

Lamarque, J. F., et al., 2013: The Atmospheric Chemistry and Climate Model Intercomparison Project (ACCMIP): Overview and description of models, simulations and climate diagnostics. *Geosci. Model Dev.*, **6**, 179–206.

Lambert, F., and M. Webb, 2008: Dependency of global mean precipitation on surface temperature. *Geophys. Res. Lett.*, **35**, L16706.
Lambert, F. H., and J. C. H. Chiang, 2007: Control of land-ocean temperature contrast by ocean heat uptake. *Geophys. Res. Lett.*, **34**, L13704.
Lambert, F. H., M. J. Webb, and M. J. Joshi, 2011: The relationship between land-ocean surface temperature contrast and radiative forcing. *J. Clim.*, **24**, 3239–3256.
Lambert, F. H., N. P. Gillett, D. A. Stone, and C. Huntingford, 2005: Attribution studies of observed land precipitation changes with nine coupled models. *Geophys. Res. Lett.*, **32**, L18704.
Lambert, F. H., G. R. Harris, M. Collins, J. M. Murphy, D. M. H. Sexton, and B. B. B. Booth, 2012: Interactions between perturbations to different Earth system components simulated by a fully-coupled climate model. *Clim. Dyn.*, doi:10.1007/s00382-012-1618-3.
Langen, P. L., and V. A. Alexeev, 2007: Polar amplification as a preferred response in an idealized aquaplanet GCM. *Clim. Dyn.*, **29**, 305–317.
Langen, P. L., A. M. Solgaard, and C. S. Hvidberg, 2012: Self-inhibiting growth of the Greenland Ice Sheet. *Geophys. Res. Lett.*, **39**, L12502.
Lapola, D. M., M. D. Oyama, and C. A. Nobre, 2009: Exploring the range of climate biome projections for tropical South America: The role of CO_2 fertilization and seasonality. *Global Biogeochem. Cycles*, **23**, GB3003.
Lau, K., M. Kim, and K. Kim, 2006: Asian summer monsoon anomalies induced by aerosol direct forcing: The role of the Tibetan Plateau. *Clim. Dyn.*, **26**, 855–864.
Lawrence, D., and A. Slater, 2010: The contribution of snow condition trends to future ground climate. *Clim. Dyn.*, **34**, 969–981.
Lawrence, D., A. Slater, and S. Swenson, 2012: Simulation of present-day and future permafrost and seasonally frozen ground conditions in CCSM4. *J. Clim.*, **25**, 2207–2225.
Lawrence, D., A. Slater, V. Romanovsky, and D. Nicolsky, 2008a: Sensitivity of a model projection of near-surface permafrost degradation to soil column depth and representation of soil organic matter. *J. Geophys. Res. Earth Surface*, **113**, F02011.
Lawrence, D., A. Slater, R. Tomas, M. Holland, and C. Deser, 2008b: Accelerated Arctic land warming and permafrost degradation during rapid sea ice loss. *Geophys. Res. Lett.*, **35**, L11506.
Lean, J., and D. Rind, 2009: How will Earth's surface temperature change in future decades? *Geophys. Res. Lett.*, **36**, L15708.
Lee, S., T. Gong, N. Johnson, S. B. Feldstein, and D. Pollard, 2011: On the possible link between tropical convection and the Northern Hemisphere Arctic surface air temperature change between 1958 and 2001. *J. Clim.*, **24**, 4350–4367.
Lefebvre, W., and H. Goosse, 2008: Analysis of the projected regional sea-ice changes in the Southern Ocean during the twenty-first century. *Clim. Dyn.*, **30**, 59–76.
Lemoine, D. M., 2010: Climate sensitivity distributions dependence on the possibility that models share biases. *J. Clim.*, **23**, 4395–4415.
Lenderink, G., and E. Van Meijgaard, 2008: Increase in hourly precipitation extremes beyond expectations from temperature changes. *Nature Geosci.*, **1**, 511–514.
Lenderink, G., A. van Ulden, B. van den Hurk, and E. van Meijgaard, 2007: Summertime inter-annual temperature variability in an ensemble of regional model simulations: Analysis of the surface energy budget. *Clim. Change*, **81**, 233–247.
Lenton, T., H. Held, E. Kriegler, J. Hall, W. Lucht, S. Rahmstorf, and H. Schellnhuber, 2008: Tipping elements in the Earth's climate system. *Proc. Natl. Acad. Sci. U.S.A.*, **105**, 1786–1793.
Lenton, T. M., 2012: Arctic climate tipping points. *Ambio*, **41**, 10–22.
Leslie, L. M., M. Leplastrier, and B. W. Buckley, 2008: Estimating future trends in severe hailstorms over the Sydney Basin: A climate modelling study. *Atmos. Res.*, **87**, 37–51.
Levermann, A., J. Schewe, V. Petoukhov, and H. Held, 2009: Basic mechanism for abrupt monsoon transitions. *Proc. Natl. Acad. Sci. U.S.A.*, **106**, 20572–20577.
Levitus, S., J. Antonov, and T. Boyer, 2005: Warming of the world ocean, 1955–2003. *Geophys. Res. Lett.*, **32**, L02604.
Levitus, S., et al., 2012: World ocean heat content and thermosteric sea level change (0–2000 m), 1955–2010. *Geophys. Res. Lett.*, **39**, L10603.
Levy II, H., L. W. Horowitz, M. D. Schwarzkopf, Y. Ming, J.-C. Golaz, V. Naik, and V. Ramaswamy, 2013: The roles of aerosol direct and indirect effects in past and future climate change. *J. Geophys. Res.*, doi:10.1002/jgrd.50192.
Li, C., J. S. von Storch, and J. Marotzke, 2013a: Deep-ocean heat uptake and equilibrium climate response. *Clim. Dyn.*, **40**, 1071–1086.
Li, C., D. Notz, S. Tietsche, and J. Marotzke, 2013b: The transient versus the equilibrium response of sea ice to global warming. *J. Clim.*, doi:10.1175/JCLI-D-12-00492.1.
Li, F., J. Austin, and J. Wilson, 2008: The strength of the Brewer-Dobson circulation in a changing climate: Coupled chemistry-climate model simulations. *J. Clim.*, **21**, 40–57.
Li, F., W. Collins, M. Wehner, D. Williamson, J. Olson, and C. Algieri, 2011a: Impact of horizontal resolution on simulation of precipitation extremes in an aqua-planet version of Community Atmospheric Model (CAM3). *Tellus*, **63**, 884–892.
Li, L., X. Jiang, M. Chahine, E. Olsen, E. Fetzer, L. Chen, and Y. Yung, 2011b: The recycling rate of atmospheric moisture over the past two decades (1988–2009). *Environ. Res. Lett.*, **6**, 034018.
Li, L. J., et al., 2013c: The Flexible Global Ocean-Atmosphere-Land System Model: Grid-point Version 2: FGOALS-g2. *Adv. Atmos. Sci.*, **30**, 543–560.
Liepert, B. G., and M. Previdi, 2009: Do models and observations disagree on the rainfall response to global warming? *J. Clim.*, **22**, 3156–3166.
Liepert, B. G., and M. Previdi, 2012: Inter-model variability and biases of the global water cycle in CMIP3 coupled climate models. *Environ. Res. Lett.*, **7**, 014006.
Lim, E. P., and I. Simmonds, 2009: Effect of tropospheric temperature change on the zonal mean circulation and SH winter extratropical cyclones. *Clim. Dyn.*, **33**, 19–32.
Lindsay, R., and J. Zhang, 2005: The thinning of Arctic sea ice, 1988–2003: Have we passed a tipping point? *J. Clim.*, **18**, 4879–4894.
Liu, Z., S. J. Vavrus, F. He, N. Wen, and Y. Zhong, 2005: Rethinking tropical ocean response to global warming: The enhanced equatorial warming. *J. Clim.*, **18**, 4684–4700.
Livina, V. N., and T. M. Lenton, 2013: A recent tipping point in the Arctic sea-ice cover: Abrupt and persistent increase in the seasonal cycle since 2007. *Cryosphere*, **7**, 275–286.
Loarie, S. R., D. B. Lobell, G. P. Asner, Q. Z. Mu, and C. B. Field, 2011: Direct impacts on local climate of sugar-cane expansion in Brazil. *Nature Clim. Change*, **1**, 105–109.
Loeb, N. G., et al., 2009: Toward optimal closure of the Earth's Top-of-Atmosphere radiation budget. *J. Clim.*, **22**, 748–766.
Long, M. C., K. Lindsay, S. Peacock, J. K. Moore, and S. C. Doney, 2013: Twentieth-century oceanic carbon uptake and storage in CESM1(BGC). *J. Clim.*, doi:10.1175/JCLI-D-12-00184.1.
Lorenz, D. J., and E. T. DeWeaver, 2007: Tropopause height and zonal wind response to global warming in the IPCC scenario integrations. *J. Geophys. Res. Atmos.*, **112**, D10119.
Lowe, J., C. Huntingford, S. Raper, C. Jones, S. Liddicoat, and L. Gohar, 2009: How difficult is it to recover from dangerous levels of global warming? *Environ. Res. Lett.*, **4**, 014012.
Lowe, J. A., and J. M. Gregory, 2006: Understanding projections of sea level rise in a Hadley Centre coupled climate model. *J. Geophys. Res.*, **111**, C11014.
Lu, J., and M. Cai, 2009: Seasonality of polar surface warming amplification in climate simulations. *Geophys. Res. Lett.*, **36**, L16704.
Lu, J., G. Vecchi, and T. Reichler, 2007: Expansion of the Hadley cell under global warming. *Geophys. Res. Lett.*, **34**, L06805.
Lu, J., G. Chen, and D. Frierson, 2008: Response of the zonal mean atmospheric circulation to El Niño versus global warming. *J. Clim.*, **21**, 5835–5851.
Lucht, W., S. Schaphoff, T. Ebrecht, U. Heyder, and W. Cramer, 2006: Terrestrial vegetation redistribution and carbon balance under climate change. *Carbon Balance Manage.*, **1**, 1-6.
Lunt, D., A. Haywood, G. Schmidt, U. Salzmann, P. Valdes, and H. Dowsett, 2010: Earth system sensitivity inferred from Pliocene modelling and data. *Nature Geosci.*, **3**, 60–64.
Luo, J. J., W. Sasaki, and Y. Masumoto, 2012: Indian Ocean warming modulates Pacific climate change. *Proc. Natl. Acad. Sci. U.S.A.*, **109**, 18701–18706.
Lustenberger, A., R. Knutti, and E. M. Fischer, 2013: The potential of pattern scaling for projecting temperature-related extreme indices. *Int. J. Climatol.*, doi:10.1002/joc.3659.
Ma, J., and S.-P. Xie, 2013: Regional patterns of sea surface temperature change: A source of uncertainty in future projections of precipitation and atmospheric circulation. *J. Clim.*, **26**, 2482–2501.
Ma, J., S.-P. Xie, and Y. Kosaka, 2012: Mechanisms for tropical tropospheric circulation change in response to global warming. *J. Clim.*, **25**, 2979–2994.
MacDougall, A. H., C. A. Avis, and A. J. Weaver, 2012: Significant contribution to climate warming from the permafrost carbon feedback. *Nature Geosci.*, **5**, 719–721.
Mahlstein, I., and R. Knutti, 2011: Ocean heat transport as a cause for model uncertainty in projected Arctic warming. *J. Clim.*, **24**, 1451–1460.

12

Mahlstein, I., and R. Knutti, 2012: September Arctic sea ice predicted to disappear near 2°C global warming above present. *J. Geophys. Res.*, **117**, D06104.
Mahlstein, I., R. Knutti, S. Solomon, and R. W. Portmann, 2011: Early onset of significant local warming in low latitude countries. *Environ. Res. Lett.*, **6**, 034009.
Mahlstein, I., R. W. Portmann, J. S. Daniel, S. Solomon, and R. Knutti, 2012: Perceptible changes in regional precipitation in a future climate. *Geophys. Res. Lett.*, **39**, L05701.
Maksym, T., S. E. Stammerjohn, S. Ackley, and R. Massom, 2012: Antarctic sea ice—A polar opposite? *Oceanography*, **25**, 140–151.
Malhi, Y., et al., 2009: Exploring the likelihood and mechanism of a climate-change-induced dieback of the Amazon rainforest. *Proc. Natl. Acad. Sci. U.S.A.*, **106**, 20610–20615.
Manabe, S., and R. Stouffer, 1980: Sensitivity of a global climate model to an increase of CO_2 concentration in the atmosphere. *J. Geophys. Res.*, **85**, 5529–5554.
Manabe, S., and R. T. Wetherald, 1980: Distribution of climate change resulting from an increase in CO_2 content of the atmosphere. *J. Atmos. Sci.*, **37**, 99–118.
Manabe, S., and R. Stouffer, 1994: Multiple-century response of a coupled ocean-atmosphere model to an increase of atmospheric carbon-dioxide. *J. Clim.*, **7**, 5–23.
Manabe, S., K. Bryan, and M. J. Spelman, 1990: Transient-response of a global ocean atmosphere model to a doubling of atmospheric carbon-dioxide. *J. Phys. Oceanogr.*, **20**, 722–749.
Manabe, S., R. J. Stouffer, M. J. Spelman, and K. Bryan, 1991: Transient responses of a coupled ocean atmosphere model to gradual changes of atmospheric CO_2. Part I: Annual mean response. *J. Clim.*, **4**, 785–818.
Marsh, P. T., H. E. Brooks, and D. J. Karoly, 2009: Preliminary investigation into the severe thunderstorm environment of Europe simulated by the Community Climate System Model 3. *Atmos. Res.*, **93**, 607–618.
Maslowski, W., J. C. Kinney, M. Higgins, and A. Roberts, 2012: The future of Arctic sea ice. In: *Annual Review of Earth and Planetary Sciences* [R. Jeanloz (ed.)]. Annual Reviews, Palo Alto, CA, USA, pp. 625–654.
Masson, D., and R. Knutti, 2011: Climate model genealogy. *Geophys. Res. Lett.*, **38**, L08703.
Massonnet, F., T. Fichefet, H. Goosse, C. M. Bitz, G. Philippon-Berthier, M. Holland, and P. Y. Barriat, 2012: Constraining projections of summer Arctic sea ice. *Cryosphere*, **6**, 1383–1394.
Matsuno, T., K. Maruyama, and J. Tsutsui, 2012a: Stabilization of atmospheric carbon dioxide via zero emissions-An alternative way to a stable global environment. Part 1: Examination of the traditional stabilization concept. *Proc. Jpn. Acad. B*, **88**, 368–384.
Matsuno, T., K. Maruyama, and J. Tsutsui, 2012b: Stabilization of atmospheric carbon dioxide via zero emissions-An alternative way to a stable global environment. Part 2: A practical zero-emissions scenario. *Proc. Jpn. Acad. B*, **88**, 385–395.
Matthews, H., and K. Caldeira, 2008: Stabilizing climate requires near-zero emissions. *Geophys. Res. Lett.*, **35**, L04705.
Matthews, H., N. Gillett, P. Stott, and K. Zickfeld, 2009: The proportionality of global warming to cumulative carbon emissions. *Nature*, **459**, 829–832.
Matthews, H. D., and K. Zickfeld, 2012: Climate response to zeroed emissions of greenhouse gases and aerosols. *Nature Clim. Change*, **2**, 338–341.
Matthews, H. D., S. Solomon, and R. Pierrehumbert, 2012: Cumulative carbon as a policy framework for achieving climate stabilization. *Philos. Trans. R. Soc. A*, **370**, 4365–4379.
May, W., 2002: Simulated changes of the Indian summer monsoon under enhanced greenhouse gas conditions in a global time-slice experiment. *Geophys. Res. Lett.*, **29**, 1118.
May, W., 2008a: Climatic changes associated with a global "2°C-stabilization" scenario simulated by the ECHAM5/MPI-OM coupled climate model. *Clim. Dyn.*, **31**, 283–313.
May, W., 2008b: Potential future changes in the characteristics of daily precipitation in Europe simulated by the HIRHAM regional climate model. *Clim. Dyn.*, **30**, 581–603.
May, W., 2012: Assessing the strength of regional changes in near-surface climate associated with a global warming of 2°C. *Clim. Change*, **110**, 619–644.
McCabe, G., and D. Wolock, 2007: Warming may create substantial water supply shortages in the Colorado River basin. *Geophys. Res. Lett.*, **34**, L22708.
McCollum, D., V. Krey, K. Riahi, P. Kolp, A. Grubler, M. Makowski, and N. Nakicenovic, 2013: Climate policies can help resolve energy security and air pollution challenges. *Clim. Change*, doi:10.1007/s10584-013-0710-y.
McLandress, C., and T. G. Shepherd, 2009: Simulated anthropogenic changes in the Brewer-Dobson circulation, including its extension to high latitudes. *J. Clim.*, **22**, 1516–1540.
McLandress, C., T. G. Shepherd, J. F. Scinocca, D. A. Plummer, M. Sigmond, A. I. Jonsson, and M. C. Reader, 2011: Separating the dynamical effects of climate change and ozone depletion. Part II: Southern Hemisphere troposphere. *J. Clim.*, **24**, 1850–1868.
Meehl, G., and W. Washington, 1993: South Asian summer monsoon variability in a model with doubled atmospheric carbon-dioxide concentration. *Science*, **260**, 1101–1104.
Meehl, G., J. Arblaster, and C. Tebaldi, 2005a: Understanding future patterns of increased precipitation intensity in climate model simulations. *Geophys. Res. Lett.*, **32**, L18719.
Meehl, G., J. Arblaster, and W. Collins, 2008: Effects of black carbon aerosols on the Indian monsoon. *J. Clim.*, **21**, 2869–2882.
Meehl, G., et al., 2012: Climate system response to external forcings and climate change projections in CCSM4. *J. Clim.*, **25**, 3661–3683.
Meehl, G. A., and C. Tebaldi, 2004: More intense, more frequent, and longer lasting heat waves in the 21st century. *Science*, **305**, 994–997.
Meehl, G. A., G. J. Boer, C. Covey, M. Latif, and R. J. Stouffer, 2000: The Coupled Model Intercomparison Project (CMIP). *Bull. Am. Meteorol. Soc.*, **81**, 313–318.
Meehl, G. A., C. Tebaldi, G. Walton, D. Easterling, and L. McDaniel, 2009: Relative increase of record high maximum temperatures compared to record low minimum temperatures in the U. S. *Geophys. Res. Lett.*, **36**, L23701.
Meehl, G. A., W. M. Washington, C. M. Ammann, J. M. Arblaster, T. M. L. Wigley, and C. Tebaldi, 2004: Combinations of natural and anthropogenic forcings in twentieth-century climate. *J. Clim.*, **17**, 3721–3727.
Meehl, G. A., et al., 2005b: How much more global warming and sea level rise? *Science*, **307**, 1769–1772.
Meehl, G. A., et al., 2007a: The WCRP CMIP3 multimodel dataset - A new era in climate change research. *Bull. Am. Meteorol. Soc.*, **88**, 1383–1394.
Meehl, G. A., et al., 2006: Climate change projections for the twenty-first century and climate change commitment in the CCSM3. *J. Clim.*, **19**, 2597–2616.
Meehl, G. A., et al., 2013: Climate change projections in CESM1(CAM5) compared to CCSM4. *J. Clim.*, doi:10.1175/JCLI-D-12–00572.1.
Meehl, G. A., et al., 2007b: Global climate projections. In: *Climate Change 2007: The Physical Science Basis. Contribution of Working Group I to the Fourth Assessment Report of the Intergovernmental Panel on Climate Change* [Solomon, S., D. Qin, M. Manning, Z. Chen, M. Marquis, K. B. Averyt, M. Tignor and H. L. Miller (eds.)] Cambridge University Press, Cambridge, United Kingdom and New York, NY, USA, pp. 747–846.
Meijers, A. J. S., E. Shuckburgh, N. Bruneau, J.-B. Sallee, T. J. Bracegirdle, and Z. Wang, 2012: Representation of the Antarctic Circumpolar Current in the CMIP5 climate models and future changes under warming scenarios. *J. Geophys. Res.*, **117**, C12008.
Meinshausen, M., S. Raper, and T. Wigley, 2011a: Emulating coupled atmosphere-ocean and carbon cycle models with a simpler model, MAGICC6–Part 1: Model description and calibration. *Atmos. Chem. Phys.*, **11**, 1417–1456.
Meinshausen, M., T. Wigley, and S. Raper, 2011b: Emulating atmosphere-ocean and carbon cycle models with a simpler model, MAGICC6–Part 2: Applications. *Atmos. Chem. Phys.*, **11**, 1457–1471.
Meinshausen, M., B. Hare, T. Wigley, D. Van Vuuren, M. Den Elzen, and R. Swart, 2006: Multi-gas emissions pathways to meet climate targets. *Clim. Change*, **75**, 151–194.
Meinshausen, M., et al., 2009: Greenhouse-gas emission targets for limiting global warming to 2°C. *Nature*, **458**, 1158–1162.
Meinshausen, M., et al., 2011c: The RCP greenhouse gas concentrations and their extensions from 1765 to 2300. *Clim. Change*, **109**, 213–241.
Merrifield, M. A., 2011: A shift in western tropical Pacific sea level trends during the 1990s. *J. Clim.*, **24**, 4126–4138.
Merryfield, W. J., M. M. Holland, and A. H. Monahan, 2008: Multiple equilibria and abrupt transitions in Arctic summer sea ice extent. In: *Arctic Sea Ice Decline: Observations, Projections, Mechanisms, and Implications*. American Geophysical Union, Washington, DC, pp. 151–174.
Mignone, B., R. Socolow, J. Sarmiento, and M. Oppenheimer, 2008: Atmospheric stabilization and the timing of carbon mitigation. *Clim. Change*, **88**, 251–265.
Mikolajewicz, U., M. Vizcaino, J. Jungclaus, and G. Schurgers, 2007: Effect of ice sheet interactions in anthropogenic climate change simulations. *Geophys. Res. Lett.*, **34**, L18706.

Millner, A., R. Calel, D. A. Stainforth, and G. MacKerron, 2013: Do probabilistic expert elicitations capture scientists' uncertainty about climate change? *Clim. Change*, **116**, 427–436.

Milly, P., J. Betancourt, M. Falkenmark, R. Hirsch, Z. Kundzewicz, D. Lettenmaier, and R. Stouffer, 2008: Stationarity is dead: Whither water management? *Science*, **319**, 573–574.

Min, S., X. Zhang, F. Zwiers, and G. Hegerl, 2011: Human contribution to more-intense precipitation extremes. *Nature*, **470**, 378–381.

Ming, Y., V. Ramaswamy, and G. Persad, 2010: Two opposing effects of absorbing aerosols on global-mean precipitation. *Geophys. Res. Lett.*, **37**, L13701.

Mitas, C., and A. Clement, 2006: Recent behavior of the Hadley cell and tropical thermodynamics in climate models and reanalyses. *Geophys. Res. Lett.*, **33**, L01810.

Mitchell, J. F. B., 1990: Is the Holocene a good analogue for greenhouse warming? *J. Clim.*, **3**, 1177–1192.

Mitchell, J. F. B., C. A. Wilson, and W. M. Cunnington, 1987: On CO_2 climate sensitivity and model dependence of results. *Q. J. R. Meteorol. Soc.*, **113**, 293–322.

Mitchell, J. F. B., T. C. Johns, W. J. Ingram, and J. A. Lowe, 2000: The effect of stabilising atmospheric carbon dioxide concentrations on global and regional climate change. *Geophys. Res. Lett.*, **27**, 2977–2980.

Mitchell, J. F. B., T. C. Johns, M. Eagles, W. J. Ingram, and R. A. Davis, 1999: Towards the construction of climate change scenarios. *Clim. Change*, **41**, 547–581.

Mitchell, T. D., 2003: Pattern scaling - An examination of the accuracy of the technique for describing future climates. *Clim. Change*, **60**, 217–242.

Mizuta, R., 2012: Intensification of extratropical cyclones associated with the polar jet change in the CMIP5 global warming projections. *Geophys. Res. Lett.*, **39**, L19707.

Monaghan, A., D. Bromwich, and D. Schneider, 2008: Twentieth century Antarctic air temperature and snowfall simulations by IPCC climate models. *Geophys. Res. Lett.*, **35**, L07502.

Montenegro, A., V. Brovkin, M. Eby, D. Archer, and A. Weaver, 2007: Long term fate of anthropogenic carbon. *Geophys. Res. Lett.*, **34**, L19707.

Morgan, M. G., and D. W. Keith, 1995: Climate-change - Subjective judgments by climate experts. *Environ. Sci. Technol.*, **29**, A468–A476.

Moss, R. H., et al., 2010: The next generation of scenarios for climate change research and assessment. *Nature*, **463**, 747–756.

Moss, R. H., et al., 2008: Towards new scenarios for analysis of emissions, climate change, impacts, and response strategies. In: *IPCC Expert Meeting Report: Towards New Scenarios*. Intergovernmental Panel on Climate Change, Geneva, Switzerland, 132 pp.

Muller, C. J., and P. A. O'Gorman, 2011: An energetic perspective on the regional response of precipitation to climate change. *Nature Clim. Change*, **1**, 266–271.

Murphy, D. M., S. Solomon, R. W. Portmann, K. H. Rosenlof, P. M. Forster, and T. Wong, 2009: An observationally based energy balance for the Earth since 1950. *J. Geophys. Res.*, **114**, D17107.

Murphy, J., D. Sexton, D. Barnett, G. Jones, M. Webb, and M. Collins, 2004: Quantification of modelling uncertainties in a large ensemble of climate change simulations. *Nature*, **430**, 768–772.

Murphy, J. M., B. B. B. Booth, M. Collins, G. R. Harris, D. M. H. Sexton, and M. J. Webb, 2007: A methodology for probabilistic predictions of regional climate change from perturbed physics ensembles. *Philos. Trans. R. Soc. A*, **365**, 1993–2028.

Myhre, G., E. Highwood, K. Shine, and F. Stordal, 1998: New estimates of radiative forcing due to well mixed greenhouse gases. *Geophys. Res. Lett.*, **25**, 2715–2718.

Neelin, J. D., C. Chou, and H. Su, 2003: Tropical drought regions in global warming and El Niño teleconnections. *Geophys. Res. Lett.*, **30**, 2275.

Neelin, J. D., M. Munnich, H. Su, J. E. Meyerson, and C. E. Holloway, 2006: Tropical drying trends in global warming models and observations. *Proc. Natl. Acad. Sci. U.S.A.*, **103**, 6110–6115.

Nelson, F., and S. Outcalt, 1987: A computational method for prediction and regionalization of permafrost. *Arct. Alpine Res.*, **19**, 279–288.

Newlands, N. K., G. Espino-Hernández, and R. S. Erickson, 2012: Understanding crop response to climate variability with complex agroecosystem models. *Int. J. Ecol.*, **2012**, 756242.

Niall, S., and K. Walsh, 2005: The impact of climate change on hailstorms in southeastern Australia. *Int. J. Climatol.*, **25**, 1933–1952.

Nicolsky, D., V. Romanovsky, V. Alexeev, and D. Lawrence, 2007: Improved modeling of permafrost dynamics in a GCM land-surface scheme. *Geophys. Res. Lett.*, **34**, L08501.

Niinemets, U., 2010: Responses of forest trees to single and multiple environmental stresses from seedlings to mature plants: Past stress history, stress interactions, tolerance and acclimation. *Forest Ecol. Manage.*, **260**, 1623–1639.

Nikulin, G., E. Kjellstrom, U. Hansson, G. Strandberg, and A. Ullerstig, 2011: Evaluation and future projections of temperature, precipitation and wind extremes over Europe in an ensemble of regional climate simulations. *Tellus A*, **63**, 41–55.

Nobre, C., and L. Borma, 2009: 'Tipping points' for the Amazon forest. *Curr. Opin. Environ. Sustain.*, **1**, 28–36.

North, G., 1984: The small ice cap instability in diffuse climate models. *J. Atmos. Sci.*, **41**, 3390–3395.

Notaro, M., 2008: Statistical identification of global hot spots in soil moisture feedbacks among IPCC AR4 models. *J. Geophys. Res.*, **113**, D09101.

Notz, D., 2009: The future of ice sheets and sea ice: Between reversible retreat and unstoppable loss. *Proc. Natl. Acad. Sci. U.S.A.*, **106**, 20590–20595.

NRC, 2011: *Climate Stabilization Targets: Emissions, Concentrations, and Impacts over Decades to Millennia.* National Academies Press, Washington, DC, 298 pp.

O'Connor, F., et al., 2010: Possible role of wetlands, permafrost, and methane hydrates in the methane cycle under future climate change: A review. *Rev. Geophys.*, **48**, RG4005.

O'Gorman, P., and T. Schneider, 2009a: Scaling of precipitation extremes over a wide range of climates simulated with an idealized GCM. *J. Clim.*, **22**, 5676–5685.

O'Gorman, P., and T. Schneider, 2009b: The physical basis for increases in precipitation extremes in simulations of 21st-century climate change. *Proc. Natl. Acad. Sci. U.S.A.*, **106**, 14773–14777.

O'Gorman, P., R. Allan, M. Byrne, and M. Previdi, 2012: Energetic constraints on precipitation under climate change. *Surv. Geophys.*, **33**, 585–608.

O'Gorman, P. A., 2010: Understanding the varied response of the extratropical storm tracks to climate change. *Proc. Natl. Acad. Sci. U.S.A.*, **107**, 19176–19180.

O'Gorman, P. A., and C. J. Muller, 2010: How closely do changes in surface and column water vapor follow Clausius-Clapeyron scaling in climate change simulations? *Environ. Res. Lett.*, **5**, 025207.

Orlowsky, B., and S. I. Seneviratne, 2012: Global changes in extreme events: Regional and seasonal dimension. *Clim. Change*, **110**, 669–696.

Otto, A., et al., 2013: Energy budget constraints on climate response. *Nature Geosci.*, **6,** 415-416.

Overland, J. E., and M. Wang, 2013: When will the summer Arctic be nearly sea ice free? *Geophys. Res. Lett.*, doi:10.1002/grl.50316.

Overland, J. E., M. Wang, N. A. Bond, J. E. Walsh, V. M. Kattsov, and W. L. Chapman, 2011: Considerations in the selection of global climate models for regional climate projections: The Arctic as a case study. *J. Clim.*, **24**, 1583–1597.

Oyama, M. D., and C. A. Nobre, 2003: A new climate-vegetation equilibrium state for Tropical South America. *Geophys. Res. Lett.*, **30**, 2199.

Padilla, L., G. Vallis, and C. Rowley, 2011: Probabilistic estimates of transient climate sensitivity subject to uncertainty in forcing and natural variability. *J. Clim.*, **24**, 5521–5537.

Paeth, H., and F. Pollinger, 2010: Enhanced evidence in climate models for changes in extratropical atmospheric circulation. *Tellus A*, **62**, 647–660.

Pagani, M., Z. Liu, J. LaRiviere, and A. Ravelo, 2010: High Earth-system climate sensitivity determined from Pliocene carbon dioxide concentrations. *Nature Geosci.*, **3**, 27–30.

Pall, P., M. Allen, and D. Stone, 2007: Testing the Clausius-Clapeyron constraint on changes in extreme precipitation under CO_2 warming. *Clim. Dyn.*, **28**, 351–363.

Pennell, C., and T. Reichler, 2011: On the effective number of climate models. *J. Clim.*, **24**, 2358–2367.

Perkins, S. E., L. V. Alexander, and J. R. Nairn, 2012: Increasing frequency, intensity and duration of observed global heatwaves and warm spells. *Geophys. Res. Lett.*, **39**, L20714.

Perrie, W., Y. H. Yao, and W. Q. Zhang, 2010: On the impacts of climate change and the upper ocean on midlatitude northwest Atlantic landfalling cyclones. *J. Geophys. Res.*, **115**, D23110.

Piani, C., D. J. Frame, D. A. Stainforth, and M. R. Allen, 2005: Constraints on climate change from a multi-thousand member ensemble of simulations. *Geophys. Res. Lett.*, **32**, L23825.

Pierce, D., et al., 2008: Attribution of declining Western US snowpack to human effects. *J. Clim.*, **21**, 6425–6444.

Pinto, J. G., U. Ulbrich, G. C. Leckebusch, T. Spangehl, M. Reyers, and S. Zacharias, 2007: Changes in storm track and cyclone activity in three SRES ensemble experiments with the ECHAM5/MPI-OM1 GCM. *Clim. Dyn.*, **29**, 195–210.

12

Pitman, A., et al., 2009: Uncertainties in climate responses to past land cover change: First results from the LUCID intercomparison study. *Geophys. Res. Lett.*, **36**, L14814.

Plattner, G.-K., et al., 2008: Long-term climate commitments projected with climate-carbon cycle models. *J. Clim.*, **21**, 2721– 2751.

Polvani, L. M., M. Previdi, and C. Deser, 2011: Large cancellation, due to ozone recovery, of future Southern Hemisphere atmospheric circulation trends. *Geophys. Res. Lett.*, **38**, L04707.

Pongratz, J., C. Reick, T. Raddatz, and M. Claussen, 2010: Biogeophysical versus biogeochemical climate response to historical anthropogenic land cover change. *Geophys. Res. Lett.*, **37**, L08702.

Port, U., V. Brovkin, and M. Claussen, 2012: The influence of vegetation dynamics on anthropogenic climate change. *Earth Syst. Dyn.*, **3**, 233–243.

Power, S., and G. Kociuba, 2011a: The impact of global warming on the Southern Oscillation Index. *Clim. Dyn.*, **37**, 1745–1754.

Power, S., F. Delage, R. Colman, and A. Moise, 2012: Consensus on twenty-first-century rainfall projections in climate models more widespread than previously thought. *J. Clim.*, **25**, 3792–3809.

Power, S. B., and G. Kociuba, 2011b: What caused the observed twentieth-century weakening of the Walker circulation? *J. Clim.*, **24**, 6501–6514.

Previdi, M., 2010: Radiative feedbacks on global precipitation. *Environ. Res. Lett.*, **5**, 025211.

Rahmstorf, S., et al., 2005: Thermohaline circulation hysteresis: A model intercomparison. *Geophys. Res. Lett.*, **32**, L23605.

Räisänen, J., 2007: How reliable are climate models? *Tellus A*, **59**, 2–29.

Räisänen, J., 2008: Warmer climate: Less or more snow? *Clim. Dyn.*, **30**, 307–319.

Räisänen, J., and L. Ruokolainen, 2006: Probabilistic forecasts of near-term climate change based on a resampling ensemble technique. *Tellus A*, **58**, 461–472.

Räisänen, J., and J. S. Ylhaisi, 2011: Cold months in a warming climate. *Geophys. Res. Lett.*, **38**, L22704.

Ramanathan, V., P. J. Crutzen, J. T. Kiehl, and D. Rosenfeld, 2001: Aerosols, climate, and the hydrologic cycle. *Science*, **294**, 2119–2124.

Ramaswamy, V., et al., 2001: Radiative forcing of climate change. In: *Climate Change 2001: The Scientific Basis. Contribution of Working Group I to the Third Assessment Report of the Intergovernmental Panel on Climate Change* [J. T. Houghton, Y. Ding, D. J. Griggs, M. Noquer, P. J. van der Linden, X. Dai, K. Maskell and C. A. Johnson (eds.)]. Cambridge University Press, Cambridge, United Kingdom and New York, NY, USA pp. 349-416.

Rammig, A., et al., 2010: Estimating the risk of Amazonian forest dieback. *New Phytologist*, **187**, 694–706.

Randall, D. A., et al., 2007: Climate models and their evaluation. In: *Climate Change 2007: The Physical Science Basis. Contribution of Working Group I to the Fourth Assessment Report of the Intergovernmental Panel on Climate Change* [Solomon, S., D. Qin, M. Manning, Z. Chen, M. Marquis, K. B. Averyt, M. Tignor and H. L. Miller (eds.)] Cambridge University Press, Cambridge, United Kingdom and New York, NY, USA, pp. 589–662.

Randalls, S., 2010: History of the 2°C climate target. *WIREs Climate Change*, **1**, 598–605.

Randel, W., and F. Wu, 2007: A stratospheric ozone profile data set for 1979–2005: Variability, trends, and comparisons with column ozone data. *J. Geophys. Res.*, **112**, D06313.

Randel, W. J., M. Park, F. Wu, and N. Livesey, 2007: A large annual cycle in ozone above the tropical tropopause linked to the Brewer-Dobson circulation. *J. Atmos. Sci.*, **64**, 4479–4488.

Randles, C., and V. Ramaswamy, 2008: Absorbing aerosols over Asia: A Geophysical Fluid Dynamics Laboratory general circulation model sensitivity study of model response to aerosol optical depth and aerosol absorption. *J. Geophys. Res.*, **113**, D21203.

Reagan, M., and G. Moridis, 2007: Oceanic gas hydrate instability and dissociation under climate change scenarios. *Geophys. Res. Lett.*, **34**, L22709.

Reagan, M., and G. Moridis, 2009: Large-scale simulation of methane hydrate dissociation along the West Spitsbergen Margin. *Geophys. Res. Lett.*, **36**, L23612.

Ridley, J., J. Lowe, and D. Simonin, 2008: The demise of Arctic sea ice during stabilisation at high greenhouse gas concentrations. *Clim. Dyn.*, **30**, 333–341.

Ridley, J., J. Lowe, C. Brierley, and G. Harris, 2007: Uncertainty in the sensitivity of Arctic sea ice to global warming in a perturbed parameter climate model ensemble. *Geophys. Res. Lett.*, **34**, L19704.

Ridley, J., J. Gregory, P. Huybrechts, and J. Lowe, 2010: Thresholds for irreversible decline of the Greenland ice sheet. *Clim. Dyn.*, **35**, 1049–1057.

Ridley, J. K., J. A. Lowe, and H. T. Hewitt, 2012: How reversible is sea ice loss? *Cryosphere*, **6**, 193–198.

Riley, W. J., et al., 2011: Barriers to predicting changes in global terrestrial methane fluxes: Analyses using CLM4ME, a methane biogeochemistry model integrated in CESM. *Biogeosciences*, **8**, 1925–1953.

Rind, D., 1987: The doubled CO_2 climate - Impact of the sea-surface temperature-gradient. *J. Atmos. Sci.*, **44**, 3235–3268.

Rinke, A., P. Kuhry, and K. Dethloff, 2008: Importance of a soil organic layer for Arctic climate: A sensitivity study with an Arctic RCM. *Geophys. Res. Lett.*, **35**, L13709.

Rive, N., A. Torvanger, T. Berntsen, and S. Kallbekken, 2007: To what extent can a long-term temperature target guide near-term climate change commitments? *Clim. Change*, **82**, 373–391.

Robinson, A., R. Calov, and A. Ganopolski, 2012: Multistability and critical thresholds of the Greenland ice sheet. *Nature Clim. Change*, **2**, 429–432.

Roeckner, E., M. A. Giorgetta, T. Crueger, M. Esch, and J. Pongratz, 2011: Historical and future anthropogenic emission pathways derived from coupled climate-carbon cycle simulations. *Clim. Change*, **105**, 91–108.

Roehrig, R., D. Bouniol, F. Guichard, F. Hourdin, and J.-L. Redelsperger, 2013: The present and future of the West African monsoon: A process-oriented assessment of CMIP5 simulations along the AMMA transect. *J. Clim.*, doi:10.1175/JCLI-D-12-00505.1.

Roesch, A., 2006: Evaluation of surface albedo and snow cover in AR4 coupled climate models. *J. Geophys. Res.*, **111**, D15111.

Rogelj, J., M. Meinshausen, and R. Knutti, 2012: Global warming under old and new scenarios using IPCC climate sensitivity range estimates. *Nature Clim. Change*, **2**, 248–253.

Rogelj, J., D. L. McCollum, B. C. O'Neill, and K. Riahi, 2013: 2020 emissions levels required to limit warming to below 2°C. *Nature Clim. Change*, **3**, 405–412.

Rogelj, J., et al., 2011: Emission pathways consistent with a 2°C global temperature limit. *Nature Clim. Change*, **1**, 413–418.

Rohling, E., and P. P. Members, 2012: Making sense of palaeoclimate sensitivity. *Nature*, **491**, 683–691.

Rohling, E., K. Grant, M. Bolshaw, A. Roberts, M. Siddall, C. Hemleben, and M. Kucera, 2009: Antarctic temperature and global sea level closely coupled over the past five glacial cycles. *Nature Geosci.*, **2**, 500–504.

Romanovsky, V. E., S. L. Smith, and H. H. Christiansen, 2010: Permafrost thermal state in the polar Northern Hemisphere during the international polar year 2007–2009: A synthesis. *Permafr. Periglac. Process.*, **21**, 106–116.

Rotstayn, L. D., S. J. Jeffrey, M. A. Collier, S. M. Dravitzki, A. C. Hirst, J. I. Syktus, and K. K. Wong, 2012: Aerosol- and greenhouse gas-induced changes in summer rainfall and circulation in the Australasian region: A study using single-forcing climate simulations. *Atmos. Chem. Phys.*, **12**, 6377–6404.

Rougier, J., 2007: Probabilistic inference for future climate using an ensemble of climate model evaluations. *Clim. Change*, **81**, 247–264.

Rougier, J., D. M. H. Sexton, J. M. Murphy, and D. Stainforth, 2009: Analyzing the climate sensitivity of the HadSM3 climate model using ensembles from different but related experiments. *J. Clim.*, **22**, 3540–3557.

Rowell, D. P., 2012: Sources of uncertainty in future changes in local precipitation. *Clim. Dyn.*, doi:10.1007/s00382–011–1210–2.

Rowlands, D. J., et al., 2012: Broad range of 2050 warming from an observationally constrained large climate model ensemble. *Nature Geosci.*, **5**, 256–260.

Ruosteenoja, K., H. Tuomenvirta, and K. Jylha, 2007: GCM-based regional temperature and precipitation change estimates for Europe under four SRES scenarios applying a super-ensemble pattern-scaling method. *Clim. Change*, **81**, 193–208.

Saenko, O. A., A. S. Gupta, and P. Spence, 2012: On challenges in predicting bottom water transport in the Southern Ocean. *J. Clim.*, **25**, 1349–1356.

Saito, K., M. Kimoto, T. Zhang, K. Takata, and S. Emori, 2007: Evaluating a high-resolution climate model: Simulated hydrothermal regimes in frozen ground regions and their change under the global warming scenario. *J. Geophys. Res.*, **112**, F02S11.

Sallée, J.-B., E. Shuckburgh, N. Bruneau, A. J. S. Meijers, T. Bracegirdle, and Z. Wang, 2013a: Assessment of Southern Ocean mixed-layer depths in CMIP5 models: Historical bias and forcing response. *J. Geophys. Res.*, doi:10.1002/jgrc.20157.

Sallée, J.-B., E. Shuckburgh, N. Bruneau, A. J. S. Meijers, T. J. Bracegirdle, Z. Wang, and T. Roy, 2013b: Assessment of Southern Ocean water mass circulation and characteristics in CMIP5 models: Historical bias and forcing response. *J. Geophys. Res.*, doi:10.1002/jgrc.20135.

12

Sanchez-Gomez, E., S. Somot, and A. Mariotti, 2009: Future changes in the Mediterranean water budget projected by an ensemble of regional climate models. *Geophys. Res. Lett.*, **36**, L21401.

Sanderson, B. M., 2011: A multimodel study of parametric uncertainty in predictions of climate response to rising greenhouse gas concentrations. *J. Clim.*, **25**, 1362–1377.

Sanderson, B. M., 2013: On the estimation of systematic error in regression-based predictions of climate sensitivity. *Clim. Change*, doi:10.1007/s10584–012–0671–6.

Sanderson, B. M., and R. Knutti, 2012: On the interpretation of constrained climate model ensembles. *Geophys. Res. Lett.*, **39**, L16708.

Sanderson, B. M., K. M. Shell, and W. Ingram, 2010: Climate feedbacks determined using radiative kernels in a multi-thousand member ensemble of AOGCMs. *Clim. Dyn.*, **35**, 1219–1236.

Sanderson, B. M., et al., 2008: Constraints on model response to greenhouse gas forcing and the role of subgrid-scale processes. *J. Clim.*, **21**, 2384–2400.

Sanderson, M. G., D. L. Hemming, and R. A. Betts, 2011: Regional temperature and precipitation changes under high-end (>= 4°C) global warming. *Philos. Trans. R. Soc. A*, **369**, 85–98.

Sanso, B., and C. Forest, 2009: Statistical calibration of climate system properties. *J. R. Stat. Soc. C*, **58**, 485–503.

Sanso, B., C. E. Forest, and D. Zantedeschi, 2008: Inferring climate system properties using a computer model. *Bayes. Anal.*, **3**, 1–37.

Sansom, P. G., D. B. Stephenson, C. A. T. Ferro, G. Zappa, and L. Shaffrey, 2013: Simple uncertainty frameworks for selecting weighting schemes and interpreting multi-model ensemble climate change experiments. *J. Clim.*, doi:10.1175/JCLI-D-12-00462.1.

Santer, B. D., T. M. L. Wigley, M. E. Schlesinger, and J. F. B. Mitchell, 1990: *Developing Climate Scenarios from Equilibrium GCM Results.* Max-Planck-Institut-für-Meteorologie Report. Max-Planck-Institut-für-Meteorologie, Hamburg, Germany, 29 pp.

Scaife, A. A., et al., 2012: Climate change projections and stratosphere-troposphere interaction. *Clim. Dyn.*, **38**, 2089–2097.

Schaefer, K., T. Zhang, L. Bruhwiler, and A. Barrett, 2011: Amount and timing of permafrost carbon release in response to climate warming. *Tellus B*, **63**, 165–180.

Schär, C., P. L. Vidale, D. Lüthi, C. Frei, C. Häberli, M. A. Liniger, and C. Appenzeller, 2004: The role of increasing temperature variability in European summer heatwaves. *Nature*, **427**, 332–336.

Scheff, J., and D. M. W. Frierson, 2012: Robust future precipitation declines in CMIP5 largely reflect the poleward expansion of model subtropical dry zones. *Geophys. Res. Lett.*, **39**, L18704.

Scheffer, M., et al., 2009: Early-warning signals for critical transitions. *Nature*, **461**, 53–59.

Schlesinger, M., 1986: Equilibrium and transient climatic warming induced by increased atmospheric CO_2. *Clim. Dyn.*, **1**, 35–51.

Schlesinger, M., et al., 2000: Geographical distributions of temperature change for scenarios of greenhouse gas and sulfur dioxide emissions. *Technol. Forecast. Soc. Change*, **65**, 167–193.

Schmidt, M. W. I., et al., 2011: Persistence of soil organic matter as an ecosystem property. *Nature*, **478**, 49–56.

Schmittner, A., et al., 2011: Climate sensitivity estimated from temperature reconstructions of the Last Glacial Maximum. *Science*, **334**, 1385–1388.

Schneider von Deimling, T., H. Held, A. Ganopolski, and S. Rahmstorf, 2006: Climate sensitivity estimated from ensemble simulations of glacial climate. *Clim. Dyn.*, **27**, 149–163.

Schneider von Deimling, T., M. Meinshausen, A. Levermann, V. Huber, K. Frieler, D. Lawrence, and V. Brovkin, 2012: Estimating the near-surface permafrost-carbon feedback on global warming. *Biogeosciences*, **9**, 649–665.

Schoof, C., 2007: Ice sheet grounding line dynamics: Steady states, stability, and hysteresis. *J. Geophys. Res.*, **112**, F03S28.

Schröder, D., and W. M. Connolley, 2007: Impact of instantaneous sea ice removal in a coupled general circulation model. *Geophys. Res. Lett.*, **34**, L14502.

Schuenemann, K. C., and J. J. Cassano, 2010: Changes in synoptic weather patterns and Greenland precipitation in the 20th and 21st centuries: 2. Analysis of 21st century atmospheric changes using self-organizing maps. *J. Geophys. Res.*, **115**, D05108.

Schuur, E., J. Vogel, K. Crummer, H. Lee, J. Sickman, and T. Osterkamp, 2009: The effect of permafrost thaw on old carbon release and net carbon exchange from tundra. *Nature*, **459**, 556–559.

Schwalm, C. R., et al., 2012: Reduction in carbon uptake during turn of the century drought in western North America. *Nature Geosci.*, **5**, 551–556.

Schwartz, S., R. Charlson, R. Kahn, J. Ogren, and H. Rodhe, 2010: Why hasn't Earth warmed as much as expected? *J. Clim.*, **23**, 2453–2464.

Schwartz, S., R. Charlson, R. Kahn, J. Ogren, and H. Rodhe, 2012: Reply to "Comments on 'Why hasn't Earth warmed as much as expected?'". *J. Clim.*, **25**, 2200–2204.

Schwartz, S. E., 2012: Determination of Earth's transient and equilibrium climate sensitivities from observations over the twentieth century: Strong dependence on assumed forcing. *Surv. Geophys.*, **33**, 745–777.

Schweiger, A., R. Lindsay, J. Zhang, M. Steele, H. Stern, and R. Kwok, 2011: Uncertainty in modeled Arctic sea ice volume. *J. Geophys. Res.*, **116**, C00D06.

Screen, J., and I. Simmonds, 2010: The central role of diminishing sea ice in recent Arctic temperature amplification. *Nature*, **464**, 1334–1337.

Screen, J. A., N. P. Gillett, A. Y. Karpechko, and D. P. Stevens, 2010: Mixed layer temperature response to the Southern Annular Mode: Mechanisms and model representation. *J. Clim.*, **23**, 664–678.

Seager, R., and G. A. Vecchi, 2010: Greenhouse warming and the 21st century hydroclimate of the southwestern North America. *Proc. Natl. Acad. Sci. U.S.A.*, **107**, 21277–21282.

Seager, R., and N. Naik, 2012: A mechanisms-based approach to detecting recent anthropogenic hydroclimate change. *J. Clim.*, **25**, 236–261.

Seager, R., N. Naik, and G. A. Vecchi, 2010: Thermodynamic and dynamic mechanisms for large-scale changes in the hydrological cycle in response to global warming. *J. Clim.*, **23**, 4651–4668.

Seager, R., et al., 2007: Model projections of an imminent transition to a more arid climate in southwestern North America. *Science*, **316**, 1181–1184.

Sedláček, J., R. Knutti, O. Martius, and U. Beyerle, 2011: Impact of a reduced Arctic sea ice cover on ocean and atmospheric properties. *J. Clim.*, **25**, 307–319.

Seidel, D., and W. Randel, 2007: Recent widening of the tropical belt: Evidence from tropopause observations. *J. Geophys. Res.*, **112**, D20113.

Seidel, D. J., Q. Fu, W. J. Randel, and T. J. Reichler, 2008: Widening of the tropical belt in a changing climate. *Nature Geosci.*, **1**, 21–24.

Sen Gupta, A., A. Santoso, A. Taschetto, C. Ummenhofer, J. Trevena, and M. England, 2009: Projected changes to the Southern Hemisphere ocean and sea ice in the IPCC AR4 climate models. *J. Clim.*, **22**, 3047–3078.

Seneviratne, S. I., D. Lüthi, M. Litschi, and C. Schär, 2006: Land-atmosphere coupling and climate change in Europe. *Nature*, **443**, 205–209.

Seneviratne, S. I., et al., 2010: Investigating soil moisture-climate interactions in a changing climate: A review. *Earth Sci. Rev.*, **99**, 125–161.

Seneviratne, S. I., et al., 2012: Changes in climate extremes and their impacts on the natural physical environment. In: *Managing the Risks of Extreme Events and Disasters to Advance Climate Change Adaptation. A Special Report of Working Groups I and II of the Intergovernmental Panel on Climate Change* (*IPCC*) [C. B. Field, et al. (eds.)]. Cambridge University Press, Cambridge, United Kingdom, and New York, NY, USA, pp. 109–230.

Senior, C. A., and J. F. B. Mitchell, 2000: The time-dependence of climate sensitivity. *Geophys. Res. Lett.*, **27**, 2685–2688.

Serreze, M., A. Barrett, J. Stroeve, D. Kindig, and M. Holland, 2009: The emergence of surface-based Arctic amplification. *Cryosphere*, **3**, 11–19.

Serreze, M. C., and J. A. Francis, 2006: The Arctic amplification debate. *Clim. Change*, **76**, 241–264.

Sexton, D., H. Grubb, K. Shine, and C. Folland, 2003: Design and analysis of climate model experiments for the efficient estimation of anthropogenic signals. *J. Clim.*, **16**, 1320–1336.

Sexton, D. M. H., and J. M. Murphy, 2012: Multivariate probabilistic projections using imperfect climate models. Part II: Robustness of methodological choices and consequences for climate sensitivity. *Clim. Dyn.*, 2543–2558.

Sexton, D. M. H., J. M. Murphy, M. Collins, and M. J. Webb, 2012: Multivariate probabilistic projections using imperfect climate models. Part I: Outline of methodology. *Clim. Dyn.*, 2513–2542.

Shepherd, T. G., and C. McLandress, 2011: A robust mechanism for strengthening of the Brewer-Dobson circulation in response to climate change: Critical-layer control of subtropical wave breaking. *J. Atmos. Sci.*, **68**, 784–797.

Sherwood, S. C., 2010: Direct versus indirect effects of tropospheric humidity changes on the hydrologic cycle. *Environ. Res. Lett.*, **5**, 025206.

Sherwood, S. C., and M. Huber, 2010: An adaptability limit to climate change due to heat stress. *Proc. Natl. Acad. Sci. U.S.A.*, **107**, 9552–9555.

Sherwood, S. C., W. Ingram, Y. Tsushima, M. Satoh, M. Roberts, P. L. Vidale, and P. A. O'Gorman, 2010: Relative humidity changes in a warmer climate. *J. Geophys. Res.*, **115**, D09104.

Shindell, D., et al., 2012: Simultaneously mitigating near-term climate change and improving human health and food security. *Science*, **335**, 183–189.

Shindell, D. T., et al., 2006: Simulations of preindustrial, present-day, and 2100 conditions in the NASA GISS composition and climate model G-PUCCINI. *Atmos. Chem. Phys.*, **6**, 4427–4459.

Shindell, D. T., et al., 2013a: Interactive ozone and methane chemistry in GISS-E2 historical and future climate simulations. *Atmos. Chem. Phys.*, **13**, 2653–2689.

Shindell, D. T., et al., 2013b: Radiative forcing in the ACCMIP historical and future climate simulations. *Atmos. Chem. Phys.*, **13**, 2939–2974.

Shine, K. P., J. Cook, E. J. Highwood, and M. M. Joshi, 2003: An alternative to radiative forcing for estimating the relative importance of climate change mechanisms. *Geophys. Res. Lett.*, **30**, 2047.

Shiogama, H., S. Emori, K. Takahashi, T. Nagashima, T. Ogura, T. Nozawa, and T. Takemura, 2010a: Emission scenario dependency of precipitation on global warming in the MIROC3.2 model. *J. Clim.*, **23**, 2404–2417.

Shiogama, H., et al., 2010b: Emission scenario dependencies in climate change assessments of the hydrological cycle. *Clim. Change*, **99**, 321–329.

Shkolnik, I., E. Nadyozhina, T. Pavlova, E. Molkentin, and A. Semioshina, 2010: Snow cover and permafrost evolution in Siberia as simulated by the MGO regional climate model in the 20th and 21st centuries. *Environ. Res. Lett.*, **5**, 015005.

Shongwe, M. E., G. J. van Oldenborgh, B. van den Hurk, and M. van Aalst, 2011: Projected changes in mean and extreme precipitation in Africa under global warming. Part II: East Africa. *J. Clim.*, **24**, 3718–3733.

Siegenthaler, U., and H. Oeschger, 1984: Transient temperature changes due to increasing CO_2 using simple models. *Ann. Glaciol.*, **5**, 153–159.

Sigmond, M., P. C. Siegmund, E. Manzini, and H. Kelder, 2004: A simulation of the separate climate effects of middle-atmosphere and tropospheric CO_2 doubling. *J. Clim.*, **17**, 2352–2367.

Sillmann, J., and E. Roeckner, 2008: Indices for extreme events in projections of anthropogenic climate change. *Clim. Change*, **86**, 83–104.

Sillmann, J., and M. Croci-Maspoli, 2009: Present and future atmospheric blocking and its impact on European mean and extreme climate. *Geophys. Res. Lett.*, **36**, L10702.

Sillmann, J., V. V. Kharin, F. W. Zwiers, X. Zhang, and D. Bronaugh, 2013: Climate extremes indices in the CMIP5 multimodel ensemble: Part 2. Future climate projections. *J. Geophys. Res.*, **118**, 2473–2493.

Simmons, A. J., K. M. Willett, P. D. Jones, P. W. Thorne, and D. P. Dee, 2010: Low-frequency variations in surface atmospheric humidity, temperature, and precipitation: Inferences from reanalyses and monthly gridded observational data sets. *J. Geophys. Res.*, **115**, D01110.

Simpkins, G. R., and A. Y. Karpechko, 2012: Sensitivity of the southern annular mode to greenhouse gas emission scenarios. *Clim. Dyn.*, **38**, 563–572.

Slater, A. G., and D. M. Lawrence, 2013: Diagnosing present and future permafrost from climate models. *J. Clim.*, doi:10.1175/JCLI-D-12-00341.1.

Smeets, E. M. W., L. F. Bouwmanw, E. Stehfest, D. P. van Vuuren, and A. Posthuma, 2009: Contribution of N_2O to the greenhouse gas balance of first-generation biofuels. *Global Change Biol.*, **15**, 1–23.

Smith, L., Y. Sheng, G. MacDonald, and L. Hinzman, 2005: Disappearing Arctic lakes. *Science*, **308**, 1429–1429.

Smith, L., et al., 2004: Siberian peatlands a net carbon sink and global methane source since the early Holocene. *Science*, **303**, 353–356.

Smith, R. L., C. Tebaldi, D. Nychka, and L. O. Mearns, 2009: Bayesian modeling of uncertainty in ensembles of climate models. *J. Am. Stat. Assoc.*, **104**, 97–116.

Smith, S. J., J. van Aardenne, Z. Klimont, R. J. Andres, A. Volke, and S. Delgado Arias, 2011: Anthropogenic sulfur dioxide emissions: 1850–2005. *Atmos. Chem. Phys.*, **11**, 1101–1116.

Smith, S. M., J. A. Lowe, N. H. A. Bowerman, L. K. Gohar, C. Huntingford, and M. R. Allen, 2012: Equivalence of greenhouse-gas emissions for peak temperature limits. *Nature Clim. Change*, **2**, 535–538.

Sobel, A. H., and S. J. Camargo, 2011: Projected future seasonal changes in tropical summer climate. *J. Clim.*, **24**, 473–487.

Soden, B., I. Held, R. Colman, K. Shell, J. Kiehl, and C. Shields, 2008: Quantifying climate feedbacks using radiative kernels. *J. Clim.*, **21**, 3504–3520.

Soden, B. J., and I. M. Held, 2006: An assessment of climate feedbacks in coupled ocean-atmosphere models. *J. Clim.*, **19**, 3354–3360.

Soden, B. J., and G. A. Vecchi, 2011: The vertical distribution of cloud feedback in coupled ocean-atmosphere models. *Geophys. Res. Lett.*, **38**, L12704.

Sohn, B. J., and S.-C. Park, 2010: Strengthened tropical circulations in past three decades inferred from water vapor transport. *J. Geophys. Res.*, **115**, D15112.

Sokolov, A. P., et al., 2009: Probabilistic forecast for twenty-first-century climate based on uncertainties in emissions (without policy) and climate parameters. *J. Clim.*, **23**, 2230–2231.

Solgaard, A. M., and P. L. Langen, 2012: Multistability of the Greenland ice sheet and the effects of an adaptive mass balance formulation. *Clim. Dyn.*, **39**, 1599–1612.

Solomon, S., G. Plattner, R. Knutti, and P. Friedlingstein, 2009: Irreversible climate change due to carbon dioxide emissions. *Proc. Natl. Acad. Sci. U.S.A.*, **106**, 1704–1709.

Solomon, S., J. Daniel, T. Sanford, D. Murphy, G. Plattner, R. Knutti, and P. Friedlingstein, 2010: Persistence of climate changes due to a range of greenhouse gases. *Proc. Natl. Acad. Sci. U.S.A.*, **107**, 18354–18359.

Solomon, S., et al., 2007: Technical Summary. In: *Climate Change 2007: The Physical Science Basis. Contribution of Working Group I to the Fourth Assessment Report of the Intergovernmental Panel on Climate Change* [Solomon, S., D. Qin, M. Manning, Z. Chen, M. Marquis, K. B. Averyt, M. Tignor and H. L. Miller (eds.)] Cambridge University Press, Cambridge, United Kingdom and New York, NY, USA, pp. 19–92.

Son, S. W., et al., 2010: Impact of stratospheric ozone on Southern Hemisphere circulation change: A multimodel assessment. *J. Geophys. Res.*, **115**, D00M07.

Sorensson, A., C. Menendez, R. Ruscica, P. Alexander, P. Samuelsson, and U. Willen, 2010: Projected precipitation changes in South America: A dynamical downscaling within CLARIS. *Meteorol. Z.*, **19**, 347–355.

Spence, P., O. A. Saenko, C. O. Dufour, J. Le Sommer, and M. H. England, 2012: Mechanisms maintaining Southern Ocean meridional heat transport under projected wind forcing. *J. Phys. Oceanogr.*, **42**, 1923–1931.

St. Clair, S., J. Hillier, and P. Smith, 2008: Estimating the pre-harvest greenhouse gas costs of energy crop production. *Biomass Bioenerg.*, **32**, 442–452.

Stachnik, J. P., and C. Schumacher, 2011: A comparison of the Hadley circulation in modern reanalyses. *J. Geophys. Res.*, **116**, D22102.

Stephenson, D. B., M. Collins, J. C. Rougier, and R. E. Chandler, 2012: Statistical problems in the probabilistic prediction of climate change. *Environmetrics*, **23**, 364–372.

Sterl, A., et al., 2008: When can we expect extremely high surface temperatures? *Geophys. Res. Lett.*, **35**, L14703.

Stott, P., G. Jones, and J. Mitchell, 2003: Do models underestimate the solar contribution to recent climate change? *J. Clim.*, **16**, 4079–4093.

Stott, P., P. Good, G. A. Jones, N. Gillett, and E. Hawkins, 2013: The upper end of climate model temperature projections is inconsistent with past warming. *Environ. Res. Lett.*, **8**, 014024.

Stouffer, R., 2004: Time scales of climate response. *J. Clim.*, **17**, 209–217.

Stouffer, R. J., and S. Manabe, 1999: Response of a coupled ocean-atmosphere model to increasing atmospheric carbon dioxide: Sensitivity to the rate of increase. *J. Clim.*, **12**, 2224–2237.

Stowasser, M., H. Annamalai, and J. Hafner, 2009: Response of the South Asian summer monsoon to global warming: Mean and synoptic systems. *J. Clim.*, **22**, 1014–1036.

Stroeve, J., M. Holland, W. Meier, T. Scambos, and M. Serreze, 2007: Arctic sea ice decline: Faster than forecast. *Geophys. Res. Lett.*, **34**, L09501.

Stroeve, J. C., V. Kattsov, A. Barrett, M. Serreze, T. Pavlova, M. Holland, and W. N. Meier, 2012: Trends in Arctic sea ice extent from CMIP5, CMIP3 and observations. *Geophys. Res. Lett.*, **39**, L16502.

Stuber, N., M. Ponater, and R. Sausen, 2005: Why radiative forcing might fail as a predictor of climate change. *Clim. Dyn.*, **24**, 497–510.

Sudo, K., M. Takahashi, and H. Akimoto, 2003: Future changes in stratosphere-troposphere exchange and their impacts on future tropospheric ozone simulations. *Geophys. Res. Lett.*, **30**, 2256.

Sugiyama, M., H. Shiogama, and S. Emori, 2010: Precipitation extreme changes exceeding moisture content increases in MIROC and IPCC climate models. *Proc. Natl. Acad. Sci. U.S.A.*, **107**, 571–575.

Sun, Y., S. Solomon, A. Dai, and R. W. Portmann, 2007: How often will it rain? *J. Clim.*, **20**, 4801–4818.

Sutton, R. T., B. W. Dong, and J. M. Gregory, 2007: Land/sea warming ratio in response to climate change: IPCC AR4 model results and comparison with observations. *Geophys. Res. Lett.*, **34**, L02701.

Swann, A. L., I. Y. Fung, S. Levis, G. B. Bonan, and S. C. Doney, 2010: Changes in Arctic vegetation amplify high-latitude warming through the greenhouse effect. *Proc. Natl. Acad. Sci. U.S.A.*, **107**, 1295–1300.

Swart, N. C., and J. C. Fyfe, 2012: Observed and simulated changes in the Southern Hemisphere surface westerly wind-stress. *Geophys. Res. Lett.*, **39**, L16711.

Swingedouw, D., P. Braconnot, P. Delecluse, E. Guilyardi, and O. Marti, 2007: Quantifying the AMOC feedbacks during a $2xCO_2$ stabilization experiment with land-ice melting. *Clim. Dyn.*, **29**, 521–534.

Swingedouw, D., T. Fichefet, P. Huybrechts, H. Goosse, E. Driesschaert, and M. Loutre, 2008: Antarctic ice-sheet melting provides negative feedbacks on future climate warming. *Geophys. Res. Lett.*, **35**, L17705.

Szopa, S., et al., 2013: Aerosol and ozone changes as forcing for climate evolution between 1850 and 2100. *Clim. Dyn.*, **40**, 2223–2250.

Takahashi, K., 2009a: Radiative constraints on the hydrological cycle in an idealized radiative-convective equilibrium model. *J. Atmos. Sci.*, **66**, 77–91.

Takahashi, K., 2009b: The global hydrological cycle and atmospheric shortwave absorption in climate models under CO_2 forcing. *J. Clim.*, **22**, 5667–5675.

Tanaka, K., and T. Raddatz, 2011: Correlation between climate sensitivity and aerosol forcing and its implication for the "climate trap". *Clim. Change*, **109**, 815–825.

Tarnocai, C., J. Canadell, E. Schuur, P. Kuhry, G. Mazhitova, and S. Zimov, 2009: Soil organic carbon pools in the northern circumpolar permafrost region. *Global Biogeochem. Cycles*, **23**, GB2023.

Taylor, K. E., R. J. Stouffer, and G. A. Meehl, 2012: A summary of the CMIP5 experiment design. *Bull. Am. Meteorol. Soc.*, **93**, 485–498.

Tebaldi, C., and R. Knutti, 2007: The use of the multi-model ensemble in probabilistic climate projections. *Philos. Trans. R. Soc. A*, **365**, 2053–2075.

Tebaldi, C., and D. B. Lobell, 2008: Towards probabilistic projections of climate change impacts on global crop yields. *Geophys. Res. Lett.*, **35**, L08705.

Tebaldi, C., and B. Sanso, 2009: Joint projections of temperature and precipitation change from multiple climate models: A hierarchical Bayesian approach. *J. R. Stat. Soc. A*, **172**, 83–106.

Tebaldi, C., J. M. Arblaster, and R. Knutti, 2011: Mapping model agreement on future climate projections. *Geophys. Res. Lett.*, **38**, L23701.

Tebaldi, C., K. Hayhoe, J. M. Arblaster, and G. A. Meehl, 2006: Going to the extremes. *Clim. Change*, **79**, 185–211.

Terray, L., L. Corre, S. Cravatte, T. Delcroix, G. Reverdin, and A. Ribes, 2012: Near-surface salinity as nature's rain gauge to detect human influence on the tropical water cycle. *J. Clim.*, **25**, 958–977.

Thorne, P., 2008: Arctic tropospheric warming amplification? *Nature*, **455**, E1–E2.

Tietsche, S., D. Notz, J. H. Jungclaus, and J. Marotzke, 2011: Recovery mechanisms of Arctic summer sea ice. *Geophys. Res. Lett.*, **38**, L02707.

Tjiputra, J. F., et al., 2013: Evaluation of the carbon cycle components in the Norwegian Earth System Model (NorESM). *Geosci. Model Dev.*, **6**, 301–325.

Tokinaga, H., S.-P. Xie, C. Deser, Y. Kosaka, and Y. M. Okumura, 2012: Slowdown of the Walker circulation driven by tropical Indo-Pacific warming. *Nature*, **491**, 439–443.

Trapp, R. J., N. S. Diffenbaugh, and A. Gluhovsky, 2009: Transient response of severe thunderstorm forcing to elevated greenhouse gas concentrations. *Geophys. Res. Lett.*, **36**, L01703.

Trapp, R. J., N. S. Diffenbaugh, H. E. Brooks, M. E. Baldwin, E. D. Robinson, and J. S. Pal, 2007: Changes in severe thunderstorm environment frequency during the 21st century caused by anthropogenically enhanced global radiative forcing. *Proc. Natl. Acad. Sci. U.S.A.*, **104**, 19719–19723.

Trenberth, K. E., and D. J. Shea, 2005: Relationships between precipitation and surface temperature. *Geophys. Res. Lett.*, **32**, L14703.

Trenberth, K. E., and J. T. Fasullo, 2009: Global warming due to increasing absorbed solar radiation. *Geophys. Res. Lett.*, **36**, L07706.

Trenberth, K. E., and J. T. Fasullo, 2010: Simulation of present-day and twenty-first-century energy budgets of the Southern Oceans. *J. Clim.*, **23**, 440–454.

Turner, J., T. J. Bracegirdle, T. Phillips, G. J. Marshall, and J. S. Hosking, 2013: An initial assessment of Antarctic sea ice extent in the CMIP5 models. *J. Clim.*, **26**, 1473–1484.

Ueda, H., A. Iwai, K. Kuwako, and M. Hori, 2006: Impact of anthropogenic forcing on the Asian summer monsoon as simulated by eight GCMs. *Geophys. Res. Lett.*, **33**, L06703.

Ulbrich, U., G. C. Leckebusch, and J. G. Pinto, 2009: Extra-tropical cyclones in the present and future climate: A review. *Theor. Appl. Climatol.*, **96**, 117–131.

Ulbrich, U., et al., 2013: Are greenhouse gas signals of Northern Hemisphere winter extra-tropical cyclone activity dependent on the identification and tracking algorithm? *Meteorol. Z.*, **22**, 61–68.

UNEP, 2010: The emissions gap report: Are the Copenhagen Accord pledges sufficient to limit global warming to 2°C or 1.5°C? , 55 pp.

Utsumi, N., S. Seto, S. Kanae, E. E. Maeda, and T. Oki, 2011: Does higher surface temperature intensify extreme precipitation? *Geophys. Res. Lett.*, **38**, L16708.

Vaks, A., et al., 2013: Speleothems reveal 500,000-year history of Siberian permafrost. *Science*, **340**, 183–186.

Van Klooster, S. L., and P. J. Roebber, 2009: Surface-based convective potential in the contiguous United States in a business-as-usual future climate. *J. Clim.*, **22**, 3317–3330.

van Vuuren, D. P., et al., 2011: RCP3–PD: Exploring the possibilities to limit global mean temperature change to less than 2°C. *Clim. Change*, **109**, 95–116.

Vavrus, S., M. Holland, and D. Bailey, 2011: Changes in Arctic clouds during intervals of rapid sea ice loss. *Clim. Dyn.*, **36**, 1475–1489.

Vavrus, S. J., M. M. Holland, A. Jahn, D. A. Bailey, and B. A. Blazey, 2012: Twenty-first-century Arctic climate change in CCSM4. *J. Clim.*, **25**, 2696–2710.

Vecchi, G. A., and B. J. Soden, 2007: Global warming and the weakening of the tropical circulation. *Bull. Am. Meteorol. Soc.*, **88**, 1529–1530.

Vecchi, G. A., B. J. Soden, A. T. Wittenberg, I. M. Held, A. Leetmaa, and M. J. Harrison, 2006: Weakening of tropical Pacific atmospheric circulation due to anthropogenic forcing. *Nature*, **441**, 73–76.

Vial, J., J.-L. Dufresne, and S. Bony, 2013: On the interpretation of inter-model spread in CMIP5 climate sensitivity estimates. *Clim. Dyn.*, doi:10.1007/s00382-013-1725-9.

Vidale, P. L., D. Lüthi, R. Wegmann, and C. Schär, 2007: European summer climate variability in a heterogeneous multi-model ensemble. *Clim. Change*, **81**, 209–232.

Voldoire, A., et al., 2013: The CNRM-CM5.1 global climate model: Description and basic evaluation. *Clim. Dyn.*, **40**, 2091–2121.

Voss, R., and U. Mikolajewicz, 2001: Long-term climate changes due to increased CO_2 concentration in the coupled atmosphere-ocean general circulation model ECHAM3/LSG. *Clim. Dyn.*, **17**, 45–60.

Wadhams, P., 2012: Arctic ice cover, ice thickness and tipping points. *Ambio*, **41**, 23–33.

Walker, R., et al., 2009: Protecting the Amazon with protected areas. *Proc. Natl. Acad. Sci. U.S.A.*, **106**, 10582–10586.

Wang, M., and J. Overland, 2009: A sea ice free summer Arctic within 30 years? *Geophys. Res. Lett.*, **36**, L07502.

Wang, M., and J. E. Overland, 2012: A sea ice free summer Arctic within 30 years: An update from CMIP5 models. *Geophys. Res. Lett.*, **39**, L18501.

Wania, R., I. Ross, and I. Prentice, 2009: Integrating peatlands and permafrost into a dynamic global vegetation model: 2. Evaluation and sensitivity of vegetation and carbon cycle processes. *Global Biogeochem. Cycles*, **23**, GB3015.

Washington, W., et al., 2009: How much climate change can be avoided by mitigation? *Geophys. Res. Lett.*, **36**, L08703.

Watanabe, S., et al., 2011: MIROC-ESM 2010: Model description and basic results of CMIP5-20c3m experiments. *Geosci. Model Dev.*, **4**, 845–872.

Watterson, I. G., 2008: Calculation of probability density functions for temperature and precipitation change under global warming. *J. Geophys. Res.*, **113**, D12106.

Watterson, I. G., 2011: Calculation of joint PDFs for climate change with properties matching recent Australian projections. *Aust. Meteorol. Oceanogr. J.*, **61**, 211–219.

Watterson, I. G., and P. H. Whetton, 2011a: Joint PDFs for Australian climate in future decades and an idealized application to wheat crop yield. *Aust. Meteorol. Oceanogr. J.*, **61**, 221–230.

Watterson, I. G., and P. H. Whetton, 2011b: Distributions of decadal means of temperature and precipitation change under global warming. *J. Geophys. Res.*, **116**, D07101.

Watterson, I. G., J. L. McGregor, and K. C. Nguyen, 2008: Changes in extreme temperatures of Australasian summer simulated by CCAM under global warming, and the roles of winds and land-sea contrasts. *Aust. Meteorol. Mag.*, **57**, 195–212.

WBGU, 2009: *Solving the Climate Dilemma: The Budget Approach.* German Advisory Council on Global Change, Berlin, 59 pp.

Weaver, A., K. Zickfeld, A. Montenegro, and M. Eby, 2007: Long term climate implications of 2050 emission reduction targets. *Geophys. Res. Lett.*, **34**, L19703.
Weaver, A. J., et al., 2012: Stability of the Atlantic meridional overturning circulation: A model intercomparison. *Geophys. Res. Lett.*, **39**, L20709.
Webb, M., et al., 2006: On the contribution of local feedback mechanisms to the range of climate sensitivity in two GCM ensembles. *Clim. Dyn.*, **27**, 17–38.
Webb, M. J., F. H. Lambert, and J. M. Gregory, 2013: Origins of differences in climate sensitivity, forcing and feedback in climate models. *Clim. Dyn.*, **40**, 677–707.
Weber, S., et al., 2007: The modern and glacial overturning circulation in the Atlantic Ocean in PMIP coupled model simulations. *Clim. Past*, **3**, 51–64.
Weertman, J., 1974: Stability of the junction of an ice sheet and an ice shelf. J. Glaciol., **13**, 3–11.
Wehner, M., D. Easterling, J. Lawrimore, R. Heim, R. Vose, and B. Santer, 2011: Projections of future drought in the continental United States and Mexico. *J. Hydrometeorol.*, **12**, 1359–1377.
Weigel, A., R. Knutti, M. Liniger, and C. Appenzeller, 2010: Risks of model weighting in multimodel climate projections. *J. Clim.*, **23**, 4175–4191.
Wentz, F., L. Ricciardulli, K. Hilburn, and C. Mears, 2007: How much more rain will global warming bring? *Science*, **317**, 233–235.
Wetherald, R., and S. Manabe, 1988: Cloud feedback processes in a General-Circulation Model. *J. Atmos. Sci.*, **45**, 1397–1415.
Wetherald, R. T., R. J. Stouffer, and K. W. Dixon, 2001: Committed warming and its implications for climate change. *Geophys. Res. Lett.*, **28**, 1535–1538.
Wigley, T. M. L., 2005: The climate change commitment. *Science*, **307**, 1766–1769.
Wilcox, L. J., A. J. Charlton-Perez, and L. J. Gray, 2012: Trends in Austral jet position in ensembles of high- and low-top CMIP5 models. *J. Geophys. Res.*, **117**, D13115.
Willett, K., and S. Sherwood, 2012: Exceedance of heat index thresholds for 15 regions under a warming climate using the wet-bulb globe temperature. *Int. J. Climatol.*, **32**, 161–177.
Williams, J. W., S. T. Jackson, and J. E. Kutzbach, 2007: Projected distributions of novel and disappearing climates by 2100 AD. *Proc. Natl. Acad. Sci. U.S.A.*, **104**, 5738–5742.
Williams, K. D., W. J. Ingram, and J. M. Gregory, 2008: Time variation of effective climate sensitivity in GCMs. *J. Clim.*, **21**, 5076–5090.
Winton, M., 2006a: Amplified Arctic climate change: What does surface albedo feedback have to do with it? *Geophys. Res. Lett.*, **33**, L03701.
Winton, M., 2006b: Does the Arctic sea ice have a tipping point? *Geophys. Res. Lett.*, **33**, L23504.
Winton, M., 2008: Sea ice-albedo feedback and nonlinear Arctic climate change. In: *Arctic Sea Ice Decline: Observations, Projections, Mechanisms, and Implications* [E. T. DeWeaver, C. M. Bitz and L. B. Tremblay (eds.)]. American Geophysical Union, Washington, DC, pp. 111–131.
Winton, M., 2011: Do climate models underestimate the sensitivity of Northern Hemisphere sea ice cover? *J. Clim.*, **24**, 3924–3934.
WMO, 2007: Scientific assessment of ozone depletion. In: *2006, Global Ozone Research and Monitoring Project*. World Meteorological Organization, Geneva, Switzerland, 572 pp.
Wood, R., A. Keen, J. Mitchell, and J. Gregory, 1999: Changing spatial structure of the thermohaline circulation in response to atmospheric CO_2 forcing in a climate model. *Nature*, **399**, 572–575.
Woollings, T., 2008: Vertical structure of anthropogenic zonal-mean atmospheric circulation change. *Geophys. Res. Lett.*, **35**, L19702.
Woollings, T., and M. Blackburn, 2012: The North Atlantic jet stream under climate change and its relation to the NAO and EA patterns. *J. Clim.*, **25**, 886–902.
Woollings, T., J. M. Gregory, J. G. Pinto, M. Reyers, and D. J. Brayshaw, 2012: Response of the North Atlantic storm track to climate change shaped by ocean-atmosphere coupling. *Nature Geosci.*, **5**, 313–317.
Wu, P., R. Wood, J. Ridley, and J. Lowe, 2010: Temporary acceleration of the hydrological cycle in response to a CO_2 rampdown. *Geophys. Res. Lett.*, **37**, L12705.
Wu, P., L. Jackson, A. Pardaens, and N. Schaller, 2011a: Extended warming of the northern high latitudes due to an overshoot of the Atlantic meridional overturning circulation. *Geophys. Res. Lett.*, **38**, L24704.
Wu, T., et al., 2013: Global carbon budgets simulated by the Beijing Climate Center Climate System Model for the last century. *J. Geophys. Res.*, doi:10.1002/jgrd.50320.
Wu, Y., M. Ting, R. Seager, H.-P. Huang, and M. A. Cane, 2011b: Changes in storm tracks and energy transports in a warmer climate simulated by the GFDL CM2.1 model. *Clim. Dyn.*, **37**, 53–72.
Wyant, M. C., et al., 2006: A comparison of low-latitude cloud properties and their response to climate change in three AGCMs sorted into regimes using mid-tropospheric vertical velocity. *Clim. Dyn.*, **27**, 261–279.
Xie, P., and G. Vallis, 2012: The passive and active nature of ocean heat uptake in idealized climate change experiments. *Clim. Dyn.*, **38**, 667–684.
Xie, S. P., C. Deser, G. A. Vecchi, J. Ma, H. Y. Teng, and A. T. Wittenberg, 2010: Global warming pattern formation: Sea surface temperature and rainfall. *J. Clim.*, **23**, 966–986.
Xin, X., L. Zhang, J. Zhang, T. Wu, and Y. Fang, 2013a: Climate change projections over East Asia with BCC_CSM1.1 climate model under RCP scenarios. *J. Meteorol. Soc. Jpn.*, **4**, 413-429.
Xin, X., T. Wu, J. Li, Z. Wang, W. Li, and F. Wu, 2013b: How well does BCC_CSM1.1 reproduce the 20th century climate change in China? *Atmos. Ocean. Sci. Lett.*, **6**, 21–26.
Yang, F. L., A. Kumar, M. E. Schlesinger, and W. Q. Wang, 2003: Intensity of hydrological cycles in warmer climates. *J. Clim.*, **16**, 2419–2423.
Yin, J., J. Overpeck, S. Griffies, A. Hu, J. Russell, and R. Stouffer, 2011: Different magnitudes of projected subsurface ocean warming around Greenland and Antarctica. *Nature Geosci.*, **4**, 524–528.
Yokohata, T., M. Webb, M. Collins, K. Williams, M. Yoshimori, J. Hargreaves, and J. Annan, 2010: Structural similarities and differences in climate responses to CO_2 increase between two perturbed physics ensembles. *J. Clim.*, **23**, 1392–1410.
Yokohata, T., J. D. Annan, M. Collins, C. S. Jackson, M. Tobis, M. Webb, and J. C. Hargreaves, 2012: Reliability of multi-model and structurally different single-model ensembles. *Clim. Dyn.*, **39**, 599–616.
Young, P. J., K. H. Rosenlof, S. Solomon, S. C. Sherwood, Q. Fu, and J.-F. Lamarque, 2012: Changes in stratospheric temperatures and their implications for changes in the Brewer Dobson circulation, 1979–2005. *J. Clim.*, **25**, 1759–1772.
Yukimoto, S., et al., 2012: A new global climate model of the Meteorological Research Institute: MRI-CGCM3–Model description and basic performance. *J. Meteorol. Soc. Jpn.*, **90A**, 23–64.
Zappa, G., L. C. Shaffrey, K. I. Hodges, P. G. Sansom, and D. B. Stephenson, 2013: A multi-model assessment of future projections of North Atlantic and European extratropical cyclones in the CMIP5 climate models. *J. Clim.*, doi:10.1175/JCLI-D-12-00573.1.
Zelazowski, P., Y. Malhi, C. Huntingford, S. Sitch, and J. Fisher, 2011: Changes in the potential distribution of humid tropical forests on a warmer planet. *Philos. Trans. R. Soc. A*, **369**, 137–160.
Zelinka, M., and D. Hartmann, 2010: Why is longwave cloud feedback positive? *J. Geophys. Res.*, **115**, D16117.
Zelinka, M., S. Klein, and D. Hartmann, 2012: Computing and partitioning cloud feedbacks using Cloud property histograms. Part II: Attribution to changes in cloud amount, altitude, and optical depth. *J. Clim.*, **25**, 3736–3754.
Zhang, M., and H. Song, 2006: Evidence of deceleration of atmospheric vertical overturning circulation over the tropical Pacific. *Geophys. Res. Lett.*, **33**, L12701.
Zhang, M. H., and C. Bretherton, 2008: Mechanisms of low cloud-climate feedback in idealized single-column simulations with the Community Atmospheric Model, version 3 (CAM3). *J. Clim.*, **21**, 4859–4878.
Zhang, R., 2010a: Northward intensification of anthropogenically forced changes in the Atlantic meridional overturning circulation (AMOC). *Geophys. Res. Lett.*, **37**, L24603.
Zhang, T., 2005: Influence of the seasonal snow cover on the ground thermal regime: An overview. *Rev. Geophys.*, **43**, RG4002.
Zhang, T., J. A. Heginbottom, R. G. Barry, and J. Brown, 2000: Further statistics on the distribution of permafrost and ground ice in the Northern Hemisphere 1. *Polar Geogr.*, **24**, 126–131.
Zhang, X., 2010b: Sensitivity of Arctic summer sea ice coverage to global warming forcing: Towards reducing uncertainty in arctic climate change projections. *Tellus A*, **62**, 220–227.
Zhang, X., and J. Walsh, 2006: Toward a seasonally ice-covered Arctic Ocean: Scenarios from the IPCC AR4 model simulations. *J. Clim.*, **19**, 1730–1747.
Zhang, X. B., et al., 2007: Detection of human influence on twentieth-century precipitation trends. *Nature*, **448**, 461–U464.
Zhou, L. M., R. E. Dickinson, P. Dirmeyer, A. Dai, and S. K. Min, 2009: Spatiotemporal patterns of changes in maximum and minimum temperatures in multi-model simulations. *Geophys. Res. Lett.*, **36**, L02702.

Zhuang, Q., et al., 2004: Methane fluxes between terrestrial ecosystems and the atmosphere at northern high latitudes during the past century: A retrospective analysis with a process-based biogeochemistry model. *Global Biogeochem. Cycles*, **18**, GB3010.

Zickfeld, K., V. K. Arora, and N. P. Gillett, 2012: Is the climate response to CO_2 emissions path dependent? *Geophys. Res. Lett.*, **39**, L05703.

Zickfeld, K., B. Knopf, V. Petoukhov, and H. Schellnhuber, 2005: Is the Indian summer monsoon stable against global change? *Geophys. Res. Lett.*, **32**, L15707.

Zickfeld, K., M. Eby, H. Matthews, and A. Weaver, 2009: Setting cumulative emissions targets to reduce the risk of dangerous climate change. *Proc. Natl. Acad. Sci. U.S.A.*, **106**, 16129–16134.

Zickfeld, K., M. Morgan, D. Frame, and D. Keith, 2010: Expert judgments about transient climate response to alternative future trajectories of radiative forcing. *Proc. Natl. Acad. Sci. U.S.A.*, **107**, 12451–12456.

Zickfeld, K., et al., 2013: Long-term climate change commitment and reversibility: An EMIC intercomparison. *J. Clim.*, doi:10.1175/JCLI-D-12-00584.1.

Zimov, S., S. Davydov, G. Zimova, A. Davydova, E. Schuur, K. Dutta, and F. Chapin, 2006: Permafrost carbon: Stock and decomposability of a globally significant carbon pool. *Geophys. Res. Lett.*, **33**, L20502.

Zunz, V., H. Goosse, and F. Massonnet, 2013: How does internal variability influence the ability of CMIP5 models to reproduce the recent trend in Southern Ocean sea ice extent? *Cryosphere*, **7**, 451–468.

SPM

Summary for Policymakers

Drafting Authors:
Lisa V. Alexander (Australia), Simon K. Allen (Switzerland/New Zealand), Nathaniel L. Bindoff (Australia), François-Marie Bréon (France), John A. Church (Australia), Ulrich Cubasch (Germany), Seita Emori (Japan), Piers Forster (UK), Pierre Friedlingstein (UK/Belgium), Nathan Gillett (Canada), Jonathan M. Gregory (UK), Dennis L. Hartmann (USA), Eystein Jansen (Norway), Ben Kirtman (USA), Reto Knutti (Switzerland), Krishna Kumar Kanikicharla (India), Peter Lemke (Germany), Jochem Marotzke (Germany), Valérie Masson-Delmotte (France), Gerald A. Meehl (USA), Igor I. Mokhov (Russian Federation), Shilong Piao (China), Gian-Kasper Plattner (Switzerland), Qin Dahe (China), Venkatachalam Ramaswamy (USA), David Randall (USA), Monika Rhein (Germany), Maisa Rojas (Chile), Christopher Sabine (USA), Drew Shindell (USA), Thomas F. Stocker (Switzerland), Lynne D. Talley (USA), David G. Vaughan (UK), Shang-Ping Xie (USA)

Draft Contributing Authors:
Myles R. Allen (UK), Olivier Boucher (France), Don Chambers (USA), Jens Hesselbjerg Christensen (Denmark), Philippe Ciais (France), Peter U. Clark (USA), Matthew Collins (UK), Josefino C. Comiso (USA), Viviane Vasconcellos de Menezes (Australia/Brazil), Richard A. Feely (USA), Thierry Fichefet (Belgium), Arlene M. Fiore (USA), Gregory Flato (Canada), Jan Fuglestvedt (Norway), Gabriele Hegerl (UK/Germany), Paul J. Hezel (Belgium/USA), Gregory C. Johnson (USA), Georg Kaser (Austria/Italy), Vladimir Kattsov (Russian Federation), John Kennedy (UK), Albert M. G. Klein Tank (Netherlands), Corinne Le Quéré (UK), Gunnar Myhre (Norway), Timothy Osborn (UK), Antony J. Payne (UK), Judith Perlwitz (USA), Scott Power (Australia), Michael Prather (USA), Stephen R. Rintoul (Australia), Joeri Rogelj (Switzerland/Belgium), Matilde Rusticucci (Argentina), Michael Schulz (Germany), Jan Sedláček (Switzerland), Peter A. Stott (UK), Rowan Sutton (UK), Peter W. Thorne (USA/Norway/UK), Donald Wuebbles (USA)

This Summary for Policymakers should be cited as:
IPCC, 2013: Summary for Policymakers. In: *Climate Change 2013: The Physical Science Basis. Contribution of Working Group I to the Fifth Assessment Report of the Intergovernmental Panel on Climate Change* [Stocker, T.F., D. Qin, G.-K. Plattner, M. Tignor, S.K. Allen, J. Boschung, A. Nauels, Y. Xia, V. Bex and P.M. Midgley (eds.)]. Cambridge University Press, Cambridge, United Kingdom and New York, NY, USA.

A. Introduction

The Working Group I contribution to the IPCC's Fifth Assessment Report (AR5) considers new evidence of climate change based on many independent scientific analyses from observations of the climate system, paleoclimate archives, theoretical studies of climate processes and simulations using climate models. It builds upon the Working Group I contribution to the IPCC's Fourth Assessment Report (AR4), and incorporates subsequent new findings of research. As a component of the fifth assessment cycle, the IPCC Special Report on Managing the Risks of Extreme Events and Disasters to Advance Climate Change Adaptation (SREX) is an important basis for information on changing weather and climate extremes.

This Summary for Policymakers (SPM) follows the structure of the Working Group I report. The narrative is supported by a series of overarching highlighted conclusions which, taken together, provide a concise summary. Main sections are introduced with a brief paragraph in italics which outlines the methodological basis of the assessment.

The degree of certainty in key findings in this assessment is based on the author teams' evaluations of underlying scientific understanding and is expressed as a qualitative level of confidence (from *very low* to *very high*) and, when possible, probabilistically with a quantified likelihood (from *exceptionally unlikely* to *virtually certain*). Confidence in the validity of a finding is based on the type, amount, quality, and consistency of evidence (e.g., data, mechanistic understanding, theory, models, expert judgment) and the degree of agreement[1]. Probabilistic estimates of quantified measures of uncertainty in a finding are based on statistical analysis of observations or model results, or both, and expert judgment[2]. Where appropriate, findings are also formulated as statements of fact without using uncertainty qualifiers. (See Chapter 1 and Box TS.1 for more details about the specific language the IPCC uses to communicate uncertainty).

The basis for substantive paragraphs in this Summary for Policymakers can be found in the chapter sections of the underlying report and in the Technical Summary. These references are given in curly brackets.

B. Observed Changes in the Climate System

Observations of the climate system are based on direct measurements and remote sensing from satellites and other platforms. Global-scale observations from the instrumental era began in the mid-19th century for temperature and other variables, with more comprehensive and diverse sets of observations available for the period 1950 onwards. Paleoclimate reconstructions extend some records back hundreds to millions of years. Together, they provide a comprehensive view of the variability and long-term changes in the atmosphere, the ocean, the cryosphere, and the land surface.

Warming of the climate system is unequivocal, and since the 1950s, many of the observed changes are unprecedented over decades to millennia. The atmosphere and ocean have warmed, the amounts of snow and ice have diminished, sea level has risen, and the concentrations of greenhouse gases have increased (see Figures SPM.1, SPM.2, SPM.3 and SPM.4). {2.2, 2.4, 3.2, 3.7, 4.2–4.7, 5.2, 5.3, 5.5–5.6, 6.2, 13.2}

[1] In this Summary for Policymakers, the following summary terms are used to describe the available evidence: limited, medium, or robust; and for the degree of agreement: low, medium, or high. A level of confidence is expressed using five qualifiers: very low, low, medium, high, and very high, and typeset in italics, e.g., *medium confidence*. For a given evidence and agreement statement, different confidence levels can be assigned, but increasing levels of evidence and degrees of agreement are correlated with increasing confidence (see Chapter 1 and Box TS.1 for more details).

[2] In this Summary for Policymakers, the following terms have been used to indicate the assessed likelihood of an outcome or a result: virtually certain 99–100% probability, very likely 90–100%, likely 66–100%, about as likely as not 33–66%, unlikely 0–33%, very unlikely 0–10%, exceptionally unlikely 0–1%. Additional terms (extremely likely: 95–100%, more likely than not >50–100%, and extremely unlikely 0–5%) may also be used when appropriate. Assessed likelihood is typeset in italics, e.g., *very likely* (see Chapter 1 and Box TS.1 for more details).

B.1 Atmosphere

Each of the last three decades has been successively warmer at the Earth's surface than any preceding decade since 1850 (see Figure SPM.1). In the Northern Hemisphere, 1983–2012 was *likely* the warmest 30-year period of the last 1400 years (*medium confidence*). {2.4, 5.3}

- The globally averaged combined land and ocean surface temperature data as calculated by a linear trend, show a warming of 0.85 [0.65 to 1.06] °C[3], over the period 1880 to 2012, when multiple independently produced datasets exist. The total increase between the average of the 1850–1900 period and the 2003–2012 period is 0.78 [0.72 to 0.85] °C, based on the single longest dataset available[4] (see Figure SPM.1). {2.4}

- For the longest period when calculation of regional trends is sufficiently complete (1901 to 2012), almost the entire globe has experienced surface warming (see Figure SPM.1). {2.4}

- In addition to robust multi-decadal warming, global mean surface temperature exhibits substantial decadal and interannual variability (see Figure SPM.1). Due to natural variability, trends based on short records are very sensitive to the beginning and end dates and do not in general reflect long-term climate trends. As one example, the rate of warming over the past 15 years (1998–2012; 0.05 [–0.05 to 0.15] °C per decade), which begins with a strong El Niño, is smaller than the rate calculated since 1951 (1951–2012; 0.12 [0.08 to 0.14] °C per decade)[5]. {2.4}

- Continental-scale surface temperature reconstructions show, with *high confidence*, multi-decadal periods during the Medieval Climate Anomaly (year 950 to 1250) that were in some regions as warm as in the late 20th century. These regional warm periods did not occur as coherently across regions as the warming in the late 20th century (*high confidence*). {5.5}

- It is *virtually certain* that globally the troposphere has warmed since the mid-20th century. More complete observations allow greater confidence in estimates of tropospheric temperature changes in the extratropical Northern Hemisphere than elsewhere. There is *medium confidence* in the rate of warming and its vertical structure in the Northern Hemisphere extra-tropical troposphere and *low confidence* elsewhere. {2.4}

- *Confidence* in precipitation change averaged over global land areas since 1901 is *low* prior to 1951 and *medium* afterwards. Averaged over the mid-latitude land areas of the Northern Hemisphere, precipitation has increased since 1901 (*medium confidence* before and *high confidence* after 1951). For other latitudes area-averaged long-term positive or negative trends have *low confidence* (see Figure SPM.2). {TS TFE.1, Figure 2; 2.5}

- Changes in many extreme weather and climate events have been observed since about 1950 (see Table SPM.1 for details). It is *very likely* that the number of cold days and nights has decreased and the number of warm days and nights has increased on the global scale[6]. It is *likely* that the frequency of heat waves has increased in large parts of Europe, Asia and Australia. There are *likely* more land regions where the number of heavy precipitation events has increased than where it has decreased. The frequency or intensity of heavy precipitation events has *likely* increased in North America and Europe. In other continents, *confidence* in changes in heavy precipitation events is at most *medium*. {2.6}

---

3 In the WGI contribution to the AR5, uncertainty is quantified using 90% uncertainty intervals unless otherwise stated. The 90% uncertainty interval, reported in square brackets, is expected to have a 90% likelihood of covering the value that is being estimated. Uncertainty intervals are not necessarily symmetric about the corresponding best estimate. A best estimate of that value is also given where available.

4 Both methods presented in this bullet were also used in AR4. The first calculates the difference using a best fit linear trend of all points between 1880 and 2012. The second calculates the difference between averages for the two periods 1850–1900 and 2003–2012. Therefore, the resulting values and their 90% uncertainty intervals are not directly comparable. {2.4}

5 Trends for 15-year periods starting in 1995, 1996, and 1997 are 0.13 [0.02 to 0.24] °C per decade, 0.14 [0.03 to 0.24] °C per decade, and, 0.07 [–0.02 to 0.18] °C per decade, respectively.

6 See the Glossary for the definition of these terms: cold days/cold nights, warm days/warm nights, heat waves.

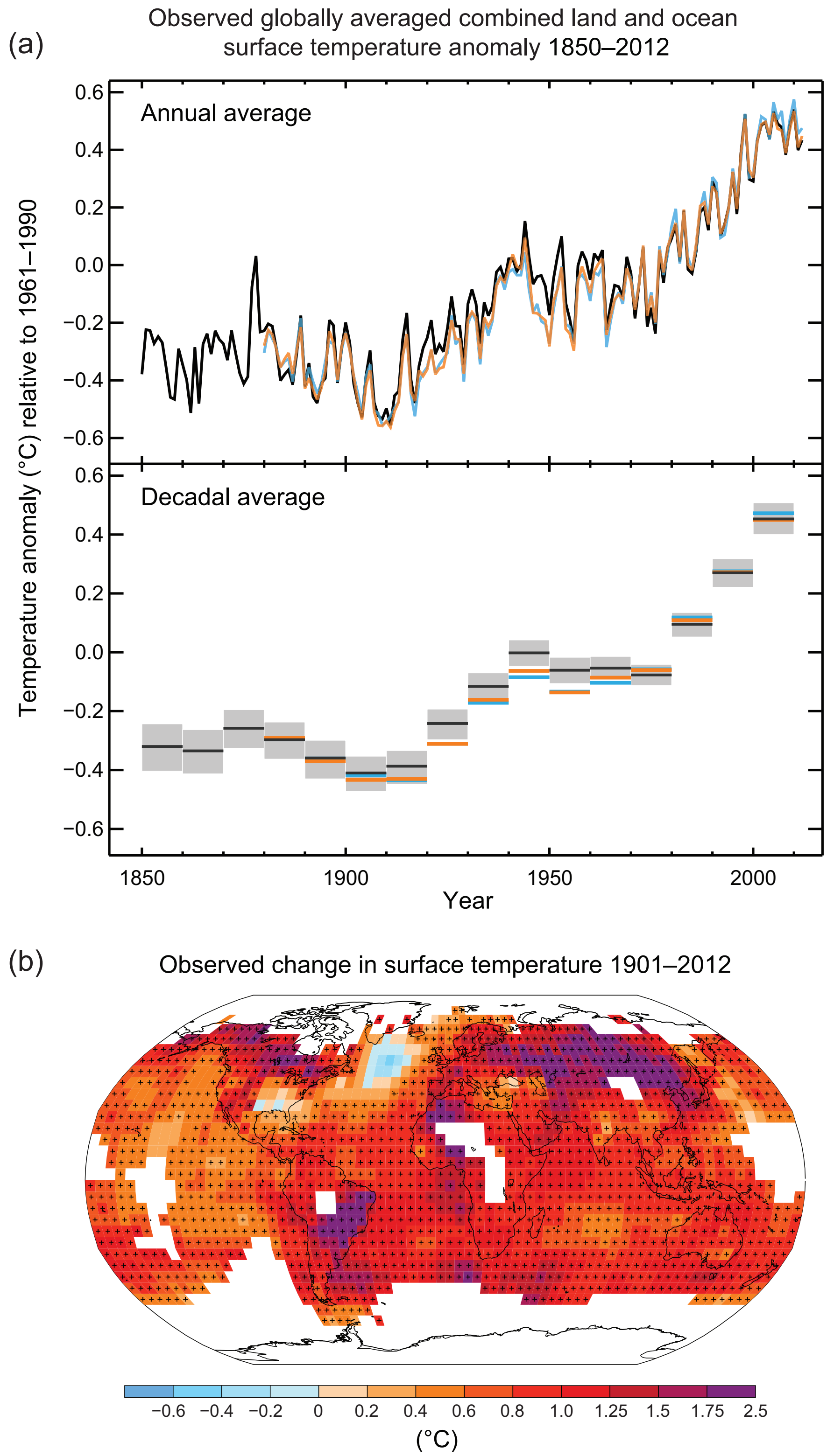

Figure SPM.1 | (a) Observed global mean combined land and ocean surface temperature anomalies, from 1850 to 2012 from three data sets. Top panel: annual mean values. Bottom panel: decadal mean values including the estimate of uncertainty for one dataset (black). Anomalies are relative to the mean of 1961−1990. (b) Map of the observed surface temperature change from 1901 to 2012 derived from temperature trends determined by linear regression from one dataset (orange line in panel a). Trends have been calculated where data availability permits a robust estimate (i.e., only for grid boxes with greater than 70% complete records and more than 20% data availability in the first and last 10% of the time period). Other areas are white. Grid boxes where the trend is significant at the 10% level are indicated by a + sign. For a listing of the datasets and further technical details see the Technical Summary Supplementary Material. {Figures 2.19–2.21; Figure TS.2}

Table SPM.1 | Extreme weather and climate events: Global-scale assessment of recent observed changes, human contribution to the changes, and projected further changes for the early (2016–2035) and late (2081–2100) 21st century. Bold indicates where the AR5 (black) provides a revised* global-scale assessment from the SREX (blue) or AR4 (red). Projections for early 21st century were not provided in previous assessment reports. Projections in the AR5 are relative to the reference period of 1986–2005, and use the new Representative Concentration Pathway (RCP) scenarios (see Box SPM.1) unless otherwise specified. See the Glossary for definitions of extreme weather and climate events.

Phenomenon and direction of trend	Assessment that changes occurred (typically since 1950 unless otherwise indicated)	Assessment of a human contribution to observed changes	Likelihood of further changes	
			Early 21st century	Late 21st century
Warmer and/or fewer cold days and nights over most land areas	*Very likely* {2.6}	***Very likely*** {10.6}	*Likely* {11.3}	*Virtually certain* {12.4}
	Very likely *Very likely*	*Likely* *Likely*		*Virtually certain* *Virtually certain*
Warmer and/or more frequent hot days and nights over most land areas	*Very likely* {2.6}	***Very likely*** {10.6}	*Likely* {11.3}	*Virtually certain* {12.4}
	Very likely *Very likely*	*Likely* *Likely* (nights only)		*Virtually certain* *Virtually certain*
Warm spells/heat waves. Frequency and/or duration increases over most land areas	***Medium confidence*** on a global scale *Likely* in large parts of Europe, Asia and Australia {2.6}	***Likely***[a] {10.6}	Not formally assessed[b] {11.3}	*Very likely* {12.4}
	Medium confidence in many (but not all) regions *Likely*	Not formally assessed *More likely than not*		*Very likely* *Very likely*
Heavy precipitation events. Increase in the frequency, intensity, and/or amount of heavy precipitation	*Likely* more land areas with increases than decreases[c] {2.6}	***Medium confidence*** {7.6, 10.6}	*Likely* over many land areas {11.3}	***Very likely*** over most of the mid-latitude land masses and over wet tropical regions {12.4}
	Likely more land areas with increases than decreases *Likely* over most land areas	*Medium confidence* *More likely than not*		*Likely* over many areas *Very likely* over most land areas
Increases in intensity and/or duration of drought	***Low confidence*** on a global scale *Likely* changes in some regions[d] {2.6}	***Low confidence*** {10.6}	*Low confidence*[g] {11.3}	***Likely*** ***(medium confidence)*** on a regional to global scale[h] {12.4}
	Medium confidence in some regions *Likely* in many regions, since 1970[e]	*Medium confidence*[f] *More likely than not*		*Medium confidence* in some regions *Likely*[e]
Increases in intense tropical cyclone activity	***Low confidence*** in long term (centennial) changes *Virtually certain* in North Atlantic since 1970 {2.6}	***Low confidence***[i] {10.6}	*Low confidence* {11.3}	***More likely than not*** in the Western North Pacific and North Atlantic[j] {14.6}
	Low confidence *Likely* in some regions, since 1970	*Low confidence* *More likely than not*		*More likely than not* in some basins *Likely*
Increased incidence and/or magnitude of extreme high sea level	*Likely* (since 1970) {3.7}	***Likely***[k] {3.7}	*Likely*[l] {13.7}	***Very likely***[l] {13.7}
	Likely (late 20th century) *Likely*	*Likely*[k] *More likely than not*[k]		*Very likely*[m] *Likely*

* The direct comparison of assessment findings between reports is difficult. For some climate variables, different aspects have been assessed, and the revised guidance note on uncertainties has been used for the SREX and AR5. The availability of new information, improved scientific understanding, continued analyses of data and models, and specific differences in methodologies applied in the assessed studies, all contribute to revised assessment findings.

Notes:

[a] Attribution is based on available case studies. It is *likely* that human influence has more than doubled the probability of occurrence of some observed heat waves in some locations.

[b] Models project near-term increases in the duration, intensity and spatial extent of heat waves and warm spells.

[c] In most continents, *confidence* in trends is not higher than *medium* except in North America and Europe where there have been *likely* increases in either the frequency or intensity of heavy precipitation with some seasonal and/or regional variation. It is *very likely* that there have been increases in central North America.

[d] The frequency and intensity of drought has *likely* increased in the Mediterranean and West Africa, and *likely* decreased in central North America and north-west Australia.

[e] AR4 assessed the area affected by drought.

[f] SREX assessed *medium confidence* that anthropogenic influence had contributed to some changes in the drought patterns observed in the second half of the 20th century, based on its attributed impact on precipitation and temperature changes. SREX assessed *low confidence* in the attribution of changes in droughts at the level of single regions.

[g] There is *low confidence* in projected changes in soil moisture.

[h] Regional to global-scale projected decreases in soil moisture and increased agricultural drought are *likely (medium confidence)* in presently dry regions by the end of this century under the RCP8.5 scenario. Soil moisture drying in the Mediterranean, Southwest US and southern African regions is consistent with projected changes in Hadley circulation and increased surface temperatures, so there is *high confidence* in *likely* surface drying in these regions by the end of this century under the RCP8.5 scenario.

[i] There is *medium confidence* that a reduction in aerosol forcing over the North Atlantic has contributed at least in part to the observed increase in tropical cyclone activity since the 1970s in this region.

[j] Based on expert judgment and assessment of projections which use an SRES A1B (or similar) scenario.

[k] Attribution is based on the close relationship between observed changes in extreme and mean sea level.

[l] There is *high confidence* that this increase in extreme high sea level will primarily be the result of an increase in mean sea level. There is *low confidence* in region-specific projections of storminess and associated storm surges.

[m] SREX assessed it to be *very likely* that mean sea level rise will contribute to future upward trends in extreme coastal high water levels.

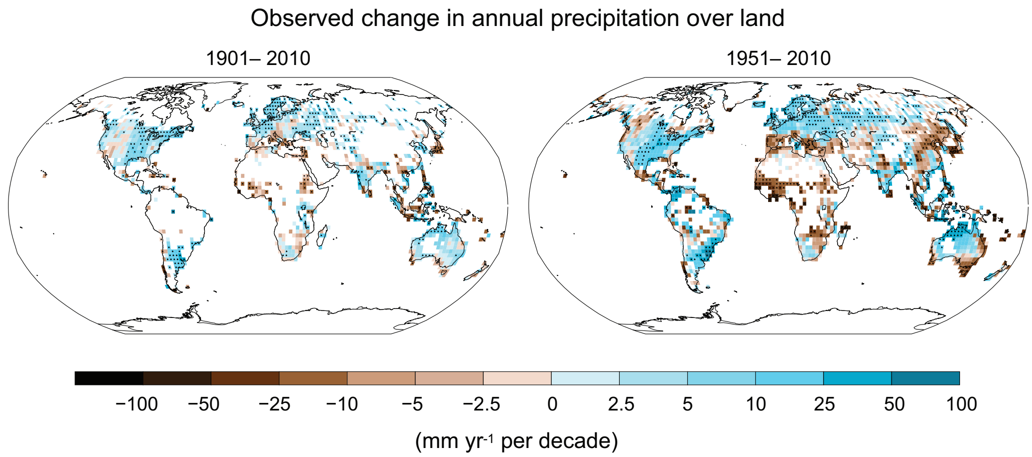

Figure SPM.2 | Maps of observed precipitation change from 1901 to 2010 and from 1951 to 2010 (trends in annual accumulation calculated using the same criteria as in Figure SPM.1) from one data set. For further technical details see the Technical Summary Supplementary Material. {TS TFE.1, Figure 2; Figure 2.29}

B.2 Ocean

Ocean warming dominates the increase in energy stored in the climate system, accounting for more than 90% of the energy accumulated between 1971 and 2010 (*high confidence*). It is *virtually certain* that the upper ocean (0–700 m) warmed from 1971 to 2010 (see Figure SPM.3), and it *likely* warmed between the 1870s and 1971. {3.2, Box 3.1}

- On a global scale, the ocean warming is largest near the surface, and the upper 75 m warmed by 0.11 [0.09 to 0.13] °C per decade over the period 1971 to 2010. Since AR4, instrumental biases in upper-ocean temperature records have been identified and reduced, enhancing confidence in the assessment of change. {3.2}

- It is *likely* that the ocean warmed between 700 and 2000 m from 1957 to 2009. Sufficient observations are available for the period 1992 to 2005 for a global assessment of temperature change below 2000 m. There were *likely* no significant observed temperature trends between 2000 and 3000 m for this period. It is *likely* that the ocean warmed from 3000 m to the bottom for this period, with the largest warming observed in the Southern Ocean. {3.2}

- More than 60% of the net energy increase in the climate system is stored in the upper ocean (0–700 m) during the relatively well-sampled 40-year period from 1971 to 2010, and about 30% is stored in the ocean below 700 m. The increase in upper ocean heat content during this time period estimated from a linear trend is *likely* 17 [15 to 19] × 10^{22} J [7] (see Figure SPM.3). {3.2, Box 3.1}

- It is *about as likely as not* that ocean heat content from 0–700 m increased more slowly during 2003 to 2010 than during 1993 to 2002 (see Figure SPM.3). Ocean heat uptake from 700–2000 m, where interannual variability is smaller, *likely* continued unabated from 1993 to 2009. {3.2, Box 9.2}

- It is *very likely* that regions of high salinity where evaporation dominates have become more saline, while regions of low salinity where precipitation dominates have become fresher since the 1950s. These regional trends in ocean salinity provide indirect evidence that evaporation and precipitation over the oceans have changed (*medium confidence*). {2.5, 3.3, 3.5}

- There is no observational evidence of a trend in the Atlantic Meridional Overturning Circulation (AMOC), based on the decade-long record of the complete AMOC and longer records of individual AMOC components. {3.6}

[7] A constant supply of heat through the ocean surface at the rate of 1 W m^{-2} for 1 year would increase the ocean heat content by 1.1 × 10^{22} J.

B.3 Cryosphere

Over the last two decades, the Greenland and Antarctic ice sheets have been losing mass, glaciers have continued to shrink almost worldwide, and Arctic sea ice and Northern Hemisphere spring snow cover have continued to decrease in extent (*high confidence*) (see Figure SPM.3). {4.2–4.7}

- The average rate of ice loss[8] from glaciers around the world, excluding glaciers on the periphery of the ice sheets[9], was *very likely* 226 [91 to 361] Gt yr^{-1} over the period 1971 to 2009, and *very likely* 275 [140 to 410] Gt yr^{-1} over the period 1993 to 2009[10]. {4.3}

- The average rate of ice loss from the Greenland ice sheet has *very likely* substantially increased from 34 [–6 to 74] Gt yr^{-1} over the period 1992 to 2001 to 215 [157 to 274] Gt yr^{-1} over the period 2002 to 2011. {4.4}

- The average rate of ice loss from the Antarctic ice sheet has *likely* increased from 30 [–37 to 97] Gt yr^{-1} over the period 1992–2001 to 147 [72 to 221] Gt yr^{-1} over the period 2002 to 2011. There is *very high confidence* that these losses are mainly from the northern Antarctic Peninsula and the Amundsen Sea sector of West Antarctica. {4.4}

- The annual mean Arctic sea ice extent decreased over the period 1979 to 2012 with a rate that was *very likely* in the range 3.5 to 4.1% per decade (range of 0.45 to 0.51 million km^2 per decade), and *very likely* in the range 9.4 to 13.6% per decade (range of 0.73 to 1.07 million km^2 per decade) for the summer sea ice minimum (perennial sea ice). The average decrease in decadal mean extent of Arctic sea ice has been most rapid in summer (*high confidence*); the spatial extent has decreased in every season, and in every successive decade since 1979 (*high confidence*) (see Figure SPM.3). There is *medium confidence* from reconstructions that over the past three decades, Arctic summer sea ice retreat was unprecedented and sea surface temperatures were anomalously high in at least the last 1,450 years. {4.2, 5.5}

- It is *very likely* that the annual mean Antarctic sea ice extent increased at a rate in the range of 1.2 to 1.8% per decade (range of 0.13 to 0.20 million km^2 per decade) between 1979 and 2012. There is *high confidence* that there are strong regional differences in this annual rate, with extent increasing in some regions and decreasing in others. {4.2}

- There is *very high confidence* that the extent of Northern Hemisphere snow cover has decreased since the mid-20th century (see Figure SPM.3). Northern Hemisphere snow cover extent decreased 1.6 [0.8 to 2.4] % per decade for March and April, and 11.7 [8.8 to 14.6] % per decade for June, over the 1967 to 2012 period. During this period, snow cover extent in the Northern Hemisphere did not show a statistically significant increase in any month. {4.5}

- There is *high confidence* that permafrost temperatures have increased in most regions since the early 1980s. Observed warming was up to 3°C in parts of Northern Alaska (early 1980s to mid-2000s) and up to 2°C in parts of the Russian European North (1971 to 2010). In the latter region, a considerable reduction in permafrost thickness and areal extent has been observed over the period 1975 to 2005 (*medium confidence*). {4.7}

- Multiple lines of evidence support very substantial Arctic warming since the mid-20th century. {Box 5.1, 10.3}

---

8 All references to 'ice loss' or 'mass loss' refer to net ice loss, i.e., accumulation minus melt and iceberg calving.

9 For methodological reasons, this assessment of ice loss from the Antarctic and Greenland ice sheets includes change in the glaciers on the periphery. These peripheral glaciers are thus excluded from the values given for glaciers.

10 100 Gt yr^{-1} of ice loss is equivalent to about 0.28 mm yr^{-1} of global mean sea level rise.

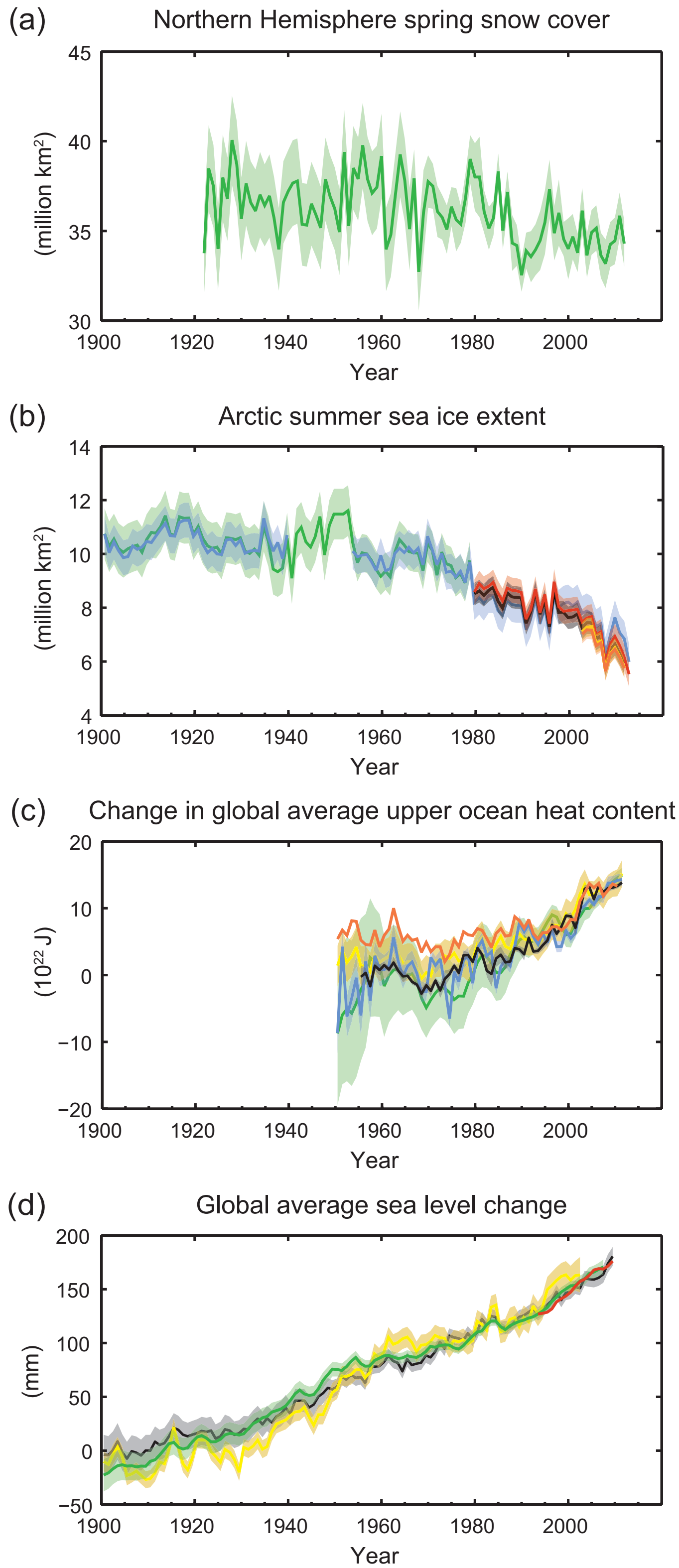

Figure SPM.3 | Multiple observed indicators of a changing global climate: (a) Extent of Northern Hemisphere March-April (spring) average snow cover; (b) extent of Arctic July-August-September (summer) average sea ice; (c) change in global mean upper ocean (0–700 m) heat content aligned to 2006–2010, and relative to the mean of all datasets for 1970; (d) global mean sea level relative to the 1900–1905 mean of the longest running dataset, and with all datasets aligned to have the same value in 1993, the first year of satellite altimetry data. All time-series (coloured lines indicating different data sets) show annual values, and where assessed, uncertainties are indicated by coloured shading. See Technical Summary Supplementary Material for a listing of the datasets. {Figures 3.2, 3.13, 4.19, and 4.3; FAQ 2.1, Figure 2; Figure TS.1}

B.4 Sea Level

The rate of sea level rise since the mid-19th century has been larger than the mean rate during the previous two millennia (*high confidence*). Over the period 1901 to 2010, global mean sea level rose by 0.19 [0.17 to 0.21] m (see Figure SPM.3). {3.7, 5.6, 13.2}

- Proxy and instrumental sea level data indicate a transition in the late 19th to the early 20th century from relatively low mean rates of rise over the previous two millennia to higher rates of rise (*high confidence*). It is *likely* that the rate of global mean sea level rise has continued to increase since the early 20th century. {3.7, 5.6, 13.2}

- It is *very likely* that the mean rate of global averaged sea level rise was 1.7 [1.5 to 1.9] mm yr^{-1} between 1901 and 2010, 2.0 [1.7 to 2.3] mm yr^{-1} between 1971 and 2010, and 3.2 [2.8 to 3.6] mm yr^{-1} between 1993 and 2010. Tide-gauge and satellite altimeter data are consistent regarding the higher rate of the latter period. It is *likely* that similarly high rates occurred between 1920 and 1950. {3.7}

- Since the early 1970s, glacier mass loss and ocean thermal expansion from warming together explain about 75% of the observed global mean sea level rise (*high confidence*). Over the period 1993 to 2010, global mean sea level rise is, with *high confidence*, consistent with the sum of the observed contributions from ocean thermal expansion due to warming (1.1 [0.8 to 1.4] mm yr^{-1}), from changes in glaciers (0.76 [0.39 to 1.13] mm yr^{-1}), Greenland ice sheet (0.33 [0.25 to 0.41] mm yr^{-1}), Antarctic ice sheet (0.27 [0.16 to 0.38] mm yr^{-1}), and land water storage (0.38 [0.26 to 0.49] mm yr^{-1}). The sum of these contributions is 2.8 [2.3 to 3.4] mm yr^{-1}. {13.3}

- There is *very high confidence* that maximum global mean sea level during the last interglacial period (129,000 to 116,000 years ago) was, for several thousand years, at least 5 m higher than present, and *high confidence* that it did not exceed 10 m above present. During the last interglacial period, the Greenland ice sheet *very likely* contributed between 1.4 and 4.3 m to the higher global mean sea level, implying with *medium confidence* an additional contribution from the Antarctic ice sheet. This change in sea level occurred in the context of different orbital forcing and with high-latitude surface temperature, averaged over several thousand years, at least 2°C warmer than present (*high confidence*). {5.3, 5.6}

B.5 Carbon and Other Biogeochemical Cycles

The atmospheric concentrations of carbon dioxide, methane, and nitrous oxide have increased to levels unprecedented in at least the last 800,000 years. Carbon dioxide concentrations have increased by 40% since pre-industrial times, primarily from fossil fuel emissions and secondarily from net land use change emissions. The ocean has absorbed about 30% of the emitted anthropogenic carbon dioxide, causing ocean acidification (see Figure SPM.4). {2.2, 3.8, 5.2, 6.2, 6.3}

- The atmospheric concentrations of the greenhouse gases carbon dioxide (CO_2), methane (CH_4), and nitrous oxide (N_2O) have all increased since 1750 due to human activity. In 2011 the concentrations of these greenhouse gases were 391 ppm[11], 1803 ppb, and 324 ppb, and exceeded the pre-industrial levels by about 40%, 150%, and 20%, respectively. {2.2, 5.2, 6.1, 6.2}

- Concentrations of CO_2, CH_4, and N_2O now substantially exceed the highest concentrations recorded in ice cores during the past 800,000 years. The mean rates of increase in atmospheric concentrations over the past century are, with *very high confidence*, unprecedented in the last 22,000 years. {5.2, 6.1, 6.2}

---

[11] ppm (parts per million) or ppb (parts per billion, 1 billion = 1,000 million) is the ratio of the number of gas molecules to the total number of molecules of dry air. For example, 300 ppm means 300 molecules of a gas per million molecules of dry air.

- Annual CO_2 emissions from fossil fuel combustion and cement production were 8.3 [7.6 to 9.0] GtC[12] yr^{-1} averaged over 2002–2011 (*high confidence*) and were 9.5 [8.7 to 10.3] GtC yr^{-1} in 2011, 54% above the 1990 level. Annual net CO_2 emissions from anthropogenic land use change were 0.9 [0.1 to 1.7] GtC yr^{-1} on average during 2002 to 2011 (*medium confidence*). {6.3}

- From 1750 to 2011, CO_2 emissions from fossil fuel combustion and cement production have released 375 [345 to 405] GtC to the atmosphere, while deforestation and other land use change are estimated to have released 180 [100 to 260] GtC. This results in cumulative anthropogenic emissions of 555 [470 to 640] GtC. {6.3}

- Of these cumulative anthropogenic CO_2 emissions, 240 [230 to 250] GtC have accumulated in the atmosphere, 155 [125 to 185] GtC have been taken up by the ocean and 160 [70 to 250] GtC have accumulated in natural terrestrial ecosystems (i.e., the cumulative residual land sink). {Figure TS.4, 3.8, 6.3}

- Ocean acidification is quantified by decreases in pH[13]. The pH of ocean surface water has decreased by 0.1 since the beginning of the industrial era (*high confidence*), corresponding to a 26% increase in hydrogen ion concentration (see Figure SPM.4). {3.8, Box 3.2}

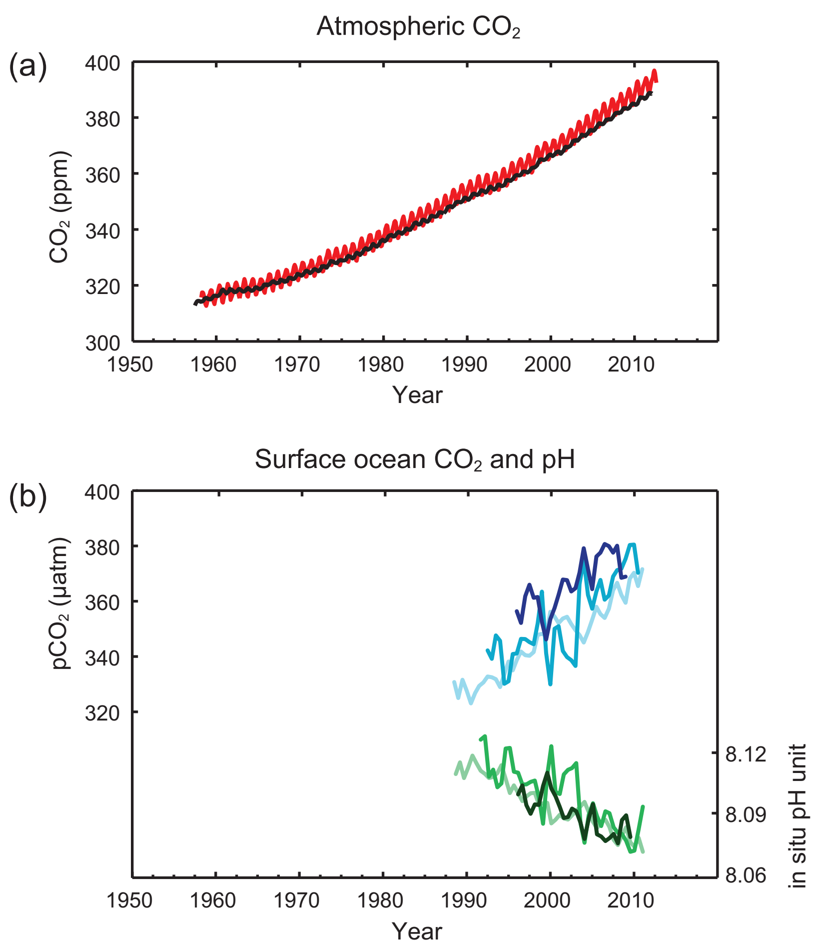

Figure SPM.4 | Multiple observed indicators of a changing global carbon cycle: (a) atmospheric concentrations of carbon dioxide (CO_2) from Mauna Loa (19°32'N, 155°34'W – red) and South Pole (89°59'S, 24°48'W – black) since 1958; (b) partial pressure of dissolved CO_2 at the ocean surface (blue curves) and in situ pH (green curves), a measure of the acidity of ocean water. Measurements are from three stations from the Atlantic (29°10'N, 15°30'W – dark blue/dark green; 31°40'N, 64°10'W – blue/green) and the Pacific Oceans (22°45'N, 158°00'W – light blue/light green). Full details of the datasets shown here are provided in the underlying report and the Technical Summary Supplementary Material. {Figures 2.1 and 3.18; Figure TS.5}

[12] 1 Gigatonne of carbon = 1 GtC = 10^{15} grams of carbon. This corresponds to 3.667 $GtCO_2$.

[13] pH is a measure of acidity using a logarithmic scale: a pH decrease of 1 unit corresponds to a 10-fold increase in hydrogen ion concentration, or acidity.

C. Drivers of Climate Change

Natural and anthropogenic substances and processes that alter the Earth's energy budget are drivers of climate change. Radiative forcing[14] (RF) quantifies the change in energy fluxes caused by changes in these drivers for 2011 relative to 1750, unless otherwise indicated. Positive RF leads to surface warming, negative RF leads to surface cooling. RF is estimated based on in-situ and remote observations, properties of greenhouse gases and aerosols, and calculations using numerical models representing observed processes. Some emitted compounds affect the atmospheric concentration of other substances. The RF can be reported based on the concentration changes of each substance[15]. Alternatively, the emission-based RF of a compound can be reported, which provides a more direct link to human activities. It includes contributions from all substances affected by that emission. The total anthropogenic RF of the two approaches are identical when considering all drivers. Though both approaches are used in this Summary for Policymakers, emission-based RFs are emphasized.

Total radiative forcing is positive, and has led to an uptake of energy by the climate system. The largest contribution to total radiative forcing is caused by the increase in the atmospheric concentration of CO_2 since 1750 (see Figure SPM.5). {3.2, Box 3.1, 8.3, 8.5}

- The total anthropogenic RF for 2011 relative to 1750 is 2.29 [1.13 to 3.33] W m^{-2} (see Figure SPM.5), and it has increased more rapidly since 1970 than during prior decades. The total anthropogenic RF best estimate for 2011 is 43% higher than that reported in AR4 for the year 2005. This is caused by a combination of continued growth in most greenhouse gas concentrations and improved estimates of RF by aerosols indicating a weaker net cooling effect (negative RF). {8.5}

- The RF from emissions of well-mixed greenhouse gases (CO_2, CH_4, N_2O, and Halocarbons) for 2011 relative to 1750 is 3.00 [2.22 to 3.78] W m^{-2} (see Figure SPM.5). The RF from changes in concentrations in these gases is 2.83 [2.26 to 3.40] W m^{-2}. {8.5}

- Emissions of CO_2 alone have caused an RF of 1.68 [1.33 to 2.03] W m^{-2} (see Figure SPM.5). Including emissions of other carbon-containing gases, which also contributed to the increase in CO_2 concentrations, the RF of CO_2 is 1.82 [1.46 to 2.18] W m^{-2}. {8.3, 8.5}

- Emissions of CH_4 alone have caused an RF of 0.97 [0.74 to 1.20] W m^{-2} (see Figure SPM.5). This is much larger than the concentration-based estimate of 0.48 [0.38 to 0.58] W m^{-2} (unchanged from AR4). This difference in estimates is caused by concentration changes in ozone and stratospheric water vapour due to CH_4 emissions and other emissions indirectly affecting CH_4. {8.3, 8.5}

- Emissions of stratospheric ozone-depleting halocarbons have caused a net positive RF of 0.18 [0.01 to 0.35] W m^{-2} (see Figure SPM.5). Their own positive RF has outweighed the negative RF from the ozone depletion that they have induced. The positive RF from all halocarbons is similar to the value in AR4, with a reduced RF from CFCs but increases from many of their substitutes. {8.3, 8.5}

- Emissions of short-lived gases contribute to the total anthropogenic RF. Emissions of carbon monoxide (CO) are *virtually certain* to have induced a positive RF, while emissions of nitrogen oxides (NO_x) are *likely* to have induced a net negative RF (see Figure SPM.5). {8.3, 8.5}

- The RF of the total aerosol effect in the atmosphere, which includes cloud adjustments due to aerosols, is –0.9 [–1.9 to –0.1] W m^{-2} (*medium confidence*), and results from a negative forcing from most aerosols and a positive contribution

---

[14] The strength of drivers is quantified as Radiative Forcing (RF) in units watts per square metre (W m^{-2}) as in previous IPCC assessments. RF is the change in energy flux caused by a driver, and is calculated at the tropopause or at the top of the atmosphere. In the traditional RF concept employed in previous IPCC reports all surface and tropospheric conditions are kept fixed. In calculations of RF for well-mixed greenhouse gases and aerosols in this report, physical variables, except for the ocean and sea ice, are allowed to respond to perturbations with rapid adjustments. The resulting forcing is called Effective Radiative Forcing (ERF) in the underlying report. This change reflects the scientific progress from previous assessments and results in a better indication of the eventual temperature response for these drivers. For all drivers other than well-mixed greenhouse gases and aerosols, rapid adjustments are less well characterized and assumed to be small, and thus the traditional RF is used. {8.1}

[15] This approach was used to report RF in the AR4 Summary for Policymakers.

from black carbon absorption of solar radiation. There is *high confidence* that aerosols and their interactions with clouds have offset a substantial portion of global mean forcing from well-mixed greenhouse gases. They continue to contribute the largest uncertainty to the total RF estimate. {7.5, 8.3, 8.5}

- The forcing from stratospheric volcanic aerosols can have a large impact on the climate for some years after volcanic eruptions. Several small eruptions have caused an RF of –0.11 [–0.15 to –0.08] W m^{-2} for the years 2008 to 2011, which is approximately twice as strong as during the years 1999 to 2002. {8.4}

- The RF due to changes in solar irradiance is estimated as 0.05 [0.00 to 0.10] W m^{-2} (see Figure SPM.5). Satellite observations of total solar irradiance changes from 1978 to 2011 indicate that the last solar minimum was lower than the previous two. This results in an RF of –0.04 [–0.08 to 0.00] W m^{-2} between the most recent minimum in 2008 and the 1986 minimum. {8.4}

- The total natural RF from solar irradiance changes and stratospheric volcanic aerosols made only a small contribution to the net radiative forcing throughout the last century, except for brief periods after large volcanic eruptions. {8.5}

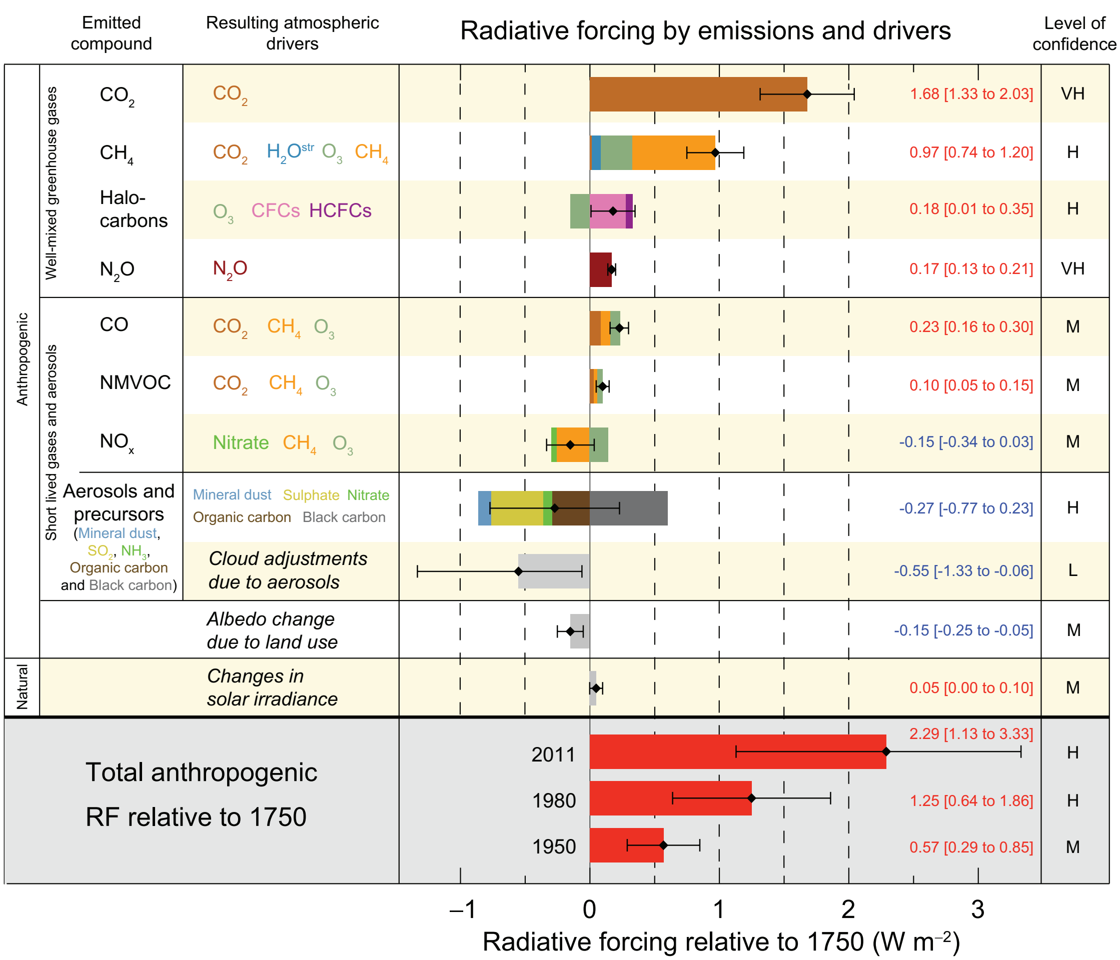

Figure SPM.5 | Radiative forcing estimates in 2011 relative to 1750 and aggregated uncertainties for the main drivers of climate change. Values are global average radiative forcing (RF[14]), partitioned according to the emitted compounds or processes that result in a combination of drivers. The best estimates of the net radiative forcing are shown as black diamonds with corresponding uncertainty intervals; the numerical values are provided on the right of the figure, together with the confidence level in the net forcing (VH – *very high*, H – *high*, M – *medium*, L – *low*, VL – *very low*). Albedo forcing due to black carbon on snow and ice is included in the black carbon aerosol bar. Small forcings due to contrails (0.05 W m^{-2}, including contrail induced cirrus), and HFCs, PFCs and SF_6 (total 0.03 W m^{-2}) are not shown. Concentration-based RFs for gases can be obtained by summing the like-coloured bars. Volcanic forcing is not included as its episodic nature makes is difficult to compare to other forcing mechanisms. Total anthropogenic radiative forcing is provided for three different years relative to 1750. For further technical details, including uncertainty ranges associated with individual components and processes, see the Technical Summary Supplementary Material. {8.5; Figures 8.14–8.18; Figures TS.6 and TS.7}

SPM

D. Understanding the Climate System and its Recent Changes

Understanding recent changes in the climate system results from combining observations, studies of feedback processes, and model simulations. Evaluation of the ability of climate models to simulate recent changes requires consideration of the state of all modelled climate system components at the start of the simulation and the natural and anthropogenic forcing used to drive the models. Compared to AR4, more detailed and longer observations and improved climate models now enable the attribution of a human contribution to detected changes in more climate system components.

Human influence on the climate system is clear. This is evident from the increasing greenhouse gas concentrations in the atmosphere, positive radiative forcing, observed warming, and understanding of the climate system. {2–14}

D.1 Evaluation of Climate Models

Climate models have improved since the AR4. Models reproduce observed continental-scale surface temperature patterns and trends over many decades, including the more rapid warming since the mid-20th century and the cooling immediately following large volcanic eruptions (*very high confidence*). {9.4, 9.6, 9.8}

- The long-term climate model simulations show a trend in global-mean surface temperature from 1951 to 2012 that agrees with the observed trend (*very high confidence*). There are, however, differences between simulated and observed trends over periods as short as 10 to 15 years (e.g., 1998 to 2012). {9.4, Box 9.2}

- The observed reduction in surface warming trend over the period 1998 to 2012 as compared to the period 1951 to 2012, is due in roughly equal measure to a reduced trend in radiative forcing and a cooling contribution from natural internal variability, which includes a possible redistribution of heat within the ocean (*medium confidence*). The reduced trend in radiative forcing is primarily due to volcanic eruptions and the timing of the downward phase of the 11-year solar cycle. However, there is *low confidence* in quantifying the role of changes in radiative forcing in causing the reduced warming trend. There is *medium confidence* that natural internal decadal variability causes to a substantial degree the difference between observations and the simulations; the latter are not expected to reproduce the timing of natural internal variability. There may also be a contribution from forcing inadequacies and, in some models, an overestimate of the response to increasing greenhouse gas and other anthropogenic forcing (dominated by the effects of aerosols). {9.4, Box 9.2, 10.3, Box 10.2, 11.3}

- On regional scales, the confidence in model capability to simulate surface temperature is less than for the larger scales. However, there is *high confidence* that regional-scale surface temperature is better simulated than at the time of the AR4. {9.4, 9.6}

- There has been substantial progress in the assessment of extreme weather and climate events since AR4. Simulated global-mean trends in the frequency of extreme warm and cold days and nights over the second half of the 20th century are generally consistent with observations. {9.5}

- There has been some improvement in the simulation of continental-scale patterns of precipitation since the AR4. At regional scales, precipitation is not simulated as well, and the assessment is hampered by observational uncertainties. {9.4, 9.6}

- Some important climate phenomena are now better reproduced by models. There is *high confidence* that the statistics of monsoon and El Niño-Southern Oscillation (ENSO) based on multi-model simulations have improved since AR4. {9.5}

- Climate models now include more cloud and aerosol processes, and their interactions, than at the time of the AR4, but there remains *low confidence* in the representation and quantification of these processes in models. {7.3, 7.6, 9.4, 9.7}

- There is robust evidence that the downward trend in Arctic summer sea ice extent since 1979 is now reproduced by more models than at the time of the AR4, with about one-quarter of the models showing a trend as large as, or larger than, the trend in the observations. Most models simulate a small downward trend in Antarctic sea ice extent, albeit with large inter-model spread, in contrast to the small upward trend in observations. {9.4}

- Many models reproduce the observed changes in upper-ocean heat content (0–700 m) from 1961 to 2005 (*high confidence*), with the multi-model mean time series falling within the range of the available observational estimates for most of the period. {9.4}

- Climate models that include the carbon cycle (Earth System Models) simulate the global pattern of ocean-atmosphere CO_2 fluxes, with outgassing in the tropics and uptake in the mid and high latitudes. In the majority of these models the sizes of the simulated global land and ocean carbon sinks over the latter part of the 20th century are within the range of observational estimates. {9.4}

D.2 Quantification of Climate System Responses

Observational and model studies of temperature change, climate feedbacks and changes in the Earth's energy budget together provide confidence in the magnitude of global warming in response to past and future forcing. {Box 12.2, Box 13.1}

- The net feedback from the combined effect of changes in water vapour, and differences between atmospheric and surface warming is *extremely likely* positive and therefore amplifies changes in climate. The net radiative feedback due to all cloud types combined is *likely* positive. Uncertainty in the sign and magnitude of the cloud feedback is due primarily to continuing uncertainty in the impact of warming on low clouds. {7.2}

- The equilibrium climate sensitivity quantifies the response of the climate system to constant radiative forcing on multi-century time scales. It is defined as the change in global mean surface temperature at equilibrium that is caused by a doubling of the atmospheric CO_2 concentration. Equilibrium climate sensitivity is *likely* in the range 1.5°C to 4.5°C (*high confidence*), *extremely unlikely* less than 1°C (*high confidence*), and *very unlikely* greater than 6°C (*medium confidence*)[16]. The lower temperature limit of the assessed *likely* range is thus less than the 2°C in the AR4, but the upper limit is the same. This assessment reflects improved understanding, the extended temperature record in the atmosphere and ocean, and new estimates of radiative forcing. {TS TFE.6, Figure 1; Box 12.2}

- The rate and magnitude of global climate change is determined by radiative forcing, climate feedbacks and the storage of energy by the climate system. Estimates of these quantities for recent decades are consistent with the assessed *likely* range of the equilibrium climate sensitivity to within assessed uncertainties, providing strong evidence for our understanding of anthropogenic climate change. {Box 12.2, Box 13.1}

- The transient climate response quantifies the response of the climate system to an increasing radiative forcing on a decadal to century timescale. It is defined as the change in global mean surface temperature at the time when the atmospheric CO_2 concentration has doubled in a scenario of concentration increasing at 1% per year. The transient climate response is *likely* in the range of 1.0°C to 2.5°C (*high confidence*) and *extremely unlikely* greater than 3°C. {Box 12.2}

- A related quantity is the transient climate response to cumulative carbon emissions (TCRE). It quantifies the transient response of the climate system to cumulative carbon emissions (see Section E.8). TCRE is defined as the global mean

[16] No best estimate for equilibrium climate sensitivity can now be given because of a lack of agreement on values across assessed lines of evidence and studies.

surface temperature change per 1000 GtC emitted to the atmosphere. TCRE is *likely* in the range of 0.8°C to 2.5°C per 1000 GtC and applies for cumulative emissions up to about 2000 GtC until the time temperatures peak (see Figure SPM.10). {12.5, Box 12.2}

- Various metrics can be used to compare the contributions to climate change of emissions of different substances. The most appropriate metric and time horizon will depend on which aspects of climate change are considered most important to a particular application. No single metric can accurately compare all consequences of different emissions, and all have limitations and uncertainties. The Global Warming Potential is based on the cumulative radiative forcing over a particular time horizon, and the Global Temperature Change Potential is based on the change in global mean surface temperature at a chosen point in time. Updated values are provided in the underlying Report. {8.7}

D.3 Detection and Attribution of Climate Change

Human influence has been detected in warming of the atmosphere and the ocean, in changes in the global water cycle, in reductions in snow and ice, in global mean sea level rise, and in changes in some climate extremes (see Figure SPM.6 and Table SPM.1). This evidence for human influence has grown since AR4. It is *extremely likely* that human influence has been the dominant cause of the observed warming since the mid-20th century. {10.3–10.6, 10.9}

- It is *extremely likely* that more than half of the observed increase in global average surface temperature from 1951 to 2010 was caused by the anthropogenic increase in greenhouse gas concentrations and other anthropogenic forcings together. The best estimate of the human-induced contribution to warming is similar to the observed warming over this period. {10.3}

- Greenhouse gases contributed a global mean surface warming *likely* to be in the range of 0.5°C to 1.3°C over the period 1951 to 2010, with the contributions from other anthropogenic forcings, including the cooling effect of aerosols, *likely* to be in the range of –0.6°C to 0.1°C. The contribution from natural forcings is *likely* to be in the range of –0.1°C to 0.1°C, and from natural internal variability is *likely* to be in the range of –0.1°C to 0.1°C. Together these assessed contributions are consistent with the observed warming of approximately 0.6°C to 0.7°C over this period. {10.3}

- Over every continental region except Antarctica, anthropogenic forcings have *likely* made a substantial contribution to surface temperature increases since the mid-20th century (see Figure SPM.6). For Antarctica, large observational uncertainties result in *low confidence* that anthropogenic forcings have contributed to the observed warming averaged over available stations. It is *likely* that there has been an anthropogenic contribution to the very substantial Arctic warming since the mid-20th century. {2.4, 10.3}

- It is *very likely* that anthropogenic influence, particularly greenhouse gases and stratospheric ozone depletion, has led to a detectable observed pattern of tropospheric warming and a corresponding cooling in the lower stratosphere since 1961. {2.4, 9.4, 10.3}

- It is *very likely* that anthropogenic forcings have made a substantial contribution to increases in global upper ocean heat content (0–700 m) observed since the 1970s (see Figure SPM.6). There is evidence for human influence in some individual ocean basins. {3.2, 10.4}

- It is *likely* that anthropogenic influences have affected the global water cycle since 1960. Anthropogenic influences have contributed to observed increases in atmospheric moisture content in the atmosphere (*medium confidence*), to global-scale changes in precipitation patterns over land (*medium confidence*), to intensification of heavy precipitation over land regions where data are sufficient (*medium confidence*), and to changes in surface and sub-surface ocean salinity (*very likely*). {2.5, 2.6, 3.3, 7.6, 10.3, 10.4}

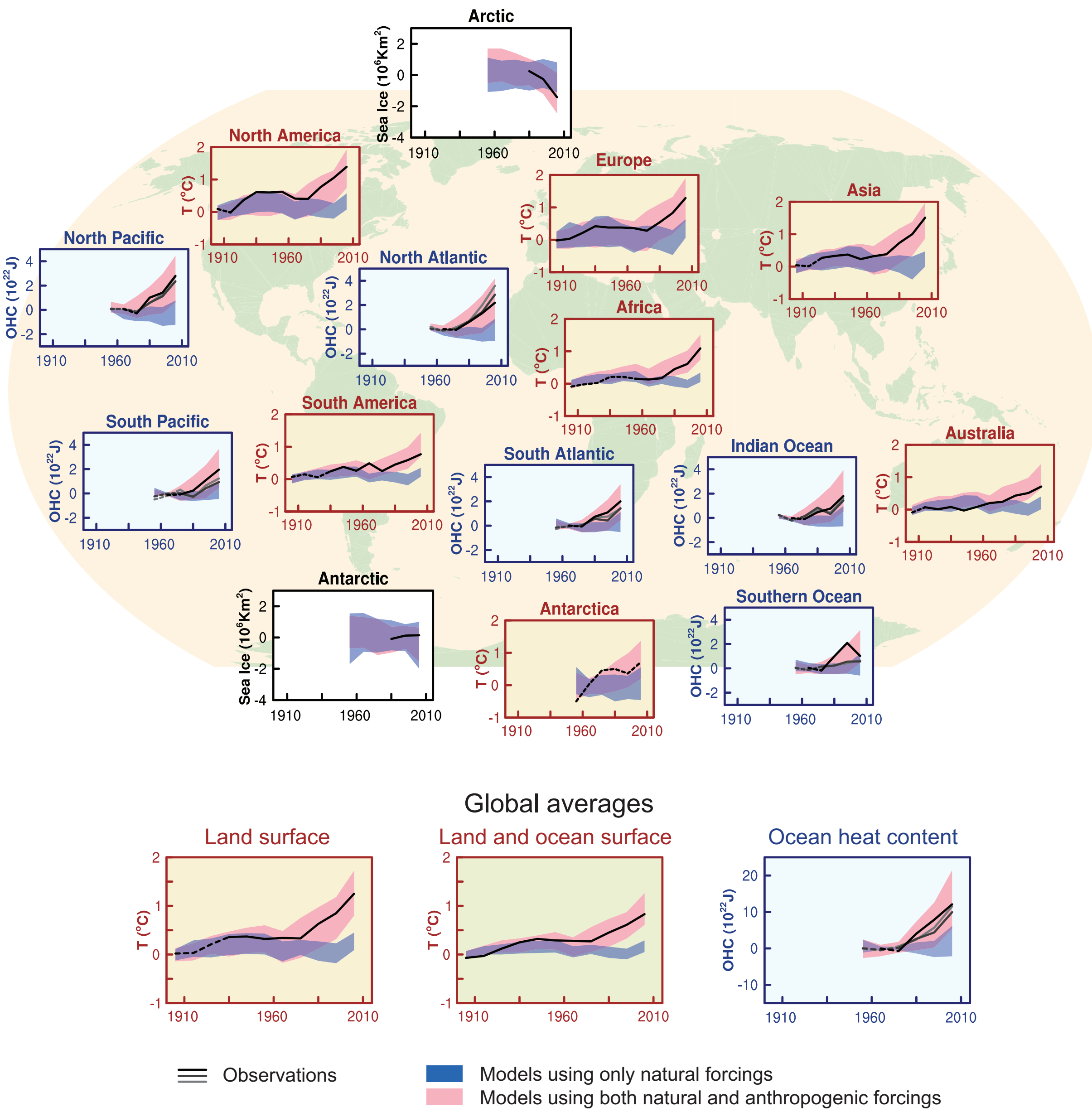

Figure SPM.6 | Comparison of observed and simulated climate change based on three large-scale indicators in the atmosphere, the cryosphere and the ocean: change in continental land surface air temperatures (yellow panels), Arctic and Antarctic September sea ice extent (white panels), and upper ocean heat content in the major ocean basins (blue panels). Global average changes are also given. Anomalies are given relative to 1880–1919 for surface temperatures, 1960–1980 for ocean heat content and 1979–1999 for sea ice. All time-series are decadal averages, plotted at the centre of the decade. For temperature panels, observations are dashed lines if the spatial coverage of areas being examined is below 50%. For ocean heat content and sea ice panels the solid line is where the coverage of data is good and higher in quality, and the dashed line is where the data coverage is only adequate, and thus, uncertainty is larger. Model results shown are Coupled Model Intercomparison Project Phase 5 (CMIP5) multi-model ensemble ranges, with shaded bands indicating the 5 to 95% confidence intervals. For further technical details, including region definitions see the Technical Summary Supplementary Material. {Figure 10.21; Figure TS.12}

- There has been further strengthening of the evidence for human influence on temperature extremes since the SREX. It is now *very likely* that human influence has contributed to observed global scale changes in the frequency and intensity of daily temperature extremes since the mid-20th century, and *likely* that human influence has more than doubled the probability of occurrence of heat waves in some locations (see Table SPM.1). {10.6}

- Anthropogenic influences have *very likely* contributed to Arctic sea ice loss since 1979. There is *low confidence* in the scientific understanding of the small observed increase in Antarctic sea ice extent due to the incomplete and competing scientific explanations for the causes of change and *low confidence* in estimates of natural internal variability in that region (see Figure SPM.6). {10.5}

- Anthropogenic influences *likely* contributed to the retreat of glaciers since the 1960s and to the increased surface mass loss of the Greenland ice sheet since 1993. Due to a low level of scientific understanding there is *low confidence* in attributing the causes of the observed loss of mass from the Antarctic ice sheet over the past two decades. {4.3, 10.5}

- It is *likely* that there has been an anthropogenic contribution to observed reductions in Northern Hemisphere spring snow cover since 1970. {10.5}

- It is *very likely* that there is a substantial anthropogenic contribution to the global mean sea level rise since the 1970s. This is based on the *high confidence* in an anthropogenic influence on the two largest contributions to sea level rise, that is thermal expansion and glacier mass loss. {10.4, 10.5, 13.3}

- There is *high confidence* that changes in total solar irradiance have not contributed to the increase in global mean surface temperature over the period 1986 to 2008, based on direct satellite measurements of total solar irradiance. There is *medium confidence* that the 11-year cycle of solar variability influences decadal climate fluctuations in some regions. No robust association between changes in cosmic rays and cloudiness has been identified. {7.4, 10.3, Box 10.2}

E. Future Global and Regional Climate Change

Projections of changes in the climate system are made using a hierarchy of climate models ranging from simple climate models, to models of intermediate complexity, to comprehensive climate models, and Earth System Models. These models simulate changes based on a set of scenarios of anthropogenic forcings. A new set of scenarios, the Representative Concentration Pathways (RCPs), was used for the new climate model simulations carried out under the framework of the Coupled Model Intercomparison Project Phase 5 (CMIP5) of the World Climate Research Programme. In all RCPs, atmospheric CO_2 concentrations are higher in 2100 relative to present day as a result of a further increase of cumulative emissions of CO_2 to the atmosphere during the 21st century (see Box SPM.1). Projections in this Summary for Policymakers are for the end of the 21st century (2081–2100) given relative to 1986–2005, unless otherwise stated. To place such projections in historical context, it is necessary to consider observed changes between different periods. Based on the longest global surface temperature dataset available, the observed change between the average of the period 1850–1900 and of the AR5 reference period is 0.61 [0.55 to 0.67] °C. However, warming has occurred beyond the average of the AR5 reference period. Hence this is not an estimate of historical warming to present (see Chapter 2) .

Continued emissions of greenhouse gases will cause further warming and changes in all components of the climate system. Limiting climate change will require substantial and sustained reductions of greenhouse gas emissions. {6, 11–14}

- Projections for the next few decades show spatial patterns of climate change similar to those projected for the later 21st century but with smaller magnitude. Natural internal variability will continue to be a major influence on climate, particularly in the near-term and at the regional scale. By the mid-21st century the magnitudes of the projected changes are substantially affected by the choice of emissions scenario (Box SPM.1). {11.3, Box 11.1, Annex I}

- Projected climate change based on RCPs is similar to AR4 in both patterns and magnitude, after accounting for scenario differences. The overall spread of projections for the high RCPs is narrower than for comparable scenarios used in AR4 because in contrast to the SRES emission scenarios used in AR4, the RCPs used in AR5 are defined as concentration pathways and thus carbon cycle uncertainties affecting atmospheric CO_2 concentrations are not considered in the concentration-driven CMIP5 simulations. Projections of sea level rise are larger than in the AR4, primarily because of improved modelling of land-ice contributions.{11.3, 12.3, 12.4, 13.4, 13.5}

E.1 Atmosphere: Temperature

Global surface temperature change for the end of the 21st century is *likely* to exceed 1.5°C relative to 1850 to 1900 for all RCP scenarios except RCP2.6. It is *likely* to exceed 2°C for RCP6.0 and RCP8.5, and *more likely than not* to exceed 2°C for RCP4.5. Warming will continue beyond 2100 under all RCP scenarios except RCP2.6. Warming will continue to exhibit interannual-to-decadal variability and will not be regionally uniform (see Figures SPM.7 and SPM.8). {11.3, 12.3, 12.4, 14.8}

- The global mean surface temperature change for the period 2016–2035 relative to 1986–2005 will *likely* be in the range of 0.3°C to 0.7°C (*medium confidence*). This assessment is based on multiple lines of evidence and assumes there will be no major volcanic eruptions or secular changes in total solar irradiance. Relative to natural internal variability, near-term increases in seasonal mean and annual mean temperatures are expected to be larger in the tropics and subtropics than in mid-latitudes (*high confidence*). {11.3}

- Increase of global mean surface temperatures for 2081–2100 relative to 1986–2005 is projected to *likely* be in the ranges derived from the concentration-driven CMIP5 model simulations, that is, 0.3°C to 1.7°C (RCP2.6), 1.1°C to 2.6°C (RCP4.5), 1.4°C to 3.1°C (RCP6.0), 2.6°C to 4.8°C (RCP8.5). The Arctic region will warm more rapidly than the global mean, and mean warming over land will be larger than over the ocean (*very high confidence*) (see Figures SPM.7 and SPM.8, and Table SPM.2). {12.4, 14.8}

- Relative to the average from year 1850 to 1900, global surface temperature change by the end of the 21st century is projected to *likely* exceed 1.5°C for RCP4.5, RCP6.0 and RCP8.5 (*high confidence*). Warming is *likely* to exceed 2°C for RCP6.0 and RCP8.5 (*high confidence*), *more likely than not* to exceed 2°C for RCP4.5 (*high confidence*), but *unlikely* to exceed 2°C for RCP2.6 (*medium confidence*). Warming is *unlikely* to exceed 4°C for RCP2.6, RCP4.5 and RCP6.0 (*high confidence*) and is *about as likely as not* to exceed 4°C for RCP8.5 (*medium confidence*). {12.4}

- It is *virtually certain* that there will be more frequent hot and fewer cold temperature extremes over most land areas on daily and seasonal timescales as global mean temperatures increase. It is *very likely* that heat waves will occur with a higher frequency and duration. Occasional cold winter extremes will continue to occur (see Table SPM.1). {12.4}

E.2 Atmosphere: Water Cycle

Changes in the global water cycle in response to the warming over the 21st century will not be uniform. The contrast in precipitation between wet and dry regions and between wet and dry seasons will increase, although there may be regional exceptions (see Figure SPM.8). {12.4, 14.3}

- Projected changes in the water cycle over the next few decades show similar large-scale patterns to those towards the end of the century, but with smaller magnitude. Changes in the near-term, and at the regional scale will be strongly influenced by natural internal variability and may be affected by anthropogenic aerosol emissions. {11.3}

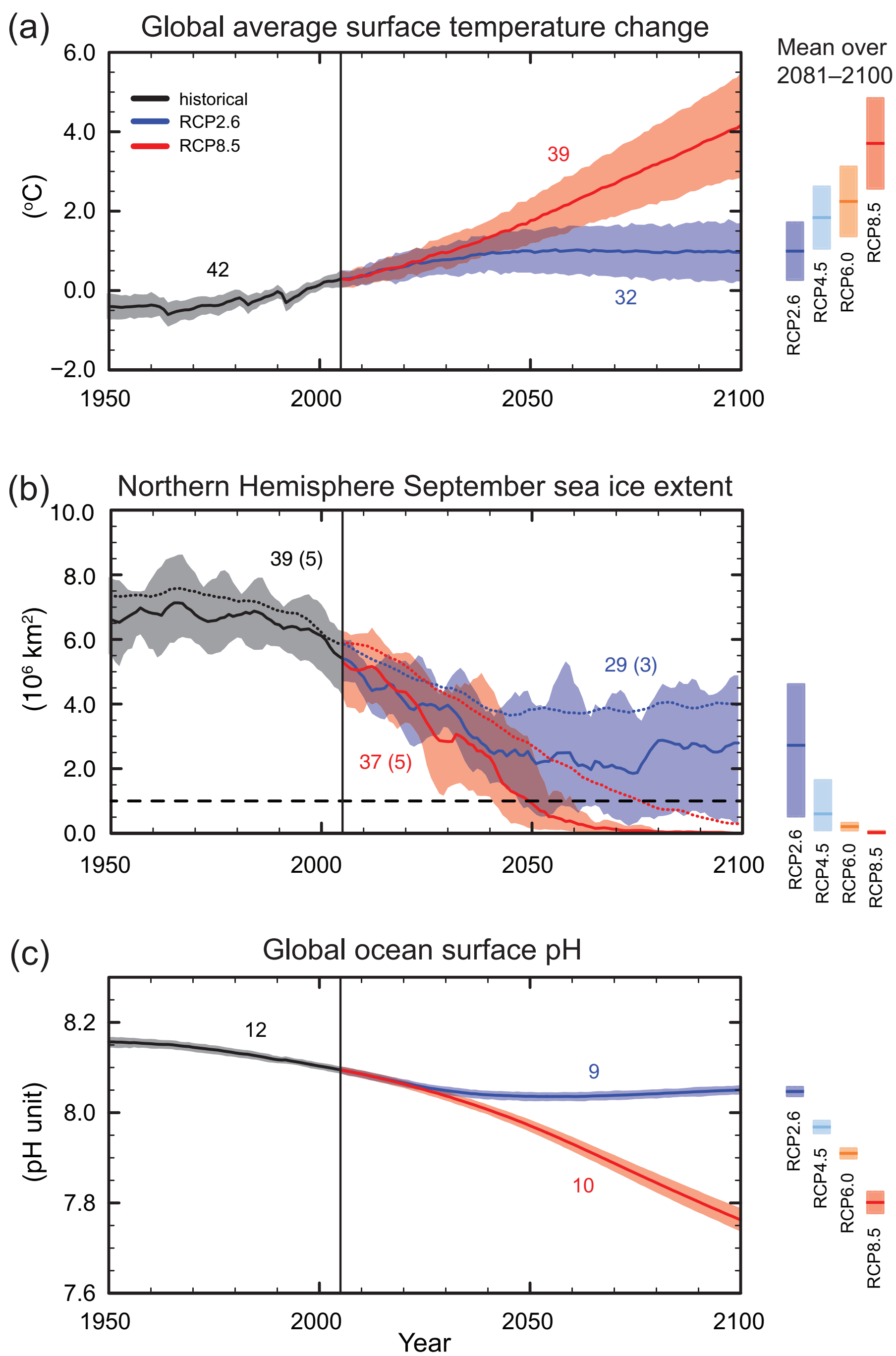

Figure SPM.7 | CMIP5 multi-model simulated time series from 1950 to 2100 for (a) change in global annual mean surface temperature relative to 1986–2005, (b) Northern Hemisphere September sea ice extent (5-year running mean), and (c) global mean ocean surface pH. Time series of projections and a measure of uncertainty (shading) are shown for scenarios RCP2.6 (blue) and RCP8.5 (red). Black (grey shading) is the modelled historical evolution using historical reconstructed forcings. The mean and associated uncertainties averaged over 2081–2100 are given for all RCP scenarios as colored vertical bars. The numbers of CMIP5 models used to calculate the multi-model mean is indicated. For sea ice extent (b), the projected mean and uncertainty (minimum-maximum range) of the subset of models that most closely reproduce the climatological mean state and 1979 to 2012 trend of the Arctic sea ice is given (number of models given in brackets). For completeness, the CMIP5 multi-model mean is also indicated with dotted lines. The dashed line represents nearly ice-free conditions (i.e., when sea ice extent is less than 10^6 km^2 for at least five consecutive years). For further technical details see the Technical Summary Supplementary Material {Figures 6.28, 12.5, and 12.28–12.31; Figures TS.15, TS.17, and TS.20}

SPM

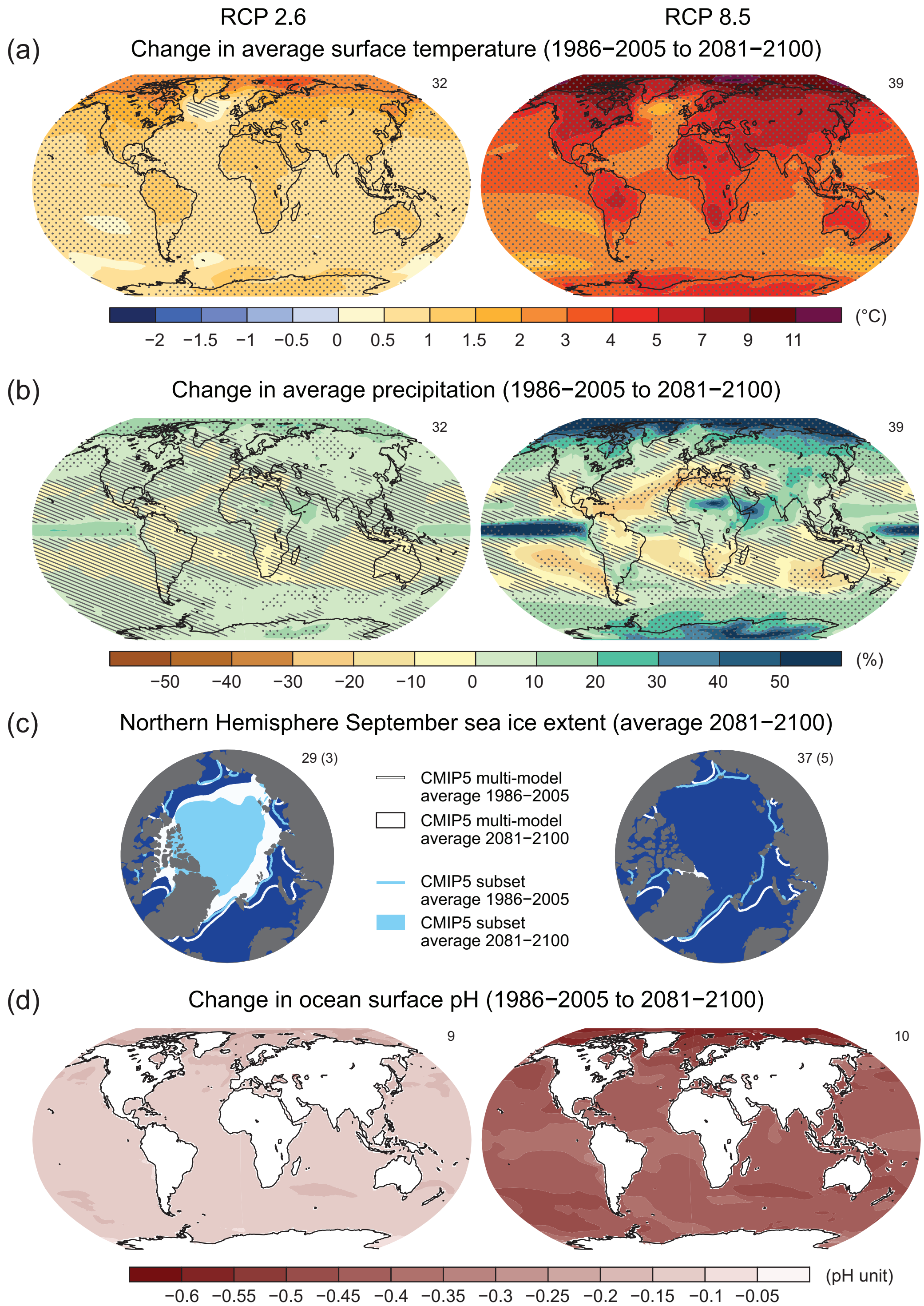

Figure SPM.8 | Maps of CMIP5 multi-model mean results for the scenarios RCP2.6 and RCP8.5 in 2081–2100 of (a) annual mean surface temperature change, (b) average percent change in annual mean precipitation, (c) Northern Hemisphere September sea ice extent, and (d) change in ocean surface pH. Changes in panels (a), (b) and (d) are shown relative to 1986–2005. The number of CMIP5 models used to calculate the multi-model mean is indicated in the upper right corner of each panel. For panels (a) and (b), hatching indicates regions where the multi-model mean is small compared to natural internal variability (i.e., less than one standard deviation of natural internal variability in 20-year means). Stippling indicates regions where the multi-model mean is large compared to natural internal variability (i.e., greater than two standard deviations of natural internal variability in 20-year means) and where at least 90% of models agree on the sign of change (see Box 12.1). In panel (c), the lines are the modelled means for 1986–2005; the filled areas are for the end of the century. The CMIP5 multi-model mean is given in white colour, the projected mean sea ice extent of a subset of models (number of models given in brackets) that most closely reproduce the climatological mean state and 1979 to 2012 trend of the Arctic sea ice extent is given in light blue colour. For further technical details see the Technical Summary Supplementary Material. {Figures 6.28, 12.11, 12.22, and 12.29; Figures TS.15, TS.16, TS.17, and TS.20}

- The high latitudes and the equatorial Pacific Ocean are *likely* to experience an increase in annual mean precipitation by the end of this century under the RCP8.5 scenario. In many mid-latitude and subtropical dry regions, mean precipitation will *likely* decrease, while in many mid-latitude wet regions, mean precipitation will *likely* increase by the end of this century under the RCP8.5 scenario (see Figure SPM.8). {7.6, 12.4, 14.3}

- Extreme precipitation events over most of the mid-latitude land masses and over wet tropical regions will *very likely* become more intense and more frequent by the end of this century, as global mean surface temperature increases (see Table SPM.1). {7.6, 12.4}

- Globally, it is *likely* that the area encompassed by monsoon systems will increase over the 21st century. While monsoon winds are *likely* to weaken, monsoon precipitation is *likely* to intensify due to the increase in atmospheric moisture. Monsoon onset dates are *likely* to become earlier or not to change much. Monsoon retreat dates will *likely* be delayed, resulting in lengthening of the monsoon season in many regions. {14.2}

- There is *high confidence* that the El Niño-Southern Oscillation (ENSO) will remain the dominant mode of interannual variability in the tropical Pacific, with global effects in the 21st century. Due to the increase in moisture availability, ENSO-related precipitation variability on regional scales will *likely* intensify. Natural variations of the amplitude and spatial pattern of ENSO are large and thus *confidence* in any specific projected change in ENSO and related regional phenomena for the 21st century remains *low*. {5.4, 14.4}

Table SPM.2 | Projected change in global mean surface air temperature and global mean sea level rise for the mid- and late 21st century relative to the reference period of 1986–2005. {12.4; Table 12.2, Table 13.5}

		2046–2065		2081–2100	
	Scenario	**Mean**	***Likely* range[c]**	**Mean**	***Likely* range[c]**
Global Mean Surface Temperature Change (°C)[a]	RCP2.6	1.0	0.4 to 1.6	1.0	0.3 to 1.7
	RCP4.5	1.4	0.9 to 2.0	1.8	1.1 to 2.6
	RCP6.0	1.3	0.8 to 1.8	2.2	1.4 to 3.1
	RCP8.5	2.0	1.4 to 2.6	3.7	2.6 to 4.8
	Scenario	**Mean**	***Likely* range[d]**	**Mean**	***Likely* range[d]**
Global Mean Sea Level Rise (m)[b]	RCP2.6	0.24	0.17 to 0.32	0.40	0.26 to 0.55
	RCP4.5	0.26	0.19 to 0.33	0.47	0.32 to 0.63
	RCP6.0	0.25	0.18 to 0.32	0.48	0.33 to 0.63
	RCP8.5	0.30	0.22 to 0.38	0.63	0.45 to 0.82

Notes:

[a] Based on the CMIP5 ensemble; anomalies calculated with respect to 1986–2005. Using HadCRUT4 and its uncertainty estimate (5–95% confidence interval), the observed warming to the reference period 1986–2005 is 0.61 [0.55 to 0.67] °C from 1850–1900, and 0.11 [0.09 to 0.13] °C from 1980–1999, the reference period for projections used in AR4. *Likely* ranges have not been assessed here with respect to earlier reference periods because methods are not generally available in the literature for combining the uncertainties in models and observations. Adding projected and observed changes does not account for potential effects of model biases compared to observations, and for natural internal variability during the observational reference period {2.4; 11.2; Tables 12.2 and 12.3}

[b] Based on 21 CMIP5 models; anomalies calculated with respect to 1986–2005. Where CMIP5 results were not available for a particular AOGCM and scenario, they were estimated as explained in Chapter 13, Table 13.5. The contributions from ice sheet rapid dynamical change and anthropogenic land water storage are treated as having uniform probability distributions, and as largely independent of scenario. This treatment does not imply that the contributions concerned will not depend on the scenario followed, only that the current state of knowledge does not permit a quantitative assessment of the dependence. Based on current understanding, only the collapse of marine-based sectors of the Antarctic ice sheet, if initiated, could cause global mean sea level to rise substantially above the *likely* range during the 21st century. There is *medium confidence* that this additional contribution would not exceed several tenths of a meter of sea level rise during the 21st century.

[c] Calculated from projections as 5−95% model ranges. These ranges are then assessed to be *likely* ranges after accounting for additional uncertainties or different levels of confidence in models. For projections of global mean surface temperature change in 2046−2065 *confidence* is *medium*, because the relative importance of natural internal variability, and uncertainty in non-greenhouse gas forcing and response, are larger than for 2081−2100. The *likely* ranges for 2046−2065 do not take into account the possible influence of factors that lead to the assessed range for near-term (2016−2035) global mean surface temperature change that is lower than the 5−95% model range, because the influence of these factors on longer term projections has not been quantified due to insufficient scientific understanding. {11.3}

[d] Calculated from projections as 5−95% model ranges. These ranges are then assessed to be *likely* ranges after accounting for additional uncertainties or different levels of confidence in models. For projections of global mean sea level rise *confidence* is *medium* for both time horizons.

SPM

E.3 Atmosphere: Air Quality

- The range in projections of air quality (ozone and PM2.5[17] in near-surface air) is driven primarily by emissions (including CH_4), rather than by physical climate change (*medium confidence*). There is *high confidence* that globally, warming decreases background surface ozone. High CH_4 levels (as in RCP8.5) can offset this decrease, raising background surface ozone by year 2100 on average by about 8 ppb (25% of current levels) relative to scenarios with small CH_4 changes (as in RCP4.5 and RCP6.0) (*high confidence*). {11.3}

- Observational and modelling evidence indicates that, all else being equal, locally higher surface temperatures in polluted regions will trigger regional feedbacks in chemistry and local emissions that will increase peak levels of ozone and PM2.5 (*medium confidence*). For PM2.5, climate change may alter natural aerosol sources as well as removal by precipitation, but no confidence level is attached to the overall impact of climate change on PM2.5 distributions. {11.3}

E.4 Ocean

The global ocean will continue to warm during the 21st century. Heat will penetrate from the surface to the deep ocean and affect ocean circulation. {11.3, 12.4}

- The strongest ocean warming is projected for the surface in tropical and Northern Hemisphere subtropical regions. At greater depth the warming will be most pronounced in the Southern Ocean (*high confidence*). Best estimates of ocean warming in the top one hundred meters are about 0.6°C (RCP2.6) to 2.0°C (RCP8.5), and about 0.3°C (RCP2.6) to 0.6°C (RCP8.5) at a depth of about 1000 m by the end of the 21st century. {12.4, 14.3}

- It is *very likely* that the Atlantic Meridional Overturning Circulation (AMOC) will weaken over the 21st century. Best estimates and ranges[18] for the reduction are 11% (1 to 24%) in RCP2.6 and 34% (12 to 54%) in RCP8.5. It is *likely* that there will be some decline in the AMOC by about 2050, but there may be some decades when the AMOC increases due to large natural internal variability. {11.3, 12.4}

- It is *very unlikely* that the AMOC will undergo an abrupt transition or collapse in the 21st century for the scenarios considered. There is *low confidence* in assessing the evolution of the AMOC beyond the 21st century because of the limited number of analyses and equivocal results. However, a collapse beyond the 21st century for large sustained warming cannot be excluded. {12.5}

E.5 Cryosphere

It is *very likely* that the Arctic sea ice cover will continue to shrink and thin and that Northern Hemisphere spring snow cover will decrease during the 21st century as global mean surface temperature rises. Global glacier volume will further decrease. {12.4, 13.4}

- Year-round reductions in Arctic sea ice extent are projected by the end of the 21st century from multi-model averages. These reductions range from 43% for RCP2.6 to 94% for RCP8.5 in September and from 8% for RCP2.6 to 34% for RCP8.5 in February (*medium confidence*) (see Figures SPM.7 and SPM.8). {12.4}

---

[17] PM2.5 refers to particulate matter with a diameter of less than 2.5 micrometres, a measure of atmospheric aerosol concentration.

[18] The ranges in this paragraph indicate a CMIP5 model spread.

- Based on an assessment of the subset of models that most closely reproduce the climatological mean state and 1979 to 2012 trend of the Arctic sea ice extent, a nearly ice-free Arctic Ocean[19] in September before mid-century is *likely* for RCP8.5 (*medium confidence*) (see Figures SPM.7 and SPM.8). A projection of when the Arctic might become nearly ice-free in September in the 21st century cannot be made with confidence for the other scenarios. {11.3, 12.4, 12.5}

- In the Antarctic, a decrease in sea ice extent and volume is projected with *low confidence* for the end of the 21st century as global mean surface temperature rises. {12.4}

- By the end of the 21st century, the global glacier volume, excluding glaciers on the periphery of Antarctica, is projected to decrease by 15 to 55% for RCP2.6, and by 35 to 85% for RCP8.5 (*medium confidence*). {13.4, 13.5}

- The area of Northern Hemisphere spring snow cover is projected to decrease by 7% for RCP2.6 and by 25% in RCP8.5 by the end of the 21st century for the model average (*medium confidence*). {12.4}

- It is *virtually certain* that near-surface permafrost extent at high northern latitudes will be reduced as global mean surface temperature increases. By the end of the 21st century, the area of permafrost near the surface (upper 3.5 m) is projected to decrease by between 37% (RCP2.6) to 81% (RCP8.5) for the model average (*medium confidence*). {12.4}

E.6 Sea Level

Global mean sea level will continue to rise during the 21st century (see Figure SPM.9). Under all RCP scenarios, the rate of sea level rise will *very likely* exceed that observed during 1971 to 2010 due to increased ocean warming and increased loss of mass from glaciers and ice sheets. {13.3–13.5}

- Confidence in projections of global mean sea level rise has increased since the AR4 because of the improved physical understanding of the components of sea level, the improved agreement of process-based models with observations, and the inclusion of ice-sheet dynamical changes. {13.3–13.5}

- Global mean sea level rise for 2081–2100 relative to 1986–2005 will *likely* be in the ranges of 0.26 to 0.55 m for RCP2.6, 0.32 to 0.63 m for RCP4.5, 0.33 to 0.63 m for RCP6.0, and 0.45 to 0.82 m for RCP8.5 (*medium confidence*). For RCP8.5, the rise by the year 2100 is 0.52 to 0.98 m, with a rate during 2081 to 2100 of 8 to 16 mm yr^{-1} (*medium confidence*). These ranges are derived from CMIP5 climate projections in combination with process-based models and literature assessment of glacier and ice sheet contributions (see Figure SPM.9, Table SPM.2). {13.5}

- In the RCP projections, thermal expansion accounts for 30 to 55% of 21st century global mean sea level rise, and glaciers for 15 to 35%. The increase in surface melting of the Greenland ice sheet will exceed the increase in snowfall, leading to a positive contribution from changes in surface mass balance to future sea level (*high confidence*). While surface melting will remain small, an increase in snowfall on the Antarctic ice sheet is expected (*medium confidence*), resulting in a negative contribution to future sea level from changes in surface mass balance. Changes in outflow from both ice sheets combined will *likely* make a contribution in the range of 0.03 to 0.20 m by 2081–2100 (*medium confidence*). {13.3–13.5}

- Based on current understanding, only the collapse of marine-based sectors of the Antarctic ice sheet, if initiated, could cause global mean sea level to rise substantially above the *likely* range during the 21st century. However, there is *medium confidence* that this additional contribution would not exceed several tenths of a meter of sea level rise during the 21st century. {13.4, 13.5}

[19] Conditions in the Arctic Ocean are referred to as nearly ice-free when the sea ice extent is less than 10^6 km² for at least five consecutive years.

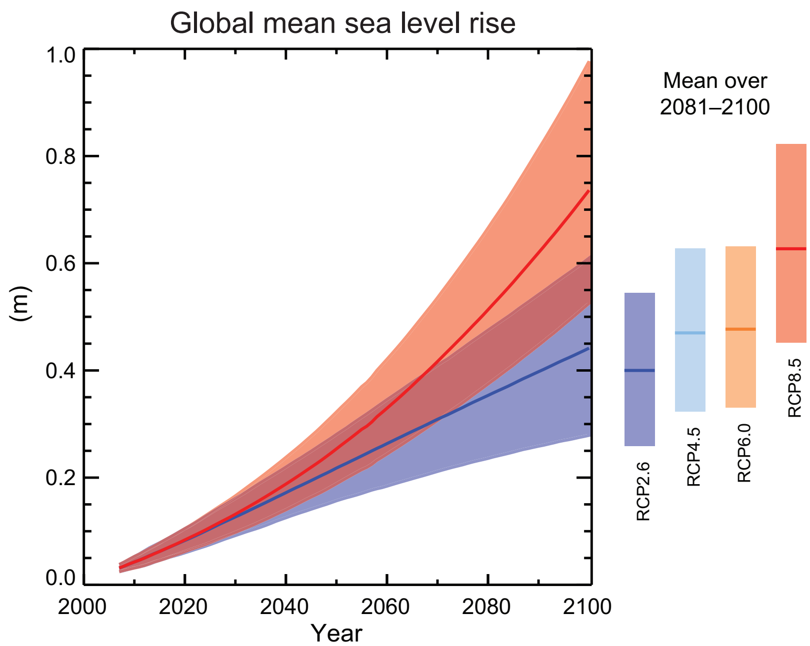

Figure SPM.9 | Projections of global mean sea level rise over the 21st century relative to 1986–2005 from the combination of the CMIP5 ensemble with process-based models, for RCP2.6 and RCP8.5. The assessed *likely* range is shown as a shaded band. The assessed *likely* ranges for the mean over the period 2081–2100 for all RCP scenarios are given as coloured vertical bars, with the corresponding median value given as a horizontal line. For further technical details see the Technical Summary Supplementary Material {Table 13.5, Figures 13.10 and 13.11; Figures TS.21 and TS.22}

- The basis for higher projections of global mean sea level rise in the 21st century has been considered and it has been concluded that there is currently insufficient evidence to evaluate the probability of specific levels above the assessed *likely* range. Many semi-empirical model projections of global mean sea level rise are higher than process-based model projections (up to about twice as large), but there is no consensus in the scientific community about their reliability and there is thus *low confidence* in their projections. {13.5}

- Sea level rise will not be uniform. By the end of the 21st century, it is *very likely* that sea level will rise in more than about 95% of the ocean area. About 70% of the coastlines worldwide are projected to experience sea level change within 20% of the global mean sea level change. {13.1, 13.6}

E.7 Carbon and Other Biogeochemical Cycles

Climate change will affect carbon cycle processes in a way that will exacerbate the increase of CO_2 in the atmosphere (*high confidence*). Further uptake of carbon by the ocean will increase ocean acidification. {6.4}

- Ocean uptake of anthropogenic CO_2 will continue under all four RCPs through to 2100, with higher uptake for higher concentration pathways (*very high confidence*). The future evolution of the land carbon uptake is less certain. A majority of models projects a continued land carbon uptake under all RCPs, but some models simulate a land carbon loss due to the combined effect of climate change and land use change. {6.4}

- Based on Earth System Models, there is *high confidence* that the feedback between climate and the carbon cycle is positive in the 21st century; that is, climate change will partially offset increases in land and ocean carbon sinks caused by rising atmospheric CO_2. As a result more of the emitted anthropogenic CO_2 will remain in the atmosphere. A positive feedback between climate and the carbon cycle on century to millennial time scales is supported by paleoclimate observations and modelling. {6.2, 6.4}

Table SPM.3 | Cumulative CO_2 emissions for the 2012 to 2100 period compatible with the RCP atmospheric concentrations simulated by the CMIP5 Earth System Models. {6.4, Table 6.12, Figure TS.19}

Scenario	Cumulative CO_2 Emissions 2012 to 2100[a]			
	GtC		$GtCO_2$	
	Mean	Range	Mean	Range
RCP2.6	270	140 to 410	990	510 to 1505
RCP4.5	780	595 to 1005	2860	2180 to 3690
RCP6.0	1060	840 to 1250	3885	3080 to 4585
RCP8.5	1685	1415 to 1910	6180	5185 to 7005

Notes:
[a] 1 Gigatonne of carbon = 1 GtC = 10^{15} grams of carbon. This corresponds to 3.667 $GtCO_2$.

- Earth System Models project a global increase in ocean acidification for all RCP scenarios. The corresponding decrease in surface ocean pH by the end of 21st century is in the range[18] of 0.06 to 0.07 for RCP2.6, 0.14 to 0.15 for RCP4.5, 0.20 to 0.21 for RCP6.0, and 0.30 to 0.32 for RCP8.5 (see Figures SPM.7 and SPM.8). {6.4}

- Cumulative CO_2 emissions[20] for the 2012 to 2100 period compatible with the RCP atmospheric CO_2 concentrations, as derived from 15 Earth System Models, range[18] from 140 to 410 GtC for RCP2.6, 595 to 1005 GtC for RCP4.5, 840 to 1250 GtC for RCP6.0, and 1415 to 1910 GtC for RCP8.5 (see Table SPM.3). {6.4}

- By 2050, annual CO_2 emissions derived from Earth System Models following RCP2.6 are smaller than 1990 emissions (by 14 to 96%). By the end of the 21st century, about half of the models infer emissions slightly above zero, while the other half infer a net removal of CO_2 from the atmosphere. {6.4, Figure TS.19}

- The release of CO_2 or CH_4 to the atmosphere from thawing permafrost carbon stocks over the 21st century is assessed to be in the range of 50 to 250 GtC for RCP8.5 (*low confidence*). {6.4}

E.8 Climate Stabilization, Climate Change Commitment and Irreversibility

Cumulative emissions of CO_2 largely determine global mean surface warming by the late 21st century and beyond (see Figure SPM.10). Most aspects of climate change will persist for many centuries even if emissions of CO_2 are stopped. This represents a substantial multi-century climate change commitment created by past, present and future emissions of CO_2. {12.5}

- Cumulative total emissions of CO_2 and global mean surface temperature response are approximately linearly related (see Figure SPM.10). Any given level of warming is associated with a range of cumulative CO_2 emissions[21], and therefore, e.g., higher emissions in earlier decades imply lower emissions later. {12.5}

- Limiting the warming caused by anthropogenic CO_2 emissions alone with a probability of >33%, >50%, and >66% to less than 2°C since the period 1861–1880[22], will require cumulative CO_2 emissions from all anthropogenic sources to stay between 0 and about 1570 GtC (5760 $GtCO_2$), 0 and about 1210 GtC (4440 $GtCO_2$), and 0 and about 1000 GtC (3670 $GtCO_2$) since that period, respectively[23]. These upper amounts are reduced to about 900 GtC (3300 $GtCO_2$), 820 GtC (3010 $GtCO_2$), and 790 GtC (2900 $GtCO_2$), respectively, when accounting for non-CO_2 forcings as in RCP2.6. An amount of 515 [445 to 585] GtC (1890 [1630 to 2150] $GtCO_2$), was already emitted by 2011. {12.5}

[20] From fossil fuel, cement, industry, and waste sectors.

[21] Quantification of this range of CO_2 emissions requires taking into account non-CO_2 drivers.

[22] The first 20-year period available from the models.

[23] This is based on the assessment of the transient climate response to cumulative carbon emissions (TCRE, see Section D.2).

SPM

- A lower warming target, or a higher likelihood of remaining below a specific warming target, will require lower cumulative CO_2 emissions. Accounting for warming effects of increases in non-CO_2 greenhouse gases, reductions in aerosols, or the release of greenhouse gases from permafrost will also lower the cumulative CO_2 emissions for a specific warming target (see Figure SPM.10). {12.5}

- A large fraction of anthropogenic climate change resulting from CO_2 emissions is irreversible on a multi-century to millennial time scale, except in the case of a large net removal of CO_2 from the atmosphere over a sustained period. Surface temperatures will remain approximately constant at elevated levels for many centuries after a complete cessation of net anthropogenic CO_2 emissions. Due to the long time scales of heat transfer from the ocean surface to depth, ocean warming will continue for centuries. Depending on the scenario, about 15 to 40% of emitted CO_2 will remain in the atmosphere longer than 1,000 years. {Box 6.1, 12.4, 12.5}

- It is *virtually certain* that global mean sea level rise will continue beyond 2100, with sea level rise due to thermal expansion to continue for many centuries. The few available model results that go beyond 2100 indicate global mean sea level rise above the pre-industrial level by 2300 to be less than 1 m for a radiative forcing that corresponds to CO_2 concentrations that peak and decline and remain below 500 ppm, as in the scenario RCP2.6. For a radiative forcing that corresponds to a CO_2 concentration that is above 700 ppm but below 1500 ppm, as in the scenario RCP8.5, the projected rise is 1 m to more than 3 m (*medium confidence*). {13.5}

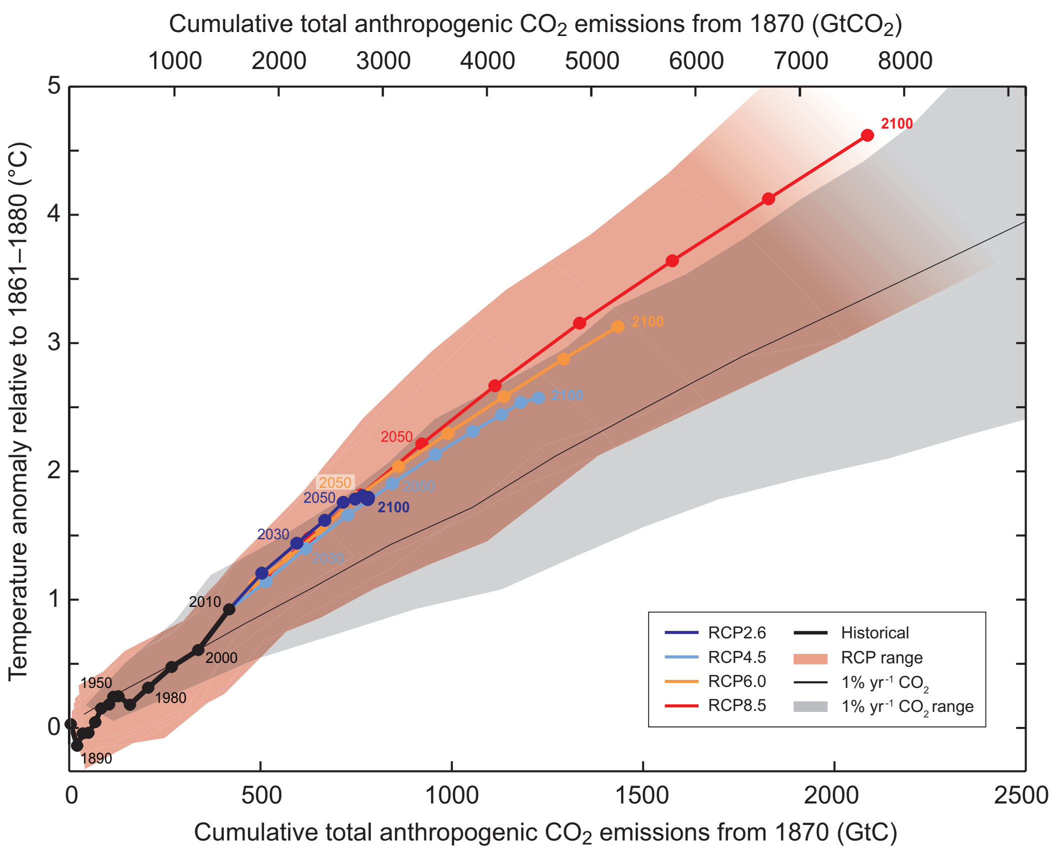

Figure SPM.10 | Global mean surface temperature increase as a function of cumulative total global CO_2 emissions from various lines of evidence. Multi-model results from a hierarchy of climate-carbon cycle models for each RCP until 2100 are shown with coloured lines and decadal means (dots). Some decadal means are labeled for clarity (e.g., 2050 indicating the decade 2040–2049). Model results over the historical period (1860 to 2010) are indicated in black. The coloured plume illustrates the multi-model spread over the four RCP scenarios and fades with the decreasing number of available models in RCP8.5. The multi-model mean and range simulated by CMIP5 models, forced by a CO_2 increase of 1% per year (1% yr^{-1} CO_2 simulations), is given by the thin black line and grey area. For a specific amount of cumulative CO_2 emissions, the 1% per year CO_2 simulations exhibit lower warming than those driven by RCPs, which include additional non-CO_2 forcings. Temperature values are given relative to the 1861–1880 base period, emissions relative to 1870. Decadal averages are connected by straight lines. For further technical details see the Technical Summary Supplementary Material. {Figure 12.45; TS TFE.8, Figure 1}

- Sustained mass loss by ice sheets would cause larger sea level rise, and some part of the mass loss might be irreversible. There is *high confidence* that sustained warming greater than some threshold would lead to the near-complete loss of the Greenland ice sheet over a millennium or more, causing a global mean sea level rise of up to 7 m. Current estimates indicate that the threshold is greater than about 1°C (*low confidence*) but less than about 4°C (*medium confidence*) global mean warming with respect to pre-industrial. Abrupt and irreversible ice loss from a potential instability of marine-based sectors of the Antarctic ice sheet in response to climate forcing is possible, but current evidence and understanding is insufficient to make a quantitative assessment. {5.8, 13.4, 13.5}

- Methods that aim to deliberately alter the climate system to counter climate change, termed geoengineering, have been proposed. Limited evidence precludes a comprehensive quantitative assessment of both Solar Radiation Management (SRM) and Carbon D ioxide Removal (CDR) and their impact on the climate system. CDR methods have biogeochemical and technological limitations to their potential on a global scale. There is insufficient knowledge to quantify how much CO_2 emissions could be partially offset by CDR on a century timescale. Modelling indicates that SRM methods, if realizable, have the potential to substantially offset a global temperature rise, but they would also modify the global water cycle, and would not reduce ocean acidification. If SRM were terminated for any reason, there is *high confidence* that global surface temperatures would rise very rapidly to values consistent with the greenhouse gas forcing. CDR and SRM methods carry side effects and long-term consequences on a global scale. {6.5, 7.7}

Box SPM.1: Representative Concentration Pathways (RCPs)

Climate change projections in IPCC Working Group I require information about future emissions or concentrations of greenhouse gases, aerosols and other climate drivers. This information is often expressed as a scenario of human activities, which are not assessed in this report. Scenarios used in Working Group I have focused on anthropogenic emissions and do not include changes in natural drivers such as solar or volcanic forcing or natural emissions, for example, of CH_4 and N_2O.

For the Fifth Assessment Report of IPCC, the scientific community has defined a set of four new scenarios, denoted Representative Concentration Pathways (RCPs, see Glossary). They are identified by their approximate total radiative forcing in year 2100 relative to 1750: 2.6 W m^{-2} for RCP2.6, 4.5 W m^{-2} for RCP4.5, 6.0 W m^{-2} for RCP6.0, and 8.5 W m^{-2} for RCP8.5. For the Coupled Model Intercomparison Project Phase 5 (CMIP5) results, these values should be understood as indicative only, as the climate forcing resulting from all drivers varies between models due to specific model characteristics and treatment of short-lived climate forcers. These four RCPs include one mitigation scenario leading to a very low forcing level (RCP2.6), two stabilization scenarios (RCP4.5 and RCP6), and one scenario with very high greenhouse gas emissions (RCP8.5). The RCPs can thus represent a range of 21st century climate policies, as compared with the no-climate policy of the Special Report on Emissions Scenarios (SRES) used in the Third Assessment Report and the Fourth Assessment Report. For RCP6.0 and RCP8.5, radiative forcing does not peak by year 2100; for RCP2.6 it peaks and declines; and for RCP4.5 it stabilizes by 2100. Each RCP provides spatially resolved data sets of land use change and sector-based emissions of air pollutants, and it specifies annual greenhouse gas concentrations and anthropogenic emissions up to 2100. RCPs are based on a combination of integrated assessment models, simple climate models, atmospheric chemistry and global carbon cycle models. While the RCPs span a wide range of total forcing values, they do not cover the full range of emissions in the literature, particularly for aerosols.

Most of the CMIP5 and Earth System Model simulations were performed with prescribed CO_2 concentrations reaching 421 ppm (RCP2.6), 538 ppm (RCP4.5), 670 ppm (RCP6.0), and 936 ppm (RCP 8.5) by the year 2100. Including also the prescribed concentrations of CH_4 and N_2O, the combined CO_2-equivalent concentrations are 475 ppm (RCP2.6), 630 ppm (RCP4.5), 800 ppm (RCP6.0), and 1313 ppm (RCP8.5). For RCP8.5, additional CMIP5 Earth System Model simulations are performed with prescribed CO_2 emissions as provided by the integrated assessment models. For all RCPs, additional calculations were made with updated atmospheric chemistry data and models (including the Atmospheric Chemistry and Climate component of CMIP5) using the RCP prescribed emissions of the chemically reactive gases (CH_4, N_2O, HFCs, NO_x, CO, NMVOC). These simulations enable investigation of uncertainties related to carbon cycle feedbacks and atmospheric chemistry.

Climate Change 2014
Synthesis Report
Summary for Policymakers

Introduction

This Synthesis Report is based on the reports of the three Working Groups of the Intergovernmental Panel on Climate Change (IPCC), including relevant Special Reports. It provides an integrated view of climate change as the final part of the IPCC's Fifth Assessment Report (AR5).

This summary follows the structure of the longer report which addresses the following topics: Observed changes and their causes; Future climate change, risks and impacts; Future pathways for adaptation, mitigation and sustainable development; Adaptation and mitigation.

In the Synthesis Report, the certainty in key assessment findings is communicated as in the Working Group Reports and Special Reports. It is based on the author teams' evaluations of underlying scientific understanding and is expressed as a qualitative level of confidence (from *very low* to *very high*) and, when possible, probabilistically with a quantified likelihood (from *exceptionally unlikely* to *virtually certain*)[1]. Where appropriate, findings are also formulated as statements of fact without using uncertainty qualifiers.

This report includes information relevant to Article 2 of the United Nations Framework Convention on Climate Change (UNFCCC).

SPM 1. Observed Changes and their Causes

Human influence on the climate system is clear, and recent anthropogenic emissions of greenhouse gases are the highest in history. Recent climate changes have had widespread impacts on human and natural systems. *{1}*

SPM 1.1 Observed changes in the climate system

Warming of the climate system is unequivocal, and since the 1950s, many of the observed changes are unprecedented over decades to millennia. The atmosphere and ocean have warmed, the amounts of snow and ice have diminished, and sea level has risen. *{1.1}*

Each of the last three decades has been successively warmer at the Earth's surface than any preceding decade since 1850. The period from 1983 to 2012 was *likely* the warmest 30-year period of the last 1400 years in the Northern Hemisphere, where such assessment is possible (*medium confidence*). The globally averaged combined land and ocean surface temperature data as calculated by a linear trend show a warming of 0.85 [0.65 to 1.06] °C[2] over the period 1880 to 2012, when multiple independently produced datasets exist (Figure SPM.1a). *{1.1.1, Figure 1.1}*

In addition to robust multi-decadal warming, the globally averaged surface temperature exhibits substantial decadal and interannual variability (Figure SPM.1a). Due to this natural variability, trends based on short records are very sensitive to the beginning and end dates and do not in general reflect long-term climate trends. As one example, the rate of warming over

---

[1] Each finding is grounded in an evaluation of underlying evidence and agreement. In many cases, a synthesis of evidence and agreement supports an assignment of confidence. The summary terms for evidence are: limited, medium or robust. For agreement, they are low, medium or high. A level of confidence is expressed using five qualifiers: very low, low, medium, high and very high, and typeset in italics, e.g., *medium confidence*. The following terms have been used to indicate the assessed likelihood of an outcome or a result: virtually certain 99–100% probability, very likely 90–100%, likely 66–100%, about as likely as not 33–66%, unlikely 0–33%, very unlikely 0–10%, exceptionally unlikely 0–1%. Additional terms (extremely likely 95–100%, more likely than not >50–100%, more unlikely than likely 0–<50%, extremely unlikely 0–5%) may also be used when appropriate. Assessed likelihood is typeset in italics, e.g., *very likely*. See for more details: Mastrandrea, M.D., C.B. Field, T.F. Stocker, O. Edenhofer, K.L. Ebi, D.J. Frame, H. Held, E. Kriegler, K.J. Mach, P.R. Matschoss, G.-K. Plattner, G.W. Yohe and F.W. Zwiers, 2010: Guidance Note for Lead Authors of the IPCC Fifth Assessment Report on Consistent Treatment of Uncertainties, Intergovernmental Panel on Climate Change (IPCC), Geneva, Switzerland, 4 pp.

[2] Ranges in square brackets or following '±' are expected to have a 90% likelihood of including the value that is being estimated, unless otherwise stated.

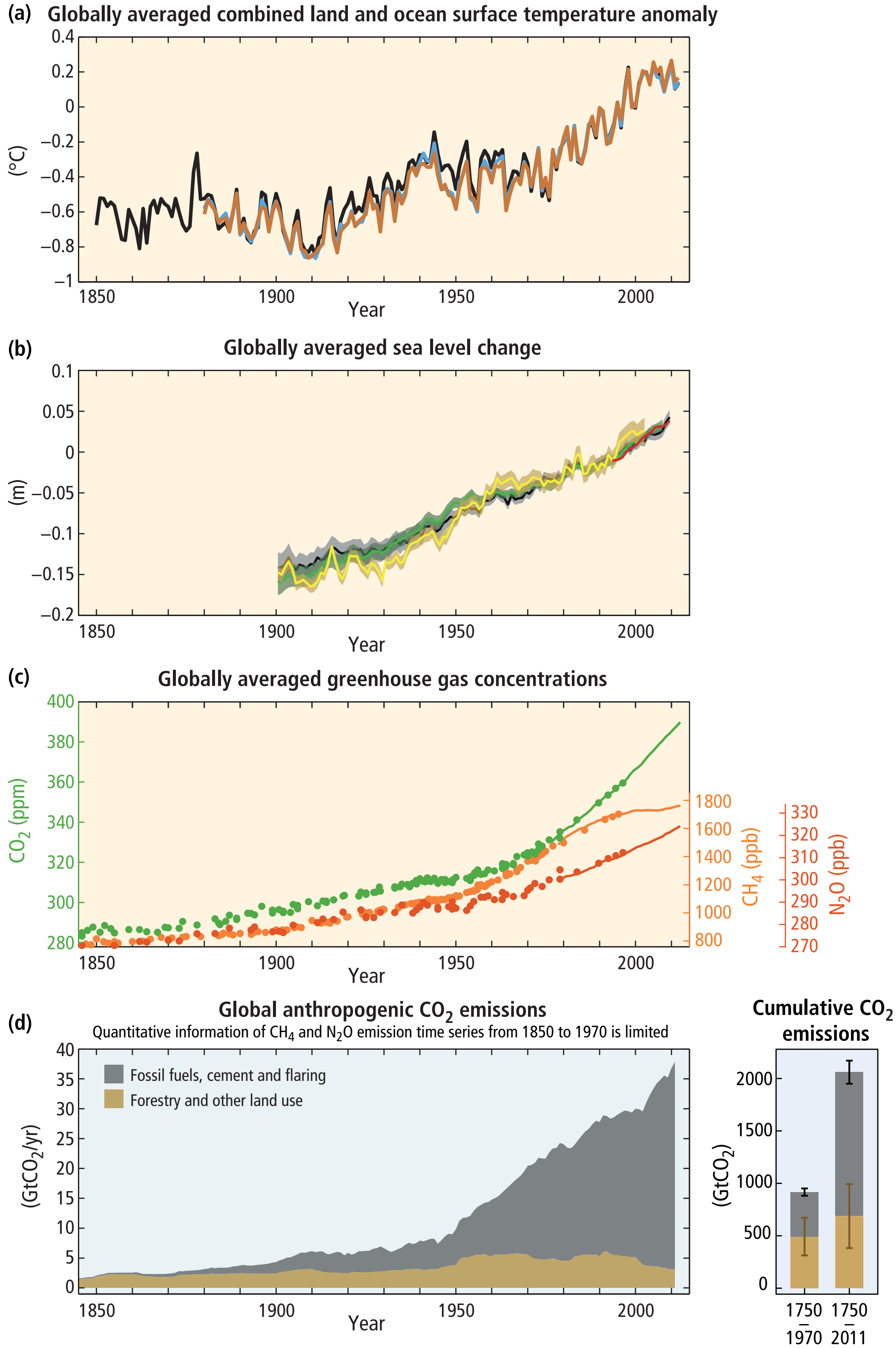

Figure SPM.1 | The complex relationship between the observations (panels a, b, c, yellow background) and the emissions (panel d, light blue background) is addressed in Section 1.2 and Topic 1. Observations and other indicators of a changing global climate system. Observations: **(a)** Annually and globally averaged combined land and ocean surface temperature anomalies relative to the average over the period 1986 to 2005. Colours indicate different data sets. **(b)** Annually and globally averaged sea level change relative to the average over the period 1986 to 2005 in the longest-running dataset. Colours indicate different data sets. All datasets are aligned to have the same value in 1993, the first year of satellite altimetry data (red). Where assessed, uncertainties are indicated by coloured shading. **(c)** Atmospheric concentrations of the greenhouse gases carbon dioxide (CO_2, green), methane (CH_4, orange) and nitrous oxide (N_2O, red) determined from ice core data (dots) and from direct atmospheric measurements (lines). Indicators: **(d)** Global anthropogenic CO_2 emissions from forestry and other land use as well as from burning of fossil fuel, cement production and flaring. Cumulative emissions of CO_2 from these sources and their uncertainties are shown as bars and whiskers, respectively, on the right hand side. The global effects of the accumulation of CH_4 and N_2O emissions are shown in panel c. Greenhouse gas emission data from 1970 to 2010 are shown in Figure SPM.2. *{Figures 1.1, 1.3, 1.5}* the past 15 years (1998–2012; 0.05 [–0.05 to 0.15] °C per decade), which begins with a strong El Niño, is smaller than the rate calculated since 1951 (1951–2012; 0.12 [0.08 to 0.14] °C per decade). *{1.1.1, Box 1.1}*

Ocean warming dominates the increase in energy stored in the climate system, accounting for more than 90% of the energy accumulated between 1971 and 2010 (*high confidence*), with only about 1% stored in the atmosphere. On a global scale, the ocean warming is largest near the surface, and the upper 75 m warmed by 0.11 [0.09 to 0.13] °C per decade over the period 1971 to 2010. It is *virtually certain* that the upper ocean (0–700 m) warmed from 1971 to 2010, and it *likely* warmed between the 1870s and 1971. *{1.1.2, Figure 1.2}*

Averaged over the mid-latitude land areas of the Northern Hemisphere, precipitation has increased since 1901 (*medium confidence* before and *high confidence* after 1951). For other latitudes, area-averaged long-term positive or negative trends have *low confidence*. Observations of changes in ocean surface salinity also provide indirect evidence for changes in the global water cycle over the ocean (*medium confidence*). It is *very likely* that regions of high salinity, where evaporation dominates, have become more saline, while regions of low salinity, where precipitation dominates, have become fresher since the 1950s. *{1.1.1, 1.1.2}*

Since the beginning of the industrial era, oceanic uptake of CO_2 has resulted in acidification of the ocean; the pH of ocean surface water has decreased by 0.1 (*high confidence*), corresponding to a 26% increase in acidity, measured as hydrogen ion concentration. *{1.1.2}*

Over the period 1992 to 2011, the Greenland and Antarctic ice sheets have been losing mass (*high confidence*), *likely* at a larger rate over 2002 to 2011. Glaciers have continued to shrink almost worldwide (*high confidence*). Northern Hemisphere spring snow cover has continued to decrease in extent (*high confidence*). There is *high confidence* that permafrost temperatures have increased in most regions since the early 1980s in response to increased surface temperature and changing snow cover. *{1.1.3}*

The annual mean Arctic sea-ice extent decreased over the period 1979 to 2012, with a rate that was *very likely* in the range 3.5 to 4.1% per decade. Arctic sea-ice extent has decreased in every season and in every successive decade since 1979, with the most rapid decrease in decadal mean extent in summer (*high confidence*). It is *very likely* that the annual mean Antarctic sea-ice extent increased in the range of 1.2 to 1.8% per decade between 1979 and 2012. However, there is *high confidence* that there are strong regional differences in Antarctica, with extent increasing in some regions and decreasing in others. *{1.1.3, Figure 1.1}*

Over the period 1901 to 2010, global mean sea level rose by 0.19 [0.17 to 0.21] m (Figure SPM.1b). The rate of sea level rise since the mid-19th century has been larger than the mean rate during the previous two millennia (*high confidence*). *{1.1.4, Figure 1.1}*

SPM 1.2 Causes of climate change

Anthropogenic greenhouse gas emissions have increased since the pre-industrial era, driven largely by economic and population growth, and are now higher than ever. This has led to atmospheric concentrations of carbon dioxide, methane and nitrous oxide that are unprecedented in at least the last 800,000 years. Their effects, together with those of other anthropogenic drivers, have been detected throughout the climate system and are *extremely likely* to have been the dominant cause of the observed warming since the mid-20th century. *{1.2, 1.3.1}*

Anthropogenic greenhouse gas (GHG) emissions since the pre-industrial era have driven large increases in the atmospheric concentrations of carbon dioxide (CO_2), methane (CH_4) and nitrous oxide (N_2O) (Figure SPM.1c). Between 1750 and 2011, cumulative anthropogenic CO_2 emissions to the atmosphere were 2040 ± 310 $GtCO_2$. About 40% of these emissions have remained in the atmosphere (880 ± 35 $GtCO_2$); the rest was removed from the atmosphere and stored on land (in plants and soils) and in the ocean. The ocean has absorbed about 30% of the emitted anthropogenic CO_2, causing ocean acidification. About half of the anthropogenic CO_2 emissions between 1750 and 2011 have occurred in the last 40 years (*high confidence*) (Figure SPM.1d). *{1.2.1, 1.2.2}*

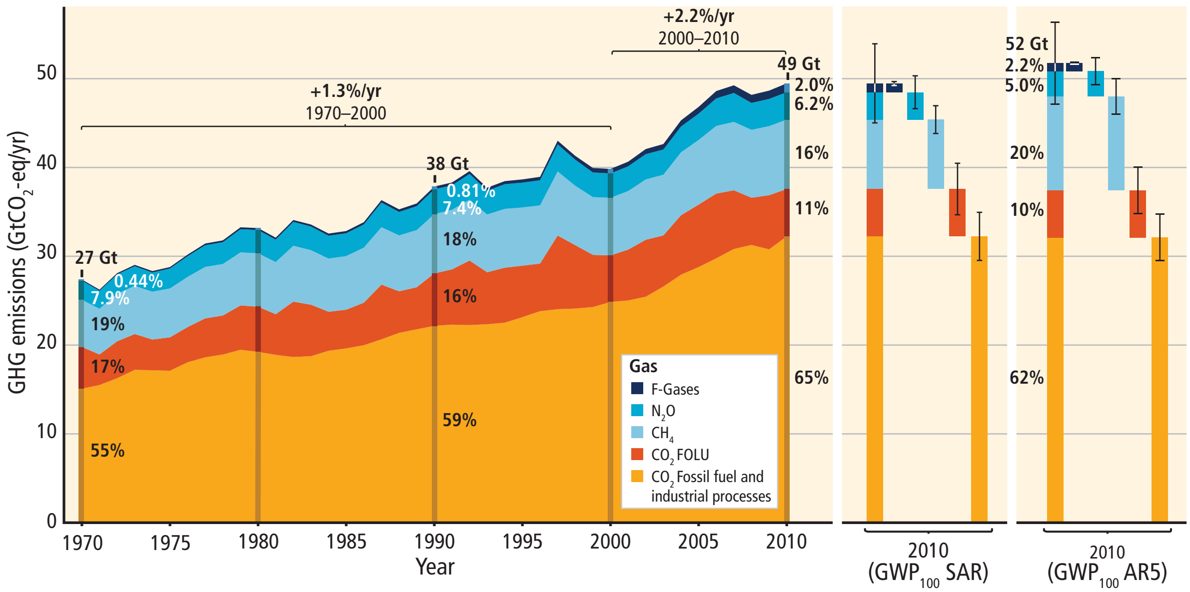

Figure SPM.2 | Total annual anthropogenic greenhouse gas (GHG) emissions (gigatonne of CO_2-equivalent per year, $GtCO_2$-eq/yr) for the period 1970 to 2010 by gases: CO_2 from fossil fuel combustion and industrial processes; CO_2 from Forestry and Other Land Use (FOLU); methane (CH_4); nitrous oxide (N_2O); fluorinated gases covered under the Kyoto Protocol (F-gases). Right hand side shows 2010 emissions, using alternatively CO_2-equivalent emission weightings based on IPCC Second Assessment Report (SAR) and AR5 values. Unless otherwise stated, CO_2-equivalent emissions in this report include the basket of Kyoto gases (CO_2, CH_4, N_2O as well as F-gases) calculated based on 100-year Global Warming Potential (GWP_{100}) values from the SAR (see Glossary). Using the most recent GWP_{100} values from the AR5 (right-hand bars) would result in higher total annual GHG emissions (52 $GtCO_2$-eq/yr) from an increased contribution of methane, but does not change the long-term trend significantly. *{Figure 1.6, Box 3.2}*

Total anthropogenic GHG emissions have continued to increase over 1970 to 2010 with larger absolute increases between 2000 and 2010, despite a growing number of climate change mitigation policies. Anthropogenic GHG emissions in 2010 have reached 49 ± 4.5 $GtCO_2$-eq/yr [3]. Emissions of CO_2 from fossil fuel combustion and industrial processes contributed about 78% of the total GHG emissions increase from 1970 to 2010, with a similar percentage contribution for the increase during the period 2000 to 2010 (*high confidence*) (Figure SPM.2). Globally, economic and population growth continued to be the most important drivers of increases in CO_2 emissions from fossil fuel combustion. The contribution of population growth between 2000 and 2010 remained roughly identical to the previous three decades, while the contribution of economic growth has risen sharply. Increased use of coal has reversed the long-standing trend of gradual decarbonization (i.e., reducing the carbon intensity of energy) of the world's energy supply (*high confidence*). *{1.2.2}*

The evidence for human influence on the climate system has grown since the IPCC Fourth Assessment Report (AR4). It is *extremely likely* that more than half of the observed increase in global average surface temperature from 1951 to 2010 was caused by the anthropogenic increase in GHG concentrations and other anthropogenic forcings together. The best estimate of the human-induced contribution to warming is similar to the observed warming over this period (Figure SPM.3). Anthropogenic forcings have *likely* made a substantial contribution to surface temperature increases since the mid-20th century over every continental region except Antarctica[4]. Anthropogenic influences have *likely* affected the global water cycle since 1960 and contributed to the retreat of glaciers since the 1960s and to the increased surface melting of the Greenland ice sheet since 1993. Anthropogenic influences have *very likely* contributed to Arctic sea-ice loss since 1979 and have *very likely* made a substantial contribution to increases in global upper ocean heat content (0–700 m) and to global mean sea level rise observed since the 1970s. *{1.3, Figure 1.10}*

---

3 Greenhouse gas emissions are quantified as CO_2-equivalent ($GtCO_2$-eq) emissions using weightings based on the 100-year Global Warming Potentials, using IPCC Second Assessment Report values unless otherwise stated. *{Box 3.2}*

4 For Antarctica, large observational uncertainties result in *low confidence* that anthropogenic forcings have contributed to the observed warming averaged over available stations.

SPM

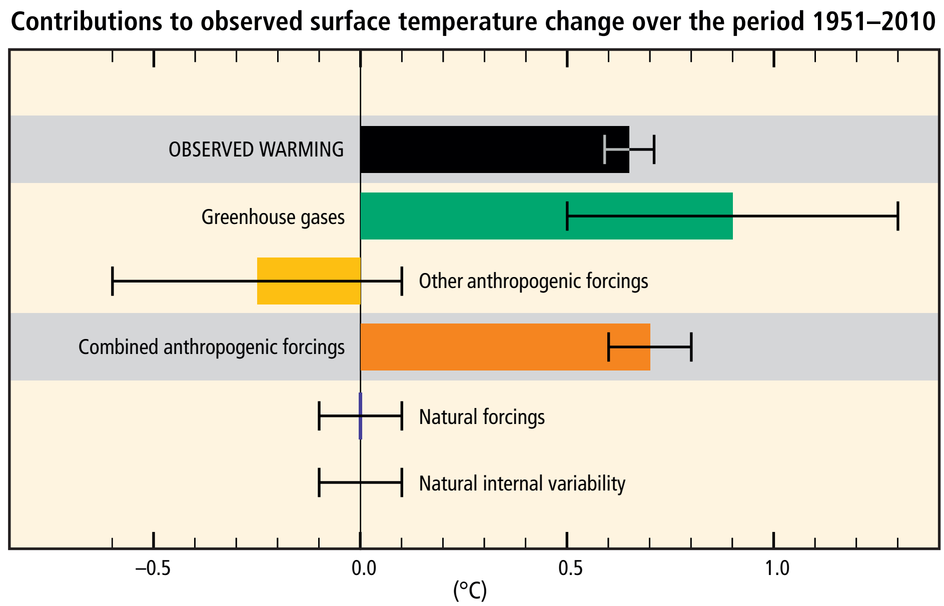

Figure SPM.3 | Assessed *likely* ranges (whiskers) and their mid-points (bars) for warming trends over the 1951–2010 period from well-mixed greenhouse gases, other anthropogenic forcings (including the cooling effect of aerosols and the effect of land use change), combined anthropogenic forcings, natural forcings and natural internal climate variability (which is the element of climate variability that arises spontaneously within the climate system even in the absence of forcings). The observed surface temperature change is shown in black, with the 5 to 95% uncertainty range due to observational uncertainty. The attributed warming ranges (colours) are based on observations combined with climate model simulations, in order to estimate the contribution of an individual external forcing to the observed warming. The contribution from the combined anthropogenic forcings can be estimated with less uncertainty than the contributions from greenhouse gases and from other anthropogenic forcings separately. This is because these two contributions partially compensate, resulting in a combined signal that is better constrained by observations. *{Figure 1.9}*

SPM 1.3 Impacts of climate change

In recent decades, changes in climate have caused impacts on natural and human systems on all continents and across the oceans. Impacts are due to observed climate change, irrespective of its cause, indicating the sensitivity of natural and human systems to changing climate. ***{1.3.2}***

Evidence of observed climate change impacts is strongest and most comprehensive for natural systems. In many regions, changing precipitation or melting snow and ice are altering hydrological systems, affecting water resources in terms of quantity and quality (*medium confidence*). Many terrestrial, freshwater and marine species have shifted their geographic ranges, seasonal activities, migration patterns, abundances and species interactions in response to ongoing climate change (*high confidence*). Some impacts on human systems have also been attributed to climate change, with a major or minor contribution of climate change distinguishable from other influences (Figure SPM.4). Assessment of many studies covering a wide range of regions and crops shows that negative impacts of climate change on crop yields have been more common than positive impacts (*high confidence*). Some impacts of ocean acidification on marine organisms have been attributed to human influence (*medium confidence*). *{1.3.2}*

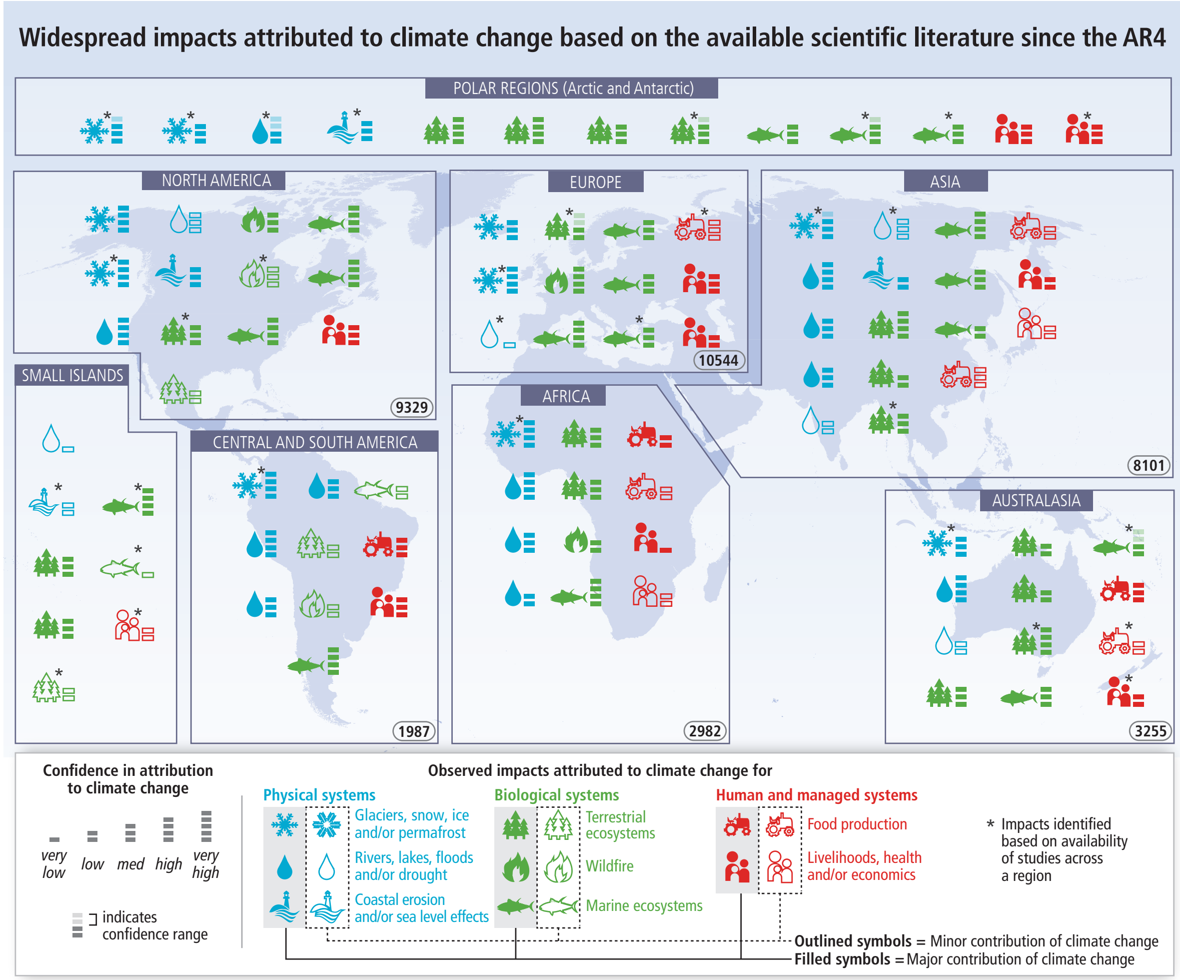

Figure SPM.4 | Based on the available scientific literature since the IPCC Fourth Assessment Report (AR4), there are substantially more impacts in recent decades now attributed to climate change. Attribution requires defined scientific evidence on the role of climate change. Absence from the map of additional impacts attributed to climate change does not imply that such impacts have not occurred. The publications supporting attributed impacts reflect a growing knowledge base, but publications are still limited for many regions, systems and processes, highlighting gaps in data and studies. Symbols indicate categories of attributed impacts, the relative contribution of climate change (major or minor) to the observed impact and confidence in attribution. Each symbol refers to one or more entries in WGII Table SPM.A1, grouping related regional-scale impacts. Numbers in ovals indicate regional totals of climate change publications from 2001 to 2010, based on the Scopus bibliographic database for publications in English with individual countries mentioned in title, abstract or key words (as of July 2011). These numbers provide an overall measure of the available scientific literature on climate change across regions; they do not indicate the number of publications supporting attribution of climate change impacts in each region. Studies for polar regions and small islands are grouped with neighbouring continental regions. The inclusion of publications for assessment of attribution followed IPCC scientific evidence criteria defined in WGII Chapter 18. Publications considered in the attribution analyses come from a broader range of literature assessed in the WGII AR5. See WGII Table SPM.A1 for descriptions of the attributed impacts. *{Figure 1.11}*

SPM 1.4 Extreme events

Changes in many extreme weather and climate events have been observed since about 1950. Some of these changes have been linked to human influences, including a decrease in cold temperature extremes, an increase in warm temperature extremes, an increase in extreme high sea levels and an increase in the number of heavy precipitation events in a number of regions. *{1.4}*

It is *very likely* that the number of cold days and nights has decreased and the number of warm days and nights has increased on the global scale. It is *likely* that the frequency of heat waves has increased in large parts of Europe, Asia and Australia. It is *very likely* that human influence has contributed to the observed global scale changes in the frequency and intensity of daily temperature extremes since the mid-20th century. It is *likely* that human influence has more than doubled the probability of occurrence of heat waves in some locations. There is *medium confidence* that the observed warming has increased heat-related human mortality and decreased cold-related human mortality in some regions. *{1.4}*

There are *likely* more land regions where the number of heavy precipitation events has increased than where it has decreased. Recent detection of increasing trends in extreme precipitation and discharge in some catchments implies greater risks of flooding at regional scale (*medium confidence*). It is *likely* that extreme sea levels (for example, as experienced in storm surges) have increased since 1970, being mainly a result of rising mean sea level. *{1.4}*

Impacts from recent climate-related extremes, such as heat waves, droughts, floods, cyclones and wildfires, reveal significant vulnerability and exposure of some ecosystems and many human systems to current climate variability (*very high confidence*). *{1.4}*

SPM 2. Future Climate Changes, Risks and Impacts

Continued emission of greenhouse gases will cause further warming and long-lasting changes in all components of the climate system, increasing the likelihood of severe, pervasive and irreversible impacts for people and ecosystems. Limiting climate change would require substantial and sustained reductions in greenhouse gas emissions which, together with adaptation, can limit climate change risks. *{2}*

SPM 2.1 Key drivers of future climate

Cumulative emissions of CO_2 largely determine global mean surface warming by the late 21st century and beyond. Projections of greenhouse gas emissions vary over a wide range, depending on both socio-economic development and climate policy. *{2.1}*

Anthropogenic GHG emissions are mainly driven by population size, economic activity, lifestyle, energy use, land use patterns, technology and climate policy. The Representative Concentration Pathways (RCPs), which are used for making projections based on these factors, describe four different 21st century pathways of GHG emissions and atmospheric concentrations, air pollutant emissions and land use. The RCPs include a stringent mitigation scenario (RCP2.6), two intermediate scenarios (RCP4.5 and RCP6.0) and one scenario with very high GHG emissions (RCP8.5). Scenarios without additional efforts to constrain emissions ('baseline scenarios') lead to pathways ranging between RCP6.0 and RCP8.5 (Figure SPM.5a). RCP2.6 is representative of a scenario that aims to keep global warming *likely* below 2°C above pre-industrial temperatures. The RCPs are consistent with the wide range of scenarios in the literature as assessed by WGIII[5]. *{2.1, Box 2.2, 4.3}*

Multiple lines of evidence indicate a strong, consistent, almost linear relationship between cumulative CO_2 emissions and projected global temperature change to the year 2100 in both the RCPs and the wider set of mitigation scenarios analysed in WGIII (Figure SPM.5b). Any given level of warming is associated with a range of cumulative CO_2 emissions[6], and therefore, e.g., higher emissions in earlier decades imply lower emissions later. *{2.2.5, Table 2.2}*

5 Roughly 300 baseline scenarios and 900 mitigation scenarios are categorized by CO_2-equivalent concentration (CO_2-eq) by 2100. The CO_2-eq includes the forcing due to all GHGs (including halogenated gases and tropospheric ozone), aerosols and albedo change.

6 Quantification of this range of CO_2 emissions requires taking into account non-CO_2 drivers.

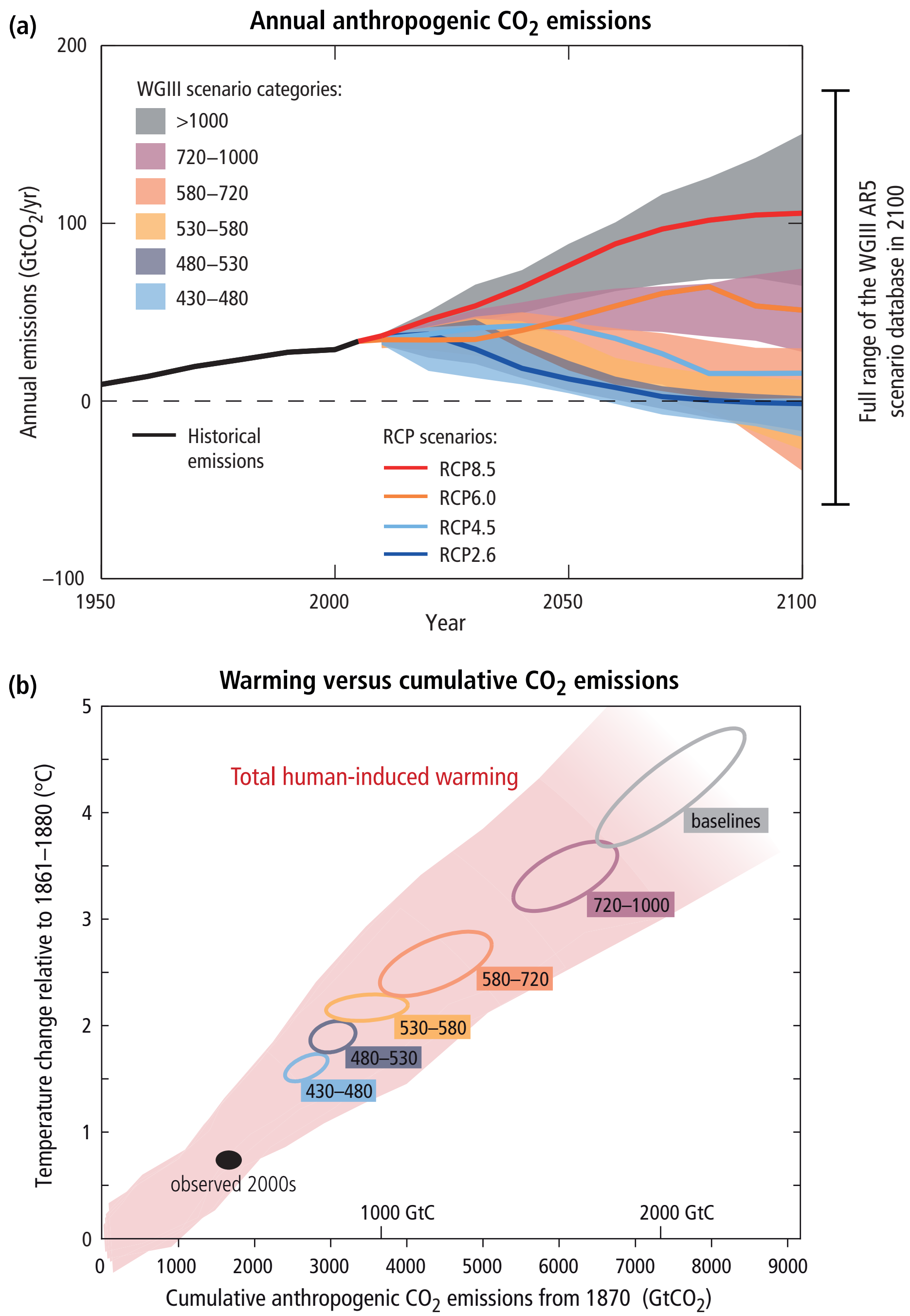

Figure SPM.5 | **(a)** Emissions of carbon dioxide (CO_2) alone in the Representative Concentration Pathways (RCPs) (lines) and the associated scenario categories used in WGIII (coloured areas show 5 to 95% range). The WGIII scenario categories summarize the wide range of emission scenarios published in the scientific literature and are defined on the basis of CO_2-eq concentration levels (in ppm) in 2100. The time series of other greenhouse gas emissions are shown in Box 2.2, Figure 1. **(b)** Global mean surface temperature increase at the time global CO_2 emissions reach a given net cumulative total, plotted as a function of that total, from various lines of evidence. Coloured plume shows the spread of past and future projections from a hierarchy of climate-carbon cycle models driven by historical emissions and the four RCPs over all times out to 2100, and fades with the decreasing number of available models. Ellipses show total anthropogenic warming in 2100 versus cumulative CO_2 emissions from 1870 to 2100 from a simple climate model (median climate response) under the scenario categories used in WGIII. The width of the ellipses in terms of temperature is caused by the impact of different scenarios for non-CO_2 climate drivers. The filled black ellipse shows observed emissions to 2005 and observed temperatures in the decade 2000–2009 with associated uncertainties. *{Box 2.2, Figure 1; Figure 2.3}*

Multi-model results show that limiting total human-induced warming to less than 2°C relative to the period 1861–1880 with a probability of >66%[7] would require cumulative CO_2 emissions from all anthropogenic sources since 1870 to remain below about 2900 $GtCO_2$ (with a range of 2550 to 3150 $GtCO_2$ depending on non-CO_2 drivers). About 1900 $GtCO_2$[8] had already been emitted by 2011. For additional context see Table 2.2. *{2.2.5}*

SPM 2.2 Projected changes in the climate system

Surface temperature is projected to rise over the 21st century under all assessed emission scenarios. It is *very likely* that heat waves will occur more often and last longer, and that extreme precipitation events will become more intense and frequent in many regions. The ocean will continue to warm and acidify, and global mean sea level to rise. *{2.2}*

The projected changes in Section SPM 2.2 are for 2081–2100 relative to 1986–2005, unless otherwise indicated.

Future climate will depend on committed warming caused by past anthropogenic emissions, as well as future anthropogenic emissions and natural climate variability. The global mean surface temperature change for the period 2016–2035 relative to 1986–2005 is similar for the four RCPs and will *likely* be in the range 0.3°C to 0.7°C (*medium confidence*). This assumes that there will be no major volcanic eruptions or changes in some natural sources (e.g., CH_4 and N_2O), or unexpected changes in total solar irradiance. By mid-21st century, the magnitude of the projected climate change is substantially affected by the choice of emissions scenario. *{2.2.1, Table 2.1}*

Relative to 1850–1900, global surface temperature change for the end of the 21st century (2081–2100) is projected to *likely* exceed 1.5°C for RCP4.5, RCP6.0 and RCP8.5 (*high confidence*). Warming is *likely* to exceed 2°C for RCP6.0 and RCP8.5 (*high confidence*), *more likely than not* to exceed 2°C for RCP4.5 (*medium confidence*), but *unlikely* to exceed 2°C for RCP2.6 (*medium confidence*). *{2.2.1}*

The increase of global mean surface temperature by the end of the 21st century (2081–2100) relative to 1986–2005 is *likely* to be 0.3°C to 1.7°C under RCP2.6, 1.1°C to 2.6°C under RCP4.5, 1.4°C to 3.1°C under RCP6.0 and 2.6°C to 4.8°C under RCP8.5[9]. The Arctic region will continue to warm more rapidly than the global mean (Figure SPM.6a, Figure SPM.7a). *{2.2.1, Figure 2.1, Figure 2.2, Table 2.1}*

It is *virtually certain* that there will be more frequent hot and fewer cold temperature extremes over most land areas on daily and seasonal timescales, as global mean surface temperature increases. It is *very likely* that heat waves will occur with a higher frequency and longer duration. Occasional cold winter extremes will continue to occur. *{2.2.1}*

---

7 Corresponding figures for limiting warming to 2°C with a probability of >50% and >33% are 3000 $GtCO_2$ (range of 2900 to 3200 $GtCO_2$) and 3300 $GtCO_2$ (range of 2950 to 3800 $GtCO_2$) respectively. Higher or lower temperature limits would imply larger or lower cumulative emissions respectively.

8 This corresponds to about two thirds of the 2900 $GtCO_2$ that would limit warming to less than 2°C with a probability of >66%; to about 63% of the total amount of 3000 $GtCO_2$ that would limit warming to less than 2°C with a probability of >50%; and to about 58% of the total amount of 3300 $GtCO_2$ that would limit warming to less than 2°C with a probability of >33%.

9 The period 1986–2005 is approximately 0.61 [0.55 to 0.67] °C warmer than 1850–1900. *{2.2.1}*

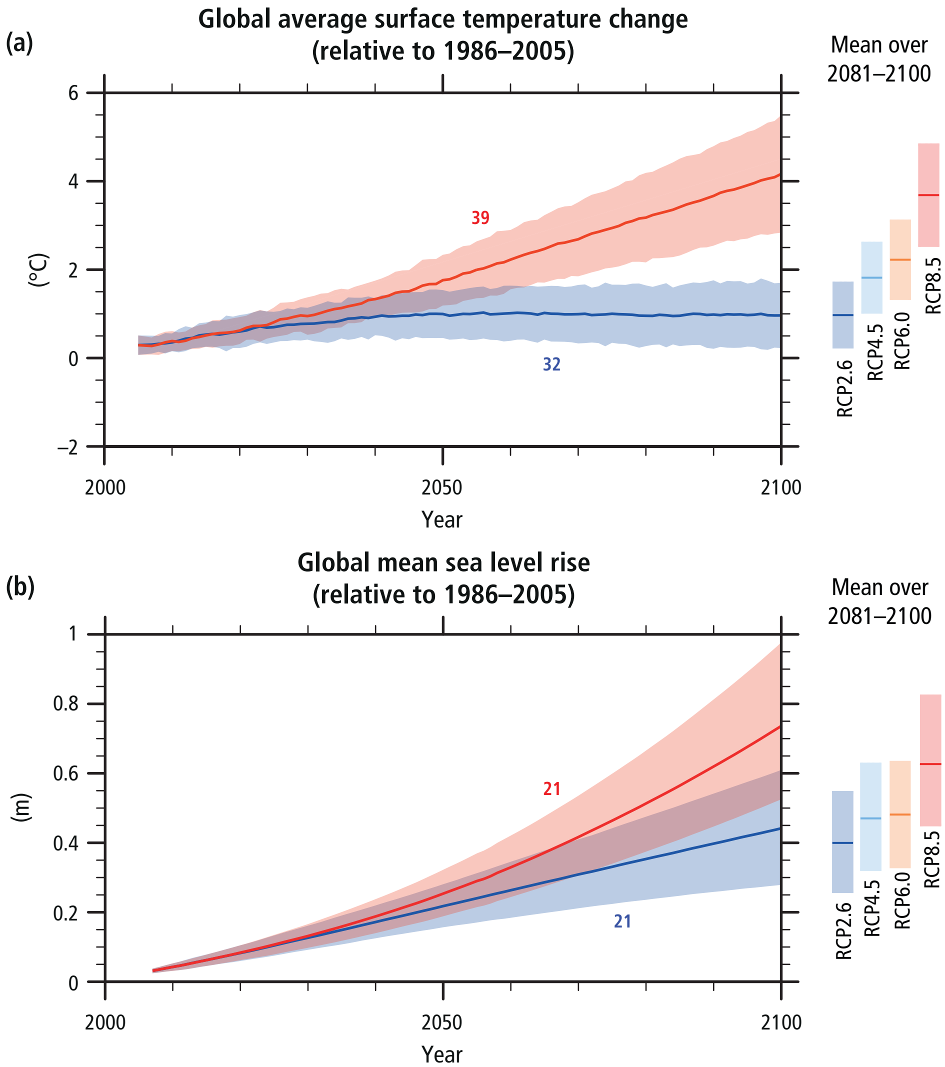

Figure SPM.6 | Global average surface temperature change **(a)** and global mean sea level rise[10] **(b)** from 2006 to 2100 as determined by multi-model simulations. All changes are relative to 1986–2005. Time series of projections and a measure of uncertainty (shading) are shown for scenarios RCP2.6 (blue) and RCP8.5 (red). The mean and associated uncertainties averaged over 2081–2100 are given for all RCP scenarios as coloured vertical bars at the right hand side of each panel. The number of Coupled Model Intercomparison Project Phase 5 (CMIP5) models used to calculate the multi-model mean is indicated. *{2.2, Figure 2.1}*

Changes in precipitation will not be uniform. The high latitudes and the equatorial Pacific are *likely* to experience an increase in annual mean precipitation under the RCP8.5 scenario. In many mid-latitude and subtropical dry regions, mean precipitation will *likely* decrease, while in many mid-latitude wet regions, mean precipitation will *likely* increase under the RCP8.5 scenario (Figure SPM.7b). Extreme precipitation events over most of the mid-latitude land masses and over wet tropical regions will *very likely* become more intense and more frequent. *{2.2.2, Figure 2.2}*

The global ocean will continue to warm during the 21st century, with the strongest warming projected for the surface in tropical and Northern Hemisphere subtropical regions (Figure SPM.7a). *{2.2.3, Figure 2.2}*

---

[10] Based on current understanding (from observations, physical understanding and modelling), only the collapse of marine-based sectors of the Antarctic ice sheet, if initiated, could cause global mean sea level to rise substantially above the *likely* range during the 21st century. There is *medium confidence* that this additional contribution would not exceed several tenths of a meter of sea level rise during the 21st century.

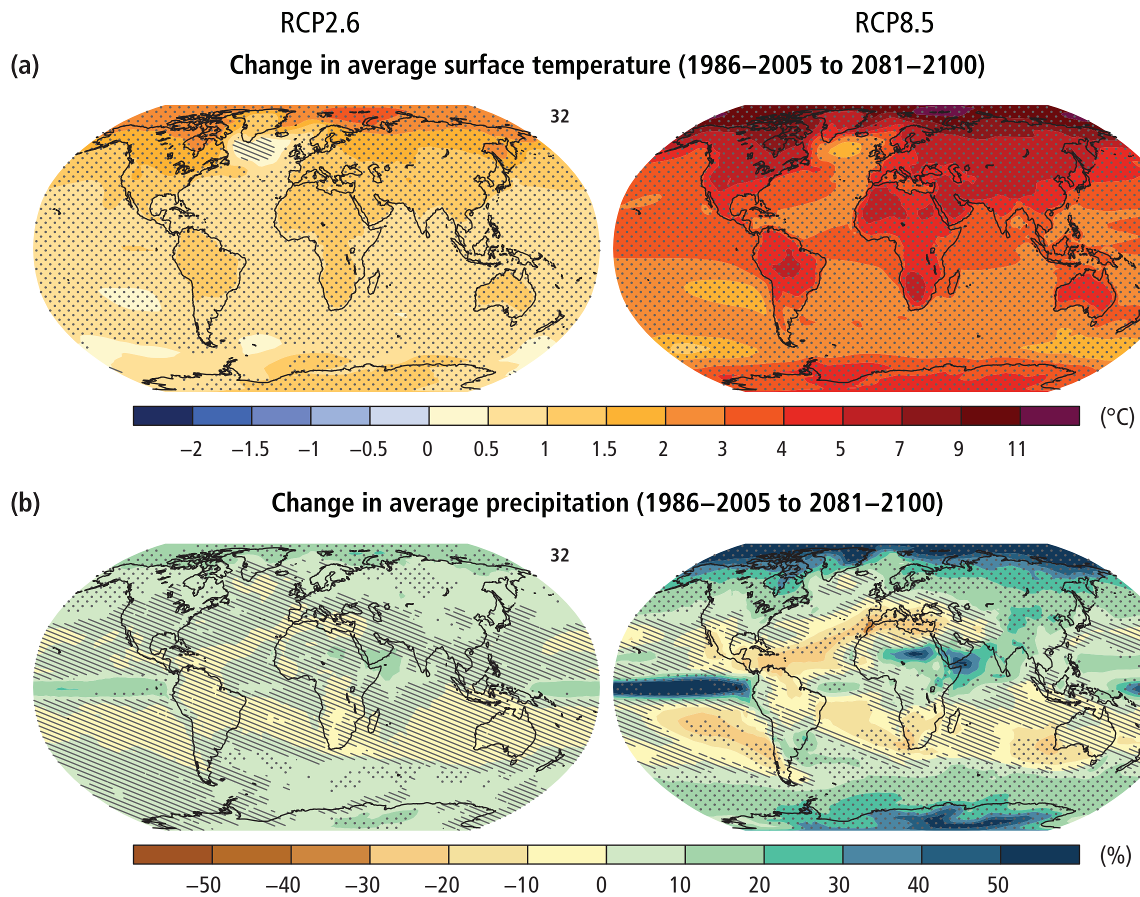

Figure SPM.7 | Change in average surface temperature **(a)** and change in average precipitation **(b)** based on multi-model mean projections for 2081–2100 relative to 1986–2005 under the RCP2.6 (left) and RCP8.5 (right) scenarios. The number of models used to calculate the multi-model mean is indicated in the upper right corner of each panel. Stippling (i.e., dots) shows regions where the projected change is large compared to natural internal variability and where at least 90% of models agree on the sign of change. Hatching (i.e., diagonal lines) shows regions where the projected change is less than one standard deviation of the natural internal variability. *{2.2, Figure 2.2}*

Earth System Models project a global increase in ocean acidification for all RCP scenarios by the end of the 21st century, with a slow recovery after mid-century under RCP2.6. The decrease in surface ocean pH is in the range of 0.06 to 0.07 (15 to 17% increase in acidity) for RCP2.6, 0.14 to 0.15 (38 to 41%) for RCP4.5, 0.20 to 0.21 (58 to 62%) for RCP6.0 and 0.30 to 0.32 (100 to 109%) for RCP8.5. *{2.2.4, Figure 2.1}*

Year-round reductions in Arctic sea ice are projected for all RCP scenarios. A nearly ice-free[11] Arctic Ocean in the summer sea-ice minimum in September before mid-century is *likely* for RCP8.5[12] (*medium confidence*). *{2.2.3, Figure 2.1}*

It is *virtually certain* that near-surface permafrost extent at high northern latitudes will be reduced as global mean surface temperature increases, with the area of permafrost near the surface (upper 3.5 m) projected to decrease by 37% (RCP2.6) to 81% (RCP8.5) for the multi-model average (*medium confidence*). *{2.2.3}*

The global glacier volume, excluding glaciers on the periphery of Antarctica (and excluding the Greenland and Antarctic ice sheets), is projected to decrease by 15 to 55% for RCP2.6 and by 35 to 85% for RCP8.5 (*medium confidence*). *{2.2.3}*

[11] When sea-ice extent is less than one million km^2 for at least five consecutive years.

[12] Based on an assessment of the subset of models that most closely reproduce the climatological mean state and 1979–2012 trend of the Arctic sea-ice extent.

There has been significant improvement in understanding and projection of sea level change since the AR4. Global mean sea level rise will continue during the 21st century, *very likely* at a faster rate than observed from 1971 to 2010. For the period 2081–2100 relative to 1986–2005, the rise will *likely* be in the ranges of 0.26 to 0.55 m for RCP2.6, and of 0.45 to 0.82 m for RCP8.5 (*medium confidence*)[10] (Figure SPM.6b). Sea level rise will not be uniform across regions. By the end of the 21st century, it is *very likely* that sea level will rise in more than about 95% of the ocean area. About 70% of the coastlines worldwide are projected to experience a sea level change within ±20% of the global mean. *{2.2.3}*

SPM 2.3 Future risks and impacts caused by a changing climate

Climate change will amplify existing risks and create new risks for natural and human systems. Risks are unevenly distributed and are generally greater for disadvantaged people and communities in countries at all levels of development. *{2.3}*

Risk of climate-related impacts results from the interaction of climate-related hazards (including hazardous events and trends) with the vulnerability and exposure of human and natural systems, including their ability to adapt. Rising rates and magnitudes of warming and other changes in the climate system, accompanied by ocean acidification, increase the risk of severe, pervasive and in some cases irreversible detrimental impacts. Some risks are particularly relevant for individual regions (Figure SPM.8), while others are global. The overall risks of future climate change impacts can be reduced by limiting the rate and magnitude of climate change, including ocean acidification. The precise levels of climate change sufficient to trigger abrupt and irreversible change remain uncertain, but the risk associated with crossing such thresholds increases with rising temperature (*medium confidence*). For risk assessment, it is important to evaluate the widest possible range of impacts, including low-probability outcomes with large consequences. *{1.5, 2.3, 2.4, 3.3, Box Introduction.1, Box 2.3, Box 2.4}*

A large fraction of species faces increased extinction risk due to climate change during and beyond the 21st century, especially as climate change interacts with other stressors (*high confidence*). Most plant species cannot naturally shift their geographical ranges sufficiently fast to keep up with current and high projected rates of climate change in most landscapes; most small mammals and freshwater molluscs will not be able to keep up at the rates projected under RCP4.5 and above in flat landscapes in this century (*high confidence*). Future risk is indicated to be high by the observation that natural global climate change at rates lower than current anthropogenic climate change caused significant ecosystem shifts and species extinctions during the past millions of years. Marine organisms will face progressively lower oxygen levels and high rates and magnitudes of ocean acidification (*high confidence*), with associated risks exacerbated by rising ocean temperature extremes (*medium confidence*). Coral reefs and polar ecosystems are highly vulnerable. Coastal systems and low-lying areas are at risk from sea level rise, which will continue for centuries even if the global mean temperature is stabilized (*high confidence*). *{2.3, 2.4, Figure 2.5}*

Climate change is projected to undermine food security (Figure SPM.9). Due to projected climate change by the mid-21st century and beyond, global marine species redistribution and marine biodiversity reduction in sensitive regions will challenge the sustained provision of fisheries productivity and other ecosystem services (*high confidence*). For wheat, rice and maize in tropical and temperate regions, climate change without adaptation is projected to negatively impact production for local temperature increases of 2°C or more above late 20th century levels, although individual locations may benefit (*medium confidence*). Global temperature increases of ~4°C or more[13] above late 20th century levels, combined with increasing food demand, would pose large risks to food security globally (*high confidence*). Climate change is projected to reduce renewable surface water and groundwater resources in most dry subtropical regions (*robust evidence*, *high agreement*), intensifying competition for water among sectors (*limited evidence*, *medium agreement*). *{2.3.1, 2.3.2}*

---

[13] Projected warming averaged over land is larger than global average warming for all RCP scenarios for the period 2081–2100 relative to 1986–2005. For regional projections, see Figure SPM.7. *{2.2}*

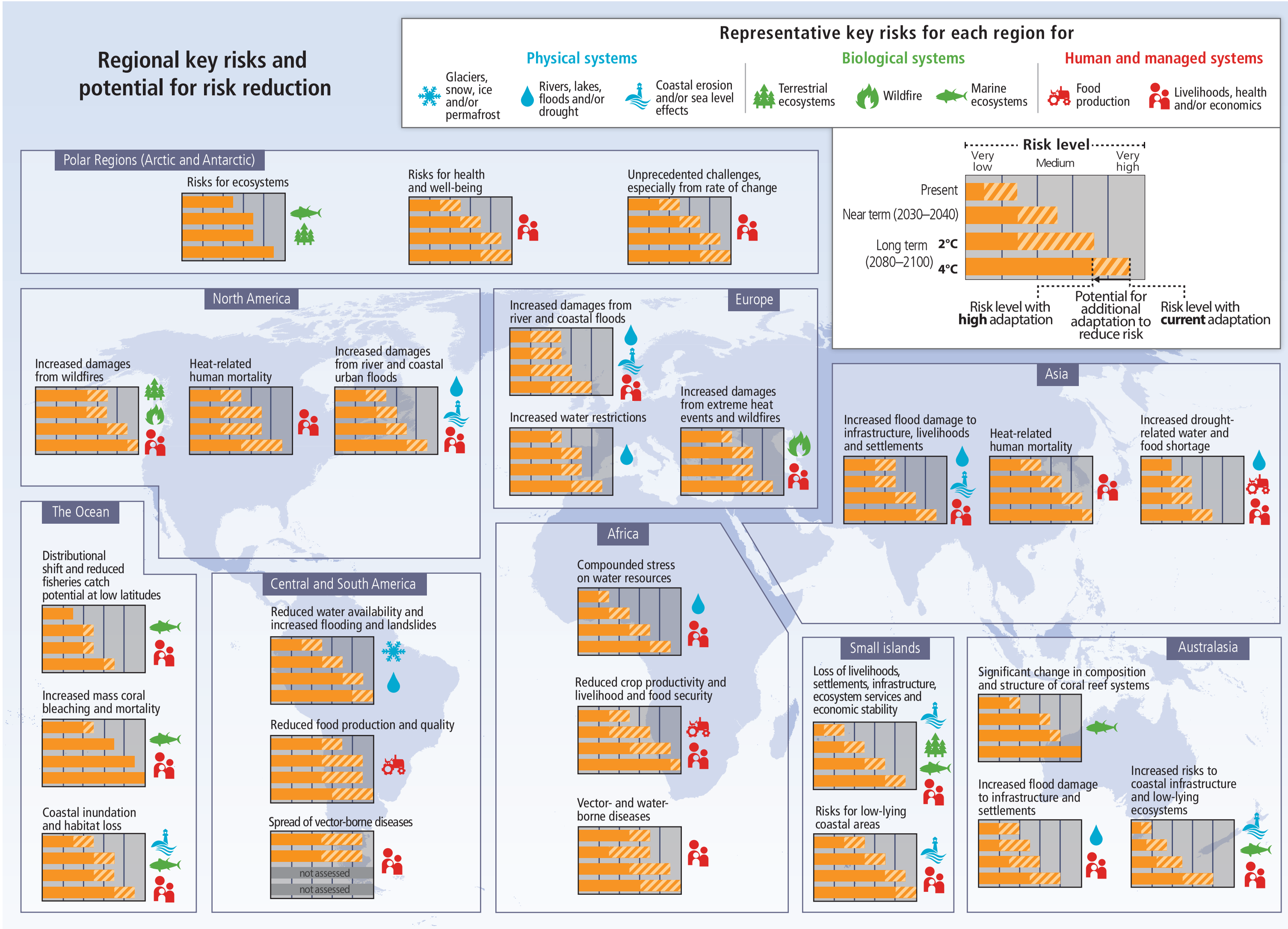

Figure SPM.8 | Representative key risks[14] for each region, including the potential for risk reduction through adaptation and mitigation, as well as limits to adaptation. Each key risk is assessed as very low, low, medium, high or very high. Risk levels are presented for three time frames: present, near term (here, for 2030–2040) and long term (here, for 2080–2100). In the near term, projected levels of global mean temperature increase do not diverge substantially across different emission scenarios. For the long term, risk levels are presented for two possible futures (2°C and 4°C global mean temperature increase above pre-industrial levels). For each timeframe, risk levels are indicated for a continuation of current adaptation and assuming high levels of current or future adaptation. Risk levels are not necessarily comparable, especially across regions. *{Figure 2.4}*

14 Identification of key risks was based on expert judgment using the following specific criteria: large magnitude, high probability or irreversibility of impacts; timing of impacts; persistent vulnerability or exposure contributing to risks; or limited potential to reduce risks through adaptation or mitigation.

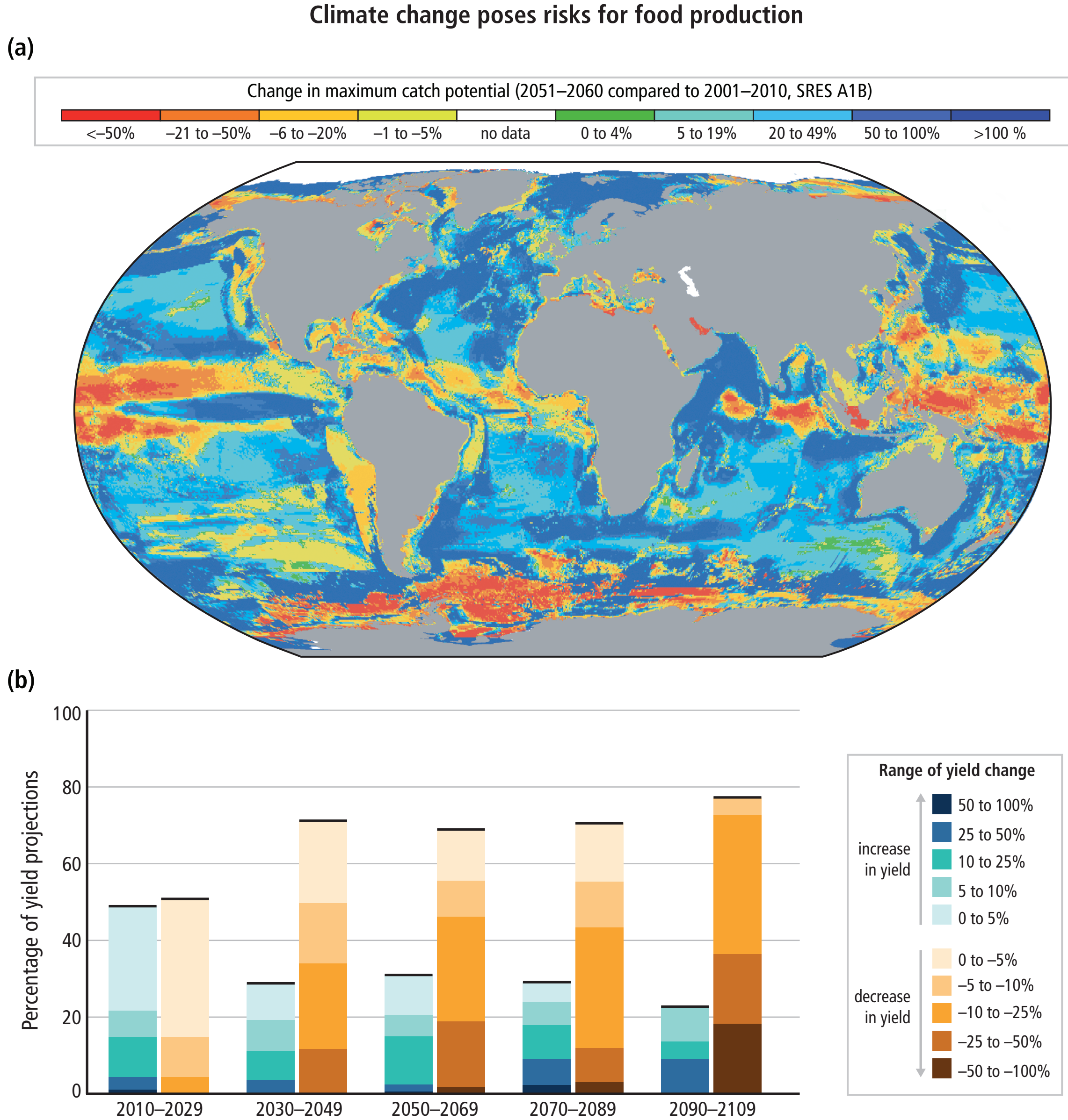

Figure SPM.9 | **(a)** Projected global redistribution of maximum catch potential of ~1000 exploited marine fish and invertebrate species. Projections compare the 10-year averages 2001–2010 and 2051–2060 using ocean conditions based on a single climate model under a moderate to high warming scenario, without analysis of potential impacts of overfishing or ocean acidification. **(b)** Summary of projected changes in crop yields (mostly wheat, maize, rice and soy), due to climate change over the 21st century. Data for each timeframe sum to 100%, indicating the percentage of projections showing yield increases versus decreases. The figure includes projections (based on 1090 data points) for different emission scenarios, for tropical and temperate regions and for adaptation and no-adaptation cases combined. Changes in crop yields are relative to late 20th century levels. *{Figure 2.6a, Figure 2.7}*

Until mid-century, projected climate change will impact human health mainly by exacerbating health problems that already exist (*very high confidence*). Throughout the 21st century, climate change is expected to lead to increases in ill-health in many regions and especially in developing countries with low income, as compared to a baseline without climate change (*high confidence*). By 2100 for RCP8.5, the combination of high temperature and humidity in some areas for parts of the year is expected to compromise common human activities, including growing food and working outdoors (*high confidence*). *{2.3.2}*

In urban areas climate change is projected to increase risks for people, assets, economies and ecosystems, including risks from heat stress, storms and extreme precipitation, inland and coastal flooding, landslides, air pollution, drought, water scarcity, sea level rise and storm surges (*very high confidence*). These risks are amplified for those lacking essential infrastructure and services or living in exposed areas. *{2.3.2}*

Rural areas are expected to experience major impacts on water availability and supply, food security, infrastructure and agricultural incomes, including shifts in the production areas of food and non-food crops around the world (*high confidence*). *{2.3.2}*

Aggregate economic losses accelerate with increasing temperature (*limited evidence, high agreement*), but global economic impacts from climate change are currently difficult to estimate. From a poverty perspective, climate change impacts are projected to slow down economic growth, make poverty reduction more difficult, further erode food security and prolong existing and create new poverty traps, the latter particularly in urban areas and emerging hotspots of hunger (*medium confidence*). International dimensions such as trade and relations among states are also important for understanding the risks of climate change at regional scales. *{2.3.2}*

Climate change is projected to increase displacement of people (*medium evidence, high agreement*). Populations that lack the resources for planned migration experience higher exposure to extreme weather events, particularly in developing countries with low income. Climate change can indirectly increase risks of violent conflicts by amplifying well-documented drivers of these conflicts such as poverty and economic shocks (*medium confidence*). *{2.3.2}*

SPM 2.4 Climate change beyond 2100, irreversibility and abrupt changes

Many aspects of climate change and associated impacts will continue for centuries, even if anthropogenic emissions of greenhouse gases are stopped. The risks of abrupt or irreversible changes increase as the magnitude of the warming increases. *{2.4}*

Warming will continue beyond 2100 under all RCP scenarios except RCP2.6. Surface temperatures will remain approximately constant at elevated levels for many centuries after a complete cessation of net anthropogenic CO_2 emissions. A large fraction of anthropogenic climate change resulting from CO_2 emissions is irreversible on a multi-century to millennial timescale, except in the case of a large net removal of CO_2 from the atmosphere over a sustained period. *{2.4, Figure 2.8}*

Stabilization of global average surface temperature does not imply stabilization for all aspects of the climate system. Shifting biomes, soil carbon, ice sheets, ocean temperatures and associated sea level rise all have their own intrinsic long timescales which will result in changes lasting hundreds to thousands of years after global surface temperature is stabilized. *{2.1, 2.4}*

There is *high confidence* that ocean acidification will increase for centuries if CO_2 emissions continue, and will strongly affect marine ecosystems. *{2.4}*

It is *virtually certain* that global mean sea level rise will continue for many centuries beyond 2100, with the amount of rise dependent on future emissions. The threshold for the loss of the Greenland ice sheet over a millennium or more, and an associated sea level rise of up to 7 m, is greater than about 1°C (*low confidence*) but less than about 4°C (*medium confidence*) of global warming with respect to pre-industrial temperatures. Abrupt and irreversible ice loss from the Antarctic ice sheet is possible, but current evidence and understanding is insufficient to make a quantitative assessment. *{2.4}*

Magnitudes and rates of climate change associated with medium- to high-emission scenarios pose an increased risk of abrupt and irreversible regional-scale change in the composition, structure and function of marine, terrestrial and freshwater ecosystems, including wetlands (*medium confidence*). A reduction in permafrost extent is *virtually certain* with continued rise in global temperatures. *{2.4}*

SPM 3. Future Pathways for Adaptation, Mitigation and Sustainable Development

Adaptation and mitigation are complementary strategies for reducing and managing the risks of climate change. Substantial emissions reductions over the next few decades can reduce climate risks in the 21st century and beyond, increase prospects for effective adaptation, reduce the costs and challenges of mitigation in the longer term and contribute to climate-resilient pathways for sustainable development. *{3.2, 3.3, 3.4}*

SPM 3.1 Foundations of decision-making about climate change

Effective decision-making to limit climate change and its effects can be informed by a wide range of analytical approaches for evaluating expected risks and benefits, recognizing the importance of governance, ethical dimensions, equity, value judgments, economic assessments and diverse perceptions and responses to risk and uncertainty. *{3.1}*

Sustainable development and equity provide a basis for assessing climate policies. Limiting the effects of climate change is necessary to achieve sustainable development and equity, including poverty eradication. Countries' past and future contributions to the accumulation of GHGs in the atmosphere are different, and countries also face varying challenges and circumstances and have different capacities to address mitigation and adaptation. Mitigation and adaptation raise issues of equity, justice and fairness. Many of those most vulnerable to climate change have contributed and contribute little to GHG emissions. Delaying mitigation shifts burdens from the present to the future, and insufficient adaptation responses to emerging impacts are already eroding the basis for sustainable development. Comprehensive strategies in response to climate change that are consistent with sustainable development take into account the co-benefits, adverse side effects and risks that may arise from both adaptation and mitigation options. *{3.1, 3.5, Box 3.4}*

The design of climate policy is influenced by how individuals and organizations perceive risks and uncertainties and take them into account. Methods of valuation from economic, social and ethical analysis are available to assist decision-making. These methods can take account of a wide range of possible impacts, including low-probability outcomes with large consequences. But they cannot identify a single best balance between mitigation, adaptation and residual climate impacts. *{3.1}*

Climate change has the characteristics of a collective action problem at the global scale, because most GHGs accumulate over time and mix globally, and emissions by any agent (e.g., individual, community, company, country) affect other agents. Effective mitigation will not be achieved if individual agents advance their own interests independently. Cooperative responses, including international cooperation, are therefore required to effectively mitigate GHG emissions and address other climate change issues. The effectiveness of adaptation can be enhanced through complementary actions across levels, including international cooperation. The evidence suggests that outcomes seen as equitable can lead to more effective cooperation. *{3.1}*

SPM 3.2 Climate change risks reduced by mitigation and adaptation

Without additional mitigation efforts beyond those in place today, and even with adaptation, warming by the end of the 21st century will lead to high to very high risk of severe, widespread and irreversible impacts globally (*high confidence*). Mitigation involves some level of co-benefits and of risks due to adverse side effects, but these risks do not involve the same possibility of severe, widespread and irreversible impacts as risks from climate change, increasing the benefits from near-term mitigation efforts. *{3.2, 3.4}*

Mitigation and adaptation are complementary approaches for reducing risks of climate change impacts over different timescales (*high confidence*). Mitigation, in the near term and through the century, can substantially reduce climate change impacts in the latter decades of the 21st century and beyond. Benefits from adaptation can already be realized in addressing current risks, and can be realized in the future for addressing emerging risks. *{3.2, 4.5}*

Five Reasons For Concern (RFCs) aggregate climate change risks and illustrate the implications of warming and of adaptation limits for people, economies and ecosystems across sectors and regions. The five RFCs are associated with: (1) Unique and threatened systems, (2) Extreme weather events, (3) Distribution of impacts, (4) Global aggregate impacts, and (5) Large-scale singular events. In this report, the RFCs provide information relevant to Article 2 of UNFCCC. *{Box 2.4}*

Without additional mitigation efforts beyond those in place today, and even with adaptation, warming by the end of the 21st century will lead to high to very high risk of severe, widespread and irreversible impacts globally (*high confidence*) (Figure SPM.10). In most scenarios without additional mitigation efforts (those with 2100 atmospheric concentrations

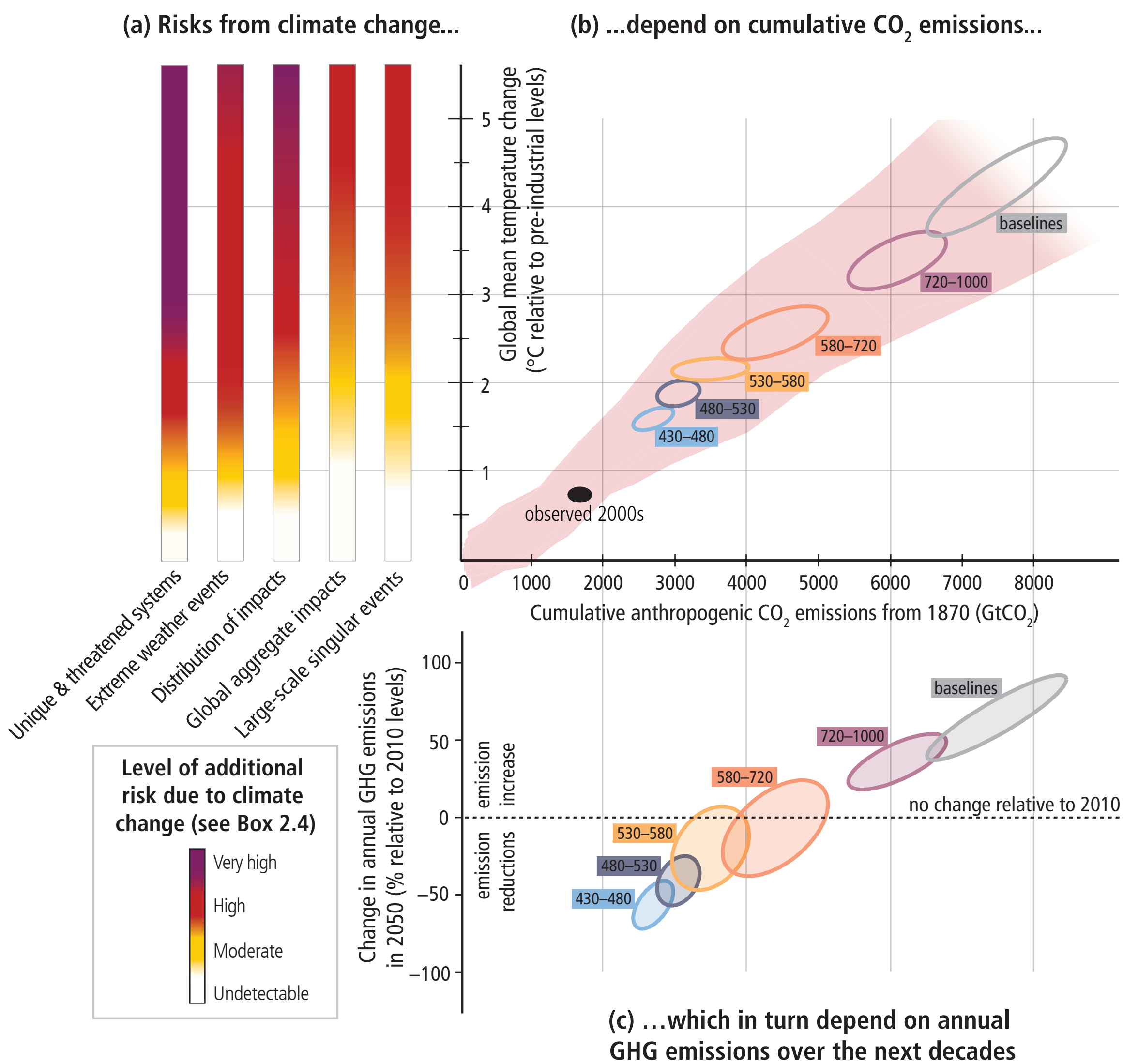

Figure SPM.10 | The relationship between risks from climate change, temperature change, cumulative carbon dioxide (CO_2) emissions and changes in annual greenhouse gas (GHG) emissions by 2050. Limiting risks across Reasons For Concern **(a)** would imply a limit for cumulative emissions of CO_2 **(b)** which would constrain annual GHG emissions over the next few decades **(c)**. **Panel a** reproduces the five Reasons For Concern *{Box 2.4}*. **Panel b** links temperature changes to cumulative CO_2 emissions (in $GtCO_2$) from 1870. They are based on Coupled Model Intercomparison Project Phase 5 (CMIP5) simulations (pink plume) and on a simple climate model (median climate response in 2100), for the baselines and five mitigation scenario categories (six ellipses). Details are provided in Figure SPM.5. **Panel c** shows the relationship between the cumulative CO_2 emissions (in $GtCO_2$) of the scenario categories and their associated change in annual GHG emissions by 2050, expressed in percentage change (in percent $GtCO_2$-eq per year) relative to 2010. The ellipses correspond to the same scenario categories as in Panel b, and are built with a similar method (see details in Figure SPM.5). *{Figure 3.1}*

>1000 ppm CO_2-eq), warming is *more likely than not* to exceed 4°C above pre-industrial levels by 2100 (Table SPM.1). The risks associated with temperatures at or above 4°C include substantial species extinction, global and regional food insecurity, consequential constraints on common human activities and limited potential for adaptation in some cases (*high confidence*). Some risks of climate change, such as risks to unique and threatened systems and risks associated with extreme weather events, are moderate to high at temperatures 1°C to 2°C above pre-industrial levels. *{2.3, Figure 2.5, 3.2, 3.4, Box 2.4, Table SPM.1}*

Substantial cuts in GHG emissions over the next few decades can substantially reduce risks of climate change by limiting warming in the second half of the 21st century and beyond. Cumulative emissions of CO_2 largely determine global mean surface warming by the late 21st century and beyond. Limiting risks across RFCs would imply a limit for cumulative emissions of CO_2. Such a limit would require that global net emissions of CO_2 eventually decrease to zero and would constrain annual emissions over the next few decades (Figure SPM.10) (*high confidence*). But some risks from climate damages are unavoidable, even with mitigation and adaptation. *{2.2.5, 3.2, 3.4}*

Mitigation involves some level of co-benefits and risks, but these risks do not involve the same possibility of severe, widespread and irreversible impacts as risks from climate change. Inertia in the economic and climate system and the possibility of irreversible impacts from climate change increase the benefits from near-term mitigation efforts (*high confidence*). Delays in additional mitigation or constraints on technological options increase the longer-term mitigation costs to hold climate change risks at a given level (Table SPM.2). *{3.2, 3.4}*

SPM 3.3 Characteristics of adaptation pathways

Adaptation can reduce the risks of climate change impacts, but there are limits to its effectiveness, especially with greater magnitudes and rates of climate change. Taking a longer-term perspective, in the context of sustainable development, increases the likelihood that more immediate adaptation actions will also enhance future options and preparedness. *{3.3}*

Adaptation can contribute to the well-being of populations, the security of assets and the maintenance of ecosystem goods, functions and services now and in the future. Adaptation is place- and context-specific (*high confidence*). A first step towards adaptation to future climate change is reducing vulnerability and exposure to present climate variability (*high confidence*). Integration of adaptation into planning, including policy design, and decision-making can promote synergies with development and disaster risk reduction. Building adaptive capacity is crucial for effective selection and implementation of adaptation options (*robust evidence, high agreement*). *{3.3}*

Adaptation planning and implementation can be enhanced through complementary actions across levels, from individuals to governments (*high confidence*). National governments can coordinate adaptation efforts of local and sub-national governments, for example by protecting vulnerable groups, by supporting economic diversification and by providing information, policy and legal frameworks and financial support (*robust evidence*, *high agreement*). Local government and the private sector are increasingly recognized as critical to progress in adaptation, given their roles in scaling up adaptation of communities, households and civil society and in managing risk information and financing (*medium evidence*, *high agreement*). *{3.3}*

Adaptation planning and implementation at all levels of governance are contingent on societal values, objectives and risk perceptions (*high confidence*). Recognition of diverse interests, circumstances, social-cultural contexts and expectations can benefit decision-making processes. Indigenous, local and traditional knowledge systems and practices, including indigenous peoples' holistic view of community and environment, are a major resource for adapting to climate change, but these have not been used consistently in existing adaptation efforts. Integrating such forms of knowledge with existing practices increases the effectiveness of adaptation. *{3.3}*

Constraints can interact to impede adaptation planning and implementation (*high confidence*). Common constraints on implementation arise from the following: limited financial and human resources; limited integration or coordination of governance; uncertainties about projected impacts; different perceptions of risks; competing values; absence of key adaptation leaders and advocates; and limited tools to monitor adaptation effectiveness. Another constraint includes insufficient research, monitoring, and observation and the finance to maintain them. *{3.3}*

Greater rates and magnitude of climate change increase the likelihood of exceeding adaptation limits (*high confidence*). Limits to adaptation emerge from the interaction among climate change and biophysical and/or socio-economic constraints. Further, poor planning or implementation, overemphasizing short-term outcomes or failing to sufficiently anticipate consequences can result in maladaptation, increasing the vulnerability or exposure of the target group in the future or the vulnerability of other people, places or sectors (*medium evidence, high agreement*). Underestimating the complexity of adaptation as a social process can create unrealistic expectations about achieving intended adaptation outcomes. *{3.3}*

Significant co-benefits, synergies and trade-offs exist between mitigation and adaptation and among different adaptation responses; interactions occur both within and across regions (*very high confidence*). Increasing efforts to mitigate and adapt to climate change imply an increasing complexity of interactions, particularly at the intersections among water, energy, land use and biodiversity, but tools to understand and manage these interactions remain limited. Examples of actions with co-benefits include (i) improved energy efficiency and cleaner energy sources, leading to reduced emissions of health-damaging, climate-altering air pollutants; (ii) reduced energy and water consumption in urban areas through greening cities and recycling water; (iii) sustainable agriculture and forestry; and (iv) protection of ecosystems for carbon storage and other ecosystem services. *{3.3}*

Transformations in economic, social, technological and political decisions and actions can enhance adaptation and promote sustainable development (*high confidence*). At the national level, transformation is considered most effective when it reflects a country's own visions and approaches to achieving sustainable development in accordance with its national circumstances and priorities. Restricting adaptation responses to incremental changes to existing systems and structures, without considering transformational change, may increase costs and losses and miss opportunities. Planning and implementation of transformational adaptation could reflect strengthened, altered or aligned paradigms and may place new and increased demands on governance structures to reconcile different goals and visions for the future and to address possible equity and ethical implications. Adaptation pathways are enhanced by iterative learning, deliberative processes and innovation. *{3.3}*

SPM 3.4 Characteristics of mitigation pathways

There are multiple mitigation pathways that are *likely* to limit warming to below 2°C relative to pre-industrial levels. These pathways would require substantial emissions reductions over the next few decades and near zero emissions of CO_2 and other long-lived greenhouse gases by the end of the century. Implementing such reductions poses substantial technological, economic, social and institutional challenges, which increase with delays in additional mitigation and if key technologies are not available. Limiting warming to lower or higher levels involves similar challenges but on different timescales. *{3.4}*

Without additional efforts to reduce GHG emissions beyond those in place today, global emissions growth is expected to persist, driven by growth in global population and economic activities. Global mean surface temperature increases in 2100 in baseline scenarios—those without additional mitigation—range from 3.7°C to 4.8°C above the average for 1850–1900 for a median climate response. They range from 2.5°C to 7.8°C when including climate uncertainty (5th to 95th percentile range) (*high confidence*). *{3.4}*

Emissions scenarios leading to CO_2-equivalent concentrations in 2100 of about 450 ppm or lower are *likely* to maintain warming below 2°C over the 21st century relative to pre-industrial levels[15]. These scenarios are characterized by 40 to 70% global anthropogenic GHG emissions reductions by 2050 compared to 2010[16], and emissions levels near zero or below in 2100. Mitigation scenarios reaching concentration levels of about 500 ppm CO_2-eq by 2100 are *more likely than not* to limit temperature change to less than 2°C, unless they temporarily overshoot concentration levels of roughly 530 ppm CO_2-eq

[15] For comparison, the CO_2-eq concentration in 2011 is estimated to be 430 ppm (uncertainty range 340 to 520 ppm)

[16] This range differs from the range provided for a similar concentration category in the AR4 (50 to 85% lower than 2000 for CO_2 only). Reasons for this difference include that this report has assessed a substantially larger number of scenarios than in the AR4 and looks at all GHGs. In addition, a large proportion of the new scenarios include Carbon Dioxide Removal (CDR) technologies (see below). Other factors include the use of 2100 concentration levels instead of stabilization levels and the shift in reference year from 2000 to 2010.

before 2100, in which case they are *about as likely as not* to achieve that goal. In these 500 ppm CO_2-eq scenarios, global 2050 emissions levels are 25 to 55% lower than in 2010. Scenarios with higher emissions in 2050 are characterized by a greater reliance on Carbon Dioxide Removal (CDR) technologies beyond mid-century (and vice versa). Trajectories that are *likely* to limit warming to 3°C relative to pre-industrial levels reduce emissions less rapidly than those limiting warming to 2°C. A limited number of studies provide scenarios that are *more likely than not* to limit warming to 1.5°C by 2100; these scenarios are characterized by concentrations below 430 ppm CO_2-eq by 2100 and 2050 emission reduction between 70% and 95% below 2010. For a comprehensive overview of the characteristics of emissions scenarios, their CO_2-equivalent concentrations and their likelihood to keep warming to below a range of temperature levels, see Figure SPM.11 and Table SPM.1. *{3.4}*

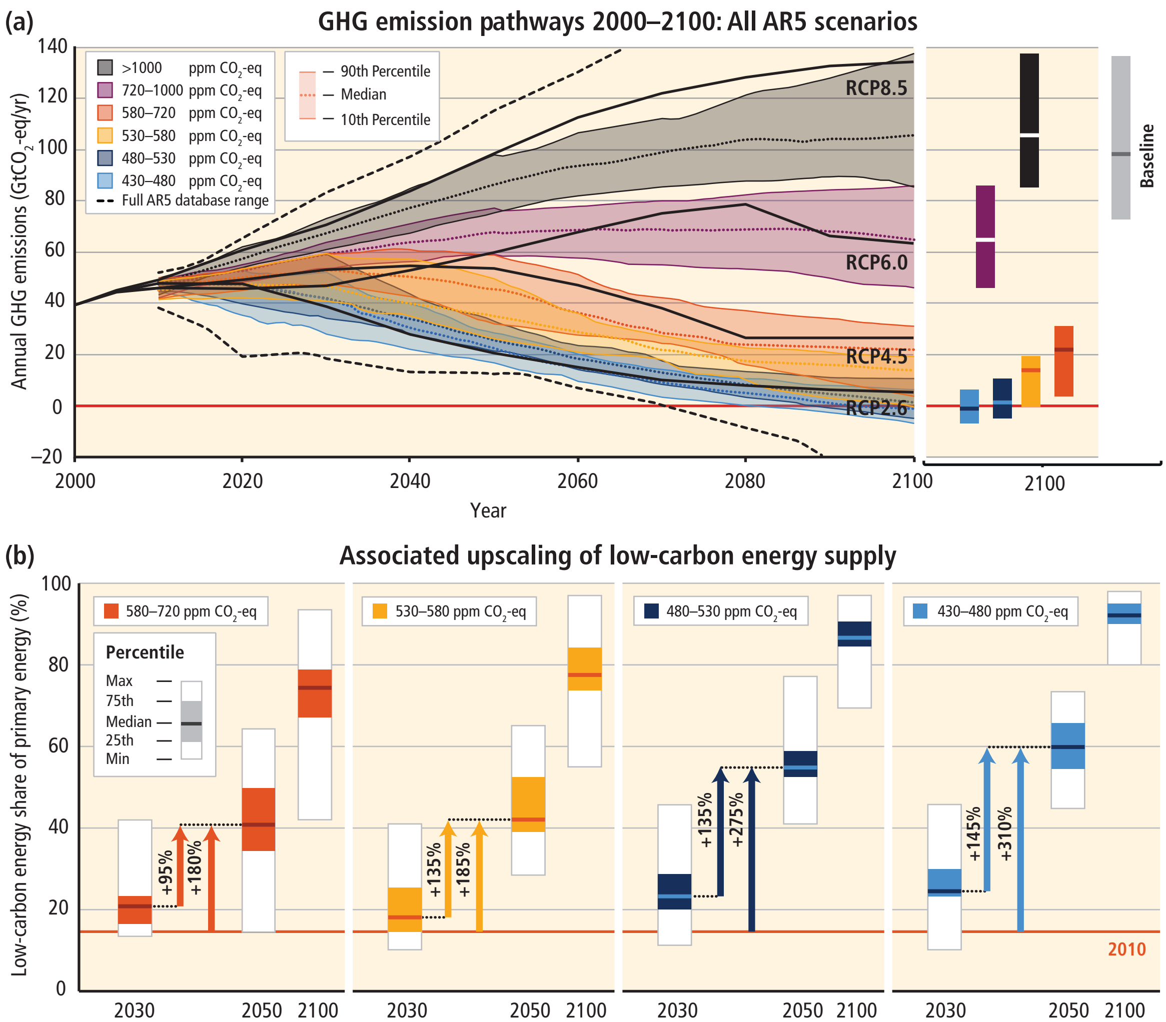

Figure SPM.11 | Global greenhouse gas emissions (gigatonne of CO_2-equivalent per year, $GtCO_2$-eq/yr) in baseline and mitigation scenarios for different long-term concentration levels **(a)** and associated upscaling requirements of low-carbon energy (% of primary energy) for 2030, 2050 and 2100 compared to 2010 levels in mitigation scenarios **(b)**. *{Figure 3.2}*

Table SPM.1 | Key characteristics of the scenarios collected and assessed for WGIII AR5. For all parameters the 10th to 90th percentile of the scenarios is shown [a]. *{Table 3.1}*

<table>
<tr><th rowspan="2">CO_2-eq Concentrations in 2100 (ppm CO_2-eq) [f]

Category label (conc. range)</th><th rowspan="2">Subcategories</th><th rowspan="2">Relative position of the RCPs [d]</th><th colspan="2">Change in CO_2-eq emissions compared to 2010 (in %) [c]</th><th colspan="4">Likelihood of staying below a specific temperature level over the 21st century (relative to 1850–1900) [d, e]</th></tr>
<tr><th>2050</th><th>2100</th><th>1.5°C</th><th>2°C</th><th>3°C</th><th>4°C</th></tr>
<tr><td><430</td><td colspan="8">Only a limited number of individual model studies have explored levels below 430 ppm CO_2-eq [j]</td></tr>
<tr><td>450
(430 to 480)</td><td>Total range [a, g]</td><td>RCP2.6</td><td>–72 to –41</td><td>–118 to –78</td><td>More unlikely than likely</td><td>Likely</td><td rowspan="6">Likely</td><td rowspan="8">Likely</td></tr>
<tr><td rowspan="2">500
(480 to 530)</td><td>No overshoot of 530 ppm CO_2-eq</td><td></td><td>–57 to –42</td><td>–107 to –73</td><td rowspan="6">Unlikely</td><td>More likely than not</td></tr>
<tr><td>Overshoot of 530 ppm CO_2-eq</td><td></td><td>–55 to –25</td><td>–114 to –90</td><td>About as likely as not</td></tr>
<tr><td rowspan="2">550
(530 to 580)</td><td>No overshoot of 580 ppm CO_2-eq</td><td></td><td>–47 to –19</td><td>–81 to –59</td><td rowspan="3">More unlikely than likely [i]</td></tr>
<tr><td>Overshoot of 580 ppm CO_2-eq</td><td></td><td>–16 to 7</td><td>–183 to –86</td></tr>
<tr><td>(580 to 650)</td><td>Total range</td><td rowspan="2">RCP4.5</td><td>–38 to 24</td><td>–134 to –50</td></tr>
<tr><td>(650 to 720)</td><td>Total range</td><td>–11 to 17</td><td>–54 to –21</td><td rowspan="2">Unlikely</td><td>More likely than not</td></tr>
<tr><td>(720 to 1000) [b]</td><td>Total range</td><td>RCP6.0</td><td>18 to 54</td><td>–7 to 72</td><td rowspan="2">Unlikely [h]</td><td>More unlikely than likely</td></tr>
<tr><td>>1000 [b]</td><td>Total range</td><td>RCP8.5</td><td>52 to 95</td><td>74 to 178</td><td>Unlikely [h]</td><td>Unlikely</td><td>More unlikely than likely</td></tr>
</table>

Notes:

[a] The 'total range' for the 430 to 480 ppm CO_2-eq concentrations scenarios corresponds to the range of the 10th to 90th percentile of the subcategory of these scenarios shown in Table 6.3 of the Working Group III Report.

[b] Baseline scenarios fall into the >1000 and 720 to 1000 ppm CO_2-eq categories. The latter category also includes mitigation scenarios. The baseline scenarios in the latter category reach a temperature change of 2.5°C to 5.8°C above the average for 1850–1900 in 2100. Together with the baseline scenarios in the >1000 ppm CO_2-eq category, this leads to an overall 2100 temperature range of 2.5°C to 7.8°C (range based on median climate response: 3.7°C to 4.8°C) for baseline scenarios across both concentration categories.

[c] The global 2010 emissions are 31% above the 1990 emissions (consistent with the historic greenhouse gas emission estimates presented in this report). CO_2-eq emissions include the basket of Kyoto gases (carbon dioxide (CO_2), methane (CH_4), nitrous oxide (N_2O) as well as fluorinated gases).

[d] The assessment here involves a large number of scenarios published in the scientific literature and is thus not limited to the Representative Concentration Pathways (RCPs). To evaluate the CO_2-eq concentration and climate implications of these scenarios, the Model for the Assessment of Greenhouse Gas Induced Climate Change (MAGICC) was used in a probabilistic mode. For a comparison between MAGICC model results and the outcomes of the models used in WGI, see WGI 12.4.1.2, 12.4.8 and WGIII 6.3.2.6.

[e] The assessment in this table is based on the probabilities calculated for the full ensemble of scenarios in WGIII AR5 using MAGICC and the assessment in WGI of the uncertainty of the temperature projections not covered by climate models. The statements are therefore consistent with the statements in WGI, which are based on the Coupled Model Intercomparison Project Phase 5 (CMIP5) runs of the RCPs and the assessed uncertainties. Hence, the likelihood statements reflect different lines of evidence from both WGs. This WGI method was also applied for scenarios with intermediate concentration levels where no CMIP5 runs are available. The likelihood statements are indicative only *{WGIII 6.3}* and follow broadly the terms used by the WGI SPM for temperature projections: likely 66–100%, more likely than not >50–100%, about as likely as not 33–66%, and unlikely 0–33%. In addition the term more unlikely than likely 0–<50% is used.

[f] The CO_2-equivalent concentration (see Glossary) is calculated on the basis of the total forcing from a simple carbon cycle/climate model, MAGICC. The CO_2-equivalent concentration in 2011 is estimated to be 430 ppm (uncertainty range 340 to 520 ppm). This is based on the assessment of total anthropogenic radiative forcing for 2011 relative to 1750 in WGI, i.e., 2.3 W/m^2, uncertainty range 1.1 to 3.3 W/m^2.

[g] The vast majority of scenarios in this category overshoot the category boundary of 480 ppm CO_2-eq concentration.

[h] For scenarios in this category, no CMIP5 run or MAGICC realization stays below the respective temperature level. Still, an *unlikely* assignment is given to reflect uncertainties that may not be reflected by the current climate models.

[i] Scenarios in the 580 to 650 ppm CO_2-eq category include both overshoot scenarios and scenarios that do not exceed the concentration level at the high end of the category (e.g., RCP4.5). The latter type of scenarios, in general, have an assessed probability of *more unlikely than likely* to stay below the 2°C temperature level, while the former are mostly assessed to have an *unlikely* probability of staying below this level.

[j] In these scenarios, global CO_2-eq emissions in 2050 are between 70 to 95% below 2010 emissions, and they are between 110 to 120% below 2010 emissions in 2100.

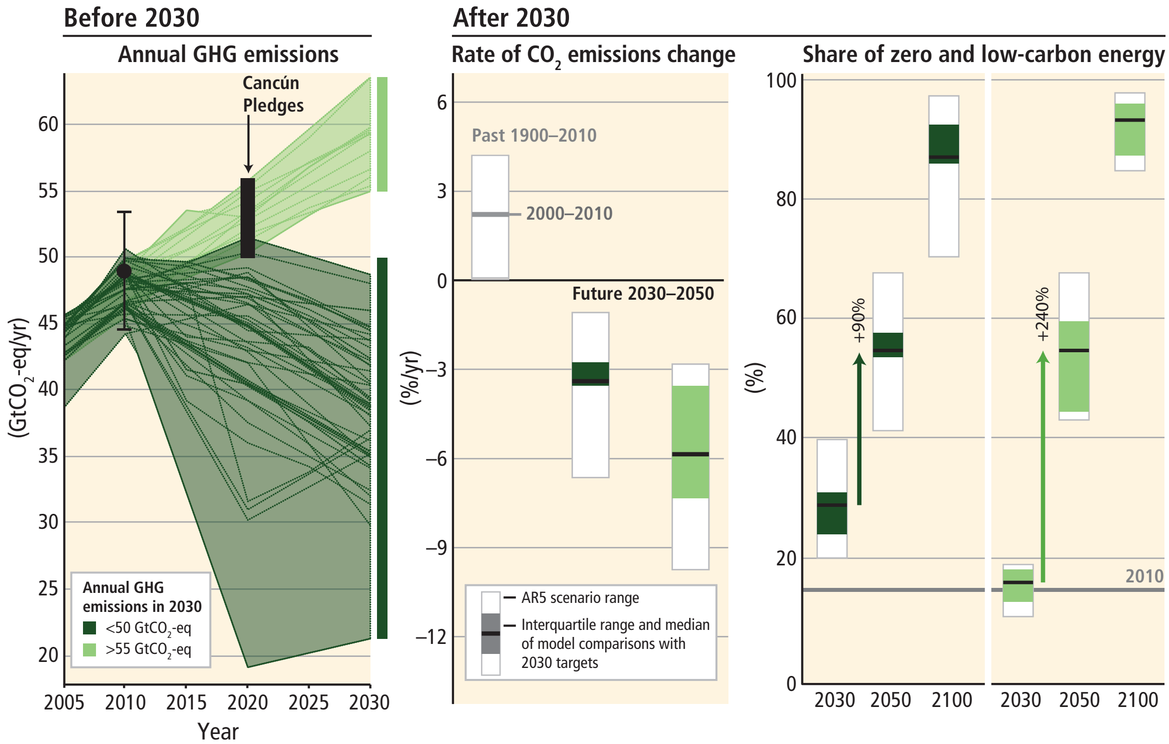

Figure SPM.12 | The implications of different 2030 greenhouse gas (GHG) emissions levels for the rate of carbon dioxide (CO_2) emissions reductions and low-carbon energy upscaling in mitigation scenarios that are at least *about as likely as not* to keep warming throughout the 21st century below 2°C relative to pre-industrial levels (2100 CO_2-equivalent concentrations of 430 to 530 ppm). The scenarios are grouped according to different emissions levels by 2030 (coloured in different shades of green). The left panel shows the pathways of GHG emissions (gigatonne of CO_2-equivalent per year, $GtCO_2$-eq/yr) leading to these 2030 levels. The black dot with whiskers gives historic GHG emission levels and associated uncertainties in 2010 as reported in Figure SPM.2. The black bar shows the estimated uncertainty range of GHG emissions implied by the Cancún Pledges. The middle panel denotes the average annual CO_2 emissions reduction rates for the period 2030–2050. It compares the median and interquartile range across scenarios from recent inter-model comparisons with explicit 2030 interim goals to the range of scenarios in the Scenario Database for WGIII AR5. Annual rates of historical emissions change (sustained over a period of 20 years) and the average annual CO_2 emission change between 2000 and 2010 are shown as well. The arrows in the right panel show the magnitude of zero and low-carbon energy supply upscaling from 2030 to 2050 subject to different 2030 GHG emissions levels. Zero- and low-carbon energy supply includes renewables, nuclear energy and fossil energy with carbon dioxide capture and storage (CCS) or bioenergy with CCS (BECCS). [Note: Only scenarios that apply the full, unconstrained mitigation technology portfolio of the underlying models (default technology assumption) are shown. Scenarios with large net negative global emissions (>20 $GtCO_2$-eq/yr), scenarios with exogenous carbon price assumptions and scenarios with 2010 emissions significantly outside the historical range are excluded.] *{Figure 3.3}*

Mitigation scenarios reaching about 450 ppm CO_2-eq in 2100 (consistent with a *likely* chance to keep warming below 2°C relative to pre-industrial levels) typically involve temporary overshoot[17] of atmospheric concentrations, as do many scenarios reaching about 500 ppm CO_2-eq to about 550 ppm CO_2-eq in 2100 (Table SPM.1). Depending on the level of overshoot, overshoot scenarios typically rely on the availability and widespread deployment of bioenergy with carbon dioxide capture and storage (BECCS) and afforestation in the second half of the century. The availability and scale of these and other CDR technologies and methods are uncertain and CDR technologies are, to varying degrees, associated with challenges and risks[18]. CDR is also prevalent in many scenarios without overshoot to compensate for residual emissions from sectors where mitigation is more expensive (*high confidence*). *{3.4, Box 3.3}*

Reducing emissions of non-CO_2 agents can be an important element of mitigation strategies. All current GHG emissions and other forcing agents affect the rate and magnitude of climate change over the next few decades, although long-term warming is mainly driven by CO_2 emissions. Emissions of non-CO_2 forcers are often expressed as 'CO_2-equivalent emissions', but the choice of metric to calculate these emissions, and the implications for the emphasis and timing of abatement of the various climate forcers, depends on application and policy context and contains value judgments. *{3.4, Box 3.2}*

[17] In concentration 'overshoot' scenarios, concentrations peak during the century and then decline.

[18] CDR methods have biogeochemical and technological limitations to their potential on the global scale. There is insufficient knowledge to quantify how much CO_2 emissions could be partially offset by CDR on a century timescale. CDR methods may carry side effects and long-term consequences on a global scale.

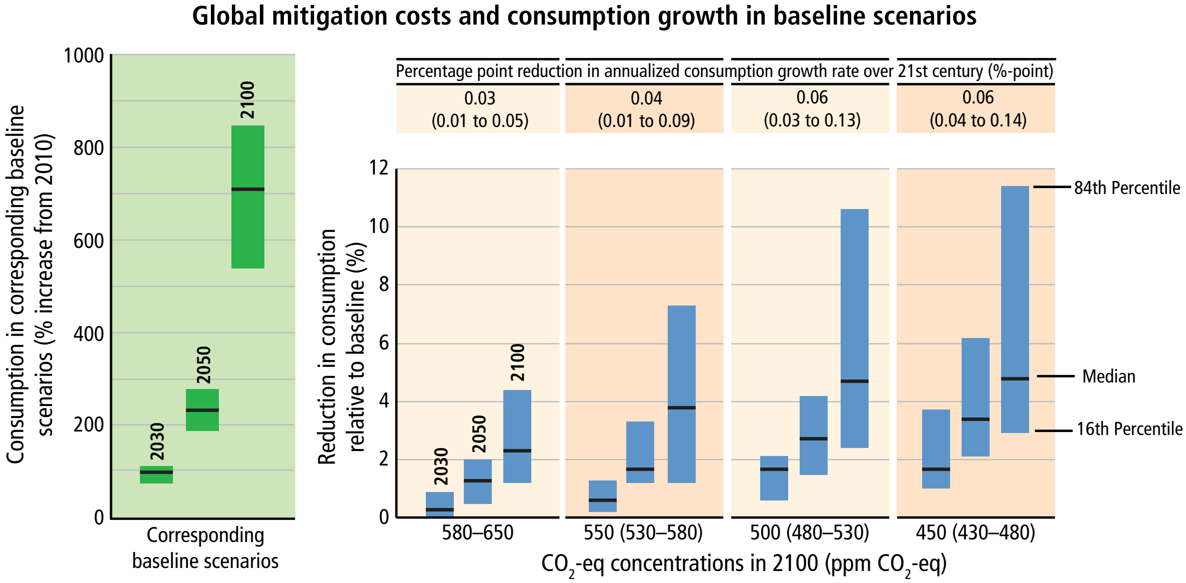

Figure SPM.13 | Global mitigation costs in cost-effective scenarios at different atmospheric concentrations levels in 2100. Cost-effective scenarios assume immediate mitigation in all countries and a single global carbon price, and impose no additional limitations on technology relative to the models' default technology assumptions. Consumption losses are shown relative to a baseline development without climate policy (left panel). The table at the top shows percentage points of annualized consumption growth reductions relative to consumption growth in the baseline of 1.6 to 3% per year (e.g., if the reduction is 0.06 percentage points per year due to mitigation, and baseline growth is 2.0% per year, then the growth rate with mitigation would be 1.94% per year). Cost estimates shown in this table do not consider the benefits of reduced climate change or co-benefits and adverse side effects of mitigation. Estimates at the high end of these cost ranges are from models that are relatively inflexible to achieve the deep emissions reductions required in the long run to meet these goals and/or include assumptions about market imperfections that would raise costs. *{Figure 3.4}*

Delaying additional mitigation to 2030 will substantially increase the challenges associated with limiting warming over the 21st century to below 2°C relative to pre-industrial levels. It will require substantially higher rates of emissions reductions from 2030 to 2050; a much more rapid scale-up of low-carbon energy over this period; a larger reliance on CDR in the long term; and higher transitional and long-term economic impacts. Estimated global emissions levels in 2020 based on the Cancún Pledges are not consistent with cost-effective mitigation trajectories that are at least *about as likely as not* to limit warming to below 2°C relative to pre-industrial levels, but they do not preclude the option to meet this goal (*high confidence*) (Figure SPM.12, Table SPM.2). *{3.4}*

Estimates of the aggregate economic costs of mitigation vary widely depending on methodologies and assumptions, but increase with the stringency of mitigation. Scenarios in which all countries of the world begin mitigation immediately, in which there is a single global carbon price, and in which all key technologies are available have been used as a cost-effective benchmark for estimating macro-economic mitigation costs (Figure SPM.13). Under these assumptions mitigation scenarios that are *likely* to limit warming to below 2°C through the 21st century relative to pre-industrial levels entail losses in global consumption—not including benefits of reduced climate change as well as co-benefits and adverse side effects of mitigation—of 1 to 4% (median: 1.7%) in 2030, 2 to 6% (median: 3.4%) in 2050 and 3 to 11% (median: 4.8%) in 2100 relative to consumption in baseline scenarios that grows anywhere from 300% to more than 900% over the century (Figure SPM.13). These numbers correspond to an annualized reduction of consumption growth by 0.04 to 0.14 (median: 0.06) percentage points over the century relative to annualized consumption growth in the baseline that is between 1.6 and 3% per year (*high confidence*). *{3.4}*

In the absence or under limited availability of mitigation technologies (such as bioenergy, CCS and their combination BECCS, nuclear, wind/solar), mitigation costs can increase substantially depending on the technology considered. Delaying additional mitigation increases mitigation costs in the medium to long term. Many models could not limit *likely* warming to below 2°C over the 21st century relative to pre-industrial levels if additional mitigation is considerably delayed. Many models could not limit *likely* warming to below 2°C if bioenergy, CCS and their combination (BECCS) are limited (*high confidence*) (Table SPM.2). *{3.4}*

Table SPM.2 | Increase in global mitigation costs due to either limited availability of specific technologies or delays in additional mitigation [a] relative to cost-effective scenarios [b]. The increase in costs is given for the median estimate and the 16th to 84th percentile range of the scenarios (in parentheses) [c]. In addition, the sample size of each scenario set is provided in the coloured symbols. The colours of the symbols indicate the fraction of models from systematic model comparison exercises that could successfully reach the targeted concentration level. *{Table 3.2}*

	Mitigation cost increases in scenarios with limited availability of technologies [d] *[% increase in total discounted [e] mitigation costs (2015–2100) relative to default technology assumptions]*				**Mitigation cost increases due to delayed additional mitigation until 2030** *[% increase in mitigation costs relative to immediate mitigation]*	
2100 concentrations (ppm CO_2-eq)	no CCS	nuclear phase out	limited solar/wind	limited bioenergy	medium term costs (2030–2050)	long term costs (2050–2100)
450 (430 to 480)	138% (29 to 297%) 4	7% (4 to 18%) 8	6% (2 to 29%) 8	64% (44 to 78%) 8	44% (2 to 78%) 29	37% (16 to 82%) 29
500 (480 to 530)	not available (n.a.)	n.a.	n.a.	n.a.		
550 (530 to 580)	39% (18 to 78%) 11	13% (2 to 23%) 10	8% (5 to 15%) 10	18% (4 to 66%) 12	15% (3 to 32%)	16% (5 to 24%)
580 to 650	n.a.	n.a.	n.a.	n.a.		

Symbol legend—fraction of models successful in producing scenarios (numbers indicate the number of successful models)

: all models successful	: between 50 and 80% of models successful
: between 80 and 100% of models successful	: less than 50% of models successful

Notes:

[a] Delayed mitigation scenarios are associated with greenhouse gas emission of more than 55 $GtCO_2$-eq in 2030, and the increase in mitigation costs is measured relative to cost-effective mitigation scenarios for the same long-term concentration level.

[b] Cost-effective scenarios assume immediate mitigation in all countries and a single global carbon price, and impose no additional limitations on technology relative to the models' default technology assumptions.

[c] The range is determined by the central scenarios encompassing the 16th to 84th percentile range of the scenario set. Only scenarios with a time horizon until 2100 are included. Some models that are included in the cost ranges for concentration levels above 530 ppm CO_2-eq in 2100 could not produce associated scenarios for concentration levels below 530 ppm CO_2-eq in 2100 with assumptions about limited availability of technologies and/or delayed additional mitigation.

[d] No CCS: carbon dioxide capture and storage is not included in these scenarios. Nuclear phase out: no addition of nuclear power plants beyond those under construction, and operation of existing plants until the end of their lifetime. Limited Solar/Wind: a maximum of 20% global electricity generation from solar and wind power in any year of these scenarios. Limited Bioenergy: a maximum of 100 EJ/yr modern bioenergy supply globally (modern bioenergy used for heat, power, combinations and industry was around 18 EJ/yr in 2008). EJ = Exajoule = 10^{18} Joule.

[e] Percentage increase of net present value of consumption losses in percent of baseline consumption (for scenarios from general equilibrium models) and abatement costs in percent of baseline gross domestic product (GDP, for scenarios from partial equilibrium models) for the period 2015–2100, discounted at 5% per year.

Mitigation scenarios reaching about 450 or 500 ppm CO_2-eq by 2100 show reduced costs for achieving air quality and energy security objectives, with significant co-benefits for human health, ecosystem impacts and sufficiency of resources and resilience of the energy system. *{4.4.2.2}*

Mitigation policy could devalue fossil fuel assets and reduce revenues for fossil fuel exporters, but differences between regions and fuels exist (*high confidence*). Most mitigation scenarios are associated with reduced revenues from coal and oil trade for major exporters (*high confidence*). The availability of CCS would reduce the adverse effects of mitigation on the value of fossil fuel assets (*medium confidence*). *{4.4.2.2}*

Solar Radiation Management (SRM) involves large-scale methods that seek to reduce the amount of absorbed solar energy in the climate system. SRM is untested and is not included in any of the mitigation scenarios. If it were deployed, SRM would entail numerous uncertainties, side effects, risks and shortcomings and has particular governance and ethical implications. SRM would not reduce ocean acidification. If it were terminated, there is *high confidence* that surface temperatures would rise very rapidly impacting ecosystems susceptible to rapid rates of change. *{Box 3.3}*

SPM 4. Adaptation and Mitigation

Many adaptation and mitigation options can help address climate change, but no single option is sufficient by itself. Effective implementation depends on policies and cooperation at all scales and can be enhanced through integrated responses that link adaptation and mitigation with other societal objectives. *{4}*

SPM 4.1 Common enabling factors and constraints for adaptation and mitigation responses

Adaptation and mitigation responses are underpinned by common enabling factors. These include effective institutions and governance, innovation and investments in environmentally sound technologies and infrastructure, sustainable livelihoods and behavioural and lifestyle choices. *{4.1}*

Inertia in many aspects of the socio-economic system constrains adaptation and mitigation options (*medium evidence, high agreement*). Innovation and investments in environmentally sound infrastructure and technologies can reduce GHG emissions and enhance resilience to climate change (*very high confidence*). *{4.1}*

Vulnerability to climate change, GHG emissions and the capacity for adaptation and mitigation are strongly influenced by livelihoods, lifestyles, behaviour and culture (*medium evidence, medium agreement*). Also, the social acceptability and/or effectiveness of climate policies are influenced by the extent to which they incentivize or depend on regionally appropriate changes in lifestyles or behaviours. *{4.1}*

For many regions and sectors, enhanced capacities to mitigate and adapt are part of the foundation essential for managing climate change risks (*high confidence*). Improving institutions as well as coordination and cooperation in governance can help overcome regional constraints associated with mitigation, adaptation and disaster risk reduction (*very high confidence*). *{4.1}*

SPM 4.2 Response options for adaptation

Adaptation options exist in all sectors, but their context for implementation and potential to reduce climate-related risks differs across sectors and regions. Some adaptation responses involve significant co-benefits, synergies and trade-offs. Increasing climate change will increase challenges for many adaptation options. *{4.2}*

Adaptation experience is accumulating across regions in the public and private sectors and within communities. There is increasing recognition of the value of social (including local and indigenous), institutional, and ecosystem-based measures and of the extent of constraints to adaptation. Adaptation is becoming embedded in some planning processes, with more limited implementation of responses (*high confidence*). *{1.6, 4.2, 4.4.2.1}*

The need for adaptation along with associated challenges is expected to increase with climate change (*very high confidence*). Adaptation options exist in all sectors and regions, with diverse potential and approaches depending on their context in vulnerability reduction, disaster risk management or proactive adaptation planning (Table SPM.3). Effective strategies and actions consider the potential for co-benefits and opportunities within wider strategic goals and development plans. *{4.2}*

Table SPM.3 | Approaches for managing the risks of climate change through adaptation. These approaches should be considered overlapping rather than discrete, and they are often pursued simultaneously. Examples are presented in no specific order and can be relevant to more than one category. *{Table 4.2}*

Overlapping Approaches	Category	Examples
Vulnerability & Exposure Reduction through development, planning & practices including many low-regrets measures	Human development	Improved access to education, nutrition, health facilities, energy, safe housing & settlement structures, & social support structures; Reduced gender inequality & marginalization in other forms.
	Poverty alleviation	Improved access to & control of local resources; Land tenure; Disaster risk reduction; Social safety nets & social protection; Insurance schemes.
	Livelihood security	Income, asset & livelihood diversification; Improved infrastructure; Access to technology & decision-making fora; Increased decision-making power; Changed cropping, livestock & aquaculture practices; Reliance on social networks.
	Disaster risk management	Early warning systems; Hazard & vulnerability mapping; Diversifying water resources; Improved drainage; Flood & cyclone shelters; Building codes & practices; Storm & wastewater management; Transport & road infrastructure improvements.
Adaptation including incremental & transformational adjustments	Ecosystem management	Maintaining wetlands & urban green spaces; Coastal afforestation; Watershed & reservoir management; Reduction of other stressors on ecosystems & of habitat fragmentation; Maintenance of genetic diversity; Manipulation of disturbance regimes; Community-based natural resource management.
	Spatial or land-use planning	Provisioning of adequate housing, infrastructure & services; Managing development in flood prone & other high risk areas; Urban planning & upgrading programs; Land zoning laws; Easements; Protected areas.
	Structural/physical	***Engineered & built-environment options***: Sea walls & coastal protection structures; Flood levees; Water storage; Improved drainage; Flood & cyclone shelters; Building codes & practices; Storm & wastewater management; Transport & road infrastructure improvements; Floating houses; Power plant & electricity grid adjustments.
		Technological options: New crop & animal varieties; Indigenous, traditional & local knowledge, technologies & methods; Efficient irrigation; Water-saving technologies; Desalinisation; Conservation agriculture; Food storage & preservation facilities; Hazard & vulnerability mapping & monitoring; Early warning systems; Building insulation; Mechanical & passive cooling; Technology development, transfer & diffusion.
		Ecosystem-based options: Ecological restoration; Soil conservation; Afforestation & reforestation; Mangrove conservation & replanting; Green infrastructure (e.g., shade trees, green roofs); Controlling overfishing; Fisheries co-management; Assisted species migration & dispersal; Ecological corridors; Seed banks, gene banks & other *ex situ* conservation; Community-based natural resource management.
		Services: Social safety nets & social protection; Food banks & distribution of food surplus; Municipal services including water & sanitation; Vaccination programs; Essential public health services; Enhanced emergency medical services.
	Institutional	***Economic options***: Financial incentives; Insurance; Catastrophe bonds; Payments for ecosystem services; Pricing water to encourage universal provision and careful use; Microfinance; Disaster contingency funds; Cash transfers; Public-private partnerships.
		Laws & regulations: Land zoning laws; Building standards & practices; Easements; Water regulations & agreements; Laws to support disaster risk reduction; Laws to encourage insurance purchasing; Defined property rights & land tenure security; Protected areas; Fishing quotas; Patent pools & technology transfer.
		National & government policies & programs: National & regional adaptation plans including mainstreaming; Sub-national & local adaptation plans; Economic diversification; Urban upgrading programs; Municipal water management programs; Disaster planning & preparedness; Integrated water resource management; Integrated coastal zone management; Ecosystem-based management; Community-based adaptation.
	Social	***Educational options***: Awareness raising & integrating into education; Gender equity in education; Extension services; Sharing indigenous, traditional & local knowledge; Participatory action research & social learning; Knowledge-sharing & learning platforms.
		Informational options: Hazard & vulnerability mapping; Early warning & response systems; Systematic monitoring & remote sensing; Climate services; Use of indigenous climate observations; Participatory scenario development; Integrated assessments.
		Behavioural options: Household preparation & evacuation planning; Migration; Soil & water conservation; Storm drain clearance; Livelihood diversification; Changed cropping, livestock & aquaculture practices; Reliance on social networks.
Transformation	Spheres of change	***Practical***: Social & technical innovations, behavioural shifts, or institutional & managerial changes that produce substantial shifts in outcomes.
		Political: Political, social, cultural & ecological decisions & actions consistent with reducing vulnerability & risk & supporting adaptation, mitigation & sustainable development.
		Personal: Individual & collective assumptions, beliefs, values & worldviews influencing climate-change responses.

SPM

SPM 4.3 Response options for mitigation

Mitigation options are available in every major sector. Mitigation can be more cost-effective if using an integrated approach that combines measures to reduce energy use and the greenhouse gas intensity of end-use sectors, decarbonize energy supply, reduce net emissions and enhance carbon sinks in land-based sectors. *{4.3}*

Well-designed systemic and cross-sectoral mitigation strategies are more cost-effective in cutting emissions than a focus on individual technologies and sectors, with efforts in one sector affecting the need for mitigation in others (*medium confidence*). Mitigation measures intersect with other societal goals, creating the possibility of co-benefits or adverse side effects. These intersections, if well-managed, can strengthen the basis for undertaking climate action. *{4.3}*

Emissions ranges for baseline scenarios and mitigation scenarios that limit CO_2-equivalent concentrations to low levels (about 450 ppm CO_2-eq, *likely* to limit warming to 2°C above pre-industrial levels) are shown for different sectors and gases in Figure SPM.14. Key measures to achieve such mitigation goals include decarbonizing (i.e., reducing the carbon intensity of) electricity generation (*medium evidence, high agreement*) as well as efficiency enhancements and behavioural changes, in order to reduce energy demand compared to baseline scenarios without compromising development (*robust evidence, high agreement*). In scenarios reaching 450 ppm CO_2-eq concentrations by 2100, global CO_2 emissions from the energy supply sector are projected to decline over the next decade and are characterized by reductions of 90% or more below 2010 levels between 2040 and 2070. In the majority of low-concentration stabilization scenarios (about 450 to about 500 ppm CO_2-eq, at least *about as likely as not* to limit warming to 2°C above pre-industrial levels), the share of low-carbon electricity supply (comprising renewable energy (RE), nuclear and carbon dioxide capture and storage (CCS) including bioenergy with carbon dioxide capture and storage (BECCS)) increases from the current share of approximately 30% to more than 80% by 2050, and fossil fuel power generation without CCS is phased out almost entirely by 2100. *{4.3}*

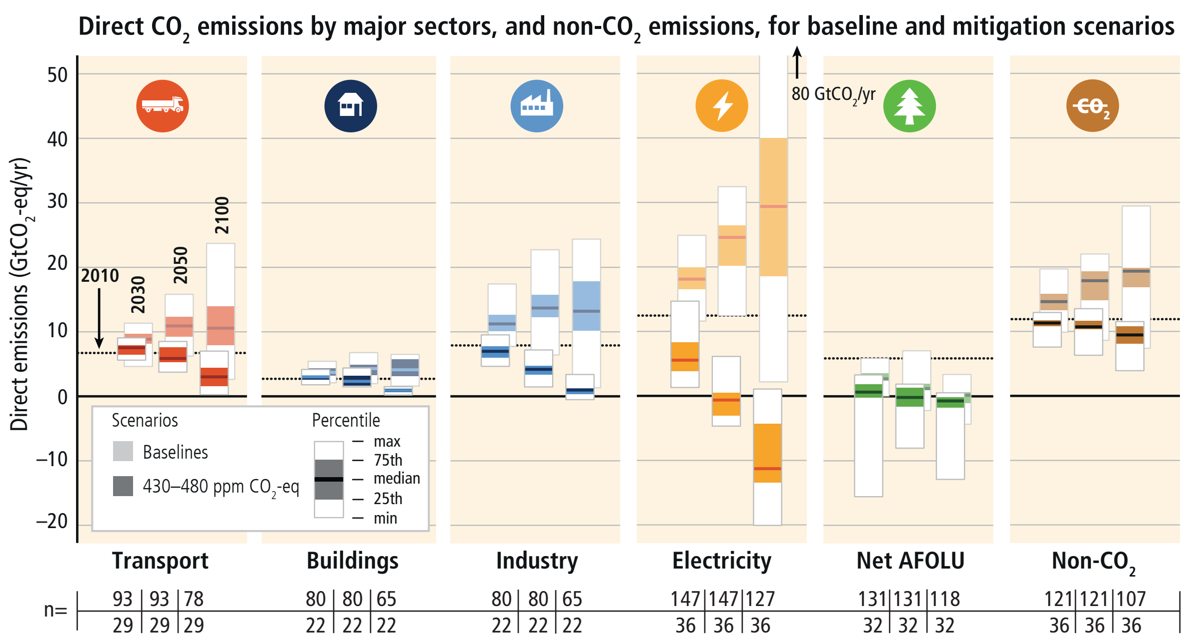

Figure SPM.14 | Carbon dioxide (CO_2) emissions by sector and total non-CO_2 greenhouse gases (Kyoto gases) across sectors in baseline (faded bars) and mitigation scenarios (solid colour bars) that reach about 450 (430 to 480) ppm CO_2-eq concentrations in 2100 (*likely* to limit warming to 2°C above pre-industrial levels). Mitigation in the end-use sectors leads also to indirect emissions reductions in the upstream energy supply sector. Direct emissions of the end-use sectors thus do not include the emission reduction potential at the supply-side due to, for example, reduced electricity demand. The numbers at the bottom of the graphs refer to the number of scenarios included in the range (upper row: baseline scenarios; lower row: mitigation scenarios), which differs across sectors and time due to different sectoral resolution and time horizon of models. Emissions ranges for mitigation scenarios include the full portfolio of mitigation options; many models cannot reach 450 ppm CO_2-eq concentration by 2100 in the absence of carbon dioxide capture and storage (CCS). Negative emissions in the electricity sector are due to the application of bioenergy with carbon dioxide capture and storage (BECCS). 'Net' agriculture, forestry and other land use (AFOLU) emissions consider afforestation, reforestation as well as deforestation activities. *{4.3, Figure 4.1}*

Near-term reductions in energy demand are an important element of cost-effective mitigation strategies, provide more flexibility for reducing carbon intensity in the energy supply sector, hedge against related supply-side risks, avoid lock-in to carbon-intensive infrastructures, and are associated with important co-benefits. The most cost-effective mitigation options in forestry are afforestation, sustainable forest management and reducing deforestation, with large differences in their relative importance across regions; and in agriculture, cropland management, grazing land management and restoration of organic soils (*medium evidence, high agreement*). *{4.3, Figures 4.1, 4.2, Table 4.3}*

Behaviour, lifestyle and culture have a considerable influence on energy use and associated emissions, with high mitigation potential in some sectors, in particular when complementing technological and structural change (*medium evidence, medium agreement*). Emissions can be substantially lowered through changes in consumption patterns, adoption of energy savings measures, dietary change and reduction in food wastes. *{4.1, 4.3}*

SPM 4.4 Policy approaches for adaptation and mitigation, technology and finance

Effective adaptation and mitigation responses will depend on policies and measures across multiple scales: international, regional, national and sub-national. Policies across all scales supporting technology development, diffusion and transfer, as well as finance for responses to climate change, can complement and enhance the effectiveness of policies that directly promote adaptation and mitigation. *{4.4}*

International cooperation is critical for effective mitigation, even though mitigation can also have local co-benefits. Adaptation focuses primarily on local to national scale outcomes, but its effectiveness can be enhanced through coordination across governance scales, including international cooperation: *{3.1, 4.4.1}*

- The United Nations Framework Convention on Climate Change (UNFCCC) is the main multilateral forum focused on addressing climate change, with nearly universal participation. Other institutions organized at different levels of governance have resulted in diversifying international climate change cooperation. *{4.4.1}*

- The Kyoto Protocol offers lessons towards achieving the ultimate objective of the UNFCCC, particularly with respect to participation, implementation, flexibility mechanisms and environmental effectiveness (*medium evidence, low agreement*). *{4.4.1}*

- Policy linkages among regional, national and sub-national climate policies offer potential climate change mitigation benefits (*medium evidence, medium agreement*). Potential advantages include lower mitigation costs, decreased emission leakage and increased market liquidity. *{4.4.1}*

- International cooperation for supporting adaptation planning and implementation has received less attention historically than mitigation but is increasing and has assisted in the creation of adaptation strategies, plans and actions at the national, sub-national and local level (*high confidence*). *{4.4.1}*

There has been a considerable increase in national and sub-national plans and strategies on both adaptation and mitigation since the AR4, with an increased focus on policies designed to integrate multiple objectives, increase co-benefits and reduce adverse side effects (*high confidence*): *{4.4.2.1, 4.4.2.2}*

- National governments play key roles in adaptation planning and implementation (*robust evidence, high agreement*) through coordinating actions and providing frameworks and support. While local government and the private sector have different functions, which vary regionally, they are increasingly recognized as critical to progress in adaptation, given their roles in scaling up adaptation of communities, households and civil society and in managing risk information and financing (*medium evidence, high agreement*). *{4.4.2.1}*

- Institutional dimensions of adaptation governance, including the integration of adaptation into planning and decision-making, play a key role in promoting the transition from planning to implementation of adaptation (*robust evidence,* *high agreement*). Examples of institutional approaches to adaptation involving multiple actors include economic options (e.g., insurance, public-private partnerships), laws and regulations (e.g., land-zoning laws) and national and government policies and programmes (e.g., economic diversification). *{4.2, 4.4.2.1, Table SPM.3}*

- In principle, mechanisms that set a carbon price, including cap and trade systems and carbon taxes, can achieve mitigation in a cost-effective way but have been implemented with diverse effects due in part to national circumstances as well as policy design. The short-run effects of cap and trade systems have been limited as a result of loose caps or caps that have not proved to be constraining (*limited evidence, medium agreement*). In some countries, tax-based policies specifically aimed at reducing GHG emissions—alongside technology and other policies—have helped to weaken the link between GHG emissions and GDP (*high confidence*). In addition, in a large group of countries, fuel taxes (although not necessarily designed for the purpose of mitigation) have had effects that are akin to sectoral carbon taxes. *{4.4.2.2}*

- Regulatory approaches and information measures are widely used and are often environmentally effective (*medium evidence, medium agreement*). Examples of regulatory approaches include energy efficiency standards; examples of information programmes include labelling programmes that can help consumers make better-informed decisions. *{4.4.2.2}*

- Sector-specific mitigation policies have been more widely used than economy-wide policies (*medium evidence, high agreement*). Sector-specific policies may be better suited to address sector-specific barriers or market failures and may be bundled in packages of complementary policies. Although theoretically more cost-effective, administrative and political barriers may make economy-wide policies harder to implement. Interactions between or among mitigation policies may be synergistic or may have no additive effect on reducing emissions. *{4.4.2.2}*

- Economic instruments in the form of subsidies may be applied across sectors, and include a variety of policy designs, such as tax rebates or exemptions, grants, loans and credit lines. An increasing number and variety of renewable energy (RE) policies including subsidies—motivated by many factors—have driven escalated growth of RE technologies in recent years. At the same time, reducing subsidies for GHG-related activities in various sectors can achieve emission reductions, depending on the social and economic context (*high confidence*). *{4.4.2.2}*

Co-benefits and adverse side effects of mitigation could affect achievement of other objectives such as those related to human health, food security, biodiversity, local environmental quality, energy access, livelihoods and equitable sustainable development. The potential for co-benefits for energy end-use measures outweighs the potential for adverse side effects whereas the evidence suggests this may not be the case for all energy supply and agriculture, forestry and other land use (AFOLU) measures. Some mitigation policies raise the prices for some energy services and could hamper the ability of societies to expand access to modern energy services to underserved populations (*low confidence*). These potential adverse side effects on energy access can be avoided with the adoption of complementary policies such as income tax rebates or other benefit transfer mechanisms (*medium confidence*). Whether or not side effects materialize, and to what extent side effects materialize, will be case- and site-specific, and depend on local circumstances and the scale, scope and pace of implementation. Many co-benefits and adverse side effects have not been well-quantified. *{4.3, 4.4.2.2, Box 3.4}*

Technology policy (development, diffusion and transfer) complements other mitigation policies across all scales, from international to sub-national; many adaptation efforts also critically rely on diffusion and transfer of technologies and management practices (*high confidence*). Policies exist to address market failures in R&D, but the effective use of technologies can also depend on capacities to adopt technologies appropriate to local circumstances. *{4.4.3}*

Substantial reductions in emissions would require large changes in investment patterns (*high confidence*). For mitigation scenarios that stabilize concentrations (without overshoot) in the range of 430 to 530 ppm CO_2-eq by 2100[19], annual investments in low carbon electricity supply and energy efficiency in key sectors (transport, industry and buildings) are projected in the scenarios to rise by several hundred billion dollars per year before 2030. Within appropriate enabling environments, the private sector, along with the public sector, can play important roles in financing mitigation and adaptation (*medium evidence, high agreement*). *{4.4.4}*

---

[19] This range comprises scenarios that reach 430 to 480 ppm CO_2-eq by 2100 (*likely* to limit warming to 2°C above pre-industrial levels) and scenarios that reach 480 to 530 ppm CO_2-eq by 2100 (without overshoot: *more likely than* not to limit warming to 2°C above pre-industrial levels).

Financial resources for adaptation have become available more slowly than for mitigation in both developed and developing countries. Limited evidence indicates that there is a gap between global adaptation needs and the funds available for adaptation (*medium confidence*). There is a need for better assessment of global adaptation costs, funding and investment. Potential synergies between international finance for disaster risk management and adaptation have not yet been fully realized (*high confidence*). *{4.4.4}*

SPM 4.5 Trade-offs, synergies and interactions with sustainable development

Climate change is a threat to sustainable development. Nonetheless, there are many opportunities to link mitigation, adaptation and the pursuit of other societal objectives through integrated responses (*high confidence*). Successful implementation relies on relevant tools, suitable governance structures and enhanced capacity to respond (*medium confidence*). *{3.5, 4.5}*

Climate change exacerbates other threats to social and natural systems, placing additional burdens particularly on the poor (*high confidence*). Aligning climate policy with sustainable development requires attention to both adaptation and mitigation (*high confidence*). Delaying global mitigation actions may reduce options for climate-resilient pathways and adaptation in the future. Opportunities to take advantage of positive synergies between adaptation and mitigation may decrease with time, particularly if limits to adaptation are exceeded. Increasing efforts to mitigate and adapt to climate change imply an increasing complexity of interactions, encompassing connections among human health, water, energy, land use and biodiversity (*medium evidence, high agreement*). *{3.1, 3.5, 4.5}*

Strategies and actions can be pursued now which will move towards climate-resilient pathways for sustainable development, while at the same time helping to improve livelihoods, social and economic well-being and effective environmental management. In some cases, economic diversification can be an important element of such strategies. The effectiveness of integrated responses can be enhanced by relevant tools, suitable governance structures and adequate institutional and human capacity (*medium confidence*). Integrated responses are especially relevant to energy planning and implementation; interactions among water, food, energy and biological carbon sequestration; and urban planning, which provides substantial opportunities for enhanced resilience, reduced emissions and more sustainable development (*medium confidence*). *{3.5, 4.4, 4.5}*

ipcc
INTERGOVERNMENTAL PANEL ON climate change

Global Warming of 1.5°C

An IPCC Special Report on the impacts of global warming of 1.5°C above pre-industrial levels and related global greenhouse gas emission pathways, in the context of strengthening the global response to the threat of climate change, sustainable development, and efforts to eradicate poverty

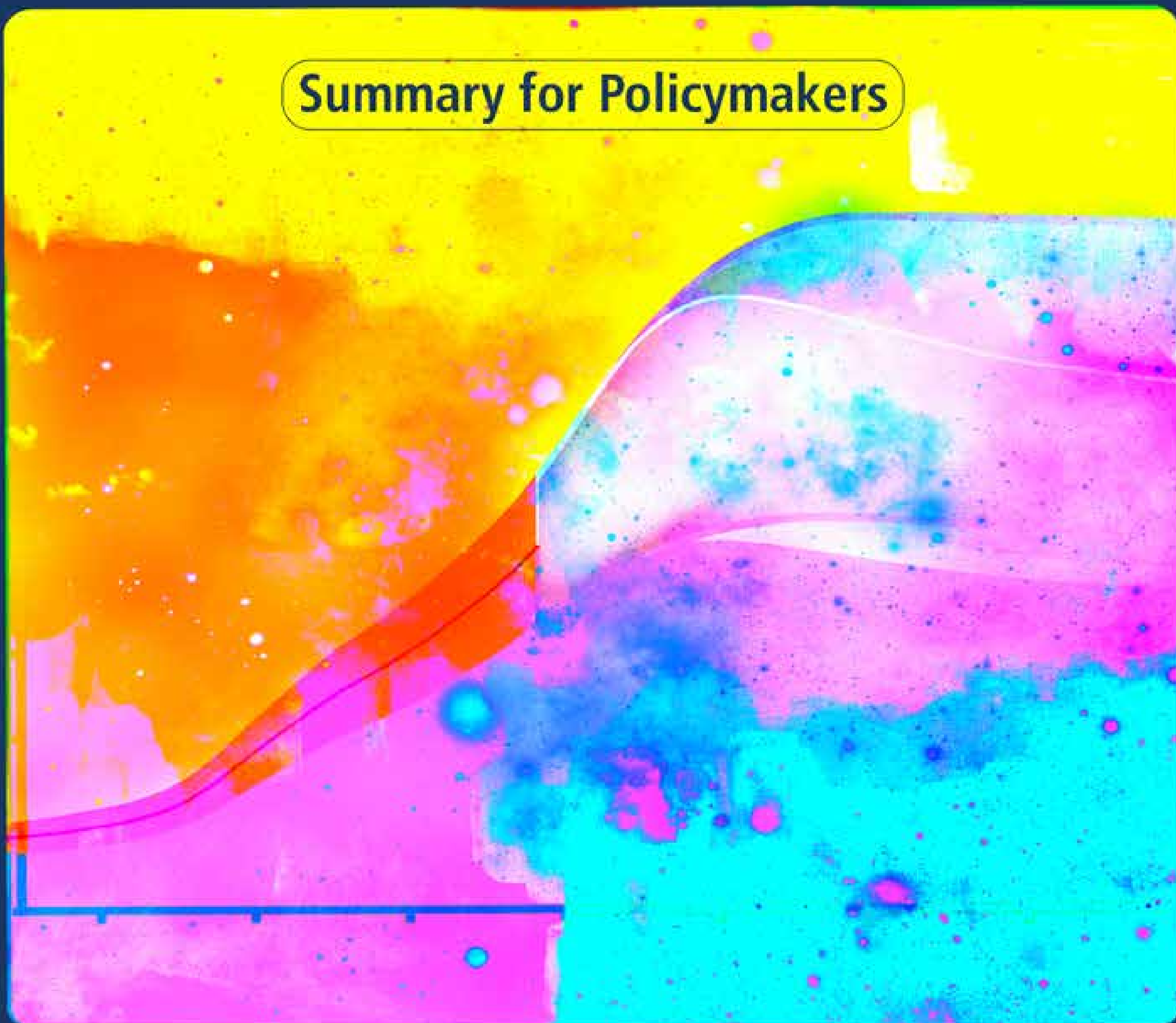

WG I WG II WG III

WMO UNEP

Global warming of 1.5°C

An IPCC Special Report on the impacts of global warming of 1.5°C above pre-industrial levels and related global greenhouse gas emission pathways, in the context of strengthening the global response to the threat of climate change, sustainable development, and efforts to eradicate poverty

Summary for Policymakers

Edited by

Valérie Masson-Delmotte
Co-Chair Working Group I

Panmao Zhai
Co-Chair Working Group I

Hans-Otto Pörtner
Co-Chair Working Group II

Debra Roberts
Co-Chair Working Group II

Jim Skea
Co-Chair Working Group III

Priyadarshi R. Shukla
Co-Chair Working Group III

Anna Pirani
Head of WGI TSU

Wilfran Moufouma-Okia
Head of Science

Clotilde Péan
Head of Operations

Roz Pidcock
Head of Communication

Sarah Connors
Science Officer

J. B. Robin Matthews
Science Officer

Yang Chen
Science Officer

Xiao Zhou
Science Assistant

Melissa I. Gomis
Graphics Officer

Elisabeth Lonnoy
Project Assistant

Tom Maycock
Science Editor

Melinda Tignor
Head of WGII TSU

Tim Waterfield
IT Officer

Working Group I Technical Support Unit

Front cover layout: Nigel Hawtin
Front cover artwork: *Time to Choose* by Alisa Singer - www.environmentalgraphiti.org - © Intergovernmental Panel on Climate Change.
The artwork was inspired by a graphic from the SPM (Figure SPM.1).

Revised on January 2019 by the IPCC, Switzerland.
Electronic copies of this Summary for Policymakers are available from the IPCC website www.ipcc.ch

ISBN 978-92-9169-151-7

Summary for Policymakers

SPM

Summary for Policymakers

Drafting Authors:

Myles R. Allen (UK), Mustafa Babiker (Sudan), Yang Chen (China), Heleen de Coninck (Netherlands/EU), Sarah Connors (UK), Renée van Diemen (Netherlands), Opha Pauline Dube (Botswana), Kristie L. Ebi (USA), Francois Engelbrecht (South Africa), Marion Ferrat (UK/France), James Ford (UK/Canada), Piers Forster (UK), Sabine Fuss (Germany), Tania Guillén Bolaños (Germany/Nicaragua), Jordan Harold (UK), Ove Hoegh-Guldberg (Australia), Jean-Charles Hourcade (France), Daniel Huppmann (Austria), Daniela Jacob (Germany), Kejun Jiang (China), Tom Gabriel Johansen (Norway), Mikiko Kainuma (Japan), Kiane de Kleijne (Netherlands/EU), Elmar Kriegler (Germany), Debora Ley (Guatemala/Mexico), Diana Liverman (USA), Natalie Mahowald (USA), Valérie Masson-Delmotte (France), J. B. Robin Matthews (UK), Richard Millar (UK), Katja Mintenbeck (Germany), Angela Morelli (Norway/Italy), Wilfran Moufouma-Okia (France/Congo), Luis Mundaca (Sweden/Chile), Maike Nicolai (Germany), Chukwumerije Okereke (UK/Nigeria), Minal Pathak (India), Antony Payne (UK), Roz Pidcock (UK), Anna Pirani (Italy), Elvira Poloczanska (UK/Australia), Hans-Otto Pörtner (Germany), Aromar Revi (India), Keywan Riahi (Austria), Debra C. Roberts (South Africa), Joeri Rogelj (Austria/Belgium), Joyashree Roy (India), Sonia I. Seneviratne (Switzerland), Priyadarshi R. Shukla (India), James Skea (UK), Raphael Slade (UK), Drew Shindell (USA), Chandni Singh (India), William Solecki (USA), Linda Steg (Netherlands), Michael Taylor (Jamaica), Petra Tschakert (Australia/Austria), Henri Waisman (France), Rachel Warren (UK), Panmao Zhai (China), Kirsten Zickfeld (Canada).

This Summary for Policymakers should be cited as:

IPCC, 2018: Summary for Policymakers. In: *Global Warming of 1.5°C. An IPCC Special Report on the impacts of global warming of 1.5°C above pre-industrial levels and related global greenhouse gas emission pathways, in the context of strengthening the global response to the threat of climate change, sustainable development, and efforts to eradicate poverty* [Masson-Delmotte, V., P. Zhai, H.-O. Pörtner, D. Roberts, J. Skea, P.R. Shukla, A. Pirani, W. Moufouma-Okia, C. Péan, R. Pidcock, S. Connors, J.B.R. Matthews, Y. Chen, X. Zhou, M.I. Gomis, E. Lonnoy, T. Maycock, M. Tignor, and T. Waterfield (eds.)]. *World Meteorological Organization, Geneva, Switzerland, 32 pp.*

Acknowledgements

We are very grateful for the expertise, rigour and dedication shown throughout by the volunteer Coordinating Lead Authors and Lead Authors, working across scientific disciplines in each chapter of the report, with essential help by the many Contributing Authors. The Review Editors have played a critical role in assisting the author teams and ensuring the integrity of the review process. We express our sincere appreciation to all the expert and government reviewers. A special thanks goes to the Chapter Scientists of this report who went above and beyond what was expected of them: Neville Ellis, Tania Guillén Bolaños, Daniel Huppmann, Kiane de Kleijne, Richard Millar and Chandni Singh.

We would also like to thank the three Intergovernmental Panel on Climate Change (IPCC) Vice-Chairs Ko Barrett, Thelma Krug, and Youba Sokona as well as the members of the WGI, WGII and WGIII Bureaux for their assistance, guidance, and wisdom throughout the preparation of the Report: Amjad Abdulla, Edvin Aldrian, Carlo Carraro, Diriba Korecha Dadi, Fatima Driouech, Andreas Fischlin, Gregory Flato, Jan Fuglestvedt, Mark Howden, Nagmeldin G. E. Mahmoud, Carlos Mendez, Joy Jacqueline Pereira, Ramón Pichs-Madruga, Andy Reisinger, Roberto Sánchez Rodríguez, Sergey Semenov, Muhammad I. Tariq, Diana Ürge-Vorsatz, Carolina Vera, Pius Yanda, Noureddine Yassaa, and Taha Zatari.

Our heartfelt thanks go to the hosts and organizers of the scoping meeting, the four Special Report on 1.5°C Lead Author Meetings and the 48th Session of the IPCC. We gratefully acknowledge the support from the host countries and institutions: World Meteorological Organization, Switzerland; Ministry of Foreign Affairs, and the National Institute for Space Research (INPE), Brazil; Met Office and the University of Exeter, the United Kingdom; Swedish Meteorological and Hydrological Institute (SMHI), Sweden; the Ministry of Environment Natural Resources Conservation and Tourism, the National Climate Change Committee in the Department of Meteorological Services and the Botswana Global Environmental Change Committee at the University of Botswana, Botswana; and Korea Meteorological Administration (KMA) and Incheon Metropolitan City, the Republic of Korea. The support provided by governments and institutions, as well as through contributions to the IPCC Trust Fund, is thankfully acknowledged as it enabled the participation of the author teams in the preparation of the Report. The efficient operation of the Working Group I Technical Support Unit was made possible by the generous financial support provided by the government of France and administrative and information technology support from the Université Paris Saclay (France), Institut Pierre Simon Laplace (IPSL) and the Laboratoire des Sciences du Climat et de l'Environnement (LSCE). We thank the Norwegian Environment Agency for supporting the preparation of the graphics for the Summary for Policymakers. We thank the UNEP Library, who supported authors throughout the drafting process by providing literature for the assessment.

We would also like to thank Abdalah Mokssit, Secretary of the IPCC, and the staff of the IPCC Secretariat: Kerstin Stendahl, Jonathan Lynn, Sophie Schlingemann, Judith Ewa, Mxolisi Shongwe, Jesbin Baidya, Werani Zabula, Nina Peeva, Joelle Fernandez, Annie Courtin, Laura Biagioni and Oksana Ekzarkho. Thanks are due to Elhousseine Gouaini who served as the conference officer for the 48th Session of the IPCC.

Finally, our particular appreciation goes to the Working Group Technical Support Units whose tireless dedication, professionalism and enthusiasm led the production of this Special Report. This report could not have been prepared without the commitment of members of the Working Group I Technical Support Unit, all new to the IPCC, who rose to the unprecedented Sixth Assessment Report challenge and were pivotal in all aspects of the preparation of the Report: Yang Chen, Sarah Connors, Melissa Gomis, Elisabeth Lonnoy, Robin Matthews, Wilfran Moufouma-Okia, Clotilde Péan, Roz Pidcock, Anna Pirani, Nicholas Reay, Tim Waterfield, and Xiao Zhou. Our warmest thanks go to the collegial and collaborative support provided by Marlies Craig, Andrew Okem, Jan Petzold, Melinda Tignor and Nora Weyer from the WGII Technical Support Unit and Bhushan Kankal, Suvadip Neogi and Joana Portugal Pereira from the WGIII Technical Support Unit. A special thanks goes to Kenny Coventry, Harmen Gudde, Irene Lorenzoni, and Stuart Jenkins for their support with the figures in the Summary for Policymakers, as well as Nigel Hawtin for graphical support of the Report. In addition, the following contributions are gratefully acknowledged: Jatinder Padda (copy edit), Melissa Dawes (copy edit), Marilyn Anderson (index), Vincent Grégoire (layout) and Sarah le Rouzic (intern).

The Special Report website has been developed by Habitat 7, led by Jamie Herring, and the report content has been prepared and managed for the website by Nicholas Reay and Tim Waterfield. We gratefully acknowledge the UN Foundation for supporting the website development.

SPM

Introduction

This Report responds to the invitation for IPCC '... to provide a Special Report in 2018 on the impacts of global warming of 1.5°C above pre-industrial levels and related global greenhouse gas emission pathways' contained in the Decision of the 21st Conference of Parties of the United Nations Framework Convention on Climate Change to adopt the Paris Agreement.[1]

The IPCC accepted the invitation in April 2016, deciding to prepare this Special Report on the impacts of global warming of 1.5°C above pre-industrial levels and related global greenhouse gas emission pathways, in the context of strengthening the global response to the threat of climate change, sustainable development, and efforts to eradicate poverty.

This Summary for Policymakers (SPM) presents the key findings of the Special Report, based on the assessment of the available scientific, technical and socio-economic literature[2] relevant to global warming of 1.5°C and for the comparison between global warming of 1.5°C and 2°C above pre-industrial levels. The level of confidence associated with each key finding is reported using the IPCC calibrated language.[3] The underlying scientific basis of each key finding is indicated by references provided to chapter elements. In the SPM, knowledge gaps are identified associated with the underlying chapters of the Report.

A. Understanding Global Warming of 1.5°C[4]

A.1 Human activities are estimated to have caused approximately 1.0°C of global warming[5] above pre-industrial levels, with a *likely* range of 0.8°C to 1.2°C. Global warming is *likely* to reach 1.5°C between 2030 and 2052 if it continues to increase at the current rate. (*high confidence*) (Figure SPM.1) {1.2}

A.1.1 Reflecting the long-term warming trend since pre-industrial times, observed global mean surface temperature (GMST) for the decade 2006–2015 was 0.87°C (*likely* between 0.75°C and 0.99°C)[6] higher than the average over the 1850–1900 period (*very high confidence*). Estimated anthropogenic global warming matches the level of observed warming to within ±20% (*likely range*). Estimated anthropogenic global warming is currently increasing at 0.2°C (*likely* between 0.1°C and 0.3°C) per decade due to past and ongoing emissions (*high confidence*). {1.2.1, Table 1.1, 1.2.4}

A.1.2 Warming greater than the global annual average is being experienced in many land regions and seasons, including two to three times higher in the Arctic. Warming is generally higher over land than over the ocean. (*high confidence*) {1.2.1, 1.2.2, Figure 1.1, Figure 1.3, 3.3.1, 3.3.2}

A.1.3 Trends in intensity and frequency of some climate and weather extremes have been detected over time spans during which about 0.5°C of global warming occurred (*medium confidence*). This assessment is based on several lines of evidence, including attribution studies for changes in extremes since 1950. {3.3.1, 3.3.2, 3.3.3}

---

1 Decision 1/CP.21, paragraph 21.

2 The assessment covers literature accepted for publication by 15 May 2018.

3 Each finding is grounded in an evaluation of underlying evidence and agreement. A level of confidence is expressed using five qualifiers: very low, low, medium, high and very high, and typeset in italics, for example, *medium confidence*. The following terms have been used to indicate the assessed likelihood of an outcome or a result: virtually certain 99–100% probability, very likely 90–100%, likely 66–100%, about as likely as not 33–66%, unlikely 0–33%, very unlikely 0–10%, exceptionally unlikely 0–1%. Additional terms (extremely likely 95–100%, more likely than not >50–100%, more unlikely than likely 0–<50%, extremely unlikely 0–5%) may also be used when appropriate. Assessed likelihood is typeset in italics, for example, *very likely*. This is consistent with AR5.

4 See also Box SPM.1: Core Concepts Central to this Special Report.

5 Present level of global warming is defined as the average of a 30-year period centred on 2017 assuming the recent rate of warming continues.

6 This range spans the four available peer-reviewed estimates of the observed GMST change and also accounts for additional uncertainty due to possible short-term natural variability. {1.2.1, Table 1.1}

A.2 Warming from anthropogenic emissions from the pre-industrial period to the present will persist for centuries to millennia and will continue to cause further long-term changes in the climate system, such as sea level rise, with associated impacts (*high confidence*), but these emissions alone are *unlikely* to cause global warming of 1.5°C (*medium confidence*). (Figure SPM.1) {1.2, 3.3, Figure 1.5}

A.2.1 Anthropogenic emissions (including greenhouse gases, aerosols and their precursors) up to the present are *unlikely* to cause further warming of more than 0.5°C over the next two to three decades (*high confidence*) or on a century time scale (*medium confidence*). {1.2.4, Figure 1.5}

A.2.2 Reaching and sustaining net zero global anthropogenic CO_2 emissions and declining net non-CO_2 radiative forcing would halt anthropogenic global warming on multi-decadal time scales (*high confidence*). The maximum temperature reached is then determined by cumulative net global anthropogenic CO_2 emissions up to the time of net zero CO_2 emissions (*high confidence*) and the level of non-CO_2 radiative forcing in the decades prior to the time that maximum temperatures are reached (*medium confidence*). On longer time scales, sustained net negative global anthropogenic CO_2 emissions and/or further reductions in non-CO_2 radiative forcing may still be required to prevent further warming due to Earth system feedbacks and to reverse ocean acidification (*medium confidence*) and will be required to minimize sea level rise (*high confidence*). {Cross-Chapter Box 2 in Chapter 1, 1.2.3, 1.2.4, Figure 1.4, 2.2.1, 2.2.2, 3.4.4.8, 3.4.5.1, 3.6.3.2}

A.3 Climate-related risks for natural and human systems are higher for global warming of 1.5°C than at present, but lower than at 2°C (*high confidence*). These risks depend on the magnitude and rate of warming, geographic location, levels of development and vulnerability, and on the choices and implementation of adaptation and mitigation options (*high confidence*). (Figure SPM.2) {1.3, 3.3, 3.4, 5.6}

A.3.1 Impacts on natural and human systems from global warming have already been observed (*high confidence*). Many land and ocean ecosystems and some of the services they provide have already changed due to global warming (*high confidence*). (Figure SPM.2) {1.4, 3.4, 3.5}

A.3.2 Future climate-related risks depend on the rate, peak and duration of warming. In the aggregate, they are larger if global warming exceeds 1.5°C before returning to that level by 2100 than if global warming gradually stabilizes at 1.5°C, especially if the peak temperature is high (e.g., about 2°C) (*high confidence*). Some impacts may be long-lasting or irreversible, such as the loss of some ecosystems (*high confidence*). {3.2, 3.4.4, 3.6.3, Cross-Chapter Box 8 in Chapter 3}

A.3.3 Adaptation and mitigation are already occurring (*high confidence*). Future climate-related risks would be reduced by the upscaling and acceleration of far-reaching, multilevel and cross-sectoral climate mitigation and by both incremental and transformational adaptation (*high confidence*). {1.2, 1.3, Table 3.5, 4.2.2, Cross-Chapter Box 9 in Chapter 4, Box 4.2, Box 4.3, Box 4.6, 4.3.1, 4.3.2, 4.3.3, 4.3.4, 4.3.5, 4.4.1, 4.4.4, 4.4.5, 4.5.3}

SPM

Cumulative emissions of CO_2 and future non-CO_2 radiative forcing determine the probability of limiting warming to 1.5°C

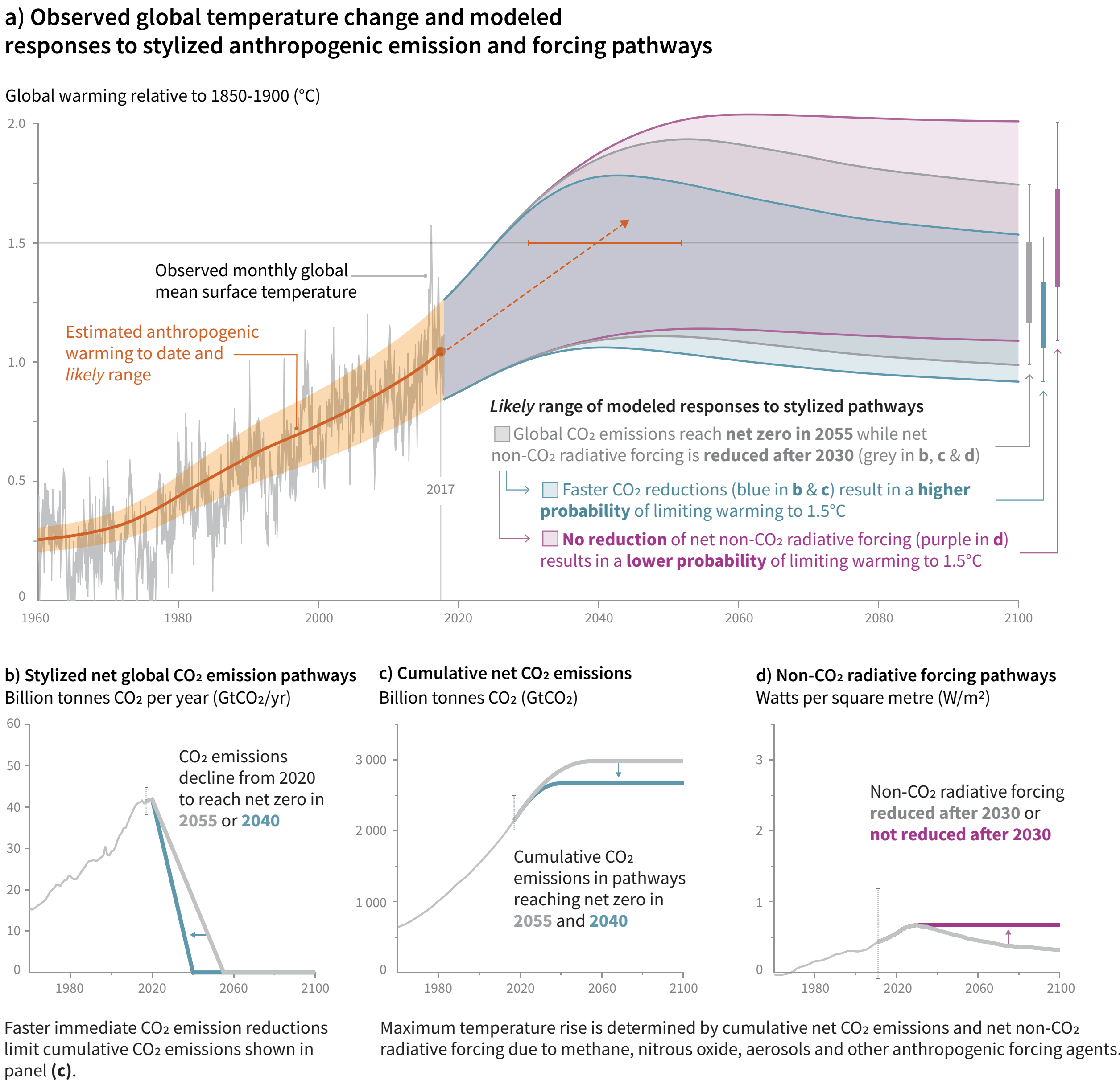

Figure SPM.1 | Panel a: Observed monthly global mean surface temperature (GMST, grey line up to 2017, from the HadCRUT4, GISTEMP, Cowtan–Way, and NOAA datasets) change and estimated anthropogenic global warming (solid orange line up to 2017, with orange shading indicating assessed *likely* range). Orange dashed arrow and horizontal orange error bar show respectively the central estimate and *likely* range of the time at which 1.5°C is reached if the current rate of warming continues. The grey plume on the right of panel a shows the *likely* range of warming responses, computed with a simple climate model, to a stylized pathway (hypothetical future) in which net CO_2 emissions (grey line in panels b and c) decline in a straight line from 2020 to reach net zero in 2055 and net non-CO_2 radiative forcing (grey line in panel d) increases to 2030 and then declines. The blue plume in panel a) shows the response to faster CO_2 emissions reductions (blue line in panel b), reaching net zero in 2040, reducing cumulative CO_2 emissions (panel c). The purple plume shows the response to net CO_2 emissions declining to zero in 2055, with net non-CO_2 forcing remaining constant after 2030. The vertical error bars on right of panel a) show the *likely* ranges (thin lines) and central terciles (33rd – 66th percentiles, thick lines) of the estimated distribution of warming in 2100 under these three stylized pathways. Vertical dotted error bars in panels b, c and d show the *likely* range of historical annual and cumulative global net CO_2 emissions in 2017 (data from the Global Carbon Project) and of net non-CO_2 radiative forcing in 2011 from AR5, respectively. Vertical axes in panels c and d are scaled to represent approximately equal effects on GMST. {1.2.1, 1.2.3, 1.2.4, 2.3, Figure 1.2 and Chapter 1 Supplementary Material, Cross-Chapter Box 2 in Chapter 1}

B. Projected Climate Change, Potential Impacts and Associated Risks

B.1 Climate models project robust[7] differences in regional climate characteristics between present-day and global warming of 1.5°C,[8] and between 1.5°C and 2°C.[8] These differences include increases in: mean temperature in most land and ocean regions (*high confidence*), hot extremes in most inhabited regions (*high confidence*), heavy precipitation in several regions (*medium confidence*), and the probability of drought and precipitation deficits in some regions (*medium confidence*). {3.3}

B.1.1 Evidence from attributed changes in some climate and weather extremes for a global warming of about 0.5°C supports the assessment that an additional 0.5°C of warming compared to present is associated with further detectable changes in these extremes (*medium confidence*). Several regional changes in climate are assessed to occur with global warming up to 1.5°C compared to pre-industrial levels, including warming of extreme temperatures in many regions (*high confidence*), increases in frequency, intensity, and/or amount of heavy precipitation in several regions (*high confidence*), and an increase in intensity or frequency of droughts in some regions (*medium confidence*). {3.2, 3.3.1, 3.3.2, 3.3.3, 3.3.4, Table 3.2}

B.1.2 Temperature extremes on land are projected to warm more than GMST (*high confidence*): extreme hot days in mid-latitudes warm by up to about 3°C at global warming of 1.5°C and about 4°C at 2°C, and extreme cold nights in high latitudes warm by up to about 4.5°C at 1.5°C and about 6°C at 2°C (*high confidence*). The number of hot days is projected to increase in most land regions, with highest increases in the tropics (*high confidence*). {3.3.1, 3.3.2, Cross-Chapter Box 8 in Chapter 3}

B.1.3 Risks from droughts and precipitation deficits are projected to be higher at 2°C compared to 1.5°C of global warming in some regions (*medium confidence*). Risks from heavy precipitation events are projected to be higher at 2°C compared to 1.5°C of global warming in several northern hemisphere high-latitude and/or high-elevation regions, eastern Asia and eastern North America (*medium confidence)*. Heavy precipitation associated with tropical cyclones is projected to be higher at 2°C compared to 1.5°C global warming (*medium confidence*). There is generally *low confidence* in projected changes in heavy precipitation at 2°C compared to 1.5°C in other regions. Heavy precipitation when aggregated at global scale is projected to be higher at 2°C than at 1.5°C of global warming (*medium confidence*). As a consequence of heavy precipitation, the fraction of the global land area affected by flood hazards is projected to be larger at 2°C compared to 1.5°C of global warming (*medium confidence*). {3.3.1, 3.3.3, 3.3.4, 3.3.5, 3.3.6}

B.2 By 2100, global mean sea level rise is projected to be around 0.1 metre lower with global warming of 1.5°C compared to 2°C (*medium confidence*). Sea level will continue to rise well beyond 2100 (*high confidence*), and the magnitude and rate of this rise depend on future emission pathways. A slower rate of sea level rise enables greater opportunities for adaptation in the human and ecological systems of small islands, low-lying coastal areas and deltas (*medium confidence*). {3.3, 3.4, 3.6}

B.2.1 Model-based projections of global mean sea level rise (relative to 1986–2005) suggest an indicative range of 0.26 to 0.77 m by 2100 for 1.5°C of global warming, 0.1 m (0.04–0.16 m) less than for a global warming of 2°C (*medium confidence*). A reduction of 0.1 m in global sea level rise implies that up to 10 million fewer people would be exposed to related risks, based on population in the year 2010 and assuming no adaptation (*medium confidence*). {3.4.4, 3.4.5, 4.3.2}

B.2.2 Sea level rise will continue beyond 2100 even if global warming is limited to 1.5°C in the 21st century (*high confidence*). Marine ice sheet instability in Antarctica and/or irreversible loss of the Greenland ice sheet could result in multi-metre rise in sea level over hundreds to thousands of years. These instabilities could be triggered at around 1.5°C to 2°C of global warming (*medium confidence*). (Figure SPM.2) {3.3.9, 3.4.5, 3.5.2, 3.6.3, Box 3.3}

7 Robust is here used to mean that at least two thirds of climate models show the same sign of changes at the grid point scale, and that differences in large regions are statistically significant.

8 Projected changes in impacts between different levels of global warming are determined with respect to changes in global mean surface air temperature.

B.2.3 Increasing warming amplifies the exposure of small islands, low-lying coastal areas and deltas to the risks associated with sea level rise for many human and ecological systems, including increased saltwater intrusion, flooding and damage to infrastructure (*high confidence*). Risks associated with sea level rise are higher at 2°C compared to 1.5°C. The slower rate of sea level rise at global warming of 1.5°C reduces these risks, enabling greater opportunities for adaptation including managing and restoring natural coastal ecosystems and infrastructure reinforcement (*medium confidence*). (Figure SPM.2) {3.4.5, Box 3.5}

B.3 On land, impacts on biodiversity and ecosystems, including species loss and extinction, are projected to be lower at 1.5°C of global warming compared to 2°C. Limiting global warming to 1.5°C compared to 2°C is projected to lower the impacts on terrestrial, freshwater and coastal ecosystems and to retain more of their services to humans (*high confidence*). (Figure SPM.2) {3.4, 3.5, Box 3.4, Box 4.2, Cross-Chapter Box 8 in Chapter 3}

B.3.1 Of 105,000 species studied,[9] 6% of insects, 8% of plants and 4% of vertebrates are projected to lose over half of their climatically determined geographic range for global warming of 1.5°C, compared with 18% of insects, 16% of plants and 8% of vertebrates for global warming of 2°C (*medium confidence*). Impacts associated with other biodiversity-related risks such as forest fires and the spread of invasive species are lower at 1.5°C compared to 2°C of global warming (*high confidence*). {3.4.3, 3.5.2}

B.3.2 Approximately 4% (interquartile range 2–7%) of the global terrestrial land area is projected to undergo a transformation of ecosystems from one type to another at 1°C of global warming, compared with 13% (interquartile range 8–20%) at 2°C (*medium confidence*). This indicates that the area at risk is projected to be approximately 50% lower at 1.5°C compared to 2°C (*medium confidence*). {3.4.3.1, 3.4.3.5}

B.3.3 High-latitude tundra and boreal forests are particularly at risk of climate change-induced degradation and loss, with woody shrubs already encroaching into the tundra (*high confidence*) and this will proceed with further warming. Limiting global warming to 1.5°C rather than 2°C is projected to prevent the thawing over centuries of a permafrost area in the range of 1.5 to 2.5 million km^2 (*medium confidence*). {3.3.2, 3.4.3, 3.5.5}

B.4 Limiting global warming to 1.5°C compared to 2°C is projected to reduce increases in ocean temperature as well as associated increases in ocean acidity and decreases in ocean oxygen levels (*high confidence*). Consequently, limiting global warming to 1.5°C is projected to reduce risks to marine biodiversity, fisheries, and ecosystems, and their functions and services to humans, as illustrated by recent changes to Arctic sea ice and warm-water coral reef ecosystems (*high confidence*). {3.3, 3.4, 3.5, Box 3.4, Box 3.5}

B.4.1 There is *high confidence* that the probability of a sea ice-free Arctic Ocean during summer is substantially lower at global warming of 1.5°C when compared to 2°C. With 1.5°C of global warming, one sea ice-free Arctic summer is projected per century. This likelihood is increased to at least one per decade with 2°C global warming. Effects of a temperature overshoot are reversible for Arctic sea ice cover on decadal time scales (*high confidence*). {3.3.8, 3.4.4.7}

B.4.2 Global warming of 1.5°C is projected to shift the ranges of many marine species to higher latitudes as well as increase the amount of damage to many ecosystems. It is also expected to drive the loss of coastal resources and reduce the productivity of fisheries and aquaculture (especially at low latitudes). The risks of climate-induced impacts are projected to be higher at 2°C than those at global warming of 1.5°C (*high confidence*). Coral reefs, for example, are projected to decline by a further 70–90% at 1.5°C (*high confidence*) with larger losses (>99%) at 2°C (*very high confidence*). The risk of irreversible loss of many marine and coastal ecosystems increases with global warming, especially at 2°C or more (*high confidence*). {3.4.4, Box 3.4}

9 Consistent with earlier studies, illustrative numbers were adopted from one recent meta-study.

B.4.3 The level of ocean acidification due to increasing CO_2 concentrations associated with global warming of 1.5°C is projected to amplify the adverse effects of warming, and even further at 2°C, impacting the growth, development, calcification, survival, and thus abundance of a broad range of species, for example, from algae to fish (*high confidence*). {3.3.10, 3.4.4}

B.4.4 Impacts of climate change in the ocean are increasing risks to fisheries and aquaculture via impacts on the physiology, survivorship, habitat, reproduction, disease incidence, and risk of invasive species (*medium confidence*) but are projected to be less at 1.5°C of global warming than at 2°C. One global fishery model, for example, projected a decrease in global annual catch for marine fisheries of about 1.5 million tonnes for 1.5°C of global warming compared to a loss of more than 3 million tonnes for 2°C of global warming (*medium confidence*). {3.4.4, Box 3.4}

B.5 Climate-related risks to health, livelihoods, food security, water supply, human security, and economic growth are projected to increase with global warming of 1.5°C and increase further with 2°C. (Figure SPM.2) {3.4, 3.5, 5.2, Box 3.2, Box 3.3, Box 3.5, Box 3.6, Cross-Chapter Box 6 in Chapter 3, Cross-Chapter Box 9 in Chapter 4, Cross-Chapter Box 12 in Chapter 5, 5.2}

B.5.1 Populations at disproportionately higher risk of adverse consequences with global warming of 1.5°C and beyond include disadvantaged and vulnerable populations, some indigenous peoples, and local communities dependent on agricultural or coastal livelihoods (*high confidence*). Regions at disproportionately higher risk include Arctic ecosystems, dryland regions, small island developing states, and Least Developed Countries (*high confidence*). Poverty and disadvantage are expected to increase in some populations as global warming increases; limiting global warming to 1.5°C, compared with 2°C, could reduce the number of people both exposed to climate-related risks and susceptible to poverty by up to several hundred million by 2050 (*medium confidence*). {3.4.10, 3.4.11, Box 3.5, Cross-Chapter Box 6 in Chapter 3, Cross-Chapter Box 9 in Chapter 4, Cross-Chapter Box 12 in Chapter 5, 4.2.2.2, 5.2.1, 5.2.2, 5.2.3, 5.6.3}

B.5.2 Any increase in global warming is projected to affect human health, with primarily negative consequences (*high confidence*). Lower risks are projected at 1.5°C than at 2°C for heat-related morbidity and mortality (*very high confidence*) and for ozone-related mortality if emissions needed for ozone formation remain high (*high confidence*). Urban heat islands often amplify the impacts of heatwaves in cities (*high confidence*). Risks from some vector-borne diseases, such as malaria and dengue fever, are projected to increase with warming from 1.5°C to 2°C, including potential shifts in their geographic range (*high confidence*). {3.4.7, 3.4.8, 3.5.5.8}

B.5.3 Limiting warming to 1.5°C compared with 2°C is projected to result in smaller net reductions in yields of maize, rice, wheat, and potentially other cereal crops, particularly in sub-Saharan Africa, Southeast Asia, and Central and South America, and in the CO_2-dependent nutritional quality of rice and wheat (*high confidence*). Reductions in projected food availability are larger at 2°C than at 1.5°C of global warming in the Sahel, southern Africa, the Mediterranean, central Europe, and the Amazon (*medium confidence*). Livestock are projected to be adversely affected with rising temperatures, depending on the extent of changes in feed quality, spread of diseases, and water resource availability (*high confidence*). {3.4.6, 3.5.4, 3.5.5, Box 3.1, Cross-Chapter Box 6 in Chapter 3, Cross-Chapter Box 9 in Chapter 4}

B.5.4 Depending on future socio-economic conditions, limiting global warming to 1.5°C compared to 2°C may reduce the proportion of the world population exposed to a climate change-induced increase in water stress by up to 50%, although there is considerable variability between regions (*medium confidence*). Many small island developing states could experience lower water stress as a result of projected changes in aridity when global warming is limited to 1.5°C, as compared to 2°C (*medium confidence*). {3.3.5, 3.4.2, 3.4.8, 3.5.5, Box 3.2, Box 3.5, Cross-Chapter Box 9 in Chapter 4}

B.5.5 Risks to global aggregated economic growth due to climate change impacts are projected to be lower at 1.5°C than at 2°C by the end of this century[10] (*medium confidence*). This excludes the costs of mitigation, adaptation investments and the benefits of adaptation. Countries in the tropics and Southern Hemisphere subtropics are projected to experience the largest impacts on economic growth due to climate change should global warming increase from 1.5°C to 2°C (*medium confidence*). {3.5.2, 3.5.3}

10 Here, impacts on economic growth refer to changes in gross domestic product (GDP). Many impacts, such as loss of human lives, cultural heritage and ecosystem services, are difficult to value and monetize.

B.5.6 Exposure to multiple and compound climate-related risks increases between 1.5°C and 2°C of global warming, with greater proportions of people both so exposed and susceptible to poverty in Africa and Asia (*high confidence*). For global warming from 1.5°C to 2°C, risks across energy, food, and water sectors could overlap spatially and temporally, creating new and exacerbating current hazards, exposures, and vulnerabilities that could affect increasing numbers of people and regions (*medium confidence*). {Box 3.5, 3.3.1, 3.4.5.3, 3.4.5.6, 3.4.11, 3.5.4.9}

B.5.7 There are multiple lines of evidence that since AR5 the assessed levels of risk increased for four of the five Reasons for Concern (RFCs) for global warming to 2°C (*high confidence*). The risk transitions by degrees of global warming are now: from high to very high risk between 1.5°C and 2°C for RFC1 (Unique and threatened systems) (*high confidence*); from moderate to high risk between 1°C and 1.5°C for RFC2 (Extreme weather events) (*medium confidence*); from moderate to high risk between 1.5°C and 2°C for RFC3 (Distribution of impacts) (*high confidence*); from moderate to high risk between 1.5°C and 2.5°C for RFC4 (Global aggregate impacts) (*medium confidence*); and from moderate to high risk between 1°C and 2.5°C for RFC5 (Large-scale singular events) (*medium confidence*). (Figure SPM.2) {3.4.13; 3.5, 3.5.2}

B.6 Most adaptation needs will be lower for global warming of 1.5°C compared to 2°C (*high confidence*). There are a wide range of adaptation options that can reduce the risks of climate change (*high confidence*). There are limits to adaptation and adaptive capacity for some human and natural systems at global warming of 1.5°C, with associated losses (*medium confidence*). The number and availability of adaptation options vary by sector (*medium confidence*). {Table 3.5, 4.3, 4.5, Cross-Chapter Box 9 in Chapter 4, Cross-Chapter Box 12 in Chapter 5}

B.6.1 A wide range of adaptation options are available to reduce the risks to natural and managed ecosystems (e.g., ecosystem-based adaptation, ecosystem restoration and avoided degradation and deforestation, biodiversity management, sustainable aquaculture, and local knowledge and indigenous knowledge), the risks of sea level rise (e.g., coastal defence and hardening), and the risks to health, livelihoods, food, water, and economic growth, especially in rural landscapes (e.g., efficient irrigation, social safety nets, disaster risk management, risk spreading and sharing, and community-based adaptation) and urban areas (e.g., green infrastructure, sustainable land use and planning, and sustainable water management) (*medium confidence*). {4.3.1, 4.3.2, 4.3.3, 4.3.5, 4.5.3, 4.5.4, 5.3.2, Box 4.2, Box 4.3, Box 4.6, Cross-Chapter Box 9 in Chapter 4}.

B.6.2 Adaptation is expected to be more challenging for ecosystems, food and health systems at 2°C of global warming than for 1.5°C (*medium confidence*). Some vulnerable regions, including small islands and Least Developed Countries, are projected to experience high multiple interrelated climate risks even at global warming of 1.5°C (*high confidence*). {3.3.1, 3.4.5, Box 3.5, Table 3.5, Cross-Chapter Box 9 in Chapter 4, 5.6, Cross-Chapter Box 12 in Chapter 5, Box 5.3}

B.6.3 Limits to adaptive capacity exist at 1.5°C of global warming, become more pronounced at higher levels of warming and vary by sector, with site-specific implications for vulnerable regions, ecosystems and human health (*medium confidence*). {Cross-Chapter Box 12 in Chapter 5, Box 3.5, Table 3.5}

How the level of global warming affects impacts and/or risks associated with the Reasons for Concern (RFCs) and selected natural, managed and human systems

Five Reasons For Concern (RFCs) illustrate the impacts and risks of different levels of global warming for people, economies and ecosystems across sectors and regions.

Impacts and risks associated with the Reasons for Concern (RFCs)

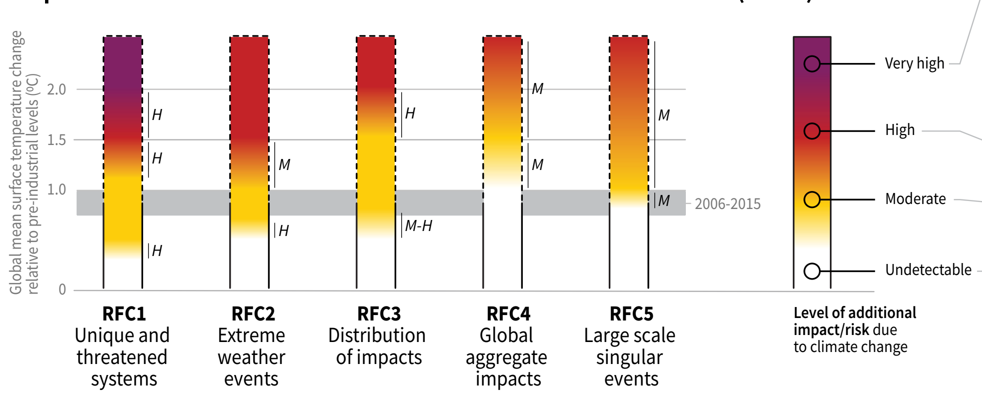

Purple indicates very high risks of severe impacts/risks and the presence of significant irreversibility or the persistence of climate-related hazards, combined with limited ability to adapt due to the nature of the hazard or impacts/risks.
Red indicates severe and widespread impacts/risks.
Yellow indicates that impacts/risks are detectable and attributable to climate change with at least medium confidence.
White indicates that no impacts are detectable and attributable to climate change.

Impacts and risks for selected natural, managed and human systems

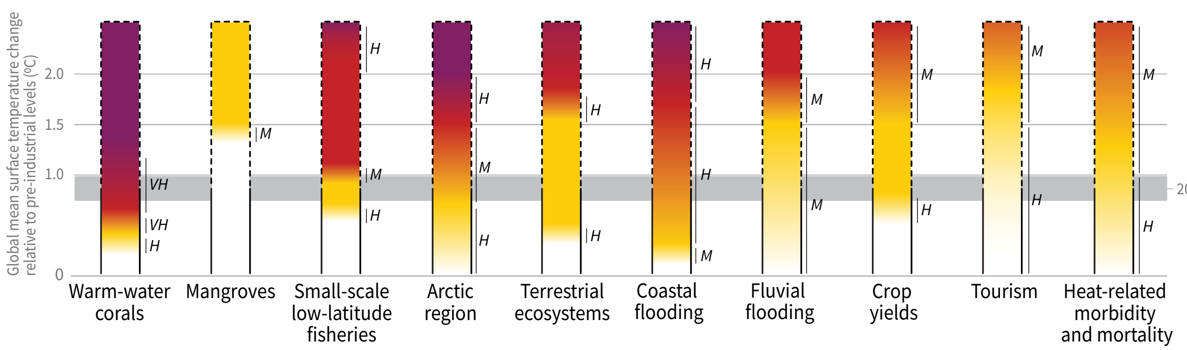

Confidence level for transition: *L*=Low, *M*=Medium, *H*=High and *VH*=Very high

Figure SPM.2 | Five integrative reasons for concern (RFCs) provide a framework for summarizing key impacts and risks across sectors and regions, and were introduced in the IPCC Third Assessment Report. RFCs illustrate the implications of global warming for people, economies and ecosystems. Impacts and/or risks for each RFC are based on assessment of the new literature that has appeared. As in AR5, this literature was used to make expert judgments to assess the levels of global warming at which levels of impact and/or risk are undetectable, moderate, high or very high. The selection of impacts and risks to natural, managed and human systems in the lower panel is illustrative and is not intended to be fully comprehensive. {3.4, 3.5, 3.5.2.1, 3.5.2.2, 3.5.2.3, 3.5.2.4, 3.5.2.5, 5.4.1, 5.5.3, 5.6.1, Box 3.4}
RFC1 Unique and threatened systems: ecological and human systems that have restricted geographic ranges constrained by climate-related conditions and have high endemism or other distinctive properties. Examples include coral reefs, the Arctic and its indigenous people, mountain glaciers and biodiversity hotspots.
RFC2 Extreme weather events: risks/impacts to human health, livelihoods, assets and ecosystems from extreme weather events such as heat waves, heavy rain, drought and associated wildfires, and coastal flooding.
RFC3 Distribution of impacts: risks/impacts that disproportionately affect particular groups due to uneven distribution of physical climate change hazards, exposure or vulnerability.
RFC4 Global aggregate impacts: global monetary damage, global-scale degradation and loss of ecosystems and biodiversity.
RFC5 Large-scale singular events: are relatively large, abrupt and sometimes irreversible changes in systems that are caused by global warming. Examples include disintegration of the Greenland and Antarctic ice sheets.

C. Emission Pathways and System Transitions Consistent with 1.5°C Global Warming

C.1 In model pathways with no or limited overshoot of 1.5°C, global net anthropogenic CO_2 emissions decline by about 45% from 2010 levels by 2030 (40–60% interquartile range), reaching net zero around 2050 (2045–2055 interquartile range). For limiting global warming to below 2°C[11] CO_2 emissions are projected to decline by about 25% by 2030 in most pathways (10–30% interquartile range) and reach net zero around 2070 (2065–2080 interquartile range). Non-CO_2 emissions in pathways that limit global warming to 1.5°C show deep reductions that are similar to those in pathways limiting warming to 2°C. (*high confidence*) (Figure SPM.3a) {2.1, 2.3, Table 2.4}

C.1.1 CO_2 emissions reductions that limit global warming to 1.5°C with no or limited overshoot can involve different portfolios of mitigation measures, striking different balances between lowering energy and resource intensity, rate of decarbonization, and the reliance on carbon dioxide removal. Different portfolios face different implementation challenges and potential synergies and trade-offs with sustainable development. (*high confidence*) (Figure SPM.3b) {2.3.2, 2.3.4, 2.4, 2.5.3}

C.1.2 Modelled pathways that limit global warming to 1.5°C with no or limited overshoot involve deep reductions in emissions of methane and black carbon (35% or more of both by 2050 relative to 2010). These pathways also reduce most of the cooling aerosols, which partially offsets mitigation effects for two to three decades. Non-CO_2 emissions[12] can be reduced as a result of broad mitigation measures in the energy sector. In addition, targeted non-CO_2 mitigation measures can reduce nitrous oxide and methane from agriculture, methane from the waste sector, some sources of black carbon, and hydrofluorocarbons. High bioenergy demand can increase emissions of nitrous oxide in some 1.5°C pathways, highlighting the importance of appropriate management approaches. Improved air quality resulting from projected reductions in many non-CO_2 emissions provide direct and immediate population health benefits in all 1.5°C model pathways. (*high confidence*) (Figure SPM.3a) {2.2.1, 2.3.3, 2.4.4, 2.5.3, 4.3.6, 5.4.2}

C.1.3 Limiting global warming requires limiting the total cumulative global anthropogenic emissions of CO_2 since the pre-industrial period, that is, staying within a total carbon budget (*high confidence*).[13] By the end of 2017, anthropogenic CO_2 emissions since the pre-industrial period are estimated to have reduced the total carbon budget for 1.5°C by approximately 2200 ± 320 $GtCO_2$ (*medium confidence*). The associated remaining budget is being depleted by current emissions of 42 ± 3 $GtCO_2$ per year (*high confidence*). The choice of the measure of global temperature affects the estimated remaining carbon budget. Using global mean surface air temperature, as in AR5, gives an estimate of the remaining carbon budget of 580 $GtCO_2$ for a 50% probability of limiting warming to 1.5°C, and 420 $GtCO_2$ for a 66% probability (*medium confidence*).[14] Alternatively, using GMST gives estimates of 770 and 570 $GtCO_2$, for 50% and 66% probabilities,[15] respectively (*medium confidence*). Uncertainties in the size of these estimated remaining carbon budgets are substantial and depend on several factors. Uncertainties in the climate response to CO_2 and non-CO_2 emissions contribute ±400 $GtCO_2$ and the level of historic warming contributes ±250 $GtCO_2$ (*medium confidence*). Potential additional carbon release from future permafrost thawing and methane release from wetlands would reduce budgets by up to 100 $GtCO_2$ over the course of this century and more thereafter (*medium confidence*). In addition, the level of non-CO_2 mitigation in the future could alter the remaining carbon budget by 250 $GtCO_2$ in either direction (*medium confidence*). {1.2.4, 2.2.2, 2.6.1, Table 2.2, Chapter 2 Supplementary Material}

C.1.4 Solar radiation modification (SRM) measures are not included in any of the available assessed pathways. Although some SRM measures may be theoretically effective in reducing an overshoot, they face large uncertainties and knowledge gaps

11 References to pathways limiting global warming to 2°C are based on a 66% probability of staying below 2°C.

12 Non-CO_2 emissions included in this Report are all anthropogenic emissions other than CO_2 that result in radiative forcing. These include short-lived climate forcers, such as methane, some fluorinated gases, ozone precursors, aerosols or aerosol precursors, such as black carbon and sulphur dioxide, respectively, as well as long-lived greenhouse gases, such as nitrous oxide or some fluorinated gases. The radiative forcing associated with non-CO_2 emissions and changes in surface albedo is referred to as non-CO_2 radiative forcing. {2.2.1}

13 There is a clear scientific basis for a total carbon budget consistent with limiting global warming to 1.5°C. However, neither this total carbon budget nor the fraction of this budget taken up by past emissions were assessed in this Report.

14 Irrespective of the measure of global temperature used, updated understanding and further advances in methods have led to an increase in the estimated remaining carbon budget of about 300 $GtCO_2$ compared to AR5. (*medium confidence*) {2.2.2}

15 These estimates use observed GMST to 2006–2015 and estimate future temperature changes using near surface air temperatures.

as well as substantial risks and institutional and social constraints to deployment related to governance, ethics, and impacts on sustainable development. They also do not mitigate ocean acidification. (*medium confidence*) {4.3.8, Cross-Chapter Box 10 in Chapter 4}

Global emissions pathway characteristics

General characteristics of the evolution of anthropogenic net emissions of CO_2, and total emissions of methane, black carbon, and nitrous oxide in model pathways that limit global warming to 1.5°C with no or limited overshoot. Net emissions are defined as anthropogenic emissions reduced by anthropogenic removals. Reductions in net emissions can be achieved through different portfolios of mitigation measures illustrated in Figure SPM.3b.

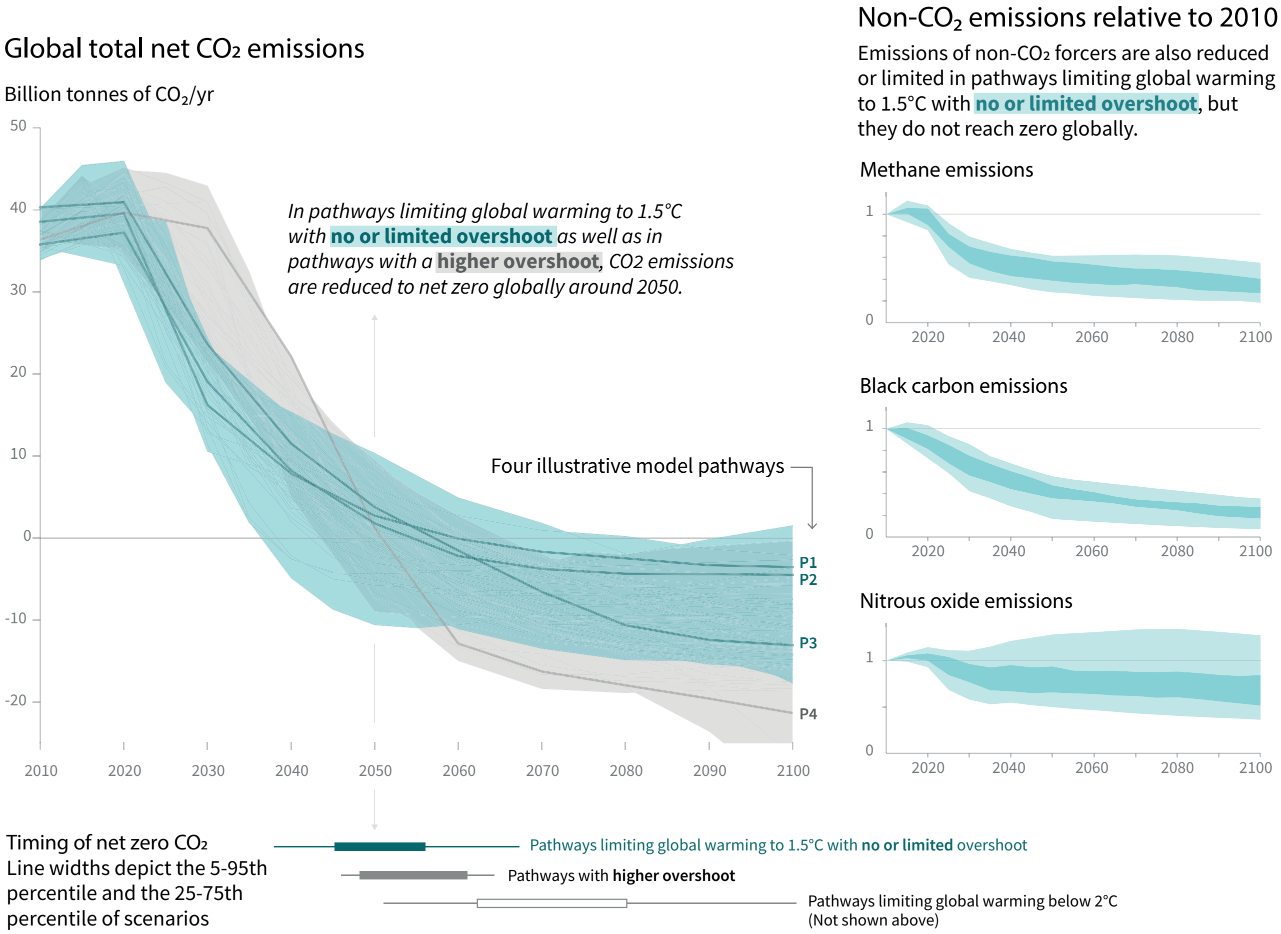

Figure SPM.3a | Global emissions pathway characteristics. The main panel shows global net anthropogenic CO_2 emissions in pathways limiting global warming to 1.5°C with no or limited (less than 0.1°C) overshoot and pathways with higher overshoot. The shaded area shows the full range for pathways analysed in this Report. The panels on the right show non-CO_2 emissions ranges for three compounds with large historical forcing and a substantial portion of emissions coming from sources distinct from those central to CO_2 mitigation. Shaded areas in these panels show the 5–95% (light shading) and interquartile (dark shading) ranges of pathways limiting global warming to 1.5°C with no or limited overshoot. Box and whiskers at the bottom of the figure show the timing of pathways reaching global net zero CO_2 emission levels, and a comparison with pathways limiting global warming to 2°C with at least 66% probability. Four illustrative model pathways are highlighted in the main panel and are labelled P1, P2, P3 and P4, corresponding to the LED, S1, S2, and S5 pathways assessed in Chapter 2. Descriptions and characteristics of these pathways are available in Figure SPM.3b. {2.1, 2.2, 2.3, Figure 2.5, Figure 2.10, Figure 2.11}

SPM

Characteristics of four illustrative model pathways

Different mitigation strategies can achieve the net emissions reductions that would be required to follow a pathway that limits global warming to 1.5°C with no or limited overshoot. All pathways use Carbon Dioxide Removal (CDR), but the amount varies across pathways, as do the relative contributions of Bioenergy with Carbon Capture and Storage (BECCS) and removals in the Agriculture, Forestry and Other Land Use (AFOLU) sector. This has implications for emissions and several other pathway characteristics.

Breakdown of contributions to global net CO_2 emissions in four illustrative model pathways

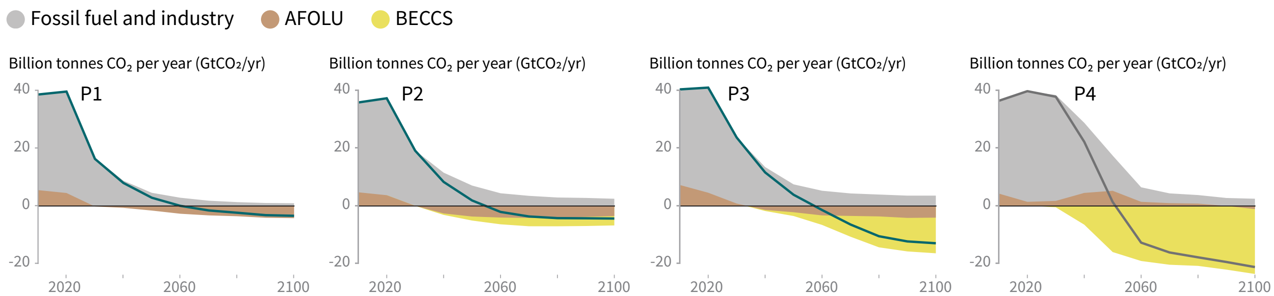

P1: A scenario in which social, business and technological innovations result in lower energy demand up to 2050 while living standards rise, especially in the global South. A downsized energy system enables rapid decarbonization of energy supply. Afforestation is the only CDR option considered; neither fossil fuels with CCS nor BECCS are used.

P2: A scenario with a broad focus on sustainability including energy intensity, human development, economic convergence and international cooperation, as well as shifts towards sustainable and healthy consumption patterns, low-carbon technology innovation, and well-managed land systems with limited societal acceptability for BECCS.

P3: A middle-of-the-road scenario in which societal as well as technological development follows historical patterns. Emissions reductions are mainly achieved by changing the way in which energy and products are produced, and to a lesser degree by reductions in demand.

P4: A resource- and energy-intensive scenario in which economic growth and globalization lead to widespread adoption of greenhouse-gas-intensive lifestyles, including high demand for transportation fuels and livestock products. Emissions reductions are mainly achieved through technological means, making strong use of CDR through the deployment of BECCS.

Global indicators	P1	P2	P3	P4	**Interquartile range**
Pathway classification	No or limited overshoot	No or limited overshoot	No or limited overshoot	Higher overshoot	No or limited overshoot
CO_2 emission change in 2030 (% rel to 2010)	-58	-47	-41	4	(-58,-40)
└ in 2050 (% rel to 2010)	-93	-95	-91	-97	(-107,-94)
Kyoto-GHG emissions in 2030 (% rel to 2010)*	-50	-49	-35	-2	(-51,-39)
└ in 2050 (% rel to 2010)	-82	-89	-78	-80	(-93,-81)
*Final energy demand** in 2030 (% rel to 2010)*	-15	-5	17	39	(-12,7)
└ in 2050 (% rel to 2010)	-32	2	21	44	(-11,22)
Renewable share in electricity in 2030 (%)	60	58	48	25	(47,65)
└ in 2050 (%)	77	81	63	70	(69,86)
Primary energy from coal in 2030 (% rel to 2010)	-78	-61	-75	-59	(-78, -59)
└ in 2050 (% rel to 2010)	-97	-77	-73	-97	(-95, -74)
from oil in 2030 (% rel to 2010)	-37	-13	-3	86	(-34,3)
└ in 2050 (% rel to 2010)	-87	-50	-81	-32	(-78,-31)
from gas in 2030 (% rel to 2010)	-25	-20	33	37	(-26,21)
└ in 2050 (% rel to 2010)	-74	-53	21	-48	(-56,6)
from nuclear in 2030 (% rel to 2010)	59	83	98	106	(44,102)
└ in 2050 (% rel to 2010)	150	98	501	468	(91,190)
from biomass in 2030 (% rel to 2010)	-11	0	36	-1	(29,80)
└ in 2050 (% rel to 2010)	-16	49	121	418	(123,261)
from non-biomass renewables in 2030 (% rel to 2010)	430	470	315	110	(245,436)
└ in 2050 (% rel to 2010)	833	1327	878	1137	(576,1299)
Cumulative CCS until 2100 ($GtCO_2$)	0	348	687	1218	(550,1017)
└ of which BECCS ($GtCO_2$)	0	151	414	1191	(364,662)
Land area of bioenergy crops in 2050 (million km²)	0.2	0.9	2.8	7.2	(1.5,3.2)
Agricultural CH_4 emissions in 2030 (% rel to 2010)	-24	-48	1	14	(-30,-11)
in 2050 (% rel to 2010)	-33	-69	-23	2	(-47,-24)
Agricultural N_2O emissions in 2030 (% rel to 2010)	5	-26	15	3	(-21,3)
in 2050 (% rel to 2010)	6	-26	0	39	(-26,1)

NOTE: Indicators have been selected to show global trends identified by the Chapter 2 assessment. National and sectoral characteristics can differ substantially from the global trends shown above.

** Kyoto-gas emissions are based on IPCC Second Assessment Report GWP-100*
*** Changes in energy demand are associated with improvements in energy efficiency and behaviour change*

Figure SPM.3b | Characteristics of four illustrative model pathways in relation to global warming of 1.5°C introduced in Figure SPM.3a. These pathways were selected to show a range of potential mitigation approaches and vary widely in their projected energy and land use, as well as their assumptions about future socio-economic developments, including economic and population growth, equity and sustainability. A breakdown of the global net anthropogenic CO_2 emissions into the contributions in terms of CO_2 emissions from fossil fuel and industry; agriculture, forestry and other land use (AFOLU); and bioenergy with carbon capture and storage (BECCS) is shown. AFOLU estimates reported here are not necessarily comparable with countries' estimates. Further characteristics for each of these pathways are listed below each pathway. These pathways illustrate relative global differences in mitigation strategies, but do not represent central estimates, national strategies, and do not indicate requirements. For comparison, the right-most column shows the interquartile ranges across pathways with no or limited overshoot of 1.5°C. Pathways P1, P2, P3 and P4 correspond to the LED, S1, S2 and S5 pathways assessed in Chapter 2 (Figure SPM.3a). {2.2.1, 2.3.1, 2.3.2, 2.3.3, 2.3.4, 2.4.1, 2.4.2, 2.4.4, 2.5.3, Figure 2.5, Figure 2.6, Figure 2.9, Figure 2.10, Figure 2.11, Figure 2.14, Figure 2.15, Figure 2.16, Figure 2.17, Figure 2.24, Figure 2.25, Table 2.4, Table 2.6, Table 2.7, Table 2.9, Table 4.1}

C.2 Pathways limiting global warming to 1.5°C with no or limited overshoot would require rapid and far-reaching transitions in energy, land, urban and infrastructure (including transport and buildings), and industrial systems (*high confidence*). These systems transitions are unprecedented in terms of scale, but not necessarily in terms of speed, and imply deep emissions reductions in all sectors, a wide portfolio of mitigation options and a significant upscaling of investments in those options (*medium confidence*). {2.3, 2.4, 2.5, 4.2, 4.3, 4.4, 4.5}

C.2.1 Pathways that limit global warming to 1.5°C with no or limited overshoot show system changes that are more rapid and pronounced over the next two decades than in 2°C pathways (*high confidence*). The rates of system changes associated with limiting global warming to 1.5°C with no or limited overshoot have occurred in the past within specific sectors, technologies and spatial contexts, but there is no documented historic precedent for their scale (*medium confidence*). {2.3.3, 2.3.4, 2.4, 2.5, 4.2.1, 4.2.2, Cross-Chapter Box 11 in Chapter 4}

C.2.2 In energy systems, modelled global pathways (considered in the literature) limiting global warming to 1.5°C with no or limited overshoot (for more details see Figure SPM.3b) generally meet energy service demand with lower energy use, including through enhanced energy efficiency, and show faster electrification of energy end use compared to 2°C (*high confidence*). In 1.5°C pathways with no or limited overshoot, low-emission energy sources are projected to have a higher share, compared with 2°C pathways, particularly before 2050 (*high confidence*). In 1.5°C pathways with no or limited overshoot, renewables are projected to supply 70–85% (interquartile range) of electricity in 2050 (*high confidence*). In electricity generation, shares of nuclear and fossil fuels with carbon dioxide capture and storage (CCS) are modelled to increase in most 1.5°C pathways with no or limited overshoot. In modelled 1.5°C pathways with limited or no overshoot, the use of CCS would allow the electricity generation share of gas to be approximately 8% (3–11% interquartile range) of global electricity in 2050, while the use of coal shows a steep reduction in all pathways and would be reduced to close to 0% (0–2% interquartile range) of electricity (*high confidence*). While acknowledging the challenges, and differences between the options and national circumstances, political, economic, social and technical feasibility of solar energy, wind energy and electricity storage technologies have substantially improved over the past few years (*high confidence*). These improvements signal a potential system transition in electricity generation. (Figure SPM.3b) {2.4.1, 2.4.2, Figure 2.1, Table 2.6, Table 2.7, Cross-Chapter Box 6 in Chapter 3, 4.2.1, 4.3.1, 4.3.3, 4.5.2}

C.2.3 CO_2 emissions from industry in pathways limiting global warming to 1.5°C with no or limited overshoot are projected to be about 65–90% (interquartile range) lower in 2050 relative to 2010, as compared to 50–80% for global warming of 2°C (*medium confidence*). Such reductions can be achieved through combinations of new and existing technologies and practices, including electrification, hydrogen, sustainable bio-based feedstocks, product substitution, and carbon capture, utilization and storage (CCUS). These options are technically proven at various scales but their large-scale deployment may be limited by economic, financial, human capacity and institutional constraints in specific contexts, and specific characteristics of large-scale industrial installations. In industry, emissions reductions by energy and process efficiency by themselves are insufficient for limiting warming to 1.5°C with no or limited overshoot (*high confidence*). {2.4.3, 4.2.1, Table 4.1, Table 4.3, 4.3.3, 4.3.4, 4.5.2}

C.2.4 The urban and infrastructure system transition consistent with limiting global warming to 1.5°C with no or limited overshoot would imply, for example, changes in land and urban planning practices, as well as deeper emissions reductions in transport and buildings compared to pathways that limit global warming below 2°C (*medium confidence*). Technical measures and practices enabling deep emissions reductions include various energy efficiency options. In pathways limiting global warming to 1.5°C with no or limited overshoot, the electricity share of energy demand in buildings would be about 55–75% in 2050 compared to 50–70% in 2050 for 2°C global warming (*medium confidence*). In the transport sector, the share of low-emission final energy would rise from less than 5% in 2020 to about 35–65% in 2050 compared to 25–45% for 2°C of global warming (*medium confidence*). Economic, institutional and socio-cultural barriers may inhibit these urban and infrastructure system transitions, depending on national, regional and local circumstances, capabilities and the availability of capital (*high confidence*). {2.3.4, 2.4.3, 4.2.1, Table 4.1, 4.3.3, 4.5.2}

C.2.5 Transitions in global and regional land use are found in all pathways limiting global warming to 1.5°C with no or limited overshoot, but their scale depends on the pursued mitigation portfolio. Model pathways that limit global warming to 1.5°C with no or limited overshoot project a 4 million km^2 reduction to a 2.5 million km^2 increase of non-pasture agricultural land for food and feed crops and a 0.5–11 million km^2 reduction of pasture land, to be converted into a 0–6 million km^2 increase of agricultural land for energy crops and a 2 million km^2 reduction to 9.5 million km^2 increase in forests by 2050 relative to 2010 (*medium confidence*).[16] Land-use transitions of similar magnitude can be observed in modelled 2°C pathways (*medium confidence*). Such large transitions pose profound challenges for sustainable management of the various demands on land for human settlements, food, livestock feed, fibre, bioenergy, carbon storage, biodiversity and other ecosystem services (*high confidence*). Mitigation options limiting the demand for land include sustainable intensification of land-use practices, ecosystem restoration and changes towards less resource-intensive diets (*high confidence*). The implementation of land-based mitigation options would require overcoming socio-economic, institutional, technological, financing and environmental barriers that differ across regions (*high confidence*). {2.4.4, Figure 2.24, 4.3.2, 4.3.7, 4.5.2, Cross-Chapter Box 7 in Chapter 3}

C.2.6 Additional annual average energy-related investments for the period 2016 to 2050 in pathways limiting warming to 1.5°C compared to pathways without new climate policies beyond those in place today are estimated to be around 830 billion USD2010 (range of 150 billion to 1700 billion USD2010 across six models[17]). This compares to total annual average energy supply investments in 1.5°C pathways of 1460 to 3510 billion USD2010 and total annual average energy demand investments of 640 to 910 billion USD2010 for the period 2016 to 2050. Total energy-related investments increase by about 12% (range of 3% to 24%) in 1.5°C pathways relative to 2°C pathways. Annual investments in low-carbon energy technologies and energy efficiency are upscaled by roughly a factor of six (range of factor of 4 to 10) by 2050 compared to 2015 (*medium confidence*). {2.5.2, Box 4.8, Figure 2.27}

C.2.7 Modelled pathways limiting global warming to 1.5°C with no or limited overshoot project a wide range of global average discounted marginal abatement costs over the 21st century. They are roughly 3-4 times higher than in pathways limiting global warming to below 2°C (*high confidence*). The economic literature distinguishes marginal abatement costs from total mitigation costs in the economy. The literature on total mitigation costs of 1.5°C mitigation pathways is limited and was not assessed in this Report. Knowledge gaps remain in the integrated assessment of the economy-wide costs and benefits of mitigation in line with pathways limiting warming to 1.5°C. {2.5.2; 2.6; Figure 2.26}

16 The projected land-use changes presented are not deployed to their upper limits simultaneously in a single pathway.

17 Including two pathways limiting warming to 1.5°C with no or limited overshoot and four pathways with higher overshoot.

C.3 All pathways that limit global warming to 1.5°C with limited or no overshoot project the use of carbon dioxide removal (CDR) on the order of 100–1000 $GtCO_2$ over the 21st century. CDR would be used to compensate for residual emissions and, in most cases, achieve net negative emissions to return global warming to 1.5°C following a peak (*high confidence*). CDR deployment of several hundreds of $GtCO_2$ is subject to multiple feasibility and sustainability constraints (*high confidence*). Significant near-term emissions reductions and measures to lower energy and land demand can limit CDR deployment to a few hundred $GtCO_2$ without reliance on bioenergy with carbon capture and storage (BECCS) (*high confidence*). {2.3, 2.4, 3.6.2, 4.3, 5.4}

C.3.1 Existing and potential CDR measures include afforestation and reforestation, land restoration and soil carbon sequestration, BECCS, direct air carbon capture and storage (DACCS), enhanced weathering and ocean alkalinization. These differ widely in terms of maturity, potentials, costs, risks, co-benefits and trade-offs (*high confidence*). To date, only a few published pathways include CDR measures other than afforestation and BECCS. {2.3.4, 3.6.2, 4.3.2, 4.3.7}

C.3.2 In pathways limiting global warming to 1.5°C with limited or no overshoot, BECCS deployment is projected to range from 0–1, 0–8, and 0–16 $GtCO_2$ yr^{-1} in 2030, 2050, and 2100, respectively, while agriculture, forestry and land-use (AFOLU) related CDR measures are projected to remove 0–5, 1–11, and 1–5 $GtCO_2$ yr^{-1} in these years (*medium confidence*). The upper end of these deployment ranges by mid-century exceeds the BECCS potential of up to 5 $GtCO_2$ yr^{-1} and afforestation potential of up to 3.6 $GtCO_2$ yr^{-1} assessed based on recent literature (*medium confidence*). Some pathways avoid BECCS deployment completely through demand-side measures and greater reliance on AFOLU-related CDR measures (*medium confidence*). The use of bioenergy can be as high or even higher when BECCS is excluded compared to when it is included due to its potential for replacing fossil fuels across sectors (*high confidence*). (Figure SPM.3b) {2.3.3, 2.3.4, 2.4.2, 3.6.2, 4.3.1, 4.2.3, 4.3.2, 4.3.7, 4.4.3, Table 2.4}

C.3.3 Pathways that overshoot 1.5°C of global warming rely on CDR exceeding residual CO_2 emissions later in the century to return to below 1.5°C by 2100, with larger overshoots requiring greater amounts of CDR (Figure SPM.3b) (*high confidence*). Limitations on the speed, scale, and societal acceptability of CDR deployment hence determine the ability to return global warming to below 1.5°C following an overshoot. Carbon cycle and climate system understanding is still limited about the effectiveness of net negative emissions to reduce temperatures after they peak (*high confidence*). {2.2, 2.3.4, 2.3.5, 2.6, 4.3.7, 4.5.2, Table 4.11}

C.3.4 Most current and potential CDR measures could have significant impacts on land, energy, water or nutrients if deployed at large scale (*high confidence*). Afforestation and bioenergy may compete with other land uses and may have significant impacts on agricultural and food systems, biodiversity, and other ecosystem functions and services (*high confidence*). Effective governance is needed to limit such trade-offs and ensure permanence of carbon removal in terrestrial, geological and ocean reservoirs (*high confidence*). Feasibility and sustainability of CDR use could be enhanced by a portfolio of options deployed at substantial, but lesser scales, rather than a single option at very large scale (*high confidence*). (Figure SPM.3b) {2.3.4, 2.4.4, 2.5.3, 2.6, 3.6.2, 4.3.2, 4.3.7, 4.5.2, 5.4.1, 5.4.2; Cross-Chapter Boxes 7 and 8 in Chapter 3, Table 4.11, Table 5.3, Figure 5.3}

C.3.5 Some AFOLU-related CDR measures such as restoration of natural ecosystems and soil carbon sequestration could provide co-benefits such as improved biodiversity, soil quality, and local food security. If deployed at large scale, they would require governance systems enabling sustainable land management to conserve and protect land carbon stocks and other ecosystem functions and services (*medium confidence*). (Figure SPM.4) {2.3.3, 2.3.4, 2.4.2, 2.4.4, 3.6.2, 5.4.1, Cross-Chapter Boxes 3 in Chapter 1 and 7 in Chapter 3, 4.3.2, 4.3.7, 4.4.1, 4.5.2, Table 2.4}

SPM

D. Strengthening the Global Response in the Context of Sustainable Development and Efforts to Eradicate Poverty

D.1 Estimates of the global emissions outcome of current nationally stated mitigation ambitions as submitted under the Paris Agreement would lead to global greenhouse gas emissions[18] in 2030 of 52–58 $GtCO_2eq\ yr^{-1}$ (*medium confidence*). Pathways reflecting these ambitions would not limit global warming to 1.5°C, even if supplemented by very challenging increases in the scale and ambition of emissions reductions after 2030 (*high confidence*). Avoiding overshoot and reliance on future large-scale deployment of carbon dioxide removal (CDR) can only be achieved if global CO_2 emissions start to decline well before 2030 (*high confidence*). {1.2, 2.3, 3.3, 3.4, 4.2, 4.4, Cross-Chapter Box 11 in Chapter 4}

D.1.1 Pathways that limit global warming to 1.5°C with no or limited overshoot show clear emission reductions by 2030 (*high confidence*). All but one show a decline in global greenhouse gas emissions to below 35 $GtCO_2eq\ yr^{-1}$ in 2030, and half of available pathways fall within the 25–30 $GtCO_2eq\ yr^{-1}$ range (interquartile range), a 40–50% reduction from 2010 levels (*high confidence*). Pathways reflecting current nationally stated mitigation ambition until 2030 are broadly consistent with cost-effective pathways that result in a global warming of about 3°C by 2100, with warming continuing afterwards (*medium confidence*). {2.3.3, 2.3.5, Cross-Chapter Box 11 in Chapter 4, 5.5.3.2}

D.1.2 Overshoot trajectories result in higher impacts and associated challenges compared to pathways that limit global warming to 1.5°C with no or limited overshoot (*high confidence*). Reversing warming after an overshoot of 0.2°C or larger during this century would require upscaling and deployment of CDR at rates and volumes that might not be achievable given considerable implementation challenges (*medium confidence*). {1.3.3, 2.3.4, 2.3.5, 2.5.1, 3.3, 4.3.7, Cross-Chapter Box 8 in Chapter 3, Cross-Chapter Box 11 in Chapter 4}

D.1.3 The lower the emissions in 2030, the lower the challenge in limiting global warming to 1.5°C after 2030 with no or limited overshoot (*high confidence*). The challenges from delayed actions to reduce greenhouse gas emissions include the risk of cost escalation, lock-in in carbon-emitting infrastructure, stranded assets, and reduced flexibility in future response options in the medium to long term (*high confidence*). These may increase uneven distributional impacts between countries at different stages of development (*medium confidence*). {2.3.5, 4.4.5, 5.4.2}

D.2 The avoided climate change impacts on sustainable development, eradication of poverty and reducing inequalities would be greater if global warming were limited to 1.5°C rather than 2°C, if mitigation and adaptation synergies are maximized while trade-offs are minimized (*high confidence*). {1.1, 1.4, 2.5, 3.3, 3.4, 5.2, Table 5.1}

D.2.1 Climate change impacts and responses are closely linked to sustainable development which balances social well-being, economic prosperity and environmental protection. The United Nations Sustainable Development Goals (SDGs), adopted in 2015, provide an established framework for assessing the links between global warming of 1.5°C or 2°C and development goals that include poverty eradication, reducing inequalities, and climate action. (*high confidence*) {Cross-Chapter Box 4 in Chapter 1, 1.4, 5.1}

D.2.2 The consideration of ethics and equity can help address the uneven distribution of adverse impacts associated with 1.5°C and higher levels of global warming, as well as those from mitigation and adaptation, particularly for poor and disadvantaged populations, in all societies (*high confidence*). {1.1.1, 1.1.2, 1.4.3, 2.5.3, 3.4.10, 5.1, 5.2, 5.3. 5.4, Cross-Chapter Box 4 in Chapter 1, Cross-Chapter Boxes 6 and 8 in Chapter 3, and Cross-Chapter Box 12 in Chapter 5}

D.2.3 Mitigation and adaptation consistent with limiting global warming to 1.5°C are underpinned by enabling conditions, assessed in this Report across the geophysical, environmental-ecological, technological, economic, socio-cultural and institutional

18 GHG emissions have been aggregated with 100-year GWP values as introduced in the IPCC Second Assessment Report.

dimensions of feasibility. Strengthened multilevel governance, institutional capacity, policy instruments, technological innovation and transfer and mobilization of finance, and changes in human behaviour and lifestyles are enabling conditions that enhance the feasibility of mitigation and adaptation options for 1.5°C-consistent systems transitions. (*high confidence*) {1.4, Cross-Chapter Box 3 in Chapter 1, 2.5.1, 4.4, 4.5, 5.6}

D.3 Adaptation options specific to national contexts, if carefully selected together with enabling conditions, will have benefits for sustainable development and poverty reduction with global warming of 1.5°C, although trade-offs are possible (*high confidence*). {1.4, 4.3, 4.5}

D.3.1 Adaptation options that reduce the vulnerability of human and natural systems have many synergies with sustainable development, if well managed, such as ensuring food and water security, reducing disaster risks, improving health conditions, maintaining ecosystem services and reducing poverty and inequality (*high confidence*). Increasing investment in physical and social infrastructure is a key enabling condition to enhance the resilience and the adaptive capacities of societies. These benefits can occur in most regions with adaptation to 1.5°C of global warming (*high confidence*). {1.4.3, 4.2.2, 4.3.1, 4.3.2, 4.3.3, 4.3.5, 4.4.1, 4.4.3, 4.5.3, 5.3.1, 5.3.2}

D.3.2 Adaptation to 1.5°C global warming can also result in trade-offs or maladaptations with adverse impacts for sustainable development. For example, if poorly designed or implemented, adaptation projects in a range of sectors can increase greenhouse gas emissions and water use, increase gender and social inequality, undermine health conditions, and encroach on natural ecosystems (*high confidence*). These trade-offs can be reduced by adaptations that include attention to poverty and sustainable development (*high confidence*). {4.3.2, 4.3.3, 4.5.4, 5.3.2; Cross-Chapter Boxes 6 and 7 in Chapter 3}

D.3.3 A mix of adaptation and mitigation options to limit global warming to 1.5°C, implemented in a participatory and integrated manner, can enable rapid, systemic transitions in urban and rural areas (*high confidence*). These are most effective when aligned with economic and sustainable development, and when local and regional governments and decision makers are supported by national governments (*medium confidence*). {4.3.2, 4.3.3, 4.4.1, 4.4.2}

D.3.4 Adaptation options that also mitigate emissions can provide synergies and cost savings in most sectors and system transitions, such as when land management reduces emissions and disaster risk, or when low-carbon buildings are also designed for efficient cooling. Trade-offs between mitigation and adaptation, when limiting global warming to 1.5°C, such as when bioenergy crops, reforestation or afforestation encroach on land needed for agricultural adaptation, can undermine food security, livelihoods, ecosystem functions and services and other aspects of sustainable development. (*high confidence*) {3.4.3, 4.3.2, 4.3.4, 4.4.1, 4.5.2, 4.5.3, 4.5.4}

D.4 Mitigation options consistent with 1.5°C pathways are associated with multiple synergies and trade-offs across the Sustainable Development Goals (SDGs). While the total number of possible synergies exceeds the number of trade-offs, their net effect will depend on the pace and magnitude of changes, the composition of the mitigation portfolio and the management of the transition. (*high confidence*) (Figure SPM.4) {2.5, 4.5, 5.4}

D.4.1 1.5°C pathways have robust synergies particularly for the SDGs 3 (health), 7 (clean energy), 11 (cities and communities), 12 (responsible consumption and production) and 14 (oceans) (*very high confidence*). Some 1.5°C pathways show potential trade-offs with mitigation for SDGs 1 (poverty), 2 (hunger), 6 (water) and 7 (energy access), if not managed carefully (*high confidence*). (Figure SPM.4) {5.4.2; Figure 5.4, Cross-Chapter Boxes 7 and 8 in Chapter 3}

D.4.2 1.5°C pathways that include low energy demand (e.g., see P1 in Figure SPM.3a and SPM.3b), low material consumption, and low GHG-intensive food consumption have the most pronounced synergies and the lowest number of trade-offs with respect to sustainable development and the SDGs (*high confidence*). Such pathways would reduce dependence on CDR. In modelled pathways, sustainable development, eradicating poverty and reducing inequality can support limiting warming to 1.5°C (*high confidence*). (Figure SPM.3b, Figure SPM.4) {2.4.3, 2.5.1, 2.5.3, Figure 2.4, Figure 2.28, 5.4.1, 5.4.2, Figure 5.4}

Indicative linkages between mitigation options and sustainable development using SDGs (The linkages do not show costs and benefits)

Mitigation options deployed in each sector can be associated with potential positive effects (synergies) or negative effects (trade-offs) with the Sustainable Development Goals (SDGs). The degree to which this potential is realized will depend on the selected portfolio of mitigation options, mitigation policy design, and local circumstances and context. Particularly in the energy-demand sector, the potential for synergies is larger than for trade-offs. The bars group individually assessed options by level of confidence and take into account the relative strength of the assessed mitigation-SDG connections.

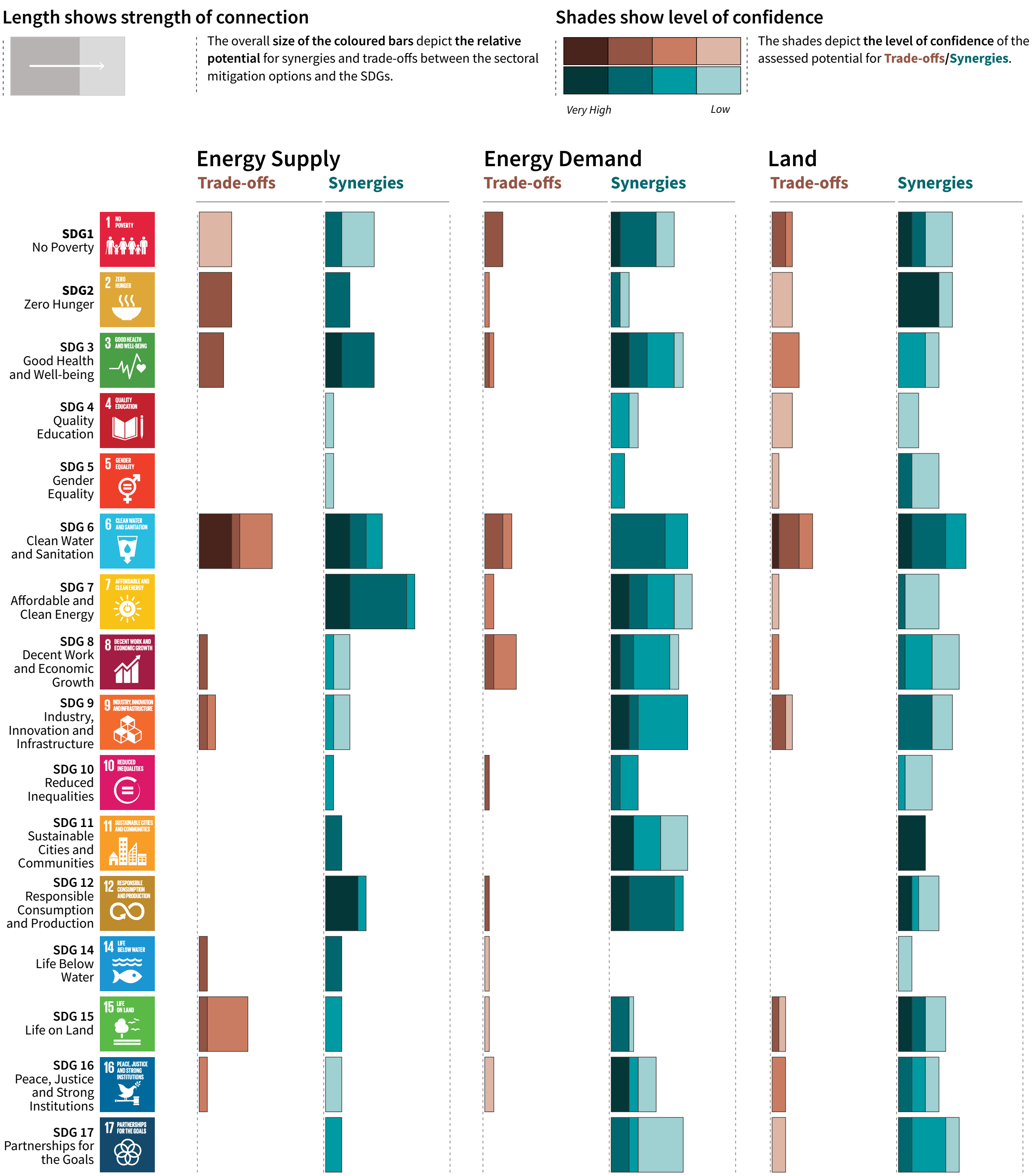

Figure SPM.4 | Potential synergies and trade-offs between the sectoral portfolio of climate change mitigation options and the Sustainable Development Goals (SDGs). The SDGs serve as an analytical framework for the assessment of the different sustainable development dimensions, which extend beyond the time frame of the 2030 SDG targets. The assessment is based on literature on mitigation options that are considered relevant for 1.5°C. The assessed strength of the SDG interactions is based on the qualitative and quantitative assessment of individual mitigation options listed in Table 5.2. For each mitigation option, the strength of the SDG-connection as well as the associated confidence of the underlying literature (shades of green and red) was assessed. The strength of positive connections (synergies) and negative connections (trade-offs) across all individual options within a sector (see Table 5.2) are aggregated into sectoral potentials for the whole mitigation portfolio. The (white) areas outside the bars, which indicate no interactions, have *low confidence* due to the uncertainty and limited number of studies exploring indirect effects. The strength of the connection considers only the effect of mitigation and does not include benefits of avoided impacts. SDG 13 (climate action) is not listed because mitigation is being considered in terms of interactions with SDGs and not vice versa. The bars denote the strength of the connection, and do not consider the strength of the impact on the SDGs. The energy demand sector comprises behavioural responses, fuel switching and efficiency options in the transport, industry and building sector as well as carbon capture options in the industry sector. Options assessed in the energy supply sector comprise biomass and non-biomass renewables, nuclear, carbon capture and storage (CCS) with bioenergy, and CCS with fossil fuels. Options in the land sector comprise agricultural and forest options, sustainable diets and reduced food waste, soil sequestration, livestock and manure management, reduced deforestation, afforestation and reforestation, and responsible sourcing. In addition to this figure, options in the ocean sector are discussed in the underlying report. {5.4, Table 5.2, Figure 5.2}

Information about the net impacts of mitigation on sustainable development in 1.5°C pathways is available only for a limited number of SDGs and mitigation options. Only a limited number of studies have assessed the benefits of avoided climate change impacts of 1.5°C pathways for the SDGs, and the co-effects of adaptation for mitigation and the SDGs. The assessment of the indicative mitigation potentials in Figure SPM.4 is a step further from AR5 towards a more comprehensive and integrated assessment in the future.

D.4.3 1.5°C and 2°C modelled pathways often rely on the deployment of large-scale land-related measures like afforestation and bioenergy supply, which, if poorly managed, can compete with food production and hence raise food security concerns (*high confidence*). The impacts of carbon dioxide removal (CDR) options on SDGs depend on the type of options and the scale of deployment (*high confidence*). If poorly implemented, CDR options such as BECCS and AFOLU options would lead to trade-offs. Context-relevant design and implementation requires considering people's needs, biodiversity, and other sustainable development dimensions (*very high confidence*). (Figure SPM.4) {5.4.1.3, Cross-Chapter Box 7 in Chapter 3}

D.4.4 Mitigation consistent with 1.5°C pathways creates risks for sustainable development in regions with high dependency on fossil fuels for revenue and employment generation (*high confidence*). Policies that promote diversification of the economy and the energy sector can address the associated challenges (*high confidence*). {5.4.1.2, Box 5.2}

D.4.5 Redistributive policies across sectors and populations that shield the poor and vulnerable can resolve trade-offs for a range of SDGs, particularly hunger, poverty and energy access. Investment needs for such complementary policies are only a small fraction of the overall mitigation investments in 1.5°C pathways. (*high confidence*) {2.4.3, 5.4.2, Figure 5.5}

D.5 Limiting the risks from global warming of 1.5°C in the context of sustainable development and poverty eradication implies system transitions that can be enabled by an increase of adaptation and mitigation investments, policy instruments, the acceleration of technological innovation and behaviour changes (*high confidence*). {2.3, 2.4, 2.5, 3.2, 4.2, 4.4, 4.5, 5.2, 5.5, 5.6}

D.5.1 Directing finance towards investment in infrastructure for mitigation and adaptation could provide additional resources. This could involve the mobilization of private funds by institutional investors, asset managers and development or investment banks, as well as the provision of public funds. Government policies that lower the risk of low-emission and adaptation investments can facilitate the mobilization of private funds and enhance the effectiveness of other public policies. Studies indicate a number of challenges, including access to finance and mobilization of funds. (*high confidence*) {2.5.1, 2.5.2, 4.4.5}

D.5.2 Adaptation finance consistent with global warming of 1.5°C is difficult to quantify and compare with 2°C. Knowledge gaps include insufficient data to calculate specific climate resilience-enhancing investments from the provision of currently underinvested basic infrastructure. Estimates of the costs of adaptation might be lower at global warming of 1.5°C than for 2°C. Adaptation needs have typically been supported by public sector sources such as national and subnational government budgets, and in developing countries together with support from development assistance, multilateral development banks, and United Nations Framework Convention on Climate Change channels (*medium confidence*). More recently there is a growing understanding of the scale and increase in non-governmental organizations and private funding in some regions (*medium confidence*). Barriers include the scale of adaptation financing, limited capacity and access to adaptation finance (*medium confidence*). {4.4.5, 4.6}

D.5.3 Global model pathways limiting global warming to 1.5°C are projected to involve the annual average investment needs in the energy system of around 2.4 trillion USD2010 between 2016 and 2035, representing about 2.5% of the world GDP (*medium confidence*). {4.4.5, Box 4.8}

D.5.4 Policy tools can help mobilize incremental resources, including through shifting global investments and savings and through market and non-market based instruments as well as accompanying measures to secure the equity of the transition, acknowledging the challenges related with implementation, including those of energy costs, depreciation of assets and impacts on international competition, and utilizing the opportunities to maximize co-benefits (*high confidence*). {1.3.3, 2.3.4, 2.3.5, 2.5.1, 2.5.2, Cross-Chapter Box 8 in Chapter 3, Cross-Chapter Box 11 in Chapter 4, 4.4.5, 5.5.2}

D.5.5 The systems transitions consistent with adapting to and limiting global warming to 1.5°C include the widespread adoption of new and possibly disruptive technologies and practices and enhanced climate-driven innovation. These imply enhanced technological innovation capabilities, including in industry and finance. Both national innovation policies and international cooperation can contribute to the development, commercialization and widespread adoption of mitigation and adaptation technologies. Innovation policies may be more effective when they combine public support for research and development with policy mixes that provide incentives for technology diffusion. (*high confidence*) {4.4.4, 4.4.5}.

D.5.6 Education, information, and community approaches, including those that are informed by indigenous knowledge and local knowledge, can accelerate the wide-scale behaviour changes consistent with adapting to and limiting global warming to 1.5°C. These approaches are more effective when combined with other policies and tailored to the motivations, capabilities and resources of specific actors and contexts (*high confidence*). Public acceptability can enable or inhibit the implementation of policies and measures to limit global warming to 1.5°C and to adapt to the consequences. Public acceptability depends on the individual's evaluation of expected policy consequences, the perceived fairness of the distribution of these consequences, and perceived fairness of decision procedures (*high confidence*). {1.1, 1.5, 4.3.5, 4.4.1, 4.4.3, Box 4.3, 5.5.3, 5.6.5}

D.6 Sustainable development supports, and often enables, the fundamental societal and systems transitions and transformations that help limit global warming to 1.5°C. Such changes facilitate the pursuit of climate-resilient development pathways that achieve ambitious mitigation and adaptation in conjunction with poverty eradication and efforts to reduce inequalities (*high confidence*). {Box 1.1, 1.4.3, Figure 5.1, 5.5.3, Box 5.3}

D.6.1 Social justice and equity are core aspects of climate-resilient development pathways that aim to limit global warming to 1.5°C as they address challenges and inevitable trade-offs, widen opportunities, and ensure that options, visions, and values are deliberated, between and within countries and communities, without making the poor and disadvantaged worse off (*high confidence*). {5.5.2, 5.5.3, Box 5.3, Figure 5.1, Figure 5.6, Cross-Chapter Boxes 12 and 13 in Chapter 5}

D.6.2 The potential for climate-resilient development pathways differs between and within regions and nations, due to different development contexts and systemic vulnerabilities (*very high confidence*). Efforts along such pathways to date have been limited (*medium confidence*) and enhanced efforts would involve strengthened and timely action from all countries and non-state actors (*high confidence*). {5.5.1, 5.5.3, Figure 5.1}

D.6.3 Pathways that are consistent with sustainable development show fewer mitigation and adaptation challenges and are associated with lower mitigation costs. The large majority of modelling studies could not construct pathways characterized by lack of international cooperation, inequality and poverty that were able to limit global warming to 1.5°C. (*high confidence*) {2.3.1, 2.5.1, 2.5.3, 5.5.2}

D.7 Strengthening the capacities for climate action of national and sub-national authorities, civil society, the private sector, indigenous peoples and local communities can support the implementation of ambitious actions implied by limiting global warming to 1.5°C (*high confidence*). International cooperation can provide an enabling environment for this to be achieved in all countries and for all people, in the context of sustainable development. International cooperation is a critical enabler for developing countries and vulnerable regions (*high confidence*). {1.4, 2.3, 2.5, 4.2, 4.4, 4.5, 5.3, 5.4, 5.5, 5.6, 5, Box 4.1, Box 4.2, Box 4.7, Box 5.3, Cross-Chapter Box 9 in Chapter 4, Cross-Chapter Box 13 in Chapter 5}

D.7.1 Partnerships involving non-state public and private actors, institutional investors, the banking system, civil society and scientific institutions would facilitate actions and responses consistent with limiting global warming to 1.5°C (*very high confidence*). {1.4, 4.4.1, 4.2.2, 4.4.3, 4.4.5, 4.5.3, 5.4.1, 5.6.2, Box 5.3}.

D.7.2 Cooperation on strengthened accountable multilevel governance that includes non-state actors such as industry, civil society and scientific institutions, coordinated sectoral and cross-sectoral policies at various governance levels, gender-sensitive policies, finance including innovative financing, and cooperation on technology development and transfer can ensure participation, transparency, capacity building and learning among different players (*high confidence*). {2.5.1, 2.5.2, 4.2.2, 4.4.1, 4.4.2, 4.4.3, 4.4.4, 4.4.5, 4.5.3, Cross-Chapter Box 9 in Chapter 4, 5.3.1, 5.5.3, Cross-Chapter Box 13 in Chapter 5, 5.6.1, 5.6.3}

D.7.3 International cooperation is a critical enabler for developing countries and vulnerable regions to strengthen their action for the implementation of 1.5°C-consistent climate responses, including through enhancing access to finance and technology and enhancing domestic capacities, taking into account national and local circumstances and needs (*high confidence*). {2.3.1, 2.5.1, 4.4.1, 4.4.2, 4.4.4, 4.4.5, 5.4.1 5.5.3, 5.6.1, Box 4.1, Box 4.2, Box 4.7}.

D.7.4 Collective efforts at all levels, in ways that reflect different circumstances and capabilities, in the pursuit of limiting global warming to 1.5°C, taking into account equity as well as effectiveness, can facilitate strengthening the global response to climate change, achieving sustainable development and eradicating poverty (*high confidence*). {1.4.2, 2.3.1, 2.5.1, 2.5.2, 2.5.3, 4.2.2, 4.4.1, 4.4.2, 4.4.3, 4.4.4, 4.4.5, 4.5.3, 5.3.1, 5.4.1, 5.5.3, 5.6.1, 5.6.2, 5.6.3}

Box SPM.1: Core Concepts Central to this Special Report

Global mean surface temperature (GMST): Estimated global average of near-surface air temperatures over land and sea ice, and sea surface temperatures over ice-free ocean regions, with changes normally expressed as departures from a value over a specified reference period. When estimating changes in GMST, near-surface air temperature over both land and oceans are also used.[19] {1.2.1.1}

Pre-industrial: The multi-century period prior to the onset of large-scale industrial activity around 1750. The reference period 1850–1900 is used to approximate pre-industrial GMST. {1.2.1.2}

Global warming: The estimated increase in GMST averaged over a 30-year period, or the 30-year period centred on a particular year or decade, expressed relative to pre-industrial levels unless otherwise specified. For 30-year periods that span past and future years, the current multi-decadal warming trend is assumed to continue. {1.2.1}

Net zero CO_2 emissions: Net zero carbon dioxide (CO_2) emissions are achieved when anthropogenic CO_2 emissions are balanced globally by anthropogenic CO_2 removals over a specified period.

Carbon dioxide removal (CDR): Anthropogenic activities removing CO_2 from the atmosphere and durably storing it in geological, terrestrial, or ocean reservoirs, or in products. It includes existing and potential anthropogenic enhancement of biological or geochemical sinks and direct air capture and storage, but excludes natural CO_2 uptake not directly caused by human activities.

Total carbon budget: Estimated cumulative net global anthropogenic CO_2 emissions from the pre-industrial period to the time that anthropogenic CO_2 emissions reach net zero that would result, at some probability, in limiting global warming to a given level, accounting for the impact of other anthropogenic emissions. {2.2.2}

Remaining carbon budget: Estimated cumulative net global anthropogenic CO_2 emissions from a given start date to the time that anthropogenic CO_2 emissions reach net zero that would result, at some probability, in limiting global warming to a given level, accounting for the impact of other anthropogenic emissions. {2.2.2}

Temperature overshoot: The temporary exceedance of a specified level of global warming.

Emission pathways: In this Summary for Policymakers, the modelled trajectories of global anthropogenic emissions over the 21st century are termed emission pathways. Emission pathways are classified by their temperature trajectory over the 21st century: pathways giving at least 50% probability based on current knowledge of limiting global warming to below 1.5°C are classified as 'no overshoot'; those limiting warming to below 1.6°C and returning to 1.5°C by 2100 are classified as '1.5°C limited-overshoot'; while those exceeding 1.6°C but still returning to 1.5°C by 2100 are classified as 'higher-overshoot'.

Impacts: Effects of climate change on human and natural systems. Impacts can have beneficial or adverse outcomes for livelihoods, health and well-being, ecosystems and species, services, infrastructure, and economic, social and cultural assets.

Risk: The potential for adverse consequences from a climate-related hazard for human and natural systems, resulting from the interactions between the hazard and the vulnerability and exposure of the affected system. Risk integrates the likelihood of exposure to a hazard and the magnitude of its impact. Risk also can describe the potential for adverse consequences of adaptation or mitigation responses to climate change.

Climate-resilient development pathways (CRDPs): Trajectories that strengthen sustainable development at multiple scales and efforts to eradicate poverty through equitable societal and systems transitions and transformations while reducing the threat of climate change through ambitious mitigation, adaptation and climate resilience.

19 Past IPCC reports, reflecting the literature, have used a variety of approximately equivalent metrics of GMST change.

Earth Syst. Sci. Data, 10, 405–448, 2018
https://doi.org/10.5194/essd-10-405-2018

Open Access Earth System Science Data

Global Carbon Budget 2017

Corinne Le Quéré[1], Robbie M. Andrew[2], Pierre Friedlingstein[3], Stephen Sitch[4], Julia Pongratz[5], Andrew C. Manning[6], Jan Ivar Korsbakken[2], Glen P. Peters[2], Josep G. Canadell[7], Robert B. Jackson[8], Thomas A. Boden[9], Pieter P. Tans[10], Oliver D. Andrews[1], Vivek K. Arora[11], Dorothee C. E. Bakker[6], Leticia Barbero[12,13], Meike Becker[14,15], Richard A. Betts[16,4], Laurent Bopp[17], Frédéric Chevallier[18], Louise P. Chini[19], Philippe Ciais[18], Catherine E. Cosca[20], Jessica Cross[20], Kim Currie[21], Thomas Gasser[22], Ian Harris[23], Judith Hauck[24], Vanessa Haverd[25], Richard A. Houghton[26], Christopher W. Hunt[27], George Hurtt[19], Tatiana Ilyina[5], Atul K. Jain[28], Etsushi Kato[29], Markus Kautz[30], Ralph F. Keeling[31], Kees Klein Goldewijk[32,33], Arne Körtzinger[34], Peter Landschützer[5], Nathalie Lefèvre[35], Andrew Lenton[36,37], Sebastian Lienert[38,39], Ivan Lima[40], Danica Lombardozzi[41], Nicolas Metzl[35], Frank Millero[42], Pedro M. S. Monteiro[43], David R. Munro[44], Julia E. M. S. Nabel[5], Shin-ichiro Nakaoka[45], Yukihiro Nojiri[45], X. Antonio Padin[46], Anna Peregon[18], Benjamin Pfeil[14,15], Denis Pierrot[12,13], Benjamin Poulter[47,48], Gregor Rehder[49], Janet Reimer[50], Christian Rödenbeck[51], Jörg Schwinger[52], Roland Séférian[53], Ingunn Skjelvan[52], Benjamin D. Stocker[54], Hanqin Tian[55], Bronte Tilbrook[36,37], Francesco N. Tubiello[56], Ingrid T. van der Laan-Luijkx[57], Guido R. van der Werf[58], Steven van Heuven[59], Nicolas Viovy[18], Nicolas Vuichard[18], Anthony P. Walker[60], Andrew J. Watson[4], Andrew J. Wiltshire[16], Sönke Zaehle[51], and Dan Zhu[18]

[1]Tyndall Centre for Climate Change Research, University of East Anglia, Norwich Research Park, Norwich NR4 7TJ, UK
[2]CICERO Center for International Climate Research, 0349 Oslo, Norway
[3]College of Engineering, Mathematics and Physical Sciences, University of Exeter, Exeter EX4 4QF, UK
[4]College of Life and Environmental Sciences, University of Exeter, Exeter EX4 4RJ, UK
[5]Max Planck Institute for Meteorology, Hamburg, Germany
[6]Centre for Ocean and Atmospheric Sciences, School of Environmental Sciences, University of East Anglia, Norwich Research Park, Norwich NR4 7TJ, UK
[7]Global Carbon Project, CSIRO Oceans and Atmosphere, GPO Box 1700, Canberra, ACT 2601, Australia
[8]Department of Earth System Science, Woods Institute for the Environment and Precourt Institute for Energy, Stanford University, Stanford, CA 94305, USA
[9]Climate Change Science Institute, Oak Ridge National Laboratory, Oak Ridge, TN 37831, USA
[10]National Oceanic and Atmospheric Administration, Earth System Research Laboratory (NOAA/ESRL), Boulder, CO 80305, USA
[11]Canadian Centre for Climate Modelling and Analysis, Climate Research Division, Environment and Climate Change Canada, Victoria, BC, Canada
[12]Cooperative Institute for Marine and Atmospheric Studies, Rosenstiel School for Marine and Atmospheric Science, University of Miami, Miami, FL 33149, USA
[13]National Oceanic and Atmospheric Administration/Atlantic Oceanographic and Meteorological Laboratory (NOAA/AOML), Miami, FL 33149, USA
[14]Geophysical Institute, University of Bergen, 5020 Bergen, Norway
[15]Bjerknes Centre for Climate Research, 5007 Bergen, Norway
[16]Met Office Hadley Centre, FitzRoy Road, Exeter EX1 3PB, UK
[17]Laboratoire de Météorologie Dynamique, Institut Pierre-Simon Laplace, CNRS-ENS-UPMC-X, Département de Géosciences, École Normale Supérieure, 24 rue Lhomond, 75005 Paris, France
[18]Laboratoire des Sciences du Climat et de l'Environnement, Institut Pierre-Simon Laplace, CEA-CNRS-UVSQ, CE Orme des Merisiers, 91191 Gif-sur-Yvette CEDEX, France

[19]Department of Geographical Sciences, University of Maryland, College Park, MD 20742, USA
[20]Pacific Marine Environmental Laboratory, National Oceanic and Atmospheric Administration, Seattle, WA 98115, USA
[21]National Institute of Water and Atmospheric Research (NIWA), Dunedin 9054, New Zealand
[22]International Institute for Applied Systems Analysis (IIASA), 2361 Laxenburg, Austria
[23]NCAS-Climate, Climatic Research Unit, School of Environmental Sciences, University of East Anglia, Norwich Research Park, Norwich, NR4 7TJ, UK
[24]Alfred Wegener Institute Helmholtz Centre for Polar and Marine Research, Postfach 120161, 27515 Bremerhaven, Germany
[25]CSIRO Oceans and Atmosphere, GPO Box 1700, Canberra, ACT 2601, Australia
[26]Woods Hole Research Centre (WHRC), Falmouth, MA 02540, USA
[27]Ocean Process Analysis Laboratory, University of New Hampshire, Durham, NH 03824, USA
[28]Department of Atmospheric Sciences, University of Illinois, Urbana, IL 61801, USA
[29]Institute of Applied Energy (IAE), Minato-ku, Tokyo 105-0003, Japan
[30]Karlsruhe Institute of Technology, Institute of Meteorology and Climate Research/Atmospheric Environmental Research, 82467 Garmisch-Partenkirchen, Germany
[31]University of California, San Diego, Scripps Institution of Oceanography, La Jolla, CA 92093-0244, USA
[32]PBL Netherlands Environmental Assessment Agency, Bezuidenhoutseweg 30, P.O. Box 30314, 2500 GH, The Hague, the Netherlands
[33]Faculty of Geosciences, Department IMEW, Copernicus Institute of Sustainable Development, Heidelberglaan 2, P.O. Box 80115, 3508 TC, Utrecht, the Netherlands
[34]GEOMAR Helmholtz Centre for Ocean Research Kiel, Düsternbrooker Weg 20, 24105 Kiel, Germany
[35]Sorbonne Universités (UPMC, Univ Paris 06), CNRS, IRD, MNHN, LOCEAN/IPSL Laboratory, 75252 Paris, France
[36]CSIRO Oceans and Atmosphere, P.O. Box 1538, Hobart, TAS, Australia
[37]Antarctic Climate and Ecosystem Cooperative Research Centre, University of Tasmania, Hobart, TAS, Australia
[38]Climate and Environmental Physics, Physics Institute, University of Bern, Bern, Switzerland
[39]Oeschger Centre for Climate Change Research, University of Bern, Bern, Switzerland
[40]Woods Hole Oceanographic Institution (WHOI), Woods Hole, MA 02543, USA
[41]National Center for Atmospheric Research, Climate and Global Dynamics, Terrestrial Sciences Section, Boulder, CO 80305, USA
[42]Department of Ocean Sciences, RSMAS/MAC, University of Miami, 4600 Rickenbacker Causeway, Miami, FL 33149, USA
[43]Ocean Systems and Climate, CSIR-CHPC, Cape Town, 7700, South Africa
[44]Department of Atmospheric and Oceanic Sciences and Institute of Arctic and Alpine Research, University of Colorado, Campus Box 450, Boulder, CO 80309-0450, USA
[45]Center for Global Environmental Research, National Institute for Environmental Studies (NIES), 16-2 Onogawa, Tsukuba, Ibaraki 305-8506, Japan
[46]Instituto de Investigacións Mariñas (CSIC), Vigo 36208, Spain
[47]NASA Goddard Space Flight Center, Biospheric Science Laboratory, Greenbelt, MD 20771, USA
[48]Department of Ecology, Montana State University, Bozeman, MT 59717, USA
[49]Leibniz Institute for Baltic Sea Research Warnemünde, 18119 Rostock, Germany
[50]School of Marine Science and Policy, University of Delaware, Newark, DE 19716, USA
[51]Max Planck Institute for Biogeochemistry, P.O. Box 600164, Hans-Knöll-Str. 10, 07745 Jena, Germany
[52]Uni Research Climate, Bjerknes Centre for Climate Research, 5007 Bergen, Norway
[53]Centre National de Recherche Météorologique, Unite mixte de recherche 3589 Météo-France/CNRS, 42 Avenue Gaspard Coriolis, 31100 Toulouse, France
[54]CREAF, E08193 Bellaterra (Cerdanyola del Vallès), Catalonia, Spain
[55]School of Forestry and Wildlife Sciences, Auburn University, 602 Ducan Drive, Auburn, AL 36849, USA
[56]Statistics Division, Food and Agriculture Organization of the United Nations, Via Terme di Caracalla, Rome 00153, Italy
[57]Department of Meteorology and Air Quality, Wageningen University & Research, P.O. Box 47, 6700AA Wageningen, the Netherlands
[58]Faculty of Science, Vrije Universiteit Amsterdam, Amsterdam, the Netherlands

[59]Energy and Sustainability Research Institute Groningen (ESRIG), University of Groningen, Groningen, the Netherlands
[60]Environmental Sciences Division & Climate Change Science Institute, Oak Ridge National Laboratory, Oak Ridge, TN, USA

Correspondence: Corinne Le Quéré (c.lequere@uea.ac.uk)

Received: 1 November 2017 – Discussion started: 13 November 2017
Revised: 16 February 2018 – Accepted: 19 February 2018 – Published: 12 March 2018

Abstract. Accurate assessment of anthropogenic carbon dioxide (CO_2) emissions and their redistribution among the atmosphere, ocean, and terrestrial biosphere – the "global carbon budget" – is important to better understand the global carbon cycle, support the development of climate policies, and project future climate change. Here we describe data sets and methodology to quantify the five major components of the global carbon budget and their uncertainties. CO_2 emissions from fossil fuels and industry (E_{FF}) are based on energy statistics and cement production data, respectively, while emissions from land-use change (E_{LUC}), mainly deforestation, are based on land-cover change data and bookkeeping models. The global atmospheric CO_2 concentration is measured directly and its rate of growth (G_{ATM}) is computed from the annual changes in concentration. The ocean CO_2 sink (S_{OCEAN}) and terrestrial CO_2 sink (S_{LAND}) are estimated with global process models constrained by observations. The resulting carbon budget imbalance (B_{IM}), the difference between the estimated total emissions and the estimated changes in the atmosphere, ocean, and terrestrial biosphere, is a measure of imperfect data and understanding of the contemporary carbon cycle. All uncertainties are reported as $\pm 1\sigma$. For the last decade available (2007–2016), E_{FF} was 9.4 ± 0.5 GtC yr^{-1}, E_{LUC} 1.3 ± 0.7 GtC yr^{-1}, G_{ATM} 4.7 ± 0.1 GtC yr^{-1}, S_{OCEAN} 2.4 ± 0.5 GtC yr^{-1}, and S_{LAND} 3.0 ± 0.8 GtC yr^{-1}, with a budget imbalance B_{IM} of 0.6 GtC yr^{-1} indicating overestimated emissions and/or underestimated sinks. For year 2016 alone, the growth in E_{FF} was approximately zero and emissions remained at 9.9 ± 0.5 GtC yr^{-1}. Also for 2016, E_{LUC} was 1.3 ± 0.7 GtC yr^{-1}, G_{ATM} was 6.1 ± 0.2 GtC yr^{-1}, S_{OCEAN} was 2.6 ± 0.5 GtC yr^{-1}, and S_{LAND} was 2.7 ± 1.0 GtC yr^{-1}, with a small B_{IM} of -0.3 GtC. G_{ATM} continued to be higher in 2016 compared to the past decade (2007–2016), reflecting in part the high fossil emissions and the small S_{LAND} consistent with El Niño conditions. The global atmospheric CO_2 concentration reached 402.8 ± 0.1 ppm averaged over 2016. For 2017, preliminary data for the first 6–9 months indicate a renewed growth in E_{FF} of +2.0 % (range of 0.8 to 3.0 %) based on national emissions projections for China, USA, and India, and projections of gross domestic product (GDP) corrected for recent changes in the carbon intensity of the economy for the rest of the world. This living data update documents changes in the methods and data sets used in this new global carbon budget compared with previous publications of this data set (Le Quéré et al., 2016, 2015b, a, 2014, 2013). All results presented here can be downloaded from https://doi.org/10.18160/GCP-2017 (GCP, 2017).

1 Introduction

The concentration of carbon dioxide (CO_2) in the atmosphere has increased from approximately 277 parts per million (ppm) in 1750 (Joos and Spahni, 2008), the beginning of the industrial era, to 402.8 ± 0.1 ppm in 2016 (Dlugokencky and Tans, 2018; Fig. 1). The atmospheric CO_2 increase above pre-industrial levels was, initially, primarily caused by the release of carbon to the atmosphere from deforestation and other land-use change activities (Ciais et al., 2013). While emissions from fossil fuels started before the industrial era, they only became the dominant source of anthropogenic emissions to the atmosphere from around 1920 and their relative share has continued to increase until present. Anthropogenic emissions occur on top of an active natural carbon cycle that circulates carbon between the reservoirs of the atmosphere, ocean, and terrestrial biosphere on timescales from sub-daily to millennia, while exchanges with geologic reservoirs occur on longer timescales (Archer et al., 2009).

The global carbon budget presented here refers to the mean, variations, and trends in the perturbation of CO_2 in the environment, referenced to the beginning of the industrial era. It quantifies the input of CO_2 to the atmosphere by emissions from human activities, the growth rate of atmospheric CO_2 concentration, and the resulting changes in the storage of carbon in the land and ocean reservoirs in response to increasing atmospheric CO_2 levels, climate change and variability, and other anthropogenic and natural changes (Fig. 2). An understanding of this perturbation budget over time and the underlying variability and trends of the natural carbon cycle are necessary to understand the response of natural sinks to changes in climate, CO_2 and land-use change

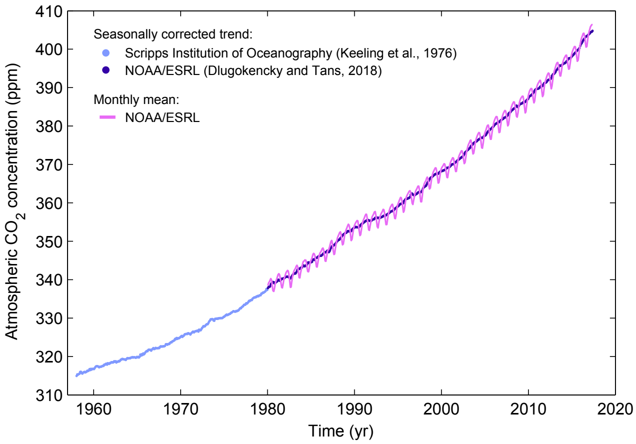

Figure 1. Surface average atmospheric CO_2 concentration (ppm). The 1980–2017 monthly data are from NOAA/ESRL (Dlugokencky and Tans, 2018) and are based on an average of direct atmospheric CO_2 measurements from multiple stations in the marine boundary layer (Masarie and Tans, 1995). The 1958–1979 monthly data are from the Scripps Institution of Oceanography, based on an average of direct atmospheric CO_2 measurements from the Mauna Loa and South Pole stations (Keeling et al., 1976). To take into account the difference of mean CO_2 and seasonality between the NOAA/ESRL and the Scripps station networks used here, the Scripps surface average (from two stations) was deseasonalised and harmonised to match the NOAA/ESRL surface average (from multiple stations) by adding the mean difference of 0.542 ppm, calculated here from overlapping data during 1980–2012.

drivers, and the permissible emissions for a given climate stabilisation target.

The components of the CO_2 budget that are reported annually in this paper include separate estimates for the CO_2 emissions from (1) fossil fuel combustion and oxidation and cement production (E_{FF}; GtC yr^{-1}) and (2) the emissions resulting from deliberate human activities on land, including those leading to land-use change (E_{LUC}; GtC yr^{-1}); and their partitioning among (3) the growth rate of atmospheric CO_2 concentration (G_{ATM}; GtC yr^{-1}); and the uptake of CO_2 (the "CO_2 sinks") in (4) the ocean (S_{OCEAN}; GtC yr^{-1}) and (5) on land (S_{LAND}; GtC yr^{-1}). The CO_2 sinks as defined here conceptually include the response of the land (including inland waters and estuaries) and ocean (including coasts and territorial sea) to elevated CO_2 and changes in climate, rivers, and other environmental conditions, although in practice not all processes are accounted for (see Sect. 2.7). The global emissions and their partitioning among the atmosphere, ocean, and land are in reality in balance; however, due to imperfect spatial and/or temporal data coverage, errors in each estimate, and smaller terms not included in our budget estimate (discussed in Sect. 2.7), their sum does not necessarily add up to zero. We introduce here a budget imbalance (B_{IM}), which is a measure of the mismatch between the estimated emissions and the estimated changes in the atmosphere, land, and ocean. This is an important change in calculation of the global carbon budget, which opens up new insights in the assessment of each term individually (Schimel et al., 2015). With this change, the full global carbon budget now reads as follows:

$$E_{FF} + E_{LUC} = G_{ATM} + S_{OCEAN} + S_{LAND} + B_{IM}. \quad (1)$$

G_{ATM} is usually reported in ppm yr^{-1}, which we convert to units of carbon mass per year, GtC yr^{-1}, using 1 ppm = 2.12 GtC (Table 1). We also include a quantification of E_{FF} by country, computed with both territorial and consumption-based accounting (see Sect. 2), and discuss missing terms from sources other than the combustion of fossil fuels (see Sect. 2.7).

The CO_2 budget has been assessed by the Intergovernmental Panel on Climate Change (IPCC) in all assessment reports (Ciais et al., 2013; Denman et al., 2007; Prentice et al., 2001; Schimel et al., 1995; Watson et al., 1990) and by others (e.g. Ballantyne et al., 2012). The IPCC methodology has been adapted and used by the Global Carbon Project (GCP, http://www.globalcarbonproject.org), which has coordinated a cooperative community effort for the annual publication of global carbon budgets up to year 2005 (Raupach et al., 2007; including fossil emissions only), year 2006 (Canadell et al., 2007), year 2007 (published online; GCP, 2007), year 2008 (Le Quéré et al., 2009), year 2009 (Friedlingstein et al., 2010), year 2010 (Peters et al., 2012b), year 2012 (Le Quéré et al., 2013; Peters et al., 2013), year 2013 (Le Quéré et al., 2014), year 2014 (Friedlingstein et al., 2014; Le Quéré et al., 2015b), year 2015 (Jackson et al., 2016; Le Quéré et al., 2015a), and most recently year 2016 (Le Quéré et al., 2016). Each of these papers updated previous estimates with the latest available information for the entire time series.

We adopt a range of ±1 standard deviation (σ) to report the uncertainties in our estimates, representing a likelihood of 68 % that the true value will be within the provided range if the errors have a Gaussian distribution. This choice reflects the difficulty of characterising the uncertainty in the CO_2 fluxes between the atmosphere and the ocean and land reservoirs individually, particularly on an annual basis, as well as the difficulty of updating the CO_2 emissions from land-use change. A likelihood of 68 % provides an indication of our current capability to quantify each term and its uncertainty given the available information. For comparison, the Fifth Assessment Report of the IPCC (AR5) generally reported a likelihood of 90 % for large data sets whose uncertainty is well characterised, or for long time intervals less affected by year-to-year variability. Our 68 % uncertainty value is near the 66 % which the IPCC characterises as "likely" for values falling into the $\pm 1\sigma$ interval. The uncertainties reported here combine statistical analysis of the underlying data and expert judgement of the likelihood of results lying outside this range. The limitations of current information are discussed in the paper and have been examined in detail elsewhere (Ballantyne et al., 2015; Zscheischler et al., 2017). We also use a

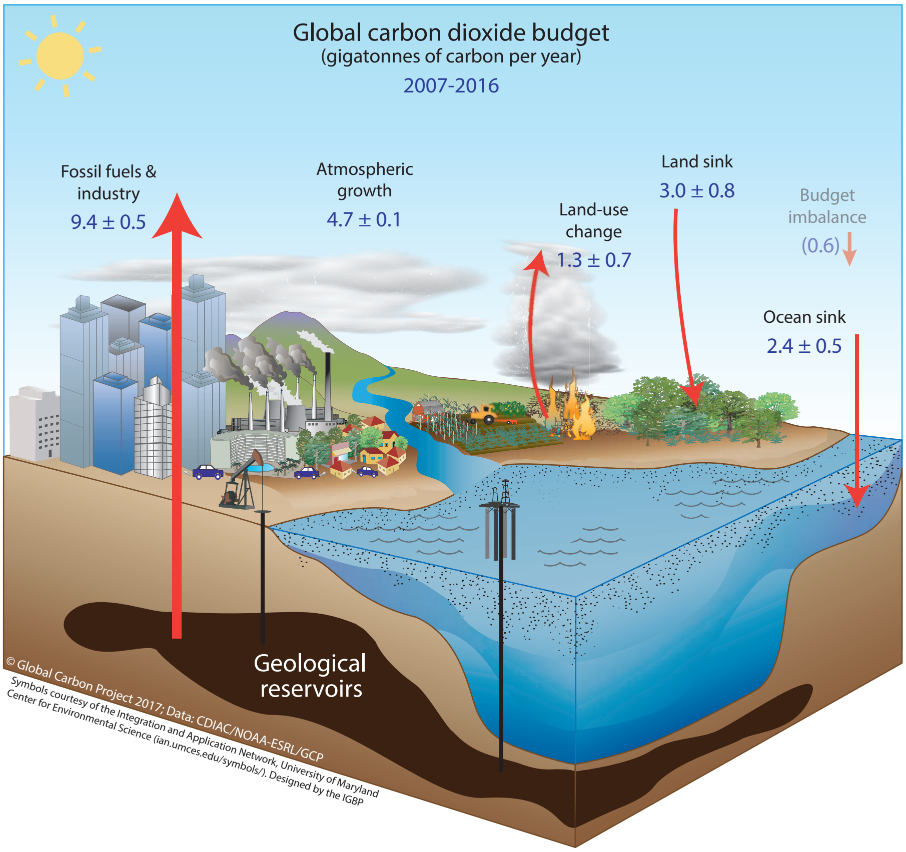

Figure 2. Schematic representation of the overall perturbation of the global carbon cycle caused by anthropogenic activities, averaged globally for the decade 2007–2016. The values represent emission from fossil fuels and industry (E_{FF}), emissions from deforestation and other land-use change (E_{LUC}), the growth rate in atmospheric CO_2 concentration (G_{ATM}), and the uptake of carbon by the sinks in the ocean (S_{OCEAN}) and land (S_{LAND}) reservoirs. The budget imbalance (B_{IM}) is also shown. All fluxes are in units of $GtC\,yr^{-1}$, with uncertainties reported as $\pm 1\sigma$ (68 % confidence that the real value lies within the given interval) as described in the text. This figure is an update of one prepared by the International Geosphere-Biosphere Programme for the GCP, using diagrams created with symbols from the Integration and Application Network, University of Maryland Center for Environmental Science (http://ian.umces.edu/symbols/), first presented in Le Quéré (2009).

Table 1. Factors used to convert carbon in various units (by convention, Unit 1 = Unit 2 conversion).

Unit 1	Unit 2	Conversion	Source
GtC (gigatonnes of carbon)	ppm (parts per million)[a]	2.12[b]	Ballantyne et al. (2012)
GtC (gigatonnes of carbon)	PgC (petagrams of carbon)	1	SI unit conversion
$GtCO_2$ (gigatonnes of carbon dioxide)	GtC (gigatonnes of carbon)	3.664	44.01/12.011 in mass equivalent
GtC (gigatonnes of carbon)	MtC (megatonnes of carbon)	1000	SI unit conversion

[a] Measurements of atmospheric CO_2 concentration have units of dry-air mole fraction. "ppm" is an abbreviation for micromole per mol of dry air.
[b] The use of a factor of 2.12 assumes that all the atmosphere is well mixed within 1 year. In reality, only the troposphere is well mixed and the growth rate of CO_2 concentration in the less well-mixed stratosphere is not measured by sites from the NOAA network. Using a factor of 2.12 makes the approximation that the growth rate of CO_2 concentration in the stratosphere equals that of the troposphere on a yearly basis.

qualitative assessment of confidence level to characterise the annual estimates from each term based on the type, amount, quality, and consistency of the evidence as defined by the IPCC (Stocker et al., 2013).

All quantities are presented in units of gigatonnes of carbon (GtC, 10^{15} gC), which is the same as petagrams of carbon (PgC; Table 1). Units of gigatonnes of CO_2 (or billion tonnes of CO_2) used in policy are equal to 3.664 multiplied by the value in units of GtC.

This paper provides a detailed description of the data sets and methodology used to compute the global carbon budget estimates for the period pre-industrial (1750) to 2016

Table 2. How to cite the individual components of the global carbon budget presented here.

Component	Primary reference
Global emissions from fossil fuels and industry (E_{FF}), total and by fuel type	Boden et al. (2017)
National territorial emissions from fossil fuels and industry (E_{FF})	CDIAC source: Boden et al. (2017), UNFCCC (2017)
National consumption-based emissions from fossil fuels and industry (E_{FF}) by country (consumption)	Peters et al. (2011b) updated as described in this paper
Land-use change emissions (E_{LUC})	Average from Houghton and Nassikas (2017) and Hansis et al. (2015), both updated as described in this paper
Growth rate in atmospheric CO_2 concentration (G_{ATM})	Dlugokencky and Tans (2018)
Ocean and land CO_2 sinks (S_{OCEAN} and S_{LAND})	This paper for S_{OCEAN} and S_{LAND} and references in Table 4 for individual models

and in more detail for the period 1959 to 2016. It also provides decadal averages starting in 1960 including the last decade (2007–2016), results for the year 2016, and a projection for year 2017. Finally it provides cumulative emissions from fossil fuels and land-use change since year 1750, the pre-industrial period, and since year 1870, the reference year for the cumulative carbon estimate used by the IPCC (AR5) based on the availability of global temperature data (Stocker et al., 2013). This paper is updated every year using the format of "living data" to keep a record of budget versions and the changes in new data, revision of data, and changes in methodology that lead to changes in estimates of the carbon budget. Additional materials associated with the release of each new version will be posted at the Global Carbon Project website (http://www.globalcarbonproject.org/carbonbudget), with fossil fuel emissions also available through the Global Carbon Atlas (http://www.globalcarbonatlas.org). With this approach, we aim to provide the highest transparency and traceability in the reporting of CO_2, the key driver of climate change.

2 Methods

Multiple organisations and research groups around the world generated the original measurements and data used to complete the global carbon budget. The effort presented here is thus mainly one of synthesis, where results from individual groups are collated, analysed, and evaluated for consistency. We facilitate access to original data with the understanding that primary data sets will be referenced in future work (see Table 2 for how to cite the data sets). Descriptions of the measurements, models, and methodologies follow below and in depth descriptions of each component are described elsewhere.

This is the 12th version of the global carbon budget and the sixth revised version in the format of a living data update. It builds on the latest published global carbon budget of Le Quéré et al. (2016). The main changes are (1) the inclusion of data to year 2016 (inclusive) and a projection for the global carbon budget for year 2017; (2) the use of two bookkeeping models to assess E_{LUC} (instead of one); (3) the use of dynamic global vegetation models (DGVMs) to assess S_{LAND}; (4) the direct use of global ocean biogeochemistry models (GOBMs) to assess S_{OCEAN} with no normalisation to observations; (5) the introduction of the budget imbalance B_{IM} as the difference between the estimated emissions and sinks, thus removing the assumption in previous global carbon budgets that the main uncertainties are primarily on the land sink (S_{LAND}) and recognising uncertainties in the estimate of S_{OCEAN}, particularly on decadal timescales; (6) the addition of a table presenting the major known sources of uncertainties; and (7) the expansion of the model descriptions. The main methodological differences between annual carbon budgets are summarised in Table 3.

The use of DGVMs and GOBMs to assess S_{LAND} and S_{OCEAN} with the introduction of the B_{IM} (3–5 above) is a substantial difference from previous global carbon budget publications. This change was introduced after a community discussion held at the 10th International CO_2 Conference in 2017, in recognition of two arguments brought forward by the community. First, recent evidence based on observed oceanic constraints suggests that the ocean models used in our global carbon budget may be underestimating the decadal and semi-decadal variability in the ocean sink (Landschützer et al., 2015; DeVries et al., 2017). Second, the

Table 3. Main methodological changes in the global carbon budget since first publication. Unless specified below, the methodology was identical to that described in the current paper. Furthermore, methodological changes introduced in one year are kept for the following years unless noted. Empty cells mean there were no methodological changes introduced that year.

Publication year[a]	Fossil fuel emissions			LUC emissions	Reservoirs			Uncertainty and other changes
	Global	Country (territorial)	Country (consumption)		Atmosphere	Ocean	Land	
2006 Raupach et al. (2007)		Split in regions						
2007 Canadell et al. (2007)				E_{LUC} based on FAO-FRA 2005; constant E_{LUC} for 2006	1959–1979 data from Mauna Loa; data after 1980 from global average	Based on one ocean model tuned to reproduced observed 1990s sink		$\pm 1\sigma$ provided for all components
2008 (online)				Constant E_{LUC} for 2007				
2009 Le Quéré et al. (2009)		Split between Annex B and non-Annex B	Results from an independent study discussed	Fire-based emission anomalies used for 2006–2008		Based on four ocean models normalised to observations with constant delta	First use of five DGVMs to compare with budget residual	
2010 Friedlingstein et al. (2010)	Projection for current year based on GDP	Emissions for top emitters		E_{LUC} updated with FAO-FRA 2010				
2011 Peters et al. (2012b)			Split between Annex B and non-Annex B					
2012 Le Quéré et al. (2013) Peters et al. (2013)		129 countries from 1959	129 countries and regions from 1990 to 2010 based on GTAP8.0	E_{LUC} for 1997–2011 includes interannual anomalies from fire-based emissions	All years from global average	Based on five ocean models normalised to observations with ratio	Ten DGVMs available for S_{LAND}; first use of four models to compare with E_{LUC}	
2013 Le Quéré et al. (2014)		250 countries[b]	134 countries and regions 1990–2011 based on GTAP8.1, with detailed estimates for years 1997, 2001, 2004, and 2007	E_{LUC} for 2012 estimated from 2001 to 2010 average		Based on six models compared with two data products to year 2011	Coordinated DGVM experiments for S_{LAND} and E_{LUC}	Confidence levels; cumulative emissions; budget from 1750
2014 Le Quéré et al. (2015b)	Three years of BP data	Three years of BP data	Extended to 2012 with updated GDP data	E_{LUC} for 1997–2013 includes interannual anomalies from fire-based emissions		Based on seven models	Based on 10 models	Inclusion of breakdown of the sinks in three latitude bands and comparison with three atmospheric inversions
2015 Le Quéré et al. (2015a) Jackson et al. (2016)	Projection for current year based on January–August data	National emissions from UNFCCC extended to 2014 also provided	Detailed estimates introduced for 2011 based on GTAP9			Based on eight models	Based on 10 models with assessment of minimum realism	The decadal uncertainty for the DGVM ensemble mean now uses $\pm 1\sigma$ of the decadal spread across models
2016 Le Quéré et al. (2016)	Two years of BP data	Added three small countries; CHN emissions from 1990 from BP data (this release only)		Preliminary E_{LUC} using FRA-2015 shown for comparison; use of five DGVMs		Based on seven models	Based on 14 models	Discussion of projection for full budget for current year
2017 (this study)	Projection includes India-specific data			Average of two bookkeeping models; use of 12 DGVMs		Based on eight models that match the observed sink for the 1990s; no longer normalised	Based on 15 models that meet observation-based criteria (see Sect. 2.5)	Land multi-model average now used in main carbon budget, with the carbon imbalance presented separately; new table of key uncertainties

[a] The naming convention of the budgets has changed. Up to and including 2010, the budget year (Carbon Budget 2010) represented the latest year of the data. From 2012, the budget year (Carbon Budget 2012) refers to the initial publication year.
[b] The CDIAC database has about 250 countries, but we show data for 219 countries since we aggregate and disaggregate some countries to be consistent with current country definitions (see Sect. 2.1.1 for more details).

growing need to verify reported emissions with Earth system observations requires that we progress rapidly towards the resolution of remaining inconsistencies in the global carbon budget (Peters et al., 2017). Furthermore, reviewers of Le Quéré et al. (2016) requested that this new edition of the global carbon budget focuses on what we do not know, rather than on what we know. We introduce this change in anticipation that it will trigger new ideas in the way we think about the global carbon budget; produce new, more stringent constraints on each of its components; and result in more evident and transparent attribution of uncertainties.

2.1 CO_2 emissions from fossil fuels and industry (E_{FF})

2.1.1 Emissions estimates

The estimates of global and national CO_2 emissions from fossil fuels, including gas flaring and cement production (E_{FF}), rely primarily on energy consumption data, specifically data on hydrocarbon fuels, collated and archived by several organisations (Andres et al., 2012). We use four main data sets for historical emissions (1751–2016):

1. Global and national emission estimates from CDIAC for the time period 1751–2014 (Boden et al., 2017), as it is the only data set that extends back to 1751 by country.

2. Official UNFCCC national inventory reports for 1990–2015 for the 42 Annex I countries in the UNFCCC (UNFCCC, 2017), as we assess these to be the most accurate estimates because they are compiled by experts within countries which have access to detailed energy data, and they are periodically reviewed.

3. The BP Statistical Review of World Energy (BP, 2017), to project the emissions forward to 2016 to ensure the most recent estimates possible.

4. The US Geological Survey estimates of cement production (USGS, 2017), to estimate cement emissions.

In the following we provide more details in each data set and additional modifications that are required to make the data set consistent and usable.

CDIAC. The CDIAC estimates have been updated annually to include the most recent year (2014) and to include statistical revisions to recent historical data (UN, 2017). Fuel masses and volumes are converted to fuel energy content using country-level coefficients provided by the UN and then converted to CO_2 emissions using conversion factors that take into account the relationship between carbon content and energy (heat) content of the different fuel types (coal, oil, gas, gas flaring) and the combustion efficiency (Marland and Rotty, 1984).

UNFCCC. Estimates from the UNFCCC national inventory reports follow the IPCC guidelines (IPCC, 2006) but have a slightly larger system boundary than CDIAC by including emissions coming from carbonates other than in cement manufacturing. We reallocate the detailed UNFCCC estimates to the CDIAC definitions of coal, oil, gas, cement, and other to allow consistent comparisons over time and between countries.

BP. For the most recent period when the UNFCCC (2017) and CDIAC (2015–2016) estimates are not available, we generate preliminary estimates using the BP Statistical Review of World Energy (Andres et al., 2014; Myhre et al., 2009). We apply the BP growth rates by fuel type (coal, oil, gas) to estimate 2016 emissions based on 2015 estimates (UNFCCC) and to estimate 2015 and 2016 based on 2014 estimates (CDIAC). BP's data set explicitly covers about 70 countries (96 % of global emissions), and for the remaining countries we use growth rates from the subregion the country belongs to. For the most recent years, flaring is assumed constant from the most recent available year of data (2015 for countries that report to the UNFCCC, 2014 for the remainder).

USGS. Estimates of emissions from cement production are based on USGS (USGS, 2017), applying the emission factors from CDIAC (Marland and Rotty, 1984). The CDIAC cement emissions are known to be high and are likely to be revised downwards next year (Andrew, 2018). Some fraction of the CaO and MgO in cement is returned to the carbonate form during cement weathering but this is omitted here (Xi et al., 2016).

Country mappings. The published CDIAC data set includes 256 countries and regions. This list includes countries that no longer exist, such as the USSR and Yugoslavia. We reduce the list to 220 countries by reallocating emissions to the currently defined territories, using mass-preserving aggregation or disaggregation. Examples of aggregation include merging East and West Germany to the currently defined Germany. Examples of disaggregation include reallocating the emissions from the former USSR to the resulting independent countries. For disaggregation, we use the emission shares when the current territories first appeared, and thus historical estimates of disaggregated countries should be treated with extreme care.

Global total. Our global estimate is based on CDIAC, and this is greater than the sum of emissions from all countries. This is largely attributable to emissions that occur in international territory, in particular the combustion of fuels used in international shipping and aviation (bunker fuels). The emissions from international bunker fuels are calculated based on where the fuels were loaded, but we do not include them in the national emissions estimates. Other differences occur (1) because the sum of imports in all countries is not equal to the sum of exports and (2) because of inconsistent national reporting, differing treatment of oxidation of non-fuel uses of hydrocarbons (e.g. as solvents, lubricants, feedstocks), and (3) changes in fuel stored (Andres et al., 2012).

2.1.2 Uncertainty assessment for E_{FF}

We estimate the uncertainty of the global emissions from fossil fuels and industry at ±5 % (scaled down from the published ±10 % at ±2σ to the use of ±1σ bounds reported here; Andres et al., 2012). This is consistent with a more detailed recent analysis of uncertainty of ±8.4 % at ±2σ (Andres et al., 2014) and at the high-end of the range of ±5–10 % at ±2σ reported by Ballantyne et al. (2015). This includes an assessment of uncertainties in the amounts of fuel consumed, the carbon and heat contents of fuels, and the combustion efficiency. While we consider a fixed uncertainty of ±5 % for all years, the uncertainty as a percentage of the emissions is growing with time because of the larger share of global emissions from emerging economies and developing countries (Marland et al., 2009). Generally, emissions from mature economies with good statistical processes have an uncertainty of only a few per cent (Marland, 2008), while developing countries such as China have uncertainties of around ±10 % (for ±1σ; Gregg et al., 2008). Uncertainties of emissions are likely to be mainly systematic errors related to underlying biases of energy statistics and to the accounting method used by each country.

We assign a medium confidence to the results presented here because they are based on indirect estimates of emissions using energy data (Durant et al., 2011). There is only limited and indirect evidence for emissions, although there is a high agreement among the available estimates within the given uncertainty (Andres et al., 2014, 2012), and emission estimates are consistent with a range of other observations (Ciais et al., 2013), even though their regional and national partitioning is more uncertain (Francey et al., 2013).

2.1.3 Emissions embodied in goods and services

CDIAC, UNFCCC, and BP national emission statistics “include greenhouse gas emissions and removals taking place within national territory and offshore areas over which the country has jurisdiction” (Rypdal et al., 2006) and are called territorial emission inventories. Consumption-based emission inventories allocate emissions to products that are consumed within a country and are conceptually calculated as the territorial emissions minus the “embodied” territorial emissions to produce exported products plus the emissions in other countries to produce imported products (consumption = territorial − exports + imports). Consumption-based emission attribution results (e.g. Davis and Caldeira, 2010) provide additional information to territorial-based emissions that can be used to understand emission drivers (Hertwich and Peters, 2009) and quantify emission transfers by the trade of products between countries (Peters et al., 2011b). The consumption-based emissions have the same global total but reflect the trade-driven movement of emissions across the Earth’s surface in response to human activities.

We estimate consumption-based emissions from 1990 to 2015 by enumerating the global supply chain using a global model of the economic relationships between economic sectors within and between every country (Andrew and Peters, 2013; Peters et al., 2011a). Our analysis is based on the economic and trade data from the Global Trade and Analysis Project (GTAP; Narayanan et al., 2015), and we make detailed estimates for the years 1997 (GTAP version 5), 2001 (GTAP6), and 2004, 2007, and 2011 (GTAP9.2), covering 57 sectors and 141 countries and regions. The detailed results are then extended into an annual time series from 1990 to the latest year of the gross domestic product (GDP) data (2015 in this budget), using GDP data by expenditure in current exchange rate of US dollars (USD; from the UN National Accounts Main Aggregates Database; UN, 2016) and time series of trade data from GTAP (based on the methodology in Peters et al., 2011b). We estimate the sector-level CO_2 emissions using the GTAP data and methodology, include flaring and cement emissions from CDIAC, and then scale the national totals (excluding bunker fuels) to match the emission estimates from the carbon budget. We do not provide a separate uncertainty estimate for the consumption-based emissions, but based on model comparisons and sensitivity analysis, they are unlikely to be significantly different than for the territorial emission estimates (Peters et al., 2012a).

2.1.4 Growth rate in emissions

We report the annual growth rate in emissions for adjacent years (in percent per year) by calculating the difference between the two years and then normalising to the emissions in the first year: $(E_{FF}(t_{0+1}) - E_{FF}(t_0))/E_{FF}(t_0) \times 100\,\%$. We apply a leap-year adjustment to ensure valid interpretations of annual growth rates. This affects the growth rate by about 0.3 % (1/365) and causes growth rates to go up approximately 0.3 % if the first year is a leap year and down 0.3 % if the second year is a leap year.

The relative growth rate of E_{FF} over time periods of greater than 1 year can be rewritten using its logarithm equivalent as follows:

$$\frac{1}{E_{FF}}\frac{\mathrm{d}E_{FF}}{\mathrm{d}t} = \frac{\mathrm{d}(\ln E_{FF})}{\mathrm{d}t}. \qquad (2)$$

Here we calculate relative growth rates in emissions for multi-year periods (e.g. a decade) by fitting a linear trend to $\ln(E_{FF})$ in Eq. (2), reported in percent per year.

2.1.5 Emissions projections

To gain insight on emission trends for the current year (2017), we provide an assessment of global fossil fuel and industry emissions, E_{FF}, by combining individual assessments of emissions for China, USA, India (the three countries with the largest emissions), and the rest of the world. Although the

EU in aggregate emits more than India, neither official forecasts nor monthly energy statistics are available for the EU as a whole to make a projection for 2017. In consequence, we use GDP projections to infer the emissions for this region.

Our 2017 estimate for China uses (1) estimates of coal consumption, production, imports, and inventory changes from the China Coal Industry Association (CCIA) and the National Energy Agency of China (NEA) for January through June (CCIA, 2017; NEA, 2017); (2) estimated consumption of natural gas and petroleum for January through June from NEA (CCIA, 2017; NEA, 2017); and (3) production of cement reported for January through August (NBS, 2017). Using these data, we estimate the change in emissions for the corresponding months in 2017 compared to 2016 assuming no change in the energy and carbon content of coal for 2017. We then use a central estimate for the growth rate of the whole year that is adjusted down somewhat relative to the first half of the year to account for a slowing trend in industrial growth observed since July and qualitative statements from the NEA saying that they expect oil and coal consumption to be relatively stable for the second half of the year. The main sources of uncertainty are from inconsistencies between available data sources, incomplete data on inventory changes, the carbon content of coal, and the assumptions for the behaviour for the rest of the year. These are discussed further in Sect. 3.2.1.

For the USA, we use the forecast of the US Energy Information Administration (EIA) for emissions from fossil fuels (EIA, 2017). This is based on an energy forecasting model which is revised monthly and takes into account heating-degree days, household expenditures by fuel type, energy markets, policies, and other effects. We combine this with our estimate of emissions from cement production using the monthly US cement data from USGS for January–June, assuming changes in cement production over the first part of the year apply throughout the year. While the EIA's forecasts for current full-year emissions have on average been revised downwards, only nine such forecasts are available, so we conservatively use the full range of adjustments following revision and additionally assume symmetrical uncertainty to give ±2.7 % around the central forecast.

For India, we use (1) coal production and sales data from the Ministry of Mines, Coal India Limited (CIL, 2017; Ministry of Mines, 2017) and Singareni Collieries Company Limited (SCCL, 2017), combined with imports data from the Ministry of Commerce and Industry (MCI, 2017) and power station stocks data from the Central Electricity Authority (CEA, 2017); (2) oil production and consumption data from the Ministry of Petroleum and Natural Gas (PPAC, 2017b); (3) natural gas production and import data from the Ministry of Petroleum and Natural Gas (PPAC, 2017a); and (4) cement production data from the Office of the Economic Advisor (OEA, 2017). The main source of uncertainty in the projection of India's emissions is the assumption of persistent growth for the rest of the year.

For the rest of the world, we use the close relationship between the growth in GDP and the growth in emissions (Raupach et al., 2007) to project emissions for the current year. This is based on a simplified Kaya identity, whereby E_{FF} (GtC yr^{-1}) is decomposed by the product of GDP (USD yr^{-1}) and the fossil fuel carbon intensity of the economy (I_{FF}; GtC USD^{-1}) as follows:

$$E_{FF} = \mathrm{GDP} \times I_{FF}. \quad (3)$$

Taking a time derivative of Eq. (3) and rearranging gives

$$\frac{1}{E_{FF}}\frac{\mathrm{d}E_{FF}}{\mathrm{d}t} = \frac{1}{\mathrm{GDP}}\frac{\mathrm{dGDP}}{\mathrm{d}t} + \frac{1}{I_{FF}}\frac{\mathrm{d}I_{FF}}{\mathrm{d}t}, \quad (4)$$

where the left-hand term is the relative growth rate of E_{FF} and the right-hand terms are the relative growth rates of GDP and I_{FF}, respectively, which can simply be added linearly to give the overall growth rate.

The growth rates are reported in percent by multiplying each term by 100. As preliminary estimates of annual change in GDP are made well before the end of a calendar year, making assumptions on the growth rate of I_{FF} allows us to make projections of the annual change in CO_2 emissions well before the end of a calendar year. The I_{FF} is based on GDP in constant PPP (purchasing power parity) from the IEA up to 2014 (IEA/OECD, 2016) and extended using the IMF growth rates for 2015 and 2016 (IMF, 2017). Interannual variability in I_{FF} is the largest source of uncertainty in the GDP-based emissions projections. We thus use the standard deviation of the annual I_{FF} for the period 2006–2016 as a measure of uncertainty, reflecting a $\pm 1\sigma$ as in the rest of the carbon budget. This is ±1.1 % yr^{-1} for the rest of the world (global emissions minus China, USA, and India).

The 2017 projection for the world is made of the sum of the projections for China, USA, India, and the rest. The uncertainty is added in quadrature among the three regions. The uncertainty here reflects the best of our expert opinion.

2.2 CO_2 emissions from land use, land-use change, and forestry (E_{LUC})

The net CO_2 flux from land use, land-use change, and forestry reported here (E_{LUC}, called land-use change emissions in the following) include CO_2 fluxes from deforestation, afforestation, logging and forest degradation (including harvest activity), shifting cultivation (cycle of cutting forest for agriculture, then abandoning), and regrowth of forests following wood harvest or abandonment of agriculture. Only some land management activities are included in our land-use change emissions estimates (Table A1). Some of these activities lead to emissions of CO_2 to the atmosphere, while others lead to CO_2 sinks. E_{LUC} is the net sum of all anthropogenic activities considered. Our annual estimate for 1959–2016 is provided as the average of results from two bookkeeping models (Sect. 2.2.1): the estimate published by Houghton and Nassikas (2017; hereafter H&N2017) extended here to 2016 and the average of two simulations done with the BLUE model (bookkeeping of land-use emissions; Hansis et al., 2015). In addition, we use results from DGVMs (see Sect. 2.2.3 and Table A1) to help quantify the uncertainty in E_{LUC} and to explore the consistency of our understanding. The three methods are described below, and differences are discussed in Sect. 3.2.

2.2.1 Bookkeeping models

Land-use change CO_2 emissions and uptake fluxes are calculated by two bookkeeping models. Both are based on the original bookkeeping approach of Houghton (2003) that keeps track of the carbon stored in vegetation and soils before and after a land-use change (transitions between various natural vegetation types, croplands, and pastures). Literature-based response curves describe decay of vegetation and soil carbon, including transfer to product pools of different lifetimes, as well as carbon uptake due to regrowth. Additionally, they represents permanent degradation of forests by lower vegetation and soil carbon stocks for secondary as compared to the primary forests and forest management such as wood harvest.

The bookkeeping models do not include land ecosystems' transient response to changes in climate, atmospheric CO_2, and other environmental factors, and the carbon densities are based on contemporary data reflecting stable environmental conditions at that time. Since carbon densities remain fixed over time in bookkeeping models, the additional sink capacity that ecosystems provide in response to CO_2 fertilisation and some other environmental changes is not captured by these models (Pongratz et al., 2014; see Sect. 2.7.3).

The H&N2017 and BLUE models differ in (1) computational units (country-level vs. spatially explicit treatment of land-use change), (2) processes represented (see Table A1), and (3) carbon densities assigned to vegetation and soil of each vegetation type. A notable change in H&N2017 over the original approach by Houghton (2003) used in earlier budget estimates is that no shifting cultivation or other back and forth transitions at a level below country level are included. Only a decline in forest area in a country as indicated by the Forest Resource Assessment of the FAO that exceeds the expansion of agricultural area as indicated by the FAO is assumed to represent a concurrent expansion and abandonment of cropland. In contrast, the BLUE model includes sub-grid-scale transitions at the grid level between all vegetation types as indicated by the harmonised land-use change data (LUH2) data set (Hurtt et al., 2018). Furthermore, H&N2017 assume conversion of natural grasslands to pasture, while BLUE allocates pasture proportionally on all natural vegetation that exists in a grid cell. This is one reason for generally higher emissions in BLUE. H&N2017 add carbon emissions from peat burning, based on the Global Fire Emissions Database (GFED4s; van der Werf et al., 2017), and peat drainage, based on estimates by Hooijer et al. (2010), to the output of their bookkeeping model for the countries of Indonesia and Malaysia. Peat burning and emissions from the organic layers of drained peat soils, which are not captured by bookkeeping methods directly, need to be included to represent the substantially larger emissions and interannual variability due to synergies of land-use and climate variability in Southeast Asia, in particular during El-Niño events. Similarly to H&N2017, peat burning and drainage-related emissions are also added to the BLUE estimate based on GFED4s (van der Werf et al., 2017), adding the peat burning for the GFED region of equatorial Asia and the peat drainage for Southeast Asia from Hooijer et al. (2010).

The two bookkeeping estimates used in this study also differ with respect to the land-use change data used to drive the models. H&N2017 base their estimates directly on the Forest Resource Assessment of the FAO which provides statistics on forest-cover change and management at intervals of 5 years (FAO, 2015). The data are based on countries' self-reporting, some of which include satellite data in more recent assessments. Changes in land use other than forests are based on annual, national changes in cropland and pasture areas reported by FAO (FAOSTAT, 2015). BLUE uses the harmonised land-use change data LUH2 (Hurtt et al., 2018) which describes land-use change, also based on the FAO data, but downscaled at a quarter-degree spatial resolution, considering sub-grid-scale transitions between primary forest, secondary forest, cropland, pasture, and rangeland. The new LUH2 data provide a new distinction between rangelands and pasture. This is implemented by assuming rangelands are treated either all as pastures or all as natural vegetation. These two assumptions are then averaged to provide the BLUE result that is closest to the expected real value.

The estimate of H&N2017 was extended here by 1 year (to 2016) by adding the anomaly of total peat emissions (burning and drainage) from GFED4s over the previous decade (2006–2015) to the decadal average of the bookkeeping result. A small correction to their 2015 value was also made based on the updated peat burning of GFED4s.

2.2.2 Dynamic global vegetation models (DGVMs)

Land-use change CO_2 emissions have also been estimated using an ensemble of 12 DGVM simulations. The DGVMs account for deforestation and regrowth, the most important components of E_{LUC}, but they do not represent all processes resulting directly from human activities on land (Table A1). All DGVMs represent processes of vegetation growth and mortality, as well as decomposition of dead organic matter associated with natural cycles, and include the vegetation and soil carbon response to increasing atmospheric CO_2 levels and to climate variability and change. Some models explicitly simulate the coupling of carbon and nitrogen cycles and account for atmospheric N deposition (Table A1). The DGVMs are independent from the other budget terms except

Table 4. References for the process models, $p\mathrm{CO_2}$-based ocean flux products, and atmospheric inversions included in Figs. 6–8. All models and products are updated with new data to end of year 2016.

Model/data name	Reference	Change from Le Quéré et al. (2016)
Bookkeeping models for land-use change emissions		
BLUE	Hansis et al. (2015)	Not applicable (not used in previous carbon budgets)
H&N2017	Houghton and Nassikas (2017)	Updated from Houghton et al. (2012); key differences include revised land-use change data to FAO2015, revised vegetation carbon densities, Indonesian and Malaysian peat burning and drainage added, and removal of shifting cultivation.
Dynamic global vegetation models		
CABLE	Haverd et al. (2017)	Optimisation of plant investment in rubisco- vs. electron-transport-limited photosynthesis; temperature-dependent onset of spring recovery in evergreen needle leaves.
CLASS-CTEM	Melton and Arora (2016)	A soil colour index is now used to determine soil albedo as opposed to soil texture. Soil albedo still gets modulated by other factors including soil moisture.
CLM4.5(BGC)	Oleson et al. (2013)	No change.
DLEM	Tian et al. (2015)	Consideration of the expansion of cropland and pasture, compared with no pasture expansion in previous version.
ISAM	Jain et al. (2013)	No change.
JSBACH	Reick et al. (2013)[a]	Adapted the preprocessing of the LUH data; scaling of crop and pasture states and transitions with the desert fractions in JSBACH in order to maintain as much of the prescribed agricultural areas as possible.
JULES[b]	Clark et al. (2011)[c]	No Change.
LPJ-GUESS	Smith et al. (2014)[d]	LUH2 with land use aggregated to LPJ-GUESS land cover inputs, shifting cultivation based on LUH2 gross transitions matrix, and wood harvest based on LUH2 area fractions of wood harvest; α_a reduction by 15 %.
LPJ[e]	Sitch et al. (2003)[f]	No change.
LPX-Bern	Keller et al. (2017)	Updated model parameter values (Keller et al., 2017) due to assimilation of observational data.
OCN	Zaehle and Friend (2010)[g]	Uses r293, including minor bug fixes; use of the CMIP6 N deposition data set
ORCHIDEE	Krinner et al. (2005)[h]	Improved water stress, new soil albedo, improved snow scheme.
ORCHIDEE-MICT	Guimberteau et al. (2018)	New version of ORCHIDEE including fires, permafrost regions coupling between soil thermodynamics and carbon dynamics, and managed grasslands.
SDGVM	Woodward et al. (1995)[i]	Uses Kattge et al. (2009) Vcmax∼ leaf N relationships (with Oxisol relationship for evergreen broad leaves).
VISIT	Kato et al. (2013)[j]	LUH2 is applied for land use, wood harvest, and land-use change. Sensitivity of soil decomposition parameters from Lloyd and Taylor (1994) are modified.

Table 4. Continued.

Model/data name	Reference	Change from Le Quéré et al. (2016)
Global ocean biogeochemistry models		
CCSM-BEC	Doney et al. (2009)	Change in atmospheric CO_2 concentration[k].
CSIRO	Law et al. (2017)	Physical model change from MOM4 to MOM5 and atmospheric forcing from JRA-55.
MITgcm-REcoM2	Hauck et al. (2016)	1 % iron solubility and atmospheric forcing from JRA-55.
MPIOM-HAMOCC[l]	Ilyina et al. (2013)	Cyanobacteria added to HAMOCC (Paulsen et al., 2017).
NEMO-PISCES (CNRM)	Séférian et al. (2013)	No change.
NEMO-PISCES (IPSL)	Aumont and Bopp (2006)	No change.
NEMO-PlankTOM5	Buitenhuis et al. (2010)[m]	No change.
NorESM-OC	Schwinger et al. (2016)	No change.
pCO$_2$-based flux ocean products		
Landschützer	Landschützer et al. (2016)	No change.
Jena CarboScope	Rödenbeck et al. (2014)	Updated to version oc_1.5.
Atmospheric inversions		
CarbonTracker Europe (CTE)	van der Laan-Luijkx et al. (2017)	Minor changes in the inversion setup.
Jena CarboScope	Rödenbeck et al. (2003)	Prior fluxes, outlier removal, changes in atmospheric observations station suite.
CAMS	Chevallier et al. (2005)	Change from half-hourly observations to daily averages of well-mixed conditions.

[a] See also Goll et al. (2015).
[b] Joint UK Land Environment Simulator.
[c] See also Best et al. (2011).
[d] To account for the differences between the derivation of shortwave radiation (SWRAD) from CRU cloudiness and SWRAD from CRU-NCEP, the photosynthesis scaling parameter α_a was modified (−15 %) to yield similar results.
[e] Lund–Potsdam–Jena.
[f] Compared to published version, decreased LPJ wood harvest efficiency so that 50 % of biomass was removed off-site compared to 85 % used in the 2012 budget. Residue management of managed grasslands increased so that 100 % of harvested grass enters the litter pool.
[g] See also Zaehle et al. (2011).
[h] Compared to published version, revised parameters values for photosynthetic capacity for boreal forests (following assimilation of FLUXNET data), updated parameters values for stem allocation, maintenance respiration and biomass export for tropical forests (based on literature), and CO_2 down-regulation process added to photosynthesis.
[i] See also Woodward and Lomas (2004) and Walker et al. (2017).
[j] See also Ito and Inatomi (2012).
[k] Previous simulations used atmospheric CO_2 concentration from the IPCC IS92a scenario. This has been rerun using observed atmospheric CO_2 concentration consistent with the protocol used here.
[l] Last included in Le Quéré et al. (2015a).
[m] With no nutrient restoring below the mixed layer depth.

for their use of atmospheric CO_2 concentration to calculate the fertilisation effect of CO_2 on plant photosynthesis.

The DGVMs used the HYDE land-use change data set (Klein Goldewijk et al., 2017a, b), which provides annual, half-degree, fractional data on cropland and pasture. These data are based on annual FAO statistics of change in agricultural area available to 2012 (FAOSTAT, 2015). For the years 2015 and 2016, the HYDE data were extrapolated by country for pastures and cropland separately based on the trend in agricultural area over the previous 5 years. Some models also use an update of the more comprehensive harmonised land-use data set (Hurtt et al., 2011), that further includes fractional data on primary vegetation and secondary vegetation, as well as all underlying transitions between land-use states (Hurtt et al., 2018). This new data set is of quarter-degree fractional areas of land-use states and all transitions between those states, including a new wood harvest reconstruction, new representation of shifting cultivation, crop rotations, management information including irrigation, and fertiliser application. The land-use states now include five different crop types in addition to the pasture–rangeland split discussed before. Wood harvest patterns are constrained with Landsat forest loss data.

DGVMs implement land-use change differently (e.g. an increased cropland fraction in a grid cell can either be at the expense of grassland or shrubs, or forest, the latter resulting in deforestation; land cover fractions of the non-agricultural land differ between models). Similarly, model-specific assumptions are applied to convert deforested biomass or deforested area, and other forest product pools into carbon, and different choices are made regarding the allocation of rangelands as natural vegetation or pastures.

The DGVM model runs were forced by either 6-hourly CRU-NCEP or by monthly CRU temperature, precipitation, and cloud cover fields (transformed into incoming surface radiation) based on observations and provided on a $0.5° \times 0.5°$ grid and updated to 2016 (Harris et al., 2014; Viovy, 2016). The forcing data include both gridded observations of climate and global atmospheric CO_2, which change over time (Dlugokencky and Tans, 2018), and N deposition (as used in some models; Table A1).

Two sets of simulations were performed with the DGVMs. The first forced initially with historical changes in land cover distribution, climate, atmospheric CO_2 concentration, and N deposition and the second, as further described below, with a time-invariant pre-industrial land cover distribution, allowing the models to estimate, by difference with the first simulation, the dynamic evolution of biomass and soil carbon pools in response to prescribed land-cover change. E_{LUC} is diagnosed in each model by the difference between these two simulations. We only retain model outputs with positive E_{LUC} during the 1990s (Table A1). Using the difference between these two DGVM simulations to diagnose E_{LUC} means the DGVMs account for the loss of additional sink capacity (around 0.3 GtC yr^{-1}; see Sect. 2.7.3), while the bookkeeping models do not.

2.2.3 Uncertainty assessment for E_{LUC}

Differences between the bookkeeping models and DGVM models originate from three main sources: the different methodologies, the land-use and land-cover data set, and the different processes represented (Table A1). We examine the results from the DGVM models and of the bookkeeping method to assess the uncertainty in E_{LUC}.

The E_{LUC} estimate from the DGVMs' multi-model mean is consistent with the average of the emissions from the bookkeeping models (Table 5). However, there are large differences among individual DGVMs (standard deviation at around 0.5–0.6 GtC yr^{-1}; Table 5), between the two bookkeeping models (average of 0.5 GtC yr^{-1}), and between the current estimate of H&N2017 and its previous model version (Houghton et al., 2012) as used in past global carbon budgets (Le Quéré et al., 2016; average of 0.3 GtC yr^{-1}). Given the large spread in new estimates we raise our assessment of uncertainty in E_{LUC} to ± 0.7 GtC yr^{-1} (from ± 0.5 GtC yr^{-1}) as a semi-quantitative measure of uncertainty for annual and decadal emissions. This reflects our best value judgment that there is at least a 68 % chance ($\pm 1\sigma$) that the true land-use change emission lies within the given range, for the range of processes considered here. Prior to 1959, the uncertainty in E_{LUC} was taken from the standard deviation of the DGVMs. We assign low confidence to the annual estimates of E_{LUC} because of the inconsistencies among estimates and of the difficulties in quantifying some of the processes in DGVMs.

2.2.4 Emissions projections

We provide an assessment of E_{LUC} for 2017 by adding the anomaly of fire emissions in deforestation areas, including those from peat fires, from GFED4s (van der Werf et al., 2017) over the last year available. Emissions are estimated using active fire data (MCD14ML; Giglio et al., 2003), which are available in near-real time, and correlations between those and GFED4s emissions for the 2001–2016 period for the 12 corresponding months. Emissions during January–October cover most of the fire season in the Amazon and Southeast Asia, where a large part of the global deforestation takes place.

2.3 Growth rate in atmospheric CO_2 concentration (G_{ATM})

2.3.1 Global growth rate in atmospheric CO_2 concentration

The rate of growth of the atmospheric CO_2 concentration is provided by the US National Oceanic and Atmospheric Administration Earth System Research Laboratory (NOAA/ESRL; Dlugokencky and Tans, 2018), which is updated from Ballantyne et al. (2012). For the 1959–1980 period, the global growth rate is based on measurements of atmospheric CO_2 concentration averaged from the Mauna Loa and South Pole stations, as observed by the CO_2 Program at Scripps Institution of Oceanography (Keeling et al., 1976). For the 1980–2016 time period, the global growth rate is based on the average of multiple stations selected from the marine boundary layer sites with well-mixed background air (Ballantyne et al., 2012), after fitting each station with a smoothed curve as a function of time and averaging by latitude band (Masarie and Tans, 1995). The annual growth rate is estimated by Dlugokencky and Tans (2018) from atmospheric CO_2 concentration by taking the average of the most recent December–January months corrected for the average seasonal cycle and subtracting this same average 1 year earlier. The growth rate in units of ppm yr^{-1} is converted to units of GtC yr^{-1} by multiplying by a factor of 2.12 GtC ppm^{-1} (Ballantyne et al., 2012).

Table 5. Comparison of results from the bookkeeping method and budget residuals with results from the DGVMs and inverse estimates for different periods, last decade, and last year available. All values are in $GtC\,yr^{-1}$. The DGVM uncertainties represent $\pm1\sigma$ of the decadal or annual (for 2016 only) estimates from the individual DGVMs; for the inverse models all three results are given where available.

	Mean ($GtC\,yr^{-1}$)						
	1960–1969	1970–1979	1980–1989	1990–1999	2000–2009	2007–2016	2016
Land-use change emissions (E_{LUC})							
Bookkeeping methods	1.4 ± 0.7	1.1 ± 0.7	1.2 ± 0.7	1.3 ± 0.7	1.2 ± 0.7	1.3 ± 0.7	1.3 ± 0.7
DGVMs	1.3 ± 0.5	1.2 ± 0.5	1.2 ± 0.4	1.2 ± 0.3	1.2 ± 0.4	1.3 ± 0.4	1.4 ± 0.8
Terrestrial sink (S_{LAND})							
Residual sink from global budget ($E_{FF}+E_{LUC}-G_{ATM}-S_{OCEAN}$)	1.8 ± 0.9	1.8 ± 0.9	1.5 ± 0.9	2.6 ± 0.9	3.0 ± 0.9	3.6 ± 1.0	2.4 ± 1.0
DGVMs	1.4 ± 0.7	2.4 ± 0.6	2.0 ± 0.6	2.5 ± 0.5	2.9 ± 0.8	3.0 ± 0.8	2.7 ± 1.0
Total land fluxes ($S_{LAND}-E_{LUC}$)							
Budget constraint ($E_{FF}-G_{ATM}-S_{OCEAN}$)	0.4 ± 0.5	0.7 ± 0.6	0.4 ± 0.6	1.3 ± 0.6	1.7 ± 0.6	2.3 ± 0.7	1.1 ± 0.7
DGVMs	0.1 ± 0.9	1.2 ± 0.8	0.7 ± 0.7	1.2 ± 0.5	1.7 ± 0.8	1.7 ± 0.7	1.3 ± 1.0
Inversions (CTE/Jena CarboScope/CAMS)*	–/–/–	–/–/–	–/–/0.2	–/0.6/1.3	1.4/1.1/1.9	1.8/1.4/2.3	0.0/0.0/2.2

* Estimates are corrected for the pre-industrial influence of river fluxes (Sect. 2.7.2). See Tables A3 and 4 for references.

The uncertainty around the atmospheric growth rate is due to three main factors: first, the long-term reproducibility of reference gas standards (around 0.03 ppm for 1σ from the 1980s); second, the network composition of the marine boundary layer with some sites coming or going, gaps in the time series at each site, etc. (Dlugokencky and Tans, 2018) – the latter uncertainty was estimated by NOAA/ESRL with a Monte Carlo method by constructing 100 alternative networks (around 0.1 ppm; NOAA/ESRL, 2017; Masarie, and Tans, 1995); third, the uncertainty associated with using the average CO_2 concentration from a surface network to approximate the true atmospheric average CO_2 concentration (mass-weighted, in three dimensions) as needed to assess the total atmospheric CO_2 burden. In reality these will differ, especially owing to the finite rates of vertical mixing and stratosphere–troposphere exchange. For example, excess CO_2 from tropical emissions will arrive at stations in the network after a delay of months or more, and the signals will continue to evolve as the excess mixes throughout the troposphere and the stratosphere. The excess measured at the stations will not exactly track changes in total atmospheric burden, with offsets in magnitude and phasing. This effect must be very small on decadal and longer timescales, when the atmosphere can be considered well mixed. Preliminary estimates suggest this effect would increase the annual uncertainty, but a full analysis is not yet available. We therefore maintain an uncertainty around the annual growth rate based on the multiple stations data set ranges between 0.11 and 0.72 $GtC\,yr^{-1}$, with a mean of 0.61 $GtC\,yr^{-1}$ for 1959–1979 and 0.19 $GtC\,yr^{-1}$ for 1980–2016, when a larger set of stations were available as provided by Dlugokencky and Tans (2018). We also maintain the uncertainty of the decadal averaged growth rate at $\pm0.1\,GtC\,yr^{-1}$ as in Le Quéré et al. (2016) based on previous IPCC assessments, but recognising further exploration of this uncertainty is required.

We assign a high confidence to the annual estimates of G_{ATM} because they are based on direct measurements from multiple and consistent instruments and stations distributed around the world (Ballantyne et al., 2012).

In order to estimate the total carbon accumulated in the atmosphere since 1750 or 1870, we use an atmospheric CO_2 concentration of 277 ± 3 or 288 ± 3 ppm, respectively, based on a cubic spline fit to ice core data (Joos and Spahni, 2008). The uncertainty of ±3 ppm (converted to $\pm1\sigma$) is taken directly from the IPCC's assessment (Ciais et al., 2013). Typical uncertainties in the growth rate in atmospheric CO_2 concentration from ice core data are equivalent to ±0.1–$0.15\,GtC\,yr^{-1}$ as evaluated from the Law Dome data (Etheridge et al., 1996) for individual 20-year intervals over the period from 1870 to 1960 (Bruno and Joos, 1997).

2.3.2 Growth rate projection

We provide an assessment of G_{ATM} for 2017 based on the observed increase in atmospheric CO_2 concentration at the Mauna Loa station for January to September and monthly forecasts for October to December updated from Betts et al. (2016). The forecast uses a statistical relationship between annual CO_2 growth rate and sea surface temperatures (SSTs) in the Niño3.4 region. The forecast SSTs from the

GloSea seasonal forecast model were then used to estimate monthly CO_2 concentrations at Mauna Loa throughout the following calendar year, assuming a stationary seasonal cycle. The forecast CO_2 concentrations for January to August 2017 were close to the observations, so updating the 2017 forecast by simply averaging the observed and forecast values is considered justified. Growth at Mauna Loa is closely correlated with the global growth ($r = 0.95$) and is used here as a proxy for global growth.

2.4 Ocean CO_2 sink

Estimates of the global ocean CO_2 sink S_{OCEAN} are from an ensemble of global ocean biogeochemistry models that meet observational constraints over the 1990s (see below). We use observation-based estimates of S_{OCEAN} to provide a qualitative assessment of confidence in the reported results and to estimate the cumulative accumulation of S_{OCEAN} over the pre-industrial period.

2.4.1 Observation-based estimates

We use the observational constraints assessed by IPCC of a mean ocean CO_2 sink of $2.2 \pm 0.4\,\mathrm{GtC\,yr^{-1}}$ for the 1990s (Denman et al., 2007) to verify that the GOBMs provide a realistic assessment of S_{OCEAN}. This is based on indirect observations and their spread, using the methods that are deemed most reliable for the assessment of this quantity. The IPCC did not revise its assessment in 2013. The observations are based on ocean–land CO_2 sink partitioning from observed atmospheric O_2 / N_2 concentration trends (Manning and Keeling, 2006; updated in Keeling and Manning, 2014), an oceanic inversion method constrained by ocean biogeochemistry data (Mikaloff Fletcher et al., 2006), and a method based on penetration timescale for CFCs (McNeil et al., 2003). This estimate is consistent with a range of methods (Wanninkhof et al., 2013). Here we use the IPCC confidence interval of 90 % to avoid rejecting models that may be outliers but are still plausible.

We also use two estimates of the ocean CO_2 sink and its variability based on interpolations of measurements of surface ocean fugacity of CO_2 (pCO_2 corrected for the non-ideal behaviour of the gas; Pfeil et al., 2013). We refer to these as pCO_2-based flux estimates. The measurements are from the Surface Ocean CO_2 Atlas version 5, which is an update of version 3 (Bakker et al., 2016) and contains quality-controlled data to 2016 (see data attribution Table A4). The SOCAT v5 data were mapped using a data-driven diagnostic method (Rödenbeck et al., 2013) and a combined self-organising map and feed-forward neural network (Landschützer et al., 2014). The global pCO_2-based flux estimates were adjusted to remove the pre-industrial ocean source of CO_2 to the atmosphere of $0.45\,\mathrm{GtC\,yr^{-1}}$ from river input to the ocean (Jacobson et al., 2007), per our definition of S_{OCEAN}. As this adjustment is made in figures only, we do not account for the uncertainty in the river flux. Several other ocean sink products based on observations are also available, but they show large discrepancies with observed variability that need to be resolved. Here we used the two pCO_2-based flux products that had the best fit to observations for their representation of tropical and global variability (Rödenbeck et al., 2015).

We further use results from two diagnostic ocean models of Khatiwala et al. (2013) and DeVries (2014) to estimate the anthropogenic carbon accumulated in the ocean prior to 1959. The two approaches assume constant ocean circulation and biological fluxes over the pre-industrial period, with S_{OCEAN} estimated as a response in the change in atmospheric CO_2 concentration calibrated to observations. The uncertainty in cumulative uptake of $\pm 20\,\mathrm{GtC}$ (converted to $\pm 1\sigma$) is taken directly from the IPCC's review of the literature (Rhein et al., 2013), or about $\pm 30\,\%$ for the annual values (Khatiwala et al., 2009).

2.4.2 Global ocean biogeochemistry models (GOBMs)

The ocean CO_2 sink for 1959–2016 is estimated using eight GOBMs (Table A2). All GOBMs fell within 90 % confidence of the observed range, or 1.6 to $2.8\,\mathrm{GtC\,yr^{-1}}$ for the 1990s. The GOBMs represent the physical, chemical, and biological processes that influence the surface ocean concentration of CO_2 and thus the air–sea CO_2 flux. The GOBMs are forced by meteorological reanalysis and atmospheric CO_2 concentration data available for the entire time period and mostly differ in the source of the atmospheric forcing data, spin-up strategies, and in the resolution of the oceanic physical processes (Table A2). GOBMs do not include the effects of anthropogenic changes in nutrient supply, which could lead to an increase in the ocean sink of up to about $0.3\,\mathrm{GtC\,yr^{-1}}$ over the industrial period (Duce et al., 2008). They also do not include the perturbation associated with changes in river organic carbon, which is discussed Sect. 2.7.

The ocean CO_2 sink for each GOBM is no longer normalised to the observations as in previous global carbon budgets (e.g. Le Quéré et al., 2016). The normalisation was mostly intended to ensure S_{LAND} had a realistic mean value as it was previously estimated from the budget residual. With the introduction of the budget residual (Eq. 1) all terms can be estimated independently. Instead, the oceanic observations are used in the selection of the GOBMs, by using only the GOBMs that produce an oceanic CO_2 sink over the 1990s consistent with observations within 90 % confidence intervals, as explained above.

2.4.3 Uncertainty assessment for S_{OCEAN}

The uncertainty around the mean ocean sink of anthropogenic CO_2 was quantified by Denman et al. (2007) for the 1990s (see Sect. 2.4.1). To quantify the uncertainty around annual values, we examine the standard deviation of the GOBM ensemble, which averages between 0.2 and 0.3 GtC yr^{-1} during 1959–2017. We estimate that the uncertainty in the annual ocean CO_2 sink is about ±0.5 GtC yr^{-1} from the combined uncertainty of the mean flux based on observations of ±0.4 GtC yr^{-1} and the standard deviation across GOBMs of up to ±0.3 GtC yr^{-1}, reflecting both the uncertainty in the mean sink from observations during the 1990s (Denman et al., 2007; Sect. 2.4.1) and in the interannual variability as assessed by GOBMs.

We examine the consistency between the variability of the model-based and the pCO$_2$-based flux products to assess confidence in S_{OCEAN}. The interannual variability of the ocean fluxes (quantified as the standard deviation) of the two pCO$_2$-based products for 1986–2016 (where they overlap) is ±0.35 GtC yr^{-1} (Rödenbeck et al., 2014) and ±0.36 GtC yr^{-1} (Landschützer et al., 2015), compared to ±0.27 GtC yr^{-1} for the normalised GOBM ensemble. The standard deviation includes a component of trend and decadal variability in addition to interannual variability, and their relative influence differs across estimates. The estimates generally produce a higher ocean CO_2 sink during strong El Niño events. The annual pCO$_2$-based flux products correlate with the ocean CO_2 sink estimated here with a correlation of $r = 0.75$ (0.49 to 0.84 for individual GOBMs) and $r = 0.78$ (0.46 to 0.80) for the pCO$_2$-based flux products of Rödenbeck et al. (2014) and Landschützer et al. (2015), respectively (simple linear regression), with their mutual correlation at 0.70. The agreement between models and the flux products reflects some consistency in their representation of underlying variability since there is little overlap in their methodology or use of observations. The use of annual data for the correlation may reduce the strength of the relationship because the dominant source of variability associated with El Niño events is less than 1 year. We assess a medium confidence level to the annual ocean CO_2 sink and its uncertainty because it is based on multiple lines of evidence, and the results are consistent in that the interannual variability in the GOBMs and data-based estimates are all generally small compared to the variability in the growth rate of atmospheric CO_2 concentration.

2.5 Terrestrial CO_2 sink

The terrestrial land sink (S_{LAND}) is thought to be due to the combined effects of fertilisation by rising atmospheric CO_2 and N deposition on plant growth, as well as the effects of climate change such as the lengthening of the growing season in northern temperate and boreal areas. S_{LAND} does not include gross land sinks directly resulting from land use and land-use change (e.g. regrowth of vegetation) as these are part of the net land-use flux (E_{LUC}), although system boundaries make it difficult to exactly attribute CO_2 fluxes on land between S_{LAND} and E_{LUC} (Erb et al., 2013).

New to the 2017 Global Carbon Budget, S_{LAND} is estimated from the multi-model mean of the DGVMs (Table A1). As described in Sect. 2.2.3, DGVM simulations include all climate variability and CO_2 effects over land. The DGVMs do not include the perturbation associated with changes in river organic carbon, which is discussed Sect. 2.7. We apply three criteria for minimum DGVM realism by including only those DGVMs with (1) steady state after spin up; (2) where available, net land fluxes ($S_{LAND} - E_{LUC}$), that is a carbon sink over the 1990s between −0.3 and 2.3 GtC yr^{-1}, within 90 % confidence of constraints by global atmospheric and oceanic observations (Keeling and Manning, 2014; Wanninkhof et al., 2013); and (3) global E_{LUC} that is a carbon source over the 1990s. Three DGVMs did not meet the criteria (1) for E_{LUC} because of an issue with the protocol and one did not meet the criteria (2).

The standard deviation of the annual CO_2 sink across the DGVMs averages to ±0.8 GtC yr^{-1} for the period 1959 to 2016. We attach a medium confidence level to the annual land CO_2 sink and its uncertainty because the estimates from the residual budget and averaged DGVMs match well within their respective uncertainties (Table 5).

2.6 The atmospheric perspective

The worldwide network of atmospheric measurements can be used with atmospheric inversion methods to constrain the location of the combined total surface CO_2 fluxes from all sources, including fossil and land-use change emissions and land and ocean CO_2 fluxes. The inversions assume E_{FF} to be well known, and they solve for the spatial and temporal distribution of land and ocean fluxes from the residual gradients of CO_2 between stations that are not explained by emissions.

Three atmospheric inversions (Table A3) used atmospheric CO_2 data to the end of 2016 (including preliminary values in some cases) to infer the spatio-temporal CO_2 flux field. We focus here on the largest and most consistent sources of information (namely the total CO_2 flux over land regions and the distribution of the total land and ocean CO_2 fluxes for the mid- to high-latitude Northern Hemisphere (NH), 30–90° N; tropics, 30° S–30° N; and mid- to high-latitude region of the Southern Hemisphere, 30–90° S) and use these estimates to comment on the consistency across various data streams and process-based estimates.

Atmospheric inversions

The three inversion systems used in this release are the CarbonTracker Europe (CTE; van der Laan-Luijkx et al., 2017), the Jena CarboScope (Rödenbeck, 2005), and CAMS (Chevallier et al., 2005). See Table A3 for version numbers. The three inversions are based on the same Bayesian inversion principles that interpret the same, for the most part, observed time series (or subsets thereof) but use different methodologies (Table A3). These differences mainly concern the selection of atmospheric CO_2 data, the used prior fluxes, spatial breakdown (i.e. grid size), assumed correlation structures, and mathematical approach. The details of these approaches are documented extensively in the references provided above. Each system uses a different transport model, which was demonstrated to be a driving factor behind differences in atmospherically based flux estimates, and specifically their distribution across latitudinal bands (Stephens et al., 2007).

The three inversions use atmospheric CO_2 observations from various flask and in situ networks, as detailed in Table A3. They prescribe global E_{FF}, which is scaled to the present study for CAMS and CTE, while CarboScope uses CDIAC extended after 2013 using the emission growth rate of the present study. Inversion results for the sum of natural ocean and land fluxes (Fig. 8) are more constrained in the Northern Hemisphere than in the tropics, because of the higher measurement station density in the NH. Results from atmospheric inversions, similar to the pCO$_2$-based ocean flux products, are adjusted for the river fluxes. The atmospheric inversions provide new information on the regional distribution of fluxes.

2.7 Processes not included in the global carbon budget

The contribution of anthropogenic CO and CH_4 to the global carbon budget has been partly neglected in Eq. (1) and is described in Sect. 2.7.1. The contribution of anthropogenic changes in river fluxes is conceptually included in Eq. (1) in S_{OCEAN} and in S_{LAND}, but it is not represented in the process models used to quantify these fluxes. This effect is discussed in Sect. 2.7.2. Similarly, the loss of additional sink capacity from reduced forest cover is missing in the combination of approaches used here to estimate both land fluxes (E_{LUC} and S_{LAND}) and its potential effect is discussed and quantified in Sect. 2.7.3.

2.7.1 Contribution of anthropogenic CO and CH_4 to the global carbon budget

Equation (1) includes only partly the net input of CO_2 to the atmosphere from the chemical oxidation of reactive carbon-containing gases from sources other than the combustion of fossil fuels, such as (1) cement process emissions, since these do not come from combustion of fossil fuels; (2) the oxidation of fossil fuels; and (3) the assumption of immediate oxidation of vented methane in oil production. However, it omits any other anthropogenic carbon-containing gases that are eventually oxidised in the atmosphere, such as anthropogenic emissions of CO and CH_4. An attempt is made in this section to estimate their magnitude and identify the sources of uncertainty. Anthropogenic CO emissions are from incomplete fossil fuel and biofuel burning and deforestation fires. The main anthropogenic emissions of fossil CH_4 that matter for the global carbon budget are the fugitive emissions of coal, oil, and gas upstream sectors (see below). These emissions of CO and CH_4 contribute a net addition of fossil carbon to the atmosphere.

In our estimate of E_{FF} we assumed (Sect. 2.1.1) that all the fuel burned is emitted as CO_2; thus, CO anthropogenic emissions associated with incomplete combustion and their atmospheric oxidation into CO_2 within a few months are already counted implicitly in E_{FF} and should not be counted twice (same for E_{LUC} and anthropogenic CO emissions by deforestation fires). Anthropogenic emissions of fossil CH_4 are not included in E_{FF}, because these fugitive emissions are not included in the fuel inventories. Yet they contribute to the annual CO_2 growth rate after CH_4 gets oxidised into CO_2. Anthropogenic emissions of fossil CH_4 represent 15 % of total CH_4 emissions (Kirschke et al., 2013), that is 0.061 GtC yr^{-1} for the past decade. Assuming steady state, these emissions are all converted to CO_2 by OH oxidation and thus explain 0.06 GtC yr^{-1} of the global CO_2 growth rate in the past decade, or 0.07–0.1 GtC yr^{-1} using the higher CH_4 emissions reported recently (Schwietzke et al., 2016).

Other anthropogenic changes in the sources of CO and CH_4 from wildfires, biomass, wetlands, ruminants, or permafrost changes are similarly assumed to have a small effect on the CO_2 growth rate. The CH_4 emissions and sinks are published and analysed separately in the Global Methane Budget publication that follows a similar approach to that presented here (Saunois et al., 2016).

2.7.2 Anthropogenic carbon fluxes in the land to ocean aquatic continuum

The approach used to determine the global carbon budget refers to the mean, variations, and trends in the perturbation of CO_2 in the atmosphere, referenced to the pre-industrial era. Carbon is continuously displaced from the land to the ocean through the land–ocean aquatic continuum (LOAC) comprising freshwaters, estuaries, and coastal areas (Bauer et al., 2013; Regnier et al., 2013). A significant fraction of this lateral carbon flux is entirely "natural" and is thus a steady state component of the pre-industrial carbon cycle. We account for this pre-industrial flux where appropriate in our study. However, changes in environmental conditions and land-use change have caused an increase in the lateral transport of carbon into the LOAC – a perturbation that is relevant for the global carbon budget presented here.

The results of the analysis of Regnier et al. (2013) can be summarised in two points of relevance for the anthropogenic CO_2 budget. First, the anthropogenic perturbation has increased the organic carbon export from terrestrial ecosystems to the hydrosphere at a rate of 1.0 ± 0.5 GtC yr^{-1}, mainly owing to enhanced carbon export from soils. Second, this exported anthropogenic carbon is partly respired through the LOAC; partly sequestered in sediments along the LOAC; and, to a lesser extent, transferred in the open ocean where it may accumulate. The increase in storage of land-derived organic carbon in the LOAC and open ocean combined is estimated by Regnier et al. (2013) at 0.65 ± 0.35GtC yr^{-1}. We do not attempt to incorporate the changes in LOAC in our study.

The inclusion of freshwater fluxes of anthropogenic CO_2 affects the estimates of, and partitioning between, S_{LAND} and S_{OCEAN} in Eq. (1) in complementary ways, but does not affect the other terms. This effect is not included in the GOBMs and DGVMs used in our global carbon budget analysis presented here.

2.7.3 Loss of additional sink capacity

The DGVM simulations now used to estimate S_{LAND} are carried out with a time-invariant pre-industrial land-use mask. Hence, they overestimate the land sink by ignoring historical changes in vegetation cover due to land use and how this affected the global terrestrial biosphere's capacity to remove CO_2 from the atmosphere. Historical land-cover change was dominated by transitions from vegetation types that can provide a large sink per area unit (typically forests) to others less efficient in removing CO_2 from the atmosphere (typically croplands). The resultant decrease in land sink, called the "loss of sink capacity", is calculated as the difference between the actual land sink under changing land cover and the counterfactual land sink under pre-industrial land cover.

An efficient protocol has yet to be designed to estimate the magnitude of the loss of additional sink capacity in DGVMs. Here, we provide a quantitative estimate of this term to be used in the discussion. Our estimate uses the compact Earth system model OSCAR (Gasser et al., 2017), whose land carbon cycle component is designed to emulate the behaviour of TRENDY and CMIP5 complex models. We use OSCAR v2.2.1 (an update of v2.2, with minor changes) in a probabilistic setup identical to the one of Arneth et al. (2017) but with a Monte Carlo ensemble of 2000 simulations. For each, we calculate separately S_{LAND} and the loss of additional sink capacity. We then constrain the ensemble by weighting each member to obtain a distribution of cumulative S_{LAND} over 1850–2005 close to the DGVMs used here. From this ensemble, we estimate a loss of additional sink capacity of 0.4 ± 0.3 GtC yr^{-1} on average over 2005–2014 and by extrapolation of 20 ± 15 GtC accumulated between 1870 and 2016.

3 Results

3.1 Global carbon budget mean and variability for 1959–2016

The global carbon budget averaged over the last half-century is shown in Fig. 3. For this time period, 82 % of the total emissions ($E_{FF} + E_{LUC}$) were caused by fossil fuels and industry and 18 % by land-use change. The total emissions were partitioned among the atmosphere (45 %), ocean (23 %), and land (32 %). All components except land-use change emissions have grown since 1959, with important interannual variability in the growth rate in atmospheric CO_2 concentration and in the land CO_2 sink (Fig. 4), as well as some decadal variability in all terms (Table 6).

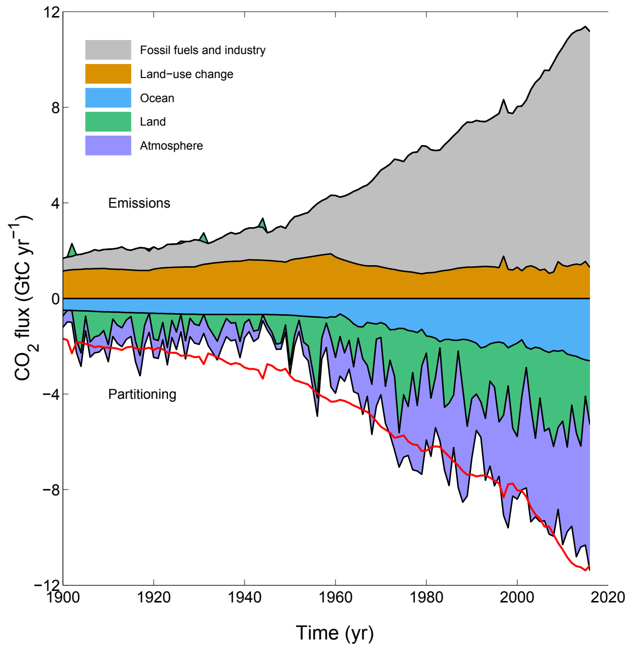

Figure 3. Combined components of the global carbon budget illustrated in Fig. 2 as a function of time, for emissions from fossil fuels and industry (E_{FF}; grey) and emissions from land-use change (E_{LUC}; brown), as well as their partitioning among the atmosphere (G_{ATM}; purple), land (S_{LAND}; green), and oceans (S_{OCEAN}; blue). The partitioning is based on nearly independent estimates from observations (for G_{ATM}) and from process model ensembles constrained by data (for S_{OCEAN} and S_{LAND}) and does not exactly add up to the sum of the emissions, resulting in a budget imbalance which is represented by the difference between the bottom red line (reflecting total emissions) and the sum of the ocean, land, and atmosphere. All time series are in GtC yr^{-1}. G_{ATM} and S_{OCEAN} prior to 1959 are based on different methods. E_{FF} is primarily from Boden et al. (2017) with uncertainty of about ± 5 % ($\pm 1\sigma$); E_{LUC} are from two bookkeeping models (Table 2) with uncertainties of about ± 50 %; G_{ATM} prior to 1959 is from Joos and Spahni (2008) with uncertainties equivalent to about ± 0.1–0.15 GtC yr^{-1}, and from Dlugokencky and Tans (2018) from 1959 with uncertainties of about ± 0.2 GtC yr^{-1}; S_{OCEAN} prior to 1959 is averaged from Khatiwala et al. (2013) and DeVries (2014) with uncertainty of about ± 30 %, and from a multi-model mean (Table 4) from 1959 with uncertainties of about ± 0.5 GtC yr^{-1}; S_{LAND} is a multi-model mean (Table 4) with uncertainties of about ± 0.9 GtC yr^{-1}. See the text for more details of each component and their uncertainties.

3.1.1 CO_2 emissions

Global CO_2 emissions from fossil fuels and industry have increased every decade from an average of 3.1 ± 0.2 GtC yr^{-1}

Table 6. Decadal mean in the five components of the anthropogenic CO_2 budget for different periods and last year available. All values are in GtC yr^{-1}, and uncertainties are reported as $\pm 1\sigma$. Unlike previous versions of the global carbon budget, the terrestrial sink (S_{LAND}) is now estimated independently from the mean of DGVM models. Therefore, the table also shows the budget imbalance (B_{IM}), which provides a measure of the discrepancies among the nearly independent estimates and has an uncertainty exceeding ± 1 GtC yr^{-1}. A positive imbalance means the emissions are overestimated and/or the sinks are too small.

	Mean (GtC yr^{-1})						
	1960–1969	1970–1979	1980–1989	1990–1999	2000–2009	2007–2016	2016
Emissions							
Fossil fuels and industry (E_{FF})	3.1 ± 0.2	4.7 ± 0.2	5.5 ± 0.3	6.3 ± 0.3	7.8 ± 0.4	9.4 ± 0.5	9.9 ± 0.5
Land-use change emissions (E_{LUC})	1.4 ± 0.7	1.1 ± 0.7	1.2 ± 0.7	1.3 ± 0.7	1.2 ± 0.7	1.3 ± 0.7	1.3 ± 0.7
Partitioning							
Growth rate in atmospheric CO_2 concentration (G_{ATM})	1.7 ± 0.1	2.8 ± 0.1	3.4 ± 0.1	3.1 ± 0.1	4.0 ± 0.1	4.7 ± 0.1	6.0 ± 0.2
Ocean sink (S_{OCEAN})	1.0 ± 0.5	1.3 ± 0.5	1.7 ± 0.5	1.9 ± 0.5	2.1 ± 0.5	2.4 ± 0.5	2.6 ± 0.5
Terrestrial sink (S_{LAND})	1.4 ± 0.7	2.4 ± 0.6	2.0 ± 0.6	2.5 ± 0.5	2.9 ± 0.8	3.0 ± 0.8	2.7 ± 1.0
Budget imbalance							
$B_{IM} = E_{FF} + E_{LUC} - (G_{ATM} + S_{OCEAN} + S_{LAND})$	(0.4)	(−0.6)	(−0.4)	(0.1)	(0.0)	(0.6)	(−0.2)

in the 1960s to an average of 9.4 ± 0.5 GtC yr^{-1} during 2007–2016 (Table 6 and Fig. 5). The growth rate in these emissions decreased between the 1960s and the 1990s, from 4.5 % yr^{-1} in the 1960s (1960–1969) to 2.8 % yr^{-1} in the 1970s (1970–1979), 1.9 % yr^{-1} in the 1980s (1980–1989), and 1.1 % yr^{-1} in the 1990s (1990–1999). After this period, the growth rate began increasing again in the 2000s at an average growth rate of 3.3 % yr^{-1}, decreasing to 1.8 % yr^{-1} for the last decade (2007–2016) and to +0.4 % yr^{-1} during 2014–2016.

In contrast, CO_2 emissions from land use, land-use change, and forestry have remained relatively constant, at around 1.3 ± 0.7 GtC yr^{-1} over the past half-century, in agreement with the DGVM ensemble of models. However, there is no agreement on the trend over the full period, with two bookkeeping models suggesting opposite trends and no coherence among DGVMs (Fig. 6).

3.1.2 Partitioning among the atmosphere, ocean, and land

The growth rate in atmospheric CO_2 level increased from 1.7 ± 0.1 GtC yr^{-1} in the 1960s to 4.7 ± 0.1 GtC yr^{-1} during 2007–2016 with important decadal variations (Table 6). Both ocean and land CO_2 sinks increased roughly in line with the atmospheric increase, but with significant decadal variability on land (Table 6) and possibly in the ocean (Fig. 7).

The ocean CO_2 sink increased from 1.0 ± 0.5 GtC yr^{-1} in the 1960s to 2.4 ± 0.5 GtC yr^{-1} during 2007–2016, with interannual variations of the order of a few tenths of GtC yr^{-1} generally showing an increased ocean sink during large El Niño events (i.e. 1997–1998) (Fig. 7; Rödenbeck et al., 2014). Note the lower ocean sink estimate compared to previous global carbon budget releases is due to the fact that ocean models are no longer normalised to observations. Although there is some coherence among the GOBMs and pCO_2-based flux products regarding the mean, there is poor agreement for interannual variability and the ocean models underestimate decadal variability (Sect. 2.4.3 and Fig. 7, also see new data-based decadal estimate of DeVries et al., 2017).

The terrestrial CO_2 sink increased from 1.4 ± 0.7 GtC yr^{-1} in the 1960s to 3.0 ± 0.8 GtC yr^{-1} during 2007–2016, with important interannual variations of up to 2 GtC yr^{-1} generally showing a decreased land sink during El Niño events, overcompensating for the increase in ocean sink and responsible for the enhanced growth rate in atmospheric CO_2 concentration during El Niño events (Fig. 6). The larger land CO_2 sink during 2007–2016 compared to the 1960s is reproduced by all the DGVMs in response to the combined atmospheric CO_2 increase and changes in climate and is consistent with constraints from the other budget terms (Table 5).

The total CO_2 fluxes on land ($S_{LAND} - E_{LUC}$) constrained by the atmospheric inversions show in general very good agreement with the global budget estimate, as expected given the strong constraints of G_{ATM} and the small relative uncertainty assumed on S_{OCEAN} and E_{FF} by inversions. The total land flux is of similar magnitude for the decadal average, with estimates for 2007–2016 from the three inversions of 1.8, 1.4, and 2.3 GtC yr^{-1} compared to 1.7 ± 0.7 GtC yr^{-1} from the DGVMs and 2.3 ± 0.7 GtC yr^{-1} for the total flux computed with the carbon budget constraints (Table 5).

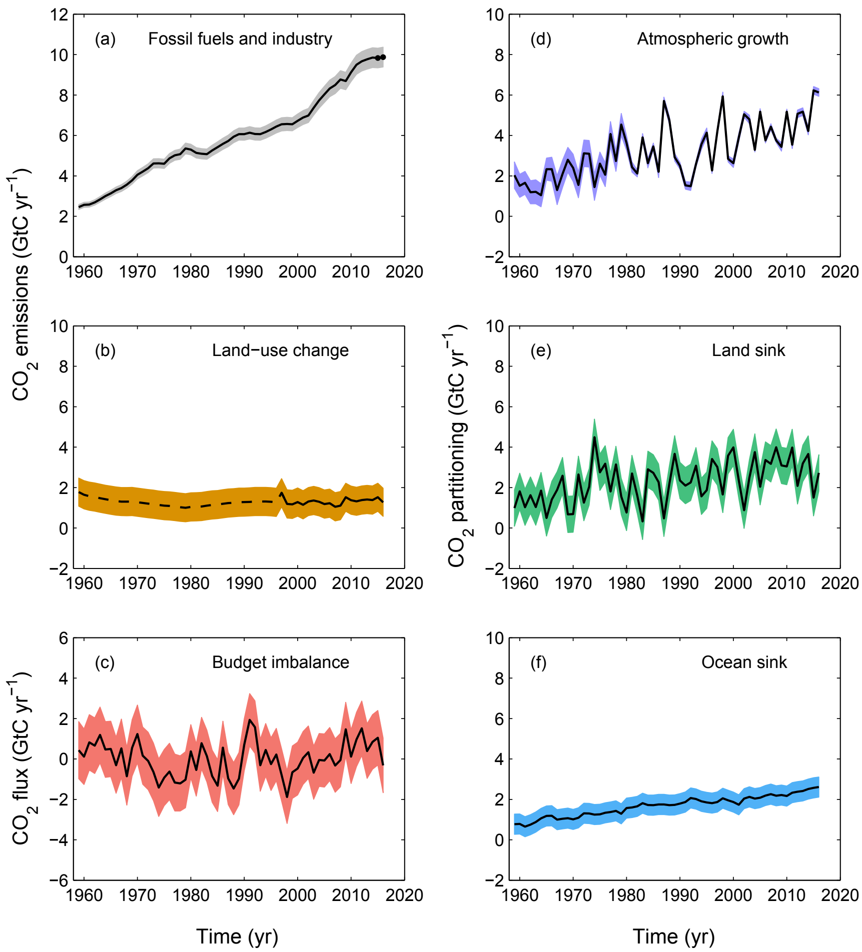

Figure 4. Components of the global carbon budget and their uncertainties as a function of time, presented individually for **(a)** emissions from fossil fuels and industry (E_{FF}), **(b)** emissions from land-use change (E_{LUC}), **(c)** the budget imbalance that is not accounted for by the other terms, **(d)** the growth rate in atmospheric CO_2 concentration (G_{ATM}), and **(e)** the land CO_2 sink (S_{LAND}; positive indicates a flux from the atmosphere to the land), **(f)** the ocean CO_2 sink (S_{OCEAN}; positive indicates a flux from the atmosphere to the ocean). All time series are in GtC yr^{-1} with the uncertainty bounds representing $\pm 1\sigma$ in shaded colour. Data sources are as in Fig. 3. The black dots in panel **(a)** show values for 2015 and 2016 that originate from a different data set to the remainder of the data (see text). The dashed line in panel **(b)** identifies the pre-satellite period before the inclusion of peatland burning.

3.1.3 Budget imbalance

The carbon budget imbalance (B_{IM}; Eq. 1) quantifies the mismatch between the estimated total emissions and the estimated changes in the atmosphere, land, and ocean reservoirs. The mean budget imbalance from 1959 to 2016 is very small (0.07 GtC yr^{-1}) and shows no trend over the full time series. The process models (GOBMs and DGVMs) have been selected to match observational constraints in the 1990s but no further constraints have been applied to their representation of trend and variability. Therefore, the near-zero mean and trend in the budget imbalance are indirect evidence of a coherent community understanding of the emissions and their partitioning on those timescales (Fig. 4). However, the budget imbalance shows substantial variability of the order of ± 1 GtC yr^{-1}, particularly over semi-decadal timescales, although most of the variability is within the uncertainty of the estimates. The imbalance during the 1960s, early 1990s, and in the last decade suggests that either the emissions were overestimated or the sinks were underestimated during these periods. The reverse is true for the 1970s and around 1995–2000 (Fig. 3).

We cannot attribute the cause of the variability in the budget imbalance with our analysis – we can only note that the budget imbalance is unlikely to be explained by errors or biases in the emissions alone because of its large semi-decadal variability component, a variability that is untypical of emissions (Fig. 4). Errors in S_{LAND} and S_{OCEAN} are more likely to be the main cause for the budget imbalance. For example, underestimation of the S_{LAND} by DGVMs has

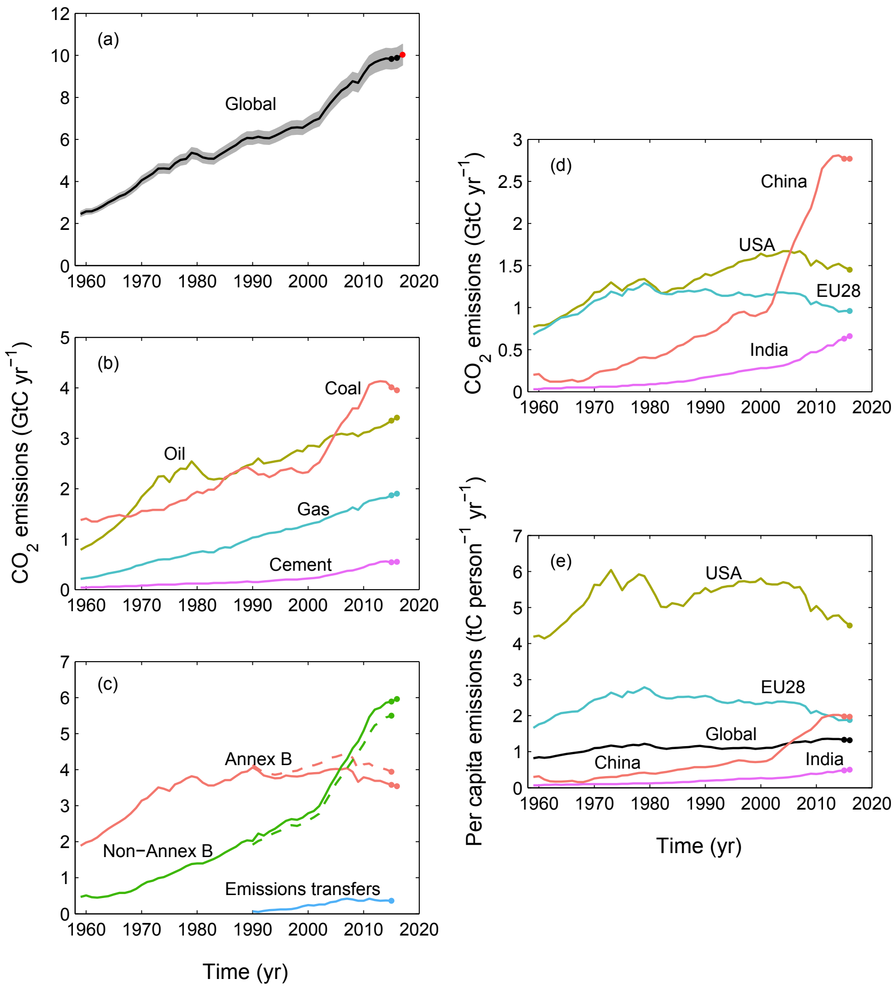

Figure 5. CO_2 emissions from fossil fuels and industry for **(a)** the globe, including an uncertainty of $\pm 5\,\%$ (grey shading), the emissions extrapolated using BP energy statistics (black dots), and the emissions projection for year 2017 based on GDP projection (red dot); **(b)** global emissions by fuel type, including coal (salmon), oil (olive), gas (turquoise), and cement (purple), and excluding gas flaring which is small (0.6 % in 2013); **(c)** territorial (solid line) and consumption (dashed line) emissions for the countries listed in Annex B of the Kyoto Protocol (salmon lines; mostly advanced economies with emissions limitations) versus non-Annex B countries (green lines) – also shown are the emissions transfer from non-Annex B to Annex B countries (light blue line); **(d)** territorial CO_2 emissions for the top three country emitters (USA – olive; China – salmon; India – purple) and for the European Union (EU; turquoise for the 28 member states of the EU as of 2012), and **(e)** per-capita emissions for the top three country emitters and the EU (all colours as in panel **d**) and the world (black). In panels **(b–e)**; the dots show the data that were extrapolated from BP energy statistics for 2014 and 2015. All time series are in GtC yr^{-1} except the per-capita emissions **(e)**, which are in tonnes of carbon per person per year (tC person^{-1} yr^{-1}). Territorial emissions are primarily from Boden et al. (2017) except national data for the USA and EU28 (the 28 member states of the EU) for 1990–2014, which are reported by the countries to the UNFCCC as detailed in the text; consumption-based emissions are updated from Peters et al. (2011a). See Sect. 2.1.1 for details of the calculations and data sources.

been reported following the eruption of Mount Pinatubo in 1991 possibly due to missing responses to changes in diffuse radiation (Mercado et al., 2009) or other yet unknown factors, and DGVMs are suspected to overestimate the land sink in response to the wet decade of the 1970s (Sitch et al., 2003). Decadal and semi-decadal variability in the ocean sink has been also reported recently (DeVries et al., 2017; Landschützer et al., 2015), with the pCO$_2$-based ocean flux products suggesting a smaller-than-expected ocean CO_2 sink in the 1990s and a larger-than-expected sink in the 2000s (Fig. 7), possibly caused by changes in ocean circulation (DeVries et al., 2017) not captured in coarse-resolution GOBMs used here (Dufour et al., 2013).

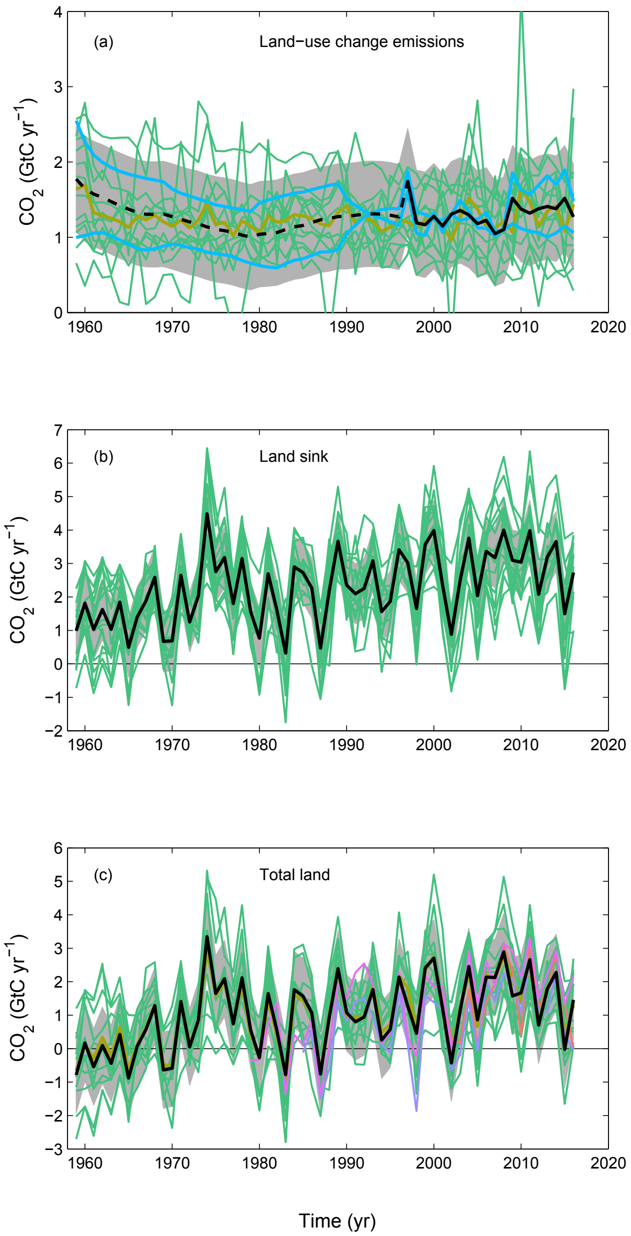

Figure 6. CO_2 exchanges between the atmosphere and the terrestrial biosphere as used in the global carbon budget (black with $\pm 1\sigma$ uncertainty in grey shading) for **(a)** CO_2 emissions from land-use change (E_{LUC}), showing also individually the two bookkeeping models (two blue lines) and the DGVM model results (green) and their multi-model mean (olive). The dashed line identifies the pre-satellite period before the inclusion of peatland burning, **(b)** land CO_2 sink (S_{LAND}) with individual DGVMs (green), and **(c)** total land CO_2 fluxes (**b** minus **a**) with individual DGVMs (green) and their multi-model mean (olive) and atmospheric inversions (CAMS in purple, Jena CarboScope in pink, CTE in salmon; see details in Table 4). In panel **(c)** the inversions were adjusted for the pre-industrial land sink of CO_2 from river input, by removing a sink of 0.45 GtC yr^{-1} (Jacobson et al., 2007), but not for the anthropogenic contribution to river fluxes (see Sect. 2.7.2).

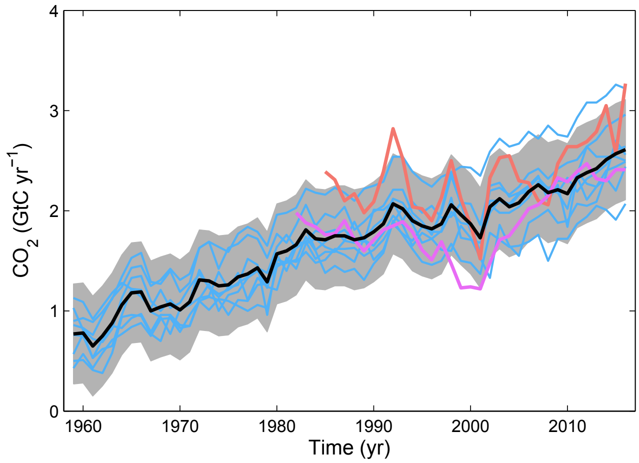

Figure 7. Comparison of the anthropogenic atmosphere–ocean CO_2 flux showing the budget values of S_{OCEAN} (black; with $\pm 1\sigma$ uncertainty in grey shading), individual ocean models (blue), and the two ocean pCO_2-based flux products (Rödenbeck et al., 2014, in salmon and Landschützer et al., 2015, in pink; see Table 4). Both pCO_2-based flux products were adjusted for the pre-industrial ocean source of CO_2 from river input to the ocean, which is not present in the ocean models, by adding a sink of 0.45 GtC yr^{-1} (Jacobson et al., 2007) to make them comparable to S_{OCEAN}. This adjustment does not take into account the anthropogenic contribution to river fluxes (see Sect. 2.7.2).

3.1.4 Regional distribution

Figure 8 shows the partitioning of the total surface fluxes excluding emissions from fossil fuels and industry ($S_{LAND} + S_{OCEAN} - E_{LUC}$) according to the multi-model average of the process models in the ocean and on land (GOBMs and DGVMs) and to the three atmospheric inversions. The total surface fluxes provide information on the regional distribution of those fluxes by latitude bands (Fig. 8). The global mean CO_2 fluxes from process models for 2007–2016 is 4.1 ± 1.0 GtC yr^{-1}. This is comparable to the fluxes of 4.6 ± 0.5 GtC yr^{-1} inferred from the remainder of the carbon budget ($E_{FF} - G_{ATM}$ in Eq. 1; Table 6) within their respective uncertainties. The total CO_2 fluxes from the three inversions range between 4.1 and 5.0 GtC yr^{-1}, consistent with the carbon budget as expected from the constraints on the inversions.

In the south (south of 30° S), the atmospheric inversions and process models all suggest a CO_2 sink for 2007–2016 around 1.3–1.4 GtC yr^{-1} (Fig. 8), although interannual to decadal variability is not fully consistent across methods. The interannual variability in the south is low because of the dominance of ocean area with low variability compared to land areas.

In the tropics (30° S–30° N), both the atmospheric inversions and process models suggest the carbon balance in this region is close to neutral on average over the past

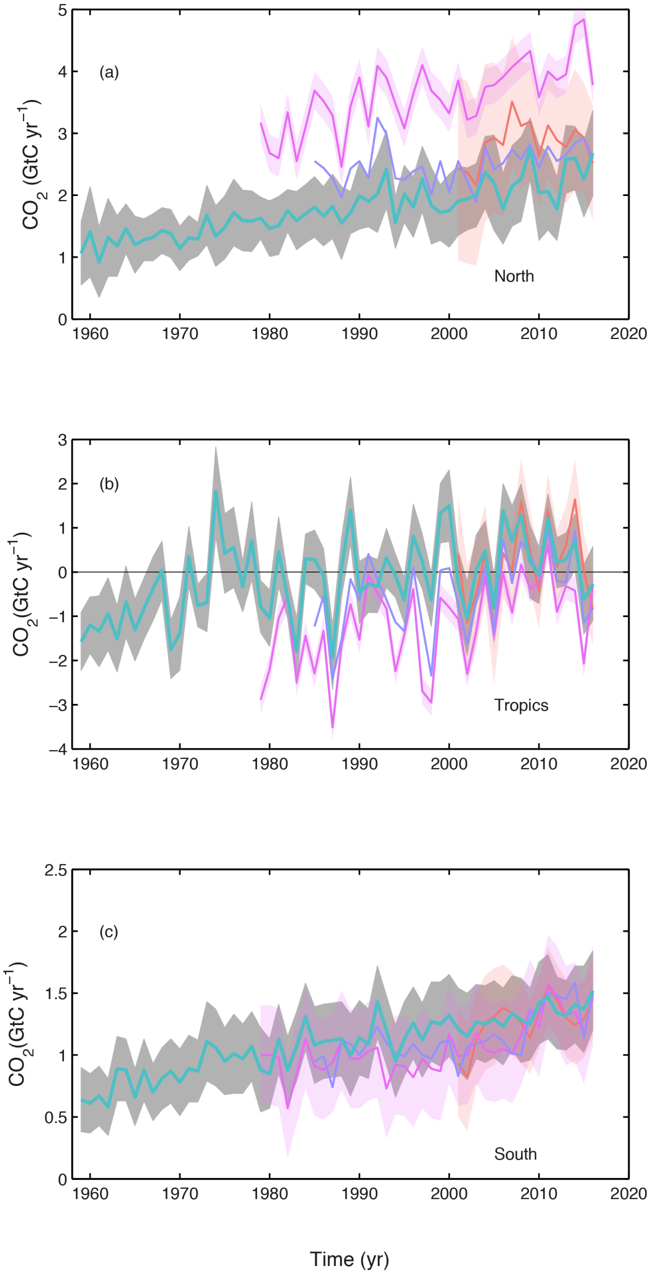

Figure 8. CO_2 fluxes between the atmosphere and the surface ($S_{OCEAN} + S_{LAND} - E_{LUC}$) by latitude bands for the **(a)** north (north of 30° N), **(b)** tropics (30° S–30° N), and **(c)** south (south of 30° S). Estimates from the combination of the process models for the land and oceans are shown (turquoise) with $\pm 1\sigma$ of the model ensemble (in grey). Results from the three atmospheric inversions are also shown (CAMS in purple, Jena CarboScope in pink, CTE in salmon; references and version number in Table 4). Where available the uncertainty in the inversions are also shown. Positive values indicate a flux from the atmosphere to the land and/or ocean.

decade, with fluxes for 2007–2016 ranging between −0.5 and +0.5 GtC yr^{-1}. Both the process models and the inversions consistently allocate more year-to-year variability of CO_2 fluxes to the tropics compared to the north (north of 30° N; Fig. 8), with this variability being dominated by land fluxes.

In the north (north of 30° N), the inversions and process models are not in agreement on the magnitude of the CO_2 sink, with the ensemble mean of the process models suggesting a total Northern Hemisphere sink for 2007–2016 of 2.3 ± 0.6 GtC yr^{-1}, below the estimates from the three inversions that estimate a sink of 2.7, 3.0, and 4.1 GtC yr^{-1} (Fig. 8). The mean difference can only partly be explained by the influence of river fluxes, which is seen by the inversions but not included in the process models; this flux in the Northern Hemisphere would be less than 0.45 GtC yr^{-1} because only the anthropogenic contribution to river fluxes needs to be accounted for. The CTE and Jena CarboScope inversions are within the 1 standard deviation of the process models for the mean sink during their overlap period, while the CAMS inversion gives a higher sink in the north than the process models and a correspondingly higher source in the tropics.

Differences between CTE, CAMS, and Jena CarboScope may be related, for example, to differences in their interhemispheric transport and other inversion settings (Table A3). Separate analysis has shown that the influence of the chosen prior land and ocean fluxes is minor compared to other aspects of each inversion. In comparison to the previous global carbon budget publication, the fossil fuel inputs for CarboScope changed to lower emissions in the north compared to CTE and CAMS, resulting in a smaller northern sink for CarboScope compared to the previous estimate. Differences between the mean fluxes of CAMS in the north and the ensemble of process models cannot be simply explained. They could either reflect a bias in this inversion or missing processes or biases in the process models, such as the lack of adequate parameterisations for forest management in the north and for forest degradation emissions in the tropics for the DGVMs. The estimated contribution of the north and its uncertainty from process models is sensitive both to the ensemble of process models used and to the specifics of each inversion.

3.2 Global carbon budget for the last decade (2007–2016)

The global carbon budget averaged over the last decade (2007–2016) is shown in Fig. 2. For this time period, 88 % of the total emissions ($E_{FF} + E_{LUC}$) were from fossil fuels and industry (E_{FF}) and 12 % from land-use change (E_{LUC}). The total emissions were partitioned among the atmosphere (44 %), ocean (22 %), and land (28 %), with a remaining unattributed budget imbalance (5 %).

3.2.1 CO_2 emissions

Global CO_2 emissions from fossil fuels and industry grew at a rate of 1.8 % yr^{-1} for the last decade (2007–2016), slowing down to $+0.4\,\%\,yr^{-1}$ during 2014–2016. China's emissions increased by $+3.8\,\%\,yr^{-1}$ on average (increasing by $+1.7\,GtC\,yr^{-1}$ during the 10-year period) dominating the global trends, followed by India's emissions increase by $+5.8\,\%\,yr^{-1}$ (increasing by $+0.30\,GtC\,yr^{-1}$), while emissions decreased in EU28 by $2.2\,\%\,yr^{-1}$ (decreasing by $-0.23\,GtC\,yr^{-1}$) and in the USA by $1.0\,\%\,yr^{-1}$ (decreasing by $-0.19\,GtC\,yr^{-1}$). In the past decade, emissions from fossil fuels and industry decreased significantly (at the 95 % level) in 26 countries. A total of 21 of these countries had positive growth in GDP over the same time period, representing 21 % of global emissions (Croatia, Czech Republic, Denmark, France, Germany, Greece, Ireland, Jamaica, Latvia, Luxembourg, Malta, Poland, Romania, Serbia, Slovakia, Slovenia, Sweden, Switzerland, Ukraine, United Kingdom, USA), while 5 countries had both declining GDP and emissions (Andorra, Aruba, North Korea, Greenland, and Syria).

In contrast, there is no apparent trend in CO_2 emissions from land-use change (Fig. 6), though the data are very uncertain.

3.2.2 Partitioning among the atmosphere, ocean, and land

The growth rate in atmospheric CO_2 concentration was initially constant and then increased during the later part of the decade 2007–2016, reflecting a similar constant level followed by a decrease in the land sink, albeit with large interannual variability (Fig. 4). During the same period, the ocean CO_2 sink appears to have intensified, an effect which is particularly apparent in the $p$$CO_2$-based flux products (Fig. 7) and is thought to originate at least in part in the Southern Ocean (Landschützer et al., 2015).

3.2.3 Budget imbalance

The budget imbalance was $0.6\,GtC\,yr^{-1}$ on average over 2007–2016. Although the uncertainties are large in each term, the sustained imbalance over a decade suggests an overestimation of the emissions and/or an underestimation of the sinks. Such a large imbalance is unlikely to originate from the emissions alone because it would indicate sustained bias in emissions over a 10-year period that is as large as the 1σ uncertainty. An origin in the land and/or ocean sink is more likely, given the large variability of the land sink and the suspected underestimation of decadal variability in the ocean sink. More integrated use of observations in the global carbon budget, either on their own or for further constraining model results, should help resolve some of the budget imbalance (Peters et al., 2017; Sect. 4).

3.3 Global carbon budget for year 2016

3.3.1 CO_2 emissions

Preliminary estimates of global CO_2 emissions from fossil fuels and industry based on BP energy statistics are for emissions remaining nearly constant between 2015 and 2016 at $9.9 \pm 0.5\,GtC$ in 2016 (Fig. 5), distributed among coal (40 %), oil (34 %), gas (19 %), cement (5.6 %), and gas flaring (0.7 %). Compared to the previous year, emissions from coal decreased by $-1.7\,\%$, while emissions from oil, gas, and cement increased by 1.5, 1.5, and 1.0 %, respectively. All growth rates presented are adjusted for the leap year, unless stated otherwise.

Emissions in 2016 were 0.2 % higher than in 2015, continuing the low growth trends observed in 2014 and 2015. This growth rate is as projected in Le Quéré et al. (2016) based on national emissions projections for China and the USA and projections of gross domestic product corrected for I_{FF} trends for the rest of the world. The specific projection for 2016 for China made last year of $-0.5\,\%$ (range of -3.8 to $+1.3\,\%$) is within the uncertainty of the realised growth rate of $-0.3\,\%$. Similarly, the projected growth for the US of $-1.7\,\%$ (range of -4.0 to $+0.6\,\%$) is very close to the realised growth rate of $-2.1\,\%$, and the projected growth for the rest of the world of $+1.0\,\%$ (range of -0.4 to 2.5 %) matches the realised rate of 1.3 %.

In 2016, the largest absolute contributions to global CO_2 emissions were from China (28 %), the USA (15 %), the EU (28 member states; 10 %), and India (6.7 %). The percentages are the fraction of the global emissions including bunker fuels (3.1 %). These four regions account for 59 % of global CO_2 emissions. Growth rates for these countries from 2015 to 2016 were $-0.3\,\%$ (China), $-2.1\,\%$ (USA), $-0.3\,\%$ (EU28), and $+4.5\,\%$ (India). The per-capita CO_2 emissions in 2016 were $1.1\,tC\,person^{-1}\,yr^{-1}$ for the globe and were 4.5 (USA), 2.0 (China), 1.9 (EU28), and 0.5 (India) $tC\,person^{-1}\,yr^{-1}$ for the four highest emitting countries (Fig. 5e).

Territorial emissions in Annex B countries (developed countries as per the Kyoto Protocol which initially had binding mitigation targets) decreased by $-0.2\,\%\,yr^{-1}$ on average during 1990–2015. Trends observed for consumption emissions were less monotonic, with $0.7\,\%\,yr^{-1}$ growth over 1990–2007 and a $-1.2\,\%\,yr^{-1}$ decrease over 2007–2015 (Fig. 5c). In non-Annex B countries (emerging economies and less developed countries as per the Kyoto Protocol with no binding mitigation commitments) territorial emissions grew at $4.6\,\%\,yr^{-1}$ during 1990–2015, while consumption emissions grew at $4.5\,\%\,yr^{-1}$. In 1990, 65 % of global territorial emissions were emitted in Annex B countries (32 % in non-Annex B and 2 % in bunker fuels used for international shipping and aviation), while in 2015 this had reduced to 37 % (60 % in non-Annex B and 3 % in bunker fuels). For consumption emissions, this split was 68 % in 1990 and 42 %

in 2015 (32 to 58 % in non-Annex B). The difference between territorial and consumption emissions (the net emission transfer via international trade) from non-Annex B to Annex B countries has increased from near zero in 1990 to 0.3 $GtC\,yr^{-1}$ around 2005 and remained relatively stable afterwards until the last year available (2015; Fig. 5). The increase in net emission transfers of 0.28 $GtC\,yr^{-1}$ between 1990 and 2015 compares with the emission reduction of 0.5 $GtC\,yr^{-1}$ in Annex B countries. These results show the importance of net emission transfer via international trade from non-Annex B to Annex B countries, as well as the stabilisation of emissions transfer when averaged over Annex B countries during the past decade. In 2015, the biggest emitters from a consumption perspective were China (23 % of the global total), USA (16 %), EU28 (12 %), and India (6 %).

The global CO_2 emissions from land-use change are estimated as 1.3 ± 0.5 GtC in 2016, as for the previous decade but with low confidence in the annual change.

3.3.2 Partitioning among the atmosphere, ocean, and land

The growth rate in atmospheric CO_2 concentration was 6.0 ± 0.2 GtC in 2016 (2.85 ± 0.09 ppm; Fig. 4; Dlugokencky and Tans, 2018). This is well above the 2007–2016 average of $4.7 \pm 0.1\,GtC\,yr^{-1}$ and reflects the large interannual variability in the growth rate of atmospheric CO_2 concentration associated with El Niño and La Niña events.

The estimated ocean CO_2 sink was $2.6 \pm 0.5\,GtC\,yr^{-1}$ in 2016, only marginally above 2015 according to the average of the ocean models but with large differences among estimates (Fig. 7).

The terrestrial CO_2 sink from the model ensemble was 2.7 ± 1.0 GtC in 2016, near the decadal average (Fig. 4) and consistent with constraints from the rest of the budget (Table 5).

The budget imbalance was -0.2 GtC in 2016, indicating a small overestimation of the emissions and/or underestimation of the sink for that year, with large uncertainties.

3.4 Global carbon budget projection for year 2017

3.4.1 CO_2 emissions

Emissions from fossil fuels and industry (E_{FF}) for 2017 are projected to increase by +2.0 % (range of 0.8 to +3.0 %; Table 7; Jackson et al., 2017; Peters et al., 2017). Our method contains several assumptions that could influence the estimate beyond the given range, and as such, it has an indicative value only. Within the given assumptions, global emissions would increase to 10.0 ± 0.5 GtC ($36.8 \pm 1.8\,GtCO_2$) in 2017. (At the time of going to press, the growth in E_{FF} for 2017 had been revised to 1.5 % (range of 0.7 to 2.4 %). A detailed update will be provided in the Global Carbon Budget 2018.)

For China, the expected change based on available data as of 19 September 2017 (see Sect. 2.1.4) is for an increase in emissions of +3.5 % (range of +0.7 to +5.4 %) in 2017 compared to 2016. This is based on estimated growth in coal (+3 %; the main fuel source in China), oil (+5.0 %), and natural gas (+11.7 %) consumption and a decline in cement production (−0.5 %). The uncertainty range considers the spread between different data sources and variances of typical revisions of Chinese data over time. The uncertainty in the growth rate of coal consumption also reflects uncertainty in the evolution of energy density and carbon content of coal.

For the USA, the EIA emissions projection for 2017 combined with cement data from USGS gives a decrease of −0.4 % (range of −2.7 to +1.9 %) compared to 2016.

For India, our projection for 2017 gives an increase of +2.0 % (range of 0.2 to +3.8 %) over 2016.

For the rest of the world (including EU28), the expected growth for 2017 is +1.6 % (range of 0.0 to +3.2 %). This is computed using the GDP projection for the world excluding China, USA, and India of 2.4 % made by the IMF (IMF, 2017) and a decrease in I_{FF} of $-1.1\,\%\,yr^{-1}$ which is the average from 2007 to 2016. The uncertainty range is based on the standard deviation of the interannual variability in I_{FF} during 2007–2016 of $\pm 1.0\,\%\,yr^{-1}$ and our estimate of uncertainty in the IMF's GDP forecast of ±0.5 %. Applying the method to the EU28 individually would give a projection of −0.2 % (range of −2.0 to +1.6 %) for EU28 and +2.3 % (range of +0.5 to +4.0 %) for the remaining countries, though the uncertainties grow with the level of disaggregation.

Emissions from land-use change (E_{LUC}) for 2017 are projected to remain in line with or slightly lower than their 2016 level of 1.3 GtC, based on active fire detections by October.

3.4.2 Partitioning among the atmosphere, ocean, and land

The 2017 growth in atmospheric CO_2 concentration (G_{ATM}) is projected to be 5.3 GtC with uncertainty around ±1 GtC (2.5 ± 0.5 ppm). Combining projected E_{FF}, E_{LUC}, and G_{ATM} suggests a combined land and ocean sink ($S_{LAND} + S_{OCEAN}$) of about 6 GtC for 2017. Although each term has large uncertainty, the oceanic sink S_{OCEAN} has generally low interannual variability and is likely to remain close to its 2016 value of around 2.6 GtC, leaving a rough estimated land sink S_{LAND} of around 3.4 GtC, near its decadal average (Table 5). This behaviour of the sink is expected due to the El Niño neutral conditions that prevailed during 2017, in stark contrast to the strong El Niño conditions in 2015 and 2016 that reduced the land sink. (At the time of going to press, the G_{ATM} for 2017 number had been revised to 2.38 ± 0.1 ppm with preliminary data to the end of 2017.)

Table 7. Comparison of the projection with realised emissions from fossil fuels and industry (E_{FF}). The "Actual" values are first estimate available using actual data, and the "Projected" values refer to the estimate made before the end of the year for each publication. Projections based on a different method from that described here during 2008–2014 are available in Le Quéré et al. (2016). All values are adjusted for leap years.

	World		China		USA		India		Rest of world	
	Projected	Actual	Projected	Actual	Projected	Actual	Projected	Actual	Projected	Actual
2015[a]	−0.6 % (−1.6 to 0.5)	0.06 %	−3.9 % (−4.6 to −1.1)	−0.7 %	−1.5 % (−5.5 to 0.3)	−2.5 %	–	–	1.2 % (−0.2 to 2.6)	1.2 %
2016[b]	−0.2 % (−1.0 to +1.8)	+0.18 %	−0.5 % (−3.8 to +1.3)	−0.3 %	−1.7 % (−4.0 to +0.6)	−2.1 %	–	–	+1.0 % (−0.4 to +2.5)	1.3 %
2017[c]	+2.0 % (+0.8 to +3.0)	–	+3.5 % (+0.7 to +5.4)	–	−0.4 % (−2.7 to +1.0)	–	+2.0 % (+0.2 to +3.8)	–	+1.6 % (0.0 to +3.2)	–

[a] Jackson et al. (2016) and Le Quéré et al. (2015a). [b] Le Quéré et al. (2016). [c] This study.

Table 8. Cumulative CO_2 for different time periods in gigatonnes of carbon (GtC). All uncertainties are reported as $\pm 1\sigma$. E_{LUC} and S_{OCEAN} have been revised to incorporate multiple estimates (Sect. 3.5), and, unlike previous versions of the global carbon budget, the terrestrial sink (S_{LAND}) is now estimated independently from the mean of the DGVM. Therefore, the table also shows the budget imbalance, which provides a measure of the discrepancies among the nearly independent estimates. Its uncertainty exceeds ±60 GtC. The method used here does not capture the loss of additional sink capacity from reduced forest cover, which is about 15 GtC and would exacerbate the budget imbalance (see Sect. 2.7.3). All values are rounded to the nearest 5 GtC and therefore columns do not necessarily add to zero.

Units of GtC	1750–2016	1850–2005	1959–2016	1870–2016	1870–2017[a]
Emissions					
Fossil fuels and industry (E_{FF})	420 ± 20	320 ± 15	345 ± 15	420 ± 20	430 ± 20
Land-use change emissions (E_{LUC})	225 ± 75	180 ± 60	75 ± 40	180 ± 60	180 ± 60
Total emissions	645 ± 80	500 ± 60	415 ± 45	600 ± 65	610 ± 65
Partitioning					
Growth rate in atmospheric CO_2 concentration (G_{ATM})[b]	270 ± 5	200 ± 5	185 ± 5	245 ± 5	250 ± 5
Ocean sink (S_{OCEAN})	160 ± 20	145 ± 20	95 ± 20	145 ± 20	150 ± 20
Terrestrial sink (S_{LAND})[c]	205 ± 55	155 ± 45	135 ± 35	190 ± 55	190 ± 55
Budget imbalance					
$B_{IM} = E_{FF} + E_{LUC} - (G_{ATM} + S_{OCEAN} + S_{LAND})$	(15)	(0)	(0)	(20)	(20)

[a] Using projections for year 2017 (Sect. 3.3).
[b] A small change was introduced from Le Quéré et al. (2016) to be consistent with the annual analysis, whereby the growth in atmospheric CO_2 concentration is calculated from the difference between concentrations at the end of the year (deseasonalised), rather than averaged over the year.
[c] Assuming S_{LAND} increases proportionally to G_{ATM} prior to 1860 when the DGVM estimates start.

3.5 Cumulative sources and sinks

Cumulative historical sources and sinks have been revised compared to the previous global carbon budgets. This version of the global carbon budget uses two updated bookkeeping models instead of one bookkeeping model only, uses two ocean sink data products instead of one data product only, and uses multiple DGVMs for the land sink instead of deriving the land sink from the residual of the other terms. As a result of these methodological changes, the cumulative emissions and their partitioning are significantly larger (by about 50 GtC) than our previous estimates. This large difference highlights the uncertainty in reconstructing historical emission sources and sinks, and this is noted through the large uncertainty associated with each term.

Cumulative fossil fuel and industry emissions for 1870–2016 were 420 ± 20 GtC for E_{FF} and, with the revised bookkeeping models, 180 ± 60 GtC for E_{LUC} (Table 8), for a total of 600 ± 65 GtC. The cumulative emissions from E_{LUC} are particularly uncertain, with a large spread among individual estimates of 135 GtC (Houghton) and 225 GtC (BLUE) for the two bookkeeping models and a range of 70 to 230 GtC for the 12 DGVMs. These estimates are consistent with indirect constraints from biomass observations (Li et al., 2017), but given the large spread a best estimate is difficult to ascertain.

With the revised methodology, emissions were partitioned among the atmosphere (245 ± 5 GtC), ocean (145 ± 20 GtC), and the land (190 ± 55 GtC). The use of nearly independent estimates for the individual terms shows a cumulative budget imbalance of 20 GtC during 1870–2016, which, if correct, suggests emissions are too high by the same proportion or the land or ocean sinks are underestimated. The imbalance originates largely from the large E_{LUC} during the mid-1920s and the mid-1960s which is unmatched by a growth in atmospheric CO_2 concentration as recorded in ice cores (Fig. 3). The known loss of additional sink capacity of about 15 GtC due to reduced forest cover has not been accounted for in our method and further exacerbates the budget imbalance (Sect. 2.7.3).

Cumulative emissions through to year 2017 increase to 610 ± 65 GtC (2235 ± 240 $GtCO_2$), with about 70 % contribution from E_{FF} and about 30 % contribution from E_{LUC}. Cumulative emissions and their partitioning for different periods are provided in Table 8.

Given the large revision in cumulative emissions, and its persistent uncertainties, we suggest extreme caution is needed if using cumulative emission estimate to determine the remaining carbon budget to stay below the given temperature limit (Rogelj et al., 2016). We suggest estimating the remaining carbon budget by integrating scenario data from the current time to some time in the future as proposed recently (Millar et al., 2017).

4 Discussion

Each year when the global carbon budget is published, each component for all previous years is updated to take into account corrections that are the result of further scrutiny and verification of the underlying data in the primary input data sets. The updates have generally been relatively small (Fig. 9). However, this year, we introduced a major methodological change to assess both S_{OCEAN} and S_{LAND} directly using multiple process models constrained by observations and to keep track of the budget imbalance separately. We also use multiple bookkeeping estimates for E_{LUC}. Therefore, the update compared to previous years has led to more substantial revisions, particularly concerning the mean S_{OCEAN}, the variability of S_{LAND}, and the trends in E_{LUC} (Fig. 9).

The budget imbalance provides a measure of the limitations in observations, in understanding or full representation of processes in models, and/or in the integration of the carbon budget components. The mismatch between the total emissions (red line in Fig. 3) and the total sinks (including the atmosphere) illustrates the need to explicitly identify imbalances separately rather than assigning residuals to the land sink as was done in the past. The mean global budget imbalance is close to zero and there is no trend over the entire time period (Fig. 4). However, the budget imbalance reaches as much as ±2 GtC yr^{-1} in individual years and ±0.6 GtC yr^{-1} in individual decades (Table 6). Such large budget imbalance limits our ability to verify reported emissions and limits our confidence in the underlying processes regulating the carbon cycle feedbacks with climate change (Peters et al., 2017).

Another semi-independent way to evaluate the carbon budget results is provided through the use of atmospheric and oceanic CO_2 data in data products (atmospheric inversions and pCO_2-based ocean flux products). The comparison shows a first-order consistency between pCO_2-based data products and process models but with substantial discrepancies, particularly for the allocation of the mean surface fluxes between the tropics and the Northern Hemisphere and for highlighting underestimated decadal variability in S_{OCEAN}. Understanding the causes of these discrepancies and further analysis of regional carbon budgets would provide additional information to quantify and improve our estimates, as has been shown by the project REgional Carbon Cycle Assessment and Processes (RECCAP; Canadell et al., 2012).

To help improve the global carbon budget components, we provide a list of the major known uncertainties for each component, defined as those uncertainties that have been a demonstrated effect of at least 0.3 GtC yr^{-1} (Table 9). We identified multiple sources of uncertainties for E_{LUC}, including in the land-cover and land-use change statistics, representation of management processes, and methodologies (e.g. Arneth et al., 2017). There are also multiple sources of uncertainties in S_{LAND} and S_{OCEAN}. When assessing S_{LAND} using DGVMs, uncertainties mostly related to the understanding and representation of processes as evidenced by the large model spread presented here. Similarly, when assessing S_{OCEAN} with GOBMs, multiple studies based on observations have shown variability in the ocean CO_2 sink larger than estimated by the models presented here, particularly related to representing the effects of variable ocean circulation in models (e.g. DeVries et al., 2017; Landschützer et al., 2015; Keeling and Manning, 2014). Finally, the quality of the energy statistics and of the emissions factors is the largest source of uncertainties for E_{FF}. There are no demonstrated uncertainties in G_{ATM} larger than 0.3 GtC yr^{-1}, although the conversion of the growth rate into a global annual flux assuming instantaneous mixing throughout the atmosphere introduces additional errors that have not yet been quantified. Multiple other sources of uncertainties have been identified (i.e. in cement emissions) that could add up to significant contributions but are unlikely to be the main sources of the budget imbalance.

Although multiple processes have been identified here, some will increase variability (e.g. land management processes, ocean circulation) while others might decrease it (e.g. better energy statistics, response to rainfall variability), and processes would not be all acting simultaneously. It is also possible that further yet unknown processes are not taken

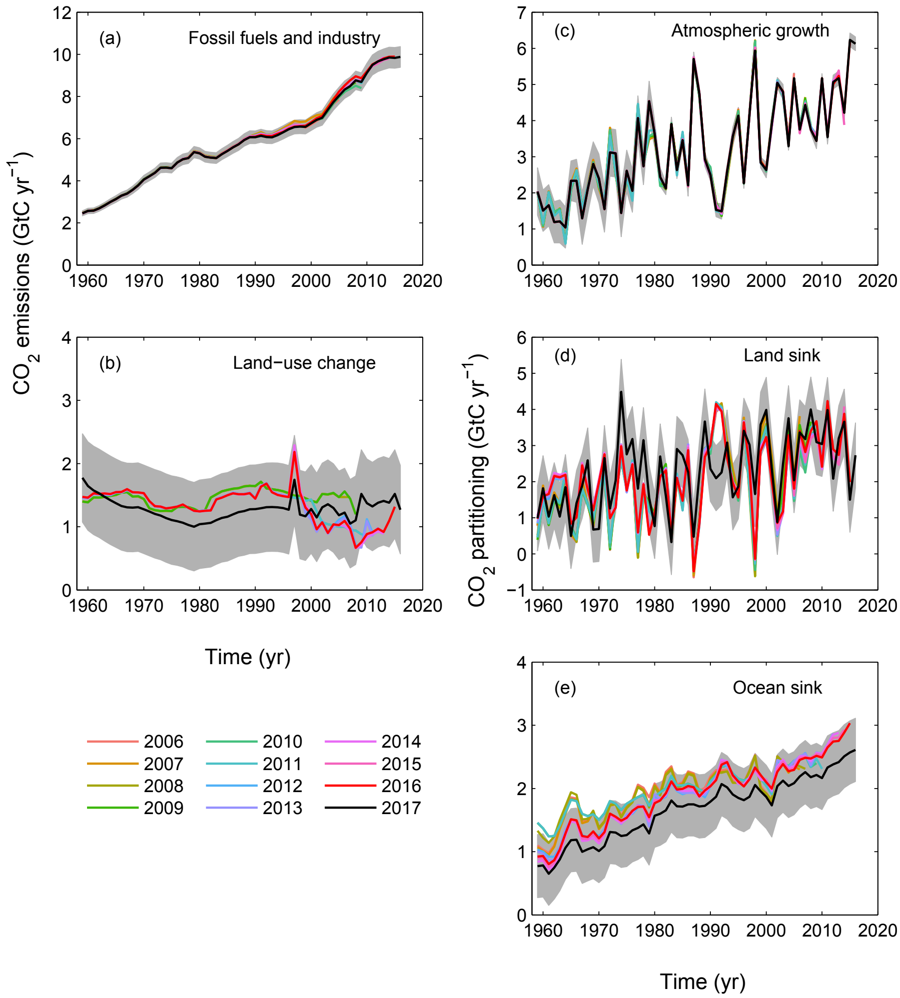

Figure 9. Comparison of global carbon budget components released annually by GCP since 2006. CO_2 emissions from **(a)** fossil fuels and industry (E_{FF}) and **(b)** land-use change (E_{LUC}), as well as their partitioning among **(c)** the atmosphere (G_{ATM}), **(d)** the land (S_{LAND}), and **(e)** the ocean (S_{OCEAN}). See legend for the corresponding years, and Table 3 for references. The budget year corresponds to the year when the budget was first released. All values are in GtC yr^{-1}. Grey shading shows the uncertainty bounds representing $\pm 1\sigma$ of the current global carbon budget.

into account. Better understanding the source of the carbon imbalance and how to resolve it is critical to progress further in the understanding of the contemporary carbon budget.

Although we have presented six components of the global carbon budget individually, different aggregations of terms are possible. In particular S_{LAND}, E_{LUC}, and B_{IM} could be aggregated into land fluxes and total uncertainty, as traditionally done, which would result in generally lower uncertainty compared to each term individually (see Table 5). This information is limited in usefulness, however, as it mixes direct and indirect processes and bring in errors from other components and hence the signal becomes difficult to interpret. However, providing a realistic assessment of uncertainties for S_{LAND} and E_{LUC} is also difficult. Here we have used the model spread as a measure of uncertainty, which may be, on the one hand, underestimated because it includes only partly uncertainty in the underlying observations and, on the other hand, overestimated as it includes artificial spread from different boundary limits among models. Therefore, further work is needed not only to better quantify the fluxes but also to better describe and quantify the uncertainty and reduce them where possible.

There are many more uncertainties affecting the annual estimates compared to the mean and trend, some of which could be improved with better data. Of the various terms in the global budget, only the emissions from fossil fuels and industry and the growth rate in atmospheric CO_2 concentration are based primarily on empirical inputs supporting annual estimates in this carbon budget. pCO_2-based flux products for the ocean CO_2 sink and atmospheric inversions based on ob-

Table 9. Major known sources of uncertainties in each component of the global carbon budget, defined as input data or processes that have a demonstrated effect of at least 0.3 $GtC\,yr^{-1}$.

Source of uncertainty	Timescale (years)	Location	Status	Evidence
Emissions from fossil fuels and industry (E_{FF}; Sect. 2.1)				
energy statistics	annual to decadal	mainly China	see Sect. 2.1	Korsbakken et al. (2016)
carbon content of coal	decadal	mainly China	see Sect. 2.1	Liu et al. (2015)
Emissions from land-use change (E_{LUC}; Sect. 2.2)				
land-cover and land-use change statistics	continuous	global, in particular tropics	see Sect. 2.2	Houghton et al. (2012)
sub-grid-scale transitions	annual to decadal	global	see Table 4	Wilkenskjeld et al. (2014)
vegetation biomass	annual to decadal	global, in particular tropics	see Table 4	Houghton et al. (2012)
wood and crop harvest	annual to decadal	global; SE Asia	see Table 4	Arneth et al. (2017)
peat burning[a]	multi-decadal trend	global	see Table 4	van der Werf et al. (2010)
loss of additional sink capacity	multi-decadal trend	global	not included; Sect. 2.7.3	Gitz and Ciais (2003)
Atmospheric growth rate (G_{ATM}) → no demonstrated uncertainties larger than ±0.3 $GtC\,yr^{-1}$[b]				
Ocean sink (S_{OCEAN})				
variability in oceanic circulation[c]	semi-decadal to decadal	global, in particular Southern Ocean	see Sect. 2.4.2	DeVries et al. (2017)
anthropogenic changes in nutrient supply	multi-decadal trend	global	not included	Duce et al. (2008)
Land sink (S_{LAND})				
strength of CO_2 fertilisation	multi-decadal trend	global	see Sect. 2.5	Wenzel et al. (2016)
response to variability in temperature and rainfall	annual to decadal	global, in particular tropics	see Sect. 2.5	Cox et al. (2013)
nutrient limitation and supply	multi-decadal trend	global	see Sect. 2.5	Zaehle et al. (2011)
response to diffuse radiation	annual	global	see Sect. 2.5	Mercado et al. (2009)

[a] As result of interactions between land use and climate.
[b] The uncertainties in G_{ATM} have been estimated as ±0.2 $GtC\,yr^{-1}$, although the conversion of the growth rate into a global annual flux assuming instantaneous mixing throughout the atmosphere introduces additional errors that have not yet been quantified.
[c] Could in part be due to uncertainties in atmospheric forcing (Swart et al., 2014).

served atmospheric CO_2 concentrations provide new ways to evaluate the model results, but there are still large discrepancies among estimates. Given the growing reliance on process models and $p$$CO_2$-based flux products in our global carbon budget, it is critical that data-based metrics are developed and used to inform the selection of models and the improvement of their process representation in the long term.

5 Data availability

The data presented here are made available in the belief that their wide dissemination will lead to greater understanding and new scientific insights of how the carbon cycle works, how humans are altering it, and how we can mitigate the resulting human-driven climate change. The free availability of these data does not constitute permission for publication of the data. For research projects, if the data are essential to the work, or if an important result or conclusion depends on the data, co-authorship may need to be considered. Full contact details and information on how to cite the data included in the GCP (2017) release are given at the top of each page in the accompanying database and summarised in Table 2.

The accompanying database includes two Excel files organised in the following spreadsheets (accessible with the free viewer at http://www.microsoft.com/en-us/download/details.aspx?id=10).

File Global_Carbon_Budget_2017v1.0.xlsx includes the following:

1. Summary

2. The global carbon budget (1959–2016)

3. Global CO_2 emissions from fossil fuels and cement production by fuel type, and the per-capita emissions (1959–2016)

4. CO_2 emissions from land-use change from the individual methods and models (1959–2016)

5. Ocean CO_2 sink from the individual ocean models and $p$$CO_2$-based products (1959–2016)

6. Terrestrial CO_2 sink from the DGVMs (1959–2016)

7. Additional information on the carbon balance prior to 1959 (1750–2016)

File National_Carbon_Emissions_2017v1.0.xlsx includes the following:

1. Summary

2. Territorial country CO_2 emissions from fossil fuels and industry (1959–2016) from CDIAC, extended to 2016 using BP data

3. Territorial country CO_2 emissions from fossil fuels and industry (1959–2016) from CDIAC with UNFCCC data overwritten where available, extended to 2016 using BP data

4. Consumption country CO_2 emissions from fossil fuels and industry and emissions transfer from the international trade of goods and services (1990–2015) using CDIAC/UNFCCC data (worksheet 3 above) as reference

5. Emissions transfers (consumption minus territorial emissions; 1990–2015)

6. Country definitions

7. Details of disaggregated countries

8. Details of aggregated countries

National emissions data are also available from the Global Carbon Atlas (http://globalcarbonatlas.org).

6 Conclusions

The estimation of global CO_2 emissions and sinks is a major effort by the carbon cycle research community that requires a combination of measurements and compilation of statistical estimates and results from models. The delivery of an annual carbon budget serves two purposes. First, there is a large demand for up-to-date information on the state of the anthropogenic perturbation of the climate system and its underpinning causes. A broad stakeholder community relies on the data sets associated with the annual carbon budget including scientists, policy makers, businesses, journalists, and the broader society increasingly engaged in adapting to and mitigating human-driven climate change. Second, over the last decade we have seen unprecedented changes in the human and biophysical environments (e.g. changes in the growth of fossil fuel emissions, ocean temperatures, and strength of the sink), which call for frequent assessments of the state of the planet and, by implication, a better understanding of the future evolution of the carbon cycle. Both the ocean and the land surface presently remove a large fraction of anthropogenic emissions. Any significant change in the function of carbon sinks is of great importance to climate policymaking, as they affect the excess CO_2 remaining in the atmosphere and therefore the compatible emissions for any climate stabilisation target. Better constraints of carbon cycle models against contemporary data sets raise the capacity for the models to become more accurate at future projections. This all requires more frequent, robust, and transparent data sets and methods that can be scrutinised and replicated. This paper via "living data" will help to keep track of new budget updates.

Appendix A

Table A1. Comparison of the processes included (Y) or not (N) in the bookkeeping and dynamic global vegetation models for their estimates of E_{LUC} and S_{LAND}. See Table 4 for model references. All models include deforestation and forest regrowth after abandonment of agriculture (or from afforestation activities on agricultural land).

(a)	Bookkeeping models		DGVMs														
	H&N2017	BLUE	CABLE	CLASS-CTEM	CLM4.5(BGC)	DLEM	ISAM	JSBACH[j]	JULES	LPJ-GUESS[j]	LPJ	LPX-Bern	OCN	ORCHIDEE	ORCHIDEE-MICT	SDGVM	VISIT[j]
Processes relevant for E_{LUC}																	
Wood harvest and forest degradation[a]	Y	Y	Y	N	Y	Y	Y		N		N	N[d]	Y	Y	N	N	
Shifting cultivation/ subgrid scale transitions	N[b]	Y	Y	N	Y	N	N		N		N	N[d]	N	N	N	N	
Cropland harvest	Y[i]	Y[i]	N	L	N	Y	Y		N		Y	Y	Y	Y	Y	Y	
Peat fires	Y	Y	N	N	Y	N	N		N		N	N	N	N	N	N	
Fire as a management tool	Y[i]	Y[i]	N	N	N	N	N		N		N	N	N	N	N	N	
N fertilisation	Y[i]	Y[i]	N	N	N	Y	Y		N		N	Y	Y	N	N	N	
Tillage	Y[i]	Y[i]	N	Y[f]	N	N	N		N		N	N	N	Y[h]	Y[h]	N	
Irrigation	Y[i]	Y[i]	N	N	N	Y	Y		N		N	N	N	N	N	N	
Wetland drainage	Y[i]	Y[i]	N	N	N	N	N		N		N	N	N	N	N	N	
Erosion	Y[i]	Y[i]	N	N	N	N	N		N		N	N	N	N	N	N	
Southeast Asia peat drainage	Y	Y	N	N	N	N	N		N		N	N	N	N	N	N	
Grazing and mowing harvest	Y[i]	Y[i]	N	N	N	N	Y		N		Y	N	N	N	N	N	
Processes relevant also for S_{LAND}																	
Fire simulation	US only	N	N	Y	Y	Y	N	Y	N	Y	Y	Y	N	N	Y	Y	Y
Climate and variability	N	N	Y	Y	Y	Y	Y	Y	Y	Y	Y	Y	Y	Y	Y	Y	Y
CO_2 fertilisation	N[g]	N[g]	Y	Y	Y	Y	Y	Y	Y	Y	Y	Y	Y	Y	Y	Y	Y
Carbon–nitrogen interactions, including N deposition	N[i]	N[i]	Y	N[e]	Y	Y	Y	N	N	Y	N	Y	Y	N[e]	N	Y[c]	N

[a] Refers to the routine harvest of established managed forests rather than pools of harvested products.
[b] No back and forth transitions between vegetation types at the country level, but if forest loss based on FRA exceeded agricultural expansion based on FAO, then this amount of area.
[c] Limited. Nitrogen uptake is simulated as a function of soil C, and Vcmax is an empirical function of canopy N. Does not consider N deposition.
[d] Available but not active for comparability between the two LU forcings.
[e] Although C–N cycle interactions are not represented, the model includes a parameterisation of down-regulation of photosynthesis as CO_2 increases to emulate nutrient constraints (Arora et al., 2009).
[f] Tillage is represented over croplands by increased soil carbon decomposition rate and reduced humification of litter to soil carbon.
[g] Bookkeeping models include effect of CO_2 fertilisation as captured by observed carbon densities, but not as an effect transient in time.
[h] 20 % reduction of active soil organic carbon (SOC) pool turnover time for C3 crop and 40 % reduction for C4 crops.
[i] Process captured implicitly by use of observed carbon densities.
[j] Three DGVMs were excluded from the E_{LUC} estimate due to an initial peak of E_{LUC} emissions caused by a cold start of shifting cultivation in 1860.

Table A2. Comparison of the processes included in the global ocean biogeochemistry models for their estimates of S_{OCEAN}. See Table 4 for model references.

	CCSM-BEC	CSIRO	NorESM-OC	MITgcm-REcoM2	MPIOM-HAMOCC	NEMO-PISCES (CNRM)	NEMO-PISCES (IPSL)	NEMO-PlankTOM5
Atmospheric forcing	NCEP	JRA-55	CORE-I (spin up)/NCEP with CORE-II corrections	JRA-55	ERA-20C	NCEP	NCEP	NCEP
Initialisation of carbon chemistry	GLODAP	GLODAP + spin up 1000+ years	GLODAP v1 + spin up 1000 years	GLODAP, then spin up 116 years (2 cycles JRA-55)	from previous model runs with > 1000 years spin-up	spin up 3000 years offline + 300 years online	GLODAP from 1948 onwards	GLODAP + spin up 30 years
Physical ocean model	POP Version *1.4.3*	MOM5	MICOM	MITgcm 65n	MPIOM	NEMOv2.4-ORCA1L42	NEMOv3.2-ORCA2L31	NEMOv2.3-ORCA2
Resolution	3.6° long, 0.8 to 1.8° lat	1° × 1° with enhanced resolution at the tropics and high-lat S. Ocean; 50 levels	1° long, 0.17 to 0.25 lat; 51 isopycnic layers + 2 bulk mixed layer	2° long, 0.38–2° lat; 30 levels	1.5°; 40 levels	2° long, 0.3 to 1° lat; 42 levels, 5 m at surface	2° long, 0.3 to 1.5° lat; 31 levels	2° long, 0.3 to 1.5° lat; 31 levels

Table A3. Comparison of the inversion setup and input fields for the atmospheric inversions. Atmospheric inversions see the full CO_2 fluxes, including the anthropogenic and pre-industrial fluxes. Hence, they need to be adjusted for the pre-industrial flux of CO_2 from the land to the ocean that is part of the natural carbon cycle before they can be compared with S_{OCEAN} and S_{LAND} from process models. See Table 4 for references.

	CarbonTracker Europe (CTE)	Jena CarboScope	CAMS
Version number	CTE2017-FT	s85oc_v4.1s	v16r1
Observations			
Atmospheric observations	Hourly resolution (well-mixed conditions) ObsPack GLOBALVIEWplus v2.1 and NRTv3.3[a]	Flasks and hourly (outliers removed by 2σ criterion)	Daily averages of well-mixed conditions – ObsPack GLOBALVIEW-plus v2.1 and NRT v3.2.3, WD-CGG, RAMCES, and ICOS ATC
Prior fluxes			
Biosphere and fires	SiBCASA-GFED4s[b]	Zero	ORCHIDEE (climatological), GFEDv4 and GFAS
Ocean	Ocean inversion by Jacobson et al. (2007)	pCO$_2$-based ocean flux product oc_v1.5 (update of Rödenbeck et al., 2014)	Landschützer et al. (2015)
Fossil fuels	EDGAR and IER, scaled to CDIAC	CDIAC (extended after 2013 with GCP totals)	EDGAR scaled to CDIAC
Transport and optimisation			
Transport model	TM5	TM3	LMDZ v5A
Weather forcing	ECMWF	NCEP	ECMWF
Resolution (degrees)	Global: 3° × 2°, Europe: 1° × 1°, North America: 1° × 1°	Global: 4° × 5°	Global: 3.75° × 1.875°
Optimisation	Ensemble Kalman filter	Conjugate gradient (re-orthonormalisation)	Variational

[a] CarbonTracker Team (2017), GLOBALVIEW (2016). [b] van der Velde et al. (2014).

Table A4. Attribution of fCO_2 measurements for the year 2016 included in SOCAT v5 (Bakker et al., 2016) to inform ocean pCO_2-based flux products.

Platform (vessel or time-series station)	Regions	No. of samples	Principal investigators	Number of data sets
Allure of the Seas	North Atlantic, Tropical Atlantic	71 744	Wanninkhof, R.; Pierrot, D.	36
Atlantic Cartier	North Atlantic	44 302	Steinhoff, T.; Körtzinger, A.; Becker, M.; Wallace, D.	12
Aurora Australis	Southern Ocean	43 885	Tilbrook, B.	2
Benguela Stream	North Atlantic, Tropical Atlantic	137 902	Schuster, U.; Watson, A. J.	21
Cap Blanche	North Pacific, Tropical Pacific	17 913	Cosca, C.; Alin, S.; Feely, R.; Herndon, J.	3
Cap San Lorenzo	North Atlantic, Tropical Atlantic	9126	Lefèvre, N.	3
Colibri	North Atlantic, Tropical Atlantic	27 780	Lefèvre, N.	6
Equinox	North Atlantic, Tropical Atlantic	97 106	Wanninkhof, R.; Pierrot, D.	35
F.G. Walton Smith	North Atlantic, Tropical Atlantic	43 222	Millero, F.; Wanninkhof, R.	16
Finnmaid	North Atlantic	34 303	Rehder, G.; Glockzin, M.	3
G.O. Sars	Arctic, North Atlantic	109 125	Skjelvan, I.	13
GAKOA_149W_60N	North Pacific	488	Cross, J.; Mathis, J.; Monacci, N.; Musielewicz, S.; Maenner, S.; Osborne, J.	1
Gordon Gunter	North Atlantic, Tropical Atlantic	59 310	Wanninkhof, R.; Pierrot, D.	13
Henry B. Bigelow	North Atlantic	61 021	Wanninkhof, R.	13
Investigator	Southern Ocean, Tropical Pacific	108 721	Tilbrook, B.	3
Laurence M. Gould	Southern Ocean	26 150	Sweeney, C.; Takahashi, T.; Newberger, T.; Sutherland, S. C.; Munro, D.	5
Marion Dufresne	Southern Ocean	3214	Metzl, N.; Lo Monaco, C.	1
New Century 2	North Atlantic, North Pacific, Tropical Pacific	25 222	Nakaoka, S.	15
Nuka Arctica	North Atlantic	47 392	Becker, M.; Olsen, A.; Omar, A.; Johannessen, T.	12
Polarstern	Arctic, North Atlantic, Southern Ocean, Tropical Atlantic	164 407	van Heuven, S.; Hoppema, M.	5
Roger Revelle	Indian Ocean, Southern Ocean, Tropical Pacific	93 689	Wanninkhof, R.; Pierrot, D.	8
Ronald H. Brown	North Pacific, Tropical Pacific	52 267	Wanninkhof, R.; Pierrot, D.	8
S.A. Agulhas II	Southern Ocean	27 851	Monteiro, P. M. S.; Joubert, W. R.	
Sarmiento de Gamboa	North Atlantic, Southern Ocean, Tropical Atlantic	16 122	Padin, X. A.	2
Savannah	North Atlantic	2803	Cai, W.-J.; Reimer, J. J.	1
SEAK	North Pacific	271	Cross, J.; Mathis, J.; Monacci, N.; Musielewicz, S.; Maenner, S.; Osborne, J.	1
Skogafoss	North Atlantic	22 541	Wanninkhof, R.; Pierrot, D.	4
Tangaroa	Southern Ocean	118 997	Currie, K.	7
Thomas G. Thompson	North Pacific, Tropical Pacific	14 656	Alin, S.; Cosca, C.; Herndon, J.; Feely, R.	1
Trans Future 5	North Pacific, Tropical Pacific, Southern Ocean	23 087	Nakaoka, S.; Nojiri, Y.	21
UNH *Gulf Challenger*	North Atlantic	2984	Hunt, C. W.	3

Table A5. Funding supporting the production of the various components of the global carbon budget in addition to the authors' supporting institutions (see also acknowledgements).

Funder and grant number (where relevant)	Author initials
Australia, Integrated Marine Observing System (IMOS)	BT
Australian National Environment Science Program (NESP)	JGC, VH
EC H2020 European Research Council (ERC) (QUINCY; grant no. 647204).	SZ
EC H2020 ERC Synergy grant (IMBALANCE-P; grant no. ERC-2013-SyG-610028)	DZ
EC H2020 project CRESCENDO (grant no. 641816)	PF, RS
EC H2020-MSCA-IF-2015 ERC (FIBER; grant no. 701329)	BDS
EC FP7 project HELIX (grant no. 603864)	PF, RAB, SS
EU FP7 project LUC4C (grant no. 603542)	PF, MK, SS
French Institut National des Sciences de l'Univers (INSU) and Institut Paul Emile Victor (IPEV), Sorbonne Universités (UPMC, Univ Paris 06)	NM
German Federal Ministry for Education and Research (BMBF)	GR, AK, SVH
German Federal Ministry of Transport and Digital Infrastructure (BMVI)	AK, SVH
German Research Foundation's Emmy Noether Programme (grant no. PO1751/1-1)	JEMSN, JP
IRD, Integrated Carbon Observation System (ICOS) RI	NL
Japan National Institute for Environmental Studies (NIES), Ministry of Environment (MOE)	SK, YN
NASA LCLUC programme (grant no. NASA NNX14AD94G)	AJ
Netherlands Organisation for Scientific Research (NWO) Veni grant (016.Veni.171.095)	IvdLL
Netherlands Organisation for Scientific Research (NWO) Veni grant (016.Veni.158.021)	KKG
New Zealand National Institute of Water and Atmospheric Research (NIWA) Core Funding	KC
Norwegian Research Council, Norwegian Environmental Agency	IS
Norwegian Research Council (ICOS 245927)	BP, MB
Norwegian Research Council (grant no. 229771)	JS
Norwegian Research Council (grant no. 209701)	RMA, JIK, GPP
RI Integrated Carbon Observation System (ICOS)	AW, GR, AK, SVH, IS, BP, MB
South Africa Council for Scientific and Industrial Research, Department of Science and Technology (DST)	PMSM
Swiss National Science Foundation (grant no.200020_172476)	SL
The Copernicus Atmosphere Monitoring Service, implemented by the European Centre for Medium-Range Weather Forecasts (ECMWF) on behalf of the European Commission	FC
UK BEIS/Defra Met Office Hadley Centre Climate Programme (grant no. GA01101)	RAB
UK Natural Environment Research Council (SONATA: grant no. NE/P021417/1)	CLQ, OA
UK NERC, EU FP7, EU Horizon2020	AW
USA Department of Energy, Office of Science and BER programme (grant no. DE-SC000 0016323)	ATJ
USA National Oceanographic and Atmospheric Administration (NOAA) Ocean Acidification Program (OAP) NA16NOS0120023	CWH
USA National Science Foundation (grant no. OPP 1543457)	DRM
USA National Science Foundation (grant no. AGS 12-43071)	AKJ
Computing resources	
Grand Équipement National de Calcul Intensif (allocation x2016016328), France	NV
HPC resources of TGCC under allocation 2017-A0010102201 made by GENCI	FC
Météo-France/DSI supercomputing centre	RS
Netherlands Organisation for Scientific Research (NWO) (SH-312-14)	IvdLL
UEA High Performance Computing Cluster, UK	ODA, CLQ

Competing interests. The authors declare that they have no conflict of interest.

Acknowledgements. We thank all people and institutions who provided the data used in this carbon budget; Clare Enright, Wouter Peters, and Shijie Shu for their involvement in the development, use, and analysis of the models and data products used here; and Fortunat Joos, Samar Khatiwala, and Timothy DeVries for providing historical data. We thank Ed Dlugokencky, who provided the atmospheric CO_2 measurements used here; Camilla Stegen Landa, Christophe Bernard, and Steve Jones of the Bjerknes Climate Data Centre and the ICOS Ocean Thematic Centre data management at the University of Bergen, who helped with gathering information from the SOCAT community; and all those involved in collecting and providing oceanographic CO_2 measurements used here, in particular for the new ocean data for year 2016 (see Table A4). This is NOAA-PMEL contribution number 4728. We thank the institutions and funding agencies responsible for the collection and quality control of the data included in SOCAT, as well as the support of the International Ocean Carbon Coordination Project (IOCCP), the Surface Ocean Lower Atmosphere Study (SOLAS), and the Integrated Marine Biogeochemistry and Ecosystem Research (IMBER) programme. We thank FAO and its member countries for the collection, analysis, and dissemination of national data through FAOSTAT.

Finally, we thank all funders who have supported the individual and joint contributions to this work (see Appendix Table A5), as well as Martin Heimann, Han Dolman, and Britton Stephens, who reviewed the manuscript and previous versions, and the many researchers who have provided feedback during the GCP community consultation held at the 10th International CO_2 Conference in Interlaken, Switzerland, and elsewhere.

Edited by: David Carlson
Reviewed by: Britton Stephens, Albertus J. (Han) Dolman, and one anonymous referee

References

Andres, R. J., Boden, T. A., Bréon, F.-M., Ciais, P., Davis, S., Erickson, D., Gregg, J. S., Jacobson, A., Marland, G., Miller, J., Oda, T., Olivier, J. G. J., Raupach, M. R., Rayner, P., and Treanton, K.: A synthesis of carbon dioxide emissions from fossil-fuel combustion, Biogeosciences, 9, 1845–1871, https://doi.org/10.5194/bg-9-1845-2012, 2012.

Andres, R. J., Boden, T., and Higdon, D.: A new evaluation of the uncertainty associated with CDIAC estimates of fossil fuel carbon dioxide emission, Tellus B, 66, 23616, https://doi.org/10.3402/tellusb.v66.23616, 2014.

Andrew, R. M.: Global CO_2 emissions from cement production, Earth Syst. Sci. Data, 10, 195–217, https://doi.org/10.5194/essd-10-195-2018, 2018.

Andrew, R. M. and Peters, G. P.: A multi-region input-output table based on the Global Trade Analysis Project Database (GTAP-MRIO), Econ. Syst. Res., 25, 99–121, 2013.

Archer, D., Eby, M., Brovkin, V., Ridgwell, A., Cao, L., Mikolajewicz, U., Caldeira, K. M., K., Munhoven, G., Montenegro, A., and Tokos, K.: Atmospheric Lifetime of Fossil Fuel Carbon Dioxide, Annu. Rev. Earth Pl. Sc., 37, 117–134, 2009.

Arneth, A., Sitch, S., Pongratz, J., Stocker, B. D., Ciais, P., Poulter, B., Bayer, A. D., Bondeau, A., Calle, L., Chini, L. P., Gasser, T., Fader, M., Friedlingstein, P., Kato, E., Li, W., Lindeskog, M., Nabel, J. E. M. S., Pugh, T. A. M., Robertson, E., Viovy, N., Yue, C., and Zaehle, S.: Historical carbon dioxide emissions caused by land-use changes are possibly larger than assumed, Nat. Geosci., 10, 79–84, 2017.

Arora, V. K., Boer, G. J., Christian, J. R., Curry, C. L., Denman, K. L., Zahariev, K., Flato, G. M., Scinocca, J. F., Merryfield, W. J., and Lee, W. G.: The Effect of Terrestrial Photosynthesis Down Regulation on the Twentieth-Century Carbon Budget Simulated with the CCCma Earth System Model, J. Climate, 22, 6066–6088, 2009.

Aumont, O. and Bopp, L.: Globalizing results from ocean in situ iron fertilization studies, Global Biogeochem. Cy., 20, GB2017, https://doi.org/10.1029/2005GB002591, 2006.

Bakker, D. C. E., Pfeil, B., Landa, C. S., Metzl, N., O'Brien, K. M., Olsen, A., Smith, K., Cosca, C., Harasawa, S., Jones, S. D., Nakaoka, S.-I., Nojiri, Y., Schuster, U., Steinhoff, T., Sweeney, C., Takahashi, T., Tilbrook, B., Wada, C., Wanninkhof, R., Alin, S. R., Balestrini, C. F., Barbero, L., Bates, N. R., Bianchi, A. A., Bonou, F., Boutin, J., Bozec, Y., Burger, E. F., Cai, W.-J., Castle, R. D., Chen, L., Chierici, M., Currie, K., Evans, W., Featherstone, C., Feely, R. A., Fransson, A., Goyet, C., Greenwood, N., Gregor, L., Hankin, S., Hardman-Mountford, N. J., Harlay, J., Hauck, J., Hoppema, M., Humphreys, M. P., Hunt, C. W., Huss, B., Ibánhez, J. S. P., Johannessen, T., Keeling, R., Kitidis, V., Körtzinger, A., Kozyr, A., Krasakopoulou, E., Kuwata, A., Landschützer, P., Lauvset, S. K., Lefèvre, N., Lo Monaco, C., Manke, A., Mathis, J. T., Merlivat, L., Millero, F. J., Monteiro, P. M. S., Munro, D. R., Murata, A., Newberger, T., Omar, A. M., Ono, T., Paterson, K., Pearce, D., Pierrot, D., Robbins, L. L., Saito, S., Salisbury, J., Schlitzer, R., Schneider, B., Schweitzer, R., Sieger, R., Skjelvan, I., Sullivan, K. F., Sutherland, S. C., Sutton, A. J., Tadokoro, K., Telszewski, M., Tuma, M., van Heuven, S. M. A. C., Vandemark, D., Ward, B., Watson, A. J., and Xu, S.: A multi-decade record of high-quality fCO_2 data in version 3 of the Surface Ocean CO_2 Atlas (SOCAT), Earth Syst. Sci. Data, 8, 383–413, https://doi.org/10.5194/essd-8-383-2016, 2016.

Ballantyne, A. P., Alden, C. B., Miller, J. B., Tans, P. P., and White, J. W. C.: Increase in observed net carbon dioxide uptake by land and oceans during the last 50 years, Nature, 488, 70–72, 2012.

Ballantyne, A. P., Andres, R., Houghton, R., Stocker, B. D., Wanninkhof, R., Anderegg, W., Cooper, L. A., DeGrandpre, M., Tans, P. P., Miller, J. B., Alden, C., and White, J. W. C.: Audit of the global carbon budget: estimate errors and their impact on uptake uncertainty, Biogeosciences, 12, 2565–2584, https://doi.org/10.5194/bg-12-2565-2015, 2015.

Bauer, J. E., Cai, W.-J., Raymond, P. A., Bianchi, T. S., Hopkinson, C. S., and Regnier, P. A. G.: The changing carbon cycle of the coastal ocean, Nature, 504, 61–70, 2013.

Best, M. J., Pryor, M., Clark, D. B., Rooney, G. G., Essery, R. L. H., Ménard, C. B., Edwards, J. M., Hendry, M. A., Porson, A., Gedney, N., Mercado, L. M., Sitch, S., Blyth, E., Boucher, O., Cox, P. M., Grimmond, C. S. B., and Harding, R. J.: The Joint UK Land Environment Simulator (JULES), model description –

Part 1: Energy and water fluxes, Geosci. Model Dev., 4, 677–699, https://doi.org/10.5194/gmd-4-677-2011, 2011.

Betts, R. A., Jones, C. D., Knight, J. R., Keeling, R. F., and Kennedy, J. J.: El Nino and a record CO_2 rise, Nature Clim. Change, 6, 806–810, 2016.

Boden, T. A., Marland, G., and Andres, R. J.: Global, Regional, and National Fossil-Fuel CO_2 Emissions, Oak Ridge National Laboratory, U.S. Department of Energy, Oak Ridge, Tenn., USA, available at: http://cdiac.ornl.gov/trends/emis/overview_2014.html, last access: 28 June 2017.

BP: BP Statistical Review of World Energy June 2017, available at: https://www.bp.com/content/dam/bp/en/corporate/pdf/energy-economics/statistical-review-2017/bp-statistical-review-of-world-energy-2017-full-report.pdf, last access: 13 June 2017.

Bruno, M. and Joos, F.: Terrestrial carbon storage during the past 200 years: A monte carlo analysis of CO_2 data from ice core and atmospheric measurements, Global Biogeochem. Cy., 11, 111–124, 1997.

Buitenhuis, E. T., Rivkin, R. B., Sailley, S., and Le Quéré, C.: Biogeochemical fluxes through microzooplankton, Global Biogeochem. Cy., 24, GB4015, https://doi.org/10.1029/2009GB003601, 2010.

Canadell, J. G., Le Quéré, C., Raupach, M. R., Field, C. B., Buitenhuis, E. T., Ciais, P., Conway, T. J., Gillett, N. P., Houghton, R. A., and Marland, G.: Contributions to accelerating atmospheric CO_2 growth from economic activity, carbon intensity, and efficiency of natural sinks, P. Natl. Acad. Sci. USA, 104, 18866–18870, 2007.

Canadell, J. G., Ciais, P., Sabine, C., and Joos, F. (Eds.): REgional Carbon Cycle Assessment and Processes (RECCAP), Biogeosciences, http://www.biogeosciences.net/special_issue107.html, 2012.

CarbonTracker Team: Compilation of near real time atmospheric carbon dioxide data provided by NOAA and EC; obspack_co2_1_NRT_v3.3_2017-04-19; NOAA Earth System Research Laboratory, Global Monitoring Division, https://doi.org/10.15138/G3G01J, 2017.

CCIA: Analysis of current economic trend of coal in China, China Coal Industry Association (CCIA), 2017, available at: http://www.coalchina.org.cn/detail/17/07/24/00000025/content.html, last access: 15 September 2017 (in Chinese).

CEA: Daily Coal – Archive, Central Electricity Authority (CEA), 2017, available at: http://www.cea.nic.in/dailyarchive.html, last access: 2 October 2017.

Chevallier, F.: On the statistical optimality of CO_2 atmospheric inversions assimilating CO_2 column retrievals, Atmos. Chem. Phys., 15, 11133–11145, https://doi.org/10.5194/acp-15-11133-2015, 2015.

Chevallier, F., Fisher, M., Peylin, P., Serrar, S., Bousquet, P., Bréon, F.-M., Chédin, A., and Ciais, P.: Inferring CO_2 sources and sinks from satellite observations: Method and application to TOVS data, J. Geophys. Res., 110, D24309, https://doi.org/10.1029/2005JD006390, 2005.

Ciais, P., Sabine, C., Govindasamy, B., Bopp, L., Brovkin, V., Canadell, J., Chhabra, A., DeFries, R., Galloway, J., Heimann, M., Jones, C., Le Quéré, C., Myneni, R., Piao, S., and Thornton, P.: Chapter 6: Carbon and Other Biogeochemical Cycles, in: Climate Change 2013 The Physical Science Basis, edited by: Stocker, T., Qin, D., and Platner, G.-K., Cambridge University Press, Cambridge, UK, 2013.

CIL: Production and Offtake Performance of CIL and Subsidiary Companies, Coal India Limited, 2017, available at: https://www.coalindia.in/en-us/performance/physical.aspx, last access: 2 October 2017.

Clark, D. B., Mercado, L. M., Sitch, S., Jones, C. D., Gedney, N., Best, M. J., Pryor, M., Rooney, G. G., Essery, R. L. H., Blyth, E., Boucher, O., Harding, R. J., Huntingford, C., and Cox, P. M.: The Joint UK Land Environment Simulator (JULES), model description – Part 2: Carbon fluxes and vegetation dynamics, Geosci. Model Dev., 4, 701–722, https://doi.org/10.5194/gmd-4-701-2011, 2011.

Cox, P. M., Pearson, D., Booth, B. B., Friedlingstein, P., Huntingford, C., Jones, C. D., and Luke, C. M.: Sensitivity of tropical carbon to climate change constrained by carbon dioxide variability, Nature, 494, 341–344, 2013.

Davis, S. J. and Caldeira, K.: Consumption-based accounting of CO_2 emissions, P. Natl. Acad. Sci. USA, 107, 5687–5692, 2010.

Denman, K. L., Brasseur, G., Chidthaisong, A., Ciais, P., Cox, P. M., Dickinson, R. E., Hauglustaine, D., Heinze, C., Holland, E., Jacob, D., Lohmann, U., Ramachandran, S., Leite da Silva Dias, P., Wofsy, S. C., and Zhang, X.: Couplings Between Changes in the Climate System and Biogeochemistry. In: Climate Change 2007: The Physical Science Basis. Contribution of Working Group I to the Fourth Assessment Report of the Intergovernmental Panel on Climate Change, edited by: Solomon, S., Qin, D., Manning, M., Marquis, M., Averyt, K., Tignor, M. M. B., Miller, H. L., and Chen, Z. L., Cambridge University Press, Cambridge, UK and New York, USA, 2007.

DeVries, T.: The oceanic anthropogenic CO_2 sink: Storage, air-sea fluxes, and transports over the industrial era, Global Biogeochem. Cy., 28, 631–647, 2014.

DeVries, T., Holzer, M., and Primeau, F.: Recent increase in oceanic carbon uptake driven by weaker upper-ocean overturning, Nature, 542, 215–218, 2017.

Dlugokencky, E. and Tans, P.: Trends in atmospheric carbon dioxide, National Oceanic & Atmospheric Administration, Earth System Research Laboratory (NOAA/ESRL), available at: http://www.esrl.noaa.gov/gmd/ccgg/trends/global.html, last access: 9 March 2018.

Doney, S. C., Lima, I., Feely, R. A., Glover, D. M., Lindsay, K., Mahowald, N., Moore, J. K., and Wanninkhof, R.: Mechanisms governing interannual variability in upper-ocean inorganic carbon system and air–sea CO_2 fluxes: Physical climate and atmospheric dust, Deep-Sea Res. Pt. II, 56, 640–655, 2009.

Duce, R. A., LaRoche, J., Altieri, K., Arrigo, K. R., Baker, A. R., Capone, D. G., Cornell, S., Dentener, F., Galloway, J., Ganeshram, R. S., Geider, R. J., Jickells, T., Kuypers, M. M., Langlois, R., Liss, P. S., Liu, S. M., Middelburg, J. J., Moore, C. M., Nickovic, S., Oschlies, A., Pedersen, T., Prospero, J., Schlitzer, R., Seitzinger, S., Sorensen, L. L., Uematsu, M., Ulloa, O., Voss, M., Ward, B., and Zamora, L.: Impacts of atmospheric anthropogenic nitrogen on the open ocean, Science, 320, 893–897, 2008.

Dufour, C. O., Le Sommer, J., Gehlen, M., Orr, J. C., Molines, J. M., Simeon, J., and Barnier, B.: Eddy compensation and controls of the enhanced sea-to-air CO_2 flux during positive phases of the

Southern Annular Mode, Global Biogeochem. Cy., 27, 950–961, 2013.

Durant, A. J., Le Quéré, C., Hope, C., and Friend, A. D.: Economic value of improved quantification in global sources and sinks of carbon dioxide, Phil. Trans. A, 269, 1967–1979, 2011.

EIA: Short-Term Energy and Winter Fuels Outlook, U.S. Energy Information Administration, available at: http://www.eia.gov/forecasts/steo/outlook.cfm, last access: 11 October 2017.

Erb, K.-H., Kastner, T., Luyssaert, S., Houghton, R. A., Kuemmerle, T., Olofsson, P., and Haberl, H.: Bias in the attribution of forest carbon sinks, Nature Clim. Change, 3, 854–856, 2013.

Etheridge, D. M., Steele, L. P., Langenfelds, R. L., and Francey, R. J.: Natural and anthropogenic changes in atmospheric CO_2 over the last 1000 years from air in Antarctic ice and firn, J. Geophys. Res., 101, 4115–4128, 1996.

FAO: Global Forest Resources Assessment 2015, Food and Agriculture Organization of the United Nations, Rome, Italy, 2015.

FAOSTAT: Land Use Dataset, Food and Agriculture Organization Statistics Division, available at: http://www.fao.org/faostat/en/#data/RL (last access: March 2017), 2015.

Francey, R. J., Trudinger, C. M., van der Schoot, M., Law, R. M., Krummel, P. B., Langenfelds, R. L., Steele, L. P., Allison, C. E., Stavert, A. R., Andres, R. J., and Rodenbeck, C.: Reply to "Anthropogenic CO_2 emissions", Nature Clim. Change, 3, 604–604, 2013.

Friedlingstein, P., Houghton, R. A., Marland, G., Hackler, J., Boden, T. A., Conway, T. J., Canadell, J. G., Raupach, M. R., Ciais, P., and Le Quéré, C.: Update on CO_2 emissions, Nat. Geosci., 3, 811–812, 2010.

Friedlingstein, P., Andrew, R. M., Rogelj, J., Peters, G. P., Canadell, J. G., Knutti, R., Luderer, G., Raupach, M. R., Schaeffer, M., van Vuuren, D. P., and Le Quéré, C.: Persistent growth of CO_2 emissions and implications for reaching climate targets, Nat. Geosci., 7, 709–715, 2014.

Gasser, T., Ciais, P., Boucher, O., Quilcaille, Y., Tortora, M., Bopp, L., and Hauglustaine, D.: The compact Earth system model OSCAR v2.2: description and first results, Geosci. Model Dev., 10, 271–319, https://doi.org/10.5194/gmd-10-271-2017, 2017.

GCP: The Global Carbon Budget 2007, available at: http://www.globalcarbonproject.org/carbonbudget/archive.htm (last access: 7 November 2016), 2007.

GCP: Global Carbon Budget 2017, ICOS Carbon Portal, https://doi.org/10.18160/GCP-2017, 2017.

Giglio, L., Descloitres, J., Justice, C. O., and Kaufman, Y. J.: An enhanced contextual fire detection algorithm for MODIS, Remote Sens. Environ., 87, 273–282, 2003.

Gitz, V. and Ciais, P.: Amplifying effects of land-use change on future atmospheric CO_2 levels, Global Biogeochem. Cy., 17, 1024, https://doi.org/10.1029/2002GB001963, 2003.

GLOBALVIEW: Cooperative Global Atmospheric Data Integration Project; Multi-laboratory compilation of atmospheric carbon dioxide data for the period 1957–2015; obspack_co2_1_GLOBALVIEWplus_v2.1_2016_09_02; NOAA Earth System Research Laboratory, Global Monitoring Division, https://doi.org/10.15138/G3059Z, 2016.

Goll, D. S., Brovkin, V., Liski, J., Raddatz, T., Thum, T., and Todd-Brown, K. E. O.: Strong dependence of CO_2 emissions from anthropogenic land cover change on initial land cover and soil carbon parametrization, Global Biogeochem. Cy., 29, 1511–1523, https://doi.org/10.1002/2014GB004988, 2015.

Gregg, J. S., Andres, R. J., and Marland, G.: China: Emissions pattern of the world leader in CO_2 emissions from fossil fuel consumption and cement production, Geophys. Res. Lett., 35, L08806, https://doi.org/10.1029/2007GL032887, 2008.

Guimberteau, M., Zhu, D., Maignan, F., Huang, Y., Yue, C., Dantec-Nédélec, S., Ottlé, C., Jornet-Puig, A., Bastos, A., Laurent, P., Goll, D., Bowring, S., Chang, J., Guenet, B., Tifafi, M., Peng, S., Krinner, G., Ducharne, A., Wang, F., Wang, T., Wang, X., Wang, Y., Yin, Z., Lauerwald, R., Joetzjer, E., Qiu, C., Kim, H., and Ciais, P.: ORCHIDEE-MICT (v8.4.1), a land surface model for the high latitudes: model description and validation, Geosci. Model Dev., 11, 121–163, https://doi.org/10.5194/gmd-11-121-2018, 2018.

Hansis, E., Davis, S. J., and Pongratz, J.: Relevance of methodological choices for accounting of land use change carbon fluxes, Global Biogeochem. Cy., 29, 1230–1246, 2015.

Harris, I., Jones, P. D., Osborn, T. J., and Lister, D. H.: Updated high-resolution grids of monthly climatic observations – the CRU TS3.10 Dataset, Int. J. Climatol., 34, 623–642, 2014.

Hauck, J., Köhler, P., Wolf-Gladrow, D., and Völker, C.: Iron fertilisation and century-scale effects of open ocean dissolution of olivine in a simulated CO_2 removal experiment, Environ. Res. Lett., 11, 024007, https://doi.org/10.1088/1748-9326/11/2/024007, 2016.

Haverd, V., Smith, B., Nieradzik, L., Briggs, P. R., Woodgate, W., Trudinger, C. M., and Canadell, J. G.: A new version of the CABLE land surface model (Subversion revision r4546), incorporating land use and land cover change, woody vegetation demography and a novel optimisation-based approach to plant coordination of electron transport and carboxylation capacity-limited photosynthesis, Geosci. Model Dev. Discuss., https://doi.org/10.5194/gmd-2017-265, in review, 2017.

Hertwich, E. G. and Peters, G. P.: Carbon Footprint of Nations: A Global, Trade-Linked Analysis, Environ. Sci. Technol., 43, 6414–6420, https://doi.org/10.1021/es803496a, 2009.

Hooijer, A., Page, S., Canadell, J. G., Silvius, M., Kwadijk, J., Wösten, H., and Jauhiainen, J.: Current and future CO_2 emissions from drained peatlands in Southeast Asia, Biogeosciences, 7, 1505–1514, https://doi.org/10.5194/bg-7-1505-2010, 2010.

Houghton, R. A.: Revised estimates of the annual net flux of carbon to the atmosphere from changes in land use and land management 1850–2000, Tellus B, 55, 378–390, 2003.

Houghton, R. A. and Nassikas, A. A.: Global and regional fluxes of carbon from land use and land cover change 1850–2015, Global Biogeochem. Cy., 31, 456–472, 2017.

Houghton, R. A., House, J. I., Pongratz, J., van der Werf, G. R., DeFries, R. S., Hansen, M. C., Le Quéré, C., and Ramankutty, N.: Carbon emissions from land use and land-cover change, Biogeosciences, 9, 5125–5142, https://doi.org/10.5194/bg-9-5125-2012, 2012.

Hourdin, F., Musat, I., Bony, S., Braconnot, P., Codron, F., Dufresne, J.-l., Fairhead, L., Filiberti, M.-A., Freidlingstein, P., Grandpeix, J.-Y., Krinner, G., LeVan, P., Li, Z.-X., and Lott, F.: The LMDZ4 general circulation model: climate performance and sensitivity to parametrized physics with emphasis on tropical convection, Clim. Dynam., 27, 787–813, 2006.

Hurtt, G. C., Chini, L. P., Frolking, S., Betts, R. A., Feddema, J., Fischer, G., Fisk, J. P., Hibbard, K., Houghton, R. A., Janetos, A., Jones, C. D., Kindermann, G., Kinoshita, T., Klein Goldewijk, K., Riahi, K., Shevliakova, E., Smith, S., Stehfest, E., Thomson, A., Thornton, P., van Vuuren, D. P., and Wang, Y. P.: Harmonization of land-use scenarios for the period 1500–2100: 600 years of global gridded annual land-use transitions, wood harvest, and resulting secondary lands, Climatic Change, 109, 117–161, 2011.

Hurtt, G. C., Chini, L., Sahajpal, R., and Frolking, S.: Harmonization of global land-use change and management for the period 850–2100, Geosci. Model Dev., in preparation, 2018.

IEA/OECD: CO_2 emissions from fuel combustion, International Energy Agency/Organisation for Economic Cooperation and Development, Paris, France, 2016.

Ilyina, T., Six, K., Segschneider, J., Maier-Reimer, E., Li, H., and Núñez-Riboni, I.: The global ocean biogeochemistry model HAMOCC: Model architecture and performance as component of the MPI-Earth System Model in different CMIP5 experimental realizations, J. Adv. Model. Earth Sy., 5, 287–315, 2013.

IMF: World Economic Outlook of the International Monetary Fund, available at: http://www.imf.org/external/ns/cs.aspx?id=29, last access: 10 October 2017.

IPCC: 2006 IPCC Guidelines for National Greenhouse Gas Inventories, Prepared by the National Greenhouse Gas Inventories Programme, Institute for Global Environmental Strategies (IGES), Hayama, Kanagawa, Japan, 2006.

Ito, A. and Inatomi, M.: Use of a process-based model for assessing the methane budgets of global terrestrial ecosystems and evaluation of uncertainty, Biogeosciences, 9, 759–773, https://doi.org/10.5194/bg-9-759-2012, 2012.

Jackson, R. B., Canadell, J. G., Le Quéré, C., Andrew, R. M., Korsbakken, J. I., Peters, G. P., and Nakicenovic, N.: Reaching peak emissions, Nature Clim. Change, 6, 7–10, 2016.

Jackson, R. B., Le Quéré, C., Andrew, R. M., Canadell, J. G., Peters, G. P., Roy, J., and Wu, L.: Warning signs for stabilizing global CO_2 emissions, Environ. Res. Lett., 12, 110202, https://doi.org/10.1088/1748-9326/aa9662, 2017.

Jacobson, A. R., Mikaloff Fletcher, S. E., Gruber, N., Sarmiento, J. L., and Gloor, M.: A joint atmosphere-ocean inversion for surface fluxes of carbon dioxide: 1. Methods and global-scale fluxes, Global Biogeochem. Cy., 21, GB1019, https://doi.org/10.1029/2005GB002556, 2007.

Jain, A. K., Meiyappan, P., Song, Y., and House, J. I.: CO_2 Emissions from Land-Use Change Affected More by Nitrogen Cycle, than by the Choice of Land Cover Data, Glob. Change Biol., 9, 2893–2906, 2013.

Joos, F. and Spahni, R.: Rates of change in natural and anthropogenic radiative forcing over the past 20 000 years, P. Natl. Acad. Sci. USA, 105, 1425–1430, 2008.

Kato, E., Kinoshita, T., Ito, A., Kawamiya, M., and Yamagata, Y.: Evaluation of spatially explicit emission scenario of land-use change and biomass burning using a process-based biogeochemical model, J. Land Use Sci., 8, 104–122, 2013.

Kattge, J., Knorr, W., Raddatz, T., and Wirth, C.: Quantifying photosynthetic capacity and its relationship to leaf nitrogen content for global-scale terrestrial biosphere models, Glob. Change Biol., 15, 976–991, https://doi.org/10.1111/j.1365-2486.2008.01744.x, 2009.

Keeling, C. D., Bacastow, R. B., Bainbridge, A. E., Ekdhal, C. A., Guenther, P. R., and Waterman, L. S.: Atmospheric carbon dioxide variations at Mauna Loa Observatory, Hawaii, Tellus, 28, 538–551, 1976.

Keeling, R. F. and Manning, A. C.: 5.15 – Studies of Recent Changes in Atmospheric O_2 Content. In: Treatise on Geochemistry: Second Edition, edited by: Holland, H. D. and Turekian, K. K., Elsevier, Oxford, UK, 2014.

Keller, K. M., Lienert, S., Bozbiyik, A., Stocker, T. F., Churakova (Sidorova), O. V., Frank, D. C., Klesse, S., Koven, C. D., Leuenberger, M., Riley, W. J., Saurer, M., Siegwolf, R., Weigt, R. B., and Joos, F.: 20th century changes in carbon isotopes and water-use efficiency: tree-ring-based evaluation of the CLM4.5 and LPX-Bern models, Biogeosciences, 14, 2641–2673, https://doi.org/10.5194/bg-14-2641-2017, 2017.

Khatiwala, S., Primeau, F., and Hall, T.: Reconstruction of the history of anthropogenic CO_2 concentrations in the ocean, Nature, 462, 346–350, 2009.

Khatiwala, S., Tanhua, T., Mikaloff Fletcher, S., Gerber, M., Doney, S. C., Graven, H. D., Gruber, N., McKinley, G. A., Murata, A., Ríos, A. F., and Sabine, C. L.: Global ocean storage of anthropogenic carbon, Biogeosciences, 10, 2169–2191, https://doi.org/10.5194/bg-10-2169-2013, 2013.

Kirschke, S., Bousquet, P., Ciais, P., Saunois, M., Canadell, J. G., Dlugokencky, E. J., Bergamaschi, P., Bergmann, D., Blake, D. R., Bruhwiler, L., Cameron Smith, P., Castaldi, S., Chevallier, F., Feng, L., Fraser, A., Heimann, M., Hodson, E. L., Houweling, S., Josse, B., Fraser, P. J., Krummel, P. B., Lamarque, J., Langenfelds, R. L., Le Quéré, C., Naik, V., O'Doherty, S., Palmer, P. I., Pison, I., Plummer, D., Poulter, B., Prinn, R. G., Rigby, M., Ringeval, B., Santini, M., Schmidt, M., Shindell, D. T., Simpson, I. J., Spahni, R., Steele, L. P., Strode, S. A., Sudo, K., Szopa, S., van der Werf, G. R., Voulgarakis, A., van Weele, M., Weiss, R. F., Williams, J. E., and Zeng, G.: Three decades of global methane sources and sinks, Nat. Geosci., 6, 813–823, 2013.

Klein Goldewijk, K., Beusen, A., Doelman, J., and Stehfest, E.: Anthropogenic land use estimates for the Holocene – HYDE 3.2, Earth Syst. Sci. Data, 9, 927–953, https://doi.org/10.5194/essd-9-927-2017, 2017a.

Klein Goldewijk, K., Dekker, S. C., and van Zanden, J. L.: Percapita estimations of long-term historical land use and the consequences for global change research, J. Land Use Sci., 12, 313–337, 2017b.

Korsbakken, J. I., Peters, G. P., and Andrew, R. M.: Uncertainties around reductions in China's coal use and CO_2 emissions, Nature Clim. Change, 6, 687–690, 2016.

Krinner, G., Viovy, N., de Noblet, N., Ogée, J., Friedlingstein, P., Ciais, P., Sitch, S., Polcher, J., and Prentice, I. C.: A dynamic global vegetation model for studies of the coupled atmosphere-biosphere system, Global Biogeochem. Cy., 19, 1–33, 2005.

Landschützer, P., Gruber, N., Bakker, D. C. E., and Schuster, U.: Recent variability of the global ocean carbon sink, Global Biogeochem. Cy., 28, 927–949, https://doi.org/10.1002/2014GB004853, 2014.

Landschützer, P., Gruber, N., Haumann, A., Rödenbeck, C., Bakker, D. C. E., van Heuven, S., Hoppema, M., Metzl, N., Sweeney, C., Takahashi, T., Tilbrook, B., and Wanninkhof, R.: The reinvigoration of the Southern Ocean carbon sink, Science, 349, 1221–1224, 2015.

Landschützer, P., Gruber, N., and Bakker, D. C. E.: Decadal variations and trends of the global ocean carbon sink, Global Biogeochem. Cy., 30, 1396–1417, 2016.

Law, R. M., Ziehn, T., Matear, R. J., Lenton, A., Chamberlain, M. A., Stevens, L. E., Wang, Y.-P., Srbinovsky, J., Bi, D., Yan, H., and Vohralik, P. F.: The carbon cycle in the Australian Community Climate and Earth System Simulator (ACCESS-ESM1) – Part 1: Model description and pre-industrial simulation, Geosci. Model Dev., 10, 2567–2590, https://doi.org/10.5194/gmd-10-2567-2017, 2017.

Le Quéré, C.: Closing the global budget for CO_2, Global Change, 74, 28–31, 2009.

Le Quéré, C., Raupach, M. R., Canadell, J. G., Marland, G., Bopp, L., Ciais, P., Conway, T. J., Doney, S. C., Feely, R. A., Foster, P., Friedlingstein, P., Gurney, K., Houghton, R. A., House, J. I., Huntingford, C., Levy, P. E., Lomas, M. R., Majkut, J., Metzl, N., Ometto, J. P., Peters, G. P., Prentice, I. C., Randerson, J. T., Running, S. W., Sarmiento, J. L., Schuster, U., Sitch, S., Takahashi, T., Viovy, N., van der Werf, G. R., and Woodward, F. I.: Trends in the sources and sinks of carbon dioxide, Nat. Geosci., 2, 831–836, 2009.

Le Quéré, C., Andres, R. J., Boden, T., Conway, T., Houghton, R. A., House, J. I., Marland, G., Peters, G. P., van der Werf, G. R., Ahlström, A., Andrew, R. M., Bopp, L., Canadell, J. G., Ciais, P., Doney, S. C., Enright, C., Friedlingstein, P., Huntingford, C., Jain, A. K., Jourdain, C., Kato, E., Keeling, R. F., Klein Goldewijk, K., Levis, S., Levy, P., Lomas, M., Poulter, B., Raupach, M. R., Schwinger, J., Sitch, S., Stocker, B. D., Viovy, N., Zaehle, S., and Zeng, N.: The global carbon budget 1959–2011, Earth Syst. Sci. Data, 5, 165–185, https://doi.org/10.5194/essd-5-165-2013, 2013.

Le Quéré, C., Peters, G. P., Andres, R. J., Andrew, R. M., Boden, T. A., Ciais, P., Friedlingstein, P., Houghton, R. A., Marland, G., Moriarty, R., Sitch, S., Tans, P., Arneth, A., Arvanitis, A., Bakker, D. C. E., Bopp, L., Canadell, J. G., Chini, L. P., Doney, S. C., Harper, A., Harris, I., House, J. I., Jain, A. K., Jones, S. D., Kato, E., Keeling, R. F., Klein Goldewijk, K., Körtzinger, A., Koven, C., Lefèvre, N., Maignan, F., Omar, A., Ono, T., Park, G.-H., Pfeil, B., Poulter, B., Raupach, M. R., Regnier, P., Rödenbeck, C., Saito, S., Schwinger, J., Segschneider, J., Stocker, B. D., Takahashi, T., Tilbrook, B., van Heuven, S., Viovy, N., Wanninkhof, R., Wiltshire, A., and Zaehle, S.: Global carbon budget 2013, Earth Syst. Sci. Data, 6, 235–263, https://doi.org/10.5194/essd-6-235-2014, 2014.

Le Quéré, C., Moriarty, R., Andrew, R. M., Canadell, J. G., Sitch, S., Korsbakken, J. I., Friedlingstein, P., Peters, G. P., Andres, R. J., Boden, T. A., Houghton, R. A., House, J. I., Keeling, R. F., Tans, P., Arneth, A., Bakker, D. C. E., Barbero, L., Bopp, L., Chang, J., Chevallier, F., Chini, L. P., Ciais, P., Fader, M., Feely, R. A., Gkritzalis, T., Harris, I., Hauck, J., Ilyina, T., Jain, A. K., Kato, E., Kitidis, V., Klein Goldewijk, K., Koven, C., Landschützer, P., Lauvset, S. K., Lefèvre, N., Lenton, A., Lima, I. D., Metzl, N., Millero, F., Munro, D. R., Murata, A., Nabel, J. E. M. S., Nakaoka, S., Nojiri, Y., O'Brien, K., Olsen, A., Ono, T., Pérez, F. F., Pfeil, B., Pierrot, D., Poulter, B., Rehder, G., Rödenbeck, C., Saito, S., Schuster, U., Schwinger, J., Séférian, R., Steinhoff, T., Stocker, B. D., Sutton, A. J., Takahashi, T., Tilbrook, B., van der Laan-Luijkx, I. T., van der Werf, G. R., van Heuven, S., Vandemark, D., Viovy, N., Wiltshire, A., Zaehle, S., and Zeng, N.: Global Carbon Budget 2015, Earth Syst. Sci. Data, 7, 349–396, https://doi.org/10.5194/essd-7-349-2015, 2015a.

Le Quéré, C., Moriarty, R., Andrew, R. M., Peters, G. P., Ciais, P., Friedlingstein, P., Jones, S. D., Sitch, S., Tans, P., Arneth, A., Boden, T. A., Bopp, L., Bozec, Y., Canadell, J. G., Chini, L. P., Chevallier, F., Cosca, C. E., Harris, I., Hoppema, M., Houghton, R. A., House, J. I., Jain, A. K., Johannessen, T., Kato, E., Keeling, R. F., Kitidis, V., Klein Goldewijk, K., Koven, C., Landa, C. S., Landschützer, P., Lenton, A., Lima, I. D., Marland, G., Mathis, J. T., Metzl, N., Nojiri, Y., Olsen, A., Ono, T., Peng, S., Peters, W., Pfeil, B., Poulter, B., Raupach, M. R., Regnier, P., Rödenbeck, C., Saito, S., Salisbury, J. E., Schuster, U., Schwinger, J., Séférian, R., Segschneider, J., Steinhoff, T., Stocker, B. D., Sutton, A. J., Takahashi, T., Tilbrook, B., van der Werf, G. R., Viovy, N., Wang, Y.-P., Wanninkhof, R., Wiltshire, A., and Zeng, N.: Global carbon budget 2014, Earth Syst. Sci. Data, 7, 47–85, https://doi.org/10.5194/essd-7-47-2015, 2015b.

Le Quéré, C., Andrew, R. M., Canadell, J. G., Sitch, S., Korsbakken, J. I., Peters, G. P., Manning, A. C., Boden, T. A., Tans, P. P., Houghton, R. A., Keeling, R. F., Alin, S., Andrews, O. D., Anthoni, P., Barbero, L., Bopp, L., Chevallier, F., Chini, L. P., Ciais, P., Currie, K., Delire, C., Doney, S. C., Friedlingstein, P., Gkritzalis, T., Harris, I., Hauck, J., Haverd, V., Hoppema, M., Klein Goldewijk, K., Jain, A. K., Kato, E., Körtzinger, A., Landschützer, P., Lefèvre, N., Lenton, A., Lienert, S., Lombardozzi, D., Melton, J. R., Metzl, N., Millero, F., Monteiro, P. M. S., Munro, D. R., Nabel, J. E. M. S., Nakaoka, S.-I., O'Brien, K., Olsen, A., Omar, A. M., Ono, T., Pierrot, D., Poulter, B., Rödenbeck, C., Salisbury, J., Schuster, U., Schwinger, J., Séférian, R., Skjelvan, I., Stocker, B. D., Sutton, A. J., Takahashi, T., Tian, H., Tilbrook, B., van der Laan-Luijkx, I. T., van der Werf, G. R., Viovy, N., Walker, A. P., Wiltshire, A. J., and Zaehle, S.: Global Carbon Budget 2016, Earth Syst. Sci. Data, 8, 605–649, https://doi.org/10.5194/essd-8-605-2016, 2016.

Li, W., Ciais, P., Peng, S., Yue, C., Wang, Y., Thurner, M., Saatchi, S. S., Arneth, A., Avitabile, V., Carvalhais, N., Harper, A. B., Kato, E., Koven, C., Liu, Y. Y., Nabel, J. E. M. S., Pan, Y., Pongratz, J., Poulter, B., Pugh, T. A. M., Santoro, M., Sitch, S., Stocker, B. D., Viovy, N., Wiltshire, A., Yousefpour, R., and Zaehle, S.: Land-use and land-cover change carbon emissions between 1901 and 2012 constrained by biomass observations, Biogeosciences, 14, 5053–5067, https://doi.org/10.5194/bg-14-5053-2017, 2017.

Liu, Z., Guan, D., Wei, W., Davis, S. J., Ciais, P., Bai, J., Peng, S., Zhang, Q., Hubacek, K., Marland, G., Andres, R. J., Crawford-Brown, D., Lin, J., Zhao, H., Hong, C., Boden, T. A., Feng, K., Peters, G. P., Xi, F., Liu, J., Li, Y., Zhao, Y., Zeng, N., and He, K.: Reduced carbon emission estimates from fossil fuel combustion and cement production in China, Nature, 524, 335–338, 2015.

Lloyd, J. and Taylor, J.: On the Temperature Dependence of Soil Respiration, Funct. Ecol., 8, 315–323, https://doi.org/10.2307/2389824, 1994.

Manning, A. C. and Keeling, R. F.: Global oceanic and land biotic carbon sinks from the Scripps atmospheric oxygen flask sampling network, Tellus B, 58, 95–116, 2006.

Marland, G.: Uncertainties in accounting for CO_2 from fossil fuels, J. Ind. Ecol., 12, 136–139, 2008.

Marland, G. and Rotty, R. M.: Carbon-Dioxide Emissions from Fossil-Fuels – a Procedure for Estimation and Results for 1950-1982, Tellus B, 36, 232–261, 1984.

Marland, G., Hamal, K., and Jonas, M.: How Uncertain Are Estimates of CO_2 Emissions?, J. Ind. Ecol., 13, 4–7, 2009.

Masarie, K. A. and Tans, P. P.: Extension and integratino of atmospheric carbon dioxide data into a globally consistent measurement record, J. Geophys. Res.-Atmos., 100, 11593–11610, 1995.

MCI: Foreign Trade Data Dissemination Portal, Ministry of Commerce and Industry, 2017, available at: http://121.241.212.146/, last access: September 2017.

McNeil, B. I., Matear, R. J., Key, R. M., Bullister, J. L., and Sarmiento, J. L.: Anthropogenic CO_2 uptake by the ocean based on the global chlorofluorocarbon data set, Science, 299, 235–239, 2003.

Melton, J. R. and Arora, V. K.: Competition between plant functional types in the Canadian Terrestrial Ecosystem Model (CTEM) v. 2.0, Geosci. Model Dev., 9, 323–361, https://doi.org/10.5194/gmd-9-323-2016, 2016.

Mercado, L. M., Bellouin, N., Sitch, S., Boucher, O., Huntingford, C., Wild, M., and Cox, P. M.: Impact of changes in diffuse radiation on the global land carbon sink, Nature, 458, 1014–1018, 2009.

Mikaloff Fletcher, S. E., Gruber, N., Jacobson, A. R., Doney, S. C., Dutkiewicz, S., Gerber, M., Follows, M., Joos, F., Lindsay, K., Menemenlis, D., Mouchet, A., Müller, S. A., and Sarmiento, J. L.: Inverse estimates of anthropogenic CO_2 uptake, transport, and storage by the oceans, Global Biogeochem. Cy., 20, GB2002, https://doi.org/10.1029/2005GB002530, 2006.

Millar, R. J., Fuglestvedt, J. S., Friedlingstein, P., Rogelj, J., Grubb, M. J., Matthews, H. D., Skeie, R. B., Forster, P. M., Frame, D. J., and Allen, A. R.: Emission budgets and pathways consistent with limiting warming to 1.5 degrees C, Nat. Geosci., 10, 741–747, 2017.

Ministry of Mines: Mineral Production, Ministry of Mines, 2017, available at: http://ibm.nic.in/, last access: 25 September 2017.

Myhre, G., Alterskjær, K., and Lowe, D.: A fast method for updating global fossil fuel carbon dioxide emissions, Environ. Res. Lett., 4, 034012, https://doi.org/10.1088/1748-9326/4/3/034012, 2009.

Narayanan, B., Aguiar, A., and McDougall, R.: GTAP 9 Data Base, available at: https://www.gtap.agecon.purdue.edu/databases/v9/default.asp (last access: 10 September 2017), 2015.

NBS: Value added in Industrial enterprises above the reporting limit grew 7.6 % in August 2017, National Bureau of Statistics of China (NBS), 2017, available at: http://www.stats.gov.cn/tjsj/zxfb/201707/t20170717_1513524.html, (last access: 15 September 2016), 2017 (in Chinese).

NEA: News conference on the energy situation in the first half of 2017, National Energy Administration of China (NEA), 2017, available at: http://mp.weixin.qq.com/s/DlMA4Zod2y_nG8pely_iQw, last access: 15 September 2017 (in Chinese).

NOAA/ESRL: NOAA Greenhouse Gas Marine Boundary Layer Reference, available at: https://www.esrl.noaa.gov/gmd/ccgg/mbl/mbl.html, last access: 30 January 2017.

OEA: Index of Eight Core Industries. Office of the Economic Advisor, Office of the Economic Advisor (OEA), 2017, available at: http://eaindustry.nic.in/home.asp, last access: 4 September 2017.

Oleson, K., Lawrence, D., Bonan, G., Drewniak, B., Huang, M., Koven, C., Levis, S., Li, F., Riley, W., Subin, Z., Swenson, S., Thornton, P., Bozbiyik, A., Fisher, R., Heald, C., Kluzek, E., Lamarque, J., Lawrence, P., Leung, L., Lipscomb, W., Muszala, S., Ricciuto, D., Sacks, W., Tang, J., and Yang, Z.: Technical Description of version 4.5 of the Community Land Model (CLM), NCAR, Boulder, Colorado, USA, 2013.

Paulsen, H., Ilyina, T., Six, K. D., and Stemmler, I.: Incorporating a prognostic representation of marine nitrogen fixers into the global ocean biogeochemical model HAMOCC, J. Adv. Model. Earth Sy., 9, 438–464, 2017.

Peters, G. P., Andrew, R., and Lennos, J.: Constructing a multi-regional input-output table using the GTAP database, Econ. Syst. Res., 23, 131–152, 2011a.

Peters, G. P., Minx, J. C., Weber, C. L., and Edenhofer, O.: Growth in emission transfers via international trade from 1990 to 2008, P. Natl. Acad. Sci. USA, 108, 8903–8908, 2011b.

Peters, G. P., Davis, S. J., and Andrew, R.: A synthesis of carbon in international trade, Biogeosciences, 9, 3247–3276, https://doi.org/10.5194/bg-9-3247-2012, 2012a.

Peters, G. P., Marland, G., Le Quéré, C., Boden, T. A., Canadell, J. G., and Raupach, M. R.: Correspondence: Rapid growth in CO_2 emissions after the 2008-2009 global financial crisis, Nature Clim. Change, 2, 2–4, 2012b.

Peters, G. P., Andrew, R. M., Boden, T., Canadell, J. G., Ciais, P., Le Quéré, C., Marland, G., Raupach, M. R., and Wilson, C.: The challenge to keep global warming below 2 °C, Nature Clim. Change, 3, 4–6, 2013.

Peters, G. P., Le Quéré, C., Andrew, R. M., Canadell, J. G., Friedlingstein, P., Ilyina, T., Jackson, R. B., Korsbakken, J. I., McKinley, G., Sitch, S., and Tans, P.: Towards real-time verification of carbon dioxide emissions, Nature Clim. Change, 7, 848–850, https://doi.org/10.1038/s41558-017-0013-9, 2017.

Pfeil, B., Olsen, A., Bakker, D. C. E., Hankin, S., Koyuk, H., Kozyr, A., Malczyk, J., Manke, A., Metzl, N., Sabine, C. L., Akl, J., Alin, S. R., Bates, N., Bellerby, R. G. J., Borges, A., Boutin, J., Brown, P. J., Cai, W.-J., Chavez, F. P., Chen, A., Cosca, C., Fassbender, A. J., Feely, R. A., González-Dávila, M., Goyet, C., Hales, B., Hardman-Mountford, N., Heinze, C., Hood, M., Hoppema, M., Hunt, C. W., Hydes, D., Ishii, M., Johannessen, T., Jones, S. D., Key, R. M., Körtzinger, A., Landschützer, P., Lauvset, S. K., Lefèvre, N., Lenton, A., Lourantou, A., Merlivat, L., Midorikawa, T., Mintrop, L., Miyazaki, C., Murata, A., Nakadate, A., Nakano, Y., Nakaoka, S., Nojiri, Y., Omar, A. M., Padin, X. A., Park, G.-H., Paterson, K., Perez, F. F., Pierrot, D., Poisson, A., Ríos, A. F., Santana-Casiano, J. M., Salisbury, J., Sarma, V. V. S. S., Schlitzer, R., Schneider, B., Schuster, U., Sieger, R., Skjelvan, I., Steinhoff, T., Suzuki, T., Takahashi, T., Tedesco, K., Telszewski, M., Thomas, H., Tilbrook, B., Tjiputra, J., Vandemark, D., Veness, T., Wanninkhof, R., Watson, A. J., Weiss, R., Wong, C. S., and Yoshikawa-Inoue, H.: A uniform, quality controlled Surface Ocean CO_2 Atlas (SOCAT), Earth Syst. Sci. Data, 5, 125–143, https://doi.org/10.5194/essd-5-125-2013, 2013.

Pongratz, J., Reick, C. H., Houghton, R. A., and House, J. I.: Terminology as a key uncertainty in net land use and land cover change carbon flux estimates, Earth Syst. Dynam., 5, 177–195, https://doi.org/10.5194/esd-5-177-2014, 2014.

PPAC: Natural Gas, Petroleum Planning and Analysis Cell, Ministry of Petroleum and Natural Gas, available at: http://eaindustry.nic.in/home.asp, last access: 25 September 2017a.

PPAC: Petroleum, Petroleum Planning and Analysis Cell, Ministry of Petroleum and Natural Gas, availble at: http://eaindustry.nic.in/home.asp, last access: 15 September 2017b.

Prentice, I. C., Farquhar, G. D., Fasham, M. J. R., Goulden, M. L., Heimann, M., Jaramillo, V. J., Kheshgi, H. S., Le Quéré, C., Scholes, R. J., and Wallace, D. W. R.: The Carbon Cycle and Atmospheric Carbon Dioxide, in: Climate Change 2001: The Scientific Basis. Contribution of Working Group I to the Third Assessment Report of the Intergovernmental Panel on Climate Change, edited by: Houghton, J. T., Ding, Y., Griggs, D. J., Noguer, M., van der Linden, P. J., Dai, X., Maskell, K., and Johnson, C. A., Cambridge University Press, Cambridge, UK and New York, NY, USA, 2001.

Raupach, M. R., Marland, G., Ciais, P., Le Quéré, C., Canadell, J. G., Klepper, G., and Field, C. B.: Global and regional drivers of accelerating CO_2 emissions, P. Natl. Acad. Sci. USA, 104, 10288–10293, 2007.

Regnier, P., Friedlingstein, P., Ciais, P., Mackenzie, F. T., Gruber, N., Janssens, I. A., Laruelle, G. G., Lauerwald, R., Luyssaert, S., Andersson, A. J., Arndt, S., Arnosti, C., Borges, A. V., Dale, A. W., Gallego-Sala, A., Goddéris, Y., Goossens, N., Hartmann, J., Heinze, C., Ilyina, T., Joos, F., La Rowe, D. E., Leifeld, J., Meysman, F. J. R., Munhoven, G., Raymond, P. A., Spahni, R., Suntharalingam, P., and Thullner M.: Anthropogenic perturbation of the carbon fluxes from land to ocean, Nat. Geosci., 6, 597–607, 2013.

Reick, C. H., Raddatz, T., Brovkin, V., and Gayler, V.: The representation of natural and anthropogenic land cover change in MPI-ESM, J. Adv. Model. Earth Sy., 5, 459–482, 2013.

Rhein, M., Rintoul, S. R., Aoki, S., Campos, E., Chambers, D., Feely, R. A., Gulev, S., Johnson, G. C., Josey, S. A., Kostianoy, A., Mauritzen, C., Roemmich, D., Talley, L. D., and Wang, F.: Observations: Ocean, chap. 3, in: Climate Change 2013 The Physical Science Basis, Cambridge University Press, Cambridge, UK and New York, NY, USA, 2013.

Rödenbeck, C.: Estimating CO_2 sources and sinks from atmospheric mixing ratio measurements using a global inversion of atmospheric transport, Max Plank Institute, MPI-BGC, Jena, Germany, 2005.

Rödenbeck, C., Houweling, S., Gloor, M., and Heimann, M.: CO_2 flux history 1982–2001 inferred from atmospheric data using a global inversion of atmospheric transport, Atmos. Chem. Phys., 3, 1919–1964, https://doi.org/10.5194/acp-3-1919-2003, 2003.

Rödenbeck, C., Keeling, R. F., Bakker, D. C. E., Metzl, N., Olsen, A., Sabine, C., and Heimann, M.: Global surface-ocean $p\mathrm{CO}_2$ and sea–air CO_2 flux variability from an observation-driven ocean mixed-layer scheme, Ocean Sci., 9, 193–216, https://doi.org/10.5194/os-9-193-2013, 2013.

Rödenbeck, C., Bakker, D. C. E., Metzl, N., Olsen, A., Sabine, C., Cassar, N., Reum, F., Keeling, R. F., and Heimann, M.: Interannual sea–air CO_2 flux variability from an observation-driven ocean mixed-layer scheme, Biogeosciences, 11, 4599–4613, https://doi.org/10.5194/bg-11-4599-2014, 2014.

Rödenbeck, C., Bakker, D. C. E., Gruber, N., Iida, Y., Jacobson, A. R., Jones, S., Landschützer, P., Metzl, N., Nakaoka, S., Olsen, A., Park, G.-H., Peylin, P., Rodgers, K. B., Sasse, T. P., Schuster, U., Shutler, J. D., Valsala, V., Wanninkhof, R., and Zeng, J.: Data-based estimates of the ocean carbon sink variability – first results of the Surface Ocean $p\mathrm{CO}_2$ Mapping intercomparison (SOCOM), Biogeosciences, 12, 7251–7278, https://doi.org/10.5194/bg-12-7251-2015, 2015.

Rogelj, J., Schaeffer, M., Friedlingstein, P., Gillett, N. P., van Vuuren, D. P., Riahi, K., Allen, M., and Knutti, R.: Differences between carbon budget estimates unravelled, Nature Clim. Change, 6, 245–252, 2016.

Rypdal, K., Paciomik, N., Eggleston, S., Goodwin, J., Irving, W., Penman, J., and Woodfield, M.: Introduction to the 2006 Guidelines, chap. 1, in: 2006 IPCC Guidelines for National Greenhouse Gas Inventories, edited by: Eggleston, S., Buendia, L., Miwa, K., Ngara, T., and Tanabe, K., Institute for Global Environmental Strategies (IGES), Hayama, Kanagawa, Japan, 2006.

Saunois, M., Bousquet, P., Poulter, B., Peregon, A., Ciais, P., Canadell, J. G., Dlugokencky, E. J., Etiope, G., Bastviken, D., Houweling, S., Janssens-Maenhout, G., Tubiello, F. N., Castaldi, S., Jackson, R. B., Alexe, M., Arora, V. K., Beerling, D. J., Bergamaschi, P., Blake, D. R., Brailsford, G., Brovkin, V., Bruhwiler, L., Crevoisier, C., Crill, P., Covey, K., Curry, C., Frankenberg, C., Gedney, N., Höglund-Isaksson, L., Ishizawa, M., Ito, A., Joos, F., Kim, H.-S., Kleinen, T., Krummel, P., Lamarque, J.-F., Langenfelds, R., Locatelli, R., Machida, T., Maksyutov, S., McDonald, K. C., Marshall, J., Melton, J. R., Morino, I., Naik, V., O'Doherty, S., Parmentier, F.-J. W., Patra, P. K., Peng, C., Peng, S., Peters, G. P., Pison, I., Prigent, C., Prinn, R., Ramonet, M., Riley, W. J., Saito, M., Santini, M., Schroeder, R., Simpson, I. J., Spahni, R., Steele, P., Takizawa, A., Thornton, B. F., Tian, H., Tohjima, Y., Viovy, N., Voulgarakis, A., van Weele, M., van der Werf, G. R., Weiss, R., Wiedinmyer, C., Wilton, D. J., Wiltshire, A., Worthy, D., Wunch, D., Xu, X., Yoshida, Y., Zhang, B., Zhang, Z., and Zhu, Q.: The global methane budget 2000–2012, Earth Syst. Sci. Data, 8, 697–751, https://doi.org/10.5194/essd-8-697-2016, 2016.

SCCL: Provisional Production and Dispatches Performance, Singareni Collieries Company Limited (SCCL), 2017, available at: https://scclmines.com/scclnew/performance_production.asp, last access: 2 October 2017.

Schimel, D., Alves, D., Enting, I., Heimann, M., Joos, F., Raynaud, D., Wigley, T., Prater, M., Derwent, R., Ehhalt, D., Fraser, P., Sanhueza, E., Zhou, X., Jonas, P., Charlson, R., Rodhe, H., Sadasivan, S., Shine, K. P., Fouquart, Y., Ramaswamy, V., Solomon, S., Srinivasan, J., Albritton, D., Derwent, R., Isaksen, I., Lal, M., and Wuebbles, D.: Radiative Forcing of Climate Change, in: Climate Change 1995 The Science of Climate Change. Contribution of Working Group I to the Second Assessment Report of the Intergovernmental Panel on Climate Change, edited by: Houghton, J. T., Meira Rilho, L. G., Callander, B. A., Harris, N., Kattenberg, A., and Maskell, K., Cambridge University Press, Cambridge, UK and New York, NY, USA, 1995.

Schimel, D., Stephens, B. B., and Fisher, J. B.: Effect of increasing CO_2 on the terrestrial carbon sink, P. Natl. Acad. Sci. USA, 112, 436–441, 2015.

Schwietzke, S., Sherwood, O. A., Bruhwiler, L. M. P., Miller, J. B., Etiope, G., Dlugokencky, E. J., Michel, S. E., Arling, V. A., Vaughn, B. H., White, J. W. C., and Tans, P. P.: Upward revision of global fossil fuel methane emissions based on isotope database, Nature, 538, 88–91, 2016.

Schwinger, J., Goris, N., Tjiputra, J. F., Kriest, I., Bentsen, M., Bethke, I., Ilicak, M., Assmann, K. M., and Heinze, C.: Evaluation of NorESM-OC (versions 1 and 1.2), the ocean carbon-cycle stand-alone configuration of the Norwegian Earth System Model (NorESM1), Geosci. Model Dev., 9, 2589–2622, https://doi.org/10.5194/gmd-9-2589-2016, 2016.

Séférian, R., Bopp, L., Gehlen, M., Orr, J., Ethé, C., Cadule, P., Aumont, O., Salas y Mélia, D., Voldoire, A., and Madec, G.: Skill assessment of three earth system models with common marine biogeochemistry, Clim. Dynam., 40, 2549–2573, 2013.

Sitch, S., Smith, B., Prentice, I. C., Arneth, A., Bondeau, A., Cramer, W., Kaplan, J. O., Levis, S., Lucht, W., Sykes, M. T., Thonicke, K., and Venevsky, S.: Evaluation of ecosystem dynamics, plant geography and terrestrial carbon cycling in the LPJ dynamic global vegetation model, Glob. Change Biol., 9, 161–185, 2003.

Smith, B., Wårlind, D., Arneth, A., Hickler, T., Leadley, P., Siltberg, J., and Zaehle, S.: Implications of incorporating N cycling and N limitations on primary production in an individual-based dynamic vegetation model, Biogeosciences, 11, 2027–2054, https://doi.org/10.5194/bg-11-2027-2014, 2014.

Stephens, B. B., Gurney, K. R., Tans, P. P., Sweeney, C., Peters, W., Bruhwiler, L., Ciais, P., Ramonet, M., Bousquet, P., Nakazawa, T., Aoki, S., Machida, T., Inoue, G., Vinnichenko, N., Lloyd, J., Jordan, A., Heimann, M., Shibistova, O., Langenfelds, R. L., Steele, L. P., Francey, R. J., and Denning, A. S.: Weak northern and strong tropical land carbon uptake from vertical profiles of atmospheric CO_2, Science, 316, 1732–1735, 2007.

Stocker, T., Qin, D., and Platner, G.-K.: Climate Change 2013 The Physical Science Basis, Cambridge University Press, Cambridge, UK and New York, NY, USA, 2013.

Swart, N. C., Fyfe, J. C., Saenko, O. A., and Eby, M.: Wind-driven changes in the ocean carbon sink, Biogeosciences, 11, 6107–6117, https://doi.org/10.5194/bg-11-6107-2014, 2014.

Tian, H. Q., Chen, G. S., Lu, C. Q., Xu, X. F., Hayes, D. J., Ren, W., Pan, S. F., Huntzinger, D. N., and Wofsy, S. C.: North American terrestrial CO_2 uptake largely offset by CH_4 and N_2O emissions: toward a full accounting of the greenhouse gas budget, Climatic Change, 129, 413–426, 2015.

UN: National Accounts Main Aggregates Database, United Nations Statistics Division, available at: http://unstats.un.org/unsd/snaama/Introduction.asp (last access: 2 February 2017), 2016.

UN: Energy Statistics, United Nations Statistics Division, available at: http://unstats.un.org/unsd/energy/, last access: June 2017.

UNFCCC: National Inventory Submissions, available at: http://unfccc.int/national_reports/annex_i_ghg_inventories/national_inventories_submissions/items/10116.php, last access: 7 June 2017.

USGS: 2014 Minerals Yearbook – Cement, US Geological Survey, Reston, Virginia, USA, 2017.

van der Laan-Luijkx, I. T., van der Velde, I. R., van der Veen, E., Tsuruta, A., Stanislawska, K., Babenhauserheide, A., Zhang, H. F., Liu, Y., He, W., Chen, H., Masarie, K. A., Krol, M. C., and Peters, W.: The CarbonTracker Data Assimilation Shell (CTDAS) v1.0: implementation and global carbon balance 2001–2015, Geosci. Model Dev., 10, 2785–2800, https://doi.org/10.5194/gmd-10-2785-2017, 2017.

van der Velde, I. R., Miller, J. B., Schaefer, K., van der Werf, G. R., Krol, M. C., and Peters, W.: Terrestrial cycling of $^{13}CO_2$ by photosynthesis, respiration, and biomass burning in SiBCASA, Biogeosciences, 11, 6553–6571, https://doi.org/10.5194/bg-11-6553-2014, 2014.

van der Werf, G. R., Randerson, J. T., Giglio, L., Collatz, G. J., Mu, M., Kasibhatla, P. S., Morton, D. C., DeFries, R. S., Jin, Y., and van Leeuwen, T. T.: Global fire emissions and the contribution of deforestation, savanna, forest, agricultural, and peat fires (1997–2009), Atmos. Chem. Phys., 10, 11707–11735, https://doi.org/10.5194/acp-10-11707-2010, 2010.

van der Werf, G. R., Randerson, J. T., Giglio, L., van Leeuwen, T. T., Chen, Y., Rogers, B. M., Mu, M., van Marle, M. J. E., Morton, D. C., Collatz, G. J., Yokelson, R. J., and Kasibhatla, P. S.: Global fire emissions estimates during 1997–2016, Earth Syst. Sci. Data, 9, 697–720, https://doi.org/10.5194/essd-9-697-2017, 2017.

Viovy, N.: CRUNCEP data set, available at: ftp://nacp.ornl.gov/synthesis/2009/frescati/temp/land_use_change/original/readme.htm, last access: June 2016.

Walker, A. P., Quaife, T., van Bodegom, P. M., De Kauwe, M. G., Keenan, T. F., Joiner, J., Lomas, M. R., MacBean, N., Xu, C. G., Yang, X. J., and Woodward, F. I.: The impact of alternative trait-scaling hypotheses for the maximum photosynthetic carboxylation rate (V-cmax) on global gross primary production, New Phytol., 215, 1370–1386, 2017.

Wanninkhof, R., Park, G.-H., Takahashi, T., Sweeney, C., Feely, R., Nojiri, Y., Gruber, N., Doney, S. C., McKinley, G. A., Lenton, A., Le Quéré, C., Heinze, C., Schwinger, J., Graven, H., and Khatiwala, S.: Global ocean carbon uptake: magnitude, variability and trends, Biogeosciences, 10, 1983–2000, https://doi.org/10.5194/bg-10-1983-2013, 2013.

Watson, R. T., Rodhe, H., Oeschger, H., and Siegenthaler, U.: Greenhouse Gases and Aerosols, in: Climate Change: The IPCC Scientific Assessment. Intergovernmental Panel on Climate Change (IPCC), edited by: Houghton, J. T., Jenkins, G. J., and Ephraums, J. J., Cambridge University Press, Cambridge, UK, 1990.

Wenzel, S., Cox, P. M., Eyring, V., and Friedlingstein, P.: Projected land photosynthesis constrained by changes in the seasonal cycle of atmospheric CO_2, Nature, 538, 499–501, 2016.

Wilkenskjeld, S., Kloster, S., Pongratz, J., Raddatz, T., and Reick, C. H.: Comparing the influence of net and gross anthropogenic land-use and land-cover changes on the carbon cycle in the MPI-ESM, Biogeosciences, 11, 4817–4828, https://doi.org/10.5194/bg-11-4817-2014, 2014.

Woodward, F. I. and Lomas, M. R.: Vegetation dynamics – simulating responses to climatic change, Biol. Rev., 79, 643–670, 2004.

Woodward, F. I., Smith, T. M., and Emanuel, W. R.: A global land primary productivity and phytogeography model, Global Biogeochem. Cy., 9, 471–490, 1995.

Xi, F., Davis, S. J., Ciais, P., Crawford-Brown, D., Guan, D., Pade, C., Shi, T., Syddall, M., Lv, J., Ji, L., Bing, L., Wang, J., Wei, W., Yang, K.-H., Lagerblad, B., Galan, I., Andrade, C., Zhang, Y., and Liu, Z.: Substantial global carbon uptake by cement carbonation, Nat. Geosci., 9, 880–883, 2016.

Zaehle, S. and Friend, A. D.: Carbon and nitrogen cycle dynamics in the O-CN land surface model: 1. Model description, site-scale evaluation, and sensitivity to parameter estimates, Global Biogeochem. Cy., 24, GB1005, https://doi.org/10.1029/2009GB003521, 2010.

Zaehle, S., Ciais, P., Friend, A. D., and Prieur, V.: Carbon benefits of anthropogenic reactive nitrogen offset by nitrous oxide emissions, Nat. Geosci., 4, 601–605, 2011.

Zscheischler, J., Mahecha, M. D., Avitabile, V., Calle, L., Carvalhais, N., Ciais, P., Gans, F., Gruber, N., Hartmann, J., Herold, M., Ichii, K., Jung, M., Landschützer, P., Laruelle, G. G., Lauerwald, R., Papale, D., Peylin, P., Poulter, B., Ray, D., Regnier, P., Rödenbeck, C., Roman-Cuesta, R. M., Schwalm, C., Tramontana, G., Tyukavina, A., Valentini, R., van der Werf, G., West, T. O., Wolf, J. E., and Reichstein, M.: Reviews and syntheses: An empirical spatiotemporal description of the global surface–atmosphere carbon fluxes: opportunities and data limitations, Biogeosciences, 14, 3685–3703, https://doi.org/10.5194/bg-14-3685-2017, 2017.

doi:10.1038/nature14016

The geographical distribution of fossil fuels unused when limiting global warming to 2 °C

Christophe McGlade[1] & Paul Ekins[1]

Policy makers have generally agreed that the average global temperature rise caused by greenhouse gas emissions should not exceed 2 °C above the average global temperature of pre-industrial times[1]. It has been estimated that to have at least a 50 per cent chance of keeping warming below 2 °C throughout the twenty-first century, the cumulative carbon emissions between 2011 and 2050 need to be limited to around 1,100 gigatonnes of carbon dioxide (Gt CO_2)[2,3]. However, the greenhouse gas emissions contained in present estimates of global fossil fuel reserves are around three times higher than this[2,4], and so the unabated use of all current fossil fuel reserves is incompatible with a warming limit of 2 °C. Here we use a single integrated assessment model that contains estimates of the quantities, locations and nature of the world's oil, gas and coal reserves and resources, and which is shown to be consistent with a wide variety of modelling approaches with different assumptions[5], to explore the implications of this emissions limit for fossil fuel production in different regions. Our results suggest that, globally, a third of oil reserves, half of gas reserves and over 80 per cent of current coal reserves should remain unused from 2010 to 2050 in order to meet the target of 2 °C. We show that development of resources in the Arctic and any increase in unconventional oil production are incommensurate with efforts to limit average global warming to 2 °C. Our results show that policy makers' instincts to exploit rapidly and completely their territorial fossil fuels are, in aggregate, inconsistent with their commitments to this temperature limit. Implementation of this policy commitment would also render unnecessary continued substantial expenditure on fossil fuel exploration, because any new discoveries could not lead to increased aggregate production.

Recent climate studies have demonstrated that average global temperature rises are closely related to cumulative emissions of greenhouse gases emitted over a given timeframe[2,6,7]. This has resulted in the concept of the remaining global 'carbon budget' associated with the probability of successfully keeping the global temperature rise below a certain level[4,8,9]. The Intergovernmental Panel on Climate Change (IPCC)[3] recently suggested that to have a better-than-even chance of avoiding more than a 2 °C temperature rise, the carbon budget between 2011 and 2050 is around 870–1,240 Gt CO_2.

Such a carbon budget will have profound implications for the future utilization of oil, gas and coal. However, to understand the quantities that are required, and are not required, under different scenarios, we first

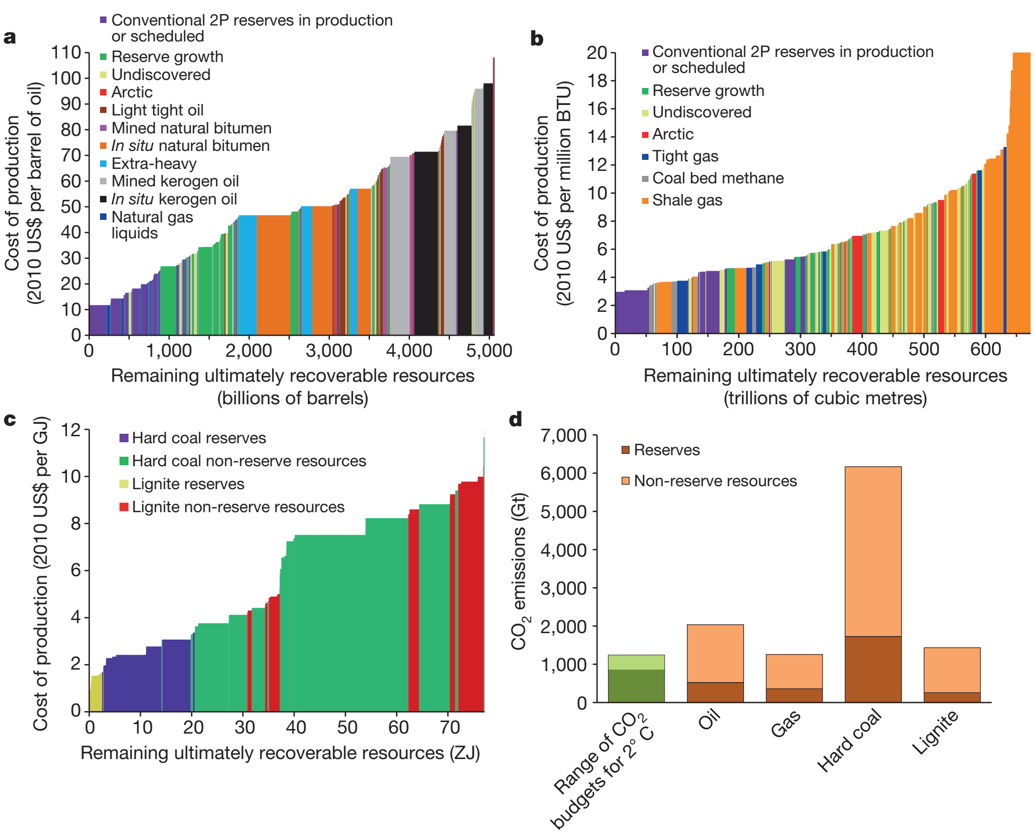

Figure 1 | Supply cost curves for oil, gas and coal and the combustion CO_2 emissions for these resources. **a**–**c**, Supply cost curves for oil (**a**), gas (**b**) and coal (**c**). **d**, The combustion CO_2 emissions for these resources. Within these resource estimates, 1,294 billion barrels of oil, 192 trillion cubic metres of gas, 728 Gt of hard coal, and 276 Gt of lignite are classified as reserves globally. These reserves would result in 2,900 Gt of CO_2 if combusted unabated. The range of carbon budgets between 2011 and 2050 that are approximately commensurate with limiting the temperature rise to 2 °C (870–1,240 Gt of CO_2) is also shown. 2P, 'proved plus probable' reserves; BTU, British thermal units (one BTU is equal to 1,055 J). One zettajoule (ZJ) is equal to one sextillion (10^{21}) joules. Annual global primary energy production is approximately 0.5 ZJ.

[1]University College London (UCL), Institute for Sustainable Resources, Central House, 14 Upper Woburn Place, London WC1H 0NN, UK.

need to establish the quantities and location of those currently estimated to exist. A variety of metrics with disparate nomenclature are relied upon to report the availability of fossil fuels[10,11], but the two most common are 'resources' and 'reserves'. In this work 'resources' are taken to be the remaining ultimately recoverable resources (RURR)—the quantity of oil, gas or coal remaining that is recoverable over all time with both current and future technology, irrespective of current economic conditions. 'Reserves' are a subset of resources that are defined to be recoverable under current economic conditions and have a specific probability of being produced[11]. Our best estimates of the reserves and resources are presented in Fig. 1 and, at the regional level, in Extended Data Table 1.

Figure 1 also compares the above carbon budget with the CO_2 emissions that would result from the combustion of our estimate of remaining fossil fuel resources (nearly 11,000 Gt CO_2). With the combustion emissions of the remaining reserves alone totalling nearly 2,900 Gt CO_2, the disparity between what resources and reserves exist and what can be emitted while avoiding a temperature rise greater than the agreed 2 °C limit is therefore stark.

Although previous research[12] has examined the implications that emissions mitigation might have on the rents collected by fossil fuel resource owners, more pertinent to policy and industry are the quantities of fossil fuel that are not used before 2050 in scenarios that limit the average global surface temperature rise to 2 °C. Such geographically disaggregated estimates of 'unburnable' reserves and resources are provided here using the linear optimization, integrated assessment model TIAM-UCL[13].

To provide context to the issue of unburnable fossil fuels and our results, it is useful to examine scenarios provided by other models that quantify separately the volumes of oil, gas and coal produced globally under a range of future emissions trajectories[5]. Cumulative production between 2010 and 2050 from these are presented in Fig. 2. Since they have very different future greenhouse gas emissions profiles, we have converted them to approximate temperature rise trajectories. These have been calculated using the climate model MAGICC[14], which generates a probability distribution over temperature rise trajectories for a given emissions profile. We use the 60th percentile temperature trajectory (to correspond with assumptions within TIAM-UCL) and then group the scenarios by the final temperature rise in 2100: below 2 °C, between 2 °C and 3 °C, or exceeding 3 °C.

In this work we have constructed three core scenarios that are constrained to limit the average surface temperature rise in all time periods to 2 °C, to 3 °C, and to 5 °C. Cumulative production of each fossil fuel between 2010 and 2050 in each of these scenarios can be identified within each of the three temperature groupings in Fig. 2.

The global reserves of oil, gas and coal included in Fig. 1 total approximately 7.4 ZJ, 7.1 ZJ and 20 ZJ, respectively. With narrow inter-quartile ranges, relative to the level of reserves available, Fig. 2 shows good agreement on the levels of fossil fuels produced within the temperature groups, despite the range of modelling methodologies and assumptions included.

Since assumptions in modelling the energy system are subject to wide bands of uncertainty[15], we further constructed a number of sensitivity scenarios using TIAM-UCL that remain within a 2 °C temperature rise. These span a broad range of assumptions on production costs, the availability of bio-energy, oil and gas, demand projections, and technology availability (one with no negative emissions technologies, and one with no carbon capture and storage (CCS)) (Extended Data Table 2). The availability of CCS has the largest effect on cumulative production levels (Extended Data Fig. 1); however, there is little variability in the total production of fossil fuels if the world is to have a good chance of staying within the agreed 2 °C limit.

Global production of oil, gas and coal over time in our main 2 °C scenario is given in Fig. 3. This separates production by category, that is, by the individual kinds of oil and gas that make up the global resource base, and compares total production with the projections from the 2 °C scenarios in Fig. 2. The results generated using TIAM-UCL are a product

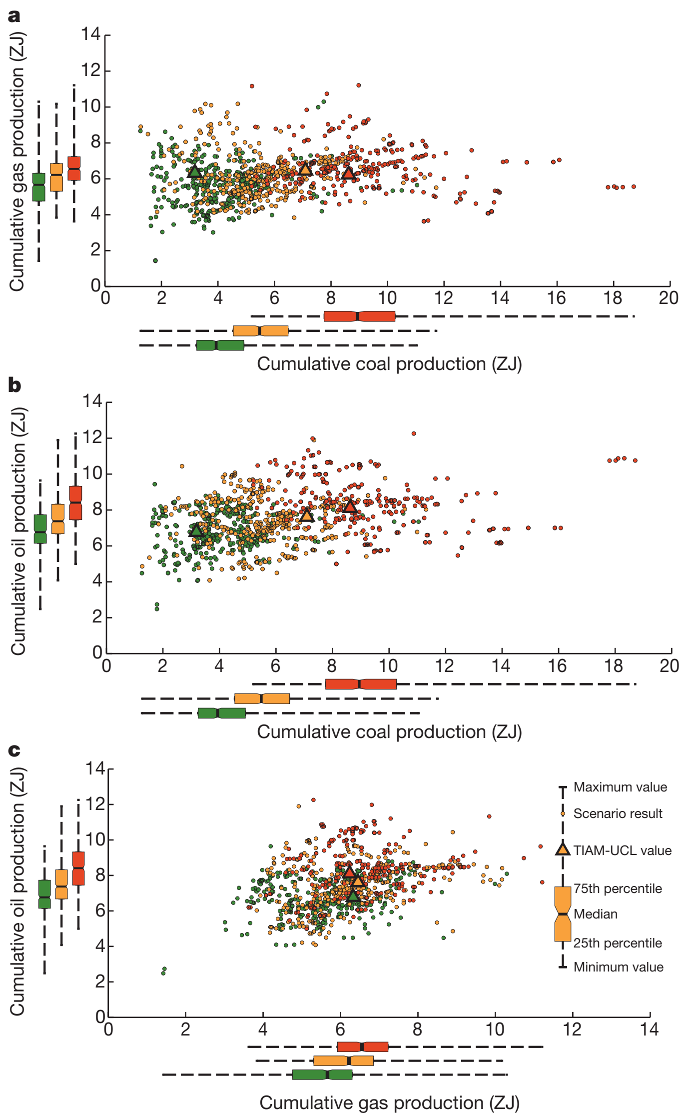

Figure 2 | Cumulative production between 2010 and 2050 from a range of long-term energy scenarios. Panels refer to coal and gas (**a**), coal and oil (**b**), and gas and oil (**c**). Scenarios[5] are coloured according to their approximate resultant 2100 temperature rise above pre-industrial levels. 379 individual scenarios result in a temperature rise of less than 2 °C (green), 366 of between 2 °C and 3 °C (orange), and 284 of more than 3 °C (red). Triangles are the values from the 2 °C (with CCS), 3 °C and 5 °C TIAM-UCL scenarios. Ranges and symbols are as shown in the key in **c**.

of the economically-optimal solution, and other regional distributions of unburnable reserves are possible while still remaining within the 2 °C limit (even though these would have a lower social welfare). A future multi-model analysis could therefore usefully build on and extend the work that is presented here, but results at the aggregate level can be seen to lie within range of the ensemble of models and scenarios that also give no more than a 2 °C temperature rise.

In the TIAM-UCL scenarios, production of reserves and non-reserve resources occurs contemporaneously. It is therefore important to recognize that it would be inappropriate simply to compare the cumulative production figures in Fig. 2 with the reserve estimates from Fig. 1 and declare any reserves not used as 'unburnable'. Although there may be sufficient reserves to cover cumulative production between 2010 and 2050, it does not follow that only reserves should be developed and all other resources should remain unused. For oil and gas, resources that are not currently reserves may turn out to be cheaper to produce than some reserves, while new resources will also be developed to maintain

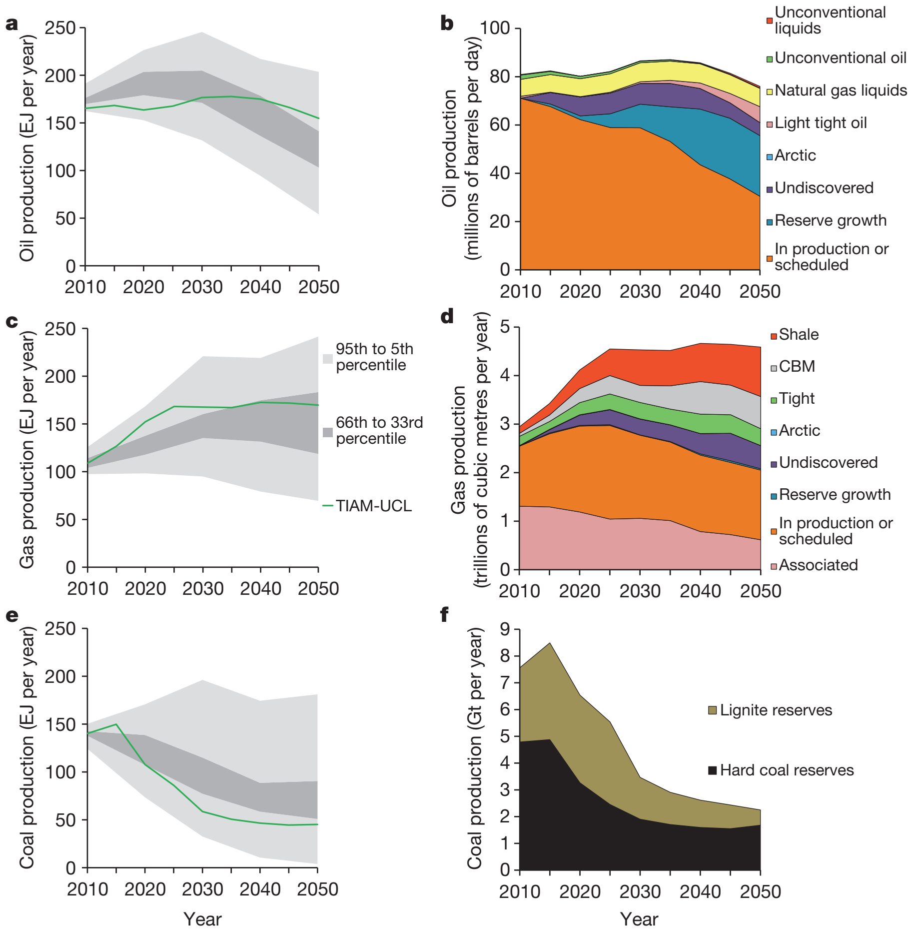

Figure 3 | Oil, gas and coal production in the TIAM-UCL 2 °C scenario (with CCS) and comparison with all other 2 °C scenarios in the Intergovernmental Panel on Climate Change Fifth Assessment Report (AR5) database[5]. **a**, **c** and **e** compare total production by oil, gas and coal with the AR5 database; **b**, **d** and **f** provide a disaggregated view of production for the TIAM-UCL 2 °C scenario separated by category. Associated gas is gas produced alongside crude oil from oil fields. One exajoule (EJ) is equal to one quintillion (10^{18}) joules.

the flow rates demanded by end-use sectors. However, if resources that are currently non-reserves are produced, a greater proportion of reserves must not be produced to stay within the carbon budget.

The reserves of oil, gas and coal that should be classified as unburnable within each region, and the percentage of current reserves that remain unused, are set out in Table 1. Since total production is most sensitive to assumptions on CCS, and since it has been suggested that the deployment of CCS will permit wider exploitation of the fossil fuel resource base[16], Table 1 includes the unburnable reserves from two alternative 2 °C scenarios. One scenario permits the widespread deployment of CCS from 2025 onwards, and the other assumes that CCS is unavailable in any time period.

Globally, when CCS is permitted, over 430 billion barrels of oil and 95 trillion cubic metres of gas currently classified as reserves should remain unburned by 2050. The Middle East, although using over 60% of its oil reserves, carries over half of the unburnable oil globally, leaving over 260 billions of barrels in the ground. Canada has the lowest utilization of its oil reserves (25%), as its natural bitumen[17] deposits remain largely undeveloped (see below) while the United States has the highest, given the proximity of supply and demand centres. The Middle East also holds half of unburnable global gas reserves, with Former Soviet Union countries accounting for another third, meaning that they can use only half their current reserves.

Coal reserves are by far the least-used fossil fuel, with a global total of 82% remaining unburned before 2050. The United States and the Former Soviet Union countries each use less than 10% of their current reserves, meaning that they should leave over 200 billion tonnes (Gt) coal (both hard and lignite) reserves unburned. Coal reserve utilization

Table 1 | Regional distribution of reserves unburnable before 2050 for the 2 °C scenarios with and without CCS

	2 °C with CCS						2 °C without CCS					
	Oil		Gas		Coal		Oil		Gas		Coal	
Country or region	Billions of barrels	%	Trillions of cubic metres	%	Gt	%	Billions of barrels	%	Trillions of cubic metres	%	Gt	%
Africa	23	21%	4.4	33%	28	85%	28	26%	4.4	34%	30	90%
Canada	39	74%	0.3	24%	5.0	75%	40	75%	0.3	24%	5.4	82%
China and India	9	25%	2.9	63%	180	66%	9	25%	2.5	53%	207	77%
FSU	27	18%	31	50%	203	94%	28	19%	36	59%	209	97%
CSA	58	39%	4.8	53%	8	51%	63	42%	5.0	56%	11	73%
Europe	5.0	20%	0.6	11%	65	78%	5.3	21%	0.3	6%	74	89%
Middle East	263	38%	46	61%	3.4	99%	264	38%	47	61%	3.4	99%
OECD Pacific	2.1	37%	2.2	56%	83	93%	2.7	46%	2.0	51%	85	95%
ODA	2.0	9%	2.2	24%	10	34%	2.8	12%	2.1	22%	17	60%
United States of America	2.8	6%	0.3	4%	235	92%	4.6	9%	0.5	6%	245	95%
Global	431	33%	95	49%	819	82%	449	35%	100	52%	887	88%

FSU, the former Soviet Union countries; CSA, Central and South America; ODA, Other developing Asian countries; OECD, the Organisation for Economic Co-operation and Development. A barrel of oil is 0.159 m^3; %, Reserves unburnable before 2050 as a percentage of current reserves.

is twenty-five percentage points higher in China and India, but still they should also leave nearly 200 Gt of their current coal reserves unburned.

The utilization of current reserves is lower in nearly all regions for all of the fossil fuels when CCS is not available, although there is a slight increase in gas production in some regions to offset some of the larger drop in coal production. Nevertheless, Table 1 demonstrates that the reserves of coal that can be burned are only six percentage points higher when CCS is allowed, with the utilization of gas and oil increasing by an even smaller fraction (around two percentage points). Because of the expense of CCS, its relatively late date of introduction (2025), and the assumed maximum rate at which it can be built, CCS has a relatively modest effect on the overall levels of fossil fuel that can be produced before 2050 in a 2 °C scenario.

As shown in Fig. 3, there is substantial production of many of the non-reserve resource categories of oil and gas. Extended Data Table 3 sets out the regional unburnable resources of all coal, gas and oil in the scenario that allows CCS by comparing cumulative production of all fossil fuel resources with the resource estimates in Fig. 1.

The RURR of both types of coal and unconventional oil vastly exceed cumulative production between 2010 and 2050, with the overwhelming majority remaining unburned. Resources of conventional oil are used to the greatest extent, with just under 350 billion barrels of non-reserve resources produced over the model timeframe. The Middle East again holds the largest share of the unburnable resources of conventional oil, but there is a much wider geographical distribution of these unburnable resources than was the case for oil reserves.

Regarding the production of unconventional oil, open-pit mining of natural bitumen in Canada soon drops to negligible levels after 2020 in all scenarios because it is considerably less economic than other methods of production. Production by *in situ* technologies continues in the 2 °C scenario that allows CCS, but this is accompanied by a rapid and total decarbonization of the auxiliary energy inputs required (Extended Data Fig. 2). Although such a decarbonization would be extremely challenging in reality, cumulative production of Canadian bitumen between 2010 and 2050 is still only 7.5 billion barrels. 85% of its 48 billion of barrels of bitumen reserves thus remain unburnable if the 2 °C limit is not to be exceeded. When CCS is not available, all bitumen production ceases by 2040. In both cases, the RURR of Canadian bitumen dwarfs cumulative production, so that around 99% of our estimate of its resources (640 billion barrels), remains unburnable. Similar results are seen for extra-heavy oil in Venezuela. Cumulative production is 3 billion barrels, meaning that almost 95% of its extra-heavy reserves and 99% of the RURR are unburnable, even when CCS is available.

The utilization of unconventional gas resources is considerably higher than unconventional oil. Under the 2 °C scenario, gas plays an important part in displacing coal from the electrical and industrial sectors and so there is over 50 trillion cubic metres unconventional gas production globally, over half of which occurs in North America. Nevertheless, there is a low level of utilization of the large potential unconventional gas resources held by China and India, Africa and the Middle East, and so over 80% of unconventional gas resources (247 trillion cubic metres) are unburnable before 2050. Production of these unconventional gas resources is, however, only possible if the levels of coal reserves identified in Table 1 are not developed: that is, it is not possible for unconventional gas to be additional to current levels of coal production.

Finally, we estimate there to be 100 billion barrels of oil (including natural gas liquids) and 35 trillion cubic metres of gas in fields within the Arctic Circle that are not being produced as of 2010. However, none is produced in any region in either of the 2 °C scenarios before 2050. These results indicate to us that all Arctic resources should be classified as unburnable.

To conclude, these results demonstrate that a stark transformation in our understanding of fossil fuel availability is necessary. Although there have previously been fears over the scarcity of fossil fuels[18], in a climate-constrained world this is no longer a relevant concern: large portions of the reserve base and an even greater proportion of the resource base should not be produced if the temperature rise is to remain below 2 °C.

Online Content Methods, along with any additional Extended Data display items and Source Data, are available in the online version of the paper; references unique to these sections appear only in the online paper.

Received 18 February; accepted 27 October 2014.

1. United Nations Framework Convention on Climate Change (UNFCC). *Report of the Conference of the Parties on its Fifteenth Session, held in Copenhagen from 7 to 19 December 2009. Part Two: Action taken by the Conference of the Parties at its Fifteenth Session.* United Nations Climate Change Conf. Report 43 http://unfccc.int/resource/docs/2009/cop15/eng/11a01.pdf (UNFCC, 2009).
2. Meinshausen, M. *et al.* Greenhouse gas emission targets for limiting global warming to 2 °C. *Nature* **458,** 1158–1162 (2009).
3. Clarke, L. *et al.* in *Climate Change 2014: Mitigation of Climate Change* (Edenhofer, O. *et al.*) Ch. 6 (Cambridge Univ. Press, 2014).
4. Raupach, M. R. *et al.* Sharing a quota on cumulative carbon emissions. *Nature Clim. Chang.* **4,** 873–879 (2014).
5. IPCC Working Group III. *Integrated Assessment Modelling Consortium (IAMC) AR5 Scenario Database* https://secure.iiasa.ac.at/web-apps/ene/AR5DB/ (International Institute for Applied Systems Analysis, 2014).
6. Allen, M. R. *et al.* Warming caused by cumulative carbon emissions towards the trillionth tonne. *Nature* **458,** 1163–1166 (2009).
7. Matthews, H. D., Gillett, N. P., Stott, P. A. & Zickfeld, K. The proportionality of global warming to cumulative carbon emissions. *Nature* **459,** 829–832 (2009).
8. Friedlingstein, P. *et al.* Persistent growth of CO_2 emissions and implications for reaching climate targets. *Nature Geosci.* **7,** 709–715 (2014).
9. Leaton, J. *Unburnable Carbon—Are the World's Financial Markets Carrying a Carbon Bubble?* http://www.carbontracker.org/wp-content/uploads/2014/09/Unburnable-Carbon-Full-rev2-1.pdf (Investor Watch, 2011).
10. McGlade, C. E. A review of the uncertainties in estimates of global oil resources. *Energy* **47,** 262–270 (2012).
11. Society of Petroleum Engineers (SPE). *Petroleum Resources Management System.* www.spe.org/industry/docs/Petroleum_Resources_Management_System_2007.pdf (SPE, 2008).
12. Bauer, N. *et al.* Global fossil energy markets and climate change mitigation—an analysis with REMIND. *Clim. Change* http://dx.doi.org/10.1007/s10584-013-0901-6 (2013).
13. Anandarajah, G., Pye, S., Usher, W., Kesicki, F. & McGlade, C. E. *TIAM-UCL Global Model Documentation.* http://www.ucl.ac.uk/energy-models/models/tiam-ucl/tiam-ucl-manual (University College London, 2011).
14. Meinshausen, M., Raper, S. C. B. & Wigley, T. M. L. Emulating atmosphere–ocean and carbon cycle models with a simpler model, MAGICC6—Part 1: Model description and calibration. *Atmos. Chem. Phys.* **11,** 1417–1456 (2011).
15. Usher, W. & Strachan, N. Critical mid-term uncertainties in long-term decarbonisation pathways. *Energy Policy* **41,** 433–444 (2012).
16. IEA. *Resources to Reserves* Ch. 8 (International Energy Agency, 2013).
17. Alberta Energy Regulator (AER). *Alberta's Energy Reserves 2013 and Supply/Demand Outlook 2014–2023.* www.aer.ca/documents/sts/ST98/ST98-2014.pdf (AER, 2014).
18. Yergin, D. *The Prize: the Epic Quest for Oil, Money and Power* Epilogue (Simon and Schuster, 2009).

Acknowledgements We thank I. Keppo at the UCL Energy Institute, E. Trutnevyte at ETH Zurich, and A.-M. Lyne at the UCL Department of Statistical Science. This research formed part of the programme of the UK Energy Research Centre and was supported by the UK Research Councils under Natural Environment Research Council award NE/G007748/1.

Author Contributions Both authors contributed equally to this work.

Author Information Reprints and permissions information is available at www.nature.com/reprints. The authors declare no competing financial interests. Readers are welcome to comment on the online version of the paper. Correspondence and requests for materials should be addressed to C.M. (christophe.mcglade@ucl.ac.uk).

METHODS

Fossil fuel definitions. A 'McKelvey' box[19] is often used to provide an overview of the relationship between different resource and reserve estimates[20]. The best estimates of current oil and gas reserves in Extended Data Table 1 were of the 'proved plus probable' or '2P' quantities. Since 2P reserve estimates are rare for coal and none are in the public domain, the best estimates shown for coal were of the 'proved' or '1P' reserves. Broadly speaking, 1P estimates are more conservative, often corresponding to an estimate with a 90% probability of being exceeded, while 2P estimates are the median estimate of the reserves for a given field or region[11].

Oil and gas can be further separated into 'conventional' and 'unconventional' reserves and resources. Again, there is no single definition of these terms, but here we define oil with density greater than water (often standardized as '10°API') to be unconventional and all other quantities as conventional. We therefore categorize the 'light tight oil' extracted from impermeable shale formations using hydraulic fracturing as conventional oil.

For gas, tight gas (gas trapped in relatively impermeable hard rock, limestone or sandstone), coal-bed methane (gas trapped in coal seams that is adsorbed in the solid matrix of the coal), and shale gas (gas trapped in fine-grained shale) are considered as the three 'unconventional gases'; all other quantities are considered to be conventional.

Coal is distinguished by its energy density following the definitions used by the Federal Institute for Geosciences and Natural Resources (BGR)[21]. Hard coal has an energy density greater than 16.5 MJ kg^{-1}; any quantities with energy density less than this are classified as lignite.

Derivation of reserve and resource estimates. The estimated oil and gas reserves and resources shown in Extended Data Table 1 were derived in the following manner[22]. We first identified the individual elements or categories of oil and gas that make up the global resource base. For oil these are: current conventional 2P reserves in fields that are in production or are scheduled to be developed, reserve growth, undiscovered oil, Arctic oil, light tight oil, natural gas liquids, natural bitumen, extra-heavy oil, and kerogen oil. The latter three of these are the unconventional oil categories.

Reserve growth is defined to be 'the commonly observed increase in recoverable resources in previously discovered fields through time'[23]. Quantities in this category here include any contributions from reserves in fields that have been discovered but are not scheduled to be developed ('fallow fields'), the new implementation of advanced production technologies such as enhanced oil recovery, changes in geological understanding, and changes in regional definitions.

There are eight categories of conventional and unconventional gas: current conventional 2P reserves that are in fields in production or are scheduled to be developed, reserve growth, undiscovered gas, Arctic gas, associated gas, tight gas, coal-bed methane, and shale gas. As noted above, the latter three of these are collectively referred to as unconventional gas.

We then selected the most robust data sources that provide estimates of the resource potential of each individual category within each country; these sources are set out in Extended Data Table 4. Taken together, differences between these sources provide a spread of discrete quantitative resource estimates for each category within each country. We also differentiated between the quantities of conventional oil that are natural gas liquids, and the quantities of natural gas that are associated with oil fields; these distinctions are important for modelling purposes but are rarely made in the literature.

For unconventional oil, we first generated a range of estimates for the in-place resources of natural bitumen, extra-heavy oil, and kerogen oil, and a range of potential recovery factors for different extraction technologies. We separately characterized the natural bitumen and kerogen oil resources that are extractable using mining technologies and those resources that are extractable using *in situ* technologies because the resource potential, costs, and energy requirements of these technologies are very different.

Continuous distributions were next constructed across these data ranges. Since there is no empirical basis for the choice of a suitable shape or form for such distributions, we used both the triangular and the beta distributions, chosen because they can be skewed both positively and negatively, and because they allow identical distributions to be used across all of the ranges derived. With equal weighting for each distribution, we combined these into a single individual resource distribution for each category within each country.

We then estimated the production costs of each of the oil and gas resource categories. Taking account of the resource uncertainty, these were used to develop supply cost curves for each category of oil and gas within each country.

We finally used a Monte Carlo selection process to combine these country-level supply cost curves. Regional supply cost curves were thus formed from aggregated supply cost curves for individual countries, and similarly supply cost curves formed for multiple categories of oil or gas within one or more countries. Data in Fig. 1 are the median values from these aggregate distributions with Extended Data Table 4 giving high (95th percentile), median, and low (5th percentile) estimates for each category at the global level.

In most industry databases of oil and gas reserves (for example, the database produced by the consultancy IHS CERA[24,25]), some of the quantities classified as reserves lie in fields that were discovered over ten years ago, yet these fields have not been developed and there are no plans at present to do so. These are sometimes referred to as 'fallow fields'. For gas these quantities can also be called 'stranded gas', and they can be quite substantial; for example ref. 24 suggests that 50% gas reserves outside of North America are in stranded fields. Strictly, oil and gas in such fields should not be classified as reserves (for example, ref. 11 states that reserve quantities must have a 'reasonable timetable for development'). However, in this work, to ensure that the reserve estimates provided in Table 1 are not substantially different from the global totals provided by these industry databases, we follow their convention of classifying these quantities as reserves.

There are fewer independent estimates of reserves for coal and so we simply relied upon the estimates provided by the BGR[21] for the reserve figures in Extended Data Table 1. The RURR of coal are more problematic to characterize, however. The 'resource' estimates provided by the BGR are not estimates of the quantities that can actually be extracted but are the in-place quantities; large portions of these are unlikely ever to be technically recoverable.

We therefore used the proved, probable and possible reserve estimates for hard coal and lignite provided by the World Energy Council[26] for a selection of countries. The sum of these three figures gives an estimate of the 'tonnage within the estimated additional amount in place that geological and engineering information indicates with reasonable certainty might be recovered in the future' (the definition provided by the World Energy Council). Since the sum of these three figures takes account of technical recoverability, we consider that, while imperfect, they provide a better estimate of the ultimately recoverable resources of coal than either the (narrower) proved reserve or the (broader) in-place resource estimates.

There are a number of countries that are estimated by the BGR to hold large quantities of coal in place but for which no probable and possible reserve estimates are provided by the World Energy Council. The ratio of the World Energy Council resource estimate to the BGR in-place estimate in countries that have estimates provided by both sources can vary substantially, but the average ratio is 16% for hard coal and 31% for lignite. We therefore assumed this ratio to generate resource estimates for all countries for which only BGR in-place estimates are provided. The proved reserve estimates of coal are so large themselves that the resource estimates are less important than is the case for oil and gas resource estimates.

There are few other sources providing a comprehensive overview of fossil fuel availability. Further, these often do not provide their sources or the methods used to generate estimates, do not define fully what categories or elements are included or excluded, and do not indicate sufficient conversion factors that would allow a like-with-like comparison. Some exceptions, however, are the IEA[27,28], the IIASA Global Energy Assessment (GEA)[29], and the BGR[21]. Their estimates are shown together with our aggregated reserve and resource estimates in Extended Data Table 5.

A number of factors contribute to the large variation between these estimates. A key reason is that the definitions of 'reserves' and 'resources' differ among sources, and so it is problematic to seek to compare them directly. For example, as noted above, the BGR, whose estimates are followed closely by the other sources, gives the total coal in place rather than an estimate of the resources that can be recovered, as in our study. Other reasons for the differences seen include: (1) the exclusion or inclusion of certain categories of fossil fuels such as light tight oil, aquifer gas, and methane hydrates; (2) whether proved (1P) or proved plus probable (2P) reserves are reported, and the methods used to generate the 1P reserve estimates; (3) the potential inflation of reserve estimates for political reasons, and whether they should consequently be increased or reduced[30]; (4) the inclusion of stranded gas volumes in gas reserve estimates; (5) differences in the functional form used to estimate volumes of reserve growth (if reserve growth is included at all); (6) the difficulty in estimating current recovery factors (the ratio of recoverable resources to total resources in place), and how these may increase in the future; (7) differences between the methods used to estimate undiscovered oil and gas volumes; (8) the scarcity of reports providing reliable estimates of the potential resources of Arctic oil and gas, light tight oil, tight gas and coal bed methane, and the frequent consequent reliance upon expert judgement; (9) variation in what unconventional oil production technologies, which vary considerably in their recovery factors, will be used in the future; and (10) the chosen cut-off 'yield' (the volume of synthetic oil produced from a given weight of shale rock) for kerogen oil.

The estimates considered in our model are the result of careful and explicit consideration of all these issues, with our choices justified in the light of available knowledge. It can be seen in Extended Data Table 5, however, that our median figures are generally lower than the estimates provided by the other sources shown there. Therefore, although we consider our median resource estimates to be more robust than the figures used by these other sources, if in fact these other estimates were found to be closer to being correct, then the unburnable resources given in Extended Data Table 3 would also be larger. For example, if total gas resources are actually at the GEA high estimate, then the percentage that should be classified as unburnable before 2050 under the 2 °C scenario would increase to 99% rather than our estimate of 75%.

The cut-off date after which quantities that have not been produced should be considered 'unburnable' is also an important assumption. While there are no specific timeframes attached to the definition of reserves, quantities are usually required to be developed within, for example, a 'reasonable timeframe'[11]. It is doubtful whether any reserves not produced by 2050 would fulfil this criterion. We therefore take cumulative production of reserves between 2010 and 2050 as the reserve 'utilization', and classify any quantities not used within this time as those that should be 'unburnable' if a certain temperature rise is not to be exceeded. Similarly, if none, or only a minor proportion, of a certain non-reserve resource is produced before 2050, then any current interest in developing it would be questionable. We thus also rely on 2050 as the cut-off date for classifying resources that should be considered as unburnable.

Description and key assumptions in TIAM-UCL. The TIMES Integrated Assessment Model in University College London ('TIAM-UCL') is a technology-rich, bottom-up, whole-system model that maximizes social welfare under a number of imposed constraints. It models all primary energy sources (oil, gas, coal, nuclear, biomass, and renewables) from resource production through to their conversion, infrastructure requirements, and finally to sectoral end-use. An extended explanation of input assumptions, approaches and data sources can be found in ref. 13. The base year of TIAM-UCL is 2005, the model is run in full to 2100, and thereafter the climate module is run to 2200. Results are presented here only between 2010 and 2050 (and are reported in five-year increments). All scenarios in this paper are run with the assumption of perfect foresight.

Resources and costs of all primary energy production are specified separately within 16 regions covering the world, and separately within the regions that contain members of the Organisation of Petroleum Exporting Countries (OPEC); the names of these are presented in Extended Data Table 6. For clarity in the main text, we have aggregated some of these regions into ten more-encompassing groups.

The climate module of TIAM-UCL is calibrated to the MAGICC model[14]. This module can be used to project the effects of greenhouse gas emissions on: atmospheric concentrations of greenhouse gas, radiative forcing, and average global temperature rises. It can also be used to constrain the model to certain bounds on these variables. In this work, the climate module is used to restrict the temperature rise to certain levels (as explained below). For the calibration to MAGICC, values from the probability distributions of climate parameters in MAGICC were selected so that there is a 60% chance that the temperature rise will remain below any level reported. Any constraints imposed using the TIAM-UCL climate module thus also correspond to this probability.

The emissions profiles[5] used in Fig. 2 were converted to temperature rises using MAGICC. To ensure consistency with TIAM-UCL, we use the 60th percentile temperature trajectory from MAGICC and then group by the final temperature rise in 2100; there is therefore also a 60% chance that the temperature rise will be below the level indicated.

For each of the scenarios run in this paper using TIAM-UCL, a 'base case' is first formed that incorporates no greenhouse gas abatement policies. This base case uses the standard version of the model that relies upon minimizing the discounted system cost. This is used to generate base prices for each commodity in the model. TIAM-UCL is then re-run using the elastic-demand version with the greenhouse gas abatement policies introduced. This version of the model maximizes social welfare (the sum of consumer and producer surplus) and allows the energy-service demands to respond to changes in the endogenously determined prices resulting from these new constraints.

Fossil fuel modelling in TIAM-UCL. Oil and gas are both modelled in a similar manner in TIAM-UCL. The nine categories of conventional and unconventional oil and eight categories of conventional and unconventional gas identified above are all modelled separately. Coal production in TIAM-UCL is modelled more collectively, with only two categories, reserves and resources, for hard coal and lignite.

Natural bitumen and kerogen oil resources can be produced using either mining or *in situ* means, the technologies for which have different costs, efficiencies, and energy inputs. Although natural gas is predominantly used at present for the energy inputs to these unconventional resources, the model is free to choose any source of heat, electricity and hydrogen to allow greater flexibility. The costs of the auxiliary energy inputs required to extract and upgrade the native unconventional oils are determined endogenously by the model.

Each of the coal, gas and oil categories are modelled separately within the regions listed in Extended Data Table 6, with each resource category within each region split into three cost steps. As discussed above, the supply cost curves given in Fig. 1 comprise the data input to TIAM-UCL.

After processing, oil is next refined into products (gasoline, diesel, naphtha and so on), whereas processed gas and coal can be used directly. Fuel switching to and from all of the fossil fuels is possible. Trade of hard coal, crude oil, refined products, natural gas, both in pipelines and as liquefied natural gas, is allowed. Lignite cannot be traded between the regions.

Refined oil products can also be produced directly using Fischer–Tropsch processes with possible feedstocks of coal, gas, or biomass; these technologies can also be employed either with or without carbon capture and storage. Regional coal, oil and gas prices are generated endogenously within the model. These incorporate the marginal cost of production, scarcity rents, rents arising from other imposed constraints, and transportation costs.

A new key aspect of TIAM-UCL is the imposition of asymmetric constraints on the rate of production of oil and gas given a certain resource availability; these are intended to represent 'depletion rate constraints'. In TIAM-UCL, these constraints are modelled through introducing maximum annual production growth and maximum 'decline rate' restrictions. These are imposed on each cost step of each category of both oil and gas in each region, and ensure that the production follows a more realistic profile over time.

Data for these constraints are available at the field level from the bottom-up economic and geological oil field production model ('BUEGO')[31]. BUEGO contains a data-rich representation of 7,000 producing 'undiscovered' and discovered but undeveloped oil fields. These data include each field's 2P reserves, potential production capacity increases, water depth, capital and operating costs, and natural decline rate (the rate at which production would decline in the absence of any additional capital investment).

We used production-weighted averages (as of 2010) of the individual fields within each region to give average regional natural decline rates, which were imposed as maximum decline constraints in TIAM-UCL in the form of equal maximum annual percentage reductions. Although data on gas natural decline rates are much more sparse, some are available at a regional level[32], which can be compared with similar results for oil natural decline rates[25]. This comparison suggests that gas natural decline rates are on average 1% per year greater than for oil, with similar distributions for location (onshore/offshore) and size. The constraints placed on the maximum annual reductions in natural gas production were thus assumed to be 1% higher than those derived for oil.

As identified in the main text, to understand the quantities of reserves of oil and gas that are unburnable, production of reserve sources only should be compared with reserve estimates, while cumulative production of all sources should be compared with the resource estimates. For coal, the reserves are so much greater than cumulative production under any scenario that this distinction is not as important.

The base year of TIAM-UCL is 2005, but the base year of this study is 2010. Since reserves have grown, and oil and gas have been discovered in the intervening five years, some quantities that were classified as reserve growth and undiscovered oil and gas in 2005 should be classified as reserves in 2010. Within each region, the cumulative production figures to which the reserve estimates in Extended Data Table 1 are compared therefore contain production from the conventional 2P reserves in the 'fields in production or scheduled to be developed' category, as well as some portions of production from the 'reserve growth' and 'undiscovered' categories. In addition, since, for example, reserves of natural bitumen are included in the reserves figures of Canada and unconventional gas reserves are included in the reserves figures of the United States, production of some of the unconventional categories are also included in these cumulative production figures. To ensure consistency within each region, the maximum production potentials over the modelling period from the categories included in the cumulative production figures are equal to the reserve estimates given in Extended Data Table 1.

Overview of scenarios implemented. A brief overview of the main assumptions within the four scenarios run as part of this work is provided in Extended Data Table 7. For the emissions mitigation scenarios (those that limit the temperature rise to 3 °C and 2 °C), we assume that there are only relatively modest efforts to limit emissions in early periods as explained. The assumptions within the 2 °C sensitivity scenarios used to construct Extended Data Fig. 1 are provided in Extended Data Table 2.

19. McKelvey, V. E. Mineral resource estimates and public policy. *Am. Sci.* **60,** 32–40 (1972).
20. McGlade, C. E., Speirs, J. & Sorrell, S. Unconventional gas—a review of regional and global resource estimates. *Energy* **55,** 571–584 (2013).
21. Federal Institute for Geosciences and Natural Resources (BGR). *Energy Study 2012. Reserves, Resources and Availability of Energy Resources.* http://www.bgr.bund.de/DE/Gemeinsames/Produkte/Downloads/DERA_Rohstoffinformationen/rohstoffinformationen-15e.pdf?__blob=publicationFile&v=3 (BGR, 2012).
22. McGlade, C. E. *Uncertainties in the outlook for oil and gas.* PhD thesis, UCL, http://discovery.ucl.ac.uk/1418473/2/131106%20Christophe%20McGlade_PhD%20Thesis.pdf (2013).

23. Klett, T. & Schmoker, J. in *Giant Oil and Gas fields of the Decade 1990–1999* (ed. Halbouty, M. T.) 107–122 (The American Association of Petroleum Geologists, 2003).
24. Attanasi, E. D. & Freeman, P. A. Survey of Stranded Gas and Delivered Costs to Europe of Selected Gas Resources. *SPE Econ. Manag.* **3,** 149–162 (2011).
25. International Energy Agency (IEA). *World Energy Outlook.* http://www.worldenergyoutlook.org/media/weowebsite/2008-1994/weo2008.pdf (IEA, 2008).
26. Trinnaman, J. & Clarke, A. *Survey of Energy Resources* http://www.worldenergy.org/wp-content/uploads/2012/09/ser_2010_report_1.pdf (World Energy Council, 2010).
27. International Energy Agency (IEA). *World Energy Outlook*. http://www.worldenergyoutlook.org/publications/weo-2013/ (IEA, 2013).
28. International Energy Agency (IEA). *World Energy Outlook*. http://www.iea.org/publications/freepublications/publication/weo2011_web.pdf (IEA, 2011).
29. Rogner, H.-H. *et al.* in *Global Energy Assessment—Towards a Sustainable Future* Ch. 7, 423–512 (Cambridge University Press, 2012).
30. Owen, N. A., Inderwildi, O. R. & King, D. A. The status of conventional world oil reserves—hype or cause for concern? *Energy Policy* **38,** 4743–4749 (2010).
31. McGlade, C. & Ekins, P. Un-burnable oil: an examination of oil resource utilisation in a decarbonised energy system. *Energy Policy* **64,** 102–112 (2014).
32. International Energy Agency (IEA). *World Energy Outlook*. http://www.worldenergyoutlook.org/media/weowebsite/2009/WEO2009.pdf (IEA, 2009).
33. Leatherdale, A. *et al. Bioenergy Review: Technical Paper 2—Global and UK Bioenergy Supply Scenarios.* http://archive.theccc.org.uk/aws2/Bioenergy/1463%20CCC_Bio-TP2_supply-scen_FINALwithBkMks.pdf (Committee on Climate Change, 2011).
34. O'Neill, B. C. *et al.* A new scenario framework for climate change research: the concept of shared socioeconomic pathways. *Clim. Change* **122,** 387–400 (2014).
35. Campbell, C. J. *Atlas of Oil and Gas Depletion* (Springer, 2013).
36. Herrmann, L. *et al. Oil and Gas for Beginners* 270–413 (Deutsche Bank, 2013).
37. Klett, T. R. *et al.* An Assessment of Potential Additions to Conventional Oil and Gas Resources of the World (outside the United States) from Reserve Growth. http://pubs.usgs.gov/fs/2012/3052/fs2012-3052.pdf (USGS, 2012).
38. Klett, T. R. *et al. Potential Additions to Conventional Oil and Gas Resources in Discovered Fields of the United States from Reserve Growth, 2012*. http://pubs.usgs.gov/fs/2012/3108/ (USGS, 2012).
39. Ahlbrandt, T., Charpentier, R., Klett, T., Schmoker, J. & Schenk, C. *USGS World Petroleum Assessment 2000.* http://pubs.usgs.gov/dds/dds-060/ (USGS, 2000).
40. Bentley, R., Miller, R., Wheeler, S. & Boyle, G. *UKERC Review of Evidence on Global Oil Depletion: Annex 1—Models of global oil supply for the period 2008-2030.* http://www.ukerc.ac.uk/support/tiki-download_file.php?fileId=292 (UKERC, 2009).
41. Brownfield, M., Charpentier, R. R., Cook, T., Gautier, D. L. & Higley, D. K. *An Estimate of Undiscovered Conventional Oil and Gas Resources of the World, 2012.* http://pubs.usgs.gov/fs/2012/3042/fs2012-3042.pdf (USGS, 2012).
42. Gautier, D. L. *et al.* Assessment of undiscovered oil and gas in the Arctic. *Science* **324,** 1175–1179 (2009).
43. Smith, T. Arctic dreams—a reality check. Geo ExPro **4,** 16–24 (2007).
44. Shah, A. *et al.* A review of novel techniques for heavy oil and bitumen extraction and upgrading. *Energy Environ. Sci.* **3,** 700–714 (2010).
45. Clarke, B. *NPC Global Oil and Gas Study: Topic Paper 22—Heavy Oil.* www.npc.org/study_topic_papers/22-ttg-heavy-oil.pdf (National Petroleum Council, 2007).
46. Schenk, C. *et al. An Estimate of Recoverable Heavy Oil Resources of the Orinoco Oil Belt, Venezuela.* http://pubs.usgs.gov/fs/2009/3028/pdf/FS09-3028.pdf (USGS, 2009).
47. Attanasi, E. D. & Meyer, R. F. in *2010 Survey of Energy Resources* 123–150 (World Energy Council, 2010).
48. Johnson, R. C., Mercier, T. J. & Brownfield, M. Assessment of in-place oil shale resources of the Green River Formation, Greater Green River Basin in Wyoming, Colorado, and Utah. http://pubs.usgs.gov/fs/2011/3063/pdf/FS11-3063.pdf (USGS, 2011).
49. Dyni, J. *Geology and Resources of Some World Oil-Shale Deposits.* http://pubs.usgs.gov/sir/2005/5294/pdf/sir5294_508.pdf (USGS, 2006).
50. Biglarbigi, K., Mohan, H. & Carolus, M. *Potential for Oil Shale Development in the United States.* http://www.inteki.com/reports.html (INTEK, 2009).
51. CEDIGAZ. *Natural Gas in the World, End of July 2008* (Centre International d'Information sur le Gaz Naturel et tous Hydrocarbures Gazeux (CEDIGAZ), 2009).

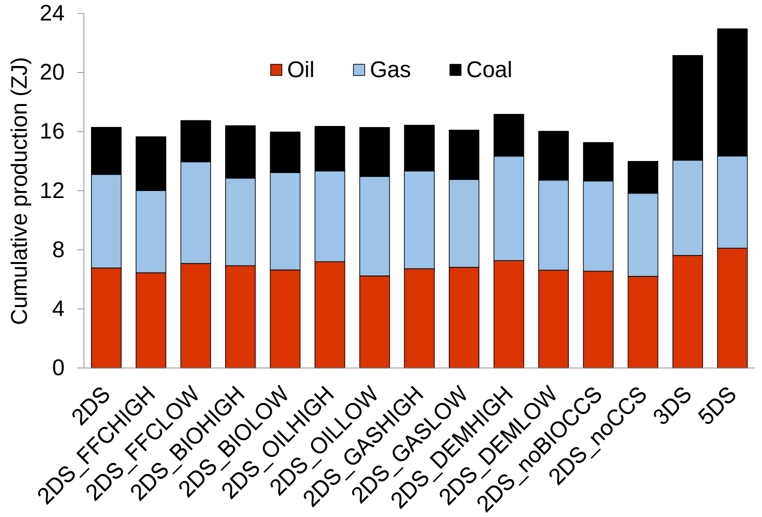

Extended Data Figure 1 | Cumulative fossil fuel production under a range of sensitivity scenarios run using TIAM-UCL. Scenario names and characteristics are given in Extended Data Table 2.

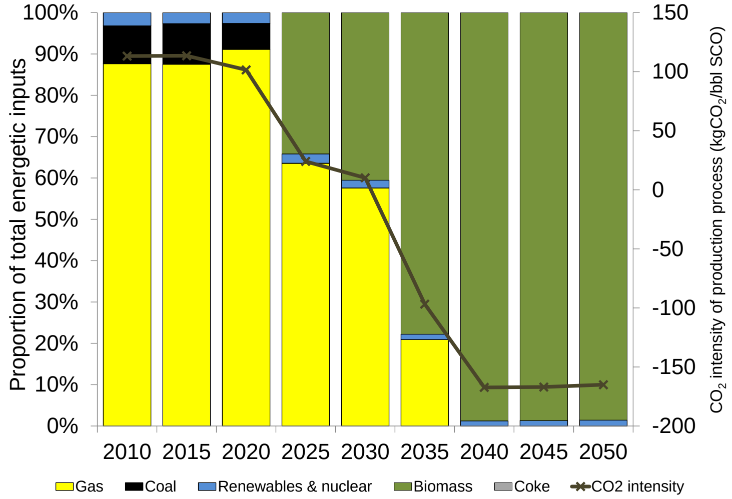

Extended Data Figure 2 | The auxiliary energy inputs for natural bitumen production in Canada by *in situ* technologies in the 2 °C scenario and the CO_2 intensity of these. bbl SCO, a barrel of synthetic crude oil, the oil that results after upgrading the natural bitumen.

Extended Data Table 1 | Best estimates of remaining reserves and remaining ultimately recoverable resources from 2010

	Oil (Gb)			Gas (Tcm)			Hard coal (Gt)		Lignite (Gt)	
Country or region	Res	Con RURR	Uncon RURR	Res	Con RURR	Uncon RURR	Res	RURR	Res	RURR
Africa	111	280	70	13	45	35	31	45	2	5
Canada	53	60	640	1	5	25	4	35	2	40
China and India	38	90	110	5	10	40	255	1,080	16	120
FSU	152	370	360	61	95	30	123	580	94	490
CSA	148	360	450	9	30	55	10	25	5	10
Europe	25	110	30	6	25	20	17	70	66	160
Middle East	689	1,050	10	76	105	20	2	10	2	5
OECD Pacific	6	30	130	4	10	20	45	120	44	200
ODA	23	75	5	9	25	15	15	40	14	155
United States	50	190	650	8	25	40	226	560	31	335
Global	1,294	2,615	2,455	192	375	300	728	2,565	276	1,520

'Con' and 'Uncon' stand for conventional and unconventional sources, respectively. Coal is specified in billions of tonnes (Gt), gas in trillions of cubic metres (Tcm) and oil in billions of barrels (Gb). Res, reserves.

Extended Data Table 2 | Labels and description of the sensitivity scenarios modelled in this project

Sensitivity Name	Description
2DS_FFCHIGH	Production costs of all fossil fuel technologies are 50% larger in 2015 and 100% larger in 2020 than in 2DS, with equal annual percentage changes between these dates and remaining at this level for the model horizon
2DS_FFCLOW	Production costs of all fossil fuel technologies are 33% lower in 2015 and 50% lower in 2020 than in 2DS, with equal annual percentage changes between these dates and remaining at this level for the model horizon
2DS_BIOHIGH	The maximum annual production of solid biomass and bio-crops in 2050 is assumed to be 350 EJ. This is close to the highest level of production of bio-energy in any of the scenarios from the AR5 scenario database[5] and is around three times the equivalent figure in 2DS (119 EJ).
2DS_BIOLOW	The maximum annual production of solid biomass and bio-crop in 2050 is assumed to be 38 EJ. This is similar to the figure given in the central scenario from [33] and is around a third of the equivalent figure in 2DS (119 EJ).
2DS_OILHIGH	Uses the high values of each category of oil in each region from the aggregate resource distributions described in the methods section (Extended Data Table 4)
2DS_OILLOW	Uses the low values of each category of oil in each region (Extended Data Table 4)
2DS_GASHIGH	Uses the high values of each category of gas in each region (Extended Data Table 4)
2DS_GASLOW	Uses the low values of each category of gas in each region (Extended Data Table 4)
2DS_DEMHIGH	The major drivers of energy service demands in TIAM-UCL are growth in GDP, population, and GDP/capita. Future regional growth in GDP and population are therefore modified to the values given in Shared Socioeconomic Pathway (SSP) number 5[34] the SSP with the highest GDP and GDP/capita growth by 2050 (a 240% increase in the global average; cf. a 120% increase in 2DS). All other energy service demands (not relying on GDP or population) are also modified commensurately.
2DS_DEMLOW	Future regional growth in GDP and population are modified to the values given in Shared Socioeconomic Pathway (SSP) number 3:[34] the SSP with the lowest GDP and GDP/capita growth by 2050 (a 50% increase in the global average).
2DS_NOBIOCCS	No negative emissions technologies are permitted i.e. carbon capture and storage (CCS) cannot be applied to any electrical or industrial process that uses biomass or bio-energy as feedstock in any period.
2DS_NOCCS	CCS is not permitted to be applied to any electrical or industrial process in any period.

Data for bio-energy sensitivities from refs 5 and 33, and for demand sensitivities from ref. 34.

Extended Data Table 3 | Regional distribution of resources unburnable before 2050 in absolute terms and as a percentage of current resources under the 2 °C scenario that allows CCS

	Conven oil		Unconven oil		Conven Gas		Unconven Gas		Hard Coal		Lignite	
Country or region	Gb	%	Gb	%	Tcm	%	Tcm	%	Gt	%	Gt	%
Africa	141	50%	70	100%	28	61%	35	100%	42	94%	2.8	56%
Canada	43	72%	633	99%	3.6	73%	18	71%	34	98%	39	97%
China and India	54	60%	110	100%	8.0	80%	35	88%	1,003	93%	106	88%
FSU	201	54%	360	100%	63	67%	27	89%	576	99%	480	98%
CSA	198	55%	447	99%	23	76%	51	92%	21	85%	6.3	63%
Europe	64	58%	30	100%	18	72%	16	78%	69	99%	142	89%
Middle East	554	53%	10	100%	72	68%	20	100%	10	100%	5.0	99%
OECD Pacific	23	77%	130	100%	9.0	90%	15	74%	116	97%	198	99%
ODA	38	51%	5.0	100%	14	55%	12	78%	34	84%	142	92%
United States	99	52%	650	100%	19	75%	20	50%	556	99%	317	95%
Global	1,417	54%	2,445	100%	257	69%	247	82%	2,462	96%	1,438	95%

'Conven' and 'Unconven' stand for conventional and unconventional resources, respectively.

Extended Data Table 4 | Principal data sources used to derive reserve and resource estimates and estimates at the global level for each category of production

Category	Data sources used to provide country-level estimates of resources	Aggregated high estimate	Aggregated median estimate	Aggregated low estimate
Oil		(in Gb)	(in Gb)	(in Gb)
Current conventional 2P reserves in fields in production or scheduled to be developed	[21,31,35,36]	950	820	620
Reserve growth	[37,38]	1,200	850	610
Undiscovered oil	Fact sheets since USGS World Petroleum Assessment [39] and [35,40,41]	580	300	180
Arctic oil	[42,43]	80	65	40
Light tight oil	[10]	470	300	150
Natural gas liquids (NGL)	[26] Ancillary data associated with [39]	380	280	170
Natural bitumen	Oil in place estimates [17,26]	Mined RURR 130	Mined RURR 100	Mined RURR 70
	Extraction technologies [44–46]	*In situ* RURR 1290	*In situ* RURR 840	*In situ* RURR 520
Extra-heavy oil	Oil in place estimates [47,48] Extraction technologies [47] and refs for bitumen	750	440	230
Kerogen oil	Oil in place estimates [49,50]	Mined RURR 740	Mined RURR 485	Mined RURR 270
	Extraction technologies [51]	*In situ* RURR 1,080	*In situ* RURR 590	*In situ* RURR 190
Total		7,650	5,070	3,050
Gas		(in tcm)	(in tcm)	(in tcm)
Current conventional 2P reserves in fields in production or scheduled to be developed	[35,52]	140	130	110
Reserve growth	[24,37,38]	125	90	60
Undiscovered gas	Fact sheets since USGS World Petroleum Assessment [39] and [35,41]	180	120	80
Arctic gas	[42,43]	40	35	25
Tight gas	[20]	60	60	60
Coal-bed methane	[20]	45	40	20
Shale gas	[20]	310	200	120
Associated gas	[36,37,44]	Included in the above		
Total		900	675	475

High and low values are the aggregated 95th and 5th percentile estimates, respectively. 'tcm', trillions of cubic metres. Data are from references 10, 17, 20, 21, 31, 35, 36, 37, 38, 39, 40, 41, 42, 43, 44, 45, 46, 47, 48, 49, 50 and 51.

Extended Data Table 5 | Global aggregated oil, gas and coal reserve and resource estimates from a selection of data sources

	Oil (Gb)		Gas (Tcm)		Coal (Gt)	
Organisation	Reserves	Resources	Reserves	Resources	Reserves	Resources
BGR	1,600	4,750	195	825	1,000	23,500
IEA	1,700	5,950	190	810	1,000	21,000
GEA	1,500 - 2,300	4,200 - 6,000	670 - 2,000	2,000 - 12,500	850 - 1,000	14,000 - 20,000
This study's median figures	1,300	5,070	190	675	1,000	4,085

BGR, Federal Institute for Geosciences and Natural Resources[21]; IEA, International Energy Agency[27,28]; GEA, Global Energy Assessment[29].

Extended Data Table 6 | Regions included in TIAM-UCL and their aggregation to the regions given in the main text

Region	Aggregated region in main text
Non-OPEC Africa	Africa
OPEC Africa	Africa
Australia	OECD Pacific
Canada	Canada
Non-OPEC Central and South America	Central and South America (CSA)
OPEC Central and South America	Central and South America (CSA)
China	China and India
Eastern Europe	Europe
Former Soviet Union	Former Soviet Union (FSU)
India	China and India
Japan	OECD Pacific
Non-OPEC Middle	Middle East
OPEC Middle East	Middle East
Mexico	Central and South America (CSA)
Other Developing Asia	Other Developing Asia (ODA)
South Korea	OECD Pacific
United Kingdom	Europe
United States	United States
Western Europe	Europe

Extended Data Table 7 | Labels and description of the four core scenarios modelled in this project

Scenario Name	Description
5DS	The model is constrained to keep the average global surface temperature rise to less than 5°C in all years to 2200. No other emissions constraints are imposed, and since allowed emissions under this scenario are so high (i.e. the constraint is very lax), no real emissions mitigation is required. These constraints result in 2050 GHG emissions of 71 Gt CO_2-eq (up from around 48 Gt CO_2-eq in 2010).
3DS	From 2005 to 2010, the model is fixed to the solution given in the 5°C temperature i.e. we assume that no emissions reductions are required. From 2010-2015, it is assumed that the model must be on track to achieve the emissions reduction pledges set out in the Copenhagen Accord[1], but no other emissions reductions are required. From 2015 onwards the model must meet the Copenhagen Accord emissions reductions in 2020, and emissions must be such as to keep the average global surface temperature rise below 3°C in all years to 2200. These constraints result in 2050 GHG emissions of 54 Gt CO_2-eq
2DS	The constraints between 2005 and 2015 in this scenario are identical to the 3DS. From 2015 onwards the model must meet the Copenhagen Accord emissions reductions in 2020, and emissions must be such as to keep the average global surface temperature rise below 2°C in all years to 2200. These constraints result in 2050 GHG emissions of 21 Gt CO_2-eq
2DS-noCCS	Emissions reduction requirements are identical to 2DS. Carbon capture and storage (CCS) is not permitted to be applied to any electricity or industrial process in any period.

GHG, greenhouse gas measured in tonnes of CO_2 equivalent (CO_2-eq). Data from ref. 1.

PERSPECTIVE

Trajectories of the Earth System in the Anthropocene

Will Steffen[a,b,1], Johan Rockström[a], Katherine Richardson[c], Timothy M. Lenton[d], Carl Folke[a,e], Diana Liverman[f], Colin P. Summerhayes[g], Anthony D. Barnosky[h], Sarah E. Cornell[a], Michel Crucifix[i,j], Jonathan F. Donges[a,k], Ingo Fetzer[a], Steven J. Lade[a,b], Marten Scheffer[l], Ricarda Winkelmann[k,m], and Hans Joachim Schellnhuber[a,k,m,1]

Edited by William C. Clark, Harvard University, Cambridge, MA, and approved July 6, 2018 (received for review June 19, 2018)

We explore the risk that self-reinforcing feedbacks could push the Earth System toward a planetary threshold that, if crossed, could prevent stabilization of the climate at intermediate temperature rises and cause continued warming on a "Hothouse Earth" pathway even as human emissions are reduced. Crossing the threshold would lead to a much higher global average temperature than any interglacial in the past 1.2 million years and to sea levels significantly higher than at any time in the Holocene. We examine the evidence that such a threshold might exist and where it might be. If the threshold is crossed, the resulting trajectory would likely cause serious disruptions to ecosystems, society, and economies. Collective human action is required to steer the Earth System away from a potential threshold and stabilize it in a habitable interglacial-like state. Such action entails stewardship of the entire Earth System—biosphere, climate, and societies—and could include decarbonization of the global economy, enhancement of biosphere carbon sinks, behavioral changes, technological innovations, new governance arrangements, and transformed social values.

Earth System trajectories | climate change | Anthropocene | biosphere feedbacks | tipping elements

The Anthropocene is a proposed new geological epoch (1) based on the observation that human impacts on essential planetary processes have become so profound (2) that they have driven the Earth out of the Holocene epoch in which agriculture, sedentary communities, and eventually, socially and technologically complex human societies developed. The formalization of the Anthropocene as a new geological epoch is being considered by the stratigraphic community (3), but regardless of the outcome of that process, it is becoming apparent that Anthropocene conditions transgress Holocene conditions in several respects (2). The knowledge that human activity now rivals geological forces in influencing the trajectory of the Earth System has important implications for both Earth System science and societal decision making. While recognizing that different societies around the world have contributed differently and unequally to pressures on the Earth System and will have varied capabilities to alter future trajectories (4), the sum total of human impacts on the system needs to be taken into account for analyzing future trajectories of the Earth System.

Here, we explore potential future trajectories of the Earth System by addressing the following questions.

> Is there a planetary threshold in the trajectory of the Earth System that, if crossed, could prevent stabilization in a range of intermediate temperature rises?

> Given our understanding of geophysical and biosphere feedbacks intrinsic to the Earth System, where might such a threshold be?

[a]Stockholm Resilience Centre, Stockholm University, 10691 Stockholm, Sweden; [b]Fenner School of Environment and Society, The Australian National University, Canberra, ACT 2601, Australia; [c]Center for Macroecology, Evolution, and Climate, University of Copenhagen, Natural History Museum of Denmark, 2100 Copenhagen, Denmark; [d]Earth System Science Group, College of Life and Environmental Sciences, University of Exeter, EX4 4QE Exeter, United Kingdom; [e]The Beijer Institute of Ecological Economics, The Royal Swedish Academy of Science, SE-10405 Stockholm, Sweden; [f]School of Geography and Development, The University of Arizona, Tucson, AZ 85721; [g]Scott Polar Research Institute, Cambridge University, CB2 1ER Cambridge, United Kingdom; [h]Jasper Ridge Biological Preserve, Stanford University, Stanford, CA 94305; [i]Earth and Life Institute, Université catholique de Louvain, 1348 Louvain-la-Neuve, Belgium; [j]Belgian National Fund of Scientific Research, 1000 Brussels, Belgium; [k]Research Domain Earth System Analysis, Potsdam Institute for Climate Impact Research, 14473 Potsdam, Germany; [l]Department of Environmental Sciences, Wageningen University & Research, 6700AA Wageningen, The Netherlands; and [m]Department of Physics and Astronomy, University of Potsdam, 14469 Potsdam, Germany

Author contributions: W.S., J.R., K.R., T.M.L., C.F., D.L., C.P.S., A.D.B., S.E.C., M.C., J.F.D., I.F., S.J.L., M.S., R.W., and H.J.S. wrote the paper.

The authors declare no conflict of interest.

This article is a PNAS Direct Submission.

[1]To whom correspondence may be addressed. Email: will.steffen@anu.edu.au or john@pik-potsdam.de.

This article contains supporting information online at www.pnas.org/lookup/suppl/doi:10.1073/pnas.1810141115/-/DCSupplemental.

Published online August 6, 2018.

If a threshold is crossed, what are the implications, especially for the wellbeing of human societies?

What human actions could create a pathway that would steer the Earth System away from the potential threshold and toward the maintenance of interglacial-like conditions?

Addressing these questions requires a deep integration of knowledge from biogeophysical Earth System science with that from the social sciences and humanities on the development and functioning of human societies (5). Integrating the requisite knowledge can be difficult, especially in light of the formidable range of timescales involved. Increasingly, concepts from complex systems analysis provide a framework that unites the diverse fields of inquiry relevant to the Anthropocene (6). Earth System dynamics can be described, studied, and understood in terms of trajectories between alternate states separated by thresholds that are controlled by nonlinear processes, interactions, and feedbacks. Based on this framework, we argue that social and technological trends and decisions occurring over the next decade or two could significantly influence the trajectory of the Earth System for tens to hundreds of thousands of years and potentially lead to conditions that resemble planetary states that were last seen several millions of years ago, conditions that would be inhospitable to current human societies and to many other contemporary species.

Risk of a Hothouse Earth Pathway

Limit Cycles and Planetary Thresholds. The trajectory of the Earth System through the Late Quaternary, particularly the Holocene, provides the context for exploring the human-driven changes of the Anthropocene and the future trajectories of the system (*SI Appendix* has more detail). Fig. 1 shows a simplified representation of complex Earth System dynamics, where the physical climate system is subjected to the effects of slow changes in Earth's orbit and inclination. Over the Late Quaternary (past 1.2 million years), the system has remained bounded between glacial and interglacial extremes. Not every glacial–interglacial cycle of the past million years follows precisely the same trajectory (7), but the cycles follow the same overall pathway (a term that we use to refer to a family of broadly similar trajectories). The full glacial and interglacial states and the ca. 100,000-years oscillations between them in the Late Quaternary loosely constitute limit cycles (technically, the asymptotic dynamics of ice ages are best modeled as pullback attractors in a nonautonomous dynamical system). This limit cycle is shown in a schematic fashion in blue in Fig. 1, *Lower Left* using temperature and sea level as the axes. The Holocene is represented by the top of the limit cycle loop near the label A.

The current position of the Earth System in the Anthropocene is shown in Fig. 1, *Upper Right* by the small ball on the pathway that leads away from the glacial–interglacial limit cycle. In Fig. 2, a stability landscape, the current position of the Earth System is represented by the globe at the end of the solid arrow in the deepening Anthropocene basin of attraction.

The Anthropocene represents the beginning of a very rapid human-driven trajectory of the Earth System away from the glacial–interglacial limit cycle toward new, hotter climatic conditions and a profoundly different biosphere (2, 8, 9) (*SI Appendix*). The current position, at over 1 °C above a preindustrial baseline (10), is nearing the upper envelope of interglacial conditions over the past 1.2 million years (*SI Appendix*, Table S1). More importantly, the rapid trajectory of the climate system over the past half-century along with technological lock in and socioeconomic

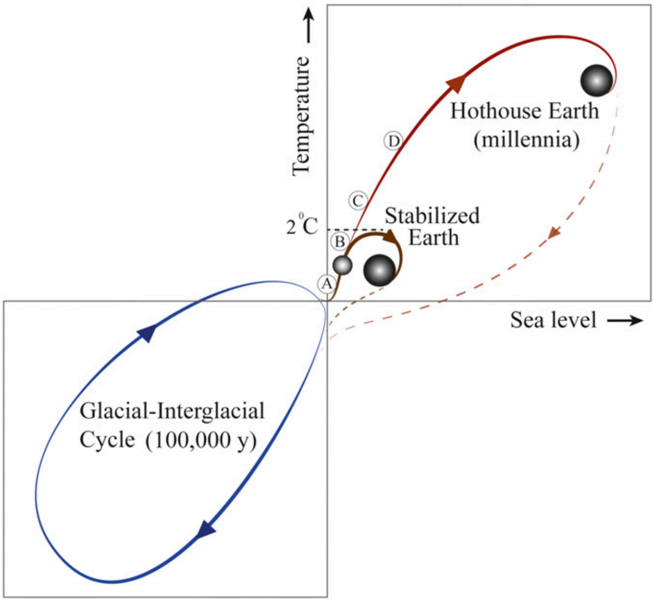

Fig. 1. A schematic illustration of possible future pathways of the climate against the background of the typical glacial–interglacial cycles (*Lower Left*). The interglacial state of the Earth System is at the top of the glacial–interglacial cycle, while the glacial state is at the bottom. Sea level follows temperature change relatively slowly through thermal expansion and the melting of glaciers and ice caps. The horizontal line in the middle of the figure represents the preindustrial temperature level, and the current position of the Earth System is shown by the small sphere on the red line close to the divergence between the Stabilized Earth and Hothouse Earth pathways. The proposed planetary threshold at ∼2 °C above the preindustrial level is also shown. The letters along the Stabilized Earth/Hothouse Earth pathways represent four time periods in Earth's recent past that may give insights into positions along these pathways (*SI Appendix*): A, Mid-Holocene; B, Eemian; C, Mid-Pliocene; and D, Mid-Miocene. Their positions on the pathway are approximate only. Their temperature ranges relative to preindustrial are given in *SI Appendix*, Table S1.

inertia in human systems commit the climate system to conditions beyond the envelope of past interglacial conditions. We, therefore, suggest that the Earth System may already have passed one "fork in the road" of potential pathways, a bifurcation (near A in Fig. 1) taking the Earth System out of the next glaciation cycle (11).

In the future, the Earth System could potentially follow many trajectories (12, 13), often represented by the large range of global temperature rises simulated by climate models (14). In most analyses, these trajectories are largely driven by the amount of greenhouse gases that human activities have already emitted and will continue to emit into the atmosphere over the rest of this century and beyond—with a presumed quasilinear relationship between cumulative carbon dioxide emissions and global temperature rise (14). However, here we suggest that biogeophysical feedback processes within the Earth System coupled with direct human degradation of the biosphere may play a more important role than normally assumed, limiting the range of potential future trajectories and potentially eliminating the possibility of the intermediate trajectories. We argue that there is a significant risk that these internal dynamics, especially strong nonlinearities in feedback processes, could become an important or perhaps, even dominant factor in steering the trajectory that the Earth System actually follows over coming centuries.

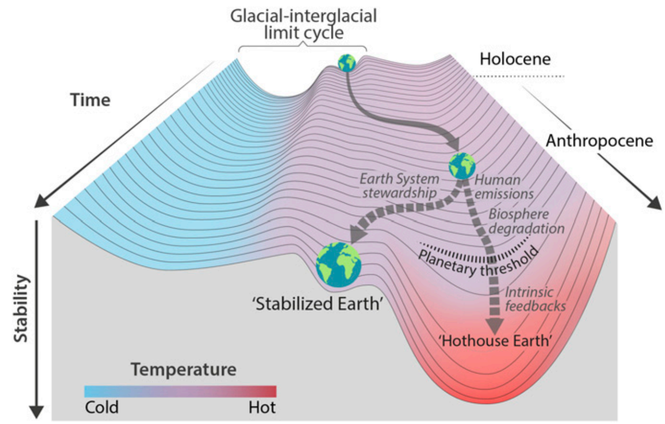

Fig. 2. Stability landscape showing the pathway of the Earth System out of the Holocene and thus, out of the glacial–interglacial limit cycle to its present position in the hotter Anthropocene. The fork in the road in Fig. 1 is shown here as the two divergent pathways of the Earth System in the future (broken arrows). Currently, the Earth System is on a Hothouse Earth pathway driven by human emissions of greenhouse gases and biosphere degradation toward a planetary threshold at ∼2 °C (horizontal broken line at 2 °C in Fig. 1), beyond which the system follows an essentially irreversible pathway driven by intrinsic biogeophysical feedbacks. The other pathway leads to Stabilized Earth, a pathway of Earth System stewardship guided by human-created feedbacks to a quasistable, human-maintained basin of attraction. "Stability" (vertical axis) is defined here as the inverse of the potential energy of the system. Systems in a highly stable state (deep valley) have low potential energy, and considerable energy is required to move them out of this stable state. Systems in an unstable state (top of a hill) have high potential energy, and they require only a little additional energy to push them off the hill and down toward a valley of lower potential energy.

This risk is represented in Figs. 1 and 2 by a planetary threshold (horizontal broken line in Fig. 1 on the Hothouse Earth pathway around 2 °C above preindustrial temperature). Beyond this threshold, intrinsic biogeophysical feedbacks in the Earth System (*Biogeophysical Feedbacks*) could become the dominant processes controlling the system's trajectory. Precisely where a potential planetary threshold might be is uncertain (15, 16). We suggest 2 °C because of the risk that a 2 °C warming could activate important tipping elements (12, 17), raising the temperature further to activate other tipping elements in a domino-like cascade that could take the Earth System to even higher temperatures (*Tipping Cascades*). Such cascades comprise, in essence, the dynamical process that leads to thresholds in complex systems (section 4.2 in ref. 18).

This analysis implies that, even if the Paris Accord target of a 1.5 °C to 2.0 °C rise in temperature is met, we cannot exclude the risk that a cascade of feedbacks could push the Earth System irreversibly onto a "Hothouse Earth" pathway. The challenge that humanity faces is to create a "Stabilized Earth" pathway that steers the Earth System away from its current trajectory toward the threshold beyond which is Hothouse Earth (Fig. 2). The human-created Stabilized Earth pathway leads to a basin of attraction that is not likely to exist in the Earth System's stability landscape without human stewardship to create and maintain it. Creating such a pathway and basin of attraction requires a fundamental change in the role of humans on the planet. This stewardship role requires deliberate and sustained action to become an integral, adaptive part of Earth System dynamics, creating feedbacks that keep the system on a Stabilized Earth pathway (*Alternative Stabilized Earth Pathway*).

We now explore this critical question in more detail by considering the relevant biogeophysical feedbacks (*Biogeophysical Feedbacks*) and the risk of tipping cascades (*Tipping Cascades*).

Biogeophysical Feedbacks. The trajectory of the Earth System is influenced by biogeophysical feedbacks within the system that can maintain it in a given state (negative feedbacks) and those that can amplify a perturbation and drive a transition to a different state (positive feedbacks). Some of the key negative feedbacks that could maintain the Earth System in Holocene-like conditions—notably, carbon uptake by land and ocean systems—are weakening relative to human forcing (19), increasing the risk that positive feedbacks could play an important role in determining the Earth System's trajectory. Table 1 summarizes carbon cycle feedbacks that could accelerate warming, while *SI Appendix*, Table S2 describes in detail a more complete set of biogeophysical feedbacks that can be triggered by forcing levels likely to be reached within the rest of the century.

Most of the feedbacks can show both continuous responses and tipping point behavior in which the feedback process becomes self-perpetuating after a critical threshold is crossed; subsystems exhibiting this behavior are often called "tipping elements" (17). The type of behavior—continuous response or tipping point/abrupt change—can depend on the magnitude or the rate of forcing, or both. Many feedbacks will show some gradual change before the tipping point is reached.

A few of the changes associated with the feedbacks are reversible on short timeframes of 50–100 years (e.g., change in Arctic sea ice extent with a warming or cooling of the climate; Antarctic sea ice may be less reversible because of heat accumulation in the Southern Ocean), but most changes are largely irreversible on timeframes that matter to contemporary societies (e.g., loss of permafrost carbon). A few of the feedbacks do not have apparent thresholds (e.g., change in the land and ocean physiological carbon sinks, such as increasing carbon uptake due

Table 1. Carbon cycle feedbacks in the Earth System that could accelerate global warming

Feedback	Strength of feedback by 2100,* °C	Refs. (*SI Appendix*, Table S2 has more details)
Permafrost thawing	0.09 (0.04–0.16)	20–23
Relative weakening of land and ocean physiological C sinks	0.25 (0.13–0.37)	24
Increased bacterial respiration in the ocean	0.02	25, 26
Amazon forest dieback	0.05 (0.03–0.11)	27
Boreal forest dieback	0.06 (0.02–0.10)	28
Total	0.47 (0.24–0.66)	

The strength of the feedback is estimated at 2100 for an ∼2 °C warming.
*The additional temperature rise (degrees Celsius) by 2100 arising from the feedback.

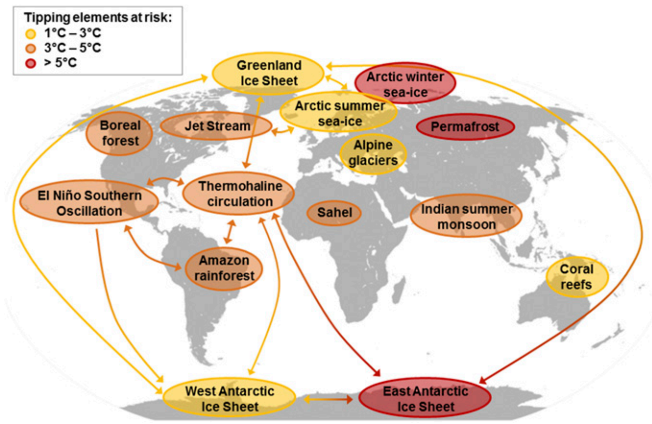

Fig. 3. Global map of potential tipping cascades. The individual tipping elements are color- coded according to estimated thresholds in global average surface temperature (tipping points) (12, 34). Arrows show the potential interactions among the tipping elements based on expert elicitation that could generate cascades. Note that, although the risk for tipping (loss of) the East Antarctic Ice Sheet is proposed at >5 °C, some marine-based sectors in East Antarctica may be vulnerable at lower temperatures (35–38).

to the CO_2 fertilization effect or decreasing uptake due to a decrease in rainfall). For some of the tipping elements, crossing the tipping point could trigger an abrupt, nonlinear response (e.g., conversion of large areas of the Amazon rainforest to a savanna or seasonally dry forest), while for others, crossing the tipping point would lead to a more gradual but self-perpetuating response (large-scale loss of permafrost). There could also be considerable lags after the crossing of a threshold, particularly for those tipping elements that involve the melting of large masses of ice. However, in some cases, ice loss can be very rapid when occurring as massive iceberg outbreaks (e.g., Heinrich Events).

For some feedback processes, the magnitude—and even the direction—depend on the rate of climate change. If the rate of climate change is small, the shift in biomes can track the change in temperature/moisture, and the biomes may shift gradually, potentially taking up carbon from the atmosphere as the climate warms and atmospheric CO_2 concentration increases. However, if the rate of climate change is too large or too fast, a tipping point can be crossed, and a rapid biome shift may occur via extensive disturbances (e.g., wildfires, insect attacks, droughts) that can abruptly remove an existing biome. In some terrestrial cases, such as widespread wildfires, there could be a pulse of carbon to the atmosphere, which if large enough, could influence the trajectory of the Earth System (29).

Varying response rates to a changing climate could lead to complex biosphere dynamics with implications for feedback processes. For example, delays in permafrost thawing would most likely delay the projected northward migration of boreal forests (30), while warming of the southern areas of these forests could result in their conversion to steppe grasslands of significantly lower carbon storage capacity. The overall result would be a positive feedback to the climate system.

The so-called "greening" of the planet, caused by enhanced plant growth due to increasing atmospheric CO_2 concentration (31), has increased the land carbon sink in recent decades (32). However, increasing atmospheric CO_2 raises temperature, and hotter leaves photosynthesize less well. Other feedbacks are also involved—for instance, warming the soil increases microbial respiration, releasing CO_2 back into the atmosphere.

Our analysis focuses on the strength of the feedback between now and 2100. However, several of the feedbacks that show negligible or very small magnitude by 2100 could nevertheless be triggered well before then, and they could eventually generate significant feedback strength over longer timeframes—centuries and even millennia—and thus, influence the long-term trajectory of the Earth System. These feedback processes include permafrost thawing, decomposition of ocean methane hydrates, increased marine bacterial respiration, and loss of polar ice sheets accompanied by a rise in sea levels and potential amplification of temperature rise through changes in ocean circulation (33).

Tipping Cascades. Fig. 3 shows a global map of some potential tipping cascades. The tipping elements fall into three clusters based on their estimated threshold temperature (12, 17, 39). Cascades could be formed when a rise in global temperature reaches the level of the lower-temperature cluster, activating tipping elements, such as loss of the Greenland Ice Sheet or Arctic sea ice. These tipping elements, along with some of the non-tipping element feedbacks (e.g., gradual weakening of land and ocean physiological carbon sinks), could push the global average temperature even higher, inducing tipping in mid- and higher-temperature clusters. For example, tipping (loss) of the Greenland Ice Sheet could trigger a critical transition in the Atlantic Meridional Ocean Circulation (AMOC), which could together, by causing sea-level rise and Southern Ocean heat accumulation, accelerate ice loss from the East Antarctic Ice Sheet (32, 40) on timescales of centuries (41).

Observations of past behavior support an important contribution of changes in ocean circulation to such feedback cascades. During previous glaciations, the climate system flickered between two states that seem to reflect changes in convective activity in the Nordic seas and changes in the activity of the AMOC. These variations caused typical temperature response patterns called the "bipolar seesaw" (42–44). During extremely cold conditions in the north, heat accumulated in the Southern Ocean, and Antarctica warmed. Eventually, the heat made its way north and generated subsurface warming that may have been instrumental in destabilizing the edges of the Northern Hemisphere ice sheets (45).

If Greenland and the West Antarctic Ice Sheet melt in the future, the freshening and cooling of nearby surface waters will have significant effects on the ocean circulation. While the probability of significant circulation changes is difficult to quantify, climate model simulations suggest that freshwater inputs compatible with current rates of Greenland melting are sufficient to have measurable effects on ocean temperature and circulation (46, 47). Sustained warming of the northern high latitudes as a result of this process could accelerate feedbacks or activate tipping elements in that region, such as permafrost degradation, loss of Arctic sea ice, and boreal forest dieback.

While this may seem to be an extreme scenario, it illustrates that a warming into the range of even the lower-temperature cluster (i.e., the Paris targets) could lead to tipping in the mid- and higher-temperature clusters via cascade effects. Based on this analysis of tipping cascades and taking a risk-averse approach, we suggest that a potential planetary threshold could occur at a temperature rise as low as ~2.0 °C above preindustrial (Fig. 1).

Alternative Stabilized Earth Pathway

If the world's societies want to avoid crossing a potential threshold that locks the Earth System into the Hothouse Earth pathway, then it is critical that they make deliberate decisions to avoid this risk and maintain the Earth System in Holocene-like conditions. This human-created pathway is represented in Figs. 1 and 2 by what we call Stabilized Earth (small loop at the bottom of Fig. 1, *Upper Right*), in which the Earth System is maintained in a state with a temperature rise no greater than 2 °C above preindustrial (a "super-Holocene" state) (11). Stabilized Earth would require deep cuts in greenhouse gas emissions, protection and enhancement of biosphere carbon sinks, efforts to remove CO_2 from the atmosphere, possibly solar radiation management, and adaptation to unavoidable impacts of the warming already occurring (48). The short broken red line beyond Stabilized Earth in Fig. 1, *Upper Right* represents a potential return to interglacial-like conditions in the longer term.

In essence, the Stabilized Earth pathway could be conceptualized as a regime of the Earth System in which humanity plays an active planetary stewardship role in maintaining a state intermediate between the glacial–interglacial limit cycle of the Late Quaternary and a Hothouse Earth (Fig. 2). We emphasize that Stabilized Earth is not an intrinsic state of the Earth System but rather, one in which humanity commits to a pathway of ongoing management of its relationship with the rest of the Earth System.

A critical issue is that, if a planetary threshold is crossed toward the Hothouse Earth pathway, accessing the Stabilized Earth pathway would become very difficult no matter what actions human societies might take. Beyond the threshold, positive (reinforcing) feedbacks within the Earth System—outside of human influence or control—could become the dominant driver of the system's pathway, as individual tipping elements create linked cascades through time and with rising temperature (Fig. 3). In other words, after the Earth System is committed to the Hothouse Earth pathway, the alternative Stabilized Earth pathway would very likely become inaccessible as illustrated in Fig. 2.

What Is at Stake? Hothouse Earth is likely to be uncontrollable and dangerous to many, particularly if we transition into it in only a century or two, and it poses severe risks for health, economies, political stability (12, 39, 49, 50) (especially for the most climate vulnerable), and ultimately, the habitability of the planet for humans.

Insights into the risks posed by the rapid climatic changes emerging in the Anthropocene can be obtained not only from contemporary observations (51–55) but also, from interactions in the past between human societies and regional and seasonal hydroclimate variability. This variability was often much more pronounced than global, longer-term Holocene variability (*SI Appendix*). Agricultural production and water supplies are especially vulnerable to changes in the hydroclimate, leading to hot/dry or cool/wet extremes. Societal declines, collapses, migrations/resettlements, reorganizations, and cultural changes were often associated with severe regional droughts and with the global megadrought at 4.2–3.9 thousand years before present, all occurring within the relative stability of the narrow global Holocene temperature range of approximately ±1 °C (56).

SI Appendix, Table S4 summarizes biomes and regional biosphere–physical climate subsystems critical for human wellbeing and the resultant risks if the Earth System follows a Hothouse Earth pathway. While most of these biomes or regional systems may be retained in a Stabilized Earth pathway, most or all of them would likely be substantially changed or degraded in a Hothouse Earth pathway, with serious challenges for the viability of human societies.

For example, agricultural systems are particularly vulnerable, because they are spatially organized around the relatively stable Holocene patterns of terrestrial primary productivity, which depend on a well-established and predictable spatial distribution of temperature and precipitation in relation to the location of fertile soils as well as on a particular atmospheric CO_2 concentration. Current understanding suggests that, while a Stabilized Earth pathway could result in an approximate balance between increases and decreases in regional production as human systems adapt, a Hothouse Earth trajectory will likely exceed the limits of adaptation and result in a substantial overall decrease in agricultural production, increased prices, and even more disparity between wealthy and poor countries (57).

The world's coastal zones, especially low-lying deltas and the adjacent coastal seas and ecosystems, are particularly important for human wellbeing. These areas are home to much of the world's population, most of the emerging megacities, and a significant amount of infrastructure vital for both national economies and international trade. A Hothouse Earth trajectory would almost certainly flood deltaic environments, increase the risk of damage from coastal storms, and eliminate coral reefs (and all of the benefits that they provide for societies) by the end of this century or earlier (58).

Human Feedbacks in the Earth System. In the dominant climate change narrative, humans are an external force driving change to the Earth System in a largely linear, deterministic way; the higher the forcing in terms of anthropogenic greenhouse gas emissions, the higher the global average temperature. However, our analysis argues that human societies and our activities need to be recast as an integral, interacting component of a complex, adaptive Earth System. This framing puts the focus not only on human system dynamics that reduce greenhouse gas emissions but also, on those that create or enhance negative feedbacks that reduce the risk that the Earth System will cross a planetary threshold and lock into a Hothouse Earth pathway.

Humanity's challenge then is to influence the dynamical properties of the Earth System in such a way that the emerging unstable conditions in the zone between the Holocene and a very hot state become a de facto stable intermediate state (Stabilized Earth) (Fig. 2). This requires that humans take deliberate, integral, and adaptive steps to reduce dangerous impacts on the Earth System, effectively monitoring and changing behavior to form feedback loops that stabilize this intermediate state.

There is much uncertainty and debate about how this can be done—technically, ethically, equitably, and economically—and there is no doubt that the normative, policy, and institutional aspects are highly challenging. However, societies could take a wide range of actions that constitute negative feedbacks, summarized in *SI Appendix*, Table S5, to steer the Earth System toward Stabilized Earth. Some of these actions are already altering emission trajectories. The negative feedback actions fall into three broad categories: (*i*) reducing greenhouse gas emissions, (*ii*) enhancing or creating carbon sinks (e.g., protecting and enhancing biosphere carbon sinks and creating new types of sinks) (59), and (*iii*) modifying Earth's energy balance (for example, via solar radiation management, although that particular feedback entails very large risks of destabilization or degradation of several key processes in the Earth System) (60, 61). While reducing emissions is a priority, much more could be done to reduce direct human pressures on critical biomes that contribute to the regulation of the state of the Earth System through carbon sinks and moisture feedbacks, such as the Amazon and boreal forests (Table 1), and to build much more effective stewardship of the marine and terrestrial biospheres in general.

The present dominant socioeconomic system, however, is based on high-carbon economic growth and exploitative resource use (9). Attempts to modify this system have met with some success locally but little success globally in reducing greenhouse gas emissions or building more effective stewardship of the biosphere. Incremental linear changes to the present socioeconomic system are not enough to stabilize the Earth System. Widespread, rapid, and fundamental transformations will likely be required to reduce the risk of crossing the threshold and locking in the Hothouse Earth pathway; these include changes in behavior, technology and innovation, governance, and values (48, 62, 63).

International efforts to reduce human impacts on the Earth System while improving wellbeing include the United Nations Sustainable Development Goals and the commitment in the Paris agreement to keep warming below 2 °C. These international governance initiatives are matched by carbon reduction commitments by countries, cities, businesses, and individuals (64–66) , but as yet, these are not enough to meet the Paris target. Enhanced ambition will need new collectively shared values, principles, and frameworks as well as education to support such changes (67, 68). In essence, effective Earth System stewardship is an essential precondition for the prosperous development of human societies in a Stabilized Earth pathway (69, 70).

In addition to institutional and social innovation at the global governance level, changes in demographics, consumption, behavior, attitudes, education, institutions, and socially embedded technologies are all important to maximize the chances of achieving a Stabilized Earth pathway (71). Many of the needed shifts may take decades to have a globally aggregated impact (*SI Appendix*, Table S5), but there are indications that society may be reaching some important societal tipping points. For example, there has been relatively rapid progress toward slowing or reversing population growth through declining fertility resulting from the empowerment of women, access to birth control technologies, expansion of educational opportunities, and rising income levels (72, 73). These demographic changes must be complemented by sustainable per capita consumption patterns, especially among the higher per capita consumers. Some changes in consumer behavior have been observed (74, 75), and opportunities for consequent major transitions in social norms over broad scales may arise (76). Technological innovation is contributing to more rapid decarbonization and the possibility for removing CO_2 from the atmosphere (48).

Ultimately, the transformations necessary to achieve the Stabilized Earth pathway require a fundamental reorientation and restructuring of national and international institutions toward more effective governance at the Earth System level (77), with a much stronger emphasis on planetary concerns in economic governance, global trade, investments and finance, and technological development (78).

Building Resilience in a Rapidly Changing Earth System. Even if a Stabilized Earth pathway is achieved, humanity will face a turbulent road of rapid and profound changes and uncertainties on route to it—politically, socially, and environmentally—that challenge the resilience of human societies (79–82). Stabilized Earth will likely be warmer than any other time over the last 800,000 years at least (83) (that is, warmer than at any other time in which fully modern humans have existed).

In addition, the Stabilized Earth trajectory will almost surely be characterized by the activation of some tipping elements (*Tipping Cascades* and Fig. 3) and by nonlinear dynamics and abrupt shifts at the level of critical biomes that support humanity (*SI Appendix*, Table S4). Current rates of change of important features of the Earth System already match or exceed those of abrupt geophysical events in the past (*SI Appendix*). With these trends likely to continue for the next several decades at least, the contemporary way of guiding development founded on theories, tools, and beliefs of gradual or incremental change, with a focus on economy efficiency, will likely not be adequate to cope with this trajectory. Thus, in addition to adaptation, increasing resilience will become a key strategy for navigating the future.

Generic resilience-building strategies include developing insurance, buffers, redundancy, diversity, and other features of resilience that are critical for transforming human systems in the face of warming and possible surprise associated with tipping points (84). Features of such a strategy include (*i*) maintenance of diversity, modularity, and redundancy; (*ii*) management of connectivity, openness, slow variables, and feedbacks; (*iii*) understanding social–ecological systems as complex adaptive systems, especially at the level of the Earth System as a whole (85); (*iv*) encouraging learning and experimentation; and (*v*) broadening of participation and building of trust to promote polycentric governance systems (86, 87).

Conclusions

Our systems approach, focusing on feedbacks, tipping points, and nonlinear dynamics, has addressed the four questions posed in the Introduction.

Our analysis suggests that the Earth System may be approaching a planetary threshold that could lock in a continuing rapid pathway toward much hotter conditions—Hothouse Earth. This pathway would be propelled by strong, intrinsic, biogeophysical feedbacks difficult to influence by human actions, a pathway that could not be reversed, steered, or substantially slowed.

Where such a threshold might be is uncertain, but it could be only decades ahead at a temperature rise of ~2.0 °C above preindustrial, and thus, it could be within the range of the Paris Accord temperature targets.

The impacts of a Hothouse Earth pathway on human societies would likely be massive, sometimes abrupt, and undoubtedly disruptive.

Avoiding this threshold by creating a Stabilized Earth pathway can only be achieved and maintained by a coordinated, deliberate effort by human societies to manage our relationship with the rest of the Earth System, recognizing that humanity is an integral, interacting component of the system. Humanity is now facing the need for critical decisions and actions that could influence our future for centuries, if not millennia (88).

How credible is this analysis? There is significant evidence from a number of sources that the risk of a planetary threshold and thus, the need to create a divergent pathway should be taken seriously:

First, the complex system behavior of the Earth System in the Late Quaternary is well-documented and understood. The two bounding states of the system—glacial and interglacial—are reasonably well-defined, the ca. 100,000-years periodicity of the limit cycle is established, and internal (carbon cycle and ice albedo feedbacks) and external (changes in insolation caused by changes in Earth's orbital parameters) driving processes are generally well-known. Furthermore, we know with high confidence that the progressive disintegration of ice sheets and the transgression of other tipping elements are difficult to reverse after critical levels of warming are reached.

Second, insights from Earth's recent geological past (*SI Appendix*) suggest that conditions consistent with the Hothouse Earth pathway are accessible with levels of atmospheric CO_2 concentration and temperature rise either already realized or projected for this century (*SI Appendix*, Table S1).

Third, the tipping elements and feedback processes that operated over Quaternary glacial–interglacial cycles are the same as several of those proposed as critical for the future trajectory of the Earth System (*Biogeophysical Feedbacks*, *Tipping Cascades*, Fig. 3, Table 1, and *SI Appendix*, Table S2).

Fourth, contemporary observations (29, 38) (*SI Appendix*) of tipping element behavior at an observed temperature anomaly of about 1 °C above preindustrial suggest that some of these elements are vulnerable to tipping within just a 1 °C to 3 °C increase in global temperature, with many more of them vulnerable at higher temperatures (*Biogeophysical Feedbacks* and *Tipping Cascades*) (12, 17, 39). This suggests that the risk of tipping cascades could be significant at a 2 °C temperature rise and could increase sharply beyond that point. We argue that a planetary threshold in the Earth System could exist at a temperature rise as low as 2 °C above preindustrial.

The Stabilized Earth trajectory requires deliberate management of humanity's relationship with the rest of the Earth System if the world is to avoid crossing a planetary threshold. We suggest that a deep transformation based on a fundamental reorientation of human values, equity, behavior, institutions, economies, and technologies is required. Even so, the pathway toward Stabilized Earth will involve considerable changes to the structure and functioning of the Earth System, suggesting that resilience-building strategies be given much higher priority than at present in decision making. Some signs are emerging that societies are initiating some of the necessary transformations. However, these transformations are still in initial stages, and the social/political tipping points that definitively move the current trajectory away from Hothouse Earth have not yet been crossed, while the door to the Stabilized Earth pathway may be rapidly closing.

Our initial analysis here needs to be underpinned by more in-depth, quantitative Earth System analysis and modeling studies to address three critical questions. (*i*) Is humanity at risk for pushing the system across a planetary threshold and irreversibly down a Hothouse Earth pathway? (*ii*) What other pathways might be possible in the complex stability landscape of the Earth System, and what risks might they entail? (*iii*) What planetary stewardship strategies are required to maintain the Earth System in a manageable Stabilized Earth state?

Acknowledgments

We thank the three reviewers for their comments on the first version of the manuscript and two of the reviewers for further comments on a revised version of the manuscript. These comments were very helpful in the revisions. We thank a member of the PNAS editorial board for a comprehensive and very helpful review. W.S. and C.P.S. are members of the Anthropocene Working Group. W.S., J.R., K.R., S.E.C., J.F.D., I.F., S.J.L., R.W. and H.J.S. are members of the Planetary Boundaries Research Network PB.net and the Earth League's EarthDoc Programme supported by the Stordalen Foundation. T.M.L. was supported by a Royal Society Wolfson Research Merit Award and the European Union Framework Programme 7 Project HELIX. C.F. was supported by the Erling–Persson Family Foundation. The participation of D.L. was supported by the Haury Program in Environment and Social Justice and National Science Foundation (USA) Decadal and Regional Climate Prediction using Earth System Models Grant 1243125. S.E.C. was supported in part by Swedish Research Council Formas Grant 2012-742. J.F.D. and R.W. were supported by Leibniz Association Project DOMINOES. S.J.L. receives funding from Formas Grant 2014-589. This paper is a contribution to European Research Council Advanced Grant 2016, Earth Resilience in the Anthropocene Project 743080.

1 Crutzen PJ (2002) Geology of mankind. *Nature* 415:23.
2 Steffen W, Broadgate W, Deutsch L, Gaffney O, Ludwig C (2015) The trajectory of the Anthropocene: The great acceleration. *Anthropocene Rev* 2:81–98.
3 Waters CN, et al. (2016) The Anthropocene is functionally and stratigraphically distinct from the Holocene. *Science* 351:aad2622.
4 Malm A, Hornborg A (2014) The geology of mankind? A critique of the Anthropocene narrative. *Anthropocene Rev* 1:62–69.
5 Donges JF, et al. (2017) Closing the loop: Reconnecting human dynamics to Earth System science. *Anthropocene Rev* 4:151–157.
6 Levin SA (2003) Complex adaptive systems: Exploring the known, the unknown and the unknowable. *Bull Am Math Soc* 40:3–20.
7 Past Interglacial Working Group of PAGES (2016) Interglacials of the last 800,000 years. *Rev Geophys* 54:162–219.
8 Williams M, et al. (2015) The Anthropocene biosphere. *Anthropocene Rev* 2:196–219.
9 McNeill JR, Engelke P (2016) *The Great Acceleration* (Harvard Univ Press, Cambridge, MA).
10 Hawkins E, et al. (2017) Estimating changes in global temperature since the pre-industrial period. *Bull Am Meteorol Soc* 98:1841–1856.
11 Ganopolski A, Winkelmann R, Schellnhuber HJ (2016) Critical insolation-CO_2 relation for diagnosing past and future glacial inception. *Nature* 529:200–203.
12 Schellnhuber HJ, Rahmstorf S, Winkelmann R (2016) Why the right climate target was agreed in Paris. *Nat Clim Change* 6:649–653.
13 Schellnhuber HJ (1999) 'Earth system' analysis and the second Copernican revolution. *Nature* 402(Suppl):C19–C23.
14 IPCC (2013) Summary for policymakers. *Climate Change 2013: The Physical Science Basis, Contribution of Working Group I to the Fifth Assessment Report of the Intergovernmental Panel on Climate Change*, eds Stocker TF, et al. (Cambridge Univ Press, Cambridge, UK), pp 3–29.
15 Drijfhout S, et al. (2015) Catalogue of abrupt shifts in Intergovernmental Panel on Climate Change climate models. *Proc Natl Acad Sci USA* 112:E5777–E5786.
16 Stocker TF, et al. (2013) Technical summary. *Climate Change 2013: The Physical Science Basis. Contribution of Working Group I to the Fifth Assessment Report of the Intergovernmental Panel on Climate Change*, eds Stocker TF, et al. (Cambridge Univ Press, Cambridge, UK).
17 Lenton TM, et al. (2008) Tipping elements in the Earth's climate system. *Proc Natl Acad Sci USA* 105:1786–1793.
18 Scheffer M (2009) *Critical Transitions in Nature and Society* (Princeton Univ Press, Princeton).
19 Raupach MR, et al. (2014) The declining uptake rate of atmospheric CO_2 by land and ocean sinks. *Biogeosciences* 11:3453–3475.
20 Schaefer K, Lantuit H, Romanovsky VE, Schuur EAG, Witt R (2014) The impact of the permafrost carbon feedback on global climate. *Environ Res Lett* 9:085003.
21 Schneider von Deimling T, et al. (2015) Observation-based modelling of permafrost carbon fluxes with accounting for deep carbon deposits and thermokarst activity. *Biogeosciences* 12:3469–3488.
22 Koven CD, et al. (2015) A simplified, data-constrained approach to estimate the permafrost carbon-climate feedback. *Philos Trans A Math Phys Eng Sci* 373:20140423.
23 Chadburn SE, et al. (2017) An observation-based constraint on permafrost loss as a function of global warming. *Nat Clim Change* 7:340–344.
24 Ciais P, et al. (2013) Carbon and other biogeochemical cycles. *Climate Change 2013: The Physical Science Basis, Contribution of Working Group I to the Fifth Assessment Report of the Intergovernmental Panel on Climate Change*, eds Stocker TF, et al. (Cambridge Univ Press, Cambridge, UK), pp 465–570.
25 Segschneider J, Bendtsen J (2013) Temperature-dependent remineralization in a warming ocean increases surface pCO_2 through changes in marine ecosystem composition. *Global Biogeochem Cycles* 27:1214–1225.
26 Bendtsen J, Hilligsøe KM, Hansen J, Richardson K (2015) Analysis of remineralisation, lability, temperature sensitivity and structural composition of organic matter from the upper ocean. *Prog Oceanogr* 130:125–145.
27 Jones C, Lowe J, Liddicoat S, Betts R (2009) Committed terrestrial ecosystem changes due to climate change. *Nat Geosci* 2:484–487.
28 Kurz WA, Apps MJ (1999) A 70-year retrospective analysis of carbon fluxes in the Canadian forest sector. *Ecol Appl* 9:526–547.
29 Lewis SL, Brando PM, Phillips OL, van der Heijden GMF, Nepstad D (2011) The 2010 Amazon drought. *Science* 331:554.
30 Herzschuh U, et al. (2016) Glacial legacies on interglacial vegetation at the Pliocene-Pleistocene transition in NE Asia. *Nature Commun* 7:11967.

31 Mao J, et al. (2016) Human-induced greening of the northern extratropical land surface. *Nat Clim Change* 6:959–963.
32 Keenan TF, et al. (2016) Recent pause in the growth rate of atmospheric CO_2 due to enhanced terrestrial carbon uptake. *Nature Commun* 7:13428, and erratum (2017) 8:16137.
33 Hansen J, et al. (2016) Ice melt, sea level rise and superstorms: Evidence from paleoclimatedata, climate modeling, and modern observations that 2 °C global warming could be dangerous. *Atmos Chem Phys* 16:3761–3812.
34 Kriegler E, Hall JW, Held H, Dawson R, Schellnhuber HJ (2009) Imprecise probability assessment of tipping points in the climate system. *Proc Natl Acad Sci USA* 106:5041–5046.
35 Pollard D, DeConto RM (2009) Modelling West Antarctic ice sheet growth and collapse through the past five million years. *Nature* 458:329–332.
36 Pollard D, DeConto RM, Alley RB (2015) Potential Antarctic Ice Sheet retreat driven by hydrofracturing and ice cliff failure. *Earth Planet Sci Lett* 412:112–121.
37 DeConto RM, Pollard D (2016) Contribution of Antarctica to past and future sea-level rise. *Nature* 531:591–597.
38 Rintoul SR, et al. (2016) Ocean heat drives rapid basal melt of the Totten Ice Shelf. *Sci Adv* 2:e1601610.
39 US Department of Defense (2015) National security implications of climate-related risks and a changing climate. Available at archive.defense.gov/pubs/150724-congressional-report-on-national-implications-of-climate-change.pdf?source=govdelivery. Accessed February 7, 2018.
40 Mengel M, Levermann A (2014) Ice plug prevents irreversible discharge from East Antarctica. *Nat Clim Change* 4:451–455.
41 Armour KC, et al. (2016) Southern Ocean warming delayed by circumpolar upwelling and equatorward transport. *Nat Geosci* 9:549–554.
42 Stocker TF, Johnsen SJ (2003) A minimum thermodynamic model for the bipolar seesaw. *Paleoceanography* 18:1087.
43 Rahmstorf S (2002) Ocean circulation and climate during the past 120,000 years. *Nature* 419:207–214.
44 Hemming SR (2004) Heinrich events: Massive late Pleistocene detritus layers of the North Atlantic and their global climate imprint. *Rev Geophys* 42:1–43.
45 Alvarez-Solas J, et al. (2010) Link between ocean temperature and iceberg discharge during Heinrich events. *Nat Geosci* 3:122–126.
46 Stouffer RJ, et al. (2006) Investigating the causes of the response of the thermohaline circulation to past and future climate changes. *J Clim* 19:1365–1387.
47 Swingedow D, et al. (2013) Decadal fingerprints of freshwater discharge around Greenland in a multi-model ensemble. *Clim Dyn* 41:695–720.
48 Rockström J, et al. (2017) A roadmap for rapid decarbonization. *Science* 355:1269–1271.
49 Schleussner C-F, Donges JF, Donner RV, Schellnhuber HJ (2016) Armed-conflict risks enhanced by climate-related disasters in ethnically fractionalized countries. *Proc Natl Acad Sci USA* 113:9216–9221.
50 McMichael AJ, et al., eds (2003) *Climate Change and Human Health: Risks and Responses* (WHO, Geneva).
51 Udmale PD, et al. (2015) How did the 2012 drought affect rural livelihoods in vulnerable areas? Empirical evidence from India. *Int J Disaster Risk Reduct* 13:454–469.
52 Maldonado JK, Shearer C, Bronen R, Peterson K, Lazrus H (2013) The impact of climate change on tribal communities in the US: Displacement, relocation, and human rights. *Clim Change* 120:601–614.
53 Warner K, Afifi T (2014) Where the rain falls: Evidence from 8 countries on how vulnerable households use migration to manage the risk of rainfall variability and food insecurity. *Clim Dev* 6:1–17.
54 Cheung WW, Watson R, Pauly D (2013) Signature of ocean warming in global fisheries catch. *Nature* 497:365–368.
55 Nakano K (2017) Screening of climatic impacts on a country's international supply chains: Japan as a case study. *Mitig Adapt Strategies Glob Change* 22:651–667.
56 Latorre C, Wilmshurst J, von Gunten L, eds (2016) Climate change and cultural evolution. *PAGES (Past Global Changes) Magazine* 24:1–32.
57 IPCC (2014) Summary for policymakers. *Climate Change 2014: Impacts, Adaptation, and Vulnerability. Part A: Global and Sectoral Aspects. Contribution of Working Group II to the Fifth Assessment Report of the Intergovernmental Panel on Climate Change*, eds Field CB, et al. (Cambridge Univ Press, Cambridge, UK), pp 1–32.
58 Schleussner C-F, et al. (2016) Science and policy characteristics of the Paris Agreement temperature goal. *Nat Clim Change* 6:827–835.
59 Griscom BW, et al. (2017) Natural climate solutions. *Proc Natl Acad Sci USA* 114:11645–11650.
60 Barrett S, et al. (2014) Climate engineering reconsidered. *Nat Clim Change* 4:527–529.
61 Mathesius S, Hofmann M, Calderia K, Schellnhuber HJ (2015) Long-term response of oceans to CO_2 removal from the atmosphere. *Nat Clim Change* 5:1107–1113.
62 Geels FW, Sovacool BK, Schwanen T, Sorrell S (2017) Sociotechnical transitions for deep decarbonization. *Science* 357:1242–1244.
63 O'Brien K (2018) Is the 1.5 °C target possible? Exploring the three spheres of transformation. *Curr Opin Environ Sustain* 31:153–160.
64 Young OR, et al. (2006) The globalization of socioecological systems: An agenda for scientific research. *Glob Environ Change* 16:304–316.
65 Adger NW, Eakin H, Winkels A (2009) Nested and teleconnected vulnerabilities to environmental change. *Front Ecol Environ* 7:150–157.
66 UN General Assembly (2015) *Transforming Our World: The 2030 Agenda for Sustainable Development*, A/RES/70/1. Available at https://sustainabledevelopment.un.org/content/documents/21252030%20Agenda%20for%20Sustainable%20Development%20web.pdf. Accessed July 18, 2018.
67 Wals AE, Brody M, Dillon J, Stevenson RB (2014) Science education. Convergence between science and environmental education. *Science* 344:583–584.
68 O'Brien K, et al. (2013) You say you want a revolution? Transforming education and capacity building in response to global change. *Environ Sci Policy* 28:48–59.
69 Chapin FS, III, et al. (2011) Earth stewardship: A strategy for social–ecological transformation to reverse planetary degradation. *J Environ Stud Sci* 1:44–53.
70 Folke C, Biggs R, Norström AV, Reyers B, Rockström J (2016) Social-ecological resilience and biosphere-based sustainability science. *Ecol Soc* 21:41.
71 Westley F, et al. (2011) Tipping toward sustainability: Emerging pathways of transformation. *Ambio* 40:762–780.
72 Lutz W, Muttarak R, Striessnig E (2014) Environment and development. Universal education is key to enhanced climate adaptation. *Science* 346:1061–1062.
73 Bongaarts J (2016) Development: Slow down population growth. *Nature* 530:409–412.
74 Defila R, Di Giulio A, Kaufmann-Hayoz R, eds (2012) *The Nature of Sustainable Consumption and How to Achieve It: Results from the Focal Topic "From Knowledge to Action–New Paths Towards Sustainable Consumption"* (Oakum, Munich).
75 Cohen MJ, Szejnwald Brown H, Vergragt P, eds (2013) *Innovations in Sustainable Consumption: New Economics, Socio-Technical Transitions and Social Practices* (Edward Elgar, Cheltenham, UK).
76 Nyborg K, et al. (2016) Social norms as solutions. *Science* 354:42–43.
77 Biermann F, et al. (2012) Science and government. Navigating the anthropocene: Improving Earth system governance. *Science* 335:1306–1307.
78 Galaz V (2014) *Global Environmental Governance, Technology and Politics: The Anthropocene Gap* (Edward Elgar, Cheltenham, UK).
79 Peters DPC, et al. (2004) Cross-scale interactions, nonlinearities, and forecasting catastrophic events. *Proc Natl Acad Sci USA* 101:15130–15135.
80 Walker B, et al. (2009) Environment. Looming global-scale failures and missing institutions. *Science* 325:1345–1346.
81 Hansen J, Sato M, Ruedy R (2012) Perception of climate change. *Proc Natl Acad Sci USA* 109:E2415–E2423.
82 Galaz V, et al. (2017) Global governance dimensions of globally networked risks: The state of the art in social science research. *Risks Hazards Crisis Public Policy* 8:4–27.
83 Augustin L, et al.; EPICA community members (2004) Eight glacial cycles from an Antarctic ice core. *Nature* 429:623–628.
84 Polasky S, Carpenter SR, Folke C, Keeler B (2011) Decision-making under great uncertainty: Environmental management in an era of global change. *Trends Ecol Evol* 26:398–404.
85 Capra F, Luisi PL (2014) *The Systems View of Life; A Unifying Vision* (Cambridge Univ Press, Cambridge, UK).
86 Carpenter SR, et al. (2012) General resilience to cope with extreme events. *Sustainability* 4:3248–3259.
87 Biggs R, et al. (2012) Toward principles for enhancing the resilience of ecosystem services. *Annu Rev Environ Resour* 37:421–448.
88 Figueres C, et al. (2017) Three years to safeguard our climate. *Nature* 546:593–595.